1st Virtual International Conference
on
# GREEN TECHNOLOGIES FOR SUSTAINABLE DEVELOPMENT
(ICON-GTSD 2021)

# E-Proceeding

9th - 11th March, 2021

ORGANIZED BY:

## Dharmsinh Desai University(DDU)
College Road, Nadiad-387001, Gujarat, India

# Organizing *Committee*

| Position | Name of Authority |
|---|---|
| **Patron** | Dr. H. M.Desai, Vice Chancellor,Dharmsinh Desai University(DDU),Nadiad. |
| **Vice Patrons** | Mr. Ankur Desai, Campus Director, Dharmsinh Desai University, Nadiad<br>Mr. Narottam Sahoo, Advisor, Gujrat Council on Science and Technology, Gandhinargar |
| **Mentor** | Dr. Dinesh O. Shah, Founding Director of SSCSSN, DDU, Nadiad |
| **Conveners** | Dr. B.N. Suhagia, Dean, Faculty of Pharmacy, DDU, Nadiad<br>Dr. P.A. Joshi, Chairman & Professor, Anchor Institute, Department of Chemical Engineering, Nadiad |
| **Coordinator** | Dr. M.S.Rao, Professor and Head, Department of Chemical Engineering, DDU, Nadiad<br>Dr. Tejal Soni, Professor, Faculty of Pharmacy, DDU, Nadiad |
| **Organizing Secretory** | Dr. Atindra Shukla, Director, SSCSSN, DDU, Nadiad<br>Dr. Vimal Gandhi, Department of Chemical Engineering, DDU, Nadiad |
| **Organizing Committee** | Prof P C Chiang, National Taiwan University, Taipei, Taiwan<br>Prof P. Musonge, Researcher in Residence, Institute of Systems Science, Durban University of Technology, South Africa<br>Dr. Hyunook Kim, School of Environmental Engineering, University of Seoul, Seoul,South Korea.<br>Dr R V Jasra, Sr. Vice President, Research & Development, Reliance Industries Ltd,Vadodara<br>Mr. Ashok Panjwani, Director, BEIL Infrastructure Ltd, 9701-16, G.I.D.C., Ankleshwar, Gujarat - 393002<br>Mr Ketan Patel, CMD, Troikaa Pharmaceutical Limited, Ahmedabad<br>Dr. Sunil Bhagwat, Institute of Chemical Technology, Mumbai<br>Prof Sachin Parikh, Joint Director, Directorate of Technical Education, Gandhinagar<br>Dr. Bharat Jain, Member Secretary, GCPC, Gandhinagar<br>Dr Jaimin Vasa, President, Gujarat Chemical Association, Ahmedabad<br>Mr. Shital Patwa, Heatchem Engineers Pvt. Ltd., Ahmedabad<br>Dr. Manish Mishra, Department of Chemistry, S.P. University, Vidyanagar<br>Mr Shwetal Shah, Climate Change Department, Government of Gujarat.<br>Dr. Prachi Thareja, Department of Chemical Engineering, IIT, Gandhinagar.<br>Mr. Jaimin Shah, Co-founder and MD, Dev Infotech North America Ltd, Canada<br>Mr. Shrenik Trivedi, Syntron Industries Pvt Ltd., Ahmedabad.<br>Dr. Nitin Bhate, Department of Chemical Engineering, Faculty of Technology, M S University, Vadodara<br>Dr. Kaushik Nath, Department of Chemical Engineering, G.H. Patel Institute of Technology, Vidyanagar<br>Dr. Sanjay Patel, Department of Chemical Engineering, Institute of Technology, Nirma University, Ahmedabad |

| | | |
|---|---|---|
| | Dr. Kinjal Shah, College of Urban Construction, Nanjing Tech University, Nanjing, China.<br>Dr. Brajeshkumar, Head, PG Department of Chemistry, Tata College, Chaibasa, INDIA | |
| **Local Action Committee** | Dr. Avinash Deshmukh | Mehul Patel |
| | Dr. Jalesh Purohit | Dr. Tejas Patel |
| | Dr. Anand Dhanwani | Dr. R.B.Mardia |
| | Ms. Dipali Shah | Mr. Jagat Upadhyay |
| | Mr. Mihir Shah | Ms. Mayuri Patel |
| | Mr. Nirav Bhavsar | Ms. C.P.Macwan |
| | Mr. Siddharth Modi | Mr. V.T. Prajapati |
| | Mr. Hitesh Panchal | Dr. Kishor Sorathia |
| | Dr. Anand Tiwari | Dr. Arup Ghosh |
| | Dr. Mahendra Gaikwad | Ms. Charmy Malde |
| | Mr. Dhrumil Gandhi | Mr. Rignesh Patel |
| | Mr. Niraj Nair | Dr. Chirag Patel |
| | Dr. Bhupendra Suryanshi | Dr. Hemantkumar |
| | Dr. Krishna Chauhan | Ms. Mudita Garg |
| | Mr. Jaydeep Jivani | Ms. Jalpa Patel |
| | Ms. Gita Gohel | Mr. Vashisth Bhavsar |
| | Mr. Vasim Babuna | |

# <u>Chief Editors</u>

Dr. M.S. Rao (Head, Department of Chemical Engineering, DDU)

Dr. Jalesh Purohit (Professor, Department of Chemical Engineering, DDU)

Dr. Vimal Gandhi (Associate Professor, Department of Chemical Engineering, DDU)

## <u>Editors:</u>

# Preface

Green Technology for Sustainable Development - 2021 is a global event designed to provide platform for the deliberations on the Theme: "Sustainable development through green and clean technology for better future business". The main focus is to make a forum for professionals at all levels of the Chemical and Petrochemical industry, Petroleum Refining industry, Polymer industry, Pharmaceutical industry, and Speciality chemicals industry along with the support of Academia, with an objective to enhance their understanding of what will drive and shape the future of the Chemical Process Industries. The Conference is expected to have the participation of organizations and individuals from a wide variety of sector and countries. The renowned speakers from industry and academia and the panellist will help in making the sessions interactive and encourages a strong level of dialogue and discussion, thus maximising the benefits of attendance. Gujarat being a hub of chemical, petrochemical and allied chemical industries will surely be giving an investment and business opportunity to the participants.

Dharmsinh Desai University (DDU) has been a pioneer in chemical technology in Gujarat since 1968 and has evolved in to a full-fledged professional university offering variety of engineering, management and medical courses. The University was established in 1968 with diploma and degree program in just one engineering discipline, chemical engineering and continued to be so till 1981. Since then it has made tremendous growth and today it is a State University with five different faculties, viz. Technology, Pharmacy, Management & Information Technology, Dentistry and Medicine. In 2008 the university has been awarded recognition as a Centre of Excellence from Dept. of Industries and Mines, Govt. of Gujarat to carryout cutting edge R&D activities in the area of Nanotechnology Also it was granted status of Anchor Institute (Chemicals & Petrochemicals) to impart training to the trainers and employees of the industries.

Dharmsinh Desai University, a leading technology university of Gujarat, is organized an international conference on Green Technologies for Sustainable Development at Nadiad from 9-11 March, 2021 with the support of various government agencies and industries. This is one of the first such conferences to be held in probably the most relevant area of concern as the need for sustainable development was never felt to the extent it is felt now. This international conference supported by speakers of stellar quality from abroad and India. Total 9 plenary sessions, 13 Keynote Talk and 10 Industrial case studies were conducted along with 13 parallel sessions included more than 120 oral presentations from young researchers. More than 500 professionals and academicians were participated in the conference. The success of the conference has not been possible without the visionary guidance of Padmshri Dr. H. M. Desai, Vice Chancellor of the University and Campus Director, Shri Ankurbhai Desai. We acknowledge the support and guidance of Prof. R K Jain (Registrar,DDU) and Prof. K N Sheth(Dean, FoT,DDU).

We are thankful to GUJCOST, Climate change department and industrial groups like Ami Organics, ColourTex, Filter cocept, and Yash Chemicals for providing us financial supports.

We are thankful to all the Plenary speakers, namely, Dr. D O Shah( USA), Prof. Hyunook Kim ( South Korea), Prof. Klemes Jiri( Czech Republic), Prof. P C Chiang( Taiwan), Prof. Sunil Bhagwat(ICT-Bombay), Prof. Yogendra Shastri(IIT-Bombay),  Prof. Shantanu Bandopadhyay (IIT-Bombay)and Dr. Bharat Jain (GCPC,Gandhinagar) for their inspirational talk on

various aspects of Green Technologies for the sustainable development of the world. We appreciate the efforts of all the keynote speakers and session chairs for their talks and valuable inputs to evaluate the research work during parallel sessions of the conference on various sub themes.

We acknowledged the efforts of young researchers from various University of India and abroad along with Research Institutions and Industries for sharing their research works and joined hands with us to create awareness about green technologies.

The unique concept of Industrial Knowledge partners are appreciated by all major Chemical Process Industries like Reliance, UOP Honeywell, GCPC, Solvay, Sanofi India, Navin Florine, SoliQz BV, UPL, PI Industry and ColorTex. We are thankful to industrial representatives for sharing their experience in terms of case studies with the participants.

All the faculty members and students of Chemical Engineering department act as backbone of the conference and tried their best to convert dreams into realities. We apprentice the support of each one in the grand success of virtual conference.

# PHOTO CATALYSIS

## GREEN SYNTHESIS USING BIOTECH & BIOCATALYSIS

# Simultaneous removal of chromium and nickel from aqueous solution by electrocoagulation

Sunil R. Patel[1*], Mahirkhan Pathan[1], Sachin P. Parikh[2]

[1*] Chemical Engineering Department, V.G.E.C.-Chandkheda, Gujarat Technological University, Ahmedabad-382424, Gujarat, India
[2] Chemical Engineering Department, L. D.C.E. - Navaranpura, Gujarat Technological University, Ahmedabad 380015, Gujarat, India

*Corresponding author: srp@vgec.ac.in, sunilpatel.juet@gmail.com, mobile number: +919426215788

## Abstract

This article reports the Nickel (Ni) and chromium [Cr (VI)] removal by electrocoagulation (EC) from synthetic solution in a batch reactor using iron electrodes. In present work, electrocoagulation process was applied to evaluate the impact of process variables such as pH, current density, composition of Ni and Cr(VI) and electrode distance for the removal of Ni and Cr(VI) from solution. The experimental investigation shows that, current density (CD) value of 89.45 A/m$^2$, electrode distance (ED) value of 0.7 cm, pH value of 4.5, operating time of 60 minutes, are the optimal operating parameters to achieve 88.45 % and 95.47 % removal efficiency of Ni and Cr(VI) respectively. In additional, when the current density increased the increase of Ni and Cr(VI) removal and specific electrical energy consumption (SEEC). It was also observed that the lower electrode distance and lower composition of Ni and Cr(VI) favors higher removal efficiency of Ni and Cr(VI). The Cr(VI) and Ni removal was confirmed by mass balance of Cr(VI) and Ni in filtrate and residue after electrocoagulation.

**Keywords:** Electrocoagulation, iron electrode, Ni and Cr(VI) removal, energy consumption.

## 1. Introduction

Now days the advancement of industry is manor issues about the pollution of water and lack of energy. Heavy metals are used for production and manufacturing of various industrial product in several industries like paints, leather, dyes and pigments, metallurgical industry, mining, electroplating, cosmetics etc (Wang et al., 2020). This generates large amount of wastewater containing nickel and chromium. These metal ions have fatal effects on environment and human life and it is very carcinogenic and toxic even presence in low concentration (Zhou et al., 2020). Therefore, it is necessary to treatment of effluents containing heavy metal ions that coming from various industry. So that these metal ions do not cause health effect and harm to the environment. Various methods are available for the treatment of chromium and nickel which include photocatalysis, precipitation /coagulation, membrane separation, ion exchange, biological treatment, adsorption, electrocoagulation (Darban, Shahedi, Ph, & Taghipour, 2020). All method has own set of advantages and disadvantages for example membrane separation, photocatalysis and ion exchange are costly processes (Kobya, Darvishi, Soltani, & Isaac, 2020). Precipitation /coagulation are less costly but it required large amount of additional chemicals and generate secondary pollutant (Sharma, Chaudhari, & Prajapati, 2019). Adsorption technique takes short time for treatment of heavy metal ions but its produce high amount of sludge as high adsorbent used for treatment(Nandi & Patel, 2013). Biological processes are less efficient for the removal of heavy metal ions and required more time (Tahreen, Jami, & Ali, 2020). At present the industries generating wastewater which contains more than one metal ion. So it is necessary to treat these metal ions. Electrocoagulation (EC) gives additional benefits as compare to other techniques for example gives high removal efficiency in less time, no addition chemicals required, easy operation, very less amount of sludge produce (Patel & Parikh, 2020).

EC has been successfully applied for the removal of heavy metals such as nickel (Akbal & Camcidotless, 2011), arsenic (Mohora et al., 2014), cadmium (Xu et al., 2018), copper (Kilany, Nosier, Hussein, Abdel-Aziz, & Sedahmed, 2020), zinc and lead (Mansoorian, Mahvi, & Jafari, 2014). In the current state, work has been done on single metal ion removal, very less literatures are available for the removal of more than one metal ion. Generally the industries having effluent contains more than one metal ions. So the present work will be helpful for real application of EC process in industrial application. A summary of the literature review is presented in Table 1.

Table1: Literature summary

| Type of wastewater | Current | Electrode | pH | EC time | Heavy meatls | Removal efficiency % | References |
|---|---|---|---|---|---|---|---|
| Metal plating plant. | 10 mA/cm$^2$ | Fe-Al | 3 | 20 min | Cu, Cr, Ni | 100, 100, 100 | (Akbal & Camcidotless, 2011) |
| Artificial wastewater | 4 mA/cm$^2$ | Fe-Al | 9 | 60 min | Cu, Ni, Zn, Cr) | >95 | (Kim, Kim, & Zoh, 2020) |
| Artificial wastewater | 98 A/m$^2$ | Al | 4.5 | 30 min | Zn(II), Cu(II), Ni(II), Ag(I) | - | (Heidmann & Calmano, 2008) |

| | | | | and Cr(VI) | | |
|---|---|---|---|---|---|---|
| Surface finishing plant | 77.29 mA/cm$^2$ | Fe | 7 | 20 min | Zn, Ni, Cr, Fe | 87.6, 44.7, 100,100 | (Ya et al., 2018) |
| Metal plant | 50 A/m$^2$ | Fe-Fe, Fe-Al | 2.42 | 60 min | Cu(II), Cr(VI), Ni(II) | 100,100,100 | (Beyazit, 2014) |

The present work aims to simultaneously removal of (Ni) and chromium [Cr (VI)] from synthetic wastewater by EC using iron electrodes. The present study is focused on investigating the impact of composition of Ni and Cr (VI) on its removal percentage. Also check the impact of other like pH, current density, electrode distance for Ni and Cr (VI) removal percentage. Electrical energy utilization was calculated for the removal of Ni and Cr (VI). Mass balance of Ni and Cr (VI) was carried out for its removal.

## 2. Theory

Electrocoagulation (EC) process is based on in-situ generation of coagulants as a form of metal ions by applies a direct current across electrodes surface in a solution, this result in the dissolution of the anode. These ions then form hydroxides complex which absorb contaminants and precipitate from wastewater. Following reactions will takes place during the EC with Fe electrode(Nandi & Patel, 2013):

*Mechanism 1*

Anode: $4Fe_{(s)} \rightarrow 4Fe_{(aq)}^{2+} + 8e-$       (1)

Bulk of solution: $4Fe_{(aq)}^{2+} + 10H_2O_{(l)} + O_{2(aq)} \rightarrow 4Fe(OH)_{3(s)} + 8H^+_{(aq)}$  (2)

Cathode: $8H^+_{(aq)} + 8e- \rightarrow 4H_{2(g)}$       (3)

Overall: $4Fe_{(s)} + 10H_2O_{(l)} + O_{2(aq)} \rightarrow 4Fe(OH)_{3(s)} + 4H_{2(g)}$  (4)

*Mechanism 2*

Anode: $Fe_{(s)} \rightarrow Fe^{2+}_{(aq)} + 2e-$       (5)

Bulk of solution: $Fe_{(aq)}^{2+} + OH^-_{(aq)} \rightarrow Fe(OH)_{2(s)}$   (6)

Cathode: $2H_2O_{(l)} + 2e- \rightarrow H_{2(g)} + 2OH^-_{(aq)}$   (7)

Overall: $Fe_{(s)} + 2H_2O_{(l)} \rightarrow Fe(OH)_{2(s)} + H_{2(g)}$   (8)
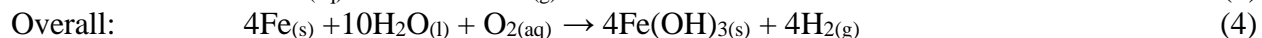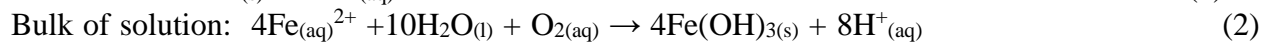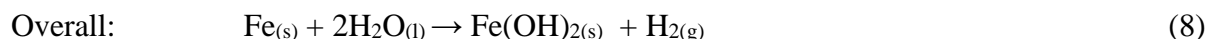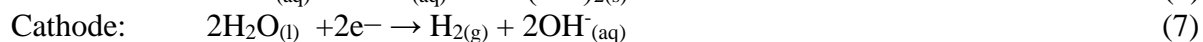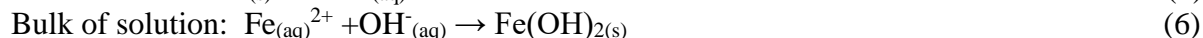
The $Fe(OH)_{n(s)}$ produced in the solution as a gelatinous suspension, which can remove the impurities from effluent by coagulation. These polymeric hydroxides are act as a coagulant (El-Taweel, Nassef, Elkheriany, & Sayed, 2015).

## 3. Materials and methods

The experimental setup is shown in figure 1. Cylindrical glass vessel having a capacity of 1 L was utilized for experiment with volume of 500 ml. All experiments were performed at room temperature ($\pm 25$ $^0$C). Rectangular iron plates were utilized as electrodes for the EC process which were purchased from the local market of Ahmedabad, Gujarat. The dimensions of the

electrodes were 0.15 m $\times$ 0.043 m $\times$ 0.001 m. The effective area of electrode was 0.00559 m$^2$ (55.9 cm$^2$). Both electrodes (Anode & Cathode) were connected to the DC power supply (Aplab, India, Model: L-1285) as shown in figure 1. Distances between two electrodes were maintained by 0.7 cm thick wooden box. The synthetic solutions containing Nickel and Chromium were made by dissolving (in 500ml distilled water) required quantity of Nickel sulphate heptahydrate (NiSO$_4$. 7H$_2$O) (Central Drug House Ltd., 99%) and Potassium Dichromate (K$_2$Cr$_2$O$_7$) (NICE Chemicals Pvt. Ltd., 99.50%), respectively. Weights of the chemicals and electrodes were measured by Electronic Weight Balance (WENSAR, Model: 77252). HCl and NaOH were used for adjusting the pH for the solution. pH of the solutions measured by digital pH meter (CHEMI LINE, India, CL110). Various parameters studied for the Cr (VI) and Ni removal are presented in Table 2. Each experiment was executed twice and average experimental error was found approximately 3%. The concentration of Cr (VI) and Ni was measured by Atomic Absorption Spectroscopy (CHEMITO AA201). After completion of 60 minutes the residue was filtered by filter paper and sludge was separated for mass balance of Cr (VI) and Ni. The removal efficiencies of Cr (VI) and Ni were calculated from the following equation:

$$\text{Cr (VI) and Ni removal efficiency (\%)} = \frac{Ca - Cb}{Ca} \times 100 \tag{9}$$

Where; $C_a$ is initial the concentration and $C_b$ is final concentration of Cr (VI) and Ni respectively.

The specific electrical energy consumption (SEEC) in kWh/ (kg Fe) and electrical energy consumption (EEC) in (kWh m$^{-3}$) was calculated as per the equations available in literature (Akbal & Camcidotless, 2011; Patel & Parikh, 2020).

$$\varphi = \frac{\Delta M_{\text{experimental}}}{\Delta M_{\text{theoritical}}} \times 100 \tag{10}$$

$$\Delta M_{\text{theoritical}} = \frac{M.I.t_{EC}}{n.F} \tag{11}$$

$\Delta M_{\text{experimental}}$ is weight loss of iron electrode during EC. $\Delta M_{\text{theoretical}}$ is theoretical weight loss of iron electrode and it was calculated according to the Faraday's law equation (11).

$$SEEC = \frac{n \times F \times U}{3600 \times M \times \varphi} \tag{12}$$

$$\text{Energy consumption (E)} = \frac{U I t_{EC}}{V} \tag{13}$$

where F is Faraday constant (F = 96487 C mol$^{-1}$), I is current (A), U is voltage (volt), M is molecular weight of iron (g mol$^{-1}$), $\varphi$ is current efficiency, n is moles of electron, V indicates volume of effluent (L), and $t_{EC}$ is the time of EC.
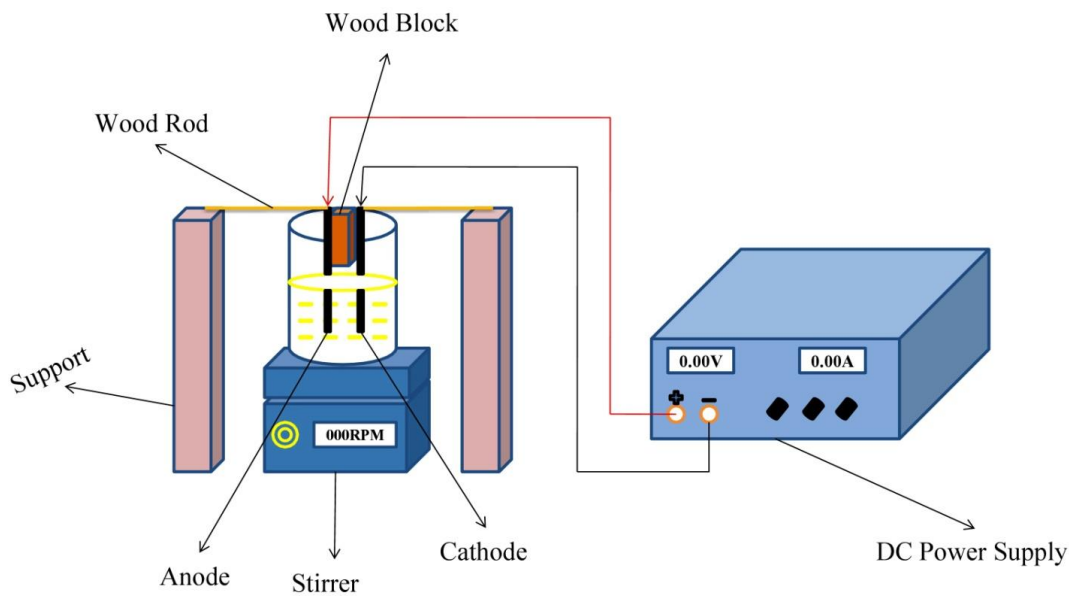
Figure 1. Experimental setup of EC process

Table 2. Variables studied for the EC process.

| Parameter | Deviation in parameter | Fix parameter |
|---|---|---|
| Composition of Cr(VI) and Ni (mg/L) | 20:80, 40:60, 60:40, 80:20, 100:100 | Current= 0.5 A,  ED= 0.7 cm, pH= 4.5, |
| pH | 2, 4, 6, 8, 10 | Cr(VI) and Ni concentration= 100 mg/L, Current= 0.5 A,   ED= 0.7 cm, |
| Electrode distance (ED) (cm) | 0.7, 1.4, 2.1 | Cr(VI) and Ni concentration= 100 mg/L, Current= 0.5 A, pH= 4.5 |
| Current (A) | 0.10, 0.30, 0.50 | Cr(VI) and Ni concentration= 100 mg/L, Current= 0.5 A,   ED= 0.7 cm, pH= 4.5, |
| EC time (minute) | 60 | |

## 4.  Results and discussions

### 4.1 Effect of composition of Cr (IV) and Ni

To examine the effect of composition of Cr (VI) and Ni on EC method, the composition of Cr (VI) and Ni was varied in the ratio of 20:80, 40:60, 60:40, and 80:20 mg/L respectively. Figure 2a, 2b, 2c and 2d are shows the impact of composition of Cr (VI) and Ni on removal percentage with time. Figure 2a, 2b, 2c and 2d are shows the initial concentration of Cr (VI)

and Ni decrease with increase time of EC up to 60 minutes. Figure 2a demonstrates when the initial concentration of Cr (VI) and Ni was 20 and 80 mg/L, the removal percentage 99.8 % and 99.65 % was achieved in 40 and 60 minutes respectively. Figure 2b illustrates when the initial concentration of Cr (VI) and Ni was 40 and 60 mg/L, the removal percentage 99.87 % and 99.53 % was achieved in 50 and 60 minutes respectively. Figure 2c demonstrates when the initial concentration of Cr (VI) and Ni was 60 and 40 mg/L, the removal percentage 99.95 % and 99.87 % was achieved in 50 minutes respectively. Figure 2d demonstrates when the initial concentration of Cr (VI) and Ni was 80 and 20 mg/L, the removal percentage 99.93 % and 99.9 % was achieved in 50 and 40 minutes respectively. The motive for all can be explained as present of metal ions is higher while the Cr (VI) and Ni concentration is lower as a result production of iron hydroxide monomers and polymers are high. So at lower concentration of Cr (VI) and Ni, the higher removal percentage was achieved in a short time period. But at a higher concentration of Cr (VI) and Ni, the iron hydroxide complexes are insufficient to adsorb all the Cr (VI) and Ni ions present in the solution. It resulted in to the increases residual concentration with increases Cr (VI) and Ni concentration (Aber, Amani-Ghadim, & Mirzajani, 2009).
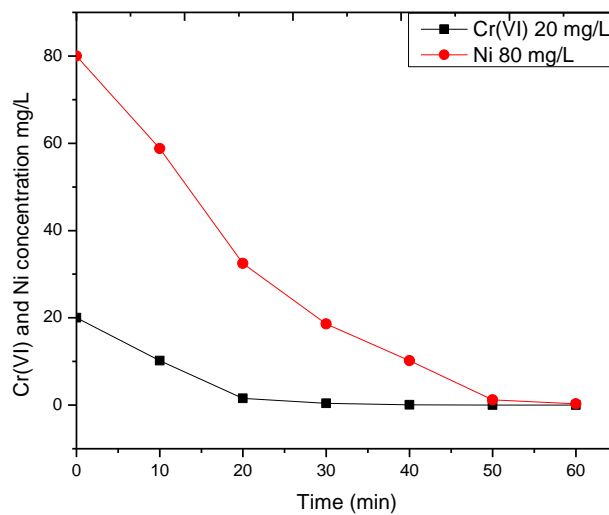


Figure 2a. Effect of composition of Cr(VI) and Ni on its removal.
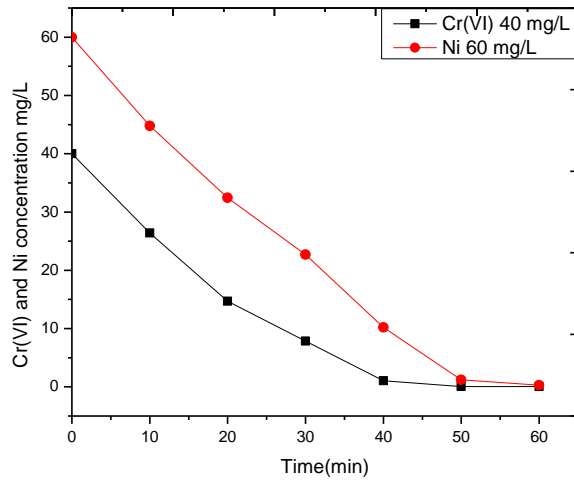
Figure 2b. Effect of composition of Cr(VI) and Ni on its removal.
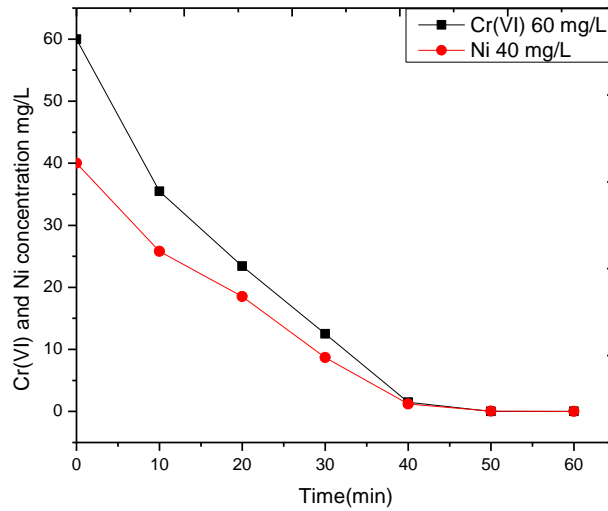


Figure 2c. Effect of composition of Cr(VI) and Ni on its removal.
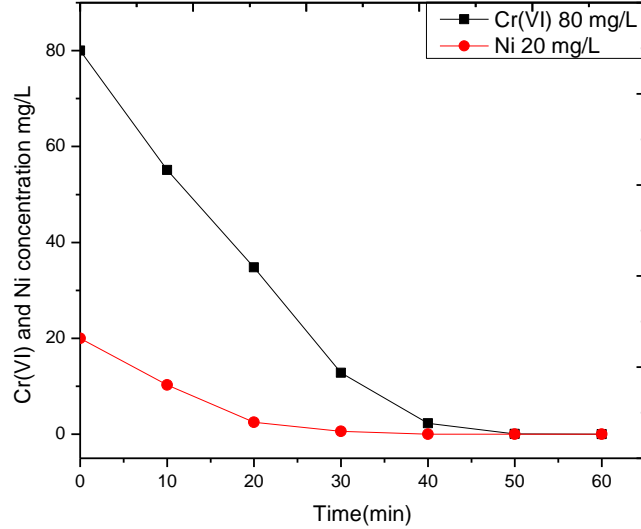
Figure 2d. Effect of composition of Cr(VI) and Ni on its removal.


## *4.2 Effect of current density*

Current is very important parameter for EC process. It increases the removal percentage as well as energy consumption. To observe the impact of current density CD, the experiments were carried out at CD range from 17.88 to 89.45 A/m$^2$ at an initial concentration of 100 mg/L of Cr (VI) and Ni. Figure 3a and 3b shows the variation in the removal percentage at various CD. From Figure 3a, it can be observed that the Cr (VI) removal percentage increase from 68.3 to 95.47 % as CD increasing from 17.88 to 89.45 A/m$^2$. Similarly from Figure 3b, it can be observed that the Ni removal percentage increase from 61.67 to 88.45 % as CD increasing from 17.88 to 89.45 A/m$^2$. The reason can be given by the Faraday's law (Eq. 11). The rate of metal ions production is directly proposnal to the CD.  As the CD increases metal ions production rate also increases. It resulted in to increases the rate of iron hydroxides production which absorb metal ions from wastewater (Zhou et al., 2020).
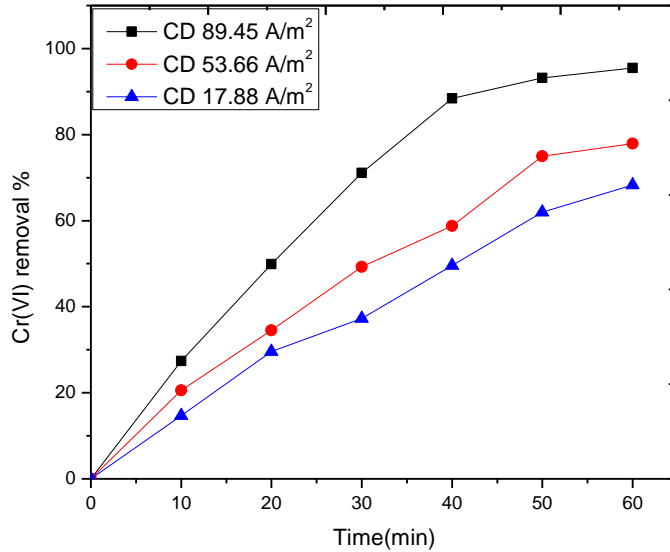
Figure 3a. Effect of current density on Cr(VI) removal.


### 4.3 Effect of pH

pH is key parameter for EC process. So, to find the optimum value of pH for removal of Cr (VI) and Ni, pH was varied from 2 to 10 for the experiments. Figure 4a and 4b shows the effect of pH on the removal percentage of Cr (VI) and Ni. From Figure 4a and 4b it was observed that as pH increased from 2 to 6, the removal percentage of Cr (VI) and Ni increased from 78.6 to 97.8 % and 66.79 to 91.3 % respectively and the maximum removal was achieved at pH 6. The removal percentage of Cr (VI) and Ni decreased as pH increased up to 10. The reason may be due to generation of iron hydroxide and it depends on the pH of wastewater during EC process. The balance among $H^+$ ions and iron ions is required for the optimal productions of hydroxide. In other words various percentage of Cr (VI) and Ni removal at different pH were because of amount of iron hydroxide ions produced at particular pH (Prajapati, Chaudhari, Pal, Chandrakar, & Choudhary, 2016). It is reported by various investigator that the higher amount of metal hydroxides formed in the range of pH 6 to 9 (Kim et al., 2020; Vasudevan, Lakshmi, & Sozhan, 2012).
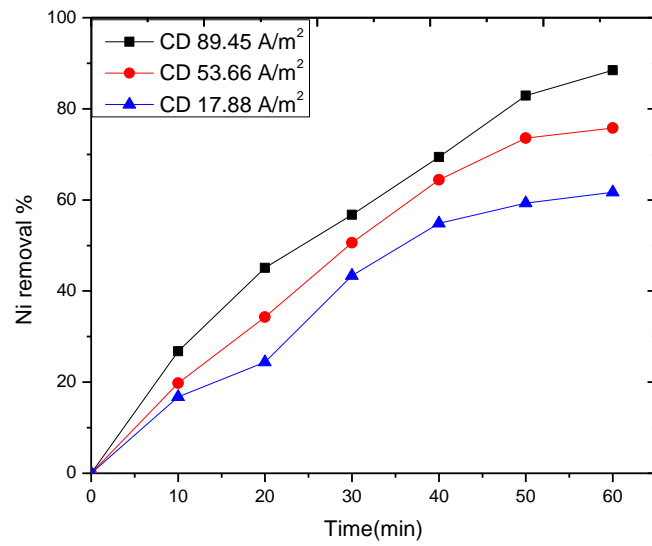
Figure 3b. Effect of current density on Ni removal.
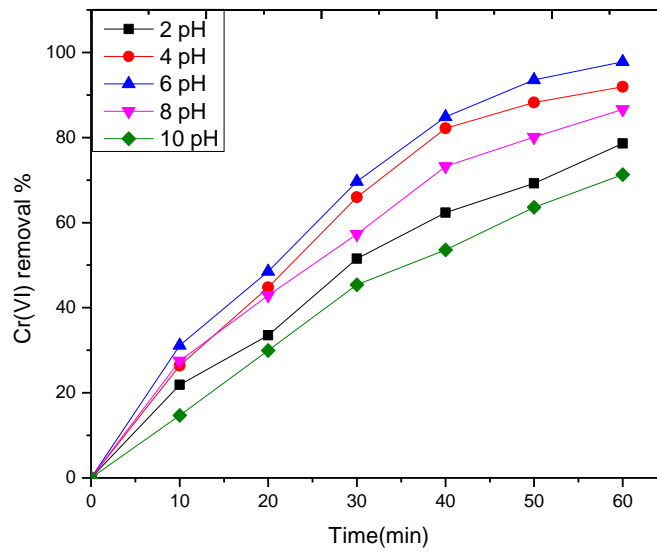


Figure 4a. Effect of pH on Cr(VI) removal.
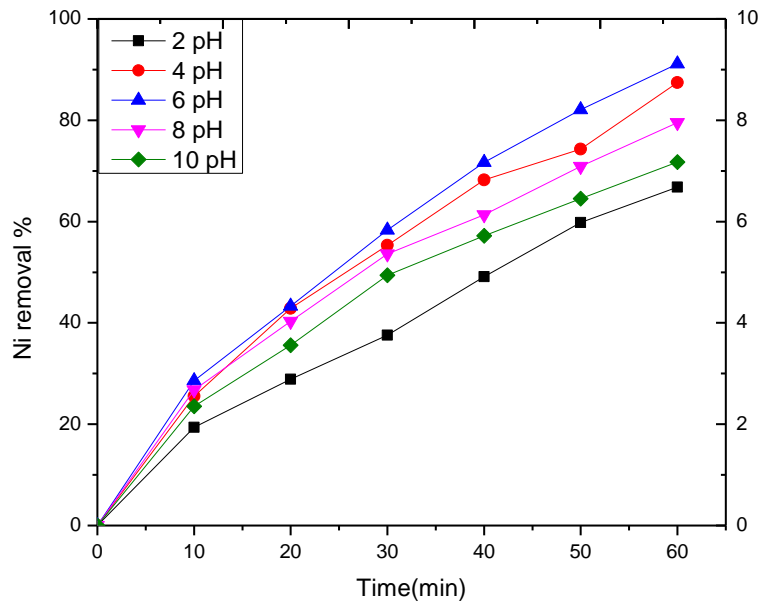
Figure 4b. Effect of pH on Ni removal.

## 4.4 Effect of Electrode distance

The impact of ED on removal of Cr (VI) and Ni shown in figure 5a and 5b. It was seen from figure 5a and 5b that the Cr (VI) and Ni removal decrease with increasing in ED. Figure 5a shows the ED effect on the Cr (VI) removal and it was observed that the Cr (VI) removal decreased from 95.47 % to 77.11 % with increasing ED from 0.7 to 2.1 cm. corresponding the residual Cr (VI) concentration increased from 4.53 to 22.89 mg/L. Figure 5b shows the ED effect on the Ni removal and it was observed that the Ni removal decreased from 88.45 % to 72.49 % with increasing ED from 0.7 to 2.1 cm. corresponding the residual Ni concentration increased from 11.55 to 27.51 mg/L. This was because of decrease in $Fe(OH)_2$ flocs in the solution (Das & Nandi, 2019). The electrical resistance among the both electrode increases with increases in ED. So contact with $Fe^{2+}$ and $OH^-$ ions generated during EC gets delayed. As a resulted in to the rate of $Fe(OH)_2$ production reduces and therefore, the removal percentage decreases (Patel & Parikh, 2020).

The electrical energy consumption (EEC) in $kWh/m^3$ and specific electrical energy consumption (SEEC) in kWh/kg Fe calculated for the removal of Cr (VI) and Ni at various ED. The variation in EEC and SEEC shows in figure 5c at different ED. It was observed from figure 5c that the EEC increased from 14 to 38 $kWh/m^3$ and SEEC increased from 1.16 to 3.15 kWh/kg Fe as ED increased from 0.7 to 2.1 cm respectively. The reason was that the voltage drop rises as the raises of ED. So at constant CD, the electrical resistance among the both electrode increases. It resulted in to increase EEC and SEEC (Das & Nandi, 2019b).
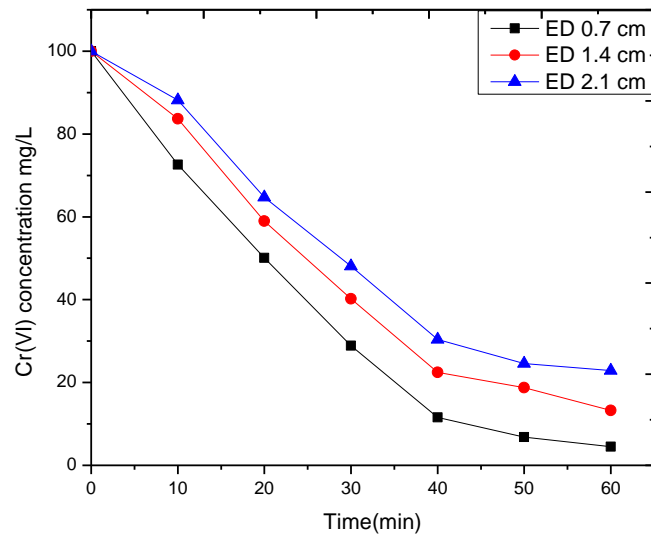
Figure 5a. Impact of ED on Cr(VI) removal.
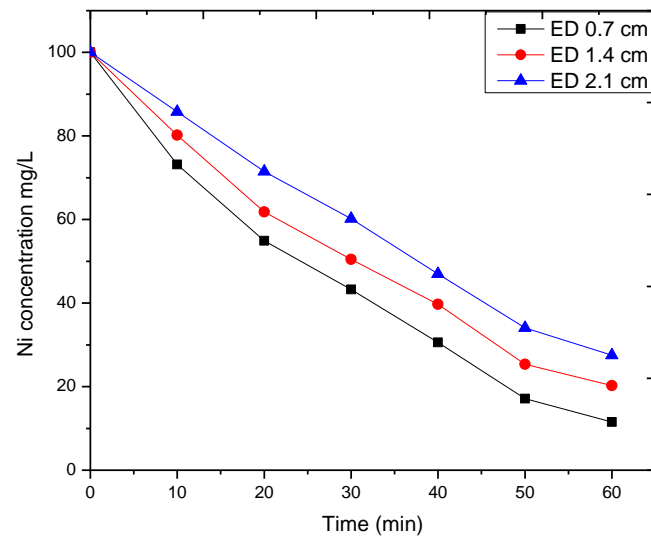


Figure 5b. Impact of ED on Ni removal.
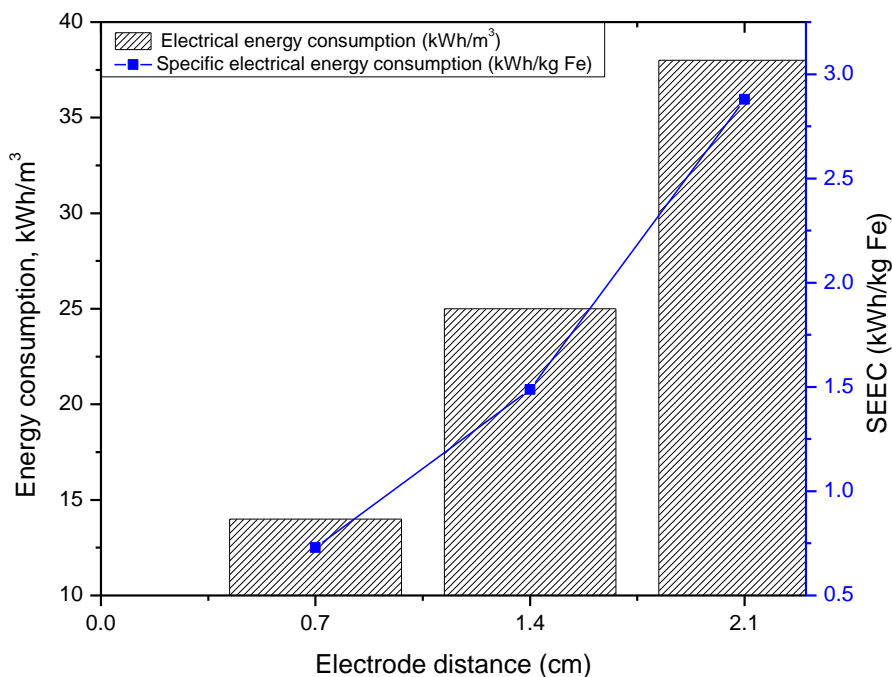
Figure 5c. Energy consumption and SEEC at various ED.

### 4.5 Mass balance of Cr (VI) and Ni

Mass balance of Ni and Cr (VI) has been carried out for the confirmation of present in sludge.  The residue was filtered using filter paper and dried. This dried residue was dissolved in aquarezia with slowly heating (at temperature $80\ ^0C$) until the residue mixed completely. Ni and Cr (VI) concentration was measured using AAS. The mass balance of Ni and Cr (VI) is presented in Table 3 and Table 4 respectively. Mass balance of Ni and Cr (VI) shows same amount present in filtrate and residue with maximum error of 4.93% and 5.36% respectively.

Table 3. Mass balance of Ni at various pH

| pH | Initial Ni in solution (mg/L) | Ni in residue (mg/L) | Ni in filtrate (mg/L) | Total Ni (mg/L) (Residue + Filtrate) | Error % |
|---|---|---|---|---|---|
| 2 | 100 | 62.47 | 33.21 | 95.68 | 4.32 |
| 4 | 100 | 83.79 | 12.57 | 96.36 | 3.64 |
| 6 | 100 | 88.4 | 8.87 | 97.27 | 2.73 |
| 8 | 100 | 75.52 | 20.47 | 95.99 | 4.01 |
| 10 | 100 | 66.84 | 28.23 | 95.07 | 4.93 |

Table 4. Mass balance of Cr (VI) at various pH

| pH | Initial Cr (VI) in solution (mg/L) | Cr (VI) in residue (mg/L) | Cr (VI) in filtrate (mg/L) | Total Cr (VI) (mg/L) (Residue + Filtrate) | Error % |
|---|---|---|---|---|---|
| 2 | 100 | 73.24 | 21.4 | 94.64 | 5.36 |
| 4 | 100 | 88.65 | 8.1 | 96.75 | 3.25 |
| 6 | 100 | 93.22 | 2.2 | 95.42 | 4.58 |
| 8 | 100 | 83.57 | 13.41 | 96.98 | 3.02 |
| 10 | 100 | 66.87 | 28.7 | 95.57 | 4.43 |

## 5. Conclusions

EC process using iron electrode for the simultaneously removal of Cr (VI) and Ni resulted as an effective treatment method. The impact of various operating parameters of EC process for Cr (VI) and Ni removal were evaluated. It was concluded that the highest Cr (VI) and Ni i.e. 95.47 % and 88.45 % respectively was achieved at CD value of 89.45 A/m$^2$, pH value of 4.5 with ED of 0.7 cm and EC time of 60 minutes. It was also observed that the lower ED and lower composition of Cr (VI) and Ni, favors higher removal efficiency of Cr (VI) and Ni. EEC and SEEC of EC process for removal of Cr (VI) and Ni was 14 kWh/m$^3$ and 1.16 kWh/kg Fe respectively. The Cr (VI) and Ni removal was confirmed by mass balance of Cr (VI) and Ni in filtrate and residue after electrocoagulation.

## Acknowledgements

# References

Aber, S., Amani-Ghadim, A. R., & Mirzajani, V. (2009). Removal of Cr(VI) from polluted solutions by electrocoagulation: Modeling of experimental results using artificial neural network. *Journal of Hazardous Materials*, *171*(1–3), 484–490. https://doi.org/10.1016/j.jhazmat.2009.06.025

Akbal, F., & Camcidotless, S. (2011). Copper, chromium and nickel removal from metal plating wastewater by electrocoagulation. *Desalination*, *269*(1–3), 214–222. https://doi.org/10.1016/j.desal.2010.11.001

Beyazit, N. (2014). Copper(II), chromium(VI) and nickel(II) removal from metal plating effluent by electrocoagulation. *International Journal of Electrochemical Science*, *9*(8), 4315–4330.

Darban, A. K., Shahedi, A., Ph, D., & Taghipour, F. (2020). A review on industrial wastewater treatment via electrocoagulation processes. *Current Opinion in Electrochemistry*. https://doi.org/10.1016/j.coelec.2020.05.009

Das, D., & Nandi, B. K. (2019). Arsenic removal from tap water by electrocoagulation: investigation of process parameters, kinetic analysis, and operating cost. *Journal of Dispersion Science and Technology*, *0*(0), 1–10. https://doi.org/10.1080/01932691.2019.1681280

El-Taweel, Y. A., Nassef, E. M., Elkheriany, I., & Sayed, D. (2015). Removal of Cr(VI) ions from waste water by electrocoagulation using iron electrode. *Egyptian Journal of Petroleum*, *24*(2), 183–192. https://doi.org/10.1016/j.ejpe.2015.05.011

Heidmann, I., & Calmano, W. (2008). Removal of Zn(II), Cu(II), Ni(II), Ag(I) and Cr(VI) present in aqueous solutions by aluminium electrocoagulation. *Journal of Hazardous Materials*, *152*(3), 934–941. https://doi.org/10.1016/j.jhazmat.2007.07.068

Kilany, A. Y., Nosier, S. A., Hussein, M., Abdel-Aziz, M. H., & Sedahmed, G. H. (2020). Combined oil demulsification and copper removal from copper plating plant effluents by electrocoagulation in a new cell design. *Separation and Purification Technology*, *248*(May), 117056. https://doi.org/10.1016/j.seppur.2020.117056

Kim, T., Kim, T. K., & Zoh, K. D. (2020). Removal mechanism of heavy metal (Cu, Ni, Zn, and Cr) in the presence of cyanide during electrocoagulation using Fe and Al electrodes. *Journal of Water Process Engineering*, *33*(July 2019), 101109. https://doi.org/10.1016/j.jwpe.2019.101109

Kobya, M., Darvishi, R., Soltani, C., & Isaac, P. (2020). Environmental Technology & Innovation A review on decontamination of arsenic-contained water by electrocoagulation : Reactor configurations and operating cost along with removal mechanisms. *Environmental Technology & Innovation*, *17*, 100519. https://doi.org/10.1016/j.eti.2019.100519

Mansoorian, H. J., Mahvi, A. H., & Jafari, A. J. (2014). Removal of lead and zinc from battery industry wastewater using electrocoagulation process: Influence of direct and alternating current by using iron and stainless steel rod electrodes. *Separation and Purification Technology*, *135*, 165–175. https://doi.org/10.1016/j.seppur.2014.08.012

Mohora, E., Rončević, S., Agbaba, J., Tubić, A., Mitić, M., Klašnja, M., & Dalmacija, B. (2014). Removal of arsenic from groundwater rich in natural organic matter (NOM) by continuous electrocoagulation/flocculation (ECF). *Separation and Purification Technology*, *136*, 150–156. https://doi.org/10.1016/j.seppur.2014.09.006

Nandi, B. K., & Patel, S. (2013). Effects of operational parameters on the removal of brilliant green dye from aqueous solutions by electrocoagulation. *ARABIAN JOURNAL OF CHEMISTRY*. https://doi.org/10.1016/j.arabjc.2013.11.032

Patel, S. R., & Parikh, S. P. (2020). Statistical optimizing of electrocoagulation process for the removal of Cr ( VI ) using response surface methodology and kinetic study. *Arabian Journal of Chemistry*, (Vi). https://doi.org/10.1016/j.arabjc.2020.07.009

Prajapati, A. K., Chaudhari, P. K., Pal, D., Chandrakar, A., & Choudhary, R. (2016). Electrocoagulation treatment of rice grain based distillery effluent using copper electrode. *Journal of Water Process Engineering*, *11*, 1–7. https://doi.org/10.1016/j.jwpe.2016.03.008

Sharma, D., Chaudhari, P. K., & Prajapati, A. K. (2019). Removal of chromium ( VI ) and lead from electroplating effluent using electrocoagulation. *Separation Science and Technology*, *00*(00), 1–11. https://doi.org/10.1080/01496395.2018.1563157

Tahreen, A., Jami, M. S., & Ali, F. (2020). Role of electrocoagulation in wastewater treatment: A developmental review. *Journal of Water Process Engineering*, *37*(May), 101440. https://doi.org/10.1016/j.jwpe.2020.101440

Vasudevan, S., Lakshmi, J., & Sozhan, G. (2012). Simultaneous removal of Co, Cu, and Cr from water by electrocoagulation. *Toxicological and Environmental Chemistry*, *94*(10), 1930–1940. https://doi.org/10.1080/02772248.2012.742898

Wang, Z., Shen, Q., Xue, J., Guan, R., Li, Q., Jia, H., … Wu, Y. (2020). 3D Hierarchically Porous NiO/NF Electrode for the Removal of Chromium(VI) from Wastewater by

Electrocoagulation. https://doi.org/10.1016/j.cej.2020.126151

Xu, L., Cao, G., Xu, X., He, C., Wang, Y., Huang, Q., & Yang, M. (2018). Sulfite assisted rotating disc electrocoagulation on cadmium removal: Parameter optimization and response surface methodology. *Separation and Purification Technology*, *195*, 121–129. https://doi.org/10.1016/j.seppur.2017.12.010

Ya, V., Martin, N., Chou, Y. H., Chen, Y. M., Choo, K. H., Chen, S. S., & Li, C. W. (2018). Electrochemical treatment for simultaneous removal of heavy metals and organics from surface finishing wastewater using sacrificial iron anode. *Journal of the Taiwan Institute of Chemical Engineers*, *83*, 107–114. https://doi.org/10.1016/j.jtice.2017.12.004

Zhou, R., Liu, F., Wei, N., Yang, C., Yang, J., Wu, Y., … Zhang, C. (2020). Comparison of Cr(VI) removal by direct and pulse current electrocoagulation: Implications for energy consumption optimization, sludge reduction and floc magnetism. *Journal of Water Process Engineering*, *37*(February), 101387. https://doi.org/10.1016/j.jwpe.2020.101387

# Reduction of COD from waste water by sustainable adsorbent: Experimental and Modelling.

*Dr.Latesh Chaudhari 1, Sunil Valand 2*

[1]*Principal,  R. N. G. Patel Institute of Technology.Bardoli – Navsari Road, Isroli, Afwa, Bardoli, Surat, Gujarat 394620*

[2]*Dept. of Chemical Engineering, Chhotubhai Gopalbhai Patel Institute of Technology, UTU-Bardoli, Surat, Gujarat 394350*
*sunilvaland99@gmail.com , +919033253202*

**Abstract**

Industrial, agricultural, and domestic activities of humans have affected the environmental system, resulting in drastic problems such as wastewater containing high concentration of COD, Colour etc. Various methods are utilized that reduction of pollutants by using ion exchange, reverse osmosis, electro dialysis, ultrafiltration, etc. However, most of them above depend on the substantial financial input and their use isrestricted because of cost factors. Adsorption process being very simple,economical, effective and versatile has become the most preferred methods for removal of toxic contaminants from wastewater. An efforthas to brief idea about such as the low-cost alternative adsorbents with view to utilizing in the treatment of wastewater.

The objective of this work is to study adsoprtion process which benefit to environment usings sustainable adsorbent  like  fullers eartth  to reduction of  COD  from waste water. Experimental adsorption was carried out with the acidic sample collected from dye producing industry in Gujarat having varied nature from acidic sample (before primary treatment)   and Neutralised Nature of the effluent. COD and %COD reduction values using two different adsorbents like activated carbon and Fullers earth were studied for different types of conditions viz. effect of time of contact and effect of quantity

The result were studied by mathematical modeling such as Rathi-Puranik model, Weber-Morri'smodel and Lagregean model, which suggest that Rathi - Puranik model is more effective  compare to Weber-Morri's model and Lagregean model to predict the COD value at different time interval in a given system.

**Key words** - Waste water, COD, Activated carbon, Fullers earth, Rathi-Puranik model, Weber-Morri'smodel, Lagregean model.

## 1 Introduction:

Water is the most important and it is used in all type of s different industrie processes such as Cleaning , dilution  etc . Generally all industry generates waste water that needs urgent attention. Wastewater discharged by industrial activities is often contaminated by a variety of toxic or otherwise harmful substances which have negative effects on the water environment. Pollution of water by organic and inorganic chemicals is of serious environmental concern

[2] Waste water generated from different industry has a high concentrated of COD and other different contamination available in waste water which cannot be discharged in water resources without any treatment. In order to meet the growing demand for potable water and water of good quality for industrial use, it has become necessary to treat wastewaters for reuse, and minimize  pollutants before mixing with natural water bodies.A number of conventional treatment technologies have been considered for treatment of wastewater such as coagulation process , membrane filtration  and oxidation process . These methods are generally expensive. Among them, adsorption process is found to be the most effective method and better alternative in waste water treatment because of convenience, ease to use, high efficiency , sustainable and simplicity of design [16].  In Effluent treatment plant, adsorption processes are applied for the reduction  of dissolved pollutants that remain from the subsequent biological phases or a chemical oxidation treatments. Now a days, the most of the industries have commonly adopted adsorbent such as activated carbon. It is commonly used for the reduction  of various pollutants from waste water such as metal , colour etc. However, its widespread use in  wastewater treatment is sometimes restricted due to its high cost . The high cost of coal-based activated carbons has stimulated the search for cheaper alternatives[2]. Various low- cost adsorbents such as Lignite, fullers earth, can be used as adsorbents for reduction of pollutants in waste water.

**2 Scope of Experimental Workn**:
**2.1  Objective:**
Activated carbon is the most widely used as adsorbent but it is found to be quite expensive . Considering the resource constraints experienced by the small scale industries, they use adsorption technique only if it is cost effective. Inexpensive adsorbent like fullers earth can be considered for detailed studies with respect to their performance in treating waste water effluent.

**2.2  Approach**:
The conventional flow-sheets  refer figure.1 of industrial wastewater treatment shown below include the primary treatment of pH adjustment and clarification, the secondary treatment which may consist of biological/chemical treatment and clarification, and depending on the quality of the waste water and the statutory discharge standards, tertiary treatment with activated carbon.
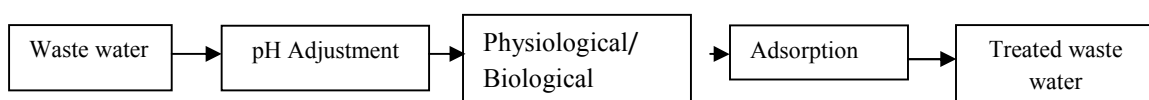


Fig.A.1. Conventional Flow sheet of waste water   treatment [6].

During primary treatment, neutralization of the waste water results in to increase of salts. Salts in high concentration inhibit biological activity and may cause an increase in non-settle able suspended solids in the treated waste water.

```
┌────────────┐   ┌────────────┐   ┌────────────┐   ┌──────────────┐   ┌────────────┐
│ Waste water│──▶│ Adsorption │──▶│     pH     │──▶│Physiological/│──▶│Treated waste│
│            │   │            │   │ Adjustment │   │  Biological  │   │    water   │
│            │   │            │   │            │   │  Treatment   │   │            │
└────────────┘   └────────────┘   └────────────┘   └──────────────┘   └────────────┘
```
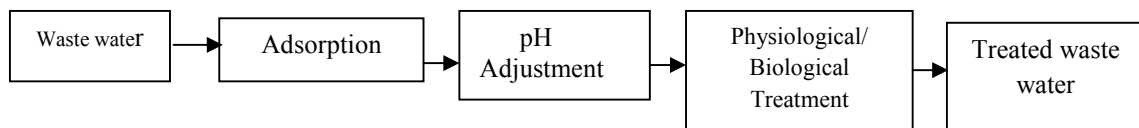
Fig.A.2. Modified flow sheet of Waste water treatment [15].

The flow sheet shown figure 2 above is therefore proposed wherein adsorption with inexpensive adsorbents is employed prior to the conventional primary treatment for increasing the efficiency of subsequent biological treatment.

## 3 Experimental procedures:

### 3.1 Sampling collection

The samples were collected from the ETP inlet stream (that is acidic sample) in bottle and then sealeed. Samples were stored at room temperature. The acidic samples were neutralised by using Caustic soda (NaOH) in a laboratory.

### 3.2 Procedure

During experiment 100 ml of sample and 1% (1gm) of Activated carbon (A/C) was taken in a flask and mixed with the help of magnetic stirrer for 2 hours. Same procedure were repeated for 2% A/C, 3% A/C and 4% A/C, by keeping constant quantity of sample (i.e.100 ml). And same produre were followed by using fuller earth adsorbent inplace of activated carbon. All the experiments were carried out at room temperature.

### 4. Results and Discussion:

### 4.1 Effect of Quantity of adsorbent

| Fig.A.3 Comparison between fullers earth and activated carbon for COD Results from plant producing Vinyl sulfone ester (Acidic sample) | | |
|---|---|---|
| | Fullers earth | Activated carbon |

| % Adsorbents | COD (mg/lit) | % COD Reduction | COD (mg/lit) | % COD Reduction |
|---|---|---|---|---|
| Raw sample | 3664 | - | 3664 | - |
| 1% | 3572 | 2.51 | 3475 | 5.15 |
| 2% | 3232 | 11.79 | 3127 | 14.65 |
| 3% | 3061 | 16.45 | 2891 | 21.09 |
| 4% | 2381 | 35.01 | 2041 | 44.29 |

| Fig.A.4 Comparison between fullers earth and activated carbon for COD Results from plant producing Vinyl sulfone ester (Neutralised sample ) | | | | |
|---|---|---|---|---|
| | Fullers earth | | Activated carbon | |
| % Adsorbents | COD (mg/lit) | % COD Reduction | COD (mg/lit) | % COD Reduction |
| Raw sample | 3116 | - | 3116 | - |
| 1% | 2967 | 4.78 | 2770 | 11.10 |
| 2% | 2444 | 21.56 | 2251 | 27.75 |
| 3% | 1778 | 42.93 | 1500 | 51.86 |
| 4% | 1422 | 54.36 | 1166 | 62.58 |

COD Reduction for acidic sample (Vinyl sulfone ester) of using fullers earth is 2.51 % to 11.79 % for 1% fullers earth to 2% fullers earth and using Activated cabon is 5.15 % to 14.65 % for 1% Activated carbon to 2% Activated carbon .

COD Reduction for acidic sample (Vinyl sulfone ester) of using fullers earth is 16.45 % to 35 % for 3% fullers earth to 4% fullers earth and using Activated cabon is 21.09 % to 44.29 % for 3% Activated carbon to 4% Activated carbon .

COD Reduction for neutralised (Vinyl sulfone ester) Sample using fullers earth is 4.78 % to 21.56 % for 1% to 2% Fullers earth and using Activated carbon is 11.10 % to 27.75 % for 1% Activated carbon to 2% Activated carbon .

COD Reduction for neutralised (Vinyl sulfone ester) Sample using fullers earth is 42.93 % to 54.36 % for 3 % to 4% Fullers earth and using Activated carbon is 51.86 % to 62.58 % for 3% Activated carbon to 4% Activated carbon .

The above observations were made for two different adsorbents such as Fullers earth and Activated carbon , it was found that the value of percentage COD reduction for the case of acidic effluent are lower than the values of COD reduction for the case of neutralised effluent.

| Fig.A.5 Comparing between Fullers earth and Activated carbon | | |
| --- | --- | --- |
| | Fullers earth | Activated carbon |
| Surface area (m²/g) | 120-140 | 500-1200 |
| Cost (Rs/kg) | 30-40 | 450-600 |
| COD Results for acidic sample ( for 4% adsorbent ) | 35.01% | 44.29 % |
| COD Results for Neutralised sample ( for 4% adsorbent ) | 54.36% | 62.58% |
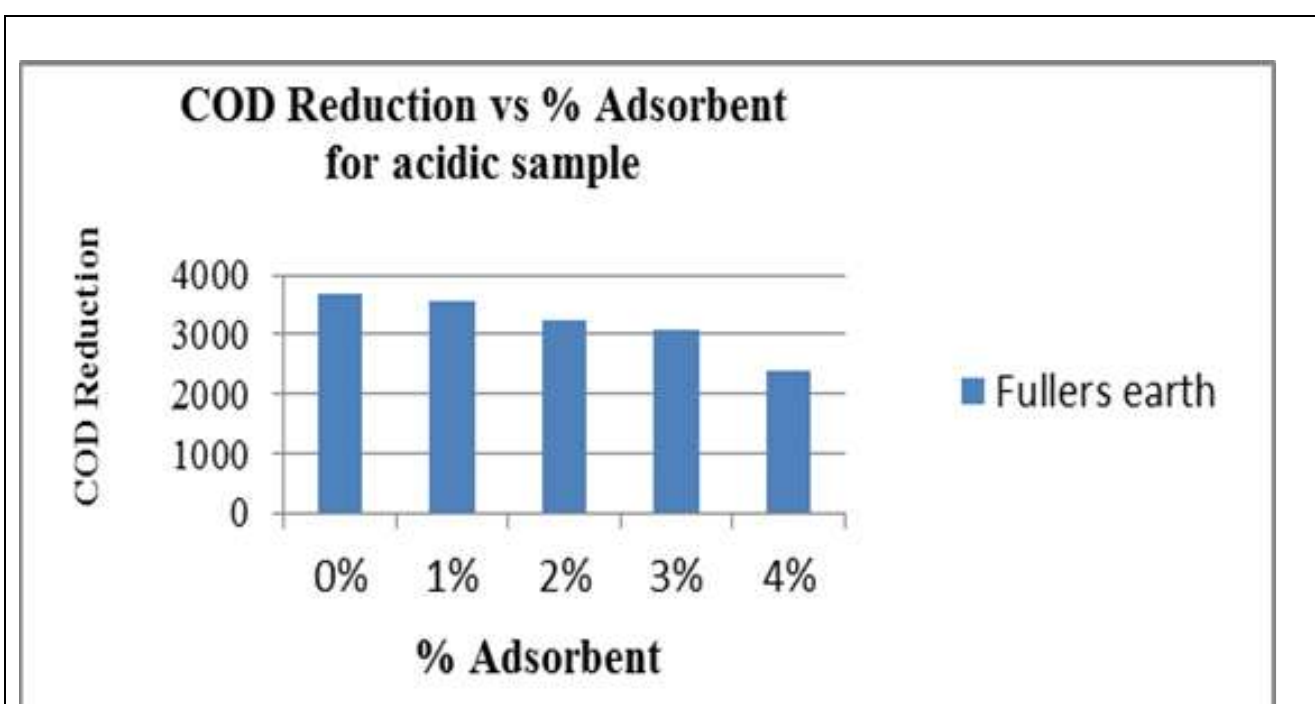


Fig.A.6.COD reduction Vs.%Adsorbent for acidic sample using Fullers earth.
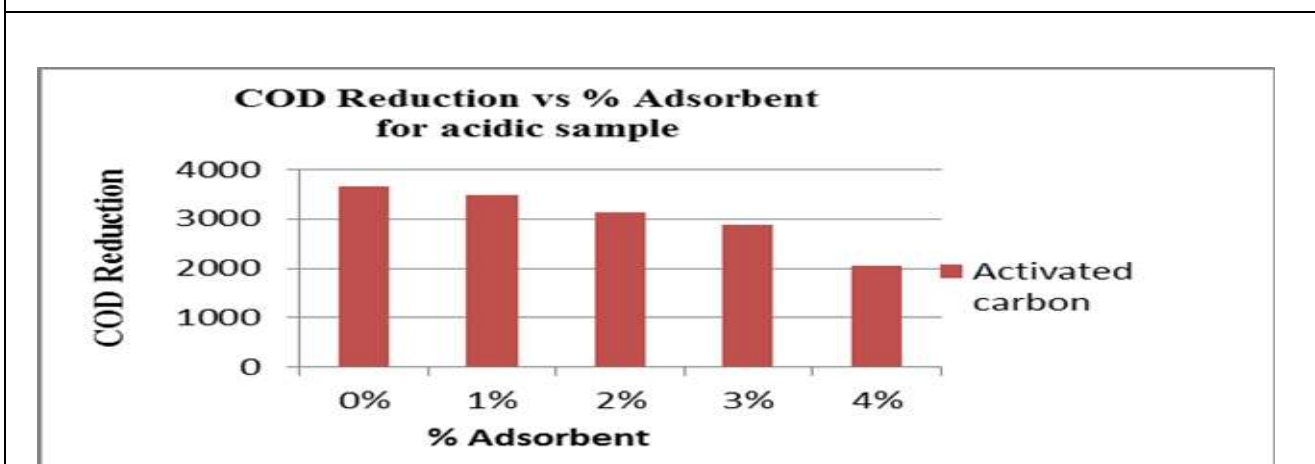


Fig.A.7 COD reduction Vs.%Adsorbent for acidic sample using Activated carbon.
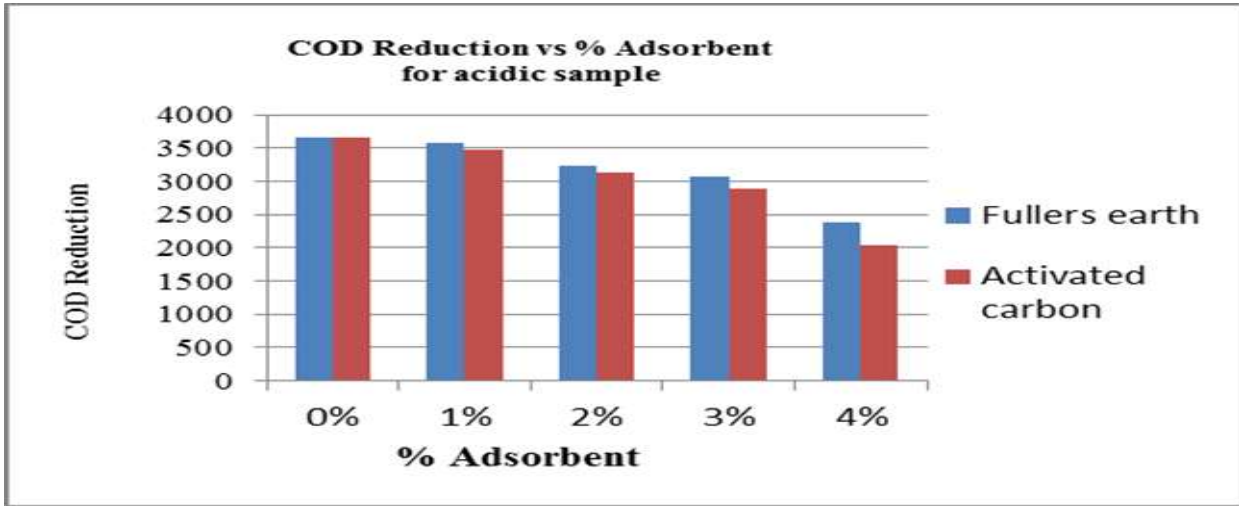
Fig.A.8  COD reduction Vs.%Adsorbent for acidic sample using Fullers earth and Activated carbon.
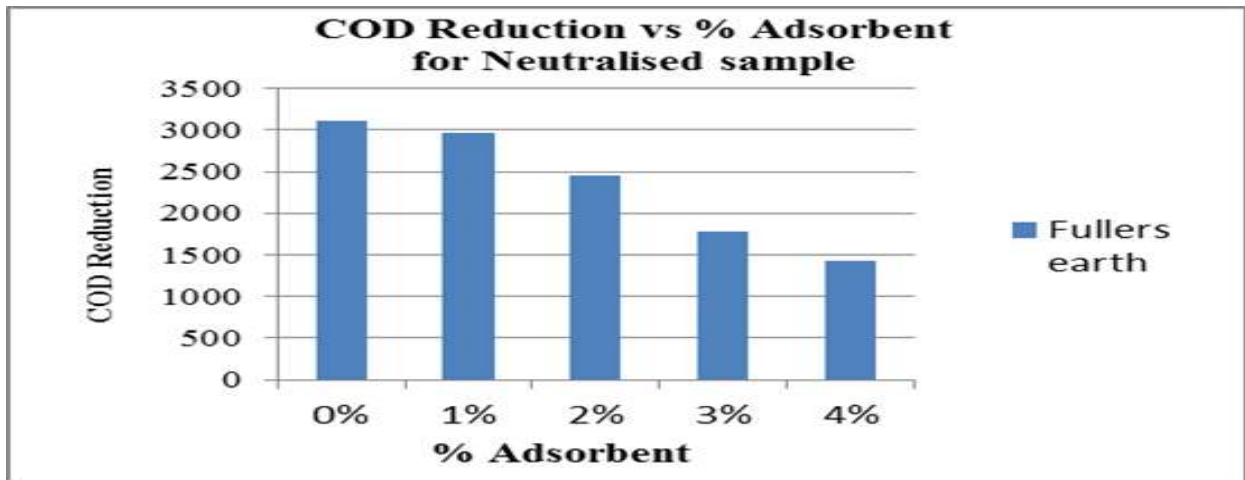


Fig.A.9  COD reduction Vs.%Adsorbent for Neutralised sample using Fullers earth.
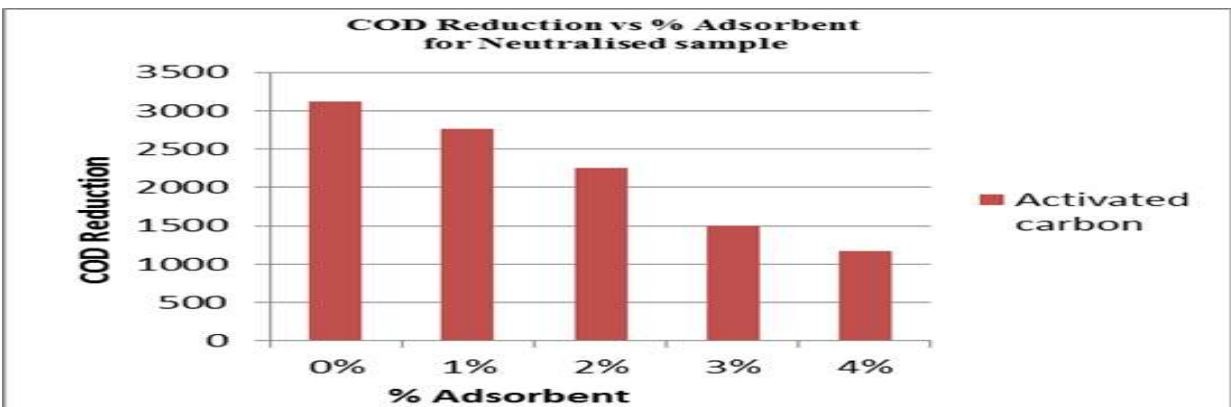


Fig.A.10  COD reduction Vs.%Adsorbent for Neutralised sample using Activated carbon.
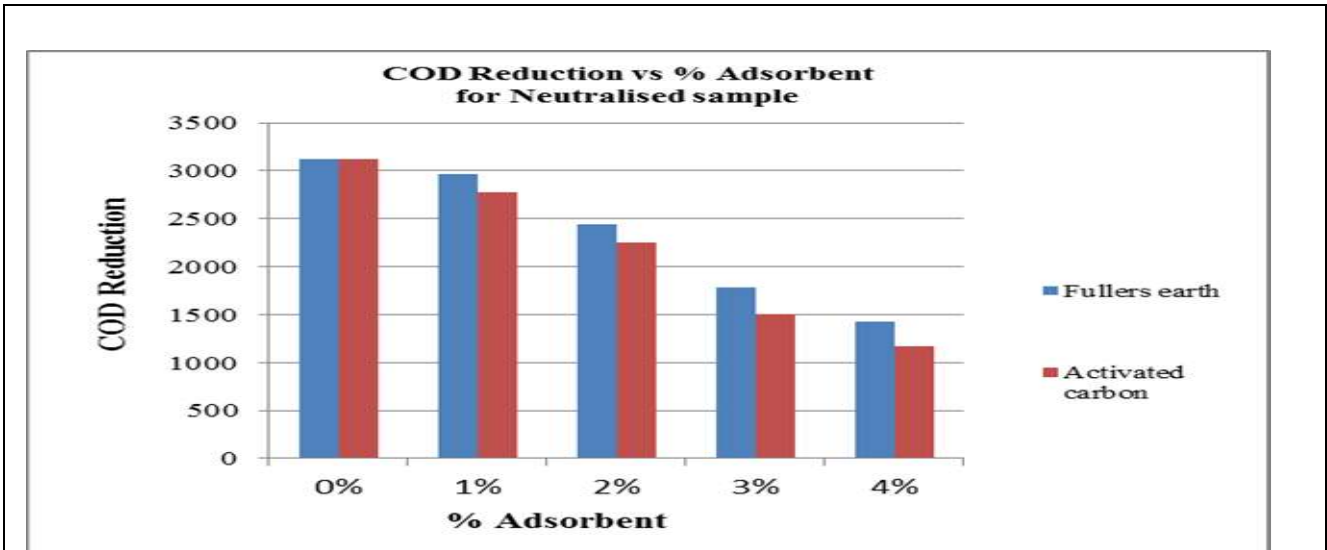
Fig.A.11  COD reduction Vs.%Adsorbent for Neutralised sample using Fullers earth and activated carbon
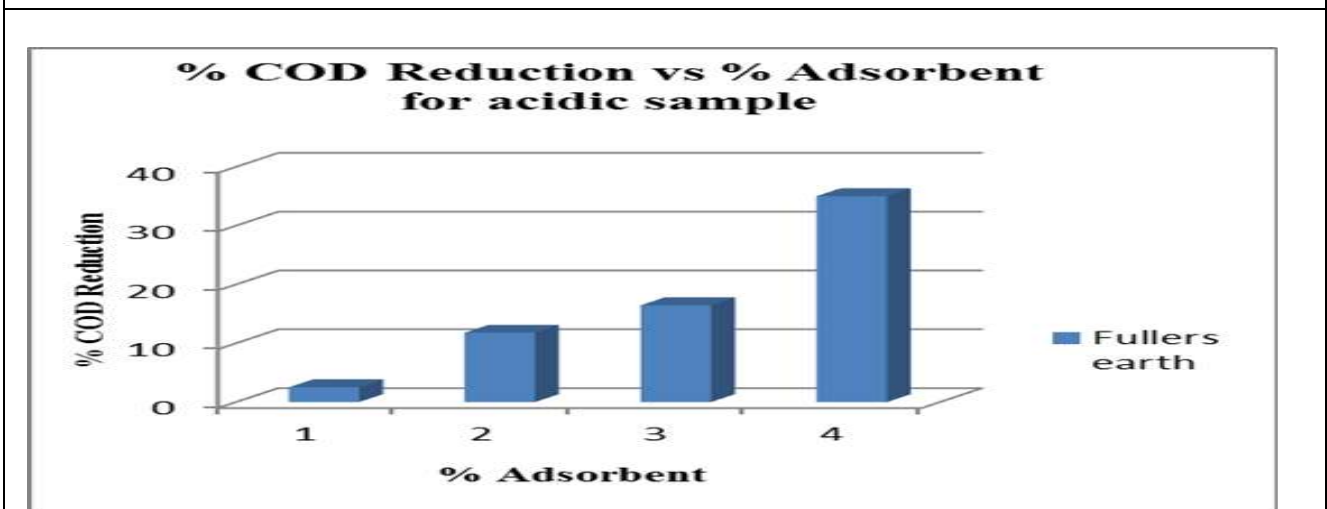


Fig.A.12   %COD reduction Vs.%Adsorbent for acidic sample using Fullers earth
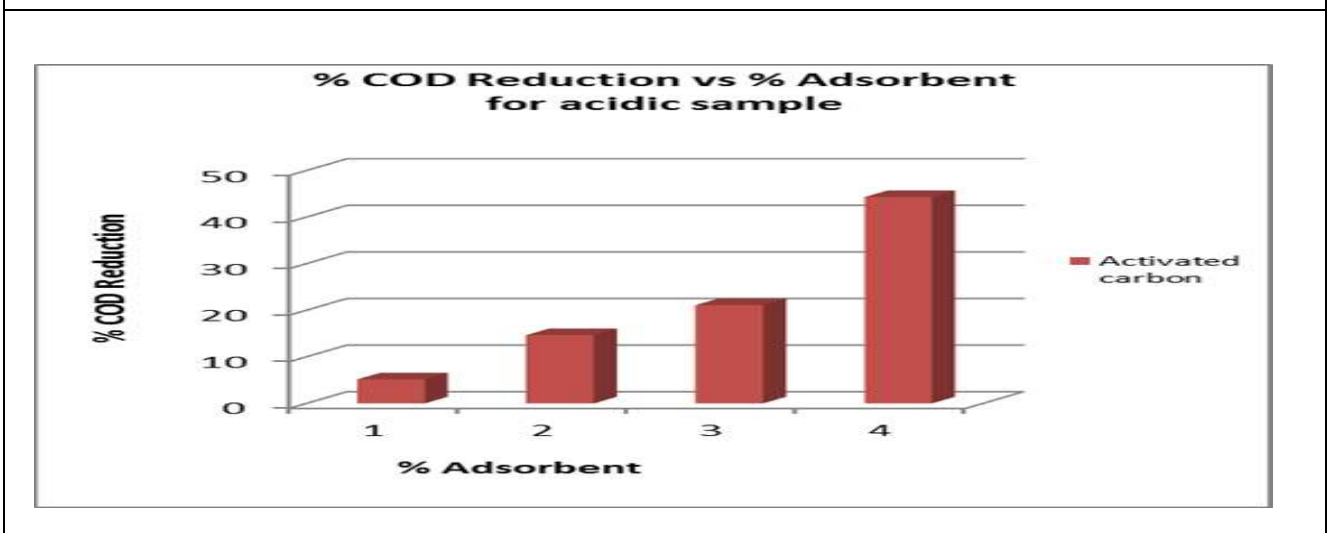
Fig.A.13   %COD reduction Vs.%Adsorbent for acidic sample using Activated carbon
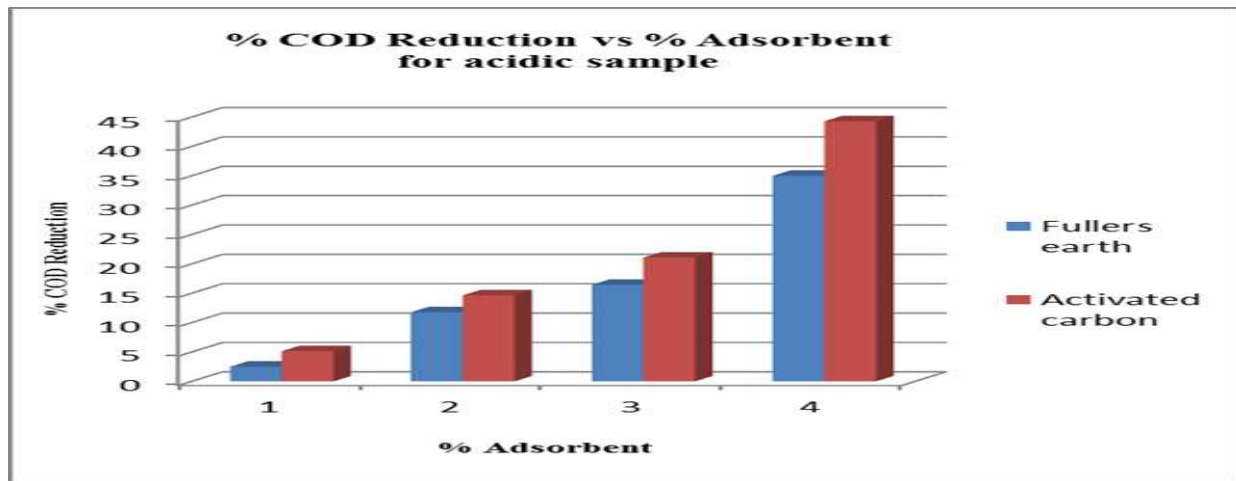


Fig.A.14  %COD reduction Vs.%Adsorbent for acicic sample using Fulllers earh and  Activated carbon
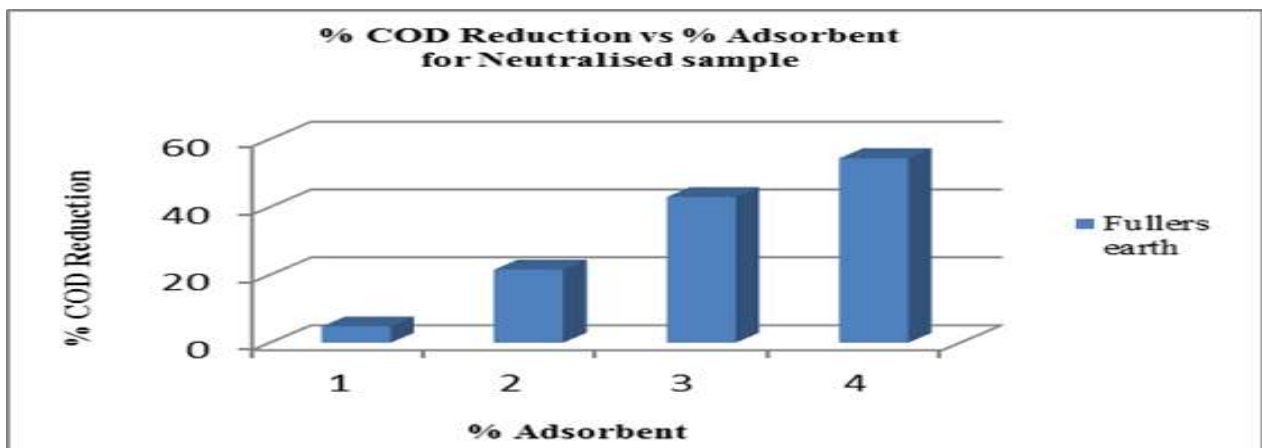


Fig.A.15   %COD reduction Vs.%Adsorbent for Neutralised  sample using Fullers earth.
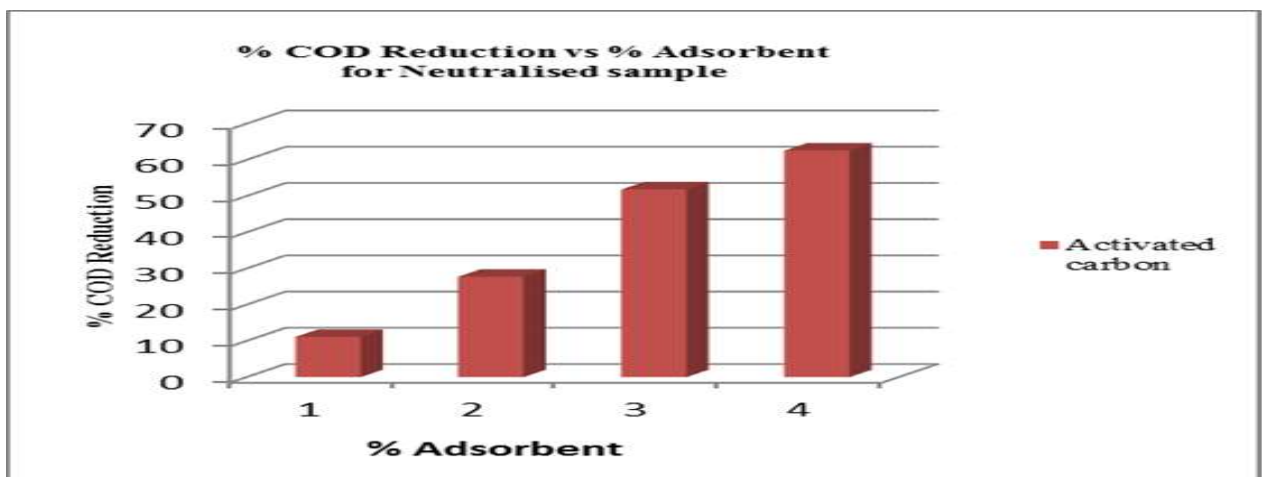
Fig.A.16 % COD reduction Vs.%Adsorbent for Neutralised sample using Activated carbon.
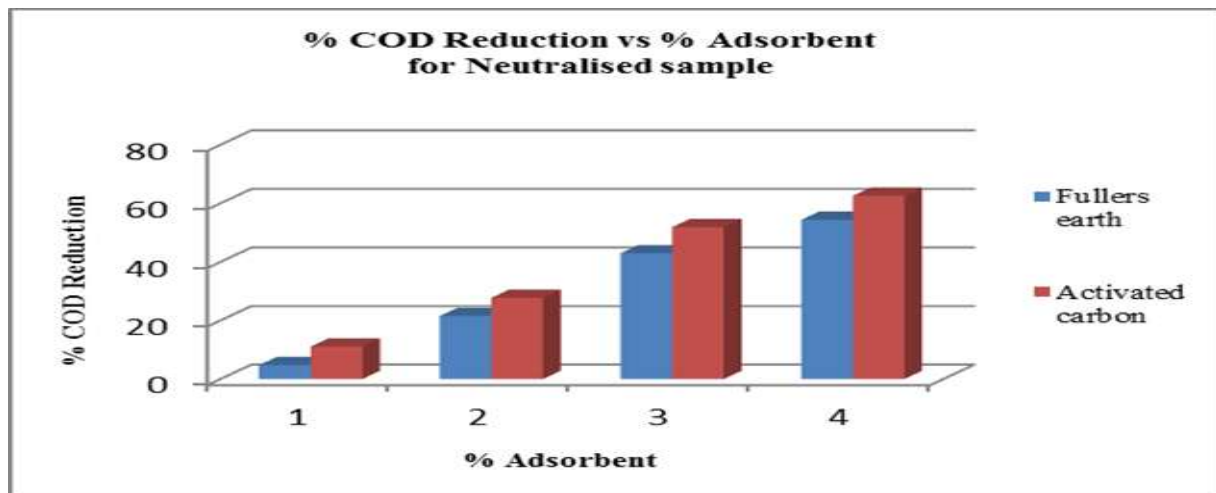


Fig.A.17  % COD reduction Vs.%Adsorbent for Neutralised sample using Fulllers earh and  Activated carbon

## 5 Mathematical Models:

Various mathematical models to predict the behaviour various adsorbents are available which includes.

### 5.1 Rathi-Puranik equation

$Log (CODRT) = m t + c$

Where, $CODRT = (Ci-C)/t$

$Ci$ = Initial concentration

$C$= Concentration at time t

$t$ = time in minute

$m$ = slope

$c$ = constant

### 5.2 Weber - Morri's equation

$(Ci-C)/Ci = m_1 t^{0.5} + c_1$

Where, $Ci$ = initial concentration

$C$= Concentration at time t

### 5.3  Lagregean equation

$log (C-C_{eq}) = m_2 + c_2$

Where,

$C$=Concentration at time t

Ceq= Equilibrium concentration

These model are useful to predict COD value



$$y = -0.0045x + 0.5458$$
$$R^2 = 0.992$$
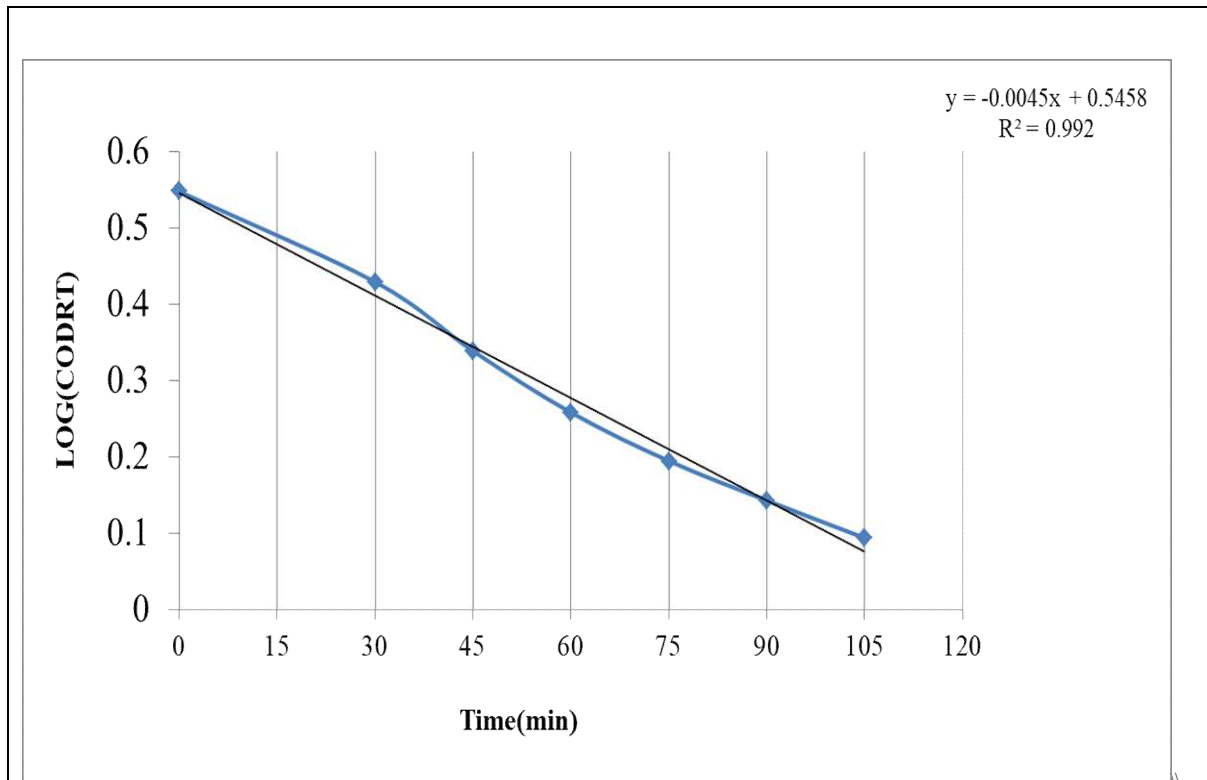
Fig.A.18  Rathi-puranik model  for LOG(CODRT)  vs  Time(min) .



$$y = -0.0045x + 2.1658$$
$$R^2 = 0.8559$$
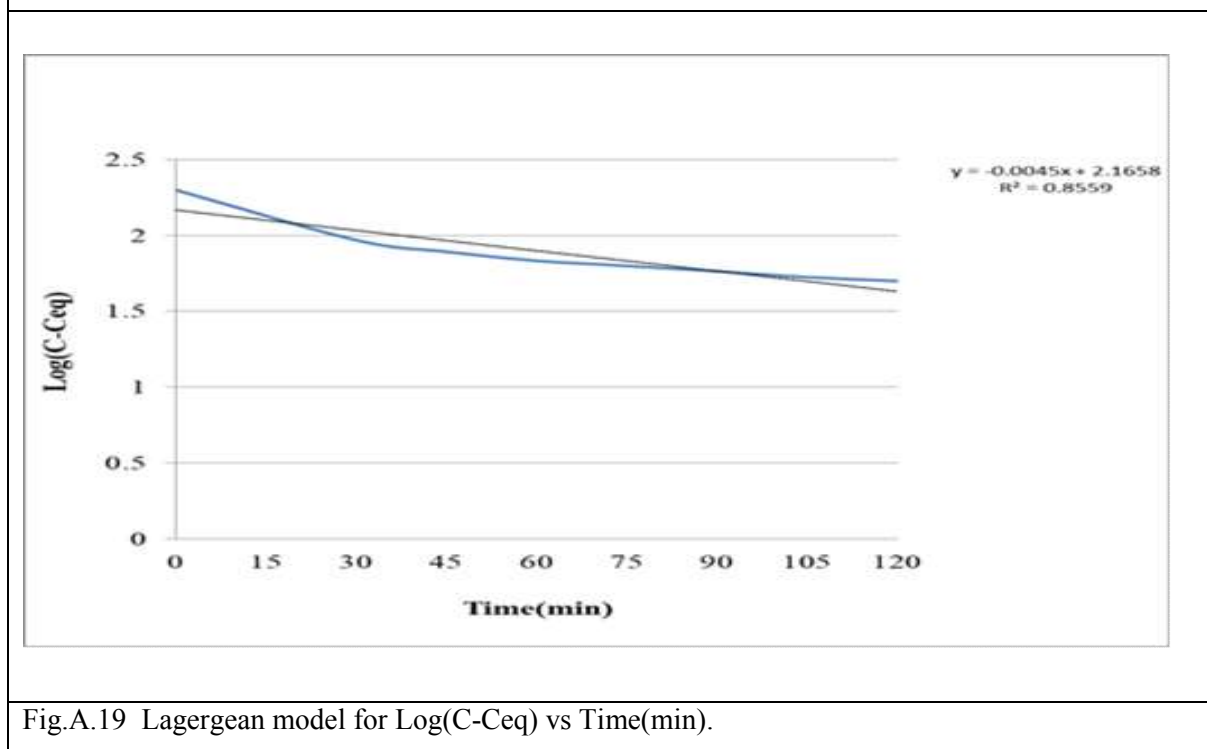
Fig.A.19  Lagergean model for Log(C-Ceq) vs Time(min).
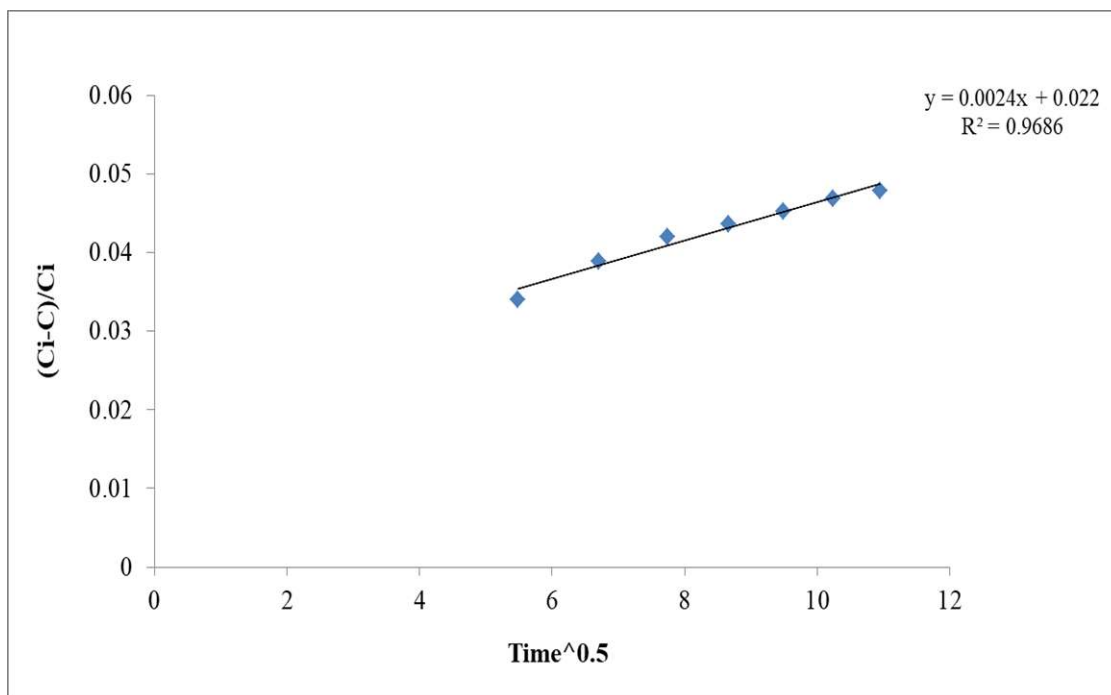
Fig.A.20 Weber and Morri's model for $(C_i-C)/C_i$ vs Time^0.5

The graph shows:
$$y = 0.0024x + 0.022$$
$$R^2 = 0.9686$$

## 6.Conclusion

- The above observations were made for two different adsorbents such as Fullers earth and Activated carbon, it was found that the value of COD reduction for the case of acidic effluent are lower than the values of COD reduction for the case of neutralised effluent.

- From the comparison of COD and %COD reduction values for Acidic and Neutralized sample, we can conclude that, as time and adsorbent quantity increases, COD value decreases and % COD reduction value increases.

- From the comparison of COD values and %COD reduction values of Fullers earth and Activated carbon it is found that, %COD reduction value are higher for Activated carbon. Owing to the cost of activated carbon it is not suitable for small scale industry Considering this factor it can be replaced by Fullers earth

- Study on mathematical modelling for three mathematical models- Rathi Puranik model, Weber-Morri's model and Lagergean Model we conclude that Rathi-Puranik model is more appropiate than Weber- Morri's model and Lagergean model ( As shown Fig.A.18, A.19, A.20) to predict the COD value at any time in a given system.

**References**

[1]N.B.Prakash, Vimala Sockan, and P.Jayakaran, Waste Water Treatment by Coagulation and Flocculation" *International Journal of Engineering Science and Innovative*

[2]Imran Ali, Mohd. Asim, Tabrez A. Khan, *Low cost adsorbents for the removal of organic pollutants from wastewater*, Journal of Environmental Management 113 (2012) 170-183.

[3]Parsons, S. "Advanced oxidation processes for water and wastewater treatment". *Water Intelligence Online*, *4*, p.9781780403076.2005

[4]Zularisam, A. W., A. F. Ismail, and Razman Salim. "Behaviours of natural organic matter in membrane filtration for surface water treatment—a review. *"Desalination* 194.1 (2006): 211-231.

[5] Crini, Gregorio. "Non-conventional low-cost adsorbents for dye removal: a review." *Bioresource technology* 97, no. 9 (2006), pp. 1061-1085.

[6] Vinesh V. Rakhodiya, Dr.S.A.Puranik " COD Reduction using modified industrial effluent flow sheet and low cost adsorbents as a part of cleaner production''Pelagia Research library, *Advance in Applied Science research*,2012.

[7]McDougall, G.J., 1991. The physical nature and manufacture of activated carbon. *Journal of the South African institute of mining and metallurgy*, *91*(4), pp.109-120.

[8] Bajpai, A.K. and Vishwakarma, N., 2000. Adsorption of polyacrylamide onto Fuller's earth surface. *INDIAN JOURNAL OF CHEMISTRY SECTION A*,*39*(12), pp.1248 1257.

[9] Babel, Sandhya, and Tonni Agustiono Kurniawan. "Low-cost adsorbents for heavy metals uptake from contaminated water: a review." *Journal of Hazardous materials* 97, no. 1 (2003) .pp.219-243.

[10]  V. K Gupta. "Application of low-cost adsorbents for dye removal–A review. "*Journal of environmental management* ''90.8 (2009), pp.2313-2342.

[11] Mohammed, M. A., A. Shitu, and A. Ibrahim. "Removal of methylene blue using low cost    adsorbent: a review." *Research Journal of Chemical Science,* (2014).

[12] Lokeshwari, N., and Keshna Joshi. "Low Cost Adsorbent for Reducing Organic Components."*Jr. of Industrial Pollution Control* 30(1) pp 53-58. 2014.

[13] A.K.A.Rathi, S.A.Puranik, "Chemical industry waste water treatment using Adsorption'' *Journal of scientific & Industrial Research*, vol-61, January 2002.

[14] Akhilesh R. Yadav, Dr. S. A. Puranik," Industrial Waste Water Treatment by Adsorption", *Asian International Conference on Science, Engineering & Technology*, 2015.

[15] Dasani Khushboo B, Dr. S. A. Puranik, "Modification in COD Reduction By Adsorption in Dyes & Dyes Intermediate Industry*", Global Research Analysis*, vol-II, Issue: V, May, 2013.

[16] De Gisi, Sabino, et al. "Characteristics and adsorption capacities of low-cost sorbents for wastewater treatment: a review." Sustainable Materials and Technologies 9 (2016): 10-40.

# Effect of sound waves and inclination of membrane on the performance of the osmotic microbial fuel cell

*Mandar S. Bhagat[1], Arvind K. Mungray[1], Alka A. Mungray[1]\**

[1]Department of Chemical Engineering, Sardar Vallabhbhai National Institute of Technology, Surat, Gujrat, India.
*Corresponding author: bag@ched.svnit.ac.in

## Abstract

This study aimed to explore the effect of the sound wave and membrane inclination i.e., 45° and 90° (MI45 and MI90) on the performance of osmotic microbial fuel cell (OMFC). The vibrations were given by a sound intensity of 60-80 dB and 20-1000 Hz in an anode compartment for a period of 5-6 (h) per day. Membrane inclination was given to maximizing the effective surface area under a fixed plane without changing its volumetric capacity to enhance water flux. Membrane inclination increased the effective surface area up to 33.33 %, therefore, Water flux was increased by 10% by using 45° inclination. The OMFC produced maximum water flux, reverse salt flux and power density of $0.750 \pm 0.02$ and $0.666 \pm 0.02$ $Lm^{-2}h^{-1}$, $3.18 \pm 0.02$ and $3.10 \pm 0.02$ $gm^{-2}h^{-1}$, $35.22 \pm 12$ and $24.22 \pm 08$ $mW.m^{-2}$ for MI45 and MI90 respectively with the effect of sound. The chemical oxygen demand (COD) removal was found $66.85 \pm 1$ % and $59.51 \pm 1$ % with and without the effect of sound. Therefore, sound reduced the OMFC start-up time by 2-3 days based on OCV data and also increased the anaerobic degradation by 6-9 %.

**Keywords:** Sound wave; Membrane inclination; Osmotic microbial fuel cell; Forward osmosis; Microbial fuel cell.

## Graphical Abstract
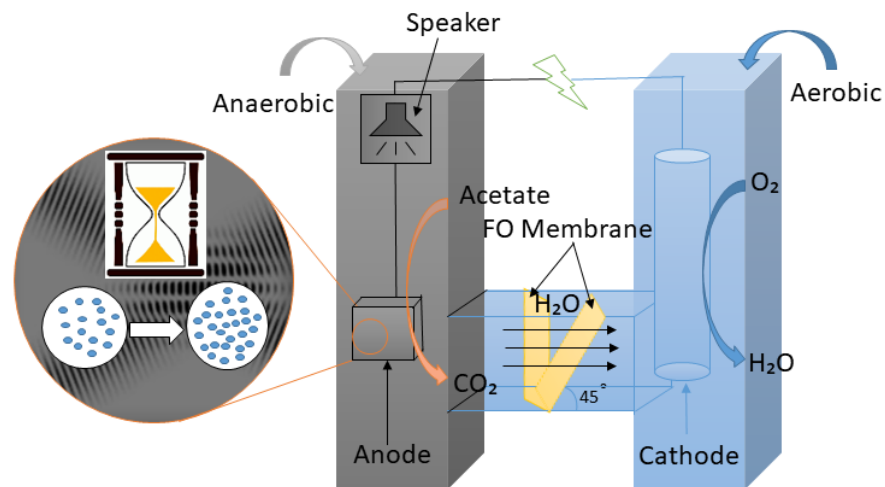
**Abbreviations**

MI = Membrane inclination
MI90 = Membrane inclination at 90°
MI45 = Membrane inclination at 45°
WOS = Without effect of sound
WS = With effect of sound
WF = Water flux
RSF = Reverse salt flux
PD = Power density
OCV = Open circuit voltage
CCV = Closed circuit voltage
BGR = Bacterial Growth Rate
SEM = Scanning Electron Microscope
COD = Chemical Oxygen Demand
TFC = Thin film composite
HRT = Hydraulic retention time

## 1. Introduction

Forward osmosis (FO) is an emerging technology based on the principle of naturally occurring osmosis, in which diffusion of a solvent through a semi-permeable membrane from a high to low water chemical potential difference (Awad et al., 2019). Osmosis has been increasing steadily over recent years with applications mainly focusing on desalination and wastewater treatment processes to power generation (Cath et al., 2006).

In Microbial fuel cell (MFC), microorganisms produce electricity by utilizing biodegradable substrates as a source from wastewater (Rahimnejad et al., 2015; Slate et al., 2019). In the anode compartment, the oxidation reaction takes place by electrochemically active bacteria using substrate/acetate as a fuel source (Logan, 2007). In the cathode compartment, the protons diffused through proton exchange membrane and combine with oxygen (and electron through an external circuit) leads to the generation of electricity and water via the following oxygen reduction reaction (ORR) (Logan, 2007);
Anode chamber reaction:

$$CH_3COO^- + 4H_2O \rightarrow 2HCO_3^- + 9H^+ + 8e^-$$   -------------- (1)
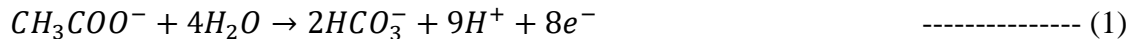
Cathode chamber reaction:

$$O_2 + 4H^+ + 4e^- \rightarrow 2H_2O$$   -------------- (2)

The combination of the natural osmosis concept and microbial fuel cell creates a novel term known as osmotic microbial fuel cell (Al-mamun et al., 2017; Yang et al., 2017; Zhu et al., 2015). Osmotic microbial fuel cell (OMFC) performs water treatment along with the recovery of water and energy by the combination of electrochemistry and microbiology (Yang et al., 2017). OMFC is able to produce more electricity than that of conventional MFC because of its low membrane resistance and water flux with the ion transport and/or higher level of concentration polarization that further reduces internal resistance (Qin et al., 2017). The practical application of the OMFC system will require to develop a design first to produce high power, coulombic efficiency, and pure water. And

secondly, it should be financially feasible to work on a large scale (Logan, 2007). The researcher proposed many modifications in OMFC design to improve its efficiency but still, it is not up to the mark. There is a need to increase the efficiency of exoelectrogens for better bacterial performance and membrane area for better flux for proton and water.

Sound creates a vibration or vice-versa that has been employed in various studies from plant to bacteria (Cho and Ying, 2009). The frequency of sound was able to shorten the lag phase and increased the growth rate of the bacterial cells (Juergensmeyer, 2004). The vibration effect provides the working condition for bacterial cell membrane to enhance the growth as well as metabolic activity (Cho and Ying, 2009; Shaobin et al., 2010). Therefore, the effect of sound in OMFC can have two distinct advantages; (1) lesser start-up time due to growth, and (2) enhance substrate degradation efficiency due to metabolic acceleration. Till date, no data is available on OMFC for these two effects.

In membrane separation processes, various membrane modules are used. Those are generally hollow fiber, tubular, plate, and frame, spiral wound, etc. for providing maximum effective surface area without changing its volumetric capacity, maximum flux, easy handling, and back-flushing (Rautenbach et al., 1994; Thakur and De, 2012). But for increasing the effective surface area, the membrane is replaced. Therefore, just by changing membrane inclination what would be the performance is still not known.

To the best of the author's knowledge, no data is available regarding the influence of sound waves on the degradation efficiency and viability of microorganisms in the OMFC reactor. Also, instead of changing the membrane module, the effect of membrane inclination towards the flux and ultimately on the performance of OMFC is not known. Therefore, this study was designed to investigate the effect of sound waves on biodegradation characteristics and membrane inclination (45˚ and 90˚) on the performance of OMFC i.e. power density, columbic efficiency, water flux, reverse salt flux, COD removal, etc.

## 2. Materials and Methods

### 2.1 Materials

Thin-film composite FO membrane manufactured by HTI, Inc. USA was used for all experimentation. All the chemicals used were research grade. Distilled water used in this study was collected from Milli-Q Millipore with an initial TDS of 0-5 ppm. The material used for making anode and cathode were carbon cloth and graphite rod having a surface area of 36.85 cm$^2$ and 56.52 cm$^2$ respectively.

### 2.2 Design of OMFC set-up

The fabricated OMFC with a different inclination of the membrane module is shown in Fig. 1. This OMFC set-up had two equal-size compartments of 140 mL each with the size of (16 x 3 x 3 cm$^3$) for anode and cathode respectively. The surface area of membranes with an inclination of 45˚ and 90˚ were 13.5 cm$^2$ and 9 cm$^2$ respectively. The geometry of the membrane inclination under the fixed plane is shown in Fig. 2.
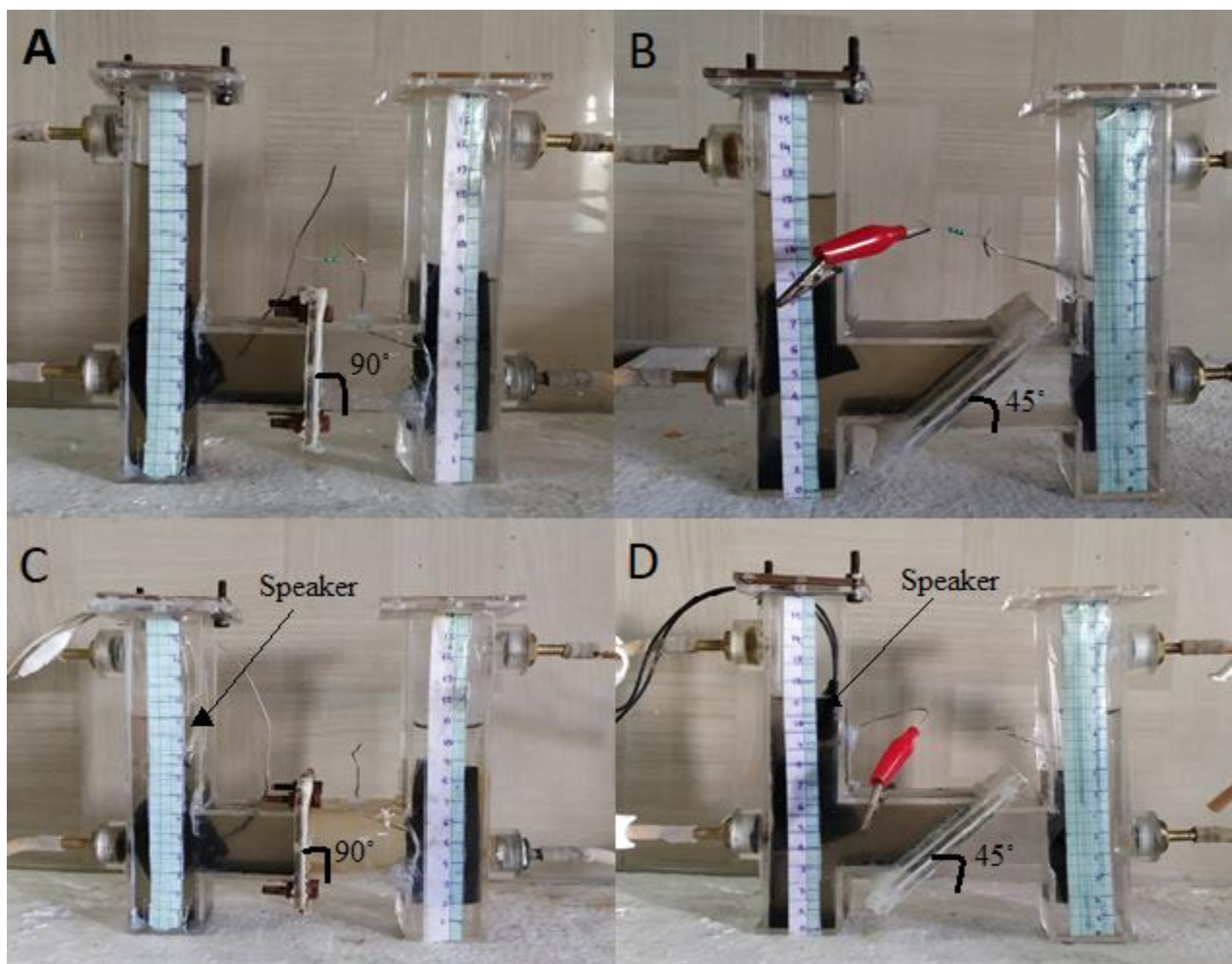
Figure 1. Real images for OMFC set-up (A-MI90, B-MI45 for WOS and C-MI90, D-MI45 for WS)
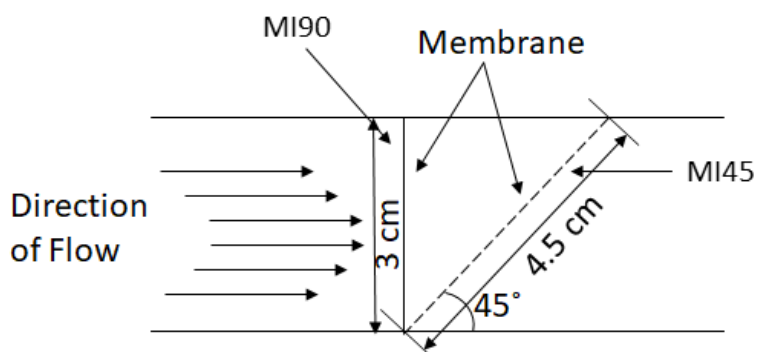


Figure 2. Geometry of angle inclination

The OMFC reactors were operated at room temperature ($25 \pm 2$ °C) throughout all experiments. The anode was fed with synthetic wastewater prepared by the distilled water as $1000 \pm 5$ mL; sodium acetate, $1000 \pm 20$ mg; $NH_4Cl$, $70 \pm 5$ mg; $CaCl_2$, $20 \pm 5$ mg; $MgSO_4$, $15 \pm 5$ mg; $NaHCO_3$,

$100 \pm 5$ mg; $K_2HPO_4$, $5.4 \pm 5$ mg; $KH_2PO_4$, $2.6 \pm 0.5$ mg; and trace element, 1 mL (Angenent and Sung, 2001). The anaerobic sludge (5% v/v) obtained from the local domestic wastewater treatment plant was chosen as the inoculation source of the anodic compartment. The actual set-up of OMFC is shown in Fig. 1 (A, B, C, and D for the study with and without the effect of sound). Table 1, shows the characteristics of synthetic wastewater.

Table 1 Properties of synthetic wastewater

| Properties | Range |
|---|---|
| Chemical oxygen demand | $1010$ mg. $L^{-1}$ |
| pH | $6.52$ |
| Oxygen reduction potential | $28$ mV |
| Conductivity | $5854$ $\mu s.cm^{-1}$ |
| Dissolved oxygen | $4.95$ mg. $L^{-1}$ |

## 2.3 OMFC startup

The FO membrane was used from the start of the run to separate anode and cathode compartments of OMFC to develop biofilm on the anode surface. The anode was inoculated by using synthetic wastewater, sludge, and the cathode chamber was filled with distilled water and kept in an open circuit. During the biofilm development phase, negligible changes in liquid volume were observed in both the compartment. After achieving a constant OCV value the catholyte was replaced by 1 M NaCl solution as a draw solution. The active layer of the membrane was facing on the anode side throughout all the experiments. The stainless steel wires were used to complete the external circuit and a polarization study was performed to find external registers for both reactors.

## 2.4 Sound treatment on OMFC

Sound stimulation for bacteria on the degradation of organic matter was performed in the reactor as shown in Fig. 1 (C and D). Waterproof speakers were kept in the anodic chamber to provide a vibrational effect of sound. The bacteria was stimulated by sound wave with an intensity of 60-80 dB where frequency range from 20-1000 Hz throughout the experiment for an interval of 5-6 hrs. per day (Yi et al., 2003). The distance of the speaker from the anode was 2 cm. The bacterial degradation of the substrate was studied by COD removal for WOS and WS conditions.

## 2.5 Measurement of OMFC parameters

### 2.5.1 Water flux and reverse salt flux

The water flux (Jw) was calculated from equation (3); the volume change of the draw or feed solution. The unit for water flux is $Lm^{-2} h^{-1}$, abbreviated as LMH (Pardeshi and Mungray, 2014).

$$J_w = \frac{\Delta V}{\Delta t A_m} \qquad \text{---------------- (3)}$$

where $\Delta V$ is the volume change of feed solution, $A_m$ is an effective membrane area and $\Delta t$ is the time interval between volume change of feed or draw solution.

Reverse salt diffusion was calculated by using equation (4); it is defined as the permeation of solute from draw solution to feed solution was calculated from the changes in concentration of draw solution ($J_s$, $gm^{-2}h^{-1}$, abbreviated as gMH) (Wang et al., 2019):

$$J_s = \frac{\Delta C \Delta V}{\Delta t A_m} \qquad \text{----------------- (4)}$$

where $\Delta C$ is the change in the concentration of salt.

## 2.5.2 Columbic efficiency

The ratio of coulombs recovered by a system to the total coulombs in the substrate is defined as columbic efficiency (CE). Coulombic efficiency also represents the recovery of the electron in the system. For the measurement of coulombic efficiency UNI-T brand Digital Multi-meter (1000 V) was used across the external resistors of anode and cathode at an interval of 3 minutes and converted to current and power using equation (5 and 6). Equation (7) was used to calculate columbic efficiency ($C_E$) (Pardeshi and Mungray, 2014):

$$V = IR \qquad \text{--------------- (5)}$$

$$P = IV \qquad \text{-------------- (6)}$$

$$C_E = \frac{8 \int_0^b I \, dt}{F \vartheta_{an} \Delta COD} \qquad \text{-------------- (7)}$$

where I is the current in amperes, F is the Faraday constant, $\Delta COD$ is the change in substrate concentration in terms of COD for batch feed mode system by time $t_b$, and $\vartheta_{an}$ liquid volume in the anode chamber.

Energy recovery is expressed in kilowatt-hour per cubic meter or kilowatt-hour per kilogram of COD (Ge et al., 2014):

$$Energy\ recovery = \frac{Power \times Time}{\Delta COD} \qquad \text{--------------- (8)}$$

## 2.5.3 Polarization curve analysis

The voltage across the series of different resistances was measured to obtain the polarization curve. The equation (9) was used to calculate the current. The polarization curve gives us an idea about at what resistor the OMFC system gives maximum power density so the system can work well on that resistance. The power density was obtained by using equation (10) and the plot of power density versus current was prepared (Pardeshi and Mungray, 2014).

$$I = V/R_{ext} \qquad \text{------------- (9)}$$

$$P = V^2/RA \qquad \text{------------- (10)}$$

## 2.5.4 Chemical oxygen demand

The closed reflux colorimetric method was used for measuring chemical oxygen demand (COD). The percentage of COD removal was calculated by using equation (11) (McCrady, 2008).

$$\%E_{COD} = \frac{COD_{in} - COD_{out}}{COD_{in}} \times 100 \qquad \text{------------------ (11)}$$

where, $COD_{in}$ = the influent COD; $COD_{out}$ = the effluent COD.

## 3. Results

### 3.1 Effect of sound and membrane inclination (MI) on open circuit voltage

The maximum voltage that can be obtained by the OMFC system without closing the external circuit is measured as open-circuit voltage (OCV) (Pardeshi and Mungray, 2014). The infinite resistance condition has to be maintained to measure OCV. The stable OCV for MI90 WS and WOS stimulation was $0.800 \pm 0.02$ V and $0.788 \pm 0.02$ V respectively. And the stable OCV for MI45 WS and WOS stimulation were $0.805 \pm 0.02$ V and $0.785 \pm 0.02$ V respectively as shown in Fig. 3. Almost 14-15 days are required for enrichment of biofilm on anode surfaces (Ge et al., 2013; Pardeshi and Mungray, 2014; Yang et al., 2016). In our experiments, the time required for the enrichment of bacteria on an anode surface was found to be shortened by 2-3 days with the effect of sound. Hence the start-up time for OMFC set-up was reduced. Fig. 3, shows the fluctuation in OCV of WOS and WS system. Less fluctuation was observed in OCV with the effect of sound. This shows the sound not only had an influence on the growth of bacteria but also accelerate the metabolic activity (Bochu et al., 2001; Cho and Ying, 2009; Juergensmeyer, 2004) for faster degradation. The average OCV observed is less by about 30% to that of the theoretical value of 1.14 V obtained by the $O_2/H_2O$ (+0.82 V) and the NAD/NADH (-0.32 V) redox potential (Liu and Cheng, 2005; Sun et al., 2015).
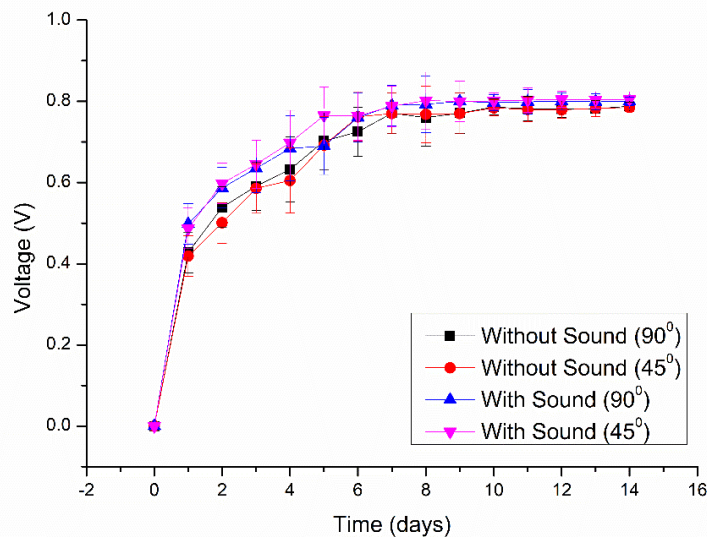


Figure 3. Graph represents open-circuit voltage in MFC before conversion of OMFC

### 3.2 Effect of sound and membrane inclination on electricity generation

The desirable operating conditions for OMFC to improve the performance are: (a) increased interaction of microorganism with wastewater to enhance the degradation rate of wastewater treatment or decreasing the HRT by stimulating the growth of microorganism for faster

degradation of organic matter (Pardeshi and Mungray, 2014), and (b) increase the movement of the proton through FO membrane or by increasing membrane area without changing its volumetric capacity.

Fig. 4 (a, b, c, d) shows polarization and for 4 distinct conditions of WOS (MI45 and MI90) and WS (MI45 and MI90). The application of sound in the OMFC system results in higher values of current and power than those of conventional systems (Tables 1). In the batch mode having HRT of 72 hrs, this system with the sound produced close circuit voltage (CCV) of $0.361 \pm 0.02$ V by using external resistance 1000 $\Omega$, the maximum current density of $97.56 \pm 22$ mA m$^{-2}$ and maximum power density of $35.22 \pm 12$ mW.m$^{-2}$ at MI45 and CCV of $0.3 \pm 0.2$ V, the maximum current density of $81.08 \pm 15$ mA.m$^{-2}$ and maximum power density of $24.32 \pm 08$ mW.m$^{-2}$ at MI90. However, WOS system by using 1000 $\Omega$ external resistor produced CCV $0.304 \pm 0.2$, the maximum current density of $43.78 \pm 09$ mA m$^{-2}$ and maximum power density $21.27 \pm 07$ mW m$^{-2}$ at MI45 and CCV of $0.402 \pm 0.02$ V, the maximum current density of $41.26 \pm 04$ mA.m$^{-2}$ and maximum power density of $18.89 \pm 04$ mW.m$^{-2}$ at MI90 with synthetic wastewater.

The maximum power and current production by the system were two times higher than that produced by WOS system. Here the WS system gave a more stable curve of power and current than WOS system (discussed in section 4). Coulombic efficiency up to $4.49 \pm 0.1\%$ and $5.52 \pm 0.1\%$ (for WOS) and $8.81 \pm 0.1\%$ and $8.46 \pm 0.1\%$ (for WS) at MI 45° and 90° respectively using acetate as a substrate. WS system had more electron recovery up to 35-45% higher than WOS system. Energy production was exactly double in WS case as shown in Table 1. In batch mode, for WOS system $0.002 \pm 0.0006$ kWh.kg$^{-1}$ and $0.001 \pm 0.0002$ kWh.kg$^{-1}$ of COD at MI45 and MI90 respectively and for WS system $0.0045 \pm 0.0014$ kWh.kg$^{-1}$ and $0.0032 \pm 0.0006$ kWh.kg$^{-1}$ of COD at MI45 and MI90 respectively. The energy production is higher for WS system than WOS system.

Table 2 OMFC performance with acetate as a substrate with WS and WOS system ($R_{ext}$ = 1000 $\Omega$)

| Condition | pH | | COD removal (%) | Current density (mA.m$^{-2}$) | Power density (mW.m$^{-2}$) | Energy Production (kWh.kg$^{-1}$) | CE (%) | Average flux (LMH) |
|---|---|---|---|---|---|---|---|---|
| | Anode | Cathode | | | | | | |
| **WSB 45°** | 6.52 | 7.52 | 63.33 ± 1 | 97.56 ± 22 | 35.22 ± 12 | 0.0045 ± 0.0014 | 8.81 ± 0.1 | 0.750 ± 0.02 |
| **WSB 90°** | 6.64 | 7.62 | 64.11 ± 1 | 81.08 ± 15 | 24.32 ± 08 | 0.0032 ± 0.0008 | 8.46 ± 0.1 | 0.666 ± 0.02 |
| **WOSB 45°** | 6.52 | 7.52 | 59.42 ± 1 | 43.78 ± 09 | 21.27 ± 07 | 0.002 ± 0.0006 | 4.49 ± 0.1 | 0.694 ± 0.02 |
| **WOSB 90°** | 6.64 | 7.62 | 59.43 ± 1 | 41.26 ± 04 | 18.89 ± 04 | 0.001 ± 0.0002 | 5.52 ± 0.1 | 0.625 ± 0.02 |

WSB- With Sound Batch (HRT: 72 hrs.); WOSB- Without Sound Batch (HRT: 72 hrs.)
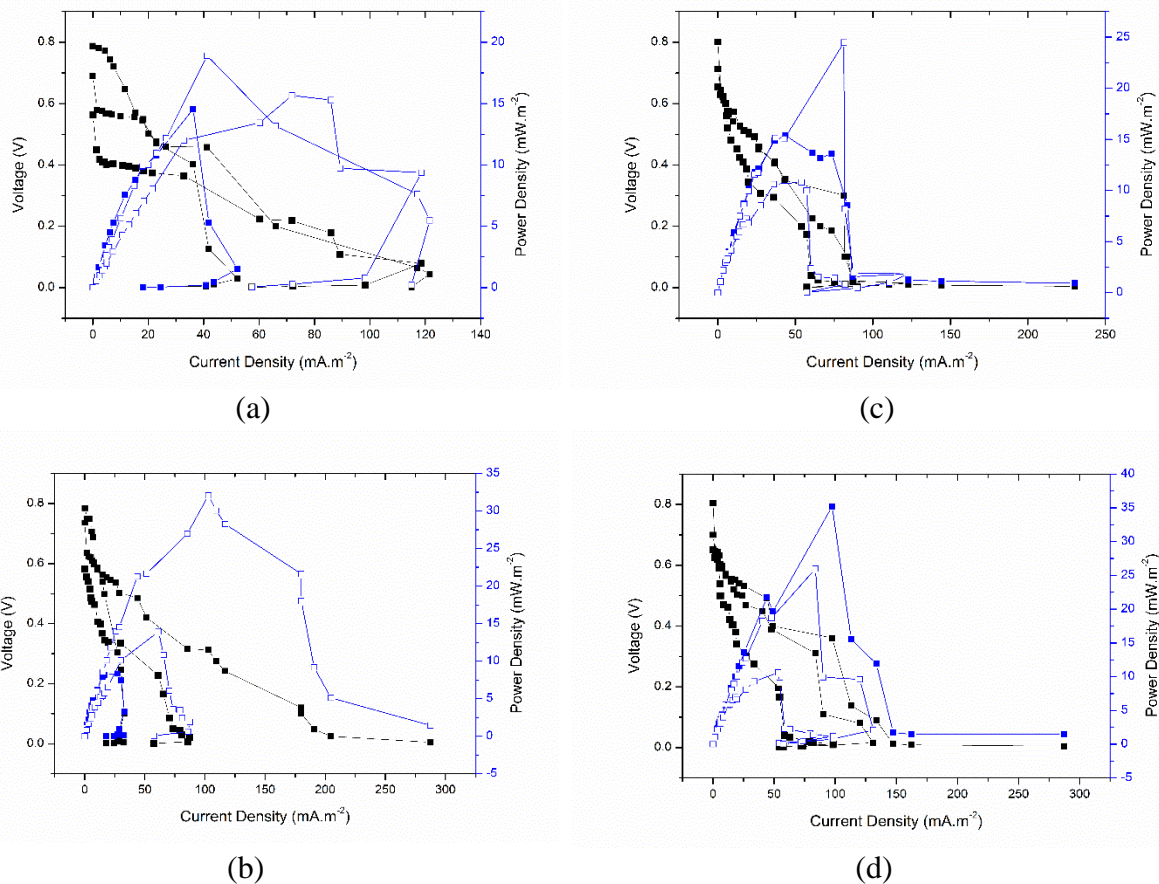
Figure 4. (a, b, c, d) Polarization curve for WOS (fig. a:MI90 and fig. b:MI45) and WS (fig. c:MI90 and fig. d:MI45) respectively with an interval of 3 days

### 3.3 Effect on the degradation efficiency of wastewater

The degradation of sodium acetate was monitored by COD removal as shown in Fig. 5 (a and b). The difference in COD pattern WOS and WS on bacteria represents the effect of sound on the degradation of organic matter. In batch mode, the COD removal efficiency for MI45 is $59.42 \pm 1$ % and $63.33 \pm 1\%$ for WOS and WS respectively. However, the COD removal for MI90 was $59.43 \pm 1\%$ and $64.11 \pm 1\%$ for WOS and WS respectively. Here we observed that the sound improves the degradation efficiency by up to 6 to 9 %. As substrate concentration decreases the growth of bacteria will be increased. The growth rate depends on substrate concentration only when most of the substrate will be consumed. At this point, the culture has practically reached its maximum biomass density (López et al., 2017). If the growth is more in less time the food (means the acetate) is consumed faster than usual. Therefore, the degradation rate is the function of the growth of bacteria (discussed in section 4).
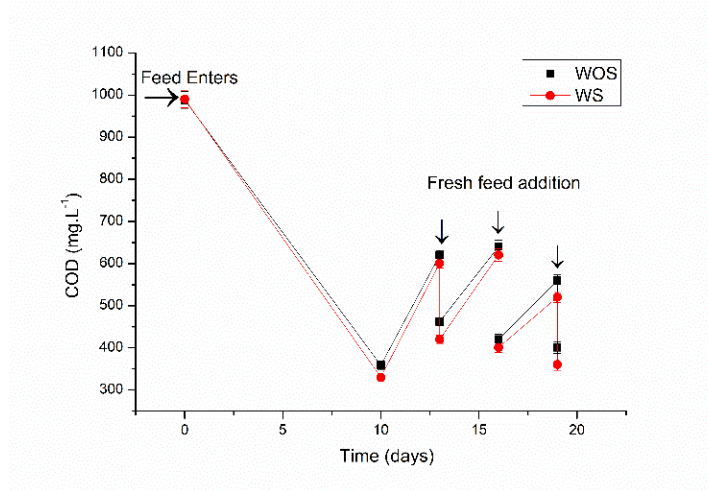
(a)
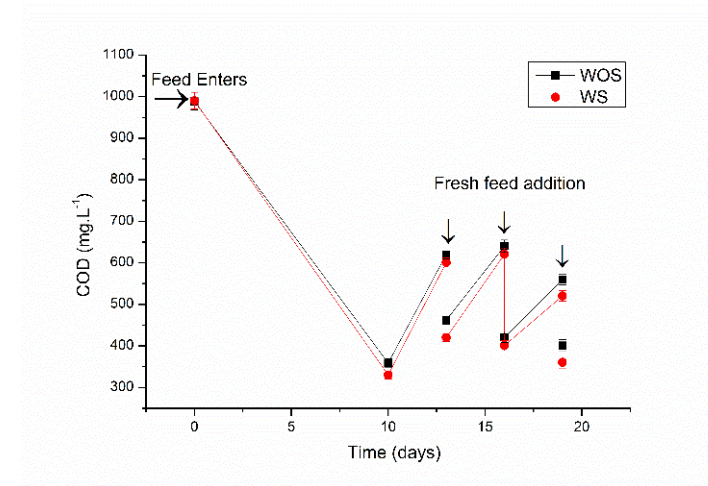


(b)

Figure 5. (a and b) Difference in COD (WOS and WS) at (MI90 and MI45) respectively

## 4. Discussion

### 4.1 Effect of sound on various parameters of the OMFC system

In OMFC, the natural catalyst (such as enzymes) is used by bacteria to produce electricity by degrading the organic matter present in the wastewater. Biofilms on an anode surface give an electron to the electrode with the help of metabolic activity through the cell membrane (nanowire) (Al-mamun et al., 2017). The basic structure of the bacterial cell membrane is shown in Fig. 6. The polar hydrophilic glycerol head attached through an ester bond to two nonpolar hydrophobic fatty acid tails, which naturally form a bilayer in aqueous environments (He and Angenent, 2009).
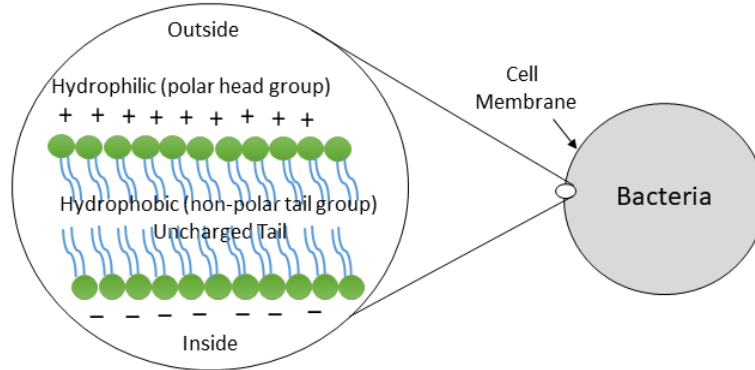
Figure 6. Schematic of cell membrane structure

The dimensions of the plasma membrane in bacteria are thus similar to membrane structures in animal and plant cells associated with the osmotic or secretory function (Williams and Rickaby, 2012). A glycoprotein across the membrane (H+-ATPase, a kind of glycoprotein across a membrane) is the plasma membrane (PM), which plays an important role in the processes of growth and development of plants as well as bacteria. The plasma membrane targets the cell function regulation and its activity is affected by light, hormone, fungal toxin, and other environmental factors. A sound wave is a definite form of discontinuous stress, which has great effects on the growth of plants and bacteria (Hughes, 2009). It is well known that environmental stresses induce and select physiological, metabolic, and/or genetic variations in micro-organisms (Wang et al., 2002). The vibration creates mechanical stress to the bacterial cell membrane, resulting in alternate contraction and expansion in membrane structure as shown in Fig. 7. The alternative stress triggers the internal fluid and its deformation of the cellular plasma membrane, while its fluidity increases with sound vibrations. Furthermore, stimulation of sound changes the membrane protein structure (Ackerman, 1951; Bochu et al., 2001; Leys et al., 2004). These processes are useful for membrane operating mechanism, and to accelerate metabolic activity (Apodaca, 2002).
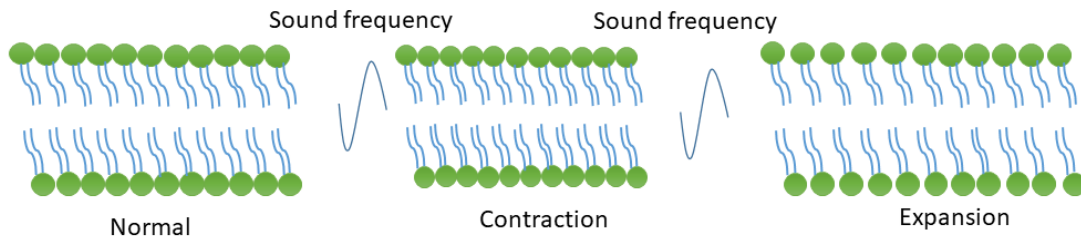

Figure 7. Cell membrane under vibrational stress

## 4.2 Stimulation processes of Endocytosis and Exocytosis

The tension in the plasma membrane can affect the processes of endocytosis and exocytosis. Endocytosis is a process in which a substance from outside the cell (outside of cell membrane) is captured and brings them into the cell (inside of the cell membrane). And exocytosis is a process in which material from inside the cell membrane is released to the outside of the cell membrane. Laplace's law in-plane tension (for simple thin-walled sphere), is given by equation (12) (Apodaca, 2002).

$$Tension = \frac{1}{2} \times radius\ of\ curvature\ \times pressure \qquad\qquad \text{----------- (12)}$$
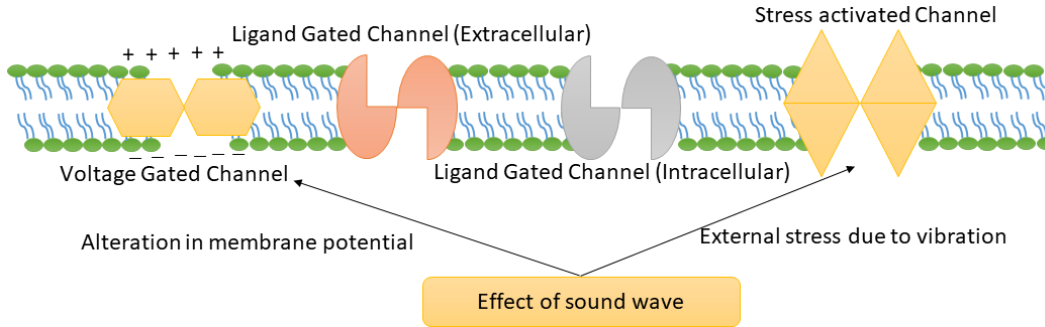
Figure 8. Effect of sound on the ion channel present in the cell membrane

There are four types of ion channels in a cell membrane (1) voltage-gated channel (2) ligand-gated channel (intracellular) (3) ligand-gated channel (extracellular) and (4) stress-activated channel. Fig. 8, shows the effect of sound waves on the ion channel present in a cell membrane. The main types of stimuli that are known to cause ion channels to open are changing membrane potential, mechanical stress (e.g. sound, temperature, ultraviolet light, magnetic field, etc.), or binding of ligands (Bruce Alberts et. al., 2002).

The area of the plasma membrane can be increased up to 2-3% before it breaks and its slimness makes the bilayer an active capacitor. The specific capacitance for the plasma membrane is 0.7 $\mu F/cm^2$. The surface area (SA) plasma membrane governs the absolute magnitude of ionic flux needed for any given voltage change and the rate at which transmembrane voltage can change (Apodaca, 2002; Morris and Homann, 2001). Therefore: (i) cell surface area affects the speed of electrical signaling means maximum power and current density can be obtained by using the sound system and (ii) cell surface area affects metabolic load means the degradation capacity can be increased by using a sound system since the amount of "pump" energy required to boost cellular batteries (after capacitive release) depends on the total number of ions pumped. Therefore, a large SA/volume ratio aids in facilitated transport as shown in Fig. 9.
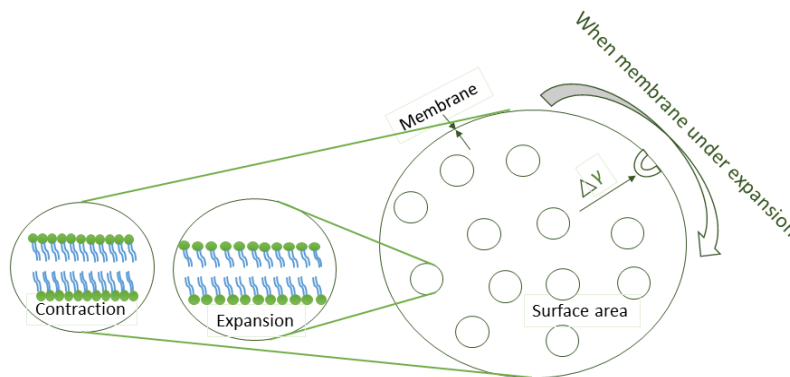


Figure 9. Bacterial cell exocytosis process: by increasing membrane tension ($\Delta\gamma$)

Fig. 10, explains the signaling pathways link with sound/vibration stimulation changes in endocytosis and exocytosis process (1) intermediate filaments, actin and microtubules are part of the cytoskeleton, and its function is affected by external vibration. The plasma membrane is attached to the cytoskeleton and it responds or reorganized when the membrane is under contraction and expansion. Therefore, the tension in the membrane changes the cytoskeleton ultimately affects the processes of endocytosis and exocytosis; (2) entry of $Ca^{2+}$ through plasma

membrane channel can also regulate endocytosis and increased intracellular $Ca^{2+}$ triggers exocytosis in many cells; (3) integrins are another class of vibration sensor which link extracellular matrix molecules to the intracellular actin cytoskeleton. An integrin ligand is capable of transmitting vibrational stress to the primary skeleton coated with magnetic beads; (4) the Rho family of GTP-ases regulates the formation of focal complexes; (5) tyrosine kinase and phospholipases are also plays a significant role in mechano-transduction receptor and nonreceptor; (6) vibrational stretch stimulate cAMP in some cell type including uroepithelium; (7) vibrational stretch of cardiac myocytes activates phospholipase C which in turn creates diacylglycerol (DAG) and inositol 1,4,5-triphosphate. DAG activates protein kinase (PKC) a known regulator of endocytosis and exocytosis process. inositol 1,4,5-triphosphate promotes $Ca^{2+}$ release which inspires the exocytosis process; (8) sound stimulus also increased production or secretion of multiple growth hormones (GF-R) (Berridge et al., 2000; Maria A. D. M., Giovanna S., Rechard A. K., 1993; Sadoshima and Izumo, 1997; Wang et al., 1993).
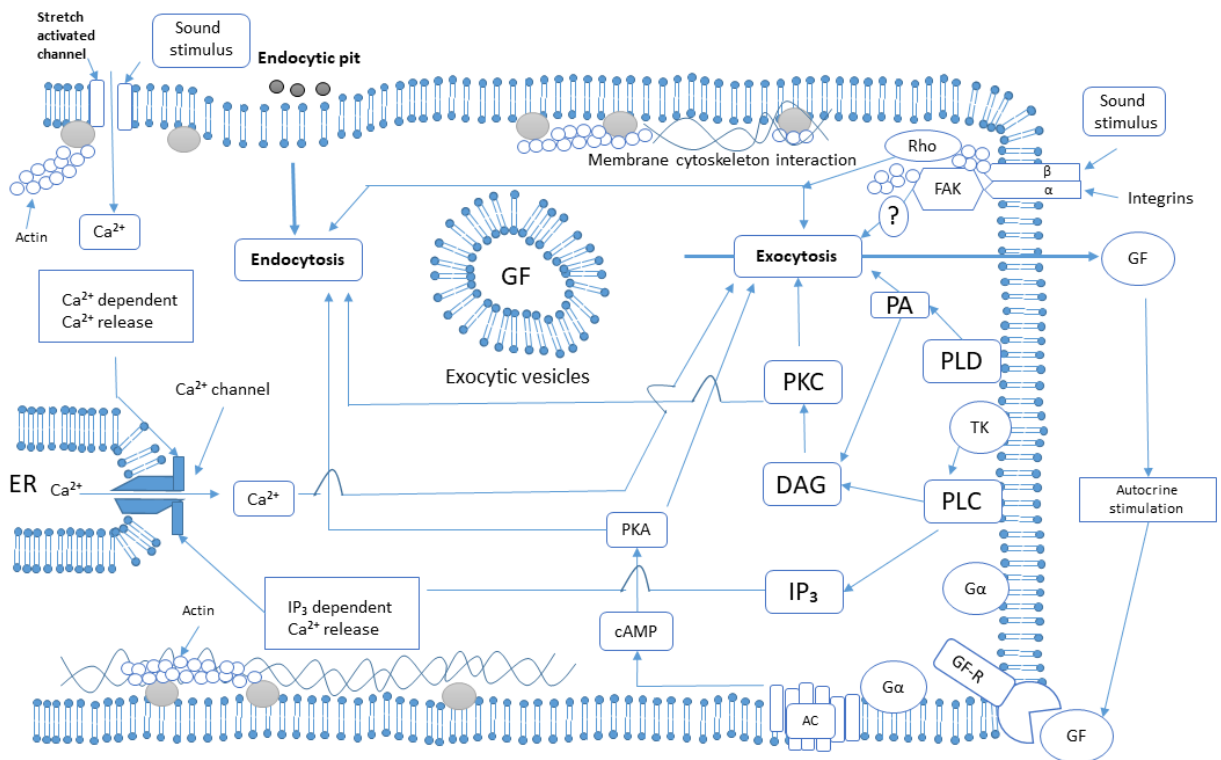


Figure 10. Signaling pathways link with sound stimulation in endocytosis and exocytosis. DAG: diacylglycerol; ER: endoplasmic reticulum; Gα: heterotrimeric G protein α-subunit; FAK: focal adhesion kinase; GF: growth factor/hormone receptor; IP$_3$: inositol 1,4,5-triphosphate; PA: phosphatidic acid; PLD: phospholipase D; PKC: protein kinase C; PLC: phospholipase C; Rho: Rho family GTPase; TK: tyrosine kinase; cAMP: e.g., forskolin; AC: adenylyl cyclase.

## 5. Effect of angle inclination on water flux

The water flux through the FO membrane was determined from the increased or decreased mass of water in the vessel containing cathodic or anodic effluent respectively. The draw solution at the end of each operation cycle is diluted by the osmotic water flux. The anolyte stream became concentrated due to reverse permeation of draw solute into it and water losses (Hancock and Cath,

2009). Fig. 11 (a, b, c, d), showed 72 h average water flux through FO membrane for four different OMFC systems. The maximum water flux (WF) achieved by OMFC WOS is $0.694 \pm 0.02$ Lm$^{-2}$h$^{-1}$ and $0.625 \pm 0.02$ Lm$^{-2}$h$^{-1}$ and the RSF $3.27 \pm 0.02$ g m$^{-2}$h$^{-1}$ and $3.14 \pm 0.02$ g m$^{-2}$h$^{-1}$ having MI 45˚ and 90˚ respectively. The maximum WF achieved by OMFC WS is $0.750 \pm 0.02$ L m$^{-2}$h$^{-1}$ and $0.666 \pm 0.02$ L m$^{-2}$h$^{-1}$ and the RSF $3.18 \pm 0.02$ g m$^{-2}$h$^{-1}$ and $3.10 \pm 0.02$ g m$^{-2}$h$^{-1}$ having MI 45˚ and 90˚ respectively. The highest water flux achieved in OMFC in literature was 1.06-1.49 by using a 2 M sodium chloride solution (Ge et al., 2013). Our observed value is nearby half due to the difference in osmotic pressure between 1 M NaCl and 2 M NaCl solution. The inclination of the membrane under the fixed plane gives maximum surface area without changing its volumetric capacity to obtain maximum water flux. In our case, the area of a membrane is increased from 9 to 13.5 cm$^2$. The water flux is increased from 9.94% and 11.2% for WOS and WS respectively for MI45.



(a)

(b)

(c)

(d)
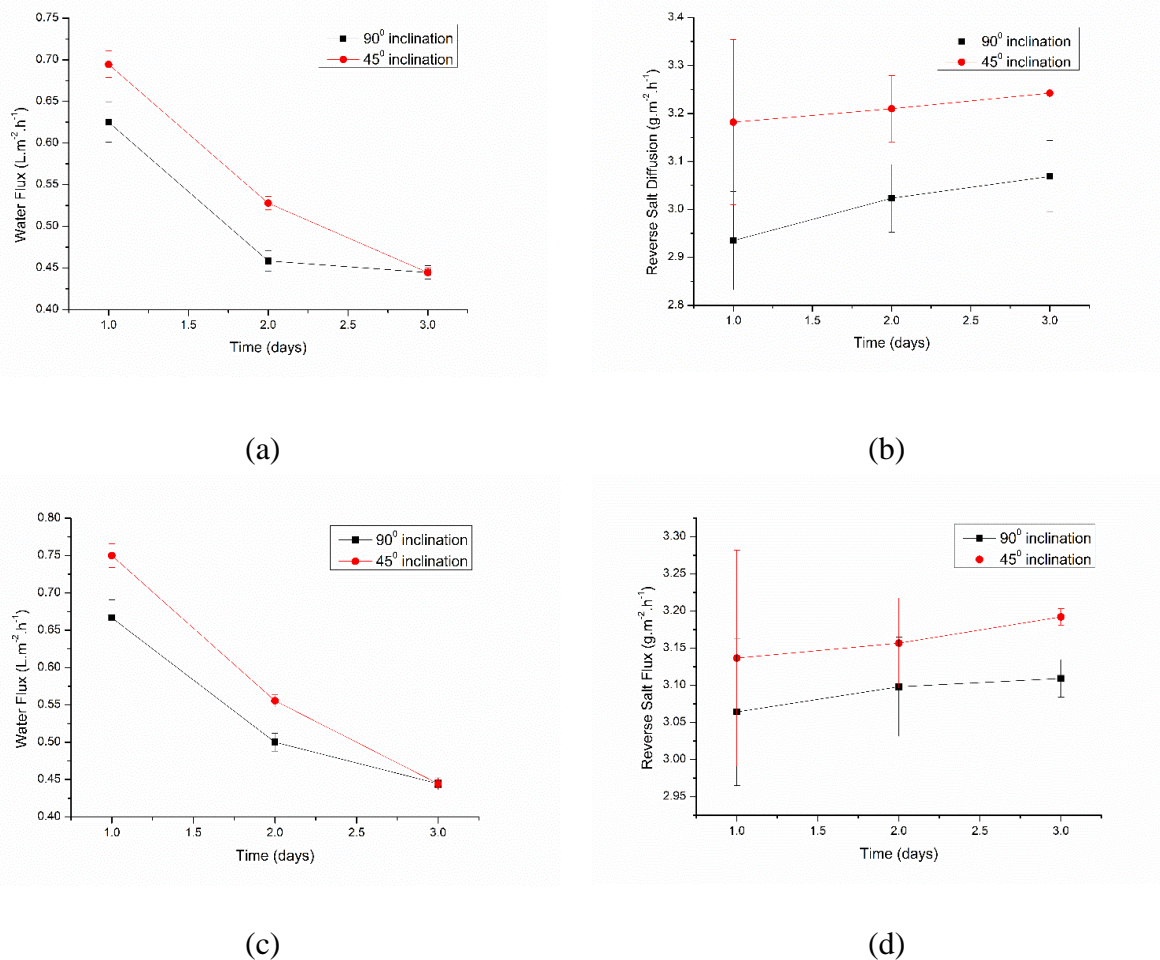
Figure 11. (a, b, c, d) Difference in WF and RSF of OMFC (WOS: a and b) and (WS: c and d) respectively

## 6. Scanning Electron Microscopy of Membrane surface

After operating the OMFC for more than 45 days in between backwash was given to the FO membrane to reduce fouling for better performance. The FO membrane was removed to analyze fouling as shown in Figure 12. The scanning electron microscopy (SEM) image shows the fouling of the FO membrane on the active side of the FO membrane. The fouling of the membrane is the

major challenge while applying the FO membrane in wastewater treatment. Our results give an idea about biofouling which occurred due to microorganisms and organic/inorganic compounds in synthetic wastewater, which can adversely affect the performance of the membrane (Mondal and De, 2009). The fouling is more in MI45 than MI90 because of inclination more solids in wastewater were stuck to the membrane surface so the water flux is declined and reverse salt flux is inclined as shown in Fig. 11 (a, b, c, d). The fouling can be more serious on the anode of an OMFC due to the anaerobic condition and no gas bubbling. (Ge and He, 2012).

The membrane-based process is becoming an attractive alternative to conventional separation processes. The decline of permeate flux is the major issue in the membrane separation which can occur due to the adsorption of solute components inside the pores causing pore blocking and accumulation of solute components on the membrane surface (known as concentration polarization). There are three types of pore-blocking (1) complete, (2) intermediate, and (3) partial. Each of these fouling mechanisms affects flux decline which is dependent on various factors such as the nature of solute, operating conditions, membrane material pore size, and the size distribution of solutes, etc. (Mondal and De, 2009).
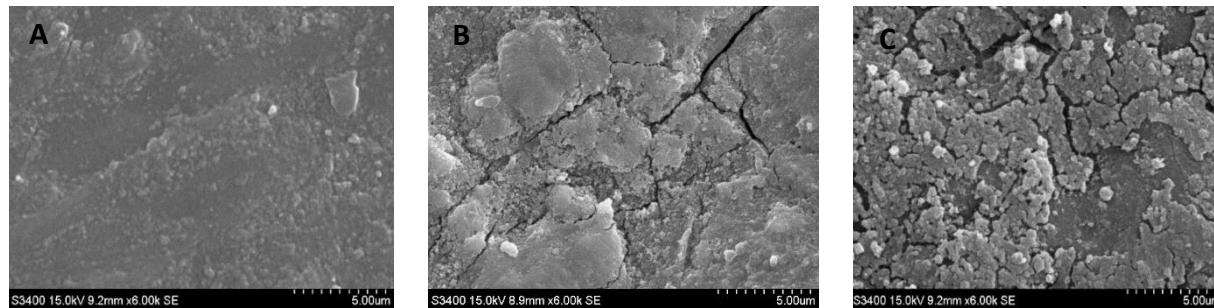


Figure 12. Scanning electron microscopy of forward osmosis membrane-active surface (A for raw membrane, B for MI90, and C for MI45)

## 7. Conclusion

The most important part of OMFC is bacteria which plays an important role in the performance of the overall system. This study investigates that using sound wave stimulation, bacteria accelerates degradation rate which ultimately affects the performance of OMFC. Degradation of organic matter with the corresponding release of energy leads to the growth of bacteria with respect to time. The OMFC produced maximum water flux, reverse salt flux and power density of $0.750 \pm 0.02$ $Lm^{-2}h^{-1}$, $3.18 \pm 0.02$ $gm^{-2}h^{-1}$, $35.22 \pm 12$ $mW.m^{-2}$ for MI45 with WS system. We obtained maximum current up to 1.5 mA and 1.4 mA (WOS), 2.8 mA, and 2.5 mA (WS) at MI 45˚ and 90˚ respectively. Therefore, OMFC was able to achieve coulombic efficiency up to $4.49 \pm 0.1\%$ and $5.52 \pm 0.1\%$ (WOS) and $8.81 \pm 0.1\%$ and $8.46 \pm 0.1\%$ (WS) at MI 45˚ and 90˚ respectively using acetate as a substrate. The understanding of vibration effect and inclination of membrane on the performance of OMFC was observed through this study.

## References

1. Ackerman, E., 1951. Resonances of biological cells at audible frequencies. Bull. Math. Biophys. 13, 93–94. https://doi.org/10.1007/BF02478356
2. Al-mamun, A., Said, M., Ranjan, B., Kim, I.S., 2017. Improved recovery of bioenergy and osmotic water in an osmotic microbial fuel cell using micro-diffuser assisted marine aerobic

biofilm on cathode. Biochem. Eng. J. 128, 235–242. https://doi.org/10.1016/j.bej.2017.09.020

3. Angenent, L.T., Sung, S., 2001. Development of anaerobic migrating blanket reactor ( ambr ), a novel anaerobic treatment system. Wat. Res. 35, 1739–1747. https://doi.org/https://doi.org/10.1016/S0043-1354(00)00447-4

4. Apodaca, G., 2002. Modulation of membrane traffic by mechanical stimuli. Am. J. Physiol. - Ren. Physiol. 282. https://doi.org/10.1152/ajprenal.2002.282.2.f179

5. Awad, A.M., Jalab, R., Minier-Matar, J., Adham, S., Nasser, M.S., Judd, S.J., 2019. The status of forward osmosis technology implementation. Desalination 461, 10–21. https://doi.org/10.1016/j.desal.2019.03.013

6. Berridge, M.J., Lipp, P., Bootman, M.D., 2000. The versatility and universality of calcium signalling. Nat. Rev. Mol. Cell Biol. 1, 11–21. https://doi.org/10.1038/35036035

7. Bochu, W., Hucheng, Z., Yiyao, L., Yi, J., Sakanishi, A., 2001. The effects of alternative stress on the cell membrane deformability of chrysanthemum callus cells. Colloids Surfaces B Biointerfaces 20, 321–325. https://doi.org/https://doi.org/10.1016/S0927-7765(00)00181-8

8. Bruce Alberts, Alexander Johnson, Julian Lewis, Martin Raff, Keith Roberts, and P.W., 2002. Molecular biology of the cell. Garland Science, New York.

9. Cath, T.Y., Childress, A.E., Elimelech, M., 2006. Forward osmosis: Principles, applications, and recent developments. J. Memb. Sci. 281, 70–87. https://doi.org/10.1016/j.memsci.2006.05.048

10. Cho, J., Ying, L., 2009. Experimental Investigation on the Effects of Audible Sound to the Growth of Escherichia coli. Mod. Appl. Sci. 3, 124–127. https://doi.org/10.5539/mas.v3n3p124

11. Ge, Z., He, Z., 2012. Effects of draw solutions and membrane conditions on electricity generation and water flux in osmotic microbial fuel cells. Bioresour. Technol. 109, 70–76. https://doi.org/10.1016/j.biortech.2012.01.044

12. Ge, Z., Li, J., Xiao, L., Tong, Y., He, Z., 2014. Recovery of Electrical Energy in Microbial Fuel Cells. https://doi.org/10.1021/ez4000324

13. Ge, Z., Ping, Q., Xiao, L., He, Z., 2013. Reducing ef fl uent discharge and recovering bioenergy in an osmotic microbial fuel cell treating domestic wastewater. DES 312, 52–59. https://doi.org/10.1016/j.desal.2012.08.036

14. Hancock, N.T., Cath, T.Y., 2009. Solute coupled diffusion in osmotically driven membrane processes. Environ. Sci. Technol. 43, 6769–6775. https://doi.org/10.1021/es901132x

15. He, Z., Angenent, L.T., 2009. Application of Bacterial Biocathodes in Microbial Fuel Cells. Electroanalysis 18, 2009–2015. https://doi.org/10.1002/elan.200603628

16. Hughes, D.E., 2009. The Bacterial Cytoplasmic Membrane. J. gen. Microbiol. 29, 39–46. https://doi.org/10.1099/00221287-29-1-39

17. Juergensmeyer, E.A., 2004. Effect of vibration on bacterial growth and antibiotic resistance. University in Elgin, Illinois.

18. Leys, N., Nuclear, B., Boever, P. De, Baatout, S., Nuclear, B., Mergeay, M., Nuclear, B., 2004. Space flight effects on bacterial physiology. J. Biol. Regul. Homeost. Agents. https://doi.org/https://doi.org/pubmed/15471227

19. Liu, H., Cheng, S., 2005. Production of Electricity from Acetate or Butyrate Using a Single-Chamber Microbial Fuel Cell. Environ. Sci. Technol. 39, 658–662. https://doi.org/10.1021/es048927c

20. Logan, B.E., 2007. Microbial Fuel Cells. John Wiley & Sons, Inc., New Jersey.

21. López, M., Santos, V., Javier, F., Valadéz, R., Solís, V.M., Nava, C.G., Jacob, A., Martell, C.,

Hensel, O., 2017. Performance of a microbial fuel cell operated with vinasses using different cod concentrations. Rev. Int. Contam. Ambie 33, 521–528. https://doi.org/10.20937/RICA.2017.33.03.14

22. Maria A. D. M., Giovanna S., Rechard A. K., G.D.T. and A.L., 1993. Receptor and protein kinase C-mediated regulation of ARF binding to the Golgi complex. Nature 363, 210–211.

23. McCrady, M.H., 2008. Standard methods for the examination of water and waste-water (12th ed.), American Journal of Public Health and the Nations Health. Washington DC. https://doi.org/10.2105/ajph.56.4.684-a

24. Mondal, S., De, S., 2009. Generalized criteria for identification of fouling mechanism under steady state membrane filtration. J. Memb. Sci. 344, 6–13. https://doi.org/10.1016/j.memsci.2009.08.015

25. Morris, C.E., Homann, U., 2001. Cell surface area regulation and membrane tension. J. Membr. Biol. 179, 79–102. https://doi.org/10.1007/s002320010040

26. Pardeshi P. and Mungray A., 2014. High Flux Layer by Layer Polyelectrolyte FO Membrane : Toward Enhanced Performance for Osmotic Microbial Fuel C. Int. J. Polym. Mater. Polym. Biomater. 37–41. https://doi.org/10.1080/00914037.2013.854232

27. Qin, M., Hynes, E.A., Abu-reesh, I.M., He, Z., 2017. Ammonium removal from synthetic wastewater promoted by current generation and water fl ux in an osmotic microbial fuel cell. J. Clean. Prod. 149, 856–862. https://doi.org/10.1016/j.jclepro.2017.02.169

28. Rahimnejad, M., Adhami, A., Darvari, S., Zirepour, A., Oh, S.E., 2015. Microbial fuel cell as new technol ogy for bioelectricity generation: A review. Alexandria Eng. J. https://doi.org/10.1016/j.aej.2015.03.031

29. Rautenbach, R., Albrezht, R., Wiley, J., 1994. Uk (1989,. Membr. Process. 236–237. https://doi.org/https://doi.org/10.1002/apj.5500030310

30. Sadoshima, J., Izumo, S., 1997. The cellular and molecular response of cardiac myocytes to mechanical stress. Annu. Rev. Physiol. 59, 551–571. https://doi.org/10.1146/annurev.physiol.59.1.551

31. Shaobin, G., Wu, Y., Li, K., Li, S., Ma, S., Wang, Q., Wang, R., 2010. A pilot study of the effect of audible sound on the growth of Escherichia coli. Colloids Surfaces B Biointerfaces 78, 367–371. https://doi.org/10.1016/j.colsurfb.2010.02.028

32. Slate, A.J., Whitehead, K.A., Brownson, D.A.C., Banks, C.E., 2019. Microbial fuel cells: An overview of current technology. Renew. Sustain. Energy Rev. 101, 60–81. https://doi.org/10.1016/j.rser.2018.09.044

33. Sun, G., Thygesen, A., Meyer, A.S., 2015. Acetate is a superior substrate for microbial fuel cell initiation preceding bioethanol effluent utilization. Appl Microbiol Biotechnol 99, 4905–4915. https://doi.org/10.1007/s00253-015-6513-5

34. Thakur, B.K., De, S., 2012. A novel method for spinning hollow fiber membrane and its application for treatment of turbid water. Sep. Purif. Technol. 93, 67–74. https://doi.org/10.1016/j.seppur.2012.03.032

35. Wang, B., Zhao, H., Wang, X., Duan, C., Wang, D., Sakanishi, A., 2002. Influence of sound stimulation on plasma membrane H + -ATPase activity. Colloids Surfaces B Biointerfaces 25, 183–188. https://doi.org/https://doi.org/10.1016/S0927-7765(01)00320-4

36. Wang, N., Butler, J.P., Ingber, D.E., 1993. Mechanotransduction across the cell surface and through the cytoskeleton. Science. 260, 1124–1127. https://doi.org/10.1126/science.7684161

37. Wang, Z., Wu, S., He, Z., 2019. Science of the Total Environment Production of electricity and water in an osmotic microbial fuel cell by using EDTA-Na 2 as a recoverable draw solute.

Sci. Total Environ. 677, 382–389. https://doi.org/10.1016/j.scitotenv.2019.04.319

38. Yang, E., Chae, K., Babatunde, A., Kim, K., Kim, I.S., 2016. Concurrent performance improvement and biofouling mitigation in osmotic microbial fuel cells using a silver nanoparticle-polydopamine coated forward osmosis membrane. J. Memb. Sci. 513, 217–225. https://doi.org/10.1016/j.memsci.2016.04.028

39. Yang, Y., Qin, M., Yang, X., He, Z., 2017. Sustainable Operation of Osmotic Microbial Fuel Cells through Effective Reproduction of Polyelectrolyte Draw Solutes Facilitated by Cathodic pH Increase. J. Clean. Prod. https://doi.org/10.1016/j.jclepro.2017.09.107

40. Yi, J., Bochu, W., Xiujuan, W., Daohong, W., Chuanren, D., 2003. Effect of sound wa v e on the metabolism of chrysanthemum roots. Colloids Surfaces B Biointerfaces 29, 115–118. https://doi.org/https://doi.org/10.1016/S0927-7765(02)00155-8

41. Zhu, X., Zhang, F., Li, W., Li, J., Li, L., Yu, H., Huang, M., Huang, T., 2015. Insights into enhanced current generation of an osmotic microbial fuel cell under membrane fouling condition Xian-Zheng. J. Memb. Sci. https://doi.org/10.1016/j.memsci.2015.12.050

# Application of Ionic Liquids as Draw Solute in Natural Osmosis

*Harshkumar Panchal [1]\*, Supritam Dutta[2]*

[1]Department of Chemical Engineering, L.J Institute of Engineering and Technology, Ahmedabad- 382210, Gujarat, India

[2]Department of Chemical Engineering, L.D Collage of Engineering, Ahmedabad- 380015, Gujarat, India

\*Corresponding author: hp28298@yahoo.com, mobile number: +91-7405504215

## Abstract

Water is one of the prime and principal solvent in industry and it is essential requirement for all living being on the planet Earth. At present, reverse osmosis is being extensively used for the water refinement, however It is believed that Natural osmosis being low energy technology can replace it. Natural osmosis is inchoate membrane technologies in which, concentration difference of solute in feed solution and draw solution, induce difference in osmotic potential, which is the driving force for the entire operation. Water is transferred from higher solute concentration to lower solute concentration via a specially design membrane. Main components to natural osmosis process are the draw solution (DS) and the membrane as both play a substantial role in performance of system. Hence, the selection of an appropriate DS is vital for process efficiency. This research work is focused on the preparation of deep eutectic solvents (DES) (i.e. Choline chloride and Glycerol) and to check its suitability as draw solution in natural osmosis. Sequence of experiments are conducted on laboratory scale set up for different concentration, temperature, flow rate and membrane orientation. The performance of selected DES was assessed in terms of water flux and reverse draw solute flux. 14.98486 lit/(m$^2$*hr) of water flux was obtained with 20% concentrated DES solution, this result indicate that DES can generate high osmotic potential and it can be implemented as Draw solute. Further to this, recovery of Choline chloride and Glycerol by thermal separation is also investigated in this study.

## Keywords

Water treatment, Desalination, Forward osmosis, membrane technology, Deep eutectic solvent, Waste water treatment.

## Abbreviations

DES: Deep Eutectic solvent
IL: Ionic liquid
FO: Natural osmosis
RO: Reverse osmosis
FS: Feed solution
DS: Draw solution
DI water: deionized water
LMH: $Lm^{-2}\,h^{-1}$
GMH: $gm^{-2}\,h^{-1}$
RSF: Reverse solute flux
CTA: Cellulose tri acetate

## 1. Introduction

One of the foremost significant challenges of this century is in meeting the increasing freshwater demand for drinkable supplies, food production and different industrial must support the large population growth [1]. In the field of water treatment, reverse osmosis is generally a more familiar process than Natural osmosis. RO uses hydraulic pressure to oppose, and exceed, the osmotic pressure of an aqueous feed solution to produce purified water [2]. Both the RO and natural osmosis processes use a semi-permeable membrane to separate water from dissolved solutes effectively, although their driving forces are different. In RO, the applied pressure is the driving force for mass transport through the membrane. While in the natural osmosis process osmotic pressure itself is the driving force for mass transport of solute form one side of semi-permeable membrane to the other side of it. Fig. 1 explains the fundamentals of the natural osmotic processes and revers osmosis process
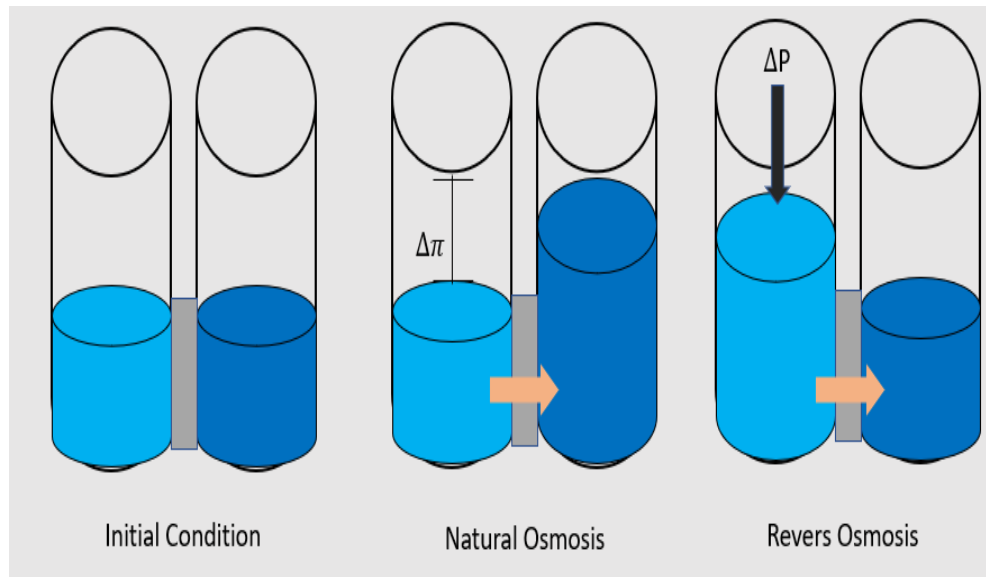


Figure 1. Principles of osmotic Processes

Although the performance of RO desalination plants now consumes significantly lower energy than the other desalination over several decades ago, the energy required for purification still remains high due to the thermodynamic limit of the membrane desalination processes. Therefore, in order to comply with water, energy and environmental issues, a wastewater technology that consumes much lower energy is essential. Natural osmosis (FO), despite being old in its concept, has spurred a renewed interest, both academically and commercially in last two decades [3]. Being natural, clean and eco-friendly process, natural osmosis has remarkable potential in substituting or complementing many conventional separation systems.

In a Natural osmosis process, a semipermeable membrane is positioned in between two solutions of different concentrations more precisely of different osmotic pressure a concentrated solution known as draw solution and a dilute solution known as feed solution. The concentration difference between the two solutions generates the required osmotic potential which provides the driving

force to attract fresh water from a feed solution on the other side of the membrane. As a result, the process can concentrate a solution of lower osmotic pressure with that of a higher osmotic pressure. The DS becomes diluted and loses its osmotic pressure gradually. In order to reuse the DS, the draw solutes must be separated and recycled back to the FO unit using a suitable post treatment process (Fig. 2).
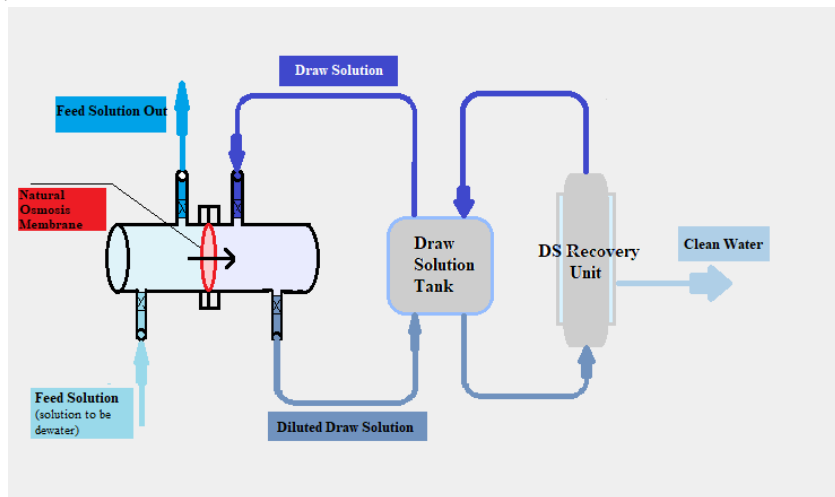


Figure 2. General schematic outline of a natural osmosis process

The purity of the water thus generated depends on the separation efficiency of the post treatment process which is essential yet energy consuming. Therefore, the selection of draw solute is of paramount importance for the success of FO process. An ideal draw solution should be able to generate high osmotic pressure and consequently high-water flux. Also, it should be easily recoverable using minimum energy. However, these two requirements are contradictory as high osmotic potential needs strong affinity between the draw solute and water molecules which subsequently renders recovery process difficult [4]. Besides, the DS should be endowed with other attributes such as high solubility, minimal toxicity, non-reactivity and wider availability at low cost. Another important aspect which determines the selection of draw solute is reverse solute flux (RSF) in which draw solute migrates from DS side to FS side through the membrane. Occurrence of RSF not only diminishes the driving force [5] but also contaminates the FS (e.g., dewatering of pharmaceuticals, proteins, fruit juice etc.). RSF results in the loss of precious draw solute which needs replenishment and can cause severe membrane fouling [6]. Hence, finding draw solutes which can facilitate water flux but mitigate RSF is decisive for the success of FO.

Numerous inorganic compounds have been reported and explored in membrane literature as potential candidates for draw solutions [4,7]. Nonetheless, many of these compounds have exhibited a high reverse draw solute flux or are expensive to recycle, leave aside their toxic potency at times. Therefore, the search for a compatible and efficient draw solution assumes paramount importance in view of the wider industrial acceptance of forward osmosis [8].

Ionic liquids (IL) and deep eutectic solvents (DES) are lately touted as green solvents to be used in a variety of separation processes [9]. These are a few of the latest class of draw solutes which has caught researchers' attention. The wide array of choice of hydrogen bond donor makes easier to develop DESs with required properties. The same characteristics and properties which make ILs

attractive for industrial application are also shared by DESs. DESs exhibit negligible vapor pressure, high ionic conductivity, high solubility, nonflammability, bio-degradability, chemical and thermal stability making them highly acceptable as solvents, (Table 1).

Table 1 DES used in natural osmosis

| Process | Membranes | Draw solute (DES) | DS Recovery | Water flux rates $(Lm^{-2}\,h^{-1})$ | Ref. |
|---|---|---|---|---|---|
| Desalination of brackish water | TFC Polyamide | Ch-Cl-EG (1:2) | Chilling | 7.85 | 9,10 |
| Dewatering of DNA & Conc. Of protein | TFC Polyamide | Ch-Cl-EG (1:2) | Chilling | 3.10 | 9,10 |
| Desalination (0.6M NaCl) | CTA, HTI Inc | Glycol ethers | Heating | 0.62 | 11 |
| Desalination (0.6–1.6M NaCl) | TFC Polyamide | P$^{4444}$ DMBS (70%wt) | Heating | 4.0 | 4 |

In this research work DES of Choline chloride – glycerol (Ch-Cl-glycerol) has been attempted as potential draw solutes. It has shown to possess high osmotic potential and can be easily recovered rendering better energy efficiency of the overall process. it is also economically competitive and environmentally benign. Although there are quite a good number of reviews on various aspects of Natural Osmosis in recent literature, encompassing membrane development, area specific applications, selection of draw solutions and few more, applicability of IL and DES, in particular, as draw solution have not been surveyed so far.

This paper focuses on is focused on the preparation of deep eutectic solvents (DES) (i.e., Choline chloride and Glycerol) and to check its suitability as draw solution in natural osmosis. Sequence of experiments are conducted on laboratory scale set up for different concentration, temperature, flow rate and membrane orientation.  synthesis and recovery of draw solutes and economic aspects are adequately reviewed in the following sections.

## 2.  Materials and methods

### 2.1 Chemicals

Laboratory grade (LR), Choline Chloride 98% EP (Cas - 67-48-1) manufactured by Loba was purchased from M/s Lab-Chem corporation, Ahmedabad were used as received without further purification as a Hydrogen bond acceptor and LR grade Glycerol from M/s SD Fine was use as a hydrogen bond donor. Stock solutions of deionized (DI) water with negligible dissolved solid content was purchased of M/s Merck. 0.25M NaCl solution was simulated as brackish water and 0.6M NaCl solution was simulated as sea water for experimentation purpose.

## 2.2 Preparation of DES

To produce Deep Eutectic Solvents, one hydrogen Bond Donor and Hydrogen Bond Acceptor are stirred for a specific time at appropriate Temperature until transparent liquid is being formed. This can be done by three methods [12].

Method 1: Hydrogen bond donor is Bring to the temperature of DES formation and Then after appropriate temperature, Hydrogen Bond acceptor is added. Then, the mixture is stirred.

Method 2: Hydrogen bond Acceptor is Bring to the temperature of DES formation and Then after appropriate temperature, Hydrogen Bond Donor is added. Then, the mixture is stirred.

Method 3: Both Hydrogen Bond Donor and Hydrogen Bond Acceptor are mixed at normal temperature and then sudden heating and stirring are applied for the time required to get Transparent Liquid.

All the three methods were tried, sudden heating method was found successful. Initially liquid Glycerol was heated to normal temperature and after that powder of Choline Chloride was slowly added to it. This initial mixture was wax kind of solution, which is transferred to three neck round bottom flask for further heating. To maintain the temperature of 80°C the flask was put on heating mental with vertical condenser to provide total reflux. Continuous stirring was also provided for two hours. After it the mixture took the transformation to homogenous transparent liquid form.



Figure 3. Choline Chloride- Glycerol DES

## 2.3 Membrane

An indigenously developed membrane was prepared by CSIR Hyderabad and was used as received. This membrane was produced by the addition of excess m-phenylenediamine along with a small quantity of dipolar dimethyl sulfoxide solvent in the aqueous reaction bath [12].

A support layer for the membrane was synthesized by adding Polyethersulfone powder into a solution containing dimethyl formamide (DMF) and propionic acid; the obtained homogenous solution was cast onto a polyester fabric support and immersed in a water bath to get an ultra-porous PES support layer.

For the synthesis of Hydrophilized active layer interfacial polymerization technique was used. The synthesized Polyethersulfone support layer was immersed in an aqueous bath containing of m-phenylenediamine (MPD) and dimethyl sulfoxide (DMSO) was added to enhance hydrophilicity. After that, the membrane was dried in the open atmosphere and in an oven at 60–70°C to obtain the hydrophilized TFC polyamide membrane. More detaile is explain in by S Sridhar et al. [12] about the manufacturing of the hydrophilized TFC polyamide membrane in there research work.

## 2.4 Experimental setup

The experiments were conducted on a bench-scale laboratory system as shown in Fig. Two mild-steel flanged, sandwiching membrane and gaskets served as central unit for this natural osmosis experimentation. The module has 13.19 cm$^2$ of active membrane surface area (4.1 cm diameter. Both pipes were bolted together tightly to prevent any leakage of mixing. Each pipe carries two opening for inlet and outlet respectively. Two valves were inserted in inlet flow stream to keep flow rate within the range. Installation of submersible pump of requisite capacity in both the containers allowed for the circulation of Feed solution and Draw solution in both the chambers. All experiments were performed in AL-FS orientation (FO mode) and Flow rate of 14 L min$^{-1}$ was maintained on both sides unless otherwise mentioned. As we know, as the natural osmosis occurs, water moves from the feed side to draw side. To measure this reduction precision balance of 0.1 gm accuracy was used as shown in fig.4. All the experiments were performed for 4 h continuous run. A fresh membrane piece was used for experiment each time after soaking for 30 min in DI water. The decrease in weight of FS was measured at a regular interval of 10 min. The change in weight of FS is converted to volume and then the value is divided by the membrane area and time duration to calculate the water flux as shown in (Eq. (1))

$J_w = w_i - w_f / \rho A_m t$ ....... (1)

where $J_w$ is the water flux, wi is the initial weight of the FS, wf is the final weight of the FS, $\rho$ is the density of the FS, Am is the membrane area and t is the time of operation.
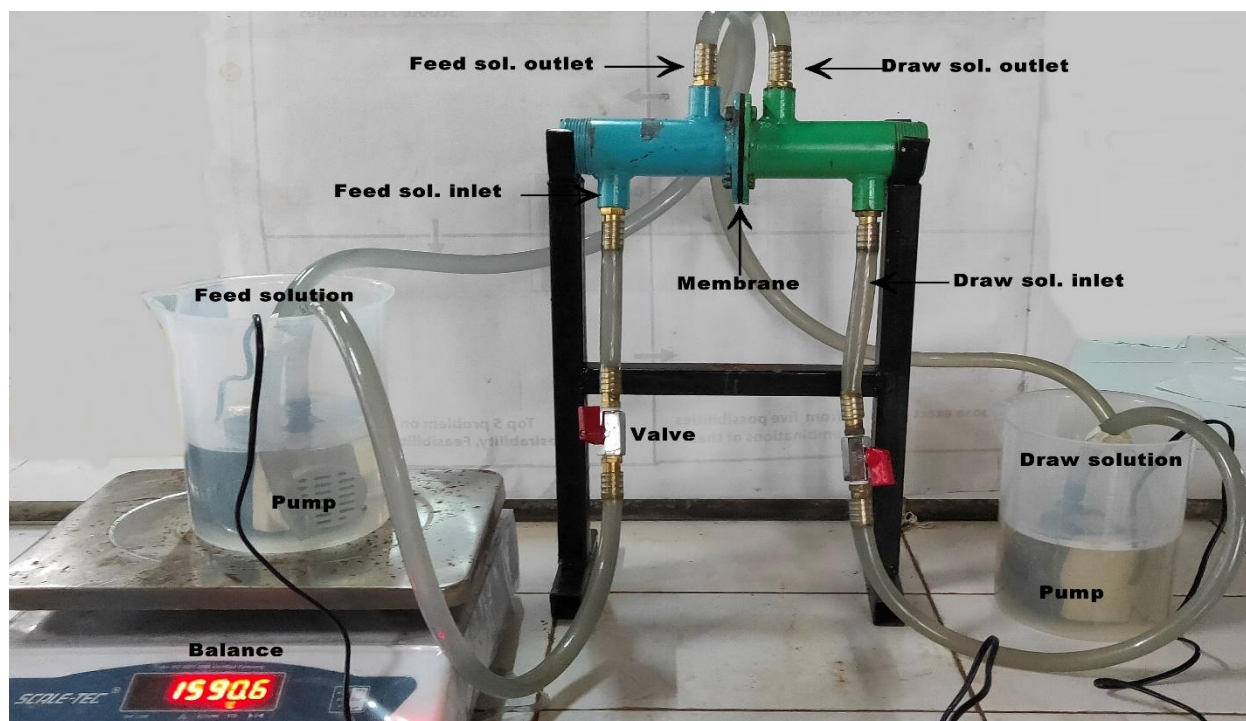
Figure 4. Experimental setup

## 2.5 Experimental Procedure:

Before installation in set-up, membrane was soaked in distilled water for about 30 minutes. After that membrane was load between two flanges as shown in eperimental setup. DES of Choline Chloride and Glycerol was diluted by adding measure quantity of distilled water to make draw solution of 20%, 22.5%, 255, 28.5% by weight. DI water was used as feed solution. Before starting the experiment temperature and conductivity of FS and DS was noted down. Pumps and piping network was arranged to circulate streams of DS and FS. Switch-on the pump and allow the operation to stabilize. Once the stability is attained, note down the reduction in weight of feed solution. This setup of natural osmosis was run for 4 hours for every experiments and reduction in weight was note down on interval of 10 minutes. At the end of 4 hour sample of feed solution and draw solution was taken out for the analysis.

## 3. Results and Discussion

### 3.1 Effect of Concentration on Water Flux in Natural Osmosis

The mass transfer has ruled that with the higher concentration of the solution, the mass transfer gradient will become high. This is also true in natural osmosis. So, the higher the concentration, the higher the flux rate [13]. This should be natural behavior of draw solute too. Draw solution should give a higher flux rate with high concentration.

To verify this, four solutions of different concentration Ch-Cl-Glycerol DES was prepared with DI water. Having concentration 20%, 22.5%, 25%, 28.5%. This experiment was done on the natural osmosis membrane. After the experiment, it was observed that water flux deacreses with increase in the concentration, this is mainly due to the increment in viscocity of draw solution with

concentration. For natural osmosis membrane, at 20%, 22.5%, 25%, 28.5% concentration of DES, identified flux rate of 14.98486 L/ (m$^2$×hr), 13.98587 L/ (m$^2$×hr), 13.0041 L/ (m$^2$×hr), 12.52183 L/ (m$^2$×hr) was obtained respectively.

Initially a standard salt solution was taken for reference data collation, for this purpose four different salt solution of concentration 0.25N, 0.5N, 0.5N and 1N was prepared and flux with this standard salt solution was compared with DES flux.
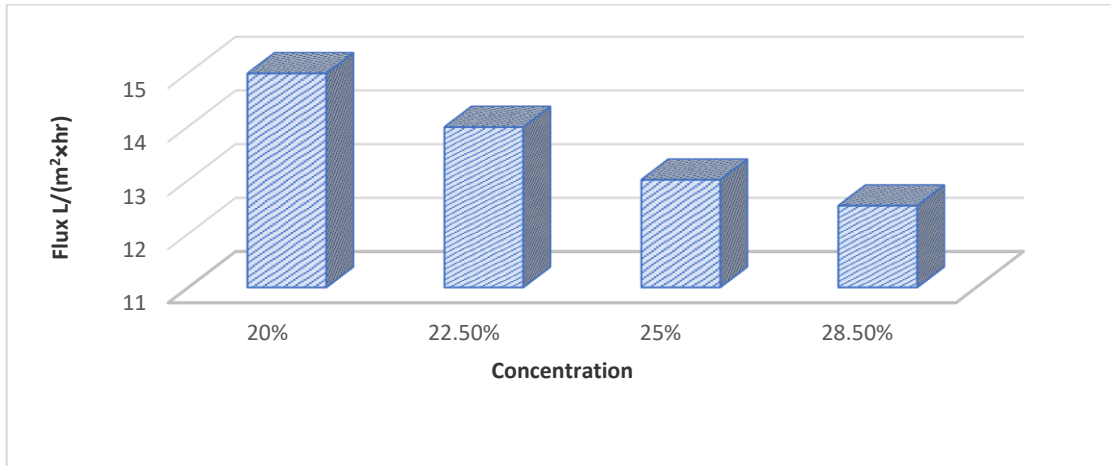
Figure 5. Plot of Concentration vs Flux (DES)
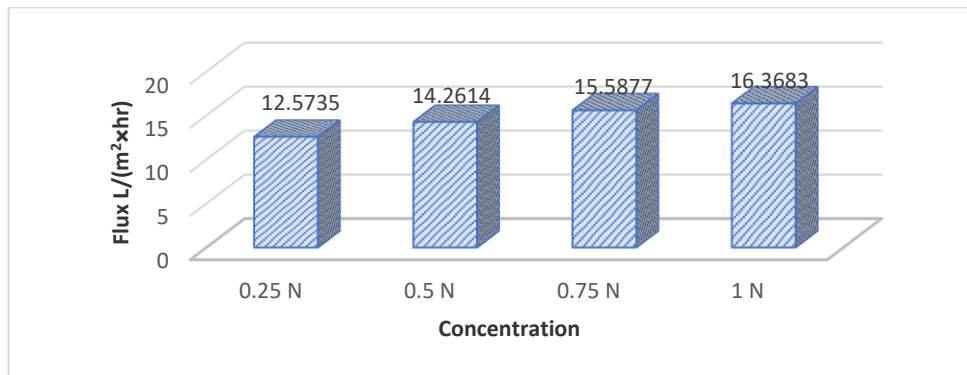
Figure 6. Plot of Concentration vs Flux (NaCl)

## 3.2 Effect of Variation on Temperature on Natural Osmosis:

For this experiment, 20% of concentration of DES Ch-Cl-Glycerol was taken as a fixed solution for all the experiments. Experiments was carried out at four different temperature of draw solution 20°C, 30°C, 40°C and 50°C with the help of hot plate at bottom. And flux was calculated as per the standard procedure. It is clear from the data below that for natural osmosis membrane, with an increase in the temperature, Flux rate also increases.

For DS temperature, at 20°C, 30°C, 40°C and 50°C flux rates after 4 hr of practical 14.98486 L/ (m$^2$×hr), 16.19054 L/ (m$^2$×hr) 16.89672 L/ (m$^2$×hr) and 19.15306 L/ (m$^2$×hr) was found which is in successive order.
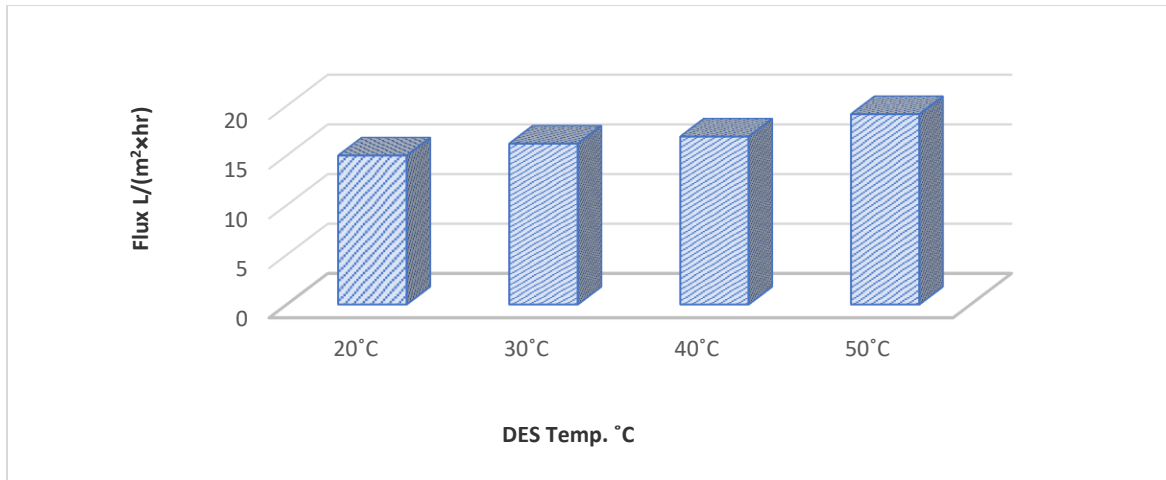
Figure 7. Effect of Temperature on flux rate for natural osmosis membrane

## 3.3 Effect of Orientation Change on Natural Osmosis:

The membrane has two sides; one is Active layer and one is the support layer. By a combination of these two layers, one membrane can be made. Based on this, there are two kinds of orientation available. One is an active layer-feed solution (AL-FS) in which the active layer of material will come into the contact with Feed solution whereas the support layer will come in to contact with Draw solution. The other orientation is called Active Layer-Draw solution (AL-DS) in which the active layer of the membrane will come in to contact with Draw solution whereas the support layer will come in to contact with feed solution. Now, it is observed in the kinds of literature that by altering the side of the membrane, the flux rate can become different. Here, 20% concentrated Ch-Cl Glycerol DES was taken as Draw solute and then checked the performance of it with both orientation, AL-DS & AL-FS for natural osmosis membrane. The result verifies the ability of DES as draw solute as it gives a higher flux rate for AL-FS side then AL-DS. For natural osmosis membrane, average flux rate after 4 hr of experiments in AL-FS & AL-DS is 14.98486 L/ (m$^2$×hr) and 9.662651 v respectively. This shows AL-FS gives higher flux rate than AL-DS.
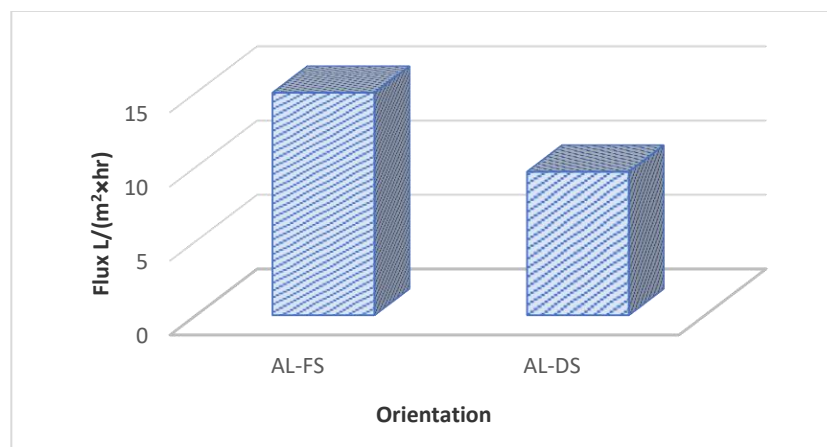


Figure 8. Effect of Membrane orientation on Flux rate for FO membrane

## 3.4 Effect of Flow Rate on Water Flux in Natural Osmosis:

For this experiment, 20% of concentration of DES Ch-Cl-Glycerol was taken as a fixed solution. After then this, flow rate of 0.1369 lit/sec, 0.05720 lit/sec, 0.01785 lit/sec and 0.01225 lit/sec were set with help of the valve at inlet section of system. It is clear from the data below that for natural osmosis membrane, with an increase in the flow rate, Flux rate also increases. For Flow rate, at 0.1369 lit/sec, 0.05720 lit/sec, 0.01785 lit/sec and 0.01225 lit/sec flux rates after 4 hr of practical 14.98486 L/ (m$^2$×hr),13.8136 L/ (m$^2$×hr), 12.78019 L/ (m$^2$×hr) and 10.57552 L/ (m$^2$×hr) was found which is in successive order.
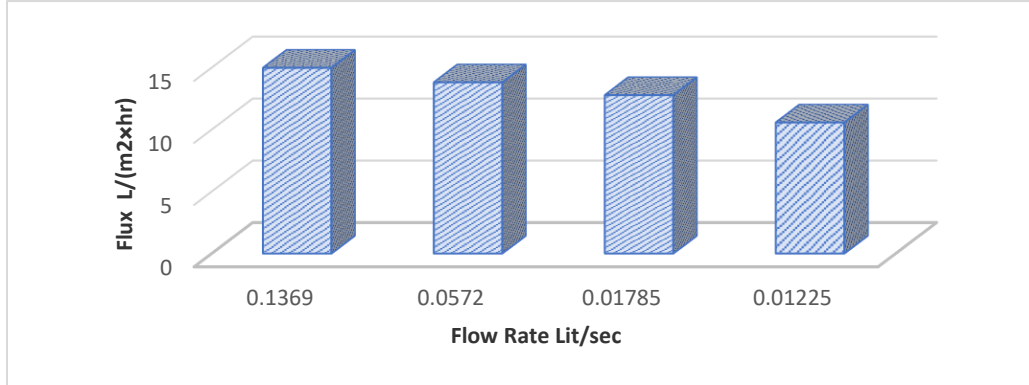


Figure 9. Effect of Flow Rate on Water Flux in Natural osmosis

## 3.5 Draw solute recovery by chilling:

In the present work, we attempt to demonstrate the use of DESs, choline chloride glycerol (ChCl-Gly 1:2) as efficient and recyclable energy resource in natural osmosis process. Choline Chloride-Glycerol DES has the freezing point of -40°C [14]. As this DES has this much lower freezing point, then if the temperature decrease blow -10°C the DES solution will be separated in two layers. One will have water in form of ice where as other part will be pure DES. This how, by creating the temperature difference, the recovery of DES can be done. The separated ice will have the water migrated from the feed solution. This how water can be utilized form the feed solution. In order to check recovery of DES from water, a mixture of 50 ml of DES and water was prepared in lab. In proportion of 10% DES and 90% water and other mixture of 20% DES and 80% water. This two-mixture ware kept in the ice chiller for overnight at -23˚C and clear separation of DES and water (in the form of ice) was observed.
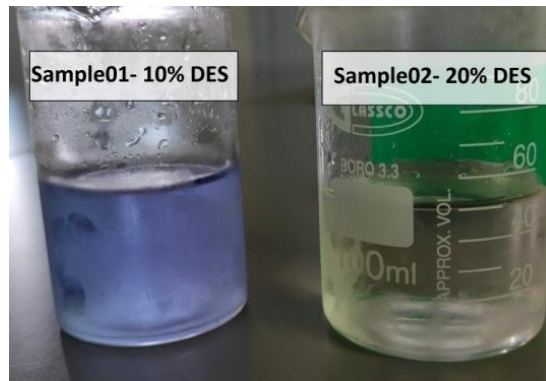


Figure 10. Initial DES Solution
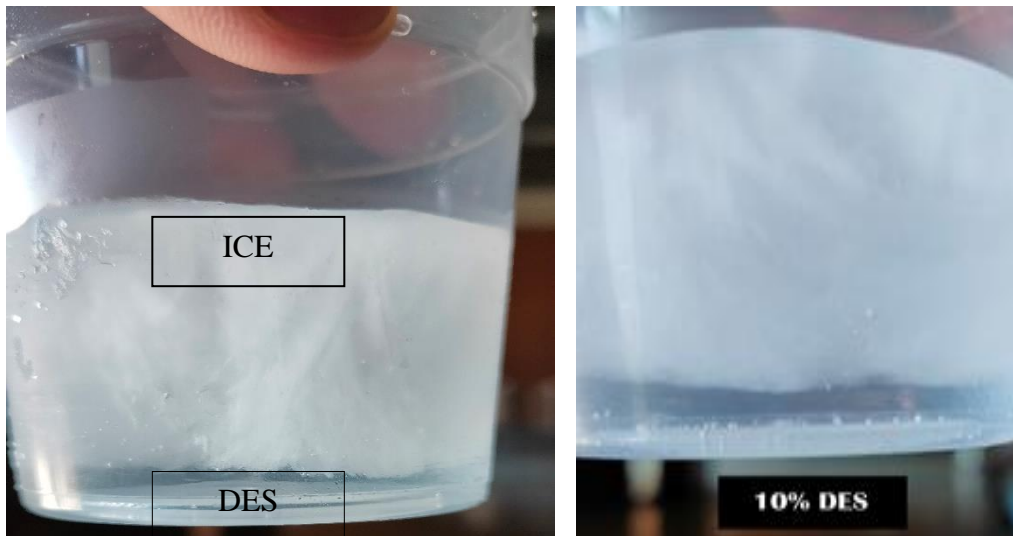
Figure 11. final DES Solution

## 4. Conclusions

The performance of Choline Chloride- Glycerol DES as DS in natural osmosis process using a natural osmosis membrane was evaluated. Choline Chloride- Glycerol DES is inexpensive and easily manufactured along with other favourable advantages like high solubility, minimal toxicity, non-reactivity, high osmotic potential and further to this high-water flux with very low RSF was found in all cases making it suitable for draw solute. The water flux was observed to decrease with increase in Choline Chloride- Glycerol DES concentration this is because as the concentration of DES increases the viscosity of the draw solution also increases and that lead to decrement in the osmotic pressure and ultimately pure water flux. Water flux of 14.98486 L/ (m$^2$×hr), 13.98587 L/ (m$^2$×hr) 13.0041 L/ (m$^2$×hr) and 12.52183 L/ (m$^2$×hr) were obtained using 20%, 22.5%, 25% and 28.5% DES concentration respectively as draw solution. The water flux was observed to increase with Choline Chloride- Glycerol DES temperature because as the temperature of DES increases the diffusivity of molecules also increases. Water flux of 14.98486 L/ (m$^2$×hr), 16.19054 L/ (m$^2$×hr), 16.89672 L/ (m$^2$×hr) and 19.15306 L/ (m$^2$×hr) were obtained with 20 °C, 30°C, 40°C and 50°C temperature of draw solution respectively. It also observes that water flux increases as the flow rate of DS increases. Water flux of 10.57552 L/ (m$^2$×hr), 12.78019 L/ (m$^2$×hr) 12.78019 L/ (m$^2$×hr) and 14.98486 L/ (m$^2$×hr) were obtained with flow rate of 0.01225 lit/sec, 0.01785 lit/sec, 0.05720 lit/sec and 0.136920 lit/sec respectively. Choline Chloride- Glycerol DES was successfully recovered by thermal separation in form of chilling at -20°C. After chilling the water was separated out from DS in the form of the ice.

## Acknowledgements

**References**

1. F. A. Ward and M. Pulido-Velazquez, "Water conservation in irrigation can increase water use," *Proc. Natl. Acad. Sci. U. S. A.*, vol. 105, no. 47, pp. 18215–18220, 2008, doi: 10.1073/pnas.0805554105.
2. J. A. Schufle, "Reverse Osmosis(Sourirajan, S.)," *J. Chem. Educ.*, vol. 48, no. 9, p. A565, 1971, doi: 10.1021/ed048pa565.
3. S. Dutta and K. Nath, "Prospect of ionic liquids and deep eutectic solvents as new generation draw solution in forward osmosis process," *J. Water Process Eng.*, vol. 21, no. August 2017, pp. 163–176, 2018, doi: 10.1016/j.jwpe.2017.12.012.
4. Y. Cai and X. M. Hu, "A critical review on draw solutes development for forward osmosis," *Desalination*, vol. 391, pp. 16–29, 2016, doi: 10.1016/j.desal.2016.03.021.
5. K. Lutchmiah, A. R. D. Verliefde, K. Roest, L. C. Rietveld, and E. R. Cornelissen, "Forward osmosis for application in wastewater treatment: A review," *Water Res.*, vol. 58, no. December 2015, pp. 179–197, 2014, doi: 10.1016/j.watres.2014.03.045.
6. S. Lee, C. Boo, M. Elimelech, S. Hong, "Comparison of fouling behavior in forward osmosis (FO) and reverse osmosis (RO), J. Membr. Sci. 365 (2010) 34–39, doi.org/10.1016/j.memsci.2010.08.036.
7. L. Chekli, S. Phuntsho, H. K. Shon, S. Vigneswaran, J. Kandasamy, and A. Chanan, "A review of draw solutes in forward osmosis process and their use in modern applications," *Desalin. Water Treat.*, vol. 43, no. 1–3, pp. 167–184, 2012, doi: 10.1080/19443994.2012.672168.
8. C. Bhattacharjee, V. K. Saxena, and S. Dutta, "Fruit juice processing using membrane technology: A review," *Innovative Food Science and Emerging Technologies*. 2017, doi: 10.1016/j.ifset.2017.08.002.
9. D. Mondal, A. Mahto, P. Veerababu, J. Bhatt, K. Prasad, and S. K. Nataraj, "Deep eutectic solvents as a new class of draw agent to enrich low abundance DNA and proteins using forward osmosis," *RSC Adv.*, 2015, doi: 10.1039/c5ra20735e.
10. S.K. Alamaru, K. Prasad, D. Mondal, J. Polisetti, A. Mahto, Dewatering Process Through Forward Osmosis Using Deep Eutectic Solvents with or Without Dispersed Magnetic Nanoparticles as Novel Draw Solutions, (2016).
11. D. Nakayama, Y. Mok, M. Noh, J. Park, S. Kang, Y. Lee, Lower critical solution temperature (LCST) phase separation of glycol ethers for forward osmotic control, Phys. Chem. Chem. Phys. 16 (2014) 5319.
12. M. Madhumala, S. Moulik, T. Sankarshana, and S. Sridhar, "Forward-osmosis-aided concentration of fructose sugar through hydrophilized polyamide membrane: Molecular modeling and economic estimation," *J. Appl. Polym. Sci.*, 2017, doi: 10.1002/app.44649.
13. A. P. Abbott, G. Capper, D. L. Davies, R. K. Rasheed, and V. Tambyrajah, "Novel solvent properties of choline chloride/urea mixtures," *Chem. Commun.*, 2003, doi: 10.1039/b210714g.
14. A. E. Lewis *et al.*, "Design of a Eutectic Freeze Crystallization process for multicomponent waste water stream," *Chem. Eng. Res. Des.*, 2010, doi: 10.1016/j.cherd.2010.01.023.

# Substrate optimization for generation of electricity from wastewater by using microbial fuel cell (MFC)

*Bibhabasu Mohanty[*1], Kunj Patel[1], Mitul Patel[1]*

[1]Department of Civil Engineering, Sal Institute of technology and engineering research, Gujarat Technological University, Ahmedabad-380060

* Corresponding author: bibhabasu.mohanty@gmail.com, mobile number: +91-7383789601

## Abstract

Development in developing countries, such as India, depends on the energy generation required for the industrial and agricultural sectors and the efficiency of their processes in terms of energy usage. In the ongoing energy crisis, it is now a major concern of researchers to search for alternative and renewable sources of energy for the future. Fuel cell systems have dual-purpose solutions for electricity generation and waste water disposal. A microbial fuel cell (MFC) is an innovative method to compete with three-dimensional fossil fuel-based energy production problems with high-cost and pollution-generating systems. It is an emerging technology for wastewater treatment which produces energy. It has the potential to use waste water as a feed substrate for microorganisms and to generate bio-electricity. In carbon capture, bioremediation, biosensing, bio-hydrogen production, and desalination, MFCs can also be used. In this research an attempt was made to increase the efficiency of generation of electricity from wastewater by using substrates like glucose, sodium acetate. Along with generation of electricity from wastewater there are also some impurities like TDS (50 %) and COD (65 %) are also reduced from wastewater.

**Key Words:** Microbial, Fuel cell, Energy production, Sustainable, Wastewater

## 1. Introduction

As our world population grows, the industry continues to need water. Water consumption has been increasing at an appreciable rate in the past century with the population growth. Because of an increase in water usage, produced wastewater and, therefore, the demand for treatment has gone up. New wastewater treatment technologies, therefore, currently consume 3% of the electricity produced in developed countries (Das S, Mangwani N. 2010). With population growth and the need to conserve water, it is imperative to find more economical and reliable methods of treating wastewater. To balance water and energy security, development of new technologies to offset the high cost of utility payments is necessary (Mathuriya A S, Yakhmi J. 2014).

Wastewater treatment plants (WWTPs) have been implemented by many firms and municipal governments to minimise hazardous wastewater pollution and improve water quality. Rhoads et al., 2005, pointed out that most WWTPs were built with faulty energy efficiency in mind, without proper consideration of water treatment requirements. However, WWTP efficiency is now becoming important as renewable water and energy sources, related carbon emissions, and urban development are becoming increasingly important.

The quest for sustainable energy has also led to increasing energy conservation, energy quality improvements, and the pursuit of renewable energy. Water treatment plants are a common water-energy interaction (Chandra I. 2012). All water treatment plants reduce water quality in exchange for significant energy input. Wastes are also regarded by municipal governments as the main big consumers of energy. A wide array of wastewater treatment process components, including the collection, transportation and discharge of waste, require significant energy. In a traditional wastewater treatment plant, energy consumption comprises

half or more of their operating costs. In addition, WWTPs are a source of greenhouse gas emissions that are causing global concern.

Microbial fuel cells have recently shown promise as an exciting new technology with a host of benefits. In an MFC, microorganisms communicate through the use of electrons supplied from an electrical circuit formed by electrodes. Bio-electrochemical systems (BESs) are the main types of BESs that use microorganisms to create electricity through metabolic activity (Rabaey K, Verstraete W. 2005). MFC is seen as a promising sustainable technology to meet increased energy demands, especially the ability to convert wastewater into electricity and at the same time treat wastewater.

MFC is a small reactor that produces electricity by the metabolic activity of microbes (anaerobic oxidation). MFCs have been shown to be effective at extracting bio-energy from wastewater and simultaneously cleaning wastewater by removing contaminants. This application has a basic MFC configuration with an anode in anodic chamber, a cathode in cathodic chamber. MFC operates on a theory in which organic substrates are oxidised by biocatalysts in the anodic chamber and electrons and protons are released, thereby generating $CO_2$ (Zhang et al. 2007 & Zhou et al. 2011).

The anode transfers electrons to the cathode creating electrostatic forces, while simultaneously moving protons from the anode chamber to the cathode. The electrons combine at the anode to form water and oxygen (Logan B E, Regan J M. 2006). Electricity can be produced from wastewater in an MFC, and the electricity can be used directly. The hydrogen and methane can be derived from anaerobic digestion processes that do not require further separation, purification, or other auxiliary processes. MFC technology is environmentally friendly as it is technologically feasible, produces zero pollution, and has no adverse environmental impact (Cheng S, Liu H, Logan B E. 2006). Despite MFC technology being able to effectively treat wastewater, it still faces challenges in bringing this technology out of the lab and into the marketplace (Aelterman 2006). A number of factors such as electrode material costs, the need for precious metals, low performance, low power density, and expensive PEMs limit MFC technology to direct application (Shrivastava S, Bundela H. 2013).

The purpose of this study is to test lab-scale pile models containing plastic beakers full of sludge and wastewater. A MFC was fitted with a cathodic and anodic chamber connecting graphite rod electrode and an ion-selective buffer salt bridge.

## 2. Materials and methods

### 2.1 Collection of samples and its characteristics

Sludge and wastewater collected from Pirana sewage treatment plant located in Ahmedabad, Gujarat, India. The wastewaters which are collected are composite in nature, collected at an interval of 3 hrs for a 24 hrs cycle. The sample collected in a closed air tight container to avoid any atmospheric interference. For collection of sludge the collected wastewater kept in a jar for 24 hrs without any disturbance. The settled sludge then transfers to the experimental set up for further experimentation. The physiochemical characteristics were initially characterized and reported. pH, Chemical Oxygen Demand (COD), Total Dissolved Solids (TDS) were measured with help of standard procedure.

## 2.2 Microbial fuel cells reactor and experimental setup

Microbial fuel cell is composed of 2 L anodic and cathodic container. Figure 1 and 2 displays the schematic and photographic image of the MFC set up. The electrode used is a rod composed of graphite. Copper wire is used to hang the graphite rod and is used as a linker between them to transfer the electrons emitted from anode to cathode. The salt bridge is designed using the 15 cm long, 3 cm diameter PVC pipe, 10 per cent agar is used inside the PVC pipe along with 1 M KCl which forms the salt bridge and helps move the electron from anode to cathode. The anode is attached to the multimeter, and the cathode and voltage are noted down. To calculate the voltage and current generated during the process the multimeter is connected to the anode and cathode.
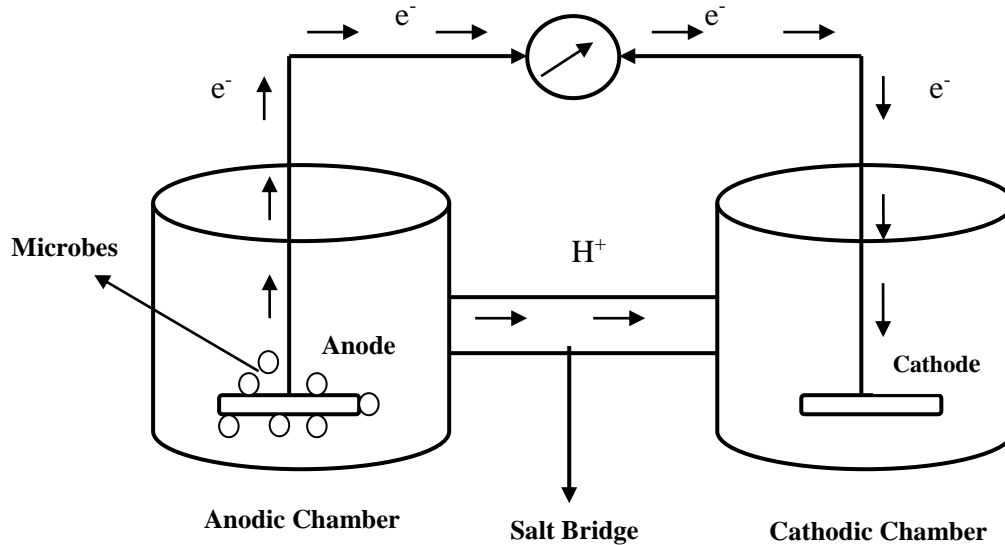


Figure 1. Schematic Diagram of Dual-Chamber Microbial Fuel Cell



Figure 2. Photographic picture of the experimental MFC set up

The experimental tests were carried out in two phases (phase I and phase II) using sludge and domestic wastewater. Microbial fuel cell worked with sludge in phase I and Microbial fuel cell operated with household wastewater in phase II. A microorganism that metabolizes the

organic matter typically found in the sludge and wastewater. 2 gm Sodium acetate and glucose was applied to 1 L of wastewater samples, used as food for microbes.

Parameters such as pH, Chemical Oxygen Demand (COD), Total Dissolved Solids (TDS) were analyzed before and after the manufactured microbial fuel cell model was operating during the experimental process. Eventually, voltage, current density and power density were calculated, compared and analyzed.

## 3. Results and Discussion

The experiment was conducted with salt water as in cathode and microbes in anode to degrade the organic matter in the first phase of experimental run using sludge substratum and second phase with domestic wastewater along with sodium acetate for the microorganism. With the aid of multimeter, the current and voltage produced by the MFC were noted down on a daily basis for about 17 days. The parameters such as voltage, power and current have been measured and the graph for detailed analysis are being plotted (Figure 3-8). Figure shows the microorganism's growth curve as the voltage rises during the exponential process then reaches a standing voltage phase and constant as the system enters the stationary period due to the nutrient depletion in the anodic chamber. After a cycle of 14 days it was observed that there is no further enhancement of production of voltage from sludge as well as from wastewater. This may be due to complete decomposition of organic matter present in sludge as well as in wastewater. So, it may be advisable that change of the feed materials i.e. sludge and wastewater after a cycle of 14 days. It was found that the average current and voltage from the sludge was 460 mA and 460 mV, and 640 mA and 640 mV for domestic wastewater. Compared with wastewater sludge generates less current, because it is difficult to degrade due to sludge nature.
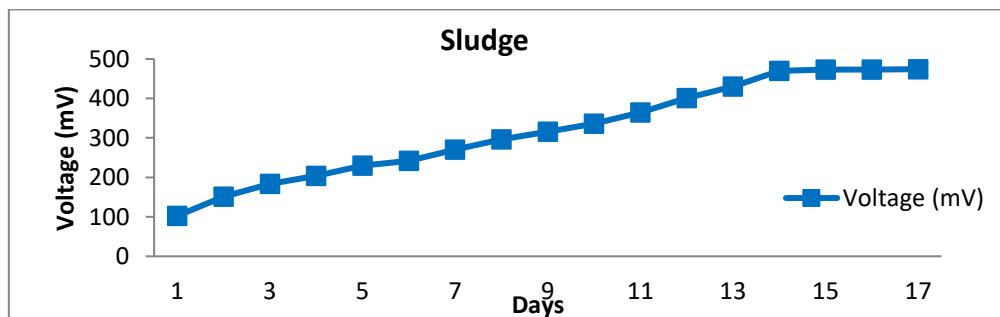


Figure 3. Production of Voltage from sludge with respect to time
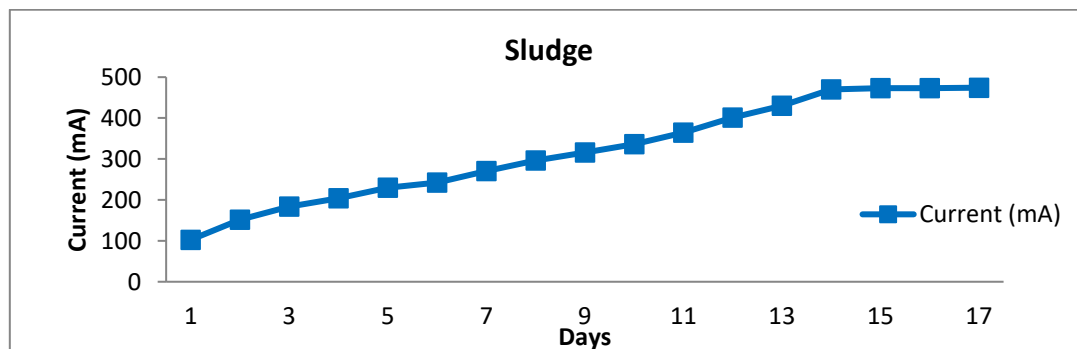


Figure 4. Production of Current from sludge with respect to time
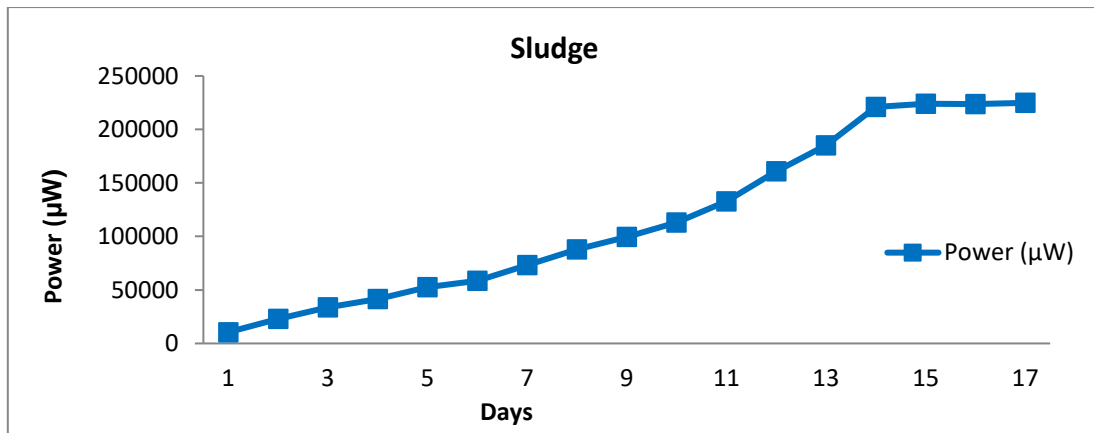
Figure 5. Production of Power from sludge with respect to time
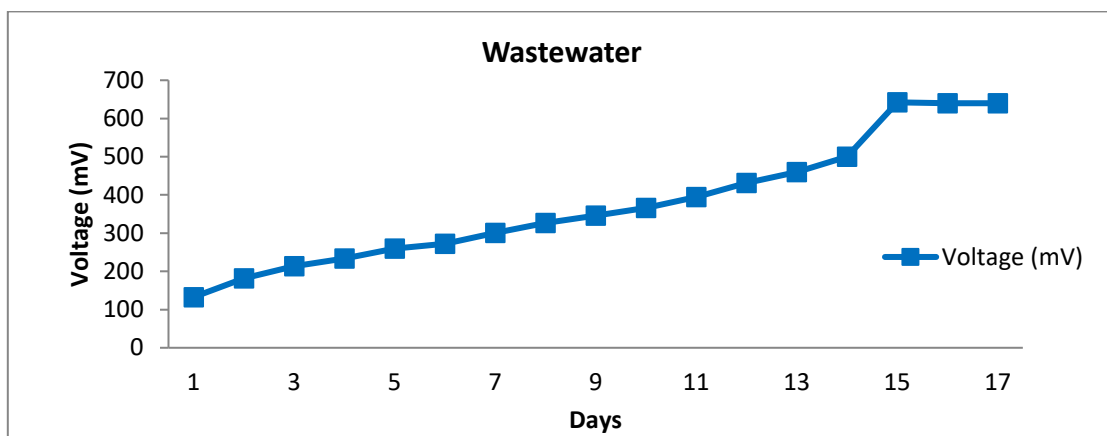


Figure 6. Production of Voltage from wastewater with respect to time
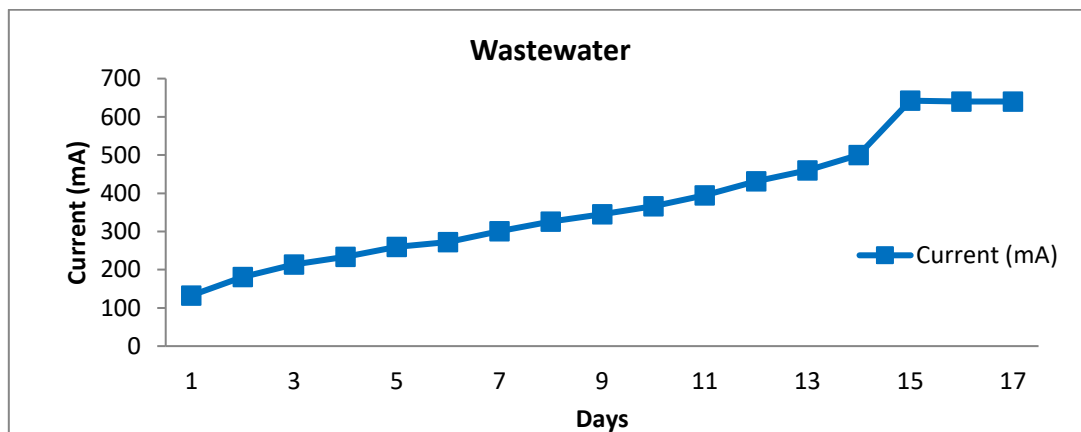


Figure 7. Production of Current from wastewater with respect to time
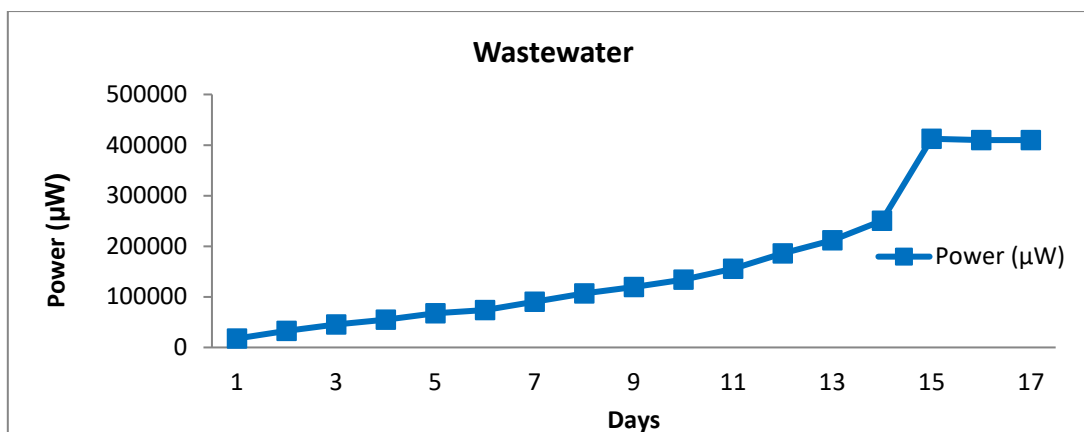
Figure 8. Production of Power from wastewater with respect to time

Physiochemical analysis: Initially, the domestic wastewater was analyzed for its physiochemical parameters, and then treated with manufactured microbial fuel cell (MFC). Table-1 demonstrates the physiochemical characteristics for household wastewater before and after treatment with MFC. The pH of untreated domestic wastewater was found to be 6.3 and the pH had risen to 7.4 after treatment which indicated that treatment of wastewater using MFC had modified the acidic nature of the effluent to a nearer neutral state. The total dissolved solids (TDS) were assessed in the effluent and 50 percent of the removal was observed. Certain parameters such as COD have also been measured and 65% of elimination has been found.

Table 1 Physiochemical characteristics of wastewater

| Parameters | Untreated wastewater | Treated wastewater |
|---|---|---|
| Colour | Greyish black | Greyish black |
| Odour | Foul | Foul |
| pH | 6.3 | 7.4 |
| COD (mg/L) | 900 | 580 |
| TDS (mg/L) | 840 | 425 |

## 4. Conclusion

Due to the capabilities of MFCs, they are attracting considerable attention from researchers globally. However, to achieve stable power production, there is a need for continued technological advancements. The microbiological organism and electrode are critical in determining the cost and efficiency of the MFC. Optimization of factors that increase a company's overall marketing application. Efforts must be made to use the most efficient microorganisms and noble electrodes to reduce the complexity of the rates limiting steps which yield higher current output. Most of the literature has recently focused on improving the efficiency of molten salt reactors by increasing peaking power. However, research and development of engineered MFC microorganisms is limited. It can be concluded that commercial application of MFC can be achieved through optimization of microorganism and new electrode design which will provide a promising alternative for cost-effective MFC electrical generation. Treatment experiments showed important reduction in COD and TDS, indicating successful treatment of domestic wastewater. This experiment demonstrated that the microorganism can efficiently remove the organic material present in the wastewater.

## References

1. Aelterman P, Rabaey K, Pham TH, Boon N, Verstraete W. 2006. Continuous electricity generation at high voltages and currents using stacked microbial fuel cells. Environ Sci Technol. 40(10):3388–3394.
2. American Public Health Association. 2005. Standard Methods for the Examination of Water and Wastewater. 19th edition. APHA, Washington, DC, USA.
3. Chandra I. 2012. Waste to energy: Microbial fuel cell a novel approach to generate bio-electricity. Int J adv Biotechnol Bioinf. 1:33-40.
4. Cheng S, Liu H, Logan B E. 2006. Increased performance of single-chamber microbial fuel cells using an improved cathode structure. Electrochem Commun. 8(3):489–494.
5. Das S, Mangwani N. 2010. Recent developments in Microbial fuel cells: A review. J Sci Indus Res. 69:727-31.
6. Logan B E, Regan J M. 2006. Electricity-producing bacterial communities in microbial fuel cells. Trends Microbiol. 14(12):512–518.
7. Mathuriya A S, Yakhmi J. 2014. Microbial fuel cells–Applications for generation of electrical power and beyond. Crit Rev Microbiol. 42:1-17.
8. Nair k, Renganathan K. Barathi S, et al. 2013. Performance of salt-bridge microbial fuel cell at various agarose concentrations using hostel sewage waste as substrate. Int J Adv Res Technol. 2:326-30.
9. Pham T H, Jang J K, Chang I S, Kim B H. 2004. Improvement of cathode reaction of a mediatorless microbial fuel cell. J Microbiol Biotechnol. 14 (2):324–329.
10. Rabaey K, Verstraete W. 2005. Microbial fuel cells: novel biotechnology for energy generation. Trends Biotechnol. 23(6):291–298.
11. Rhoads A, Beyenal H, Lewandowski Z. 2005. Microbial fuel cell using anaerobic respiration as an anodic reaction and biomineralized manganese as a cathodic reactant. Environ Sci Technol. 39(12):4666–4671.
12. Sharma Y, Li B. 2010. The variation of power generation with organic substrates in single-chamber microbial fuel cells (SCMFCs). Bioresour Technol. 101:1844–1850.
13. Shrivastava S, Bundela H. 2013. Power generation through double chamber MFC operation by slurry mixed with different substrates. Int J Eng Trends Technol. 4:4201-5.
14. Zhang T, Zeng Y, Chen S, Ai X, Yang H. 2007. Improved performances of *E. coli-*catalyzed microbial fuel cells with composite graphite/PTFE anodes. Electrochem Communs. 9(3):349–353.
15. Zhou M, Chi M, Luo J, He H, Jin T. 2011. An overview of electrode materials in microbial fuel cells. J Power Sources. 196(10):4427–4435.

# Evaluating performance of Ammonium Sulphate as Draw Solute in Fertilizer Driven Forward Osmosis for Wastewater treatment

*Rutvikkumar Bhatiya [1], Bhavsar Yash[1], Pandya Jatin[1], Patil Mitesh[1], Pankhaniya Kumbhan[1],*
*Panchal Harsh[1], Supritam Dutta[1]*

[1]Department of Chemical Engineering, L D College of Engineering, Ahmedabad.
*Corresponding author: rbhatiya194@gmail.com, mobile number: +91-8140779780

**Abstract:**

Forward osmosis (FO) is a novel and emerging low energy technology applied for the desalination of saline water and concentration of feed solution like wastewater, etc. FO process utilizes the osmotic pressure difference induced by the solute concentration difference between the feed and draw solution separated by a selectively permeable membrane. This work focus on performance of inorganic fertilizer such as ammonium sulphate as draw solution and its osmotic potential for drawing pure water from waste water by using a thin film composite (TFC) membranes. The diluted draw solutions can be used as a fertilizer solution and can be applied in drip irrigation (fertigation). Performance parameters like water flux, reverse permeation and a suitable draw solute recovery process is studied for possible industrial application.

## Keywords

Forward Osmosis, Draw solution, Irrigation, Membrane, Desalination, Waste Water, Fertilizer.

## Abbreviation

FO: Natural osmosis
RO: Reverse osmosis
FS: Feed solution
DS: Draw solution
DI Water: deionized water
RSF: Reverse solute flux
PES Membrane: Polyethersulphone Membrane

## 1. Introduction

Forward osmosis (FO) has emerged as a viable alternative to the traditional pressure-driven membrane processes with a possibility to consume lower energy in the domains of desalination and wastewater treatment. The osmotic driving force generated by means of concentrated draw solution and feed solution (FS) on either side of semi-permeable membrane eliminates the need of high-pressure pumps. The solute from diluted draw solution is recovered and recycled back to the FO process. Fertilizer-drawn forward osmosis (FDFO) process uses concentrated fertilizer solution as draw solute (DS) for drawing freshwater from sea-water and other impaired feed water. The dilute fertilizer solution thus generated can be used for fertigation, thereby eliminating the need of energy-intensive recovery process. Several fertilizers have been tested for their potential as DS in FDFO process. Inorganic fertilizers such as Urea, Ammonium Sulphate, Ammonium Chloride, Di-ammonium phosphate and Potassium Nitrate [1, 2]; blend of various fertilizers [3]; and liquid fertilizers [7] have been used as DS for desalination. FDFO can draw water from other impaired water sources [4, 5]. Practically the dilute draw solution generated needs further dilution to decrease the concentration level required for fertigation purposes. Different methods have been demonstrated for adjusting the final nutrient concentration of dilute draw solution such as microfiltration, nano-filtration and Pressure-Retarded Osmosis. Here in ammonium sulphate is checked for their suitability as DS. The

fertilizer is shortlisted based on their low cost, ease of availability and other essential properties required for FO. Ammonium Sulphate is widely used as it contains 21% nitrogen and 24% sulphur which is one of the most important micronutrient and also low cost around Rs. 300 per kg in India. Ammonium Sulphate has good osmotic potential of 92.1 atm.

Most of the commercial FO membranes produced by international water solution providers are proprietary and not easily available in an open market. Hence, the membranes which are openly available and inexpensive require study for their suitability in FO application. Based on their performance, the membranes may be used as it is or can be structurally modified to enhance their performance. In this work, a locally available, low-cost, commercial, low-pressure nanofiltration (NF) membrane of thin-film composite (TFC) [6] type is used without modification. The FO system was checked for dewatering/concentration of dye waste water. The present work aims to demonstrate the ability of low-cost integrated FDFO system using locally available membranes and ammonium sulphate as fertilizer as draw solute to generate good quality water from wastewater feed for direct application in fertigation techniques such as drip irrigation and hydroponics.

## 2. Material and method

## 2.1 FO Experimental

A laboratory-scale flat sheet membrane FO test cell providing 0.00145 $m^2$ active area was fabricated (Fig. 1). All the experiments were performed in batch mode for 4 h at 300($\pm$1) K with FO mode membrane orientation, i.e., active layer facing FS and support layer facing draw solution (AL-FS mode). The feed and draw solutions were circulated using submersible centrifugal pumps. The water transfer was measured by recording the weight of FS tank using a digital weighing balance at 10-min interval. The water flux, Jw, was measured as follows:
$J_w = (W_f - W_i)/ (\rho A_m t)$ ...... (1)
Where $W_i$ and $W_f$ are the initial and final weight of FS, respectively, $\rho$ is the density of FS, $A_m$ is the membrane area and t is the time of operation.
Reverse Solute Flux:   $J_s = \Delta (C_t * V_t)/ (A_m * \Delta t)$ ...... (2)
Where $C_t$ & $V_t$ are the DS concentration and volume of FS, respectively, at any time t.
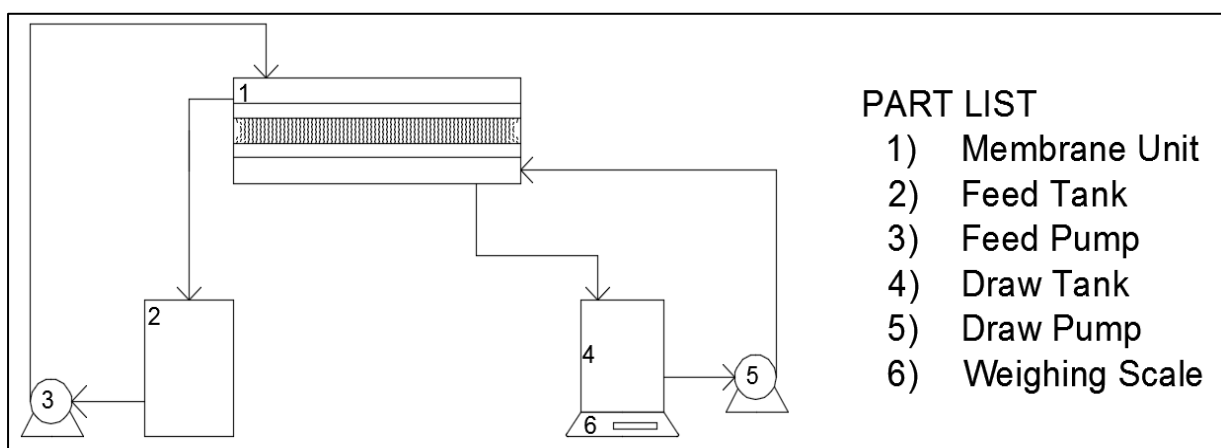


Figure 1. Schematic Representation of Experimental Setup

## 2.2 Membrane

The membrane used is a non-polyamide, cross linked PES membrane which is stable in mineral acid like Hydrochloric acid, Sulphuric acid and Phosphoric acid. Moreover, these are chlorine sanitizable therefore are ideal for food and beverage applications. It has ability to pass chlorides without much resistance coupled with high divalent salt rejection makes it an excellent membrane for separation of heavy metals and acids.

Table 1 Membrane Specification

| Type | MWCO (Delton) | % Solute rejection | | | | | Typical application |
| | | 2000 ppm $MgSO_4$ | 500 ppm NaCl | 1% PEG | 1000 ppm $Al^{3+}$ | 5% Lactose | |
| --- | --- | --- | --- | --- | --- | --- | --- |
| HFN 300 | 300-400 | Min | 40 | >95% | >75% | >96% | Color removal, spent brine Purification, whey dewashing, acid, alkali and metal recovery |
| | | 95% | 45% | | | | |

## 2.3 Chemical Specification

Table 2 Draw solute (Ammonium Sulphate) properties

| Chemical formula | $(NH_4)_2SO_4$ |
| --- | --- |
| Molecular weight | 132.1 g/mol. |
| Maximum solubility | 5.7 M (77 g/100 mL@25°C) |
| Melting point | 235 C |
| Density | 1.760 g/cm$^3$ |
| pH at 2 M | 5.46 |
| Π at 1 M (atm.) | 46.14 |
| Π at 2 M (atm.) | 92.1 |
| Π at max solubility (atm.) | 274.8 |
| Species formed in 2.0 M solution at 25°C and 1.0 atm. Pressure | $NH_4^+$: 3.07 M, $SO_4^{2-}$: 1.07 M, $NH_4SO_4^-$: 0.93 M |

Waste water contains 5 ml of dye (Ujala Fabric whitener) in 1250 ml water.

## 3. Result and Discussion

## 3.1 Water Flux

The performance of $(NH_4)_2SO_4$ as DS is checked using deionized (DI) water as feed solution and flux is compared with NaCl as a standard. As shown in Fig. 2., flux of ammonium sulfate solution as a draw solution is coming higher in comparison with sodium chloride as a draw solution.
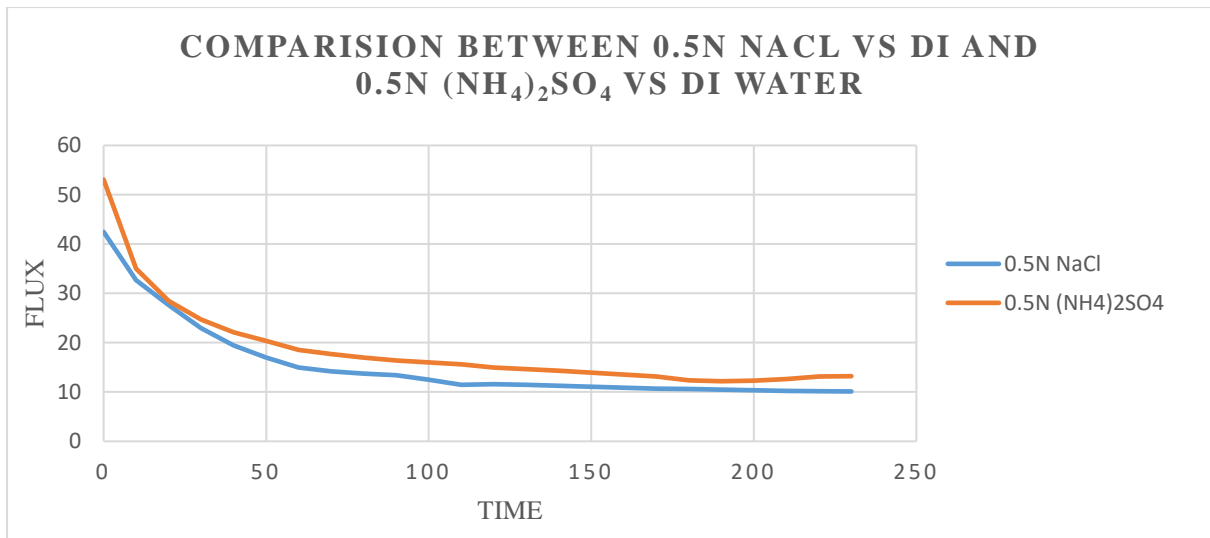
Figure 2. Comparison between 0.5N NaCl vs DI and 0.5N $(NH_4)_2SO_4$ VS DI Water

The graph below shows comparison between 0.5 N Ammonium Sulfate as a draw solution vs. DI water and 0.5 N $(NH_4)_2SO_4$ as a draw solution vs. dye waste water. Fig. 3. clearly shows that flux for $(NH_4)_2SO_4$ Vs. Dye waste water is coming higher in comparison with $(NH_4)_2SO_4$ Vs. DI water.
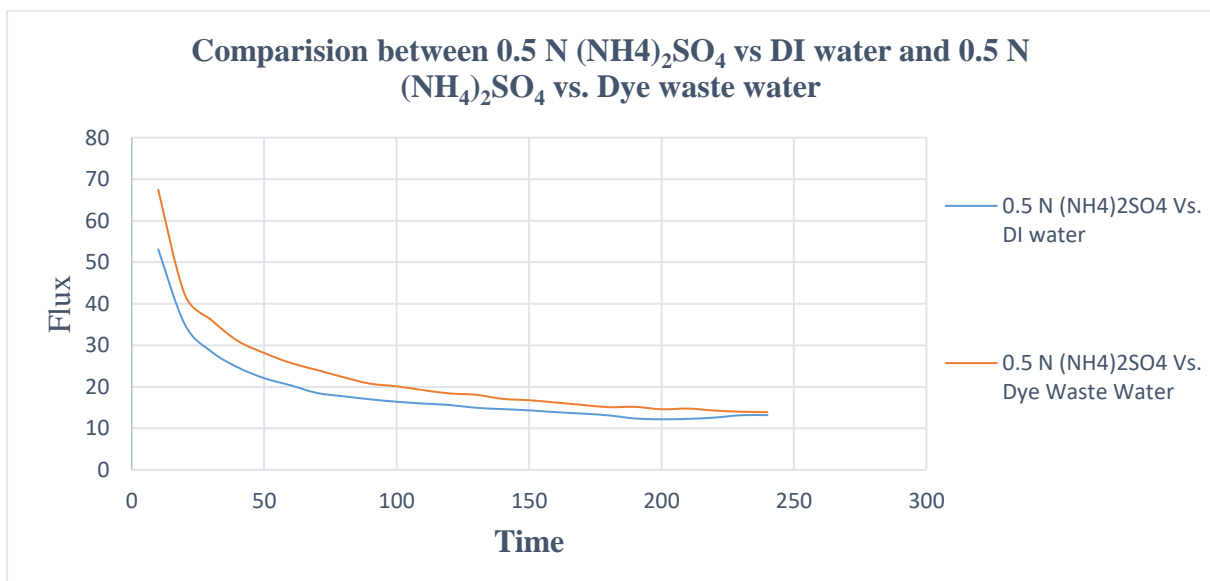


Figure 3. Comparison between 0.5 N $(NH_4)_2SO_4$ vs DI water and 0.5 N $(NH_4)_2SO_4$ vs. Dye waste water

## 4. Conclusion

The performance of Ammonium Sulphate [$(NH_4)_2SO_4$] fertilizer as draw solute in FO process using low pressure membrane was evaluated and results of which were compared with NaCl draw solution as a standard. The water flux in case of ammonium sulfate was higher than NaCl for DI feed solution. In case of dye wastewater feed solution, the water flux was little higher compared to DI water feed. When dye wastewater was used, the clear diluted draw solution at the end of FO process was obtained which showed that the membrane used can reject feed solutes effectively.

## Acknowledgement

## Reference

1. Achilli, Andrea, Tzahi Y. Cath, and Amy E. Childress. "Selection of inorganic-based draw solutions for forward osmosis applications." *Journal of membrane science* 364.1-2 (2010): 233-241.
2. Chekli, Laura, et al. "A review of draw solutes in forward osmosis process and their use in modern applications." *Desalination and Water Treatment* 43.1-3 (2012): 167-184.
3. Kim, Youngjin, et al. "Evaluation of fertilizer-drawn forward osmosis for coal seam gas reverse osmosis brine treatment and sustainable agricultural reuse." *Journal of Membrane Science* 537 (2017): 22-31.
4. Phuntsho, Sherub, et al. "A novel low energy fertilizer driven forward osmosis desalination for direct fertigation: evaluating the performance of fertilizer draw solutions." *Journal of Membrane Science* 375.1-2 (2011): 172-181.
5. Phuntsho, Sherub, et al. "Blended fertilizers as draw solutions for fertilizer-drawn forward osmosis desalination." *Environmental science & technology* 46.8 (2012): 4567-4575.
6. Nasr, Peter, and Hani Sewilam. "Investigating the performance of ammonium sulphate draw solution in fertilizer drawn forward osmosis process." *Clean Technologies and Environmental Policy* 18.3 (2016): 717-727.
7. Zou, Shiqiang, and Zhen He. "Enhancing wastewater reuse by forward osmosis with self-diluted commercial fertilizers as draw solutes." *Water research* 99 (2016): 235-243.

# Co-pyrolysis based activated bio-char assisted pulp and paper industry biologically treated waste water for removal of COD and colour

D.V. Kapatel[a], Y.C. Rotliwala[b*]

[a]Chemical Engineering Department, G H Patel College of Engineering &Technology, Gujarat Technological University, Vallabh Vidyanagar, 388120, India
[b]Chemical Engineering Department, Pacific School of Engineering, Gujarat Technological University, Surat 394305, India
*Corresponding author: yrotliwala@yahoo.com, +91 9998628041

**Abstract:**

This work addresses the preparation of activated bio-char through chemical activation method using phosphoric acid (activating agent) onthe residue obtained from co-pyrolysis of municipal sewage sludge (MSS)-sugarcane bagasse (SCB) and to determine the potential of this activated bio-char for the removal of COD and colourin biologically treated wastewater (after secondary treatment) from pulp and paper industry operating in Gujarat state, India.With the optimum dose of activated bio-char, resulting treated waste water imparted COD and colour in the range of 57-61 mg/L and 0.41-0.52 Pt-Co, respectively. Such characteristic of treated waste water was observed suitable for recycling at pulp and paper process itself. Brunauer-Emmett-Teller (BET) surface area, total pore volume and average pore diameter were 1.549 $m^2$/g, 0.0053 $cm^3$/g and 1.68 nm, respectively. Also, various functional groups on the activated bio-char were determined from the FTIR results.The Freundlinchand Langmuirisotherm model was found best to describe the obtained equilibrium adsorption data at 30 °C.

**Keywords:**Co-pyrolysis, Activated char, Paper industry effluent, Adsorption.

## 1.Introduction:

Wastewater from pulp and paper industry characterizes as toxic due to huge contamination such as chlorinated compound, fatty acid, tannin, resin acid, phenols and its derivatives, lignin and its derivatives, sulfur and sulphur compounds (Garg, 2007; Ali andSreekrishnan, 2001). The presence of lignin and its derivatives contribute to strong colourand COD in most pulp and paper waste water (Dilek and Gokcay, 1994). These represents high total organic carbon (TOC), chemical oxygen demand (COD), colour, AOX(Adsorbable organic halides), and low biodegradability index (<0.4) (Pokhrel andViraraghavan, 2004). Moreover, pulp and paper industry consumes enormous quantity of fresh water, i.e. 60-230 $m^3$ per ton of paper production, resulting to the generation of massive quantity of waste water (Büyükkamaci andKoken, 2010). It is the sixth largest polluter (after oil, cement, leather, textile and steel industries), discharging a diversified of wastes into the environment (Savant et al., 2006). In India, most modern and efficient operational technique for pulp and paper industry reported fresh water consumption to the tune of 60 $m^3$, leading to waste water generation of 50 $m^3$ per ton of paper production (Thompson et al., 2001).

The conventional treatment of such waste water comprises of various methods such as aerobic, anaerobic, photo-catalysis, electrochemical, ozonation, coagulation-flocculation and adsorption treatment processes (Hubbeet al., 2016; Amor et al., 2019; Kamali andKhodaparast, 2015). Efficient removal of suspended solids (68-87%), BOD (90%), COD (70%) and colour (80%) is reported in a conventional treatment (Junna andRuonala 1991; Peerbhoiet al., 2003; Ashrafiet al., 2015). Thus, convention treatment (primary and secondary treatment) refers to as an efficient removal of major organic load for pulp and paper industry waste water. Also, treated effluent is meeting the final discharge permissible norms of

pollution control board. In India, presently, most pulp and paper industries are discharging treated effluent in a Nalla through final discharge pipe line. Moreover, use of treated water for irrigation purpose reported. So, the attempt has been made to recycle such type of treated waste water in the process itself. However, characteristics of treated effluent (due to mainly colour and COD) is not allowing to recycle it in the process itself. Thus, the purpose of the present work was for the further reduction in COD and colour to explore its potential to recycle secondary treated waste water in the process itself.Use of activated carbon as a polishing treatment provides a solution (Razali et al.,2011).However; commercially available activated carbon is becoming too expensive. Since, growing interest in low cost activated carbon from renewable sources, especially for the application in waste water treatment, various researcher have emphasis for the production of activated carbon from various agricultural by-products and waste materials, viz., sugar cane bagasse (SCB) (Onal et al., 2017), apricot shell (Karagozoglu et al., 2007), sunflower seed hull (Thinakaran et al., 2008), coconut shells (Singh, 2008), rubber seed coat (Rengarajn et al., 2002), oil pal fiber(Tan, 2007), date stones (Hameed et al., 2009a) and palm empty fruit bunch (Hameed et al., 2009b) and sewage sludge (Agrafioti et al., 2013).

Enormous availability of sugarcane bagasse (SCB) (50 million metric tons per annum) (Yadav and Singh, 2011)and municipal sewage sludge (MSS) (4 million tonnes per annum in urban areas) (Karia and Christian, 2013) in India leading to idea of application of these both the materials for the production of activated bio-char (carbon) and its utilisation for treatment of treated waste water (after biological treatment) from pulp and paper industry effluent to refer its recycling potential for its process itself. Production of activated carbons are reported that physical or/and chemical activation methods improves its pore size, resulting to improved carbon structure and adsorption efficiency (Sudaryantoet al., 2006). The chemical activation of lignocellulosic materials with phosphoric acid has been extensively investigated for the improvement of porosity (Diao et al., 2002; Jagtoyen and Derbyshire, 1998; Suarez-Garcia et al., 2002; Vernerssonet al., 2002). Precursor degradation mechanism is also explained extensively (GuoandLua, 2003; Solum et al., 1995).The investigation of sewage sludge-SCB derived bio-char for the treatment of treated waste water from pulp and paper industry rarely reported.

This work addresses the preparation of activated bio-char through chemical activation method using phosphoric acid (activating agent) on the residue obtained from co-pyrolysis of MSS-SCB and to determine the potential of this activated bio-char for the removal of COD and colourin biologically treated wastewater (after secondary treatment) from pulp and paper industry operating in Gujarat state, India.Moreover, characterisation of activated bio-char was determined.

## 2. Materials & Methods

### 2.1 Sampling of secondary treated waste water from pulp and paper industry

Secondary treated waste water was kindly collected from JK Paper Ltd, Songadh, Gujarat, India. The key processes of this industry included with pulping, cleaning and bleaching, washing and drying. The samples were stored at ≤5 ℃ to avoid any change in its physico-chemical characteristics. Table 1 shows the characteristics of secondary treated waste water (after biological treatment)sample i.e., BOD, COD, colour, pH, temperature andconductivity were analysed according to methods prescribed in APHA. (Baird and Bridgewater, 2017). Table 1 shows COD and colour of secondary treated waste water in the range of 230-350 mg/L and 51-65 Pt/Co, respectively.

## 2.2 Residue (Bio-char) Preparation

Sewage sludge used in this work was collected from Sewage Treatment plant located at Vadodara, India. SCB used in this study was kindly provided by Shree KhedutSahakariKhandUdyogMandli Ltd., Bardoli, India. Both the materials were separated from physical impurities, sun dried, oven dried at 105 ⁰C for 24 h, crushed, sieved for particle size beingless than to 150 µm and stored in a desiccator. To produce bio-char for use in theexperiments, the dried sewage sludge and SCB were first completely mixed at the weight

**Table 1.**Characteristics of treated waste water of pulp and paper industry(After biological treatment)

| Parameters | Unit | Value |
|---|---|---|
| pH | - | 6-8 |
| Temperature | ⁰C | 25-30 ⁰C |
| BOD | mg/L | <50 |
| COD | mg/L | 230-250 |
| Colour | Pt/Co | 51-65 |
| Conductivity | µS/cm | 1.932 |

ratio of 1:1. 100 g material was taken in a stainless steel cylindrical (50 mm ID X 190 mm length) reactor (Fig.1) and it was placed in a muffle furnace. To maintain oxygen free atmosphere during the process, nitrogen was supplied to the system at a flow rate of 200 mL/min. The temperature increased to 500 ⁰C at the rate of 20 ⁰C/min and the sample was kept in furnace for 60 min in the operating furnace after reaching the target temperature (Méndez et al., 2014; Zhang et al., 2015). The bio-char was then removed from the furnace, cooled in a desiccator, weighted and stored in airtight plastic containers. The yield of bio-char was 43.8%. Bio-char was passed through a 100 mesh sieve and was stored for further characterization and use in the adsorption experiment.
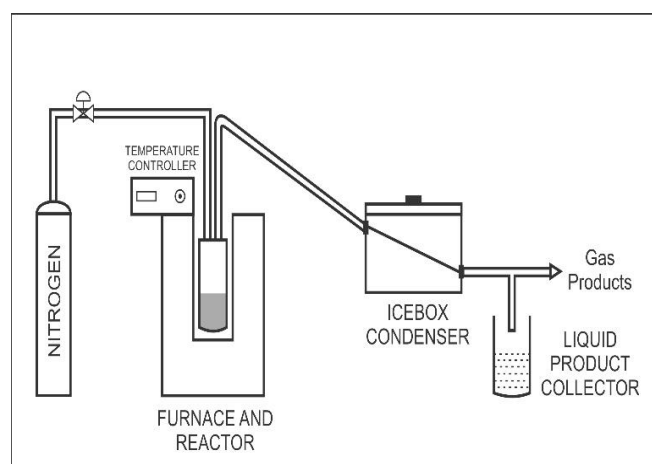


**Fig. 1.**Experimental system for MSS-SCB co-pyrolysis for biochar preparation.

## 2.3 Activation of Bio-char

Bio-char was washed with hot distilled water to remove dust-like impurities, dried at 105 °C, ground and sieved (200–300 µm) to discrete sizes. Chemical activation method using phosphoric acid (purity 85%) was used to activate the bio-char. In a typical method, 40 g of bio-char was impregnated by certain amount of 40 wt% concentrated phosphoric acid with occasional stirring. The amount of phosphoric acid solution used was adjusted to give a certain impregnation ratio. Subsequently, the impregnated samples were air dried under sunlight for 3 days. Activation of the phosphoric acid impregnated precursor was carried out at temperature of 500 °C for 2 h under purified nitrogen (99.995%) flow (150cm$^3$/g) at a heating rate of 10 °C/min in a muffle furnace. After activation, the sample was cooled to room temperature and washed sequentially several times with hot distilled water (70 °C) until the pH of the washing solution reached to 6-7. Finally the sample was dried in an oven at 110 °C for 24 h and then stored in plastic containers. The activated bio-char yield was calculated as per (1).

$$Yield\% = \frac{M_b}{M_0} * 100 \qquad (1)$$

Where $M_b$ is the dry weight of final activated bio-char and $M_0$ is the dry weight of precursor.

## 2.4 Characterization of Bio-char:

The bio-char after chemical activation was characterized by various techniques. Electrical conductivity (EC) was determined in the supernatant of a solution (solid/water, 1:5, w/v) by using a conductivity meter (Systronics µ-controller based conductivity -TDS meter 308) and pH was measured by using pH meter (Systronics digital pH meter – Model 802). A Fourier transform infrared (FTIR) spectrum of the activated bio-char was recorded on an Alpha FT-IR spectrometer Brucker at room temperature in the 400-4000 cm$^{-1}$ wave number range to determine their functional groups. Textural characterization of the activated bio-char was carried out in Nova Touch LX2 gas sorption analyzer from Quantachrome Instruments by Brunauer-Emmett-Teller (BET) method, using the software of Micromeritics. BETsurface area, total pore volume for pores, and average pore diameter were thus determined. Surface morphology and the presence of porosity of the activated carbon prepared in this work were studied using scanning electron microscopy (SEM) analysis using Model Nova NanoSEM 450.

## 2.5 Treatment of waste water:

All the adsorption experiments were carried out at temperature of 30 °C in a batch mode. The experiments were run in different flasks of 250mL capacity using an average shaker's speed of 120 rpm. The desired pH of 3 was maintained using dilute NaOH (0.1N)/HCl (0.1N) solutions. The initial COD and colour index were 234 mg/L and 51 Pt/Co, respectively. To determine the contribution of the adsorbent dose to colour and COD reduction, 100mL of sample was treated with different doses of adsorbent ranging between 0.30 and 1.4 g, the other conditions includes treatment time of 24 h, pH of 3 and initial COD and colour of the sample were 234 mg/L and 51 Pt/Co, respectively. At elapse of each set, the treated wastewater sample was filtered through 0.45µm filter paper before analyses. The samples were analysed using a Lovibond Spectrodirect Spectrophotometer at wavelength of 620 and 455nm for COD andcolour respectively. All experiments were carried out twice and the error was observed ± 5%.

The adsorption amount at equilibrium, $q_e$, and the reduction percentage was calculated from (2) and (3), respectively:

$$q_e = \frac{(C_0 - C_e)V}{m} \qquad (2)$$

$$\% \, reduciton = \frac{(C_0 - C_e)}{C_0} * 100 \qquad (3)$$

In equation (2) and (3), $C_0$ and $C_e$ are the liquid phase concentrations of adsorbate at initial and at equilibrium, respectively; V (mL) is the volume of solution and m (g) is the mass of dry adsorbent (bio-char) used.

## 3. Results and Discussion:

### 3.1 BET, SEM and FTIR of activated bio-char:

The BET surface area, total pore volumeand average pore diameter of the prepared activated bio-char were 1.549 m$^2$/g, 0.0053 cm$^3$/g and 1.68 nm, respectively.Activated bio-char characterized by electrical conductivity (EC) of 145.5 µS/cm and pH 8.2.The maximum value of activated carbon yield was found to be47.21%. Moreover, the average pore diameter of the activated carbonwas found to be 1.68 nm, indicating that the activated carbon prepared was in the microporeregion(Pores are classifiedasmicropores (<2 nm diameter), mesopores (2-50 nm diameter) andmacropores (>50 nm diameter) (IUPAC, 1972)).

The scanning electron microscopy (SEM) photo micrograph of the activated bio-char at 1,000 magnification is depicted in Fig. 2. The obtained bio-char was characteristic of irregular shape and heterogeneous pore structure.Many large pores in a honeycomb shape were found on the surface of the activated carbon.Hence, the surface structure of bio-char renders it a potentially good adsorbent.
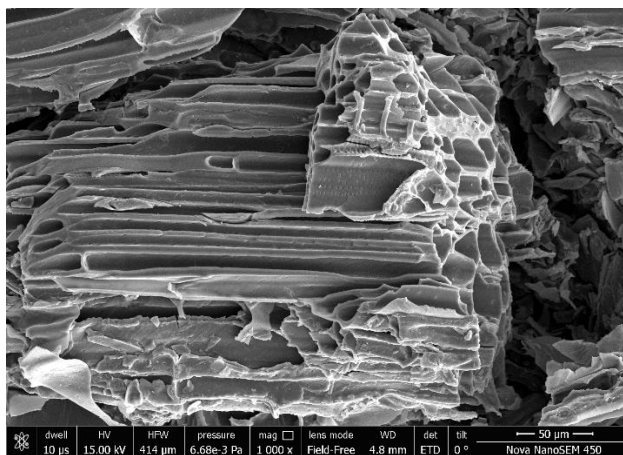


**Fig. 2.** SEM image of copyrolysis based activated bio-char (magnification = 1000×).

Fig 3, the FTIR spectra of prepared activated bio-char contained abundant functional groups displayed the following bands: 3828, 3769 and 3455 cm$^{-1}$ was recognized to bonded –OH (hydroxyl) groups, usually in the range of 3200-3750 cm$^{-1}$ for alcohols and phenols, involved in hydrogen bonding may be due to adsorbed water (Chen et al., 2002). 2942 cm$^{-1}$ denotes aliphatic C-H, 2383 cm$^{-1}$ denotes C=0 stretching from ketones, aldehydes or carboxylic groups, while 1693 is C=C stretching vibration of the aromatic rings or C=O stretch

carboxylic acid. 1434 cm$^{-1}$ denotes N-H bending 1036 C=O groups (Fan et al., 2016). In the low-wavenumber region, the shoulder peak at 887cm$^{-1}$could be attributed to the out-of-plane bending absorption of C-H in the aromatic ring (Sun et al., 2012). 674 cm$^{-1}$ denotes C-O-H twist broad. The surface of the prepared activated bio-char has rich functional groups, especially hydroxyl groups,carboxylic acid and carbonyl group. Functional groups with such a characteristics may act as active sites for the removal of colour and COD by chemical adsorption (Guo andLua 2003; Zhang et al., 2019; Luo et al., 2019).
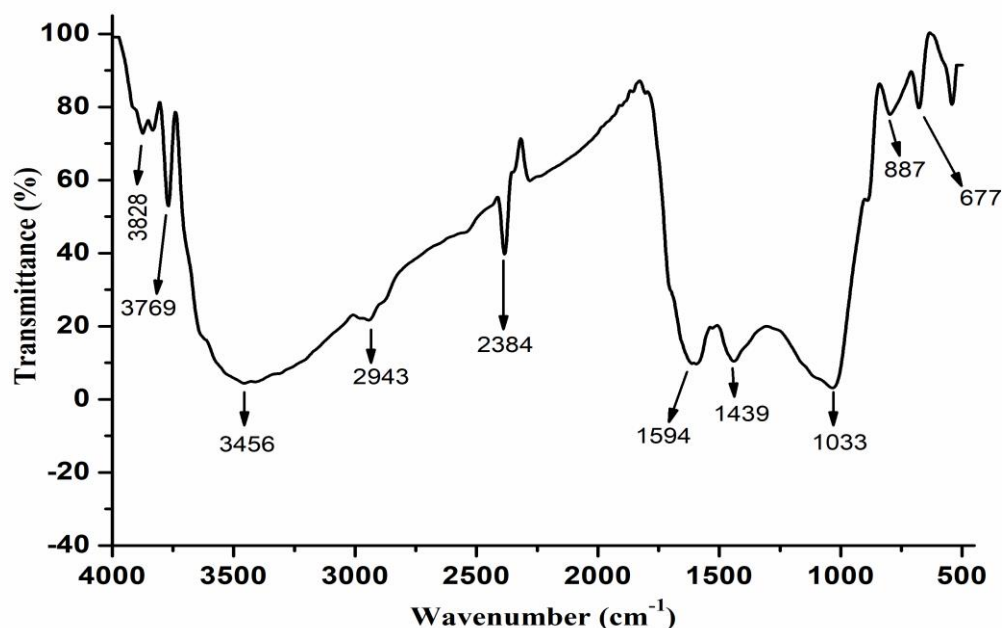


**Fig. 3.** FTIR spectra of Activated bio-char

### 3.2 Effect of activated bio-char dose

Fig. 4 shows the variation of percentage reduction for the COD and colour removal with activated bio-char dose. The COD and colour removal increased with increase in the quantity of activated bio-char. The maximum percentage of COD (optimum) and colour removed from the paper industry effluent was noted as 75.30 and 99.20, respectively, by using 1.4 g activated bio-char respectively. With this dose of bio-char, resulting treated waste water imparted COD and colour in the range of 57-61 mg/L and 0.41-0.52 Pt-Co. Such characteristic of treated waste water was observed suitable for recycling at pulp and paper process itself. A similar observation was reported for the treatment pulp and paper mill waste water with poly aluminium chloride and bagasse fly ash (Srivastava et al., 2005)and cotton textile mill effluent by using bamboo-based activated carbon (Ahmad and Hameed, 2009).
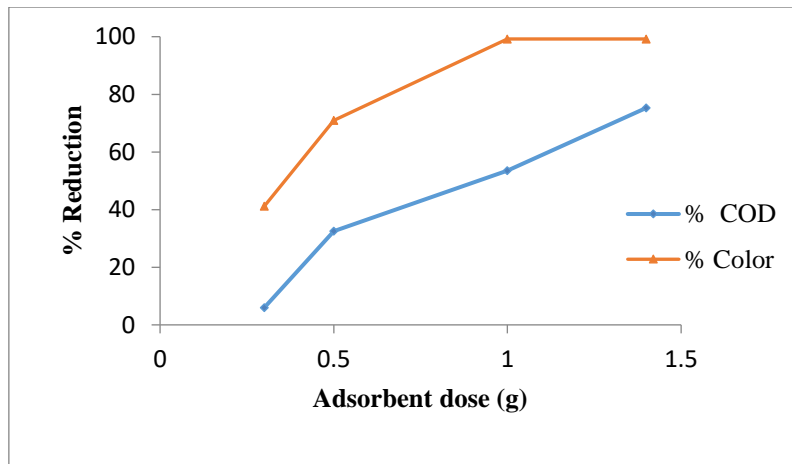
**Fig. 4.** Effect of dosage of activatedbio-char on the adsorption of COD and colour

### 3.3 Adsorption isotherms:

To study the adsorption isotherm process of COD and colour solution onto activated bio-char, Langmuir andFreundlich isotherm models, (4) and (5), respectively were examined for their abilities to accurately describe the adsorption process.

Langmuir isotherm equation.

$$\frac{C_e}{q_e} = \frac{1}{q_m} C_e + \frac{1}{K_L q_m} \qquad (4)$$

Freundlich isotherm equation

$$\log q_e = \log K_F + \frac{1}{n} log C_e \quad (5)$$

Where $C_e$ is the equilibrium concentration of adsorbate, mg/L; $q_e$ is the amount of adsorbate adsorbed per unit mass of adsorbent, mg/g; $q_m$ and $K_L$ are Langmuir constants related to adsorption capacity and rate of adsorption, respectively. $K_F$ and n are the Freundlich constants with n giving an indication of how favourable is the adsorption process and $K_F$ is the adsorption capacity of the adsorbent.Both the models, Langmuir and Freundlich are plotted for COD and Colour removal on activated bio-char (Figures not shown). Two isotherm modelswere seen to be appropriate for the experimental databecause all values of $R^2$ were higher than 0.9. The factor "1/n" given an indication of the favourability of adsorption. Values of 1/n smaller than 0.5 represents that the adsorbate is easily adsorbed; values of 1/n larger than 2 indicates the adsorbate is hardly adsorbed (Shi et al., 2014). The obtained values of 1/n (0.1 < 1/n < 1) suggested that the adsorption of COD and colour onto activated bio-char was favourable.

### 4. Conclusions:

The present study revealed that chemical activation method using phosphoric acid (activating agent) treated activated bio-char (co-pyrolysis mixture of MSS and SCB) is a promising adsorbent used to reduce the COD and colour from secondary treated (after biological treatment) pulp and paper industry waste water. FTIR study shows that activation of bio-char resulting to generation of active sites due to formation of rich-functional groups especially hydroxyl groups, carboxylic acid and carbonyl group, which were leading to reduction in

COD and colour. With the optimum dose of activated bio-char, resulting treated waste water imparted COD and colour in the range of 57-61 mg/L and 0.41-0.52 Pt-Co, respectively. Such characteristic of treated waste water was observed suitable for recycling at pulp and paper process itself. Brunauer-Emmett-Teller (BET) surface area, total pore volume and average pore diameter were 1.549 $m^2$/g, 0.0053 $cm^3$/g and 1.68 nm, respectively. The Freundlinchand Langmuirisotherm model was found best to describe the obtained equilibrium adsorption data at 30 $^{\circ}$C.

**References:**

Agrafioti, E., Bouras, G., Kalderis, D., Diamadopoulos, E., 2013. Bio-char production by sewage sludge pyrolysis. J. Anal. Appl. Pyrolysis. 102, 72-78

Ahmad, A.A., Hameed, B.H., 2009. Reduction of COD and color of dyeing effluent from a cotton textile mill byadsorption onto bamboo-based activated carbon. J. Hazard. Mater. 172, 1538–1543.

Ali, M., Sreekrishnan, T.R., 2001. Aquatic toxicity from pulp and paper mill effluents: A review. Adv. Environ. Res. 5, 175–196.

Amor, C.,Marchão, L., Lucas, M.S., Peres, J.A., 2019. Application of Advanced Oxidation Processes for the Treatment of Recalcitrant Agro-Industrial Wastewater: A Review.Water. 11, 205.

Ashrafi, O., Yerushalmi, L., Haghighat. F., 2015. Wastewater treatment in the pulp-and-paper industry: A review oftreatment processes and the associated greenhouse gas emission. J. Environ. Manage.158, 146-157.

Baird, R., & Bridgewater, L., 2017. Standard methods for the examination of water and wastewater. 23rd edition. Washington, D.C. American Public Health Association.

Büyükkamaci, N., Koken, E., 2010. Economic evaluation of alternative wastewater treatment plant options for pulpand paper industry.Sci. Total Environ.408, 6070–6078.

Chen, X., Jeyaseelan, S., Graham, N., 2002. Physical and chemical properties study of the activated carbon made from sewage sludge. Waste Manag. 22, 755–760.

Diao, Y., Walawender, W.P., Fan, L.T., 2002. Activated carbons prepared from phosphoric acid activation of grain sorghum. Bioresour. Technol. 81, 45–52.

Dilek, F.B., Gokcay, C.F., 1994. Treatment of effluents from hemp-based pulp andpaper industry: I – Thewaste characterization and physico-chemical treatability, in:Proceedings of the IAWQ International Specialized Conference on Pre-treatmentof Industrial Wastewaters. Pergamon Press Inc, Athens, Greece, pp. 161-163.

Fan, S., Tang, J., Wang, Y.,Li, H., Zhang, H., Tang, J., Wang, Z., Li. X., 2016. Bio-char prepared from co-pyrolysis of municipal sewage sludge and tea waste for the adsorption of methylene blue from aqueous solutions: Kinetics, isotherm, thermodynamic and mechanism. J. Mol. Liq. 220, 432-441.

Ferraz, F.M., Yuan, Q., 2020. Organic matter removal from landfill leachate by adsorption using spent coffee grounds activated carbon.Sustain. Mater. Technol. 23, e00141.

Garg, A., Mishra, I.M., Chand, S., 2007. Catalytic wet oxidation of the pretreated synthetic pulp and paper mill effluent under moderate conditions. Chemosphere 66, 1799–1805.

Guo, J., Lua, A.C., 2003. Textural and chemical properties of adsorbent prepared from palm shell by phosphoric acid activation. Mater. Chem. Phys. 80, 114–119.

Guo, J., Lua, A.C., 2003. Textural and chemical properties of adsorbent prepared from palm shell by phosphoric acid activation. Mater. Chem. Phys. 80, 114–119.

Hameed, B.H., Salman, J.M., Ahmad, A.L., 2009a. Adsorption isotherm and kinetic modeling of 2,4-D pesticide on activated carbon derived from date stones, J. Hazard. Mater. 163, 121–126.

Hameed, B.H., Tan, I.A.W., Ahmad, A.L., 2009b. Preparation of oil palm empty fruit bunchbased activated carbon for removal of 2,4,6-trichlorophenol: optimization using response surface methodology, J. Hazard. Mater. 164, 1316–1324.

Hubbe, M.A., Metts, J.R., Hermosilla, D., Blanco, M.A., Yerushalmi, L., Haghighat, F., Lindholm-Lehto, P., Khodaparast, Z., Kamali, M., Elliott, A., 2016. Wastewater Treatment and reclamation: A review of Pulp and paper Industry Practices and Opportunities. Bioresources. 11, 7953–8091.

IUPAC, 1972. IUPAC manual of symbols and terminology. Pure Appl. Chem. 31, pp. 587

Jagtoyen, M., Derbyshire, F.J., 1998. Activated carbons from yellow poplar and white oak by $H_3PO_4$ activation. Carbon 36, 1085–1097.

Junna, J., Ruonala, S., 1991. Trends and guidelines in water pollution control in the Finnish pulp and paper industry. Tappi J.74, 105–111.

Kamali, M., Khodaparast, Z., 2015. Review on recent developments on pulp and paper mill wastewater treatment. Ecotoxicol. Environ. Saf. 114, 326–342.

Karagozoglu, B., Tasdemir, M., Demirbas, E., Kobya M., 2007. The adsorption of basic dye (Astrazon Blue FGRL) from aqueous solutions onto sepiolite, fly ash and apricot shell activated carbon: kinetic and equilibrium studies, J. Hazard. Mater. 147, 297–306.

Karia, G.L., Christian, R.A., 2013. Wastewater treatment concept and design approach. PHI Learning, New Delhi pp. 371.

Khellouf, M., Chemini, R., Salem, Z., Khodja, M., Zeriri, D., Jada, M., 2020. A new activated carbon prepared from cypress cones and its application in the COD reduction and colour removal from industrial textile effluent. Environ. Dev. Sustain. https://doi.org/10.1007/s10668-020-00944-2.

Luo, C., Zhang, D., Lun, Z., Zhao, C., Wang, H., Pan, Z., Li, Y., Zhang, J.,Jia, S., 2019. Displacement behaviors of adsorbed coalbed methane on coals by injection of $SO_2/CO_2$ binary mixture. Fuel. 247, 356–367.

Méndez, A., Paz-Ferreiro, J., Araujo, F., Gascó, G., 2014. Bio-char from pyrolysis of deinking paper sludge and its use in the treatment of a nickel polluted soil. J. Anal. Appl. Pyrol. 107, 46–52.

Mohan, D., Kunwar, P.S., Vinod, K.S., 2008. Wastewater treatment using low cost activatedcarbons derived from agricultural byproducts - a case study. J. Hazard.Mater. 152, 1045–1053.

Onal, Y., kmil-Bas, C., Sarıcı-Ozdemir, C., Erdogan, S., 2007. Textural development of sugar beet bagasse activated with ZnCl2. J. Hazard. Mater. 142, 138–143.

Pala, A., Tokat, E., 2002. Color removal from cotton textile industry wastewater inan activated sludge system with various additives. Water Res. 36, 2920–2925.

Peerbhoi, Z.M., Mehrotra, I., Shrivastava, A.K., 2003. Treatability studies of black liquor by upflow anaerobic sludge blanket reactor. J. Environ. Eng. Sci.2, 307–313.

Pokhrel, D., Viraraghavan, T., 2004. Treatment of pulp and paper mill wastewater – A review. Sci. Total Environ. 333, 37–58.

Razali, M.A.A., Ahmad, Z., Ahmad, M.S.B., Ariffin, A., 2011. Treatment of pulp and paper mill wastewater with various molecular weight of polyDADMAC induced flocculation. Chem. Eng. J. 166, 529–535.

Rengaraj, S., Moon, S.H., Sivabalan, R., Arabindoo, B., Murugesan, V., 2002. Removal of phenol from aqueous solution and resin manufacturing industry wastewater using an agricultural waste: rubber seed coat, J. Hazard. Mater. 89, 185–196.

Savant, D., Abdulrahman, R., Ranade, D., 2006. Anaerobic degradation of adsorbable organic halides (AOX) frompulp and paper industry wastewater.Bioresour. Technol.97, 1092–1104.

Shi, L., Zhang, G., Wei, D., Yan, T., Xue, X.D., Shi, S.S., Wei, Q., 2014. Preparation and utilization of anaerobic granular sludge-based bio-char for the adsorption of methylene blue from aqueous solutions. J. Mol. Liq. 198, 334–340.

Singh, K.P., Malik A., Sinha, S., Ojha, P., 2008. Liquid-phase adsorption of phenols using activated carbons derived from agricultural waste material, J. Hazard. Mater. 150, 626–641.

Solum, M.S., Pugmire, R.J., Jagtoyen, M., Derbyshire, F., 1995. Evolution of carbon structure in chemically activated wood, Carbon 33, 1247–1254.

Srivastava, S.K., Gupta, V.K., Mohan, D., Pant, N., 1993. Removal of COD from reclaimedrubber factory effluents by using the activated carbon (developed from fertilizerwaste material) and activated slag(developed from the blast furnace wastematerial) - a case study.Fresen. Environ. Bull. 2, 394–401.

Srivastava, V.C., Mall, I.D., Mishra, I.M., 2005. Treatment of pulp and paper mill wastewaters with poly aluminium chloride and bagasse fly ash. Colloids Surf. A Physicochem. Eng. Asp. 260, 17–28.

Suarez-Garcia, F., Martinez-Alonso, A., Tascon, J.M.D., 2002. Pyrolysis of apple pulp: chemical activation with phosphoric acid. J. Anal. Appl. Pyrol. 63, 283–301.

Sudaryanto, Y., Hartono, S.B., Irawaty, W., Hindarso, H., Ismadji, S., 2006. High surface area activated carbon prepared from cassava peel by chemical activation.Bioresour. Technol. 97, 734–739.

Sun, Y., Yue, Q., Gao, B., Huang, L., Xu, X., Li, Q., 2012. Comparative study on characterization and adsorption properties of activated carbons with $H_3PO_4$ and $H_4P_2O_7$ activation employing Cyperusalternifolius as precursor. Chem. Eng. J. 181-182, 790–797.

Tan, I.A.W., Hameed, B.H., Ahmad, A.L., 2007. Equilibrium and kinetic studies on basic dye adsorption by oil palm fibre, activated carbon, Chem. Eng. J. 127, 111–119.

Thinakaran, N., Baskaralingam, P., Pulikesi, M., Panneerselvam, P., Sivanesan, S., 2008. Removal of Acid Violet 17 from aqueous solutions by adsorption onto activated carbon prepared from sunflower seed hull, J. Hazard. Mater. 151, 316–322.

Thompson, G., Swain, J., Kay, M., Forster, C.F., 2001. The treatment of pulp and paper mill effluent: a review.Bioresour. Technol.77, 275–286.

Vernersson, T., Bonelli, P.R., Cerrella, E.G., Cukierman, A.L., 2002. Arundodonax cane as a precursor for activated carbons preparation by phosphoric acid activation. Bioresour. Technol. 83, 95–104.

Yadav, J.P., and Singh, B.R., 2011. Study on Future Prospects of Power Generation by Bagasse, Rice Husk and Municipal Waste in Uttar Pradesh. SAMRIDDHI-J. Phys. Sci. Eng. Technol. (S-JPSET). 2, 2-4

Zhang, D., Liu, S., Fu, X., Jia, S., Min, C., Pan, Z., 2019. Adsorption and Desorption Behaviors of Nitrous Oxide on Various Rank Coals: Implications for Oxy-coal Combustion Flue Gas Sequestration in Deep Coal Seams.Energy Fuels. 33, 11494–11506.

Zhang, W.H., Zheng, J., Zheng, P.P., Qiu, R.L., 2015. Atrazine immobilization on sludge derived bio-char and the interactive influence of coexisting Pb(II) or Cr(VI) ions, Chemosphere. 134, 438–445.

# Phenol removal from water using choline chloride based DESs – Study on thermodynamic solvent screening model and experimental validation

*Dhruvkumar Rabadiya[a], Parth Modi[a], Krunal Suthar[b*] and Milind H. Joshipura[c]*

[a,b]Department of Chemical Engineering, Shroff S R Rotary Institute of Chemical Technology, Gujarat Technological University - 393135, Gujarat, INDIA
[c,d]Department of Chemical Engineering, Institute of Technology, Nirma University, Ahmedabad- 382481, Gujarat, INDIA

*Corresponding author: krunal.suthar@srict.in , 919974090049

## Abstract

Phenol is one of the common chemical compounds with wide application in process industries. The highly toxic phenolic compounds have the limit of 0.001 mg/L phenol content in potable water. Extensive research is done for phenol removal using various techniques viz. enzymatic polymerization, electrochemical, adsorption, and ion exchange method, and membrane-based method. These physico-chemical and biological treatments have the limitations in phenol recovery. The liquid-liquid extraction appears to have great potential in the field of phenol removal from water. An extractant selection is a key to the effective separation of liquid-liquid extraction. A wide variety of extractants are available in the market. In the present study, the attempt was to use a thermodynamic solvent selection model for environmental benign deep eutectic solvents (DESs). The model is based on the common solvent selection criteria which included selectivity, solvent power and solvent loss. These selection criteria were predicted using a limiting activity coefficient using UNIFAC in a process simulator. The thermodynamic predictive model was validated experimentally for three choline chloride based DESs for phenol removal from water. The phenol recovery was less compared to few conventional solvents.

**Keywords:** Solvent extraction, DES, thermodynamic model, phenol-water

## Introduction

The remediation of phenolic compounds is essential as the generation of highly concentrated phenolic wastewater in increasing industrialization. As per reported bulletin of Acta Technica Corviniensis, phenol is one of the major pollutants with serious threats [01]. The phenolic compound wastes are generated in various sectors of chemical process industries including petrochemical plants and refineries, coal conversion industries, pharmaceutical plants, dyes and pigment, paper and pulps, agricultural activities etc. [2,3]. Phenol is a toxic component which reaches to the ground water through the continuous release via various chemical process industries. It is essential to treat the wastewater containing phenol and phenolic compounds before discharging into the water streams.

Many treatment methods are reported for removal of phenol from wastewater which includes adsorption, extraction and microextraction, advanced oxidation, biological processes etc. [4-6].

Due to high catalyst efficiency and effective removal, the enzymatic treatment method is known to be advantageous. The disadvantages of enzymatic treatment include the slow rate, instability and non-reusability [6]. The extraction is known to be a low energy operation with high throughput and accepted separation operation worldwide [7]. Moreover, the extraction process is well adopted for separation of azeotropic mixtures and separation of mixtures with poor separation factor. An important step is designing liquid-liquid extraction is to employ an effective extractant for efficient separation. The selection of the best suitable solvent is a challenging task for an engineer due to the large range of available solvents and solvent mixtures. The screen models for solvents are reported.

The Deep Eutectic Solvents (DESs) are known to be green solvents with an easy synthesis step. The DESs are produced by mixing halide quaternary salt with hydrogen bond donors and mixing them at moderate temperature. The depression in the freezing point is lower than the freezing point of an individual component. The DESs were reported as an effective solvent alternative to ionic liquids. The application of DESs includes a wide variety of fields including alloy coatings, copper plating, synthesis applications, gas adsorption, biotransformation, purifying and manufacturing biofuel [8-10].

The main aim of the present work was to evaluate and assess the application of DESs as extractant for phenol removal. The purpose was also to test the solvent screening model which can be used to access a wide variety of tunable eutectic solvents. The scheme of the present work is shown in Figure-1.

**Materials and methods**

The quaternary salt for synthesis of DESs were purchased from Loba chemie and the analytical grade of other chemicals were purchased from Rankem chemicals. The purity of the purchased raw material was greater than 98.5%. DESs were synthesized based on choline chloride as a quaternary salt in combination with three Hydrogen Bond Donors (HBDs). The considered HBDs viz. glycerol, ethylene glycol and Triethylene glycol were mixed with quaternary salt in 1:2, 1:2 and 1:4 molar ratio. The list of DESs synthesized is listed in Table-1. The molar ratio of quaternary salt and HBDs were selected based on the studied eutectic point. The mixture was agitated at 300 rpm in a jacketed glass vessel until the homogenous transparent liquid was observed. The synthesized DESs were stored in a tight glass bottle to avoid any contamination.

The synthetic mixture of water-phenol was considered for the experimentation purpose. The mixture was synthesized using 5% wt. of phenol in demineralized water. The water-phenol mixture and the synthesized eutectic solvent were mixed in a 1:1 mass ratio. The mixture was agitated slightly before allowing it to settle overnight in a separating funnel. The two distinct layers were visible and the samples of extract and raffinate phases were collected carefully. The efficiency of the solvent of removing phenol was analyzed using gas chromatography.

The solvent screening model studied in the present work depends on estimation of solvent power, solvent loss and selectivity. Separation factors in the distillation columns should be considered in case of solvent extraction separated via distillation. The separation factor in the present study is

neglected as the primary need is to screen solvents from a larger list. Before screening the DESs, the conventional solvents were screened to check the consistency of the model studied.

The selected solvent should show high selectivity ($\alpha_{ij}$) which would reduce the number of extraction stages. The selectivity of a solvent is further predicted from the activity coefficient of water and phenol at infinite dilution ($\gamma^\infty$) in solvent.

$$\alpha_{ij} = \frac{\gamma_{i,S}^\infty}{\gamma_{j,S}^\infty}$$

Where $i$ $and$ $j$ indicate water and phenol whereas $s$ indicates the solvent.

The solvent capacity is determined as an inverse of the activity coefficient of the extracted component $i$ (phenol) at infinite dilution in the solvent ($s$). The solvent capacity positively influences the selectivity. The solvent power can be expressed as the inverse of the activity coefficient of the solvent at an infinite dilution of raffinate i.e., water.

$$S_{pi} = \frac{1}{\gamma_{i,S}^\infty}$$

In the equation, $S_{pi}$ indicates solvent power. Another criterion considered in the present study is solvent loss which depends on the size of miscibility gap. The solvent loss can be expressed as the inverse of the activity coefficient of the solvent ($s$) at an infinite dilution of raffinate.

$$S_l = \frac{1}{\gamma_{S,R}^\infty}$$

In the above equation, $S_l$ denotes solvent loss. The solvent screening criteria is expressed by combining these three terms of selectivity, solvent power and solvent loss as follows.

$$[Sa_{ij}]^{ws} \cdot \left[\frac{1}{\gamma_{E(i),S}^\infty}\right]^{wc} \cdot \left(1 - \frac{1}{\gamma_{S,R}^\infty}\right)^{wsl} = Selection\ criteria$$

In the solvent selection criteria, the $w_s$, $w_c$ and $w_{sl}$ denotes weightage factor of selectivity, solvent capacity and solvent loss respectively. The weightage factors were adopted from the work of Gmehling et. al. [11]. The weighing factor of selectivity was taken as one, weighing factor of solvent capacity is taken as 1.5 and the weighing factor of solvent loss was taken as 3.

The selected solvent screening model is dependent on the limiting activity coefficient value. The estimation of limiting activity coefficient is commonly reported using the COSMO-RS, UNIFAC or MOSCED parameter model. Before studying the solvent screening model for DESs, the model was tested for conventional solvents. The values of limiting activity coefficient for fifteen conventional solvents of different families were estimated at 298.15 K using MOSCED parameter model. The values are listed in table-2.

The contents of the MOSCED equation for DESs were not available and the estimation of these constants needs the experimental values for regression. Hence, in the present study the limiting activity coefficient of DESs was estimated using the UNIFAC model. The DESs are pure compounds that are not available in the component library of a process simulator. DESs were

hypothetically added to a process simulator DWSIM. The critical properties and acentric factor of quaternary salt and HBDs were estimated using the Lydersen, Joback and Reid (LJR) model and later the Lee–Kesler mixing rules equations were applied [12-13]. The estimated values of the normal boiling point, average molecular weight, critical properties and acentric factor are listed in table-3. hypothetical addition of DESs.

**Results and Discussion**

The solvent selection model was first employed over fifteen conventional solvents of various families. Based on the estimation of selectivity of the solvent for removal of phenol, the sequence is as follows, Alkanes>Ether>Ketones>Esters>Alcohols. The higher value of selectivity refers to the lower extraction stages. The estimated selectivity was plotted for all fifteen conventional solvents as shown in Figure-2. of Whereas the solvent power follows the order, Alcohols>Ketone>Ether>Ester>Alkanes for removal of phenol. The higher power corresponds to the less solvent consumption in extraction. The selectivity, solvent power and solvent loss of conventional solvents are tabulated in Table-3. The sequence matched the previously reported work. The estimated values were applied to solvent selection criteria for conventional solvents and the solvent ranking matched to the experimental values.

After validating the screening model, it was employed for DESs. It was essential to select DESs with low melting point which remains in liquid state while employing it for extraction of phenol from large volume water. The knowledge of DESs structure dynamics and transport properties of DESs are not known accurately. The critical properties of synthesized DESs were estimated using the NRTL model. NRTL model with parameters regressed using MODFAC-NIST showed better results than UNIFAC, UNIFAC-LL, UNIFAC-DO.

The predicted values of limiting activity coefficient were plugged on the solvent screening model. The order of a ranking based in the screening model was; $DES_1$>$DES_3$>DES2. The value of solvent loss was less for $DES_1$ compared to the other two. $DES_1$ was superior based selectivity, solvent power and solvent loss. The GC results showed the same ranking for the experimental extraction study. The GC graphs for separation of phenol using DESs were shown in Figure-3. The overall result of phenol removal experimentally and the ranking based on solvent screening model is tabulated in Table-4. The result showed that the phenol removal using DESs was not as efficient as expected. The possible reason for more efficient separation can be the induction of emulsifier agent causing the quick and efficient mass transfer between two phases. Also, the use of acid-base induced-DESs can act as the phase separation agent. The factors affecting the extraction process can be further optimized carefully. The result emphasizes the need for accurate prediction of limiting activity coefficient leading to an efficient solvent screening model. The model considered in the present study was validated by the results obtained experimentally.

**Conclusion**

DESs have shown potential as extractants in various fields of separation and purification. The property of DESs can be tuned by adjusting the type and molar ratio of HBDs. A wide variety of solvents are available. The conventional solvents were studied to verify the consistency of the solvent screening model. In the present study, an attempt was made to employ a solvent selection

model for DESs. The model was validated by the results obtained experimentally. The model can be further improved by considering the viscosity, solvent stability and accurate prediction of limiting activity coefficient. $DES_1$ showed a fair result compared to other two choline chloride based DESs. The study emphasizes the requirement of limiting activity coefficient databases for novel solvents, DESs. Being environmentally benign, DESs are potential extractant for phenol removal as it replaces the consumption of the toxic solvent and eliminates the centrifugation and other complex purification processes.

## Acknowledgement

## References

1. Tomic, M., Bujanovic, L.N., Cekerevac, M., Zdravkovic, M. 2017. Application of electrochemically synthesized ferrate (vi) in the treatment of phenol contaminated wastewater from wood industry. Acta Technica Corviniensis-Bulletin of Engineering. 39.
2. Cai, T., Qiu, H., 2019. Application of deep eutectic solvents in chromatography: A review, TrAC Trends in Analytical Chemistry. 120, 115623.
3. Qin, H., Hu, X., Wang, J., Cheng, H., Chen, L., Qi, Z., 2020. Overview of acidic deep eutectic solvents on synthesis, properties and applications. Green Energy & Environment. 5, 8-21.
4. Kulkarnia, S., Tapre, R., Patilc, S., Sawarkard, M. 2013. Adsorption of Phenol from Wastewater in Fluidized Bed Using Coconut Shell Activated Carbon. Procedia engineering.
5. Munguia, A. 2001. Residual compost of Agaricus bisporus as a source of crude laccase for enzymic oxidation of phenolic compounds. Process Biochem. Article process biochemistry.
6. González-Muñoz, M.J., Luque, S., Álvarez, J.R., Coca J. 2002. Recovery of phenol from aqueous soltions using hollow fibre contactors. Journal of membrane science.
7. Dahili, L., A., Feczko, T., 2015. Cross-linking of Horseradish Peroxidase Enzyme to Fine Particles Generated by Nano Spray Dryer B-90. Periodica Polytechnica Chemical Engineering. 59(3), 209-214.
8. Ren, S., H., Xiao, Y., Wang, Y., M., Kong, J., Hou, Y., C., Wu, Y., 2015. Effect of water on the separation of phenol from model oil with choline chloride via forming deep eutectic solvent, Fuel Processing Technology. 137, 104-108.
9. Altunay, N., Elik, A., Kaya, S., 2020. Alcohol-DES based vortex assisted homogenous liquid-liquid microextraction approach for the determination of total selenium in food samples by hydride generation AAS: Insights from theoretical and experimental studies. Talanta, 215, 120903.
10. Leron, R., B., Li, M., H., 2013. Solubility of carbon dioxide in a eutectic mixture of choline chloride and glycerol at moderate pressures, J. Chem. Thermodyn. 57,131–136.
11. Gmehling, J., Schedemann, A., 2014. Selection of Solvents or Solvent Mixtures for Liquid−Liquid Extraction Using Predictive Thermodynamic Models or Access to the Dortmund Data Bank. Ind. Eng. Chem. Res. 53, 45, 17794–17805.
12. Valderrama, J., O., Robles, P., A., 2007. Critical properties, Normal boiling temperatures, and acentric factors of fifty ionic liquids, Ind. Eng. Chem. Res. 46, 1338–1344.

13. Knapp, H., Doring, R., Oellrich, I., Plocker, U., Prausnitz, J., M., 1982. Vapor-liquid equilibria for mixtures of low boiling substances, DECHEMA Chem. Data Ser. 4.

**Figures**
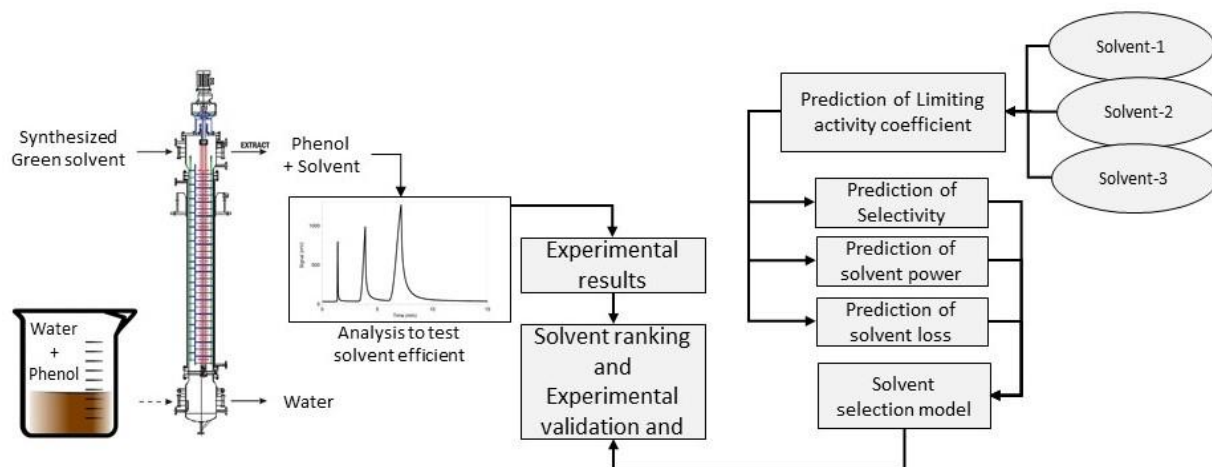


Figure-1 Scheme of the present work
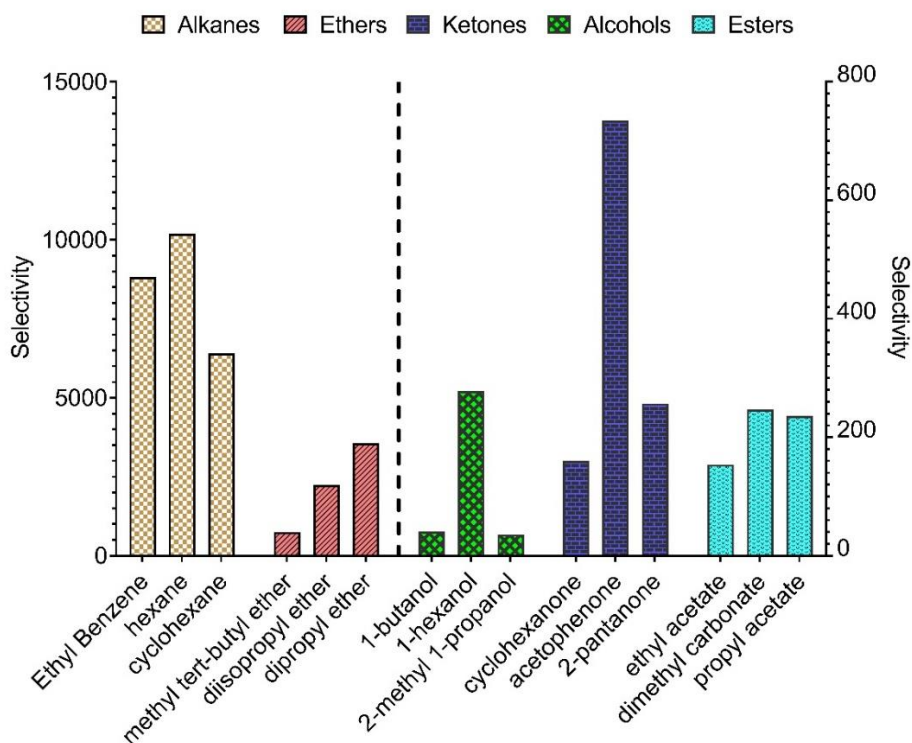


Figure-2 Estimated selectivity for fifteen conventional solvents
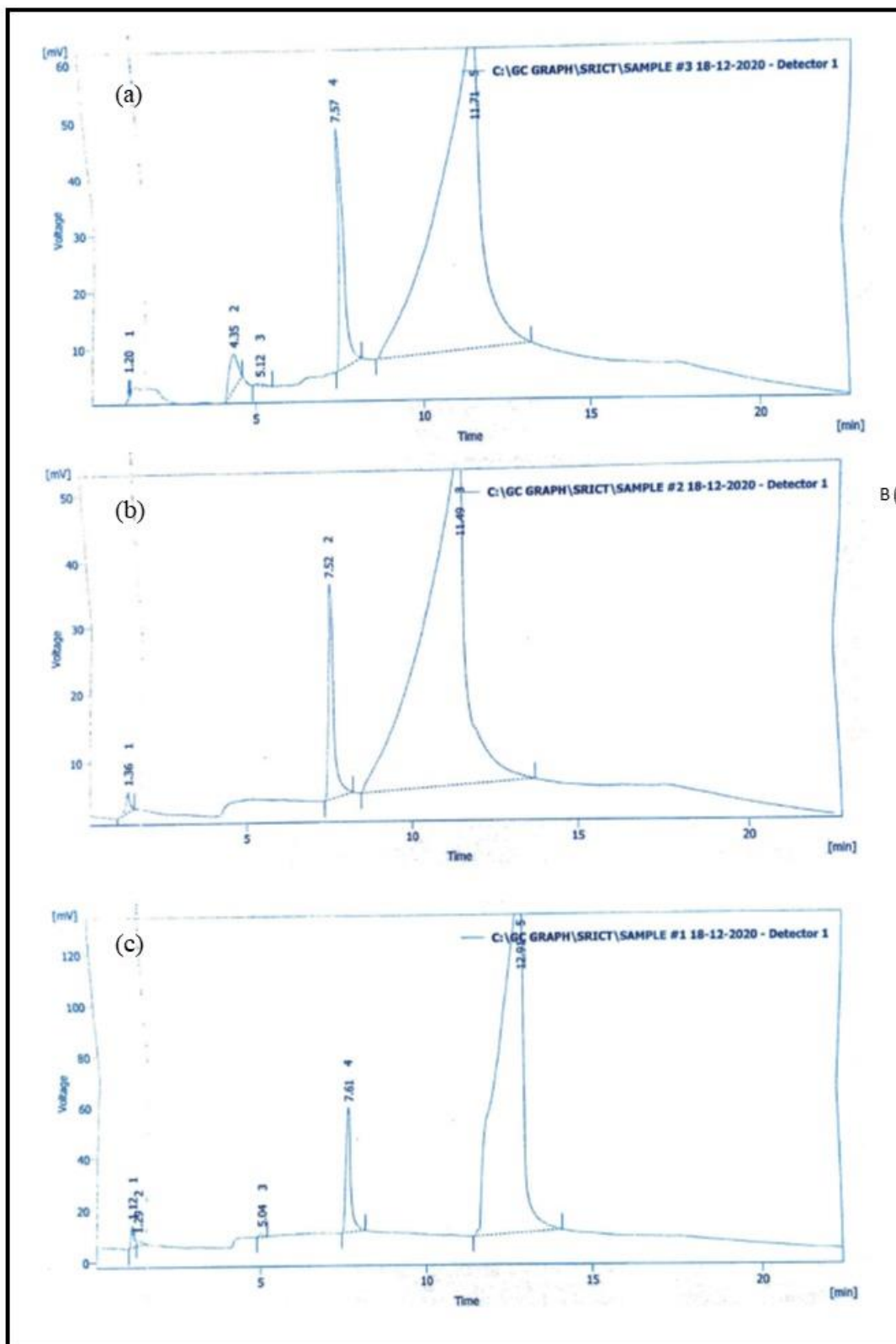
Firure-3 GC graphs of phenol removal using DESs (a) DES$_1$, (b) DES$_2$ and (c) DES$_3$

**Tables**

Table-1 List of DESs considered in the present study

| DESs | salt | HBDs | Molar ratio | Molecular weight (gm. mol$^{-1}$) |
|------|------|------|-------------|-----------------------------------|
| DES$_1$ | Choline chloride | Glycerol | 1:2 | 107.94 |
| DES$_2$ | Choline chloride | Ethylene Glycol | 1:2 | 87.92 |
| DES$_3$ | Choline chloride | Tri ethylene Glycol | 1:4 | 148.06 |

Table-3 The selectivity, solvent power and solvent loss of conventional solvents

| Solvent *(i)* | Family | $\gamma_{water,i}$ | $\gamma_{phenol,i}$ | $\gamma_{i, water}$ |
|---------------|--------|--------------------|---------------------|---------------------|
| Ethyl Benzene | Alkanes | 31476.75 | 3.57 | 12816.92 |
| hexane | Alkanes | 159190.7 | 15.62 | 106881.9 |
| cyclohexane | Alkanes | 57082.42 | 8.91 | 283862 |
| methyl tert-butyl ether | Ethers | 428.38 | 0.57 | 272.51 |
| diisopropyl ether | Ethers | 1970 | 0.88 | 339 |
| dipropyl ether | Ethers | 4555.06 | 1.28 | 921.79 |
| 1-butanol | Alcohols | 19.23 | 0.47 | 3.24 |
| 1-hexanol | Alcohols | 150.26 | 0.54 | 2.58 |
| 2-methyl 1-propanol | Alcohols | 19.89 | 0.56 | 3.37 |
| cyclohexanone | Ketones | 33.60 | 0.21 | 8.49 |
| acetophenone | Ketones | 441.11 | 0.6 | 23.94 |
| 2-pantanone | Ketones | 120.89 | 0.47 | 47.3 |
| ethyl acetate | Esters | 109.53 | 0.71 | 80.67 |
| dimethyl carbonate | Esters | 197.94 | 0.80 | 65.97 |
| propyl acetate | Esters | 155.82 | 0.66 | 46.45 |

Table-2 Estimated normal boiling point, critical properties and acentric factor of DESs

| Property | DES$_1$ | DES$_2$ | DES$_3$ | Unit |
|----------|---------|---------|---------|------|
| Normal boiling point | 502.67 | 426.25 | 536.73 | K |
| Critical temperature | 644.61 | 589.46 | 657.07 | K |
| Critical pressure | 57.04 | 59.95 | 36.61 | bar |
| Critical volume | 298.08 | 247.28 | 385.27 | cm$^3$/mol |
| Acentric factor | 1.25 | 0.94 | 1.05 | -- |

Table-4 Result summary of phenol extraction using DESs

| DESs | T (K) | Selectivity | Solvent power | Solvent loss | Selection criteria | Rank based in model | Experimental phenol removal | Rank based on experiment |
|------|-------|-------------|---------------|--------------|--------------------|--------------------|------------------------------|---------------------------|
| $DES_1$ | 298.15 | 2.035 | 0.929316 | 0.4556 | 0.294101 | 1 | 80.60% | 1 |
| $DES_2$ | 298.15 | 1.107 | 0.981104 | 0.8846 | 0.001652 | 3 | 74.40% | 3 |
| $DES_3$ | 298.15 | 1.005 | 0.764304 | 0.7583 | 0.009486 | 2 | 75.60% | 2 |

# Greywater Characterization of an Indian Household and Potential Treatment for Reuse

*Vivek P.Bhange[1]\*, Soniya S. Shende[1], Parnavi S. Ghorpade[1], Pravin D. Patil[2]*

[1]Department of Biotechnology, Priyadarshini Institute of Engineering & Technology, Hingna road, Nagpur-19.
[2]Department of Basic Science & Humanities, NMIMS Mukesh Patel School of Technology Management & Engineering, Mumbai, Maharashtra, 400056, India

**\*Corresponding author:** vivekbhange@gmail.com, telephone number with country code: +91-7104-244463

## Abstract

Inadequate water supplies recall the environmental values of recovery and reuse of limited resources. One of the exciting opportunities in these circumstances is Grey water. Wastewater is generated from household activities like bathing, kitchen sinks, washbasins, and laundry classified as greywater. Inventing a pilot-scale greywater treatment system that treats in-house generated greywater and makes it reusable by assisting the untapped potential of physical methods of greywater purification was the main aim of this study. The study results from greywater samples' characterization from various sources in an Indian middle-class single household with four residents for six months. Moreover, the designing and analyzing of a treatment system applied to treat this in-house generated greywater was conducted. A filtration system with different filter layers was designed. It was found to have a chemical oxygen demand removal efficiency of 85.98%, biochemical oxygen demand removal efficiency of 86.28%, and total suspended solids removal efficiency of 94.44%. The filter system designed in this study describes improved removal efficiency in all respects and gives an idea of the reusability of in-house treated greywater. The study concludes that greywater can be recycled and reused for toilet flushing, gardening, car washing, and fire fighting. This practice can also lead to a significant reduction in the consumption of freshwater.

**Keywords:** Greywater, Characterization, Treatment system.

## 1. Introduction

Water is needed to ensure food security, feed livestock, industrial production, and conserve biodiversity and the environment. Searching for an alternate water source to maintain the balance between the demand and the availability of freshwater is the need of the hour. To overcome the problem, recycling and reuse of wastewater have been practiced worldwide by different techniques. Wastewater usually generates in large quantities from household or industrial activities. The wastewater generated from households can be further categorized as grey water and black water.

Wastewater is produced from household activities like bathing, kitchen sinks, washbasins, and laundry, classified as greywater, whereas wastewater generated from toilets is classified as black water. Generally, greywater represents up to 70% of total consumed water but contains only 30% of organic fraction and 9% to 20% nutrients (Pidou et al., 2007). Various sources contribute towards grey water with varying compositions. In an average household, greywater is produced from washbasins, kitchen sinks, laundry, and bathing.

The characteristics of greywater vary depending on the number of family members, age, and usage. The chemicals used by an individual household also contribute towards the varying properties of greywater generated. The greywater generated from the bathroom consists of many shampoos, soaps, body care products, etc. Laundry greywater consists of a high level of different

detergents. Sink greywater has a contribution of soap, toothpaste, etc. The greywater generated from kitchen sinks has many food residues, oil, grease, etc.

Due to the increasing global shortage of water, on-site source-separated treatment and reuse of less polluted greywater is an attractive option (Vakil et al., 2014). This treated greywater can be further used for various purposes like irrigation of edible and non-edible crops, car washing, toilet flushing, fire fighting, etc. (Wanjiru and Xia 2018). Different countries have varying reasons for the adoption of treatment and reuse systems of greywater. India is a highly populated, tropical, and drought-induced country that needs greywater reuse systems (Asano 1996).

Filtration studies, being elementary, were performed by different people in different parts of the world. Gross et al. (2007) used sand filter layers and plastic filter media as filter layers. On the other hand, Finley et al. (2009) conducted studies on the shower and washing machine greywater using coarse filtration followed by slow sand filtration with a hydraulic retention time of ± 24h. Parjane and Sane (2011) tested a filtration unit consisting of coconut shell cover, coarse sawdust, charcoal, bricks, and sand. In total, the filtration systems achieved removal efficiencies of total suspended solids (TSS) 53– 93%, biological oxygen demand (BOD) 89–98 %, Chemical oxygen demand (COD) 37–94 %. Parjane and Sane (2011), in their filtration study, used only bath and washbasin greywater. Hence, there was a need for further investigations into the filtration. Other sources of greywater like laundry, kitchen, and combined greywater needed research (Ghaitidak and Yadav, 2013).

This study aims to characterize the in-house generated greywater from different sources such as kitchen sink, laundry, bathing, washbasin, and a mixed stream of these for six months from July to December. A mediocre income household in Nagpur, Maharashtra, India, was chosen as a model for this study. Designing a treatment system that is a simple filtration unit comprising various filter layers is also a part of the study. Lastly, we also aim to predict this particular unit's possible application and efficiency, along with its cost approximation.

## 2. Materials and Methods

### 2.1 Collection and Characterization of Grey Water

A mediocre income household in Nagpur, Maharashtra, India, was chosen as a model for this study. The different greywater sources were identified, such as a washbasin, kitchen sink, post bathing water, and water used for washing clothes. Drain pipes from these sources were separated from the central wastewater collection stream and made to flow individually into separate tanks of a capacity of 5L placed in the backyard of the house. This was done for the characterization of greywater from individual sources. Next, for the overall mixed greywater, the wastewater collection drains were redesigned. All the greywater generating points mentioned above, i.e., total wastewater barring the water from toilets, were integrated and led to another tank of capacity of 5L located in the backyard of the house. Samples were collected after every 12 hours from these collection tanks and analyzed in the laboratory to obtain the values of different parameters such as pH, COD, BOD, turbidity, TSS, and chlorine. The study was undertaken for six months, from July to December.

### 2.2 Sample Analysis

Analysis of samples was done before treatment and post-treatment to check different greywater parameters that determine its quality. Before treatment, samples of 1L from various sources were collected and analyzed for parameters such as pH, turbidity, TSS, COD, BOD, and chlorine according to Standard Methods methods (APHA, 2005). COD was measured using a COD digester.

## 2.3 Treatment Studies

A greywater purification system comprising of wood chips, sand filter, banana peels, sand filter, coconut husk, and sand filter layers of different filters having distinct removal efficiencies was designed. The filter unit was composed of a PVC container (to avoid rusting) of height 100 cm and width 30 cm. Different layers of materials such as sand, gravel, fly ash, banana peels, wood chips, coconut husk, etc., were laid into the container leaving a 20 cm clear space above the filter media. The specifications of these layers are given in Table 1. The raw greywater and filtered greywater were analyzed using different parameters like pH, turbidity, COD, BOD, etc.

Table 1: Height of various filter layers used

| Filter layer | Height |
|---|---|
| Large size gravel (at the bottom) | 15 cm |
| Small and medium sized gravels | 10 cm |
| Powdered fly ash bricks | 6 cm |
| Small sized gravels | 8 cm |
| Coconut husk | 10 cm |
| Wood chips | 8 cm |
| Banana peels | 8 cm |
| Fine sand (top most layer) | 20 cm |

## 2.4 Characterization of Filter Layers

Sand comprising a mixture of gravel and small pebbles was taken up from a construction site and was first washed with tap water and then sun-dried. The various components were then separated by filtration using sieves of different sizes. The gravels and stones were isolated and characterized into groups of 5-8 cm, 2 to 5 cm, i.e., the large and medium-sized gravels and small-sized gravels of 1 to 2 cm. Fine sand was obtained by separation using a sieve of 1 mm pore size. Sand filter reduces COD, BOD, and TSS levels of wastewater (Zuma et al., 2009).

Fly ash bricks can reduce the surfactants, oil, and grease present in water. Thus, fly ash bricks were taken and broken down into smaller pieces of 1 to 2cm. These clumps were used as one of the filter layers (Katukiza et al., 2014). Coconut husk was first washed with tap water and sun-dried. This acts as a promising adsorbent and can successfully remove dye components (Gisi et al., 2016). The bark of the neem (*Azadirachta indica*) tree was scraped, and wood chips of a minimum width of 1 cm were prepared. These chips were sun-dried for almost three days to evaporate the water in them and then used as a filter layer. Neem wood chips are seen to impart microbial property and reduce the nitrogen and ammonia content and water odor (Murnane et al., 2016).

Banana peels were taken from around 24 bananas and were cut into small pieces of a minimum length of 2 cm. These were then sun-dried for two days and used as an adsorbent layer. These facilitate the removal of metal ions and organic compounds (Renata et al., 2011).

## 2.5 Filter Installation

All the above filter layers were laid into the PVC container of 20 L, height 100 cm and width 30 cm, in a chronology as mentioned in Table 1, and the filter unit was prepared as shown in Figure 1. In between these filter layers, nylon meshes of pore size 1 mm were placed to hold these layers in place. The mesh was placed between the coconut husk and gravel layers and between the banana peel and subtle sand layers. The filter height and width was decided by a trial and error method wherein; similar filter units were prepared of different heights and width. The preliminary filter was ready in a 2 L coke bottle, and the filtration efficiency was checked by visual inspection of the input and output greywater. Subsequently, the filter height and width were increased using different sized containers, and its efficiency was checked. Three such filters were prepared, and finally, the filter unit with the above-said specifications was seen to give the best output, and thus it was selected for further investigations. At the bottom of the container, small holes of diameter 2 cm were made for the effluent. Sampling point P1 was provided for the influent and R1 for the effluent. The filter unit was placed at the height of 40 cm above the ground level over an iron tripod stand, and the effluent was collected from below into a collection vessel.
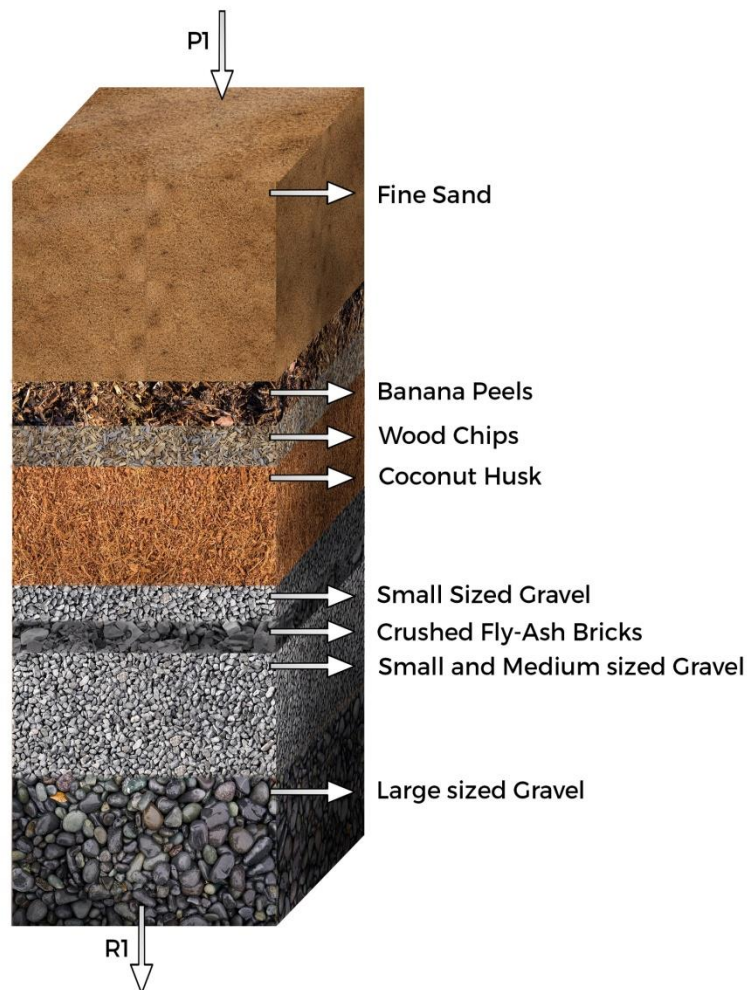


Figure 1: Filtration assembly

## 2.6 System Operation

The various filter layers were installed first in the required assembly. Water was allowed to pass through it till all the layers were stabilized. Once the system was stabilized, the greywater was allowed to pass through it. The whole assembly was monitored for a span of three months, i.e., from October to December. The hydraulic loading rate of the greywater stream was maintained at 2 L/hr. The hydraulic volume was maintained 2 L initially for the first two months. For the subsequent month, the hydraulic loading rate was held at 1 L/hr. The filter was dosed two times per day with a dosing frequency, $\Delta T= 6$ hours. The hydraulic retention time for the assembly was three minutes and eight seconds. The filter worked efficiently for a period of 80 days. After that, due to the clogging of pores and deposition of material, the filter's efficiency was reduced.

## 3. Results and Discussion
## 3.1 Characterization of Raw Grey Water

Characterization of raw greywater was carried for six months. The parameters like COD, BOD, TSS, turbidity, chlorine content and pH were analyzed. Table 2 represents the average characterization values of different parameters. It was observed that the values of COD, BOD were higher than any of the other studies. The value of TSS remained in a lower range as compared to Katukiza et al. 2014. In addition to this, the turbidity levels were also high while pH varied between the ranges of 6.8-7.8. It is essential to emphasize the significant variation in greywater quality, even when the origin is the same. This wide variation in composition, when significant chemical and physical changes may occur in short periods, is the most significant difficulty in treating greywater (Odeh R. Al-Jayyousi, 2003).

Table 2: Average Monthly Characterization of Grey Water.

| Parameters | Units | July | August | September | October | November | December |
|:---:|:---:|:---:|:---:|:---:|:---:|:---:|:---:|
| pH | - | 7.8 | 7.5 | 7.7 | 6.8 | 7.1 | 7.4 |
| COD | mg/L | 665 | 538 | 632 | 758 | 774 | 831 |
| BOD | mg/L | 303 | 243 | 290 | 276 | 255 | 245 |
| TSS | mg/L | 118 | 339 | 302 | 266 | 223 | 216 |
| TURBIDITY | NTU | 88 | 87 | 98 | 175 | 111 | 133 |
| CHLORINE | mg/L | 372 | 318 | 321 | 403 | 364 | 390 |

## 3.2 Performance and Efficiency of Treatment System

Table 3 shows the various parameters before and after treatment. The parameters evaluated had high values before the application of the treatment procedure. There was a decrease in the investigated parameters' values, which proves that the filter layers were efficient in the treatment. It can also be seen that the generation and characteristics of greywater vary greatly depending upon its source. The variation in the parameters defining greywater also depends on the time of the year, i.e., the greywater parameters vary seasonally. This occurs because of the variation in the temperature, moisture content, microbial growth, etc. There was a significant decrease in the BOD of the greywater samples in winter. The reason for this might be the decreased microbial growth in low temperatures. Even though greywater is less polluted than blackwater, it can still not be reused as it is without any treatment.

Table 3: Changes in various parameters of grey water from different sources after treatment

| Parameters | Units | Kitchen sink | | Laundry | | Wash basin | | Bathing | | Mixed | |
|---|---|---|---|---|---|---|---|---|---|---|---|
| | | Before | After | Before | After | Before | After | Before | After | Before | After |
| pH | - | 7.1 | 6.7 | 8.55 | 7.4 | 8.1 | 7.3 | 7.4 | 7.1 | 7.4 | 6.9 |
| Turbidity | NTU | 298 | 62 | 247 | 52 | 102 | 21 | 209 | 44 | 133 | 28 |
| TSS | mg/L | 717 | 40 | 266 | 15 | 181 | 10 | 256 | 14 | 216 | 12 |
| Chlorine | mg/L | 43 | 21 | 8.9 | 6.9 | 4.6 | 3.2 | 5.4 | 1.1 | 390.5 | 78.4 |
| BOD | mg/L | 998 | 126.9 | 260 | 33.0 | 252 | 32.0 | 215 | 27.3 | 245.4 | 31.2 |
| COD | mg/L | 1038 | 145.5 | 1590 | 222.9 | 424 | 59.4 | 366 | 51.3 | 831.6 | 116.5 |

Table 4 signifies the removal efficiency of the filter layers used. All the filter layers demonstrated a removal efficiency of a minimum 75%. The combined filter unit had a greater removal capacity for TSS 94.44 %. It also depicted 87.28 % and 85.98 % removal efficiency respectively of BOD and COD. The studied treatment system showed improvement in the greywater. The filtration system had a BOD removal efficiency was higher than other treatment systems. Pidou et al. (2008) treated greywater with magnetic ion exchange resins and got BOD removal rate of 83.9%. Further, Lin et al. (2005) performed electrocoagulation and got a BOD removal rate of 60.8%. Most of the estimated results had BOD value less than the studied system. The system also had a COD removal rate of 85.98%, which was higher than Ward's (2000) work, which combined a sand filter and membrane filter and performed disinfection and got a COD removal rate of 72.3%. Murnane et al. (2016) used only woodchips and got a COD removal rate of 77.98%. Techniques like electrocoagulation were also performed by Lin et al. (2005) still the BOD removal rates were low.

Table 4: Removal capacity of different filters.

| Parameters | % removed |
|---|---|
| Biological oxygen demand | 87.28% |
| Chemical oxygen demand | 85.98% |
| Turbidity | 78.94% |
| Total suspended solids(TSS) | 94.44% |
| Chlorine | 79.90% |

However, the turbidity levels showed only a slight decrease compared to other studies as the initial levels were high. Further treatment for the removal of turbidity was required. The filter worked efficiently for 80 days. After that, the pores started blocking in the sand filter, and the efficiency was reduced. In contrast, we are not aware of any reported issues with surface clogging of woodchip media, and it has been estimated that a woodchip filter may be operational for 2-3 years (Ruane et al., 2011). The banana peels can be used efficiently 11 times and can work up to 20 folds, after which they need to be replaced (Renata et al., 2011).

In this particular study, we immediately treated the collected greywater and simultaneously reused it for various applications. But in case if we need to store the collected greywater before and after treatment, then we need to consider the temperature of the greywater since storage temperatures might affect the microbial growth and contamination in it, and the temperature variation might also affect the other parameters (Li F. et al., 2009).

## 3.3 Cost Analysis

This study aimed to develop low-cost greywater recycle unit. And hence, most filter materials used were waste products generated in the house itself. These filter materials, therefore, are free of cost and readily available. The contribution to the system's cost was made only by the container inside which the filter layers are laid. The cost of this PVC container was 2.48 USD. Another addition to the filter price was the cost of the nylon mesh used inside to separate different layers. This nylon mesh of pore size 1mm was priced at 1 USD per meter. A supporting stand was also used to place the filter unit. The cost of this stand was 3.10 USD. Combining the cost of these materials, the overall cost of the system is approximately 5.73 USD. However, the supporting stand is not necessary if a house already has other arrangements to place the filter unit. Hence, the overall cost of the filtration unit is just 2.63 USD.

## 3.4 Applications and Reuse

This treated greywater, by various means, can fulfill the need for water. Not for potable purposes, but using it for various other purposes like gardening, fountains, fire fighting, car washing, etc., can reduce freshwater consumption. This will lead to a more balanced situation. The greywater generated in an individual household can vary with conditions and the number of persons. Figure 2 shows the plan of our greywater treatment and reuse system applied to a single household. Tank 1 offers the fresh water tank, and the blue pipelines represent the freshwater provided to the kitchen sink, washbasin, laundry, and bathing purposes. Separate pipelines have to be installed in the house for the collection of greywater from these individual sources.

The collection of greywater is carried out by gravitational force. The greywater generated is directed towards a tank situated underground called a collection tank, represented by tank 2 in the figure. Black pipelines represent the greywater collection pipes. Following the collection tank, the filtration unit, i.e., tank 3 in the model, has to be installed, which treats the collected greywater as and when required. The filtration unit is situated adjacent to the collection tank. The greywater moves towards the filtration unit through the pipelines. This greywater will then be treated and reused for various purposes, including toilet flushing and other house-works, by employing an attachment of separate pipelines. The water can also be used for gardening purposes in the house. Artificial or imitation fountains can also be supplied treated with greywater. Car washing can waste a large amount of fresh water. Using this treated water for car washing can also help in water conservation and reuse.
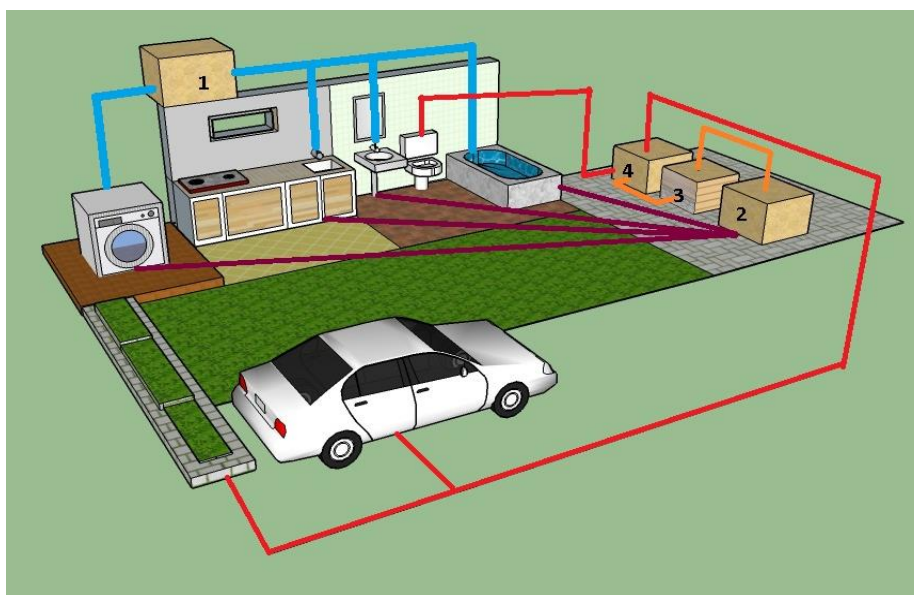
Figure 2: Grey Water Treatment and Reuse Plan.

## 4. Conclusions

From this study, it can be very well demonstrated that a filter unit integrating various filter layers proves to be a useful way of treating in-house generated greywater and using it then and there itself, which reduces the freshwater requirement and saves a significant amount of money and energy. The filter unit described in this study was found to have achieved a COD removal efficiency of 85.98%, BOD removal efficiency of 87.28%, and turbidity, which was reduced by 78.94%, and TSS were decreased by 94.44%. Removal efficiencies are higher than obtained in earlier studies. Even though this system proves to be efficient in treating greywater to levels permissible for its reuse in gardening, fire fighting, etc., it is still not yet fit for human consumption and requires further treatment. This greywater reuse method by masses would ensure a reliable water supply to our future generations. It can be concluded from this study that greywater can be recycled and reused for purposes such as toilet flushing, gardening, car washing, fire fighting, and this practice will lead to a significant reduction in the consumption of freshwater.

**Conflict of interest:** The authors declare that they have no conflict of interest.

**REFERENCES:**

Asano T., 1996. Wastewater Reclamation and Reuse. Technomic Publishing, Lancaster, PA.

Finley S, Barrington S, Lyew D., 2009. Reuse of domestic greywater for the irrigation of food crops. Water Air Soil Pollution.199, 235–245.

Ghaitidak D, Yadav K., 2013. Characteristics and treatment of greywater—a review. Environ SciPollut Res. 20, 2795-2809.

Gisi S., Lofrano G., Grassi M., Notarnicol M., 2016. Characteristics and adsorption capacities of low-cost sorbents for wastewater treatment: A review. Sustainable Materials and Technologies. 9, 10-40.

Gross A, Shmueli O, Ronen Z, Raveh E., 2007. Recycled vertical flow constructed wetland (RVFCW)-a novel method of recycling greywater for irrigation in small communities and households. Chemosphere. 66, 916–923.

Katukiza A.Y., Ronteltap M., Niwagaba C.B., Kansiime F., Lens P.N.L., 2014. Grey water treatment in urban slums by a filtration system: Optimisation of the filtration medium. Journal of Environmental Management. 146, 131-141.

Li F, Wichmann K, Otterpohl R., 2009.Review of technological approaches for grey water treatment and reuse. Science of the Total Environment. 407, 3439-49.

Lin C J, Lo S L, Kuo C Y, Wu C H., 2005. Pilot-scale electrocoagulation with bipolar aluminium electrodes for on-site domestic greywater reuse. J Environ Eng. 131, 491–495.

Murnane JG, Brennan RB, Healy MG, Fenton O., 2016. Assessment of intermittently loaded woodchip and sand filters to treat dairy soiled water. Water Research. 103, 408-415.

Odeh R. Al-Jayyousi, 2003. Greywater reuse: towards sustainable water management. Desalination. 156, 181- 192.

Parjane SB, Sane MG., 2011. Performance of grey water treatment plant by economical way for Indian rural development. Int J Chem Tech Res. 3,1808–1815.

Pidou M, Avery L, Stephenson T, Jeffrey P, Parsons SA, Liu S, Memon FA, Jefferson B., 2008 Chemical solutions for grey water recycling. Chemosphere. 71, 147-155.

Pidou M, Memon FA, Stephenson T, Jefferson B, Jeffrey P., 2007. Greywater recycling: treatment options and applications. Proc. Inst. Civil Eng. 160, 119–131.

Renata S, Ferreira G, Pedro M, Padilha, Margarida J., 2011. Banana Peel Applied to the Solid Phase Extraction of Copper and Lead from River Water: Pre concentration of Metal Ions with a Fruit Waste. Ind. Eng. Chem. Res., 50, 3446–3451.

Ruane EM, Murphy PN, Healy MG, French P, Rodgers M., 2011. On-farm treatment of dairy soiled water using aerobic woodchip filters. Water Res. 45, 6668-6676.

Standard methods for examination of water and wastewater, 21st ed., American Public Health Association (APHA), Washington DC, 2005.

Vakil K, Sharma M, Bhatia A, Kazmi A, Sarkar S., 2014. Characterization of greywater in an Indian middle-class household and investigation of physicochemical treatment using electrocoagulation. Separation and Purification Technology. 130, 160–166.

Wanjiru Evan, Xia Xiaohua, 2018. Sustainable energy-water management for residential houses with optimal integrated grey and rain water recycling. Journal of Cleaner Production. 170, 1151-1166.

Ward M., 2000. Treatment of domestic greywater using biological and membrane separation techniques. MPhil thesis, Cranfield University, UK.

Zuma BM, Tandlich R, Whittington-Jones KJ, Burgess JE., 2009. Mulch tower treatment system Part I: Overall performance in grey water treatment. Desalination. 242,38-56.

# Synthesis and characterization of Fish-Scale-Based Porous Carbon for dye removal

*Suneeta Kumari*

*Department of Chemical Engineering, BIT Sindri, Dhanbad, Jharkhand, 828123*

## ABSTRACT

The wastewater from the dyeing industry has been one of the major sources of many environmental problems. It contains dyes that are harmful to fora and fauna. In particular, some organic dyes and their products can cause mutagenic or carcinogenic effects on human beings. The presence of even very low concentrations of dyes in the effluent is highly visible and undesirable. The effluent also contains residues of reactive dyes and toxic chemicals. Therefore, wastewater with dye contaminations needs to be properly treated before its release into the environment. The main objective of this paper, synthesis of fish scale based activated carbon. The adsorption of dye from aquatic system by the fish–scale based hierarchical lamellar porous carbon was examined. Fish–scale based hierarchical lamellar porous carbon was characterization by X-ray powder diffraction (XRD), Transmission electron microscopy and (TEM). The adsorption capacity of fish -scale based carbon was shown to be better with different pH value.

**Key words:** Carbon, dye, Fish scale and heavy meta

## Introduction

The wastewater from the many industry has been one of the main sources of many environmental issues. It contains dyes and other compounds are harmful to fora and fauna. some organic dyes and their products can also cause mutagenic or carcinogenic effects on human beings. The presence of even very low concentrations of dyes in the effluent is highly visible and undesirable. The effluent also contains residues of reactive dyes and toxic chemicals. Moreover, wastewater with dye contaminations needs to be properly treated before its release into the environment. Hence, last decade in the waste water treatment, activated carbon materials are important due to their significant adsorption ability for waste water treatment. Mostly it is mostly used for adsorption capability with measure to evaluate the property of activated carbon in wastewater treatment. It reflects the quantity of mesopores on the activated carbon surface. Hence, an adsorbent, activated carbon is also treated as catalysts support, energy store in the chemical industry due to their high specific surface, high degree of surface reactivity and variable surface chemistries. Moreover, active carbon materials have high production costs, researchers focus more and more on the development of the alternative and environmentally friendly. It producing cost-effective activated carbon with high adsorption capacity. Some recent studies have concentrated on the agriculture by products like buffing dust, bamboo, counter shell, saw dust and cotton stalks [1].
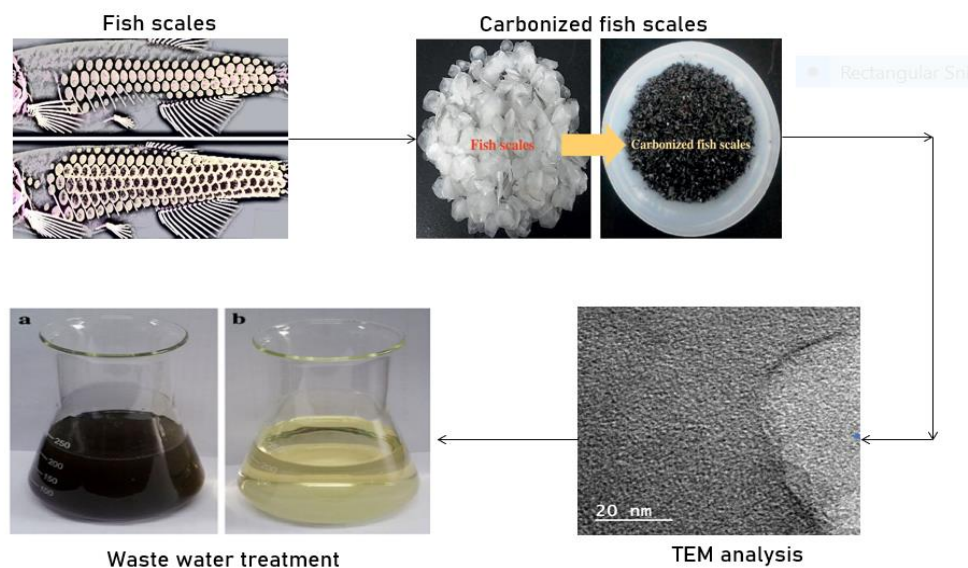
Figure 1. The preparation of activated carbon from fish scales.

Fish scales contains of ash scales are protein and hydroxyapatite. In the carbonization the protein will provide the carbon source while hydroxyapatite serves as a template to form a specific porous structure. Fish-scale-based porous carbon, it has high surface area and lamellar hierarchical structure. The main object of this research article to fish-scale-based hierarchical lamellar porous carbon (FHLC) as an adsorbent to remove the model pollutant [2].

## 2.Materials & methods

Raw fish scale was collected from local market. Cleaned and dry fish scales was percarbonate at 300°C for 3hr in air. The per-carbonized powder was mixed with KOH at a weight ration 1:1 with the presences of N2 atmosphere at 950°C for 1 hr. After the finial products were washed with 5 M HCl with hot deionized water unit the pH value become neutral and then dry in a vacuum oven at 120°C for 24 h to obtained the fish-based carbon. After that sample was by characterized by different characterization techniques.

Aqueous samples were taken from each RO16 solutions at precise time intervals. The concentrations of the RO16 in the supernatant solution before and after adsorption were determined using a double-beam UV–visible spectrophotometer (UV-1700 Shimadzu, Japan) at maximum wavelength, λmax = 493 nm. The percentage removal (%) of RO16 by the CFS adsorbent is described by the following:

$$\text{Removal (\%)} = Co - Co \times 100 \tag{2}$$

where Co and C (mg/l) are the initial and final concentrations of RO16, respectively. The adsorbed amount at equilibrium, qe (mg/g), was computed from the concentration of the dye solution according to following relation:

$$q_e = (Co - Ce)\, V/\, W \tag{3}$$

where Co and Ce (mg/l) are the initial and equilibrium liquid-phase concentrations of RO16, V is the volume of the dye solution (l), and W is the weight of CFS powder (g) [3].

### 3. Characterization of activated carbon

### 3.1 Transmission electron microscope (TEM)

The analyze in details the structure of the microscopic pores, its used transmission electron microscopy (TEM) combined with image analysis. Since the brightness variation of the boundary of pore that appear in the TEM image is very ambiguous, it is difficult to distinguish the boundary of pore.

### 3.2 X-ray powder diffraction (XRD)

XRD has been most widely employed for quantitative analysis. This technique allows researchers to calculate the structural parameters (interplanar distance and crystallite size) of carbon materials directly from their X-ray diffraction patterns, which primarily determine their structure. The interplanar distance is calculated based onthe angles of diffraction peaks, and the crystallite sizes Lc and La can be determined using the angles and full width at half maximum (FWHM) of diffraction peaks. Previous structural analyses of carbon materials using XRD methods can be categorized according to the type of carbon material used, including highly graphitizable and less graphitizable carbon materials. Many studies reported on structural parameters of highly graphitizable carbon materials, as follows: d002 ranges from 3.36 to 3.44 Å, while Lc and La are of some hundreds of Å. Other structural analyses of less graphitizable carbon materials reported that d002 ranged from 3.5 to 5.0 Å, larger than that of highly graphitizable carbon materials, and that Lc and La were very small [1,2]. This structural distinction was reportedly attributed to the use of different starting materials or heat treatment processes [4].

### 4  Results & Discussion

 Characterization of adsorbent

The structure of the microscopic pores, generally used transmission electron microscopic (TEM) combined with images analysis [5]. Since the brightness variation of the boundary of pour that appear in the TEM image is very ambiguous, it is difficult to distinguish the boundary of pores was shown in the Figure 2 [6&7].
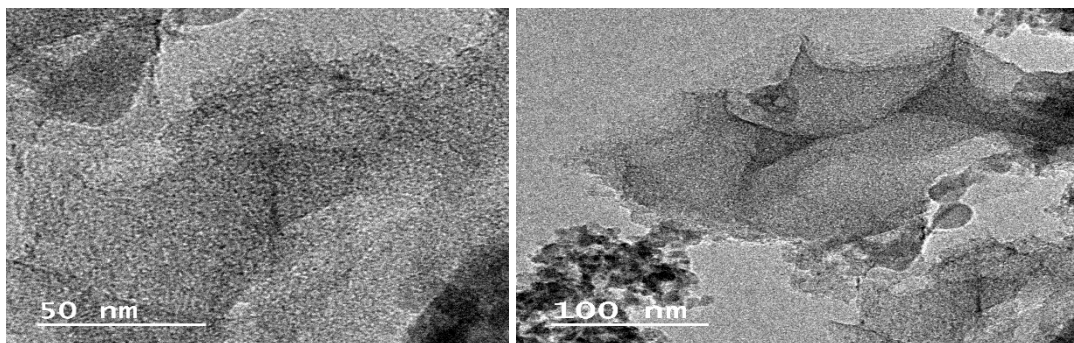


Figure 2. TEM analysis of Fish scale activated carbon.
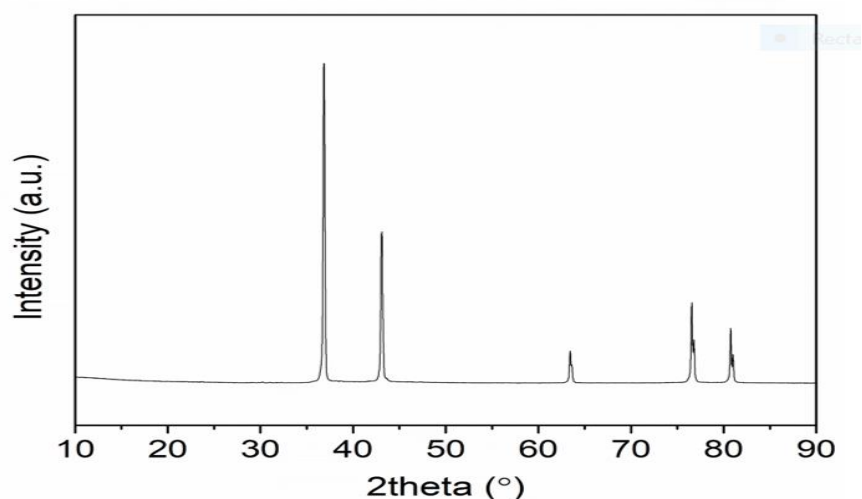
Figure 3. XRD spectra of fish based activated carbon.

The mineral composition and phase purity of the fish scale biochar's were examined by XRD and the diffraction patterns are presented in Figure 3.fish scale biochar at 400 °C exhibits broader peaks, whose peaks are sharper and more intense. This difference may be attributed to the presence of proteins and less complete decomposition of organic matter at 400 °C.

**Conclusion**

The high performance of Fish-scale-based porous carbon for the removal of methylene blue from the aqueous solution has been demonstrated. Their adsorption capacity was shown to be better for dye adsorption at different pH values. The maximum adsorption capacity of the FHLC was 400 mg/g at pH 7.07.

**Refences**

1. Zhe Huang,† Hongyuan Shao,† Bicheng Huang, Chengming Li, Yaqin Huang* and Xiaonong Chen, High-performance fish-scale-based porous carbon for the removal of methylene blue from aqueous solution, Cite this: RSC Adv., 2014, 4, 18737.
2. T. Liu, Y. Li, Q. Du, J. Sun, Y. Jiao, G. Yang and D. Wu, Adsorption of methylene blue from aqueous solution by graphene, Colloids Surf., B, 2012, 90, 197–203.
3. F. Maia, R. Silva, B. Jarrais, A. R. Silva, C. Freire, M. F. R. Pereira and J. L. Figueiredo, Pore tuned activated carbons as supports for an enantioselective molecular catalyst, J. Colloid Interface Sci., 2008, 328, 314–323.
4. B. Liu, H. Shioyama, T. Akita and Q. Xu, Metal-Organic Framework as a Template for Porous Carbon Synthesis, J. Am. Chem. Soc., 2009, 130, 5390–5391.
5. B. H. Hameed, A. T. M. Din and A. L. Ahmad, Adsorption of methylene blue onto bamboo-based activated carbon: Kinetics and equilibrium studies, J. Hazard. Mater., 2007, 141, 819–825.
6. G. Afrane and O. W. Achaw, Effect of the concentration of inherent mineral elements on the adsorption capacity of coconut shell-based activated carbons, Bioresour. Technol., 2008, 99, 6678–6682.

# Bio-sorption of Cu²⁺ ion from wastewater using (Musa acuminata) banana peels

*Felicia O Afolabi[1*], Paul Musonge[1,2], Babatunde F Bakare[3]*

[1]*Institute of Systems Science, Durban University of Technology, Durban, South Africa.*

[2] *Faculty of Engineering, Mangosuthu University of Technology, Durban, South Africa.*

[3]*Department of Chemical Engineering, Mangosuthu University of Technology, Durban, South Africa.*

Corresponding author's email: afolabiomolara1810@gmail.com, telephone: (+27) 748176612

## Abstract

Globally, environmental pollution of water bodies has become a major concern due to increased industrialization and urbanization. Treatment of industrial wastewater is highly essential before discharge into the environment. Bio-sorption has been proven as an efficient method for the treatment of wastewater with a low concentration of metal ions. In this study, the interactive effects of initial metal ion concentration, adsorbent dosage, pH, and particle size were investigated on the removal of copper ions using banana peels in a batch system using the central composite design with response surface methodology (RSM). The banana peels were characterised using FTIR and EDX to obtain the functional groups present on the surface as well as the chemical composition of the bio-sorbent. The optimum condition for the bio-sorption of copper ion gave 92.92 % with an initial concentration of 100 m/L, adsorbent dosage 1g, pH 5 and particle size 75 µm. There was good agreement between the experimental values and the predicted values with a correlation coefficient $R^2$ of 0.9889. The adsorbent dosage and pH had the greatest impact on the bio-sorption process. Ion exchange was suggested as the adsorption mechanism of copper ion bio-sorption using banana peels.

Keywords

Banana peel, Bio-sorption, heavy metals, wastewater, central composite design

## 1. Introduction

Copper is one of the most abundant metals found in municipal and industrial wastewater in South Africa. . High concentrations of $Cu^{2+}$ in public water sources cause undesirable taste and unpleasant odour. Besides, copper ions are released into water bodies through the discharge of untreated industrial effluent. The effects of high-level exposure to copper range from nausea, diarrhoea, vomiting, gastric complications to more severe health issues like liver damage and cancer depending on the period of exposure (Nguyen *et al.* 2013; Salman H. Abbas *et al.* 2014). The excessive exposure of aquatic systems to copper causes damage to the ecosystem which affects the osmoregulatory process of animals. Hence, the United State Environmental Protection Agency (US EPA) has set the discharge limit of copper as 1.3 mg/L while the World Health Organization (WHO) has specified the permissible limit of copper in drinking water as 2 mg/L (Krstić, Urošević and Pešovski 2018; Singh N.B *et al.* 2018). It is therefore important to treat wastewater to a level that it has no adverse effect on plants, animals, and humans.

Different techniques can be used to accomplish the removal of heavy metal ions from wastewater such as; solvent extraction, adsorption, membrane processes, ion exchange, chemical precipitation, reverse osmosis, electrochemical processes (Singh N.B *et al.* 2018) etc. Among these methods, adsorption has been proven lately to be more efficient and cost-effective. Researchers have focused on the use of adsorbents derived from a plant (biological source) for adsorption studies. Bio-sorption is an alternative technique for treating wastewater generated from industrial activities due to ease of operation, low-cost, reduction in chemical usage, minimal sludge production, high efficiency etc. Bio-sorbents derived from agricultural wastes contain functional groups which are obtained from cellulose, hemicellulose, lipids, lignin, hydrocarbons, and starch, thus making these waste efficient for removing several pollutants. Many bio-sorbents such as sugarcane bagasse, moringa pod, orange peels, banana peels, lemon peels, watermelon rind, potato peel etc have been explored for heavy metal removal from wastewater.

Banana is one of the major fruits largely produced and consumed in large quantities. Banana peels are unwanted waste generated from households, food and beverage industries and the marketplace; this waste constitutes 40% by weight of the fresh fruit. Hence, utilization of banana peels for adsorption will not only solve the problem of contaminated water but also reduce environmental pollution thus adding value to banana production. Banana peels have been used by many researchers for the adsorption of heavy metals (Arunakumara, Walpola and Yoon 2013). Cadmium removal from wastewater was carried out using banana peels, the maximum adsorption capacity was 5.91 mg/g (Deshmukh *et al.* 2017), banana peels nano sorbent was used for the removal of radioactive minerals (Oyewo, Onyango and Wolkersdorfer 2016), natural banana peel was used for the removal of fluoride ion from aqueous solution (Mondal 2016), banana peel biochar was used to investigate the adsorption of copper and lead (Amin, Alazba and Shafiq 2017). However, these studies did not account for the interactive effects of the operating parameters.

Many operating parameters influence the adsorption process of a system such as pH, temperature, agitation speed, contact time, initial metal concentration, adsorbent dosage and the particle size of the adsorbent (Pathak Pranav, Mandavgane Sachin and Kulkarni Bhaskar 2015). Most of the studies carried out using banana peels were done in batch mode with the effect of each operating parameter separately considered. Previously, removal of copper from water by adsorption onto banana peels was reported Hossain *et al.* (2012). It is therefore important to study the interactive effect of these operating parameters for the purpose of designing and operating industrial scale treatment plants. Also, optimization of the operating parameters is crucial to enhance the process efficiency, which can be obtained through the application of response surface methodology (RSM). The central composite, Box-Behnken and full three-level factorial designs are the commonly used design of RSM applied in environmental processes. Many studies have been reported on the application of RSM in adsorption processes such as Geyikçi *et al.* (2012), Ghosh, Sinha and Saha (2013), Afolabi, Musonge and Bakare (2021), Madala *et al.* (2015), Nair, Makwana and Ahammed (2014) etc.

This present study, therefore, investigates the interactive effects of operating parameters such as initial metal ion concentration, adsorbent dosage, pH and particle size on the bio-sorption of copper ions from aqueous solution using banana peels. RSM was used to predict and optimize the bio-sorption process of copper ions.

## 2. Materials and method

### 2.1 Bio-sorbent and preparation of the stock solution

The bio-sorbent was prepared according to the procedure followed by (Afolabi, Musonge and Bakare 2021). Copper nitrate trihydrate salt ($Cu(NO_3)_2.3H_2O$) was used for the preparation of the stock solution used in this study. 3.8g of the salt was dissolved in deionized water to make 1000mL solution in a volumetric flask. Then, different concentrations of the metal solution were prepared from the stock solution by dilution. The pH of the solution was adjusted by adding drops of 0.1 M $H_2SO_4$ or 0.1 M NaOH and the value determined by a digital pH meter (HANNA edge$^{pH}$ HI 2002, USA). All the chemicals used were of analytical grade purchased from Analytical Laboratory Supplies Limited, South Africa.

### 2.3 Characterization of bio-sorbent

The bio-sorbent was characterized using Fourier transform infrared (FT-IR) (Perkin Elmer, Waltham, USA) to determine the functional groups present in the bio-sorbent. The energy-dispersive x-ray spectroscopy (EDS) (Evo HD 15, Carlzeiss, Germany) was used to determine the elemental composition of the bio-sorbent.

### 2.4 Experimental method

All the experiments were carried out at room temperature ($27^0C$) with varying operating parameters in a batch mode using a linear shaker. The adsorption experiments were conducted using a conical flask (250mL) containing 100mL of the solution with varying initial conditions; initial concentration of copper ranged from 10 – 100 mg/L, adsorbent dose 0.1 – 1g, solution pH 2 – 6 and particle size 75 – 455 µm. The solution pH was adjusted using 0.1 M $H_2SO_4$ and 0.1 M NaOH, the contact time was 120 min and the agitation speed was set at 180 rpm. After adsorption, the supernatant portion of the solution was filtered using Whatman filter paper (150 mm) thereafter, the filtrate was filtered again using syringe filter (0.45 µm ) and analysed using micro-plasma atomic emission spectrophotometer (MP – AES, MY 18379001, Agilent, USA). The percentage removal of copper ions was determined using equation (1) below.

$$\% \, Removal \, of \, Cu = \frac{(C_0 - C_e)}{C_0} * 100 \qquad (1)$$

Where Co and Ce are the initial and final concentration of $Cu^{2+}$ in the solution (ppm), respectively. The quantity of copper ion adsorbed onto banana peels was determined using the mass balance represented by equation (2).

$$q_e = \frac{(C_0 - C_e)}{m} V \qquad (2)$$

Where $q_e$ is the quantity of copper ion adsorbed at equilibrium (mg/g), V is the volume of the solution (L) and m is the mass of the adsorbent (g).

## 2.5 Adsorption process optimization using central composite design (CCD)

The central composite design with face centred was used for the optimization of copper ion bio-sorption with four variables. CCD is a factorial design comprising of three levels, a centre point, and two axial points. The statistically designed matrix depicting the experimental runs was generated using design expert software (11.1.0.1). The operating parameters are initial concentration ($X_1$), adsorbent dosage ($X_2$), pH ($X_3$) and particle size ($X_4$). These variables were coded in three-levels (-1, 0 and +1) and a total of 30 experimental runs were generated from the CCD design. The levels of the independent variables and the experimental range are represented in Table 1. The optimization of the adsorption process was determined by a second-order polynomial equation stated below (equation 3). The quadratic equation also reflects the influence of the independent variables as well as their interactions.

$$Y = \beta_o + \sum_{i=1}^{k} \beta_i X_i + \sum_{i=1}^{k} \beta_{ii} X_i^2 + \sum_{i=1} \sum_{j=i+1} \beta_{ij} X_i X_j + \in \qquad (3)$$

Where, Y is the yield/response (dependent factor), Xi and Xj are the independent parameters, $\beta_o$, $\beta_i$, $\beta_{ii}$ and $\beta_{ij}$ are the regression coefficient and $\mathcal{E}$ is the residual error (Jaafari and Yaghmaeian 2019). The analysis of variance (ANOVA) was used to explain the significance of the parameters and the correlation of the experimental results. Also, the model equation fitness and the importance of each variable in the model is determined by the F-value and p-value.

**Table 1:** Independent variables levels and experimental range

| Independent Variables | Factor | Range and level | | |
|---|---|---|---|---|
| | | -1 | 0 | +1 |
| Initial metal concentration (mg/L) | X1 | 10 | 55 | 100 |
| Adsorbent dosage (g) | X2 | 0.1 | 0.55 | 1 |
| pH | X3 | 2 | 4 | 6 |
| Particle size (µm) | X4 | 75 | 265* | 455 |

*250 micron was used in the experiment due to available sieve sizes

## 3. Results and discussion

### 3.1 Characterization of the bio-sorbent

3.1.1 Fourier Transform Infrared Spectroscopy (FTIR)

The FTIR is a plot of percentage transmittance against the wavenumber, the wavenumber of banana peels ranges from 4000 cm$^{-1}$ to 500 cm$^{-1}$ (Fig. 1). This analysis is a technique used to determine the functional groups present on the surface of a bio-sorbent before and after the adsorption process. Besides, this method reveals the changes in the peaks of the functional groups and their impacts on the adsorption process. The FTIR analysis of banana peels before adsorption revealed the availability of hydroxyl group (O-H), which comprise alcohols and phenols. The O-H is attributed to a broad absorption peak at 3333.62 cm$^{-1}$ with percentage transmittance of 80.62 %. The peaks representing alkyl group (C-H) are 2918.92 cm$^{-1}$, 2850.97 cm$^{-1}$, 1441.94 cm$^{-1}$, 1374.74 cm$^{-1}$ and 887.26 cm$^{-1}$. These peaks are regarded as alkanes which shows substitution bond. The carboxylic group (C=O) and carbonyl group (C=C) are depicted by the peaks at 1734.38 cm$^{-1}$ and 1607.04 cm$^{-1}$ respectively (Afolabi, Musonge and Bakare

2021). These are unsaturated hydrocarbon groups consisting of conjugated anhydride and ketones.

After copper adsorption, significant shifts were observed in the peaks of the functional groups which affected the transmittance and wavenumber accordingly. There was major shift in the broad peak representing the hydroxyl group after adsorption. The wavenumber of 3333.62cm$^{-1}$ and percentage transmittance of 80.63 % of banana peels before adsorption shifted to 3295.27 cm-1 with percentage transmittance of 90.02 %. Others peaks that were modified are; 2918.92 cm-1 (74.79 %), 2850.97 cm-1 (76.63 %), 1734.83 cm-1 (85.62 %), 1607.04 cm$^{-1}$ (79.09%), 1441.94 cm$^{-1}$ (79.80 %), 1374.74 cm$^{-1}$ (78.40%), 1029.61 cm$^{-1}$ (59.69%) and 887.26 cm$^{-1}$ (76.69%) before adsorption shifted to 2918.36 cm$^{-1}$ (87.87%), 2851 cm$^{-1}$ (90.125%), 1732.5 cm$^{-1}$ (91.83%), 1615.57 cm$^{-1}$ (88.18%), 1443.2 cm$^{-1}$ (89.135%), 1374.4 cm$^{-1}$ (87.87%), 1030.28 cm$^{-1}$ (76.50%) and 885.92 cm$^{-1}$ (85.1%) respectively after adsorption.
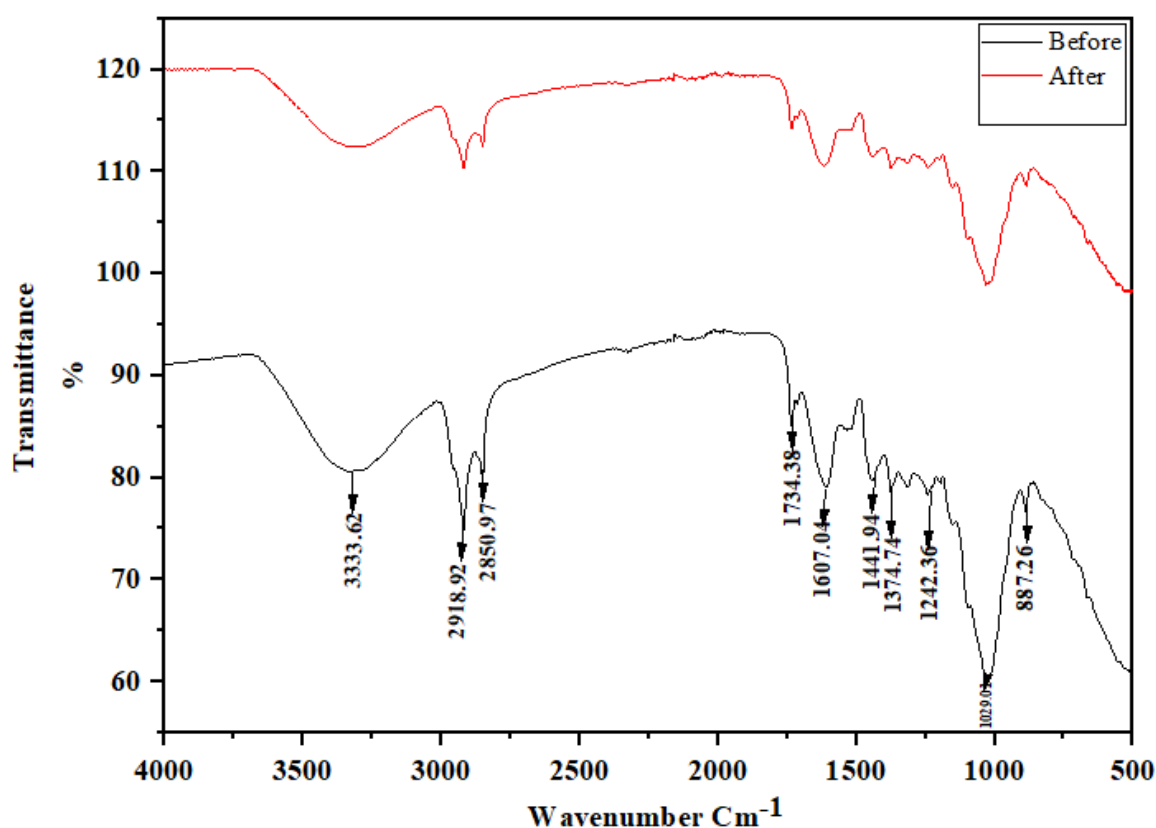


**Fig. 1:** FTIR of banana peels before and after adsorption

3.1.2 Energy Dispersive X-ray (EDX) analysis

The EDX of natural banana peels and banana peels loaded with $Cu^{2+}$ is shown in (Fig. 2). The EDX is a semi-quantitative graph which reveals the elemental composition of the adsorbent before and after adsorption as shown in Table 2. The composition of natural banana peels showed a high percentage of carbon and oxygen with a little amount of other metals (silicon and potassium). After adsorption, banana peels loaded with $Cu^{2+}$ showed the presence of carbon, oxygen, silicon and $Cu^{2+}$ ions (Fig. 2b). There were significant changes in the

compositions of carbon, oxygen, and silicon after adsorption which suggest that the carboxyl and hydroxyl functional groups present on the surface of the bio-sorbent played a major role in the adsorption of $Cu^{2+}$ while silicon also participated in ion exchange as there was a reduction in its composition after adsorption. Furthermore, the potassium in the bio-sorbent before adsorption disappeared after adsorption and was replaced with $Cu^{2+}$. This suggests ion exchange between the $Cu^{2+}$ in the solution and the potassium ion present on the surface of the bio-sorbent. Therefore, ion exchange is identified as the adsorption mechanism of $Cu^{2+}$ bio-sorption.
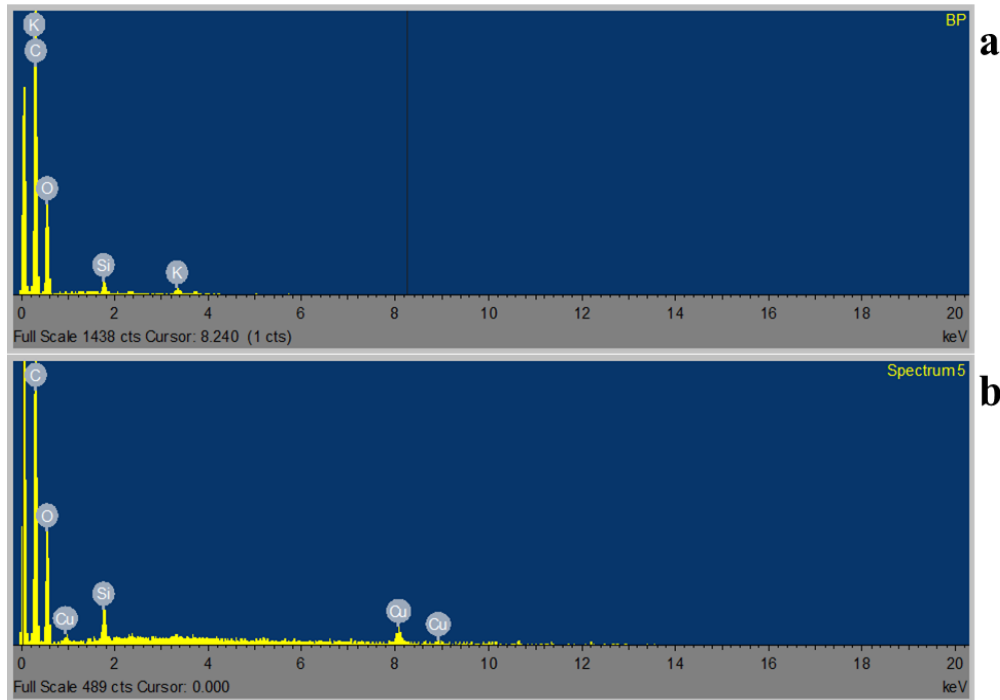


**Fig. 2:** Energy dispersive x-ray (a) natural banana peels (b) banana peels loaded with $Cu^{2+}$.

**Table 2:** Elemental composition of banana peels before and after adsorption

| Element | C | O | Si | K | Cu |
|---------|-------|-------|------|------|------|
| Before (%) | 56.43 | 38.22 | 4.74 | 0.61 | - |
| After (%) | 58.99 | 37.81 | 0.68 | - | 2.52 |

## 3.2 Experimental design

Table 3 depicts the design matrix and the response for $Cu^{2+}$ ion percentage removal. The second-order polynomial was used to express the percentage removal of $Cu^{2+}$ ion with the specified four design variables. The regression model specifies the significant variables obtained for the response ($Y_{Cu}$, %) written as a function of coded variables; initial concentration (A), adsorbent dosage (B), pH (C) and particle size (D) as stated in Equation (4).

$$Y_{Cu} = 93.35 + 6.07B + 5.76C - 0.9533D + 2.25AB + 3.46AD - 4.08BC + 1.55BD - 2.81CD + 3.76A^2 - 4.32B^2 - 4.69C^2 - 5.93D^2 \tag{4}$$

**Table 3:** Experimental design matrix with coded factors and responses

| Std | Run no | Variables | | | | Responses | |
|---|---|---|---|---|---|---|---|
| | | | | | | Cu removal (%) | |
| | | A | B | C | D | $Y_{exp}$ | $Y_{pred}$ |
| 8 | 1 | 100 | 1 | 6 | 75 | 92.65 | 91.84 |
| 28 | 2 | 55 | 0.55 | 4 | 250 | 94.20 | 93.39 |
| 18 | 3 | 100 | 0.55 | 4 | 250 | 98.12 | 97.42 |
| 30 | 4 | 55 | 0.55 | 4 | 250 | 92.80 | 93.39 |
| 5 | 5 | 10 | 0.1 | 6 | 75 | 96.25 | 96.05 |
| 11 | 6 | 10 | 1 | 2 | 455 | 85.50 | 84.06 |
| 7 | 7 | 10 | 0.1 | 6 | 75 | 91.71 | 92.44 |
| 16 | 8 | 100 | 1 | 6 | 455 | 94.52 | 94.34 |
| 13 | 9 | 10 | 0.1 | 6 | 455 | 80.10 | 78.51 |
| 14 | 10 | 100 | 0.1 | 6 | 455 | 81.67 | 82.75 |
| 19 | 11 | 55 | 0.1 | 4 | 250 | 82.21 | 83.11 |
| 20 | 12 | 55 | 1 | 4 | 250 | 94.78 | 95.01 |
| 2 | 13 | 100 | 0.1 | 2 | 75 | 59.95 | 60.43 |
| 6 | 14 | 100 | 1 | 6 | 75 | 86.05 | 86.46 |
| 17 | 15 | 10 | 0.55 | 4 | 250 | 95.04 | 96.87 |
| 29 | 16 | 55 | 0.55 | 4 | 250 | 92.98 | 93.39 |
| 9 | 17 | 10 | 0.1 | 2 | 455 | 63.55 | 65.17 |
| 3 | 18 | 10 | 1 | 2 | 75 | 84.51 | 84.17 |
| 27 | 19 | 55 | 0.55 | 4 | 250 | 92.96 | 93.39 |
| 1 | 20 | 10 | 0.1 | 2 | 75 | 72.38 | 71.47 |
| 4 | 21 | 100 | 1 | 2 | 75 | 81.57 | 82.13 |
| 15 | 22 | 10 | 1 | 6 | 455 | 80.80 | 81.10 |
| 21 | 23 | 55 | 0.55 | 2 | 250 | 81.85 | 82.71 |
| 12 | 24 | 100 | 1 | 2 | 455 | 94.91 | 95.86 |
| 23 | 25 | 55 | 0.55 | 4 | 75 | 88.30 | 88.38 |
| 26 | 26 | 55 | 0.55 | 4 | 250 | 95.01 | 93.39 |
| 10 | 27 | 100 | 0.1 | 2 | 455 | 69.75 | 67.96 |
| 24 | 28 | 55 | 0.55 | 4 | 455 | 85.41 | 86.47 |
| 22 | 29 | 55 | 0.55 | 6 | 250 | 94.41 | 94.68 |
| 25 | 30 | 55 | 0.55 | 4 | 250 | 95.78 | 93.39 |

## 3.3 Analysis of variance and model validation

Analysis of variance (ANOVA) gives information on the accuracy of the fit and its significance. The ANOVA was used to evaluate the model equation, which showed that the regression model is statistically significant. Table 4 and 5 present the ANOVA and the model variables as predicted by the quadratic model for copper bio-sorption ($Y_{Cu}$). The F-value and p-values were used to check the significance of the coefficient of each variable. The F-value compares the model variance with the residual error. In this case, the F-value for copper bio-

sorption is 92.59, which implies that the model is significant. The lack-of-fit is obtained from pure error and the residuals. The lack-of-fit F-value of 1.55 implies that the lack-of-fit is not significant relative to the pure error. A factor with a p-value less than 0.05 suggests significant model terms. In this case, B, C, D, AB, AD, BC, BD, CD, $A^2$, $B^2$, $C^2$ and $D^2$ are the significant model terms. The initial concentration (A) is the only first-order main effect term which is not significant and the interactive effect (AC). This suggests that the interaction of initial concentration with other process parameters except pH have a significant influence on the adsorption process.

The validity of the mathematical model fitness was evaluated by the comparison between the predicted values and the actual values, as depicted in Fig. 3. The coefficient of determination ($R^2$) for the relationship between the actual and predicted values for the bio-sorption efficiency of copper gave 0.9889. The value of $R^2$ close to 1 is desirable and shows a high level of agreement between the experimental values and the predicted values derived from the regression model.

**Table 4:** ANOVA for the regression model of copper bio-sorption

| Copper ion | Model variable (coded) | Coefficient value | Standard error | F-value | p-value |
|---|---|---|---|---|---|
| Cu | Intercept | 93.35 | 0.4541 | | <0.0001 |
| | B | 6.07 | 0.3434 | 312.64 | <0.0001 |
| | C | 5.76 | 0.3434 | 281.76 | <0.0001 |
| | D | -0.9533 | 0.3434 | 7.71 | 0.0141 |
| | AB | 2.25 | 0.3642 | 38.15 | <0.0001 |
| | AD | 3.46 | 0.3641 | 90.23 | <0.0001 |
| | BC | -4.08 | 0.3642 | 125.39 | <0.0001 |
| | BD | 1.55 | 0.3641 | 18.12 | 0.0007 |
| | CD | -2.81 | 0.3641 | 59.46 | <0.0001 |
| | $A^2$ | 3.76 | 0.9050 | 17.27 | 0.0008 |
| | $B^2$ | -4.32 | 0.9050 | 22.83 | 0.0002 |
| | $C^2$ | -4.69 | 0.9050 | 26.84 | 0.0001 |
| | $D^2$ | -5.93 | 0.9111 | 42.30 | <0.0001 |

**Table 5:** Validation of the model

| Metal ion | Source | Sum of squares | Degree of freedom df | Mean square | F-value | p-value |
|---|---|---|---|---|---|---|
| Cu | Model | 2825.07 | 14 | 95.09 | 92.59 | <0.0001 |
| | Residual | 31.83 | 15 | 2.12 | | |
| | Cor. Total | 2856.90 | 29 | | | |
| | Lack of fit | 24.05 | 10 | 2.41 | 1.55 | 0.3294 |

| | | | |
|---|---|---|---|
| Pure error | 7.78 | 5 | 1.55 |
| $R^2$ | 0.9889 | | |
| Adjusted $R^2$ | 0.9785 | | |
| Predicted $R^2$ | 0.9400 | | |
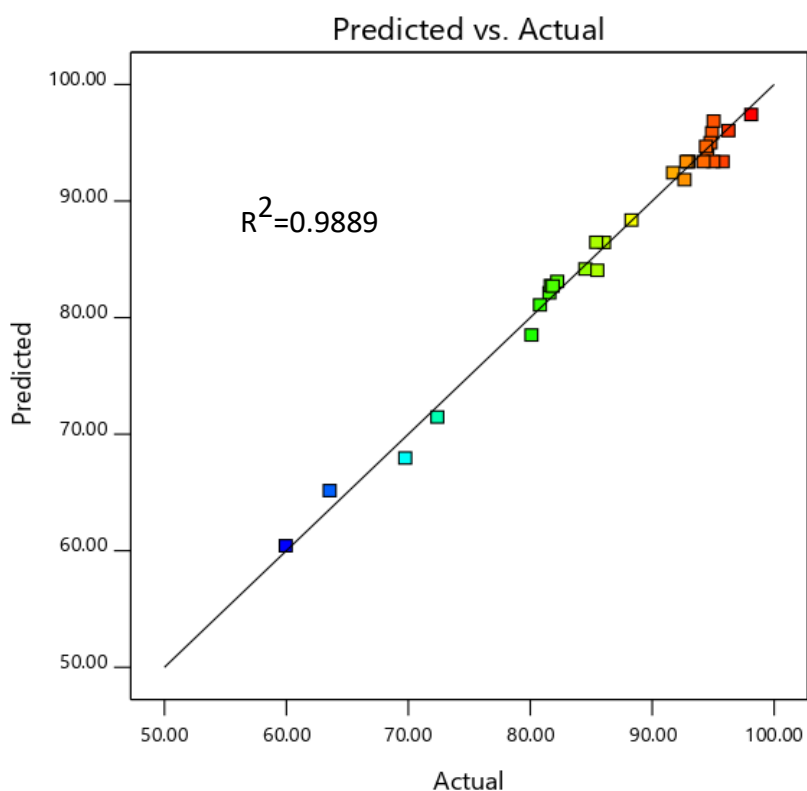


**Fig.3:** Plot of actual data (%) vs predicted data (%) by RSM for $Cu^{2+}$ bio-sorption.

### 3.4 Effect of initial concentration, adsorbent dosage, pH and particle size on $Cu^{2+}$ bio-sorption.

The experimental results showed that the highest percentage removal of 98 % was obtained at the highest concentration of 100 mg/L and a pH of 4. In this study, adsorbent dosage and the solution pH had a greater impact on the bio-sorption of $Cu^{2+}$ ions. At lower pH, the percentage removal of $Cu^{2+}$ was low which suggests that hydrogen, $H^+$ and hydronium ion, $H_3O^+$ were dominant on the active sites of banana peel. The effects of initial concentration, adsorbent dosage, pH and the particle size were explained by 3-Dimensional surface plot represented in Fig.4. Fig.4a shows the plot of initial concentration against adsorbent dosage with corresponding percentage removal of $Cu^{2+}$. The percentage removal of $Cu^{2+}$ increased with increasing adsorbent dosage which implies that the active sites on the bio-sorbent increased with increasing dosage. However, the percentage removal of $Cu^{2+}$ slightly increased when the initial concentration increased from 10 to 80 mg/L and increased significantly from 80 to 100

mg/L. In Fig. 4b, the simultaneous effect of initial concentration and pH with percentage removal of $Cu^{2+}$ was illustrated. The percentage removal increased with increasing pH and the highest removal efficiency of 98% was achieved at pH range 4 - 5.5 while the highest removal occurred at 100 mg/L. From Fig 4c, the percentage removal increased as the initial concentration increased. The interaction between the initial concentration and the particle size was significant. Similarly reported by (Afolabi, Musonge and Bakare 2021).

Fig. 4d shows the interactive effect of adsorbent dosage and pH on the percentage bio-sorption of $Cu^{2+}$. The percentage removal increased with increasing adsorbent dosage and pH. This result is significant because lower amounts of bio-sorbent mean smaller active sites. Fig. 4e depicts the interaction between the adsorbent dosage and the particle size. The graph shows that the percentage removal decreased with increased particle size while it increased with increasing adsorbent dosage. However, the maximum bio-sorption capacity of $Cu^{2+}$ was reached with a particle size between 250 – 360 microns. Finally, Fig. 4f shows the interactive effect between the adsorbent dosage and pH. At a low particle size, the bio-sorption efficiency increased with increasing pH. However, the graph shows a saddle point which suggests that the maximum bio-sorption capacity is in between a maximum and minimum point. In conclusion, from Fig(a-f) the adsorbent dosage and pH followed by particle size had a greater influence on the bio-sorption of $Cu^{2+}$ using natural banana peels.
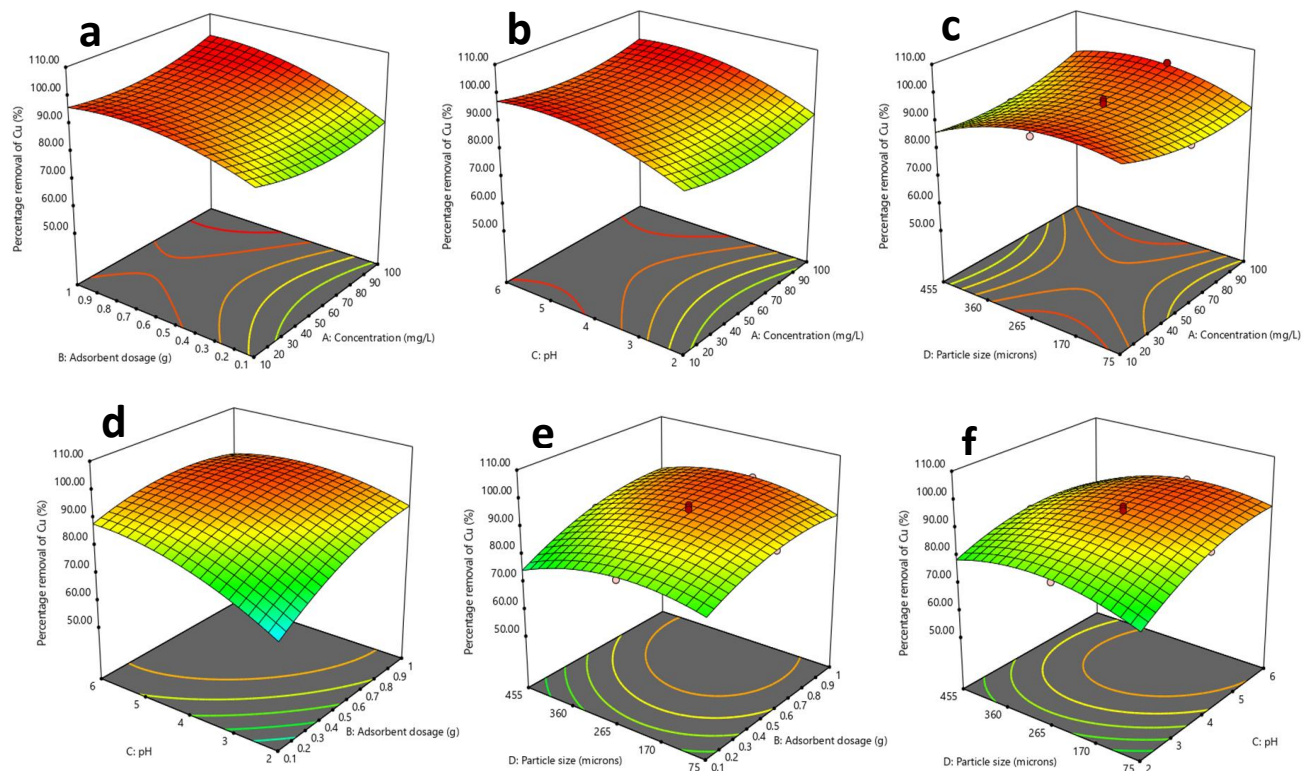


**Fig. 4:** 3D response surface plot showing interaction between operating parameters (a) initial concentration and adsorbent dosage (b) initial concentration and pH (c) initial concentration and particle size (d) adsorbent dosage and pH (c) adsorbent dosage and particle size (f) pH and particle size.

## 3.5 Optimization of process variables for the bio-sorption of $Cu^{2+}$ ion.

The goal of optimization is to predict the optimal conditions of the process variables for the bio-sorption of $Cu^{2+}$ ion using banana peels. The aim is to maximize the removal efficiency of the heavy metal ion to obtain the highest optimal bio-sorption value. The application of a desirability function helps to determine the most suitable conditions for a particular system (Witek-Krowiak *et al.* 2014). The desirability functions di ranges from di=0 for an unacceptable value to di=1 for an acceptable value.

The obtained optimized process variable conditions for the bio-sorption of $Cu^{2+}$ ion using banana peels gave 92.92% with an initial concentration of 100 mg/L, adsorbent dosage of 1g, pH 5 and particle size of 75 microns. The desirability of the above conditions gave 1.000 which suggests that the optimum condition is reasonably acceptable.

## 3.6 Mechanism of Copper ion bio-sorption

The bio-sorption mechanism of $cu^{2+}$ ion using banana peels was influenced by the combined effect of the process variables to obtain maximum bio-sorption efficiency. The characterization of banana peels before and after adsorption using FTIR showed the presence of functional groups on the surface of the bio-sorbent, however, there were significant shifts in the peaks of the functional groups after adsorption which suggests that the functional groups (OH and COOH) are responsible for the bio-sorption of copper ion. Also, the EDX graph in Fig. 2(a and b) showed the presence of potassium ion ($K^+$) on the surface of banana peels before adsorption which, disappeared after adsorption. This reveals that there was an exchange of ions between the copper ion in the aqueous solution and the ions present on the surface of the bio-sorbent.

## 3.7 Pareto chart

The Pareto chart depicts the coefficient of all the variables present in the model equation. The influences of the main variables, their interactive effects, and the quadratic terms on the percentage efficiency of $Cu^{2+}$ bio-sorption are illustrated in the graph (Fig.5). It can be concluded from Fig.5 that the adsorbent dosage (B) had the greatest influence on the bio-sorption process. The percentage removal of copper ion increased with increasing adsorbent dosage. Also, the pH of the solution (C) is significant. The quadratic term $D^2$, $C^2$, $B^2$ and $A^2$ are also significant as any changes in their coefficient value will affect the percentage removal of Cu. The interactive factors BC, AD, CD and AB also influenced the bio-sorption process.
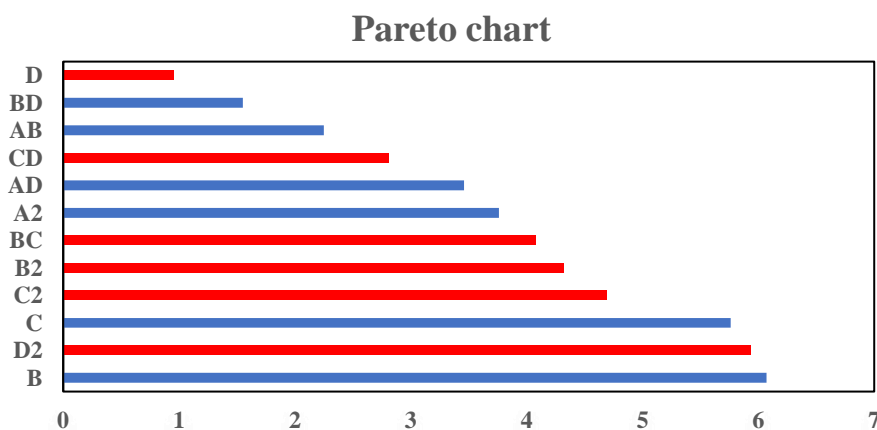


**Fig. 5:** Pareto chart of model parameters

## 4. Conclusion

The present study reports on the efficiency of banana peels in copper ion removal from wastewater using response surface methodology with the central composite design statistical analysis. The influence of operating parameters, initial metal concentration, adsorbent dosage, pH and particle size were investigated. The results showed that the central composite design can be successfully used for the modelling and optimization of the process parameters and interaction of the responses. The removal efficiency of copper ions increased with increasing adsorbent dosage and the solution pH. The quadratic regression model was validated using the ANOVA statistical analysis and the error between the observed value and predicted value obtained was in the range of 0.1 – 2.5%.

The FTIR revealed the presence of hydroxyl and carboxyl groups which enhance the bio-sorption of the metal ions. At high pH value, acidic groups (OH and COOH) on the surface of the bio-sorbent are deprotonated and the surface of the bio-sorbent becomes negatively charged. Hence, adsorption of copper ion occurs by the electrostatic attraction which occurred between the metal ion in solution and the surface of the bio-sorbent. Besides, the absence of potassium ion on the surface of bio-sorbent after adsorption also suggested ion exchange as the adsorption mechanism.

## Acknowledgements

## Conflict of interest

The authors declare no conflict of interest.

## References

Afolabi, F. O., Musonge, P. and Bakare, B. F. 2021. Evaluation of Lead (II) Removal from Wastewater Using Banana Peels: Optimization Study. *Polish Journal of Environmental Studies*, 30 (2): 1-10.

Amin, M. T., Alazba, A. A. and Shafiq, M. 2017. Removal of Copper and Lead using Banana Biochar in Batch Adsorption Systems: Isotherms and Kinetic Studies. *Arabian Journal for Science and Engineering*, 43 (11): 5711-5722.

Arunakumara, K., Walpola, B. C. and Yoon, M.-H. 2013. Banana Peel: A Green Solution for Metal Removal from Contaminated Waters. *Korean Journal of Environmental Agriculture*, 32 (2): 108-116.

Deshmukh, P. D., Khadse, G. K., Shinde, V. M. and Labhasetwar, P. 2017. Cadmium Removal from Aqueous Solutions Using Dried Banana Peels as An Adsorbent: Kinetics and Equilibrium Modeling. *Journal of Bioremediation & Biodegradation*, 08 (03): 395.

Geyikçi, F., Kılıç, E., Çoruh, S. and Elevli, S. 2012. Modelling of lead adsorption from industrial sludge leachate on red mud by using RSM and ANN. *Chemical Engineering Journal*, 183: 53-59.

Ghosh, A., Sinha, K. and Saha, P. D. 2013. Central composite design optimization and artificial neural network modeling of copper removal by chemically modified orange peel. *Desalination and Water Treatment*, 51 (40-42): 7791-7799.

Hossain, M., Ngo, H. H., Guo, W. and Nguyen, T. 2012. Removal of copper from water by adsorption onto banana peel as bioadsorbent. *International Journal of Geomate*, 2 (2): 227-234.

Jaafari, J. and Yaghmaeian, K. 2019. Optimization of heavy metal biosorption onto freshwater algae (Chlorella coloniales) using response surface methodology (RSM). *Chemosphere*, 217: 447-455.

Krstić, V., Urošević, T. and Pešovski, B. 2018. A review on adsorbents for treatment of water and wastewaters containing copper ions. *Chemical Engineering Science*, 192: 273-287.

Madala, S., Mudumala, V. N. R., Vudagandla, S. and Abburi, K. 2015. Modified leaf biomass for Pb(II) removal from aqueous solution: Application of response surface methodology. *Ecological Engineering*, 83: 218-226.

Mondal, N. K. 2016. Natural Banana (Musa acuminate) Peel: an Unconventional Adsorbent for Removal of Fluoride from Aqueous Solution through Batch Study. *Water Conservation Science and Engineering*, 1 (4): 223-232.

Nair, A. T., Makwana, A. R. and Ahammed, M. M. 2014. The use of response surface methodology for modelling and analysis of water and wastewater treatment processes: a review. *Water Science and Technology*, 69 (3): 464-478.

Nguyen, T. A. H., Ngo, H. H., Guo, W. S., Zhang, J., Liang, S., Yue, Q. Y., Li, Q. and Nguyen, T. V. 2013. Applicability of agricultural waste and by-products for adsorptive removal of heavy metals from wastewater. *Bioresource Technology*, 148: 574-585.

Oyewo, O. A., Onyango, M. S. and Wolkersdorfer, C. 2016. Application of banana peels nanosorbent for the removal of radioactive minerals from real mine water. *J Environ Radioact*, 164: 369-376.

Pathak Pranav, D., Mandavgane Sachin, A. and Kulkarni Bhaskar, D. 2015. *Fruit peel waste as a novel low-cost bio adsorbent*. Available: https://www.degruyter.com/view/j/revce.2015.31.issue-4/revce-2014-0041/revce-2014-0041.xml (Accessed 2018-08-09t06:05:05.65+02:00).

Salman H. Abbas, Ibrahim M. Ismail, Tarek M. Mostafa and Sulaymon, A. H. 2014. Biosorption of heavy metals: A review. *Journal of Chemical Science and Technology*, 3 (4): 74 - 102.

Singh N.B, Nagpal Garima, Agrawal Sonal and Rachna. 2018. Water purification by using Adsorbents: A review. *Environmental Technology and Innovation*, 11: 187-240.

Witek-Krowiak, A., Chojnacka, K., Podstawczyk, D., Dawiec, A. and Pokomeda, K. 2014. Application of response surface methodology and artificial neural network methods in modelling and optimization of biosorption process. *Bioresource Technology*, 160: 150-160.

# Biosorption of Fe (II) from wastewater using natural and alkali- modified sugarcane bagasse

N.L.G. Ndebele[1], P. Musonge[2] and B.F. Bakare[1].

[1] Department of Chemical Engineering, Mangosuthu University of Technology, Durban, South Africa.

[2] Faculty of Engineering, Mangosuthu University of Technology, Durban, South Africa.

[1]Corresponding author: ndebele.lindi@mut.ac.za

## Abstract

In this study, adsorption capacities of unmodified and modified sugarcane bagasse for the removal of Fe (II) from wastewater was investigated in batch experiments. Sugarcane comprises of cellulose, hemicellulose and lignin. To determine the adsorptive performance of the natural and de-lignified bagasse, sugarcane bagasse was modified by removing lignin in varying degress. In addition to the effect of the removal of lignin on the adsorption process the study also aims at the prospects of valorizing lignin. Removal of lignin which is an aromatic macromolecule is used widely as a raw material in agriculture, forestry and construction. The natural bagasse was modified using varying concentrations of sodium hydroxide, i.e.0.5% NaOH to 2.5% NaOH. It was observed that modification using sodium hydroxide showed better adsorption performance. The operational parameters investigated in this study to compare the performance of natural and modified sugar bagasse on the Fe (II) removal efficiency, were initial concentration, pH, contact time and adsorbent dose. The Langmuir and Freundlich kinetic isotherms were used to study the adsorption mechanisms. A good correlation coefficient (>0.95) was obtained using Langmuir isotherm for both the natural and modified sugarcane bagasse.

*Keywords***: Chemical Pretreatment; Sugarcane bagasse; Heavy metals, Cellulose; lignin**

# 1. Introduction

Industrial effluents containing non-biodegradable heavy metals are a major source of wastewater contamination. If these are left untreated, they could cause severe environmental problems and a variety of physiological and neurological damage to human health (Mohan & Sreelakshmi, 2008). According to (Babarinde, et al., 2006) heavy metals are those elements with atomic density greater than 5g/cm$^3$. Due to problems caused by these heavy metals, regulatory laws have been developed by the World Health Organisation (WHO) which stipulates the allowable concentration of these metals in wastewater as well as in drinking water. According to South African National Standard (SANS), the allowable concentration of (Fe (II) in wastewater and drinking water should be less than 0.3 and 0.04 mg/L, respectively. Above these concentrations of Fe (II), stipulated by WHO, Fe (II) becomes a toxic persistent bio-accumulative heavy metal. The sources of Fe pollution include galvanizing, copper plating, primer paints corrosion inhibitors in boiling and cooling systems. The consequence of drinking Fe-contaminated water may lead to liver, heart, pancreatic damages as well as diabetes. It is, therefore, of great importance to treat metal-contaminated wastewater prior to discharge to the environment as there are still communities who depend on water obtained from rivers, dams, boreholes for domestic use (Trgo, et al., 2011) .

Various conventional methods are currently used to remove these toxic heavy metals from wastewater. These methods include chemical precipitation, lime coagulation, solvent extraction, membrane filtration, reverse osmosis, ion exchange and adsorption on activated carbon. However, these method are disadvantaged by their high cost, high reagent and energy requirement (Balci, et al., 2011). Another disadvantage, according to (Fu & Wang, 2011), is that determination of optimum removal conditions  for the wastewater containing heavy metals can be complicated since the effectiveness of each conventional method depends on a number of  parameters. Therefore, due to these disadvantages, the development of efficient, low cost and eco-friendly technology to reduce these metals in wastewater is of great importance. Recently much focus has shifted to the use of agricultural biomass (lignocelluloses) as biosorbents, these biosorbents include eggshells and sugarcane bagasse (Harripersadth, et al., 2020), banana peels (Afolabi, et al., 2021). Biosorption is the process of rapid and reversible binding of ions from the aqueous solution onto the functional groups present on the surface of the biomass. The competiveness, effectiveness, low cost, low energy consumption, availability of agricultural biomass has made the biosorption

process to be a more viable alternative for the removal of these toxic metals (Ndlovu, et al., 2013). There are many agricultural biomasses that have been successfully used to remove toxic heavy metals, these biomasses include banana peels, orange peels, eggshells, rice husk (Afolabi, et al., 2021; Harripersadth, et al., 2020). Although biosorption is considered as an efficient process, it is also affected by many factors such as the temperature, characteristics of biomass, surface area to volume ratio, pH, biomass concentration, metal ion concentration and metal affinity to the biosorbents.

In this study, sugarcane bagasse was used as a biosorbent, in its natural as well as modified form, remove Fe (II) from waste water using the biosorption process. Sugarcane is a lignocellulosic tropical, perennial grass of the genus Saccharum, tribe Andropogoneae and grass family Poaceae. This lignocellulosic material contains cellulose, lignin and hemicellulose and its biological component polymers makes sugarcane bagasse rich in functional groups such as hydroxyl, phenolic, carbonyl and carboxylic groups. In a biosorption process, surface area is one of the major factors affecting the performance of the absorbent/adsorption capacity (Brigida, et al., 2010). When a biosorbent is used in the removal of heavy metals in wastewater, the rate of adsorption highly depends on the available surface area and therefore the greater the surface area accessible to the metal, the greater the adsorption capacity. According to (Brigida, et al., 2010) the adsorption capacity of the lignocellulosic material can be increased by physical or chemical modification of the biosorbents. When (Harripersadth, et al., 2020) used sugarcane bagasse in its natural form to remove Lead and Cadmium from wastewater, it was discovered that the maximum monolayer adsorption capacity of Pb and Cd removal using were found to be 31.45 mg/g for Pb and 19.49 mg/g for Cd. Lignin, a macromonomer, acts as a gluing substance that binds cellulose and hemicellulose fibers together. Therefore, removing this macromonomer (by chemical pretreatment) results in sugarcane bagasse bundles dismantling thus leading to an increased surface area, which in turn leads to increased adsorption capacity. Lignin is widely used as a raw material in the agriculture, forestry and construction industries (Luo, et al., 2010). According to (Rezende, et al., 2011), alkali pretreatments lead to the disruption of lignocellulosic cell walls of the biosorbent which dissolves hemicellulose, lignin and silica by hydrolyzing uronic and acetic acid and swelling cellulose. Degradation of lignin is attributed to the cleavage of the α-aryl ether bonds from its phenolic monomer (Jackson, 1977) while swelling of the cellulose is due to the weakening of the hydrogen bonds. Literature reveal that there has been a number of alkali modification i.e.

calcium hydroxide, sodium carbonate, ammonium hydroxide, that has been explored but sodium hydroxide (NaOH) presented the greatest degradation of lignin (Rodriquez-Vazquez & Diaz-Cervantes, 1994). A study done (Rodriquez-Vazquez & Diaz-Cervantes, 1994) used a 0.2g sodium hydroxide per pith gram to pretreat the pith of component of the sugarcane bagasse. This study yielded a maximum digestibility of lignin of 71% at 92℃. (Rezende, et al., 2011) also discovered that pretreatments using NaOH concentrations above 2% did not result in further removal of lignin.

The overall aim of this study was to evaluate the performance and to understand the biosorption mechanism of the natural and modified forms of the sugarcane bagasse in removing Fe (II) from wastewater. Modification of sugarcane bagasse in this study solely focused on removing lignin using different concentrations of sodium hydroxide.

In order to achieve the overall aim of this study, evaluation of the performance of the sugarcane bagasse (natural and modified) by varying the amount of the biosorbent, pH, metal concentration and contact time.

## 2. Material and methods

### 2.1 Material

The reagents used in the current study were pure sodium hydroxide (NaOH) pellets, 98% Sulphuric acid purchased from Laboratory Supplies. An appropriate amount of Sulphate salt of $FeSO_4.7H_2O$ was added to 1000mL of de-ionized water and was diluted to obtain required concentrations. Sugarcane bagasse was collected from a local sugar mill.

### 2.2 Method

The sugarcane was then washed with de-ionized water to remove any impurities and dried in an air-convention drier at 40℃ with an air velocity of 1.3 m/s until the mass remained constant. The dried sugarcane bagasse was then grounded using a kitchen blender and then sieved to the desired particle size.

An appropriate amount of pure sodium hydroxide pellets was added to 1000ml of de-ionized water in order to produce alkaline solutions of 0.5%; 1%; 1.5%; 2%; 2.5%. Then 60g of natural sugarcane bagasse was added to each solution. The solution (alkaline solution + bagasse) was left for a

duration of 24 hours (with the aim of extracting as much lignin as possible). After 24 hours, the contents were filtered using a sieve. The solid residue was then washed thoroughly with de-ionized water until neutral pH was reached. The solids were then dried in an air convention (CE130 Gunt Hamburg dryer) at 40℃ with airflow of 1.3m/s until the mass remained constant. The dried sugarcane bagasse was then grounded and sieved to desired particle size.

## 3. BATCH ADSORPTION STUDIES

Once the adsorbents (natural and modified) were characterised, the effect of operational parameters such as initial concentration, adsorbent dosage, pH, contact time and agitation speed were investigated using batch adsorption studies. These operational variations were done in order to evaluate their effect on the removal of heavy metals, in particular Fe(II) ions from wastewater.

Preparation of synthetic solutions were made by dissolving appropriate amounts of Ferrous Sulphate heptahydrate salt ($FeSO_4.7H_2O$) into 1000mL of de-ionized water. The synthetic solution was allowed to agitate in a Cole –Parmer Stuart Orbital Shaker SSL1 model at 160rpm allowing thorough mixing. The stock solution was then diluted with deionized water to the required solutions of different concentrations. These concentrations were then used in batch adsorption studies. The final concentration after each variation was obtained using the Pelkin Elmer AAnalyst 400 Absorption Atomic Spectrometry with an Iron Lamp of current of 10Amperes, a wavenumber of 248.3nm 248.3nm and a flame of Air/Acetylene flame, respectively.

The following batch studies were performed using a jar test in order to determine the effect of adsorbent loading, initial concentration, speed, pH and contact time.

### 3.1.1. Effect of speed

1g of the natural and modified bagasse was measured into different conical flasks containing a sample of 100ml of Fe (II) solution and subjected to varying agitation speeds of 140 – 240rpm while keeping the pH constant at 5, contact time constant at 200 minutes, and adsorbent dose constant at 1g. The contents were then filtered and the concentration of the filtrates was determined using AAS.

### 3.1.2. Effect of adsorbent loading

This effect was studied by varying the dosage from 0.2 -3g of natural and modified sugarcane bagasse in increments of 0.2g into 100ml of Fe (II) solution while keeping the agitation speed and initial concentration at 160rpm and 5mgL, respectively. After 200 minutes, the contents were filtered and the concentration of the filtrates was determined using Atomic Absorption Spectrometry (AAS).

### 3.1.3. Effect of initial concentration

This effect was studied by varying the initial concentration of Fe (II) ions in solution from 5-40mg/L, while keeping the other parameters constant: agitation speed, dosage, pH at 160rpm, 1g and 5; respectively. The solutions were then allowed to agitate for a period of 200 minutes. Thereafter contents were filtered and the concentration of the filtrates was determined using AAS.

### 3.1.4. Effect of contact time variation

Fe (II) solutions of 5mg/L were contacted with one gram of sugarcane bagasse while keeping pH and agitation speed constant at 5 and 160rpm. Contact time was varied from 5-200 minutes with sampling intervals of 5 minutes. The contents were then filtered and the concentration of the filtrates was determined using AAS.

For the batch experiments, percentage removal and adsorption capacities were calculated as follows:

**Percentage removal of Fe (II) was calculated as:**

$$\% \ Removal = \left( \frac{C_o - C_e}{C_o} \right) * 100 \tag{1}$$

Where, $C_o$ and $C_e$ are the initial concentration and concentration at equilibrium (mg/L); respectively.

**The adsorption capacity $(Q_e)$ was calculated as follows:**

$$Q_e = \left( \frac{C_o - C_e}{W} \right) V \tag{2}$$

Where, $C_o$ (mg/L), $C_e$ (mg/L), V and W are the initial concentration, concentration at equilibrium, Volume of the solution (ml) and Mass of adsorbent (mg), respectively.

## 3.2 Adsorption Isotherms and Kinetics

### 3.2.1 Adsorption Isotherms

Biosorption processes are usually best described through adsorption isotherms. Adsorption isotherm is a method used to determine the feasibility of using a particular adsorbent material for a certain application. It represents the equilibrium relationship between the metal concentration in the fluid phase and the adsorbate concentration in the adsorbent particles at a given temperature. This mechanism is determined by plotting the amount of adsorbate per unit weight of adsorbent (Qe) against the equilibrium concentration (Ce) of the adsorbate remaining in the solution.

Isotherm curves can be evaluated by adjusting the solute concentration while keeping the environmental parameters such as pH, temperature and metal concentration constant. The metal uptake by the biomass tends to be directly proportional to the concentration until it reaches a point of saturation at higher concentrations (Banum, 1982). The slope $\left(\frac{1}{q_L}\right)$ and intercept $\left(\frac{1}{q_L K_L}\right)$ are given by the plot of $\left(\frac{C_e}{q_e}\right)$ versus $C_e$.

In order to determine the mechanistic parameters associated with Fe (II) sorption, the results obtained by the batch adsorption experiments were analysed using the Langmuir and Freundlich models.

### 3.2.1.1 Langmuir Isotherm

The Langmuir isotherm assumes that all adsorption sites are equivalent and adsorption in active sites is independent of whether the adjacent is occupied or not.

**The linearized form of the Langmuir isotherm model is given by the following equation.**

$$\frac{Ce}{q_e} = \frac{1}{q_L K_L} + \frac{1}{q_L} C_e \tag{3}$$

Where Ce (mg/L) is the equilibrium at concentration; $q_e$ (L/mg) is the adsorption capacity of the adsorbent, $q_m$ (mg/g) is the maximum monolayer adsorption capacity and $K_L$ is the Langmuir adsorption constant (L/mg).

### 3.2.1.2. Freundlich isotherm

This model is used in the description of the equilibrium of heterogeneous surfaces and is not limited to monolayer adsorption (Dursun, et al., 2005).

$$log\ log\ Q_{eq} = logK_f + \frac{1}{n\ logC_{eq}} \tag{4}$$

Where $K_f$ (mg/g), n, Qe represent adsorption capacity, amount of metal ion adsorbed at equilibrium per unit of mass (mg/g).

## 3. RESULTS AND DISCUSSION

### 3.3.1. Effect of adsorbent dose

The number of active sites available on the surface of adsorbent depends on the amount of the adsorbent used for adsorption studies; this then makes it important for studies to verify the ideal dosage for adsorption processes. (Rubio, et al., 2015) stated that there may be decrease of amount adsorbed due to the formation of agglomerates that can then lead to the reduction of the total surface area and number of active sites available for the adsorption process. The effect of the adsorbent dose on the removal of Fe (II) was then studied by varying the amount of modified and unmodified forms of sugarcane bagasse from 0.2 to 3grams in 100mL solution, while keeping the concentration, pH and contact time at 5mg/L, 5 and 200 minutes, respectively. A difference in Fe (II) removal for the natural and modified sugarcane bagasse is shown in Fig. 1.
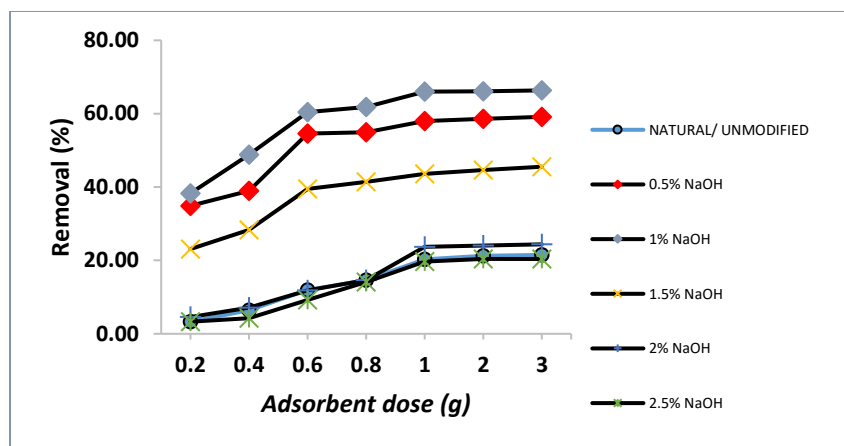
**Figure 1: Effect of adsorbent dose on Fe (II) removal onto natural and modified sugarcane bagasse (agitation speed: 160 rpm, initial concentration: 5mg/L; pH: 5).**

It can be noted from Fig.1 that the amount of Fe (II) removed increased with an increased in biomass dose for both the natural and modified adsorbent. This was expected because while increasing the amount of adsorbent, the number of adsorbent particles surrounded by Fe (II) ions also increased. The formation of clusters of Fe (II) on the surface of the adsorbent could be attributed to the subsequent decrease of the active sites of the adsorbent thus decreasing the surface area for adsorption to take place, hence no appreciable adsorption observed for adsorbent doses above 1.0g. A percentage removal of 3.30% and 22.30% Fe (II) was obtained using 0.2 and 1.0g of natural sugarcane bagasse. It was also observed that as the adsorbent dosage increased, the adsorption capacity decreased due to decrease of active sites on the surface of the adsorbent.

An increase in adsorption capacities was seen upon chemical pretreatment with alkali as illustrated by Fig. 1, which revealed that the highest removal efficiency of Fe (II) was achieved at 1wt% NaOH where 38.30 and 66.03% was obtained at 0.2 and 1g, respectively. This highest removal of 1% NaOH was followed by that of 1.5wt% NaOH with percentage removal of 34.90% and 43.56% for 0.2 and 1.0g; respectively.

It was also observed in Fig. 1 that as the concentration of alkaline solution increased above 1.0wt% NaOH, the adsorption capabilities of the adsorbent decreased because there was not much increase in percentage removal of Fe (II) using 1.5wt% NaOH. Percentage removal of Fe (II) obtained after using 1.5wt% NaOH were 23.10 and 39.5% when 0.2 and 0.6g of 1.5% NaOH were respectively

used. The least performing adsorbent in the removal of Fe (II) was that of 2.5 wt% NaOH with 3.30 and 19.69% when using 0.2 and 1.0g, respectively.

### 3.3.2. Effect of contact time

The influence of contact time on adsorption of Fe (II) onto the active sites of natural and modified sugarcane bagasse was investigated at the contact time range of 5-200 minutes, pH 5; initial concentration at 5 mg/L and 1g/L adsorbent dosage (natural and modified). Fig. 2 shows the performance of the different forms of sugarcane bagasse in the time interval of 5-200 minutes. It was observed that as the contact time increased, the percentage removal of the natural bagasse also decreased with the highest percentage removal of 15.6% obtained after 10 minutes.

A great improvement was seen on the structure of the bagasse upon chemical pretreatment with sodium hydroxide, as shown by Fig. 2. It was also observed in Fig. 2 that the highest percentage removal of Fe (II) were obtained when 1% NaOH- pretreated bagasse was used followed by 1.5% NaOH-pretreated bagasse with removal percentages of 82.98% and 65.93% at 50 and 80 minutes, respectively. It can also be seen in Fig. 2 that as the concentration of the alkali solution increased above 1wt% NaOH, the performance of the alkali pretreated adsorbent decreased. In this case 1.5wt% NaOH performed better than 2wt%NaOH, and 2wt% NaOH performed better than 2.5wt% NaOH. Removal of functional groups during delignification process may have resulted to these decreases in performance of these adsorbents.
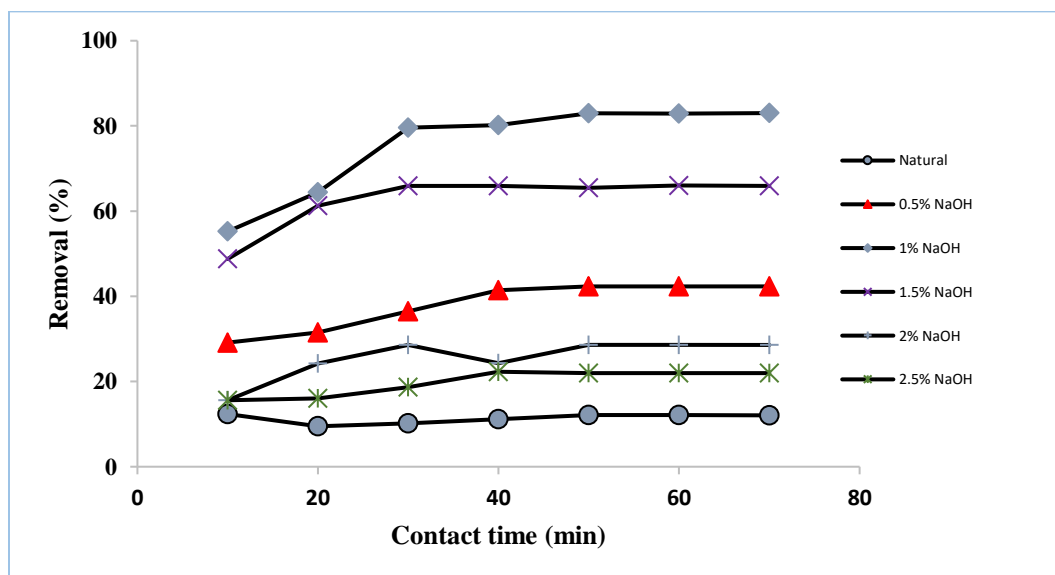
**Figure 2: Effect of contact time on Fe (II) removal onto natural and modified sugarcane bagasse (pH: 5; adsorbent dose: 1g; Initial concentration: 5mg/L)**

### 3.3.3. Effect of initial concentration

(Akgul & Karabakan, 2011) deemed the initial concentration of the solution to be the driving force in overcoming all the mass transfer resistances of the metal ions between the solid and an aqueous phase. Fig.3 3 shows the effect of Fe (II) concentration on removal of metal ion. For the initial concentrations of 5; 10; 15; 20; 30; 40mg/L, the natural bagasse was able to remove 24.07, 19.22, 7.33, 6.77, 4.97 and 4.58%; respectively. However, a great improvement was observed in adsorption capacities when sugarcane bagasse was chemically pretreated with sodium hydroxide i.e. 0.5wt% NaOH, 1.0wt% NaOH, 1.5wt% NaOH, 2wt% NaOH, 2.5wt% NaOH.

In a case of alkali modification (cellulose – hemicellulose combination) of 0.5wt% NaOH, 1.0wt% NaOH, 1.5wt% NaOH, 2.0wt% NaOH, 2.5wt% NaOH, the removal of Fe(II) increased to 48.43, 74.10, 72.51, 65.85, 62.74% and 16.17, 30.50, 26.04, 24.33, 16.48% ,respectively, for 5 and 40mg /L as depicted in Fig. 3.
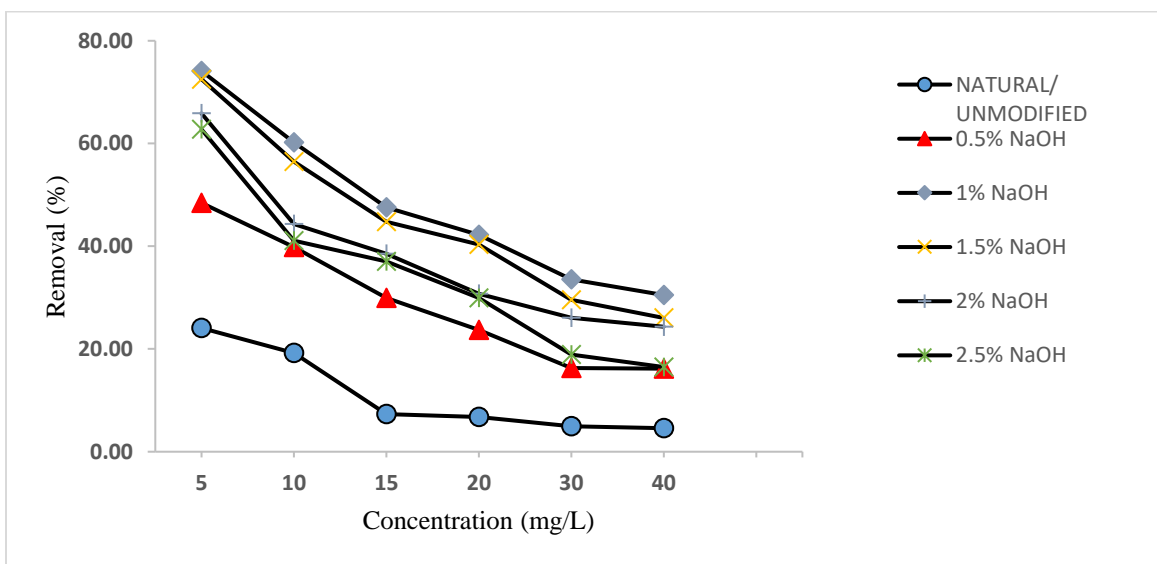


**Figure 3: Effect of initial concentration on Fe (II) removal using natural and modified sugarcane bagasse**

It is worth noting that although the percentage removal of Fe (II) increased after chemical pretreatment, but it decreased as the initial concentration increased from 5 to 40mg/L. This decrease in adsorption was due to the reduction of the active sites on the surface due to an increase in the number of ions competing for available binding sites, at higher concentration, in both the natural and modified adsorbents. The effect of initial concentration can, thus, be explained as follows: the metal ions adsorption involves higher energy binding sites at low metal ion/ biosorbent ratio, therefore an increase in metal ion/ biosorbent ratio at higher concentrations lead the saturation of binding sites, this in-turn leads saturation of active sites of the biosorbent which then results in decreased percentage removal of metal ions. The components of lignocellulosic material contains functional groups such as carboxyl, carbonyl, hydroxyl groups which promote adsorption of ions onto adsorbents. According to (Chen & Yang, 2005) alkaline pretreatment of biomass has been found to enhance the biosorption efficiencies of biosorbent due to the hydrolysis of their reactions which results in the formation of more carboxylic and hydroxyl groups. During the hydrolysis process of the chemical pretreatment, inactive superficial groups of biomass are transformed to available functional groups for interaction with metal ions thus enhancing their biosorption efficiency of the modified biosorbents.

It can be inferred from Fig. 3 that the adsorption capacity of cellulose-hemicellulose is greater compared to that of the natural bagasse. Lignin is a gluing substance which holds the cellulose and hemicellulose together. Therefore, removing lignin leads to the dismantling of lignocellulosic fibers which in-turn leads to the exposure of functional groups present both in the cellulose and the hemicellulose hence making more functional groups available for adsorption of Fe (II) ion.

It can be observed from Fig. 3 that the removal of Fe (II) of the natural and cellulose-hemicellulose combination also depends on the acidity/ alkalinity of the chemical pretreatment. As shown in Fig. 3, the percentage removal of the cellulose-hemicellulose combination increased when the sodium hydroxide concentration was 0.5 and 1.0 wt% NaOH but decreased when the concentration increased from 1.5wt% NaOH to 2.5wt% NaOH. Since the lignin contains some functional groups, therefore removal of it leads to reduction of its functional groups during the pretreatment process. A decrease in adsorption capacity was observed when the pretreatment concentration was above 1.5wt% NaOH.

### 3.3.4. Effect of pH

The pH of the solution is one of the most crucial parameters affecting the adsorption process of metal ions owing to its capability of changing the surface charge of the adsorbent. To investigate the influence this parameter has on the adsorption of metal ions; natural and alkali modified forms of sugarcane bagasse were contacted with single metal ion solution of Fe (II) at different pH values ranging from 2 - 7 for a period of 200 minutes. After the designated period of contact, the resultant pH values (equilibrium pH) were determined for each solution. Fig. 4 gives the presentation of these results which shows that the removal of Fe (II) ions increased with increasing pH for all forms of sugarcane bagasse, i.e. natural and alkali modified forms. Higher adsorption of metal ions obtained from higher pH values imply that the interaction of Fe (II) metal ions and the different forms of sugarcane bagasse is through a chelating mechanism. It can be seen from Fig. 4 that the active sites, at low pH values (<4), are less available for metal ions due to protonation of the active sites at higher concentration of $H^+$ ions, whereas at moderate pH values (4- 6), $H^+$ ions are released from the active sites thus increasing the amount of the adsorbed ions. According to (Swathandra, 2014), the dominating adsorption mechanism for the removal of metal ions from the solution at this pH range is the ion exchange and complex formation processes. Above these moderate pH range (>6), occurrence of both ion exchange and aqueous metal formation may be observed as significant mechanisms in the removal process.
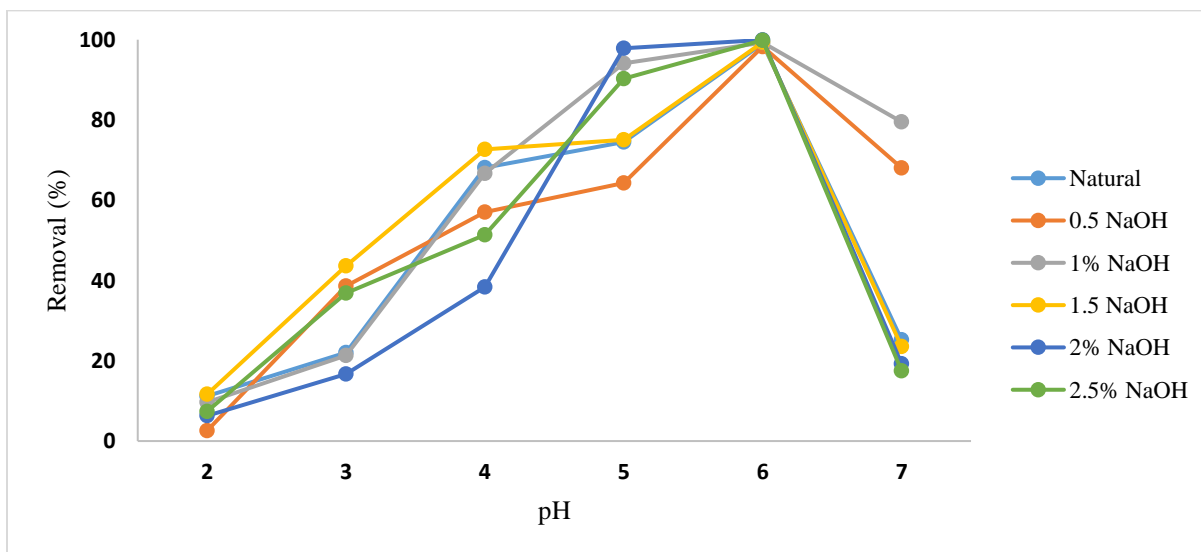


**Figure 4: Effect of pH on Fe (II) removal using natural and modified sugarcane bagasse**

## 4. Adsorption Isotherms

The correlation coefficients $(R^2)$ of the natural and modified sugarcane bagasse obtained from the batch process are given in Table 1. It can be observed in Table 1 that the Langmuir correlation coefficients of delignified bagasse is greater than 0.95, thus indicating the good fit of the monolayer Langmuir model to the a adsorption of Fe (II) by the alkali –pretreated bagasse.

**Table 1: Langmuir and Freundlich adsorption isotherms for Fe (II) adsorption**

| Adsorbent | FREUNDLICH MODEL | | | LANGMUIR MODEL | | |
|---|---|---|---|---|---|---|
| | $K_F$ | n | $R^2$ | $K_L$ | Q | $R^2$ |
| Natural | 1.875 | -40.000 | 0.003 | 0.374 | 6.064 | 0.674 |
| | | | | | | |
| 0.5% NaOH | 4.430 | 27.780 | 0.853 | 1.424 | 7.898 | 0.933 |
| 1% NaOH | 2.500 | 2.730 | 0.968 | 5.003 | 4.659 | 1.000 |
| 1.5% NaOH | 4.196 | 7.010 | 0.609 | 12.903 | 0.497 | 0.987 |
| 2% NaOH | 2.087 | 1.990 | 0.911 | 1.627 | 7.951 | 0.986 |
| 2.5% NaOH | 3.388 | 2.680 | 0.993 | 2.420 | 5.700 | 0.967 |

## 5. Conclusion

The present study on removal of Fe (II) from aqueous solution using natural and modified sugarcane bagasse was carried out in batch experiment. The operational parameters such as the initial concentration, pH, contact time, adsorbent dose had a significant effect on the Fe (II) removal efficiency. For the concentration variation using alkali pretreatment, it was discovered that the maximum removal of Fe (II) was obtained at when 1% NaOH was used at 5mg/L, above 1% NaOH the percentage removal decreased. One gram per litre of both natural and pretreated bagasse was found

to be the optimum adsorbent dosage, above this dosage, the adsorption capacity of all the adsorbents decreased. The maximum removal of Fe (II) was found to be at pH of 5. In order to examine the mechanism responsible for the adsorption process, Langmuir and Freundlich kinetic isotherms were used for this examination. For both the natural and modified sugarcane bagasse, a good correlation coefficient (>0.95) was obtained using Langmuir isotherm.

**References**

Afolabi, F., Musonge, P. & Bakare, B., 2021. Evaluation of Lead (II) Removal from Wastewater Using Banana Peels: Optizing Sudy. *Polish Journal of Environmental Studies,* 30(2), pp. 1487-1496.

Akgul, M. & Karabakan, A., 2011. Promoted dye adsorption performance over desilicated natural zeolite. *Microporous and Mesoporous Material,* Volume 145, pp. 157-164.

Babarinde, N., Babalola, J. & Sanni, R., 2006. Biosorption of lead ions from aqueous solutions by maize leaf. *Journal of Physical Science,* Volume 97, pp. 219-243.

Balci, B., Keskinkan, O. & Avci, M., 2011. Use of BDST and ANN model for prediction of dye adsorption efficiency of Eucalyptus camalduslensis barks. *Expert Systems with applications,* 38(1), pp. 949- 956.

Banum, S., 1982. *Introduction to Organic and Biological Chemistry.* Third ed. New York: Macmillan Publishing Co..

Brigida, A., V., C., Goncalves, L. & Coelho, M., 2010. Effect of chemical Pretreatment on properties of green coconut fiber. *Carbohydrate Polymers,* Volume 79, pp. 832-838.

Chen, J. & Yang, L., 2005. Chemical modification of Sargassum species for prevention of organic leachig and enhancement of uptake during metal biosorption. *Industrial Engineering of Chemical Resources,* Volume 44, pp. 9931-9942.

Dursun, G., Cicek, H. & Dursun, A., 2005. Adsorption of phenol from aqueous solutions by carbonized beet pulp. *Journal of Hazardous Materials,* Volume 125, pp. 175 - 182.

Fu, F. & Wang, Q., 2011. Removal of heavy metal ions from wastewater : A review. *Journal of Environment Management,* Volume 92, pp. 407- 418.

Harripersadth, C., Musonge, P., Isa, Y. & Morales, M., 2020. The application of eggshells and sugarcane bagasse as potential biomaterials in the removal of heavy metals from aueous solutions.. *South African Journal of Chemical Engineering,* Volume 34, pp. 142-150.

Jackson, M., 1977. Review article: the alkali treatment of straws. *Anim Feed Sci Technol,* Volume 2, pp. 105 - 130.

Luo, L., Voet, E. & Huppes, G., 2010. Biorefinering of lignocellulosic feedstock-technical, economic and environmental considerations. *Bioresource Technology,* Volume 101, pp. 5023-5032.

Mohan, S. & Sreelakshmi, G., 2008. Fixed bed column study for heavy metal removal using phosphate treated rice husk. *Journal of hazardous Material,* Volume 153, pp. 75-82.

Ndlovu, S., Simate, G., Seepe, L. & Shemi, A., 2013. The removal of Co2+, V3+ and Cr3+ from watewater using cassava waste. *South African Journal of Chemical Engineering,* 18(1), pp. 51-69.

Rezende, C., de Lima, M.A., Maziero, P., deAzevedo, E.R., Garcia W. & Polikarpov, I., 2011. Chemical and morphological characterization of sugarcane bagasse sumbitted to delignification process for enhanced enzymatic digestibility. *Biotechnology for Biofuels,* 4(54).

Rodriquez-Vazquez, R. & Diaz-Cervantes, D., 1994. Effcet of chemical solutions sprayed on sugarcane bagasse pith to produce single cell protein: physical, chemical analysis of pith.. *Bioresour. Technol.,* Volume 47, pp. 159-164.

Rubio, F.; Jr., Goncalves; Dragunski, D.C.; Meneghel, A.P.; Tarley, C.T.R.; Schwantes, D., 2015. A Crambe abyssinics seed by-product as biosorbent for Lead (II) removal from wastewater. *Desalination and Water Treatment,* 53(1), pp. 139 - 148.

Swathandra, P., 2014. Baggase as potential adsorbent of cadmium removal from aqueous solutions. *Int. J. Innov. Eng. Technol.,* Volume 4, pp. 109-115.

Trgo, M., Medvidovic, N. & Peric, J., 2011. Application of mathematical empirical models to dynamic removal of lead on zeolite clinoptilotilolite in a fixed bed column. *Indian Journal of Chemical Technology,* Volume 18, pp. 123-131.

Wan Ngah, W. & Hanafiah, M., 2008. Removal of heavy metal ions from wastewater by chemically modified plant waste as adsorbent: a review. *Bioresource Technology,* 99(10), pp. 3948 - 3958.

# ADSORPTION OF FE (II) AND MN (II) FROM WASTEWATER USING SURFACTANT MODIFIED BENTONITE AND SYNTHETIC CLAY.

*Silindile Gumede[1], Paul Musonge[2,3]*

*[1] Department of Chemical Engineering, Durban University of Technology, Durban, South Africa*

*[2] Institute of Systems Science, Durban University of Technology, Durban, South Africa*

*[3] Faculty of Engineering, Mangosuthu University of Technology, Durban, South Africa*

[1]*silindileg@dut.ac.za,* [2,3]*paulm@dut.ac.za*

## Abstract

Heavy metal pollution in the environment and its effects on human health is a global issue that needs sustainable solutions. Due to the continuous deterioration of water quality from highly contaminated waste, is it necessary to frequently research and improve the wastewater treatment technologies. It has been proven that adsorption is an effective method for purification, because of significant advantages including stability, utility, low-cost, ease of operation and performance.

The choice of adsorbent for heavy metal removal is the most critical component, environmentally and economically. Regeneratable/recyclable materials and highly efficient adsorbents are necessary in treating wastewater with high metal concentrations. The use of clays has drawn added attention to researchers because of their accessibility compared to other adsorbents.

Synthetic hydrotalcite (HT)and surfactant modified bentonite (MB) were used for this study to investigate their efficacy in removing Fe (II) and Mn (II). Iron and manganese have been found to be present in high concentrations in acid mine drainage, especially in metal producing mines and coalfields, however they vary depending on the source. Batch experiments were undertaken to study the effect of adsorbent dosage, initial concentration, and pH on the performance of the adsorbents. Results showed that the adsorbent performance is highly dependent on the initial ions concentration, with % removals decreasing with increase in initial concentration over the studied concentration range. An increase in metal removal using both adsorbents was observed with the increase in pH. Desorption studies revealed that modified bentonite may be easier to regenerate than hydrotalcite with 97.5% desorption of Fe at a concentration of 0.1N of HCl. The results of this study have shown the effectiveness of nano clays as alternative adsorbents for wastewater remediation.

Keywords*: acid mine drainage, adsorption, clays, hydrocalcite, wastewater.*

## 1. INTRODUCTION

There is a huge responsibility for researchers to investigate convenient, inexpensive and safe technology to treat acid mine drainage to meet government legislation before disposal into the receiving water bodies. Iron and manganese have been found to be present in high concentrations in acid mine drainage (AMD), especially in metal producing mines and coalfields, however they vary depending on the source (Hallberg and Johnson 2005). The problem with treating waste water contaminated with manganese and iron is that it is quite difficult to remove it without causing the secondary environmental pollution, yet consumption of these metals in high concentration may cause severe health problems (Goldani et al., 2013).

Generally, acid mine drainage does not only consist of one heavy metal but several heavy metals with different concentrations. All heavy metals are physio-chemically unique as such, the more you have them in one AMD stream the harder it is to treat the stream because they compete. (Lukman et al., 2013) reported that copper and lead are easier to remove using adsorption compared to cadmium. Therefore, there is a need to investigate the removal of cations such as iron and manganese in a binary or ternary mixture.

The international standards for consumption of iron is 0.3 mg/L while that of manganese is 0.1 mg/l (Ellis et al., 2000). Several technologies have been applied to remediate mine water and it has be found that the removal of Mn (II) is difficult because the interactions among Mn(II), Fe (II), and other metals which are very complex, affecting Mn (II) solubility. The adsorption of manganese is supressed/inhibited by a higher iron to manganese ratio (Goldani et al., 2013).

(Mulopo, 2015) reported on the different concentrations of iron and manganese from gold and coal mines in South Africa. The average total iron concentrations in both coal and gold mines were around 1000 mg/L while that of manganese was around 174 mg/l. These concentrations are way above the recommended limits for industrial effluents in South Africa, thus their removal from acid mine drainage before disposal into the receiving water bodies is mandatory.

There are many different types of technologies that are being used to treat AMD. These include chemical precipitation, membrane-filtration, ion exchange, and adsorption. The adsorption process is preferred over the traditional processes because it is cheaper to operate, efficient in treating AMD and has good metal recovery efficiency (Bhattacharyya and Susmita, 2006).

There are several adsorbents that are currently being explored for the removal of different contaminants from wastewater; however, some are reported to be not readily available, inefficient and costly for wastewater treatment. The search for low-cost adsorbents that have metal-binding capacities has intensified in recent years. The most investigated adsorbents are zeolites, activated carbon and waste sourced from agricultural activities (Barakat, 2011). A highly effective adsorbent like clay is characterised by its high surface area, stability, structure and ion exchange capacity (Bhattacharyya and Gupta, 2008). Besides their good adsorption properties, clays have also been favoured because of their ability to regenerate and de-sorb heavy metals (Adeyemo et al., 2017). The superior surface area of nanomaterials has enabled them to be researched extensively in the treatment of AMD (Yue et al., 2016)

The most common and most efficient clay for heavy metal removal from wastewater is bentonite. However, it is not very efficient in treating acid mine drainage with a very high concentration of heavy metals. Clay materials can be modified using a variety of chemical/physical treatments to achieve the desired surface properties to remove contaminants. On the other hand, synthetic clays have been chosen because of their advantages over natural

clays. Its purity, composition and chemical/physical features can be altered to improve its efficiency depending on its application.

While every adsorbent has its unique structure, characteristics and functionality, one common feature shared by all adsorbents is that they all contain rich active surface functional groups, which are crucial for the surface chemistry of materials and the adsorption of heavy metals. It is generally believed that the chemical/physical interactions between heavy metals and functional groups of adsorbents contribute significantly to the adsorption of heavy metals. Functional groups are typically bonded with heteroatoms on carbon surfaces, commonly oxygen, nitrogen, sulfur, phosphorus and halogens (Yang et al., 2019). The functionality and quantity of each type of functional groups can be enhanced by chemically and/or physically modifying the surface of carbon materials to introduce the desired heteroatoms on carbon surfaces. Thus, one key area of research deals with the modification of materials to enhance their surface chemistry for selective adsorption of target heavy metals.

As much as the adsorption process is more efficient and is one of the cost-effective technologies available the fact that the adsorbents need to be disposed of after they have been exhausted cannot be ignored, therefore it is necessary to ensure that the adsorbent can be regenerated or recyclable to minimise the disposal costs. Several researchers have reported that in order to have a highly effective adsorption system for the removal of heavy metals it is important to ensure that the regeneration of adsorbents is equally effective. After the adsorption process, the adsorbents become saturated with heavy metals which are very toxic to all living organisms including plants and animals as such the heavy metals must be recovered prior to the disposal of the adsorbent. Disposing of the heavy metal stripped adsorbents limits their environmental and pollution impact. In order to protect the environment, it is of great importance to ensure that adsorbents are disposed of after heavy metals have been stripped of them (Lata et al., 2015).

Desorption and regeneration studies do not only help cut the costs but to also understand the nature of adsorbate–adsorbent interaction. Therefore, it was of importance to explore the desorption of manganese and iron ions from the saturated adsorbents. Several studies have shown that hydrochloric acid is the most effective desorbing agent after the adsorption of heavy metals compared to other desorbing agents such as sulphuric acid, nitric acid and sodium hydroxide (Akpomie et al., 2015). The added advantage which comes with hydrochloric acid is that it is cheaper, effective and does not damage the adsorbent structure.

The main aim of this study was to investigate and explore the feasibility of using surfactant-modified bentonite and hydrotalcite nano- clays for the treatment of iron and manganese rich acid mine drainage. The objectives were to investigate and compare the performances of the adsorbents by varying pH, solution concentrations and adsorbent mass dosages in batch experiments. To investigate desorption capacities of the recommended adsorbents by washing them with hydrochloric acid and compare their respective percentage removals.

## 2.Materials and methods

### 2.1 Materials

The primary materials used as adsorbents in this study were Di(hydrogenated tallow ), dimethyl ammonium chloride (Arquad 2HT-75) , modified bentonite and hydrotalcite. Both the modified bentonite and hydrotalcite samples used in this study were produced at CSIR Nanomaterial Industrial Development Facility (South Africa).

## 2.2 Effect of adsorbent dosage

For the adsorption study of clays, a working solution was prepared by diluting each stock solution to give the desired concentrations of 800 mg/L and 50 mg/L for Fe (II) and Mn (II), respectively. Sulphuric acid was added dropwise to reach a pH of approximately 3 to mimic AMD pH. Concentrations of 800 mg/L for Fe (II) and 50 mg/L for Mn (II) and pH were prepared based on the physio-chemical characteristics of the AMD obtained from the three different mines. Different dosages of clay adsorbent ranging from 0.1 to 1 g were added to a fixed volume (50 ml) of the metal ion solutions which had fixed concentrations of 800 mg/L and 50 mg/L for Fe (II) and Mn (II), respectively. Batch adsorption studies were then performed at 25 °C, and a shaker speed of 150 rpm to investigate the effect of adsorbent mass on metals removal. After 24 hours in a shaker, the solutions were filtered, and the remaining metal ion concentrations were analysed using Inductively Coupled Plasma Mass Spectrometry.

## 2.3 Effect of pH

The effect of pH on metal removal from AMD was explored by varying the initial solution pH from 2 - 6. Since the pH of AMD fluctuates with time owing to poor buffering and varies from one location to another, it was imperative to study the effect of pH on metal removal from AMD. Solution pH has a significant effect on metal uptake since it determines the surface charge of the adsorbent and the degree of ionization and speciation of the adsorbate. In all cases, 0.1 gram of each adsorbent was contacted with 50 ml of metal ion rich solutions at 25 °C and 150 rpm.

## 2.4 Effect of concentration

When determining the effect of concentration, a 50 ml of metal test solution of varying concentrations i.e. 100-800 mg/L for Fe and 10 to 50 mg/L for Mn (II) was dosed with 0.1 g of adsorbent and mixed using a shaker at 25 °C for 24 hours at a fixed speed of 150 rpm. $H_2SO_4$ was also added to reduce the pH to 2. After 24 hours had lapsed, the solution was filtered and the concentration of the metal ions remaining in the solution was analysed by using the ICP.

The percentage removal and quantity adsorbed were calculated as follows:

$$\%removal = 100 \times \frac{C_0 - C_e}{C_0} \tag{1}$$

$$q_e = V \frac{C_0 - C_e}{m} \tag{2}$$

Where $C_o$ (mg/L) is the initial metal ion concentration, $C_e$ (mg/L) is the equilibrium metal ion concentration in solution, $Q_e$ (mg/g) is the quantity of metal ions adsorbed per unit mass of adsorbent, V (L) is the volume of solution used and m (g) is the mass of the adsorbent.

## 2.5 Desorption

Desorption studies help to understand if the adsorbent is reusable. In this study, desorption experiments were performed using HCl as a desorbing agent. The efficiency of HCl on desorption was conducted by mixing 1 g of the already used adsorbent with 50 ml of HCl concentrations ranging from 0 to 1.0 N. The mixture was then agitated for 120 minutes. The concentration of metal in the filtrate was then analysed using the AAS. The percentage of metal ions desorbed was then calculated by the following equation:

$$\%Desorption = 100 \times \frac{C_D V_D}{Qe \times m} \qquad (3)$$

where $C_D$ (mg/L) is the concentration of metal ions in the desorbed solution, $V_D$ (L) is the volume of desorbed solution, m (g) is the mass of adsorbent used for desorption studies and qe (mg/g) is the adsorption capacity of the adsorbent for metal ions.

## 3 Results and discussion

### 3.1 Effect of adsorbent mass

The synthesised AMD was prepared to reflect the concentrations and pH of the actual AMD. The effect of dosage was investigated by varying adsorbent mass from 0.1 to 1g. The adsorbent mass is an important variable because it relates to the number of active sites available and consequently affects the overall efficiency of the AMD treatment system.



a.                                                                                          b.
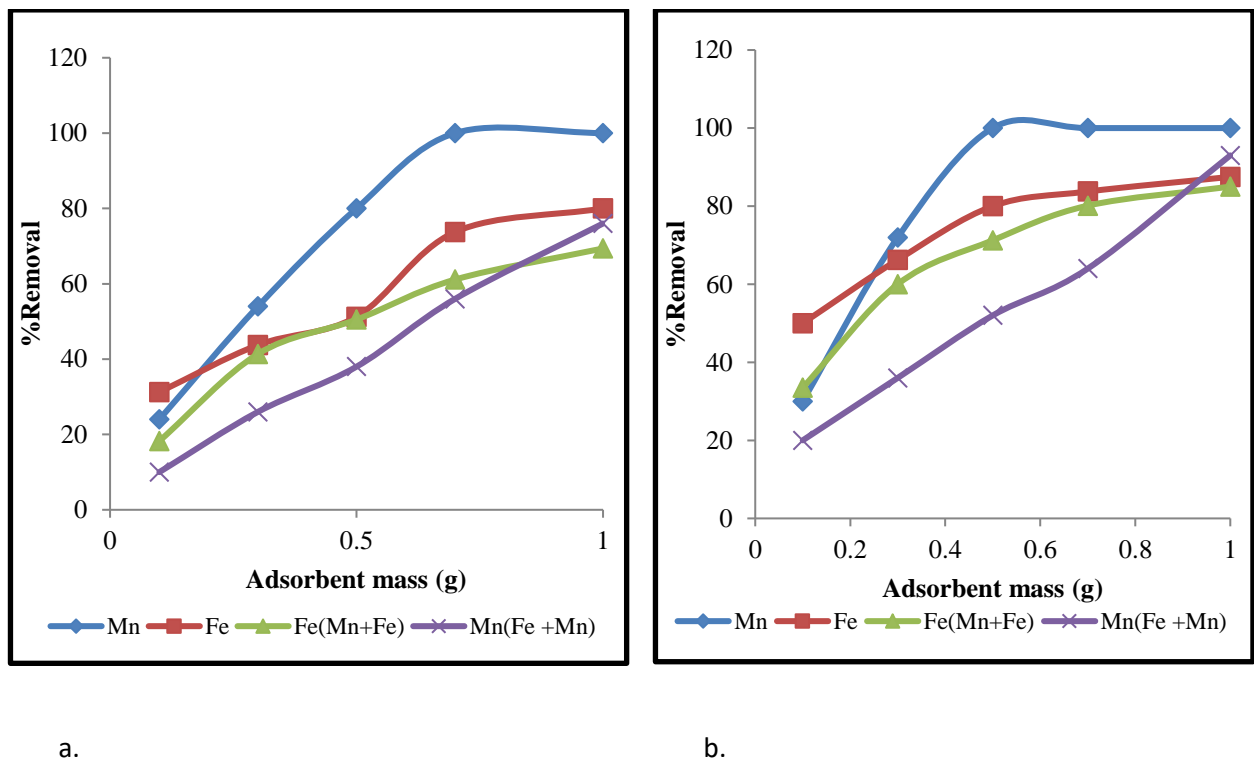
Figure 1: Effect of dosage on the adsorption of Mn and Fe for a) MB and b) HT in singular and binary solution

As shown in figure 1a, the percentage removal increased from 24% to 100% for Mn (II) removal and from 35% to 81% for the removal of Fe (II) using MB. In a binary solution, the % removal of Mn (II) increased from 10% to 76% and from 18.5% to 69% for the removal Fe (II). Figure 1b, results show an increase in % removal of Mn (II) from 30% to 100% in adsorption with 0.1g to 1g of HT and from 53% to 88% for the removal Fe (II) in a single solution. In a binary solution, % removal of Mn (II) from 20% to 93% in adsorption with 0.1g to 1g and from 33% to 85% for the removal Fe (II).

An increase in %removal as the dosage increases is due to an increase in the availability of exchangeable surface sites with the increase in the adsorbent dosage.

The % removal of Mn (II) and Fe (II) in HT and MB decreased as compared to the single adsorption and this was attributed to the fact that both Mn (II) and Fe (II) were competing for the surface binding sites and bind to different surface sites.

Comparing the adsorption of the two heavy metals, the order of the removal rates were $Fe^{2+} > Mn^{2+}$ given the fact that Fe (II) was highly concentrated than Mn (II) which was attributed to their atomic radii (Mn and Fe), Fe has the atomic radii closer to that of $Mg^{2+}$ present in both adsorbents as analysed by the EDS(Gumede and Musonge, 2020). Fe (II) and Mn (II) have ionic radii of 0.075 and 0.082 nm respectively and Mg has the ionic radii of 0.072 therefore isomorphic substitution may have taken place between Mg and Fe.

**Adsorption capacities**



a.                                                                                            b.
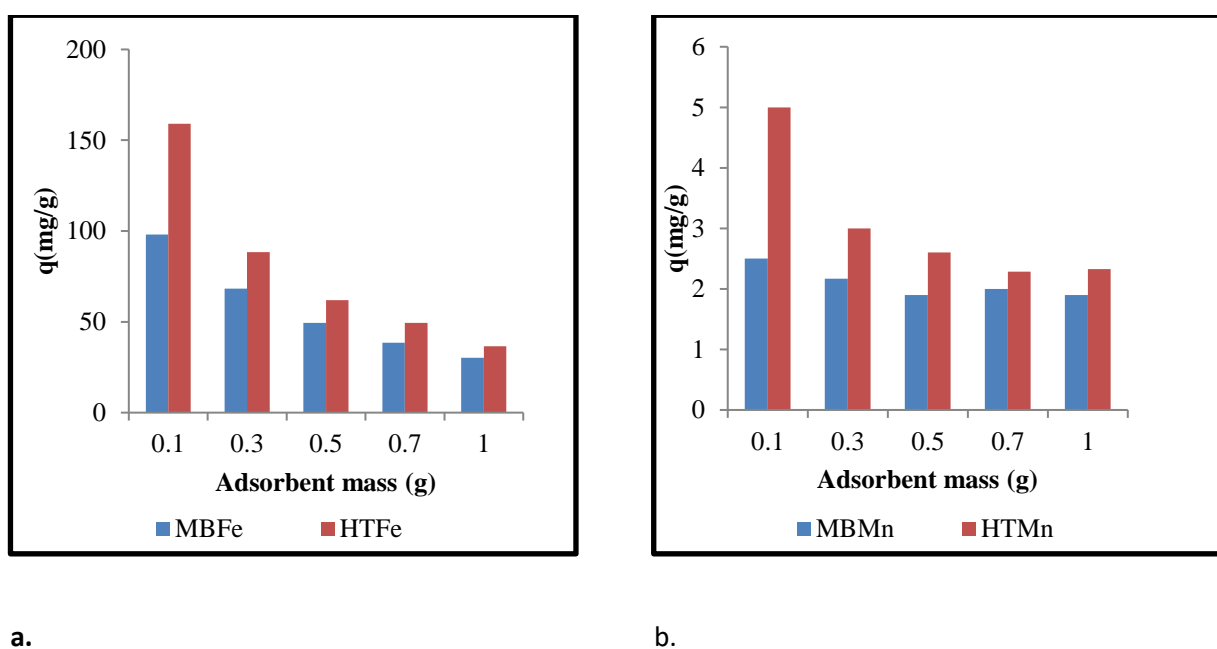
Figure 2: Adsorption capacities on the adsorption of a) Fe (II) and b) Mn (II) using MB and HT

Figure 2 shows that the amount of metals adsorbed per unit weight (adsorption capacity) at different dosage in a binary solution. While the percentage removal showed an increase with the increase in dosage, the adsorption capacity showed the opposite for both HT and MB. The adsorption capacity ($q_e$) of MB for Mn decreased from 2.5 to 1.9 mg/g when adsorbent dosage was increased from 0.1 to 1g. HT had the same trend with adsorption capacity for the removal of Mn (II) declining from 5 to 2.3 mg/g when adsorbent dosage was increased from 0.1 and 1 g. A similar trend was observed for Fe adsorption, the adsorption capacity decreased from 98 to 30mg/g and from 159 to 36.5mg/g when using MB and HT, respectively. This trend may be due to the increase in adsorption active sites as the dosage increase which results to adsorption site remaining unsaturated.

(Zubair et al., 2017) also obtained a similar trend on the effect of adsorbent dosage for the adsorption of Pb (II) on modified MgAl (LDH). An increase in adsorbent dose increased the percentage removal of Pb (II) while adsorption capacity decreased proportionally.

**3.2 Effect of pH on the adsorption of Fe (II) and Mn (II).**

The solution pH plays a vital role in the adsorption process and research has shown that it is one of the critical parameters. It influences the solubility of heavy metals and affects the concentration of the counter ions on the functional groups. It was therefore necessary to evaluate its effect on the adsorption of Fe (II) and Mn (II). During the adsorption process, as it affects the solubility of the metal ions, concentration of the counter ions on the functional groups of the adsorbent and the degree of ionization of the adsorbate during reaction. The active sites on an adsorbent can either be protonated or deprotonated depending on the pH.

Adsorption experiments were performed in the pH range of 2–6 (error of less than 0.3) in Figure 3 because at higher pH levels, Fe (II) and Mn (II) would be converted into their hydroxide forms and get precipitated.

a.                                                                                        b.
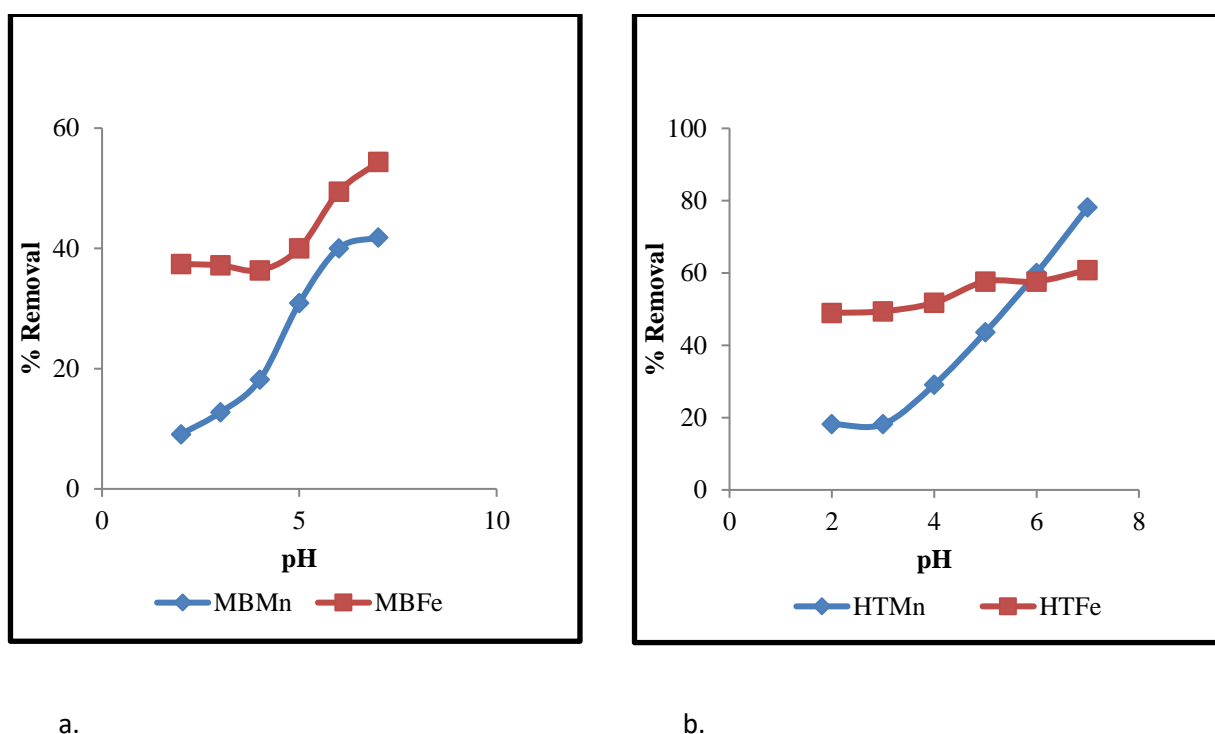
Figure 3: Effect of pH on the adsorption of Mn (II) and Fe (II) using a) MB and b) HT in a binary mixture.

The effect of pH on the removal of Fe (II) and Mn (II) from synthetic AMD using HT and MB is shown in Figures 3 for the binary solutions. It was noted in both figures that the adsorption uptake of Mn (II) was enhanced from 9 to 65 % using MB and from 23.6 to 81 % using HT. The adsorption uptake of Fe (II) was enhanced from 33.5 to 56.5 % using MB and from 50 to 73.9 % using HT with increasing pH value from 2 to 6. HT contains hydroxyl functional group and MB contains the aluminol and silanol as analysed by the FTIR, which are active sites for the metal binding(Gumede and Musonge, 2020). At low pH these functional groups are more protonated and, hence, they are less available to retain the metals. As a result, the adsorption

of Mn and Fe decreases. At a lower pH, the positive charged ion (Fe (II) and Mn (II)) species may compete with H+ and be adsorbed at the surface of the adsorbent by ion exchange mechanism (Singh et al. 2005) (Cheraghi et al., 2015).Similar findings were observed by Setshedi et al for the adsorption of $Pb^{2+}$ in hydrotalcite; it was found the removal of $Pb^{2+}$, increases with an increase in pH. As the pH increases , the active site of the adsorbent get deprotonated therefore improving the adsorption capacity (Setshedi et al., 2012), (Bradl, 2004).

### 3.3 Effect of initial concentration

The effect of concentration was investigated by varying Fe (II) concentration from 800 mg/L to 100mg/L and Mn (II) from 50 mg/L to 10mg/L while all other parameters were kept constant i.e. pH was at 2, adsorbent mass was 0,1g and temperature was 25 ºC. It was necessary to investigate the effect of concentration in adsorption because normally wastewater contains different ion concentrations depending on the source as seen from samples collected in different mines.
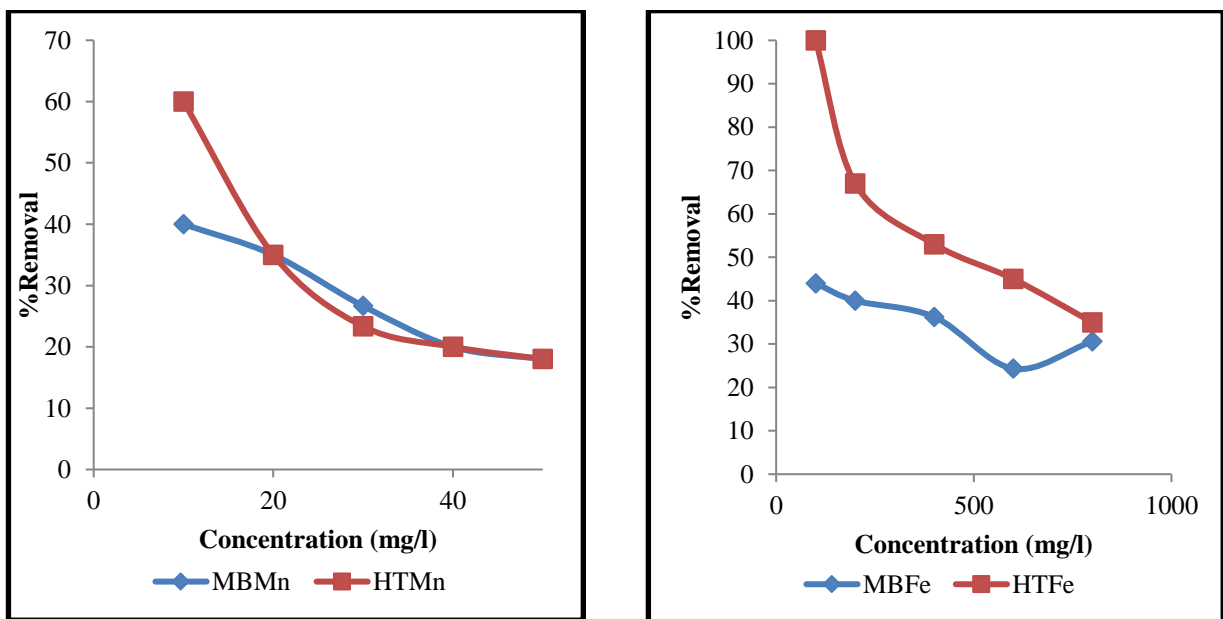


a.                                                                                              b.

Figure 4: The % removal of a) Mn (II) and b) Fe (II) of different concentrations using MB and HT in binary solution.

The percentage removal of Fe (II) and Mn (II) showed a decrease with an increase in ion concentration for both HT and MB. The percentage removal for Mn decreased from 60% to 18% and from 40% to 18% (mg/L) using HT and MB, respectively as shown in Fig. 4a.

For the removal of Fe in Fig. 4b percentage removal for Fe also decreased from 100% to 35% (HT) and from 44% to 30% (MB) binary solution of concentration of 100 mg/L to 800 mg/L. The decrease is due to the fact that all adsorbents have a fixed number of active sites and at higher concentrations, the active sites become saturated.

## 3.4 Desorption studies

In order to investigate the re-use of the adsorbents, the desorption of Fe (II) and Mn (II) from modified bentonite and hydrotalcite was studied. It is important to select an effective adsorbent that is recyclable as this has an effect on the shelf life of the adsorbent and hence the operating costs. Hydrochloric acid (HCl) was chosen as a desorbing agent because the previous studies have shown that it is the most efficient, non- damaging and cost effective agent for heavy metals as compared to other agents such as nitric acid, sodium hydroxide and sulphuric acid (Mishra, 2014). Desorption studies were carried out using 0.1- 0.5 N -HCl as an eluent and the desorption % are as shown in the succeeding graphs.
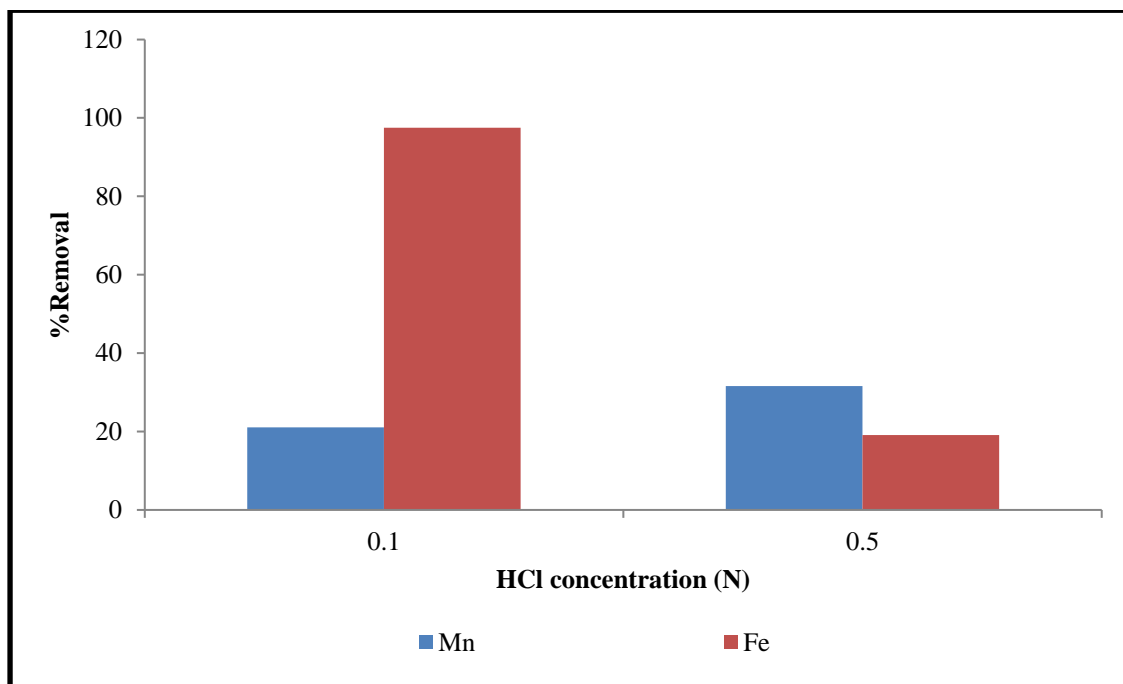


Figure 5: Desorption of Fe (II) and Mn (II) from MB for binary mixture
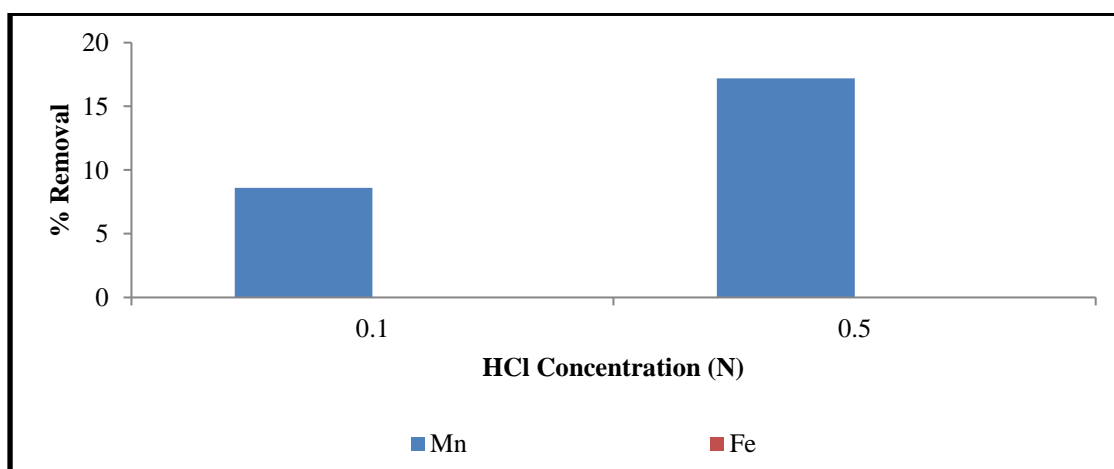


Figure 6 : Desorption of Fe (II) and Mn (II) from HT for binary mixture

For desorption of Mn (II) from HT and MB, it was found that both adsorbents can desorb Mn (II) under HCl solution as a desorbing agent. About 21% of Mn (II) was desorbed from modified bentonite and 9% from hydrotalcite when using 0.1N HCl while 0.5N HCl achieved 31 and 17%, respectively.

For the desorption of Fe(II) , it was found that Fe(II) can be desorbed from MB and not from HT and this was possibly due to the fact that most of the Fe(II) from hydrotalcite was adsorbed through precipitation process since the FTIR shows the $CO_3$ content (Gumede and Musonge, 2020) and it could not be desorbed by using HCl. Most of the metal ions are desorbed at pH < 2.0 (Mishra, 2014) and it was found that the pH of HT went up to 6.5 at a dosage of 1g. In MB, the maximum % desorption was obtained at a concentration of 0.1N as 97%. It is speculated that high acid concentration could damage the structure of the adsorbents, as reported by (Kołodyńska et al., 2017). Desorption of metals at an acidic condition is due to the fact that the adsorbent is protonated which allows desorption of positively charged ions. It is important to note that at low concentration, the desorption solution was able to quantitatively remove the metal ions from the adsorbent, thereby reducing the expenses and waste generation.

## Conclusion

Batch experiments for manganese and iron removal from AMD were undertaken by changing variables such as adsorbent dosage, initial concentration and pH. Effect of adsorbent dosage on the removal of Mn (II) and Fe (II) was investigated and concluded that the percentage removal increased with increase in mass due to an increase in active site. The percentage removal increased for Mn (II) increased from 24% to 100% and from 35% to 81% for the removal of Fe (II). Using HT an increase in % removal of Mn (II) from 30% to 100% and from 53% to 88% for the removal Fe (II) was achieved using 0.1 to 1g. The experimental results clearly show that the adsorbent performance is highly dependent on the initial solution concentration, with % removals decreasing with increase in initial solution concentration over the studied concentration ranges. Further, it was noted that HT had a higher pH buffering effect that raised the solution pH than MB. This observation is good because it eliminates the need to adjust pH after treatment. Desorption results showed that modified bentonite may be easier to regenerate than hydrotalcite.

**References**

ADEYEMO, A. A., ADEOYE, I. O. & BELLO, O. S. 2017. Adsorption of dyes using different types of clay: a review. *Applied Water Science,* 7**,** 543-568.

AKPOMIE, K. G., DAWODU, F. A. & ADEBOWALE, K. O. 2015. Mechanism on the sorption of heavy metals from binary-solution by a low cost montmorillonite and its desorption potential. *Alexandria Engineering Journal,* 54**,** 757-767.

BARAKAT, M. A. 2011. New trends in removing heavy metals from industrial wastewater. *Arabian Journal of Chemistry,* 4**,** 361–377.

BHATTACHARYYA, K. G. & GUPTA, S. S. 2008. Adsorption of a few heavy metals on natural and modified kaolinite and montmorillonite: A review. *Advances in Colloid and Interface Science* 140**,** 114–131.

BHATTACHARYYA, K. G. & SUSMITA, S. G. 2006. Kaolinite, montmorillonite, and their modified derivatives as adsorbents for removal of Cu(II) from aqueous solution. *Separation and Purification Technology,* 50**,** 388–397.

BRADL, H. B. 2004. Adsorption of heavy metal ions on soils and soils constituents. *Journal of Colloid and Interface Science,* 277**,** 1-18.

CHERAGHI, E., AMERI, E. & MOHEB, A. 2015. Adsorption of cadmium ions from aqueous solutions using sesame as a low-cost biosorbent: kinetics and equilibrium studies. *International journal of environmental science and technology,* 12**,** 2579-2592.

ELLIS, D., BOUCHARD, C. & LANTAGNE, G. 2000. Removal of iron and manganese from groundwater by oxidation and microfiltration. *Desalination,* 130**,** 255-264.

GOLDANI, E., MORO, C. C. & MAIA, S. M. 2013. A study employing differents clays for Fe and Mn removal in the treatment of acid mine drainage. *Water, Air, & Soil Pollution,* 224**,** 1401.

GUMEDE, S. & MUSONGE, P. 2020. Effects of Physiochemical Properties of Nano-Clays on the Removal of Heavy Metals from Acid Mine Drainage . *'18th JOHANNESBURG Int'l Conference on Science, Engineering, Technology & Waste Management (SETWM-20),* 16-17 November,Johannesburg (SA)

KOŁODYŃSKA, D., KRUKOWSKA, J. A. & THOMAS, P. 2017. Comparison of sorption and desorption studies of heavy metal ions from biochar and commercial active carbon. *Chemical Engineering Journal,* 307**,** 353-363.

LATA, S., SINGH, P. K. & SAMADDER, S. R. 2015. Regeneration of adsorbents and recovery of heavy metals: a review. *International Journal of Environmental Science and Technology,* 12**,** 1461-1478.

LUKMAN, S., ESSA, M., BUKHARI, A. & BASHEER, C. 2013. Adsorption and desorption of heavy metals onto natural clay material: influence of initial pH.

MISHRA, S. 2014. Adsorption–desorption of heavy metal ions. *Current Science***,** 601-612.

MULOPO, J. 2015. Making sense of our mining wastes: Removal of heavy metals from AMD using sulphidation media derived from waste gypsum. *Journal of the Southern African Institute of Mining and Metallurgy,* 115**,** 1193-1197.

SETSHEDI, K., REN, J., AOYI, O. & ONYANGO, M. 2012. *Removal of Pb(II) from aqueous solution using hydrotalcite-like nanostructured material*.

YANG, X., WAN, Y., ZHENG, Y., HE, F., YU, Z., HUANG, J., WANG, H., OK, Y. S., JIANG, Y. & GAO, B. 2019. Surface functional groups of carbon-based adsorbents and their roles in the removal of heavy metals from aqueous solutions: a critical review. *Chemical Engineering Journal,* 366**,** 608-621.

YUE, X., LIU, W., CHEN, Z. & LIN, Z. 2016. *Simultaneous removal of Cu(II) and Cr(VI) by Mg–Al–Cl layered double hydroxide and mechanism insight*.

ZUBAIR, M., DAUD, M., MCKAY, G., SHEHZAD, F. & AL-HARTHI, M. A. 2017. Recent progress in layered double hydroxides (LDH)-containing hybrids as adsorbents for water remediation. *Applied Clay Science,* 143**,** 279-292.

# Performance Evaluation of Solar Operated Forced Convective Cabinet Dryer for Drying of Ginger

*S. R. Kalbande[1], A. N. Kale[2], A. J. Dhondge[3] and A. N. Kamble[4],*

1. Registrar & Head, Department of Unconventional energy Sources and Electrical Engineering, Dr. PanjabraoDeshmukh Agricultural University, Akola, Maharashtra, India. Email: surenkalbande@gmail.com
2. Assistant Professor, Dr.RajendraGode College of Agricultural Engineering, Buldhana, Maharashtra, India. Email:kaleashwini88@gmail.com
3. Assistant Professor, Department of Unconventional energy Sources and Electrical Engineering, Dr.PanjabraoDeshmukh Agricultural University, Akola, Maharashtra, India.Email:amol.jd1107@gmail.com
4. Assistant Professor, Department of Unconventional energy Sources and Electrical Engineering, Dr.PanjabraoDeshmukh Agricultural University, Akola, Maharashtra, India. Email: anilkumar_kamble@yahoo.com

*Correspondng author: amol.jd1107@gmail.comMob.7972063761*

## Abstract

The performance of solar cabinet dryer coupled with heat storage system of capacity 10 kg was evaluated at no load and full load condition under forced convection mode at the Deptt. of UCES & EE Dr. PDKV, Akola. The maximum temperature developed in solar dryer in forced convective mode for drying of ginger slices was observed to be 45°C at tray $T_1$ (top) , 45.7°C at tray $T_2$, 46.8°C at tray $T_3$, 47.5°C at tray $T_4$ and 48.7°C attray $T_5$ (bottom) of the dryer in summer season. The flow rate of air at ambient condition and at the exhaust chimney was observed in the range of 0.2 to 1.4 and 1 to 1.7 m/s, respectively. Drying time for 10 kg ginger slices for reducing its moisture content from 79 to 9% (wb) was found to be 12 h in the forced convective solar cabinet dryer with heat storage system, whereas it was 17 h for open sun drying. The ginger powder was prepared from slices dried in solar cabinet dryer under forced convective mode was found better in quality ,colour, appearance, taste, smell and overall acceptability than the samples dried in open sun drying method. The net present worth, benefit cost ratio and payback period was found to be Rs. 259224, 1.23 and 11 months for forced convective solar cabinet dryer with heat storage system.

## Keywords

Solar dryer, Moisture content, Drying, Ginger &Cabinet dryer.

## Introduction

India has a daily solar potential of 4 to 7 kWh/m$^2$ with about 1500-2000 sunshine hours annually. This available solar potential of 600 TW (5 x 10$^{12}$ kWh/year) is much more than the current energy consu,mption (Salam *et al.*, 2012). Drying of fruit and vegetables is one of the oldest methods of food preservation. In addition, drying enhances the storability, transportability, nutritional value retention, flavour and texture of food products reducing moisture content of foodstuff down to a certain level slows down the action of enzymes, bacteria, yeasts and moulds (Jithinraj and Karim, 2014).Ginger is the rhizome of the plant *Zingiberofficinale*. It is a tropical spice and cultivated in India, China, Japan, Indonesia, Australia, Nigeria and West Indies islands. India is the largest producer and consumer of ginger in the world (UmayalSundari*et al*.,2013). Out of the total production about 50% is consumed as fresh ginger, 30% is converted into dry ginger and 20% as seed materials. Major share of the dry ginger produced is dried and exported due to its medicinal properties (Jayashree*et al*., 2012).

Active solar dryer are also called force convection solar dryer. It is generally agreed that forced convection distributed solar dryer are more effective and more controllable than the natural-circulation type. External force is provided to the solar dryer such as fans may be powered with utility electricity if available, or with a solar photovoltaic panel. (Mohanraj and Chandrasekar, 2008). The solar dryer is an energy efficient option in the drying processes. Use of forced convection solar dryers seems to be an advantage compared to traditional methods and improves the quality of the product considerably (Mohanraj and Chandrasekar, 2009). Therefore the study was undertaken on"Solar operated forced convective cabinet dryer coupled with heat storage system"

## Material & Methods

A. Experimental procedure

Ginger was thoroughly washed with tap water to remove the dirt. The fingers of ginger rhizomes were separated and the fingers were cut into slices of thickness 3 to 4 mm .Solar drying of ginger slices were carried out without any pre-treatment. In full load test the ginger samples were spread over the thin perforated dishes. The experiment was conducted in summer month of March 2015during 8:30 to 20:30 h. The initial weight of the samples was recorded. Each sample on tray was weighted regularly at an interval of 1 h and simultaneously the temperature, relative humidity, solar radiation and air velocity inside the solar cabinet dryer was measured. Rate of loading ginger slices on each tray was 1.9 kg /m$^2$.

The performance of the solar cabinet dryer with heat storage system was evaluated at no load and full load conditions for forced convective drying of ginger slices. Under the full load condition the ginger slices were spread over the stainless steel wire mesh of 22 gauge of drying trays.

### B. Formulae

Following are the different formulae used for the performance evaluation of the cabinet dryer.

### 1. Moisture content

The moisture content of the produce is computed by following formula (Chakraverty, 1988).

$$\text{M.C. (wb)\%} = \frac{(W_1 - W_2)}{W_1} \times 100$$

$$\text{M.C. (db)\%} = \frac{(W_1 - W_2)}{W_2} \times 100$$

Where,

$W_1$ - weight of sample before drying, g
$W_2$ - weight of bone dried sample, g

### 2. Moisture ratio

The moisture ratio of the produce is computed by following formula (Chakraverty, 1988).

$$\text{Moisture Ratio (M.R.)} = \frac{(M_t - M_e)}{(M_i - M_e)} = e^{-kt}$$

Where,
$M_t$ - Moisture content (db), %
$M_e$ - Equilibrium moisture content (db), %
$M_i$ - Initial moisture content(db), %

k - Drying rate constant per minute

t - Drying time, min

## 3. Drying efficiency

The drying efficiency of solar cabinet dryer was calculated by following formula (UmayalSundari*et al.*2013).

$$\eta = \frac{m_w L}{I_t \times A_c} \times 100$$

Where,

$m_w$ - Mass of water evaporated  kg/hr

$I_t$- insolation on collector surface, $kJ/m^2h$

$A_c$- Collector Area $m^2$

L- Latent heat of vaporization of water,kJ/kg

The isometric view of the existing solar cabinet dryer coupled with heat storage system is given in Fig .1.
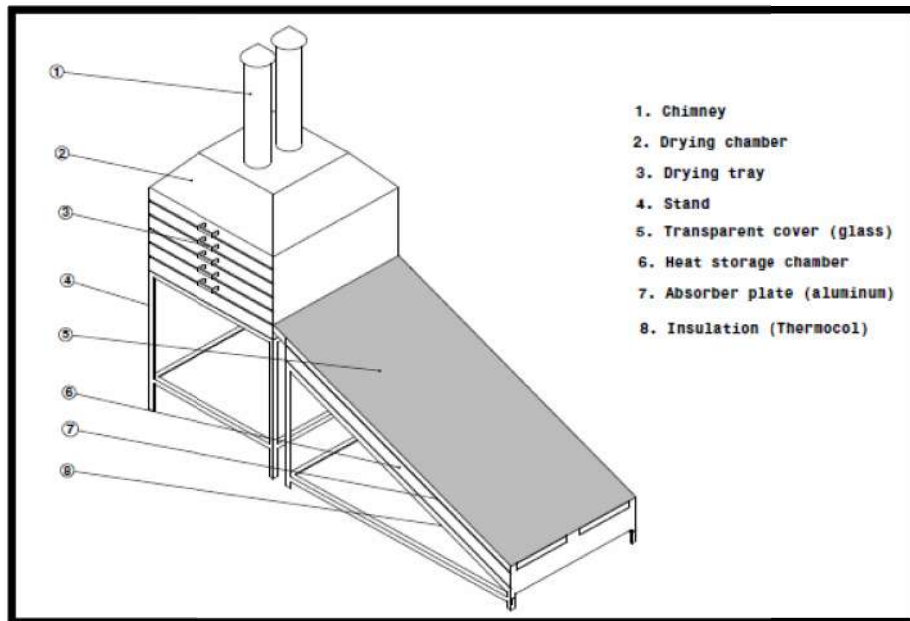


**Fig.1 Isometric view of existing solar cabinet dryer coupled with heat storage system**

## Result & discussion

A.  No load testing of forced convective solar cabinet dryer coupled with heat storage system
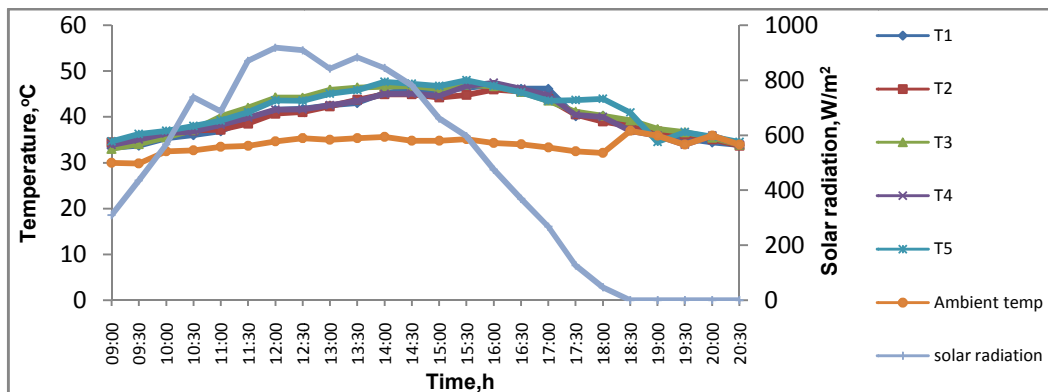


**Fig.1 Temperature variation in the forced convective solar cabinet dryer coupled with heat storage system at no load condition in March 2015.**

The average temperature in the solar cabinet dryer was observed in the range of 33.20°C to 45.17°C at Tray 1($T_1$), 33.43 to 46.08 at Tray 2($T_2$), 33.80°C to 47.52°C at Tray 3($T_3$), 34.07°C to 47.80°C at Tray 4($T_4$), 34.67°C to 48.63°C at Tray 5($T_5$) from Fig. 1. A WaheedDeshmukh et al. (2014) found the temperature range between 38 to 70° C in solar cabinet dryer. The ambient temperature, relative humidity and solar intensity were observed in the range of 30 to 35.67°C, 29 to 19% and 46.4 to 918 W/m$^2$,respectively. The flow rate of air at ambient condition and at the exhaust chimney was observed in the range of 0.4 to 1.4 and 0.5 to 1.5 m/s, respectively. The temperature rose slowly during morning till late afternoon and after that it started declining during evening and reached to near ambient temperature.

From the Fig. 1 it is clear that the temperature inside the solar cabinet drying chamber was significantly higher when compaired to OSD. It migth be due to the solar energy entering the cabinet is trapped inside the cabinet solar dryer facilitating absorption and the black surface of collector gives away of its energy to the cabinet by conduction heating.

B. Full load testing of forced convective solar cabinet dryer coupled with heat storage system

From Fig. 2 it was depicted that the average moisture content of ginger slices placed in $T_1$, $T_2$, $T_3$, $T_4$ and $T_5$ trays reduced from 411.46 to 9.67, 9.87, 9.17, 9.36 and 9.49% (db) in 12 h, respectively in forced convective solar cabinet dryer with heat storage system. Whereas, the moisture content of ginger slices was reduced from 411.46 to 9.13 % (db) in 17 h in OSD. From Fig. 3 it is seen that the drying rate of ginger slices dried in trays $T_1$, $T_2$, $T_3$, $T_4$ and $T_5$ of forced convective solar cabinet dryer coupled with heat storage system varied from 1.530 to 0.023, 1.2177 to 0.0115, 0.82 to 0.02, 1.310 to 0.01 and 1.52 to 0.030 gm/100gm bdm min, respectively. The drying rate of ginger slices dried in OSD was found to be 0.966 to 0.004 gm/100gm bdm min.
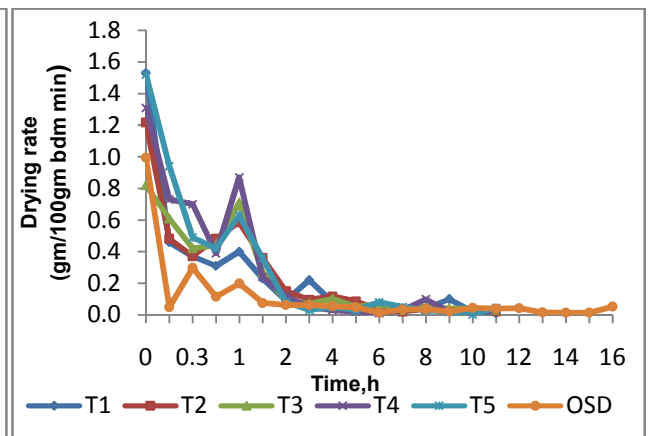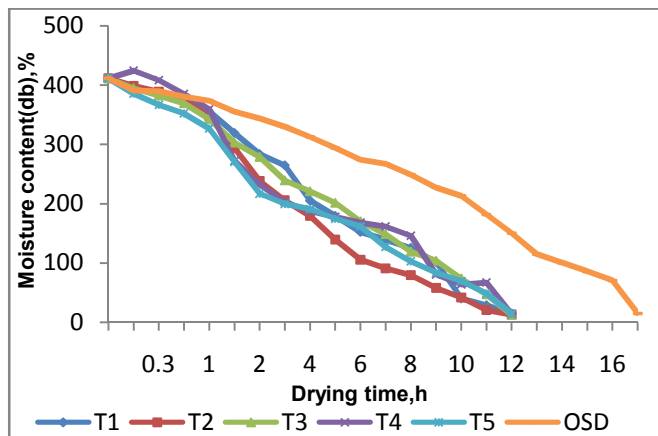


Fig. 2 Variation of moisture content of ginger slices in forced convective solar cabinet dryer coupled with heat storage system and OSD

Fig. 3 Variation of drying rate of ginger slices in forced convective solar cabinet dryer with heat storage system and OSD

The drying rate in forced convective solar cabinet dryer was found to be more as compared to OSD. Similar results were obtained by Sunil K. Sansaniwal et al. (2017). From Table 2 It is revealed that the average heat efficiency of forced convective solar cabinet dryer coupled with heat storage system was varied from28.81 to 37.22% during 8:30 to 17:30 and 28.81 to 35.82 during 17:30 to 20:30 h. it was observed in decreasing at day time and increasing at non sunshine hour mode.

**Table 2. Effective heat efficiency (EHE) of forced and natural convective solar cabinet dryer**

| Drying time, h | Drying time, h | EHE of forced convective solar cabinet dryer | Thermal efficiency, % |
|---|---|---|---|
| 0 | 8:30 | 37.22 | 14.05 |
| 1 | 9:30 | 46.54 | 19.85 |
| 2 | 10:30 | 59.21 | 26.85 |
| 3 | 11:30 | 65.15 | 34.82 |
| 4 | 12:30 | 63.17 | 30.30 |
| 5 | 13:30 | 54.44 | 17.11 |
| 6 | 14:30 | 45.45 | 13.88 |
| 7 | 15:30 | 41.81 | 10.9 |
| 8 | 16:30 | 28.57 | 7.56 |
| 9 | 17:30 | 28.81 | 6.50 |
| 10 | 18:30 | 31.89 | **Avg.= 20.28** |
| 11 | 19:30 | 33.33 | |
| 12 | 20:30 | 35.22 | |

The average thermal efficiency of forced convective solar cabinet dryer with heat storage system was found to be 20.28 %. The variation in thermal efficiency of dryer was observed may be due to variation in solar intensity, ambient temperature and temperature developed in dryer.

C. Quality analysis of the dried agricultural produce ginger

i. Protein content of ginger powder prepared from dried slices

The per cent protein content in ginger powder sample was found to be 18, 17 and 13 in forced convective, natural convective solar cabinet dryer and OSD method, respectively.

ii. Colour value of different ginger powder sample

The results in Table 3 revealed that the forced and natural convective solar cabinet dryer dried sample was very lower value of L* i.e.lightness as compared to other means implying that the powder appeared darker. The samples appear greener shown by lower a* values. The sample of natural convective solar cabinet dryer dried shown the lower value of a* so appears less green as compared to forced convection type.Similar results were obtained by A. WaheedDeshmukh et al. (2014).

**Table 3. Colour value of different ginger powder sample**

| Sample Name | X | Y | Z | L* | a* | b* |
|---|---|---|---|---|---|---|
| $S_1$ | 45.65 | 45.33 | 31.48 | 73.10 | 3.43 | 24.98 |
| $S_2$ | 43.15 | 43.04 | 28.74 | 71.83 | 2.66 | 26.10 |
| $S_3$ | 43.68 | 43.47 | 29.86 | 71.87 | 3.07 | 25.08 |

($S_1$ - Sun dried ginger powder, $S_2$ - Natural convective solar cabinet dried powder, $S_3$ - Forced convective solar cabinet dried powder, X, Y & Z are the imaginary positive primaries used by instrument for colour measurement)

## Conclusion

From the above results following conclusion are drawn.

1. The average drying time for ginger slices dried in forced convective solar cabinet dryer was found 20 % less than natural convective system.
2. Extended drying hours of 3 were obtained after sunset in solar cabinet dryer coupled with heat storage system.
3. The ginger powder obtained from forced convection was found to be dark colour, high protein content, better smell and taste as compared to natural convection.

## References

Salam, A.A., R.Anjan, B. Srivatsa and R.Senthil, 2012.Thermal performance analysis on solar integrated collector storage. Academic Research Journal (UARJ).1(2):111-114.

Jithinraj, T. and Aftab A Karim, 2014. Experimental analysis on multi pass flat plate collector solar air dryer. International Journal of Emerging Engineering Research and Technology. 2:1-11.

Umayal, Sundari, A. R. P. Neelamegam and C.V. Subramanian. 2013. Study and analysis of drying characteristics of ginger using solar drier with evacuated tube collectors. Research Journal of Pharmaceutical, Biological and Chemical Sciences 4(3):1258-1267.

Jayashree, E. andVisvanathan R. and John Zachariah T. 2012. Quality of dry ginger (Zingiberofficinale) by different drying methods.Journal of Food Science and Technology.

Mohanraj, M. and P. Chandrasekar 2009. Performance of a forced convection solar dryer integrated with Gravel as heat storage material for chilli drying. Journal of Engineering Science and Technology, Vol. 4(3), pp.305-314.

Chakraverty A.,1997. Post harvest technology of cereals ,pulses and oilseeds. Oxford and IBH publishing,49-51.

A. WaheedDeshmukh, Mahesh N. Varma, Chang KyooYoo and Kailas L.Wasewar (2014). Investigation of solar drying of ginger (Zingiberofficinale): Empricalmodelling, drying characteristics, and quality study.Chinese Journal of Engineering, Volume 2014, http://dx.doi.org/10.1155/2014/305823.

Sunil K. Sansaniwal, M. Kumar, Rajneesh and V. Kumar (2017). Investigation of indirect solar drying of ginger rhizomes (ZingiberOfficinale): A comparative study.Journal of Engineering Science and Technology Vol. 12(7), pp.1956- 1971.

# ESTIMATION OF VLE DATA OF GREEN SOLVENT SYSTEMS USING DWSIM SIMULATION SOFTWARE FOR VARIOUS THERMODYNAMIC MODELS

*Parth Shah[1*], Dr Sachin Parikh[1,2]*
*[1]Gujarat Technological University, Ahmedabad, India,*
*[2]Directorate of Technical Education Gandhinagar, India.*
*Corresponding Author :[1]parthgcet@gmail.com, +91-9429612518 (M)*
*[2]sachinparikh@hotmail.com*

**Abstract**

In present study, green solvents that are environment friendly in nature were considered because it will reduce the environment pollution by replacing the petroleum derived solvents. Solvent used in chemical industry were mostly derived from the petroleum crude oils(Sharma, 2015). Solvent emission increases the environment pollution. With the use of green solvents, closed carbon cycle will reduce the environment pollution drastically(Capello, Fischer, & Hungerbühler, 2007a). Bio-derived solvents are the recent replacement of petroleum solvents that increased the industrial attention to reduce the environment pollution and hazardous effect on the living organism(Jessop, 2011). Industrial application of solvent required laboratory data generation to design industrial equipment. The behavior of the binary liquid mixture and separation of the liquid mixture is studied with the use of the vapor liquid equilibrium (VLE) data(Parsana & Parikh, 2015). DWSIM simulation software is used to predict the binary VLE data using different thermodynamic models(Tangsriwong et al., 2020). Activity coefficient was determined based on the group contribution methods such as UNIFAC, ASOG and UNIQUAC(Wittig, Lohmann, & Gmehling, 2003). The theoretical activity coefficient helped to determine the non-ideality behavior of the mixture(Hartono, Saleem, Arshad, Usman, & Svendsen, 2013). In this study, VLE data were generated using DWSIM simulation software and activity coefficient using UNIFAC method was determined for two different binary system. Chemicals considered for the calculation were green solvents such as 2-MeTHF (2-Methyl Tetra Hydro Furan), Propylene Carbonate and Water. System considered for the data generations were 2-MeTHF – Water and Propylene Carbonate – Water. Activity coefficient and Vapor composition were determined at atmospheric pressure and at vacuum. UNIFAC parameters were found out from the literature and the interaction parameters were calculated. DWSIM simulation software is used for prediction of VLE data using various thermodynamic models.

***Key Words:*** DWSIM Simulation, UNIFAC Method, Green Solvent, VLE data, Activity coefficient.

## 1. Introduction

The environment conservation is the major challenge facing the upcoming industry(Jessop, 2011). The loss of the solvent will increase the health and environment hazard. All the government restriction will focus on the emission of the chemical in the open environment. The release of the chemical is restricted highly by the local government authority all over the world. To overcome this problem to reduce the long-term environmental effect, it is important to use a solvent that has negligible environment effect or biologically degradable compound (Capello, Fischer, & Hungerbühler, 2007b). Green solvents are the most suitable and potential solvent to reduce the environmental degradation. It is important that green solvent has the properties such as low vapor pressure, high boiling point, bio derived product(Mohammad & Inamuddin, 2012). These important properties of green solvents make it more suitable for the better eco-friendly technology development.

Based on the biodegradability of the chemical present in the waste stream, the quality of the process is identified. The separation of the organic compound from the main process is important to improve the water quality that considered as waste water. Also, it is necessary as per the government rules and regulations. For examples, for the removal of the phenol from the wastewater using cumene as solvent(Villegas et al., 2016). For the removal of aniline from wastewater, nitrobenzene is used as solvent(Li, 2010). Formic acid – water separation done effectively by butyl acetate and ethyl acetate (Timedjeghdine, Hasseine, Binous, Bacha, & Attarakih, 2016). For the separation of acetic acid from water number of solvents such as n-butanol, i-butanol, ethyl acetate used as industrial applications (Haque, Khan, Roy, & Uddin, 2013).

Major challenge for the production process is to meet the physical and ecological requirement by selecting solvent to ensure the plant safety and environment problem. The environmental assessment helping to solve this complex problem. The short-term environmental effect measures the legislative limits on the all the pollutants in three phases (Solid, Liquid, Gases). In long term environmental effects classified in two different groups such as environment concern and human health concern. The green solvent that is completely bio-degradable should select first to eliminate the long-term environment damage.(Pistikopoulos & Stefanis, 1998).

Solvents are the most inherent part of the chemical industries. Solvents are volatile organic solvents (VOCs) obtained or produced from the non-renewable sources(Bermejo, Mendiola, Ibáñez, Reglero, & Fornari, 2015). With the awareness of the pollution hazard, the use of the bio-derived and less hazardous solvents found to be potential alternative(Rapinel et al., 2020). There are number of green solvents identified in past few years such as Cyclo Pentyl methyl ether(Kobayashi, Shibukawa, Miyaguchi, & Masuyama, 2016), 2-Methyl Tetra hydro furan(Antonucci et al., 2011) and Propylene carbonate(Lu et al., 2004).

The potential solvent application is studied by finding out the behavior of the binary liquid mixture. Vapor-Liquid Equilibrium (VLE) data gives the separation efficiency of the binary mixture(Fonseca, Dohrn, & Peper, 2011). This separation gives the recoverability and the reuse of the solvent for chemical process industry. The data generated for the binary mixtures are very useful for the designing of the industrial scale equipment.

Here, binary mixture of two different organic solvents were studied. Using activity coefficient, the behavior of binary mixture and ideality of the mixture is studied. Current study aims to provide the mixture behavior of the organic chemicals.

## 2. Materials and Methodology

For the current study, two organic solvents such as 2-Methyl Tetra Hydro furan(2-MeTHF) and Propylene carbonate (PC). For two different systems, VLE data were generated using group contribution method such as UNIFAC. This data was compared with the data generated using DWSIM simulation software. It is important to compare the data of simulated data with the group contribution methods. Binary data of both chemical systems were generated for NRTL thermodynamics model(Döker & Gmehling, 2005). For the current study, atmospheric pressure is considered.


## 3. VLE Data generation Methodology


### 3.1 UNIFAC Method Calculation

For two different systems such as 2-MeTHF (1) – Water (2) and Propylene Carbonate (3)-Water (2), VLE data has been generated theoretically using UNIFAC - group contribution method. The group parameters are listed in table 1 for PC-water system. The group parameter

for 2-MeTHF – Water are listed in table 2. The group contribution components consist of volume contributor -$R_k$ and surface area contribution - $Q_k$.

Table 1 UNIFAC Sub group parameters for Propylene Carbonate (PC) -Water System(Wittig et al., 2003)

| Component Group | k | $R_k$ | $Q_k$ | $vk_1$ | $vk_2$ |
|---|---|---|---|---|---|
| $CH_3$ | 1 | 0.9011 | 0.848 | 1 | 0 |
| $CH_2CO$ | 20 | 1.4457 | 1.18 | 1 | 0 |
| CHO | 27 | 0.6908 | 0.468 | 1 | 0 |
| $H_2O$ | 17 | 0.92 | 1.4 | 0 | 1 |

Table 2 UNIFAC Sub group parameters for 2-MeTHF -Water System(Wittig et al., 2003)

| Component Group | k | $R_k$ | $Q_k$ | $vk_1$ | $vk_2$ |
|---|---|---|---|---|---|
| $CH_3$ | 1 | 0.9011 | 0.848 | 1 | 0 |
| $CH_2$ | 2 | 0.6744 | 0.54 | 2 | 0 |
| CH | 3 | 0.4469 | 0.228 | 1 | 0 |
| CHO | 26 | 0.9183 | 0.78 | 1 | 0 |
| $H_2O$ | 17 | 0.92 | 1.4 | 0 | 1 |

With the help of parameters mentioned in the Table 1 and Table 2, the activity coefficient for both the binary systems were calculated. The activity coefficients are in figure 1 and figure 2. As seen from the figure, the activity coefficient values increase drastically when approaches pure component concentration.
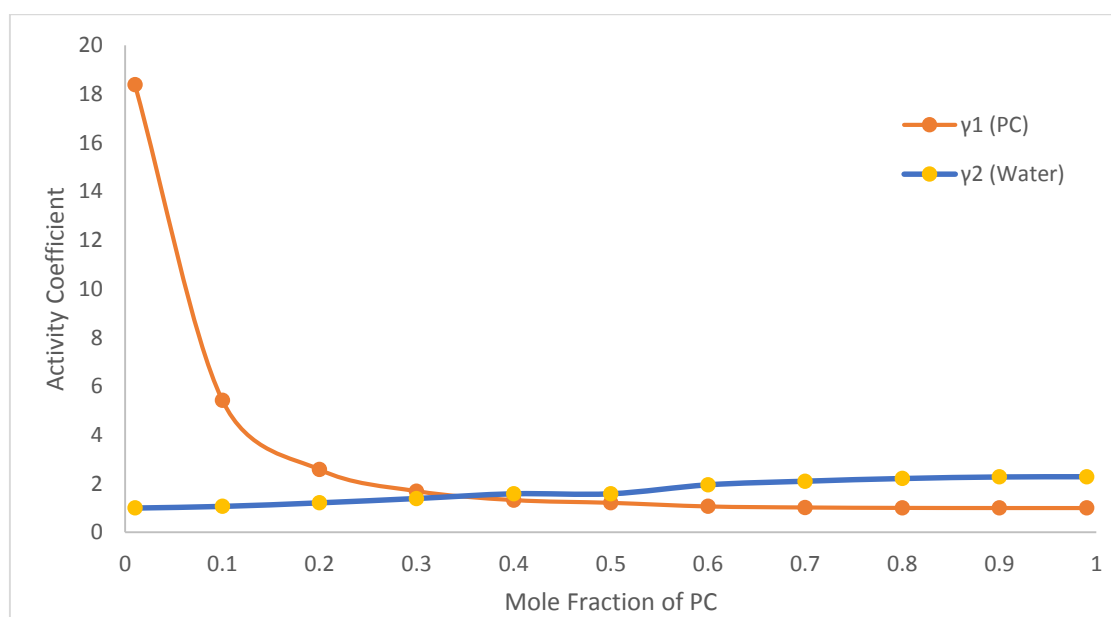


Figure 1 Activity Coefficient of PC – Water using UNIFAC method
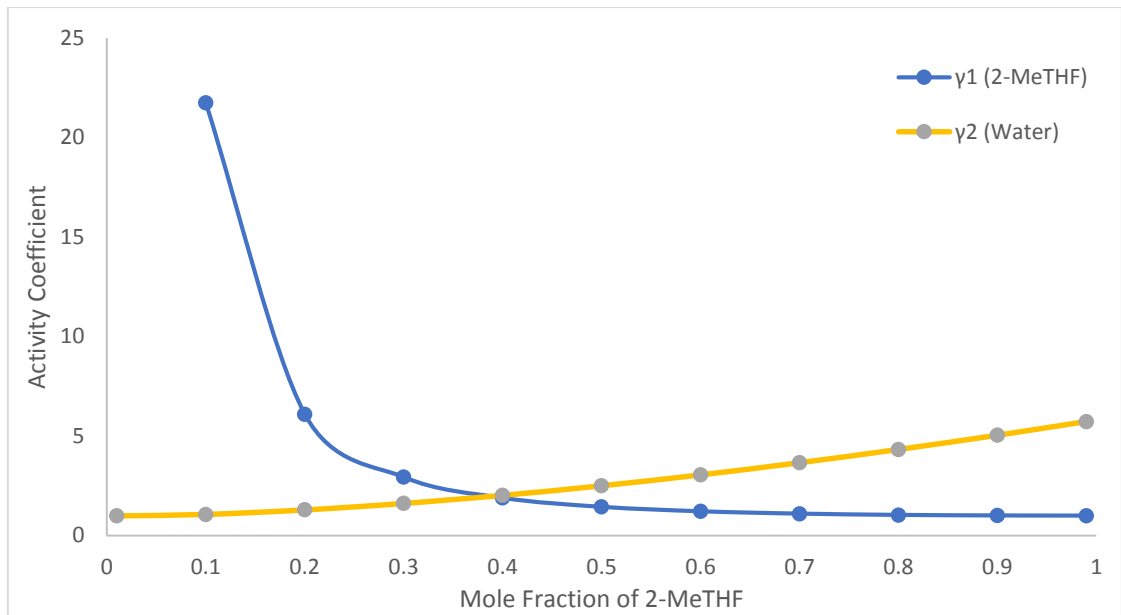
Figure 2 Figure 1 Activity Coefficient of 2-MeTHF – Water using UNIFAC method

## 3.2 DWSIM Method

DWSIM software is open-source software. DWSIM is very useful simulation software used to predict the VLE data(Jaćimović & Genić, 2018). For the prediction of VLE data, thermodynamics models have to be selected for each run of simulation. For current study, two different models have been considered for the organic solvent systems such as NRTL model. The simulation program has been programmed as per figure 3.
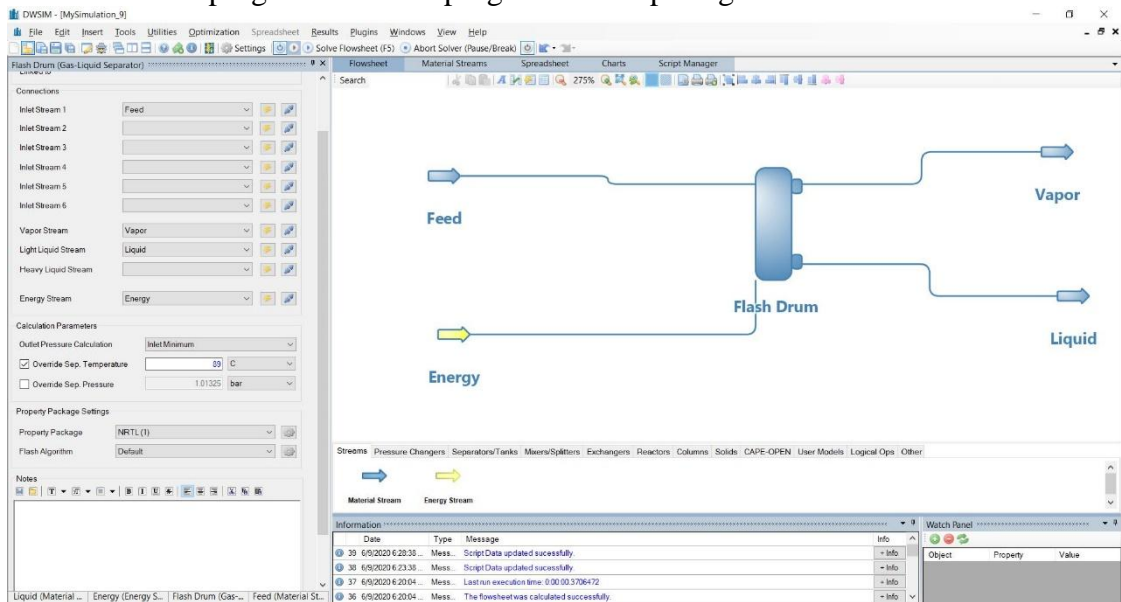


Figure 3 DWSIM simulation flow diagram

## 4. Result and Declaration

Based on the simulation, the VLE data for both the systems were generated at atmospheric pressure. At atmospheric pressure, the T(xy) plot for both the systems. The results show the very promising data using NRTL model as shown in figure 4.
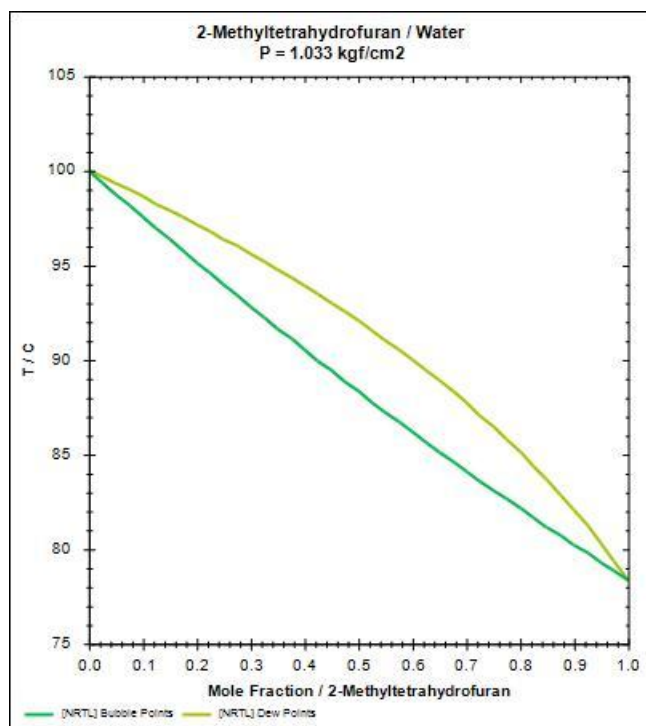
(a)
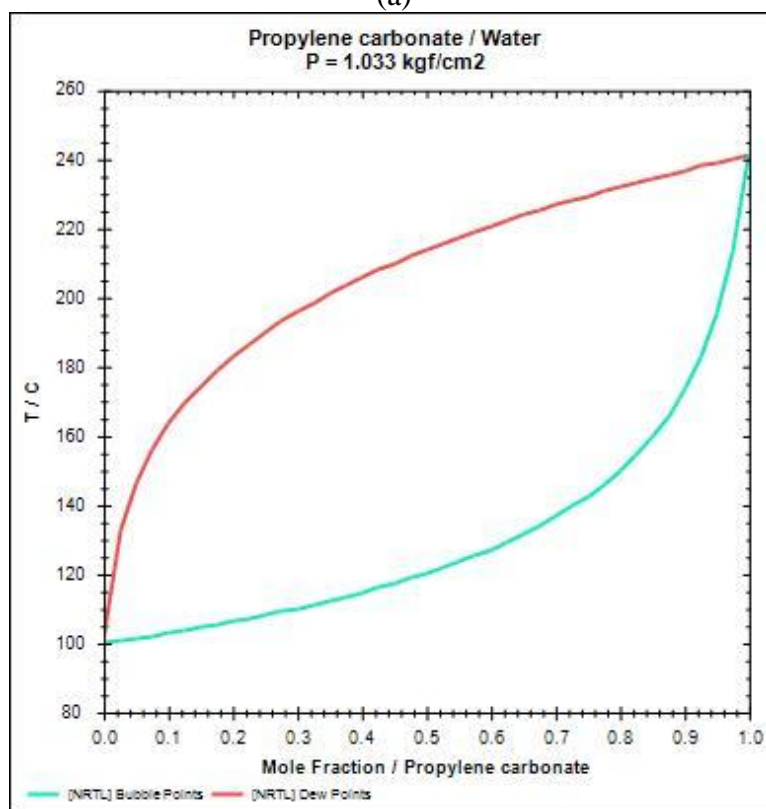


(b)

Figure 4 T-xy diagram using DWSIM method for system (a) 2-MeTHF- Water, (b) PC-Water

Similarly, xy data was generated for the for both the systems. The plot is generated isothermally. The VLE data at uniform temperature for both the systems represent very similar curve to that of the UNIFAC method. The separation of vapor and liquid mixture at

the given temperature shows the similar composition profile to the that of UNIFAC method. The plot is indicated in figure 5.
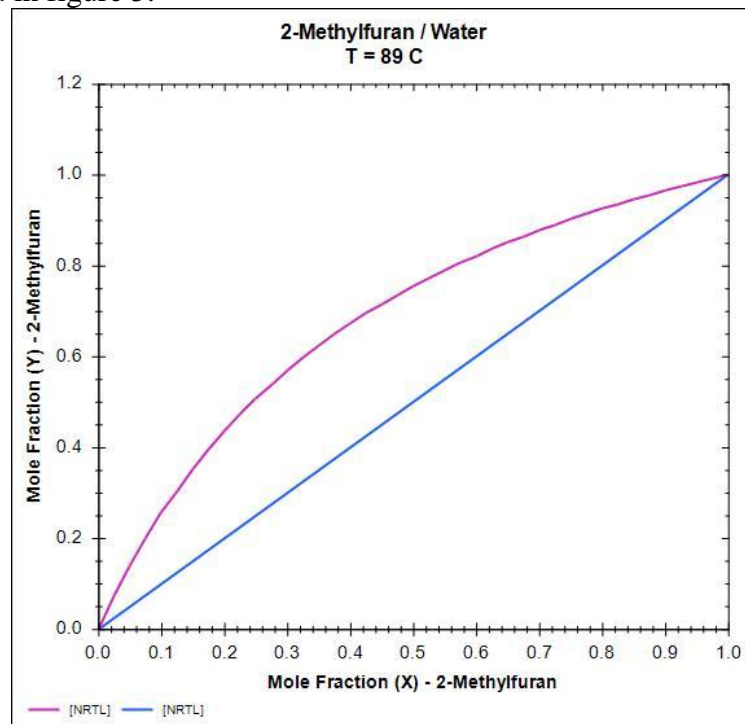


(a)
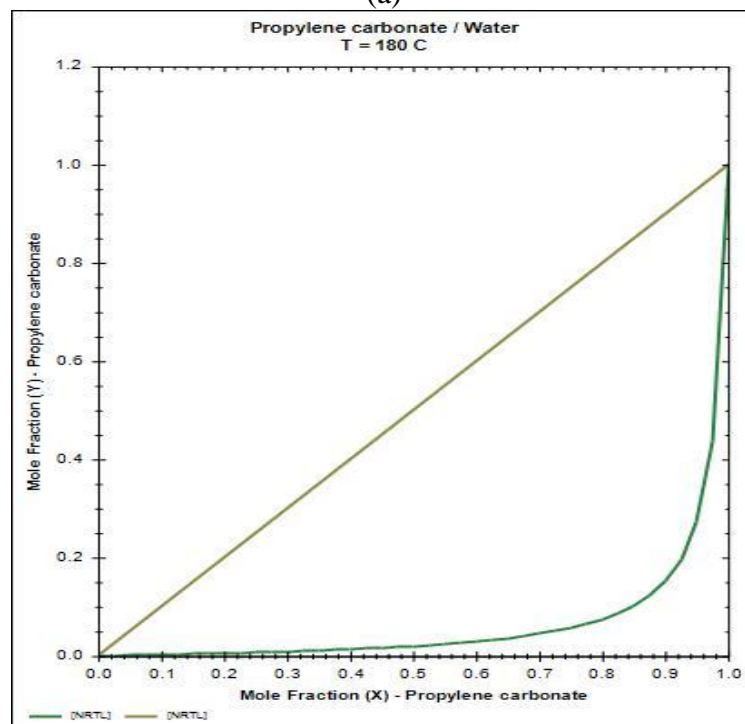


(b)

Figure 5 xy plot of the binary system using NRTL method for (a) 2-MeTHF- Water, (b) PC-Water

## 5. Conclusion

Based on the result generated, it was observed that the DWSIM method accuracy is high for the given system. The result shows that the average deviation observed for the PC-water and

2-MeTHF – water system is below 2% as compared to the UNIFAC method. The data generated to study the separation efficiency of the binary mixture are very promising for the industrial scale application.

**References:**
1.  Antonucci, V., Coleman, J., Ferry, J. B., Johnson, N., Mathe, M., Scott, J. P., & Xu, J. (2011). Toxicological assessment of 2-methyltetrahydrofuran and cyclopentyl methyl ether in support of their use in pharmaceutical chemical process development. *Organic Process Research and Development*, *15*(4), 939–941. https://doi.org/10.1021/op100303c
2.  Bermejo, D. V., Mendiola, J. A., Ibáñez, E., Reglero, G., & Fornari, T. (2015). Pressurized liquid extraction of caffeine and catechins from green tea leaves using ethyl lactate, water and ethyl lactate + water mixtures. *Food and Bioproducts Processing*, *96*, 106–112. https://doi.org/10.1016/j.fbp.2015.07.008
3.  Capello, C., Fischer, U., & Hungerbühler, K. (2007a). What is a green solvent? A comprehensive framework for the environmental assessment of solvents. *Green Chemistry*, *9*(9), 927–934. https://doi.org/10.1039/b617536h
4.  Capello, C., Fischer, U., & Hungerbühler, K. (2007b). What is a green solvent? A comprehensive framework for the environmental assessment of solvents. *Green Chemistry*, *9*(9), 927–934. https://doi.org/10.1039/b617536h
5.  Döker, M., & Gmehling, J. (2005). Measurement and prediction of vapor-liquid equilibria of ternary systems containing ionic liquids. *Fluid Phase Equilibria*, *227*(2), 255–266. https://doi.org/10.1016/j.fluid.2004.11.010
6.  Fonseca, J. M. S., Dohrn, R., & Peper, S. (2011). High-pressure fluid-phase equilibria: Experimental methods and systems investigated (2005-2008). *Fluid Phase Equilibria*, *300*(1–2), 1–69. https://doi.org/10.1016/j.fluid.2010.09.017
7.  Haque, S., Khan, M. Z. H., Roy, B. C., & Uddin, H. (2013). Separation of Acetic Acid from Aqueous Solution using Various Organic Solvents. *Journal of Science and Technology*, *5*(2). Retrieved from https://publisher.uthm.edu.my/ojs/index.php/JST/article/view/655
8.  Hartono, A., Saleem, F., Arshad, M. W., Usman, M., & Svendsen, H. F. (2013). Binary and ternary VLE of the 2-(diethylamino)-ethanol (DEEA)/3-(methylamino)-propylamine (MAPA)/water system. *Chemical Engineering Science*, *101*, 401–411. https://doi.org/10.1016/j.ces.2013.06.052
9.  Jaćimović, B., & Genić, S. (2018). Reconsideration of T–P–x–y data and correlations for ammonia–water mixture for pressures up to 100 bar. *Fluid Phase Equilibria*, *463*, 62–68. https://doi.org/10.1016/j.fluid.2018.02.007
10. Jessop, P. G. (2011). Searching for green solvents. *Green Chemistry*, *13*(6), 1391–1398. https://doi.org/10.1039/c0gc00797h
11. Kobayashi, S., Shibukawa, K., Miyaguchi, Y., & Masuyama, A. (2016). Grignard Reactions in Cyclopentyl Methyl Ether. *Asian Journal of Organic Chemistry*, *5*(5), 636–645. https://doi.org/10.1002/ajoc.201600059
12. Li, C. H. (2010). Recovery of aniline from wastewater by nitrobenzene extraction enhanced with salting-out effect. *Biomedical and Environmental Sciences*, *23*(3), 208–212. https://doi.org/10.1016/S0895-3988(10)60054-2
13. Lu, X. B., Liang, B., Zhang, Y. J., Tian, Y. Z., Wang, Y. M., Bai, C. X., … Zhang, R. (2004). Asymmetric Catalysis with CO2: Direct Synthesis of Optically Active Propylene Carbonate from Racemic Epoxides. *Journal of the American Chemical Society*, *126*(12), 3732–3733. https://doi.org/10.1021/ja049734s
14. Mohammad, A., & Inamuddin. (2012). Green Solvents. *Springer*, (September). https://doi.org/10.5281/zenodo.893346

15. Parsana, V. M., & Parikh, S. P. (2015). *Need for Vapour-Liquid Equilibrium Data Generation of Systems Involving Green Solvents*. 5(6), 55–62.
16. Pistikopoulos, E. N., & Stefanis, S. K. (1998). Optimal solvent design for environmental impact minimization. *Computers and Chemical Engineering*, 22(6), 717–733. https://doi.org/10.1016/S0098-1354(97)00255-X
17. Rapinel, V., Claux, O., Abert-Vian, M., McAlinden, C., Bartier, M., Patouillard, N., … Chemat, F. (2020). 2-methyloxolane (2-MeOx) as sustainable lipophilic solvent to substitute hexane for green extraction of natural products. Properties, applications, and perspectives. *Molecules*, 25(15). https://doi.org/10.3390/molecules25153417
18. Sharma, S. R. (2015). Green Chemistry, Green Solvents and Alternative Techniques in Organic Synthesis SONALI R. SHARMA Green Chemistry, Green Solvents and Alternative Techniques in Organic Synthesis. *International Journal of Chemical and Physical Sciences*, 4, 2319–6602. Retrieved from www.ijcps.org
19. Tangsriwong, K., Lapchit, P., Kittijungjit, T., Klamrassamee, T., Sukjai, Y., & Laoonual, Y. (2020). Modeling of chemical processes using commercial and open-source software: A comparison between Aspen plus and DWSIM. *IOP Conference Series: Earth and Environmental Science*, 463(1). https://doi.org/10.1088/1755-1315/463/1/012057
20. Timedjeghdine, M., Hasseine, A., Binous, H., Bacha, O., & Attarakih, M. (2016). Liquid-liquid equilibrium data for water + formic acid + solvent (butyl acetate, ethyl acetate, and isoamyl alcohol) at T = 291.15 K. *Fluid Phase Equilibria*, 415, 51–57. https://doi.org/10.1016/j.fluid.2016.01.045
21. Villegas, L. G. C., Mashhadi, N., Chen, M., Mukherjee, D., Taylor, K. E., & Biswas, N. (2016). A Short Review of Techniques for Phenol Removal from Wastewater. *Current Pollution Reports*, 2(3), 157–167. https://doi.org/10.1007/s40726-016-0035-3
22. Wittig, R., Lohmann, J., & Gmehling, J. (2003). Vapor-liquid equilibria by UNIFAC group contribution. 6. Revision and extension. *Industrial and Engineering Chemistry Research*, 42(1), 183–188. https://doi.org/10.1021/ie020506l

# Integrated Pest Management in cotton: Sustainable Green solution with Agricultural Mineral Oil (AMO)

**Banti Sidhiwala[1], TCSM Gupta1*, T. Saritha[1]**
[1]Research and Development Centre, APAR Industries Ltd., Navi Mumbai – 400 701, Maharashtra, INDIA.
*Corresponding author: tcsm.gupta@apar.com, mobile number: +91-7738057579

## Abstract

"PEST- RESISTANCE- PESTICIDE RESIDUE" is gaining more attention in agricultural field, directing most of the efforts towards the use of environmentally acceptable, sustainable methods of pest control. Excessive use of pesticides results in residue and resistance in pests, resulting in loss of crop to farmers; apart from human safety issues. Cotton, being one of the most important commercial crops of India, consumes over 50 % of total pesticides used in the country. Recent Field reports indicate that White fly (Bemisa Tabaci) is one of the major sucking pests infecting the cotton apart from jassids (Amrasca biguttula) causing huge economic loss to farmers in terms of quantity and quality. Integrated Pest Management (IPM) is the best tool for minimizing the risk and problems in cotton cultivation. Agricultural mineral oil (AMO) is a central component of many integrated pest and disease management programs because of their relatively minor side-effect on natural enemies, low residual effect, and their undoubted efficacy against a wide-range of pests and diseases through asphyxiation. AMO's are highly refined, food grade formulated using oils. In the recent study, Bio-efficacy analysis and quantification of residue of AMO is done from cotton; soil and leaf which showed minimal trace residues which are much below of $LD_{50}$ and $LC_{50}$ limits. Present study showed the AMO's improves the farm economics, thus offering a green and safe crop management solution.

Keywords: AMO, Bt.cotton, aphids, jassids, whiteflies, bio-efficacy, residue, yield

## 1. Introduction

Cotton (Gossypium hirsutum) is an important natural fibre crop cultivated in varying climatic conditions of tropics as well sub-tropic regions of more than 83 countries all over the world. Cotton plays a key role in the National economy in terms of generation of direct and indirect employment in the Agricultural and Industrial sectors.

Bt. cotton is a genetically modified organism (GMO) cotton variety, which produces an insecticide to bollworm. A gene from the soil bacterium Bacillus thuringiensis (Bt) was transferred to the cotton genome. This gene encodes the production of a protein that is toxic to certain lepidopteran insects. As an inbuilt pest resistance mechanism, Bt. could cause significant economic and ecological benefits, provided that pest populations would not rapidly overcome this resistance. Major pests attack on Bt.cotton are Whitefly (Bemisia tabaci), Jassid (Amrasca bigutella bigutella), Thrips (Thrips tabaci), Aphids (Aphis gossypii), Mealy bugs (Pseudococcidae) and Spider mites (Tetranychus urticae).

Leaf hoppers (Jassids) feed on cotton as well a wide range of other host plants. They apparently introduce a toxin that impair photosynthesis in proportion to the amount of feeding, and this causes the edges of leaves to curl down wards, the leaf become yellowish and then redden. The 'Honeydew' excreted by aphids and whiteflies deposited the upper surface of lower

leaves, over which sooty mould develops which interfere with photosynthesis of the plant. Heavy fungal growth on honeydew leads to premature leaf drop. Honeydew on open bolls causes stickiness of cotton which interferes with picking, ginning and spinning thus the lint value is reduced.

Currently, much attention in the agricultural industry is directed towards the use of environmentally acceptable, sustainable methods of pest control. Petroleum oils are highly refined, paraffinic oils that are used to manage pests and diseases of plants. Petroleum oils may be referred to by many names, including horticultural mineral oil (HMO), spray oil, dormant oil, summer oil, Agricultural Mineral oil (AMO) or white mineral oil.

Use of petroleum-derived oils as agricultural crop protectants dates back to the 1800s, but it was not until the latter half of the 20th century that advances in petroleum chemistry allowed substantial modification and diversification in their commercial applicability. Oils contain saturated and unsaturated hydrocarbons The Unsulfonated Residue (UR) is a measure of the degree of oil refinement and is expressed as a percentage. In general, the higher the UR, the less unsaturated hydrocarbon content in the oil and the less likelihood of plant injury Modern refining improvements of the distilled fractions progressed from solvent extraction (1950s) to hydrogenation and dewaxing to increase the UR value (1960s), and hydrocracking, which replaced solvent extraction for the production of high-UR oils (late 1960s). Modern, petroleum-based horticultural oils are refined to standard specifications. Agricultural mineral oil is gaining importance in many integrated pest and disease management programs because of the relatively minor effects on natural enemies, low residual effect, and their undoubted efficacy against a wide-range of pests and diseases through asphyxiation.

Asphyxiation (suffocation) occurs as oil moves into the pest's tracheae (breathing tubes) and clogs its respiratory system, interfering with the normal exchange of oxygen. The timing of spray oil application can be critical, with the most effective control gained when pests are young and recently hatched. AMO also interferes with the development and hatching of existing eggs on the leaf surface; in the first instance, by preventing normal oxygen exchange via the egg surface. This hardens the outer membrane, preventing hatching and by penetrating into the egg itself to cause protoplasm coagulation. [1]

AMO works by physically interrupting the process of pest respiration, not by metabolic disruption; thus, very unlikely to create resistance.

AMOs are effective in controlling Aphids (Aphis gossypii), Thrips (Thrips tabaci), Jassids (Amrasca biguttula), spider mites (Tetranychid mites), Mealybugs (Pseudococcidae), Whiteflies (Bemisia tabaci), plant bugs (Lyguslineolaris), Caterpillars (Pectinophora gossypiella), Scale, and some plant diseases like rusts and mildews.

The cost to develop new pesticide chemicals is aggravated by the rate of pest-resistance development to chemicals. These ever-increasing costs are always passed onto the farmer. Using a pesticide rotation program that includes AMO helps preserve the efficacy of chemicals for seasons to come. Repeated chemical applications can clean out beneficial insects from a crop, leaving it without natural protection and open to infestations by secondary pests. AMO causes minimal disruption to beneficial pets, allowing them to continue protecting the crop at no extra cost.

Smith and Pearce (1948) studied the respiratory effects of oils on eggs of the oriental fruit moth, Grapholita molesta (Busck) (Lepidoptera: Tortricidae) and found them to be responsible for decreased respiration rate, presumably through mechanical interference with normal gaseous exchange studied by Smith and Pearce. They further concluded that the less reactive paraffinic oils showed greater ovicidal efficacy than did the more reactive unsaturated oils.

Insect suffocation by spiracle blockage is usually held as the most accepted theory on the mode of action of mineral oils (Johnson, 1994). The tracheal inflow of oil was reported for the first time by Moore and Graham (1918), and addressed after that by several authors (Roy et al., 1943; Stadler et al., 1996; Taverner et al., 2001). Stadler et al. (1996) found evidence of the inflow of PDSOs to the trachea of Lepidoptera larvae (Anticarsia gemmatalis Hub. (Lepidoptera: Noctuidae) by looking at the air-liquid interface inside the tracheae and tracheolar tubes. In Blatella germanica L. (Blattodea: Blattellidae), oils appeared to induce mortality due to asphyxia by occlusion of tracheae and tracheoles (Stadler et al., 1996).

AMO stays on the leaf surface while the water runs off. All plant surfaces be should evenly coated with oil, including upper and lower leaf surfaces, fruit, branches and tree trunks for product performance. It is better to apply multiple sprays of lower concentrations of oil in the tank mix than to use single sprays of higher oil concentrations.

AMO poses a number of advantages over conventional pesticides and they have very low mammalian toxicity (Oral LD50>5000 mg/kg, Dermal LC50>2000 mg/kg), low residual activity. [2]

## 2. Materials and Methods

### 2.1 Bioefficacy of AMO

Agricultural Mineral Oil at different doses (1.0, 1.5 and 2.0% (v/v)) and Imidacloprid 17.8% SL @ 0.01% were evaluated against aphids, jassids and whiteflies on Bt. Cotton at Akola, Maharashtra from August-2018 to Febrauary-2019 and for each treatment replicated three times. Observations on leaves infested above Economic Threshold Level (ETL) with 1 adult or nymph jassids per leaf, 5 adult or nymph of whiteflies per leaf, 10-20% aphids affected plants were recorded and also noted down infestation at 1,3,5,7 and 9 days after the treatment.

### 2.2 Yield of cotton

For yield of cotton with seeds, randomly 10 mature plants selected with similar height and growth. Also noted down the number of cotton balls per plant with AMO @ 2.0% (v/v) v/s Imidacloprid 17.8% @ 0.01% at the harvest time from randomly selected 10 cotton plants. Total 3 applications done with both AMO 2% and Imidacloprid 17.8% done throughout the season in individual field.

### 2.3 Residue of AMO

Cotton sample of 250 gm and leaf samples were collected from upper, middle and lower part of randomly selected cotton plants after 1,3,5,7 and 9 days from application of AMO @ 2% v/v. soil and leaf samples were also collected as per standard protocol from the cotton field after 1,3,5,7 and 9 days from application of AMO @ 2% v/v.

# 3. Results and Discussion

## 3.1 Bioefficacy of AMO

During field trial, % infestation of aphids was significantly less in all the treatments than control. Among all the treatments, imidacloprid @0.01% recorded significantly less% infestation of aphids than different doses of AMO treatment at 1,3,5,7 and 9 days but was on par with 1.5% AMO at 5 Days after Treatment (DAT) and with 2% AMO at 9 DAT. At 5 DAT 1.5% and 2% AMO recorded significantly less infestation (% infestation with 1.5% AMO: 33.3-42.8%; (% infestation with 2% AMO: 16.4-29.4%). Aphid's infestation (%) at 9 DAT was significantly low at 2% AMO than 1.0% and 1.5% AMO. AMO was found effective at @2.0% against aphids up to 9 days with respect to % infestation as shown in Table no. 1.

As given in Table no. 2, Jassids population was significantly less in all the treatments than control. Jassids population was significantly less at dose 2% (% infestation with 2% AMO: 5.88-20%) at 5 DAT, similarly at 7 DAT, jassids population was also significantly less in 2% (% infestation with 2% AMO: 29.41-37.5%) than 1.0% and 1.5% AMO. Among all the treatments, imidacloprid @0.01% recorded significantly lower % of infestation of jassids than different doses of AMO treatment at 1,3,5,7 and 9 days but was on par with 2% AMO at 9 DAT. AMO was found to be effective @1.5% against jassids up to 7 days and @2.0% against jassids up to 9 days with respect to % infestation.

As shown in Table no.3, Whiteflies population was significantly less in all the treatments than control except 1% AMO. Whiteflies population was significantly less at dose 2% (% infestation with 2% AMO: 42.85-50%) at 5 DAT, similarly at 7 DAT also whiteflies population was significantly less in 2% (% infestation with 2% AMO: 55.56- 62.5%). Among all the treatments, imidacloprid @0.01% recorded significantly lower % of infestation of whiteflies than AMO at different treat dosages over  1,3,5,7 and 9 days but was on par with 1.5% AMO at 5 DAT and with 2% AMO at 9 DAT. AMO was found effective @1.5% against whiteflies up to 3 days and @2.0% against whiteflies up to 7 days with respect to % infestation. AMO @ 2.0-3.0% may give better control over whiteflies.

Table 1. Effect of AMO on aphids infestation in Bt.cotton

| Treatments | % Aphids infestation | | | | |
|---|---|---|---|---|---|
| | 1 DAT | 3 DAT | 5 DAT | 7 DAT | 9 DAT |
| AMO 1.0%(v/v) | 17.18 | 31.70 | 43.00 | 60.45 | 74.12 |
| AMO 1.50%(v/v) | 15.25 | 20.89 | 37.52 | 58.14 | 67.385 |
| AMO 2.0%(v/v) | 5.40 | 17.37 | 24.56 | 38.23 | 44.33 |
| Imidacloprid 17.8% SL @ 0.01% | 8.11 | 15.30 | 23.59 | 35.03 | 41.16 |
| Control | 65.72 | 72.23 | 76.85 | 79.52 | 82.73 |

Table 2. Effect of AMO on jassids infestation in Bt.cotton

| Treatments | % Jassids infestation | | | | |
|---|---|---|---|---|---|
| | 1 DAT | 3 DAT | 5 DAT | 7 DAT | 9 DAT |
| AMO 1.0%(v/v) | 30.91 | 29.25 | 39.26 | 56.67 | 75.00 |
| AMO 1.50%(v/v) | 14.48 | 24.36 | 33.73 | 49.16 | 71.76 |
| AMO 2.0%(v/v) | 7.03 | 13.67 | 14.88 | 34.80 | 50.12 |
| Imidacloprid 17.8% SL @ 0.01% | 6.53 | 12.01 | 13.97 | 30.56 | 46.39 |
| Control | 68.41 | 77.68 | 80.75 | 83.30 | 83.38 |

Table 3. Effect of AMO on whiteflies infestation in Bt.cotton

| Treatments | % Whiteflies infestation | | | | |
|---|---|---|---|---|---|
| | 1 DAT | 3 DAT | 5 DAT | 7 DAT | 9 DAT |
| AMO 1.0%(v/v) | 58.93 | 63.61 | 70.14 | 80.78 | 82.83 |
| AMO 1.50%(v/v) | 35.00 | 41.11 | 62.70 | 74.49 | 75.00 |
| AMO 2.0%(v/v) | 26.19 | 36.51 | 45.77 | 59.35 | 60.40 |
| Imidacloprid 17.8% SL @ 0.01% | 18.89 | 30.00 | 39.29 | 52.38 | 51.85 |
| Control | 62.88 | 65.91 | 77.02 | 80.05 | 82.83 |

## 3.2 Yield of cotton

Average weight of cotton with seed was 10-30% high with AMO @ 2% treat rate, compared with imidacloprid 17.8% SL @ 0.01% as shown in Table 4. It can also be seen that average cotton balls with AMO 5-15% high compared with imidacloprid as shown in Table 4.

Table 4. Yield Comparison of AMO v/s Imidacloprid after treatment in Bt.cotton

| | AMO 2.0% | Imidacloprid 17.8% SL @ 0.01% |
|---|---|---|
| Weight of cotton with seed/ 10 plants (gm) | 556 | 410 |
| | 430 | 390 |
| | 460 | 400 |
| Average number of cotton balls/ 10 plants | 15 | 13 |
| | 27 | 24 |
| | 26 | 22 |

## 3.3 Residue of AMO

AMO with 2% (v/v) application extracted from the cotton, leaf and soil sample using n-pentane and analyzed by FTIR. [3]

Table 5. AMO residue in cotton, soil and leaf after treatment

| Sample | 1 DAT | 3 DAT | 5 DAT | 7 DAT | 10 DAT |
|--------|-------|-------|-------|-------|--------|
| Cotton | 243.75 ppm | 183.25 ppm | 133.75 ppm | 101.25 ppm | 87.5 ppm |
| Soil | 122.25 ppm | 107.25 ppm | 83.5 ppm | 63.25 ppm | 39.25 ppm |
| leaf | 95 ppm | 73.75 ppm | 56.25 ppm | 37.75 ppm | 24.75 ppm |

The residue levels of less than 100 ppm is much lower than the LC 50 and LD 50 limits of mineral oils indicting no side effects or hazard to the user or consumer and are safer option.

## 3.4 Economics

Though the number of applications of AMO is high in comparison with Imidacloprid, but the economics of over all applications of AMO works out to be viable due to the lower per unit cost of AMO (see Table 6).

Table 6. Pesticide application cost comparison

| | Imidacloprid 17.8% SL @ 0.01% (Chemical Pesticides) | AMO |
|--------|--------|--------|
| No. of application throughout season | 4-5 | 6-7 |
| Pesticide cost / acre / season | 3500-4000 Rs. | 2500-3000 Rs. |
| Labor cost / acre (one time) | 200 Rs. | 200 Rs. |
| Total Labor cost / acre / season | (200*5 application) = 1000 Rs. | (200*7 application) = 1400 Rs. |
| Pesticide spray interval | 15 days | 7-9 days |
| Total cost / acre / season | 4500-5000 Rs. | 3900-4400 Rs. |

The total application cost works out to be economical by atleast 10% and also offers the advantages of application safety, no residue and the product also can be biodegradable leaving no residue over period of time.

## 4. Conclusion

AMO will effectively work on treating sucking pests up to 5- 7 days with 1.5-2% (v/v) and up to 7-9 days with 2-3% AMO (v/v). Average number of cotton balls and weight of cotton is high with AMO compared to the control Imidacloprid 17.8% SL. The residue on crop, leaves & soil were found to be much lower than the limits Of $LD_{50}$ and $LC_{50}$. AMO's total application cost is economical compared to chemical pesticide and offers a safe alteranative to chemical pesticides towards an IPM concept.

**References**

1. Agnello, A.M., 2002. *Petroleum-derived spray oils: chemistry, history, refining and formulation*, Spray Oils Beyond 2000, University of Western Sydney, Australia, pp. 42
2. Ebbon, G.P. ,2002. *Environmental and health aspects of agricultural spray oils* Spray Oil Beyond 2000, University of Western Sydney, Australia, pp. 232-245.
3. Johnson, D., Hodgkinson, M.C., & Nicetic, O., 2002. *Quantification of mineral oil spray deposits on foliage by solvent extraction and FTIR spectroscopy,* Spray Oils Beyond 2000, University of Western Sydney, Australia, pp. 592-594.

# Environmental Sustainability & Industry 4.0 from India perspective

*Manishkumar V Patel*

*Department of Mechanical Engineering, LJ INSTITUTE OF ENGINEERING AND TECHNOLOGY*

## Abstract

Recently, Industries worldwide are experiencing Industry 4.0 Revolution. It began in Germany where their industries main focus was on strengthening and leading their wide-reaching manufacturing expertise. Some of the key Industry 4.0 technologies like Internet of Things and Cyber-physical systems among others have already penetrated the main stream market. With rising Gross Domestic Product (GDP) and foreign direct investment, India has also lately witnessed Industry 4.0 revolution. The fast pace developments in this area have created issues related to environmental sustainability and green manufacturing. The weak sustainability framework associated with Industry 4.0 can have negative impact on environment. India is one of the biggest polluters in the world. In India, more than half of the total pollution is due to industrialization. This paper explores the context of environmental sustainability and its framework from Indian industries perspective. Obstacles, issues and possible solutions are discussed. These reforms can be considered critically and applied to reduce carbon footprint thereby creating and protecting sustainable environment.

## Keywords

Industry 4.0(I4.0), Internet of Things, Cyber-Physical System, environmental sustainability

## 1. Introduction to Industry 4.0(I4.0)

The fourth industrial revolution or Industry 4.0 can be defined as the intelligent integration of machines, services, people and processes with the help of cutting-edge networking and communication technologies. The basis of I4.0 is Cyber-physical system, Internet of Things and smart factory. According to National Science Foundation, USA - the term "cyber-physical systems" refers to the tight conjoining of and coordination between computational and physical resources. The integration is achieved through embedded control system. Emerging Technologies like 5G networking, cyber-robotics, Augmented and virtual reality, Big Data, Internet of Things, System integration, cybersecurity, Additive manufacturing, Machine to machine and human to machine communication, smart sensing, simulation, nanotechnology and cloud computing are the key components in development of I4.0. These technologies act as an addon to the automation with features such as self-optimization, self-configuration, cognition and intelligent networking.

The first industrial revolution started between 1760 and 1840 in England with the invention of steam engines, water power usage and mechanization of manufacturing. Invention of electricity along with introduction of assembly lines initiated the second industrial revolution. Digital Revolution or the third industrial revolution was introduced in the late 20th century as a result of adoption of computing technology, robotics and convergence of internet and operations technology. Fourth industrial revolution – the phrase was first familiarized by Klaus Schwab – the founder of World Economic Forum. The term "Industrie 4.0" originated visibly as a result of the focus of German Manufacturing strategy at the Hannover Fair, Germany in 2011. As a digital transformation policy of manufacturing, German Federal Ministry of Education and Research (BMBF) created work group to define and implement the I4.0 framework.

As per (Ortiz et al., n.d.), I4.0 redefines the concepts of quality, ensure the prestige of the company, increase cyber security of data and information, modify or adapt the laws of different countries to the new production model, the adaptation of international relations at the commercial level, measure the environmental impact generated by the new business model, to include concepts such as happiness, joy, well-being in the people linked to the production process. The fourth industrial revolution has paved way to another revolution in making where highly customized products catering the needs of customers are made through harmonized human machine collaboration. This revolution, also known as Industry 5.0, is already a buzzword in the industry.

### Industry 4.0 – challenges and current status

The I4.0 framework and policies provided by the German manufacturing industries have enabled industries across the globe to adopt and push the limits of I4.0 in various sectors.

For example, UK has already invested more than £150 million in 5G networking and £400 million in electric vehicle charging infrastructure. According to Markets and markets research report, global share of Internet of Things was valued at $10.1 billion in 2017 and is set to be worth $45.3 billion by the end of 2022. This is a huge boost and good news for the USA, where manufacturing sector is ailing right now. According to the recent report by International Federation of Robotics, USA has nearly 2,93,000 robots in their manufacturing units.

International Federation of Robotics, USA has nearly 2,93,000 robots in their manufacturing units.

In the era of digitalization, the implementation of I4.0 comes with roadblocks as well. These challenges hamper the adoption of the technology. Major companies and their manufacturing units have successfully integrated I4.0 enabled expertise. Specifically, for SMEs, operational prospects are the key enablers. Regardless of any organization size, environmental and social opportunities play important role in I4.0 implementation(Müller et al., 2018).

## 2. Environmental sustainability and I4.0

### 2.1 Introduction to environmental sustainability

United Nations defines sustainability as a movement for ensuring a better and more sustainable wellbeing for all, including the future generations, which aims to address the everlasting global issues of injustice, inequality, peace, climate change, pollution, and environmental degradation.

Herman Daly, one of the leading researchers in ecological sustainability, proposed that environmental sustainability is the rates of renewable resource harvest, pollution creation and non-renewable resource depletion that can be continued indefinitely. Ironically, economic growth is degrading the environment and if it continues then it can nullify the very foundation on which sustainability fosters. In this era, exponential growth in digital technology has fueled speculations that environment will be eventually destroyed. Sustainable operations, circular economy and green manufacturing are some of the areas to focus on to tackle the problems of climate change and pollution.

### 2.2 Industry 4.0 and Sustainability

Recent study in sustainable I4.0 shows that there is a considerable impact of I4.0 technology on economic, social and environmental dimensions of sustainability (Kamble, 2018). The TBL (Triple Bottom Line) performance in the form of social, economic and environmental factors has been identified by many organizations for evaluating their sustainability index.

#### 2.2.1 Economic sustainability

Lean manufacturing techniques can be applied in factories to reduce manufacturing costs. These techniques along with smart sensing and controlling operations can work towards overall cost reduction strategies in daily manufacturing operations.

#### 2.2.2 Environmental sustainability

I4.0 has enabled firms to utilize the resources such as energy, water, raw material in efficient way using innovative sensing and controlling techniques. This has resulted in green, smart and sustainable manufacturing(Stock and Seliger, 2016).

#### 2.2.3 Social sustainability

Social sustainability is the way by which a business organization identifies and manages the impact of its operations on employees, society, suppliers and customers. Social sustainability

integrates many factors and not limited to Labor rights, justice, social responsibilities, work ethics, social equity, healthy working conditions.

When the manufacturing industry strives towards digital transformation, it realizes efficient manufacturing performance with profitable business. It also enables environmental management along with energy efficient competence within the manufacturing domain which leads to environmental conservation and helps in reducing pollution (Ghobakhloo, 2019).

Studies by (Yadav et al., 2020) regarding the development of framework of sustainable I4.0 shows that the results reveal that managerial and economical enablers were found to be the most critical for sustainability adoption; while, environmental enablers also possessed a strong influence in achieving overall sustainability. It is important to notice that the adoption of sustainable energy resources systems, adoption sustainability supportive policies and effective sustainability performance metrics were among the top influencing enablers that support sustainability adoption. Accordingly, it is suggested that government policies favoring sustainability adoption through the execution of new technologies will have a positive impact on strengthening nations' economy. Similarly, the promotion of a sustainable energy resource system will create awareness among manufacturing organizations and help them improve their sustainable performance.

As per (Madan Shankar et al., 2017), promoting 6R (reduce, reuse, recycle, recover, redesign, and remanufacture) concepts reveals the greatest influence on sustainable manufacturing implementation.

I4.0 with circular economy can help in overcoming the roadblocks in transition from day-to-day manufacturing operations to I4.0 enabled technology. Circular economy enabled I4.0 are mutually beneficial and assists manufacturing sector with sustainable operations(Lopes de Sousa Jabbour et al., 2018).

## 3. Environmental sustainability and Industry 4.0 – India perspective

India is one of the fastest developing nations in the world. According to Indian Ministry of Statistics and Program Implementation – In India more than fifty eight percent population depend on agriculture for their livelihood. With world's largest crop insurance scheme and Digital India initiative, India has seen substantial growth in agricultural sector. Investment in areas such as broadband, rural transportation, electricity and education play a vital role in inclusive growth of digital India (Lele and Goswami, 2017). As the key player in manufacturing and services sector worldwide, India is slowly and steadily picking up in I4.0 adoption. India has overseen rapid growth in two key technologies – Internet of things and Big Data. For example, Indian IoT market has captured 20 percent of worldwide IoT market, which stands at around US\$ 300 billion.(Bhatia, 2016). Reports by SiliconMag India suggest that Big data analytics market in India, which is valued at Rs 13,000 crore at present, is expected to reach Rs 1,03,974 crore by the end of 2025, which is around 32% of the world-wide Big data analytics market.

To accelerate the pace of the development in smart manufacturing, Indian government has come up with many policies and schemes like National Program on Artificial Intelligence, National Manufacturing Policy – 2017, Center of Excellence on IT for I4.0 and Mission on

Cyber-Physical Systems. Additionally, private IT organizations have also started adopting and collaborating on I4.0 contributions.

Major contribution on manufacturing front in India comes from the small and medium scale industries. Ninety five percent of Indian manufacturing firms come under the category of small scale industry(Singh et al., 2012). To be able to withstand the international competition, these industries have to elevate technical and technological know-how. Apart from this, ethical and sustainable operations also aid in improving overall industry performance.

India is one of the leading polluters of environment in the world and rising industrialization and developments are worrying signs for India. According to recent study by world economic forum, Six out of 10 most polluted cities in the world are in India. More than one million people die every year due to air pollution in India. Major developments in the area of I4.0 in India should be promoted in parallel with framework development to provide concrete sustainable manufacturing and services operations.

Studies undertaken by (Kumar et al., 2020) reveal that creating awareness among SMEs, Long term planning, policies and regulations for I4.0 with ethical and sustainable footprints can reduce the challenges posed by the SMEs regarding the I4.0 implementation. Managerial and economic factors like adopting policies related to sustainability, efficient budget allocation Creating and promoting Internet of Things and Big Data and related sensing technologies are crucial for creating sustainable Industry 4.0 framework. Apart from that, encouraging environmentally sustainable activities like utilizing energy efficient resources, green product and process design and ecological initiatives in industries also contribute towards fostering overall sustainability. Lean and agile manufacturing, sustainable supply chain operations and sustainable product and process design can lead to sustainable manufacturing in India(Gupta et al., 2018).

## 4. Conclusion

As the world has already perceived the fourth industrial revolution and is marching towards Industry 5.0, the revolutionary technology has its positive impacts with own limitations with respect to sustainability issues. With India's viewpoint where pollution and natural resources degradation is a huge concern, I4.0 with circular economy is fruitful to the overall sustainable operations(Lopes de Sousa Jabbour et al., 2018). India, as an emerging player in global manufacturing arena, can foresee the benefits of I4.0 in regards with the environmental sustainability by framing policies and work groups dedicated towards sustainable actions. Digitalizing and educating rural India, creating awareness regarding sustainability and I4.0 and ditching the conventional way of make, use and throw framework, Indian manufacturing units can work collectively to come up with a regenerative framework or so called circular economic development where society, employees and the business are benefitted.

## 5. References

Bhatia, R., 2016. Top 5 Internet of Things (IoT) initiatives by Government of India. Anal. India Mag. URL https://analyticsindiamag.com/top-5-internet-things-initiatives-government-india/ (accessed 1.23.21).
Ghobakhloo, M., 2019. Industry 4.0, Digitization, and Opportunities for Sustainability. J. Clean. Prod. 252, 119869. https://doi.org/10.1016/j.jclepro.2019.119869

Gupta, D.S., Dangayach, G., Posinasetti, N., 2018. Implementation of sustainable manufacturing Practices in Indian manufacturing companies. Benchmarking Int. J. 25, 2441–2459. https://doi.org/10.1108/BIJ-12-2016-0186

India dominates the list of the world's most polluted cities [WWW Document], n.d. . World Econ. Forum. URL https://www.weforum.org/agenda/2020/03/6-of-the-world-s-10-most-polluted-cities-are-in-india/ (accessed 1.24.21).

Kamble, S.S., 2018. Sustainable Industry 4.0 framework: A systematic literature review identifying the current trends and future perspectives. Process Saf. Environ. Prot. 18.

Kumar, R., Singh, R.Kr., Dwivedi, Y.Kr., 2020. Application of industry 4.0 technologies in SMEs for ethical and sustainable operations: Analysis of challenges. J. Clean. Prod. 275, 124063. https://doi.org/10.1016/j.jclepro.2020.124063

Lele, U., Goswami, S., 2017. The fourth industrial revolution, agricultural and rural innovation, and implications for public policy and investments: a case of India. Agric. Econ. 48, 87–100. https://doi.org/10.1111/agec.12388

Lopes de Sousa Jabbour, A.B., Jabbour, C.J.C., Godinho Filho, M., Roubaud, D., 2018. Industry 4.0 and the circular economy: a proposed research agenda and original roadmap for sustainable operations. Ann. Oper. Res. 270, 273–286. https://doi.org/10.1007/s10479-018-2772-8

Madan Shankar, K., Kannan, D., Udhaya Kumar, P., 2017. Analyzing sustainable manufacturing practices – A case study in Indian context. J. Clean. Prod. 164, 1332–1343. https://doi.org/10.1016/j.jclepro.2017.05.097

Müller, J.M., Kiel, D., Voigt, K.-I., 2018. What Drives the Implementation of Industry 4.0? The Role of Opportunities and Challenges in the Context of Sustainability 24.

Ortiz, J.H., Marroquin, W.G., Cifuentes, L.Z., n.d. Industry 4.0: Current Status and Future Trends 17.

Singh, R.K., Kumar, R., Shankar, R., 2012. Supply Chain Management in SMEs: a case study. Int. J. Manuf. Res. 7, 165. https://doi.org/10.1504/IJMR.2012.046801

Stock, T., Seliger, G., 2016. Opportunities of Sustainable Manufacturing in Industry 4.0. Procedia CIRP 6.

Yadav, G., Kumar, A., Luthra, S., Garza-Reyes, J.A., Kumar, V., Batista, L., 2020. A framework to achieve sustainability in manufacturing organisations of developing economies using industry 4.0 technologies' enablers. Comput. Ind. 122, 103280. https://doi.org/10.1016/j.compind.2020.103280

# Foil Gas Bearing: An Integral Part of Green Propulsion Technology-A Review

D G Bohra[*1], Dr. G D Bassan[2],

[1]Assistant Professor, Department of Mechanical Engineering, Dharmsinh Desai University, Nadiad-387 001, Gujarat, INDIA

[2] Professor, Head of Department of Mechanical Engineering, Dharmsinh Desai University, Nadiad-387 001, Gujarat, INDIA

*Corresponding author: dgbohra.mech@ddu.ac.in, +919974942139

## Abstract

The propellant used in space programs creates exclusively three ecological concerns: Ground-based Impacts which vary from groundwater contagion to explosions caused by inconvenient management of fuels. Atmospheric Impacts are generally due to the interface of propellant exhaust with the atmosphere. Biological Impacts include toxicity and corrosiveness of propellants. This leads to the emergence of Cryogenic and Semi Cryogenic engines where the main propellants are Liquid Hydrogen and Liquid Oxygen (very effective in controlling above mentioned three environmental concerns). The operation necessities designate a need for reliable and long-life $LH_2$ & LOX turbopumps. Existing turbopumps use rolling component bearings which restrict turbopump life. Foil Gas Bearings (FGB) can be effectively used in high-speed turbomachines to attain noteworthy consistency. The present work reports how FGB can successfully replace the conventional roller bearings and prove to be a very important contribution towards Green Propulsion Technology. FGB offers elimination of oil lubrication system (an environmental concern) resulting into condensed weight and improved temperature competence. Using FGB to cryo turbopumps would lengthen turbopump life well ahead of operation necessities. This work also focuses on how Foil Gas Bearing technology can be a great prospect for Indian Space Programmes.

## Keywords

Gas Bearing, Cryogenic turbo-pump, Space Lubrication, Liquid Hydrogen, Liquid Oxygen, Rolling element bearing, green propellants.

## 1. Introduction

The Space age had carry with it many pollution and lubrication challenges that had not been witnessed in past. These challenges are worth addressing as nowadays space exploration is not limited to just a few minutes or hours. It's now getting a pace of years. Earlier space missions used to be of minutes or hours. With developing space vehicles, the life necessities for mechanical apparatus have amplified. Also, the requirements for fuel are increased. For example, the Space Station Freedom requirements dictate a life of 30 years. This has lead to the enforcement of green propulsion techniques. Green propulsion is a step towards minimizing the environmental concerns associated with space missions. This is not only restricted to reducing the exhaust plumes, soot, $CO_2$, CO, alumina and sulphuric compounds, NOx, etc. Green propulsion technology also focuses on the life enhancement of rocket engine components. Since when the discussion is about the long life of space missions, interplanetary missions, propulsive telescopes, components should be with least maintenance to zero maintenance. Here comes the need for gas-bearing technology into the picture. This paper will highlight the necessity of Foil Gas Bearing (FGB), its feasibility in space missions, its design aspects, and its upper hand over existing rolling element bearings. The paper will also focus on explaining how FGB plays an important role in fulfilling an important aspect of Green Technology i.e. removal of oil lubrication (an environmental concern) [1-4]

## 2. Necessity of Foil Gas Bearing [5, 6, 7]

The operation necessities for orbital transfer vehicles, space control schemes, launch vehicle, and trans atmospheric vehicles specify a call for consistent and long-life $LH_2$ & LOX turbopumps. Existing turbopumps use rolling component bearings that bound turbopump life. Using FGB to cryo turbopumps would lengthen turbopump life well ahead of operation necessities. This is due to its mechanical and lubrication properties. In space, oil supply can be a problem in view of the fact that there is no gravity to heave it down. This confines the usage of oil lubrication and brings the requisite of using process fluid bearings which uses the process fluid for its lubrication. Below mentioned points will try to highlight the importance of FGB in space application considering mechanical aspects and environmental aspects.

### 2.1 Mechanical Aspects

A foil gas bearing has all the vital features necessary by space-grade components. To list them, they are;
- Higher Dependability
- High-Speed Maneuver
- Low and High-Temperature Operations
- Environment Resilience
- Low Maintenance
- Soft Failure

### 2.2 Environmental Aspects

The most beneficial part of using FGB is that it uses the process fluid for lubrication and hence eliminates the use of any lubricating oil whose production causes a lot of environmental concerns. Refineries are chief cause of harmful and deadly air pollutants such as BTEX compounds. They are also a key source of particulate matter (PM), nitrogen oxides (NOx), carbon monoxide (CO), hydrogen sulfide ($H_2S$), and sulfur dioxide ($SO_2$). They are possible major contributor to groundwater and surface water flaw. Which include oil remains and numerous other perilous wastes. The pollutants released into surface waters are sulfides, ammonia, suspended solids, and other compounds that may be there in the wastewater. Soil pollution includes some unsafe wastes, spent catalysts or coke dust, tank bottoms, and sludge from the handling processes that can arise from leaks as well as accidents or spills on or off-site throughout the transport process [5].

After discussing the importance of FGB as an integral part of Green Propulsion, now let us discuss its feasibility, its construction, design aspects, manufacturing feasibility.

## 3. Foil Gas Bearing (FGB) [6, 7, 8, 10, 12, 15]

FGB are self-acting hydrodynamic bearings prepared from sheet metal foils consist of minimum two layers. The inmost "top foil" layer entraps a gas pressure film whch supports a load whereas a layer or layers beneath offer an flexible base. FGB make available a way to abolish the system of oil which results into condensed weight and superior temperature competence. Figure 1 shows a cross-section draft of the majority established types of the foil bearing blueprint in practice, the "bump" foil bearing.
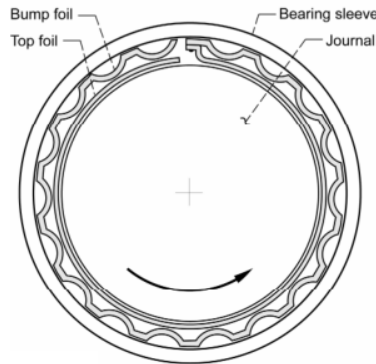
Figure 1 Schematic example of Bump type Foil Bearing [7]

In a FGB arrangement, a number of foils are wrapped and overlapped about the shaft as shown in above figure. The foils have definite thickness and curvature radius to sustain contact with the shaft during its rest position. The foils elevate due to generation of hydrodynamic film as a result of shaft movement. With least speed achievement of shaft, wear becomes zero. Shielding coating is provided on foil component to protect shaft from wearing during start-stop cycles. To protect the shaft from wear for the period of start and stop transients, a shielding coating is used on the foil component that remains in contact with the shaft at rest. To safeguard the shaft, coating is made more elastic compared to shaft, so that in any unwanted situations the coating is affected and not the shaft. Laboratory investigation specifies a competence over 1 lakh start-stop cycles, which is quite enough.

## 3.1 Feasibility of Foil Bearing

Cryogenic turbopumps are simple from mechanical aspects as they have lesser parts in comparison to rolling bearing units. In view of the fact that FGB have no speed restrictions, FGB turbopumps usually operate quicker, are extra competent, and provide lesser volumes than rolling bearing units. These characteristics propose near to the ground manufacture costs. Due to elevated consistency, these turbopumps can be reused, stitching numerous operations. The foils are more soft compared to the fluid film and deflect to accommodate thermal deformation and misalignment. This attribute is well fitting to cryogenic operation and makes the FGB advanced to existing bearings.

A distinctive rotor dynamic reaction and critical speed chart is shown in figure 2. The broad parting amid the initial two and the third critical speed offer a hefty critical speed free working choice. As of a bulky margin amid the shaft speed and the stiff body critical speeds, every mass disturbance is attenuated. Therefore, FGB components can overpower mass imbalance. The outstanding rotor dynamics, high-speed constancy, and damping distinctiveness of FGB make available the foundation for the towering consistency of these turbo-pumps.

FGB find application in high-speed aircraft air-cycle turbocompressors and supplementary purpose, such as helium compressors, gas turbines, and cryogenic turbomachines. Foil bearings has gained noteworthy trustworthiness. For aircraft turbocompressors, the mean time between failures is on average over 60K hr. In cryogenic applications, the Mini-Halo space refrigeration turbo alternator function productively over 17K hr, and the first FGB turboexpander has run constantly without any supervision in excess of 9 years. Using FGB in cryo turbopumps will lengthen turbopump life well ahead of operation necessities. [7, 12]
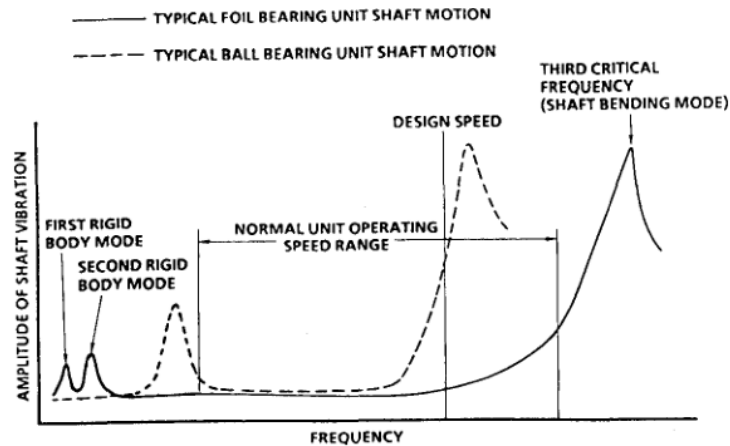
Figure 2 Rotor Dynamic response Vs Unit Speed [7]

To support the practicability of foil bearing for cryogenic turbopumps this paper highlights the thriving demonstration of this exceptional FGB perception.

## 3.1 LH$_2$ FGB Performance Test

The primary cryogenic FGB machinery has been effectively established in cooperation by AlliedSignal and NASA. A FGB was tested in LH$_2$ at NASA Lewis Research Center. The things to see of the test outcomes are scheduled in Table 1. An investigational LH$_2$ turbopump was build in 1992. The working speed varies from 20K-90K rpm. The flow rate was 8.6 lb/sec. This LH$_2$ turbopump was effectively tested in NASA Stennis Space Center. The overview of the test outcomes are scheduled in Table 2. A post test assessment signifies that all the FGB and the rotating assembly were in outstanding state past the wide-ranging test [8-11].

Table 1 LH$_2$ FGB Test Outcomes [7]

| Attained 16.8737 kgf/cm$^2$ load competence in Liquid Hydrogen |
|---|
| Worked steadily at all speeds |
| Above 150 start-stop cycles without bearing defect |
| Established insignificant cross-coupling stiffness |
| Attained 21.0921 kgf/cm$^2$ load competence in Liquid Nitrogen |
| Collective run time: 4 hour in Liquid Hydrogen and 5 hour in Liquid Nitrogen |

Table 2 LH$_2$ FGB Turbo Pump Demonstration Overview [7]

| Attained discharge near to 70.307 Kgf/cm$^2$ |
|---|
| Worked steadily commencing 14,000 rpm to 91,000 |
| Aver 100 starts-stops |
| Turbopump started effectively with no entire bearing chill down |
| Overall run time: about one hour |

## 3.2 LOX FGB Performance Test

A FGB test in LOX was accomplished in late 1992 at NASA MSFC. Analogous outcomes were obtained. The test outcomes are summed up in Table 3. The bearing operated sturdily commencing 6-35K rpm. A LOX FGB turbopump was build in 1993. It was effectively tested at NASA Marshall

Space Flight Center. The in service speed of this turbopump varied from 5-25K rpm, and the rate of flow fluctuate from 6-50 lb/sec. Over view of the test outcomes are scheduled in Table 4. [7]

Table 3 LOX FGB Test Outcomes [7]

| Attained 19.6859 kgf/cm$^2$ load competence |
|---|
| 27.7712 kgf/cm$^2$ load capability confirmed in Liquid Nitrogen |
| Extremely lofty damping noticed in Liquid Nitrogen & Oxygen Damping ratio = 0.7 - 1.4 in Liquid Nitrogen Damping data in Liquid Oxygen being condensed |
| 120 start-stop in Liquid Oxygen accomplished |
| About two hour test period in Liquid Oxygen |

Table 4 LOX FGB Turbo Pump Demonstration Overview [7]

| Worked steadily within 2-25K rpm |
|---|
| A pressure increase up to 84.36835 kgf/cm$^2$ |
| Above 100 start-stop cycles |
| Established hefty bearing load capability limits |
| Demonstrate tolerance to debris |
| Overall run duration: Ninety minutes |

There are a lot more thriving test results for foil bearing; however many are limited to high temperature maneuver. But to recapitulate the above results it's very noticeable to say that Cryo FGB turbopumps propose superior consistency and little cost. Performance of FGB in LH$_2$ and LOX has been authenticated. Elevated load competence, exceptional rotor dynamics, and minor bearing wear were experienced following above 100 cycles of operation in liquid propellants.

Now once the feasibility of FGB is understood let this paper throw some light on the design, construction, and variants of foil gas bearings.

## 4. Design of Foil Gas Bearing [6, 7, 12, 14, 15]
The feasibility of replacing cryogenic turbopump with rolling element bearing with foil bearing has been understood. Foil bearing, in addition to an extended life, can be designed to offer preferred rigidity and damping characteristics essential for optimal turbopump rotordynamic characteristics.

### 4.1 Foil Bearing Configuration and Operation

Basic elements of a FGB have been illustrated in figure 1. Among many critical features of FGB one is a dual mechanism to impart damping and stiffness. One means is through the geometry and the bump and top foil materials, which are comparable to a compliant spring support. Followed by another mechanism is hydrodynamic consequential from the fluid film sandwiched between the runner or the shaft and the top foil. Elastic deformation of foils creates the clearance geometry which is required to create load carrying hydrodynamic film. With amplification of speed the bump foil and top pad are involuntarily thrown radially outward to form a wedge action.
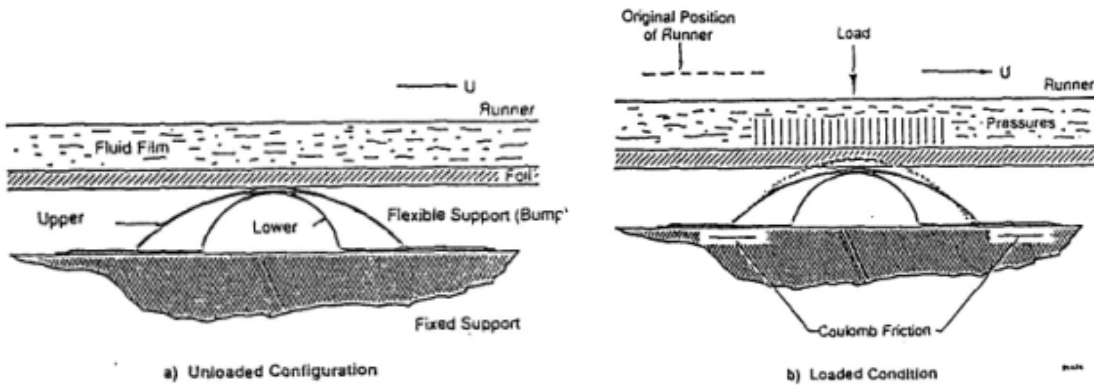
Figure 3 Principle of multistage bump foil operation under hydrodynamic loading.

As shown in Figures 1 and 3 nested or staggered bumps may be used to offer a stiffness that varies with load or deflection. This attribute is very significant in ensuring system stability and compatibility with the load variation right through the speed range.

## 4.2 Variants of Foil Gas Bearing[6,13]

The different variants of FGB include, Multipad FGB, Reversed Multilayer FGB, Hydresil FGB, Reversed Multipad FGB, etc. These variants are practiced by lots of reputed international bodies for different applications. All of them have different capabilities like, offering preload conditions, accommodating extension, digression, and any misalignment,high coloumb damping, high load bearing capacity, starting at lesser torque etc. The variants are as shown in figures below.
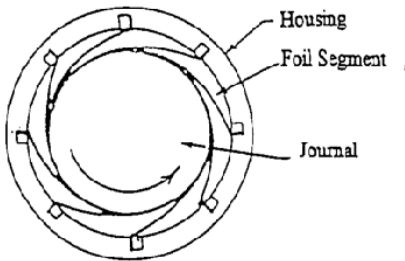


Figure 4 Multipad Foil Bearing [6]
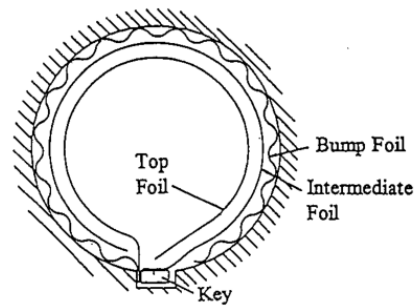


Figure 5 Reversed Multilayer Foil Journal Bear [6]
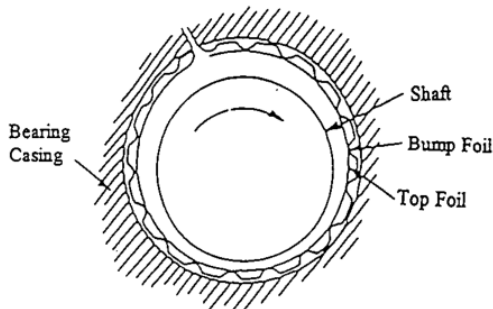


Figure 6 Hydresil Foil Journal Bearing [6]
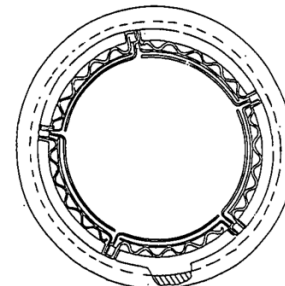


Figure 7 Reversed Multipad Foil Journal Bearing [6]

### 4.2.4 Thrust Bearings

Thrust bearings resist axial loads in rotary machinery. Their working is based on the similar hydrodynamic theory as journal bearings. In a thrust bearing the wedge action is build in considering into account any deflection due to the axial load.
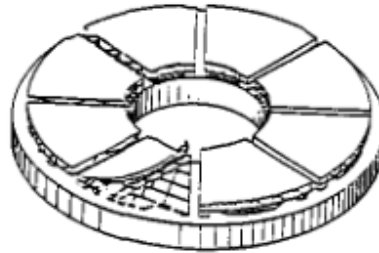


Figure 8 Thrust gas bearing [6]

### 5. Analysis and Testing of Foil Bearing

FGB analysis involves lots of iterative methods and synchronized solutions for solving elasticity and hydrodynamic equations. Former equations have nonlinearity and entail hefty deformation theory. Deformation of a foil is almost 5 times its thickness and thus no pleasing results are offered by any FEM or FDM approach. In addition to this even nonlinear Reynolds' equations with constantly changing boundary conditions make solution of hydrodynamic equations very difficult. Thus semi-empirical method can offer good results. Adequate record is composed by altering test and geometrical parameters. Outcome is linked by means of a multiple regression technique. After that a model is set by means of coefficients of the multiple regression technique. Hydrodynamic equations are cracked by means of the chosen concluding geometry. Subsequently a contrary technique is used to design the foil geometry in the unburdened arrangement. That's how a critical problem is divided into lots of easy problems. [13-15]

### 6. Developmental Stages of Foil Gas Bearing

FGB have developed all the way through three varied stages from the time when the first practical bending subjected designs. Gen-I bearings have a homogenous simple elastic base with even stiffness properties. Gen-II bearings have more intricate elastic base with personalized axial stiffness to house shaft misalignment & seepage of fluid from edges. Gen-II bearings are twice in load carrying capability as compared to Gen-I. Gen-III FGB have highly complex elastic base with stiffness customized in radial as well as axial direction. This grade of design takes care of housing edge effects & capability to take unstable loads. It has 3-4 times load bearing capacity than Gen-I bearings. Figure 9 shows all three generations bearing foil structure divergence. [14]

| (a). Gen-I Bearing Foil | (b). Gen-II Bearing Foil | (c). Gen-III Bearing Foil |

Figure 9 Variation in foil structure in all three generation bearings [14]

## 8. Conclusions

The paper summarizes the developmental path of Foil Gas Bearing as an integral part of Green propulsion technology. It focuses on how the load-carrying capacity and life of propulsion components can be increased using FGB in place of existing Rolling element bearings. It also shows how using FGB can help reduce the pollution created during the production of lubricating oil, used in rolling element bearings. It can be concluded from the above discussion that foil bearings are fit for cryogenic turbopumps used for Cryogenic Propellants which are best for Green Propulsion.

## References

[1] Rupesh Agrawal, Ishan K Patel, P B Sharma, " Green Propellant-A Study", International Journal of Latest Trends in Engineering and Technology, Sep 2015 vol 6.

[2] Desain, J.D. (2011). Green Propulsion: Trends and Perspective. Retrieved from http://www.aerospace.org/2013/07/31/green-propulsion-trends-and-perspectives

[3] HPGP – The Next Level of Propulsion. Retrieved from http://www.sscspace.com/about-the-ssc-group/ssc-companies/ecaps

[4] Rarata G., Surmacz P., Sobczak K., "Near Future Green Propellant for Space Transportation", 8th International Scientific Conference: "Development Trends in Space Propulsion Systems" Warsaw 2013.

[5] Article, "Environmental Impact of the Petroleum Industrzardous Substance Research Centre.

[6] Giri L. Agrawal,1997, "Foil Air/Gas Bearing Technology, An Overview" ASME, Publication 97-GT-347

[7] Alston Gu, "Foil Bearing Turbo pumps", AIAA Space Programs and Technologies conference and exhibition, Sept 21-23 1993.

[8] Saville, M., Gu, A., and Capaldi, R., "Liquid Hydrogen Turbopump Foil Bearing," AIAA-91-2108.

[9] Genge, G., Saville, M., and Gu, A., "Foil Bearing Performance in Liquid Nitrogen and Liquid Oxygen," AIAA-93-2536.

[10] Gilbrach, R.J., Gu, A., Rigney, T., Saville, M., and Rossoni, M., "Liquid Hydrogen Foil-Bearing Turbopump," AIAA - 93 - 2537.

[11] Gilbrach, R.J., Gu, A., Rigney, T., Saville, M., and Rossoni, M., "Liquid Hydrogen Foil-Bearing Turbopump," AIAA - 93 - 2537.

[12] H. Heshmat," A  Feasibility Study  On  The  Use  Of  Foil Bearings  In  Cryogenic Turbo pumps", AIAA, 27th  Joint Propulsion Conference June  24-26,1991.

[13]  H.  Heshmat,  J  Walton,  "Compliant  Foil  Bearings  For  Use  In  Cryogenic  Turbo  pumps", Proceedings of the conference held at NASA/MSFC May 17-19, 1994, Advanced Earth- to orbit Propulsion Technology, NASA, vol 1, pp . 372-381, Sept 19, 1994

[14] Christopher DellaCorte, Kevin C. Radil , Robert J. Bruckner & S. Adam Howard,2008, "Design, Fabrication, and Performance of Open Source Generation I and II Compliant Hydrodynamic Gas Foil Bearings" Tribology Transactions, 51: 254-264

[15] Heshmat, H., Walowit, J. A., Pinkus, O., 1983, "Analysis of Gas Lubricated Foil Journal Bearings", Journal of Lubrication Technology, 105, 647-655.

# Application of Chemical based Technologies called Surfactant(S) and Alkali-Surfactant (AS) for Enhancing Oil Production from matured fields : Case studies

*B.P.Singh\*, P.K.Sharma\*\**

**\* Ex-ONGCian, Consultant- Pan India Consultancy Ltd,Gurgaon and Domain Expert -Oil India Ltd, Address- H-53, Karnawati Socity, Chandkheda, Ahmedabad, Gujrat, India, Email:singh01bp@gmail.com , mobile-+91 9426614667**

**\*\* GM (Production),ONGC,Ahmedabad Asset.**

## Abstract

With growing global energy demand and depleting reserves, enhanced oil recovery (EOR) from existing brown fields becomes more and more important. Petroleum engineers are continually being challenged to develop new and improved techniques and strategies for hydrocarbon recovery. Enhanced Oil Recovery (EOR) methods enable us to optimise the extraction of your oil beyond that recoverable by primary and secondary methods. Technological interventions have significant potential in stimulating the recovery of hydrocarbon reserves from the matured/aging fields. Among various EOR processes, chemical EOR process have edge over other techniques to boost the oil production. At present three chemicals viz alkali, surfactant and polymer are being used in oil industry, either as a single one or in the combination of two and three to improve the oil production.

Present paper is concerned with single well treatment based on use of two chemicals EOR technologies called Surfactant (S) and Alkali - Surfactant (AS) for low to heavy oil reservoir. These two innovative technologies has been used for the first time in different fields of Ahmedabad Asset in ONGC. These were applied on trial basis in ceased and low potential wells at the time of workover to reduce the operation cost and few jobs were done without using rig. The jobs were completed in two phases, in first phase-I only surfactant (S) jobs were done in 5 wells for light oil reservoirs and in second phase-II ,out of 15 jobs 5 jobs were done for Alkaline-Surfactant (AS) for viscous crude oil . The results of phase-1 are highly encouraging as cumulative incremental oil gain was found 27562 $m^3$ as on Sept-2020 (42 months). The liquid rate increased to 93 $m^3$/d from 54 $m^3$/d , oil rate become double ,which increased to 65 $m^3$/d from 31 $m^3$/d and decrease in average water cut of 20 % was observed. The life of job and its effectiveness was found more than three years, which is equivalent of life of Chemical Pilot done in pattern form using 1 injector and 4 producers or vice-versa. Therefore, these single well surfactant jobs are just like a mini pilot testing. These mini pilots conducted in huff n puff mode are highly cost effective as mainly chemical cost is involved. The other advantages are saving of huge time as job can be completed in one day, either during workover job or using minimum infrastructure just like dosing pump and some tanks. Return is very high as well can be put on production with improved production parameters on next day of job.

In second phase-II for the first time Alkali -Surfactant (AS) technology was implemented in 5 wells to test the process for high viscous crude oil. The oil viscosity of three wells is in range of 4000 to 6000 cP . Generally thermal EOR processes are most suitable for viscous oil, but due to technological development and other limitations such as isolated single well and limited payzone thickness etc, the chemical EOR processes were found more advantageous. Practically these wells were not contributing much oil and oil production rate was in fraction and less than1 $m^3$/d. The

results of phase-II are highly encouraging as cumulative incremental oil gain was found 2576 m$^3$ as on Sept-2020 (18 months). The liquid rate increased to 25 m3/d from 10 m$^3$/d , oil rate become double ,which has increased to 13 m$^3$/d from 5 m$^3$/d and decrease in average water cut of 5 % was observed. Thus, liquid influx has almost become double just after treatment which is due to change in rheological properties and reduction in oil viscosity of crude oil by chemical reactivity. It is obvious that Alkali-Surfactant (AS) technology is emerging and promising process for enhancing oil production of viscous oil. The technology is highly useful for small reservoir or fields in which wells are lying in isolated area or 3 to 4 wells are completed in single block.

Present paper contains the details of the selection of surfactant, theoretical aspect, laboratory studies for optimisation of chemical doses, mechanism involved, production performance of individual well, cost benefits and future scope of application of these two emerging technologies.

## 1. Experimental Details

### 1.1 Selection of surfactant and availability

Chemical Technology has a long track record of success and it depends upon the available technology and quality of chemicals used in formulation. Today we have both technology and chemicals. The surfactant used in present treatment is selected based on various screening tests in Institute of Reservoir Studies. Among various surfactant samples , anionic type of surfactant was found most suitable based on screening results of thermal stability, critical micellar Concentration(CMC) value , Interfacial tension (IFT) measurement and emulsion formulation studies. Finally tested on core flood experiment on native sand pack at reservoir temperature. The active content in used surfactant is 36-38%. It is commercially available in India and manufactured by many companies.

### 1.2 Concept and mechanism of Surfactant

Surfactant are surface acting agents that creates miscibility between two immiscible phases such as oil and water. The surfactant consisting of two parts namely water loving termed as head and oil loving termed as tail. Generally, surfactants are categorized into four type called as anionic, cationic, nonionic and amphoteric. In oil industry these surfactants are used for different works and have wide application. For EOR application in Sandstone reservoir the anionic type is mostly used as it has negative charge. In present treatment anionic surfactant was used after detailed study in Institute of Reservoir Study .Due to dual nature surfactant always remains at interface of two immiscible liquid i.e water and oil and formed emulsion by solubilization of oil and water due to IFT reduction. The working principle of surfactant is due to two principles one is emulsification and entrainment and other is emulsification and entrapment

Emulsification and entrainment involve formation of emulsion by reduction of interfacial tension between oil and water. This emulsified oil entrained in pore throat and plug it due to which injected fluid diverted into porous media previously not contacted. Emulsification and entrapment involve the production of oil droplets from pore throats as a result of increase in capillary number. As the front move the capillary pressure changes due to loss of surfactant by adsorption, resulting change in interfacial activity. In this manner incremental oil is produced by sweeping oil from pores which have not previously swept.

## 2. Results and Discussion

The results of mini pilots testing using surfactant for EOR for a wide range of oil viscosity are mentioned below. The jobs were done in 2 phases. The phase wise results are given below.

### 2.1 Results of 5 Surfactant Jobs done in First Phase-I ( Kalol and Limbodara Field)

In first phase-I, a total five surfactant jobs were done on trial basis in two fields namely Kalol and Limbodara of Ahmedabad Asset. These jobs were done for the first time in history of ONGC , Ahmedabad. Jobs were carried out almost three years back in year -2017. Out of 5 jobs , 4 numbers of jobs were done in a largest and matured Kalol field. It is multilayer heterogenous and a complex field, where average oil recovery is below 15% of OIIP. Therefore, sufficient amount of remaining oil is left in reservoir even after water injection is continued from last many years. In view of low oil recovery, a suitable EOR process is highly required for Kalol field. As per EOR screening criteria, thermal method is not suitable and gas injection process can not be done due to low reservoir pressure and non availability of gas for injection. In this situation chemical EOR method is only option left for such type of reservoir. Among chemical EOR processes, Polymer can not be injected in this field due to low permeability. Therefore. ,only surfactant (S) and alkali mixed with surfactant (AS) is suitable EOR technologies for Kalol field. Laboratory studies were carried out long back both for ASP and AS processes. ASP pilot was conducted in K-XII sand of Kalol Field and preliminary results of ASP injection were found encouraging (Ref-1,2) but as ASP solution was followed by polymer solution, severe injectivity problems were observed and polymer solution could not be injected further. Thus Polymer flooding is ruled out EOR technology for this field. Based on experiences gained, and keeping in mind that generally pilot testing takes long period of 5-10 years, mini pilot testing for surfactant (S) was chosen the suitable EOR process to enhance oil production. Kalol is a complex field has wide variation in permeability 20-700 mD and oil viscosity varied from few centipoise to thousand centipoise. In first phase-I , those wells were selected which has light oil viscosity and completed in different reservoirs of Kalol field. The summary of results of production performance both pretreatment and post treatment are given in Table-1.

**Table-1: Summary of results of pre and post production performance(Phase-1)**

| Month | Well Name | Pre -Job | | | Post -Job | | | Cumulative Incremental Oil,m$^3$ |
|---|---|---|---|---|---|---|---|---|
| | | QL, m$^3$/d | Qo, m$^3$/d | W/C,% | QL, m$^3$/d | Qo, m$^3$/d | W/C,% | as on 1.09.2020 |
| | | | | | | | | |
| Feb-17 | Kalol well#A/185A | 12 | 10 | 40 | 25 | 23 | 2 | 12513 |
| Apr-17 | Kalol well#B/124 | 10 | 3 | 60 | 15 | 9 | 40 | 6278 |
| Jan-17 | Kalol well#C/68 | 5 | 3 | 40 | 10 | 6 | 20 | 2278 |
| Jan-17 | Kalol well#D/506 | 10 | 9 | 20 | 18 | 15 | 15 | 4191 |
| Nov-17 | Limbodara well#A/507 | 17 | 6 | 70 | 25 | 12 | 50 | 2302 |

| | Total | 54 | 31 | 49 | 93 | 65 | 30 | 27562 |
|---|---|---|---|---|---|---|---|---|

## 2.2 Production performance of Kalol well KL #A/185A

The Kalol well #A/185A was treated in February-2017. It is completed in sand of K-IX+X of Kalol field and operating with Gas lift Valve (GLV) installation. Before workover job the well was not flowing, due to choking of perforation . It is important to mentioned here that Foam +N$_2$ job through CTU was carried out repeatedly three times for clearing the wellbore from sand and wax deposition. But could not get the success, finally surfactant treatment was carried out which was found very much effective as it has not only removed the sand/wax deposition but improve the production performance of the well by reduction in water cut and increase in liquid and oil production.

The Production Performance graphs of Kalol well #A/185A is shown in Figure-1. It shows that there is drastic reduction in water cut , which has reduced to 2% from 40% . The level of water cut is still in range of 2-3% even after completion of three years .There is also good gain in liquid and oil production rate. The oil rate increased to 23 m$^3$/d from 10 m$^3$/d and liquid rate improved to 25 m$^3$/d from 12 m$^3$/d. The incremental cumulative oil production over base is 12513 m$^3$ till 30th Sept-2020. This well is star performer as huge amount of oil has already been produced and still producing oil without any decline from last 38 months,



**Figure-1: Production Performance of Kalol Well#A/185A**

**Figure-2: Reduction in Viscosity and change in Rheological Properties of Produced crude**

## 2.3 Production performance of Kalol Well#B/124

The Second Kalol well #B/124 was treated in April-2017. It is completed in sand of K-XII and operated with SRP installation. Present jobs was done at the time of workover job for tubing replacement and reinstallation of SRP. The new formulation consisting of anionic surfactant and EGMBE was tried in the well. The results were found encouraging. The oil rate increased to 9 $m^3$/d from 3 $m^3$/d and liquid rate improved to 15 $m^3$/d from 10 $m^3$/d , water cut reduces from 60 % to 40%.The incremental cumulative oil production over base is 6278 $m^3$ till 30th Sept-2020. The improvement in production data is due to effectiveness of surfactant job. The surfactant has mobilized the oil contacted by it and formed emulsion by solubilization of oil due to IFT reduction. The Production Performance graphs of Kalol well #B/124 is shown in Figure-3



**Figure-3: Production Performance of Kalol Well#B/124**

## 2.4 Production performance  of Kalol Well #C/68

The Kalol well #C/68 was treated in January-2017. It is completed in sand of  K-VII+IX+X  and operating with  GLVS installation. Present job was done  at the time of work over operation  for GLVs repairing. The well #A/68 , was  closed  since long back say 2 years , due to GLV service. It was also suspected the wax deposition in tubing due to closer of the well for long time. The new formulation consisting of anionic surfactant and EGMBE was tried in the well. The results were found encouraging. The oil rate increased to 6 $m^3$/d from 3 $m^3$/d and liquid rate improved to 10 $m^3$/d from 6 $m^3$/d , water cut reduced from 40 % to 10%.The incremental cumulative oil production over base was 2278 $m^3$ till 30th Sept-2020.The enhancement in production data is due to effectiveness of surfactant job. The surfactant has mobilized  the oil by formation of emulsion due to IFT reduction. The Production Performance graphs of well #A/68 is shown in Figure-4
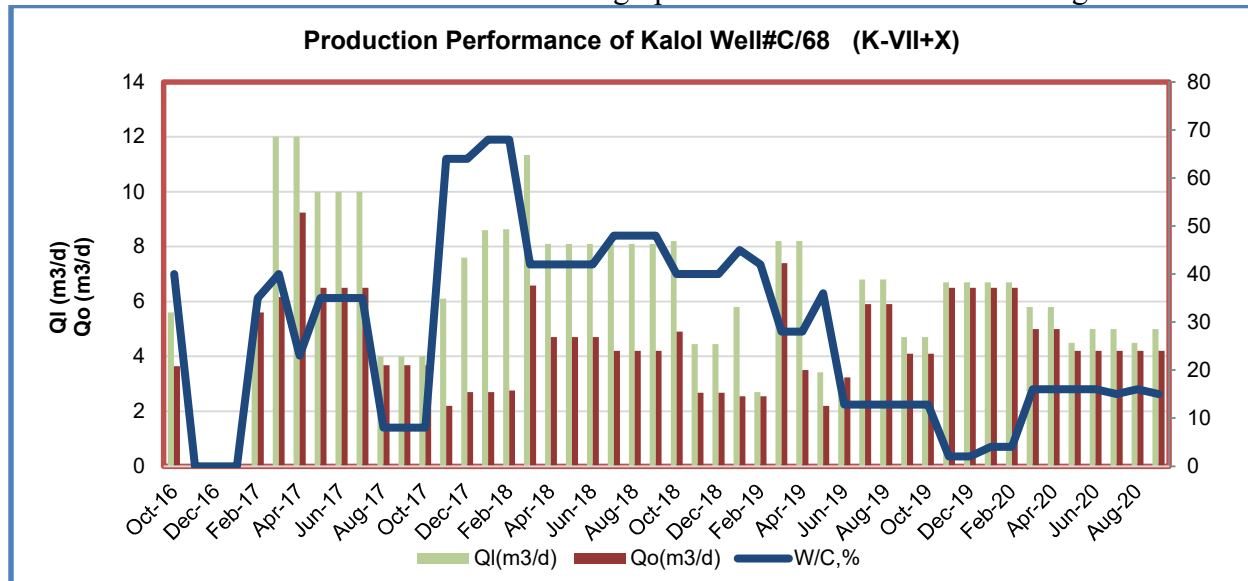


**Figure-4**: **Production Performance of  Kalol Well#C/68**

## 2.5 Production performance  of  Kalol well #D/506

The Kalol well #D/506 was treated in January-2017.  It is completed in sand of  K-XII and operating  with  SRP. Present jobs was done at the time of workover operation. Rig was deployed for tubing replacement and installation of SRP. The well was closed since long back for more than one year, due to GLV service. It was also suspected the wax deposition in tubing due to closer of the well for long time. The new formulation consisting of anionic surfactant mixed in filtered injection water was tried in the well. The results were found encouraging. The oil rate increased to 15 $m^3$/d from  9 $m^3$/d and liquid rate improved to 18 $m^3$/d from 10 $m^3$/d , water cut reduced from 20 % to 15%. The incremental gain in cumulative oil production 4191 $m^3$ till 30th Sept-2020. The improved performance of the well is due to formation of good emulsion by solubilization of more oil  by IFT reduction. The Production Performance graphs of the is shown in Figure-5.
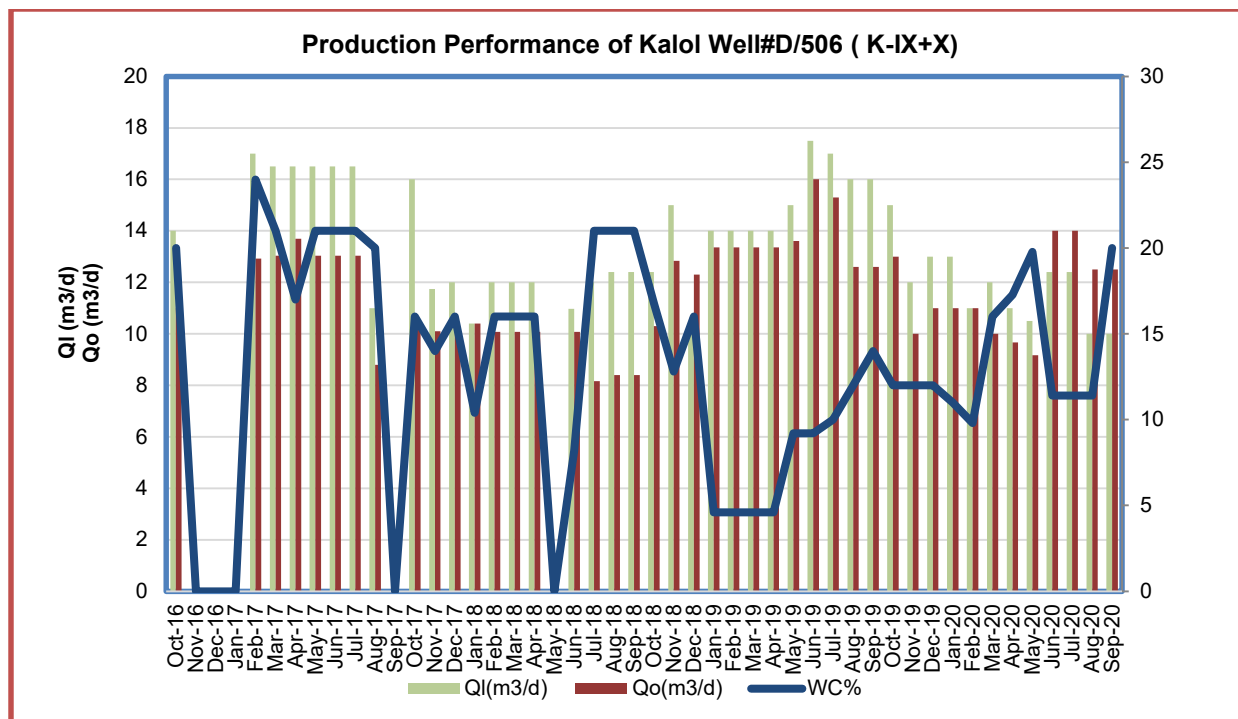
**Figure-5**: **Production Performance of well Kalol Well#D/506**

## 2.6 Production performance of Limbodra well#A/85

The Limbodra well #A/85 in was treated in November-2017. This job was done at the time of workover job for tubing Replacement and installation of SRP. Limbodra is second field in which Surfactant treatment jobs was carried in first well on trial basis. In Limbodra field about 45 wells are being treated with Zylene/ Naptha for mitigating the flow assurance problem. This Well #A/85 was also being treated occasionally for Zylene/Naptha. The crude is waxy in nature and wax content varies from 18 to 36%. The production performance of the well improved significantly after treatment. The oil rate increased to 12 m³/d from 6 m³/d and liquid rate improved to 25 m³/d from 17 m³/d , water cut reduced from 70 % to 50% . The incremental cumulative oil production 2302 m³ till 30th Sept-2020. The Production Performance graphs of well #A/85 is shown in Figure-6.
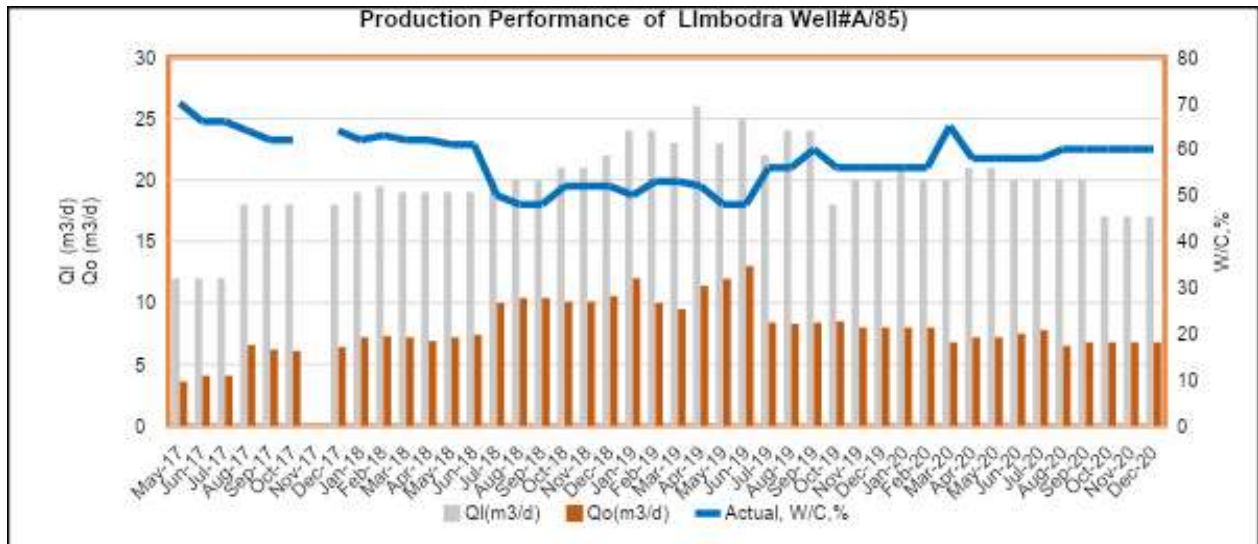
**Figure-6**: **Production Performance of well Limbodra Well#A/85**

## 2.7 Results of 5 Jobs done in Second Phase-II for High viscous crude ( Kalol, Wadsar, Gamij Field)

 Generally thermal methods are considered most suitable EOR processes for high viscous crude. Initially chemical EOR methods were applicable to the crude oil have maximum viscosity of 350 cP. Literature surveys and field application of chemical EOR methods has opened the wide scope for its application to high viscous crude (Ref-3,4).With this confidence and finding favorable screening laboratory results the Alkali- Surfactant (AS) technology was implemented  in 3 wells of Kalol field, 1 well in Wadsar and  1 well in Gamij field of Ahmedabad Asset. Technology was applied as single well mini pilot form on  trial basis for the first time in ONGC, Ahmedabad Asset. In high viscous crude, oil recovery is low due to adverse mobility contrast existing in reservoir. The surfactant control adverse mobility ratio by decreasing  oil viscosity and also changing the relative permeability of  oil and water  in reservoir rock. This phenomena is due to reduction in interfacial tension (IFT) and increase in capillary number by surfactant. Mostly high viscous crude are acidic in nature, therefore alkali is used as it  helping in generating in-situ surfactant by neutralization process.  Both the chemical are forming very good emulsion with crude oil, also solubilize more oil, resulting more oil production. AS technology  is termed as low cost  high efficiency EOR process.  The summary of results  of  production pretreatment and post treatment are given in  Table-2. The  details of production performance of these  wells are mentioned below.

Table-2: Summary of results of pre and post production performance (Phase-II)

| Sr No | Well no | Date of Job | Pre Treatment | | | Post Treatment | | | Cumulative incremental Oil on m$^3$(30$^{th}$ Sept-2020) |
|---|---|---|---|---|---|---|---|---|---|
| | | | Ql,m$^3$/d | Qo , m$^3$/d | W/C,% | Ql,m$^3$/d | Qo , m$^3$/d | W/C,% | |

| | | | | | | | | | |
|---|---|---|---|---|---|---|---|---|---|
| 1 | Kalol well#E/612 | Jan,-2019 | 3.1 | 0.8 | 76 | 4.5 | 2.3 | 45 | 671 |
| 2 | Kalol well#F/636 | Jan-2019 | 1.8 | 0.35 | 75 | 4 | 2.5 | 45 | 311 |
| 3 | Kalol well#G/530 | Jan-2020 | 1.4 | 0.7 | 60 | 5 | 2.5 | 42 | 974 |
| 4 | Wadsar well#A/1 | Jan-2019 | 3.6 | 3 | 12 | 11 | 5.5 | 9 | 621 |
| | | | **10** | **5** | **51** | **25** | **13** | **48** | **2576** |

## 2.8 Production Performance of Kalol well #E/612

The Kalol well #E/612 was treated in February-2019. This is low potential well and producing oil and liquid rate of @0.7 $m^3/d$ and @ 3 $m^3/d$ respectively . The crude oil is collected in open tank and operating with tanker loading system due to very low potential. The oil is highly viscous and viscosity is 5123 cP at 40 degree centigrade. This high viscosity is main production problem identified of this well. This well is being treated with dosing of Zylene/naptha to improve the production performance but no significant improvement was obtained. However hot water treatment is going on in this well just as routine practice. As per literature survey and laboratory studies conducted, the Alkali -Surfactant (AS) technology is best process for such type of reservoir. Therefore, mixture of alkali and surfactant solution was squeezed into formation. Next day well was activated and opened for flow.

The production performance of the well improved due to gain in liquid and oil rate and reduction in water production. As on date in well #E/612, there is good gain in oil rate, which increased to 2.3 $m^3/d$ from 0.8 $m^3/d$, water cut reduced from 76 % to 45% with cumulative oil production 671 $m^3$ till 30th Sept-2020 . The production performance of this well is shown in Figure-7. Change in rheological properties of crude oil sample collected at the surface after job is shown in Figure-8. This behavior is pseudo-plastic in nature just like polymer. The viscosity has also reduced to 1000 cP from 5123 cP. The reduction in viscosity and change in flow behavior is responsible for good liquid influx and water control by clearing the wellbore and mobility control in this well.
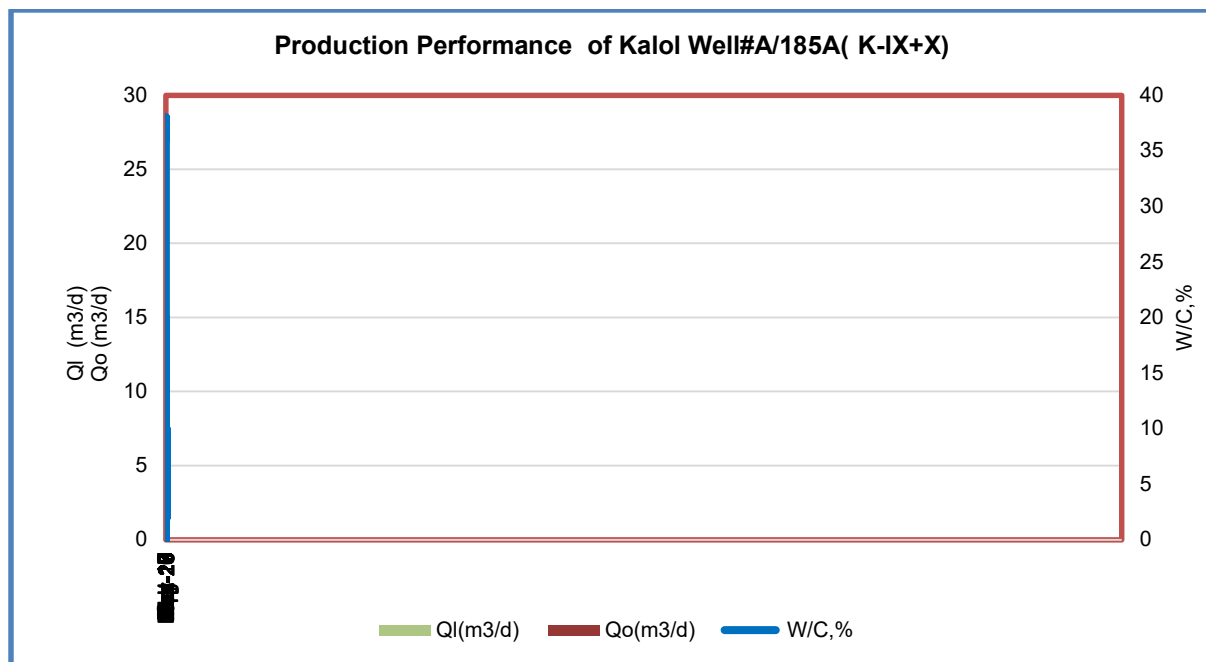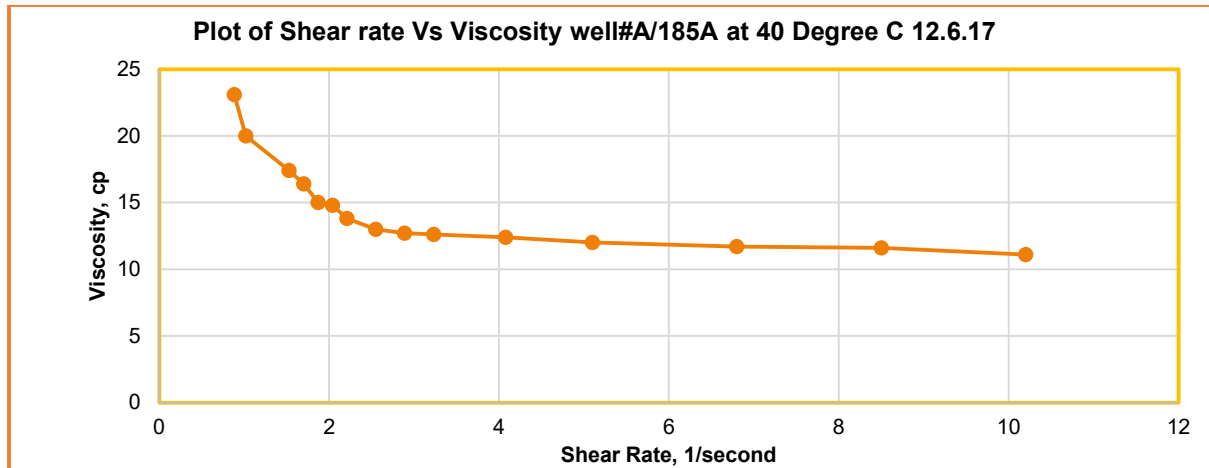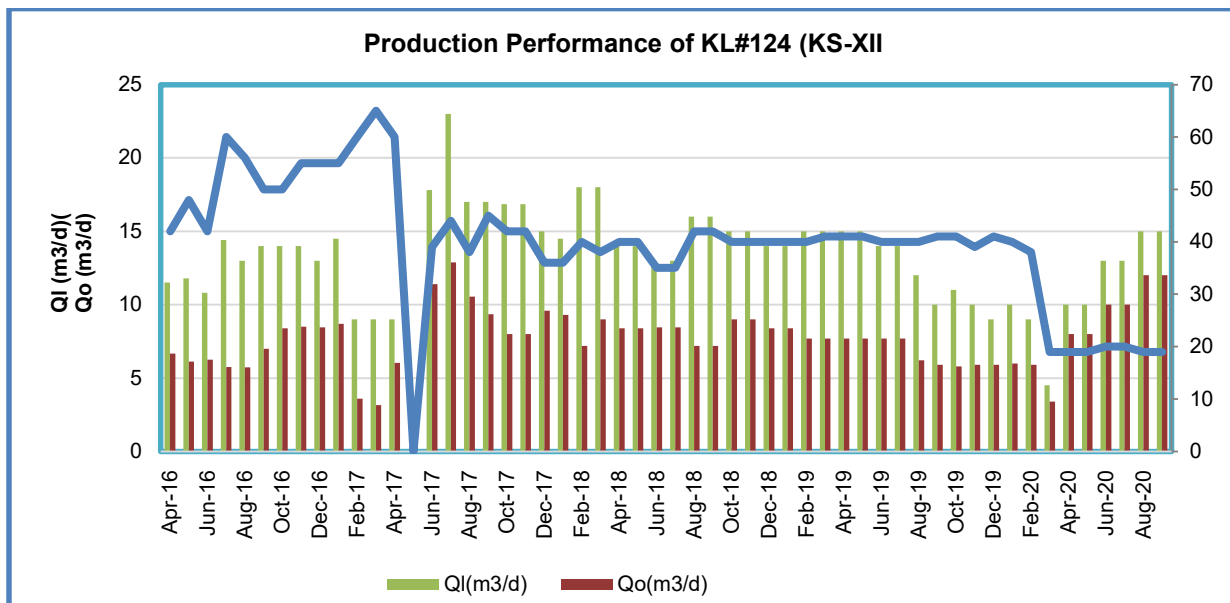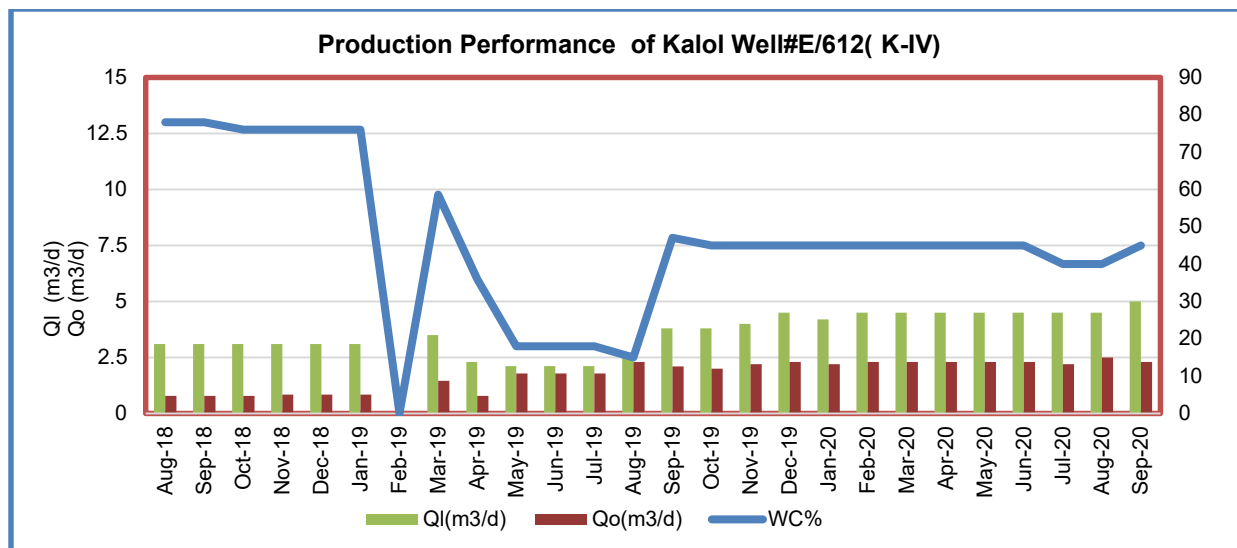
**Figure-7**: **Production Performance of Kalol Well#E/612**
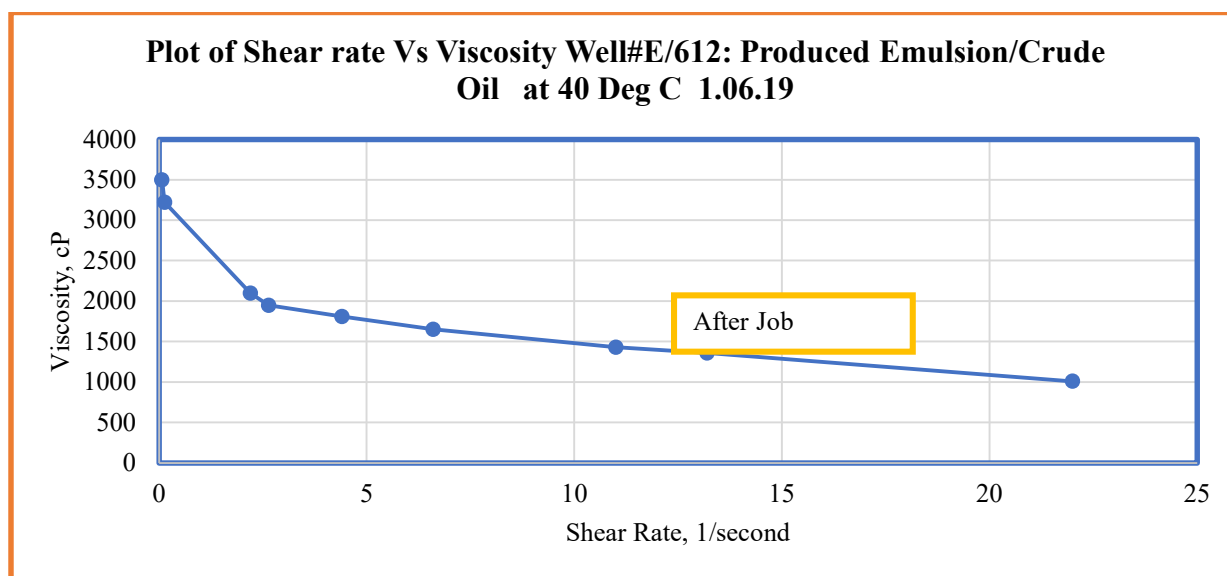


**Figure-8: Reduction in Viscosity and change in Rheological Properties of Produced crude**

## 2.9 Production Performance of Kalol well #E/612

The   Kalol well #F/636 was treated in February-2019. This is also a low potential well which producing oil and liquid rate of @0.35 m³/d and @ 2 m³/d  respectively.The  crude oil is collected in  open tank  and operating with tanker loading system  due to very low potential. The oil is highly viscous and viscosity is  3299 cP at 40 degree centigrade. This high viscosity is main production problem identified of this well .This well is being treated with dosing of Zylene/naptha to improve the production performance but no improvement was obtained. Therefore, mixture of Alkali and Surfactant solution  was squeezed into formation. Next day well was activated and opened for flow.

After treatment the production performance of the well improved significantly. In well#F/636, oil rate increased to 2.5 m³/d from 0.35 m³/d, liquid rate increased to 4 m³/d from 1.8 m³/d and water cut reduces from 75 % to 45%. The incremental cumulative oil production is 671 m³ till 30th Sept-2020 . The production performance of this well is shown in Figure-9. Change in rheological properties of crude oil sample collected at the surface after job is shown in Figure-10. This behavior is pseudo-plastic in nature just like polymer. The viscosity has also reduced to 1200 cP from 3299 cP. This reduction in viscosity and change in flow behavior is responsible for good liquid influx and water control by clearing the wellbore and mobility control in this well. Well is closed due to tubing annulus communication since December-2019.
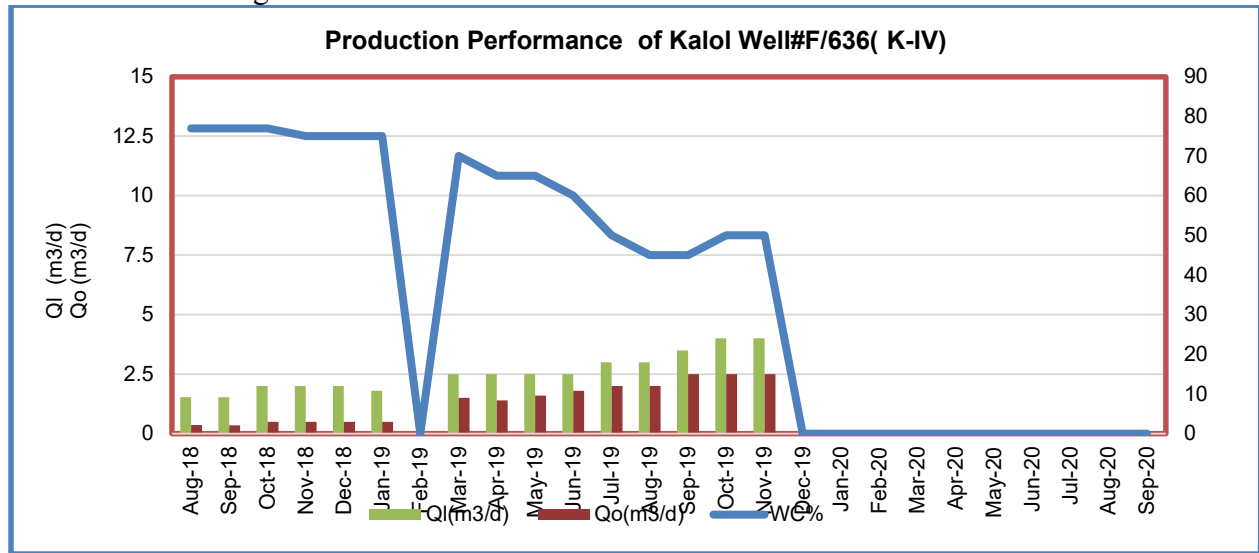


**Figure-9**: Production Performance of Kalol Well#F/636
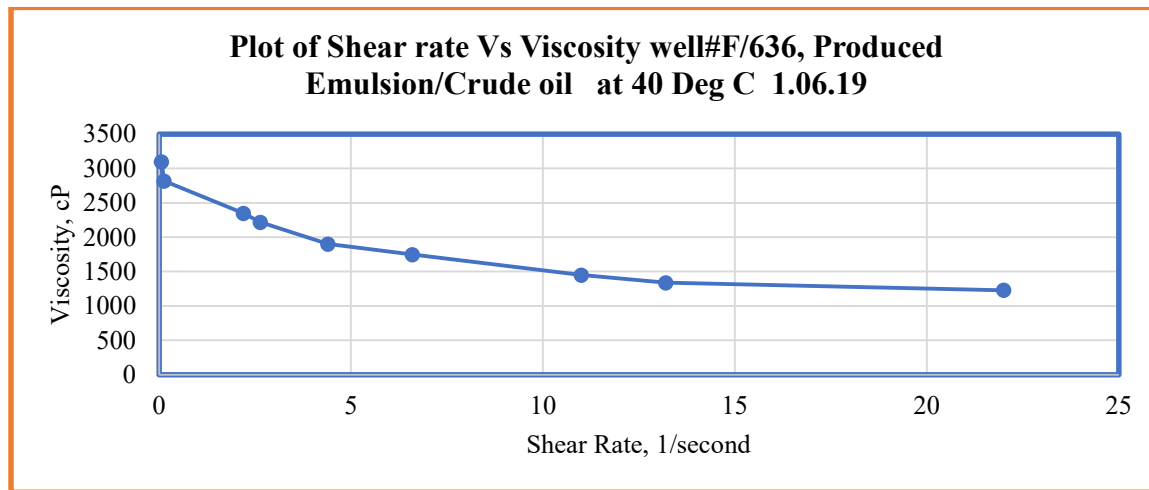


**Figure-10: Reduction in Viscosity and change in Rheological Properties of Produced crude**

## 2.10 Production Performance of Kalol Well#G/530

The Kalol Well #G/530 was treated in March-2019.This is a low potential and producing oil and liquid rate of @0.7 m³/d and @ 1.4 m³/d respectively . The crude oil is collected in open tank

and operating with tanker loading system due to very low potential. The effort were made to major the crude oil viscosity but could not be measured even at high temperature. Dosing of Zylene/naptha is being done but could not improved flow condition due to very high viscosity. A mixture of Alkali and Surfactant (AS) solution was squeezed into formation. Next day well was activated and opened for flow. Production performance improved drastically, there is good gain in oil rate, which increased to 2.5 m$^3$/d from 0.7 m$^3$/d, liquid rate jumped to 5 m$^3$/d from 1.4 m$^3$/d and water cut reduces from 60 % to 42%. The cumulative incremental oil gain was obtained 974 m$^3$ till 30$^{th}$ Sept-2020 . The production performance of this well is shown in Figure-11. The oil sample collected at the surface and measured oil viscosity with time is shown in Figure-12. Change in crude oil viscosity was observed and lowest measured value was 1823 cP at 60 degree centigrade. This reduction in viscosity and change in flow behavior is responsible for good liquid influx and water control by clearing the wellbore and mobility control in this well.
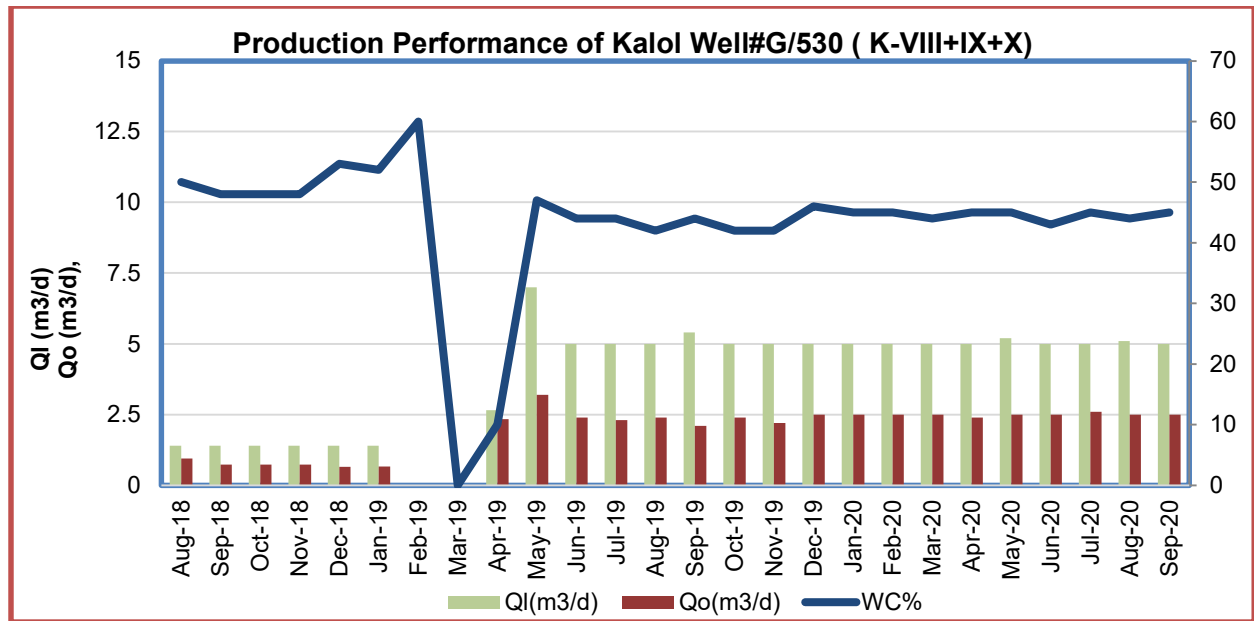


**Figure-11**: **Production Performance of Kalol Well#G/530**
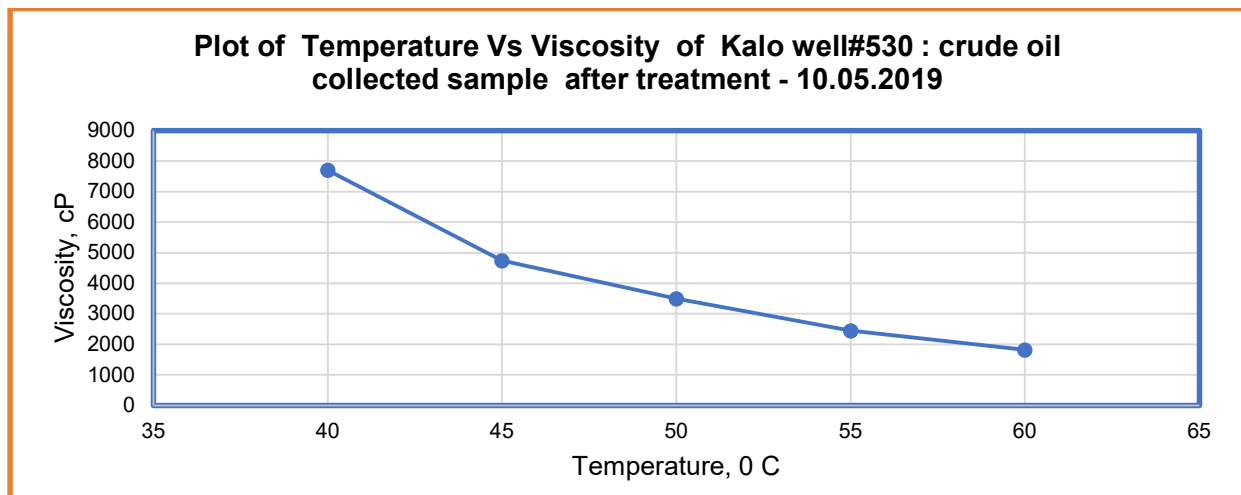


**Figure-12: Reduction in Viscosity of Produced crude**

## 2.11 Production Performance of Wadsar Well#A/1

The Wadsar Well#A/1 was treated in January-2019. This well producing oil and liquid rate of @ 3 $m^3$/d and @ 3.6 $m^3$/d respectively. The crude oil is collected in open tank and operating with tanker loading system due to very low potential. The oil is viscous and viscosity is 74.4 cP at 40 degree centigrade. The crude is waxy in nature and it is range 26-42%. This high viscosity is main production problem identified of this well initially. This well is being treated with dosing of Zylene/Naptha to improve the production performance but no improvement was obtained. Therefore, mixture of Alkali and Surfactant solution was squeezed into formation. Next day well was activated and opened for flow. Production performance improved drastically, there is good gain in oil rate, which increased to 5.5$m^3$/d from 3.0 $m^3$/d, liquid rate increased to 11 $m^3$/d from 3.7 $m^3$/d and water cut reduced from 12 % to 9%. The cumulative incremental oil gain was obtained 621 till 30th Sept-2020.The production performance of this well is shown in Figure-13.
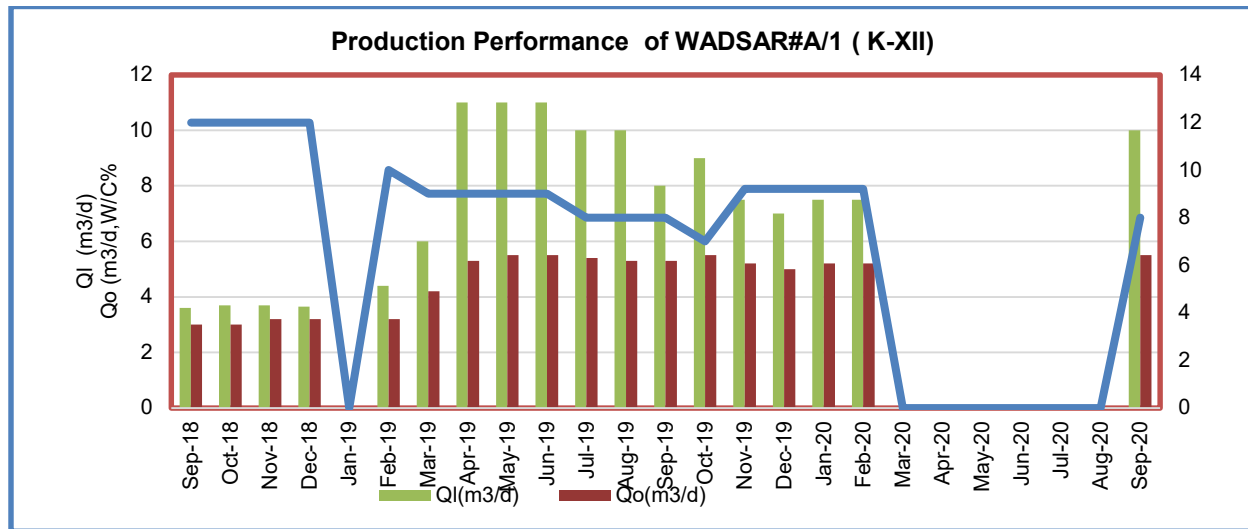


**Figure-13**: Production Performance of well Wadsar Well#A/1

## 2.12 Production Performance of Gamij Well#A/233

The Gamij Well#A/1 in Gamij Field was treated in March-2020. This is exploratory well and completed at shallow depth of about 700 m. The crude is highly viscous in nature. The viscosity was found 7900 cP at 27 degree centigrade and 5200 cP at 30 degree centigrade. The measured viscosity values at different temperature is shown in Figure-14. During activation the well has produced 2-3 lts of oil in application of different compressors. The nature of crude is very thick and it is in lumb form . Free flow of crude oil was not observed. Efforts has been made to reduce the viscosity of this well and to produce the oil ,but could not get successes. Based on encouraging results in viscous oil of Kalol and Wadsar fields, the Alkali-Surfactant (AS) treatment was carried in this well. After 2 days the well was activated and got the crude oil samples. Measured the viscosity of collected crude oil and also investigated the changes in rheological properties of crude oil as a monitoring tool. A significant reduction from 7900 cP to 200 cP in crude oil viscosity was observed. The crude behaviour was pseudo plastic in nature as viscosity reduction was observed with increased in shear rate as depicted in Figure-15.

Physically free flow was observed in behavior of crude oil collected and shown in Figure-. Based on these observations it is concluded that Alkali-Surfactant (AS) treatment is quite effective and to be put on regular production on suitable artificial lift system.

**Plot of Viscosity Vs temperature of Gamij well# A/233 : crude oil before treatment - 02.04.2019**
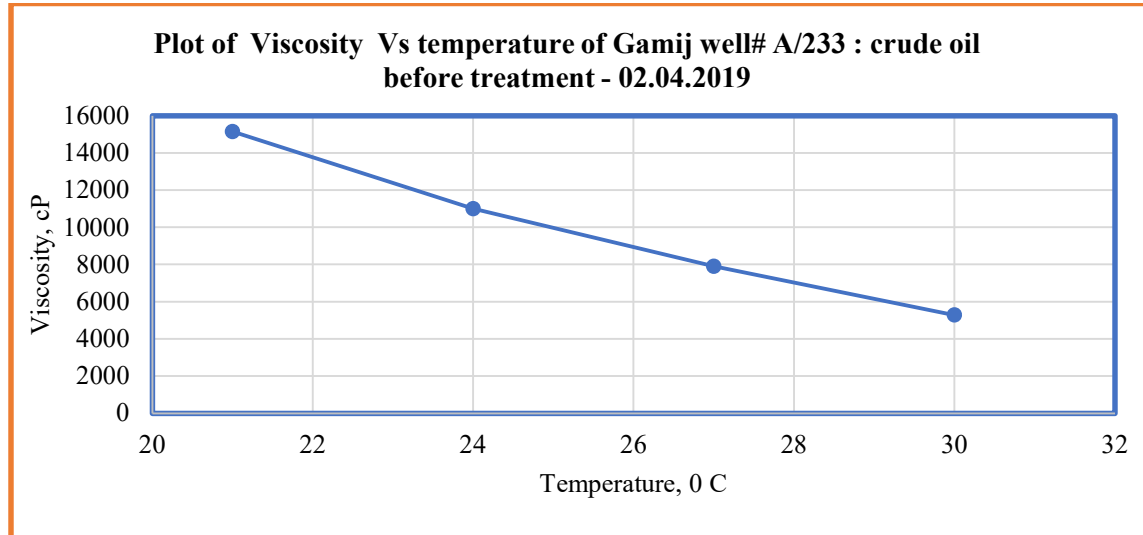
**Figure-14**: **Viscosity of crude oil before job Gamij well#A/233**

**Plot of Shear rate Vs Viscosity Gamij Well#A/233: Crude oil emulsion collected after treatment at 30 0C-15.03.2020**
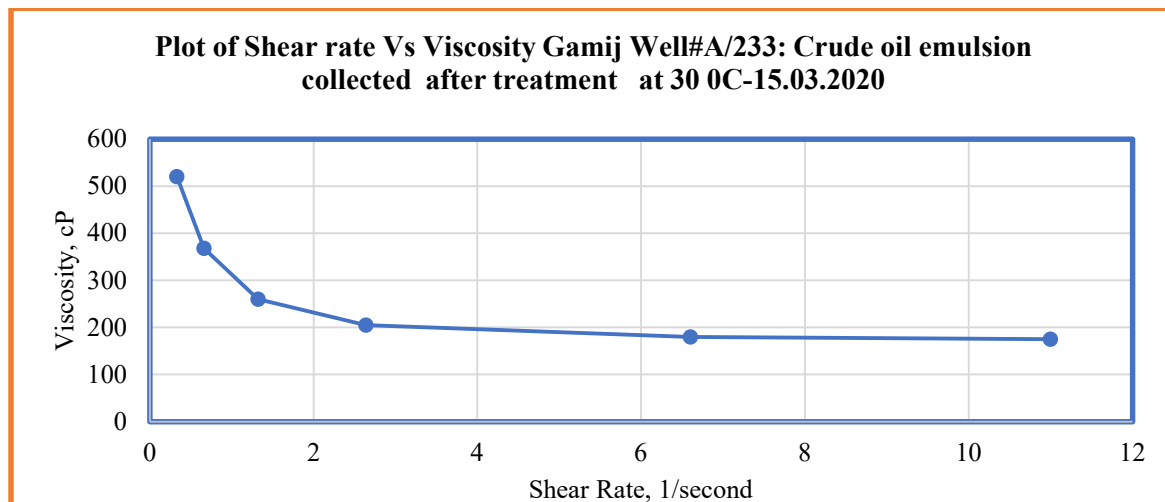
**Figure-15**: **Viscosity Reduction and change in rheological properties of produced oil Gamij well#A/233**

## 2.13 Cost Effectiveness of Surfactant Treatment Jobs

Single well mini pilot testing by use of Surfactant (S) and Alkali -Surfactant (AS) technologies for EOR was found highly cost incentive. The average per well chemical cost is of the order of 2-4 lakhs. Both the chemical are easily available in Ahmedabad, Gujrat. The Operation cost is

nominal as job can be done at the time of workover operation or with use of pump and small tanks in a single day. Moreover, displacing fluid used was process water, instead of oil used in conventional solvent system in these both technologies, which further reduced the operation cost.The per well incremental oil gain is expected to minimum 1000 m$^3$ to 5000 m$^3$ which is worth of Rs. 2.5 crs to 10.0 crs. by considering oil price of Rs 25000/m$^3$ of oil. In simple way, chemical cost is paid up ,if well produced 10-15 m$^3$ of oil. Thus both the technologies are low cost high efficiency EOR processes and applicable over a wider range of oil viscosity. Moreover, chemical EOR processes are cheapest methods than thermal EOR methods for heavy oil. It is more beneficial for the limited and isolated oil pools, having 3-4 oil producing wells.

## 3 Conclusions

1. For the first time in the history of ONGC, Ahmedabad Asset ,Single well mini pilot testing by use of surfactant for EOR was carried out on trial basis for wider range of oil viscosity. The results of all jobs were found encouraging.

2. The Surfactant (S) technology for EOR was done in 4 Kalol wells and 1 well of Limbodara field in First phase-I for light oil crude.Significant improvement in oil production was obtained with cumulative incremental oil gain of 27562 m$^3$ in last 3.5 years.

3. For the first time Alkali -Surfactant (AS) technology was implemented by single well treatment in 3 wells of Kalol field and 1 well in Wadsar field in Second phase-II. The viscosity of Kalol wells was in range of 3000 cP to 5500 cP and 75 cP in Wadsar well.

4. Significant improvement in liquid influx and oil gain for high viscous crude was obtained in these 4 wells which were basically very low potential oil well. A cumulative incremental oil gain of 2576 m$^3$ was obtained in last 1.5 years.

5. The change in rheological properties and decrease in viscosity of produced crude oil was observed, it has confirmed that AS technology is effective in controlling of high mobility contrast in viscous crude oil reservoir.

6. The longevity and job life of single well mini pilot testing is unbelievable as job can sustained for minimum 1 year to 3 years. Effectiveness for longer period makes the technologies very cost effective, besides cheaper chemical cost and nominal operation cost.

7. This single well mini pilot testing gave lot of confidence and experience in applying these chemical EOR technologies in pattern form in full field in quicker mode to enhance the oil production.

8. Thus, chemical EOR technologies are quite effective and applicable for a wider range of crude oil viscosity. Oil production can be quickly increased of the wells lying in isolate pool or in the reservoir have limited 3 to 4 wells.

### Nomenclature

ASP     Alkali Surfactant-Polymer
CMC    Critical MicelleConcentration
EOR     Enhance oil recovery
CEOR   Chemical Enhanced Oil Recovery
AS      Alkali -Surfactant

S        Surfactant

EGMBE Ethylene Glycol Methylene Butyl Ethane

OIIP     Oil Initial In placed

WOJ    Work Over Job

GLV     Gas Lift valve

QL      Liquid Rate

Qo      Oil Rate

W/C     water cut

IFT      Interfacial tension

SRP     Sucker Rod Pump

IRS     Institute of Reservoir Studies

ppm    Parts per-million

Wt.%   Percent weight

cP      Centipo

**References**

1. Ankit Hanotia, B.P Singh, Supriyo Samanta, Oil and Natural Gas Corporation Ltd." ASP Flood Pilot Test at Tertiary Stage in Kalol Field – A Case History Presented at SPE  Oil and Gas India Conference and Exhibition held in Mumbai, India, 24-26 November 2015. SPE-178083-MS

2. Singh,B.P, Saxena M.K, Kumar, Anil, "Laboratory Evaluation for Applicability of ASP/AS Flood Process for Kalol Horizons K-IX+X & XII", Research Report, IRS, ONGC, 1999.

3. James J. Sheng, "A Comprehensive Review of Alkaline-Surfactant-Polymer (ASP) flooding ", SPE-165358, Presented at the SPE Western Regional & AAPG Pacific Section meeting,2013 Joint Technical Conference held in Monterey, California, USA, 19-25 April,2013

4. R.V. Poptani, L.Mishra, A.K.Gupta. et al  cairn India Limited. " Field trial of Surfactant in Low PI and Intermittently Flowing PCP Wells: A successful case Study of  Bhagyam Field" .Presented at SPE  Oil and Gas India Conference and Exhibition held in Mumbai, India, 4-6 April 2017. SPE-185403-MS

5. B.P.Singh, V.P.Singh , ONGC Ltd "Single well Anionic Surfactant Treatment an Innovative Technology for Productivity enhancement through flow assurance, stimulation and water control in two fields of Ahmedabad Asset. A Successful case Study" presented in Petro-tech 2019 Delhi, 10-12 Feb-2019, Paper ID-1550

6. Jain, A.K. Dhawan, A.K. Misra, T.R. 2012. "ASP Flood Pilot in Jhalora(K-IV) – A Case Study. Presented at SPE Oil and Gas Conference and Exhibition, Mumbai, India, 28-30 March. SPE 153667

7. B. P. Singh, S. Parulkar, and Aditya Kumar, Oil and Natural Gas Corporation Ltd" Successful Pilot Implementation of ASP Flooding through CEOR/IOR Application – A Case Study" SPE Oil and Gas India Conference and Exhibition held in Mumbai, India, 4–6 April 2017. SPE185409MS

8. Singh, B.P and Kumar, A.".Initial Six Month Results of First Chemical EOR(ASP) Pilot Test in Viraj Field in India:" A field experience. Presented at India Oil & Gas Review Summit, Mumbai, 8-9 September2011.

# Evaluation and Characterisation of Polymer Chemicals for Enhancing Oil Recovery

*B.P.Singh\*, B Sai Rohit Yadav\*\**

*\* Ex-ONGCian, Consultant- Pan India Consultancy Ltd,Gurgaon and Domain Expert -Oil India Ltd, Address- H-53, Karnawati Socity, Chandkheda, Ahmedabad, Gujrat, India, Email:singh01bp@gmail.com , mobile-+91 9426614667*

*\*\* M.Tech Student( June-2016) , Andhara University, Visakhapatnam, India, Research done in IRS,ONGC,Ahmedabad under supervision of B P Singh*

*Email:singh01bp@gmail.com \**

## Abstract

It is well known fact that the Primary Recovery in most of the fields which have mobility contrast, permeability variation and operating under pressure depletion of drive mechanism is not sufficient and below 15% of Original Oil In Place (OIIP) even with water injection. Water injection in not adequate to control the viscosity contrast, in turn resulting into poor volumetric sweep efficiency in such heterogenous reservoirs. In these reservoirs use of suitable polymer is essential to increase recovery factor. Besides screening of fields, proper selection of suitable polymer chemical and its concentration through laboratory evaluation is highly needed to take the full benefit of polymer EOR technology. There are many applications of polymer in oil industry for which different type of polymer are being used. In enhanced oil recovery (EOR) processes partially hydrolysed poly acrylamide polymer (PHPA) is mostly used. These polymer have high molecular weight of the order of $15\text{-}25*10^5$ Dalton and degree of hydrolysis more then 20. The implementation of polymer flooding in a particular field depends upon certain steps like first is feasibility study of screening of field, secondly laboratory evaluation of polymer, thirdly core flood studies and finally pilot design and implementation. The laboratory evaluation through polymer characterisation and core flood studies play a dominant role in polymer based chemical EOR process. Present paper is dealing with characterisation of seven commercially available polymer samples for their use in ONGC fields for EOR process. These samples were characterised by determination of various properties like moisture content, insoluble residue, Brookfield viscosity, Cannon Fenske relative viscosity, screen factor, intrinsic viscosity, filter ratio, thermal stability, compatibility, static adsorption and rheological study. Finally core flood studies were done for determination of incremental oil recovery over water flooding , adsorption loses and residual resistance factor (RRF). Three type of process water/brines used viz soft brine (2% NaCl), hard brine (2% NaCl+0.05% $CaCL_2.2H_2O$) and Sanand tube well water (SND-Tube well) were used in the study.

The experimental results were found encouraging of all seven samples. The average moisture content was found about 6% and insoluble residue was nominal i.e 0.09% and 0.13 % in soft and hard brine respectively. The Brookfield viscosity (spindle-1 at $40^0$C) was in order of 6 to 8 cP against the required minimum value of 5 cP. The other Brookfield viscosity (UL Adapter at 60 rpm and $40^0$C) was found more as against the specified value of 3.2 cP for soft brine and 2.9 cP for hard brine. Relative viscosity (Cannon Fenske at $40^0$C) was also obtained more then the specified value of 3.1 cP and 2.8 cP for soft and hard brine respectively. The screen factor at 40 0C was found in specified ranges for both brines. Intrinsic viscosity at $40^0$C (dl/g) in soft brine was in order of 21.9 to 25.8 as desired value of 16.9 to 27.1.The filter ratio was within the limit and less then 1.5. All polymer samples were thermally stable at $82^0$C having more then 80% retention in viscosity after 7 days. Seven samples showed good rheological properties as viscosity decreases with increases of shear rate, which is good for oil recovery. Finally core flood studies were carried out by taking Berea core. The incremental displacement efficiency was obtained more then 14% of HCPV (hydro carbon pore volume) with Residual Resistance Factor (RRF) of 2.5. The dynamic adsorption losses was nominal i.e 0.01 mg/g of Berea rock.

Present paper related with detailed knowledge of characterisation of polymer chemicals for their use in Indian oil industry specially ONGC and Oil India limited (OIL) for enhancing the secondary and tertiary recovery .Today, polymer EOR chemicals are available in India at a reasonable cost, therefore, polymer technology should be use for enhancing oil recovery in those fields, which have mobilty contrast ,permeability variation and are under water injection but obtained low recovery of less than 15% of OIIP. Success of polymer in specific field depends upon selection of suitable polymer and its concentration through laboratory evaluation. Moreover, as on date EOR is mandatory and not a choice for matured/aged fields as per government guidelines. The government formed a technical committee to monitor EOR activities and job of feasibility study of screening out suitable EOR process was assigned to 4 IITs, PDPU and IRS in India. Selection of suitable EOR process will be carried out by evaluation by reservoir data and laboratory studies for a particular field. Chemical based EOR processes has a wide scope of their application as compared to other processes in India. Availability of CO2 gas for gas injection and suitability of limited reservoirs for thermal methods are main constraints for their application. Therefore, industry and academia should give more attention on chemical based EOR processes to improve the recovery at global level of 35-40%.

## 2. Experimental Details

### 2.1 Selection of Polymer and availability

Chemical Technology has a long track record of success and it depends upon the available technology and quality of chemicals used in formulation. Today we have both technology and chemicals. The polymers used were selected based on various screening tests in Institute of Reservoir Studies (IRS). Among various polymer samples, partially hydrolyzed poly acrylamide (PHPA) was found most suitable based on screening results of thermal stability, static adsorption, rheological study, screen factor, filter ration and finally core flood experiments for determination of displacement efficiency over water flooding, relative permeability of oil and water at the ends point, mobility ratio, dynamic adsorption, resistance factor(RF) and residual resistance factor (RRF). At present polymers are commercially available in India and manufactured by different companies. A total seven polymer samples namely PT-353,206,402,350,403,617 and 618 were evaluated.

### 2.2 Concept and mechanism of Polymer

The polymer (PHPA) is used in oil industry to control the mobility ratio. Mobility ratio is ratio of mobility of displacing fluid (water) and mobility of displaced fluid(oil). Mobility is again ratio of relative permeability of oil and water at the end points saturation and viscosity values respectively. In simple way, polymer used to increase the viscosity of water, in turn helping to reduce mobility contrast between the two fluids. In general, if mobility ratio is more than one/ unity, it is termed as adverse mobility ratio. It is found in all medium and high viscous crude oil reservoirs. The other important mechanism is polymer changed the relative permeability of water by adsorption on reservoir rock and also due to its pseudo-plastic behavior in porous media. Thus polymer is changing both viscosity and relative permeability in reservoir, in turn controlling mobility contrast and reservoir heterogeneity. It improves both areal and vertical sweep efficiency, resulting increases in volumetric sweep efficiency. Generally, polymer is applied at the secondary stage, but in case of high mobility contrast reservoir, it can be applied at a early stage.

## 3. Experimental Results and Discussions

Evaluation and characterization of polymer samples are carried out for samples received in two heads the first one is bonded/tender samples called EOR polymer and they are evaluated for specifications parameters. The study of EOR Polymer were conducted using soft and hard brines. The polymer of second category were evaluated for a particular field using its formation and tube well water/process water. The studies are carried out by using oil, water and native core samples of targeted reservoir at particular temperature of the field.

Experimental studies for polymer evaluation were completed in two heads namely screening studies and core flooding studies. The details are described below

### 3.1 Screening Studies

### 3.1.1 Moisture content

Moisture content which provides directly the amount of moisture present in polymer sample**.** If it is more ,it means active matter of polymer is less and there is requirement to add more polymer to get desired concentration of polymer solution. The other disadvantages are that it formed lumps and rise in fish eyes in solution, which effect other factors such as increase in filter ratio and screen factor.

Moisture content limit is 10% in common for the EOR polymer like PHPA.The average moisture content was found about 6% of all the polymer samples as shown in Figure-1.
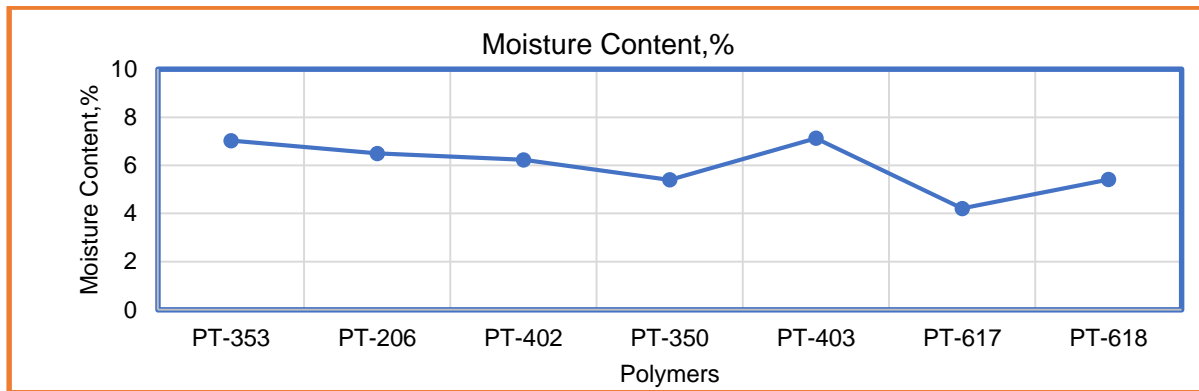


Figure-1: Moisture Content of Seven Polymers

### 3.1.2 Insoluble Residue

This is calculated  by preparing 1000 ppm (100%AM) polymer solution both using soft and hard brine. Polymer solution is filtered with 120 mesh stainless steel screen. Dry the residue in oven and determine the weight. This should be estimated, if not then higher value of it may results in the chocking  at the well bottom  hole there by causing  injectivity problems.

The maximum value of insoluble residues were nominal i.e 0.09% and 0.13% in soft and hard brine respectively, whereas maximum specified value is 0.3%. Values are shown in Figure-2.
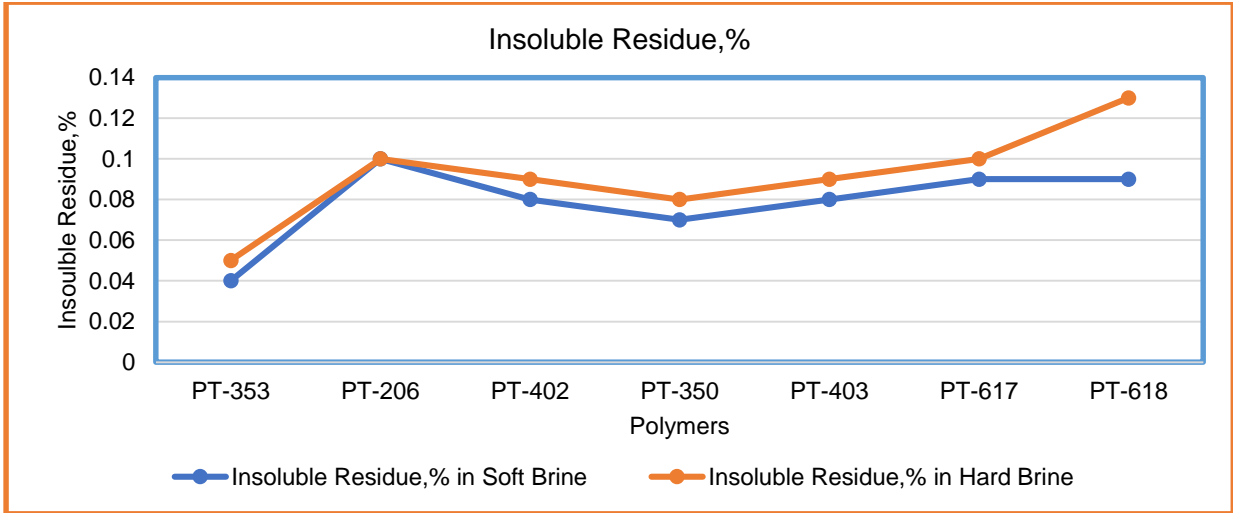
Figure-2: Insoluble Residue of Seven Polymers

### 3.1.3 Brook Field Viscosity

Viscosity is the measure of the internal friction of a fluid. This friction becomes apparent when a layer of fluid is made to move in relation to another layer. The greater the friction , the greater the amount of force required to cause its movement , which is called " shear". Shearing occurs whenever the fluid is physically m,oved as in pouring , missing etc. The measure of speed at which these layers move with respect to each other is called the "shear rate". This has a unit of measurement called the "reciprocal second"($sec^{-1}$).

The Brookfield viscosity (spindle-1 at $40^0$C) was in order of 6 to 8 cP against the required minimum value of 5 cP, the values are plotted in Figure-3.The other Brookfield viscosity (UL Adapter at 60 rpm and $40^0$C) was more as against the specified value of 3.2 cP for soft brine and 2.9 cP for hard brine, the values are plotted are shown in Figure-4.
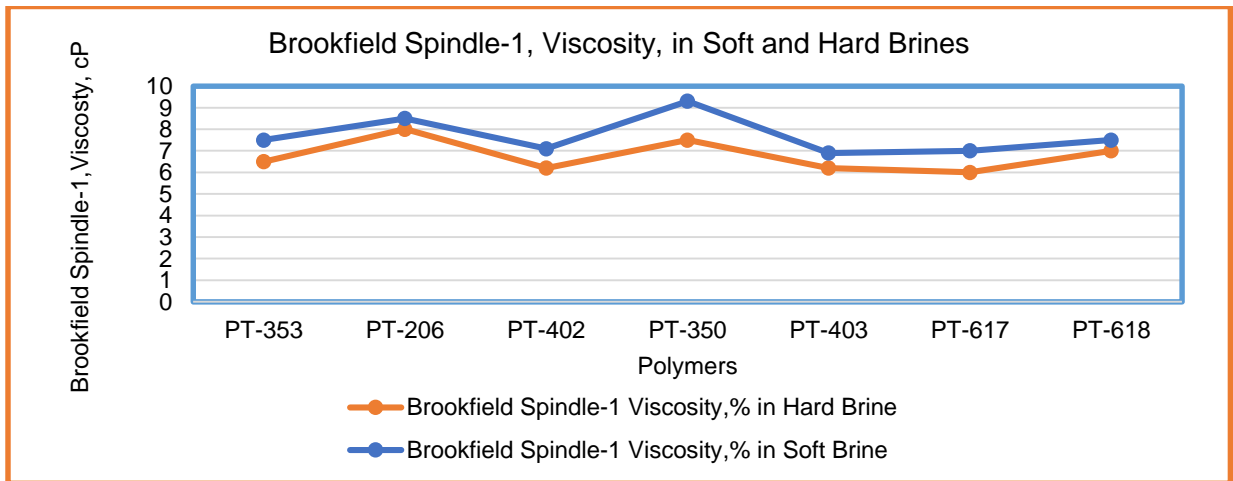


Figure-3: Brookfield Spindle-1 Viscosity of Seven Polymers
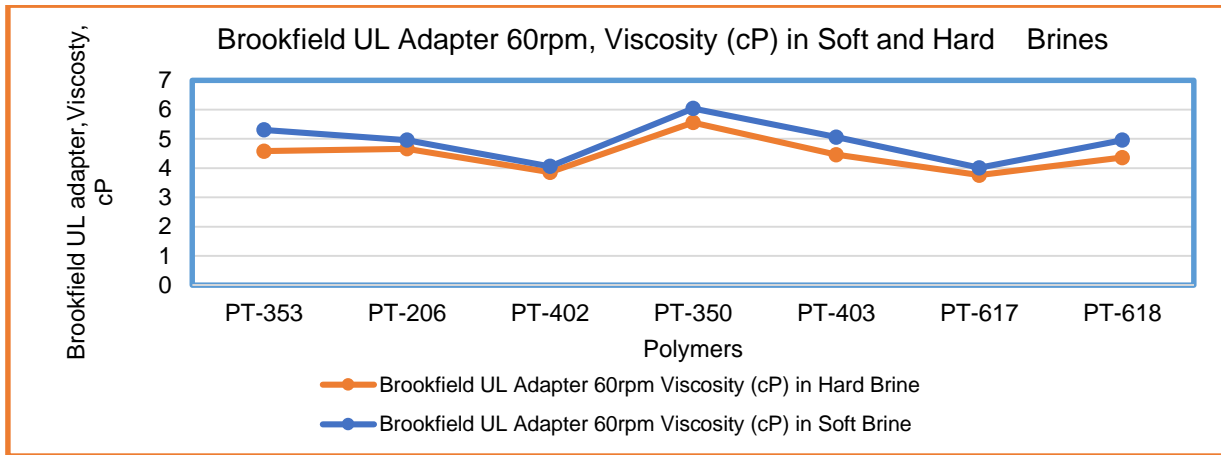
Figure-4: Brookfield UL Adapter, 600rpmViscosity of Seven Polymers

### 3.1.4 Canon Fenske -Relative Viscosity

Relative viscosity of polymer solution is determined by Cannon Fenske routine viscometer of size 75 at $40^{0}$C by taking 7 ml of 1000 ppm of polymer solution. Flow time is measured by allowing the sampler to flow freely and measuring the time taken in flowing from marked upper point to lower point on viscometer. The relative viscosity was determined by ratio of the time taken by polymer solution and brine solution in which it is prepared. The specified minimum values are 3.1 and 2.8 for soft brine and hard brines respectively. Against of these the minimum relative viscosity values were found 3.5 for soft brine and 3,2 for hard brine. The values of viscosity of seven polymers are shown in Figure-5.
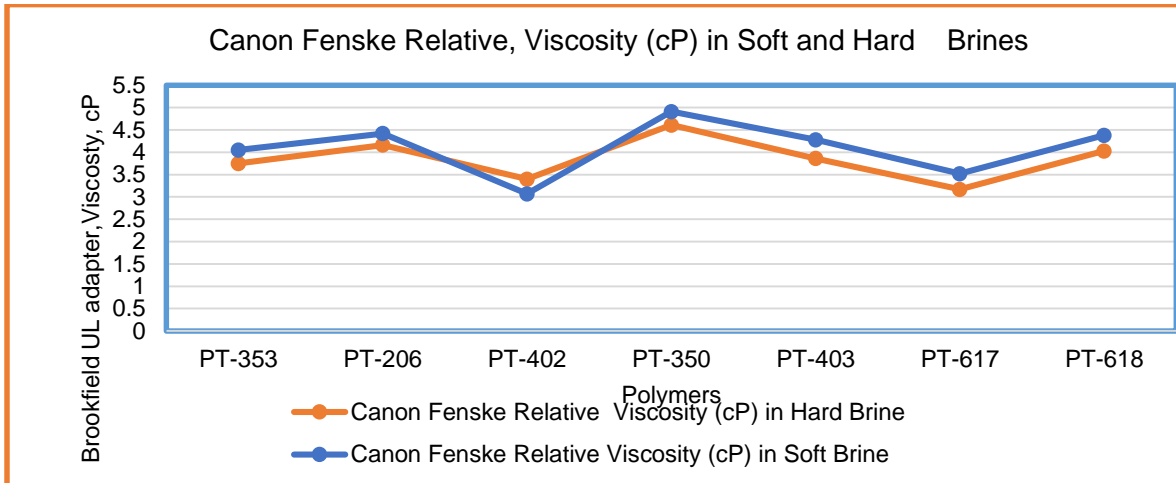


Figure-5: Canon Fenske Viscosity of Seven Polymers

### 3.1.5 Screen Factor

The screen factor was measured by preparation of 1000 ppm polymer solution from stock concentrated polymer solution through dilution by adding 0.45 micron filtered brine and mixing on magnetic stirrer till homogenized solution was obtained. The polymer solution was filtered through 120 mesh screen.

Sample of polymer was equilibrated in water bath at $40^{0}$C with the attached screen (120 mesh) and about 60 ml of the polymer solution was taken into the top bulb by suction. A little of the solution was released

to fill the attached section. Air was removed which might be trapped in the screen by gently tapping and/or blowing some solution through the screen in such a way that no air bubble was present in either the solution or the screen during the measurement. Solution was allowed to run freely and the time taken by the solution to pass from first timing mark to the second timing mark was recorded, for both the both brines and the polymer solution. The average of 3 runs was taken for calculating screen factor.

The screen factor is measure of resistance factor that reflect both viscosity and the viscoelasticity of a solution. Viscoelasticity drops much more rapidly and is reflected by a drop in resistance factor in porous media as well as a drop in screen factor. Thus screen factor is useful tool to measure the viscoelasticity in the field and to detect the polymer degradation. Very high value is also not advisable and can creates injectivity problem in field.

The screen factor at 40 $^0$C was found in same order for all samples as compared to in specified ranges viz 19.6-29.3 for soft brine and 17.46-25.5 for hard brine respectively. The values are shown Figure-6

Screen factor = Polymer Solution time/Brine time
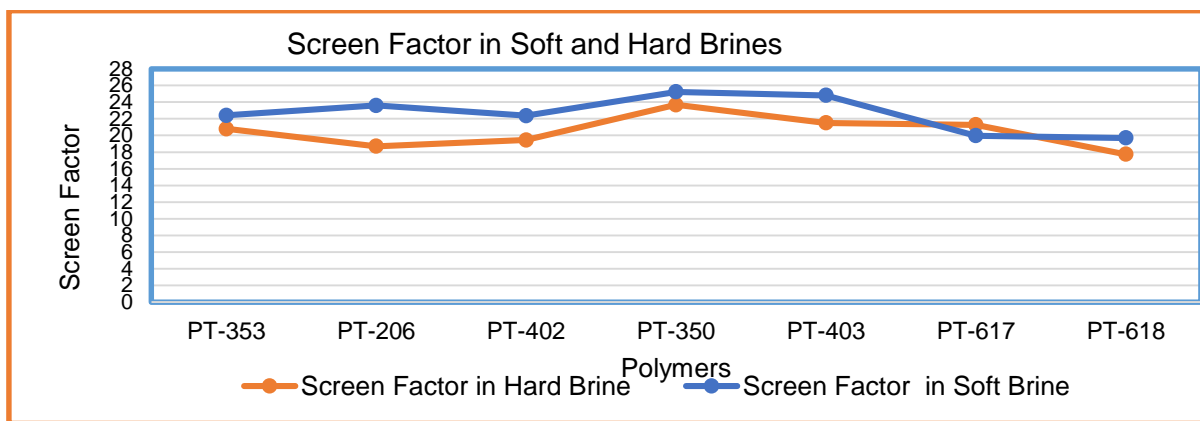


Figure-6: Screen Factor of Seven Polymers

### 3.1.6 Intrinsic Viscosity at 40$^0$C (dl/g)

The intrinsic viscosity is a hypothetical viscosity at a hypothetical "zero concentration". This intrinsic viscosity indicates the molecular weight of the polymer as it directly proportional to the molecular weight. It is determined by measuring the polymer solution of various concentration such as 150, 200,300,400,500,750 and 1000 ppm ,which are prepared in soft brine. The viscosity is measured through Brookfield viscometer and using UL Adapter at 60 rpm and 40$^0$C. This viscosity of soft brine (2%NaCL) is also measured. The other four viscosity named as specific viscosity , reduced , relative and inherent viscosities are measure using brine viscosity and polymer concentration. The formule are mentioned below.

Specific viscosity (nsp)= (polymer viscosity/brine viscosity)-1= (n/ns)-1

Reduced viscosity (nr)=specific viscosity/polymer concentration in gm/dl (gram per decilitre)=ns/c

Relative viscosity =polymer viscosity/brine viscosity=n/ns

Inherent viscosity (ni)=ln *relative viscosity/concentration

Plot reduced and inherent viscosities as a function of polymer concentration in ppm. Fit to separate straight lines and extra plot to polymer concentration of zero. The y-intersept at zero concentration is called Intrinsic viscosity. The unit of intrinsic viscosity is inverse of concentration is dl/gm, where dl is decilitre and equal to 100cc. Data for calculation of Intrinsic viscosity of polymer sample (PT-353) is shown in Table-1. Plots for determination of intrinsic viscosity of one polymer sample, PT-353 is shown in Figure-7.

Intrinsic viscosity at 40 $^0$C (dl/g) in soft brine was found in order of 21.9 to 25.8 against desired value of 16.9 to 27.1. Thus all seven sample have molecular weight of same order and found suitable for field implementation. The values of seven polymer samples are shown in Figure-8.

Table-1: Data for calculation of Intrinsic Viscosity of polymer sample(PT-353)

| Data for calculation of Intrinsic Viscosity of Polymer Sample(PT-353) | | | | | | | |
|---|---|---|---|---|---|---|---|
| Conc,% | Conc,ppm | Dial reading | Viscosity, polymer | Viscosity of blank(soft brine) | Specific Viscosity | Reduced Viscosity | Inherent Viscosity |
| | | | n | ns | nsp | nr | ni |
| | | | | 0.87 | | | |
| 0.015 | 150 | 12 | 1.16 | | 0.33 | 22.22 | 19.18 |
| 0.02 | 200 | 14.5 | 1.41 | | 0.62 | 31.03 | 24.14 |
| 0.03 | 300 | 16.5 | 1.61 | | 0.85 | 28.35 | 20.52 |
| 0.04 | 400 | 20 | 1.96 | | 1.25 | 31.12 | 20.31 |
| 0.05 | 500 | 24 | 2.36 | | 1.71 | 34.25 | 19.96 |
| 0.075 | 750 | 33 | 3.26 | | 2.75 | 36.63 | 17.61 |
| 0.1 | 1000 | 48 | 4.76 | | 4.47 | 44.71 | 17 |
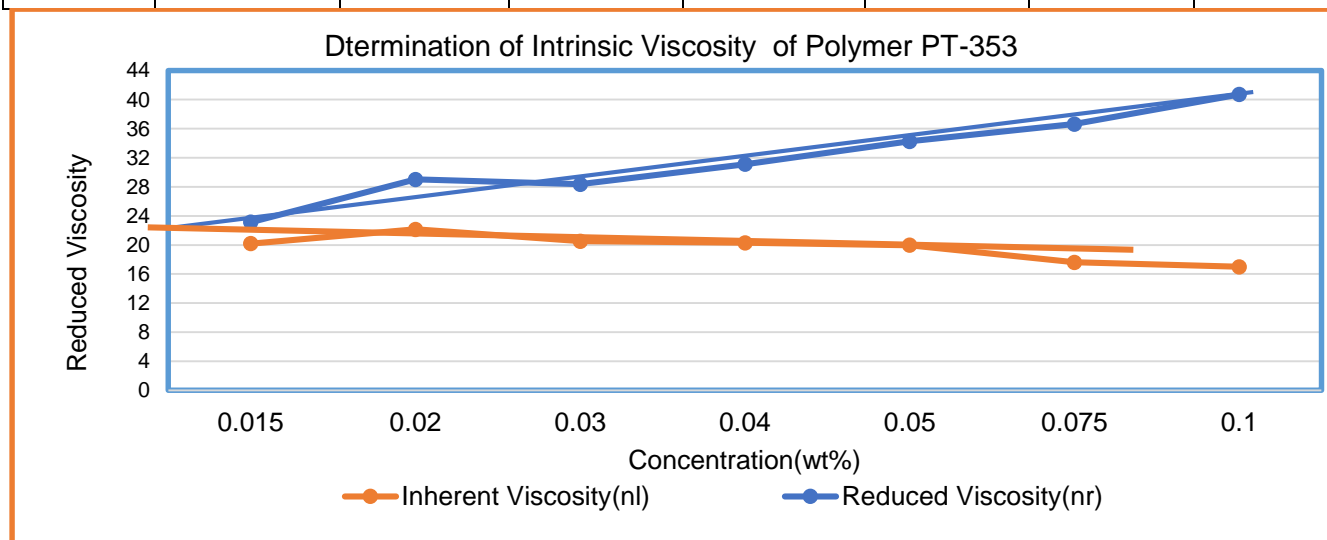


Figure-7: Plots for Determination of Intrinsic Viscosity of one polymer sample, PT-353
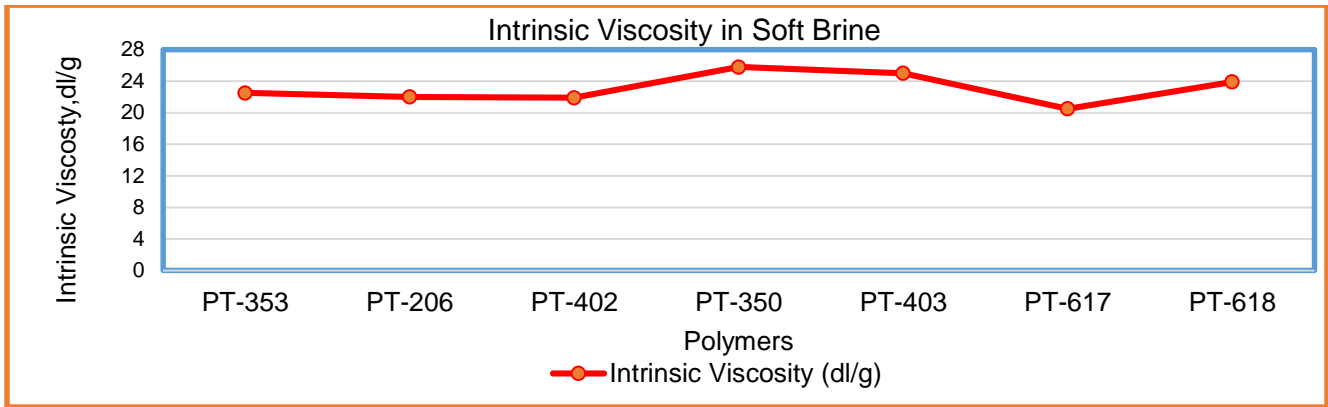
Figure-8: Intrinsic Viscosity of polymer samples

### 3.1.7 Filter ratio

It is another efficient method to detect formation of microgel or insoluble particles in polymer solution. If value of filter ratio is more then 0.5, then polymer solution is not suitable to inject in reservoir rock and may create injectivity problem. It is calculate as follows

Filter ratio=$(t_{500ml}-t_{400ml})/ (t_{200ml}-t_{100ml})$

Where, $t_{500ml}$, $t_{400ml}$, $t_{200ml}$, $t_{100ml}$ are times in seconds required to filter 500,400,200 and 100 ml of polymer solution of 1000 ppm concentration. Generally 550-600 ml polymer is taken in cylinder of apparatus and pressurised by constant pressure of 20 psig and record the time taken by filteration of polymer solution of 500,400,200 and 100ml through. Suitable pore size membrane filters viz 5 micron or smaller 1 micron are fitted in the apparatus. Filter ratio of polymer samples is shown in Figure-9.
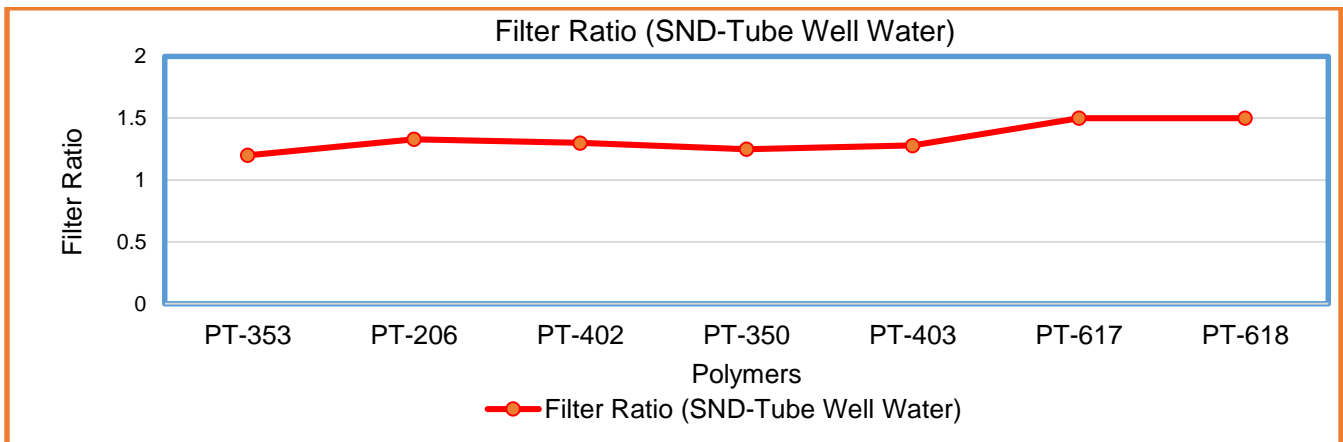


Figure-9: Filter ratio of polymer samples

### 3.1.8 Thermal Stability Studies

If a polymer solution is kept for a longer period at high temperatures, it can degrade and loose its viscosity. The degradation may coincide with a precipitation. Detecting the thermal stability of a polymer is usually accomplished by measuring the viscosity loss of a polymer solution. Thus thermal stability is the most critical screening criterion. Measure the relative viscosity of 1000 ppm polymer solution through Canon Fenske of 75 number at $40^0$C. Take 25 m polymer solution in 50 ml volumetric flask ,sealed it properly

and put in oven at $82^0$C for 7 days. Again measure the relative viscosity after seven days. Calculate the percentage retention in viscosity , which should be more then 60%.

All the seven sample were found thermally stable at $82^0$C as viscosity retention was found above 80% after 7 days.
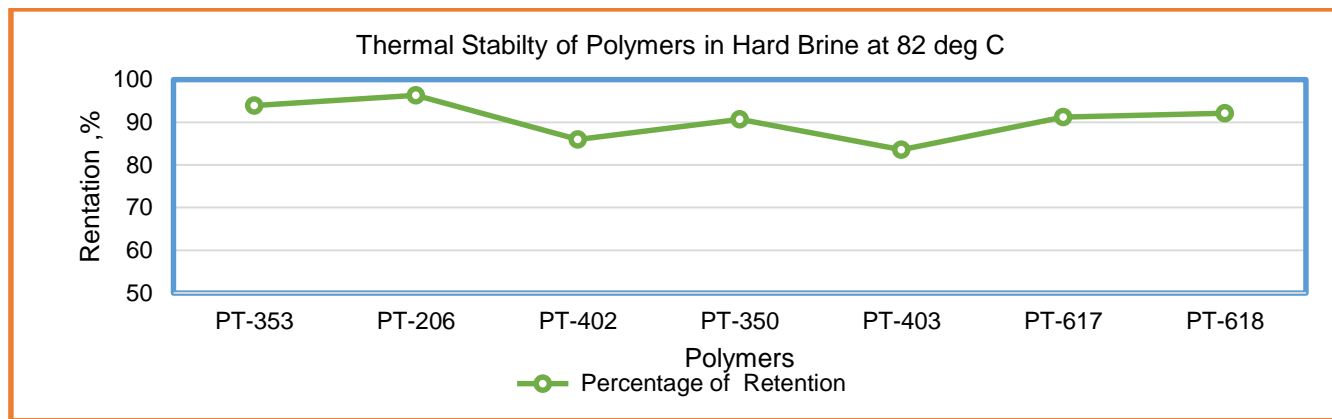


Figure-10: Thermal Stability (Retention in percent) of polymer samples

### 3.1.9 Rheological Study

Polymer solution rheology is fundamental to the evaluation and design of a polymer flood. Rheology of the polymer is to find the viscoelastic property of the polymer solution. Usually polymers are non - Newtonian which means shear thinning behavior is found in the polymer. It means viscosity of polymer solution decreases with increases of shear rate, which helps in easily flow of polymer solution in reservoir, due to variation in shear rate. Solution rheology is a function of many factors such as polymer type, polymer concentration, brine composition and temperature. Polymer solutions used in polymer flooding should maintain solution viscosity and should exhibit sufficient resistance to shear forces induced in the reservoir, surface equipment and tubular. Thus, polymer solution viscosities of different concentrations are measured as a function of varying shear rates using Brookfield viscometer (UL adaptor) at reservoir temperature. Dial reading below 10 is not considered as it have error as per the manufacturing standards.

The plots of different concentrations of polymer and shear rates are used to select the polymer concentration required for conducting core flood studies. The viscosity values of seven polymer samples measured for 800 and 1000ppm polymer solutions which are prepared in Sanand tube well water(SND-Tube well water) are shown in Figure-11 and Figure-12 respectively. All polymer samples showing shear thinning behavior, which is good for oil recovery.
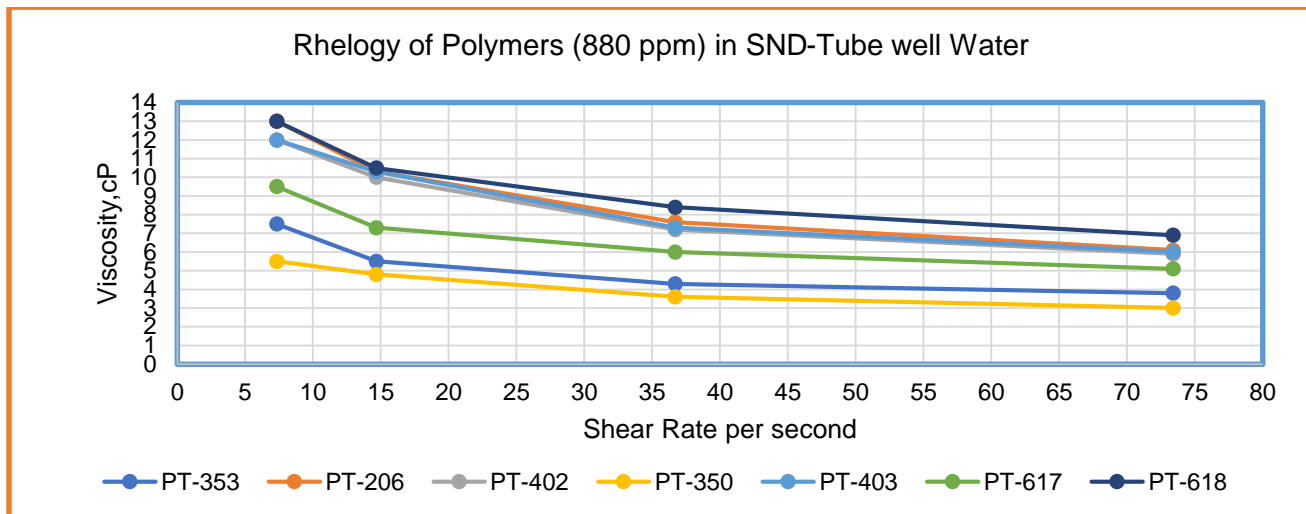
Figure-11: Rheology of Polymers (800 ppm)
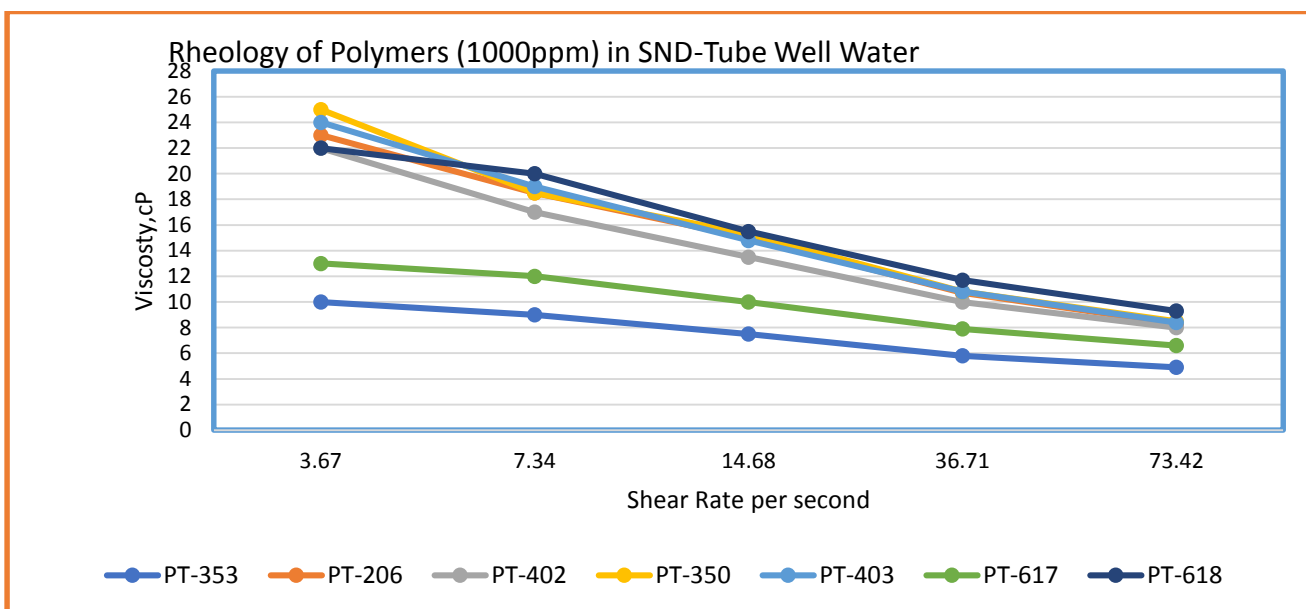


Figure-12: Rheology of Polymers (1000ppm)

### 3.1.10 Compatibility Study

Compatibility study for the polymer solutions is a visual observation for the appearance of any precipitate or generation of turbidity at reservoir temperature and at ambient temperature. Compatibility of polymer solution was checked in process water and formation water of a field.

All these seven polymer samples were found compatible in soft and hard brines and also in formation and tube well/process water at ambient and reservoir temperature.

### 3.1.11 Static Adsorption Study

This study is generally carried out for screening out the polymer samples before doing extensive core flood studies on native reservoir rock. The adsorption of polymer should be of such a level that the polymer

solution is not rapidly depleted and the polymer loss is limited. To ascertain this, static adsorption study was performed with all the polymers to assess the adsorption of polymer on the reservoir minerals. These tests are qualitative in nature since experimental results are very sensitive to rock particle size and preparation. These results may be used to screen out certain polymers showing particularly high retention. (ref IPTC 11200)

The experiment used to determine static adsorption involves polymer solution in contact with the crushed sample of reservoir rock. Studies have shown that mineralogy of the rock has adverse effect on the efficiency of the polymer flooding. For this study, core pieces of reservoir rock were soxhlated with 80% Toluene and 20% Methanol mixture. The pieces were air dried and powdered. 35 gram of crushed core powder was wetted with minimum amount of formation water and then 90 ml of 1000ppm polymer solution was added and kept in oven at 80ºC. Samples were tested for polymer concentration using Canon-Fenske viscometer size no-75.

## 4 Evaluation of Polymer through Core flood Studies

After getting desired results of all screening studies, the polymer sample is finally evaluated through conducting core flood studies. All bonded/tender samples viz seven samples are evaluated by taking standard Berea core of nominal permeability of 1000 mD and bearing length of 7.8 cm with cross sectional area of 11.33 cm$^2$ . Polymer solution of 800 ppm prepared in Sanand tube well water (SND-Tube well) was used. Sanand Oil , which have viscosity of 18cP at 80$^0$C.Sanand tube water was used , which have salinity 296 ppm as NaCL and calcium and magnesium ions concentration of 52 ppm and 38.4 ppm respectively. Following are the results of parameters of two polymer samples namely PT-353 and PT-206 evaluated through core flood experiments.

## 4.1 Core flood Linear Displacement Efficiency(LCDE)

In the case of polymer samples PT-353, the incremental displacement efficiency by injecting of 25% polymer slug of 800ppm , followed by chase water , was obtained 14% HCPV over water flood displacement efficiency of 60.4%HCPV and shown in Figure-13. In case of other samples PT-206, it was obtained 14.6% HCPV over water flood displacement efficiency of 59.5%HCPV and shown in Figure-14. Thus, in both the samples displacement efficiency was more then 14%HCPV, which is minimum desired value fixed for evaluation.
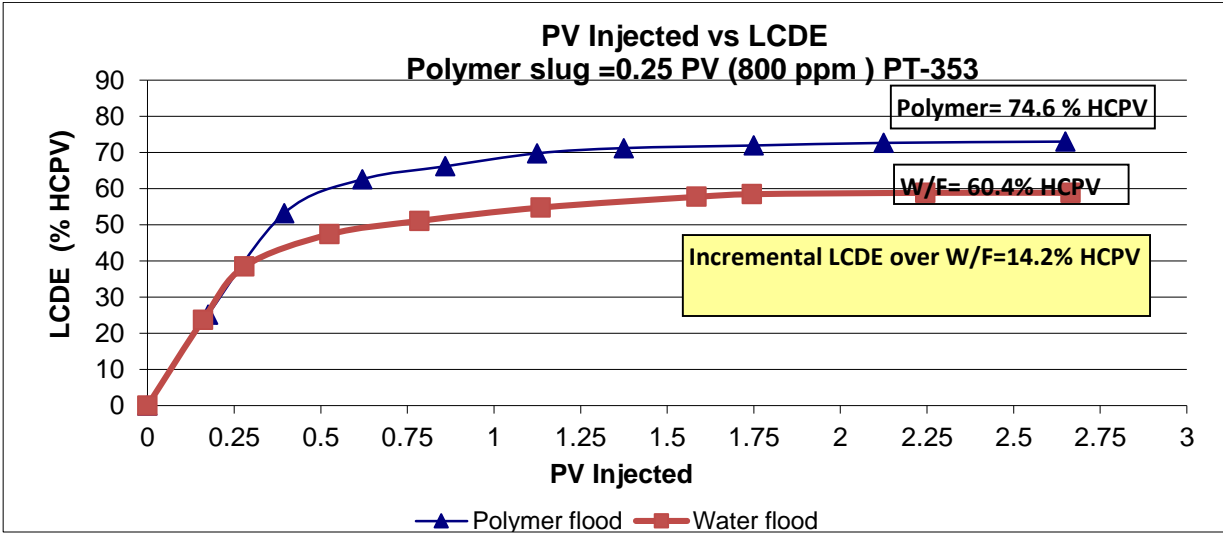
Figure-13: Core Flood Displacement Efficiency of Polymer PT-353



**PV Injected vs LCDE**
**Polymer slug =0.25 PV (800 ppm) PT-206**

Polymer= 75.1 % HCPV

W/F= 59.5% HCPV

Incremental LCDE over W/F=14.6% HCPV
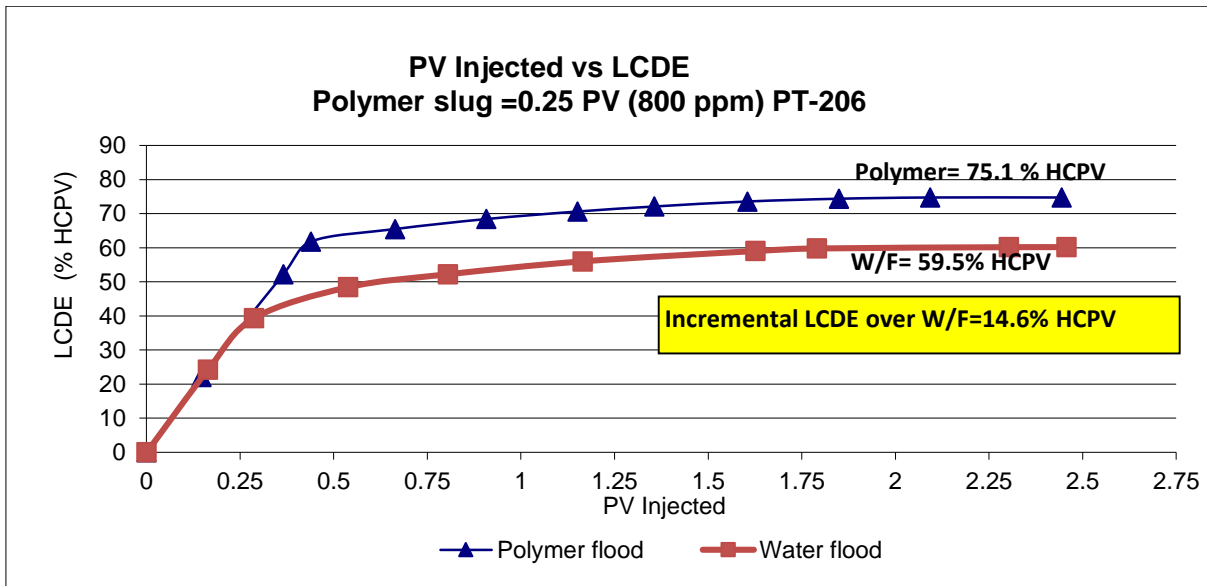
Figure-14: Core Flood Displacement Efficiency of Polymer PT-206

## 4.2 Residual Resistance Factor (RRF)

The residual resistance factor is measure of reduction in permeability of the porous media caused by flowing the polymer solution through the reservoir rock matrix. This is basic characteristics of a polymer by which it control heterogeneities or permeability variation in reservoir rock and resulting improvement in oil recovery. The values of residual resistance factor was found 2.3 for polymer sample of PT-353 and 2.5 for sample PT-206 respectively. These values were also found in desired range of 2.0-2.5.

## 4.3 Dynamic Adsorption

Polymer adsorption is also an important parameter and play a key role in polymer selection. The adsorption of polymer on reservoir rock is a natural process , which helps in permeability reduction. But, high adsorption value has detrimental effect on polymer EOR process as effecting economic of polymer flooding. Dynamic adsorption values was found in order of 0.01-0.014 gm per gm of rock, which is nominal and minimum value.

## 5. Conclusions

1. The experimental results were found encouraging of all seven samples. These polymers were evaluated and characterised by conducting both screening and core flood studies for there use in different fields of ONGC, Ahmedabad, specially in Sanand Polymer Flood Project.
2. The average moisture content was found about 6% and insoluble residue was nominal i.e 0.09% and 0.13 % in soft and hard brine respectively.
3. The Brookfield viscosity (spindle-1 at $40^0$C) was in order of 6 to 8 cP against the required minimum value of 5 cP. The other Brookfield viscosity (UL Adapter at 60 rpm and $40^0$C) was more as against the specified value of 3.2 cP for soft brine and 2.9 cP for hard brine.Relative viscosity (Cannon Fenske at $40^0$C) was also obtained more then the specified value of 3.1 cP and 2.8 cP for soft and hard brine respectively. These Viscosity values are good for enhancing oil recovery.

4.  The screen factor at 40 $^0$C was found in specified ranges for both brines. The filter ratio was within the limit and less then 1.5. Therefore, injectivity problem are not expected by these seven polymers.
5.  Intrinsic viscosity at 40 $^0$C (dl/g) in soft brine was in order of 21.9 to 25.8 as desired value of 16.9 to 27.1. Thus, all polymers have molecular weight in same order.
6.  All polymer samples were thermally stable at 80$^0$C having more than 80% retention in viscosity after 7 days.
7.  All samples showed good rheological properties as viscosity decreases with increases of shear rate, which is good characteristic of polymer samples and necessary to control mobility contrast in reservoir.
8.  Core flood studies were carried out by taking Berea core. The incremental displacement efficiency was obtained more then 14% of HCPV (hydro carbon pore volume) with Residual Resistance Factor (RRF) of 2.5. The adsorption loses was nominal i.e 0.01 mg/g of rock

## Nomenclature

PHPA    Partially Hydrolyzed Poly Acrylamide

AM       Active Matter

ASP      Alkali SurfactantPolymer

$t_{500ml}$    Time to Filter 500 ml polymer solution

SND      Sanand

EOR      Enhance oil recovery

LCDE     Linear Core Displacement Efficiency

HCPV     Hydrocarbon Pore Volume

IRS        Institute of Reservoir Studies

IIT        Indian Institute of Technology

PDPU     Pandit Deendayal Petroleum University

OIIP      Oil Initial In placed

RRF       Residual Resistance Factor

IRS        Institute of Reservoir Studies

ONGC  Oil and Natural Gas Commision

OIL       Oil India Limited

ppm       Parts per-million

Wt.%     Percent weight

cP        Centipoise

**References**

1. B .Sai Rohit Yadav, B.P.Singh" Laboratory characterization for evaluation of suitable polymer for chemical EOR" Research Report for Dissertation work ,June-2016
2. Applied Enhanced Oil Recovery by Aurel Carcoana
3. Modern Chemical Oil; Recovery Theory and Practice by James .J Sheng
4. David B .Levitt, University of Texas" Selection and Screening of Polymerts for Enhanced Oil Recovery" SPE 113845, April2008.
5. W.C Foshee Dow Chemicals USA" Preparation and Testing of Partially Hydrolysed Polyacrylamide Solution" SPE-6202.
6. Russell D, Shupe Conoco Inc "Chemical Stability of Polyacrylamide Polymers" Journal of Petroleum Technology August 1981.
7. Santhosh K Veerabhadrappa , SPE, University of Alberta" Polymer Screening criteria for EOR application-A Rheological characterization approach" SPE 144570, May2011.
8. H.L Chang Cities Service Oil Co. " Polymer Flooding Technology-Yesterday, Today and Tomorrow" SPE 7043.
9. Lvonete P. Gonzalez da Silava Federal University of Rio De Janerio" Polymer Flooding: A sustainable Oil Recovery in the Current Scenario" SPE107727.
10. Nazita Yacob (et. Al)" Determination of viscosity- Average molecular weight of chitosan using intrinsic viscosity measurement "Malaysian Nuclear Agency ( Nuclear Malaysia), Bangi, 43000, Kajang, Malaysia).
11. Monitoring of Polymer flood Project at Sanand field by A.K.Dhawan , Chanchal Dass, Manisha Jain , A.K.Jain SPE 113552-MS.

# Pyrolysis of metal free-shredded WPCBs in fixed cum fluidized bed pyrolyser

*Vaibhav Pandere\*, Dr. Shina Gautam, Dr. Alok Gautam*

*Department of Chemical Engineering, Shroff SR Rotary Institute of Chemical Technology, Vataria-393 135, Gujarat, INDIA*

*\*Corresponding author: [vaibhav.pandere@yahoo.com](mailto:vaibhav.pandere@yahoo.com), Mobile number with country code:+91 808 050 9818*

## Abstract

Waste plastic is a global problem for its disposal. It becomes more difficult when it comes to thermosetting plastic. E waste contains 30-40 % thermosetting plastic. To utilize this plastic a fixed-cum-fluidized bed pyrolyser was used to study pyrolysis of metal free-shredded WPCBs. Series of experiments were carried out at various operating parameters to understand their effect on yield of pyrolysis products such as oil, gas and solid residue. Operating parameters like pyrolysis temperatures, heating rates, reaction times, nitrogen velocities etc. were varied and resulting yield of solids, oils and gases were calculated. Higher reaction times, heating rates, temperatures and nitrogen velocities reduced solid yield and proportionately increased oil and gas yield. Effect of increased nitrogen velocity showed significant effect on increased yield of oils and gases compared to other parameters.

**Keywords:** Fluidized bed, Fixed bed, Fuel oil, WPCBs, Pyrolysis, WEEE.

## 1. Introduction

Use of electrical and electronic equipment increasing worldwide day by day. Aggressive research and competition in market is reducing cost and increasing availability of such equipment every day. Average life of such equipment is decreasing which is creating waste of electrical and electronic equipment (WEEE) at a very high rate. Waste of electrical and electronic equipment (WEEE) made 5% of municipal solid waste (MSW) in 1997 and it has rose to 10% in 2020 (Marco et. al 2015). It showed annual growth of 7% from 2007 to 2012 (Hense et. al. 2015). India is second largest country in the world in terms of population and industrial growth in India has been significant in last few years. Hence India has witnessed rapid growth in use of electrical equipment and ultimately in rapid generation of WEEE in last few years. WEEE recycling is one of the major concerns in India. About 95 % of WEEE recycling operations in India are managed by informal and unorganized institutes and people. (Awasthi et.al. 2016) As per ASSOCHAM-KPMG study conducted in 2016, India is fifth largest producer of WEEE in world. This study states that computer and telecommunication equipment make around 70% and 12% of nations WEEE, respectively.

Printed circuit boards (PCBs) are backbone of computers and telecommunication equipment. PCBs constitute of very complex combination of metals, plastics and glass fibers. Plastic in PCBs is thermosetting in nature, it does not melt upon heating instead it converts directly into volatiles. Such properties of WPCBs (waste printed circuit boards) make it very difficult to recycle. (Hall et. al. 2007). Some WPCBs contain halogenated compounds as fire retardants, which may release toxic brominated compounds when combusted (Hao et.al. 2014). Like other WEEEs, WPCBs are conventionally recycled for metal recovery and remaining part is either combusted or landfilled. Such practice posses' hazard of seriously polluting air, soil and ground water (Kim et.al. 2017).

WPCBs are composed of about 30 to 40 % of hydrocarbon reach plastic part. Recycling WPCBs to separate energy and metals is quite difficult using conventional methods. WPCBs can be

pyrolysed to produce fuel oils and gases from its plastic part. (Evangelopoulos et.al. 2015). In this study we have established pyrolysis as process to recycle hydrocarbon energy in form of fuel oils and gases from WPCBs. We have conducted series of experiment to understand effect of different process parameters such as reaction temperature, reaction time, heating rate and nature of feed bed (fixed vs fluidized) on yield of pyrolysis products such as char, oils and gases and same is reported here.

## 2. Material and Method
### 2.1 Material

WPCBs are most complex among all categories of WEEEs. WPCBs are made up of very complex structure of metals, plastics and other non-metallic, non-organic materials which are used for its construction. Plastic used in PCBs is thermosetting type of plastic. Such nature makes its recovery very difficult. Shredded and metal-free part of WPCBs received from Punjab based small scale solid waste management company named M/s Shivalik solid waste management ltd. Received material had particles in size range of 300 to 500 μ.



Figure 1 Metal free-shredded WPCB sample

### 2.2 Experimental setup

Inhouse developed fixed cum fluidized bed pyrolyser used for pyrolyzing WPCB samples at various parameters. Pyrolyser is made up of SS-316. Its cylindrical shell is having diameter of 100 mm, height of 320 mm and thickness of 7 mm. Pyrolyser top is semispherical in shape which is designed to collect and guide vapors out of the reactor. Provision for entering nitrogen given at bottom of pyrolyser. Internal part of pyrolyser equipped with system to distribute nitrogen and accommodate feed and catalysts. Nitrogen velocity can be increased and decreased to convert feed bed into fluidized bed and fixed bed, respectively. Pyrolyser is heated using electrical heater. Pyrolyser attached with nitrogen cylinder and regulator to control nitrogen flow in it. Also, series of condensers provided to condensate vapors formed during pyrolysis and convert them into fuel oil. Schematic of pyrolysis set-up given in below figure.
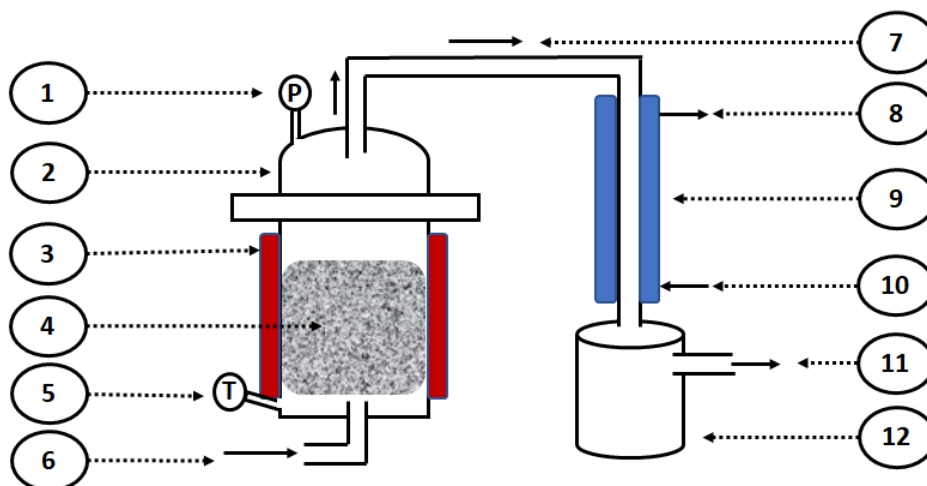
Figure 2 Pyrolysis set up 1) Pressure gauge, 2)Pyrolyser, 3) Electrical heater, 4) Feed bed, 5) Temperature sensor, 6) Nitrogen entry, 7) Vapors leaving pyrolyser, 8) Chilled water outlet, 9) Condenser, 10) Chilled water inlet, 11) Gases collection, 12) Oil collection

## 2.3 Experimental procedure

In this study four process parameters viz. temperature, heating rate, reaction time and fluidization gas (nitrogen) velocity were varied in series of experiments to study effect of each on reaction completion and yield of different products.

Pyrolysis experiments conducted in four sets to study effect of each parameter on yield of different products. The parameter under study in a particular set varied in each experiment while other parameters maintained constant. In first set, effect of temperature studied at three reaction temperatures. Entire system inertized using nitrogen and heating rate of 10 $^OC$/min maintained for all experiments. In three experiments, entire system heated to 400 $^OC$, 500 $^OC$ and 600 $^OC$ and this temperature maintained for 60 mins. In case of second set of experiments, effect of heating rate studied at three different heating rates. Entire system inertized using nitrogen. In three experiments, pyrolyser heated with heating rates of 5 $^OC$/min, 10 $^OC$/min and 15 $^OC$/min to 500 $^OC$ and this temperature maintained for 60 minutes. In third set of experiments, effect of reaction time studied at four different reaction times. Entire system inertized using nitrogen. Pyrolyser heated up to 500 $^OC$ at heating rate of 10 $^OC$/min and this temperature maintained for 30 mins, 45 mins, 60 mins and 75 mins in four experiments. In fourth set of experiments, effect of fluidized bed vs fixed bed on product yield studied. Entire system inertized using nitrogen. Heating rate of 10 $^OC$/min, reaction temperature of 500 $^OC$ and reaction time of 60 mins maintained for both experiments. One experiment carried out with nitrogen velocity of 0.2 m/s. At this velocity feed bed was in fluidized state. Another experiment carried out without providing nitrogen during reaction. Without flow of any nitrogen, feed bed was in fixed state. Oil and char from pyrolysis experiments measured and yield of gases determined by difference in quantity of feed and that of oil and char. Pyrolysis oil analyzed for properties of crude oil.

## 3 Results and discussion

Table 1 Temperature Vs Yield

| Sr. No. | Temperature ($^O$C) | Mass (%) | | |
| --- | --- | --- | --- | --- |
| | | Solids | Oil | Gas (By difference) |
| 1 | 400 | 72.5 | 12.1 | 15.4 |
| 2 | 500 | 60.2 | 19.8 | 20.0 |
| 3 | 600 | 60.0 | 19.8 | 20.2 |

Temperature Versus Yield data for first set of experiments shown in Table 1. For experiment with reaction temperature 400$^O$C, solid yield is higher while Liquid and gaseous yield is lower than other two experiments. Solid yield of experiments at 500$^O$C and 600$^O$C is somewhat closer to each other. Similar trend observed for oil and gaseous yield of experiments at 500$^O$C and 600$^O$C. Higher solid yield and lower liquid and gas yield of first experiment implies that pyrolysis reaction does not complete at 400$^O$C. Non-significant difference between yield of experiments at 500$^O$C and 600$^O$C suggest that reaction can be considered completed at 500$^O$C and the energy required to reach 600$^O$C is very high against low output of oil and gases.

Table 2 Heating rate Vs Yield

| Sr. No. | Heating rate ($^O$C/min) | Mass (%) | | |
| --- | --- | --- | --- | --- |
| | | Solids | Oil | Gas (By difference) |
| 1 | 5 | 62.5 | 18.4 | 19.1 |
| 2 | 10 | 60.2 | 19.8 | 20.0 |
| 3 | 15 | 59.9 | 20.0 | 20.1 |

Heating rate versus Yield data shown in Table 2. Although Heating rate of 5 $^O$C/min had slightly higher solid yield and lower liquid and gas yield when compared with other two heating rates. There was no significant difference in yield of solids, liquids and gases of all three experiment. It can be explained by the fact that plastic in PCBs is thermosetting in nature. Thermosetting plastics do not melt upon heating, instead they instantly convert into volatiles after reaching certain temperature. Thus, it can be concluded that heating rates does not affect much in yield of WPCB pyrolysis. However same cannot be said for components in oil and gases and it needs to be determined experimentally.

Table 3 Reaction Time Vs Yield

| Sr. No. | Reaction Time (mins) | Mass (%) | | |
|---|---|---|---|---|
| | | Solids | Oil | Gas (By difference) |
| 1 | 30 | 65.8 | 16.9 | 17.3 |
| 2 | 45 | 63.1 | 18.3 | 18.6 |
| 3 | 60 | 60.2 | 19.8 | 20.0 |
| 4 | 75 | 60.1 | 19.9 | 20.0 |

Reaction time versus Yield data shown in Table 3. As seen in table, Solid yield decreases, and liquid and gas yields increase with increase in reaction time up to reaction time of 60 minutes. Yields of all three products are same for 60 minutes and 75 minutes reaction time. It is observed that pyrolysis reaction completes after 60 minutes and there is no need of further heating.

Table 4 Nitrogen flow rate Vs Yield

| Sr. No. | Nitrogen Flow rate (m/s) | Mass (%) | | |
|---|---|---|---|---|
| | | Solids | Oil | Gas (By difference) |
| 1 | 0.2 (Fluidized bed) | 56.8 | 21.2 | 22.0 |
| 2 | 0.0 (Fixed bed) | 60.2 | 19.8 | 20.0 |

Nitrogen flow rate vs Yield data shown in Table 4. It was observed that yield of solid decreases and that of oil and gas increases proportionately in fluidized bed experiment when compared with yields of fixed bed experiment. WPCB particles in fluidized state decompose more efficiently due to better heat transfer. Temperature gradient in fixed bed reactions limits heat transfer causing comparatively lower yield of oil and gases. Even though fluidization increases yields in pyrolysis reactions, considering pyrolysis to be energy intensive process, additional cost of nitrogen which is required for fluidization may make overall process economically unviable. However, introduction of certain techniques to recycle nitrogen may help in making process economically viable and increase yield of oil and gases.

Pyrolysis oil analyzed for properties of crude oil. Table 5 shows results obtained from analysis. It can be seen from GCV value that, pyrolysis oil can be used as fuel if processed further.

Table 5 Properties of pyrolysis oil

| Sr. No. | Parameter | Results | Unit |
|---|---|---|---|
| 1 | Kinematic viscosity at 40 $^O$C | 20.31 | Cst |
| 2 | Viscosity index | 58.21 | - |
| 3 | Flash point (COC) | 168 | $^O$C |
| 4 | Pour point | 10 | $^O$C |
| 5 | Ash content | Nil | % (w/w) |
| 6 | Moisture | 0.05 | % (w/w) |
| 7 | Total acidity | 0.14 | MgKOH/gm |
| 8 | GCV | 32000 | kJ/kg |

## 4 Conclusion

WPCBs are made up of complex structure of metals, thermosetting plastics and non-metallic, non-organic compounds. Plastic part of WPCBs can be pyrolysed to produce fuel oils and gases. Effect of various process parameters such as reaction temperature, heating rate, reaction time and fixed vs fluidized bed studied. Reaction temperature of 500$^O$C is optimum for completing pyrolysis reaction. Due to thermosetting nature of plastic, heating rate does not have significant effect on yield of liquid and gases. Reaction time of 60 minutes is sufficient to complete pyrolysis reaction. Yield of oils and gases increases when pyrolysis conducted with feed bed in fluidized state. However, process with fluidized bed will be economically viable when fluidizing fluid recycled or reused. Oil obtained from pyrolysis had GCV of 32000 kJ/kg, this implies that it can be used as fuel if processed further.

## References

1) Awashthi, A. K., Xeng, X., Li, J., 2016. Relationship between e-waste recycling and human health risk in India: a critical review. Environ. Sci. Pollut. Res. 23 (12):11509-11532. DOI: 10.1007/s11356-016-6085-7

2) Guo, Q., Yue, X., Wang, M., Liu, Y., 2010. Pyrolysis of scrap printed circuit board plastic particles in a fluidized bed. Powder Technology 198, 422–428. DOI: https://doi.org/10.1016/j.powtec.2009.12.011

3) Hall, W.J., Williams, P.T., 2007. Separation and recovery of materials from scrap printed circuit boards. Resources, Conservation and Recycling. 51: 691-709. DOI: https://doi.org/10.1016/j.resconrec.2006.11.010

4) Hall, W.J., Williams, P.T., 2006a. Pyrolysis of brominated feedstock plastic in a fluidized bed reactor. J. Anal. Appl. Pyrolysis 77, 75–82. DOI: https://doi.org/10.1016/j.jaap.2006.01.006

5) Hall, W.J., Williams, P.T., 2007. Analysis of products from the pyrolysis of plastics recovered from the commercial scale recycling of waste electrical and electronic equipment. J. Anal. Appl. Pyrolysis 79, 375–386. DOI: https://doi.org/10.1016/j.jaap.2006.10.006

6) Hao, J., Wang, H., Che, S., Cai, B., Ge, L., Xia, W.,2013. Pyrolysis characteristics of the mixture of printed circuit board scraps and coal powder. Waste Management. 34: 1763-1769. DOI: http://dx.doi.org/10.1016/j.wasman.2013.10.043

7) Hense, P., Reh, K., Franke, M., Aigner, J., Hornung, A., Contin, A., 2015. Pyrolysis of waste electrical and electronic equipment (WEEE) for recovering metals and energy: previous achievements and current approaches. Env. Eng. Management Journal 7, 1637-1647. DOI: http://publica.fraunhofer.de/documents/N-369645.html

8) Kim, Y. M., Kim, S., Lee, J. Y., Park Y. K., 2013. Pyrolysis Reaction Pathways of Waste Epoxy-Printed Circuit Board. Env. Engg. Sci. 30: 11. DOI: https://doi.org/10.1089/ees.2013.0166

9) Marco,I., Caballero, B., Choman, M., Laresgoiti, M., Torres, A., Fernandez, G., Arnaiz, S., 2008. Pyrolysis of electrical and electronic wastes. J. Anal. Appl. Pyrolysis 81, 179-183. DOI: https://doi.org/10.1016/j.jaap.2008.03.011

10) Evangelopoulos, P., Kantarelis, E., Yang, W., 2015. Investigation of the thermal decomposition of printed circuit boards (PCBs) via thermogravimetric analysis (TGA) and analytical pyrolysis (Py–GC/MS). J. Anal. Appl. Pyrol. 115: 337-343. DOI: http://dx.doi.org/10.1016/j.jaap.2015.08.012

11) Sun, J., Wang, W., Liu, Z., Ma, C., 2011. Recycling of Waste Printed Circuit Boards by Microwave-Induced Pyrolysis and Featured Mechanical Processing. Ind. Eng. chem. Res. 50, 11763-11769. DOI: https://doi.org/10.1021/ie2013407

12) Sun, L., Lu, J., Wang, S., Zeng, L., Zhang, J., 2002. Experimental research on pyrolysis of printed circuit board wastes and analysis of characteristics of products. J. Fuel Chem. Technol. 30, 285–288. DOI: https://www.researchgate.net/publication/303249054

13) Sun, L., Lu, J., Wang, S., Zhang, J., Zhou, H., 2003b. Experimental research on pyrolysis characteristics of printed circuit board wastes. J. Chem. Ind. Eng. (China) 54, 419–423. DOI: https://www.researchgate.net/publication/284155221

14) Yang, X., Sun, L., Xiang, J., Hu, S., Su, S., 2013. Pyrolysis and dehalogenation of plastics from waste electrical and electronic equipment (WEEE): A review. Waste Management 33, 462-473. DOI: https://doi.org/10.1016/j.wasman.2012.07.025

15) https://www.assocham.org

# Investigate the Behavior of concrete at Elevated temperature by using CFG

*Mr. Jenil Patel[1], Prof. Gaurav Vyas[2]*
*[1]Civil Engineering, Gujarat Power Engineering and Research Institute, Mewad, Mehsana, Gujarat, India: - 384460*
*[1]Email Id: - 171040106018@gperi.ac.in, Mo: - 9924470762*
*[2]Civil Engineering, Gujarat Power Engineering and Research Institute, Mewad, Mehsana, Gujarat, India: - 384460*
*[2]Email Id: - gaurav.vyas@gperi.ac.in, Mo:- 9033992273*

## Abstract

As concrete is the most commonly used material in construction, improvement of cemetitious material become more and more essential. Conventional concrete has two major drawbacks: low tensile strength and a destructive and brittle failure. In an attempt to increase concrete ductility and energy absorption, Fibre Reinforced Concrete (FRC) has been introduced. By studying the research paper, it is clear that by using synthetic fibre, steel fiber in concrete it gives better result. And we also used this kind of fibre in concrete where required high strength. The purpose of this work was to study production technologies, properties of carbon fibers, methods of construction, using this material, compare carbon fiber and structures, using carbon fiber with traditional materials and structures and find out reasons for application in construction. As per literature survey many work given conclusion that by using fibres in concrete it will gives better strength properties. So here in this paper work is carried out to determine effect of using carbon fibre grid (CFG) in concrete at elevated temperature. Measurement of cracks development in specimen and its strength and durability properties were determined.

And provide a comparison of strength, durability results before applying elevated temperature (about 100°C) and after applying elevated temperature, of normal concrete (NC) and Carbon fibre grid concrete (CFGC).

**Keywords:** Normal concrete (NC), Carbon fibre (CF), Carbon fibre grid (CFD), Carbon fibre grid concrete (CFGC), Fibre reinforced Concrete (FRC).

## 1. INTRODUCTION

Concrete is mixture of cement, sand, aggregates and water. Concrete is proven to be weak in tension and strong in compression. So to provide strength to the leading construction material many contractors, builders, government and non government agencies are using fibres in the concrete. Many types of fibres used in construction field like steel, glass, composite etc.

Here in this work carbon fibre used in the concrete construction in the form of grid. Many physical and chemical properties of concrete effect by using fibres in to concrete mixes.

### 1.1 Carbon fibres

Carbon fibers are a type of high-performance fiber available for civil engineering application. It is also called graphite fiber or carbon graphite; carbon fiber consists of very thin strands of the element carbon. Carbon fibers have high tensile strength and are very strong for their size. In fact, carbon fiber might be the strongest material. Carbon fibers have high elastic modulus and fatigue strength than those of glass fibers. Considering service life, studies suggests that carbon fiber reinforced polymers have more potential than agamid and glass fibers. They also are highly chemically resistant and have high temperature tolerance with low thermal expansion. and corrosion resistance. Each fiber is 5-10 microns in diameter. To give a sense of how small that is,

one micron (um) is 0.000039 inches. One strand of spider web silk is usually between 3-8 microns. Carbon fibers are twice as stiff as steel and five times as strong as steel, (per unit of weight). The most important factors determining the physical properties of carbon fiber are degree of carbonization (carbon content, usually more than 92% by weight) and orientation of the layered carbon planes (the ribbons). Carbon fiber-reinforced composite materials are used to make aircraft and spacecraft parts, racing car bodies, golf club shafts, bicycle frames, fishing rods, automobile springs, sailboat masts, and many other components where light weight and high strength are needed. Carbon fiber's high strength, light weight and resistance to corrosion make it an ideal reinforcing material.


Fig. 1 (carbon fibre grid)

## 2. LITERATURE REVIEW

In the literature review there are many papers studied and as per their view here following comparison carried out.

**2.1** "Strengthening of Normal and High Strength Concrete Corbels with Horizontal and Inclined Stripes of Carbon Fiber". Prof.AamerNajim Abbas and et al. They suggest in this paper The ultimate carrying capacity of tested corbels is affected positively by using carbon fiber strips as a strengthening method. The cracking capacity of normal strength concrete corbels does not affect by using carbon fiber strips, while the high strength concrete corbels achieved good improvement.The amount of energy absorption increased as a result of using carbon fiber strips. The strengthened corbels by carbon fiber strips have a good stiffness in comparison with un-strengthened corbels.

**2.2** "Determination of Thermal Diffusivity of Carbon/Epoxy Composites with different Fiber Content using Transient Thermography", G. Wróbel et al, provides valuable conclusion by using epoxy type of fibre is that, In the present study, the transient thermography was used to measure the thermal diffusivity of CFRP composites with different fibre content. The method initially proposed by Parker et al. as "flash method" for the thermal diffusivity measurements of homogeneous solids was successfully applied to determine thermal diffusivity values of non-homogeneous carbon/epoxy composites. Relationship showed that the thermal diffusivity is linear function of carbon content in considered materials.

**2.3** "Use of CFRP Grid for Precast Concrete Piles", Hatem M. Seliem et al, contribute in the field of fibre concrete and used type of concrete in foundation work. Their concluding remarks like, Bond length equivalent to twice the grid spacing can develop the full tensile strength of the strands of the CFRP grid. The confinement provided by one layer of CFRP grid was the same as

that provided by steel square spirals with a pitch of 75 mm, typically used in at the ends of precast piles subjected to impact from driving forces. Use of two layers of CFRP grid does not increase the confinement effect. Uses of two continuous layers of the CFRP grid are more effective than using two separate layers of the CFRP Grid. Use of CFRP grid provides slight enhancements to the moment capacity of prestressed concrete piles. The use of the CFRP grid slightly increases the flexural stiffness of prestressed concrete piles due to the presence of the longitudinal strands. Further research is required to address any possible galvanic corrosion potentials between CFRP grid and steel prestressing strands.

**2.4 "**Effect of Different Dispersants in Compressive Strength of Carbon Fiber Cementations Composites", Yulinda Lestari et al. In this work authors were trying to use types of fibres in the concrete mixes and their critical conclusions are, Carbon Fiber tend to aggregate due to the Vander Waals forces, the dispersion carbon fiber in cement matrixes is a key problem in the fabrication of piezoresistive CFCC. The use of methylcellulose and deformer to disperse carbon fiber has a negative effect on the hydration of cement and will cause a decrease in the mechanical properties of cementations composites. In this study, a super plasticizer, as a additive component in cementations material formulas, was employed to disperse carbon fiber that make good bonding with aggregate and cementations materials in the fabrication of piezoresistive CFCC.

**2.5 "**Elevated Temperature Strength and Thermal Shock Behavior of Hot-Pressed Carbon Fiber Reinforced TiC Composites", Gui-Ming Song et al, Here in this work researchers work on finding effect of elevated temperature on concrete. Their concluding remarks are, The addition of 20 vol.% short carbon fiber increases the room temperature flexural strength from 471 MPa for monolithic TiC to 593 MPa for the composite. The fracture strength of the composite at 1400_C is 439 MPa, an increase of 78% over that of monolithic TiC. A role-of-mixture formulation is proposed to calculate the strengthening effect of the carbon fibers, the calculated results of the strength of the composite in the range of room temperature to 1400_C agree well with the experimental results. With carbon fiber addition, the fracture toughness of TiC is increased remarkably, and the elastic modulus and thermal expansion coefficient are decreased. The thermal stress fracture resistance parameter, R, thermal stress damage resistance parameter, RIV, and thermal stress crack stability parameter, Rst, are all increased. The residual strength of the composite decreases significantly when the thermal shock temperature difference, _T, is higher than 900_C, and the residual strength is 252 MPa when _T is 1400_C. Carbon fiber Reinforced-TiC composite exhibits superior resistance to thermal shock damage compared with monolithic TiC. Catastrophic failure induced by severe thermal stresses can be prevented in the Cf/TiC composite.

**2.6 "**Residual Strength of Hybrid-Fiber-Reinforced High-Strength Concrete after Exposure to High Temperatures", Bing Chena et al. This paper gives information on variation in strength properties of concrete by using fibers and effect under elevated temperature conditions. There is explosive spalling for normal HSC when exposure to high temperatures. The higher the temperature, the severer the explosion. Adding carbon and steel fibers in HSC can delay the time when spalling occurs, while adding PP fibers can eliminate the spalling under high temperatures. That higher residual compressive strengths and splitting tensile strengths of fiber-reinforced HSC than those of normal HSC indicates that adding fibers in HSC can alleviate the deterioration of mechanical properties of HSC exposure to high temperatures. For concretes with hybrid fibers, especially mixing with PP fiber, their properties exposure to high temperatures improve

significantly because the high vapor pressure due to inner moisture of concrete is released by microchannels due to melting of PP fiber under high temperatures.

## 3. Material Used
### 3.1 Cement:
The cement used was Ordinary Portland cement (OPC) of 43 grades conforming to IS 12269-2013 is used. Specific gravity of cement is 3.05.

The Tests includes (I) Fineness of Cement, (II) Standard Consistency, (III) Soundness of Cement, and (IV) compressive Strength of Mortar Cubes for O.P.C. The test results are above the limiting value.

### 3.2 Coarse Aggregates:

Table 3.1 Properties of coarse aggregates

| Property | NCA |
|---|---|
| Impact value | 17.18 |
| Abrasion value | 22.56 |
| Crushing value | 23.54 |
| Specific gravity | 2.61 |
| Water absorption | 0.48 |
| Fineness modulus | 7.42 |

### 3.3 Fine Aggregates:
Table 3.2 Properties of fine aggregates

| Properties | Sand |
|---|---|
| Fineness Modulus | 3.23 |
| Water Absorption | 0.38 |
| Specific gravity | 2.64 |
| Silt content | 1.07 |

### 3.4 Carbon fibre grid:-

The carbon fibre used is obtained from NIRALI CONSTRUCTION MATERIAL, Vasna, Ahmadabad. The density of carbon fibre is about 1800 kg/m$^3$ and tensile strength of fibre is 4137 N/mm$^2$.

### 3.5 Concrete Mix Design:-

In this work M20 grade of concrete used. Mix proportion were found out by using IS-10262 and IS code method is used. Final proportion is 1:1.67:3.06 with 0.5 W/C ratio.

### 4. RESULTS AND DISCUSSION

Table 4.1 Compressive Strength after 7, 28 days Results

| Sr. | Designation | Mix | Comp. Strength At 7 days | Comp. Strength At 28 |
|---|---|---|---|---|

| no. | | | (N/mm²) | days (N/mm²) |
|---|---|---|---|---|
| 1 | Normal Concrete | M20 | 20.31 | 24.99 |
| 2 | Carbon Fibre Concrete | M20 | 23.73 | 28.13 |
| 3 | Carbon Fibre Concrete by 1% of Volume | M20 | 13.82 | 19.45 |

## 4.1 Comparison Chart of Compressive Strength
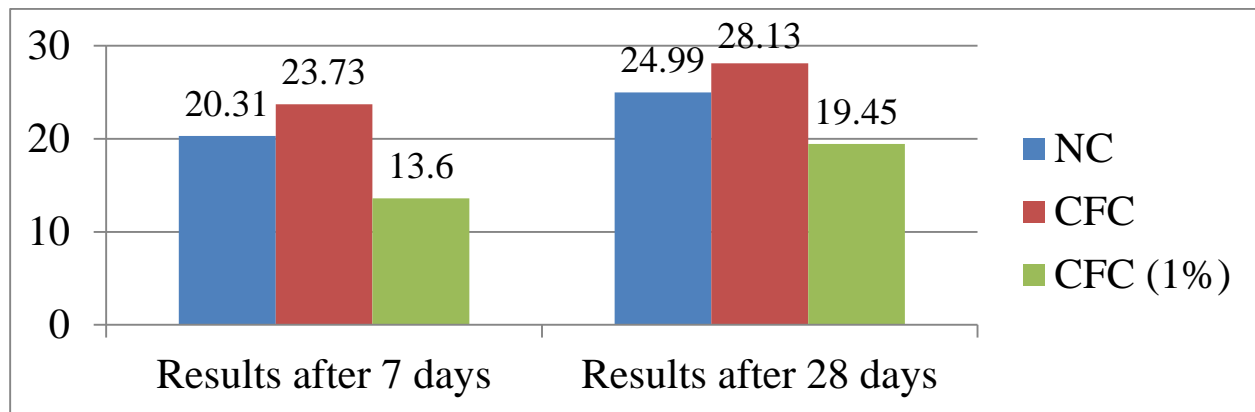


## 4.2 Thermal Variation Test Result

### 4.2.1 Thermal Variation test after 7 days

Table 4.2 Thermal Variation Test After 7 Days

| Day Cycle | Concrete | Oven Temperature (℃) | Crack in Cube (mm) |
|---|---|---|---|
| 1 to 9 | NC | 100 | 0 |
| 10 | NC | 100 | 0.038 |
| 10 | CFG | 100 | 0 |
| 11 | NC | 100 | 0.052 |
| 11 | CFG | 100 | 0 |
| 12 | NC | 100 | 0.076 |
| 12 | CFG | 100 | 0 |

| 13 | NC | 100 | 0.103 |
|----|-----|-----|-------|
| 13 | CFG | 100 | 0 |
| 14 | NC | 100 | 0.143 |
| 14 | CFG | 100 | 0 |
| 15 | NC | 100 | 0.152 |
| 15 | CFG | 100 | 0 |
| 16 | NC | 100 | 0.155 |
| 16 | CFG | 100 | 0 |
| 17 | NC | 100 | 0.190 |
| 17 | CFG | 100 | 0 |
| 18 | NC | 100 | 0.229 |
| 18 | CFG | 100 | 0 |
| 19 | NC | 100 | 0.281 |
| 19 | CFG | 100 | 0 |
| 20 | NC | 100 | 0.305 |
| 20 | CFG | 100 | 0 |
| 21 | NC | 150 | 0.381 |
| 21 | CFG | 150 | 0 |
| 22 | NC | 150 | 0.383 |
| 22 | CFG | 150 | 0 |
| 23 | NC | 150 | 0.390 |
| 23 | CFG | 150 | 0 |
| 24 | NC | 150 | 0.395 |
| 24 | CFG | 150 | 0 |
| 25 | NC | 150 | 0.402 |
| 25 | CFG | 150 | 0 |
| 26 | NC | 150 | 0.410 |
| 26 | CFG | 150 | 0 |
| 27 | NC | 150 | 0.440 |

| 27 | CFG | 150 | 0 |
| 28 | NC | 150 | 0.490 |
| 28 | CFG | 150 | 0 |

**NOTE**

NC = NORMAL CONCRETE

CFG = CARBON FIBRE GRID CONCRETE

CU = CUBE

ALL DIMENSIONS ARE IN MM

### 4.2.2 Thermal Variation test after 28 days

**Table 4.3 Thermal Variation Test after 28 Days**

| Day Cycle | Concrete | Oven Temperature (℃) | Crack in Cube (mm) |
| --- | --- | --- | --- |
| 1 to 11 | NC | 100 | 0 |
| 12 | NC | 100 | 0.090 |
| 12 | CFG | 100 | 0 |
| 13 | NC | 100 | 0.102 |
| 13 | CFG | 100 | 0 |
| 14 | NC | 100 | 0.107 |
| 14 | CFG | 100 | 0 |
| 15 | NC | 100 | 0.115 |
| 15 | CFG | 100 | 0 |
| 16 | NC | 100 | 0.178 |
| 16 | CFG | 100 | 0 |
| 17 | NC | 100 | 0.188 |
| 17 | CFG | 100 | 0 |
| 18 | NC | 100 | 0.196 |
| 18 | CFG | 100 | 0 |
| 19 | NC | 100 | 0.203 |

| 19 | CFG | 100 | 0 |
|----|-----|-----|-----|
| 20 | NC | 100 | 0.221 |
| 20 | CFG | 100 | 0 |
| 21 | NC | 150 | 0.235 |
| 21 | CFG | 150 | 0 |
| 22 | NC | 150 | 0.253 |
| 22 | CFG | 150 | 0 |
| 23 | NC | 150 | 0.278 |
| 23 | CFG | 150 | 0 |
| 24 | NC | 150 | 0.293 |
| 24 | CFG | 150 | 0 |
| 25 | NC | 150 | 0.307 |
| 25 | CFG | 150 | 0 |
| 26 | NC | 150 | 0.322 |
| 26 | CFG | 150 | 0 |
| 27 | NC | 150 | 0.350 |
| 27 | CFG | 150 | 0 |
| 28 | NC | 150 | 0.390 |
| 28 | CFG | 150 | 0 |

**NOTE**                                                                                                          -

1. NC = NORMAL CONCRETE

2. CC = CARBON FIBRE GRID CONCRETE

3. CU = CUBE

4. ALL DIMENSIONS ARE IN MM

**4.2.3 Chart for Thermal Cracks of 7 & 28 Days**
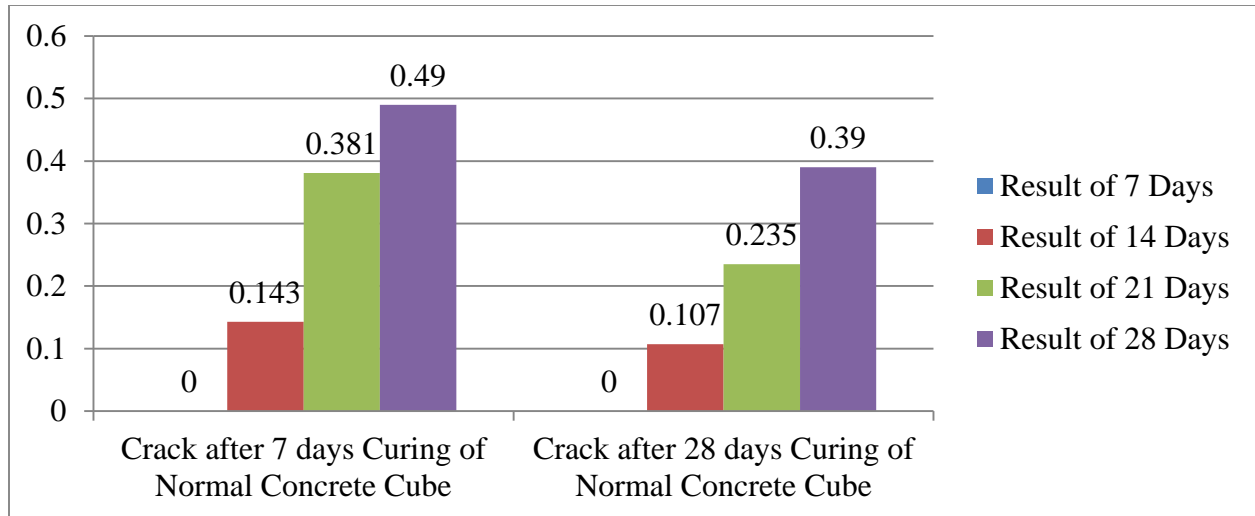
**4.3 Durability Test result**

Loss of Weight and Strength

10% HCL

Acid Attack Test Results After 56 days Results M20 grade mix the Loss of Weight and Strength as per follows:

Table 4.4 56 Days of Acid Attack

| Concrete | Initial Weight | 10% HCL Solution | |
| --- | --- | --- | --- |
| | | Weight | Comp.          Strength (N/mm$^2$) |
| Normal | 8.232 | 8.016 | 29.73 |
| Carbon Fiber | 8.245 | 8.043 | 32.34 |

Table 4.5 Comparison of Normal and Acid Attack Test

| Concrete | 10% HCL Solution | |
| --- | --- | --- |
| | Weight loss | Strength Loss |
| Normal | 2.62% | 8.01% |
| Carbon Fibre | 2.45% | 6.02% |

**Figure: - 5.5.1 Crack measurement with Gauge meter.**

## 5. CONCLUSION

- ➢ In the Study, no crack exceeds limit of 0.5mm at 100°C freezing and thawing cycle. Moreover, permissible limit of 0.5mm exceeds at 150°C freezing and thawing cycle.
- ➢ Compressive strength increase by use of carbon fibre with respect to normal concrete.
- ➢ The increment in the compressive strength by 12.56% by using carbon fibre grid as a layer in concrete cube. If we add carbon fibre grid as a volume in concrete mix then there is decrement in cube compressive strength observed and the decrement is about 22.16%.
- ➢ More the curing period, the probability of time of initiation of cracks increases in freezing and thawing effect of environmental cycle.
- ➢ As we compare results of durability test there increment in the strength of 9% after acid attack test. Also strength loss measured it reduced by 2% as we compare NC and CFGC.
- ➢ No cracks observed on use of carbon fibre. **Hence the use of carbon fibre makes concrete durable.**

## 6. REFERENCES

1) Kinayekar, S.M., Gundakalle, V.D. And Kulkarni, K., 2014. The Effect of Addition of Carbon Fibers On Mechanical Properties of High Strength Concrete. International Journal of Innovative Research in Science, Engineering and Technology, 3, Pp.8777-8784.
2) Kumar, I.P., Mohite, P.M. And Kamle, S., 2013. Axial Compressive Strength Testing of Single Carbon Fibres. Archives of Mechanics, 65(1), Pp.27-43.
3) Chen, B. And Liu, J., 2004. Residual Strength of Hybrid-Fiber-Reinforced High-Strength Concrete After Exposure to High Temperatures. Cement and Concrete Research, 34(6), Pp.1065-1069.
4) Hambach, M., Möller, H., Neumann, T. And Volkmer, D., 2016. Carbon Fibre Reinforced Cement-Based Composites as Smart Floor Heating Materials. Composites Part B: Engineering, 90, Pp.465-470.
5) Xu, Y., Wong, Y.L., Poon, C.S. And Anson, M., 2001. Impact of High Temperature On PFA Concrete. Cement and Concrete Research, 31(7), Pp.1065-1073.
6) Breitenbücher, R., 1990. Investigation of Thermal Cracking with The Cracking-Frame. Materials and Structures, 23(3), Pp.172-177.

7) Kalifa, P., Chene, G. And Galle, C., 2001. High-Temperature Behaviour of HPC with Polypropylene Fibres: From Spalling to Microstructure. Cement and Concrete Research, 31(10), Pp.1487-1499.

8) Yokozeki, T., Iwahori, Y. And Ishiwata, S., 2007. Matrix Cracking Behaviours in Carbon Fiber/Epoxy Laminates Filled with Cup-Stacked Carbon Nanotubes (Cscnts). Composites Part A: Applied Science and Manufacturing, 38(3), Pp.917-924.

9) Is: 383-1970, Specifications for Coarse and Fine Aggregates from Natural Sources for Concrete, Bureau of Indian Standards, New Delhi, India.

10) Is 516:1959, "Methods Of Tests for Strength Of Concrete"

11) Is 2386 (Part –I)-1963, "Methods Of Test For Aggregates For Concrete, Part I -  Particle Size And Shape"

12) Is 2386 (Part –Ii)-1963, "Methods Of Test For Aggregates For Concrete, Part Ill - Specific Gravity, Density, Voids,Absorption And Bulking"

13) Is 2386 (Part –Ii)-1963, "Methods of Test for Aggregates for Concrete, Part Iv - Mechanical Properties"

14) Is 10262-2009, "Concrete Mix Proportioning – Guidelines"

15) Is 269-2015, "Ordinary Portland Cement, 43 Grade"

16) Is 4031: Part 5 – 1988, "Methods of Physical Tests for Hydraulic Cement: Part 6 Determination of Compressive Strength of Hydraulic Cement (Other Than Masonry Cement)"

# Rheological and Surface Property Study of Novel Green Surfactants and Biopolymer Blend Used in Enhanced Oil Recovery

*Nirav J. Bhavsar [1], *, Dr. Atindra Shukla [2], Dr. M. S. Rao [1]*

[1] Department of Chemical Engineering, Dharmsinh Desai University, Nadiad-387 001, Gujarat, INDIA

[2] Shah-Schulman Center for Surface Science & Nanotechnology, Dharmsinh Desai University, Nadiad-387 001, Gujarat, INDIA

*Corresponding author: njbhavsar.ch@ddu.ac.in, mobile number: +919426391115

**ABSTRACT**

Surfactant – polymer flooding has been shown to be promising chemical flooding method to recover tertiary oil in Enhanced Oil Recovery (EOR). The interaction between surfactant and polymer plays a vital role for efficient displacement of oil. Wettability alteration and Interfacial Tension (IFT) reduction are two main recovery mechanisms that are achieved by injecting Surfactants. On other hand, the mobilization of oil is obtained by addition of appropriate polymer by increasing viscous forces. The main objective of this work is to identify a novel green surfactant-polymer blend that can efficiently improve oil recovery beneath earth's surface. The study of the rheological and surface properties of surfactant along with the polymer provides the idea about the effectiveness and potentiality of the novel green surfactant-polymer blend in EOR. In this study, Guar gum is selected as a biopolymer and surfactants synthesized from the sulfonation of oleic acid, dextrin powder and cellulose are selected as green surfactants. This paper incorporates the measurement of viscosity of polymer and surfactant-polymer blend in different concentration. Presence of surfactant with Guar gum exhibits that solution viscosity increases with increasing surfactant concentration and decreasing with temperature at fixed shear rate. Equilibrium Surface Tension (EST) of green surfactants were measured in water and brine to assess their efficiency. Close proximity in results of EST were observed in comparison with proven surfactants Sodium Dodecyl Sulfate (SDS) and α – Olefin sulfonate (AOS).

**Keywords**: Enhanced Oil Recovery (EOR), Rheology, Novel Green Surfactant, Polymer, Guar gum, Interfacial Tension (IFT), Equilibrium Surface Tension (EST).

## 1. Introduction

Most of the current world oil demand depends upon the production of oil from mature oil fields. In the near future, to discover abundant substitute for crude oil to propel the economy of the world is quite difficult. Maintaining the efficient supply to boost world's economy requires both development of additional crude oil reserves and enhancement in oil recovery from the present reservoirs. To increase the recovery of oil from the aging resources is a major task for oil companies and authorities to fulfil the growing demand day by day. As the global oil supply decreases, the ability to effectively recover the oil from a particular well becomes increasingly important. Different types of effective methods have been proposed to enhance recovery of oil from mature oil fields that includes chemical flooding, microbial flooding, thermal methods and so on [1-4]. Chemical flooding plays a significant role among mentioned methods. Surfactant-polymer (SP) flooding is a very important method in chemical flooding. In recent years, more attention has been paid to study the interaction between surfactant and polymer in SP flooding. Efficient displacement of locked oil in internal structure like cracks, crevices, and pores depends upon effective interaction between surfactant and polymer with improvement in slug integrity, adsorption and mobility control [5]. The main focus of this study is to develop a green and inexpensive surfactant-polymer mixture that can efficiently help in to recover tertiary oil. Large quantities of oil remain locked after waterflooding of an oil reservoir due to capillary forces which arises due to interfacial tension (IFT) between oil and water. These capillary forces create a resistance to applied viscous forces and intend the injected water to bypass the resident oil. Therefore, it is necessary to lower capillary forces between oil and water by addition of surfactant. Excellent surface properties of surfactant have made it a good promising agent in Enhanced oil recovery (EOR) method. The main role of surfactant is to overcome the capillary force in reservoir [6]. Two main mechanisms involved with EOR by surfactant flooding are interfacial tension reduction [7] and wettability alteration [8,9]. The displacement efficiency is increased with reduction in ultra-low interfacial tension exists between surfactant solution and trapped crude oil in reservoir. Use of surfactant alter the wettability of reservoir from oil-wet surface to water-wet surface that results in to enhance the recovery efficiency. However, use of expensive traditional petroleum-based surfactants has made surfactant flooding an economically non-viable technique particularly at low crude oil price. Therefore, it is necessary to look at some green route using renewable resources to synthesise surfactant having good physiochemical properties with low production cost [10]. Lots of attention have been received now a days for effective use of such green surfactants in EOR. Many such surfactants have been synthesized recently from vegetable oils with their

successful application in EOR [11-15]. Sulfonation of ricinoleic acid methyl ester present in castor oil gives anionic surfactants that reduces the IFT to an ultra-low value with good wettability alteration of rock [16]. Negm et al. [17] synthesized biodegradable non-ionic surfactants from Jatropha oil. Synthesis and characterization of different surfactants from different vegetable oils like palm [18], mahua [19], sunflower [20,21] have also been reported. As the demand of vegetable oils as food is increasing in recent years, much attention is now given on synthesis of surfactants from non-edible oils [22]. The efficiency and yield of surfactants depend on the process of synthesis. An oleic acid that occurs naturally in different vegetable fats and oil is also considered as one of the natural sources to produce surfactant. It is classified as a monosaturated omega-9 fatty acid with molecular formula of $C_{18}H_{34}O_2$. It is the most common fatty acid found in nature.

In normal practice after addition of the surfactant, appropriate polymer is added that acts as a plug to push the oil from internal structure to the top of the surface. Trapping of resident oil is due to higher capillary forces which is in competition with the viscous forces that mobilize the oil. The mobilization of oil is obtained by increasing viscous force by addition of appropriate polymer. An important feature of an effective polymer is the desired rheological behavior when dissolved in water in presence of salts at variable temperature. So, water soluble polymers are widely used in SP flooding. In present scenario, Hydrolyzed Polyacrylamide (HPAM) and various biopolymers are potentially used in polymer flooding or SP flooding for recovery of oil. Xanthan gum and Guar gum are two potential candidates as a biopolymer.

In this study, we have chosen Guar gum as a natural biopolymer mainly consists of high molecular weight polysaccharides that are composed of galactomannans with a linear chain of (1→4)-linked β-D-mannopyranosyl units with (1→6)-linked α-D-galactopyranosyl residues as side chains. The most promising property of guar is to develop higher viscosity in fresh water or brine with lower concentration. The hydration property of Guar gum is an important characteristic in many applications where aqueous polymer solutions are used. The hydration of guar depends on pH, temperature and shear. Rheological analysis of the Guar gum solution in water and brine in different temperature and concentration range was carried out to assess its effectiveness in EOR study. Different types of surfactants are chosen to check compatibility with biopolymer candidate Guar gum in oil recovery process by studying the surface properties. In present study, Oleic acid-based surfactants with sulfonation at terminal carbon and their esters are used. The attempts were also made to design polymeric surfactants derived from sulphonation of dextrin powder and starch. The idea behind this was to achieve surfactant and polymer function in a single candidate.

## 2. Experimental

### 2.1. Materials

**Polymer:** Polymer is a high molecular weight commercial Guar gum (Viscosity = 5210 CP) provided by Syntron Industries Pvt Ltd., Vatva, Ahmedabad, INDIA.

**Surfactant:** Sodium Dodecyl Sulfate (SDS) and petroleum sulfonate named α-olefin sulfonate (AOS) were used as commercial benchmark surfactants. SDS (Merck Millipore) extra pure was purchased from Dutt Enterprise, Nadiad, Gujarat, INDIA. AOS was supplied by Syntron Industries Pvt Ltd., Vatva, Ahmedabad, INDIA. Sulphonated products of Oleic acid, Dextrin and Starch were used as novel green route surfactants in this study. These products were synthesized by Syntron Industries Pvt Ltd., Vatva, Ahmedabad, INDIA as per our requirement.

**3% Salt Solution:** 3% NaCl solution was prepared by dissolving 3 gram of sodium chloride in 100 ml of water. The main aim of using salt solution was to study the effect of salinity on viscosity of polymer solution and surface properties. Extra pure NaCl (Finar Chemicals) was purchased to prepare salt solution from Dutt Enterprise, Nadiad, Gujarat, INDIA.

### 2.2. Methods

#### 2.2.1. Surface Tension Measurement

The surface tension of synthesized surfactants was measured using DuNouy ring tensiometer (KSV NIMA) at controlled temperature 25 °C. The surfactant solutions were prepared in Millipore water in the range of 0.1 to 0.5% (w/v). Equilibrium surface tension of each sample was measured at least for three times and then average value was considered for the particular surfactant concentration. The Equilibrium surface tension of distilled water is 71.5 mN/m at $25^0$C. At the end of each measurement the platinum ring was cleaned properly using acetone and dried on burner flame before performing next experiment.

The Equilibrium surface tension in each case was measured by dipping the vertically hung ring into the solution and then subsequently it was pulled out. The maximum force required to pull the ring through the interface was considered as the Equilibrium surface tension. The Equilibrium surface tension of distilled water, 71.5 mN/m at $25^0$C, was used to calibrate the tensiometer.

#### 2.2.2. Polymer Solution Preparations

Guar gum solutions were prepared by adding calculated amount of Guar gum powder in 100 ml of water at $30^0$ C with continuous stirring action in 60 to 90 seconds. Continuous stirring was provided at least for 3-4 hours at 500-600 rpm using magnetic stirrer. Then it was

kept at lower temperature to increase the rate of hydration that results in to increase the viscosity of the solution. Guar gum solutions of different concentrations are prepared to check the viscosity of solution.

### 2.2.3. Rheological Measurements

Viscosity of the Guar gum solution and polymer-surfactant solutions of different concentration were measured as a function of shear rate ($\gamma$) using Plate and Plate type Anton Paar Rheometer MCR102 series. Temperature Sweep analysis was applied at fixed shear rate of 50 S$^{-1}$ in temperature range of 20 to 50$^0$ C.

## 3. Results and Discussion

### 3.1. Equilibrium Surface Tension of Surfactants

Equilibrium surface tension (EST) of different newly developed green route surfactants were measured to assess their surface properties with benchmark surfactants. Table 1 shows the Equilibrium surface tension of different surfactants.

**Table. 1** Equilibrium surface tension of different surfactants

| CONCENTRATION (%w/v) | DYNAMIC SURFACE TENSION (mN/m) | | | |
|---|---|---|---|---|
| | DE-SA - 20 | DE-CSA- 20 | ST-CSA- 20 | SMP-07 |
| 0.1 | 38.5 | 46.798 | 55.3 | 31.32 |
| 0.25 | 38.13 | 46.7 | 49.45 | 31.08 |
| 0.5 | 38.11 | 50.1 | 51.1 | 29.97 |

It was found that DE-SA-20 and SMP-07 exhibit good surface properties. Further investigation about Interfacial Tension properties is necessary to establish two surfactants as promising candidates in EOR study.

Normally, anionic surfactants are used for EOR applications. Petroleum Sulfonates (PS), α-olefin sulfonates (AOS), Internal olefin sulfonates (IOS), Alkyl-aryl sulfonates, Sodium Dodecyl Sulfate (SDS), Ethoxylated Alcohol (EA) are the most common types of surfactants used in EOR based on the tolerance ability to salinity and hardness, and temperature stability.

In present study, we have considered the SDS and AOS as reference surfactants and measured their Equilibrium surface tension in the concentration range of 0.1 to 0.5% (w/v). Table 2 shows the Equilibrium surface tension of SDS and AOS.

**Table. 2** Equilibrium surface Tension of SDS and AOS

| CONCENTRATION (%) | EST OF AOS (mN/M) | EST OF SDS (mN/m) |
|:---:|:---:|:---:|
| **0.1** | 31.226 | 30.22 |
| **0.2** | 31.229 | 31.45 |
| **0.25** | 31.65 | 31.83 |
| **0.3** | 31.891 | 32.218 |
| **0.4** | 31.63 | 33.019 |
| **0.5** | 32.234 | 33.014 |

The measured value of EST of synthesized surfactants are compared with these values to check the effectiveness of the newly developed surfactants. Figure 1 shows the comparison of EST of SMP-07 and DE-SA-20 with reference surfactants SDS and AOS.
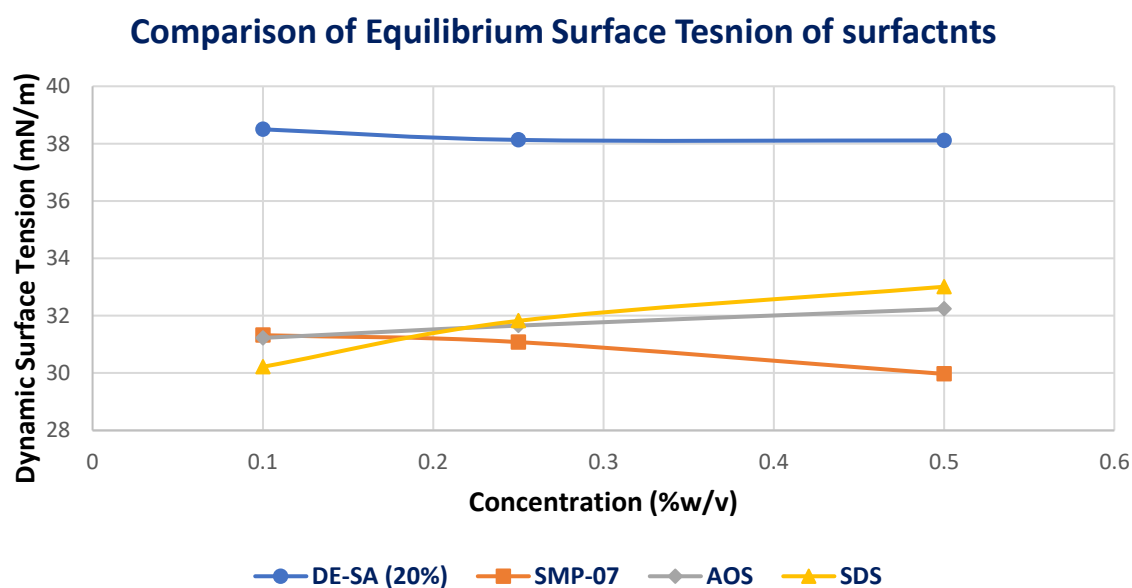


**Figure 1.** Comparison of Equilibrium surface Tension of different surfactants

Close approximation in results of the SMP-07 was observed with the SDS and AOS. Synthesized surfactant SMP-07 gave good results in comparison with SDS and AOS. Therefore, SMP-07 can be considered as an effective surfactant for EOR. However, other surface properties like Interfacial Tension (IFT), wettability alteration, CMC and surface

adsorption ability must be studied to make it more effective in polymer – surfactant flooding. Surfactant also plays a vital role in rheological study along with the selected polymer. So, it is also important to check the effect of it over the viscosity of solution.

### 3.2. Rheological Analysis of Polymer and Polymer- Surfactant blend
### 3.2.1. Viscosity measurement of Guar gum in water Solution.

Viscosity of Guar gum in water solution in different concentration (1000, 2000, 3000, 4000, 5000 ppm) were measured at constant shear rate of 50 S $^{-1}$ in the temperature range of 20 to $50^0$ C which is summarized in Table 3.

**Table 3.** Viscosity of Guar gum solutions in water at different temperature

| No | Guar Solution (PPM) | Viscosity (Centipoise) | | | |
|---|---|---|---|---|---|
| | | $20^0$ C | $30^0$ C | $40^0$ C | $50\ ^0$C |
| 1 | 1000 | 26.5 | 18.6 | 14.6 | 11.7 |
| 2 | 2000 | 85.6 | 63.6 | 50.9 | 42.7 |
| 3 | 3000 | 156.3 | 122 | 96.8 | 77.48 |
| 4 | 4000 | 494.7 | 445 | 405 | 345.9 |
| 5 | 5000 | 836 | 725 | 639 | 567 |

The main focus of this study was to observe the viscosity change with respect to variable concentration and temperature. Table 3 shows that the increasing concentration of Guar gum in water increases the viscosity of the solution. Viscosity of 4000 and 5000 ppm guar gum solution was found to be very high. For each of the five different concentration, a higher viscosity was observed at higher concentration of Guar gum. This happens because of a greater number of chains available at higher concentration and that increases the probability of interaction and entanglement between chains [23].

### 3.2.2. Viscosity measurement of Guar gum and SDS solution in water.

Series of experiments were performed to measure the viscosity of 1000 ppm Guar gum solution with surfactant SDS in different concentration range of 0.2 to 0.5% (w/v). Temperature sweep analysis test was applied in each case at constant shear rate of 50 S $^{-1}$. The main aim of this study was to assess the effect of surfactant on the viscosity of the Guar gum solution when added with polymer solution to alter the surface properties of displacing fluid in EOR.
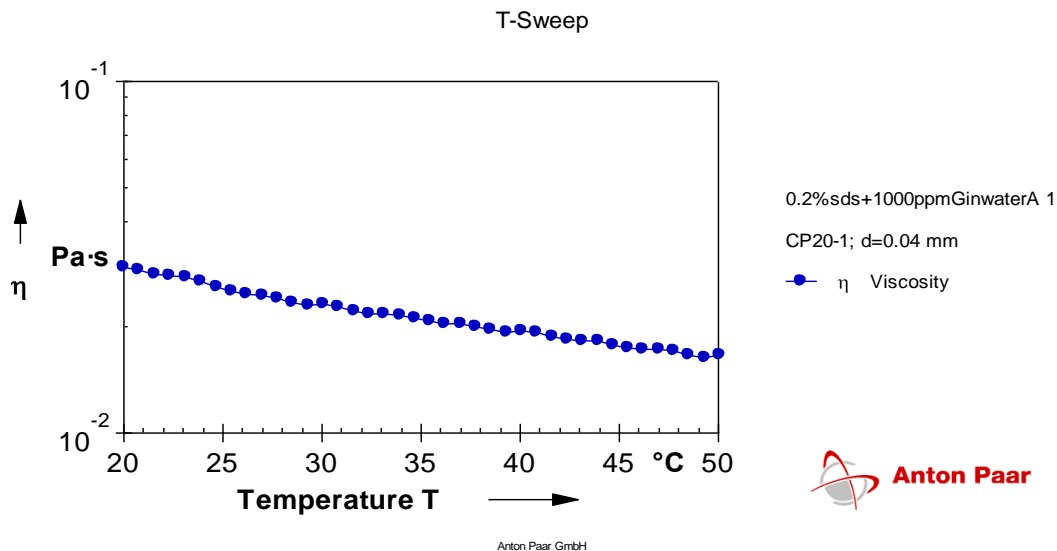
**Figure 2.** Viscosity of 1000 ppm Guar gum and 0.2% SDS solution

Figure 2 depicts the viscosity of 1000 ppm Guar gum solution with 0.2% SDS.It was found that viscosity of the solution was 0.0296 Pa.s (29.6 cP) at 20 $^0$C and 0.0116 Pa.s (11.6 cP) at 50 $^0$C. Comparison of this result with viscosity of 1000 ppm Guar gum solution indicates that there is rise in viscosity due to addition of SDS that promotes the hydration rate of Guar gum.
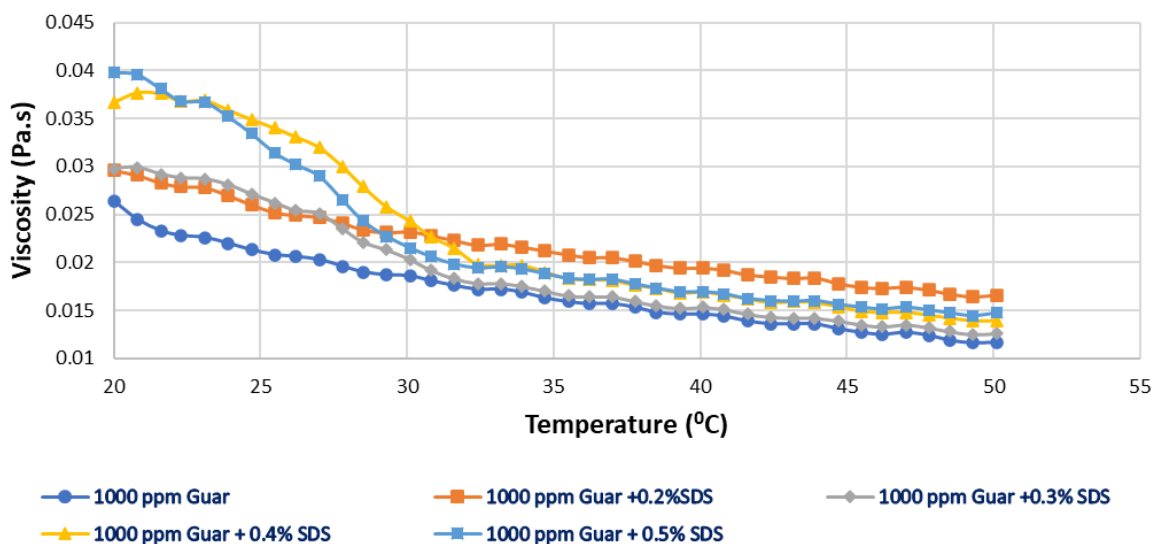


**Figure 3.** Comparative Viscosity of 1000 ppm Guar gum solution with SDS in different concentration.

Figure 3 shows comparative viscosity of 1000 ppm Guar gum solution with SDS in different concentration. It was found that viscosity of Guar gum solution increases with increasing concentration of SDS. The addition of SDS at lower concentration reveals slightly increase in

solution viscosity. However, significant rise in viscosity was observed at higher concentration of SDS. It may possible due to extension or uncoiling of the Guar gum chain due to interaction with negatively charged SDS [24-26].

### 3.2.3 Viscosity measurement of Guar gum and Oleic Acid Sulfonate (OAS) solution in water.

Experiments were conducted to study the effect of newly developed green surfactant OAS on the viscosity of the Guar gum solution in water. Figure 4 shows the change in viscosity of 1000 ppm Guar gum solution with 0.2% OAS with respect to change in temperature.
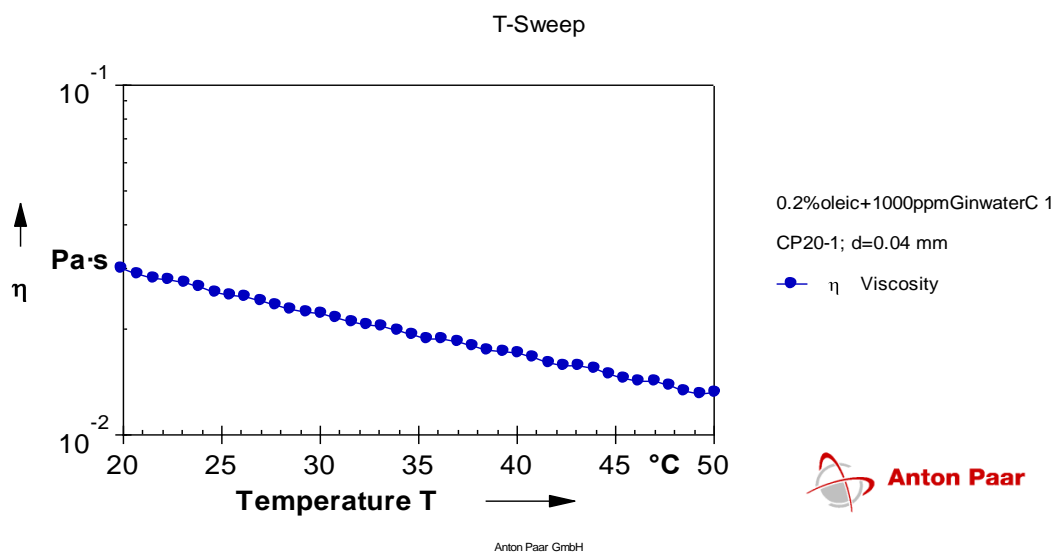


**Figure 4.** Viscosity of Guar gum Solution with 0.2% Oleic Acid Surfactant in Water

It was observed that viscosity of solution was 0.03 Pa.s (30.0 cP) at 20 $^0$C and 0.0132 Pa.s (13.2 cP) at 50 $^0$C. Comparison of this result with viscosity of 1000 ppm Guar gum solution with 0.2% SDS clearly reveals that trend of viscosity change is almost same.

Figure 5 reveals that viscosity of 1000 ppm Guar gum solution increases with increasing concentration of OAS.
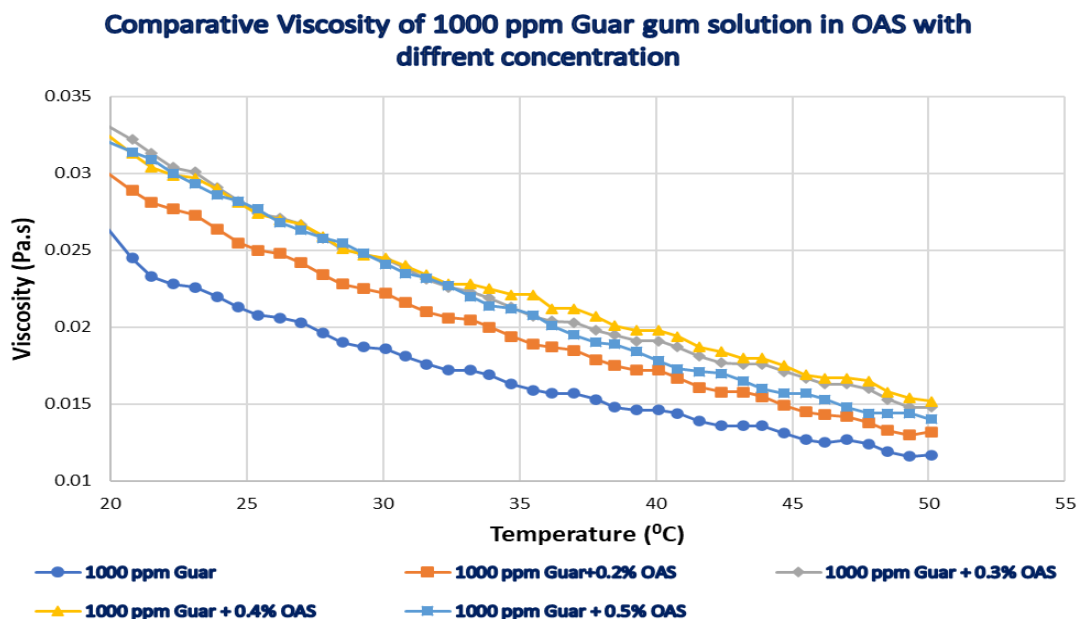
**Figure 5.** Comparative Viscosity of 1000 ppm Guar Solution with OAS

Table 4 gives information about the viscosity of Guar gum solution with surfactants in different concentration. Addition of surfactant increase the solution viscosity of the 1000 ppm Guar gum solution. However, significant rise in viscosity was observed at 0.3% concentration of OAS. An increasing concentration of OAS above 0.3% does not generate moderate rise in viscosity of solution but it remains almost uniform. This may happen due to negligible expansion or shrinkage of polymer chain when interchain association becomes weak. It was reported that no notable change in viscosity was observed above CMC of the surfactant due to micelle formation that neutralize the binding sites of polymer and break the junctions [24]. While, in case of increasing concentration of SDS, solution viscosity was found to be increased.

**Table 4.** Comparative Viscosity of 1000 ppm Guar gum solution with SDS and OAS

| Temperature ($^0$C) | Viscosity (Pa.s) | | | | | | | | |
|---|---|---|---|---|---|---|---|---|---|
| | 1000 ppm Guar | 0.20% | | 0.30% | | 0.40% | | 0.50% | |
| | | SDS | OAS | SDS | OAS | SDS | OAS | SDS | OAS |
| 20 | 0.0264 | 0.0296 | 0.03 | 0.0298 | 0.0331 | 0.0367 | 0.0325 | 0.0398 | 0.0321 |
| 30.1 | 0.0186 | 0.0232 | 0.0222 | 0.0203 | 0.0244 | 0.0243 | 0.0245 | 0.0215 | 0.0241 |
| 40.1 | 0.0146 | 0.0194 | 0.0172 | 0.0153 | 0.0191 | 0.0169 | 0.0198 | 0.0169 | 0.0178 |
| 50.1 | 0.0117 | 0.0166 | 0.0132 | 0.0126 | 0.0148 | 0.0139 | 0.0152 | 0.0147 | 0.014 |

### 3.2.4. Viscosity measurement of Guar gum and OAS in Salt solution.

In the real field application of oil recovery, solution of polymer and surfactant is prepared using ETP water or sea water (brine solution) which contains 2 to 3.5 % of sodium salt as a major compound.

In order to check the effect of salinity on the viscosity of the polymer – surfactant solution, 3% salt solution was prepared by dissolving 3 gram of sodium chloride in 100 ml of water and same salt solution was used to prepare the 1000 ppm solution of Guar gum with OAS in different concentration. Figure 6 gives information about the change in viscosity of 1000 ppm Guar gum solution with 0.2% Oleic Acid Sulfonate (OAS) with varying temperature in salt solution. It was observed that viscosity of solution was 0.0285 Pa.s (28.5 cP) at 20 $^0$C and 0.0155 Pa.s (15.5 cP) at 50 $^0$C.
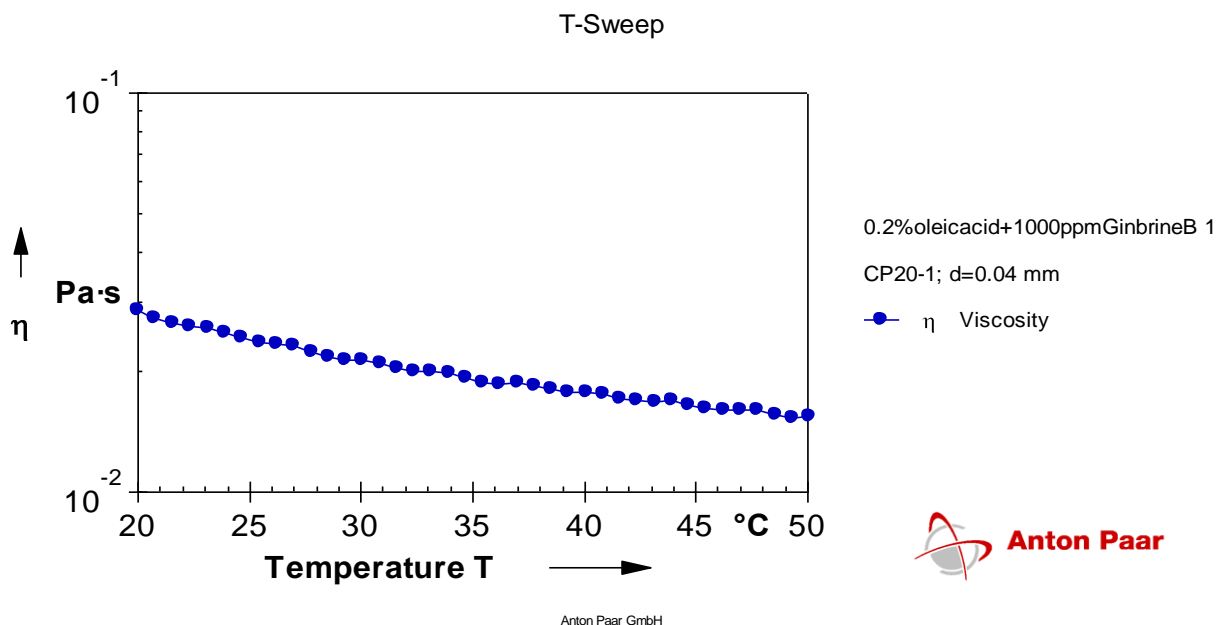


**Figure 6.** Viscosity of Guar gum Solution with 0.2% Oleic Acid Surfactant in 3% Salt Solution

Comparison of this result with viscosity of 1000 ppm Guar gum solution with 0.2% SDS in water is shown in Figure 7 which reveals that viscosity of solution was slightly lower at temperature 20 $^0$C but it was found to be higher at higher temperature at 50 $^0$C for this particular concentration.

We can observe the same trend in the 1000 ppm Guar gum solution with 0.3%, 0.4% OAS in brine as shown in Figure 8 and 9.
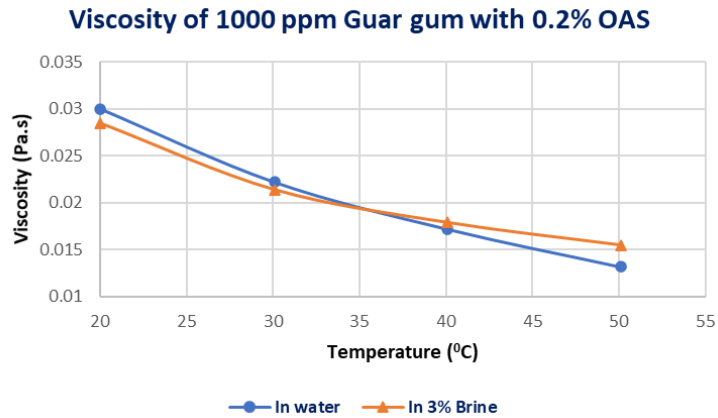
**Figure 7.** Comparison of 1000 ppm Guar gum Solution viscosity with 0.2% Oleic Acid Surfactant in salt solution and water.
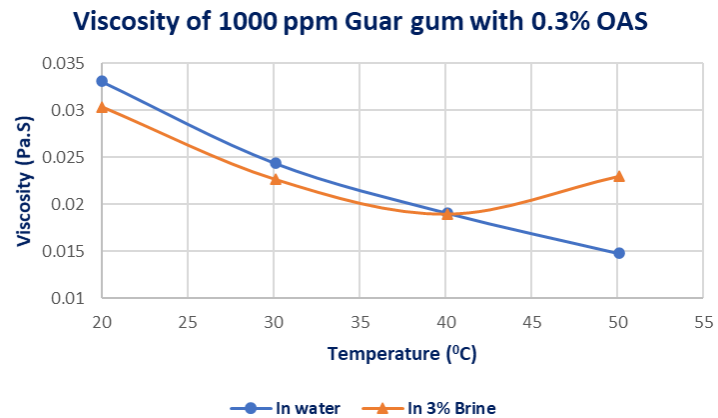


**Figure 8.** Comparison of 1000 ppm Guar gum Solution viscosity with 0.3% Oleic Acid Surfactant in salt solution and water.
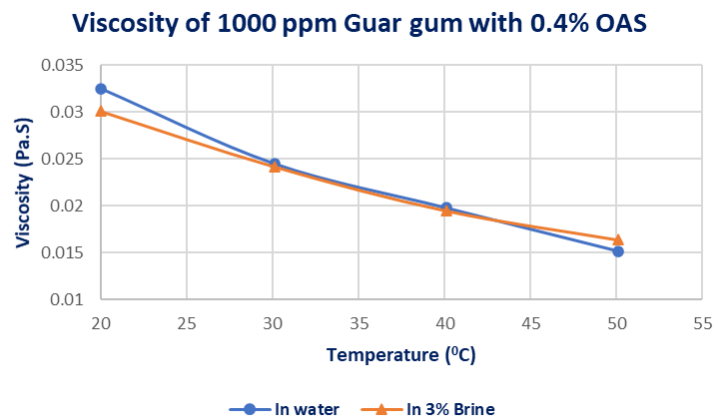


**Figure 9.** Comparison of 1000 ppm Guar gum Solution viscosity with 0.4% Oleic Acid Surfactant in salt solution and water.

There is a probability of shrinking of polymer coil due to presence of $Na^+$ in the solution at lower temperature that results in the reduction in viscosity. It was also observed that after rise in temperature, the further reduction in viscosity became slow and ultimately levels off. Continuous increase in temperature than increases the solution viscosity in brine solution in comparison to solution in water [27]. The reason behind this may be all negative charges contained by the polymer is neutralized by the $Na^+$ ions at lower temperature. At higher temperature, solution in brine exhibits higher viscosity compare to solution in water.

Figure 10 exhibit the changes in viscosity of 1000 ppm Guar gum solution with 0.5% OAS in water and salt solution. It signifies that viscosity of polymer solution in salt solution exhibit higher viscosity in comparison of polymer solution in water at any temperature. This effect is because of higher concentration of surfactant dissolved in solution.
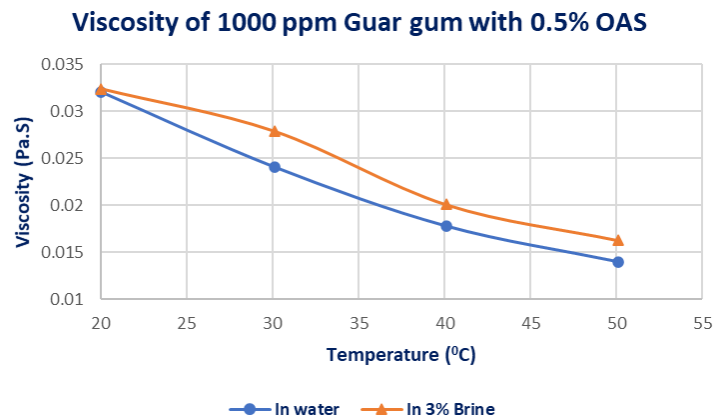


**Figure 10.** Comparison of 1000 ppm Guar gum Solution viscosity with 0.5% Oleic Acid Surfactant in salt solution and water.

## 4. Conclusion

In the present study, surfactant and polymer blends were prepared based on natural materials like Oleic acid, Dextrin, Cellulose and Guar gum. Rheological and surface properties were studied. Experimental results revealed that oleic acid derivative SMP-07 exhibits satisfactory surface property in comparison with the benchmark surfactants. Derivative of Dextrin, DE-SA-20, was found to be a good candidate having function of both polymer and surfactant. Biodegradable polymer Guar gum solutions in the concentration range of 2000-3000 ppm have shown comparable rheological properties with synthetic benchmark polymer used in EOR. Derivative of oleic acid OAS was found to be a potential replacement for SDS as it has produced similar rheological properties when added in Guar gum solution. It is

interesting to note that Guar gum – OAS surfactant blend in 3% salt solution has shown increase in viscosity with increase in temperature. All in all, Guar gum – OAS surfactant blend is found to be a potential green surfactant-polymer blend for EOR.

**Acknowledgments:**

**References:**

1. Lake, L. W., 1989. Enhanced Oil Recovery, Prentice-Hall, Englewood Cliffs, NJ.

2. Green, D. W., and Willhite, G. P., 1998. Enhanced Oil Recovery, SPE Textbook Series Vol. 6, SPE inc., Richardson, TX.

3. Alvarado, V., Manrique, E., 2010. Enhanced oil recovery: an update review, Energies 3,1529–1575.

4. Tunio, S.Q., Tunio, A.H., Ghirano, N.A. and El Adawy, Z.M., 2011. Comparison of different enhanced oil recovery techniques for better oil productivity. International Journal of Applied Science and Technology, 1(5).

5. Alban, N., Gubitta, J., 1999. Surfactant polymer interaction in enhanced oil recovery (Doctoral dissertation, Prairie View A & M University).

6. Babu, K., Pal, N., Bera, A., Saxena V. K., Mandal. A., 2015. Studies on Interfacial Tension and Contact Angle of Synthesized Surfactant and Polymeric from Castor Oil for Enhanced Oil Recovery. Applied Surface Science, 353,1126-1136.

7. Bera, A., Ojha, K., Mandal, A., Kumar, T., 2011. Interfacial tension and phase behaviour of surfactant-brine–oil system. Colloids Surfaces: A Physicochemical Engineering Aspects, 383,114-119.

8. Golabi, E., Azad, F. S., Ayatollahi, S. S., Hosseini, S. N., Akhlaghi, N., 2012. Experimental Study of Wettability Alteration of Limestone Rock from Oil- Wet to Water-Wet using Various Surfactants. SPE Heavy Oil Conference.1-16.

9. Qi. Z., Wang, Y., He, H., Li, D., Xu, X., 2013. Wettability alteration of the quartz surface in the presence of metal cations. Energy & Fuels, 27,7354-7359.

10. Foley, P., Kermanshahi Pour, A., Beach, ES., and Zimmerman, JB., 2012. Derivation and synthesis of renewable surfactants. Chemical Society Reviews, 41,1499-1518.

11. Zhang, Q-Q., Cai, B-X., Xu, W-J., Gang, H-J., Liu, J-F., Yang, S-J., Mu, B-J., 2015. Novel zwitterionic surfactant derived from castor oil and its performance evaluation for oil recovery. Colloids Surfaces A Physicochemical Engineering Aspects, 483,87-95.

12. Han, F., Deng, Y., Wang, P., Song, J., Zhou, Y., Xu, B., 2013. Synthesis and Characterization of Glucosamide Surfactant. Journal of Surfactants Detergent, 16,155-159.

13. Johansson, I., Svensson, M., 2001. Surfactants based on fatty acids and other natura hydrophobes. Current Opinion in Colloid Interface Science, 6,178-188.

14. Majidaie, S., Muhammad, M., Tan, IM., Demiral, B., 2011. Green surfactant for enhanced oil recovery. National Postgraduate Conference. IEEE.,1-5.

15. Elraies, K.A., Tan, I.M., 2012. The application of a new polymeric surfactant for chemical EOR. Introduction to Enhanced Oil Recovery (EOR) Processes and Bioremediation of Oil-Contaminated Sites.

16. Babu, K., Maurya. N.K., Mandal, A., Saxena, V. K., 2015. Synthesis and Characterization of Sodium Methyl Ester Sulfonate for Chemically-Enhanced Oil Recovery. Brazilian Journal of Chemical Engineering. 32, 795-803.

17. Negm, N.A., El-Tabl, A.S., Aiad, I.A., Zakareya, K., Moustafa, A.H., 2013. Synthesis, Characterization, Biodegradation and Evaluation of the Surface-Active Properties of Nonionic Surfactants Derived from Jatropha Oil. Journal of Surfactants Detergent, 16, 857-863.

18. Lim, SR., Park, HR., Jung, KA., 2014. Synthesis of methyl ester sulfonate surfactant from palm oil methyl ester by using UV or ozone as an initiator. Journal of Biotechnology, 185,120 -121.

19. Salimon, J., Abdullah, B., Yusop, R.M., Salih. N., 2014. Synthesis, reactivity and application studies for different bio lubricants. Chemistry Central Journal. 8, 8-16.

20. Mori. K., Matsumura, S., 2012. Chemoenzymatic synthesis and properties of novel lactone-type anionic surfactants. Journal of Oleo Science. 61, 609-620.

21. Poyarkova, T.N., Kudrina, G.V., 2010. Synthesis of surfactants from sunflower oil production wastes. Russian Journal of Applied Chemistry. 83, 1314-1317.

22. Gervajio, G.C., Withana-Gamage, T.S., Sivakumar, M., 2005. Fatty acids from derivatives from coconut oil. Baily's industrial oil and fat products, 1-45.

23. Akbari, S., Mahmood, S.M., Tan, I. M., Bharadwaj, A.M., Hematpour, H., 2017. Experimental investigation of the effect of different process variables on the viscosity of sulfonated polyacrylamide copolymers. Journal of petroleum Exploration and Production Technology, 7, 87-101.

24. Chen, X.M., Yang, H.Y., you, X., Zhu, P.P., He, P.S., 2006. Effect of anionic surfactant upon the viscosity of polymer guar gum solution. Chinese journal of polymer Science,24, 437-440.

25. Zhang, L. M., Zhou, J. F., Hui, P. S., 2005. A comparative study on viscosity behavior of water-soluble chemically modified guar gum with different functional lateral groups. Journal of the Science of Food and Agriculture, 85, 2638-2644.

26. Nasr-El-Din, H. A., Hawkins, B. F., Green, K. A., 1991. Viscosity behaviour of alkaline, surfactant, polyacrylamide solutions used for enhanced oil recovery. In SPE International Symposium on Oilfield Chemistry. Society of Petroleum Engineers.

27. Akbari, S., Mahmood, S. M., Tan, I. M., Ghaedi, H., Ling, O. L., 2017. Assessment of polyacrylamide-based co-polymers enhanced by functional group modifications with regards to salinity and hardness. Polymers, 9, 647.

# Agro-Waste Materials as Better Substitutes to Conventional Toxic Chemical Additives in Water-Based Drilling Fluids for Greener Operational Practices: A Review

Raunak Gupta[1] & Uttam K. Bhui[2]
[1]raunak.gphd19@spt.pdpu.ac.in
gupta_raunak@ongc.co.in
[2]School of Petroleum Technology, Pandit Deendayal Petroleum
University, Raisan, Gandhinagar, Gujarat 382007, India
E-mail address: Uttam.bhui@spt.pdpu.ac.in

## Abstract

As the whole world is moving towards a greener and sustainable energy needs, the oil and gas industry is also following the trend by adopting greener methods in different areas of its operational practices. The drilling activity of this industry is an expensive area where the average drilling fluid cost is considerably significant as it is almost one-tenth of the total drilling operation cost. The stringent policies regarding proper waste disposal and management of drilling fluids and various occupational hazards have inspired this industry to look into biodegradable substitutes for conventional and toxic additives. Literature survey clearly demonstrated that a plethora of researchers has been favorably disposed to analyze the use of agro-based materials for pH control, filtration control, corrosion control, and rheology modifiers in drilling fluids. Such waste materials are pervasive and at thrifty cost as compared to conventional drilling fluid additives. We have gathered data of several agro-waste materials including Corn Cob (CC), Mango Extracts (ME), Cashew Extracts (CE), Rice Husk (RH), Banana Peel Powder (BPP), Spent Tea Waste (STW), Tamarind gum (TG), Pistachio Shell Powder (PSP), Henna Leaf Extracts (HLE), Groundnut Husk (GNH), Cocoa Pod Extract (CPE), Fly Ash (FA) and Coconut Shell (CNS) through API standard experimental investigations by earlier researchers and provide a review of their applicability as green additives for future use. In this respect, fly ash and henna leaf extracts were found to be the cheapest and most expensive waste materials respectively. CC processed cellulose proved to be a better fluid loss control agent than PAC. CPE showed potentially high corrosion inhibition property in comparison to synthetic KOH (caustic potash), FA performed comparably but proved to be cost-effective over API-grade bentonite, and so on. We have further discussed various biodegradable waste materials in terms of their wide availability in India, better economics, safety with comparable/superior rheological properties than the conventional toxic chemical additives used in the water-based drilling fluids. Further research with various biodegradable agro-waste materials or their combination may be undertaken to optimize the performance of drilling fluids for various operational conditions like HPHT, oil or foam base mud, underbalanced drilling, directional drilling, etc. maintaining the stringent rule of green environment for the future.

*Keywords*: Filter loss, Rheological modifiers, Gel strength, Drilling mud, PAC (Polyanionic Cellulose), MCT (mud cake thickness)

## 1. Introduction

Drilling a well without the use of drilling fluid is unimaginable. These fluids may vary in composition but their functions stay largely the same. Drilling the wellbore is the initial and the

most costly step in the oil and gas industry. Drilling costs account for 25% of the total oil field exploitation cost and are concentrated mostly in the exploration and development of well drilling. Drilling fluids represents about one fifth (15-18%) of the total cost of oil well drilling but may cause 100% of drilling problems (Hossain ME, Al-Majed AA, 2015). Formulating the drilling fluid is the most important task in well planning as the bad design may have many direct as well as indirect impacts as shown in Figure 1. All these drilling fluids incorporate various additives that impart specific properties to the drilling mud as a whole. They clean the well, hold the cuttings in suspension, prevent caving, ensure the tightness of the well wall and form an impermeable cake near the wellbore area (rheological properties) for which rheology modifiers (viscosifiers, thinners, etc.) are needed. Moreover, they also have to cool and lubricate the tool, transfer the hydraulic power, and carry information about the drilled formation by raising the cuttings from the bottom to the surface. Conventionally, all these mud additives are chemical-based which are toxic to humans as well as the environment as these are non-biodegradable and it adds to the already maligned image of the O&G industry as the worst foe of the environment. During drilling operations, the most harmful drilling fluid chemical additives are lime, sodium hydroxide, lingo-sulphonate, chrome-lignite, and caustic soda. The most widely recognized drilling fluid additives with their potential dangers are illustrated in Table 1 (Patidar et al. 2020).

Major technical and economic challenges are faced by the corrosion of metals during the drilling operation. Hence, corrosion scavengers (like Magnetite) are commonly used in drilling fluids. Many industries all over the world have suffered significant losses due to corrosion. According to the 2002 U.S. corrosion study, the direct cost of metallic corrosion is $276 billion on an annual basis. Imported chemicals such as sodium carbonate [$Na_2CO_3$], sodium hydroxide [$NaOH$], and calcium hydroxide [$Ca(OH)_2$] are usually added to the mud to increase the mud pH to standard 8.0 or 10.5. To control corrosion of drilling materials, the corrosion inhibitor is usually used as one of the drilling mud additives. Such inhibitive substance can only be applied when it improves the rheological properties of the drilling mud.

With the stringent guidelines, standards, and environmental regulations by environmental protection agencies (EPA) and enhanced environmental concern across the O&G industry concerning drilling waste management, it is imperative for the drilling industry to pursue environmental friendly drilling practices so that the effect of generated waste on the environment from drilling can be minimized, as it counts for the second-largest volume of waste (Haute et al. 2007).

Food waste products account for about 8.2% of greenhouse gas emissions and they can be utilized for better uses such as drilling fluid additives. Regarding this, a plethora of research has been done on reducing the generated drilling waste or swapping the conventional chemical additives to locally sourced, non-toxic, and biodegradable agro-waste additives as it has multifold benefits which include, but not limited to, alleviating effect on the environment, better or comparable attributes at dirt-cheap prices to conventional chemical additives and it will encourage local content development. Agricultural wastage is India's no. 1 problem. Further, the occupational health hazards due to conventional chemical additives have been discussed. In this paper, the focus is on the latter aspect of utilizing agro-waste biodegradable additives (say, for example, studies have revealed that plant extracts are potential eco-friendly corrosion inhibitors) in the drilling mud where data of several agro-waste materials including Corn Cob (CC), Mango Extracts (ME), Cashew Extracts (CE), Rice Husk (RH), Banana Peel Powder (BPP), Spent Tea Waste (STW), Tamarind gum (TG), Pistachio Shell Powder (PSP), Henna Leaf Extracts (HLE), Groundnut Husk (GNH), Cocoa Pod Extract (CPE), Fly Ash (FA) and Coconut Shell (CNS) have

been gathered through API standard experimental investigations by earlier researchers and have been chronicled in a single paper. A summarized impact of potential agro-waste biodegradable drilling fluid additives on the specifications of water-based mud has been arrayed down in Table 2. Also, the comparative cost analysis and availability of these agro-wastes in India have been discussed in detail.

**Field Illustration of Drilling Mud Cost**
Figure 2 illustrates the costs of drilling 25 wells in the South Rumaila field, Iraq. It demonstrates a veritable concept from the South Rumaila field, Iraq, comparing the expense of drilling fluid and drilling operations. The percentage of drilling fluid cost ranges from 4.66 to 15.2%. The lowest in terms of drilling fluid cost was well 25; the drilling fluid cost around $279,000 while well 12 cost around $1,893,000, which was the highest cost for drilling fluid in this field. (Basra Oil Company, 2018). The expense of traditional chemical drilling fluid additives is a tangible cost of the drilling fluid (Al-Hameedi et al., 2019a). By utilizing waste materials, this expense can be decreased to a huge extent as waste materials are unwanted substances that are of no value and are left over after utilizing the essential product so they are available at meager costs in comparison to conventional drilling fluid additives.

**2. Experimental design, materials, methods, results, and discussion**
This segment is divided into various sub-segments to provide a comprehensive and logical insight to gauge the performances of each agro-waste material that is readily available in India. A summary of all the research findings for the aforementioned biodegradable drilling fluid additives at different concentrations and conditions in addition to the API standard experimental setup (such as rheometer/viscometer, pH meter, filter press, mud balance and retort kit) has been presented here.

**2.1. Corn Cob Cellulose (CCC)**
First of all, the reference mud sample was prepared using water, NaOH, bentonite, barite, Xanthan gum, etc. Cellulose was extracted from freshly harvested corn cobs using the Cellulose Extraction Method. Three samples (A, B, and C) of drilling fluid were prepared by mixing reference mud sample with 2.0g PAC for sample A, 2.0g corn cob cellulose for sample B, and 3.0g corn cob cellulose for sample C to precisely understand the impact of concentration variation of CCC on the reference mud. Standardized API drilling fluids testing equipment have been used to adjudge the effectiveness of Corn Cob Cellulose (CCC) over poly-anionic cellulose (PAC) to water-based mud in terms of adding various concentrations. All these tests were conducted under the surface conditions to obtain the physical properties of the mud as demonstrated by (Nmegbu et al. 2014). These results have shown that the pH, mud density, specific gravity of the mud formulated from corn cob cellulose are higher than that of the standard mud, but the rheology of the prepared mud was lower than that of the standard mud. The results show that cellulose processed from corn cob can significantly reduce a fluid loss (5.2-5.8 mls as compared to 6.6 mls for PAC) in a water-based drilling mud, suggesting CCC as a preferred fluid loss control agent over PAC.

**2.2. Mango Extracts (ME) and Cashew Extracts (CE)**
The production method of the mud and the determination of its rheological and allied properties were carried out based on the mud production standards of API. In the inspired work, the reference fluid (RF) sample was a drilling mud prepared using 245 ml water, 5.0g bentonite, 0.4g Xanthan

Gum biopolymer, 0.25g high viscosity Polyanionic Cellulose (PAC-HV), 0.1g KOH, 12.0g Sodium carbonate, 12.0g Barite as conventional chemical additives. Different concentrations of ME and CE ranging between 0% by weight to a maximum of 6% by weight were used and added separately to the reference mud, then to evaluate the effect of adding the different concentrations of ME and CE on the reference mud, full-set measurements were initially addressed for the reference mud, then the same measurements were conducted after adding ME and CE as illustrated by Omotioma et al. 2014.

Analysis of the experimental results showed that cashew and mango leaves extracts are worthy additives for the WBDM formulation. Mango leaves extract exhibited higher enhancement of the rheological properties of the drilling mud. The mud weight and pH of the formulated mud in the absence of plant extracts are 8.1 (lb/gal) and 9.1 (an alkaline state) respectively. For all the periods of gel strength determination, an increase in the concentration of cashew and mango extracts increases the gel strength of the mud. On average, mango extract gave the highest gel strength. For all samples with cashew and mango extracts, an increase in temperature decreased the yield point, plastic, and apparent viscosities of the drilling mud.

## 2.3. Rice Husk (RH)

The reference fluid (RF) sample was spud mud type and prepared using only bentonite and $Na_2CO_3$ as conventional chemical additives. The composition of the spud mud sample was 350 cc of water and 25 g of non-treated bentonite which was kept for 24 hrs to age. The mud's pH was measured and adjusted with 5 g of soda ash to enhance it's clay content and swelling. Full-set measurements were initially addressed for the reference mud. Henceforth, 12 mud samples were prepared and these mud samples were grouped into 3 batches: BATCH-1, BATCH-2, BATCH-3 with each batch constituting 4 mud samples. Different concentrations of rice husk (RH), PAC, and CMC ranging between 2.5 g to a maximum of 20 g were added separately to the reference mud and then LT-LP (low temperature - low pressure) filtration tests based on API standard were carried out to comparatively evaluate the effect of adding the different concentrations of RH, PAC, and CMC on the reference mud. The fluid loss volume and mud cake thickness of these batches were measured and results were arrayed down by Anietie et al. 2014.

Filtration action and mud cake-building attributes of drilling fluid are rudimentary to the non-damaging aspect of drilling fluid for the effective drilling operation. The variety and amount of solids, as well as, their physical and chemical interactions, present in the mud greatly impacts filtration. Therefore, RH was evaluated as the potentially better fluid loss control agent than PAC and CMC. The results obtained were compared with predilection towards RH with 64.89% reduction in the fluid loss at RH content of 20 g per 350 ml mud in comparison to 59.57% and 62.77% fluid loss reduction with 10 g -10 g of PAC and CMC respectively. As far as filter cake thickness obtained from these control additives was nearly the same, i.e., 3.2mm, 3.5mm, 3.3mm for RH, PAC, and CMC respectively. Hence, RH and CMC compare favorably. The presence of the blend silica and lignin compound provides the rice husk high resistance to water penetration, thermal and fungal decomposition (Oliveira et al., 2012). Conclusively, it can be said that, at a reasonable amount, RH can be used as a fluid loss control additive in WBDM owing to its remarkable filtration control attributes and high stability at high temperatures.

## 2.4. Banana Peels Powder (BPP)

To distinguish the effect of presenting various concentrations of Banana Peels Powder (BPP) on the physical and chemical properties of the drilling fluid, a reference fluid (RF) was prepared by

adding 0.1 gm of caustic soda (NaOH) and 36 gm of bentonite to 600 cc of water. Once the mixture is prepared full-set lab tests were conducted to find base measurements to compare to the results of adding different concentrations of BPP. From here, 1% (6 gm), 2% (12%), and 3% (18%) concentrations of BPP were separately added to the reference fluid. Once again, full-set measurements were conducted for each concentration to investigate the effect of BPP additives on the physical and chemical properties of the reference fluid. Typical API drilling mud experimentation approaches were implemented. All measurements were examined under the ambient laboratory conditions and static circumstances as demonstrated by Al-Hameedi et al. 2014.

Looking at the experimental findings, 1% (6 gm), 2% (12 gm), and 3% (18 gm) were first evaluated at room temperature and pressure. Adding BPP showed little to no effect on the mud density. However, for the rheological properties, the experimental additives resulted in increasing plastic viscosity (PV), yield point (YP), especially at 3% concentration. The BPP also showed excellent behavior for the initial and final gel strength as compared to the reference mud. Other properties that remarkably reduced were the pH levels and mud resistivity, which decreased as more BPP was added. The experimental mud filtration at 7.5 minutes and 30 minutes also showed a great improvement along with the filter cake thickness proving it to be a multipurpose effective drilling additive for water-based fluids. Additionally, other properties such as temperature, which was not affected, salinity (NaCl) and calcium content (Ca++) changed due to the increase in BPP concentration. The salinity was significantly increased for the mud, mud cake, and mud filtrate; while the calcium content was decreased from 52 mg/L to 8 mg/L by introducing a 3% BPP additive. After experimenting with different concentrations of BPP, it can be concluded that there was an overall improvement in the mud's properties. The outcomes and economic evaluation of the BPP revealed that it can possibly be used as biodegradable drilling fluid additives other than conventional chemical additives. Considering the outcomes recently expressed demonstrating the decrease in pH, filtration specifications, and Ca++; while increasing in viscosity and NaCl properties which proves BPP as a superior and economically more feasible elective than the conventional one.

## 2.5. Spent Tea Waste (STW)

Perez (2015) made an invention relating to the use of tannins as an additive and referred to it as a thinner and conditioning agent to reduce viscosity, yield point, and gel strength of drilling fluid as desired. [7] To test four concentrations of Spent Tea Waste (STW) derived calcium tannate, a reference fluid (RF) was made with basic components such as water (1000 cc), barite (60 gm), and bentonite (30 gm) which was then compared for fluid samples involving STW additives. STW was treated with calcium carbonate to precipitate out the desired calcium tannate. From here, four test samples having varying concentrations (0.5 gm to 3 gm) of STW derived calcium tannate were added to the mixture to change certain fluid properties and examine the effect of STW additives on the drilling mud characteristics. Each sample consisted of the same basic components mentioned above for RF. After mixing the powder, certain API standard tests were conducted, to help to evaluate the effectiveness of the powder within each sample. The chemical and physical properties can be found in the article by Talukdar et al. 2018.

Results from this study have shown the efficacy of Calcium Tannate as a rheology modifier or rheology control agent in water-based mud. It can be deduced that there was a decrease in the rheological properties i.e. viscosity, gel strength, and yield point with increasing concentration of Calcium Tannate. So, the optimal composition of Calcium Tannate for the favorable formulation

of an effective drilling mud can be selected. The effect of varying concentration on other properties are as follows: mud density increases with the increasing composition of Calcium Tannate and has a nearly minor effect on fluid loss. Thus, calcium tannate as an environmentally friendly drilling fluid additive, and the use of it will decrease environmental pollution since the tea waste otherwise would have disposed of directly in the environment. It is cost-effective since it is derived from the tea waste using simple procedures. There will be no scarcity of this material since the tea waste can be obtained from the abundant tea industries around the world.

## 2.6. Tamarind Gum (TG)

First of all, the spud mud sample (7% freshwater bentonite) referred to as the base mud (or reference fluid) was prepared using 325.5 cc of water and 24.5 g of bentonite. Two samples of drilling fluid were prepared by mixing 5ppb of TG and 10ppb of TG to minutely understand the impact of concentration variation on the reference mud. Standard API drilling fluids testing equipment have been used to evaluate the effectiveness of Tamarind Gum (TG) to water-based mud in terms of adding various concentrations. The fluid loss volume and mud cake thickness of these two concentrations were measured and results were demonstrated by Al-saba et al, 2018.
It is stable up to 75°C, has almost the same viscosity, and seven times cheaper than guar gum (Mahto et al. 2006). Both the fluid loss and mud cake thickness has been reduced considerably by adding the TG hence proving itself to be a worthy fluid loss control agent.

## 2.7. Pistachio Shell Powder (PSP)

To recognize the impact of adding various concentrations of PSP on the properties of the drilling mud, the reference fluid (RF) was initially prepared, and it consisted of water, caustic soda (NaOH), soda ash ($Na_2CO_3$), potassium chloride (KCl), sodium chloride (NaCl), starch HT, low viscosity polyanionic cellulose (PAC-LV), XC polymer, and limestone. Finally, different amounts of PAC-LV and/or two different sizes of PSP were added to each sample to control fluid (filtration) loss. Seven drilling mud samples were formulated which contained either polyanionic cellulose or two different PSP sizes (120–150μm and less than 75 μm). Then, full-set measurements were conducted using API standards for reference fluid (involving PAC) and the fluid with the locally sourced PSP to be compared to the effects of adding PSP vs PAC as illustrated by Davoodi et al. 2018.
The pistachio shell with two different fine particle sizes proved their inherent properties to be used as a fluid loss control agent. Thin and high-quality mud cakes produced by them corroborated their applicative field attribute. Due to the low true density of PSP, no significant change in density of mud samples was observed due to the presence of PSP. Pistachio Shell Powder (PSP) enhanced rheological properties, reduced fluid loss and mud cake thickness in both Low Pressure-Low Temperature (LP-LT) and High Pressure-High Temperature (HP-HT) conditions. Substantial fluid loss reductions by 44% and 39% in comparison to RF were observed with utilizing 9 g of PSP-1(less than 75 μm) in 350 ml drilling fluid under LP-LT and HP-HT operating conditions. The coarse size of PSP (120–150 μm) has also given the 29% API fluid loss reduction and acceptable thickness of the mud cake with fair quality. The economics of additives for the field applicable drilling fluid decreased by about 13–14 % by substituting the PSP in this formulation instead of the conventional fluid loss control additive (PAC-LV). From the field scale point of view, each half-percentage truncate expenditure plays a crucial role in the economics of drilling operation; therefore, the size of 13–14 % cost reduction emerges itself as noteworthy in the cost analysis. The presented method is successfully applied in one of the Iranian oil fields.

## 2.8. Coconut Shell (CNS)

The reference fluid (RF) sample was spud mud type and prepared using only 7% bentonite. The composition of the spud mud sample was 325.5 cc of water, and 24.5 g of bentonite. From here, two concentrations of CNS (6 ppb and 10 ppb) were added to the mixture to change certain fluid properties and examine the effect of CNS additives on the drilling mud characteristics, full-set measurements were initially addressed for the reference mud, then the same measurements were conducted after adding CNS. Each sample consisted of the same basic components mentioned above for RF. After mixing the powder, certain API standards were conducted, to help to evaluate the effectiveness of the powder within each sample. The chemical and physical properties can be found in the article by Widodo et al. 2020.

The 6 ppb CNS improved the yield point by approximately 331%. It has proved it's worth as a potential pH modifier. The 10 ppb CNS improved PV by 150%, 6 ppb CNS and 10 ppb CNS reduced fluid loss volume by 52% and 43.2% respectively so additive made from CNS can be used to improve the rheology of WBDM at high temperatures and high pressures.

## 2.9. Henna Leaf Extracts (HLE)

The additives used in this study are potassium chloride (KCl), caustic soda (NaOH), bentonite, PHPA, oxygen scavenger (OX-SCAV), barite, sodium chloride (NaCl), and PAC-LV. Rheological and filtration tests were carried out on the WBDFs to detect the effects of different concentrations (1, 2, 10, 20, 30, and 40 g) of HLE at 78 and 300 °F. The results of 1 and 2 g of the plant extracts were compared with those of low-viscosity polyanionic cellulose (PAC-LV). Compatibility test was carried out using 25 g/L of the green additives on base fluid (RF- 50 g/L KCl + 100 g/L NaCl+ 7.0 g/L PAC LV+2.0 g/L PHPA), and the swelling rate of sodium bentonite in distilled water was also considered using 1, 10, and 20 g of the green additives as demonstrated by Ismail et al, 2020.

The results showed that HLE significantly reduced the fluid loss between 62% and 67% and enhanced the rheological properties of the WBDM at higher concentrations (between 10 and 40 g) of HLE. Greater effect on the rheological properties was observed with PAC-LV than the green additives in equal amounts (1 and 2 g), but it demonstrated flat high and progressive gels which have the potential to lead to mechanical pipe sticking. It was also proved that the addition of HLE in the WBDM has a greater influence on the mud cake than PAC-LV. The cake thickness of the WBDF was reduced in the following order: 30–32% (by HLE), and 24–27% (by PAC-LV). This concludes the outstanding filtration characteristics of HLE. Further, compatibility test data established that the HLE is compatible with the other base fluid additives and the swelling behavior of sodium bentonite verified that the HLE is effective in inhibiting bentonite swelling. Notwithstanding, HLE showed excellent inhibition property and a strong viscosity enhancing effect on the WBDM system. Moslemizadeh and Shadizadeh (2017) researched the effect of using henna extract, which is a natural dye, in WBM as an environmentally friendly shale inhibitor. The results showed that the henna extract was able to reduce shale swelling effectively as well as improving the lubricity.

## 2.10. Groundnut Husk (GNH)

Simple formulations of drilling mud with water (500 ml), barite (22% equivalent to 110 g), XCP (0.4% equivalent to 2g), and GNH (at different concentrations from 1% to maximum 4%) were tested at two different particle sizes (63-74 μm and 250-297 μm). Cellulose was generated from

locally sourced groundnut husk at two varying particle sizes using mesh analysis to compare it with the commercially available PAC at different concentrations to corroborate its properties as a comparable fluid loss retarder additive as well as a rheological modifier. It was evaluated at both the fresh conditions as well as at the aged conditions to simulate both surface as well as subsurface conditions using standard API drilling fluids testing equipments as demonstrated by Patidar et al. 2020.

Proposed additive with sizes (63—74) μm and the (250—297) μm showed a decrease of 91.88% and 82.31% respectively, in the API filtration loss values from the base mud at 4% concentration as compared to 98.21% decrease by PAC-LV. The GNH acted as a filtrate retarder additive without much deviation from base rheology and with a significantly higher pH than the base mud. This investigation indicates that the proposed fluid loss additive and rheological modifier can minimize the environmental hazards and have proved to be a cost-effective eco-friendly alternative to PAC-LV.

## 2.11. Cocoa Pod Extract (CPE)

The reference fluid (RF) sample was spud mud type and prepared using only bentonite (24.5 g) and water (350 ml) as conventional chemical additives after which it was aged for 24 hours and tested for pH. then 0.41 g of sulfur was added to all the mud slurries, and initial pH was recorded accordingly. Conventional chemical additives used include viscosifiers (xanthan gum – 1.0g, PAC – 6.0g), fluid loss additives (chrome lignosulfonates, pregelatinized starch), weighing agent (barite – 75.4g), and alcoholic based defoamer. Five (5) drilling mud samples were prepared using the base mud and all the additives except the pH control additives. The different muds contained the pH control agents obtained from cocoa pod husk (CPH) and commercial potassium hydroxide (KOH). The KOH laden mud served as a reference fluid. The acidity of the mud was bound to increase in all cases after sulfurization and was regarded corrosive. Oil-well steel coupon (N-80 Steel of size 50x12x2 mm) was used for the corrosion tests by the weight loss method. This test was carried out in a small, high-temperature corrosion autoclave containing the sulphurized mud. Then an oil-well steel coupon (N-80 Steel) which had been treated according to the API specifications (API RP-13 B-1) was hung in the mud for 6 hours. The test temperatures were 27, 47, 67, and 87°C for pressures of 3000, 4000, and 5000 psi.

The result demonstrated in paper by *Arinkoola et al, 2017* that CPE showed high corrosion inhibition potential when compared to the synthetic KOH. Also, CPE has higher thermal stability and is a very efficient fluid loss reducer at high temperatures. On the flip side, it shows a thinning tendency, and hence, mud may require an additional viscosifier to improve its rheology. Further scope of study involves varying the local additive concentration and increasing the test time to beyond 6 hours.

## 2.12. Fly Ash (FA)

In the present work, a possible alternative to API-grade drilling bentonite was developed by modifying the Class-F fly ash to generate α-glycol- and amine-substituted FA. The formulated drilling fluid system included functionalized FA (2.0%, 3.0% and 4.0% ), tamarind gum (1.5 g L-1) and PAC (1.0 g L-1). Rheological behavior and filtration loss properties of the functionalized FA in aqueous suspension were determined and compared with the API-grade drilling bentonite yielding similar results. Then it's performance was studied for thermal stability, cuttings transportation ability, friction, and shelf-life properties under dynamic and static aging (i.e., downhole condition at 75°C and 100 psig) performance parameters obtained were listed in the

literature by Gautam et al. 2018. The cost of α-glycol- and amine-substituted FA was found to be 125 and 230 \$/t, respectively which was quite economical over API-grade bentonite (i.e., 250 \$/t). Although, locally sourced-based drilling fluid is more sensitive to static aging exhibiting maximum reductions in rheological, frictional, and fluid loss properties. The reduced shelf-life (i.e., the length of time that the drilling mud is compliant with all specifications for re-use) of the functionalized FA-based drilling over bentonite-based mud was mainly due to the presence of α-glycol and amine functional group on FA surface. Rheological, frictional and filtration properties under the dynamic and static aging condition suggested that a new drilling fluid system based on the functionalized FA was thermally stable, potential to lift cuttings, and has desired lubrication behavior at the downhole condition at 75°C and 100 psig. The deviation of zeta-potential from – 47.1 to – 68.1 mV in pH range 8-12 and cation exchange capacity with ~ 68.0 meq/100 g corroborated the stability of the aqueous suspension of α-glycol- and amine-substituted FA.

## 3. Availability and cost comparison of various biodegradable agro wastes

The uncertainties and deviations in crude oil prices over time have become an increasing cause of concern amongst industry players and researchers about finding innovative ways of reducing the OPEX. One aspect is to find cheaper alternative materials. As per the Bloys *et al.* (1994) drilling fluids takes up approximately 5 -15% of the total well drilling costs, hence, minimizing the economics of any drilling fluid additive becomes of utmost crucial. Table 3 illustrates the dirt-cheap prices of unprocessed agro-waste materials available in India that can act as additives performing crucial functions in drilling fluids.

### 3.1 Economic Analysis

In this section, an economic investigation for the preparation of the agro-waste material to put it into practical usage as additives imparting required properties to drilling mud is presented. For a holistic economic analysis, the cost of an industrial plant should be factored in; however, this would make the analysis complex and thus had to be overlooked. Hence, the economic investigation would be concentrated on the cost of the agro-waste material, processing costs (pulverizing and sieving), and energy costs. The cost of production of 1kg of each drilling mud additive from the agro wastes is based on the unit cost of each material, labor, and energy required. Notwithstanding being a simple analysis, it must be stated that the costs taken into consideration in the analysis refer to industrial and not laboratory quantities. The raw material costs used for this analysis were sourced from the prices as seen on the webpage of the commercial Indian suppliers of these agro wastes. The breakdown of the processing costs for the production of 1kg of locally sourced drilling fluid additive from the agro-waste materials is summarized in Table 4. To acknowledge the economic investigation as presented in Table 3 and 4, it is essential to compare the results with the cost of the conventional drilling fluid additives as illustrated in Table 5. This comparison is crucial to manifest if the costs are economically sustainable. To be competitive and economically acceptable, the total cost for processing each agro waste and the cost of the agro-waste itself must be lower than the cost of the conventional drilling fluid additive. However, for easy understanding, it is necessary to fuse Table 3, 4, and 5 into a single piece. This integration is illustrated in Figure 3. In the figure, the average cost of the processed agro-waste material is compared with the cost of the conventional drilling fluid additives. From the figure, it is categorical that fly ash is the cheapest agro waste material. However, despite the cost of the corn cob, it still competes favorably with the conventional fluid loss control agents such as CMC and xanthan gum. Thus, the low cost

of these agro-waste materials as seen in Figure 3 indicate that no matter that even if the cost differences are with the slightest margins, they could lead to huge cost savings if they are used as a replacement for the conventional fluid loss additives (Amanullah *et al*., 2016).

As illustrated (Patidar et al. 2020), the average price of Xanthum gum polymer (XCP) ranges between Rs. 200 and 225 per kg with a median price of approx. Rs. 210 per kg. Similarly, the median price of Barite is approx. Rs. 14.5 per kg, and for the PAC-LVG it is approx. Rs. 184 per kg. The median price of groundnut husk is approx. Rs. 3—3.5 per kg and the median price of sodium hydroxide is approx. Rs. 33—34 per kg. So based on these mean values of base composition, the cost of preparation of 500 ml of base fluid will be around Rs. 2. The cost of preparing 500 ml groundnut husk drilling fluid at 4% concentration will cost around Rs. 2.8, and the cost of 500 ml of drilling fluid with the same concentration of PAC-LVG will cost around Rs. 5.70. Thus, the groundnut husk additive is 50.79% more cost-efficient than the industrial PAC-LVG, and this becomes a hundredfold when used for oil and gas drilling operations.

## 4. Summary and Future Scope

Almost negligible work has been done on the occupational health hazards, economic analysis, and microscopic structure analysis of these locally sourced biodegradable agro-waste materials. Future studies should be concerned to prove the thermal stability and compatibility with other additives of these agro wastes under dynamic and HP-HT conditions in both OBDM and WBDM to ensure the relevance of these additives and to superiorize the already enhanced properties when utilized in the field. The effect of all these green additives should be studied for various operational practices like cuttings transport efficiency etc. Efforts should be made to replace all the conventional chemical additives with locally sourced biodegradable materials to formulate even more potent drilling mud which will be safer to the environment as well as rig personnel coming in direct contact with it. Interaction study of different rock types with the drilling fluids may help us to understand the effectiveness of different biodegradable agro-waste in different specific situation of drilling environment (health and environment concern).

## 5. Conflict of Interest

The authors declare that they have no known competing financial interests or personal relationships that could have appeared to influence the work reported in this paper.

## References

1. Abo Taleb T. Al-Hameedi, Husam H. Alkinani, Shari Dunn-Norman, Ebrahem Salem, Matthew D. Knickerbocker, and Naser F. Alashwak, Missouri University of Science and Technology; Rusul A. Mutar, Ministry of Communications and Technology, Iraq; Waleed H. Al-Bazzaz, Kuwait Institute for Scientific Research, Laboratory Study of Environmentally Friendly Drilling Fluid Additives Banana Peel Powder for Modifying the Drilling Fluid Characteristics in Water-Based Muds, IPTC-19964-MS, International Petroleum Technology Conference, Saudi Arabia, 13 – 15 January 2020.
2. Abo Taleb T. Al-Hameedi, Husam H. Alkinani, Shari Dunn-Norman, Hussien W. Albazzaz, and Mohammed M. Alkhamis, [2019a]Insights into Eco-Friendly and Conventional Drilling Additives: Applications, Cost Analysis, Health, Safety, and Environmental Considerations, SPE-195398-MS, SPE Symposium: Asia Pacific Health, Safety, Security, Environment and Social Responsibility, Malaysia, 23 - 24 April 2019.

3. Aghil Moslemizadeh, Seyed Reza Shadizadeh, A natural dye in water-based drilling fluids: Swelling inhibitive characteristic and side effects, Petroleum, Volume 3, Issue 3, 2017, Pages 355-366, ISSN 2405-6561, https://doi.org/10.1016/j.petlm.2016.08.007.

4. Agwu, O.E., Akpabio, J.U., Using agro-waste materials as possible filter loss control agents in drilling muds: A review, *Journal of Petroleum Science and Engineering* (2018), doi:10.1016/j.petrol.2018.01.009.

5. Al-saba, M. T., Amadi, K. W., Al-Hadramy, K. O., Dushaishi, M. F., Al-Hameedi, A., and H. Alkinani. "Experimental Investigation of Bio-Degradable Environmental Friendly Drilling Fluid Additives Generated from Waste." Paper presented at the SPE International Conference and Exhibition on Health, Safety, Security, Environment, and Social Responsibility, Abu Dhabi, UAE, April 2018. doi: https://doi.org/10.2118/190655-MS

6. Anietie N. Okon *, Julius U. Akpabio, Kilaliba W. Tugwell, Evaluating the locally sourced materials as fluid loss control additives in water-based drilling fluid, Heliyon 6 (2020) e04091

7. Anietie N. Okon, Francis D. Udoh, and Perpetua G. Bassey, Evaluation of Rice Husk as Fluid Loss Control Additive in Water-Based Drilling Mud, SPE-172379-MS**.** SPE Nigeria Annual International Conference and Exhibition Nigeria, 05–07 August 2014

8. API SPEC 13A, Specification for Drilling Fluids – Specifications and Testing. 2010. Washington, DC: API.

9. Atul Kumar Patidar, Anjali Sharma, Dev Joshi, 2020. Formulation of cellulose using groundnut husk as an environment-friendly fluid loss retarder additive and rheological modifier comparable to PAC for WBM. *J Pet Explor Prod Technol (2020)* 10:3449-3466.

10. Basra oil Company. Various Daily Reports, Final Reports, and Tests for 2017 and 2018. *Several Drilled Wells, Basra oil Fields, Iraq.*

11. Dagde, Kenneth Kekpugile, and Nmegbu, Chukwuma Godwin Jacob, DRILLING FLUID FORMULATION USING CELLULOSE GENERATED FROM GROUNDNUT HUSK, International Journal of Advancements in Research & Technology, Volume 3, Issue 6, June-2014  ISSN 2278-7763

12. file:///F:/PhD/biodegrable%20additives%20papers/corn%20availability%20reference.html, last accessed on Dec 22nd, 2020

13. Gautam, S., Guria, C., Rajak, D.K., Pathak, A.K., Functionalization of fly ash for the substitution of bentonite in drilling fluid, *Journal of Petroleum Science and Engineering* (2018), doi: 10.1016/j.petrol.2018.02.065.

14. Hossain ME, Al-Majed AA. Fundamentals of Sustainable Drilling Engineering. John Wiley & Sons, New Jersey, USA; 2015

15. http://apeda.in/agriexchange/India%20Production/India_Productions.aspx?cat=fruit&hscode=1042 last accessed on Dec 21st, 2020

16. http://apeda.in/agriexchange/India%20Production/India_Productions.aspx?cat=Spices&hscode=1111 last accessed on Dec 21st, 2020

17. https://timesofindia.indiatimes.com/business/india-business/agricultural-wastage-is-indias-problem-no-1-here-is-why/articleshow/70974705.cms last accessed on Dec 30th, 2020.

18. https://sugarcane.dac.gov.in/Mis/Docs/636988050947079153-d6011213-1f5c-47c5-8735-25157d55fe48SP_Sugarcane2017.pdf last accessed on Dec 21st, 2020

19. https://www.indiatea.org/uploads/scenerio_image/1496838969.pdf, last accessed on Jan 1st, 2021

20. Ismail, A.R., Mohd, N.M.N.A., Basir, N.F. *et al.* Improvement of rheological and filtration characteristics of water-based drilling fluids using naturally derived henna leaf and hibiscus leaf extracts. *J Petrol Explor Prod Technol* **10,** 3541–3556 (2020). https://doi.org/10.1007/s13202-020-01007-y

21. *M. O. Aremu1, A. O. Arinkoola, K. K. Salam1, and E. O. Ogunmola,* POTENTIAL OF LOCAL PH CONTROL ADDITIVES FOR CORROSION INHIBITION IN WATER BASE DRILLING FLUIDS, January 2017, Petroleum and Coal 59(5):611-619

22. MI-Drilling fluids, 2000. Drilling fluids manual.

23. Nmegbu, J., and B. A. Bekee. "Evaluation of corn cob cellulose and its suitability for drilling mud formulation." *International Journal of Engineering Research and Applications* 4.5 (2014): 112-117.

24. Omotioma M., Ejikeme P. C. N., And Mbah G. O., Comparative Analysis of the Effects of Cashew and Mango Extracts on the Rheological Properties of Water-Based Mud, *Int. Journal of Engineering Research and Applications ISSN: 2248-9622, Vol. 4, Issue 10( Part - 6), October 2014, pp.56-61*

25. Onuh C.Y, Igwilo K.C, Anawe P.A.L, Daramola Olakunle, and Ogunwomoju Omotoke, Environmentally Friendly Fluid loss Control Agent in Water-Based Mud for Oil and Gas Drilling Operations, International Journal of Applied Engineering Research ISSN 0973-4562 Volume 12, Number 8 (2017) pp. 1520-1523

26. Oseh, Jeffrey O., A. Gbadamosi, A. Ogunyemi, O. Olawale, and OMOTARA. "Transports of Different Cuttings Sizes in A Wellbore using Henna and Lignite Materials." (2018). ABUAD Journal of Engineering Research and Development (AJERD) ISSN: 2645-2685 Volume 1, Issue 3, 351-365

27. Owolabi, Ololade, Emmanuel, Ayodele, Okafor, Ikechukwu, Daniel, Ngwu, Igbine, Anita, and Maduabuchi Gloria. "The Evaluation of Coconut Fibre as a Loss Circulation Material in Drilling Operation." Paper presented at the SPE Nigeria Annual International Conference and Exhibition, Virtual, August 2020. doi: https://doi.org/10.2118/203756-MS

28. Prasenjit Talukdar*, Sudarshana Kalita, Amarjit Pandey, Upasana Dutta, Rituraj Singh, Use of Tannate derived from Tea Waste as Drilling Fluid Additive, International Journal of Applied Engineering Research ISSN 0973-4562 Volume 13, Number 16 (2018) pp. 12463-12468

29. Shadfar Davoodi, Ahmad Ramazani S.A., Saied Jamshidi, Arash Fellah Jahromi,
A novel field applicable mud formula with enhanced fluid loss properties in High Pressure-High Temperature well condition containing pistachio shell powder, J. Pet. **Sci**. **Eng**, Volume 162, 2018, Pages 378-385, ISSN 0920-4105,
https://doi.org/10.1016/j.petrol.2017.12.059.

30. Sharma, Virender Parkash, and Vikas Mahto. "Studies on Less Expansive Environmentally Safe Polymers for Development of Water-Based Drilling Fluids." Paper presented at the SPE Asia Pacific Oil & Gas Conference and Exhibition, Adelaide, Australia, September 2006. doi: https://doi.org/10.2118/100903-MS

31. Sonny Irawan, Ahmad Zakuan Ahmad Azmi, and Mohd. Saaid, Corn Cobs and Sugar Cane Waste as a Viscosivier in Drilling Fluid, *Pertanika J. Sci. & Technol.* 17 (1): 173 – 181 (2009) © Universiti Putra Malaysia Press, ISSN: 0128-7680

32. Widodo, H., Setyarto, M. R., Andhy, A., Prastya, M., & Annisa, A. (2020). Laboratory Analysis Using Coconut Shell from Bekasi Regency for Drilling Mud Additives on Oil

and Gas Wells. *Journal of Earth Energy Engineering*, *9*(1), 46-58. https://doi.org/10.25299/jeee.2020.3975

Table 1
Some of the Traditional Toxic Additives for the Drilling Fluids (Basra Oil Company, 2017; Halliburton, 2018; Baker Hughes, 2015; NewPark Company, 2018)

| Additive | Composition | Hazards |
|---|---|---|
| Bentonite | Montmorillonite >90%, Quartz <10%, Mica <10% | Respiratory effect: possible slight irritation from dust. |
| Barite | Quartz 10-12%, Barite 80-84%, Mica/illite <6%, Calcite <2% | Carcinogen, skin and eye irritant, respiratory irritant. |
| Caustic Soda | Sodium Hydroxide >97%, non-hazardous and other components 1-2.5% | Severe irritation or burns to the eyes, skin, gastrointestinal tract, and respiratory system. |
| Soda Ash | Sodium Carbonate 60-100% | May cause eye, skin, and respiratory irritation. |
| Sodium Bicarbonate | No ingredients as hazardous | Product dust may be irritating to eyes, skin, and respiratory system. |
| Calcium Carbonate | Calcium Carbonate 97-100% | Cause eye irritation. May cause skin, and respiratory tract irritation. |
| Lime | Calcium Hydroxide 100% | Harmful in contact with eyes. Risk of serious damage to eyes. Irritating to skin. Prolonged exposure may cause chronic effects. |
| Attapulgite Clay | Hydrated Aluminium- Magnesium Silicate 95-99%, Quartz 1-5% | Slightly hazardous in case of skin contact, of eye contact, of ingestion, of inhalation. |
| CMC | Sodium Carboxymethylcellulose 100% | Harmful in contact with eyes. |
| Sodium Hydroxide | Sodium Hydroxide 95-100%, Sodium Carbonate <3% | Causes eye and skin burns. Caused digestive and respiratory tract burns. Hygroscopic. |

| | | May cause eye and skin irritation. May cause irritation of digestive tract. May cause respiratory tract irritation. |
|---|---|---|
| Sodium Chloride | Sodium Chloride 100% | May cause eye and skin irritation. May cause irritation of digestive tract. May cause respiratory tract irritation. |
| Biocide | Magnesium Nitrate | May cause sensitization by skin contact. Very toxic to aquatic organisms. |
| Sodium Sulfite | Sodium Sulfite 100% | Causes eye and skin irritation. |
| Sodium Carbonate | Sodium Carbonate 100% | Harmful if inhaled. Causes eye and skin irritation. May cause respiratory tract irritation. |
| Sodium Nitrate | Sodium Nitrate 100% | Causes eye and skin irritation. Harmful if swallowed. May cause irritation of digestive tract. |

Table 2
Impact of potential agro-waste biodegradable drilling fluid additives on the specifications of water-based mud.

| Additive | Properties Improved | Description |
|---|---|---|
| CCC | Fluid loss control agent | Preferred over PAC |
| ME and CE | Gel Strength (rheology modifier) | Enhance the gel strength of WBDM; ME preferred over CE |
| RH | Filtration Control and MCT (mud cake thickness) | Preferred over PAC and CMC for filtration control and have comparable MCT |
| BPP | pH, Filtration Control, Viscosity, salinity | Decrease in pH, filtration specifications, and Ca++; while increasing in viscosity and NaCl properties |
| STW | Rheology reducer (thinner) | Decrease in the rheological properties i.e. viscosity, gel strength, and yield point |
| TG | Thermal Stability, Filtration Control and MCT | Stable up to 75°C; Potential replacement of guar gum |

| | | |
|---|---|---|
| PSP | Rheological Properties, Filtration Control and MCT | Properties enhanced in both LT-LP and HP-HT conditions. |
| HLE | Shale Inhibitor, Filtration Control and MCT | Reduced MCT: 30–32% (by HLE) v/s 24–27% (by PAC-LV), reduced fluid loss by 67%. |
| GNH | Fluid loss control and rheological modifier | Better alternative to PAC in terms of economics and biodegradability. |
| CPE | Filtration control at high temperature and corrosion inhibitor | Drawback: Thinning tendency; may require additional viscosifier. |
| FA | Rheological, filtration and frictional properties | Potential replacement of bentonite |
| CNS | Rheology and pH modifier | YP and PV was improved by 331% and 150% respectively. Reduced fluid loss volume by 52%. |

Table 3
Cost per kg of each raw agro waste (unprocessed agro-waste)

| Waste Material | Minimum Cost per Kg (Year - 2020) | Maximum cost per kg (Year - 2020) | Average cost per kg (Year - 2020) |
|---|---|---|---|
| Corn Cob | $ 0.067 Hardik Enterprises (2020) | $ 0.74 Niraj Optical Machinery (2020) | $ 0.403 |
| Sugarcane waste bagasse | $ 0.027 Manbhavan Organic (2020) | $ 0.051 Chatrapati Urja (2020) | $ 0.039 |
| Mango extract (leaves) | $ 1.085 Km Banana Leaf Merchant | $ 1.63 Agri Buy Onlines | $ 1.357 |
| Rice husk | $ 0.006 M/s Shyam Veda | $0.122 Guru Kirpa Agro Industries | $ 0.064 |
| Banana peels powder | $ 0.42 Banana Skin Powder Manufacturers Company | $ 2.03 Eklavya Biotech Private Limited | $ 1.227 |
| Spent tea waste | - | - | $ 1.24 (Tea board of India) |
| Tamarind gum | $ 0.597 Crystal Gum | $1.357 | $ 0.977 |

| | | Shri Gopal Gum Industries | |
|---|---|---|---|
| Pistachio shell powder | $ 0.135 Madan Lal Shyam Sunder | $ 0.339 Dry Luxury | $ 0.237 |
| Coconut shell | $ 0.081 Sri Murugan Oil Mill | $ 0.23 Skylark Exporter | $ 0.155 |
| Henna leaves | $ 0.746 Eastmade Spices & Herbs Private Limited | $ 2.035 Natural Herbal | $ 1.390 |
| Groundnut husk | $ 0.04 Peanuts Processing Plant, Visakhapatnam | $ 0.135 Indian SUPPLIERS | $ 0.087 |
| Cocoa pod | $ 0.271 Vital Herbs, Delhi | $ 1.71 Hill Natural Extract LLP, Greater Noida | $ 0.992 |
| Fly Ash | $ 0.002 Deepak Traders | $ 0.024 Ashcon Energy Solutions | $0.013 |

[1USD = Rs.74 was used as the conversion rate]

Table 4
Overview of processing costs for agro-waste materials

| | | **Source** |
|---|---|---|
| Estimated electrical energy required to pulverize 1kg of agro-waste (kWh) | 0.375 kWh | Chanu and Devi (2013) |
| Estimated Cost for 1 unit of electric power used for industrial purposes ($) | $ 0.0722/kWh | U.S. Energy Information Administration (2017) |
| Total Processing cost | $ 0.027 | |

Table 5
Cost per kg of conventional additives

| **Additive** | **Minimum Cost per Kg (2020)** | **Maximum Cost per kg (2020)** | **Average Cost** |
|---|---|---|---|
| Potassium hydroxide | $ 0.878 **Suvidhi Industries** | $ 1.283 **Proto Chemicals Industries** | $ 1.080 |

| | | | |
|---|---|---|---|
| Carboxymethyl cellulose (CMC) | $ 1.081 Jai Shakti Enterprises | $ 20.27 Bioven Ingredients | $ 10.675 |
| Polyanionic cellulose (PAC) | $ 1.013 **M S A TRADERS** | $ 3.378 **Perry Impex** | $ 2.195 |
| Xanthan Gum | $ 1.756 PANCHAMRUT CHEMICALS | $ 6.756 Bioven Ingredients | $ 4.256 |
| API Grade Bentonite | | | $ 0.250 |
| Starch | $ 0.520 Shree Ram Bio Starch Polymers Private Limited | $ 1.216 Shri Gajanan Laminates | $ 0.868 |
| Potassium Chloride | $ 0.189 Chirag Mineral & Chemicals | $ 0.878 Advance Inorganics | $ 0.533 |

[1USD = Rs.74 was used as the conversion rate]

**Direct Impacts**
- Financial Issues (1m$^3$ = $1000)
- Non-Productive Time (NPT)
- Formation Damage
- Hole Cleaning Problems
- Loss of Formation Evaluation
- Additional Casing String

**Indirect Impacts**
- Kick
- Collapse Issue
- Mechanical Stuck Pipe
- Bit Damage
- Wash Pipe
- Loss of Well
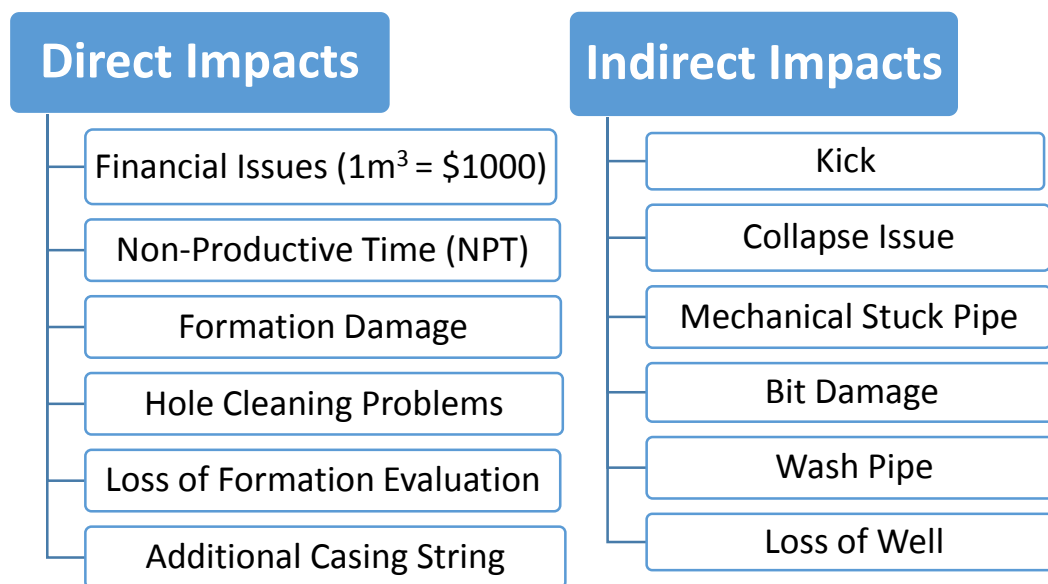
Fig 1. Impact of inappropriate formulation of drilling fluid
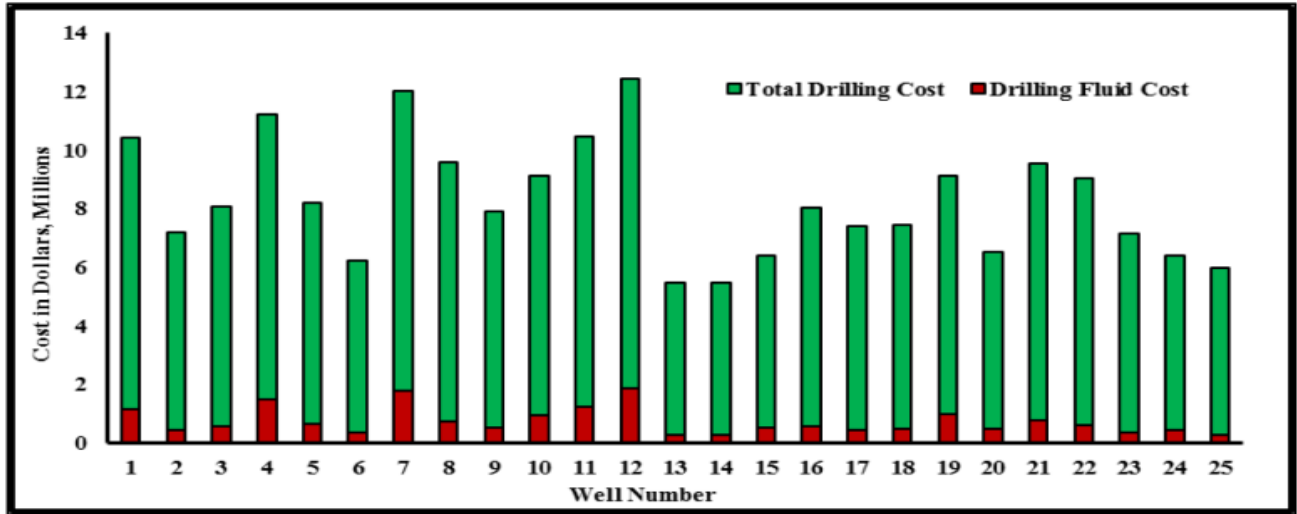
Fig 2. The South Rumaila Field Cost of Drilling Operations (Basra Oil Company, 2018).
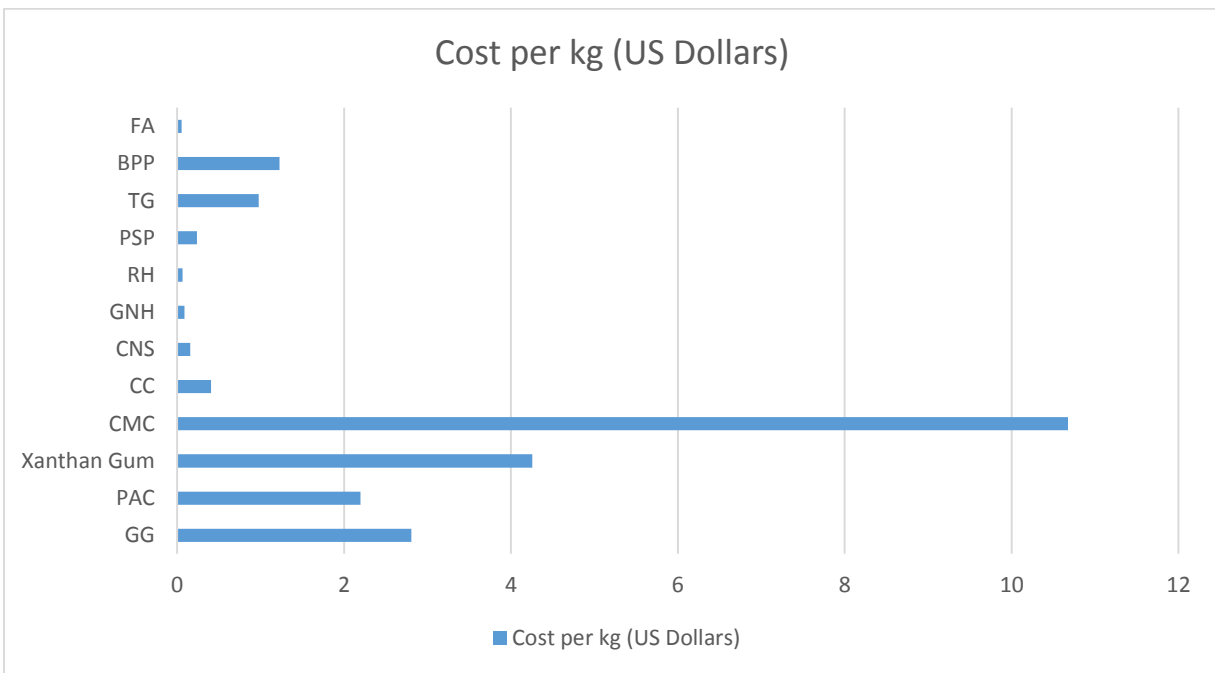


Fig 3. Cost comparison of agro wastes with conventional chemical additives.

# Energy efficient drying of potato chips using microwave

*Dipsa Patel , M S Rao*

*Department of Chemical Engineering, FOT, Dharmsinh Desai University*

## Abstract

Drying or dehydration of food is still a challenging unit operation in Food Processing. The purpose of this study is to compare conventional dryer(tray dryer) to microwave and to investigate the effect of microwave power levels on drying characteristics and quality of product. The drying experiments were conducted with domestic microwave. It was observed that time required to dry potato chips in tray dryer was very high compare to microwave drying. Also case hardening was observed in tray dried samples. The drying of potato slices in microwave was further carried out as time required by microwave for drying was lesser. Potato slices with and without pre-treatments were dried in the microwave. Drying characteristics, re-hydration characteristics and texture analysis of the same was done. It was observed that for microwave at high intensity require minimum drying time. However browning of surface of slices was observed at high intensity. Microwave at 60% intensity, with uniform slice diameter gives slightly better colored slices and drying time require was 14 minutes. Experimental study indicated that the moisture content of the sample decreases with time, Drying rate initially increases and then becomes constant with time. It was also observed that potato slices without any pre-treatment were inferior in appearance (color) than pre treated slices. Also slices dried in microwave on grill were having better acceptability in appearance than slices dried on an elevated plate. So further drying in microwave was carried out on grill only. The best results in terms of acceptability in color and drying time was found in samples treated with 5% NaCl solution and 5% Citric acid solution. Re-hydration characteristics like re-hydration ratio and co-efficient of reconstitution were found better/ higher in microwave dried samples than tray dried samples.

**Key words:** Drying, conventional drying, microwave drying, pre treatment, rehydration characteristics

## 1. Introduction

Drying is one of the oldest methods used for preservation of food sample. By drying moisture is removed from the water. This leads to slow enzymatic activity and ceases the microbial growth in the food sample. The selection of dryer required for drying depends upon the raw material, intermediate product, final product and their characteristics. Along with selection of dryer pre treatment methods are also required to be consider for partial removal of moisture from the food sample. Drying is one of the methods that consume time as well as energy.[1]

Microwave drying is newer addition to the list of conventional drying techniques. Microwave radiations have very wide range of applications in food processing like drying, blanching, cooking, tempering, pasteurization, sterilization, etc [2]. The objective of this study is to compare results of conventional dryer with the microwave dryer and investigate the effect of microwave power levels on drying characteristics as well as quality of the sample ie slices.

## 2. Materials and methods

India is second most producer of potato in the world. According to FAOSTAT India produces 45,343,600 tonnes potatoes per annum. Due to higher moisture content of potatoes it needs to be processed to store. Drying is oldest method followed for preservation of food samples which reduces space required by sample, ease of handling, reduces moisture along with microbial activity, and increases shelf life by decreasing moisture content so it is dried. Hence this study focuses on microwave as well as tray drying of potato chips. Microwave used for batch drying of potato slices was IFB (model no: 30sc3), power output is 900 W and frequency 2450 MHz, Power consumption – convection is 2000 W, Power consumption- microwave is 1400 W, Power requirement- AC 230 V, 50 Hz, Power consumption –grill-1250 W, Capacity – 30L. Venire calipers used to measure dimensions of potato slices was Mahr (16 EX).

Method to be followed for Microwave batch drying of potatoes is mentioned in chart 1. And the pretreatments to be done for potato slices are mentioned in chart 2. Potatoes were washed, peeled and sliced having diameter 3.12 cm and slice thicknesses 2mm , 1.5mm, 0.8mm. 10g of slices were uniformly distributed on grill or plate of microwave. The decrease in weight of slices with 1 min microwave drying was observed.
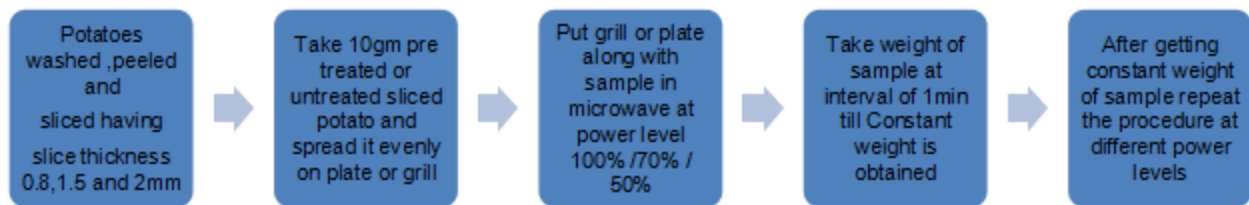


Chart 1. Microwave batch drying method
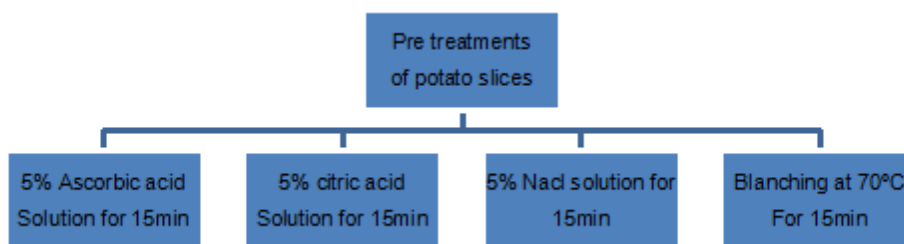


Chart 2. Pre treatments of potato slices

After comparing the results of tray dryer and microwave, microwave dryer was chosen for further work where effect of various parameters on the dried product was studied like: microwave power levels , grill and plate, slice thickness of potatoes, pre treatments.

## 2.1 Theory/calculation

Drying characteristics of the sample, like Moisture content (Dry basis), Drying rate, moisture ratio were obtained from the experiments.

## A. Moisture content

Moisture content is measure of water present in sample. Moisture content gives an idea about shelf life of sample. More the moisture content lesser the shelf life of the sample. Moisture content of a sample depends on porosity of sample as most of the food samples are hygroscopic in nature. Porosity at saturation point also affects rate of drying. Moisture content (MC or M) of sample can be calculated on dry basis (DB) as well as wet basis (WB). Moisture content on wet basis was calculated by using following relation:

M (WB) (%)= [(initial sample wt.- sample wt. at given time)/initial sample wt.]*100

Moisture ratio (MR)= (moisture at any time – equilibrium moisture) / (initial moisture – equilibrium moisture)

## B. Drying rate

It provides information about how moisture content of sample changes with respect to time.

Drying rate= $(M_{t+dt} - M_t)/dt$

Where,

$M_{t+dt}$= moisture content at time t+dt

$M_t$=moisture content at time t

dt=difference of time

Dehydration ratio= wt. of prepared material before drying / wt. of dried material

## C. Shrinkage

Shrinkage is decreasing volume of the food sample due to loss of moisture. Drying causes shrinkage. Specific volume, density and sample porosity is function of pressure and moisture present in the food sample [4]. Decrease in diameter as well as thickness of slices after drying in microwave and tray dryer was analyzed using Digital venire calipers.

% Shrikage (thickness) = ((initial thickness – thickness after drying)/ Initial thickness)*100

% Shrikage (diameter) = ((initial diameter – diameter after drying)/ Initial diameter)*100

## D. Texture and color of slices

Texture is mainly a property related to surface quality which can be sensed by hand, eyes. Texture falls under sensory evaluation. Textural properties are hardness, springiness, gumminess, chewiness, firmness, adhesiveness. These properties can be identified or quantified by shear, tension compression etc tests. Textural properties mainly gives acceptance or rejection to the dried sample [5]. Any pretreatment causes change in color and texture of sample[3]. Blanching at 70ºC to 100 ºC for 15 min causes change in

structure of sample cells and due to which textural properties changes. Acid and salt pretreatment also changes texture as moisture from sample is either removed or gained. Color is also affected by the type of treatment as different treatments have different effects on enzymatic activities/browning of sample[3]. Texture analysis of dried potato slices was done with texture analyzer using Cutting probe. The results were obtained using LLOYD LF1750 texture Analyzer using Nexion software to check viability of the results obtained.

Texture anlyzer basically detects the force applied on dried chips, where a probe is used to rupture the dried chip. The cutting probe was used to know the Hardness of dried chip and force required to rupture the dried chip.

Color of dried slices varies with microwave power level and slice's thickness along with type of pre treatment.

### E. Rehydration characteristics

Rehydration ratio of dried slices can be obtained by immersing the slices in hot water at 100°C for 5 min. Excess water should be drained and weight of sample before and after immersing in water is to be noted.

Rehydration ratio= wt. of rehydrated material / wt. of dehydrated material

Co-efficient of reconstitution = rehydration ratio / dehydration ratio

## 3. Results and Discussion

Drying characteristics along with texture, shrinkage, rehydration characteristics were studied in the present study.

In present study we have carried out drying experiments in tray dryer as well as microwave dryer with and without pre treatments of potato slices. In microwave drying the potato slices were placed on grill and elevated plate for drying where it was observed that the drying of slices on grill was better in reference to case hardening. The potato slices used for drying were 0.8mm, 1.5mm, 2mm thick and the pretreatments done were: (1)Blanching the slices at 70°C for 30minutes, (2) Treating with 5% NaCl solution for 30 minutes (3) Treating with 5% Ascorbic acid solution for 30 minutes (4) Treating with 5% citric acid solution for 30 minutes

Amount of moisture present in the sample with respect to time taken for drying in case of microwave and try drying are presented in Figures (1-2). Based on tray drying and microwave drying data it is observed that the time required for drying in microwave was very small compared to tray drying. Case hardening was observed in tray dried samples.

From Figures 1 and 2 it is observed that for micro with 100% intensity(high) we require minimum drying time. However, browning of sample slice surface was observed at high intensity. It is noted that microwave with 60% exposure time on uniform slice diameter gives slightly better colored slices and drying time require was for this case was found to be 14 minutes.
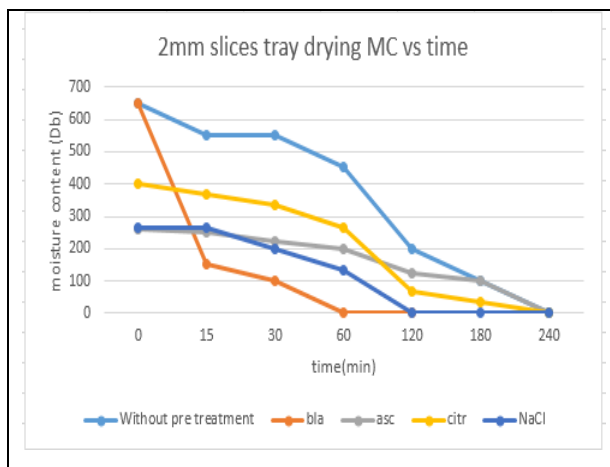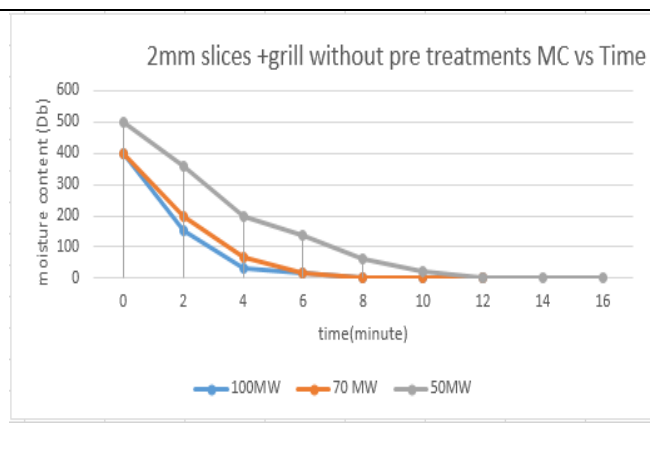
| Figure 1. Moisture Content Vs time graph of 2mm slices after tray drying | Figure 2. Moisture Content Vs time graph of 2mm slices dried in microwave on grill |

Drying rate was calculated for samples dried using try dryer, microwave drying at varies drying intensities, with and without treatment. The results obtained for try drying and microwave with frill are presented in Figures 3 and 4. Results obtained for pre-treated samples are presented in Figure 5. From these figures it is observed that drying rate initially increases and then becomes constant with time. It required less time to dry microwave when we used pre treated potato slices. The best results in terms of acceptability in color and drying time was found in samples treated with 5%NaCl solution and 5% Citric acid solution.
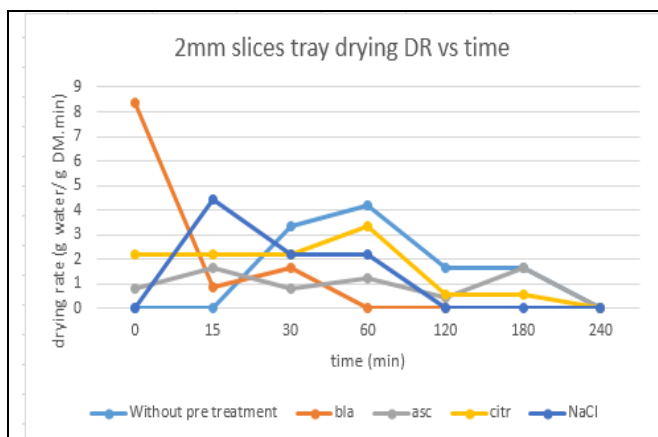


| Figure 3. Drying rate Vs time graph of 2mm slices after tray drying | Figure 4. Drying rate Vs time graph of 2mm slices dried in microwave on grill |
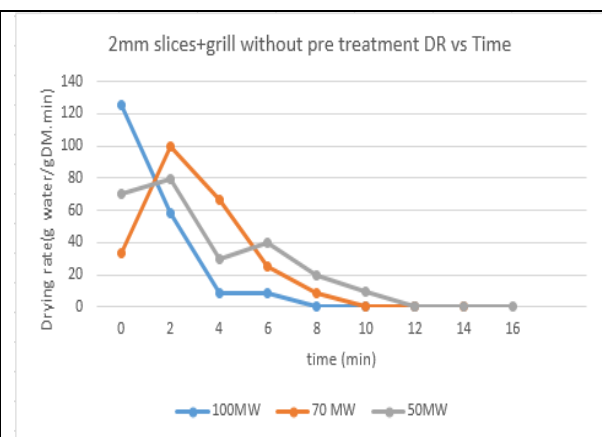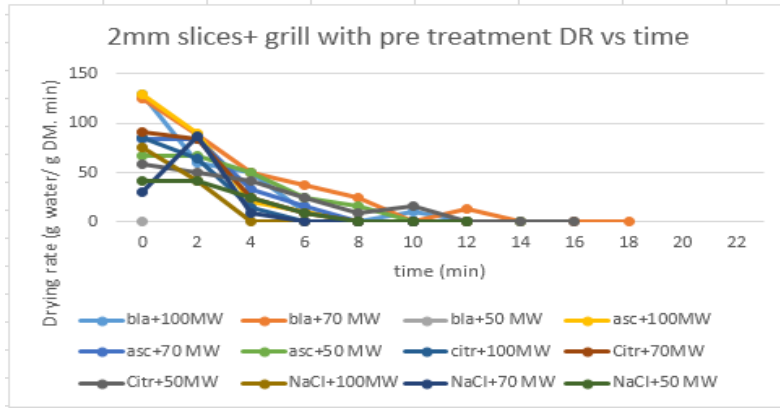
Figure 5. Drying rate Vs time graph of pre treated 2mm slices dried in microwave on grill
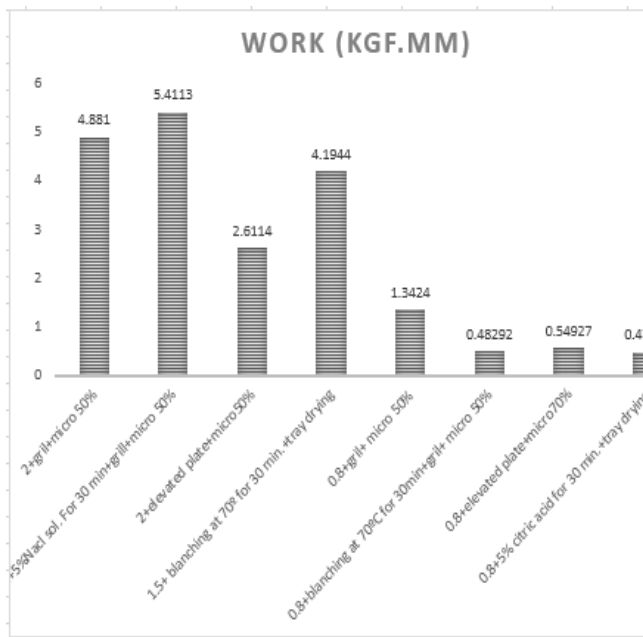




Figure 6. Comparison of work required to have a fracture(rupture) in slice for selected trials of microwave and tray drying
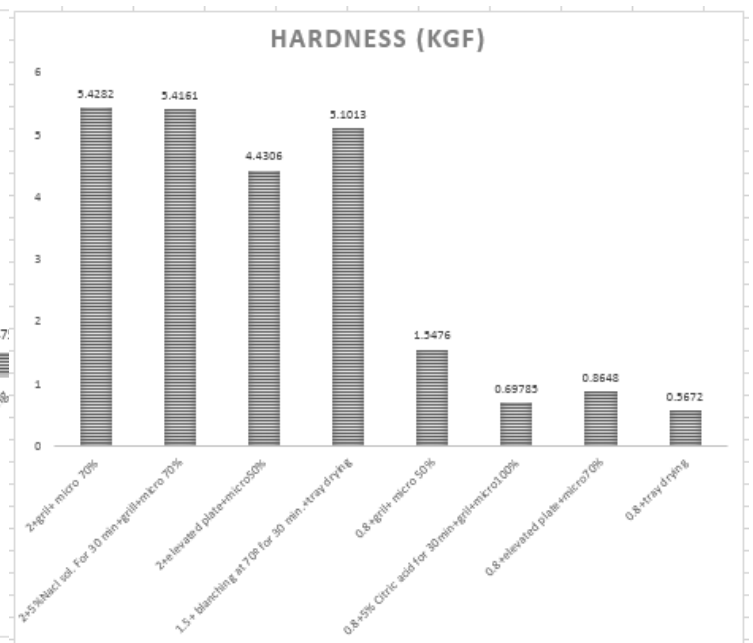
Figure 7. comparison of Hardness of slices for selected trials of microwave and tray drying

**CO-EFFICIENT OF RECONSTITUTION**

Values: 2.52, 3.40, 3.03, 2.67, 1.45, 1.11, 1.59

X-axis labels:
0.8+gril+ micro 50%
0.8+blanching at 70°C for 30min+gril+ micro 50%
0.8+elevated plate+micro70%
0.8+tray drying
0.8+gril+ micro 100%
1.5+5%NaCl sol. For 30 min+grill+micro 100%
1.5+elevated plate+micro100%
0.8+ blanching at 70ᵒ for 30 min



**REHYDRATION RATIO**

Values: 3.29, 4.26, 4.33, 3.08, 2.74, 2.43, 2.8, 1.64

X-axis labels:
0.8+ gril+ micro 50%
+5% Citric acid for 30min+ gril +micro100%
0.8 + elevated plate+micro 70%
0.8+ tray drying
2+ gril+micro 50%
2+ 5%NaCl sol. For 30min+ gril+micro 100%
2+elevated plate+ elevated plate+micro70%
2+ 5% citric acid for 30 min.+tray drying

Figure 8. values of co-efficient of reconstitution for selected trials of microwave drying and tray drying

Figure 9. values of rehydration ratio for selected trials of microwave drying and tray drying

From the texture analysis of potato slices it is concluded that work required to rupture the slice and    hardness of the slice both were find higher in potato slices of thickness 2mm  treated with 5% NaCl solution for 30min and dried on grill at microwave power level 70%.

Rehydration characteristics like rehydration ratio and co-efficient of reconstitution were found better/ higher in microwave dried samples than tray dried samples. Co-efficient of reconstitution and rehydration ratio of blanched potato slices of 0.8 mm thickness dried at microwave power 50% was found to be higher than the rest of the trials potatoes.

## 4. Conclusions

It was observed that time required to dry potato chips in tray dryer ranged from 1 hour-3 hour based on pre treated or non pre treated sample taken. Where as in microwave drying the minimum time required for drying was 4 min using microwave high power and 16 min while using microwave 50% power. It was observed that the pre treated potato slices were better in appearance compared to non pre treated slices. It was also observed that potato slices without any pre treatment were inferior in appearance (color) than pre treated slices. Also slices dried in microwave on grill were having better acceptability in appearance than slices dried on an elevated plate.

## References

[1] Humberto vega Mercado et al. (2001) Advances in dehydration of foods, journal of food engineering 49, 271-289

[2] Witkiewicz K, Nastaj JF (2010) Simulation Strategies in Mathematical Modeling of Microwave Heating in Freeze-Drying Process. Drying Technol 28: 1001-1012.

[3] Risman, P. O. and M. Celuch-Marcysiak. 2000. Electromagnetic modeling for Microwave heating applications. In 13th International Conference on Microwaves, Radar and Wireless Communications. 2000. MIKON-2000.

[4] Journal of Microwave Power and Electromagnetic Energy 39(3/4): 153.

[5] Datta, A. K. and P. M. Davidson. 2000. Microwave and radio frequency processing.Journal of Food Safety 65(s8): 32-41. Ryynänen, S. and T. Ohlsson. 1996. Microwave heating uniformity of ready meals as affected by placement, composition, and geometry. Journal of Food Science 61(3): 620-624.

# VLE Data Prediction under isobaric conditions of a binary mixture n-Hexane and CPME by using UNIFAC Method

Hitesh N. Panchal[1], M S Rao[1, *], Anand P. Dhanwani[1, *]

[1]Chemical Engineering Department, D.D. University, College Road, Nadiad-387 001, Gujarat, India.
* Corresponding author: msrao@ddu.ac.in, apdhanwani.ch@ddu.ac.in,Contact No.: 9909076070.

## Abstract

In this work, vapor-liquid equilibrium (VLE) data for the binary system n-hexane and cyclopentyl methyl ether (CPME) have been predicted under isobaric condition at 101.3 kPa. Universal Functional Activity Coefficient (UNIFAC) method is applied here for the predictions of VLE data. The UNIFAC binary interaction parameters, for ether group ($-CH_3O$) and alkane group (-CH), are taken under consideration for the prediction of VLE data. Gibbs excess models such as Van Laar & Non Random Two liquid (NRTL) models correlation are performed for the predicted VLE data. Regression analysis is also being considered to optimize the binary interaction parameters. All the predicted VLE data were tested to check their thermodynamic consistency by using Herington test method. Efficacy of data fitting is verified by average absolute deviation (AAD) values.

**Keywords:** - Vapor-liquid equilibrium, Green solvents, Cyclopentyl methyl ether, n-Hexane, UNIFAC method, Excess Gibbs models.

## 1. Introduction

Conventional solvents used in chemical industries create many harmful impact to the environment and human health. Green solvents are appearing to be environmentally friendly alternative to the conventional solvents. Cyclopentyl Methyl Ether (CPME) is an ethereal solvent and one of the green solvents that has several good properties such as low solubility in water, boiled at higher temperature, good stability in both acidic and basic medium, produce less peroxide, etc [1]. n-Hexane is a non-polar organic solvent, and used as a chemical reagent in the fields of fine chemicals [2]. CPME can be preferred an alternative for extraction of n-Hexane. As the knowledge of vapor-liquid equilibrium(VLE) data are needed in the design of separation systems mainly the distillation operation, it is imperative to separate the mixture of n-hexane and CPME. After searching DDB [6] and NIST [11], the VLE data of n-Hexane and CPME have not been reported in the literatures. Therefore, the VLE data of this binary system are appeared to be necessary. The solutions-of-groups model is to utilize for predicting phase equilibria of systems for which no experimental VLE data are available [3]. In the present work prediction of VLE data have been done for the binary system n-Hexane (1) and CPME (2) under isobaric condition using group contribution method.

## 2. UNIFAC method as a Tool for the prediction of VLE Data

A group contribution method employed for determination of activity coefficients of non-ideal solution based on the functional-groups with a UNIQUAC (Universal quasi-chemical activity coefficient) theory of liquid mixtures. The resulting model is known as the Universal Functional Activity Coefficient (UNIFAC) model which contains two adjustable parameters per pair of functional groups [4]. It has become a valuable tool in phase equilibrium calculations for systems for which little or no experimental VLE data is available [5].

## 2.1. Universal Functional Activity Coefficient (UNIFAC) method

Following is a multicomponent mixture, the generalized equation of UNIFAC method [5] of component *i* in terms of activity coefficient with the combinatorial and residual contributions:

$$\ln\gamma_i = \ln\gamma_{i(combinatorial)} + \ln\gamma_{i(residual)} \tag{1}$$

Where,

$$\ln\gamma_{i(combinatorial)} = 1 - V_i + \ln V_i - 5q_i\left(1 - \frac{V_i}{F_i} + \ln\left(\frac{V_i}{F_i}\right)\right) \tag{2}$$

$$V_i = \frac{r_i}{\sum_j X_j R_j} \tag{3}$$

$$r_i = \sum V_k^{(i)} R_k \tag{4}$$

$$F_i = \frac{q_i}{\sum_j X_j q_j} \tag{5}$$

$$q_i = \sum V_k^{(i)} Q_k \tag{6}$$

Where, $V_k^{(i)}$, is an integer, the number of groups of type k in molecule i. The group parameters $R_k$ and $Q_k$ are evaluated from the Van der Waals group volume $V_{wk}$ and surface areas $A_{wk}$. Most of other parameters are calculated in residual part as following [12]:

$$\ln\gamma_{i(residual)} = \sum_k V_k^{(i)}\left(\ln\Gamma_k - \ln\Gamma_k^{(i)}\right) \tag{7}$$

Where,

$$\ln\Gamma_k = Q_k\left(1 - \ln(\sum_m \theta_m\Psi_{mk}) - \sum_m \frac{\theta_m\Psi_{km}}{\sum_n \theta_n\Psi_{nm}}\right) \tag{8}$$

Here, $\Gamma_k$ is the group residual activity coefficient. Where $\Gamma_k^{(i)}$ is the residual activity coefficient of group k in a reference solution containing only molecule of type i.

The Eq.(9), $\theta_m$ is the area fraction of group m and Eq.(10), $X_m$ is the mole fraction of group m in the mixture. The group-interaction parameter $\Psi_{nm}$ is given by equation(11).

$$\theta_m = \frac{Q_m X_m}{\sum_n Q_n X_n} \tag{9}$$

$$X_m = \frac{\sum_j V_m^{(j)} X_j}{\sum_j \sum_n V_n^{(j)} X_j} \tag{10}$$

$$\Psi_{nm} = \exp\left(-\frac{U_{mn} - U_{nn}}{RT}\right) = \exp\left(-\frac{a_{nm}}{T}\right) \tag{11}$$

$U_{mn}$ is measure of the energy of interaction between groups m and n. The group interaction parameters $a_{mn}$ must be evaluated from experimental data having units of kelvins it is to be noted that the $a_{mn} \neq a_{nm}$. The binary interaction parameters of UNIFAC model are completely independent of temperature.

## 2.2. Group identification for n-Hexane and CPME:

The identification of functional groups for UNIFAC method is done from the literature [5] and presented in Table 1.

**Table 1. Group identification for n-Hexane and CPME**

| Component(i) | Name | M* | S* | $v_k$ (i) | $R_k$ | $Q_k$ |
|---|---|---|---|---|---|---|
| **n-Hexane(1)** | CH₃ | 1 | 1 | 2 | 0.9011 | 0.8480 |
| | CH₂ | 1 | 2 | 4 | 0.6744 | 0.5400 |
| **CPME (2 )** | CH₂ | 1 | 2 | 4 | 0.6744 | 0.5400 |
| | CH | 1 | 3 | 1 | 0.4469 | 0.2280 |
| | CH₃O | 13 | 25 | 1 | 1.1450 | 1.0880 |

## 2.3. Binary Interaction Parameters (BIPs)

UNIFAC method, Binary interaction parameters ($a_{mn}$) are obtained from the literature [5] and given in Table 2.

**Table 2. BIPs for n-Hexane and CPME**

| Group | CH₂ | CH | OH | CH₃O |
|---|---|---|---|---|
| **CH₃** | 0.0 | 0.0 | 0.0 | 251.5 |
| **CH₂** | 0.0 | 0.0 | 0.0 | 251.5 |
| **CH** | 0.0 | 0.0 | 0.0 | 251.5 |
| **CH₃O** | 83.36 | 83.36 | 83.36 | 0.0 |

## 2.4. Calculation of VLE data using Group contribution UNIFAC method

The VLE data for binary system n-Hexane(1) and CPME(2) are calculated through a spread sheet prepared in Microsoft Excel, in which temperature T and $x_1$ are given as input ,where $\gamma_1$ and $\gamma_2$ are calculated using UNIFAC method as described in the previous sections. Antoine Eq.(12) is applied to calculate $p_1^{sat}$ and $p_2^{sat}$. Total pressure P and correct temperature T are obtained by regression using Eq. (15). The generated data are presented in Table 3 using UNIFAC method.

**Table 3. VLE data of n-Hexane and CPME at 101.3kPa**

| T/ K | $x_1$ | $y_1$ | $\gamma_1$ | $\gamma_2$ |
|---|---|---|---|---|
| 379.15 | 0.0000 | 0 | -- | 1.0000 |
| 372.63 | 0.1000 | 0.3257 | 1.3596 | 1.0038 |
| 367.63 | 0.2000 | 0.5372 | 1.2779 | 1.0156 |
| 363.18 | 0.3000 | 0.6764 | 1.2088 | 1.0358 |
| 359.20 | 0.4000 | 0.7693 | 1.1511 | 1.0650 |
| 355.62 | 0.5000 | 0.8330 | 1.1037 | 1.1042 |
| 352.37 | 0.6000 | 0.8787 | 1.0659 | 1.1547 |
| 349.41 | 0.7000 | 0.9137 | 1.0369 | 1.2181 |
| 346.69 | 0.8000 | 0.9432 | 1.0164 | 1.2966 |
| 344.19 | 0.9000 | 0.9709 | 1.0041 | 1.3931 |
| 342.15 | 1.0000 | 1.0000 | 1.0000 | -- |

$$\ln p_i^{sat} = A_i - \frac{B_i}{T + C_i} \tag{12}$$

Here, Pressure in kPa and Temperature is in K. The Antoine equation parameters A, B and C of n-Hexane and CPME are listed [11] in Table 4.

**Table 4. Coefficient of Antoine's equation for n-Hexane and CPME**

| Component | Antoine constants | | | Temperature range/ K |
|---|---|---|---|---|
| | A | B | C | |
| n-Hexane | 4.0026 | 1171.5300 | -48.7840 | 286 to 342 |
| CPME | 3.6039 | 216.7424 | -242.9250 | 357 to 378 |

## 3. Thermodynamic Consistency Test of the predicted VLE data

In this paper, semi-empirical method reported by Herington is employed to examine the thermodynamic consistency of VLE data for the binary system [8]. The basic criteria of consistency of this method is that the value of D-J should not be greater than 10. D and J are obtained by Eq. (13) and (14) respectively. The values of D-J for the binary system are listed in Table 5.

$$D = 100 \frac{\left| \int_{x_1=0}^{x_1=1} \ln \frac{\gamma_1}{\gamma_2} dx_1 \right|}{\int_{x_1=0}^{x_1=1} \left| \ln \frac{\gamma_1}{\gamma_2} \right| dx_1} \tag{13}$$

$$J = 150 \frac{T_{max} - T_{min}}{T_{min}} \tag{14}$$

**Table 5. Thermodynamics consistency check by Herington Test**

| D | J | \|D-J\| | Method | Result |
|---|---|---|---|---|
| 6.3825 | 16.2210 | 9.8385 | UNIFAC | Pass |

## 4. Data reduction using $g^E$ models

The predicted VLE data are correlated using activity coefficient models such as Van Laar [9] and NRTL [10] equations. The pure components saturated vapor pressures are calculated by using Eq. (12). The regression analysis was done for optimize the BIPs by minimization of the objective function %AAD $\sum(\delta P)$. Similarly, AAD$\sum(\delta T)$ and AAD $\sum(\delta y)$ are calculated by Eq. (16) and Eq. (17) respectively. The subscript "pred." and "cald." mean the predicted and calculated data respectively, AAD, Absolute Average Deviation & n represent the number of predicted data points.

.

$$\%AAD \sum(\delta P) = \frac{100}{n} \sum_{i=1}^{n} \frac{|P_{i,pred.} - P_{i,cald.}|}{P_{i,cal.}} \tag{15}$$

$$AAD \sum(\delta T) = \frac{1}{n} \sum_{i=1}^{n} |T_{i,pred.} - T_{i,cald.}| \tag{16}$$

$$AAD \sum(\delta y) = \frac{1}{n} \sum_{i=1}^{n} |y_{i,pred.} - y_{i,cald.}| \tag{17}$$

The correlated BIPs from predicted VLE data by UNIFAC method are shown in Table 6. α is the characteristic constant of the non- randomness for the binary system. The value of α was fixed at 0.3 according to the definition in the literature [10]. The comparison of predicted data by UNIFAC method with calculated data by Van Laar, and NRTL models for binary system n-Hexane (1) + CPME (2) at 101.3 kPa is shown through Figure 1 to 5.

**Table 6. Correlated models BIPs from predicted data by UNIFAC model**

| Model | Binary Parameter | | AAD (Δy) | AAD (ΔT) |
|---|---|---|---|---|
| **Van Laar** | $A_{12}$ | $A_{21}$ | 0.0010 | 0.0021 |
| | 0.3927 | 0.3924 | | |
| **NRTL** | $b_{12}$ | $b_{21}$ | 0.0484 | 0.2159 |
| | 5075.4519 | -3275.7406 | | |

α = 0.3 for NRTL Model

## 5. Results and discussions

From Figures 1, 2 and 3, it can be clearly seen that isobaric VLE data of binary system n-Hexane(1) and CPME(2) are meeting with predicted value using UNIFAC method. Moreover, Figures 4 and 5, clearly indicate that the data predicted by UNIFAC method is compared with NRTL and Van Laar model.

The system under consideration n-Hexane(1) and CPME(2) have different dipole moments and sizes. The dipole moments for n-Hexane (1) and CPME (2) are: 0.08[13] and 1.27 [14] respectively. The system i.e., n-Hexane + CPME expected to favor the like interactions, since one component is moderately polar and the other is nonpolar. From Figure 4, it can be seen that the vapor phase predictions are satisfactory for dilute mixtures. However, for higher concentration mixtures NRTL model is under predicting vapor phase composition. Similar trend was observed by Socrates Ioannidis (1996) for R14, R23 refrigerants with dipole moments of 0, 1.65[15] respectively. However, from the results presented in Figure 5 it can be observed that vapor phase composition predictions using Van Laar model are better.
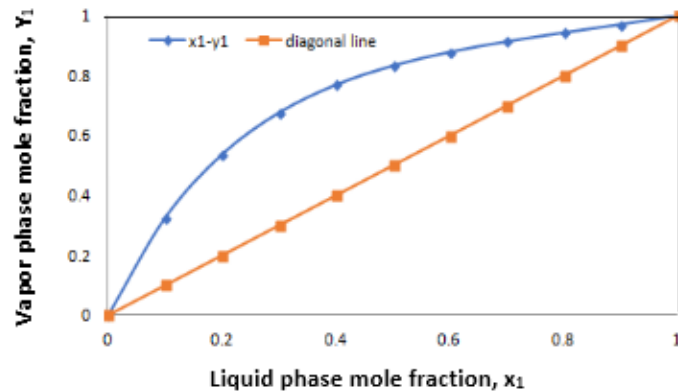


**Figure 1. $x_1$-$y_1$ Diagram for the predicted data of n-Hexane/CPME system**
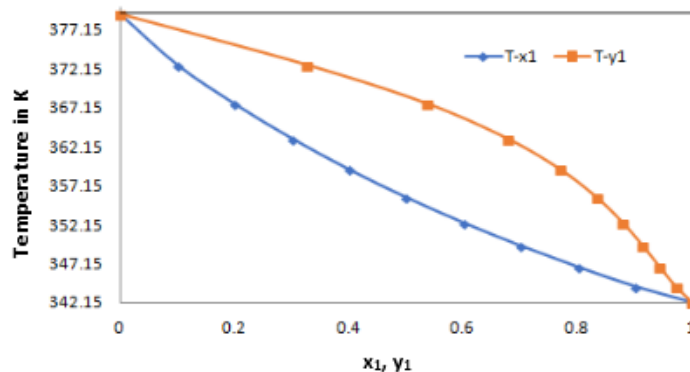


**Figure 2. T-$x_1$-$y_1$ Diagram for the predicted data of n-Hexane/CPME system**
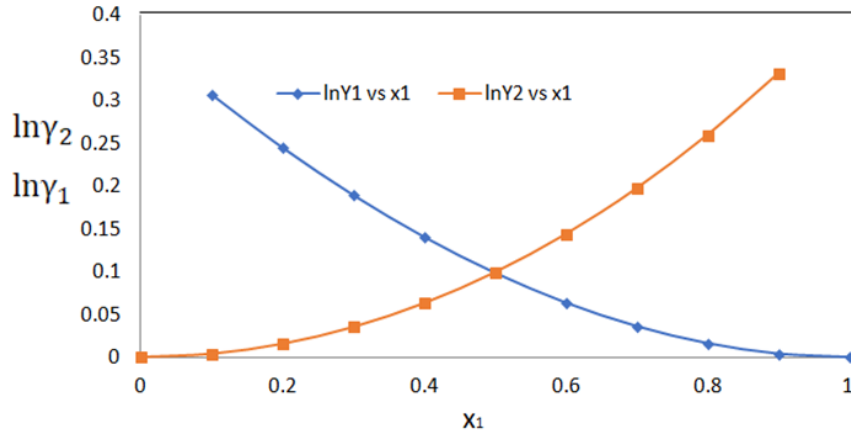
**Figure 3. $\ln\gamma_1$ vs $x_1$ & $\ln\gamma_2$ vs $x_1$ Diagram for the predicted data of n-Hexane/CPME system**
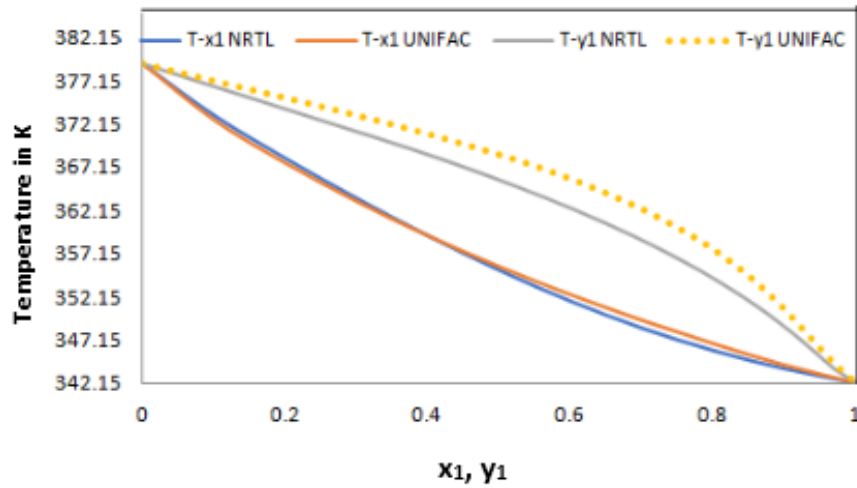


**Figure 4.T-x1-y1 Diagram for the data calculated by NRTL model and predicted by UNIFAC method**
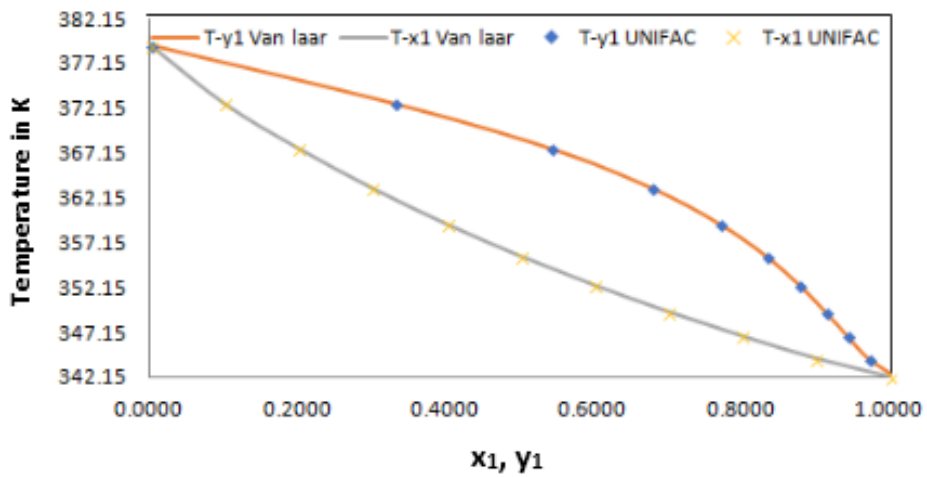


**Figure 5.T-x1-y1 Diagram for the data calculated by Van Laar model and predicted by UNIFAC method**

## 6. Conclusions

The VLE data for the binary system n-Hexane with CPME have been predicted at 101.3kPa by using UNIFAC method. Herington's test confirms the thermodynamic consistency of VLE data, which were predicted by UNIFAC method. The activity coefficient models Van Laar and NRTL were completely fitted with these predicted data by UNIFAC method. It is observed that Van Laar model is found to be better compared to NRTL model for the system under consideration. From the simulation study it was found that the n-Hexane/CPME binary system does not form azeotrope indicating feasibility of separation system design.

## Nomenclature and units

n = no. of predicted data points
P = Absolute pressure, kPa
T = Absolute temperature, K
$Q_k$ = Van der Waals surface area of subgroup k
$r_i$ = Van der Waals volume of component i
$V_i$ = Volume/ mole fraction of component i in the mixture
$q_i$ = Van der Waals surface area of compound i
ln = Natural logarithm (base e)
xi = mole fraction of $i^{th}$ component in the Liquid phase
yi = mole fraction of $i^{th}$ component in the Vapor phase
Γ = Temperature dependant integration constant
$\gamma_i$ = Activity coefficient of $i^{th}$ component
Aij = Adjustable parameters (Van laar model)
bij = Adjustable parameters (NRTL model)
$F_i$ = Surface area fraction of component i in the mixture
A, B, C = Coefficient of Antoine equation Eq. (12)

## Abbreviations

DDB = Dortmund data bank
NIST = National Institute of Standards & Technology

## Superscripts

E = Excess property
Sat = Saturated condition

## Subscripts

1 = Component 1
2 = Component 2
i = Property of $i^{th}$ component

## References

[1] Watanabe, K., Yamagiwa, N., Torisawa, Y.,2007. Cyclopentyl methyl ether as a new and alternative process solvent. Organic Process Research & Development. 11(2), 251–258.

[2] Sun, Y., Fu, D., Ma, S., Ma, Z., Sun L.,2018. Isobaric vapor–liquid equilibrium data for two binary systems n-hexane + 1,2-dimethoxyethane and methylcyclopentane + 1,2-dimethoxyethane at 101.3 kPa. Journal of Chemical and Engineering Data. 63(2), 395–401.

[3] Lohmann, J. Joh, R., Gmehling, J.,2001. From UNIFAC to modified UNIFAC (Dortmund). Industrial & Engineering Chemistry Research. 40(3), 957–964.

[4] Fredenslund, A., Jones, R.L., Prausnitz, J.M., 1975. Group-Contribution Estimation of Activity Coefficients in Non-ideal Liquid Mixtures. J. AlChE. 21 (6), 1086–99.

[5] Poling,B.E.,Prausnitz J.M.,O'Connell, J. P.,2012. The properties of gases and liquids. fifth ed. The McGraw-Hill Company limited. New York.

[6] Gmehling, J., Onken, U.,2020. Dortmund Data Bank (DDB) The University of Dortmund. http://www.ddbst.com/ddb.html (accessed March 3, 2020).

[7] Smith, J.M., Van ness, H.C., Abbott, M.,2004. Introduction to Chemical Engineering Thermodynamics. McGraw-Hill: New York.

[8] Herington, E. F. G.,1951. Tests for the consistency of experimental isobaric vapor-liquid equilibrium data. Journal of Institute of Petroleum. 37, 457–70.

[9] Gmehling et al.,1993. A modified UNIFAC model. 2. Present parameter matrix and results for different thermodynamic properties. Industrial & Engineering Chemistry Research. 32(1), 178–193.

[10] Renon,H., Prausnitz, J. M.,1968. Local compositions in thermodynamic excess functions for liquid mixtures.14(1),135-144. (doi:10.1002/aic.690140124)

[11] The NIST Bank,2020. National Institute of Standards and Technology(NIST). http://trc.nist.gov/thermolit/main/home.html (accessed March 3, 2020).

[12] Bondi, A.,1968. Physical Properties of Molecular Crystals, Liquids and Glasses Wiley. New York.

[13] Solvent Physical Properties. Retrieved February 21, 2021, from Umass.edu website: https://people.chem.umass.edu/xray/solvent.html.

[14] Cyclopentyl methyl ether (CPME). Retrieved February 21, 2021, from Lobachemie.com website: https://www.lobachemie.com/cpme/cyclopentyl-methyl-ether-CPME.aspx.

[15] Stroem, K., Gren, U., Ljungkvist, K, 1989. Representation of vapor-liquid equilibrium data for binary refrigerant mixtures. Journal of Chemical and Engineering Data. 34(2), 252–257.

# Thermal degradation kinetics of polypropylene under pyrolytic condition

*Ved Tripathi* *

Department of Chemical Engineering, Dharmsinh Desai University, Nadiad-387 001 , Gujarat, India

*Corresponding author: vedtripathi.ch@ddu.ac.in; Mobile no.: +91 9717254944

---

## Abstract

Study of thermal behaviour of polymers under pyrolytic condition is essential for recovering value from polymers through pyrolysis. In this study the thermal decomposition behaviour of polypropylene (PP) was investigated under inert condition by dynamic thermogravimetric analysis (TGA) in the temperature range of 471 K -716 K at heating rate of 10 K/min. Kinetic parameters such as activation energy and rate constant are calculated by Coats-Redfern's model fitting method. The aim of the study was to find out the model/method which can reliably predict the kinetic parameters for pyrolysis of polypropylene. Models based on Order of reaction, exponential nucleation, random nucleation and nuclei growth, diffusion controlled, and phase boundary controlled models were investigated in this study. Diffusion controlled model by Janders and Crank gave the value of $R^2 = 0.985$ for both the models for conversion($\alpha$) range from $2.7 \times 10$ -6 to 0.9997. The values of activation energy( $E_a$ ) and pre-exponential factor(A) for the Janders' model was found out to be 205.7 kJ/mol and $1.25 \times 10^{14}$ min$^{-1}$respectively and for Crank's model was found out to be 202.7 kJ/mol and $6.237 \times 10^{13}$ min$^{-1}$respectively, for the conversion range.

Keywords : pyrolysis, kinetics, polypropylene, thermogravimetric analysis, Coats-Redfern

---

## Introduction

Modern societies are still largely dependent on fossil fuels for deriving energy and other products. A broad range of applications of plastics in form of packaging films, wrapping materials, shopping and garbage bags, fluid containers, clothing, toys, household and industrial products, and building materials. Municipal solid waste generated has a large proportion of plastic.

In 2018-19, the estimated plastic waste generation in India was 33,60,043 TPA.(CPCB, 2018-19) Globally, plastic's production was over 150 million tonnes per year and in India approximately 8 Million tonnes of products made from plastics (2008) which was expected to rise 12 milllion tones by 2012. It is important to mention that no authentic estimation is available on total generation of plastic waste in the country however, considering that 70% of total plastic consumption is discarded as waste, approximately 5.6 million tons per annum (TPA) of plastic waste was generated in 2008, which is about 15342 tons per day (TPD). Tackling such a large plastic waste generation in a sustainable way remains a problem due to the heterogeneity of the waste.

Plastics degrade extremely slow and remains as it is on land, drainage systems or water-bodies, for several years. Further, due to mixing of colour, additives, stabilizers, flame retardants, the recycling of waste plastic is comparitively more harmful than that of virgin plastic. The strength of plastic material is reduced due to thermal degradation every time recycling operation is performed and thus recycling of a virgin plastic material can only be done 2-3 times. The plastic disposal through incineration is one option to reduce the volume of waste plastic generated, though it is not the preferred option in India as it releases toxic gases like chlorinated dioxins and furans, raises several environmental issues. Currently plastic waste accumulation, in several states and union territories of India, is being mitigated by the following ways:

- cement plants for co-processing
- for polymer bitumen road construction
- recycling the plastic waste
- Refuse-Derived Fuel (RDF)

Pyrolysis is a thermochemical process, which has the inherent advantage of high flexibility with respect to feedstock characteristics, so it can be applied to plastic mixtures with contaminants. In the pyrolysis process, not only industrial plastic waste mixtures but also the plastic mixtures present in municipal solid wastes can be used. This is the main advantage of this process.
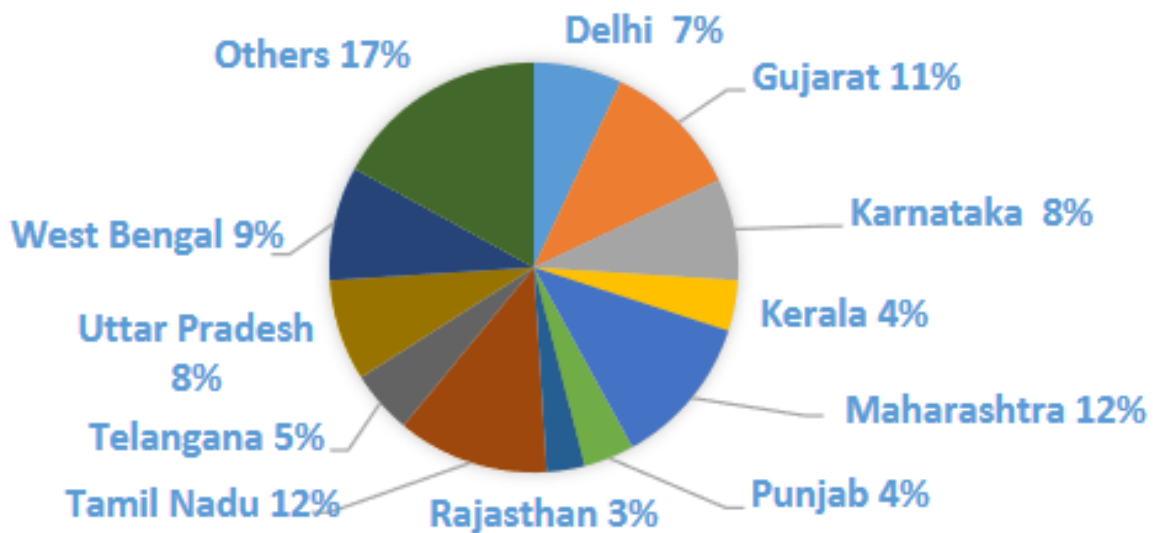


Figure 1: State/UT-wise plastic waste generation in India (CPCB, 2018-19)

**Theoretical approach**

The decomposition of waste plastic during non-isothermal pyrolysis can be represented by the following reaction:

A( solid ) → B( solid ) +C( gas )　　　　　　　　　　　　　　　　　　　　　(1)

The rate of decomposition of waste plastic can be represented in form of conversion (α):

$$\alpha = \frac{W_0 - W_t}{W_0 - W_f}$$　　　　　　　　　　　　　　　　　　　　　(2)

where ;

$W_0$= initial weight of the sample;

$W_f$ = final weight of the sample;

$W_t$= weight of the sample at any time t, $t_0 \le t \le t_f$

The rate of change of fractional conversion, r, can be expressed as a funtion of

$$r = d\alpha/dt = k(T) f(\alpha)$$　　　　　　　　　　　　　　　　　　　　　(3)

$$k(T) = A e(-E_a/RT)$$　　　　　　　　　　　　　　　　　　　　　　　　(4)

where A is the pre-exponential factor

E a is the activation energy

R is the universal gas constant

T is the absolute temperature

f( α ) is a function of kinetic mechanism dependent on conversion

Many authors have substituted this function as following:

$$f(\alpha) = (1 - \alpha)^n$$　　　　　　　　　　　　　　　　　　　　　　　(5)

For non-isothermal condition the rate of change of temperature with respect to time is β , expressed as:

$$T = T_0 + \beta t$$　　　　　　　　　　　　　　　　　　　　　　　　　　　(6)

$$\beta = dT/dt$$　　　　　　　　　　　　　　　　　　　　　　　　　　　　(7)

Substituting k( T ) , f( α ) and β in equation (2), we get:

$$d\alpha/dt => \beta \, d\alpha/dT = A e^{(-E_a/RT)} (1 - \alpha)^n$$　　　　　　　　　　(8)

Rearranging the terms, we can write equation (7) as:

$$d\alpha/(1 - \alpha)^n = A \beta \, e^{(-E_a/RT)} dT$$　　　　　　　　　　　　　　(9)

Integrating the left hand side of equation (9) over a range of conversion from 0 to $\alpha$ , we get:

$$g(\alpha) = \int_0^\alpha d\alpha/f(\alpha) = \int_0^\alpha d\alpha/(1-\alpha)^n \tag{10}$$

$$\int_0^\alpha d\alpha/(1-\alpha)^n = [1-(1-\alpha)^{1-n}]/(1-n) \tag{11}$$

Integrating the right hand side of equation (9) over a range of temperature from $T_0$ to $T_\alpha$, we get:

$$g(\alpha) = \int_{T_0}^{T_\alpha} \frac{A\, e^{(-E_a/RT)}}{\beta} \, dT \tag{12}$$

Considering a constant $\beta$ and A independent of change in temperature we can write the following equation:

$$g(\alpha) = \frac{A}{\beta} \int_{T_0}^{T_\alpha} e^{(-E_a/RT)} \, dT \tag{13}$$

$$= [1-(1-\alpha)^{1-n}]/(1-n) = = \frac{A}{\beta}[\int_0^{T_\alpha} e^{(-E_a/RT)} - \int_0^{T_0} e^{(-E_a/RT)}]\, dT \tag{14}$$

If E a /RT is replaced by x and the limits are transformed

$$x = \frac{E_a}{RT} \Rightarrow dx = \left(-\frac{E_a}{RT^2}\right) dT$$

$$\Rightarrow dT = -\frac{RT^2}{E_a} dx \Rightarrow dT = \left(-\frac{E_a}{Rx^2}\right) dx$$

Transformation of limits : As $T \to T_0$ ; $x \to \frac{E_a}{RT_0}$ and $T \to T_\alpha$ ; $x \to \frac{E_a}{RT_\alpha}$

Considering $\frac{E_a}{RT_0} = x_0$ and $\frac{E_a}{RT_\alpha} = x_\alpha$ , we get

$$g(\alpha) = \frac{AE_a}{R\beta} p(x) \tag{15}$$

Equation 15 (Flynn and Wall, 1966) involves an assumption that E a must be a constant with respect to $\alpha$ and as p( x ) has no analytical solution but has many approximations. Thus through series expansion g( $\alpha$ ) can be approximated, when value of E a is not known a priori, as in equation 16 (Coats and Redfern, 1964) and in equation 17 Agrawal et al. (1987) as following:

$$= [1-(1-\alpha)^{1-n}]/(1-n) = \frac{ART^2}{\beta E_a}\left[1-\frac{2RT}{E_a}\right] e^{(-E_a/RT)} \tag{16}$$

$$\frac{A}{\beta}\int_{T_0}^{T_\alpha} e^{(-E_a/RT)} \, dT = \frac{ART^2}{\beta E_a}\left[\frac{1-2(RT/E_a)}{1-5(RT/E_a)^2}\right] e^{(-E_a/RT)} \tag{17}$$

$$ln \frac{g(\alpha)}{T^2} = ln\left[\left[1-(1-\alpha)^{1-n}\right]/(1-n)\right] \tag{18}$$

Applying logarithm over Coats and Redfern approximation, eqn. 16, we get:

$$ln \frac{g(\alpha)}{T^2} = ln\left[\frac{AR}{\beta E_a}(1-2(RT/E_a))\right] - E_a/RT \tag{19}$$

A plot of $ln \frac{g(\alpha)}{T^2}$ vs 1/T , as in equation 19 is of the form y = mx + c where:

$$y = ln \frac{g(\alpha)}{T^2};$$

$$m = [- E_a/R];$$

x = 1/T, and can be approximated further as:

$$ln \frac{g(\alpha)}{T^2} = ln\left[\frac{AR}{\beta E_a}\right] - E_a/RT \tag{20}$$

**Materials and method**

The samples of polypropylene were procured from the Baikampady industrial estate near Surathkal, Karnataka. The waste PP was cut into small flakes of size < 5 - 10 mm was utilized for pyrolysis in a 10 Kg reactor and sample with size range < 1mm was taken for the purpose of performing TGA at Department of Chemical engineering, National Institute of Technology, Karnataka. A sample weight of 21.960 mg was taken for TGA, which was performed in the temperature range of 303 - 1173 K with a β =10 K/min under inert condition for which nitrogen gas was utilized. Thermal degradation of polypropylene started around 471 K ( α > 0) and near 715 K (α ≈ 1).

**Results**

The pyrolysis of polypropylene initiated around 471 K and has a sigmoidal curve as the temperature is increased and the conversion tends to 1 around 715 K. The data from TGA, given in Figure 1, was analyzed and plots of $ln \frac{g(\alpha)}{T^2}$ vs 1/T were used to find out the best fit model for pyrolysis of PP.
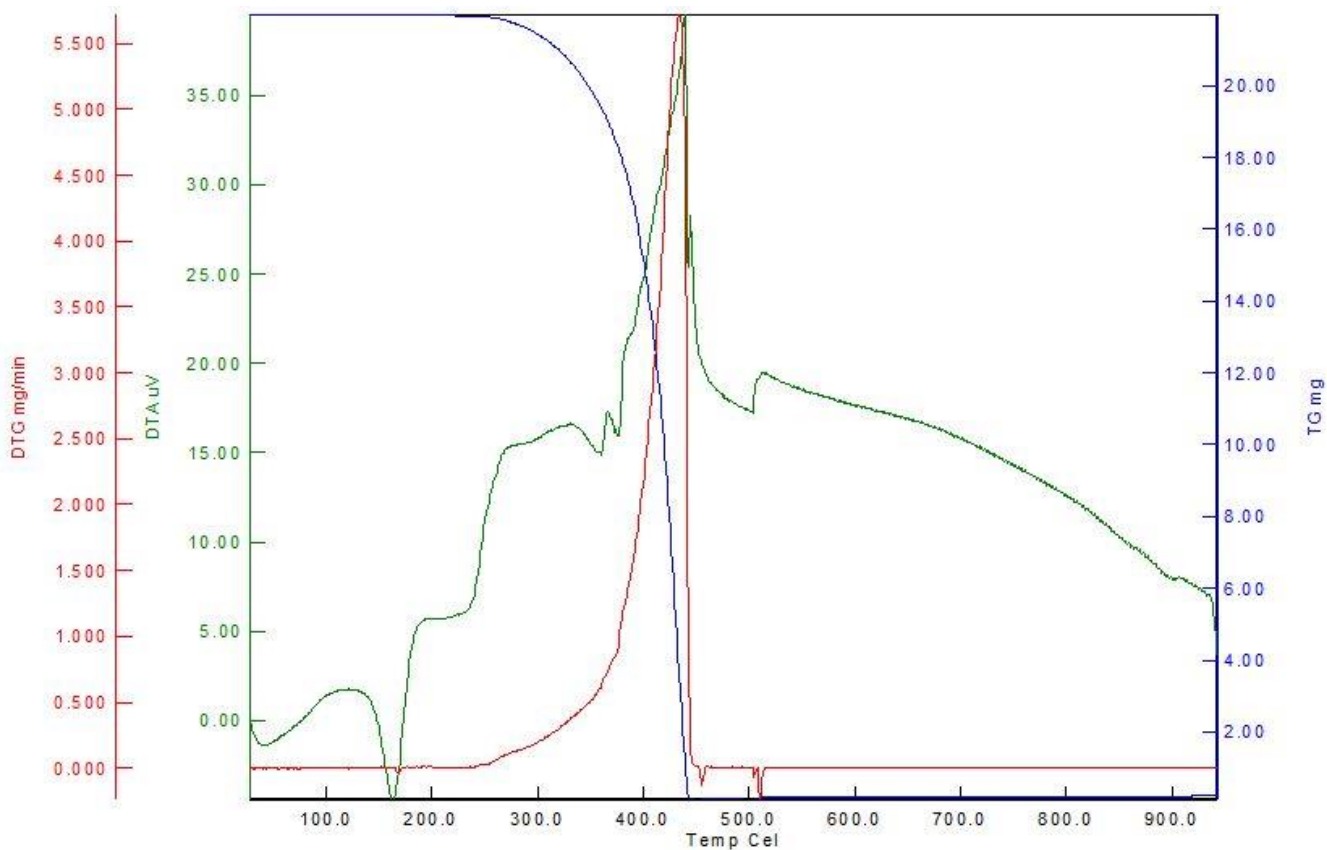
Figure 1: TGA plot obtained for PP (303 - 1173 K)

## Conclusion

From the various solid state reaction equations investigated in this study, the best fit for pyrolysis of waste polyproylene was found to be diffusion controlled model proposed by Valensi, Jander and Crank/Ginstling-Braunshtein, although one dimensional (parabolic law) and phase boundary controlled reaction models also have a good coefficient of determination. Coats and Redfern approximation was used to find out the values for $E_a$ and A, which suggests that the thermal degradation kinetics of polypropylene(PP) to be diffusion controlled.
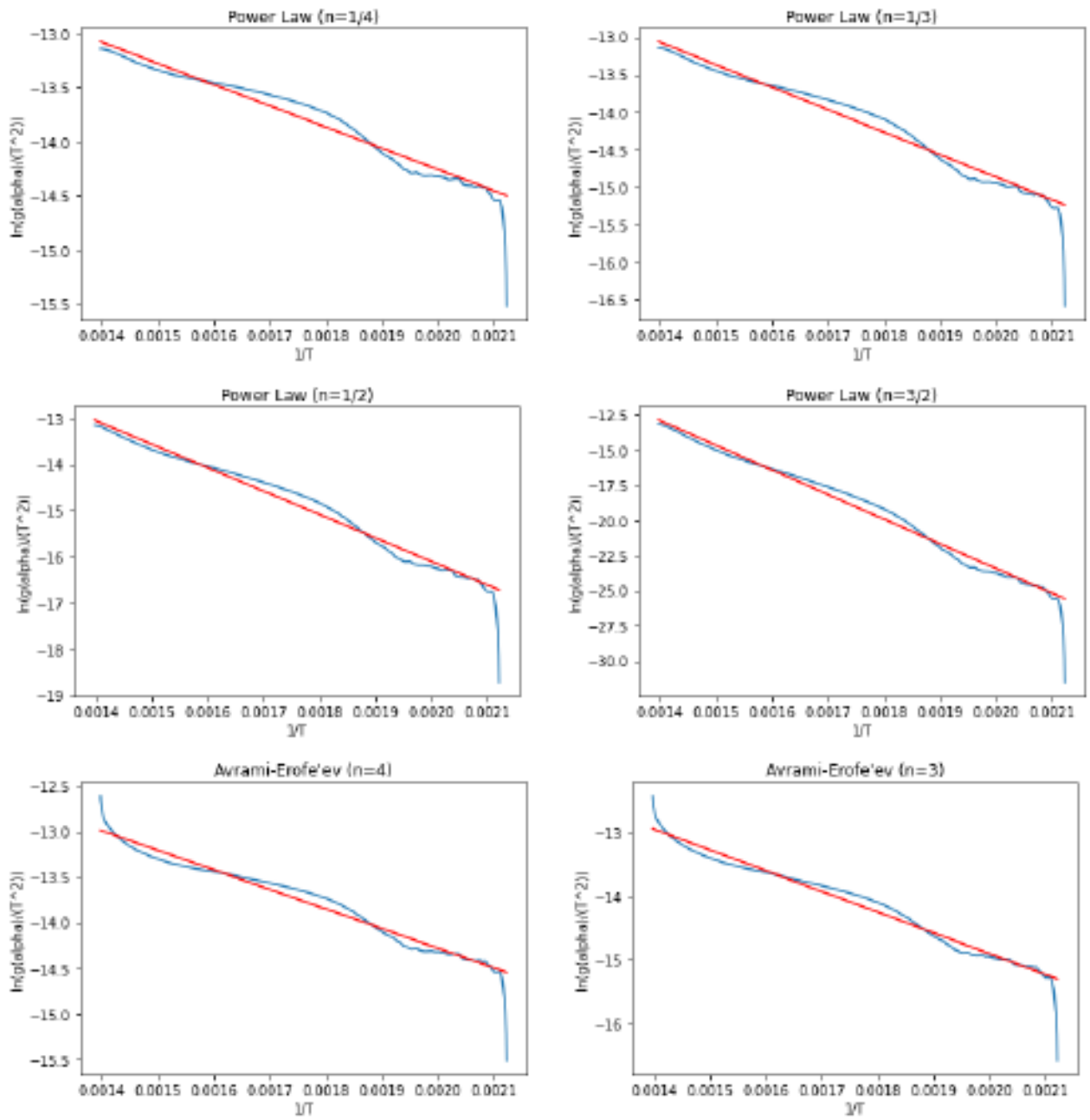
Figure 2: Plots of ln ( g( α ) T 2 ) vs 1 T for various models
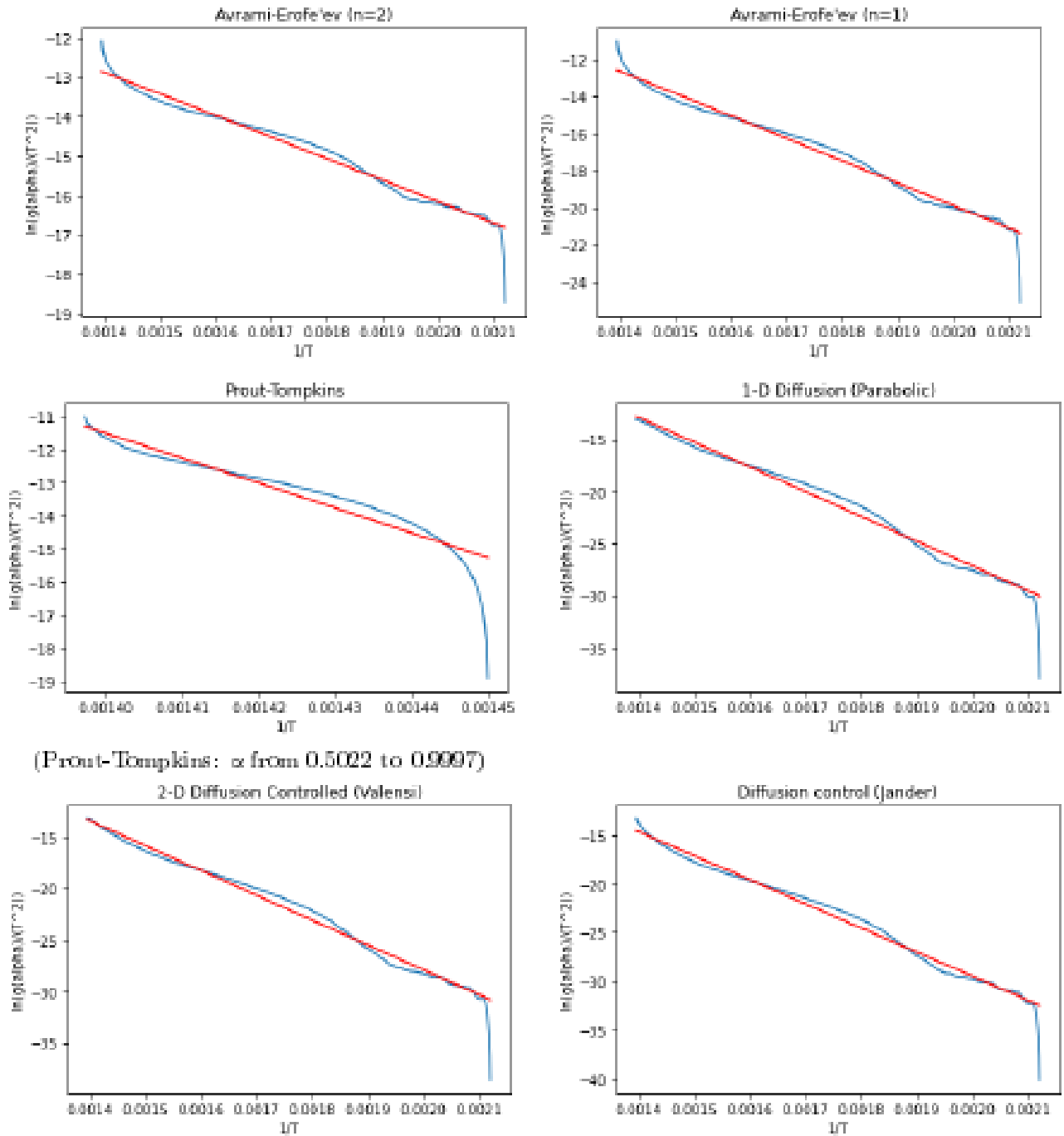
Figure 2.1: Plots of ln ( g( α ) T 2 ) vs 1 T for various models
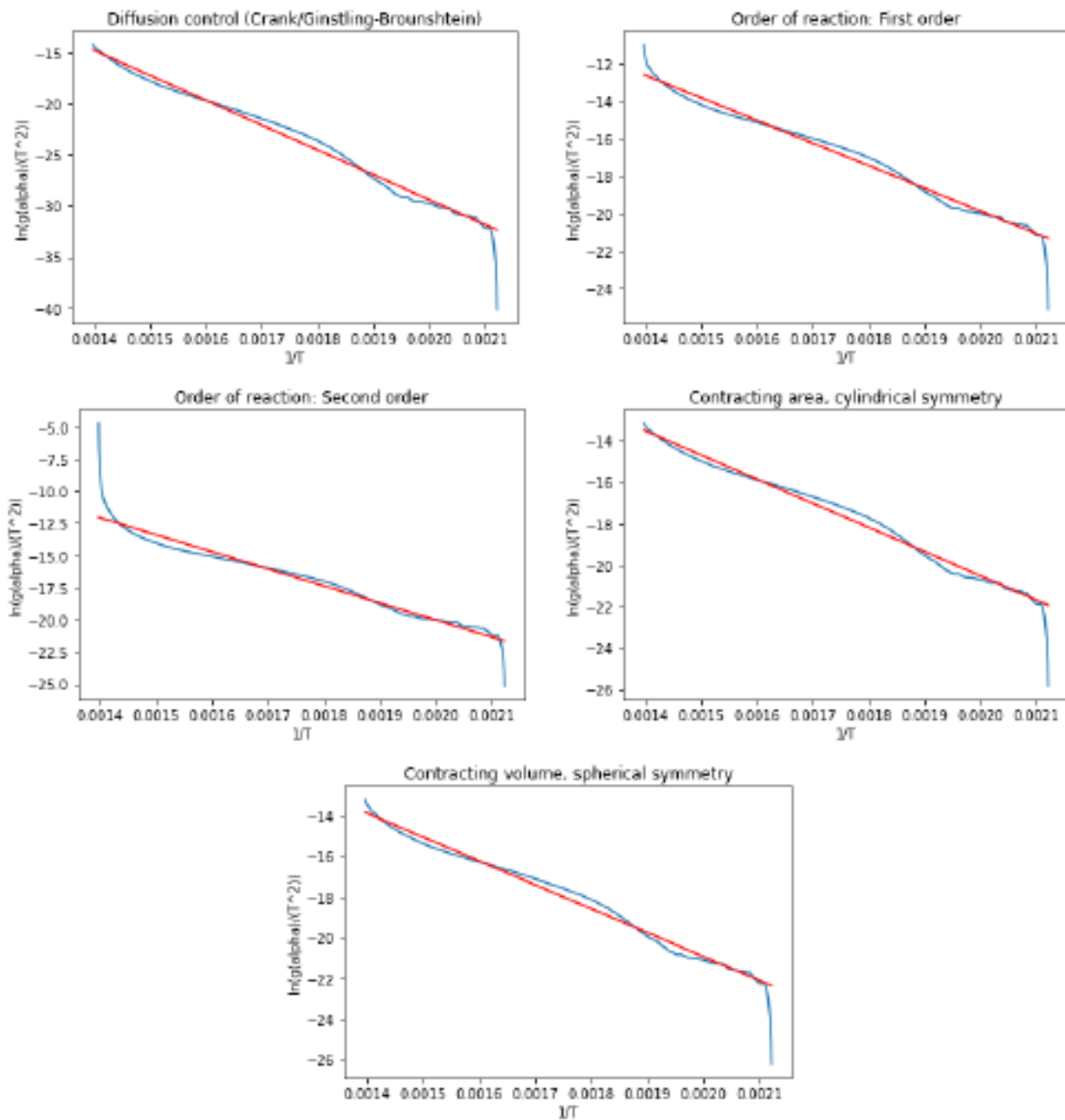
Figure 2.2: Plots of ln ( g( α ) T 2 ) vs 1 T for various models

Table 1: Solid state rate equations

| Sr. no. | Reaction Model | f(α) | g(α) | Equation obtained (y = mx + c) | R² | $E_a$(kJ/mol) | A(min⁻¹) |
|---|---|---|---|---|---|---|---|
| | **Exponential nucleation models** | | | | | | |
| 1 | Power Law (n = 1/4) | $4\alpha^{3/4}$ | $\alpha^{1/4}$ | -1966x - 10.34 | 0.956 | 16.262184 | 632.068 |
| 2 | Power Law (n = 1/3) | $3\alpha^{2/3}$ | $\alpha^{1/3}$ | -2996x - 8.879 | 0.968 | 24.908744 | 4.1729 |
| 3 | Power Law (n = 1/2) | $2\sqrt{\alpha}$ | $\alpha^{1/2}$ | -5074x - 5.948 | 0.976 | 42.185 | 132.485 |
| 4 | Power Law (n = 3/2) | $\frac{2}{3\sqrt{\alpha}}$ | $\alpha^{3/2}$ | -1754x + 11.63 | 0.983 | 145.877 | $1.9725 \times 10^{10}$ |
| | **Random nucleation & nuclei growth** | | | | | | |
| 5 | Avrami-Erofe'ev (n = 1) | $(1-\alpha)$ | $[-\ln(1-\alpha)]$ | -1205x + 4.312 | 0.981 | 100.541 | $9.020 \times 10^6$ |
| 6 | Avrami-Erofe'ev (n = 4) | $4(1-\alpha)[-\ln(1-\alpha)]^{3/4}$ | $[-\ln(1-\alpha)]^{1/4}$ | -2152x - 9.978 | 0.962 | 17.891 | $9.987 \times 10^{-1}$ |
| 7 | Avrami-Erofe'ev (n = 3) | $3(1-\alpha)[-\ln(1-\alpha)]^{2/3}$ | $[-\ln(1-\alpha)]^{1/3}$ | -3257x - 8.390 | 0.971 | 27.079 | 7.3975 |
| 8 | Avrami-Erofe'ev (n = 2) | $2(1-\alpha)[-\ln(1-\alpha)]^{1/2}$ | $[-\ln(1-\alpha)]^{1/2}$ | -5465x - 5.215 | 0.977 | 45.444 | 297.046 |
| 9 | Prout-Tompkins | $\alpha(1-\alpha)$ | $\ln[\alpha/(1-\alpha)]$ | -75193x + 93.75 | 0.890 (z = 0.502 to 0.9997) | 81.901 | $1.112 \times 10^{-3}$ |
| | **Diffusion Models** | | | | | | |
| 10 | One dimensional (Parabolic law) | $\left(\frac{1}{2\alpha}\right)$ | $\alpha^2$ | -23782x + 20.43 | 0.983 | 197.7235 | $1.774 \times 10^{14}$ |
| 11 | Two dimensional (Valensi) | $-1/\ln(1-x)$ | $(1-\alpha)\ln(1-\alpha)+\alpha$ | -24205x + 20.53 | 0.985 | 201.249 | $1.995 \times 10^{11}$ |
| 12 | Diffusion control (Jander) | $2(1-\alpha)^{2/3}[1-(1-\alpha)^{1/3}]$ | $[1-(1-\alpha)^{1/3}]^2$ | -24745x + 20.04 | 0.985 | 205.73 | $1.25 \times 10^{14}$ |
| 13 | Diffusion control (Crank/Ginstling-Brounshtein) | $\frac{3}{2(\sqrt[3]{(1-\alpha)}-1)}$ | $1-(2/3)\alpha-(1-\alpha)^{2/3}$ | -24831x + 19.95 | 0.985 | 202.704 | $6.237 \times 10^{13}$ |
| | **Order of reaction** | | | | | | |
| 14 | 1ˢᵗ order | $(1-\alpha)$ | $-\ln(1-\alpha)$ | -12063x + 4.312 | 0.981 | 100.541 | $9.020 \times 10^6$ |
| 15 | 2ⁿᵈ order | $(1-\alpha)^2$ | $(1-\alpha)^{-1}-1$ | -13258x + 6.486 | 0.938 | 110.227 | $8.696 \times 10^7$ |
| | **Phase boundary controlled** | | | | | | |
| 16 | Contracting area, cylindrical symmetry | $2\sqrt{(1-\alpha)}$ | $[1-(1-\alpha)^{1/2}]$ | -11658x + 2.905 | 0.984 | 96.925 | $1.927 \times 10^6$ |
| 17 | Contracting volume, spherical symmetry | $3\sqrt[3]{(1-\alpha)^2}$ | $[1-(1-\alpha)^{1/3}]$ | -11792x + 2.660 | 0.984 | 98.0887 | $1.669 \times 10^6$ |

## Acknowledgements

## References

Aboulkas A., Harfi K. El, Bouadili A. El, 2010. Thermal degradation behaviors of polyethylene and polypropylene. Part I: Pyrolysis kinetics and mechanisms. Energy Conversion and Management 51, 1363–1369

Agrawal R. K., Sivasubramanian M. S., 1987. Integral approximations for nonisothermal kinetics [J]. AIChE J, 33, 1212−1214.

Coats, A. W., Redfern, J. P. 1964. Kinetic analysis from thermogravimetric data. Nature. 201, 68−69.

Central Pollution Control Board. (2018-19)., Annual Report for the year 2018-19 on Implementation of Plastic Waste Management Rules, Ministry of Environment, Forest & Climate Change. https://cpcb.nic.in/uploads/plasticwaste/Annual_Report_2018-19_PWM.pdf

Flynn, J. H., Wall, L. A., 1966. A quick, direct method for the determination of activation energy from thermogravimetric data. J. Polym. Sci., Part B: Polym. Lett., 4 (5), 323−328.

Ginstling, A. M.; Braunshtein, B. I., 1950. J. Appl. Chem. USSR, 23, 1327.

Jander, W. Z., 1927. Z. Anorg. Allg. Chem., 163, 1

# Applicability of nanofluids to enhance thermal conductivity

*Anshul Sharma[1], Himanshu P. Kohli [1,2], Mousumi Chakraborty [1] \*, Parimal A. Parikh [1] \**

[1]Department of Chemical Engineering, Sardar Vallabhbhai National Institute of Technology, Surat 395007, Gujarat, India.

[2]Department of Chemical Engineering, R. N. G. Patel Institute of Technology, Bardoli 394620, Gujarat, India.

*Corresponding authors: mousumichakra1995@gmail.com, paparikh@ched.svnit.ac.in

## Abstract

Nanofluids are colloidal suspensions containing dispersed nanomaterials with improved chemical and thermo-physical properties. Nanofluid contains nanoparticles normally prepared of carbon nanotubes, metals, oxides, polymers and many more. They are in wide use as the nanoparticles incorporated in the fluid have distinctive physicochemical properties due to their size and large surface area. Nowadays more importance has been given to the fluids incorporated with nanoparticles due to their distinctive features like size, surface area, solubility, chemical composition, shape, crystal structure, morphology, energy and charge of the surface. Nanofluids include materials having various forms like nanorods, nanofibers, nanosheets, nanoparticles, nanowires, nanotubes or nanodroplets. Incorporation of nanoparticles in the fluids leads to rise in the strength of materials, lighter weight, more stable and better electrical conductors. Nanofluid is a heat transfer medium having nanoparticles (1–100 nm) which are evenly and steadily distributed in a base fluid. The nanoparticles (metal or metal oxide) significantly improve the thermal conductivity of nanofluid, increases conduction and convection coefficients, allowing for more heat transfer. Frequently used heat transfer fluids like water, ethylene glycol and engine oil have low thermal conductivities as compared to solids. The present paper focuses on the use of nanofluid containing different metal/metal oxide nanoparticles toward the sustainability development and properties improvement in the fields pertaining to thermal conductivity.

**Keywords:** Nanofluids, nanoparticles, physicochemical properties, thermal conductivity.

## 1. Introduction

The modern problems of power engineering, micro and nanotechnologies, dictates the requirement for miniaturization of cooling systems and development of effective techniques for controlling the heat transfer. Incorporation of solid particles having high thermal conductivity into a heat carrier increases its thermal conductivity significantly. This is a promising method for heat transfer intensification. As per various investigations, when micron particles are applied, they cannot lead to intensification, but vice versa reduces the rate of heat transfer due to turbulence suppression by a dispersed phase. Also, unwanted phenomenon like abrasive wearing of channel surface, particles deposition on the wall and in stagnation zones, and rise of hydraulic resistance. Hence, the transition to nanometric particles is grounded and used to resolve the crucial difficulties (Terekhov et al. 2010).

Although various researches pertaining to the field of nanofluids have been carried out but still, numerous problems are not thoroughly investigated, and results are often contradictory. The main cause for this can be attributed to complex nature of nanofluids, starting from their production, occurrence, devastation, peculiarities of experimental equipment and result consistency (Terekhov et al. 2010). A nanofluid is synthesized by the dispersion of metallic or nonmetallic nanoparticles having size less than 100 nm in a base liquid (Sidik et al. 2014). A major parameter of the working fluid in heat transfer is the thermal conductivity. In comparison to the thermal conductivities of

solids, especially metals, frequently used fluids for heat transfer applications like water, ethylene glycol and engine oil have low thermal conductivities. Due to this, researchers have tried to find a way to increase thermal conductivity of these commonly used fluids (Ozerinc et al. 2010).

In heat transfer applications, various fluids are used as heat carriers. Heat transfer fluids plays an important role in various systems that exchange heat in power stations, buildings having cooling and heating systems, transportation where vehicles consist of air conditioning system and most of the processing plants that comprises of cooling systems. In all of the above-mentioned applications, the efficiency of the heat transfer process and overall efficiency of the system is strongly affected by the thermal conductivity of heat transfer fluid. Due to this, researchers are continuously working on developing advanced heat transfer fluids which have significantly high thermal conductivities than the conventionally used fluids (Ali et al. 2018).

The commercial implementation of nanofluids is described as follows (Saidur et al. 2011): heat transfer nanofluids, surfactant and cooling nanofluids, chemical nanofluids, process/extraction nanofluids, environmental (pollution cleaning) nanofluids, bio and pharmaceutical-nanofluids, nanofluids for drug delivery and functional tissue-cell interaction.

## 2. Fate of nanofluids: Before and after thermal conductivity enhancement

In the present scenario, the need to synthesize advanced heat transfer fluids is very high. Moreover, these fluids should have high thermal conductivities and enhanced heat transfer features than the solvents which are in current use like water, ethylene glycol mixture and oil. All these solvents are poor heat transfer fluids. Although substantial amount of research work has been carried out on the industrial heat transfer requirements, but main enhancement in heat transfer capability have been suppressed due to the basic limit in the thermal conductivity of conventional fluids.

Nanofluids exhibits more improved properties than the traditional heat transfer fluids. For a particle of 10 µm diameter, surface area to volume ratio is thousand times smaller than for the particles with 10 nm diameter. Along with the enhancement in heat transfer properties, stability of the suspensions also increases because of higher surface area of nanoparticles than the conventional particles. Due the large total surface area of nanoparticles, they have immense potential for heat applications (Lee et al. 1999). The stability of a nanofluid diminishes as clusters are formed and aggregation occurs due particles coagulation after a long period of preparation (Awais et al. 2021).

Though nanofluid offers the benefits of more heat transfer than the conventional fluids but still the disposal of nanoparticles are really environmental concerns. The type of nanoparticle and its production, and production of nanofluid are the main causes of impacts. Employing green synthesis methods has a significant role in reducing the environmental impacts. So, for this nanoparticle should be environmentally friendly, low cost and readily available. Also, the base fluid should be environmentally friendly, nontoxic and nonflammable (Elsaid et al. 2021). With time, base fluid is degraded with temperature but properties of nanoparticle are unaltered. Before discarding base fluid, nanoparticles should be removed by centrifugation and nanofiltration. Nanoparticles can be reused after washing and calcination with fresh base fluid.

### 3. Heat transfer mechanisms of nanofluids

In the coolants, the heat transfer mechanism is changed by adding the nanofluids. Importantly the thermal conductivity of the coolant is enhanced (Singh et al. 2017). Free electrons (electron heat conductivity) and atom oscillations (phonon or lattice thermal conductivity) are the two main mechanisms which governs the changes in thermal conductivity of fluids and solid bodies. For dielectrics consisting of most fluids and water in pure form, phonon thermal conductivity is predominant, and for metals the thermal conductivity is altered by electron heat conductivity. Researchers have been analyzing several main mechanisms, including Brownian motion of nanoparticles, making highly heat-conductive fluid layer (the thickness of which is at molecular level) at the fluid-particle interface, ballistic transfer of heat energy inside a separate nanoparticle and between nanoparticles, when they contact, and the effects due to clustering of nanoparticles. A lot of investigation has been carried out to find the reason for an increase in thermal conductivity of nanofluids (Terekhov et al. 2010).

### 3.1 Brownian motion of particles

Here nanoparticles in liquid move through it and collide with each other allowing the direct solid to solid heat transfer. Since the particles collide in liquid, the thermal conductivity increases, temperature increases and size of nanoparticle decreases. Also, microscopic forces such as Van der Waals, electrostatic and stochastic are accountable for an increase in the Brownian motion of particles, which increases the heat transfer rate (Singh et al. 2017).

### 3.2 Layering of molecules of liquid-particles interface

An interface effect of liquid surrounding the particles could increase the thermal conductivity. A more ordered atomic structure of liquid than that of the bulk liquid is attained. The behavior of liquid shell surrounding the particles is like those of solids, which enhances the thermal conductivity (Singh et al. 2017).

### 3.3 Nature of heat transport in nanoparticles

The macroscopic transport of phonons in nanofluids carries heat. These phonons are distinguished by randomness in their creation and propagation and this gets scattered by each other and results in enhanced heat transfer (Singh et al. 2017).

### 3.4 Clustering of nanoparticles in nanofluids

Nanoparticle clustering play a significant part in thermal conductivity. Formation of a well diffused, percolated structure is achieved due to rise in temperature. Formation of isolated regions at lower temperatures occurs as the clusters start to accumulate and results in formation of disconnected cluster networks. So, "particle free-zones" and "particle rich-zones" regions are formed. Transport of heat is enlarged with a well diffused thermal pathway at higher temperatures; while isolated clusters have adverse effect on heat transport at lower temperature (Singh et al. 2017).

## 4. Synthesis of nanofluids

Nanofluid consists of the incorporation of nanoparticles (Metals, metal oxides and carbon tubes) having high heat conducting properties in a base fluid like water, ethylene glycol and engine oil. The present techniques are divided into single and two stages. In the single-stage technique, nanofluid can be synthesized by one process cycle. Due to this single-stage technology, the produced nanoparticles are usually very small (2−20 nm), agglomeration is reduced and synthesized nanofluids are stable. In single stage method, the metal (nanoparticle material) is evaporated by an electron beam in a vacuum chamber and is settled on a rotating disc covered by base fluid. In the two-stage method, the nanoparticles are first synthesized and then incorporated in the fluid. The two-stage technique is desirable for the particles of oxides due to its low affinity to agglomerate (Terekhov et al. 2010). Figure 1 shows the schematic view of nanofluid preparation.
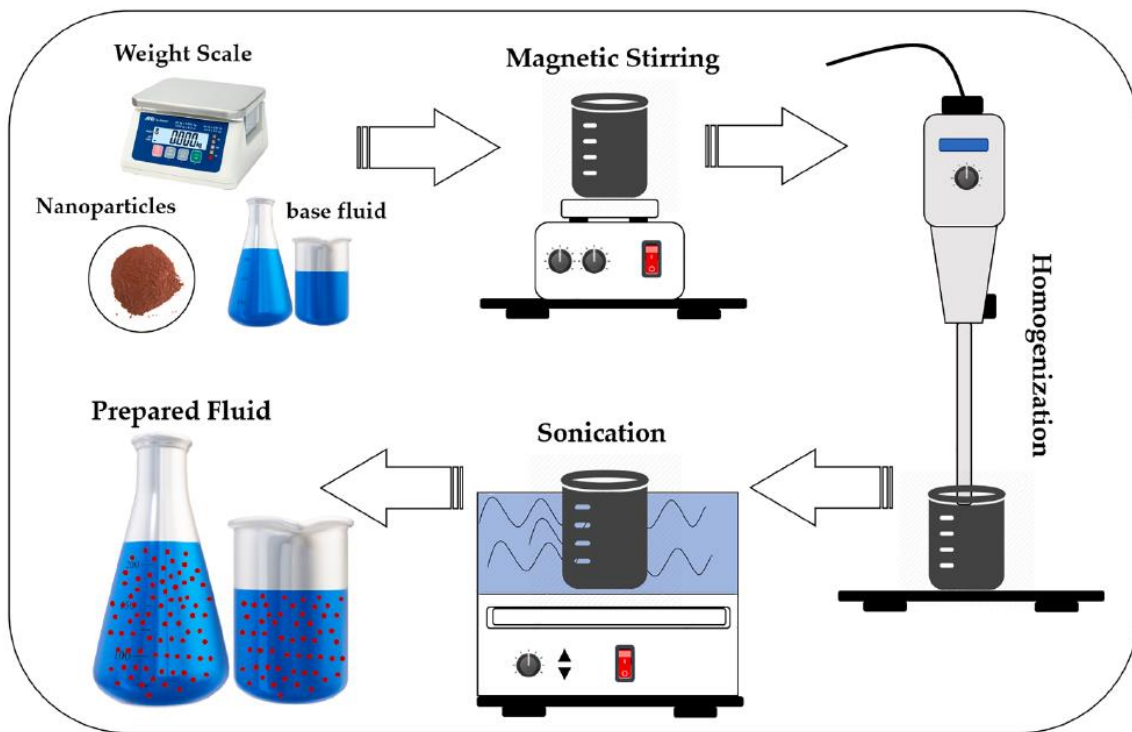


**Figure 1:** Schematic representation of preparation of nanofluid (Babar and Ali, 2019).

## 5. Thermal applications of nanofluid

Table 1 lists out the thermal applications of nanofluids.

Table 1: Thermal applications of nanofluids

| Particle type | Base Fluid | Particle size | Parameters altered | Enhancement in thermal conductivity | Reference |
|---|---|---|---|---|---|
| Al₂O₃ | Water | | | 10% | |
| Al₂O₃ | Ethylene glycol | 38.4 nm | Room temperature, particle volume fraction | 18% | Lee et al. 1999 |
| CuO | Water | 23.6 nm | | 12% | |
| CuO | Ethylene glycol | | | 23% | |
| Al₂O₃ | Water | | | 16% | |
| Al₂O₃ | Ethylene glycol | 28 nm | Room temperature, particle volume fraction | 41% | Wang et al. 1999 |
| Al₂O₃ | Engine Oil | | | 30% | |
| Al₂O₃ | Pump fluid | | | 20% | |
| CuO | Water | 23 nm | | 34% | |
| CuO | Ethylene glycol | | | 54% | |
| Cu | Ethylene glycol | < 10 nm | Room temperature, particle volume fraction | 41% | Eastmen et al. 2001 |
| Multi-walled carbon nanotubes | Poly($\alpha$-olefin) | Diameter = ~25 nm, Length= ~50 µm | Room temperature, particle volume fraction | 160% (for 1 vol%) | Choi et al. 2001 |
| SiC | Water | 26 nm (Sphere shape) | Particle volume fraction, effect of particle shape and size | 17% | Xie et al. 2002a |
| | Ethylene glycol | 600 nm (cylindrical shaped) | | 13% | |
| Al₂O₃ | Water Ethylene glycol Pump oil Glycerol | 60.4 nm | Room temperature, particle volume fraction | 23% 29% 38% 27% | Xie et al. 2002b |
| Al₂O₃ | Water | 38.4 nm | Temperature, particle volume fraction | 24% | Das et al. 2003 |
| CuO | | 28.6 nm | | 36% | |
| Multi-walled | Synthetic engine oil (N-hydroxysuccini | Inner diameter = | Volume fraction | 30% (for 2 vol%) | Liu et al. 2005 |

| Material | Base fluid | Size | Parameters | Enhancement | Reference |
|---|---|---|---|---|---|
| carbon nanotubes | mide as dispersant) | 5 to 10 nm, Outer diameter = 20 to 50 nm | | | |
| | Ethylene glycol | | | 12.4% (for1 vol%) | |
| Cu | Water | 100-200 nm | Concentrations of precursor, Amount of reducing agent, amount of water solvent, volume fraction | 23.8% (for 0.1 vol%) | Liu et al. 2006 |
| TiO$_2$ | Water | 15 nm (Sphere shaped) | | 30% | |
| TiO$_2$ | Water | Diameter= 10 nm, Length=40 nm (rod shaped) | Room temperature, particle volume fraction | 33% | Murshed et al. 2005 |
| Double-walled carbon nanotubes | Water (Hexadecyltrimethyl ammonium bromide and Nanosperse AQ as dispersants) | Outer diameter= 5 nm Inner diameter= 2.5 nm | Effect of sonication time was examined, particle volume fraction | 7.6% | Assael et al. 2005 |
| Multi-walled carbon nanotubes | | Length= >10 µm, Outer diameters =100-250 nm | | 34% | |
| Fe | Ethylene glycol | >1 µm | Effect of clustering, particle volume fraction | 18% | Hong et al. 2006 |
| Al$_2$O$_3$ | | 36 nm | Nanoparticle material, diameter, volume fraction, bulk temperature | 29% | |
| CuO | Water | 29 nm | | 51% | Li and Peterson, 2006 |
| Multi-walled | Water | | Temperature, particle volume fraction | 79% | Ding et al. 2006 |

| | | | | | |
|---|---|---|---|---|---|
| carbon nanotubes | | | | | |
| Au | Toluene | 1.65 nm | | 8% | |
| $Al_2O_3$ | | 20 nm | | No unusual enhancement | |
| $TiO_2$ | | 40 nm | Particle concentration, temperature, Volume fraction | No unusual enhancement | Xing et al. 2007 |
| CuO | water | 33 nm | | No unusual enhancement | |
| Carbon nanotubes | | Length=10 μm, Diameter= 150 nm | | No unusual enhancement | |
| Cu Ag $Al_2O_3$ CuO $TiO_2$ | water | | Volume fraction, temperature | Increment observed | Nada, 2008 |
| $Al_2Cu$ | Water (Oleic acid as surfactant) Ethlyene glycol (Oleic acid as surfactant) | | | The experimental results show that the thermal conductivity ratio, relative to that of base fluid, increases nonlinearly with the increase in volume fraction and as the size/diameter of nanoparticles was decreased. | Chopkar et al. 2008 |
| $Ag_2Al$ | Water (Oleic acid as surfactant) Ethylene glycol (Oleic acid as surfactant) | Average diameter = 30 – 40 nm | Effect of particle size is examined and particle volume fraction | | |
| $Al_2O_3$ | Water | Diameter = 36 nm | Temperature and particle volume fraction | 31% | Mintsa et al. 2009 |
| CuO | | Diameter = 29 nm | | 24% | |
| $Al_2O_3$ | Water | 8 nm-282 nm | Effect of particle size was examined and | 20% | Beck et al. 2009 |
| | Ethylene glycol | 12 nm-282 nm | | 19% | |

| | | | particle volume fraction | | |
|---|---|---|---|---|---|
| TiO$_2$ | Water | 21 nm | Temperature and particle volume fraction | 7.4% | Turgut et al. 2009 |
| Cu | Water and ethanol | 20 nm | Operational temperature, mass fraction | Heat transfer coefficient enhanced upto 38-45% | Lu et al. 2011 |
| CuO | Deionized water | 50 nm | Mass fraction, volume fraction | 42% | Liu and Zhu, 2011 |
| ZnO | Propylene glycol, water | 25-45 nm | Volume fraction | Heat transfer coefficient increased by 29% (2 vol%) | Sungathi et al. 2016 |
| Al$_2$O$_3$ | Ethylene glycol (Polyvinylpyrrolidone, Sodium dodecylbenzene sulfonate, Gum Arabic as dispersants) | 13 nm, 40 nm, 50 nm, 90 nm | Particle volume concentration, temperature, pH, type of surfactants, Particle size | Thermal conductivity enhancement by 38% | Krishnakumar et al. 2018 |
| Graphene wrapped carbon nanotubes | | | | 22.6%, 15.5% | |
| CuO/Graphene Carbonnanotubes | Deionized water, Ethylene glycol | Outer diameter = 65 nm, Thickness = 5.2 nm | Temperature, Volume fraction | 24.1%, 17.7% | Sati et al. 2018 |
| ZnO/Graphene Carbonnanotubes | | | | 26.0%, 21.2% | |

## 6. Limitations of nanofluids

Nanofluids shows lot of promise for its use in different applications but obstruction in the development of the field occurs due to: (i) The results obtained by different researchers are not in agreement with each other (ii) Suspensions being characterized at below par level; (iii) Absence of hypothetical knowledge of the mechanisms accountable for changes in properties (Saidur et al. 2011). Some of the factors that play a role in hindrance in the development in the area of nanofluid applications are mentioned as follows:

## 6.1 Poor stability of suspension

1) Nanofluids are thermodynamically unstable due to multi-phase dispersion system with great surface energies. 2) There is a high tendency of nanoparticles dispersed in the nanofluids to collide with each other. The motion of the nanoparticles can overcome their inclination to settle down caused by the gravitational field. 3) As the time progresses there is a decline in dispersion of nanoparticles in the fluids due to the assemblage of nanoparticles, caused by Van der Waals forces. 4) At the working conditions of nanofluid, there should not be any chemical reaction among the suspended nanoparticles or amid the base fluid and nanoparticles. So, aggregation and sedimentation are the two phenomena that are dictates the stability of nanofluid (Gupta et al. 2012; Haddad et al. 2014).

Thermal conductivity of ethylene glycol based nanofluids having 0.3% copper nanoparticles reduced with time. Thermal conductivity was determined twice: (i) within 2 days (ii) two months after the preparation. Fresh nanofluids showed marginally high thermal conductivities than nanofluids that were kept up to two months (Eastman et al. 2001). They explained that aggregation and sedimentation of nanoparticles would reduce thermal conductivity of nanofluids.

## 6.2 Increased pressure drop and pumping power

The effectiveness of nanofluid is evaluated by pressure drop and necessary pumping power during the flow of coolant. High pressure drops and pumping power is caused by high density and viscosity (Gupta et al. 2012).

The pumping cost in due course increased as the concentration of nanoparticles was increased that raised the single-phase pressure drops of $Al_2O_3$ nanofluids in microchannel heat sink (Lee and Mudawar, 2007).

## 7. Concluding remarks

These are the conclusions from the above study
- High surface area of nanoparticles present in nanofluids provides more heat transfer surface compared to base fluid.
- High heat transfer of nanofluids is due Brownian motion of particles, layering of molecules of liquid-particles interface and phonon heat transfer
- Clustering and agglomeration of nanoparticles causes instability of nanoparticles which eventually reduces the heat transfer.
- Higher density of nanoparticles and higher viscosity of nano fluids increases the pressure drop and pumping cost.

**References**

1. Ali, N., Teixeria, J. A., Addali, A., 2018. A review on nanofluids: Fabrication, stability, and thermophysical properties. J. Nanomater. 2018, Article ID 6978130.
2. Assael, M. J., Metaxa, I. N., Aravaniditis, J., Christofilos, D., Lioutas, C., 2005. Thermal conductivity enhancement in aqueous suspensions of carbon Multi-Walled and Double-Walled Nanotubes in the Presence of Two Different Dispersants. Int. J. Thermophys. 26, 647-664.
3. Awais. M., Ullah, N., Ahmed, J., Sikandar, F., Ehsan, M.M., Salehin, S., Bhuiyan, A.A. 2021. Heat transfer and pressure drop performance of nanofluid: A state-of-the-art review. Int. J. Thermofluids. 9, 10065.
4. Babar, H., Ali, H. M., 2019. Airfoil shaped pin-fin heat sink: potential evaluation of ferric oxide and titania nanofluids. Energy Convers. Manage. 202, 1-19.
5. Beck, M. P., Yuan, Y., Warrier, P., Teja, A. S., 2009. The effect of the particle size on the thermal conductivity of alumina nanofluids. J. Nanopart. Res. 11, 129-1136.
6. Choi, S. U. S., Zhang, Z. G., Yu, W., Lockwood, F. E., Grulke, E. A., 2001. Anomalous thermal conductivity enhancement in nanotube suspensions. Appl. Phys. Lett. 79, 2252-2254.
7. Chopkar, M., Sudarshan, S., Das, P. K., Manna, I., 2008. Effect of particle size on thermal conductivity of nanofluid, Mettal. Mater. Trans. A. 39A, 1535-1542.
8. Das, S.K., Putra, N., Thiesen, P., Roetzel, W., 2003. Temperature dependence of thermal conductivity enhancement for nanofluids. J. Heat Transfer 125, 567-574.
9. Ding, Y., Alias, H., Wen, D., William, R. A., 2006. Heat transfer of aqueous suspensions of carbon nanotubes (CNT nanofluids). Int. J. Heat Mass Transfer 49, 240-250.
10. Eastman, J. A., Choi, S. U. S., Li, S., Yu, W., Thompson, L.J., 2001. Anomalously increased effective thermal conductivities of ethylene-based nanofluids containing copper nanoparticles. Appl. Phys. Lett. 78, 718-720.
11. Elsaid, K., Olabi, A.G., Wilberforce, T., Abdelkareem, M.A., Sayed, E.T., 2021. Environmental impacts of nanofluids: a review. Sci. Total Environ 57, 582-594.
12. Gupta, H. K., Agarwal, G. D., Mathur, J., 2012. An overview of nanofluids: A new media towards green environment. Int. J. Environ. Sci. 3, 433-440.
13. Haddad, Z., Abid, C., Oztop, H. F., Mataoui, A., 2014. A review on how researchers prepare their nanofluids. Int. J. Therm. Sci. 76, 168-189.
14. Hong, K. S., Hong, T., Yang, H., 2006. Thermal conductivity of Fe nanofluids depending on the cluster size of nanoparticles. Appl. Phys. Lett. 88, 031901.
15. Krishnakumar, T.S., Vishwanath, S.P., Varghese, S.M., Prakash, J., 2018. Experimental studies on thermal and rheological properties of $Al_2O_3$-ethylene glycol nanofluid. Int. J. Refrig. 89, 122-130.
16. Lee, J., Mudawar, I., 2007. Assessment of the effectiveness of nanofluids for single phase and two-phase heat transfer in microchannels. Int. J. Heat Mass transfer 50, 452-463.
17. Lee, S., Choi, S. U. S., Li, S., Eastman, J.A., 1999. Measuring thermal conductivity of fluids containing oxide nanoparticles. J. heat transfer 121, 280-289.
18. Li, C. H., Peterson, G. P., 2006. Experimental investigation of temperature and volume fraction variations on the effective thermal conductivity of nanoparticle suspensions (nanofluids). J. Appl. Phys., 99, 084314: 1-8.
19. Liu M., Lin, M. C., Huang, I. T., Wang, C., 2005. Enhancement of thermal conductivity with carbon nanotube for nanofluids. Int. Commun. Heat Mass Transfer 32, 1202-1210.
20. Liu, M., Lin, M. C., Tsai, C. Y., Wang, C., 2006. Enhancement of thermal conductivity with Cu for nanofluids using chemical reduction method. Int. J. Heat Mass transfer 49, 3028-3033.

21. Liu, Z., Zhu, Q, 2011. Application of aqueous nanofluids in a horizontal mesh heat pipe. Energy Convers. Manage. 52, 292-300.
22. Lu, L., Lv, L., Liu, Z., 2011. Application of Cu-water and Cu-ethanol nanofluids in a small flat capillary pumped loop. Thermochim. Acta, 512 98-104.
23. Mintsa, H. A., Roy, G., Nguyen, C. T., Doucet, D., 2008. New temperature dependent thermal conductivity data for water -based nanofluids. Int. J. Therm. Sci. 48, 363-371.
24. Murshed, S. M. S., Leong, K. C., Yang, C., 2005. Enhanced thermal conductivity of $TiO_2$-water based nanofluids. Int. J. Therm. Sci. 44, 367-373.
25. Nada, E., 2008. Application of nanofluids for heat transfer enhancement of separated flows encountered in a backward facing step. Int. J. Heat Fluid Flow 29, 242-249.
26. Ozerinc, S.; Kakac, S.; Yazicioglu, A.G., 2010. Enhanced thermal conductivity of nanofluids: a state-of-the-art review, Microfluid. Nanofluid. 8, 145-170.
27. Saidur, R., Leong, K. Y., Mohammad, H. A., 2011. A review on applications and challenges of nanofluids. Renewable Sustainable Energy Rev. 15, 1646-1668.
28. Sati, P., Shende, R. S., Ramaprabhu, S., 2018. An experimental study on thermal conductivity of DI, water-EG, based ZnO (CuO)-graphene wrapped carbon nanotubes nanofluids. Therm. Acta 666, 75-81.
29. Sidik, N. A. C., Mohammed, H. A., Alawi, O. A, Samion, S., 2014. A review on preparation methods and challenges of nanofluids. Int. Commun. Heat and Mass Transfer 54, 115-125.
30. Singh, P. K., Khandelwal, D., Sidhant, C., Shubham, A., Priyanshu, N., Rasu, G., 2017. Nanofluid heat transfer mechanism and thermo-physical properties: a review. Int. J. of Mechanical Engineering Technology 8, 156-164.
31. Suganthi, K.S., Leela, V.V., Rajan, K.S., 2016. ZnO-propylene glycol–water nanofluids with improved properties for potential applications in renewable energy and thermal management. Colloids Surf., A 506, 63-73.
32. Terekhov, V. I., Kalinina, S. V., Lemanov, V. V., 2010. The mechanism of heat transfer in nanofluids: state of the art (review). Part 1. Synthesis and properties of nanofluids, Thermophys Aeromech+ 17, 1-14.
33. Turgut, A., Tavman, I., Chirtoc, M., Schuchmann, H. P., Sauter, C., Tavman, S., 2009. Thermal conductivity and viscosity measurements of water-based $TiO_2$ nanofluids. Int. J. Thermophys. 30, 1213-1226.
34. Xie, H., Wang, J., Xi, T., Liu, Y., 2002a. Thermal conductivity of suspensions containing nanosized SiC particles. Int. J. Thermophys. 23, 571-580.
35. Xie, H., Wang, J., Xi, T., Liu, Y., Al, F., 2002b. Dependence of the thermal conductivity of nanoparticle-fluid mixture on the base fluid. J. Mater. Sci. Lett. 21, 1469-1471.
36. Wang, D. Wang, L., Zhu, G., Zeng, Y.W., 2018. Magnetic photothermal nanofluids with excellent reusability for direct absorption solar collectors. ACS Appl. Energy. Mater. 1, 3860-3868.
37. Wang, X., Xu, X., Choi, S. U. S., 1999. Thermal conductivity of nanoparticle-fluid mixture. J. Thermophys. Heat Transfer. 13, 474-480.
38. Zhang, X., Gu, H., Fujii, M., 2007. Effective thermal conductivity and thermal diffusivity of nanofluids containing spherical and cylindrical nanoparticles. Exp. Therm. Fluid Sci. 31, 593-599.

# Role of molecular sieves in methanol to light olefins production

*Baljinder Kaur Riyar[1*], Vijay Kumar Agarwal[1]*
[1]Department of Chemical Engineering, Indian Institute of Technology Roorkee, Roorkee-247 667, Uttarakhand, INDIA
*Corresponding author: briyar@ch.iitr.ac.in, mobile number: +91-8279801568

## Abstract

Light olefins (ethylene and propylene) are the building blocks of the petrochemical industry. Due to the shortage of fossil fuels, conventional methods like steam cracking of naphtha are no longer interested. The methanol to olefins (MTO) process comes for rescue to normalize the demand for light olefins. The molecular sieves are highly selective to the desired products, so zeolite like ZSM- 5 and SAPO-34 is the commercialized catalyst for the methanol to olefins process. Both of them are selective to light olefins, but there are drawbacks. The ZSM-5 may produce paraffin and aromatic compounds, and SAPO-34 gets deactivated quickly by the deposition of coke. Now, the researchers are focused on enhancing the selectivity and lifetime of the catalyst. Various factors that influence the performance of catalysts are the sources of the precursors, mixing sequences of the precursor, crystallization time, crystallization temperature, and method of preparation of the catalyst. The conversion of the MTO process could reach 100 % with the excellent yield of light olefins up to more than 80 %. The present study reviews the ZSM-5 and SAPO-34 role in the methanol to olefins process.

**Keywords**: ZSM-5, SAPO-34, MTO, molecular sieves, petrochemicals

## 1. Introduction

Ethylene and propylene are essential raw materials for various polymers, resins, solvents, and fibres in the chemical industry. In 2016, the global production of ethylene and propylene was 150 and 80 million metric tons, respectively. The demand for light olefins is expected to increase in the successive years (Castellanos-Beltran et al. 2018). The commercial route for both light olefins production is well-established processes like paraffin dehydrogenation, fluid catalytic cracking, and steam cracking of ethane and naphtha (Castellanos-Beltran et al. 2018). The availability of oil resources is limited, so the researchers have been looking for alternative technology. Two groups of Mobil researchers have accidentally found olefins from methanol using ZSM-5 as a catalyst while working on different projects (Keil 1999). Nowadays, methanol is surfaced as pivotal for sustainable chemical industries (Olah 2005). Green house gases reduction in the present times is also challenging, so the conversion of carbon dioxide to methanol can also be utilized. Thus, the non-petrochemical route for producing light olefins from coal and natural gas has gained attention. For more than 40 years, researchers have been working on pure research, process development, and catalyst synthesis for the methanol to olefins process (Sun et al. 2018). The carbon dioxide emissions are also lesser, which increases the attention towards the MTO process (Chen et al. 2005). In 2010, based on the Dalian Institute of Chemical Physics MTO technology, the world's first MTO plant has been commercialized with a capacity of 600000 ton/ year in China (Tian et al. 2015). In China, 14 DMTO (Dalian Institute of Chemical Physics technology) plants with a collective production capacity of ethylene and propylene of 7670 kt/a have been put into operation, and 26 Dalian Institute of Chemical Physics MTO units had been licensed (Ye et al. 2021).

Molecular sieves are defined as porous materials with a molecular size of a diameter of 0.3-2.0 nm (Flanigen et al. 2010). Molecular sieves were developed in late 1954, and they were utilized as adsorbents for purification and industrial separation (Flanigen 1980). Due to its excellent size selectivity, acidity, and improved thermal and hydrothermal stability, along with crystallinity, molecular sieve finds application in the petrochemical industry, petroleum refining, and ion exchange applications (Flanigen 1980). The product spectrum of the MTO reaction depends on the pore size and crystal structure of the applied catalyst. The cavity structure and cage or channel of porous oxides urge spatial confinement effect on size/reactivity/shape of active intermediates, which ultimately changes the product selectivity and reaction route. The Brønsted acid sites are crucial for the MTO reaction. The active intermediate growth and generation depend on the acidic properties of the molecular sieve (Yang et al. 2019). The various molecular sieves reported in the literature are SAPO-18 (Chen et al. 2014), Mordenite (He et al. 2017), ZSM-34 (Zhou et al. 2007), RHO (Masih et al. 2013), DNL-6 (Li et al. 2012), SSZ-39 (Dusselier et al. 2015), KFI (Ji et al. 2016), ZSM-22 (Cui et al. 2008), ZSM-11(Wang et al. 2019), ZSM-58 (Selzer et al. 2018), SSZ-13 (Wu & Hensen 2014), Zeolite Beta (Zhao et al. 2017), MCM-22 (Zhang et al. 2016), TNU-9 and MCM-68 (García-Ruiz et al. 2020), H-RUB-50 (Zhang et al. 2020), ZSM-5 (Bleken et al. 2012), SAPO-18 (Chen et al. 2014), SAPO-35 (Pinilla-Herrero et al. 2016), SAPO-34 (Sun et al. 2018), SAPO-5 (Hajfarajollah et al. 2014). The ZSM-5 and SAPO-34 have frequently used catalysts for the MTO process and its framework is shown in the Fig.1. ZSM-5 is incorporated in a fixed bed reactor for methanol to propylene reaction developed by Lurgi Company. ZSM-5 is a medium pore sized zeolite, and it has been found that it is resistant to deactivation by coke formation (Dehertog & Froment 1991). SAPO-34 gets deactivated fast, so UOP/Hydro Process uses a fluidized bed reactor for the MTO reaction. The usage of ZSM-5 (MFI-type) is favored as it has ten membered pore rings, medium-sized pores molecular sieve. It is highly selective to olefins like propylene and butylene. In comparison SAPO-34 has a CHA topology and possesses eight rings. SAPO-34 has high selectivity to ethylene and propylene, along with the concern of fast deactivation (Lefevere et al. 2014).
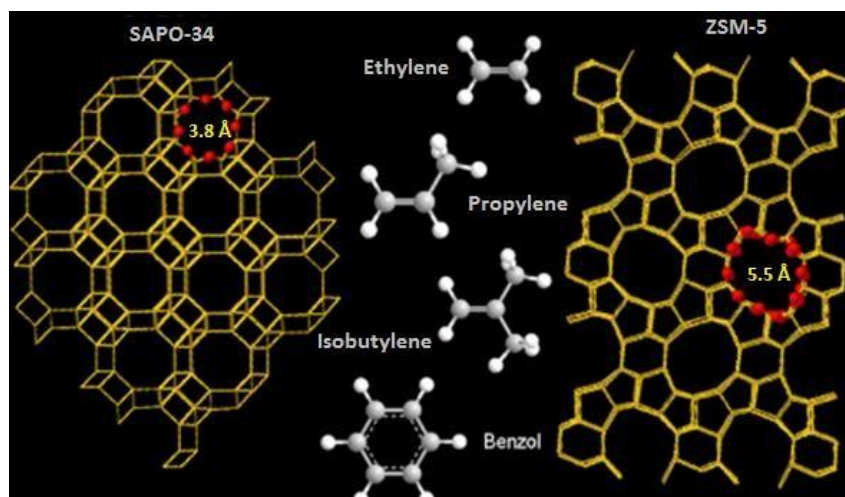


**Fig. 1** SAPO-34 and SAPO-5 framework compared to the olefins (Ethylene, Propylene) production (Chen et al. 2005)

## 2.    Factors affecting the MTO process on ZSM-5

### Reaction conditions, Si/Al ratio

Higher Si/Al ratio (lower acidity) is favorable to the production of light olefins. Dehertog & Froment 1991 reported that ZSM-5 with Si/Al ratio of 200 is highly selective to light olefins. The researchers have found that the higher temperature and low partial pressure directs the more considerable selectivity to light olefins (Dehertog & Froment 1991)

### Effect of methanol partial pressure

Wu et al. 2013 investigated the MTO reaction at different partial pressure at 460 $^{\circ}$C and various WHSV. At lower partial pressure, the methanol conversion decreases at the same WHSV. More than 5 times the earlier WHSV is required to achieve the 100 % conversion. At lower partial pressure, the selectivity of propylene, butylene, and pentene was enhanced. At higher partial pressure, the propylene selectivity is lesser, probably because of the formation of aromatics.

### Effect of water to methanol ratio

Wu et al. 2013 studied the water concentration in the methanol feed. They have found that increasing water concentration would increase ethylene formation at lower methanol conversions. There is a minute decrease in the selectivity of butylene and pentene at higher water concentrations, whereas, for different partial pressures, the selectivity curves of butylene and pentene tend to converge at 100 % methanol conversion.

### Effect of temperature

Dehertog & Froment 1991 and Wu et al. 2013 observed that increasing the temperature gives rise to methanol conversion. The distribution of the product as a function of methanol conversion varies according to the different temperatures. Propylene selectivity is increased at the higher temperature.

### Effect of impregnation on the parent catalyst

The size of the zeolite pore size is larger than the oxide molecule. Thus promoter molecules diffuse into the porous framework and introduce blank acidic sites in the zeolite (Sun et al. 2008). Gorzin & Yaripour 2019 studies the impregnation of Cs on the HZSM-5 catalyst reduces both the weak and strong acid catalytic sites. Thus conversion is dropped drastically for the Cs-HZSM-5 catalyst, as it is dependent on the Brønsted acid sites, which helps in methanol dehydration and the formation of the first carbon-carbon bond. The high desorption peak temperature corresponds to strong acidic sites of Ag-HZSM-5 and Mn-HZSM-5 reveals that some of the acidic sites are stronger than others, which leads to shortening the lifetime of the catalyst. The selectivity of light olefins for Mg-HZSM-5 is lower than the parent H-ZSM-5. The reason for the higher selectivity of light olefins is might be because of the large amount of weak acidic sites than stronger acidic sites. The proper distribution of active acidic sites possibly is the reason for the higher selectivity of light olefins in the case of P-ZSM-5 and Fe-ZSM-5.

### Factors affecting the MTO process on SAPO-34 Method of preparation of catalyst
There are various methods of preparation of catalysts reported in the literature. These synthesis methods have a notable impact on the properties of the catalyst. The various method impacts the crystallinity, size, morphology, and purity are hydrothermal synthesis (Sadeghpour & Haghighi

2015), dry gel conversion method (Hirota et al. 2010), Sonochemical synthesis (Shalmani et al. 2016), Rapid high temperature (Askari et al. 2014), Microwave synthesis (Shalmani et al. 2012), Hydrothermal method depends on the solubility of precursors in the water at a specified temperature (>100 °C).

## Crystal size

The small crystal size of SAPO-34 intensifies the methanol interaction in the cages, emanating better catalytic performance (Askari et al. 2012). Several studies observed that a crystal size of 500 nm shows the best catalytic performance. A small pore molecular sieve with a large crystal size has long intra-crystalline diffusion path that restricts the diffusion of both reactant and product molecules, resulting in the deactivation of the catalyst.

## Template and Precursor effect

Different physicochemical properties are obtained while switching to the different templates. The crystal growth and nucleation depend on the alkalinity and interaction of the reaction mixture. By using different templates and amount of template, different catalyst phases and purity is obtained. Tetraethylammonium hydroxide (TEAOH), morpholine, diethylamine (DEA), triethylamine (TEA) are the most commonly used templates. The templates can be used individually or as a combination for the synthesis of SAPO-34. It has been found that on using a single template, SAPO-34 gets deactivates quickly by the deposition of coke on the available acidic sites (Razavian et al. 2011). Various studies reported the positive impact of multi templates on the performance of the catalyst (Lee et al. 2007; Wang et al. 2012, 2018; Rostami et al. 2014). Rostami et al. 2014 have concluded that mixing of two templates promotes the decrease in crystal size, and the lifetime of the mixed template incorporated catalyst is more than 5 and 12 times the single template TEAOH and morpholine-based catalyst.

The first crystal is formed by the nucleation of the initial phase of the catalyst. The supersaturation solution is the driving force for the nucleation to place. Higher water content (100 $H_2O$ molar content instead of 60 and 75) would lead to reducing the concentration of all the precursors present in the synthesis mixture. Consequently, the crystallinity and driving force of the synthesis reaction mixture is decreased.

Higher content of Si along with template TEAOH lead to the formation of SAPO-5 as a significant phase, while lowering the Si content to half with the same concentration of TEAOH would form SAPO-34 (Lee et al. 2007), though there are reports based on TEAOH templates where SAPO-34 is formed as the single-phase using the different source of Si (Askari et al. 2012). By using the higher molar concentration of morpholine, pure SAPO-34 is formed. Similar results are retrieved for TEA and DEA.

## Effect of incorporation of metal on the parent catalysts

The addition of heteroatoms into the SAPO-34 structure can contribute to the negative charge of the framework, while divalent metal ions replace Al(III), which provides anionic; thus, brønsted acid sites are generated in which the photon charge is stabilized (Sadeghpour & Haghighi 2015). After confiscating the positively charged template that occupies the framework pores, the Brønsted acid sites are established (Rajic 2005). Amirhosseini et al. 2016 has reported that mixed metal (Ni and Mn) and mixed template (DEA, TEA, and Morpholine) incorporated SAPO-34 has higher selectivity to olefins. Though propylene selectivity is lesser than other single metal incorporated

SAPO-34, but ethylene selectivity is highest. The possible reason for the obtained results is the smaller pore size and higher crystallinity. The decrease in the propylene yield and increase in the ethylene yield might be due to the decrease of the free volume in the pore structure. Mirza et al. 2018 has synthesized the SAPO-34, K-SAPO-34, Ag-SAPO-34, and FeAPSO-34 and compared their performances. The acidic properties of FeAPSO-34 and SAPO-34 are found to be similar. The desorption peak at lower temperature helps in the conversion of methanol to dimethyl ether and desorption peak at higher temperature corresponds to bridging hydroxyl group which are linked to Al and Si atoms. These hydroxyl groups act as brønsted acidic sites and are considered responsible for MTO reaction. They concluded that adding Fe into SAPO-34, increases stability, activity, and selectivity. K-SAPO-34 exhibits the longest lifetime as it has highest crystallinity, specific surface area, and acidity concentration. At temperature 350-400 ºC, the ethylene selectivity of Ag-SAPO-34 is greater than FeAPSO-34 and SAPO-34. The weak and medium acidic sites of Ag-SAPO-34 leads to the high activity for methanol conversion and DME selectivity.

**Proposed mechanism for olefins production**

MTO is an autocatalytic reaction. Till now there are more than 20 mechanism proposed, butThe information regarding the formation of first C-C bond is still vague. Various researchers have proposed mechanism for the MTO reaction. In 1980's, Dessau & LaPierre 1982; Dessau 1986 have reported the alkene based mechanism. (Mole et al. 1983a, b) have studied the role of aromatics generation in MTO process. Hydrocarbon pool (HCP) mechanism based on the cyclic organic compounds that acts as co-catalysts confined in the zeolite cages or intersection of the channel is proposed by Dahl & Kolboe 1993, 1994a, b. After that, there are reports based on HCP mechanism, where the researchers have studied the nature of cyclic organic compounds (Hunger 1997; Wang et al. 2006; Olsbye et al. 2012). There are studies which implies that the methyl benzenes are the HCP species. (Xu & White 2004) have first reported the structure of HCP species. Haw and coworkers stated that impurities in the methanol feed or during calcination of catalyst would leads to the formation of organic species (Song et al. 2002; Haw et al. 2003).

A. Consecutive mechanism

$$2C_1 \rightarrow C_2H_4 + H_2O$$

$$C_2H_4 + C_1 \rightarrow C_3H_6$$

$$C_3H_6 + C_1 \rightarrow C_4H_8 \ldots$$

B. Parallel mechanism

$$CH_3OH \rightarrow \left(CH_2\right)_n \begin{array}{c} C_2H_4 \\ \Updownarrow \\ \rightleftharpoons C_3H_6 \\ \Updownarrow \\ C_4H_8 \end{array}$$
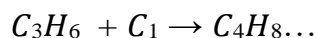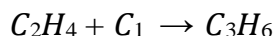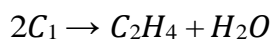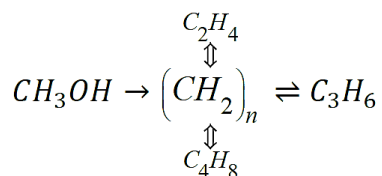
## 3. Conclusion and Outlook

The last two decades have seen excessive progress in the field of MTO. There are 14 operational DMTO units. The development of the investigations involving the first C-C bond is still in progress. The DICP researchers of China have been worked on the MTO process and synthesis of SAPO catalysts since the 1980s. The acidity and pore framework are further used for the optimization of SAPO catalyst. The acidic and pore characteristic are essential factor for the MTO reaction as they influence the performance, catalytic route and selectivity to olefins. In contrast, this catalyst is gaining more attention than ZSM-5 for the MTO process. After more than 40 years, the improvement of the SAPO-34 catalyst is still ongoing and manages to interest the researchers. The Lurgi company process is based on a fixed bed reactor, and ZSM-5, the methanol as the reactant is converted to propylene. The demand of ethylene and propylene is directed by the polymers and fibres industry. Realization of energy demand leads to the further development of the MTO process in all over the world. New catalysts are developed to bridge the gap between demand and supply. Methanol to olefins comes out as a feasible route as it is energy intensive and emission of gases is lesser. As green house gases reduction is also important for our planet, so carbon dioxide gas is also utilized for the production of methanol, which makes this process somewhat sustainable.

## References

1. Amirhosseini M, Askari S & Halladj R 2016 Incorporation of mixed metals into SAPO-34 frameworks by the dry-gel conversion method using mixed templates: Investigating catalysts characterisation and performance. *Journal of Experimental Nanoscience* 11 1032– 1043. (doi:10.1080/17458080.2016.1184767)
2. Askari S, Halladj R & Sohrabi M 2012 An overview of the effects of crystallization time, template and silicon sources on hydrothermal synthesis of SAPO-34 molecular sieve with small crystals. *Reviews on Advanced Materials Science* 32 83–93.
3. Askari S, Sedighi Z & Halladj R 2014 Rapid synthesis of SAPO-34 nanocatalyst by dry gel conversion method templated with morphline: Investigating the effects of experimental parameters. *Microporous and Mesoporous Materials* 197 229–236. (doi:10.1016/j.micromeso.2014.06.028)
4. Bleken FL, Chavan S, Olsbye U, Boltz M, Ocampo F & Louis B 2012 Conversion of methanol into light olefins over ZSM-5 zeolite: Strategy to enhance propene selectivity. *Applied Catalysis A: General* 447–448 178–185. (doi:10.1016/j.apcata.2012.09.025)
5. Castellanos-Beltran IJ, Assima GP & Lavoie JM 2018 Effect of temperature in the conversion of methanol to olefins (MTO) using an extruded SAPO-34 catalyst. *Frontiers of Chemical Science and Engineering* 12 226–238. (doi:10.1007/s11705-018-1709-8)
6. Chen JQ, Bozzano A, Glover B, Fuglerud T & Kvisle S 2005 Recent advancements in ethylene and propylene production using the UOP/Hydro MTO process. *Catalysis Today* 106 103– 107. (doi:10.1016/j.cattod.2005.07.178)
7. Chen J, Li J, Wei Y, Yuan C, Li B, Xu S, Zhou Y, Wang J, Zhang M & Liu Z 2014 Spatial confinement effects of cage-type SAPO molecular sieves on product distribution and coke formation in methanol-to-olefin reaction. *Catalysis Communications* 46 36–40. (doi:10.1016/j.catcom.2013.11.016)
8. Cui Z-M, Liu Q, Ma Z, Bian S-W & Song W-G 2008 Direct observation of olefin homologations on zeolite ZSM-22 and its implicationsto methanol to olefin conversion. *Journal of Catalysis* 258 83–86.

9.  Dahl IM & Kolboe S 1993 On the reaction mechanism for propene formation in the MTO reaction over SAPO-34. *Catalysis Letters* 20 329–336. (doi:10.1007/BF00769305)

10. Dahl IM & Kolboe S 1994a On the reaction mechanism for hydrocarbon formation from methanol over SAPO-34. I. Isotopic labeling studies of the co-reaction of ethene and methanol. *Journal of Catalysis* 149 458–464. (doi:10.1006/jcat.1994.1312)

11. Dahl IM & Kolboe S 1994b On the Reaction Mechanism for Hydrocarbon Formation from Methanol over SAPO-34: I. Isotopic Labeling Studies of the Co-Reaction of Ethene and Methanol. *Journal of Catalysis* 149 458–464.

12. Dehertog WJH & Froment GF 1991 Production of light alkenes from methanol on ZSM-5 catalysts. *Applied Catalysis* 71 153–165. (doi:10.1016/0166-9834(91)85012-K)

13. Dessau RM 1986 On the H-ZSM-5 catalyzed formation of ethylene from methanol or higher olefins. *Journal of Catalysis* 99 111–116. (doi:10.1016/0021-9517(86)90204-6)

14. Dessau RM & LaPierre RB 1982 On the mechanism of methanol conversion to hydrocarbons over HZSM-5. *Journal of Catalysis* 78 136–141. (doi:10.1016/0021-9517(82)90292-5)

15. Dusselier M, Deimund MA, Schmidt JE & Davis ME 2015 Methanol-to-Olefins Catalysis with Hydrothermally Treated Zeolite SSZ-39. *ACS Catalysis* 5 6078–6085. (doi:10.1021/acscatal.5b01577)

16. Flanigen EM 1980 Plenary Paper—Technology: Molecular sieve zeolite technology - the first twenty-five years. *Pure and Applied Chemistry* 52 2191–2211. (doi:10.1351/pac198052092191)

17. Flanigen EM, Broach RW & Wilson ST 2010 Chapter 1. In *Zeolites in Industrial Separation and Catalysis.*, pp 1–24. Ed S Kulprathipanja. WILEY-VCH Verlag GmbH & Co. KGaA, Weinheim.

18. García-Ruiz M, Solís-Casads DA, Aguilar-Pliego J, Márquez-Álvarez C, Sastre-de Andrés E, Sanjurjo-Tartalo D, Sáinz-Vaque R & Grande-Casas M 2020 Synthesis of 10 and 12 Ring Zeolites (MCM-22, TNU-9 and MCM-68) Modified with Zn and Its Potential Application in the Reaction of Methanol to Light Aromatics and Olefins. *Topics in Catalysis* 63 451– 467. (doi:10.1007/s11244-020-01242-x)

19. Gorzin F & Yaripour F 2019 Production of light olefins from methanol over modified H-ZSM-5: effect of metal impregnation in high-silica zeolite on product distribution. *Research on Chemical Intermediates* 45 261–285. (doi:10.1007/s11164-018-3601-z)

20. Hajfarajollah H, Askari S & Halladj R 2014 Effects of micro and nano-sized SAPO-34 and SAPO-5 catalysts on the conversion of methanol to light olefins. *Reaction Kinetics, Mechanisms and Catalysis* 111 723–736. (doi:10.1007/s11144-013-0650-6)

21. Haw JF, Song W, Marcus DM & Nicholas JB 2003 The Mechanism of Methanol to Hydrocarbon Catalysis. *Accounts of Chemical Research* 36 317–326.

22. He T, Hou G, Li J, Liu X, Xu S & Han X 2017 Highly selective methanol-to-olefin reaction on pyridine modified H-mordenite. *Journal of Energy Chemistry* 26 354–358. (doi:10.1016/j.jechem.2017.02.004)

23. Hirota Y, Murata K, Tanaka S, Nishiyama N, Egashira Y & Ueyama K 2010 Dry gel conversion synthesis of SAPO-34 nanocrystals. *Materials Chemistry and Physics* 123 507– 509. (doi:10.1016/j.matchemphys.2010.05.005)

24. Hunger M 1997 Brønsted acid sites in zeolites characterized by multinuclear solid-state NMR spectroscopy. *Catalysis Reviews - Science and Engineering* 39 345–393. (doi:10.1080/01614949708007100)

25. Ji Y, Birmingham J, Deimund MA, Brand SK & Davis ME 2016 Steam-dealuminated,

OSDA- free RHO and KFI-type zeolites as catalysts for the methanol-to-olefins reaction. *Microporous and Mesoporous Materials* 232 126 137. (doi:10.1016/J.MICROMESO.2016.06.012)

26. Keil FJ 1999 Methanol-to-hydrocarbons: process technology. *Microporous and Mesoporous Materials* 29 49–66. (doi:10.1016/S1387-1811(98)00320-5)

27. Lee YJ, Baek SC & Jun KW 2007 Methanol conversion on SAPO-34 catalysts prepared by mixed template method. *Applied Catalysis A: General* 329 130–136. (doi:10.1016/j.apcata.2007.06.034)

28. Lefevere J, Mullens S, Meynen V & Van Noyen J 2014 Structured catalysts for methanol-to-olefins conversion: A review. *Chemical Papers* 68 1143–1153. (doi:10.2478/s11696-014-0568-0)

29. Li J, Wei Y, Chen J, Tian P, Su X, Xu S, Qi Y, Wang Q, Zhou Y, He Y *et al.* 2012 Observation of heptamethylbenzenium cation over SAPO-type molecular sieve DNL-6 under real MTO conversion conditions. *Journal of the American Chemical Society* 134 836–839. (doi:10.1021/ja209950x)

30. Masih D, Imai H, Yokoi T, Kondo JN & Tatsumi T 2013 Methanol conversion to lower olefins over RHO type zeolite. *Catalysis Communications* 37 1–4. (doi:10.1016/j.catcom.2013.03.023)

31. Mirza K, Ghadiri Mohammad, Mohammad H & Afghan A 2018 Hydrothermal synthesize of modified Fe, Ag and K-SAPO-34 nanaostructured catalysts used in methanol conversion to light olefins. *Microporous and Mesoporous Materials* 260 155–165. (doi:10.1016/j.micromeso.2017.10.045)

32. Mole T, Whiteside JA & Seddon D 1983a Aromatic co-catalysis of methanol conversion over zeolite catalysts. *Journal of Catalysis* 82 261–266. (doi:10.1016/0021-9517(83)90192-6)

33. Mole T, Bett G & Seddon D 1983b Conversion of methanol to hydrocarbons over ZSM-5 zeolite: An examination of the role of aromatic hydrocarbons using 13carbon- and deuterium-labeled feeds. *Journal of Catalysis* 84 435–445. (doi:10.1016/0021-9517(83)90014-3)

34. Olah GA 2005 Beyond oil and gas: The methanol economy. *Angewandte Chemie - International Edition* 44 2636–2639. (doi:10.1002/anie.200462121)

35. Olsbye U, Svelle S, Bjrgen M, Beato P, Janssens TVW, Joensen F, Bordiga S & Lillerud KP 2012 Conversion of methanol to hydrocarbons: How zeolite cavity and pore size controls product selectivity. *Angewandte Chemie - International Edition* 51 5810–5831. (doi:10.1002/anie.201103657)

36. Pinilla-Herrero I, Márquez-Álvarez C & Sastre E 2016 Methanol-to-olefin reaction on SAPO-35 catalysts synthesized with controlled crystal size and using mesoporogen additives.

37. *Catalysis Today* 277 29–36. (doi:10.1016/j.cattod.2015.11.030)

38. Rajic N 2005 Open-Framework Aluminophosphates: Synthesis, Characterization and Transition Metal Modifications. *Journal of the Serbian Chemical Society* 70 371–395. (doi:10.2298/JSC0503371R)

39. Razavian M, Halladj R & Askari S 2011 Recent advances in silicoaluminophosphate nanocatalysts synthesis techniques and their effects on particle size distribution. *Reviews on Advanced Materials Science* 29 83–99.

40. Rostami RB, Ghavipour M, Behbahani RM & Aghajafari A 2014 Improvement of SAPO-34 performance in MTO reaction by utilizing mixed-template catalyst synthesis method. *Journal*

*of Natural Gas Science and Engineering* 20 312–318. (doi:10.1016/j.jngse.2014.07.015)

41. Sadeghpour P & Haghighi M 2015 DEA/TEAOH templated synthesis and characterization of nanostructured NiAPSO-34 particles: Effect of single and mixed templates on catalyst properties and performance in the methanol to olefin reaction. *Particuology* 19 69–81. (doi:10.1016/j.partic.2014.04.012)

42. Selzer C, Biemelt T, Werner A & Kaskel S 2018 Hierarchical zeolite ZSM-58 as shape selective catalyst for methanol-to-olefins reaction. *Microporous and Mesoporous Materials* 261 51– 57. (doi:10.1016/j.micromeso.2017.11.005)

43. Shalmani FM, Halladj R & Askari S 2012 Effect of contributing factors on microwave-assisted hydrothermal synthesis of nanosized SAPO-34 molecular sieves. *Powder Technology* 221 395–402.

44. Shalmani FM, Halladj R & Askari S 2016 An investigation of the crystallization kinetics of zeotype SAPO-34 crystals synthesized by hydrothermal and sonochemical methods. *Ultrasonics Sonochemistry* 29 354–362. (doi:10.1016/j.ultsonch.2015.10.011)

45. Song W, Marcus DM, Fu H, Ehresmann JO & Haw JF 2002 An oft-studied reaction that may never have been: Direct catalytic conversion of methanol or dimethyl ether to hydrocarbons on the solid acids HZSM-5 or HSAPO-34. *Journal of the American Chemical Society* 124 3844–3845. (doi:10.1021/ja016499u)

46. Sun Y, Yan H, Liu D & Zhao D 2008 A comparative study on the dehydration of monoethanolamine over cesium phosphate modified zeolite catalysts. *Catalysis Communications* 9 924–930. (doi:10.1016/j.catcom.2007.09.021)

47. Sun Q, Xie Z & Yu J 2018 The state-of-the-art synthetic strategies for SAPO-34 zeolite catalysts in methanol-to-olefin conversion. *National Science Review* 5 542–558. (doi:10.1093/nsr/nwx103)

48. Tian P, Wei Y, Ye M & Liu Z 2015 Methanol to olefins (MTO): From fundamentals to commercialization. *ACS Catalysis* 5 1922–1938. (doi:10.1021/acscatal.5b00007)

49. Wang W, Jiang Y & Hunger M 2006 Mechanistic investigations of the methanol-to-olefin (MTO) process on acidic zeolite catalysts by in situ solid-state NMR spectroscopy. *Catalysis Today* 113 02–114.

50. Wang P, Lv A, Hu J & Lu G 2012 The synthesis of SAPO-34 with mixed template and its catalytic performance for methanol to olefins reaction. *Microporous and Mesoporous Materials* 152 178–184. (doi:10.1016/j.micromeso.2011.11.037)

51. Wang X, Li R, HasnainBakhtiar S ul, Yuan F, Li Z & Zhu Y 2018 Excellent catalytic performance for methanol to olefins over SAPO-34 synthesized by controlling hydrothermal temperature. *Catalysis Communications* 108 64–67. (doi:10.1016/j.catcom.2018.01.033)

52. Wang S, Zhang L, Li S, Qin Z, Shi D, He S, Yuan K, Wang P, Zhao TS, Fan S *et al.* 2019 Tuning the siting of aluminum in ZSM-11 zeolite and regulating its catalytic performance in the conversion of methanol to olefins. *Journal of Catalysis* 377 81–97. (doi:10.1016/j.jcat.2019.07.028)

53. Wu L & Hensen EJM 2014 Comparison of mesoporous SSZ-13 and SAPO-34 zeolite catalysts for the methanol-to-olefins reaction. *Catalysis Today* 235 160–168. (doi:10.1016/j.cattod.2014.02.057)

54. Wu W, Guo W, Xiao W & Luo M 2013 Methanol conversion to olefins (MTO) over H-ZSM-5: Evidence of product distribution governed by methanol conversion. *Fuel Processing Technology* 108 19–24. (doi:10.1016/j.fuproc.2012.05.013)

55. Xu T & White JL 2004 United States Patent.

56. Yang M, Fan D, Wei Y, Tian P & Liu Z 2019 Recent Progress in Methanol-to-Olefins (MTO) Catalysts. *Advanced Materials* 31 1–15. (doi:10.1002/adma.201902181)

57. Ye M, Tian P & Liu Z 2021 DMTO: A Sustainable Methanol-to-Olefins Technology. *Engineering*. (doi:10.1016/j.eng.2020.12.001)

58. Zhang L, Wang H, Liu G, Gao K & Wu J 2016 Methanol-to-olefin conversion over H-MCM-22 catalyst. *Journal of Molecular Catalysis A: Chemical* 411 311–316.

59. Zhang W, Xu S, Zhi Y, Wei Y & Liu Z 2020 Methylcyclopentenyl cation mediated reaction route in methanol-to-olefins reaction over H-RUB-50 with small cavity. *Journal of Energy Chemistry* 45 25–30. (doi:10.1016/j.jechem.2019.09.022)

60. Zhao X, Wang L, Li J, Xu S, Zhang W, Wei Y, Guo X, Tian P & Liu Z 2017 Investigation of methanol conversion over high-Si beta zeolites and the reaction mechanism of their high propene selectivity. *Catalysis Science & Technology* 7 5882–5892. (doi:10.1039/c7cy01804e)

61. Zhou F, Tian P, Liu Z, Liu G, Chang F & Li J 2007 Synthesis of ZSM-34 and Its Catalytic Properties in Methanol-to-Olefins Reaction. *Chinese Journal of Catalysis* 28 817–822. (doi:10.1016/S1872-2067(07)60067-9)

# Review on catalytic degradation of hazardous phonolic compounds using nanocatalyst@carbon

*Aditi Singh[1], Taral D. Patel[1], Vishal J. Mayani[2] and Suranjana V. Mayani[1]\**

[1]Department of Chemistry, Marwadi University, Rajkot-Morbi Road, P.O. Gauridad, Rajkot-360003, Gujarat, India

[2]Research and Innovation Center (RIC), Ceragem Global Industries LLP, Rajkot, Gujarat, India

*Corresponding author: suranjana.mayani@marwadieducation.edu.in

## Abstract

Waste matter containing phenol is hazardous wastewater for the environment and human health. Researchers are working on the performance of several catalysts for phenol removal from wastewater from a long time. The review presents research survey of decomposition of phonolic compounds in the environment and water using nanocatalyst@carbon. Several processes such as Fenton and Fenton like reactions, photo Fenton reactions, wet oxidation and catalytic wet oxidation has also been thoroughly examined. Main aim of selection of catalyst for wet oxidation with particular reference to nano carbon materials has been highlighted. Nanoparticles exhibit significant promise for wastewater treatment, this review discusses trends and future prospects utilizing the sustainable applications of green-synthesized nanocatalysts and nanomaterials for the removal of phenol and its analogues from aqueous solutions.

## Keywords

phenolic compounds, nanocatalyst@carbon, hazardous, wet oxidation, green catalyst

## 1. Introduction

Phenol and its phenolic analogues are extensively used as designer in pharmaceuticals, personal care products and industries. These manufacturing industries generate waste streams that when set free into watercourses cause environmental problems due to their high toxicity and bio-resisting in nature. Therefore, the phenolic discharge must be treated before they liberate into watercourses to protect human health and aquatic environment. Different predictable methods were applied for degradation of phenolic compounds but incapable to completely removal of the organics instead they produce secondary contaminants (Etaiw et al., 2020). Phenolic compounds are normally generated in petrochemical industries as a derivative and, furthermore, include unwanted pyrolysis oil component. Phenolic components obtainable in excess amount in the mixture form in water and are considered as severe environmental pollution. These are corrosive to combustion engines and pipes and are difficult for transformation. This openly goes ahead to the addition of phenol-rich tar in most urbanized country environments, these results in severe pollution of the environment and unnecessary resources of valued organic carbon (Nabgan et al., 2020). The wastewater treatment is still a worldwide concern. Industrial and domestic wastewater needs to be treated correctly, which involves a wastewater treatment method to accomplish an exact minimum level to meet the environmental standards. Even though, wastewater contains different kinds of organics, phenol along with its derivative compounds, constitutes a major class of water contaminants. The main reason is that even when present at lower concentrations, these compounds are highly toxic to living organisms and have therefore been listed since 1976 on the Environmental Protection Agency (EPA) priority list (Saputra et al., 2020).

Nano catalysts doped on carbon are promising catalyst in the field of heterogeneous catalysis, adsorption, wastewater treatment, radiopharmaceutical activities, and chiral resolution. Nano catalysts are on demand everywhere due to their excellent reaction performance,

advantageous recyclability, and low cost by doping on usual carbon materials. Titanium nanoparticles (TNPs) for Ni-Pt/Al nano-sized catalysts, several nano catalysts like Au(Salen)@CC nano composites, metal incorporated composite carbon materials, nanocarbon gold composite, gold phosphorus supported carbon nanocomposites, palladium, gold and gold-palladium containing metal-carbon nanoreactors were successfully used by our research group in the field of catalysis and water treatment by degrading phonolic analogues and dyes in water which usually waste products from industries and research centers. Very few other recent literatures are available in decomposition of phenols by nonmaterial.

## 1.1 Properties that make nanocatalyst@carbon an advantageous catalyst

Salen Schiff base-transition metal complexes and their composites have been mainly scientifically examined due to its capable use as a catalyst in a broad variety of organic transformations (Abdi et al., 2009). Transition metal nanocomposites have opened huge impact over last decade because of their opportunity in applications as a solid catalyst, adsorbent, sensor, electrode, and energy storage (Mayani et al., 2015). To develop improved care of the option of this performance, we researchers have development new heterogeneous catalyst of Au(III) Salen complex onto carbon cage prepared from pyrolysis fuel oil based pitch residue using a novel and environmental friendly approach for the catalytic degradation of carcinogenic water pollutants (Mayani et al., 2017). Transition metal supported porous carbon materials have become a potential catalyst. Recyclability of the catalysts maintains no observable loss of performance during catalytic oxidation reaction. Our research group has developed transition metal supported porous carbon materials have become a promising candidate. Palladium, gold, and gold–palladium anchored carbon composites with two different sized carbon cages (~25 and ~170 nm) were synthesized using nano-silica ball (NSB) as the template and a pyrolysis fuel oil (PFO) based pitch residue as the carbon source (Mayani et al., 2016). Porous carbon materials have some inspiring properties and can be used as templates for the production of metal-carbon nanoreactors. Reusable, low-priced, and environmental friendly metal composite carbon materials have attracted considerable interest as an opportunity to unacceptable composite materials. Considerable research has been carried out to attach metal particles, such as Au, Pt, Pd, Cu, Ni, K, Mn, and Ru to the carbon frame work for prospective applications in the field of catalysis Carabineiro et al. (2013) reported that gold nano particles on carbon nanotubes achieved a combined yield of 3.6 % from cyclohexane oxidation after 6 h reaction time. Oxidative dehydrogenation of cyclohexane and cyclohexene over supported Au, Pd, and Au–Pd catalysts has been accomplished. The hybrid carbon composites with brilliant properties have been considered to gather the demands of multiple applications. These metal-doped carbon materials have potential in the field of energy storage, heterogeneous and electro-catalysis, and material science owing their individual porous structure and surface area, nano size, mass transfer capacity, and chemical and physical properties (Mayani et al., 2016).

Pyrolysis fuel oil (PFO) residue based pitch is measured the most excellent option for the well-organized and inexpensive significant production of new template-based porous carbon networks and devices. A chemically static porous carbon cage (CC) developed from low-cost petroleum pitch as a carbon source after extraction of naphthalene crystals and silica as a template can be used as a metal host, where energetic metal particles can activate along the surface/to be filled inside the carbon framework. Many techniques available for engineering metal carbon nanoreactors (MCNRs), the modern template method and metal doping approach can exceptionally produce a wide range of different sized porous structures and well-defined morphologies with metal functionalities. MCNRs also have several added features as well as the possibility for alteration the activity and selectively of nanocomposites.

Transition-metal composites (tungsten and molybdenum) have shown great significance over the past years because of their potential in applications as a sensor, photochemical device, fuel cell for power generation, adsorbent, heterogeneous catalyst or its host. Therefore, the characteristic properties of transition-metal composites have been found to be similar to those of precious metals, such as platinum (Mayani et al., 2015). Synthesized metal-attached porous carbon materials have been newly studied extensively because of their unique porous structure, peculiar surface properties, mass transfer capability and numerous applications. Among the many methods for fabricating metal carbon nanoreactors (MCNRs), the modern template method and metal doping techniques can afford a range of porous structures with a wide range of pore sizes and well-defined morphologies with metal functionality. The sets of uniform pore sizes and adequate surface areas, as well as the addition features achieved by combining active metal particles with pristine CC, highlight the possibility of improving or encouraging the activity and selectivity of MCNRs (Mayani et al., 2014 a).

Nanomaterials are a group of special material that sticks to on purpose influencing size scales (less than 100 nm). Great attempts have established that nanomaterials based catalysts such as metal/ metal oxide nanoparticles, metal/metal oxide supported nanoparticles, and nanocarbon materials can be helpful in removing organic contaminants from wastewater successfully. Normally, metal/metal oxide nanoparticles based catalysts, mainly Fe, Cu, and Mn species contained in porous solid matrices (e.g., pillared clays, activated carbon, alumina, and zeolites), are highly favorable for catalytic oxidation process. Among those nanocarbons, carbon nano tubes (CNT) are essentially appropriate for catalytic reactions, due to pore volumes, large specific surface areas as well as individual properties. In addition, the doping of nitrogen species in CNTs make them a talented candidate in catalytic wet peroxide oxidation. $Fe_3C@NCNT$ and $NiCo@NCNT$ were recognized to have equivalent activity to metal-based material in electrocatalysis, and the effectiveness is recognized to the graphitic carbon shells activated by those nanoparticles, which give carbons with high electron conductivity as well as satisfactory electron-transfer capacity. Novel nitrogen-doped carbon nanotubes on $Fe_3C$ nanocrystals coated paper-like sintered stainless steel fibers (PSSF) structured catalyst ($Fe_3C@NCNT/PSSF$) was synthesized for catalytic wet peroxide oxidation of phenol (Huang et al., 2020). Carbon-metal catalyst has attracted worldwide attentions in recent years. In this hybrid structure, carbon material has outstanding conductivity and rich chemical active sites; metal species functions as the centre of catalytic reaction and plays the role of electron transport and material transfer. Carbon-metal catalyst thus showed brilliant catalytic activities toward various reactions, including photocatalysis, electrocatalysis and asymmetric catalysis (Song et al., 2017).

## 1.2 Phenolic compounds: Effects on ecosystem and health

Phonolic compounds are characteristic pollutants that mainly come from pharmaceutical, dye, paper factories, or many other industrial sectors. They are harmful to human health and possess high toxicity and carcinogenicity, particularly, showing resistance towards various degradation technologies. Due to such properties, they are usually selected as targeted compounds in many environmental research projects (Huang et al., 2020). The effects of water pollution are not only disturbing to people but also to animals, fish, and birds. Polluted water is unsuitable for drinking, recreation, agriculture, and industry. It decreases the visual quality of lakes and rivers. Further, contaminated water destroys aquatic life and reduces its reproductive skill. In time, it is a danger to human health. Toxicity of an organic pollutant is its normal aptitude to cause an unfavorable health effect, such as the ability to induce cancer, birth defects and other illnesses in animals and humans. Phenols can cause damage to the cells of the living organisms. It has been revealed that a long-time intake of phenols by

experimental animals lead to changes in the skin, lungs, liver, mucous membranes and in the kidneys. As an outcome of phenol dispersion through the man's skin, the skin darkens and the muscles become weak. The toxicity caused by phenols irritates such symptoms as headaches, dryness of the throat, vomiting, and diarrhea. According to other reports, phenols have cytotoxic effect on skeletal muscle and neurotoxic effect on pyramidal neurones. Phenol and its derivatives also show mutagenic effects by unbinding of the DNA helix, inhibition of DNA synthesis in the human cells, and induction of gene mutations. The ingestion of 1 g of phenol is deadly for man.

Chlorophenol is one of the most toxic water pollutants, which causes damage to the critical organs of human beings. 2-chlorophenol is exceptionally corrosive and causes skin, mouth and gastrointestinal injuries. Workers exposed to pesticides that contain chlorphenols have developed acne and mild injury to their livers. In laboratory studies, animals that received high levels of chlorophenols in food or water developed liver and immune system effects, and also weight loss. High levels of chlorophenols given to pregnant female rats in their drinking water reduced the number of babies they had, and caused low birth weights. Chlorophenols have not been shown to cause birth defects in animals. There is evidence to suggest that people exposed to chlorophenols for a long time may have slightly higher cases of cancer. 4-CP is listed as hazardous for landfill disposal. 2,4-dichlorophenol (2,4-DCP) has been described to cause lethargy, tremors and convulsions in mice while workers who made pesticides or were exposed to chlorophenols developed acne and mild liver injuries. 2,4,6-TCP, caused leukemia in rats and liver cancer in mice. It can cause severe skin and eye irritation. 4-nitrophenol is more harmful than 2-nitrophenol when given in high amounts over a short time. Skin irritation has been noted in animals that had large amounts of 4-nitrophenol applied to their skin, and eye irritation when it was applied to the eye. The nitrophenols are, however, not classified as human carcinogens (Mayani et al., 2011).

## 2. Several catalytic processes for decomposition of phenols by nanocatalyst@carbon

A few methods in use for decomposition of phenols are described below:

### 2.1 Fenton and Fenton-like processes

Fenton reaction is one of the best catalytic processes for phenol oxidation. The Fenton reagent (FR) is a mixture of hydrogen peroxide ($H_2O_2$) and an iron(II) salt, which is regularly used for oxidation and degradation of organic substances owing to its high oxidizing power and simplicity. The oxidation of organic substances with FR is an induced chain reaction. Koppenol and Liebman (1984) have compared some of the thermodynamic properties of •OH and $FeO_2^+$ and found both the species to be almost equally active. The extremely reactive nature of the two species has made it very difficult to control the reactions at some desired point. Because of this, the Fenton reaction has almost no control on the product selectivity and this is also the reason for limited use of Fenton reaction for wastewater treatment and similar processes. The Fenton-like reagent, which utilizes $Fe^{3+}$ instead of $Fe^{2+}$ is also capable of oxidizing organic substrates, but it is somewhat less reactive than Fenton's reagent. As iron (III) can be produced in applications of Fenton's reagent, Fenton chemistry and Fenton-like chemistry often occur simultaneously. Therefore, Fenton and Fenton-like reactions are generally believed to continue by similar mechanisms.

Various authors have shown that several oxidation mechanisms may exist all together challenging with each other. Which mechanism overcome is determined by the reaction conditions, such as the metal ligands, the solvent, the pH and the organic substrate to be oxidized. The active species are often indefinable in nature with relatively short life-spans, making it difficult to study their activities or separate them in experiments (Mayani et al.,

2011).

## 2.2 Photo-Fenton reaction

The photo-Fenton reaction has also acknowledged enough concentration as an option, well-organized and low-cost method for wastewater and soil treatment (Chaliha and Bhattacharyya, 2006). In this process, an interaction between radiations and Fenton or Fenton-like reagents creates the conditions for more efficient oxidation of organic contaminants (Pignatello, 1992). This technique has been demonstrated to be very effective in increasing the biodegradability of chlorophenols in natural and industrial waters and has been proposed as a suitable pre-treatment step in treating industrial wastewater (Fallmann et al., 1999). The photo-Fenton method has the advantage that it has high reaction rates and can be powered by sunlight. In Fenton, Fenton-like and photo-Fenton processes, hydrogen peroxide is used which much less in cost is compared to strong oxidizing agents like per sulphate. The commonly mentioned disadvantage of the photo-Fenton method is the necessity to work at low pH (in literature normally a pH below 4 is considered to be necessary), because at higher pH, ferric ions would begin to precipitate as hydroxide. Another difficulty is to remove the added iron from the management method (Klibanov et al., 1980).

## 2.3 Wet air oxidation (WAO)

For treating wastewater full with uncontrollable organics, oxidation reactions are to be carried out in the aqueous environment. In such reactions, the dissolved oxygen can be used to react with the organics. Wet air oxidation (WAO) is thus defined as a process of oxidizing organic matter in the presence of water. Wet air oxidation of organic compounds proceeds via a free radical mechanism initiated by the reaction of the organic substrate with oxygen. WAO is considered as an ultimate process for pretreatment of wastes that are opposing to conventional biological oxidation. In the WAO, water has been shown to behave much like a catalyst and is an integral part of the reaction and the process has the capability to oxidize waste liquors, slurries, and sludges where the oxygen demanding organic matter constitutes only a few percent of the overall waste load. The organic contaminants in water are either partially degraded by means of an oxidizing agent into biodegradable intermediates or mineralized into innocuous inorganic compounds such as $CO_2$, $H_2O$ and inorganic salts, which remain in the aqueous phase. One of the main drawbacks of the WAO process is its inability to achieve complete mineralization of organics, since some low molecular weight oxygenated compounds (especially acetic and propionic acids as well as methanol, ethanol, and acetaldehyde), originally present in wastewater or build up in the liquid-phase during the oxidation process, are resistant to further transformation to carbon dioxide. Consequently, the WAO process is considered as one of the most promising and simplest techniques for partial oxidation of parent pollutants into more biologically agreeable intermediates. The efficiency of aqueous phase oxidation can be largely improved by the use of catalysts, either in the form of solids or as homogeneous catalysts (Mayani et al., 2011).

## 2.4 Catalytic wet oxidation (CWO)

The incorporation of a catalyst into the oxidation process has been considered mainly to reduce the operating temperature and pressure, and/or to treat pollutants that cannot be destroyed during non-catalytic liquid phase oxidation processes. Use of suitable heterogeneous catalysts, on the other hand, has the intrinsic advantage of easy separation of the solid catalyst from the reaction mixture. The heterogeneous oxidation process requires intensive contact between the catalyst surface and the organic contaminants in solution and the process of oxidation follows from adsorption of one or more reactants on the catalyst surface. The process thus involves the following steps (Bhargava et al., 2006): transport of

the reactants to the catalyst or support surface, adsorption of the reactants onto the surface, reaction between the adsorbed species on the surface, desorption of products off the surface, and diffusion of products from the surface to the bulk.

Phenol and its derivatives have been the subject of many studies in CWO. Studies on the mechanisms for oxidation of phenol require some knowledge of the short-lived intermediates as well as the final reaction products. Nano-architecture Cobalt (III) supramolecular coordination polymer based on host-guest has been obtained as an efficient catalyst for phenolic degradation (Etaiw et al., 2020). Saputra et al. (2020) explained carbon-supported manganese for heterogeneous activation of peroxymonosulfate for the decomposition of phenol in aqueous solutions. Novel nitrogen-doped carbon nanotubes encapsulating $Fe_3C$ nanocrystals coated paper-like sintered stainless steel fibers (PSSF) structured catalyst ($Fe_3C$@NCNT/PSSF) was designed for continuous catalytic wet peroxide oxidation of phenol (Huang et al., 2020).

## 3. Reviewed results

Researchers have been delivered continuous efforts in the field of science to develop beneficial nano carbon catalysts for heterogenous catalysis and waste water treatments.

Etaiw et al. (2020) have synthesized Nano-architecture cobalt (III) supramolecular coordination polymer based on host guest recognition as a valuable catalyst for phenolic degradation. In this research works, phenol is utilized as a pollutant pattern for the catalytic degradation experiments under normal conditions (NC), NC with UV-light irradiation and NC with ultrasonic irradiation [NC=$3.4 \times 10^{-4}$ M phenol, 0.4 M $H_2O_2$ and 0.025 g catalyst with stirring. Kinetic study exhibited degradation of phenol to follow first-order kinetics and energies of activation of 2.5 % MnOx/ACP were obtained to be 15.0 kJ/mol 2.5 % MnOx/ACP presents significantly lower activation energy than other catalysts and would be a promising catalyst Saputra et al. (2020). Huang et al. (2000) have described Novel nitrogen-doped carbon nanotubes encapsulating $Fe_3C$ nanocrystals coated paper-like sintered stainless steel fibers (PSSF) structured catalyst ($Fe_3C$@NCNT/PSSF) was designed for continuous catalytic wet peroxide oxidation of phenol. The reaction condition for catalytic degradation of phenol over $Fe_3C$@NCNT/PSSF composite catalyst (feed flow rate: 2 ml min$^{-1}$, catalyst bed height: 2 cm, temperature: 80 °C, $C_{phenol}$: 1 gL$^{-1}$ and $C_{H2O2}$ : 5.1 gL$^{-1}$) (Table 1).

Table 1 Kinetic parameters of catalytic and photocatalytic degradation of phenol using catalyst

| System/ SCP1 | $K_{obs}$ (min$^{-1}$) | $K_t$ (l mol$^{-1}$ min$^{-1}$) | $t_{1/2}$ (min) | $R^2$ | $q_e$ (mg/g) | Time (min) | D % |
|---|---|---|---|---|---|---|---|
| 1. Control experiment | 0.0002 | 0.0005 | 03450 | 0.999 | 0.506 | 1420 | 34.4 |
| 2. NC without stirring | 0.0051 | 0.0127 | 135.29 | 0.982 | 1.252 | 360 | 86.6 |
| 3. NC | 0.0053 | 0.0132 | 130.18 | 0.992 | 1.272 | 350 | 88.0 |
| 4. NC with UV-light irradiation | 0.0100 | 0.0250 | 069.00 | 0.986 | 1.324 | 240 | 96.5 |
| 5. NC with ultrasonic irradiation | 0.0143 | 0.0357 | 048.25 | 0.984 | 1.391 | 160 | 98.9 |

[NC= 3.4 X 10-4 phenol, 0.4 M H2O2 and 0.025 g catalyst with stirring]

[Control experiment = 3.4 x 10-4 M phenol and 0.4 M H2O2 with stirring]

The UV and ultrasonic radiation-catalytic processes presented a new method of elimination of hard pollutants like phenols (Etaiw et al., 2020). Carbon-supported manganese for heterogeneous activation of peroxymonosulfate has been used for the decomposition of phenol in aqueous solutions by Saputra et al. (2020). Phenol decreases with time in adsorbing and catalytic oxidation. Reaction conditions: [Phenol concentration] 75 mg/L, [Catalyst concentration] 0.4 g/L, [PMS concentration] 2 g/L, and T 25 °C.

Mayani et al. (2013) have described metal carbon nanoreactors (MCNR) samples that were made-up by (Figure 1) a nanocasting metal deposition process using pristine CC and metal nanocrystals such as gold, copper, nickel, potassium and manganese. Catalysts were well characterized by physico-chemical characterization methods (Mayani et al., 2012).
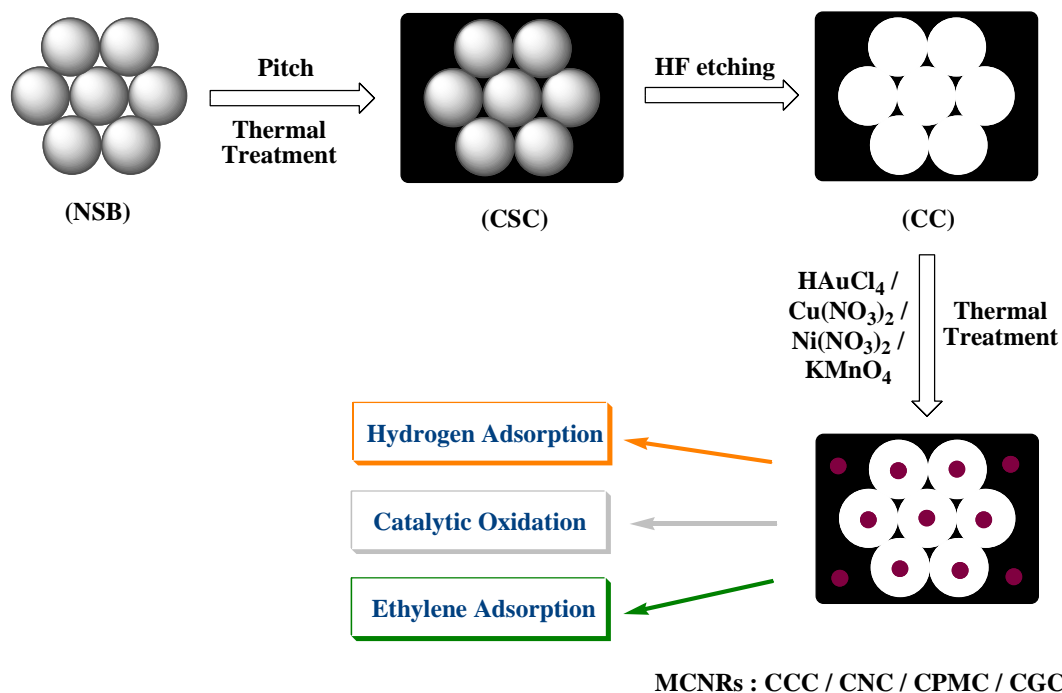


Figure 1. Schematic diagram for the synthesis of metal–carbon nanoreactors (MCNRs).

Heterogeneous catalytic oxidation of 1-phenylethanol was carried out at atmospheric pressure by solvent–free reaction condition using carbon gold composite (CGC) as an eco-friendly catalyst (Figure 2). Authors have carried out the solvent-free oxidation of 1-phenylethanol with CGC in the presence of oxygen gas at 120 °C. CGC provided the oxidation product in ~96 % yield (Table 2, entry 1). This catalytic study clearly recognized the catalytic activity to the Au supported on the CGC material and recyclability of the catalyst.
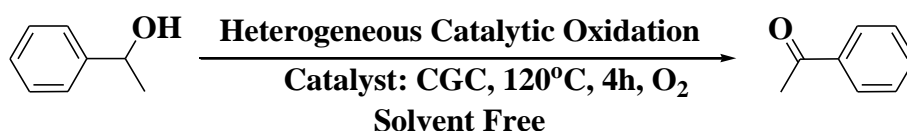


Figure 2. Heterogeneous catalytic oxidation of 1–phenylethanol using CGC.

Table 2 Heterogeneous catalytic oxidation of 1–phenylethanol using CGC and its recycling study[a]

| Entry | Materials[b] | Yield[d] (%) | Catalytic run |
|-------|--------------|--------------|---------------|
| 1 | CGC | 96 | 1 |
| 2 | CGC | 94 | 2 |
| 3 | CGC | 95 | 3 |
| 4 | CGC | 95 | 4 |
| 5 | CC | --- | --- |
| 6 | CGC + MW[c] | --- | --- |

a The reaction was carried out by using 1–phenylethanol (5.06 g) and CGC (0.1 g) in presence of O2 at 120°C for 4 h.

b Two composite materials (CC/CGC) were used as catalyst.

c The reaction was carried out by using 1–phenylethanol (5.06 g) and CGC (0.1 g) was irradiated for 1 min in a microwave oven.

d Isolated yield after column chromatography.

These MCNRs materials are found with excellent adsorption, high catalytic conversion and reasonable stability under the authors' experimental conditions.

Mayani et al.(2014 b) have synthesized Gold Phosphorus Supported Carbon Nanocomposites (Figure 3).



**NSB**  **CPN**  **CGPN**

**CSN**  **CC**  **CGN**
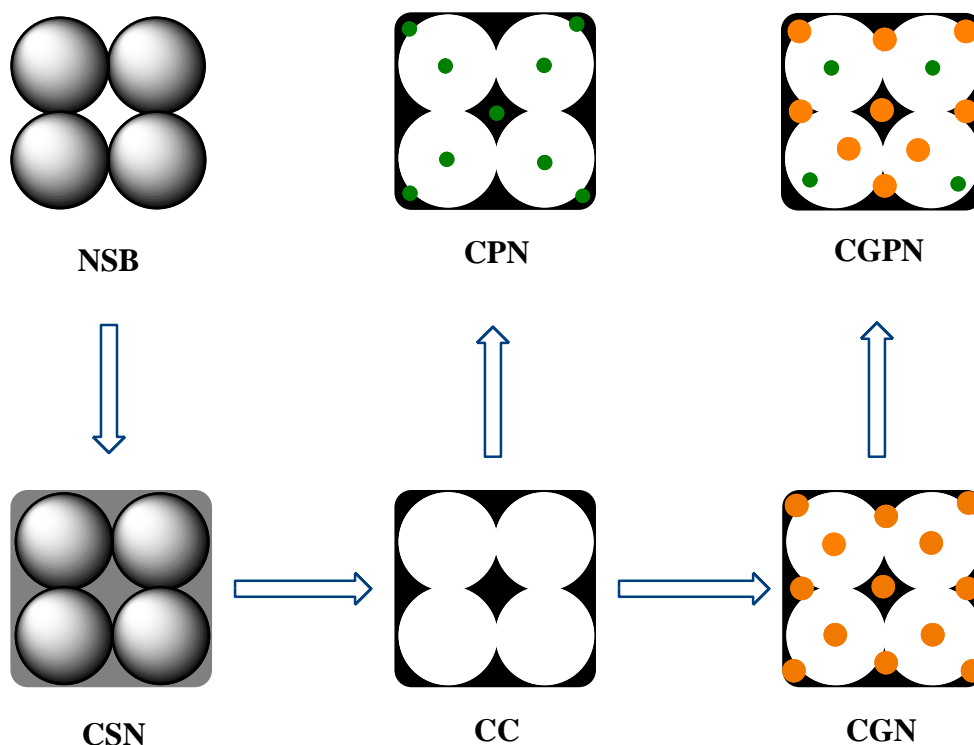
Figure 3. Schematic diagram for the synthesis of NSB, CC, CGN, CPN and CGPN.

These nanocomposite will lead to the novel applications in the field of material science with the combined property of gold and phosphorus along with carbon.

Two sized (~25 and 170 nm) porous carbon supported tungsten carbide were developed using economical petroleum residue followed by tungsten (W) doping by Mayani et al. (2015) (Table 3). Both carbon tungsten composites (CTC-25/170) showed tungsten subcarbide ($W_2C$) and monocarbide (WC) as the major and minor crystalline phase in X-ray diffraction, respectively. Schematic diagram has been discussed in Figure 4.

Table 3 Physico-chemical data and CV capacitance of nanocomposites.

| Samples | BET Surface Area ($m^2/g$) | Total Pore Volume ($cm^3/g$) | BJH Pore Diameter (Å) | Specific Capacitance (F/g) at Scan Rate (10~200 mV/s) | | | | |
|---|---|---|---|---|---|---|---|---|
| | | | | 10 | 20 | 50 | 100 | 200 |
| NSB-25 | 30 | 0.086 | 116 | | | | | |
| CC-25 | 82 | 0.120 | 58 | | | | | |
| CTC-25 | 69 | 0.107 | 61 | | | | | |
| CTCE-25 | --- | --- | --- | 957 | 873 | 780 | 590 | 468 |
| NSB-170 | 163 | 0.290 | 71 | | | | | |
| CC-170 | 212 | 0.857 | 162 | | | | | |
| CTC-170 | 180 | 0.749 | 161 | | | | | |
| CTCE-25 | --- | --- | --- | 439 | 381 | 324 | 288 | 0.2 |
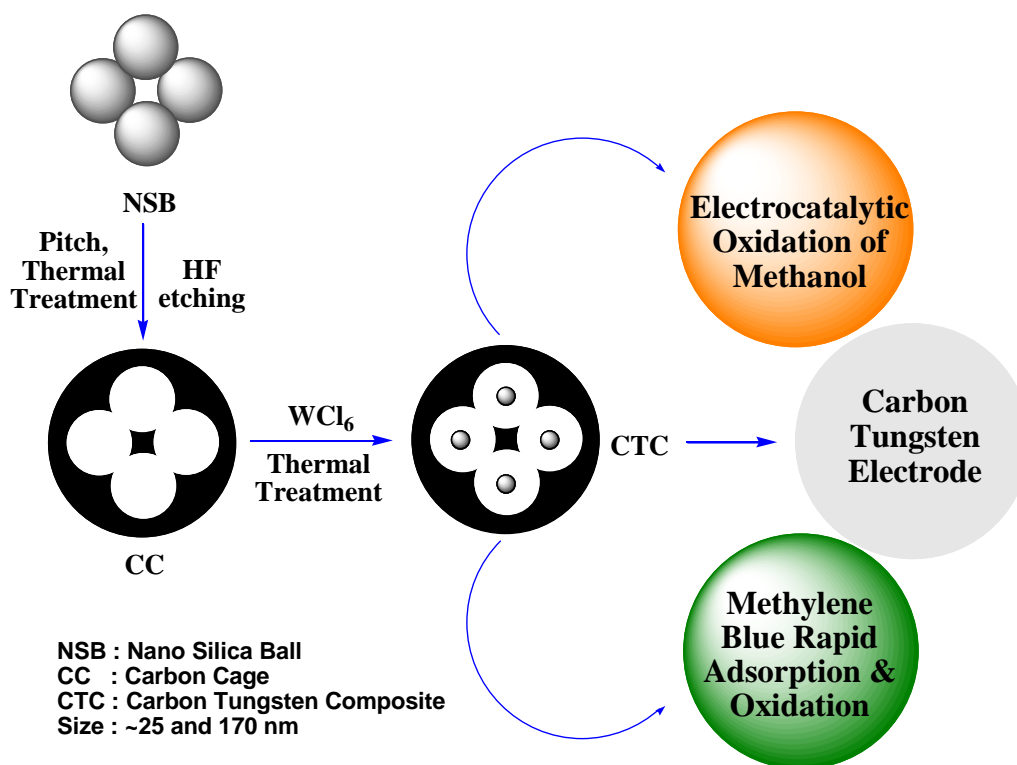


Figure 4. Schematic diagram for the preparation of NSB, CC and CTC.

Mayani et al. (2016) constructed palladium, gold and gold-palladium anchored carbon composites (CPC-25/170, CGC-25/170, and CGPC-25/170) with two different sized carbon cages (~ 25 and 170 nm) using silica spheres as the template and pyrolysis fuel oil (PFO) residue as the carbon source (Figure 5). The Pd, Au and Au-Pd doped carbon nanoreactors were well characterized. The application of catalyst in catalytic oxidation of cyclohexanol with $H_2O_2$ is described in Table 4.



**I = HAuCl$_4$, II = Pd(NO$_3$)$_2$ 2H$_2$O, III = Thermal Treatment**
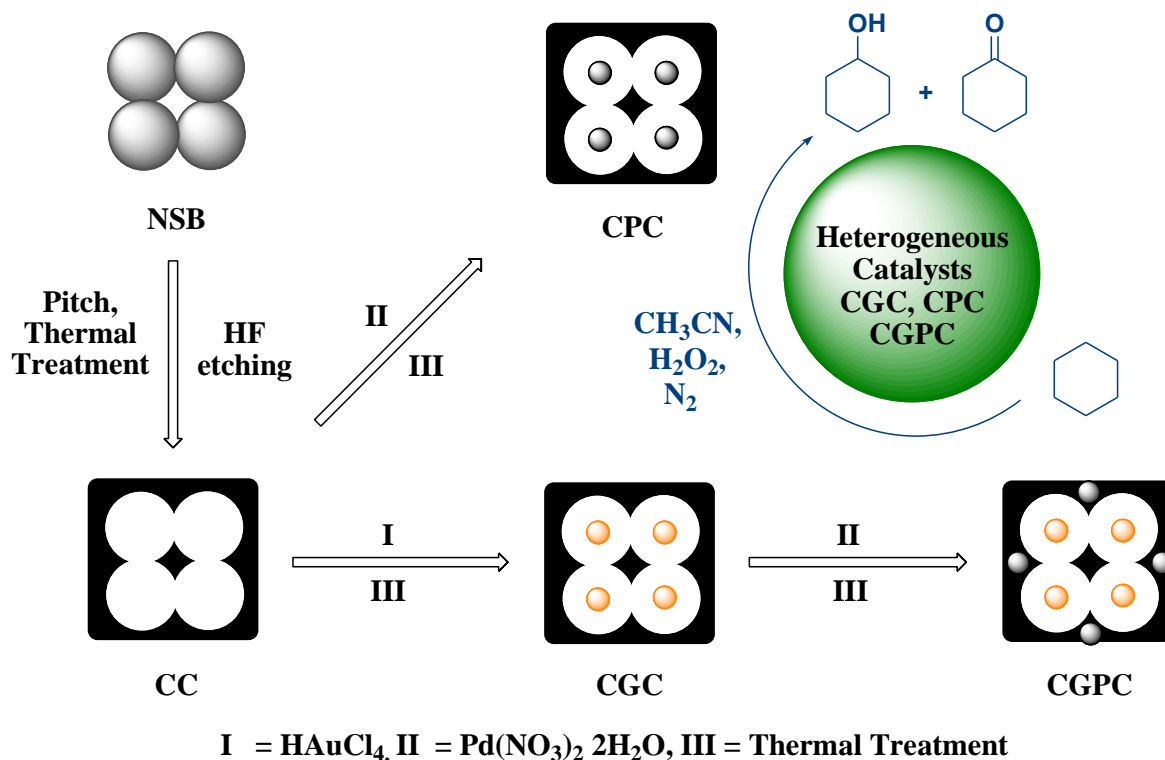
Figure 5. Schematic design for the synthesis of CGC, CPC and CGPC and its catalytic activity.

Table 4 The nanocatalyst applied in catalytic oxidation of cyclohexanol with $H_2O_2$ as given in table below:

| Sr. No. | Catalyst | Yield (%) | | |
|---------|----------|-------------|---------------|-------|
|         |          | Cyclohexanol | Cyclohexanone | Total |
| 1.      | CPC-25   | ---         | ---           | ---   |
| 2.      | CGC-25   | 0.6         | 1.8           | 2.4   |
| 3.      | CGPC-25  | 0.04        | 0.01          | 0.05  |
| 5.      | CPC-170  | ---         | ---           | ---   |
| 6.      | CGC-170  | 4.1         | 3.6           | 7.7   |
| 7.      | CGPC-170 | 0.3         | 0.02          | 0.32  |

Reaction conditions: Acetonitrile (3.0 ml), cyclohexane (5 x 10-3 mol), rt, under dinitrogen, H2O2 10x 10-3 mol, catalyst CPC-25/170 or CGC-25/170 or CGPC-25/170: 0.1 g

Mayani et al. (2018) described new gold Salen complex doped carbon nanocomposite Au(Salen)@CC which was developed by easy methodology using nano carbon cage (CC) prepared from low-priced Pyrolysis fuel oil (PFO) residue based pitch (Figure 6).
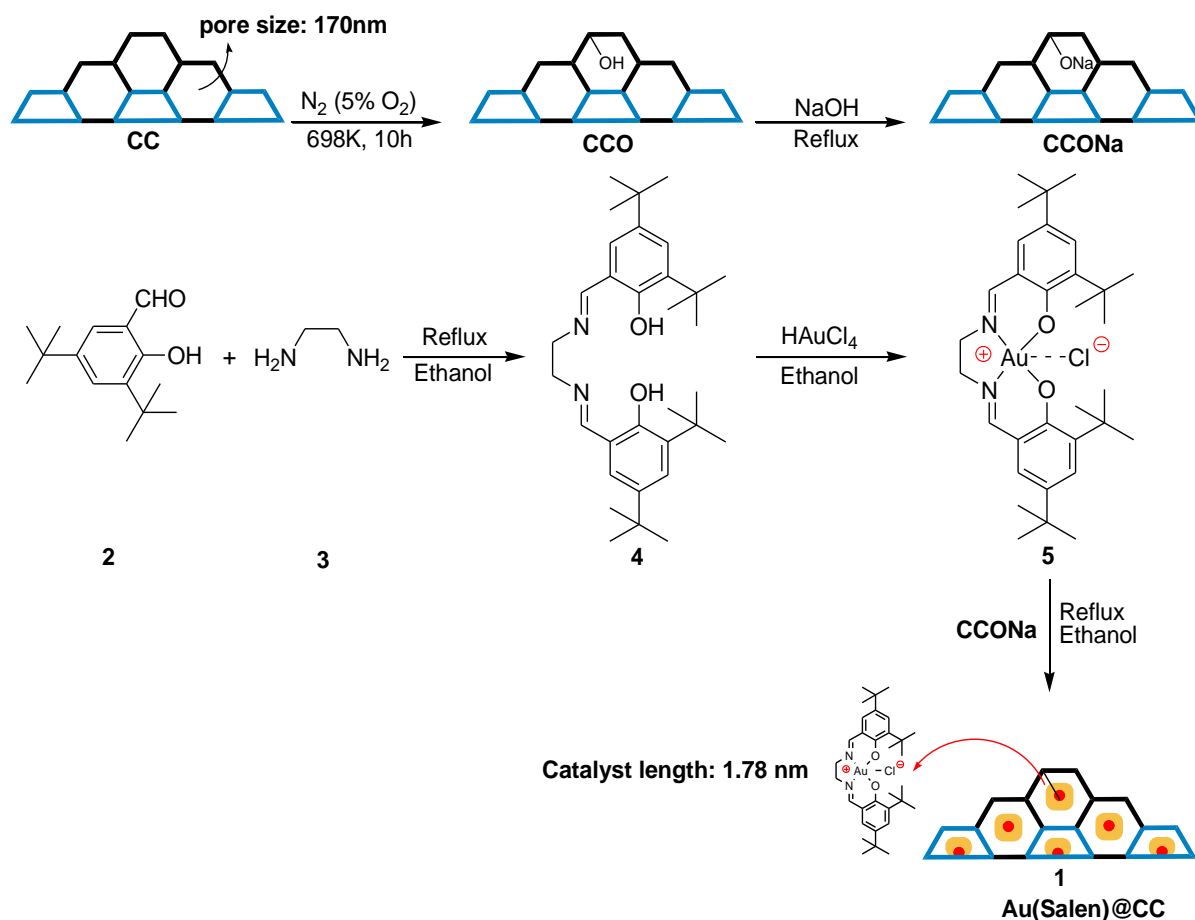


Figure 6. Synthesis path of carbon cage doped nanocomposite Au(Salen)@CC 1.

The catalyst was applied for decomposition of chromotrope 2R and Eosin-Y dyes and further works are carrying out in degradation of toxic phenolic compounds in water. It will be an advantageous and novel catalyst in the field of waste water treatment.

The eleven synthesized metal carbon nanocomposites, Au@NCC (Mayani et al., 2012 a; Mayani et al., 2013), Cu@NCC, Ni@NCC, K-Mn@NCC (Mayani et al., 2012 b; Mayani et al., 2013), P@NCC, Au-P@NCC (Mayani et al., 2014 b), Mo-V@NCC (Mayani et al., 2013), Pd@NCC, Au-Pd@NCC (Mayani et al., 2014), W@NCC (Mayani et al., 2015), and Au-Salen@NCC (Mayani et al., 2017), exhibited not only the particular physico-chemical spirit of concerned metal and nanoporous carbon cage (NCC) but also the combined characteristics of the paired composite and the happening of new behavior able of encouraging untouched procedure (Figure 7). These hybrid organic-inorganic nano catalysts have immense assurance in the field of heterogenous catalysis and water treatment (Mayani et al., March-2021).
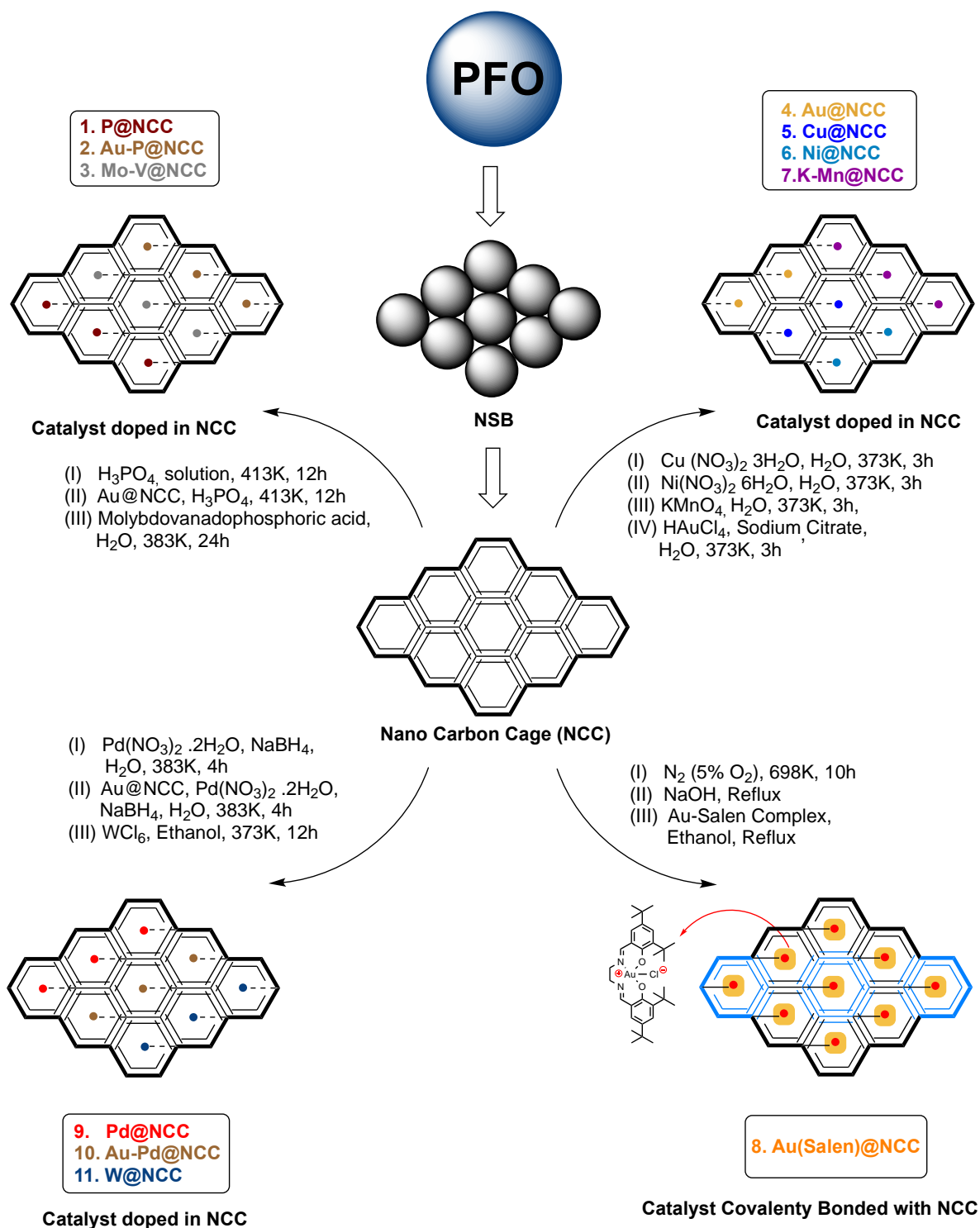
Figure 7. Synthesis route of eleven organic-inorganic metal nanocomposites 1-11.

## 4. Conclusions

The review illustrates the verification for the well-built research efforts approved in current point in time to develop new and improved methods of nanocatalyst@carbon synthesis and for the purification method of phenolic compounds. The best skill to be applied powerfully depends on single cases, in particular from the concentration of phenol in the stream and the co-presence of other contaminants. Scientifically quite simple methods are available.

However, in more complex technologies, advanced apparatus are needed, make certainly more expensive and more complex its operation, but might result very successful in the future to decrease small concentration of pollutants. In this review, opinion of the present authors, when the concentration of phenol in wastes is small, simple techniques that can be performed are preferred choices from the ecological point of view.

## References

1. Abdi, S. H. R., Kureshy, R. I., Khan, N. H., Mayani, V. J., Bajaj, H. C., 2009. Dimeric & polymeric chiral Schiff base complexes and supported BINOL complexes as potential recyclable catalysts in asymmetric kinetic resolution and C–C bond formation reactions. Catal. Surv. Asia, 13, 104–131.

2. Bhargava, S. K., Tardio, J., Prasad, J., Föger, K., Akolekar, D. B., Grocott, S. C., 2006. Reviews: Wet Oxidation and Catalytic Wet Oxidation, Indus. Eng. Chem. Res. 45, 1221-1258.

3. Carabineiro, S.A.C., Martins, L.M.D.R.S., Avalos-Borjad, M., Buijnsterse, J.G., Pombeiroc, A.J.L., Figueiredo, J.L., 2013. Gold nanoparticles supported on carbon materials for cyclohexane oxidation with hydrogen peroxide, App.Catal. A: General, 467, 279-290.

4. Chaliha, S., Bhattacharyya, K. G., 2006. Catalytic wet oxidation of phenol and its derivatives with Fe2O3 and MnO2, Ind. J. Chem. Tech.13, 499-504.

5. Etaiw, S. E. H., El-Aziz, D. M. A., Elzeny, I., 2000. Nano-architecture cobalt (III) supramolecular radation and chemical sensor. J. Organometallic Chem. doi: https://doi.org/10.1016/j.jorganchem.2020.121397.

6. Fallmann, H., Krutzler, T., Bauer, R., Malato, S., Blanco, J., 1999. Applicability of the photo-Fenton method for treating water containing pesticides, Catal. Today, 54, 309–319.

7. Huang, H., Zhang, H., Yan, Y., 2020. Preparation of novel catalyst-free Fe₃C nanocrystals encapsulated NCNT structured catalyst for continuous catalytic wet peroxide oxidation of phenol. J. Hazard. Mater. https://doi.org/10.1016/j.jhazmat.2020.124371.

8. Klibanov, A. M., Alberti, B. N., Morris, E. D., Felshin, L. M. 1980. Enzymatic Removal of Toxic Phenols and Anilines from Waste Waters, J. Appl. Biochem. 2, 414-421.

9. Koppenol, W. H., and Liebman, J. F., 1984. The oxidizing nature of the hydroxyl radical. A comparison with the ferryl ion (FeO2+), J. Phys. Chem. 88, 99-101.

10. Mayani, S. V., Mayani, V. J. Lee, J.Y., Ko, S.H., Lee, S.K., Kim, S.W., 2013. Preparation of multi metal-carbon nanoreactors for adsorption and catalysis. Adsorption, 19(2-4), 251-257.

11. Mayani, S. V., Mayani, V. J., Kim, S. W., 2014 a. SBA-15 Supported Fe, Ni, Fe-Ni Bimetallic Catalysts for Wet Oxidation of Bisphenol-A. Bull. Korean Chem.Soc. 35(12), 3535-3541.

12. Mayani, S.V., Kim, S.W., Mayani, V.J., March-2021. Sustainable Organic-Inorganic Metal Composites for Catalytic Degradation of Industrial Persistent Toxic Substances and Energy Storage, Advances in Wastewater Treatment.

13. Mayani, S.V., Mayani, V. J., Bhattacharyya, K. G., 2011. Phenol and its analogues in water: sources, environmental fate, effects and treatment. Chapter 13 "Chemistry of Phenolic Compounds: State of the Art" Nova Science Publishers, Inc., New York, USA, ISBN: 978-1-61761-335-7.

14. Mayani, S.V., Mayani, V.J., Kim, S.W., 2013. Synthesis of molybdovanadophosphoric acid supported hybrid materials and their heterogeneous catalytic activity, Mater. Lett. 111, 112–115.

15. Mayani, S.V., Mayani, V.J., Park, S.K., Kim, S.W. 2012 b. Synthesis and characterization of metal incorporated composite carbon materials from pyrolysis fuel oil, Mater. Lett. 82, 120–123.

16. Mayani, V. J., Mayani, S. V., Kim, S. W., 2012 a. Development of nanocarbon gold composite for heterogeneous catalytic oxidation. Mater. Letters, 87(1), 90–93.

17. Mayani, V. J., Mayani, S. V., Kim, S. W., 2015. Simple preparation of tungsten supported carbon nanoreactors for specific applications: adsorption, catalysis and electrochemical activity. Appl. Surf. Sci. 345, 433–439.

18. Mayani, V. J., Mayani, S. V., Kim, S. W., 2016. Palladium, Gold and Gold-palladium Nanoparticle Supported Carbon Materials for Cyclohexane Oxidation. Chem. Eng. Comm., 203(4), 539-547.

19. Mayani, V. J., Mayani, S. V., Kim, S. W., 2017. Gold Salen Complex Doped Carbon nanocomposite Au(Salen)@CC for catalytic oxidation of Eosin Y and Chromotrope 2R dyes. Nature's Sc. Rep. 7(7239), 1-9.

20. Mayani, V.J., Mayani, S.V., Kim, S.W., 2014. Development of Palladium, Gold and Gold-Palladium Containing Metal-Carbon Nanoreactors: Hydrogen Adsorption. Bull. Korean Chem. Soc. 35(5), 1312-1316.

21. Mayani, V.J., Mayani, S.V., Kim, S.W., 2014 b. Development of Gold Phosphorus Supported Carbon Nanocomposites. Bull. Korean Chem. Soc. 35(2), 401-406.

22. Nabgan, W., Nabgan, B., Abdullah, T.A., Alqaraghuli, H., Ngadi, N., Jalil, A. A., Othman, B., Ibrahim, A., Siang, T., 2020. NiePt/Al nano-sized catalyst supported on TNPs for hydrogen and valuable fuel production from the steam reforming of plastic waste dissolved in phenol. Int. J. Hydogen energy, 45, 22817-22832.

23. Pignatello, J. J., 1992. Dark and photoassisted $Fe^{3+}$ catalyzed degradation of chlorophenoxy herbicides by hydrogen peroxide, Environ. Sc. Tech. 26, 944–951.

24. Saputra, E., Pinem, J.A., Budihardjo M.A., Utama, P.S., Wang, S., 2020. Carbon-supported manganese for heterogeneous activation of peroxymonosulfate for the decomposition of phenol in aqueous solutions. Mater. Today Chem. 16, 100268.

25. Song, J., Zhang, J., Peng, Y., Zhou, J., Xu, Y., Liu, J., Liu, Q., Qian, G., 2017.Synthesis of a novel catalyst with nano metal core/carbon shell by a facile precomplexation strategy and its application in enhanced catalytic decomposition of nitric oxide. Chem Eng. J. http://dx.doi.org/10.1016/j.cej.2017.07.017.

# Reactive Distillation and Reactive Divided Wall Distillation Column Control Structures – Problems Associated and Mitigation

*Samidha Banka,[1,2] Sachin Parikh[1,3]

[1]Ph. D. Scholar, Chemical Engineering, Gujarat Technological University, Ahmedabad, Gujarat, India
[2]Department of Chemical Engineering, Shri K. J. Polytechnic, Bharuch, Gujarat, India
[3]Department of Chemical Engineering, L. D. College of Engineering, Ahmedabad, Gujarat, India
Orcid ID:[1]0000-0001-9387-7503, [2]0000-0001-9939-2822
Corresponding Author: samidhab1@yahoo.co.in, +91 8401417439

## Abstract

Process intensified technologies are being promoted globally for their better sustainability, efficiency, and economy. The idea of reactive distillation columns is now almost a century old, but its practical application is just four decades old, whereas the industrial applications of reactive divided wall columns are still at the nascent stage. The main reason behind this is the unavailability of a generic and robust optimal control structure. The simulations as well as experimental studies, done so far, clearly indicate the need for process and system-specific control structures. Besides, major sources of disturbances, required product purity, control degrees of freedom, cost, and expertise all play a significant role in the identification of the most suitable control structure. In this paper, we have tried to summarize all the studies made so far on the control structure of reactive distillation and reactive divided wall distillation columns. This paper will help in the identification and development of proper control strategies or structures while installing and operating reactive distillation columns. Moreover, this will even help researchers globally to get instant know-how about control structures for reactive separative columns, consequently promoting more and more practical, economical, and efficient applications of the processes.

## Keywords

Reactive Distillation, Control Strategies, Process Intensification, Process Control, Disturbances

## Abbreviation

| | |
|---|---|
| ATV | Auto-tune Variation |
| DWC | Divided Wall Distillation Columns |
| ETBE | ethyl *tert* – butyl ether |
| L, V, D, B | Liquid, Vapor, Distillate, Bottom Flowrates |
| MPC | Model Predictive Control |
| MTBE | methyl *tert* – butyl ether |
| NLMPC | Nonlinear Model Predictive Control |
| P | Proportional Controller |
| PI | Proportional – Integration Controller |
| PID | Proportional – Integration – Derivative Controller |
| RD | Reactive Distillation Columns |
| RDWC | Reactive Divided Wall Distillation Columns |
| TAC | Total Annual Cost |
| VLE | Vapor – Liquid Equilibrium |

## 1.Introduction

Industrial distillation columns are century old separating structures, and with ever since evolving technology and the need; the distillation processeshave been continuously re-designed and structured. Today the state–of–art technologies and the need for cleaner, efficient, robust, and economical processes have led to a whole new dimension in the field of Process Intensification.(Ramshaw 1995) The process intensification is driven with the core idea of mass and energy integration, which will result intoa hybrid process leading to costand operational benefits.(Stankiewicz and Moulijn 2000; Van Gerven and Stankiewicz 2009; Baldea 2015)Experts point out that process intensification is the vitalfor sustainability in process development sector, and the *"process control is thekey enabling technology for developing and implementing sustainable solutions in the process and energy industry sectors"*.(Daoutidis et al. 2016)

Among all the intensified distillation processes,divided wall column has its history dating back to 1930, (Luster 1930)whilereactive distillation is known since 1922(Backhaus 1922). However, it took several decades for industries to realize them.(Kiss 2014; Segovia-Hernández et al. 2015).As an advancement to these columns reactive divided wall columns was introduced in April 1983 (Kaibel 1983, 1984), nevertheless, their modeling and application started in the early 2000s(Kenig et al. 2004). The initial dynamic simulation studies for RD columns were usually generic and tried to accommodate most of the cases. However, sooner it was realized that unlike conventional distillation columns, this is precarious, as slightest deviation in reactions could produce large disturbances and dynamic instabilities in the process. (Espinosa et al. 1994; Ruiz et al. 1995; Alejski and Duprat 1996). For integrated processes, model-based control systems are not always the best choice. An optimum control system design is usually one which can manage process uncertainties and unforeseen dynamics. Control configurations and algorithms are major aspects of control system design. (Van Diggelen et al. 2010)RD and RDWC modeling and control possess a challenging problem because the parallel separation and reaction leads to complex interactions between vapor-liquid equilibrium, vapor-liquid mass transfer, and chemical kinetics, tending to inevitable nonlinearity in operations. There are three aspects that are often discussed for controlling such systems: (a) the stoichiometric balance of the reactant feed should be maintained, (b) the product quality or the limit of waste or by-product should be regulated and (c) any disturbance whether in throughput, temperature or composition should be controlled.(Kienle and Marquardt 2002; Nagy et al. 2007; Sharma and Singh 2010)Further, there are several studies that throw insight into the fact that the occurrence of multiple steady states or multiplicities is prevalent in the case of RD processes. (Nijhuis et al. 1993; Hauan et al. 1997; Sneesby et al. 1998a; Eldarsi and Douglas 1998; Güttinger and Morari 1999a, b; Scenna and Benz 2003; Pavan Kumar and Kaistha 2008a, b)The tradeoff between the robustness and control of column against input multiplicity is an obstacle. The study suggests that controlling a less sensitive tray temperature promotes better robustness, whereas controlling a high sensitive tray temperature provides control towards input multiplicity; however, it is highly recommended to control high sensitive tray temperature, as it balances feed ratio and thus, enhances overall controllability of RD. (Kumar and Kaistha 2009)

The studies done on output multiplicities in RD, present a few salient features:

- The output multiple steady state conditions are highly depended on the input parameters, this is even true for conventional distillation column.

- The studies suggest that an input multiplicity can convert into output multiplicity, provided high internal flow rates; although determination of minimal internal flow rate that

will result in output multiplicity is not necessary. However, many a times, irrespective of inputs, high internal flow rates tend to produce output multiple steady state conditions.

Not limited to a third kind of multiplicity was mentioned by Sneesby *et al.*; here, output multiplicity is observed about molar inputs, i.e., it is not visible practically, but its effects are notable, hence it is known as pseudo-multiplicity. The study also exemplifies the same using MTBE and ETBE case studies. (Sneesby et al. 1998b)Next, usually the degrees of freedom are independent of each other, but in intensified processes, there is often overlapping amongst them. However, this is discussed in detail by Nikačević *et al.*(Nikačević et al. 2012)*,* the points to ponder here are:

1. Reduced number of degrees of freedom corresponds to a decrease of actuation variables.

2. Smoothing of disturbances is not easy because of system integration.

3. These interactions lead to increased non-linearity and complexity of control systems.

4. Tiny and confined operating range limits the actuation variables' domain.

The general control design procedure for RD columns involve (not limited to): (a) identification of control objective, (b) choosing of manipulated variables, (c) determination of suitable controllers and associated parameters, (d) sending output deviations to manipulating variables (for closed loop) and (e) either control optimization or sensitivity analysis is done.

This paper begins with control strategies for batch RD, then focuses control strategies for RD – categorized into open-loop and closed-loop control structures. Next, we have made a superficial go through of control structures utilized in non-reactive divided wall columns. And finally, it describes control strategies for RDWCs, which also includes, control strategies for reactive thermally coupled distillation column and allied as they are considered equivalent to RDWC. In this paper, we have kept out other hybrid systems such as extractive distillation, azeotropic distillation, and non-reactive catalytic distillation columns, as they possess their own characteristics, which is beyond the scope of this paper and may be considered in future works.

## 2. Control strategies

### 2.1 Batch reactive distillation

The RD column in batch mode is atypicalin practice. However, due to complexities involved in continuous RD, it isoften suggested that if feasible batch and semi – batch processes should be used.(Qi 2010)The history of control of batch RD is quite long and has not been incorporated in this paper, however, we have tried to incorporate studies that are imperative industrially and are reasonably novel and reliable. Cuille and Reklaitis modeled the dynamics of batch RD column and have tried to fit them using several computer programs available then. (Cuille and Reklaitis 1986)Some of the common operational and control issues with batch RD column include:

- Due to time-dependent dynamicity of batch RD columns, use of non-linear controllers are suggested to maintain system stability.

- Identification of suitable intermediate tray temperature which will not allow the flow of heavy key component in the distillate is difficult.

- Trade-off between column temperature and batch time is one of the most difficult tasks, as number of factors must be taken into considerations.

The control strategies for basic PI controllers include – one-point top or bottom or column control and two-point control structures (distillate – reactor temperature). A comparative study suggests that out of all the four strategies formerly mentioned, one point column control is best suited for non-linear systems. (Sørensen and Skogestad 1994)Further, it also, suggest that the control of an intermediate tray temperature (chosen wisely, for most cases it is suggested towards the bottom tank), can benefit by reducing feed losses, unintended temperature gains and interactions among other loops that may cause delayed as wellas perturbed responses. (Sorensen and Skogestad 1992)As, a part of more advanced study, the researchers have tried to optimize the batch RD column, with the objective of maximum profit and minimum time control. A feedback control, implemented to keep heavy key component out of the distillate, with remaining control strategy same as before, was successful in getting high product purity and reaction conversion by measuring the reboiler temperatures.(Sørensen Leversund et al. 1994; Sørensen et al. 1996)

The various papers have been published suggesting different strategies for ethyl acetate production; Alvarez *et al.*presented output feedback controller as the robust temperature-based controller that can manipulate reflux flow rate based on reboiler temperature measurements. The damping of response has been found to be common issue with such controllers. (Pérez-Correa et al. 2008)Jana *et al.* comparedartificial neural network – based generic model controller and gain-scheduled proportional integral and proved former better than later.(Jithin Prakash et al. 2011) (A similar control structure has also been identified feasible for butyl acetate (Kathel and Jana 2010)).A study on delayed neural networks Nonlinear AutoRegressive (NAR), Nonlinear AutoRegressive with eXogenous inputs (NARX) and nonlinear I/O models proves that temperatures predicted using NAR and NARX models represents good dynamic responses. (Giwa and Karacan 2012a)Moreover, generic model controller coupled with non-linear adaptive state estimator, was better than gain-scheduled proportional integral without any doubt.(Jana 2007; Murlidhar and Jana 2007; Jana and Adari 2009)In an another approach feedback inferential control algorithm coupled with artificial neural network was found to be sufficient when composition was taken as controlled variable. (Bahar and Özgen 2010)In an additional approach, inferential state estimation scheme driven by adaptive neuro-fuzzy inference system was implemented for composition estimation with the help of temperatures. The estimations help in improving the performance either through decision making of an operator or through an automatic closed-loop control scheme.(Khazraee and Jahanmiri 2010)In an unusual approach, dynamic optimization has been done, considering maximization of conversion solved using polynomial curve fitting techniques, which consequently help in solving objective cost functions. (Mujtaba and Macchietto 1996, 1997) However, this alone is insufficient as rate parameters are inconsistent, and therefore, robustness is increased by providing an output feedback control. (Monroy-Loperena and Alvarez-Ramirez 2000) Kittisupakorn *et al.*studied the performance of batch RD column using neural network-based model predictive control, which just like all other advanced process control proved to be better than PID. (Kittisupakorn et al. 2011)

## 2.2 Reactive Distillation

### 2.2.1 Open – loop control structures

In this section, we have studied open – loop control strategies for RD processes. In an open loop control structure, output quantity has no effect upon the input. Here, the output responses are neither evaluated nor can be used for corrections in inputs or external disturbances. The open loop structures are – simple, cost efficient and suitable for both discrete and continuous process. (Sharma 2011)

**A + B ⇔ C**

The steady-state design considerations of MTBE and ETBE are quite promising in case of RD but the same is false when dynamic responses are considered; studies suggest this is either because of the presence of hysteresis or occurrence of system instability. (Jacobs and Krishna 1993; Nijhuis et al. 1993) It is, therefore, indispensable to study the dynamic responses for hybrid systems to identify the pros of integrating control system design with process design, as this can influence instrument requirements. (Sneesby et al. 1997a) For SISO control structures the studies suggest that the disturbances can be best handled using composition control, but it requires an additional online analyzer, which adds a large cost to the equipment.The studies also reveal that temperature control is easier and less expensive, and it provides adequate control as long as disturbances are not too large; although, allowing the use of feed forward control with temperature control will allow handling even for large disturbances. (Al-Arfaj and Luyben 2002a)

Sneesby *et al.* showed the results for open-loop dynamic responses for some key disturbances to the system. The step input was introduced on two fronts one-by-one namely feed rate and feed composition, keeping reflux rate, reboiler duty, and overhead pressure constant. In both the cases, the composition of the bottom product got shifted to include the additional light material and the temperature decreased,accordingly as the reboiler remained in phase equilibrium. Further, this resulted in lower recycling rates of excess component into the reactive zone and hence, lower conversion rates were seen. In addition to this, one more case was studied where step input was brought in reflux rate, keeping everything else constant, and the result was an instant response in the beginning which then came to equilibrium. Since the reboiler duty was kept constant, the column temperature quickly came down because of extra reflux, and the reactant was found in the reboiler. Although, there was a positive effect of not finding reactant in distillate as it gave higher product purity; overall the system damped as there was no reactant recycle and lower conversion rates. An additional problem may arise wherein, at higher ambient temperatures the reflux drum will go dry and the reflux rate will fall gradually; at this point in time if reboiler duty is not manipulated then there will be a significant decrease in the conversion rate and column performance. (Sneesby et al. 1997b, a) A comparative study made for one point open loop control structures for ETBE production on disturbances rejection under multi-loop structures namely, LV, DB, LB, (L/D),V suggested LV as best option, although, open loop systems are disregarded as it does not allow manipulated variable corrections. (Bisowarno and Tadé 2002)

**A + B ⇔ C + D**

Open–loopcontrol structuresto producetwo reactants – two products are found commonly in case of esters in RD.Generally, the studiesstart with the steady-state design of RD and end at the sensitivity analysis of the dynamic models. The studies clearly conclude that unlike the conventional distillation column, in RD there is no direct relationship between the temperature and product purity. Apart from this few other statements can be asserted; (i) recycling leads to higher residence time;(ii) Recycling of reflux do not lead to system instabilities; (iii) coupled systems take more time to compensate any disturbances and (iv) the stoichiometric balance in feed is extremely important as minimalist imbalance will lead to a gradual build-up of that component. They also mention that open loop control structures do not suffice the optimum need of control. (Bock et al. 1997; Sandoval-Vergara et al. 2008)

**A ⇔ B + C**

Arfaj *et al.* studied the open-loop control structures for olefin metathesis to produce 2–butane and 3–hexene. The reaction goes as $2C_2H_5 \Leftrightarrow C_4H_8 + C_6H_{12}$. In one of the control structures, where the bottom purity is controlled, the reflux rate is kept constant and disturbances in the feed are introduced; a variation from conventional distillation is found. In the case of

conventional distillation, this control structure provides consistent purity in distillate composition; whereas in case of reactive distillation, *"Changing the feed rate in a reactive column changes the load on the reactive zone."*Consequently, to maintain the product purities and conversion rates, reflux ratios must be changed in accordance with feed changes. For a single feed system, an internal composition analyzer is not required to balance stoichiometry. Furthermore, for both steady-state as well as dynamic systems, dual composition/ temperature control structure will provide the most effective control.(Al-Arfaj and Luyben 2002b)

### 2.2.2 Closed – loop control structures

In this section, we will discuss about all the possible closed loop control structures studied so far for RD processes. If the output of the process affects the input and/ or input or external disturbances, they are altered or regulated based on outputs obtained in order to maintain desired and consistent results which is known as a closed loop control structure. It is also known as feedback control as the output of the process is returned to the input.(Sharma 2011)

**A + B ⇔ C**
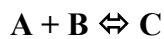
The production of epichlorohydrin using an isomeric mixture of dichloropropanols and an alkali is an apt example here. The production of epichlorohydrin is achievable in RD as the relative volatility of epichlorohydrin is considerable when compared with organic wastes received at the bottom. Further, keeping environmental considerations, it becomes necessary to have near-perfect separation of product and waste; before the waste is treated. A hybrid control structure for the same is proposed which is fed with inlet concentrations, which acts as an input variable to the black box dynamics. The controller is a linear internal model type that is capable of handling column delays. The study concluded that the combination of a black-box model with physical knowledge leads to a reduced model structure which is beneficial for systems with complex dynamics. (Chen et al. 2000)

**A + B ⇔ C + D**

The most common control structure for classical two-component reactants – two-component products system suggested with equimolar feed: A + B ⇔ C+ D for RD process is two point temperature control. (Kaymak and Luyben 2005, 2006)Al-Arfaj and Luyben (Al-Arfaj and Luyben 2000) have suggested six different control structures for RD. Their study is based on classical system with equimolar feed:(myristic acid (A) + 2 – propanol(B) ⇔ isopropyl myristate (C) + water(D))such that the relative volatilities are in order of $\alpha_C > \alpha_A > \alpha_B > \alpha_D$.Since the feed is equimolar, therefore, feedback about reactant composition inside the system is required for an effective control system. (Luyben et al. 1999) The details of the system can be referred to through the paper.

The summary of the first four composition-based control structures is given in the table 1. In the fifth control structure, a conventional method of tray temperature control is used instead of composition. Also, single-end control with constant reflux ratio control is used; the results are promising as changes are easily handled. For the last control structure, the distillate product purity is controlled by manipulating the fresh feed flow rate. The dynamics of the scheme are slower than the others because of the lags in the distillate composition to the fresh feed loop. The details of the control structure are presented in table 1. In anothercomparative study made by Luyben wherein, he has compared the aforementioned six control structure for ternary systems with and without inert; the study asserts that dual point temperature control structure is infeasible for systems with inert, however, it is readily applicable for ternary and quaternary systems without inert. The study remarks that in case of presence of inerts, their molar flow rate in feed affects the dynamics of the system and thus when designingthe

control structure a composition control loop must be present inevitably. (Luyben 2007)In addition to this, Arfaj and Olanrewaju have also proposed dual-end composition control structure with state estimator, which suggests the inherent need of controller tuning for robust process dynamics. (Olanrewaju and Al-Arfaj 2005) The two-point and three-point structures with cascade compensation of the temperature set-points effectively maintain the distillate and bottoms purity for a large throughput decrease. However, the two-point structures fail for a large increase in throughput. This is because in the kinetically controlled regime, maintaining the distillate purity requires an increase in the effective reflux ratio to internally recycle the escaping reactants back into the reactive zone. The three-point structures efficientlyretain the product purities as the reflux ratio is inexplicitly tweaked through the manipulation of the reflux rate.(Pavan Kumar and Kaistha 2008c)

Ward *et al.*studied the plant-wide control of reactive distillation process for three different systems, namely – (i) methyl acetate hydrolysis, (ii) methyl acetate – butanol transesterification and (iii) methanol – adipic acid two stage esterification, in all three cases conventional PI control structures were used with temperature as controlling variable and the results showed fast, robust, stable, economical and safe dynamics. (Hung et al. 2010)

Giwa *et al.*has proposed various control strategies for reactive distillation systems both open and closed loops ranging from P-PI controllers to MPCs. They studied the dynamics of RD for various cases:

1. In study, for biodiesel synthesis, it was found that cascaded PID control structure proves to be more suitable than conventional PID controllers, provided product purity is the controlled variable, reboiler duty is manipulated variable and disturbances are brought in reflux rate. (Giwa et al. 2018)

2. Another approach was using two-black box models (ARX and ARMAX) for ethyl acetate, and identified that ARX models had lower response times and steady states were achieved faster, whereas, ARMAX models gave better set-point controls. (Giwa and Karacan 2012b)

3. Next, when the dynamics were studied on application of decouplers in MPCs, for the production of ethyl acetate, it was found that neural network decoupling MPC out performed transfer function decoupling MPC. (Giwa and Karacan 2012c)

4. Lastly, when decoupling of PID controllers were applied for set-point tracking and disturbance rejection; the Cohen-Coon tuning technique gave more acceptable results than Ziegler-Nichols, when only set-point tracking was considered, (Giwa and Karacan 2012d) whereas Cohen-Coon tuning was more acceptable for controlling both parameters. (Abdulwahab et al. 2015)

**A ⇔ B + C**

The dual-point temperature control scheme for equimolar reversible metathesis reaction of 2–pentene to produce 2–butane and 3–hexane is studied by a group of Chinese scholars.In this study, the reflux rate and reboiler heat duty was the manipulated variables whereas, the temperature was the control parameter (tuned using Ziegler–Nichols method). The study is based on two different designs; in one case, the entire column is taken as a reactive zone with no distinct separation zones and in another case, a typical reactive distillation column is considered. The study suggested better control for step-change disturbances when separating zone is provided, as this provides a balance between mass, heat, and reaction. On the other hand, magnified deviations, and extended settling time, as in case 2, is responsible for inferior bottom product controllability. The trade-off between the two control structures is thus, dependent on the remaining factors when the column is realized.(Lin et al. 2011)

The concluding remarks for RD control structures will be: (a) Despite being simple, inexpensive, and easier in the application, open-loop control structures give no assurance for consistent output is available. (b) The unavailability of generic control structure which suffices at least the basic need of control in RD is the main reason for hurdle in RD's industrial application on a large scale. (c) It is also important to find a way to tradeoff between control structure stiffness, the robustness of process and achieving desired product purity. (d) Advanced process controls are in limelight for their benefits over conventional controllers, but their cost and skilled labor requirement is still causing hindrance in commercial activities. Moreover, detailed studies are still scope for synergic applicability of advanced process controllers along with control structure optimization and sensitivity analysis.

## 2.3 Divided Wall Distillation Column

Before we jump to reactive divided wall distillation column (RDWC), it is necessary to quickly brush through the review strategies of divided wall columns (non − reactive separation system), because in layman terms RDWC = RD + DWC. The prime purpose of using a DWC is the integration of energy, to have operational savings and hence minimization of heat utility. The earliest record of the DWC control system, to the best of our knowledge, goes back to 1978, wherein a thermally coupled column, was suggested (Seader 1978). However, the first literature on the control of the divided wall distillation column appeared in 1993 (Lestak and Smith 1993).The studies dictate that a high energy saving optimal design will cost good controllability, thus one has to trade-off between the two aspects. (Segovia-Hernández et al. 2005; Robles-Zapiain et al. 2008; Tamayo-Galván et al. 2008) Gomez Castro *et. al.*in their study concluded that the DWCs provide reasonable values for condition number andminimum singular value; eventually, closed-loop dynamics proved to be assuring. (Gómez-Castro et al. 2008) One of the simplest control structures, which is just a step ahead from the binary distillation column is a three-point control structure. The control structure suggests that distillate purity is controlled using the reflux flow rate, side stream purity is controlled using side stream flow rate and bottom purity is controlled using the boil-up ratio. The studies suggest that controllability using both linear and nonlinear models is quite satisfying to a large extent, the problem arises for extremely small changes in product purity at the extremes. To nullify this error, an additional point of control was also studied. (Wolff and Skogestad 1995) Serra *et. al.*also studied a three-point structure to control the product purity with distinct set of manipulated variables. Their results were coincident tothat of Wolff as discussed earlier. The studies also suggested that the better performance of PI is obtained using Dynamic Matrix Control. (Serra et al. 1999, 2000, 2001, 2003)An alternative is nested three control point loop wherein, side stream composition was controlled using reboiler vapor and bottom product composition was controlled using side stream flow rate. While this structure could not stand mild disturbances because of the nonlinearity of side stream composition and reboiler vapor pairing (Wolff and Skogestad 1995); a successful modification to this method was done where reflux and distillate were switched in distillate composition control loop. (Abdul Mutalib et al. 1998; Mutalib and Smith 1998)

The next set of control structures contain the liquid split ratio as an additional manipulated variable, which helps in controlling side stream impurities. One method is simple three-point control, and the results showed the difficulty of control for both linear and nonlinear models, moreover, tiny gains were achieved; and the steady-state feasibility space showed regions where no steady states existed.(Wolff and Skogestad 1995)When the liquid split control was used to control the level of heavy impurity at the top of the prefractionator the results were good and sound. (Halvorsen and Sigurd 1997; Halvorsen and Skogestad 1999; Ling and Luyben 2009, 2010)

The next set of control structures is based on inferential temperature measurements. There are two ways of implementing it, in both cases, the liquid split ratio has not been considered. The first one is controlling the temperature at the top of the prefractionator which was controlled by manipulating the reflux flow rate, as studied by Adrian *et al.*(Adrian et al. 2004); their studies remarked that the use of MPC alone is better than multi-loops PID, i.e. multi – SISO controllers. The second approach has suggested temperature control in the bottom of prefractionator which was controlled by manipulating the heat duty of reboiler. The control system worked well for disturbances in feed flow rates but not for large deviations in feed composition. The recommended solution for the problem is cascaded temperature/ composition control systems.(Wang and Wong 2007)Further, in a comparative study, the gap between PID controllers and MPC controllers has been identified and authors proposed a strategy wherein, LQG controllers have been proved better option over PID multi-loop framework, in terms of feed disturbance rejection and use of loop shaping design procedure provides additional μ-controller benefits. (Van Diggelen et al. 2010)Last but not least, there have been several advanced control techniques discussed by Kiss and Bildea. Their study also analyzed a few case studies and remarked the hierarchy of development of control structures for divided wall distillation columns.(Kiss and Bildea 2011)

## 2.4 Reactive Divided Wall Distillation Column

Prior to our study, a brief account of literature survey on control of RDWC is given by Weinfeld *et al.*, though, their study was an overall review on RDWC and thus, accounted for few papers on control. [106] In this section, we have tried to concentrate specifically on all studied control structures for RDWCs and thermally coupled RDCs. RDWC has proved to be reliable for reactions where selectivity plays an eminent role.Yuan et al. presented an ASPEN based simulation paper wherein they have utilized PI controller (P for level control) with relay feedback and Tyreus–Luyben tuning to implement composition-based controller which controls impurities in product flow. The reactions taking place here is hydrogenation of methyl acetylene and propadiene into propene and propene's hydrogenation to propane. The objective of the study is to identify control for selective hydrogenation and separation of the C3 stream. The feed stream comprises of propene, propane, butylenes, methyl acetylene and propadiene. The propene is obtained from the top, whereas here the bottom part of the column is split, thus getting two heavy products – propane and butylenes. Their study reveals the inevitable need for composition control and the inefficiency of temperature control structures. Further, the deviations in steady state despite using PIDs have made them bring an advancement. To this, they suggested model predictive control using GA to tune the parameters. In this study, there are 8 controlled variables and 8 manipulated variables; the results showed that both the number and amplitude of the oscillations of dynamic responses worked reliably for feed disturbances. The study also reflected the superiority of MPC over PI and feed-forward PI control systems. (Qian et al. 2015, 2016b, a)Moreover, for the reversible processes such as hydrolysis of methyl acetate, using a similar control strategy with just tray temperature control was found to be absolutely fit for rejecting large feed disturbances and maintain product purity. (Lee et al. 2010)

Rangaiah *et al.* have made a comparative study on control structure for production of n-propyl acetate, on four different columns, RD, RDWC, heat integrated RDWC, and vapor recompression heat pump assisted RDWC; the study mentions two controlled parameters: stoichiometric balance of feeds/reactants manipulated by sensitive tray temperature and liquid split ratio manipulated by reflux rate. Closed-loop P level controllers and PI temperature controllers were used, which were tuned by the ATV test while tuning parameters were calculated by the Tyreus-Luyben PI tuning rules and simulations carried out in ASPEN Dynamics. The results showed that the fixed liquid split ratio control strategy performs better

than control strategy wherein the ratio of the reflux rate to the sum of the two-feedreactant flowrates was fixed when the objective was smoother dynamics and lower energy consumption; with vapor recompression heat pump assisted RDWC as the best process.(Feng et al. 2019)Chien *et al.* studied the control of reactive divided wall distillation column for mixed feed alcohol (n–amyl alcohol and n– hexanol) system to produce amyl acetate and hexyl acetate, in presence of acetic acid and water as a by-product. Their control structure consisted of nine inventory loops out of which six were level and three pressure control loops. The reflux flowrate, reboiler duty, and feed ratio are other manipulated variables. The control structure was tested for three different types of disturbances: (a) Change in feed composition, (b) Change in throughput, and (c) the boil up ratio change. For all the three disturbances dual temperature control system, the temperature setpoints were achieved rapidly, although the effect on product purity is not so promising. (Wu et al. 2012)

Hernandez *et al.* provided the controllability analysis for thermally coupled RD to produce biodiesel. Their study was based on singular value decomposition for an open-loop dynamic and the underlined theory that minimum singular value is a measure of the invertibility of the system and a measure of probable troubles of the system under feedback control. The condition number determines the sensitivity of the system, during uncertainties in process parameters and modeling errors. These parameters give a qualitative judgment of the theoretical control properties of the possible designs. The systems with higher minimum singular values and lower condition numbers are anticipated to demonstrate the best dynamic performance under feedback control. Similar studies have also been identified for other systems, too.(Jantes-Jaramillo et al. 2008; Ibarra-Sánchez and Segovia-Hernández 2010)

The model benefit over here is that the dynamic responses can be first/ second-order transfer functions with/ without dead times. The study focused on the comparison of control strategies for direct RD sequences (DRDS), indirect RD sequences (IRDS), and thermally coupled RDs with side rectifier/ stripper (TCRD). The study asserted that indirect RD sequences (IRDS) had the best control properties, however, TCRD does not disappoint much, and TCRD coupled with a minimum number of reboilers will perform satisfactorily under closed-loop dynamics.(Vázquez-Ojeda et al. 2012)

It is essential to understand that in reality, it is not just individual equipment that performs but the entire plant needs adequate, efficient, and robust control and thus, a few studies have also been made in this direction. However, when processes are intensified, the overall process is primarily driven by one or two major equipments that playsa crucial role in defining the control strategies. Moreover, sustainability being the heart of process intensification, most plants work on minimum waste production, minimum utility wastage, less by-product production, and thus, fewer recovery systems. Baki and Kaymak in their study have tried to compare various Plant-wide control schemes for two reactive distillation columns for dual reaction systems such as A + B → C + D and D + E → B + F, with A and E as fresh reactants, and C and F as desired products. Here, all temperature and composition controllers are PI controllers and all liquid level controller as P controllers, except for reactor hold-up, for which a PI controller is used. All controllers are multi-loop SISO. The conventional Relay-feedback tests and Tyreus–Luyben tuning parameters were used. The details of all four control structures can be referred from the literature. However, what study reveals is noteworthy, (a) when the flow rate of a single stream taking part in both recycle loops is controlled, it offers a steady base-level regulatory control, however, the settling down process time is large and product purities aren't within the specifications; (b) if the flowrates are controlled in each recycle loop, settling time is desirably improved, however, to maintain the bottom purity,three-point temperature control is required; (c) Lastly, dual temperature control is essential for maintaining product purity in the second column.(Kaymak and Baki 2011)A

similar study has also been done by other researchers, wherein they have thermally integrated the two RDs. Here, a single reaction system is considered and as concluding remark authors suggest a pressure compensated temperature control which was able to handle feed disturbance up to 20% while maintaining the product purity, (Hsiao et al. 2017)Table 2. tries to cover papers corresponding to Plant-wide control strategies for several types of columns discussed in the paper.

Despiteadvanced control techniques being used, there are several challenges faced, during the control of RD and RDWC. These are well discussed in this paper with reasonable examples. Here is animmediate review of them, these are also discussed by Dias and Ierapetritou (Dias and Ierapetritou 2019) :

- The execution of model-based control structures is intricate and tedious, while modeling and parameter tuning is done; this is, moreover usually,expensive, and time-consuming. Such models can be developed either by first principle (black box techniques) or by system identification techniques. In each case, there are limitations; in the former case, the detailed mathematical modeling is required followed by precise experimental validations; whereas in the latter case, models identified from the experimental data are limited to certain operating conditions and are largely system and process specific, the generalization of control structures is not feasible.

- The RD processes, as discussed, tend to have steady-state multiplicities, complex phase, and higher-order nonlinearity. The studies suggest partial applicability of modified NLMPC and multi-parametric MPC. (Sharma and Singh 2010)

- For most reactive separative systems, overall degrees of freedom is minimal, as cascading of system makes it stringent to have variable measurement and manipulation of streams. (Baldea 2015)

## 3. Summary

Control of RD is a challenging problem due to process nonlinearity, complex interactions between vapor-liquid equilibrium and chemical kinetics. The presence of multiple steady states and the highly nonlinear nature of RD may impose limitations on the use of linear controllers. Multifunctional processes have an inherent disadvantage of lower degrees of freedom which restricts the flexibility of using a wide variety of controllers as well as varied process parameters. Moreover, multi-functional processes operate in a slim operating range, which is visible in actuation restriction.

Several studies, many of them mentioned in the paper, suggest that RD columns is better controlled using closed-loop cascade controllers and it is always beneficial to go for reduction of the model for control structure study.(Rouchon et al. 1991; Van Breusegem and Bastin 1992; Chen et al. 1995; Grüner et al. 2003)

In all the papers studied, it is evident that the process variables – either temperature or pressure are only to be controlled for RD and RDWC. One of the major variables to be maintained is the stoichiometric ratios of the feed, with either temperature or composition or both for the isobaric process. The basis of any control structure designed is to minimize reboiler heat duty and maintain consistent product purity. It is lucid from the study made that problem of maintaining product quality can be solved by controlling the tray or stage temperature that avoids multiplicity with the change in reboiler duty, further this temperature is robust against throughput and catalyst deactivation disturbances.(Wang et al. 2003)A study on low molecular weight alcohols with acetic acid revealed that decentralized control with

dual-temperature control and one-temperature/one-composition control suffice the non-linearity deviations of RD.(Hung and Lee 2006)

**Acknowledgement**

We would like to thank the Directorate of Technical Education and our respective institutes for permission to carry out this study as part of the doctorate program. We would also like to thank our family members, friends, and colleagues for their invaluable support, guidance, and continuous motivation, all along the process of study and writing the paper. We would even like to pay gratitude towards researchers globally who make their work available to refer to all aspirants across the globe.

**Declaration**

**Funding**: Not Applicable

**Competing Interest**

The authors declare that they have no known competing financial interests or personal relationships that could have appeared to influence the work reported in this paper.

**Availability of data and material**: Not Applicable

**Code availability**: Not Applicable

**Table 1: Describes various control structures as discussed by Arfaj et al. (Al-Arfaj and Luyben 2000)**

| Control Structure | Problem | Reason | Solution |
|---|---|---|---|
| Purities of both the product streams are measured and controlled | The system becomes unstable and cannot handle set point higher than 97%. | The reactive zone does not provide enough holdup time or catalyst to achieve the conversion required for the high purity separation | Providing excessive reaction capacity in reactive distillation such as: larger holdup, more reactive trays and large number of catalysts which makes the process easier |
| One impurity in each product stream is controlled | Here the slightest change in the top product composition brings instability in system and saturation of reflux and vapor boil up. | (1) It is practically inappropriate to assume that only one reactant (impurity) is present in either of the product stream. (2) Sometimes even if the differences in relative volatilities are low this problem will come. | This control structure should be used only in case where there are large differences in relative volatilities or reaction tends to near completion to avoid presence of reactants in both streams |
| Control one product purity and over purify the other product. (This control structure provides simple, easier, and faster response, thus bypass other control loops.) | At the higher production rates, the distillate composition falls below its specified purity | There is reduced interactions among various control loops. | The study shows that the distillate purity can be kept above the 95% specification if the tray holdups are increased. (The higher tray holdups result in higher distillate purity.) |
| Composition of lighter reactant is controlled at the bottom of reactive zone (where it is fed from in the column), and heavier reactant is controlled at the top of the reactive zone. | (1) two composition analyzers are required (2) there is no direct production-rate handle. | (1) To control composition of both the reactants in reactive zone. (2) Because control is made only within the reactive zone. | (1) The two fresh feed streams could be brought in on some type of composition control, perhaps using one composition controller and the reflux-drum level in the second column. (2) The production rate can be changed by adjusting the setpoints of either (or both) of the reaction zone composition controllers |

1

**Table 2: List of papers where Plantwide control for RD is studied**

| Column | Primary Product | Control Structure | Ref |
|---|---|---|---|
| Reactive Distillation | Methanol (via hydrolysis of Methyl Acetate). Dimethyl Adipate (via esterification). Butyl acetate (via transesterification) | PI controller (P for level control) with relay feedback and Tyreus–Luyben tuning | (Hung et al. 2010) |
| Reactive Distillation | Ethyl Acetate (via esterification) | PI controller (P for level control) with Tyreus–Luyben tuning | (Tang et al. 2005) |
| Reactive Distillation | Dimethyl Carbonate (via transesterification) | PI controller (P for level control) with relay feedback and Tyreus–Luyben tuning | (Wang et al. 2010) |
| Reactive Distillation | Butyl acetate (via transesterification) | PI controller (P for level control) with relay feedback and Tyreus–Luyben tuning | (Luyben et al. 2004) |
| Reactive Distillation | Diethyl Carbonate (via dual transesterification) | PI controller (P for level control) with suitable tuning parameters | (Wei et al. 2011) |
| Heat Integrated Reactive Distillation | Butyl acetate (via transesterification) | PI controller (P for level control) with relay feedback and Tyreus–Luyben tuning | (Wang et al. 2011) |
| Reactive Distillation | Methanol (via hydrolysis of Methyl Acetate); | PI controller (P for level control) with relay feedback and Tyreus–Luyben tuning | (Lin et al. 2008) |
| Reactive Distillation | Cumene (via Friedel-Crafts alkylation of benzene) | Dual-ended temperature inferential control system | (Pathak et al. 2011) |

**References**

Abdul Mutalib MI, Zeglam AO, Smith R (1998) Operation and control of dividing wall distillation columns: Part 2: Simulation and pilot plant studies using temperature control. Chem Eng Res Des 76:319–334

Abdulwahab G, Saidat O, Abel A (2015) Dynamics and Servo Control of Biodiesel Purity from a Reactive Distillation Process. Int J Sci Eng Res 6:146–156

Adrian T, Schoenmakers H, Boll M (2004) Model predictive control of integrated unit operations: Control of a divided wall column. Chem Eng Process Process Intensif 43:347–355. https://doi.org/10.1016/S0255-2701(03)00114-4

Al-Arfaj M, Luyben WL (2000) Comparison of Alternative Control Structures for an Ideal Two-Product Reactive Distillation Column. Ind Eng Chem Res 39:3298–3307. https://doi.org/10.1021/ie990886j

Al-Arfaj MA, Luyben WL (2002a) Control study of ethyl tert-butyl ether reactive distillation. Ind Eng Chem Res 41:3784–3796. https://doi.org/10.1021/ie010432y

Al-Arfaj MA, Luyben WL (2002b) Design and control of an olefin metathesis reactive distillation column. Chem Eng Sci 57:715–733. https://doi.org/10.1016/S0009-2509(01)00442-0

Alejski K, Duprat F (1996) Dynamic simulation of the multicomponent reactive distillation. Chem Eng Sci 51:4237–4252. https://doi.org/10.1016/0009-2509(96)00226-6

Backhaus AA (1922) Apparatus For The Manufacture Of Esters

Bahar A, Özgen C (2010) State estimation and inferential control for a reactive batch distillation column. Eng Appl Artif Intell 23:262–270. https://doi.org/10.1016/j.engappai.2009.11.003

Balasubramhanya LS, Doyle III FJ (2000) Nonlinear model-based control of a batch reactive distillation column. J Process Control 10:209–218. https://doi.org/10.14220/9783666565441.9

Baldea M (2015) From process integration to process intensification. Comput Chem Eng 81:104–114. https://doi.org/10.1016/j.compchemeng.2015.03.011

Bisowarno BH, Tadé MO (2002) The comparison of disturbance rejection properties of one-point control schemes for ETBE reactive distillation. Chem Eng Commun 189:85–100. https://doi.org/10.1080/00986440211832

Bisowarno BH, Tian YC, Tadé MO (2004) Combined gain-scheduling and multimodel control of a reactive distillation column. IFAC Proc Vol 37:791–796. https://doi.org/10.1016/s1474-6670(17)38830-4

Bock H, Wozny G, Gutsche B (1997) Design and control of a reaction distillation column including the recovery system. Chem Eng Process Process Intensif 36:101–109. https://doi.org/10.1016/S0255-2701(96)04183-9

Chen L, Bastin G, Van Breusegem V (1995) Case Study of Adaptive Nonlinear Regulation of Fed-Batch Biological Reactors. Case Study Adapt Nonlinear Regul Fed-Batch Biol React 31:55–65

Chen L, Hontoir Y, Zhang J, Bastin G (2000) Model Based Control of a Reactive Distillation Column. IFAC Proc Vol 33:99–104. https://doi.org/10.1016/s1474-6670(17)38525-7

Chiang SF, Kuo CL, Yu CC, Wong DSH (2002) Design alternatives for the amyl acetate process: Coupled reactor/column and reactive distillation. Ind Eng Chem Res 41:3233–3246. https://doi.org/10.1021/ie010358j

Cuille PE, Reklaitis G V. (1986) Dynamic simulation of multicomponent batch rectification with chemical reactions. Comput Chem Eng 10:389–398. https://doi.org/10.1016/0098-1354(86)87009-0

Daoutidis P, Zachar M, Jogwar SS (2016) Sustainability and process control: A survey and perspective. J Process Control 44:184–206.

https://doi.org/10.1016/j.jprocont.2016.06.002

Dias LS, Ierapetritou MG (2019) Optimal operation and control of intensified processes — challenges and opportunities. Curr. Opin. Chem. Eng. 25:82–86

Eldarsi HS, Douglas PL (1998) Methyl-tert-butyl-ether catalytic distillation column - Part I: Multiple steady states. Chem Eng Res Des 76:509–516. https://doi.org/10.1205/026387698524983

Espinosa J, Martfnez E, Perez G (1994) Dynamic Behavior of Reactive Distillation Columns. Equilibrium Systems. Chem Eng Commun 128:19–42. https://doi.org/10.1080/00986449408936234

Feng Z, Shen W, Rangaiah GP, et al (2019) Process Development, Assessment, and Control of Reactive Dividing-Wall Column with Vapor Recompression for Producing n -Propyl Acetate. Ind Eng Chem Res 58:276–295. https://doi.org/10.1021/acs.iecr.8b05122

Giwa A, Adeyi AA, Adeyi VA (2018) Cascade PID control of a reactive distillation process for biodiesel production: A comparison with conventional PID control. Int J Eng Res Africa 35:134–144. https://doi.org/10.4028/www.scientific.net/JERA.35.134

Giwa A, Karacan S (2012a) Modeling and Simulation of a Reactive Packed Distillation Column Using Delayed Neural Networks. In: Chaotic Modeling and Simulation International Conference. pp 129–136

Giwa A, Karacan S (2012b) Black-Box Modelling of Ethyl Acetate Reactive Packed Distillation Column Abdulwahab. AU J Technol 15:172–178

Giwa A, Karacan S (2012c) Decoupling Model Predictive Control of a Reactive Packed Distillation Column. Int J Adv Sci Technol 4:39–51

Giwa A, Karacan S (2012d) Decoupling PID Control of a Reactive Packed Distillation Column. Int J Eng Res Technol 1:1924–1933

Gómez-Castro FI, Segovia-Hernández JG, Hernández S, et al (2008) Dividing Wall Distillation Columns: Optimization and Control Properties. Chem Eng Technol 31:1246–1260. https://doi.org/10.1002/ceat.200800116

Grüner S, Mohl KD, Kienle A, et al (2003) Nonlinear control of a reactive distillation column. Control Eng Pract 11:915–925

Güttinger TE, Morari M (1999a) Predicting multiple steady states in equilibrium reactive distillation. 1. Analysis of nonhybrid systems. Ind Eng Chem Res 38:1633–1648. https://doi.org/10.1021/ie980327x

Güttinger TE, Morari M (1999b) Predicting multiple steady states in equilibrium reactive distillation. 2. Analysis of hybrid systems. Ind Eng Chem Res 38:1649–1665. https://doi.org/10.1021/ie980328p

Halvorsen IJ, Sigurd S (1997) Optimizing control of Petlyuk distillation: Understanding the steady-state behavior. Comput Chem Eng 21:S249–S254

Halvorsen IJ, Skogestad S (1999) Optimal operation of Petlyuk distillation: steady-state behavior. J Process Control 9:407–424. https://doi.org/10.1016/S0959-1524(99)00009-8

Hauan S, Schrans SM, Lien KM (1997) Dynamic Evidence of the Multiplicity Mechanism in Methyl tert-Butyl Ether Reactive Distillation. Ind Eng Chem Res 36:3995–3998. https://doi.org/10.1021/ie970237c

Hsiao TL, Weng KC, Lee HY (2017) Design and control of hybrid heat-integrated configuration for an ideal indirect reactive distillation process. J Taiwan Inst Chem Eng 73:37–49. https://doi.org/10.1016/j.jtice.2016.08.045

Hung S-B, Lee M-J (2006) Control of Different Reactive Distillation Configurations. AIChE J 52:1423–1440. https://doi.org/10.1002/aic

Hung SB, Chen JH, Lin Y Der, et al (2010) Control of plantwide reactive distillation processes: Hydrolysis, transesterification and two-stage esterification. J Taiwan Inst Chem Eng 41:382–402. https://doi.org/10.1016/j.jtice.2010.03.021

Ibarra-Sánchez J de J, Segovia-Hernández JG (2010) Reducing energy consumption and CO2 emissions in extractive distillation: Part II. Dynamic behavior. Chem Eng Res Des 88:135–145. https://doi.org/10.1016/j.cherd.2009.08.006

Jacobs R, Krishna R (1993) Multiple Solutions in Reactive Distillation for Methyl tert-Butyl Ether Synthesis. Ind Eng Chem Res 32:1706–1709. https://doi.org/10.1021/ie00020a025

Jana AK (2007) Synthesis of nonlinear adaptive controller for a batch distillation. ISA Trans 46:49–57. https://doi.org/10.1016/j.isatra.2006.05.001

Jana AK, Adari PVRK (2009) Nonlinear state estimation and control of a batch reactive distillation. Chem Eng J 150:516–526. https://doi.org/10.1016/j.cej.2009.03.015

Jantes-Jaramillo D, Segovia-Hernández JG, Hernández S (2008) Reduction of Energy Consumption and Greenhouse Gas Emissions in a Plant for the Separation of Amines. Chem Eng Technol 31:1462–1469. https://doi.org/10.1002/ceat.200800100

Jithin Prakash KJ, Patle DS, Jana AK (2011) Neuro-estimator based GMC control of a batch reactive distillation. ISA Trans 50:357–363. https://doi.org/10.1016/j.isatra.2011.01.010

Kaibel G (1984) Distillation system, consisting of two distillation columns for the distillative energy-efficient separation of a feed product consisting of several fractions

Kaibel G (1983) Method of carrying out chemical reactions and for the simultaneous fractionation of a mixture into several fractions by a distillation column

Kathel P, Jana AK (2010) Dynamic simulation and nonlinear control of a rigorous batch reactive distillation. ISA Trans 49:130–137. https://doi.org/10.1016/j.isatra.2009.09.007

Kawathekar R, Riggs JB (2007a) Nonlinear model predictive control of a reactive distillation column. Texas Tech University

Kawathekar R, Riggs JB (2007b) Nonlinear model predictive control of a reactive distillation column. Control Eng Pract 15:231–239. https://doi.org/10.1016/j.conengprac.2006.07.004

Kaymak DB, Baki RO (2011) Plantwide control of a complex process involving a reactive distillation column. Sep Div - Core Program Top 2011 AIChE Annu Meet 2:1077–1078

Kaymak DB, Luyben WL (2005) Comparison of two types of two-temperature control structures for reactive distillation columns. Ind Eng Chem Res 44:4625–4640. https://doi.org/10.1021/ie058012m

Kaymak DB, Luyben WL (2006) Evaluation of a two-temperature control structure for a two-reactant/two-product type of reactive distillation column. Chem Eng Sci 61:4432–4450. https://doi.org/10.1016/j.ces.2006.01.050

Kenig EY, Mueller I, Kloeker M (2004) Rate Based Modeling of Dividing Wall Columns – a New Application to Reactive Systems. In: Proceedings of the PRES 7th Conference. Process Engineering Publisher, Prague

Khazraee SM, Jahanmiri AH (2010) Composition Estimation of Reactive Batch Distillation by Using Adaptive Neuro-Fuzzy Inference System. Chinese J Chem Eng 18:703–710. https://doi.org/10.1016/s1004-9541(10)60278-9

Kienle A, Marquardt DW (2002) Nonlinear Dynamics and Control of Reactive Distillation Processes. In: Sundmacher K, Kienle A (eds) Reactive Distillation. Wiley-VCH Verlag GmbH & Co. KGaA, pp 241–281

Kiss AA (2014) Distillation technology - still young and full of breakthrough opportunities. J Chem Technol Biotechnol 89:479–498. https://doi.org/10.1002/jctb.4262

Kiss AA, Bildea CS (2011) A control perspective on process intensification in dividing-wall columns. Chem Eng Process Process Intensif 50:281–292. https://doi.org/10.1016/j.cep.2011.01.011

Kittisupakorn P, Konakom K, Mujtaba IM (2011) Neural network-based controller design of a batch reactive distillation column under uncertainty. Asia-Pacific J Chem Eng 7:361–377. https://doi.org/10.1002/apj

Kumar MVP, Kaistha N (2009) Reactive distillation column design for controllability: A case study. Chem Eng Process Process Intensif 48:606–616. https://doi.org/10.1016/j.cep.2008.07.004

Lee HY, Lee YC, Chien IL, Huang HP (2010) Design and control of a heat-integrated reactive distillation system for the hydrolysis of methyl acetate. Ind Eng Chem Res 49:7398–7411. https://doi.org/10.1021/ie9016754

Lestak F, Smith R (1993) The control of dividing wall column. In: IChemE Research Event. Meeting. Chemical engineering research & design, Birmingham

Lin Y Der, Chen JH, Cheng JK, et al (2008) Process alternatives for methyl acetate conversion using reactive distillation. 1. Hydrolysis. Chem Eng Sci 63:1668–1682. https://doi.org/10.1016/j.ces.2007.11.009

Lin Q, Liu G, Huang K, et al (2011) Balancing design and control of an olefin metathesis reactive distillation column through reactive section distribution. Chem Eng Sci 66:3049–3055. https://doi.org/10.1016/j.ces.2011.04.005

Ling H, Luyben WL (2010) Temperature control of the BTX divided-wall column. Ind Eng Chem Res 49:189–203. https://doi.org/10.1021/ie900125w

Ling H, Luyben WL (2009) New control structure for divided-wall Columns. Ind Eng Chem Res 48:6034–6049. https://doi.org/10.1021/ie801373b

Liu X, Cong L, Zhou Y (2013) Nonlinear model predictive control based on wave model of high-purity internal thermally coupled distillation columns. Ind Eng Chem Res 52:6470–6479. https://doi.org/10.1021/ie400033h

Lopez-Negrete R, D'Amato FJ, Biegler LT, Kumar A (2013) Fast nonlinear model predictive control: Formulation and industrial process applications. Comput Chem Eng 51:55–64. https://doi.org/10.1016/j.compchemeng.2012.06.011

Luster EW (1930) Apparatus for fractionating cracked products

Luyben WL (2007) Control of Ternary Reactive Distillation Columns with and without Chemically Inert Components. Ind Eng Chem Res 46:5576–5590

Luyben WL, Pszalgowski KM, Schaefer MR, Siddons C (2004) Design and Control of Conventional and Reactive Distillation Processes for the Production of Butyl Acetate. Ind Eng Chem Res 43:8014–8025

Luyben WL, Tyréus BD, Luyben ML (1999) Plantwide process control. McGraw-Hill Education

Monroy-Loperena R, Alvarez-Ramirez J (2000) Output-feedback control of reactive batch distillation columns. Ind Eng Chem Res 39:378–386. https://doi.org/10.1021/ie990382l

Mujtaba IM, Macchietto S (1997) Efficient optimization of batch distillation with chemical reaction using polynomial curve fitting techniques. Ind Eng Chem Res 36:2287–2295. https://doi.org/10.1021/ie960573d

Mujtaba IM, Macchietto S (1996) Simultaneous optimization of design and operation of multicomponent batch distillation column - Single and multiple separation duties. J Process Control 6:27–36. https://doi.org/10.1016/0959-1524(95)00028-3

Murlidhar GM, Jana AK (2007) Nonlinear adaptive control algorithm for a multicomponent batch distillation column. Chem Eng Sci 62:1111–1124. https://doi.org/10.1016/j.ces.2006.11.006

Mutalib MIA, Smith R (1998) Operation and Control of Dividing Wall Distillation Columns: Part 1: Degrees of Freedom and Dynamic Simulation. Chem Eng Res Des 76:308–318. https://doi.org/10.1205/026387698524956

Nagy ZK, Klein R, Kiss AA, Findeisen R (2007) Advanced Control of a Reactive Distillation Column. In: Agachi PS, Plesu V (eds) 17th European Symposium on Computer Aided Process Engineering – ESCAPE17

Nijhuis SA, Kerkhof FPJM, Mak ANS (1993) Multiple Steady States during Reactive

Distillation of Methyl tert-Butyl Ether. Ind Eng Chem Res 32:2767–2774. https://doi.org/10.1021/ie00023a045

Nikačević NM, Huesman AEM, Van den Hof PMJ, Stankiewicz AI (2012) Opportunities and challenges for process control in process intensification. Chem Eng Process Process Intensif 52:1–15. https://doi.org/10.1016/j.cep.2011.11.006

Olanrewaju MJ, Al-Arfaj MA (2005) Development and application of linear process model in estimation and control of reactive distillation. Comput Chem Eng 30:147–157. https://doi.org/10.1016/j.compchemeng.2005.08.007

Pathak AS, Agarwal S, Gera V, Kaistha N (2011) Design and Control of a Vapor-Phase Conventional Process and Reactive Distillation Process for Cumene Production. Ind Eng Chem Res 50:3312–3326

Pavan Kumar M V., Kaistha N (2008a) Steady-state multiplicity and its implications on the control of an ideal reactive distillation column. Ind Eng Chem Res 47:2778–2787. https://doi.org/10.1021/ie701720r

Pavan Kumar M V., Kaistha N (2008b) Role of multiplicity in reactive distillation control system design. J Process Control 18:692–706. https://doi.org/10.1016/j.jprocont.2007.12.001

Pavan Kumar M V., Kaistha N (2008c) Decentralized control of a kinetically controlled ideal reactive distillation column. Chem Eng Sci 63:228–243. https://doi.org/10.1016/j.ces.2007.09.029

Pérez-Correa S, González P, Alvarez J (2008) On-line optimizing control for a class of batch reactive distillation columns. IFAC Proc Vol 17:3263–3268. https://doi.org/10.3182/20080706-5-KR-1001.3708

Qi W (2010) Synthesis, design and operating strategies for batch reactive distillation. University of Massachusetts Amherst

Qian X, Jia S, Luo Y, et al (2016a) Control of reactive dividing wall column for selective hydrogenation and separation of C3 stream. Chinese J Chem Eng 24:1213–1228. https://doi.org/10.1016/j.cjche.2016.04.045

Qian X, Jia S, Luo Y, et al (2015) Selective hydrogenation and separation of C3 stream by thermally coupled reactive distillation. Chem Eng Res Des 99:176–184. https://doi.org/10.1016/j.cherd.2015.03.029

Qian X, Jia S, Skogestad S, et al (2016b) Model Predictive Control of Reactive Dividing Wall Column for the Selective Hydrogenation and Separation of a C3 Stream in an Ethylene Plant. Ind Eng Chem Res 55:9738–9748. https://doi.org/10.1021/acs.iecr.6b02112

Ramshaw C (1995) The incentive for process intensification. In: 1st International Conference on Process Intensification in the Chemical Industry. Mechanical Engineering Publications Limited.

Robles-Zapiain S, Segovia-Hernández JG, Bonilla-Petriciolet A, Maya-Yescas R (2008) Energy-efficient complex distillation sequences: Control properties. Can J Chem Eng 86:249–259. https://doi.org/10.1002/cjce.20021

Rouchon P, Creff Y, Djenab F, et al (1991) Nonlinear Quality Control of Pseudo-Binary Distillation Columns. Adv Control Chem Process 65–69

Ruiz CA, Basualdo MS, Scenna NJ (1995) Reactive Distillation Dynamic Simulation. Chem Eng Res Des 73:363–378

Sandoval-Vergara R, Barroso-Muñoz FO, Hernández-Escoto H, et al (2008) Implementation of a reactive dividing wall distillation column in a pilot plant. Comput Aided Chem Eng 25:229–234. https://doi.org/10.1016/S1570-7946(08)80043-0

Scenna NJ, Benz SJ (2003) Start-up operation of reactive columns with multiple steady states: The ethylene glycol case. Ind Eng Chem Res 42:873–882.

https://doi.org/10.1021/ie020099d

Seader JD (1978) Continuous distillation apparatus and method

Segovia-Hernández JG, Hernández S, Bonilla Petriciolet A (2015) Reactive distillation: A review of optimal design using deterministic and stochastic techniques. Chem. Eng. Process. Process Intensif. 97:134–143

Segovia-Hernández JG, Hernández S, Jiménez A (2005) Analysis of dynamic properties of alternative sequences to the Petlyuk column. In: Computers and Chemical Engineering. Elsevier Ltd, pp 1389–1399

Serra M, Espuña A, Puigjaner L (2003) Controllability of different multicomponent distillation arrangements. Ind Eng Chem Res 42:1773–1782. https://doi.org/10.1021/ie010609o

Serra M, Espuña A, Puigjaner L (1999) Control and optimization of the divided wall column. Chem Eng Process Process Intensif 38:549–562. https://doi.org/10.1016/S0255-2701(99)00052-5

Serra M, Perrier M, Espuna A, Puigjaner L (2000) Study of the divided wall column controllability: Influence of design and operation. In: Computers and Chemical Engineering. Elsevier Science Ltd, pp 901–907

Serra M, Perrier M, Espuña A, Puigjaner L (2001) Analysis of different control possibilities for the divided wall column: Feedback diagonal and dynamic matrix control. In: Computers and Chemical Engineering. Pergamon, pp 859–866

Sharma KLS (2011) Overview of Industrial Process Automation. Elsevier Inc.

Sharma N, Singh K (2010) Control of Reactive Distillation Column: A Review. Int J Chem React Eng 8:. https://doi.org/10.2202/1542-6580.2260

Sneesby MG, Tadé MO, Datta R, Smith TN (1997a) ETBE Synthesis via Reactive Distillation. 2. Dynamic Simulation and Control Aspects. Ind Eng Chem Res 36:1870–1881. https://doi.org/10.1021/ie970053y

Sneesby MG, Tadé MO, Datta R, Smith TN (1997b) ETBE Synthesis via Reactive Distillation. 1. Steady-State Simulation and Design Aspects. Ind Eng Chem Res 36:1855–1869. https://doi.org/10.1021/ie960283x

Sneesby MG, Tadé MO, Smith TN (1998a) Mechanistic Interpretation of Multiplicity in Hybrid Reactive Distillation: Physically Realizable Cases. Ind Eng Chem Res 37:4424–4433. https://doi.org/10.1021/IE970938+

Sneesby MG, Tadé MO, Smith TN (1998b) Multiplicity and pseudo-multiplicity in MTBE and ETBE reactive distillation. Chem Eng Res Des 76:525–531. https://doi.org/10.1205/026387698525009

Sørensen E, Macchietto S, Stuart G, Skogestad S (1996) Optimal control and on-line operation of reactive batch distillation. Comput Chem Eng 20:1491–1498. https://doi.org/10.1016/0098-1354(95)00234-0

Sorensen E, Skogestad S (1992) Control Strategies for a Combined Batch Reactor/Batch Distillation Process. In: Reklaitis G V., Sunol AK, Rippin DWT, Hortagsu O (eds) NATO Advanced Study Institute on Batch Processing Systems Engineering: Current Status and Future Directions. Springer-Verlag Berlin Heidelberg, Antalya, pp 274–294

Sørensen E, Skogestad S (1994) Control strategies for reactive batch distillation. J Process Control 4:205–217. https://doi.org/10.1016/0959-1524(94)80042-1

Sørensen Leversund E, Macchietto S, Stuart G, Skogestad S (1994) Optimal control and on-line operation of reactive batch distillation. Comput Chem Eng 18:S391–S395. https://doi.org/10.1016/0098-1354(94)80064-2

Stankiewicz AI, Moulijn JA (2000) Process Intensification: Transforming Chemical Engineering. Chem Eng Prog 96:22–34. https://doi.org/10.1205/psep.04241

Tamayo-Galván VE, Segovia-Hernández JG, Hernández S, et al (2008) Controllability

analysis of alternate schemes to complex column arrangements with thermal coupling for the separation of ternary mixtures. Comput Chem Eng 32:3057–3066. https://doi.org/10.1016/j.compchemeng.2008.04.007

Tang YT, Huang HP, Chien IL (2005) Plant-wide control of a complete ethyl acetate reactive distillation process. J Chem Eng Japan 38:130–146. https://doi.org/10.1252/jcej.38.130

Tatulea-Codrean A, Hakerl D, Urselmann M, Engell S (2016) Steady-state optimization and nonlinear model-predictive control of a reactive distillation process using the software platform do-mpc1. In: 2016 IEEE Conference on Control Applications, CCA 2016. Institute of Electrical and Electronics Engineers Inc., pp 1513–1518

Van Breusegem V, Bastin G (1992) Singular perturbation approach to the reduced order reaction systems. Catholic University of Louvain Belgium

Van Diggelen RC, Kiss AA, Heemink AW (2010) Comparison of control strategies for dividing-wall columns. Ind Eng Chem Res 49:288–307. https://doi.org/10.1021/ie9010673

Van Gerven T, Stankiewicz A (2009) Structure, energy, synergy, time-the fundamentals of process intensification. Ind Eng Chem Res 48:2465–2474. https://doi.org/10.1021/ie801501y

Vázquez-Ojeda M, Segovia-Hernández JG, Hernández S, et al (2012) Optimization and controllability analysis of thermally coupled reactive distillation arrangements with minimum use of reboilers. Ind Eng Chem Res 51:5856–5865. https://doi.org/10.1021/ie200929t

Venkateswarlu C, Reddy AD (2008) Nonlinear model predictive control of reactive distillation based on stochastic optimization. Ind Eng Chem Res 47:6949–6960. https://doi.org/10.1021/ie070972g

Wang SJ, Huang HP, Yu CC (2011) Design and control of a heat-integrated reactive distillation process to produce methanol and n -butyl acetate. Ind Eng Chem Res 50:1321–1329. https://doi.org/10.1021/ie100677x

Wang SJ, Wong DSH (2007) Controllability and energy efficiency of a high-purity divided wall column. Chem Eng Sci 62:1010–1025. https://doi.org/10.1016/j.ces.2006.11.002

Wang SJ, Wong DSH, Lee EK (2003) Control of a reactive distillation column in the kinetic regime for the synthesis of n-butyl acetate. Ind Eng Chem Res 42:5182–5194. https://doi.org/10.1021/ie0209172

Wang SJ, Yu CC, Huang HP (2010) Plant-wide design and control of DMC synthesis process via reactive distillation and thermally coupled extractive distillation. Comput Chem Eng 34:361–373. https://doi.org/10.1016/j.compchemeng.2009.05.002

Wei HY, Rokhmah A, Handogo R, Chien IL (2011) Design and control of reactive-distillation process for the production of diethyl carbonate via two consecutive trans-esterification reactions. J Process Control 21:1193–1207. https://doi.org/10.1016/j.jprocont.2011.06.006

Wolff EA, Skogestad S (1995) Operation of Integrated Three-Product (Petlyuk) Distillation Columns. Ind Eng Chem Res 34:2094–2103. https://doi.org/10.1021/ie00045a018

Wu YC, Lee HY, Lee CH, et al (2012) Design and Control of Reactive Divided Wall Column for Esterification with Mixed n-Amyl alcohol and n-Hexanol Feed. Comput Aided Chem Eng 31:1582–1586. https://doi.org/10.1016/B978-0-444-59506-5.50147-4

# Recent progress in the Photocatalytic Activity of Recyclable Nano-doped TiO2 for the removal of Organic Pollutants from effluent

*Darshana T. Bhatti[1*], Sachin P. Parikh[2]*
*1. Chemical Engineering Department, VVP Engineering College, Rajkot-360 005, Gujarat, INDIA*
*2. Directorate of Technical Education, Gujarat State, Gandhinagar-382 010, Gujarat, INDIA*
*[*]Corresponding author: darshana333@gmail.com, +919722243638*

**Abstract**
The world is facing climate change and a crisis of water and energy problems today. Because of this, photocatalysis research has been rapidly expanding. $TiO_2$ nanoparticles have been widely studied for photocatalysis for the removal of dyes, pesticides, insecticides, active pharmaceutical ingredients and production of solar energy devices for sustainable growth of the nation. $TiO_2$ is considered close to an ideal semiconductor for photocatalysis but possesses certain limitations such as poor absorption of visible radiation and rapid recombination of photo-generated electron/hole pairs. This review includes recent progress in the researchand application of $TiO_2$ photocatalysis for the removal of nonbiodegradable organic pollutants present in water. Various methods used to enhance the photocatalytic characteristics of $TiO_2$ including Ag and Fe doping, some composite nanostructuresand recyclability of photocatalysts are discussed. The effects of operating variables such as pH, catalyst dose and structure of catalyst on complete degradation of pollutants in addition to dopant characteristics are reviewed.

**Keywords:** Advanced Oxidation Processes,Bandgap, Solar Photocatalysis; Doped $TiO_2$; Recyclability.

## 1. Introduction

The exhaustion of non-renewable resources and global environmental problems are the major problems the world faces today. This situation enforced research towards zero effluent discharge, green technology and cleaner development mechanism. Semiconductor photocatalysis has been widely studied by many researchers for the mineralization of effluent containing refractory organics (Dubey et al., 2019; Lendzion-Bieluń et al., 2020), water splitting for hydrogen production (S. Cao et al., 2019)and solar cells(Iqbal et al., 2019). The application of $TiO_2$ as a photocatalyst is limited by UV radiations and recombination of the hole and electron pairs(Basavarajappa et al., 2020; Komaraiah et al., 2019). Rapid industrialization has vastly increased water and air pollution problems as the current generation are interested more in profit and less concerned for waste generation. This situation demands fruitful research be done on waste minimization to avoid such situations and to achieve sustainable development. Solar light driven effluent treatment methods have been focused and developed for research(Khanna & Shetty, 2014). Titanium dioxide is an N-type semiconductor having an oxygen deficit in its structure. Itis a chemically stable, nontoxic photocatalyst that provides OH radical on photocatalysis, i.e. a strong oxidizing agent with strong resistance to corrosion (D. Chen & Ray, 1999; Nagaveni, 2003). However, the $TiO_2$ photocatalyst has its limitations as follows:

- Owing to its large bandgap energy, only UV light can be used as a radiation source, as natural solar radiation encompasses only about 4–5% of UV rays.

- Low quantum yields of $TiO_2$ as electron and hole recombine, which results in the low production of OH radicals (Al-Hartomy, 2014).

In this review, we have described several recent developments in metal-doped/codoped $TiO_2$ and $TiO_2$-based hybrid photocatalysts and their physicochemical properties, bandgap, features, factors to improve catalytic efficiency and recyclability. Synthesis of nano-doped $TiO_2$, mechanism of degradation by photocatalysis, operating variables and their effects on degradation and different techniques to modify optical properties of $TiO_2$ such as the use of metal and non-metal dopants, nanofilms, nanotubes and nanowires are discussed. Feasibility and the effectiveness of recycled photocatalyst has been studied.

## 2. Titanium Dioxide Photocatalysis

Semiconductor oxides have a large number of surface atoms on their surface which enables photon absorption and performs various oxidation and reduction reactions for complete removal of a variety of organics from aqueous solutions. Titanium dioxide is widely preferred for photocatalysis due to its stability, reusability, nontoxicity, anti-corrosiveness and low cost. Different other oxides that can also be used for photocatalysis are zinc, tin, zirconium, cadmium and iron. Hydroxyl radicals react with organics to produce carbon dioxide and water(Basavarajappa et al., 2020; Huang et al., 2020). When photons bombard on $TiO_2$ surface it enables electron movement and reactions on an interface where large numbers of organic substances are absorbed from the effluent. Semiconductor $TiO_2$ absorbs photons and transfer an electron from the valance band to the conduction band. On the valence band, holes are generated which reacts with $H_2O$ or $OH^-$ to produce hydroxyl radicals. Figure 1 shows mechanism of photocatalysis.
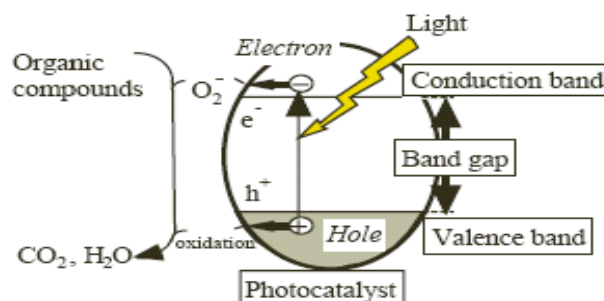


Figure 1 Mechanism of photocatalysis (Yang et al., 2006)

When semiconductors such as $TiO_2$ absorbs light e- jump from the valance band to the conduction band. Nanoparticles have a large surface-to-volume ratio and also contain more atoms on their surface which substantially absorb photons. Nanoparticles can perform photocatalysis rapidly before $e^-$ and hole recombine (Carbuloni et al., 2020; Rabbani et al., 2019).

## 3. Doping in Nano-Structured $TiO_2$ for enhanced photocatalytic activity

Doping is one of the methods to improve optical properties, reduces bandgap and overcome $e^-$/hole recombination as metals trap $e^-$ result in enhanced photocatalytic activity of semiconductor oxides. Doping will provide efficient and economical photocatalysis as it can replace UV photocatalysis with solar or visible

irradiations.Loading of TiO₂ surface with dopant will engineer the photocatalyst with improved trapping of charge carriers. Thus Doping increases organics degradation efficiency (Banerjee, 2011). Dopant will create oxygen defects and shifts light absorption from UV to the visible region by improving absorption bandwidth. The efficiency of photocatalysis may differ based on the position ofthe dopant on the TiO₂ structure. Based on synthesis methods, the dopant can take a position on the surface or it can be included in lattice structure or as core and thus these positions may lead to different photocatalytic activity and degradation efficiency. Metals and non-metals both can work as dopants but major research concludes that metal dopants possess strong surface plasmon resonance (SPR), work efficiently under solar radiations during photocatalysis (Gupta & Tripathi, 2011).

### 3.1 Synthesis of Ag and Fe doped TiO₂

Nanopowder can be synthesized using various techniques such as down to top and top to down approach (Vijayalakshmi & Rajendran, 2012). Various methods for synthesis ofnanophotocatalysts are shown in figure 2. The sol-gel method is simple, economical and provides narrow size distribution (Cui et al., 2013a). Doping of silver nanoparticles into the TiO₂ structure facilitates charge disconnection by separating e- and holes, produce more hydroxyl radicals and improve photocatalytic activity (Mohd Razip et al., 2019; Petronella et al., 2017; Zhan et al., 2014). The presence of Ag also enhances visible light photoactivity due to their peculiar plasmonic properties and decreases the bandgap of titanium dioxide(Birben et al., 2017a; Mohd Razip et al., 2019). Different methods have been used for the doping of nitrogen into the lattice of TiO₂., including microwave-assisted solvothermal method(Lendzion-Bieluń et al., 2020), sol-gel method (Jing He et al., 2019; Komaraiah et al., 2019; Nasralla et al., 2013b), hydrothermal method (Z. Chen & Fu, 2018), solvothermal method (Lendzion-Bieluń et al., 2020), and combustion sol-gel method (Aarthi & Madras, 2007; Bachvarova-Nedelcheva et al., 2013; Nagaveni, 2003). It has been reported that the synthesis of doped TiO₂ sol-gel methods are the most competent methods to produce Ag-Fe doped TiO₂ as it is simple, economical and provides narrow size distribution (Cui et al., 2013a). Typically, for the synthesis of Ag-Fe doped TiO2 nanoparticles, FeNO₃ and AgNO₃ can be used as Fe and Ag sources respectively (P. Wang et al., 2013). Several researchers proved that Ag and Fe doping in TiO₂ lattice reduces the bandgap than bare TiO2 and modifies it into a visible-light active catalyst (Tedsree et al., 2017; Zhou et al., 2018).



Figure 2 Methods for the synthesis of doped TiO₂(Basavarajappa et al., 2020)

## 3.2 Ag-Fe codoped TiO₂ for the photodegradation of pollutants

Ag and Fe co-doped $TiO_2$ haveenhanced visible light absorption and solar improved photocatalysis efficiency (Harikishore et al., 2014; Petronella et al., 2017; Zhan et al., 2014).Iron dopant stable the core-shell structure of $Ag@TiO_2$ by preventing aggregation of nanomaterials (W. Wang et al., 2008a).Core-shell structure prevents metal corrosion and its dissolution in solution hence it is important to put metals in the core during synthesis and provide shells of $TiO_2$(W. Wang et al., 2008a).$Fe_3O_4$ doped $TiO_2$ as core-shell structure prevents metal dissolution in aqueous solution during oxidation and reduction reactions also this structure providesa larger surface area for photocatalysis (Zhan et al., 2014).The well-designed nanocomposite $Fe_3O_4@SiO_2@TiO_2$-Ag showed better activity compared to Degussa P25 because of charge separation and more OH radicals availability. The catalyst provided good recyclability for 10 recycle runs (Chi et al., 2013).Greater absorption rate due to the high specific surface area of $TiO_2$ film on $Fe_3O_4$ and Ag enhanced light absorption in the visible range (Tedsree et al., 2017).

## 4. Parameters affecting photocatalysis

### 4.1 Effect of photocatalyst dose

Photocatalyst amount is one of the most significant variables that strongly affects the degradation rate of organics in $TiO_2$ photocatalysis (He et al., 2019; Komaraiah et al., 2019). The total surface available for adsorption of organics in dark depends on the dosage of the photocatalyst. The effect of catalyst dosage on the photodegradation of DFTA was studied in the range of 1-5 g/L. the photodegradation rate of DFTA and thereby COD removal efficiency as a function of photocatalyst dosage was studied. It was found that initially up to 3 g/L degradation efficiency was increased with an increase in the amount of catalyst and then further increase in the amount of the photocatalyst negatively affected degradation rate (Darshana et al., 2020). When catalyst dosage increases, it provides more sites for absorption and generates more electrons and holes, thereby increasing the production of hydroxyl radicals, but simultaneously it makes solution opaque which reduces light absorption (Nezamzadeh-Ejhieh & Hushmandrad, 2010; Sun et al., 2011). A higher amount of catalyst above optimum leads to agglomeration and sedimentation of the catalyst (Kiliç & Çinar, 2008), also it covers the catalyst surface and hence decreases the penetration of light near the catalyst and decreases photoactivation of the catalyst, which in turn reduces the generation of OH˙ radicals and thus reduction in COD removal efficiency (Nezamzadeh-Ejhieh & Amiri, 2013; Nezamzadeh-Ejhieh & Badri, 2011; Nezamzadeh-Ejhieh & Moazzeni, 2013).

### 4.2 Effect of pH

The surface charge of the photocatalyst and the protonation state of organics will depend on pH.Point of zero charge (ZPC) is defined as the condition at which the surface charge density of material equals zero and, for most of the solids it is strongly pH-dependent.It is known that oxide surfaces that are in contact with an aqueous solution or exposed to the ambient environment adsorb water molecules, followed by dissociation to OH− charged groups, resulting in chemically equivalent metal hydroxyl groups (M-OH). Due to the amphoteric behavior of most heavy metal hydroxides, the hydroxyl groups at the surface of the oxide are protonated (positively charged) at pH values below the oxide ZPC (Equation 1), and deprotonated (negatively charged) above the ZPC (Equation 2). If

the hydroxyl groups remain un-reacted in aqueous solutions, the oxide surface is said to be at its point of zero charge (zero net surface charge), meaning that at this pH the charge of the positive surface sites equals the negative ones.Most of the organics being anionic, electrostatic attraction between the positively charged $TiO_2$ and increases the removal efficiency in acidic medium. When the pH is above pHZpc, the negatively charged $TiO_2$repels the anionic form of the organics and this decreases the efficiency of photodegradation with increasing pH above 3.

$$M\text{-}OH + H^+ \rightarrow M\text{-}OH_2^+ \text{--------}(1)$$
$$M\text{--}OH^+ \rightarrow M\text{-}O^- + H^+ \text{-------}(2)$$

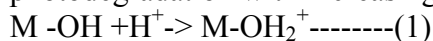Table 1 summarizes effects of parameters on photocatalytic degradation of various nonbiodegradable organics.

## 5. Recyclability of Photocatalyst

$TiO_2$ doped with 33% $Fe_2O_3$ core-shell photocatalyst has enhanced photocatalytic activity for paracetamol removal from water and the photocatalyst could be easily separated and reused for four recycle runs (Nasralla et al., 2013). Ag decorated $Fe_3O_4/TiO_2$ coated cenosphere prepared via Modified sol-gel and wet impregnation can be recycled for 8 cycles with a slight reduction in Methylene blue degradation efficiency (Zhan et al., 2014). The novel engineered photo composite core-shell structure $Fe_3O_4@SiO_2@TiO_2$ showed greater photoactivity compared to commercial $TiO_2$. The catalyst provided easy separability using a magnet and was recycled for 10 numbers of recycling runs without a decrease in efficiency (Chi et al., 2013). When the Ag-Fe codoped $TiO_2$ with Ti/Ag mole ratio 30 photocatalysts reused for six numbers of runs, 63.25% COD was removed in 5 hr solar light irradiation, indicating more deactivation of the catalyst during photocatalysis; which represented that the Ag-Fe CT 30 could be recyclable effectively for 4 cycles. The reduction in % COD removal was only less than 5% after three runs of recycling for Ag-Fe CT 30. Ag-Fe CT 30 catalyst has proved its stability even after 4 recycle runs and it can perform photocatalysis under solar radiation effectively for the photocatalysis of drug intermediates (Bhatti & Parikh, 2020). Recyclability of doped $TiO_2$ has been studied by various researchers and obtained nearly similar results (Z. Chen & Fu, 2018; Han et al., 2018). $Fe^{3+}$ doped $TiO_2$ was studied for dye degradation and there has been 9% reduction in degradation efficiency observed at the end of the sixth cycle (Han et al., 2018). Table 2 provides feasibility of catalyst recycling.

Table 1 parameters affecting photocatalysis

| Sr. No. | Parameter | catalyst | Component | Exp. conditions | result | remarks | Ref. |
|---|---|---|---|---|---|---|---|
| 1 | pH 1 to 9 | $TiO_2$ | dye ( Yellow-17) | catalyst dose 100 mg/L, dye amount 10 mg/L; time 60 min; UV and visible light | Optimum pH=3 - 100 % degradation. | Solution pH affects the surface charge of photocatalyst and thereby adsorption of organics on its surface. The pHpzc of $TiO_2$ is 6.5 when pH is less than pHpzc, the surface of photocatalyst has a positive charge and it can absorb negative charge organics on its surface. | (Khanna & Shetty K, 2013) |
|  | Catalyst loading | $Ag@TiO_2$ | AY-17 dye | Optimum pH=3. Catalyst dose=50 to 500 mg/L, time=60 min | Optimum catalyst dose=100 mg/L. | When catalyst dose increases, surface area more available and more adsorption increased degradation efficiency. When catalyst dose increases beyond optimum, it makes the system opaque and less light available for absorption results in a decrease in photocatalysis efficiency. Also, agglomeration takes place at a higher catalyst dose. |  |
|  | Addition of oxidants - $H_2O_2$ | $Ag@TiO_2$ | AY-17 dye | catalyst dose 1 g/L, pH 3, dye amount= 100 mg/L, time=60 min, $H_2O_2$ = 0 to 20 mM | Optimum oxidant $H_2O_2$ =10 mM | Oxidizing agent addition provides benefits like 1. More OH radicals generation; 2. Provide reactant for oxidation reaction; 3. Facilitate $e^-$ libration from the core; 4. Rapid reaction with CB $e^-$ and avoid $e^-$-hole recombination; 5. Reaction with $O_2^-$ anion. |  |
| 2 | pH | pH 3, 6.5, 10 | Time=350 min | Degradation was 70 %, 60 % and 30 % at pH 3, 6.5 and 10 | optimum pH=3, For acidic pH | The degradation efficiency depends on pHzpc. All photocatalysts adsorb or repel organics based on solution pH. In acidic pH, more generation of hydroxyl radicals increased photocatalytic rate. | (Yasmina et al., 2014) |
|  | Supply of external oxygen | With and without oxygen supply | $TiO_2$, UV light, time=150 min | degradation efficiency was 70 % and 80 % without and with the addition of oxygen | NA | Oxygen addition favors 1. Generation of $O_2^-$ anion; 2. Generation of OH radicals; 3. Prevents $e^-$ and hole recombination. |  |

Table 2 Feasibility and effectiveness of photocatalyst for recyclability

| Sr. No. | Catalyst | Synthesis method | Model pollutant | light | Ads in dark, min | pH | Catalyst dose, g/L | Time, min | Recyclability runs, nos. | Result | Ref. |
|---|---|---|---|---|---|---|---|---|---|---|---|
| 1 | $Fe_3O_4–TiO_2$ | Solvothermal and micro- | phenol | UV | 15 | 7 | 0.5 | 100-300 | 2 | Degradation was 100%, 70%, 32% for P25 and $Fe_3O_4–TiO_2$ | (Lendzion-Bieluń et |

| | | | | | | | | | | | |
|---|---|---|---|---|---|---|---|---|---|---|---|
| | | thermal method | | | | | | | | (3 ml titanium butoxide), $Fe_3O_4$–$TiO_2$ (10 ml Titanium butoxide) respectively | al., 2020) |
| 2 | $Fe_3O_4$@$SiO_2$/β-$NaYF_4$:$Yb^{3+}$,$Tm^{3+}$/$TiO_2$ | sol–gel process and solvo-thermal | methylene blue, rhodamine B, methyl orange and phenol under, 1-10 ppm | Laser 980 nm | 1440 | 7 | 10 | 1440 | 4 | 76.62%, 68.48%, 30.05% and 27.16% | (Z. Chen & Fu, 2018) |
| 3 | Ag-doped $TiO_2$, Ag:Ti molar ratio= 0.02, 0.04, 0.06, 0.08 and 0.12. | solgel | Acetamiprid- 20 mg/L-insecticide | UV | 10 | 6 | 0.4 | 60 | 6 | Ag/Ti = 0.06 opti, as Ag increase rutile phase increase | (Y. Cao et al., 2008) |
| 4 | $Fe^{3+}$-doped $TiO_2$-1-4 wt % | modified sol-gel | azo dye acid orange 7-50 mg/L | UV, Visible and solar | 30 | 3,5 and 9: , 5. Opt, 96%, 87%, and 40%, | 0.3 | 180 | 4 | 100 % UV, 100 % visible, 90 % solar in 2 hr, 3 wt % opt-98.9 % | (Han et al., 2018) |

## 6. Ammonical nitrogen removal using photocatalysis

. Table 3summaries research done for ammonical nitrogen removal by photocatalysis.

Table3 Ammonical nitrogen removal during photocatalysis

| Sr. No. | Catalyst | Synthesis method | Model pollutant | light | Opt pH | Catalyst dose | Time, hr | Result | Ref. |
|---|---|---|---|---|---|---|---|---|---|
| 1 | $TiO_2$ film on glass beads: to 10 layers of $TiO_2$ thin film. | Coating with sol-gel method | $NH_4Cl$ solution 300 ml, ammonia conc. 700 mg/L | UV light | 7 | film | 2 hr | 6 coating opt, 70 % removal efficiency | (Gong et al., 2017) |
| 2 | Cu/ZnO/rGO Nanocomposite | Sol-gel | Domestic wastewater $NH^{4+}$-N: 10, 30, 50, 70, and 100 mg/L | Visible-Xenon lamp | 10 | 0.2-2 g/L, opt 2 | 2 hr | Optimum : $NH^{4+}$con.= 50 mg/L, catalyst conc.= 2 g/L, pH 10. 83% removal efficiency | (S. He et al., 2018) |
| 3 | La/Fe/$TiO_2$ composite | Sol-gel | NA | 500 W mercury lamp. | 10 | 1 g/L, | 3 hr | 64.6% removal efficiency | (Luo et al., 2015) |

Batch photocatalysis experiments were performed with pharmaceutical industrial effluent having initial COD of 88660 mg/L and ammonical nitrogen (NH3-N) of 3287 mg/L under 5 hr solar irradiation. Results of COD reduction showed that the synthesized catalyst worked efficiently for actual industrial wastewater treatment for COD reduction. Ag-Fe CT 30 has removed COD ofeffluent from 88660 mg/L to 31310 mg/L, 64.69%

COD reduction. Since acidic conditions favor Organic oxidation and alkaline conditions favor $NH_3$-N reduction (Luo et al., 2015; D. Sun et al., 2015), simultaneous removal is not possible. Only 16.05% of $NH_3$-N could be removed during photocatalysis. A decrease in $NH_3$-N can be due to the stripping of dissolved ammonia from the solution due to its volatility or its reduction in nitrogen (Murgia et al., 2005). $NH_4$-N removal is higher in alkaline pH. At lower pH, the surface of photocatalyst has a positive charge whereas ammoniacal nitrogen compounds can be adsorbed only on the surface which has a negative charge (D. Sun et al., 2015).$NH_4$-N removal is more when pH is greater than 10. Researchers have reported that it is not possible to oxidize $NH_4$-N OH by radicals (Lee et al., 2002).  When pH is above 9, $NH_4$-N can be converted into $NH_3$(Xue Gong, Haifeng Wang, Chun Yang, Quan Li, 2015). Hence acidic or neutral condition does not favor $NH_3$ –N removal simultaneously with organics.


**Conclusion**

This review described various advanced oxidation processes with their merits, demerits, benefits and challenges. Various dopants have been compared for their enhanced photoactivity. The mechanism $TiO_2$ semiconductor doped with Ag and Fe has been discussed. The degradation of various chemical compounds using $TiO_2$-based photocatalysts, including mechanisms and factors affecting the process have been summarized. From the results available, it can be concluded that co-doping of $TiO_2$ with Ag and Fe generally enhances the photocatalytic efficiency of the catalyst and this merits continuing research efforts. Photocatalytic degradation using $TiO_2$ nanoparticles is found a promising technique for the treatment of effluent. Extending the wavelength for $TiO_2$ application is an area of increasing research. At last, the recyclability of photocatalyst and ammoniacal nitrogen removal has been studied. The results showed that we can separate photocatalyst after treatment and reuse photocatalyst up to several runs efficiently without much decline in treatment efficiency.

**References**

Al-Hartomy, O. A. (2014). Synthesis, characterization, photocatalytic and photovoltaic performance of Ag-doped TiO2 loaded on the Pt-carbon spheres. *Materials Science in Semiconductor Processing*, *27*(1), 71–78. https://doi.org/10.1016/j.mssp.2014.06.025

Amoli-Diva, M., Anvari, A., & Sadighi-Bonabi, R. (2019). Synthesis of magneto-plasmonic Au-Ag NPs-decorated TiO2-modified Fe3O4 nanocomposite with enhanced laser/solar-driven photocatalytic activity for degradation of dye pollutant in textile wastewater. *Ceramics International*, *45*(14), 17837–17846. https://doi.org/10.1016/j.ceramint.2019.05.355

Angela, Szabolcs, Zsuzsanna, Gábor, C. (2012). Advanced Treatment of Pharmaceutical Wastewater by Nano Filtration and Ozonation. *FASCICUIE 2012*.

Banerjee, A. N. (2011). The design, fabrication, and photocatalytic utility of nanostructured semiconductors: Focus on TiO2-based nanostructures. In *Nanotechnology, Science and Applications* (Vol. 4, Issue 1, pp. 35–65). https://doi.org/10.2147/NSA.S9040

Bansal, P., & Verma, A. (2018). Applications of sunlight responsive Fe-Ag-TiO2 composite incorporating in-situ dual effect for the degradation of pentoxifylline. *Materials Science and Engineering B: Solid-State Materials for Advanced Technology*, *236–237*, 197–207. https://doi.org/10.1016/j.mseb.2018.11.016

Basavarajappa, P. S., Patil, S. B., Ganganagappa, N., Reddy, K. R., Raghu, A. V., & Reddy, C. V. (2020). Recent progress in metal-doped TiO2, non-metal doped/codoped TiO2 and TiO2 nanostructured hybrids for enhanced photocatalysis. *International Journal of Hydrogen Energy*, *45*(13), 7764–7778. https://doi.org/10.1016/j.ijhydene.2019.07.241

Bhatti, D. T., & Parikh, S. P. (2020). Solar Light Induced Photocatalysis for Treatment of High COD Pharmaceutical Effluent with Recyclable Ag-Fe Codoped TiO2: Kinetics of COD Removal. *Current World Environment*, *15*(1), 137–150. https://doi.org/10.12944/cwe.15.1.17

Birben, N. C., Uyguner-Demirel, C. S., Kavurmaci, S. Sen, Gürkan, Y. Y., Turkten, N., Cinar, Z.,

& Bekbolet, M. (2017). Application of Fe-doped TiO2 specimens for the solar photocatalytic degradation of humic acid. *Catalysis Today*, *281*, 78–84. https://doi.org/10.1016/j.cattod.2016.06.020

Cao, S., Chan, T.-S., Lu, Y.-R., Shi, X., Fu, B., Wu, Z., Li, H., Liu, K., Alzuabi, S., Cheng, P., Liu, M., Li, T., Chen, X., & Piao, L. (2019). Photocatalytic pure water splitting with high efficiency and value by Pt/porous brookite TiO2 nanoflutes. *Nano Energy*, 104287. https://doi.org/10.1016/j.nanoen.2019.104287

Cao, Y., Tan, H., Shi, T., Tang, T., & Li, J. (2008). Preparation of Ag-doped TiO2 nanoparticles for photocatalytic degradation of acetamiprid in water. *Journal of Chemical Technology & Biotechnology*, *83*(4), 546–552. https://doi.org/10.1002/jctb.1831

Carbuloni, C. F., Savoia, J. E., Santos, J. S. P., Pereira, C. A. A., Marques, R. G., Ribeiro, V. A. S., & Ferrari, A. M. (2020). Degradation of metformin in water by TiO2–ZrO2 photocatalysis. *Journal of Environmental Management*, *262*, 110347. https://doi.org/10.1016/j.jenvman.2020.110347

Chen, D., & Ray, A. K. (1999). Photocatalytic kinetics of phenol and its derivatives over UV irradiated TiO 2. *Applied Catalysis B: Environmental*, *23*, 143–157. https://doi.org/10.1016/S0926-3373(99)00068-5

Chen, Q., Yu, Z., Pan, Y., Zeng, G., Shi, H., Yang, X., Li, F., Yang, S., & He, Y. (2017). Enhancing the photocatalytic and antibacterial property of polyvinylidene fluoride membrane by blending Ag–TiO2 nanocomposites. *Journal of Materials Science: Materials in Electronics*, *28*(4), 3865–3874. https://doi.org/10.1007/s10854-016-5999-7

Chen, Z., & Fu, M. L. (2018). Recyclable magnetic Fe3O4@SiO2/β-NaYF4:Yb3+,Tm3+/TiO2 composites with NIR enhanced photocatalytic activity. *Materials Research Bulletin*, *107*, 194–203. https://doi.org/10.1016/j.materresbull.2018.07.016

Chi, Y., Yuan, Q., Li, Y., Zhao, L., Li, N., Li, X., & Yan, W. (2013). Magnetically separable Fe3O4@SiO2@TiO2-Ag microspheres with well-designed nanostructure and enhanced photocatalytic activity. *Journal of Hazardous Materials*, *262*, 404–411. https://doi.org/10.1016/j.jhazmat.2013.08.077

Chittala, G., & Mogadati, P. S. (2012). PERFORMANCE STUDIES ON A PHARMACEUTICAL WASTEWATER TREATMENT PLANT WITH A SPECIAL REFERENCE TO TOTAL DISSOLVED SOLIDS REMOVAL. *International Journal of Life Science Biotechnology and Pharma Research*, *1*(1). www.ijlbpr.com

Cui, B., Peng, H., Xia, H., Guo, X., & Guo, H. (2013). Magnetically recoverable core-shell nanocomposites γ-Fe 2O3@SiO2@TiO2-Ag with enhanced photocatalytic activity and antibacterial activity. *Separation and Purification Technology*, *103*, 251–257. https://doi.org/10.1016/j.seppur.2012.10.008

Darshana, B., Parikh, S., & Shah, M. (2020). Potential of Ag–Fe co-doped TiO2 nanocomposite for solar photocatalysis of high COD pharmaceutical effluent and influencing factors. *Energy, Ecology and Environment*, *5*(5), 344–358. https://doi.org/10.1007/s40974-020-00162-6

Dubey, R. S., Krishnamurthy, K. V., & Singh, S. (2019). Experimental studies of TiO2 nanoparticles synthesized by sol-gel and solvothermal routes for DSSCs application. *Results in Physics*, *14*, 102390. https://doi.org/10.1016/j.rinp.2019.102390

Giampiccolo, A., Tobaldi, D. M., Leonardi, S. G., Murdoch, B. J., Seabra, M. P., Ansell, M. P., Neri, G., & Ball, R. J. (2019). Sol gel graphene/TiO2 nanoparticles for the photocatalytic-assisted sensing and abatement of NO2. *Applied Catalysis B: Environmental*, *243*, 183–194. https://doi.org/10.1016/j.apcatb.2018.10.032

Gupta, S. M., & Tripathi, M. (2011). A review of TiO2 nanoparticles. In *Chinese Science Bulletin* (Vol. 56, Issue 16, pp. 1639–1657). Springer. https://doi.org/10.1007/s11434-011-4476-1

Han, F., Kambala, V. S. R., Dharmarajan, R., Liu, Y., & Naidu, R. (2018). Photocatalytic degradation of azo dye acid orange 7 using different light sources over Fe3+-doped TiO2 nanocatalysts. *Environmental Technology and Innovation*, *12*, 27–42. https://doi.org/10.1016/j.eti.2018.07.004

Harikishore, M., Sandhyarani, M., Venkateswarlu, K., Nellaippan, T. A., & Rameshbabu, N. (2014). Effect of Ag Doping on Antibacterial and Photocatalytic Activity of Nanocrystalline TiO 2. *Procedia Materials Science*, *6*, 557–566. https://doi.org/10.1016/j.mspro.2014.07.071

He, J., Zeng, X., Lan, S., & Lo, I. M. C. (2019). Reusable magnetic Ag/Fe, N-TiO2/Fe3O4@SiO2 composite for simultaneous photocatalytic disinfection of E. coli and degradation of bisphenol A in sewage under visible light. *Chemosphere*, *217*, 869–878. https://doi.org/10.1016/j.chemosphere.2018.11.072

Huang, M., Li, J., Huang, Y., Zhou, X., Qin, Z., Tong, Z., Fan, M., Li, B., & Dong, L. (2020). Construction of g-C3N4 based heterojunction photocatalyst by coupling TiO2-SnO2 solid solution for efficient multipurpose photocatalysis. *Journal of Alloys and Compounds*, 158132. https://doi.org/10.1016/j.jallcom.2020.158132

Iqbal, M., Ali, A., Ahmad, K. S., Rana, F. M., Khan, J., Khan, K., & Thebo, K. H. (2019). Synthesis and characterization of transition metals doped CuO nanostructure and their application in hybrid bulk heterojunction solar cells. *SN Applied Sciences*, *1*(6), 1–8. https://doi.org/10.1007/s42452-019-0663-5

Jaihindh, D. P., Chen, C. C., & Fu, Y. P. (2018). Reduced graphene oxide-supported Ag-loaded Fe-doped TiO2 for the degradation mechanism of methylene blue and its electrochemical properties. *RSC Advances*, *8*(12), 6488–6501. https://doi.org/10.1039/c7ra13418e

Kaur, T., Sraw, A., Wanchoo, R. K., & Toor, A. P. (2018). Solar assisted degradation of carbendazim in water using clay beads immobilized with TiO2 & Fe doped TiO2. *Solar Energy*, *162*, 45–56. https://doi.org/10.1016/j.solener.2017.11.033

Khanna, A., & Shetty K, V. (2013). Solar photocatalysis for treatment of Acid Yellow-17 (AY-17) dye contaminated water using Ag@TiO2 core-shell structured nanoparticles. *Environmental Science and Pollution Research*, *20*(8), 5692–5707. https://doi.org/10.1007/s11356-013-1582-4

Khanna, A., & Shetty, V. K. (2014). Solar light induced photocatalytic degradation of Reactive Blue 220 (RB-220) dye with highly efficient Ag@TiO2 core-shell nanoparticles: A comparison with UV photocatalysis. *Solar Energy*, *99*, 67–76. https://doi.org/10.1016/j.solener.2013.10.032

Kiliç, M., & Çinar, Z. (2008). Hydroxyl radical reactions with 4-chlorophenol as a model for heterogeneous photocatalysis. *Journal of Molecular Structure: THEOCHEM*, *851*(1–3), 263–270. https://doi.org/10.1016/j.theochem.2007.11.022

Komaraiah, D., Radha, E., Kalarikkal, N., Sivakumar, J., Ramana Reddy, M. V., & Sayanna, R. (2019). Structural, optical and photoluminescence studies of sol-gel synthesized pure and iron doped TiO2 photocatalysts. *Ceramics International*, *45*(18), 25060–25068. https://doi.org/10.1016/j.ceramint.2019.03.170

Lendzion-Bieluń, Z., Wojciechowska, A., Grzechulska-Damszel, J., Narkiewicz, U., Śniadecki, Z., & Idzikowski, B. (2020). Effective processes of phenol degradation on Fe3O4–TiO2 nanostructured magnetic photocatalyst. *Journal of Physics and Chemistry of Solids*, *136*. https://doi.org/10.1016/j.jpcs.2019.109178

Mahy, J. G., Lambert, S. D., Léonard, G. L. M., Zubiaur, A., Olu, P. Y., Mahmoud, A., Boschini, F., & Heinrichs, B. (2016). Towards a large scale aqueous sol-gel synthesis of doped TiO2: Study of various metallic dopings for the photocatalytic degradation of p-nitrophenol. *Journal of Photochemistry and Photobiology A: Chemistry*, *329*, 189–202. https://doi.org/10.1016/j.jphotochem.2016.06.029

Makeswari, M., & Saraswathi, P. (2020). Photo catalytic degradation of methylene blue and methyl orange from aqueous solution using solar light onto chitosan bi-metal oxide composite. *SN Applied Sciences*, *2*(3). https://doi.org/10.1007/s42452-020-1980-4

Mohd Razip, N. I., Lee, K. M., Lai, C. W., & Ong, B. H. (2019). Recoverability of Fe 3 O 4 /TiO 2 nanocatalyst in methyl orange degradation. *Materials Research Express*, *6*(7). https://doi.org/10.1088/2053-1591/ab176e

Nagaveni, K. M. S. H. M. (2003). Photocatalytic degradation of various dyes by combustion

synthesized nano anatase TiO2. *Applied Catalysis B Environmental*, *45*(1), 23–28. https://doi.org/DOI: 10.1016/S0926-3373(03)00124-3

Nasralla, N., Yeganeh, M., Astuti, Y., Piticharoenphun, S., Shahtahmasebi, N., Kompany, A., Karimipour, M., Mendis, B. G., Poolton, N. R. J., & Šiller, L. (2013). Structural and spectroscopic study of Fe-doped TiO2 nanoparticles prepared by sol-gel method. *Scientia Iranica*, *20*(3), 1018–1022. https://doi.org/10.1016/j.scient.2013.05.017

Nezamzadeh-Ejhieh, A., & Amiri, M. (2013). CuO supported Clinoptilolite towards solar photocatalytic degradation of p-aminophenol. *Powder Technology*, *235*, 279–288. https://doi.org/10.1016/j.powtec.2012.10.017

Nezamzadeh-Ejhieh, A., & Badri, A. (2011). Surfactant modified ZSM-5 zeolite as an active component of membrane electrode towards thiocyanate. *Desalination*, *281*(1), 248–256. https://doi.org/10.1016/j.desal.2011.07.070

Nezamzadeh-Ejhieh, A., & Hushmandrad, S. (2010). Solar photodecolorization of methylene blue by CuO/X zeolite as a heterogeneous catalyst. *Applied Catalysis A: General*, *388*(1–2), 149–159. https://doi.org/10.1016/j.apcata.2010.08.042

Nezamzadeh-Ejhieh, A., & Moazzeni, N. (2013). Sunlight photodecolorization of a mixture of Methyl Orange and Bromocresol Green by CuS incorporated in a clinoptilolite zeolite as a heterogeneous catalyst. *Journal of Industrial and Engineering Chemistry*, *19*(5), 1433–1442. https://doi.org/10.1016/j.jiec.2013.01.006

Pant, A., Tanwar, R., Kaur, B., & Mandal, U. K. (2018). A magnetically recyclable photocatalyst with commendable dye degradation activity at ambient conditions. *Scientific Reports*, *8*(1), 1–15. https://doi.org/10.1038/s41598-018-32911-3

Petronella, F., Truppi, A., Sibillano, T., Giannini, C., Striccoli, M., Comparelli, R., & Curri, M. L. (2017). Multifunctional TiO2/FexOy/Ag based nanocrystalline heterostructures for photocatalytic degradation of a recalcitrant pollutant. *Catalysis Today*, *284*, 100–106. https://doi.org/10.1016/j.cattod.2016.11.025

R. Renugadevi1, T. V., , R. Narayanasamy, S. P., & P.Krishnamurthi. (2016). Structural, optical properties and photocatalytic activity of Fe3C doped TiO2 thin films deposited by sol-gel spin coating - Google Search. *Rasayan Journal of Chemistry*, *9*(2), 125–132. https://www.google.com/search?q=Structural%2C+optical+properties+and+photocatalytic+activity+of+Fe3C+doped+TiO2+thin+films+deposited+by+sol-gel+spin+coating&rlz=1C1SQJL_enIN871IN871&oq=Structural%2C+optical+properties+and+photocatalytic+activity+of+Fe3C+d

Rabbani, M., Safalou moghaddam, S., & Rahimi, R. (2019). Photocatalytic degradation of 4-nitrophenol in aqueous N, S-codoped TiO2 suspensions. *International Electronic Conference on Synthetic Organic Chemistry*, 1–30. https://doi.org/10.3390/ecsoc-15-00791

Sharma Sandip, jayesh ruparelia. (2011). A general review on Advanced Oxidation Processes for waste water treatment. *Chemistry*. https://www.semanticscholar.org/paper/A-general-review-on-Advanced-Oxidation-Processes-Sharma/e165f3fa23655a2af6ec0a7870b2d1982809d303

Stasinakis, 66. A.S. (2008). (PDF) Use of Selected Advanced Oxidation Processes (AOPs) for Wastewater Treatment – a Mini Review. *Global Nest*, *10*(3), 376–385. https://www.researchgate.net/publication/228474561_Use_of_Selected_Advanced_Oxidation_Processes_AOPs_for_Wastewater_Treatment_-_a_Mini_Review

Sun, W. J., Li, J., Yao, G. P., Jiang, M., & Zhang, F. X. (2011). Efficient photo-degradation of 4-nitrophenol by using new CuPp-TiO 2 photocatalyst under visible light irradiation. *Catalysis Communications*, *16*(1), 90–93. https://doi.org/10.1016/j.catcom.2011.09.013

Suwarnkar, M. B., Dhabbe, R. S., Kadam, A. N., & Garadkar, K. M. (2014). Enhanced photocatalytic activity of Ag doped TiO2 nanoparticles synthesized by a microwave assisted method. *Ceramics International*, *40*(4), 5489–5496. https://doi.org/10.1016/j.ceramint.2013.10.137

Tedsree, K., Temnuch, N., Sriplai, N., & Pinitsoontorn, S. (2017). Ag modified Fe3O4@TiO2 magnetic core-shell nanocomposites for photocatalytic degradation of methylene blue.

*Materials Today: Proceedings*, *4*(5), 6576–6584. https://doi.org/10.1016/j.matpr.2017.06.170

Trojanowicz, M., Bojanowska-Czajka, A., Bartosiewicz, I., & Kulisa, K. (2018). Advanced Oxidation/Reduction Processes treatment for aqueous perfluorooctanoate (PFOA) and perfluorooctanesulfonate (PFOS) – A review of recent advances. In *Chemical Engineering Journal* (Vol. 336, pp. 170–199). Elsevier B.V. https://doi.org/10.1016/j.cej.2017.10.153

Vijayalakshmi, R., & Rajendran, V. (2012). Synthesis and characterization of nano-TiO 2 via different methods. *Scholars Research Library Archives of Applied Science Research*, *2*, 1183–1190.

Wang, P., Tang, Y., Dong, Z., Chen, Z., & Lim, T. T. (2013). Ag-AgBr/TiO2/RGO nanocomposite for visible-light photocatalytic degradation of penicillin G. *Journal of Materials Chemistry A*, *1*(15), 4718–4727. https://doi.org/10.1039/c3ta01042b

Wang, W., Zhang, J., Chen, F., He, D., & Anpo, M. (2008a). Preparation and photocatalytic properties of Fe3+-doped Ag@TiO2 core-shell nanoparticles. *Journal of Colloid and Interface Science*, *323*(1), 182–186. https://doi.org/10.1016/j.jcis.2008.03.043

Wang, W., Zhang, J., Chen, F., He, D., & Anpo, M. (2008b). Preparation and photocatalytic properties of Fe3+-doped Ag@TiO2 core-shell nanoparticles. *Journal of Colloid and Interface Science*, *323*(1), 182–186. https://doi.org/10.1016/j.jcis.2008.03.043

Watkinson, A. J., Murby, E. J., & Costanzo, S. D. (2007). Removal of antibiotics in conventional and advanced wastewater treatment: Implications for environmental discharge and wastewater recycling. *Water Research*, *41*(18), 4164–4176. https://doi.org/10.1016/j.watres.2007.04.005

Wu, C. C., Huang, W. J., & Ji, B. H. (2015). Degradation of cyanotoxin cylindrospermopsin by TiO2-assisted ozonation in water. *Journal of Environmental Science and Health - Part A Toxic/Hazardous Substances and Environmental Engineering*, *50*(11), 1116–1126. https://doi.org/10.1080/10934529.2015.1047664

Xiu, Z., Guo, M., Zhao, T., Pan, K., Xing, Z., Li, Z., & Zhou, W. (2019). Recent advances in Ti3+ self-doped nanostructured TiO2 visible light photocatalysts for environmental and energy applications. In *Chemical Engineering Journal*. Elsevier B.V. https://doi.org/10.1016/j.cej.2019.123011

Yang, H., Zhang, K., Shi, R., Li, X., Dong, X., & Yu, Y. (2006). Sol-gel synthesis of TiO2 nanoparticles and photocatalytic degradation of methyl orange in aqueous TiO2 suspensions. *Journal of Alloys and Compounds*, *413*(1–2), 302–306. https://doi.org/10.1016/j.jallcom.2005.06.061

Yasmina, M., Mourad, K., Mohammed, S. H., & Khaoula, C. (2014). Treatment heterogeneous photocatalysis; Factors influencing the photocatalytic degradation by TiO2. *Energy Procedia*, *50*, 559–566. https://doi.org/10.1016/j.egypro.2014.06.068

Yeganeh, M., Shahtahmasebi, N., Kompany, A., Karimipour, M., Razavi, F., Nasralla, N. H. S., & Šiller, L. (2017). The magnetic characterization of Fe doped TiO2semiconducting oxide nanoparticles synthesized by sol–gel method. *Physica B: Condensed Matter*, *511*, 89–98. https://doi.org/10.1016/j.physb.2017.02.010

Zhan, J., Zhang, H., & Zhu, G. (2014). Magnetic photocatalysts of cenospheres coated with Fe3O 4/TiO2 core/shell nanoparticles decorated with Ag nanopartilces. *Ceramics International*, *40*(6), 8547–8559. https://doi.org/10.1016/j.ceramint.2014.01.069

Zhibo Zhang, †, Chen-Chi Wang, ‡, Rama Zakaria, ‡ and, & Jackie Y. Ying*, ‡. (1998). Role of Particle Size in Nanocrystalline TiO2-Based Photocatalysts. *J. Phys. Chem. B*, *102*(52), 10871–10878. https://doi.org/10.1021/JP982948+

Zhou, G., Meng, H., Cao, Y., Kou, X., Duan, S., Fan, L., Xiao, M., Zhou, F., Li, Z., & Xing, Z. (2018). Surface plasmon resonance-enhanced solar-driven photocatalytic performance from Ag nanoparticles-decorated Ti3+ self-doped porous black TiO2 pillars. *Journal of Industrial and Engineering Chemistry*, *64*, 188–193. https://doi.org/10.1016/j.jiec.2018.03.015

# Design of water ionizer for the production of alkaline water and study of its characteristics

*Parekh Akhil [1], Parmar Saurav[2], Endrick Contractor[13]*

[1] *Department of Chemical Engineering, G.H. Patel College of Engineering & Technology, Vallabh Vidyanagar, 388120 Gujarat.INDIA.*
[2]*Graduate Engineering Trainee, SaurashtraChemicals A division of Nirma Ltd. Porbandar360576.Gujarat,INDIA.*
[3]*Assistant Professor, Department of Chemical Engineering, G.H. Patel College of Engineering & Technology, Vallabh Vidyanagar, 388120 Gujarat.INDIA.*

## Abstract:

Nowadays, Electrolysis-ionized water procedure has acquired the remarkable potential to maintain environmental in its pristine state and low-cost processing. Therefore, water ionizers are highly promoted for both commercial and domestic purposes. The water ionizers have prone to manufacture alkaline water which consists of dissolved molecular hydrogen at the cathode and acidic water at the anode. Electrolysis is not only sufficient for altering pH of the sample water; almost of all these devices made with a basic semi-permeable ion-exchange membrane, which plays an indispensable role to protect the catholyte (with the alkaline OH- ions) and anolyte (with the acidic H+ ions) compartments from mixing and therefore, it yields into the production of alkaline (mild or strong) and acidic (mild or strong) water at the cathode and anode, respectively. So, in this regard, we had done a study on producing alkaline water by using cheaper electrodes like copper and aluminium. During this experimental setup, any experiments have performed with RO water and Tap water using copper and aluminium as electrodes. Here we had also changed the cross-section of electrodes and measure the effects on the production of alkaline water. To identify the optimum result and best combination, the experimental run of about 12 hours for each experiment has taken ideal. According to the experimental work on the RO water and Tap water, we can say that we are getting the positive result in pH, ORP and TDS for alkaline water and acidic water. In the initial experiments with RO water by using the copper and aluminium plate we are getting quite close results to the standard data after 12hr of the experimental run, which is quite desirable. in this set of experiments, the Copper-plate used as electrode gives the best results compared to the aluminium plate except for cost factor.

**Keywords:** Design of Water ionizer, Alkaline water, Electrolysis, Electrodes, Ion Exchange semipermeable membrane, Characteristics of alkaline water.

## Introduction:

The device which is used to produce alkaline water & acidic water is known as Water Ionizer and it works on the fundamental process of electrolysis[d]. In this process, regular tap water is allowed to pass through the ionization chamber and electricity is passed to water through its plates. The water ionizer has two electrodes put into a container having two chambers separated by a semi-permeable membrane[c]. The positive terminal produces – acidic water and the negative terminal produces – alkaline water. Here, electrolysis refers to the breakdown of a substance by passing an electric current through it. This is accomplished by placing a pair of oppositely-charged electrodes in the solution[d]. The Alkaline water which is

*Corresponding author:Endrick Contractor
endrickcontractor@gcet.ac.in , (+91) 95747 68731

also commonly known as electrolyzed reduced, reduced, and alkaline ionized water which has a pH level of more than seven [a]. It is used to balance the pH of the human body. The word "alkaline" in alkaline water refers to its pH level. However, pH is not the only parameter to impart substantiality of the alkalinity to water[a]. Alkaline water must also contain alkaline minerals and negative oxidation-reduction potential (ORP)[e]. ORP is the ability of water to act as an antioxidant. The more negative the ORP value, the more antioxidants it is.

**The objective of Experiment/Work:**

- By altering the different parameters of the process like the type of electrodes and different cross-section of the electrode, the experiment work is contending to identify the effect of these parameters on the quality of water and try to make effective and optimum alkaline water ionizer.
- Learn the feasibility study of the system through the usage of numerous electrodes and also check which electrode is more effective and economical in alkaline water production.
- Study the process performance using two different raw water with RO water and Normal tap water.

**Experimental:**

**Materials:** Electrodes (aluminium, copper), Semipermeable membrane, PVC pipes, Rectifier, Electric wire, pH meter, TDS meter, Activated carbon (depends on the condition of raw water ), ORP sensor.

**Chemicals:** Water, NaCl

**Methodology/Experimental Procedure:**

First, we complete the setup for proper operation of the water ionizer.Then We take a sample of water and analyze it (pH, TDS). If the selected water sample has solid impurities, it is removed by filtration or sedimentation process as required. Then the raw water is electrolyzed in water ionizer setup for different operating conditions such as voltage and type of electrode.
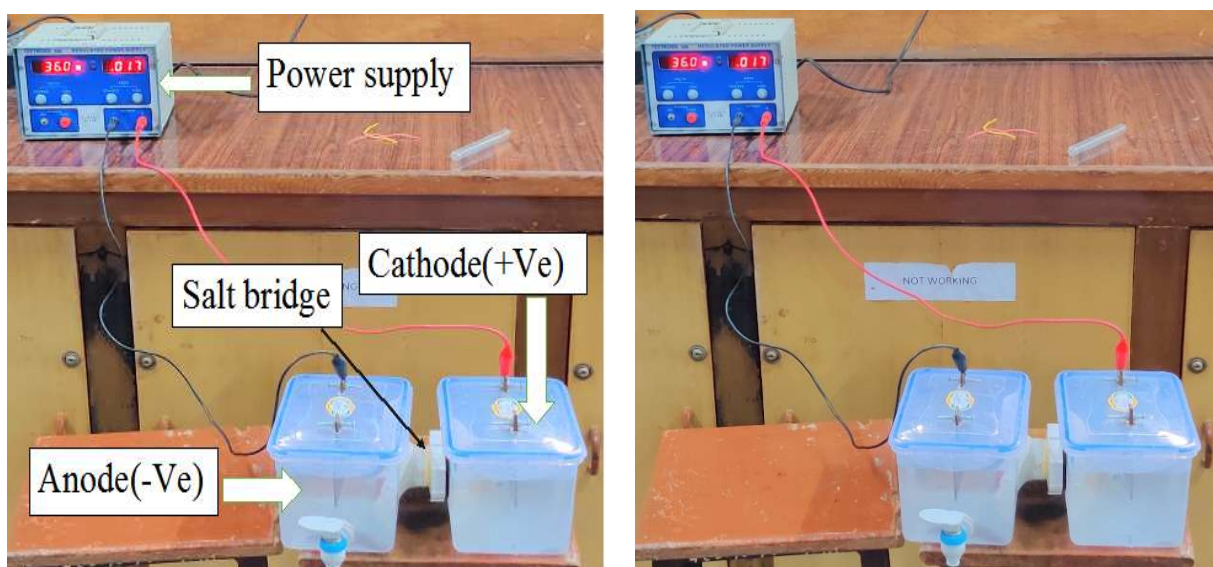


After some time the sample of electrolyzed water is taken from the anode side and cathode

side compartment. Then these samples are analyzed whether it is alkaline water, acidic water or not and ORP is also measured.

Figure 1: Complete experimental setup

**Experimental Result Tables and Graphical Presentation:**

**Set-1 Copper-plate (single c/s) experiments with RO waterpower supply = 36 volts**

| Time (hr) | Cathode side pH | Anode side pH | Cathode side ORP (mv) | Anode side ORP (mv) | | Anode side TDS (ppm) | Cathode side TDS (ppm) |
|---|---|---|---|---|---|---|---|
| 0 | 6.3 | 6.3 | 301 | 301 | **Initial** | 138 | 138 |
| 0.5 | 6.35 | 6.31 | 290 | 300 | **Final** | 151 | 149 |
| 1 | 6.5 | 6.29 | 262 | 347 | | | |
| 1.5 | 6.7 | 6.27 | 240 | 360 | | | |
| 3 | 6.79 | 6.26 | 234 | 365 | | | |
| 6 | 6.9 | 6.26 | 220 | 369 | | | |
| 8 | 6.98 | 6.25 | 211 | 372 | | | |
| 12 | 7.1 | 6.25 | 200 | 375 | | | |

Table 1 **RO water, Copper-plate (single c/s)**
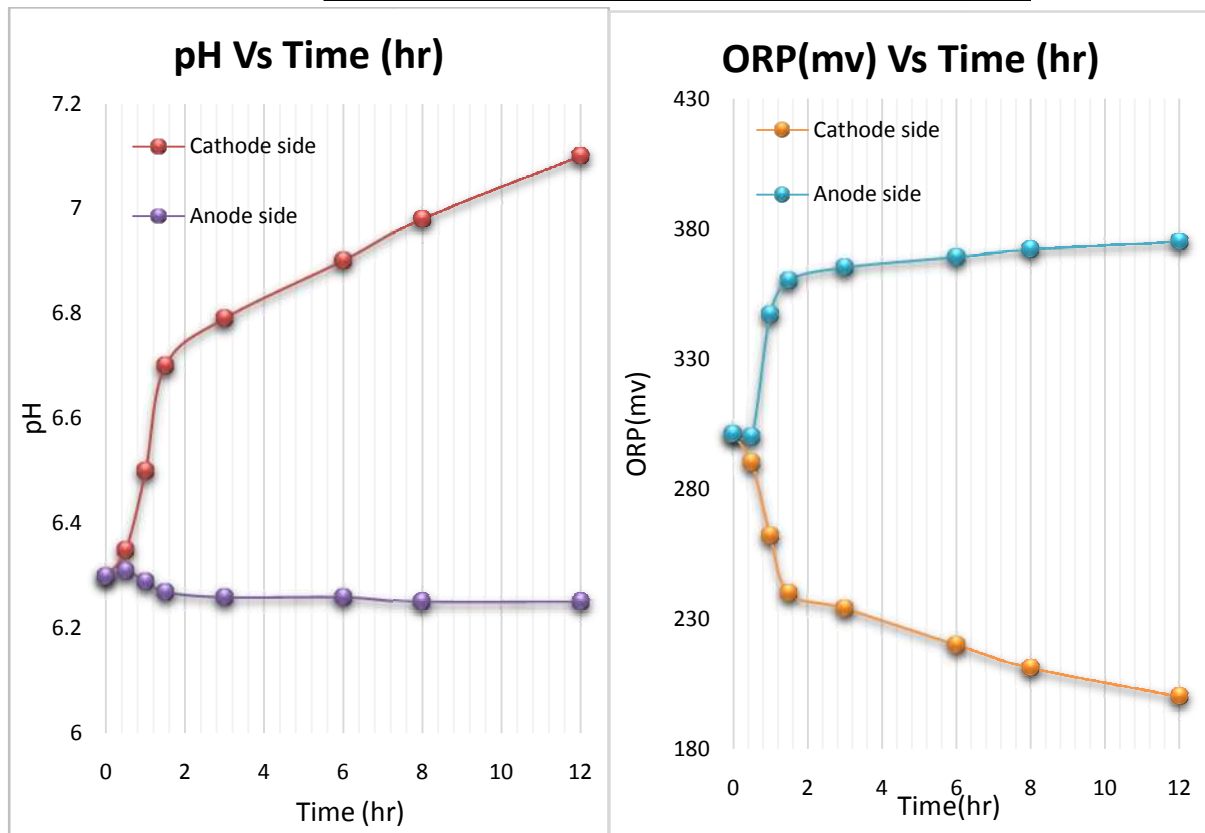


| Graph 1.1. pH Vs Time (hr) **RO water, Copper-plate (single c/s)** | Graph 1.2. ORP (mv) Vs Time (hr) **RO water, Copper-plate (single c/s)** |
|---|---|

**Set-2 Aluminium plate (single c/s) experiments with RO waterpower supply of = 36 volts**

| Time (hr) | Cathode side pH | Anode side pH | Cathode side ORP (mv) | Anode side ORP (mv) | | | Anode side TDS (ppm) | Cathode side TDS (ppm) |
|---|---|---|---|---|---|---|---|---|
| 0 | 6.42 | 6.42 | 378 | 378 | **Initial** | | 143 | 143 |
| 0.5 | 6.42 | 6.41 | 375 | 375 | **Final** | | 159 | 155 |
| 1 | 6.5 | 6.39 | 370 | 380 | | | | |
| 1.5 | 6.65 | 6.37 | 361 | 398 | | | | |
| 3 | 6.73 | 6.36 | 345 | 410 | | | | |
| 6 | 6.9 | 6.3 | 320 | 429 | | | | |
| 8 | 7.1 | 6.28 | 297 | 448 | | | | |
| 12 | 7.4 | 6.24 | 279 | 461 | | | | |

Table.2 **RO water**, **Aluminium plate (single c/s)**
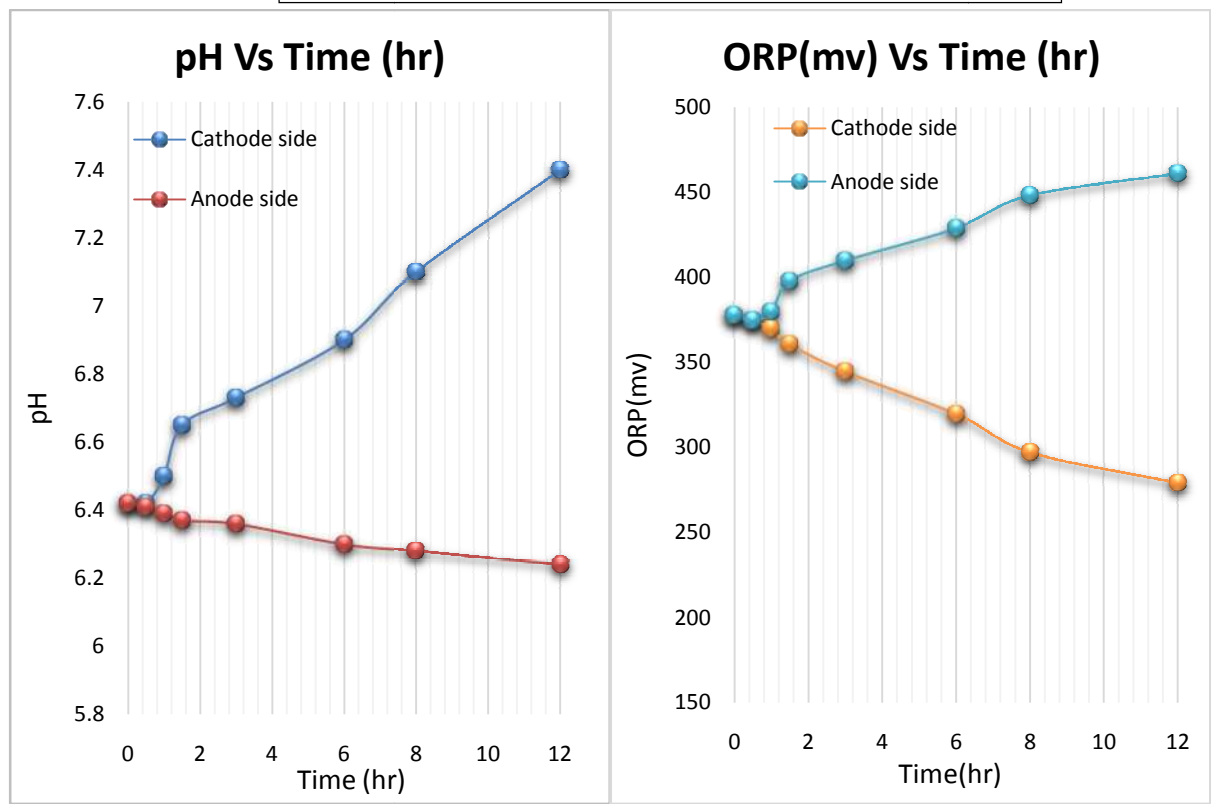


| Graph 2.1. pH Vs Time (hr)**RO water, Aluminium plate (single c/s)** | Graph 2.2 ORP (mv) Vs Time (hr)**RO water, Aluminium plate (single c/s)** |
|---|---|

**Set-3 Copper-plate (doubled cross-section area)experiments with RO water power supply = 36 volts**

| Time (hr) | Cathode side pH | Anode side pH | Cathode side ORP (mv) | Anode side ORP (mv) | | Anode side TDS (ppm) | Cathode side TDS (ppm) |
|---|---|---|---|---|---|---|---|
| 0 | 6.39 | 6.39 | 450 | 450 | **Initial** | 119 | 119 |
| 0.5 | 6.41 | 6.37 | 444 | 451 | **Final** | 137 | 133 |
| 1 | 6.45 | 6.34 | 440 | 459 | | | |
| 1.5 | 6.49 | 6.32 | 425 | 470 | | | |
| 3 | 6.6 | 6.3 | 400 | 483 | | | |
| 6 | 7 | 6.28 | 350 | 499 | | | |
| 8 | 7.4 | 6.24 | 300 | 510 | | | |
| 12 | 7.9 | 6 | 270 | 530 | | | |

Table 3 **RO water Copper-plate (doubled cross-section area)**
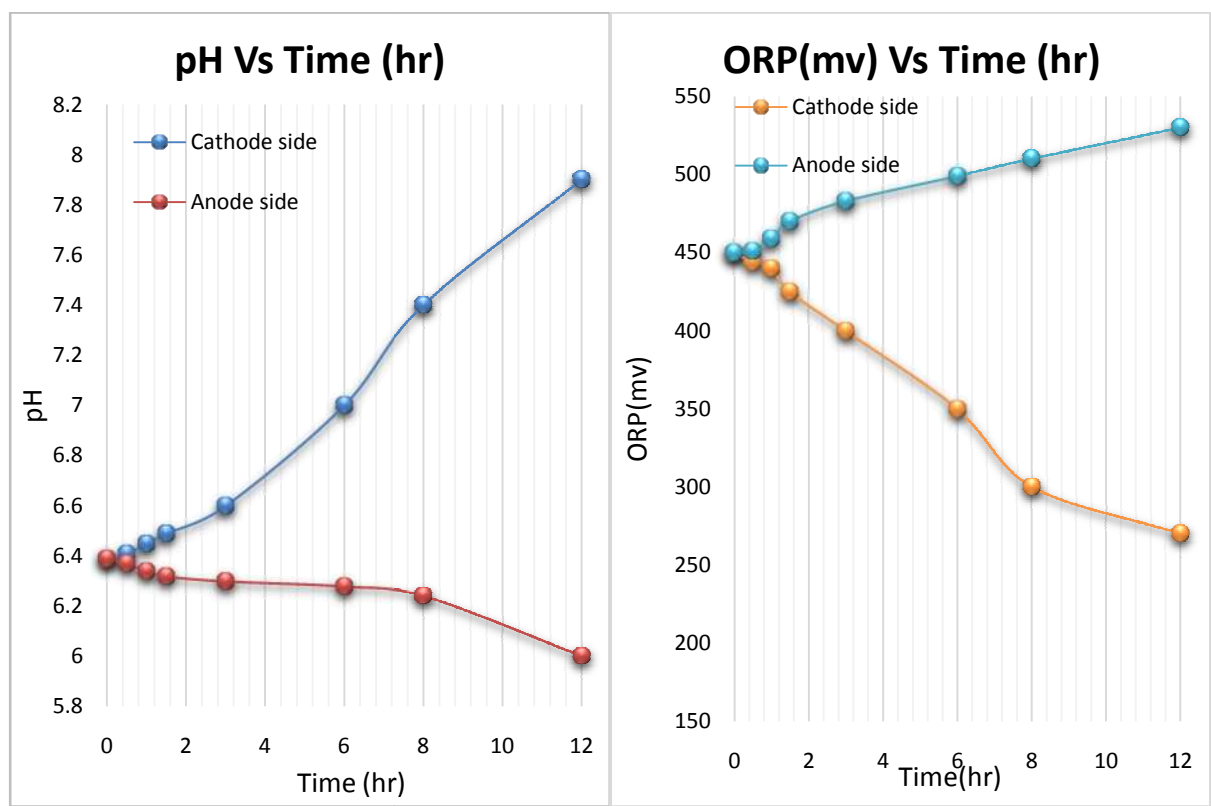


| Graph 3.1. pH Vs Time (hr) **RO water Copper-plate (doubled cross-section area)** | Graph3.2 ORP (mv) Vs Time (hr) **RO water Copper-plate (doubled cross-section area)** |
|---|---|

**Set-4 Aluminium plate (doubled cross-section area) with RO water power supply = 36 volts**

| Time (hr) | Cathode side pH | Anode side pH | Cathode side ORP (mv) | Anode side ORP (mv) | | Anode side TDS (ppm) | Cathode side TDS (ppm) |
|---|---|---|---|---|---|---|---|
| 0 | 6.26 | 6.26 | 339 | 339 | **Initial** | 138 | 138 |
| 0.5 | 6.25 | 6.24 | 335 | 340 | **Final** | 151 | 149 |
| 1 | 6.32 | 6.21 | 329 | 351 | | | |
| 1.5 | 6.49 | 6.15 | 315 | 369 | | | |
| 3 | 6.6 | 6.1 | 300 | 382 | | | |
| 6 | 6.98 | 5.9 | 291 | 398 | | | |
| 8 | 7.2 | 5.71 | 271 | 410 | | | |
| 12 | 7.56 | 5.5 | 253 | 442 | | | |

Table 4 **RO water Aluminium plate (doubled cross-section area)**
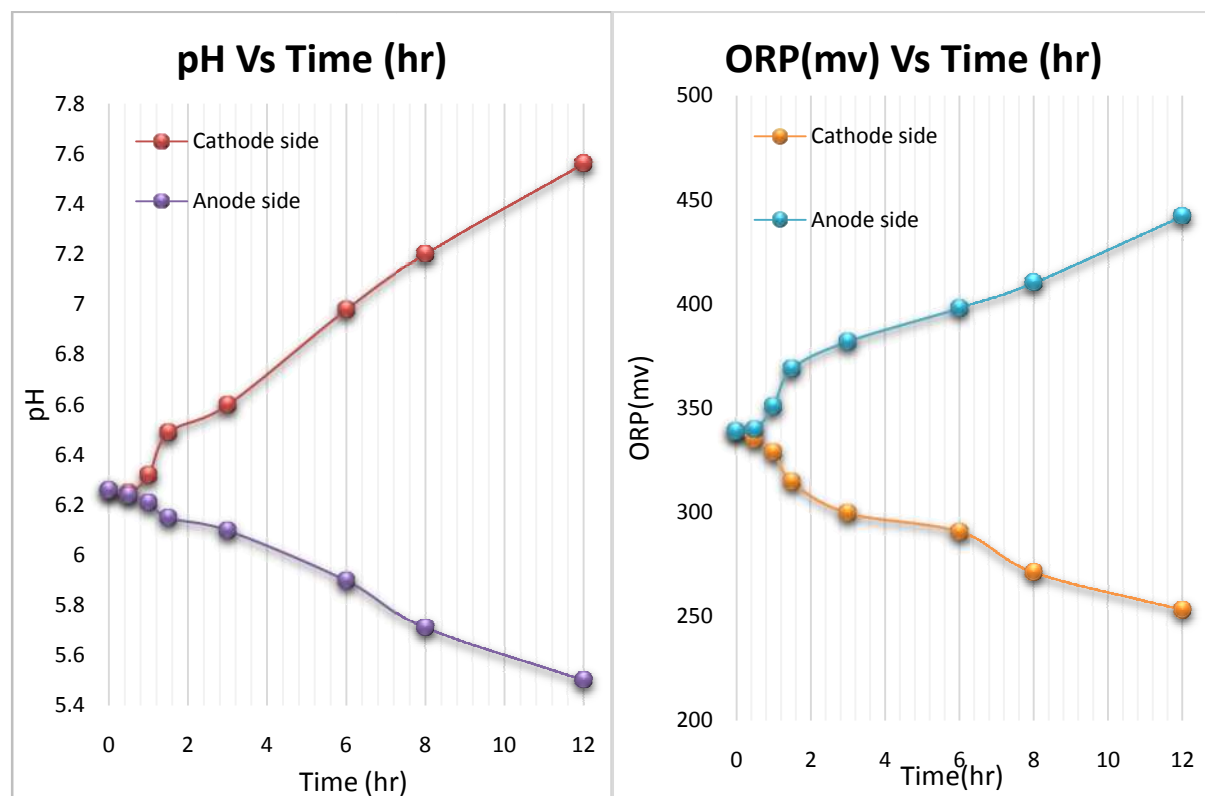
| Graph 4.1pH Vs Time (hr)**RO water Aluminium plate (doubled cross-section area)** | Graph 4.2 ORP (mv) Vs Time (hr) **RO water Aluminium plate (doubled cross-section area)** |
|---|---|
| | |

**Set-5 Copper-plate (single c/s) experiments with Tap water power supply = 36 volts**

| Time (hr) | Cathode side pH | Anode side pH | Cathode side ORP (mv) | Anode side ORP (mv) | | | Anode side TDS (ppm) | Cathode side TDS (ppm) |
|---|---|---|---|---|---|---|---|---|
| 0 | 6.7 | 6.7 | 380 | 380 | **Initial** | | 451 | 451 |
| 0.5 | 6.71 | 6.69 | 380 | 389 | **Final** | | 475 | 473 |
| 1 | 6.8 | 6.63 | 371 | 396 | | | | |
| 1.5 | 7 | 6.5 | 350 | 419 | | | | |
| 3 | 7.2 | 6.42 | 342 | 425 | | | | |
| 6 | 7.4 | 6.34 | 325 | 432 | | | | |
| 8 | 7.9 | 6.29 | 300 | 449 | | | | |
| 12 | 8.2 | 6.2 | 279 | 462 | | | | |

Table 5 **Tap water, Copper-plate (single c/s)**



Graph 5.2 ... water, C...

**Set-6 Aluminium plate (single c/s) experiments with Tap water power supply = 36 volts**
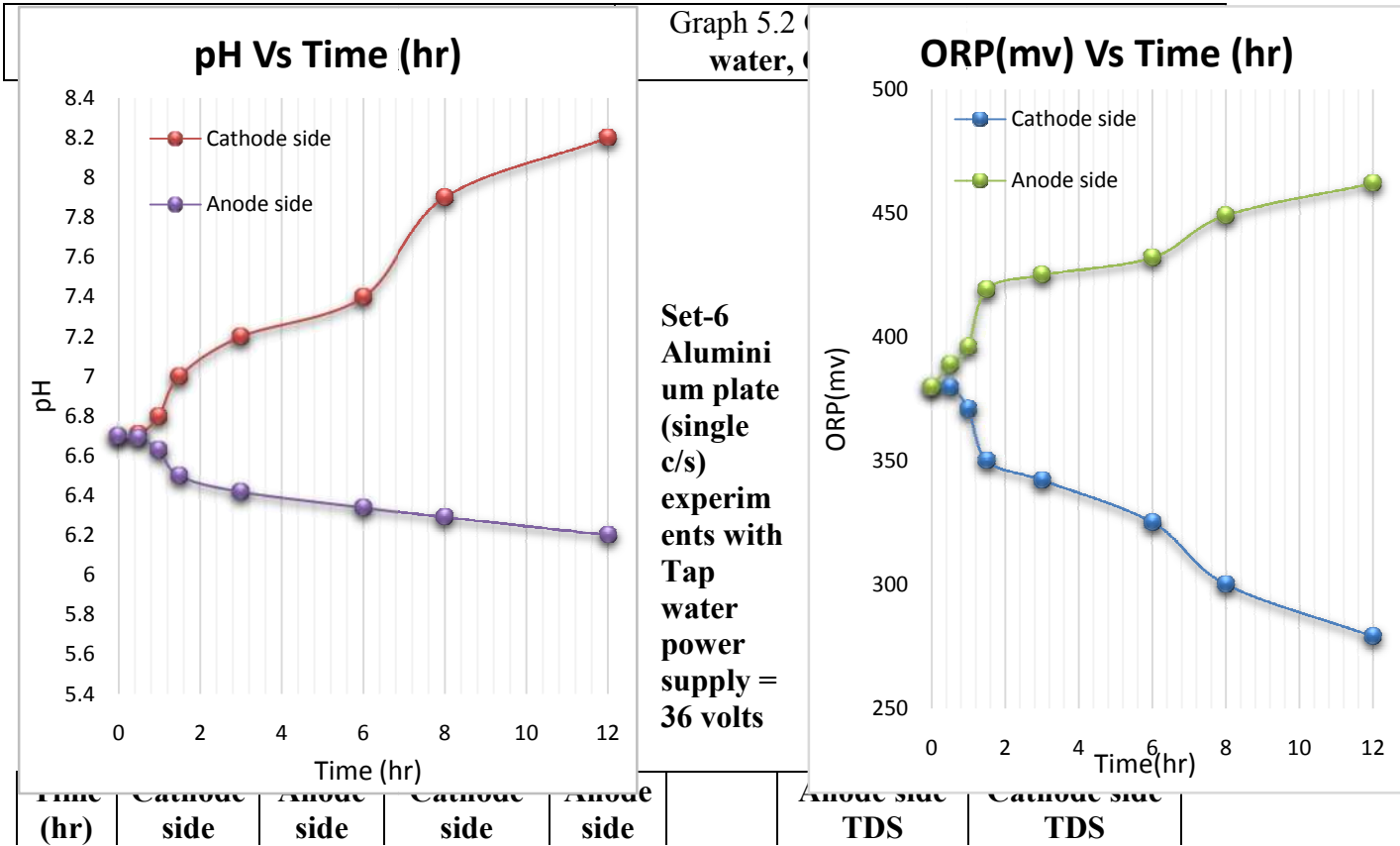
| Time (hr) | Cathode side | Anode side | Cathode side | Anode side | | Anode side TDS | Cathode side TDS |
|---|---|---|---|---|---|---|---|

|  | pH | pH | ORP (mv) | ORP (mv) |  | (ppm) | (ppm) |
|---|---|---|---|---|---|---|---|
| 0 | 6.62 | 6.62 | 371 | 371 | Initial | 471 | 471 |
| 0.5 | 6.64 | 6.6 | 370 | 375 | Final | 495 | 492 |
| 1 | 6.71 | 6.58 | 359 | 389 |  |  |  |
| 1.5 | 6.82 | 6.51 | 341 | 401 |  |  |  |
| 3 | 6.95 | 6.42 | 332 | 423 |  |  |  |
| 6 | 7.1 | 6.31 | 300 | 439 |  |  |  |
| 8 | 7.4 | 6.22 | 289 | 462 |  |  |  |
| 12 | 7.8 | 6.01 | 256 | 489 |  |  |  |

Table 6 **Tap water, Aluminium plate (single c/s)**

Graph 6.1. pH Vs Time (hr )Tap water, Aluminium plate (single c/s)



pH Vs Time (hr)

Graph 6.2. ORP (mv) Vs Time (hr) Tap water, Aluminium plate (single c/s)



ORP(mv) Vs Time (hr)

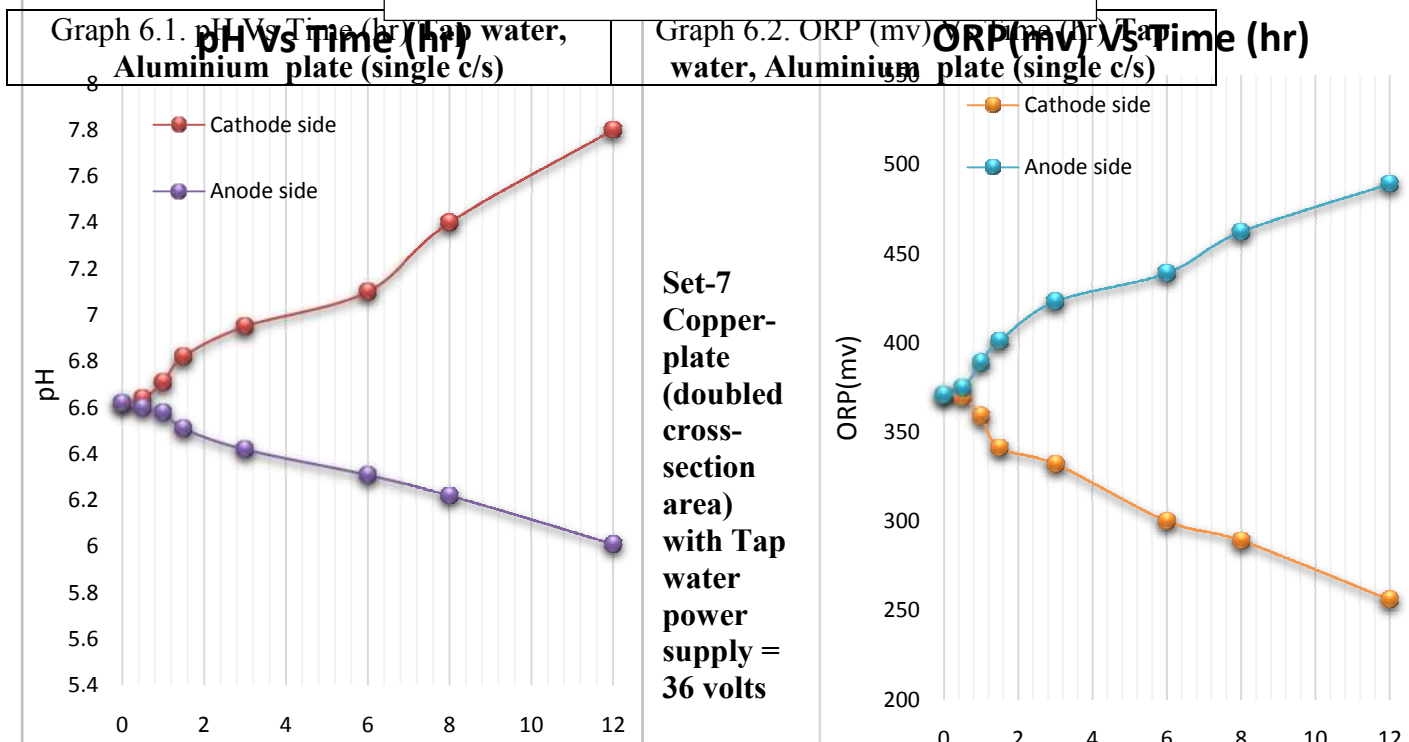**Set-7 Copper-plate (doubled cross-section area) with Tap water power supply = 36 volts**

| Time (hr) | Cathode side pH | Anode side pH | Cathode side ORP (mv) | Anode side ORP (mv) |  | Anode side TDS (ppm) | Cathode side TDS (ppm) |
|---|---|---|---|---|---|---|---|
| 0 | 6.72 | 6.72 | 387 | 387 | Initial | 428 | 428 |
| 0.5 | 6.75 | 6.7 | 380 | 393 | Final | 459 | 462 |
| 1 | 6.98 | 6.59 | 369 | 409 |  |  |  |
| 1.5 | 7.1 | 6.44 | 346 | 428 |  |  |  |
| 3 | 7.45 | 6.31 | 332 | 448 |  |  |  |
| 6 | 7.74 | 6.1 | 318 | 467 |  |  |  |
| 8 | 8.05 | 5.89 | 288 | 485 |  |  |  |

| 12 | 8.45 | 5.75 | 267 | 510 |

Table 7 **Tap water Copper-plate (doubled cross-section area)**
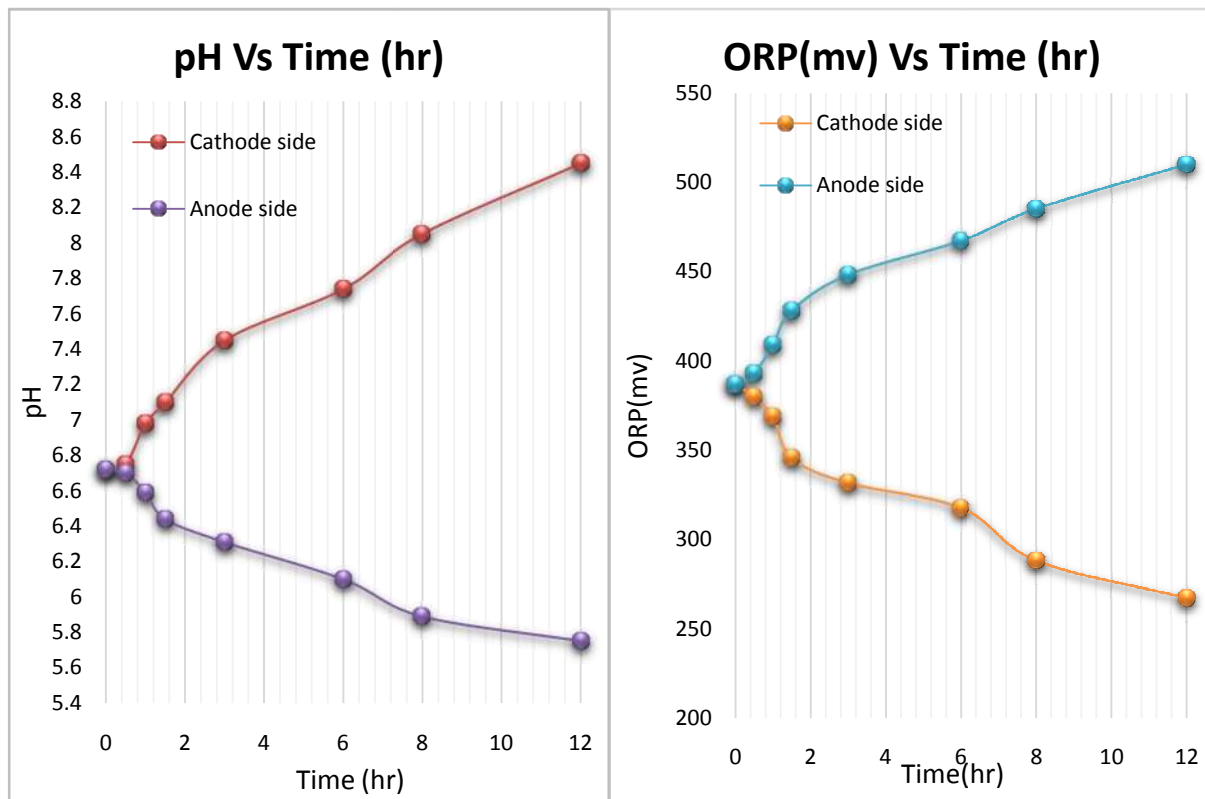


| Graph 7.1. pH Vs Time (hr) **Tap water Copper-plate (doubled cross-section area)** | Graph 7.2 ORP(mv) Vs Time (hr) **Tap water Copper-plate (doubled cross-section area)** |
|---|---|

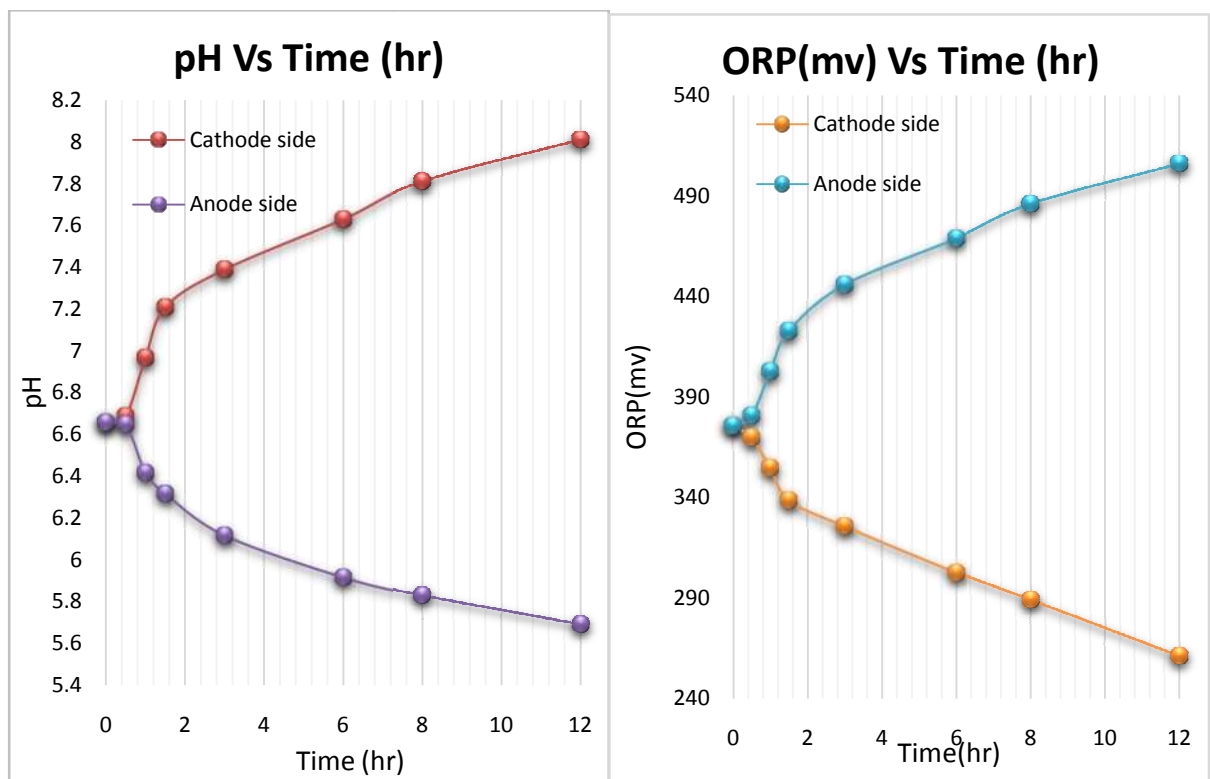**Set-8 Aluminium plate (doubled cross-section area) with Tap water power supply = 36 volts**

| Time (hr) | Cathode side pH | Anode side pH | Cathode side ORP (mv) | Anode side ORP (mv) | | Anode side TDS (ppm) | Cathode side TDS (ppm) |
|---|---|---|---|---|---|---|---|
| 0 | 6.66 | 6.66 | 376 | 376 | **Initial** | 444 | 444 |
| 0.5 | 6.69 | 6.65 | 370 | 381 | **Final** | 467 | 469 |
| 1 | 6.97 | 6.42 | 355 | 403 | | | |
| 1.5 | 7.21 | 6.32 | 339 | 423 | | | |
| 3 | 7.39 | 6.12 | 326 | 446 | | | |
| 6 | 7.63 | 5.92 | 303 | 469 | | | |
| 8 | 7.81 | 5.83 | 289 | 486 | | | |

| 12 | 8.01 | 5.69 | 261 | 506 |

Table 8 **Tap water Aluminium plate (doubled cross-section area)**



## pH Vs Time (hr)

## ORP(mv) Vs Time (hr)

| Graph 8.1pH Vs Time (hr) **Tap water Aluminium plate (doubled cross-section area)** | Graph 8.2 ORP(mv) Vs Time (hr) **Tap water Aluminium plate (doubled cross-section area)** |

**Result and Discussion**:

| Electrode Material | Cathode side  pH | | Cathode side ORP(mv) | |
|---|---|---|---|---|
| | Tap water | RO water | Tap water | RO water |
| Copper-plate (single c/s ) | 8.2 | 7.1 | 279 | 200 |
| Aluminium plate (single c/s) | 7.8 | 7.4 | 256 | 279 |
| Copper-plate (double  c/s ) | 8.45 | 7.9 | 267 | 270 |
| Aluminium plate (double c/s) | 8.01 | 7.56 | 261 | 253 |

Based on the experimental work had been done on the RO water and Tap water, the conclusion has been made that the pronounced positive result in terms of characteristic studies likepH, ORP and TDS for both the alkaline water and acidic water hasbeen achieved. Also, in the initial experiments with RO water by using the single copper and aluminium plate, the results are quite close results to the standard data (for cu plate pH7.1, for Al 7.4). Another

conclusion can be made that the Copper-plate used as the electrode gives best results compared to the aluminium plate except for cost factor.

In the next set of experiments, the cross-section of both electrode platehad turned up doubled and here also the results are quite close results to the standard data(for cu plate: pH7.9, for Al plate: pH 7.56).

Experiments on normal Tap water with single and doublecross-section of copper and aluminium plates give higher results (pH8.45for Cu plate doubled cross-section, pH8.2for Cu plate single cross-section , pH7.8 for Al plate single cross-section, pH 8.01 for Al plate doubled cross-section)than the experiments with RO water because of tap water has higher electrical conductivity than the RO water but with a quite higher level of TDS(ppm) compared to RO water.

**Conclusion**:

To conclude, after critical analysis of all experiments on this designed experimental setup we proclaimed that Copper-plate with doubled cross-section illuminates optimum results than other electrodes (cu single c/s, Al single c/s Al doubled c/s) for RO water as well as for normal Tap water.

**References:**
a) Watanabe T., Shirai W. Influence of alkaline ionized water on reproductive functions in the rat. International Journal of Fertility and Sterility. 1990;35:748–751.
b) S. Shirahata, T. Nishimura, S. Kabayama, D. Aki, K. Teruya, K. Otsubo, etal. Anti-oxidative water improves diabetes E. Lindner-Olsson, et al. (Eds.), Animal cell technology: From target to market, Kluwer Academic Publishers, Dordrecht (2001), pp. 574-577
c) Gadek Z, Hamasaki T, Shirahata S. "Nordenau Phenomenon" Application of Natural Reduced Water to Therapy. Anim Cell Tech. 2008;15:279–285.
d) R. C. Okoloekwe, J.O. Ademiluyi, C.N. Mbah, Water Ionisers and Production of Alkaline Mineral Drinking Water, International Journal of Engineering Trends and Technology (IJETT) – Volume 39 Number 5- September 2016.
e) Mehmet Faith Kaya, Nesrin Demir ,M. Salahaldin Albawabiji,Mert Tas, " Investigation of alkaline water electrolysis performance for different cost effective electrodes under magnetic field 6 February 2017.

# Determination of optimum hollowness through numerical simulation and experimental investigations of performance characteristics of optimum hollow taper roller bearing

**Rajesh M. Joshi[1*], Gurmitsingh D. Bassan[2]**

[1]Assistant Professor, Department of Mechanical Engineering, Faculty of Technology, Dharmsinh Desai University, Nadiad-387 001, Gujarat, India.
[2]Associate Professor & Head, Department of Mechanical Engineering, Faculty of Technology, Dharmsinh Desai University, Nadiad-387 001, Gujarat, India.
*Corresponding author: rmjoshi.mech@ddu.ac.in, +91 94260 47274

## Abstract

Rolling element bearings are commonly used in machines and are expected to perform better and sustain for longer life while operating under more stringent conditions. Major limitation of rolling bearings is limited fatigue life due to very high alternating stresses at contact surfaces. Recent research reveals that taper roller bearings with hollow rollers have significant advantages over bearings with solid rollers such as reduced vibration, low-radial runout, better radial stiffness, higher operating speeds, lower operating temperatures which results in longer life as compared with traditional solid taper roller bearings. Under large normal loads, a taper roller bearing with hollow rollers deflect appreciably more than a taper roller bearing with solid rollers of the same size which results in improvement in load distribution and considerable reduction in contact stresses. For taper roller bearings with hollow rollers, exact analytical method is not available for the calculation of hollowness and contact stresses. Recently, the Finite Element Analysis (FEA) has been successfully used to evaluate contact problems for the taper roller bearings and comparing results with the analytical values. In present work, determination of optimum hollowness has been done by adopting FEA for hollow tapered roller bearing. From the FEA analysis, it is investigated that Von-Mises stress is lowest for the 42% hollowness. Experimental work is carried out to study frictional torque, vibration and temperature at different speed and loading conditions for optimum 42% hollow tapered roller bearing. Optimum hollow taper roller bearing improves lubrication and cooling, reduces maintenance and replacement costs with material savings, reduced frictional losses, energy savings and enhancement of system efficiency and sustainability as compared to conventional solid taper roller bearings.

## Keywords

Taper roller bearing, Finite Element Analysis, Optimum hollowness, Fatigue life, Von-Mises stress

## 1. Introduction

Advances in many fields including gas turbine design, aeronautics, space and atomic power, involve extreme operating speeds, load, temperatures, environments which increases power and load on machinery and demand high strength to weight ratio of the rolling element bearings. To meet these great expectations, researchers have been constantly exploring new bearing designs or refining existing ones for improving the performance or increasing the fatigue life of bearings. For heavy-duty load carrying requirements, roller bearings are generally preferable as compared to the ball bearing because of the larger rolling element contact area (Palmgren, 1959). The efficiency and reliability of machines having rotating parts are strongly dependent on the choice and design of bearings used, with a direct link on safety and environment concerns. The ever increasing cost of experimental work and the need to shorten the conception stage require the development of theoretical methods and simulation tools.

Many researchers have tried the geometrical change in the design of bearing and proved that new design with hollow rollers can satisfy the today's requirement. Hollow rollers have

advantages over the solid roller bearing like more contact area, good lubricant circulation, less contact stress, less weight, lighter weight and high rotational speeds than the solid rollers. (Harris and Aaronson, 1967; U.S. patent number 4232914, Bowen, 1980; Bowen and Bhateja, 1980; Bhateja and Hahn, 1980; Murthy and Rao, 1983; Zhao, 1998). Many researchers have found that hollow rollers have longer fatigue life than solid rollers (Somasundar and Krishnamurthy, 1984; Abu Jadayil and Flugrad, 2007). U.S. patent number 4232914 (Bowen, 1980). Researchers have carried out their studies to determined optimum hollowness for cylindrical roller in pure rolling contact bearings using Finite element analysis and proved that hollow roller bearings have longer fatigue life than solid roller bearings. (Abu Jadayil, 2008; Darji and Vakharia, 2008).

The tapered roller bearings are used for carrying heavy loads. After going through the open literature, it has been observed that design of cylindrical rolling element bearings have been significantly improved, in terms of their performance and working life. However, limited attention has been paid to improve the performance of taper roller bearing. If contact stresses can be reduced by determining optimum hollowness than the taper roller bearing with optimum hollowness may result in improved lubrication and cooling, reduces maintenance and replacement costs which ultimately leads towards enhancement of system efficiency and sustainability as compared to conventional solid taper roller bearings. Standard formula (method) to find the optimum hollowness for the given loading condition and dimensions of hollow taper roller bearing is not available in open literature. Calculation of exact contact pressure for the hollow roller requires a finite element approach.

In present work, determination of optimum hollowness has been done by adopting FEA for hollow tapered roller bearing to improve the performance over solid rolling element. Experimental work is carried out to study frictional torque, vibration and temperature at different speed and loading conditions for optimum hollow tapered roller bearing.

## 2. Theoretical Analysis

The contact stresses in hollow members are often calculated by using the same equations and procedures as for solid specimens. This approach seems to be incorrect. The Hertzian theory of contact is based on several assumptions. One is that the profiles of the two bodies are continuous and can be represented to good approximation by a polynomial of second degree. Hertzian theory does not take into account a situation where the cross sections of either or both of the bodies in contact are multiply connected.

For hollow rolling element bearing no method is available for the calculation of contact stresses and deformation. Stress and displacement distributions on roller, inner and outer rings are investigated using the finite element Analysis (Darmirhan and Kanber, 2008). With the help of FEA, deformation and contact stresses are determined. FEA is also used for determining the optimum value of hollowness of the roller for which the contact stress should be minimum so ultimately there is improvement in the fatigue life of the bearing, which is the main theme of present work.

In the present analysis, first of all the contact stress was found in the heavily loaded roller of solid tapered roller bearing using Hertz equation (Harris, 2001). The same Hertz equation cannot be applied to obtain the contact stresses in the case of hollow rollers due to some assumptions therein. So, Finite Element Analysis was carried out for heavily loaded solid rollers and results obtained were compared with the results obtained by Hertz equation for validation of FEA results. After validation, the FEA approach was adopted to determine the optimum hollowness in the tapered roller bearing.

### 2.1 Analytical study of Solid Tapered Roller Bearing:

Following are the specifications of tapered roller bearing under consideration
Bearing No: 32212 (Single raw taper roller bearing)

Internal diameter of bearing: 60 mm.
Outside diameter of bearing: 110 mm
Average outer diameter of inner ring ($d_2$): 76.09 mm
Average inner diameter of outer ring: 96.65 mm
Average roller diameter ($d_1$): 12.96 mm.
Length of roller ($l$): 19.96 mm
Number of rollers: 19
Applied load on bearing ($F_r$): 30000N
Modulus of elasticity: $2.058 \times 10^5$ N/mm$^2$
Poisson's ratio ($v$): 0.3

For the rigidly supported bearing subjected to radial load under static equilibrium the applied load must be equal to the sum of vertical components of the rolling element load (Harris, 2001). For single raw taper roller bearing no. 32212; $\alpha_o = 12.57^0$, $\alpha_i = 9.07^0$ and $\alpha_f = 79.18^0$
The applied external load $F_r$ considering radial integral and thrust integral is given by,

$$F_r = ZQ_{max}J_r(\in)cos\alpha_o$$

For zero diametral clearance, the value of $\in = 0.5$ and load distribution integral,

$$J_r(\in) = 0.2453.$$

Therefore,

$Q_{max} = 6595N$ and

$F_a = F_r tan\alpha_o = 6689.3N$

$\frac{F_a}{F_r} = \frac{6689.3}{6595} = 0.2297 < e$ (0.4 from SKF bearing catalogue)

Hence, we can take $p = F_r$ and $Q_{max} = F = 6595N$

The contact width and stresses are maximum at the roller-inner race contact. Considering the heavily loaded solid roller as body I and inner race as body II (both made from the same material having $v=0.3$), the value of half contact width can be calculated as;

$$b_i = \sqrt{\frac{4F(1-v^2)}{\pi lE\left(\frac{1}{d_1}+\frac{1}{d_2}\right)}} = 0.1435mm$$

The maximum contact pressure exerted between roller-inner raceway is given as;

$$p_{max} = \frac{2F}{\pi b_i l} = 1465.83 \text{ N/mm}^2$$

### 2.2 Finite Element Analysis of Solid Tapered Roller Bearing:

The first mathematical formulation of the contact problem of ideally smooth elastic solids was presented by Hertz in 1982. Since then, significant progress has been made in the field of contact mechanics. Existing finite element models like KE model (Kogut and Etsion, 2002) and JG Model (Jackson and Green, 2005) are studied and finite element analysis for the present case is carried out.

### 2.2.1 3D Modeling:

For present study, taper roller bearing 32212 is considered and 3D axis symmetric models for solid as well as hollow taper roller bearings were developed to form single asperity contact between outer surface of the half roller and top surface of inner race using the 3D modelling software CREO.

### 2.2.2 Finite Element Model:

For Finite element analysis, ANSYS software is used. The models prepared with CREO were imported to ANSYS for performing the FEA. SOLID 185 element was used for model discretization for both roller and inner/outer race. SOLID 185 is defined by 8 nodes having 3 degree of freedom at each node and it also has plasticity, hyper elasticity, creep and stress stiffening. The coefficient of friction at contacts is considered as 0.001 and 3D model is considered symmetric from the middle plane passing through the axis of the roller.

### 2.2.3 Contact Model:

In order to create contact model in ANSYS, a contact element and a target element must be used. CONTA174 and TARGET170 elements are used to create the contact element and the target elements respectively. The outer surface of the half roller and the top surface of the inner race are selected for the contact and target element respectively. The contact model is shown in Fig. 1.
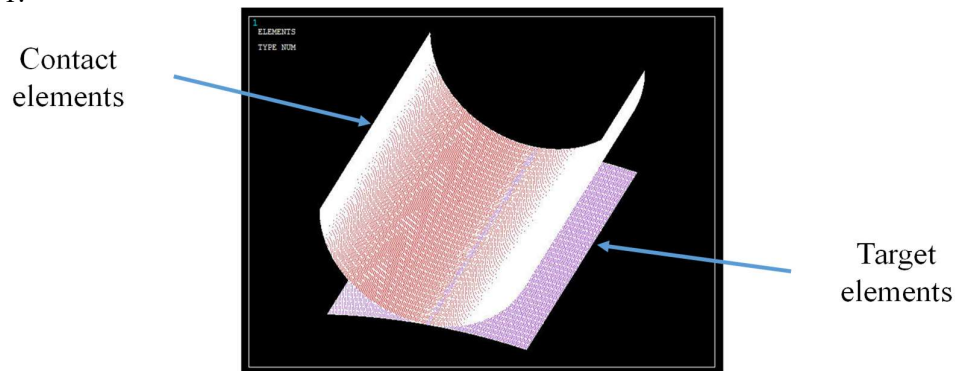


Fig. 1 Contact Model for the contact between roller and inner race

### 2.2.4 Loading and boundary conditions:

A uniform pressure which is calculated from $Q_{max}$ value and actual area is applied on top surface of the half solid roller which is at "0" position. All degrees of freedom of the nodes on the bottom surface of the inner race are restricted. The applied load is considered as a static load carrying capacity of the bearing (Abu-Jadavil et al.,2006, Prashad, 2003) and the load distribution is calculated (Dermirhan et al 2008). Solution for all models have been carried out as a 3D static analysis using the Newton Raphson method because of its fastest convergence solution.

### 2.2.5 Mesh Convergence:

In order to investigate the convergence of the solution, all models have been solved with increasing number of elements. The contact pressure values are noted for different meshing and converged values are considered for all solid as well as hollow rolling element bearings.

### 2.2.6 Validation of Finite Element adopted:

For hollow roller element, no method is available for the calculation of contact pressure and deformation like the solid rolling element bearing. In present work, contact pressure at roller and inner race contact obtained by finite element analysis is compared with analytically calculated value of contact pressure and found to be in good agreement. After validation, finite element analysis is extensively carried out for hollow roller element bearing with different hollowness ranging from 10% to 90% to obtain the contact pressure at heavily loaded roller.

**3. Experimental Performance Analysis of Hollow Tapered Roller Bearing with optimum hollowness:**

From the finite element analysis, the optimum hollowness was determined as 42%. The hollow rollers as shown in Fig. 2(a) are manufactured on EDM machine using spark erosion method.



(a)                                                          (b)
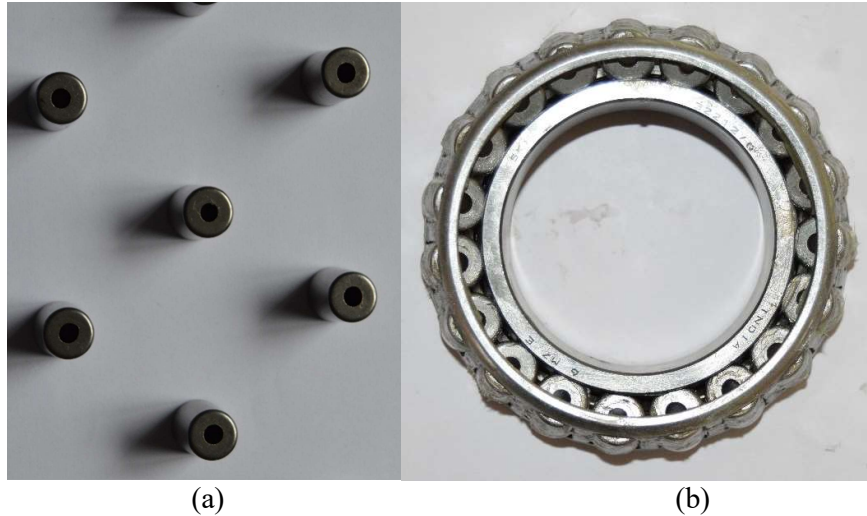
Fig. 2 (a) 42% hollow rollers (b) Bearing with 42% hollowness

For the experimental validation of the results carried out by the FE Analysis, the hollow tapered roller bearing with 42% optimum hollowness of all the rollers is developed and then experimentally tested for the dynamic loading condition based on the fatigue life. For this analysis and tests, the custom made endurance test rig as shown in Fig. 3 has been developed.



Fig. 3 Endurance test rig

Two test bearings, solid taper roller bearing and hollow taper roller bearing with 42% roller hollowness of bearing number 32212 are mounted on the shaft of the test rig. The experimentation is carried out for different load and speed conditions till the steady state condition reaches. The radial load is applied to each bearing through pneumatic bellow mounted below the housing gives exact load on each bearings. Through WINDUCOM software, the speed and load are initially being fixed before starting of each run.

The test was started with no load and 500 rpm till 10kN load and 1000 rpm. All the critical performance parameters i.e. temperature of both solid and hollow tapered roller bearings, frictional torque and vibration are continuously measured and displayed in the form of graphs on the screen. At the end of each run, the graph and readings are being stored and saved.

## 4. Results and Discussion

Finite Element Analysis has been carried out in details and results for different percentage hollowness has been given in the Table 1.

Table 1 FEA results for different percentage of hollowness

| % Hollowness | Max Deflection (mm) | Max Von mises stress (MPa) | Maximum Contact Pressure (MPa) |
|---|---|---|---|
| 0 | 0.010855 | 869.85 | 1513.13 |
| 10 | 0.011066 | 803.29 | 1179.60 |
| 20 | 0.012187 | 666.94 | 643.12 |
| 30 | 0.015202 | 834.74 | 1355.51 |
| 40 | 0.017833 | 696.82 | 957.43 |
| **42** | **0.019910** | **657.25** | **804.70** |
| 44 | 0.025683 | 704.54 | 1023.24 |
| 46 | 0.031567 | 788.00 | 1383.69 |
| 48 | 0.038429 | 859.45 | 1523.12 |
| 50 | 0.045539 | 939.30 | 1750.43 |
| 60 | 0.058190 | 730.84 | 1369.54 |
| 70 | 0.142051 | 1313.69 | 961.01 |
| 80 | 0.518408 | 2974.09 | 1531.58 |

It is seen from Table 1 results that the total deformation found to be more in case of hollow rollers as compared to the solid rollers and increases with the increase in percentage hollowness. It is also evident from simulation results that the contact pressure as well as Von Mises stresses decrease due to increase in percentage hollowness. At 42% hollowness, both contact pressure as well as maximum Von Mises stresses are at minimum after which again both rises with further increase in percentage hollowness. Hence, based on FE simulation results, 42% hollowness is considered as optimum hollowness at which both contact stresses as well as maximum Von Mises stresses are minimum.

Experimental performance analysis of Hollow Tapered Roller Bearing with optimum 42% hollowness is carried out on custom made endurance test rig. Fig. 4 to 7 show the graphs of temperature distribution for solid as well as hollow roller bearings for different speed and loading ranging from 5 to 10 kN and 500 to 1000rpm.
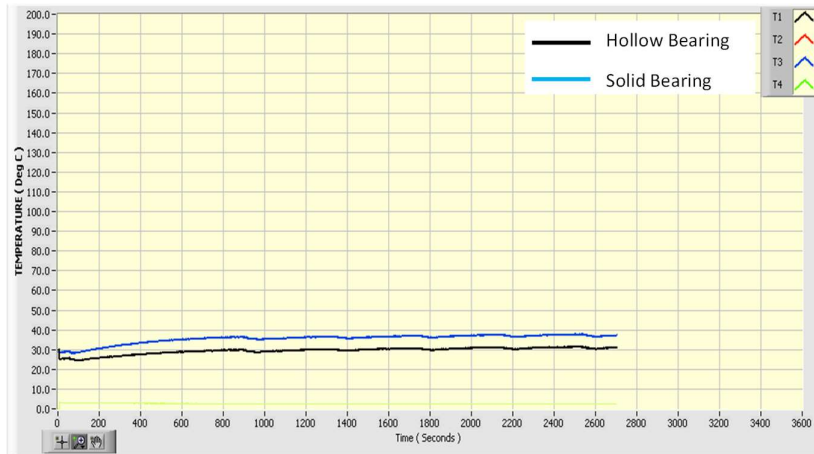
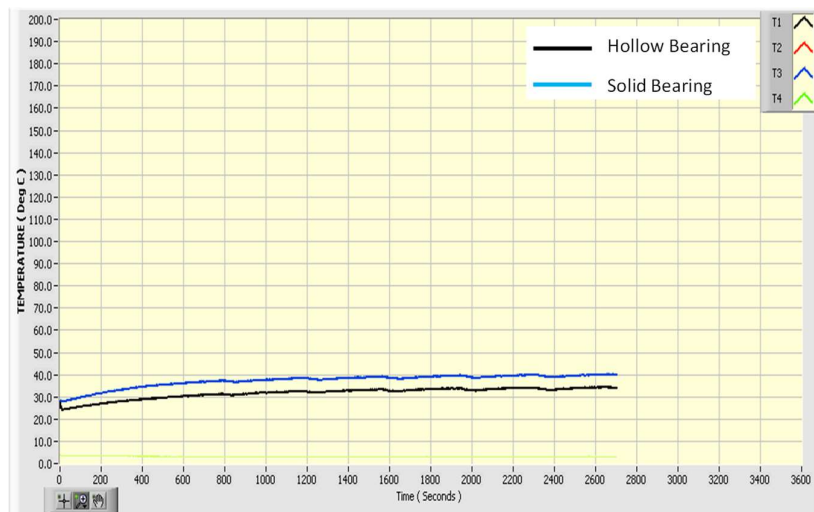Fig. 4 Temperature distribution at 500rpm and 5kN applied load



Fig. 5 Temperature distribution at 500rpm and 10kN applied load
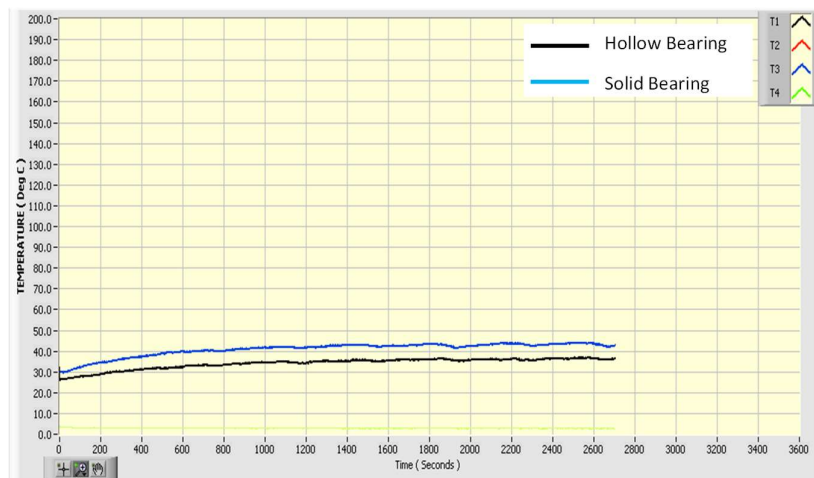


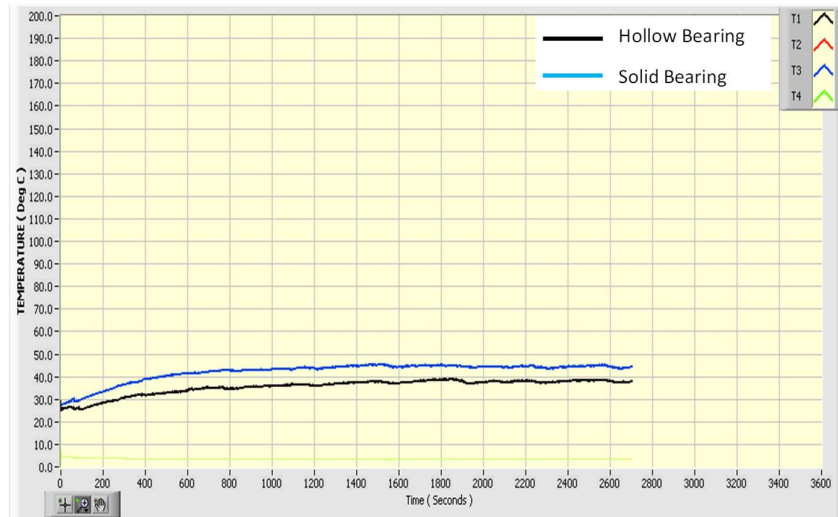Fig. 6 Temperature distribution at 1000rpm and 5kN applied load

Fig. 7 Temperature distribution at 1000rpm and 10kN applied load

From the above experimental results, it can be observed that the bearing temperature of both the bearings at the starting of experimentation is same but as we run the test, the temperature of hollow tapered roller bearing decreases than that of solid tapered roller bearing. The range of temperature rise during the entire run of solid tapered roller bearing for different speed and load conditions is from $25^0$C to $45^0$C. And the range for hollow tapered roller bearing is from $25^0$C to $38^0$C. Hence it is concluded that the total percentage fall in the temperature of hollow tapered roller bearing compared with the solid tapered roller bearing is 16% which is because of the oil circulation from the inside of the hollow roller of the bearing gives more heat transfer rate.

Fig. 8 to 10 shows the graphs of frictional for solid as well as hollow roller bearings for different speed and loading ranging from 5 to 10 kN and 500 to 1000rpm.



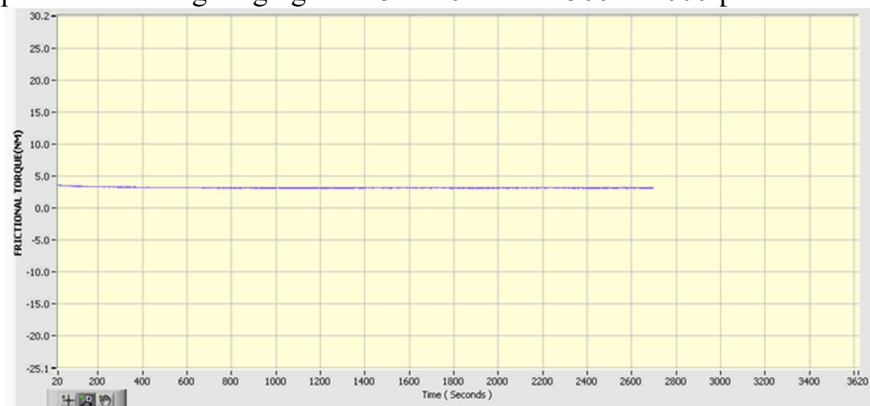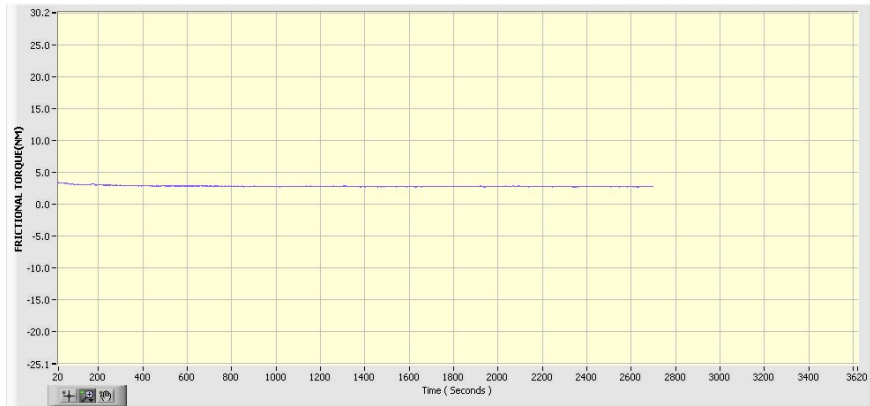Fig. 8 Friction torque at 500rpm and 10kN applied load

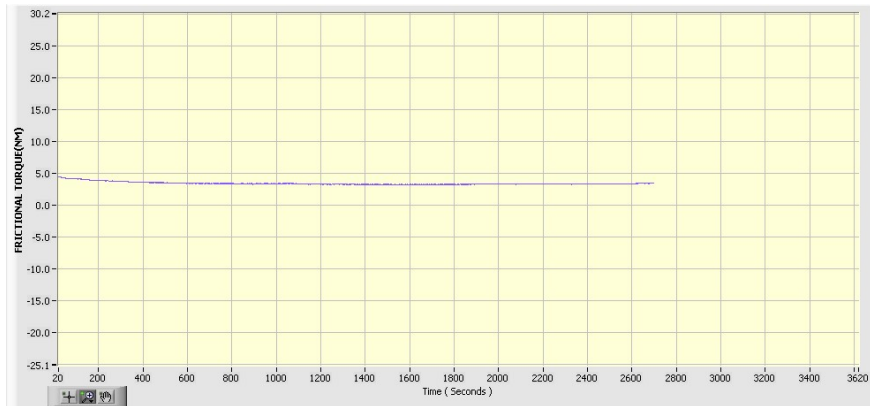Fig. 9 Friction torque at 1000rpm and 5kN applied load


Fig. 10 Friction torque at 1000 rpm and 10kN applied load

Results show that there is no deterioration in the performance due to hollow bearings.

Fig. 11 to 13 shows the graphs of vibration in hollow roller bearings for different speed and loading.
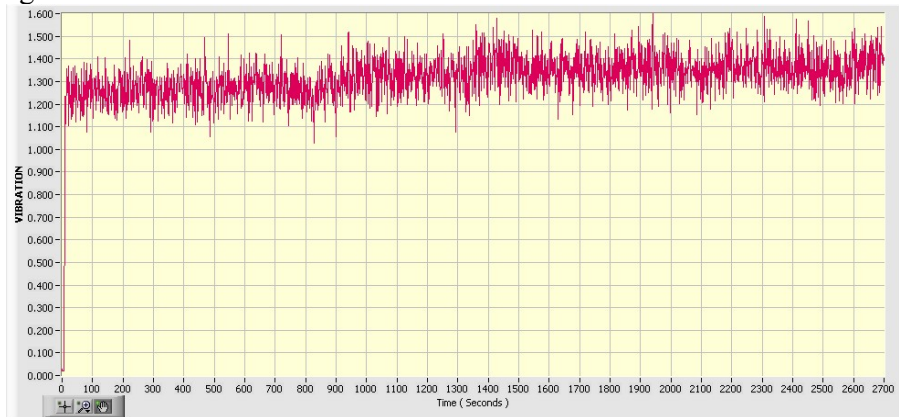

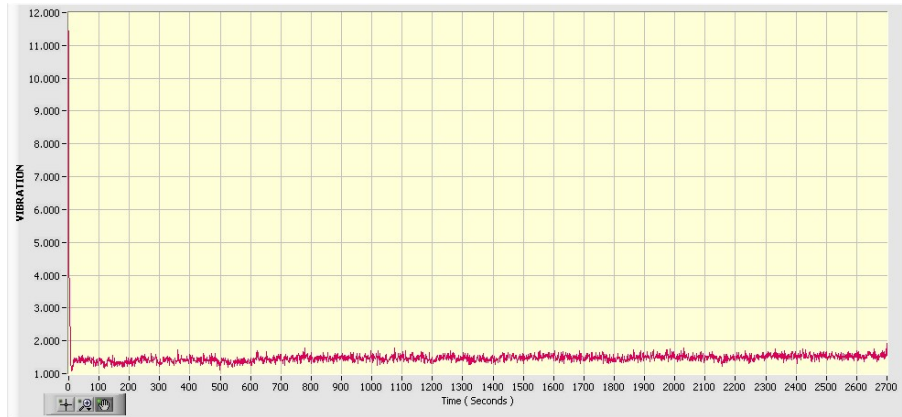Fig. 11 Vibration at 500 rpm and 5kN applied load

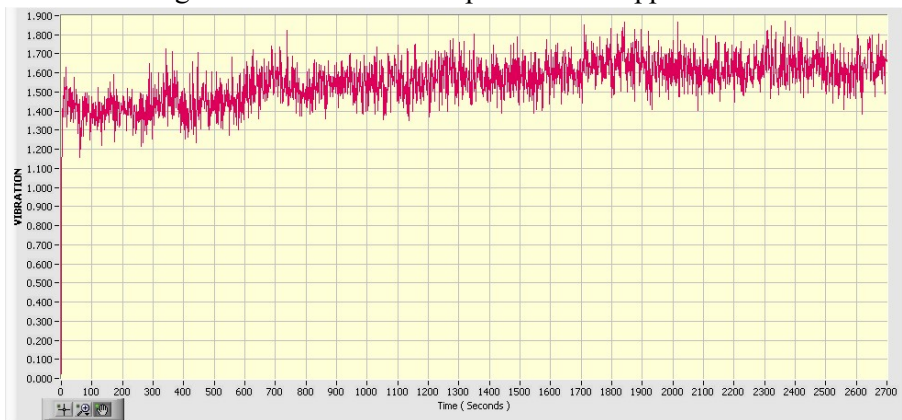Fig. 12 vibration at 1000 rpm and 5kN applied load



Fig. 13 vibration at 1000 rpm and 10kN applied load

From the above graphs of vibration level for different speed and load conditions, the range of vibration level is from 1*g* to 1.8*g*. Hence, it can be concluded that there is no measurable rise in vibration level during all the operating conditions.

## 5. Conclusions

The temperature distribution results suggest that for both solid and hollow bearing the rise in temperature is almost uniformly equal that too within the working limit. Further, profiles for frictional torque and vibration indicate that there appears no deterioration in the machine performance due to hollow bearing. In the case of hollow bearing contact area are appear expanded decreasing the contact stress substantially ultimately leading to the decrease in wear which increases the fatigue life.

In comparison with solid rolling element bearings, optimum hollow taper roller bearing results in material savings, improved lubrication and cooling, reduced losses due to friction, energy saving due to reduction in losses, reduces maintenance and replacement costs which ultimately leads towards enhancement of system efficiency and sustainability as compared to conventional solid taper roller bearings.

## 6. Nomenclature
$b$      Semi width of solid contact surfaces, mm
$b_o$      Semi width of solid contact surfaces between outer race & roller, mm
$E_1$      Modulus of elasticity of roller, N/mm$^2$
$E_2$      Modulus of elasticity of race, N/mm$^2$
$e$      Eccentricity of loading, mm

| | |
|---|---|
| $F_r$ | Radial load on bearing, N |
| $F_a$ | Axial load on bearing, N |
| $F$ | Applied load, N |
| $J_r$ | Radial load integral |
| $Q_{max}$ | Maximum, rolling contact load, N |
| $p_d$ | Diametral clearance, mm |
| Z | Number of rollers |
| $l$ | Length of the roller, mm |
| $p_{max}$ | Maximum contact pressure between roller & race, N/mm$^2$ |
| $\alpha_o$ | Contact angle between outer race and roller |
| $\alpha_i$ | Contact angle between inner race and roller |
| $\alpha_f$ | Contact angle of guide flange |
| $\epsilon$ | Load distribution factor |
| $\delta_r$ | Radial contact deflection, mm |
| $v_1$ | Poisson's ratio for roller |
| $v_2$ | Poisson's ratio for race |
| $g$ | gravitational constant, m/s$^2$ |

**References**

1. Abu-Jadavil, W.M., Flugrad, D.R. and Qamhiyah, A.Z. 2006. Fatigue life prediction of optimum hollowness of hollow cylindrical rollers in pure rolling contact, Proceedings of ASME 8th Biennial Conference on Engineering Systems Design and Analysis, Torino, 4-7 July, Paper No. ESDA2006-95036.
2. Abu Jadayil, W.M. and Flugrad, D.R., 2007. Fatigue life investigation of solid and hollow rollers under pure normal loading, Tribotest, Vol. 13(4), pp. 165-185.
3. Abu Jadayil, W.M., 2008. Relative fatigue life estimation of cylindrical hollow rollers in general pure rolling contact, Tribotest, Vol. 14, pp. 27-42.
4. Bhateja, C.P. and Hahn, R.S., 1980. A hollow roller bearing for use in precision machine tools, CIRP Annals Man Techno, Vol. 29 (1), pp. 303-307.
5. Bowen, W.L. and Bhateja, C.P., 1980. The Hollow Roller Bearing. ASME Trans., 102, pp. 222-227.
6. Bowen W.L., 1980. Hollow Tapered Roller Bearing, United States Patent, III, No. 4232914.
7. Darji, P.H. and Vakharia, D.P., 2008. Determination of optimum hollowness for hollow cylindrical rolling element bearing, ASME International Mechanical Engineering Congress and Exposition, USA.
8. Demirhan, N. and Kanber, B., 2008. Stress and Displacement Distributions of Cylindrical Roller Bearing Rings Using FEM, Mechanics Based Design of Structures and Machines, Vol. 36, pp. 86-102.
9. Demrihan, E., Trijiskens, E. and Romon, H. 2008. Stress and displacement distributions of cylindrical roller bearings rings using FEM, Mechanics Based Design of Structures and Machines, Vol. 36 (1), pp. 86-102.
10. Ducom Instruments Pvt. Ltd., Instruction Manual
11. Harris, T.A. and Aaronson, S.F., 1967. An Analytical Investigation of Cylindrical Roller Bearings Having Annular Rollers. Tribol. Trans., 10, pp. 235-242.
12. Harris, T.A., 2001. Rolling bearing analysis, Fourth ed., John Wiley & Sons, New York.
13. Jackson, R. L. and Green, I. 2005. A Finite Element Study of Elasto-Plastic Hemispherical Contact Against a Rigid Flat. Tran. ASME, J. Tribol, Vol.127, pp. 343-354
14. Kogut, L. and Etsion, I. 2002. Elastic-Plastic Contact Analysis of a Sphere and a Rigid Flat, Tran. ASME, J. Tribol, Vol. 69, pp. 657–662.

15. Murthy, C.S.C. and Rao, A.R., 1983. Mechanics and behaviour of hollow cylindrical members in rolling contact, Wear, Vol. 87, pp. 287-296.

16. Palmgren, A. (1959), Ball and Roller Bearing Engineering, SKF Industries, Philadelphia, 1.

17. Prashad, H. 2003. Determination of stiffness of roller bearings- an alternative approach, J. Inst. Eng. (India) Mech, Vol. 84(4), pp. 186-192.

18. SKF Bearing Catalogue, 1989.

19. Somasundar, H.V. and Krishnamurthy, R., 1984. Surface durability of tufftrided rolling elements, Wear, Vol. 97 (2), pp. 117-127.

20. Zhao, H. (1998) Analysis of load distributions within solid and hollow roller bearings, Transactions of the ASME, Vol. 120, pp. 134-140.

# Gasification of High Calorific Content in MSW

*Endrick Contractor[1*], Harsh Patel[2] , Shina Gautam[3], Alok Gautam[3]*

[1]Chemical Engineering Department, G.H.Patel College of Engineering & Technology, Vallabh Vidyanagar, Gujarat, India 388120
[2]BEIL Infrastructure Limited, Ankleshwar, Gujarat, India 393001
[3]Chemical Engineering Department, Shroff S.R.Rotary Institute of Chemical Technology, Ankleshwar, Gujarat, India 393001

## Abstract:

Due to the heterogeneity of municipal solid waste (MSW), it becomes challenging to use this waste for thermochemical treatment. As per previous studies, systematic segregation of high calorific contents in MSW and sampling techniques may overcome this challenge converting this waste into one of the renewable energy sources. Gasification is one of the thermochemical conversion technique for an alternative fuel from biomass and other solid wastes. In this investigation, the MSW is gasified at different temperatures, airflow to identify the behaviour of Syngas characteristic. Experiments have been performed in a laboratory-scale gasifier. The composition of the Syngas has been identified. The theoretical predictions of the amount of Syngas and composition have been identified with CHEMCAD software. It has been found that gasification temperature was the influencing parameter on syngas production and it's heating value. Experimental results are found to be in good agreement with the simulation results.

**Key words:** Gasification, MSW, Gasifier, Syngas

## Introduction:

Municipal solid wastes broadly divided into numerous items like metals, paper, textiles, plastics, wood and food garbage which consist of carbon, hydrogen, nitrogen and oxygen elements at a proportion of approximately 58.16%, 9.80%, 0.73%, and 31.31%, respectively[f]. Municipal solid waste (MSW) is considered a heterogeneous resource amid all the other wastes. Notwithstanding, segregation of MSW into several waste categories can proliferate the waste streams' homogeneity. It also permits optimization of waste reusing, recycling, appropriate treatment and lucrative yields the greatest benevolent outcomes depending on feasible treatment options for every category[d].
To deal with abovesaid problems, gasification is the process which imitates as a major troubleshooter and it is simply defined as a process of transforming organic compounds into a combination of gaseous product that is dominated by carbon dioxide ($CO_2$), carbon monoxide (CO), hydrogen ($H_2$), and methane ($CH_4$). This process uses limited amounts of air or oxygen [d]. The main objective is to convert into gaseous fuels which can be easily consolidated with existing energy production technologies[c]. The gasification is a propitious procedure with its high efficacy, the accessibility of manifold solid fuels and to produce at various capacities which are considered to be low concentrations of hazardous emissions[e]. The deciding parameters for the good quality of the syngas are feedstock, operating conditions of the gasifier, design parameters,

---

[1] Corresponding author: Endrick Contractor
edcphd@gmail.com , (+91) 95747 68731

and the gasifier agent. The gasification agent to be used in the process may differ depending on the desired syngas composition, quality, and operation cost[g].

The prime objective of this research study is to evaluate the gasification characteristics of MSW using the CHEMCAD process simulator. In this work, the effect of various temperature range and equivalence ratio on the syngas composition and also identify the feasibility of the process for better conversion of syngas.

## Materials and Methods:

## Feed characterization

Feed was received from the two different locations BEIL Ahmedabad and BEIL Ankleshwar and it was a mixed solid waste which consists of paper waste, Cotton waste and Sawdust. The particle size range between 1-50 mm. The pre-treatment was catered to this waste like drying, cutting and shredding to make it feasible for the actual gasification process.

MSW samples were marked to estimate their energetic potential. Table 1 shows the proximate and ultimate analysis of mixed solid waste. The results elucidated that MSW showcases high positive capability for energetic valorization because it has a low content of water (10.26%), high volatile content (50.4%) and high calorific value (9.81 MJ/kg). Moreover, It is a clear form that carbon and oxygen are the major components having 49.2% and 43% respectively. The sulphur is the minor component of this mixed solid waste (0.02%).

The feed characteristic analysis is shown below for the mixed solid waste material used for the experiment.

| Sr. No | Parameters | Results(%) |
|--------|------------|------------|
| 1 | Moisture Content | 10.26 |
| 2 | Ash Content | 32.84 |
| 3 | Volatile Matter | 50.4 |
| 4 | Fixed carbon | 6.5 |

| Sr. No | Parameters | Results(%) |
|--------|------------|------------|
| 1 | Hydrogen | 4.69 |
| 2 | Nitrogen | 0.18 |
| 3 | Sulphur | 0.02 |
| 4 | Oxygen | 43 |
| 5 | Carbon | 49.2 |

Table 1 Proximate and ultimate analysis

## Process Simulation of Gasification using CHEMCAD software:

The process simulation on gasification of mixed solid waste was done using the CHEMCAD software. The element composition of waste is shown below.

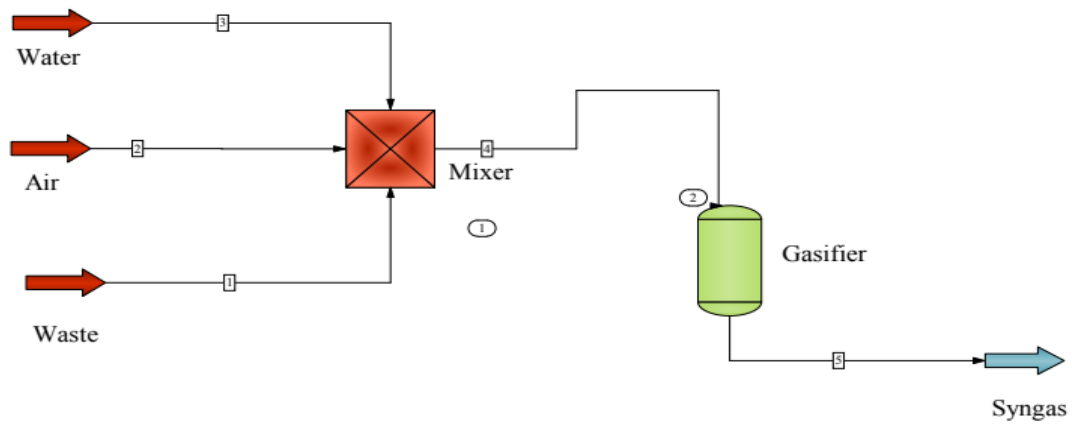| Element Composition (gm) | Carbon | Hydrogen | Oxygen | Nitrogen | Sulphur | Ash | Total |
|--------------------------|--------|----------|--------|----------|---------|-----|-------|
| | 49.2 | 4.69 | 43 | 0.18 | 0.02 | 2.9 | **99.99** |

Table 2  Element Composition of Mixed Solid Waste

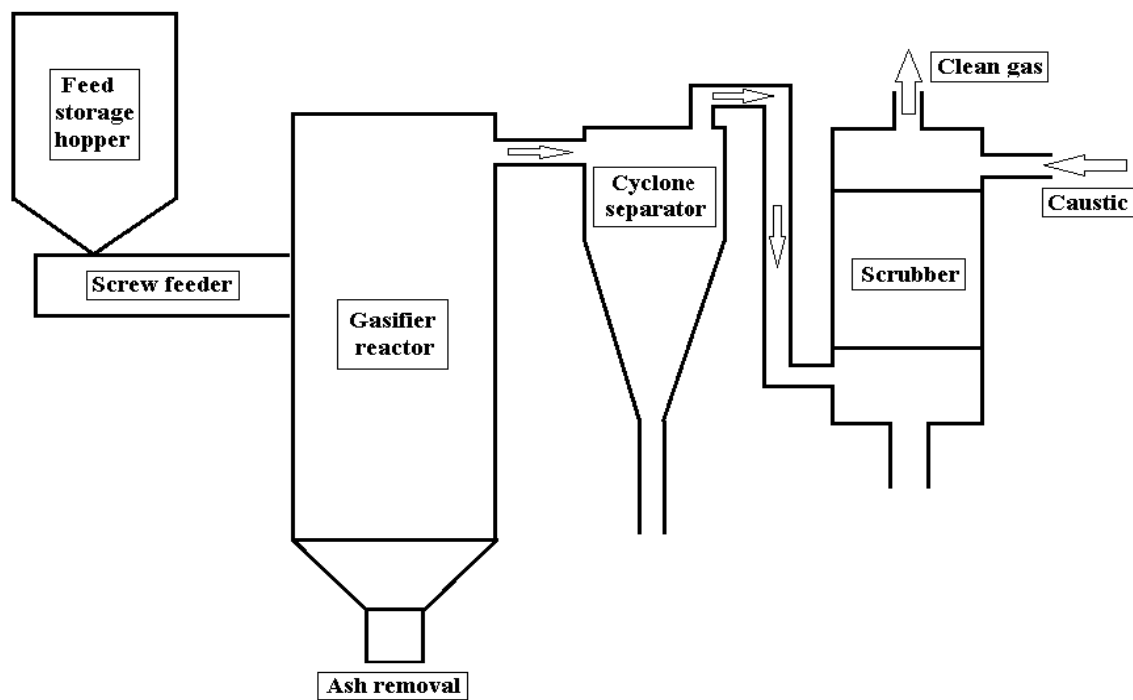Figure 1 Process flow diagram used for the Gasification of MSW using CHEMCAD.



Figure 2 Experimental setup

## Experimental procedure:

The Fixed bed air gasifier is used for the experiment and Firstly, Mixed solid waste material is stored in the hopper. The raw material is sent to the gasifier using screw conveyor and feed rate is controlled by the control unit as 10 kg/h. Here, Supply the gasification agent (air) with the electric burner into the reactor from the bottom of the reactor. Afterwards, Set the desired temperature of burner using control unit of the reactor between the ranges of 600-800 $^0$C and the ash which is generated from fixed bed gasifier is collected at bottom of the reactor. The output gas is sent to the gas cleaning equipment which is cyclone separator. For more purification purpose, the gas goes to a scrubber for scrubbing using caustic and the pure gas collected at the top of scrubber. The concentration of methane, carbon monoxide, carbon dioxide and hydrogen produced from the gasification process of mixed solid waste is measured.

## Result and Discussion:

## Simulated Results:

**Effect of Equivalence ratio:**Temperature = 1200 F & Water = 5 kg/hr & Waste = 10 kg/hr

| ER | 0.4 | 0.35 | 0.3 | 0.25 | 0.2 | 0.15 | 0.1 | 0.05 |
|---|---|---|---|---|---|---|---|---|
| Carbon | 0 | 0 | 0 | 0 | 0 | 0 | 0.28261 | 0.605394 |
| Methane | 0.054355 | 0.086195 | 0.132521 | 0.197642 | 0.285956 | 0.401505 | 0.447388 | 0.48554 |
| Carbon Monoxide | 4.60669 | 5.019414 | 5.408217 | 5.760463 | 6.062961 | 6.303218 | 5.877274 | 5.352942 |
| Carbon Dioxide | 10.64316 | 9.907333 | 9.169353 | 8.437252 | 7.719693 | 7.025215 | 6.533077 | 6.069535 |
| Hydrogen | 0.586225 | 0.61973 | 0.647677 | 0.668807 | 0.681862 | 0.685707 | 0.677651 | 0.667076 |

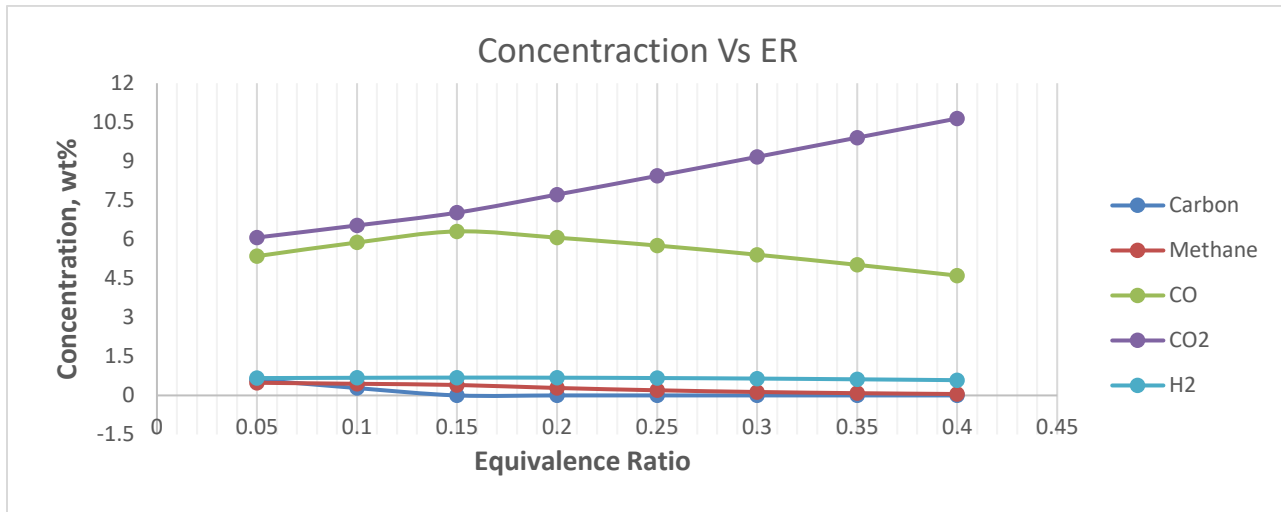Table 3 Effect of equivalence ratio on produce gases at T = 1200 F and water/waste = 0.5



Figure 3 Graphical presentation of the effect of ER to produce gases at T = 1200 F and

Water/waste = 0.5

**Effect of Temperature:** Equivalence ratio = 0.15 & Water = 5 kg/hr & Waste = 10 kg/hr

| Temperature (F) | 1300 | 1200 | 1100 | 1000 | 900 | 800 | 700 | 600 | 500 |
|---|---|---|---|---|---|---|---|---|---|
| **Carbon** | 0 | 0 | 0.756065 | 1.247499 | 1.506911 | 1.506911 | 1.768571 | 1.913292 | 2.107746 |
| **Methane** | 0.106705 | 0.401505 | 0.60314 | 0.820192 | 1.033521 | 1.033521 | 1.295442 | 1.301122 | 1.225122 |
| **Carbon Monoxide** | 7.451749 | 6.303218 | 3.285508 | 1.440991 | 0.544018 | 0.544018 | 0.04648 | 0.009707 | 0.001474 |
| **Carbon Dioxide** | 6.029325 | 7.025215 | 8.44325 | 8.94529 | 8.818894 | 8.818894 | 7.923366 | 7.435285 | 6.944201 |
| **Hydrogen** | 0.751217 | 0.685707 | 0.547761 | 0.406462 | 0.27672 | 0.27672 | 0.093057 | 0.04431 | 0.01783 |

Table 4 Effect of temperature on produce gases at ER = 0.15 and water/waste = 0.5
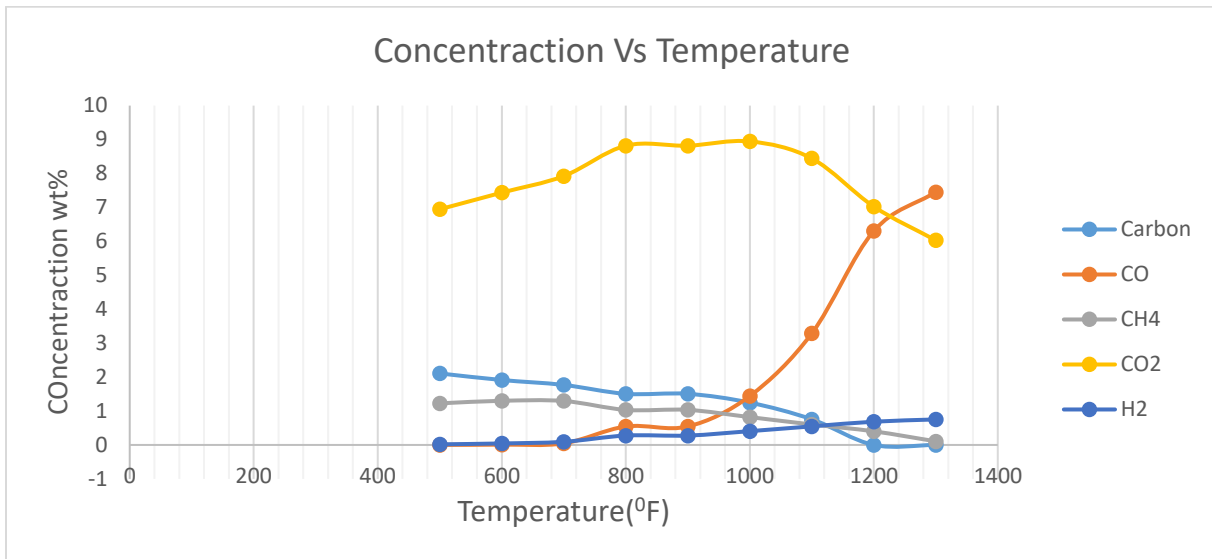


Figure 4 Graphical presentation on effect of temperature to gases at ER = 0.15 and water/waste = 0.5

**Effect of water to waste ratio:** Equivalence ratio = 0.15 & Temperature = 1200 F & Waste = 10 kg/hr

| water/waste | 0.5 | 0.6 | 0.7 | 0.8 | 0.9 | 1 |
|---|---|---|---|---|---|---|
| **Carbon** | 0 | 0 | 0 | 0 | 0 | 0 |
| **Methane** | 0.401505 | 0.337247 | 0.283163 | 0.237905 | 0.200185 | 0.168826 |
| **Carbon Monoxide** | 6.303218 | 5.92453 | 5.57922 | 5.262923 | 4.972455 | 4.705317 |
| **Carbon Dioxide** | 7.025214 | 7.796494 | 8.48742 | 9.108549 | 9.668414 | 10.17417 |
| **Hydrogen** | 0.685707 | 0.745256 | 0.79729 | 0.8428 | 0.882662 | 0.917648 |

Table 5 Effect water/ waste ration on produce gases at ER = 0.15 and T = 1200 F

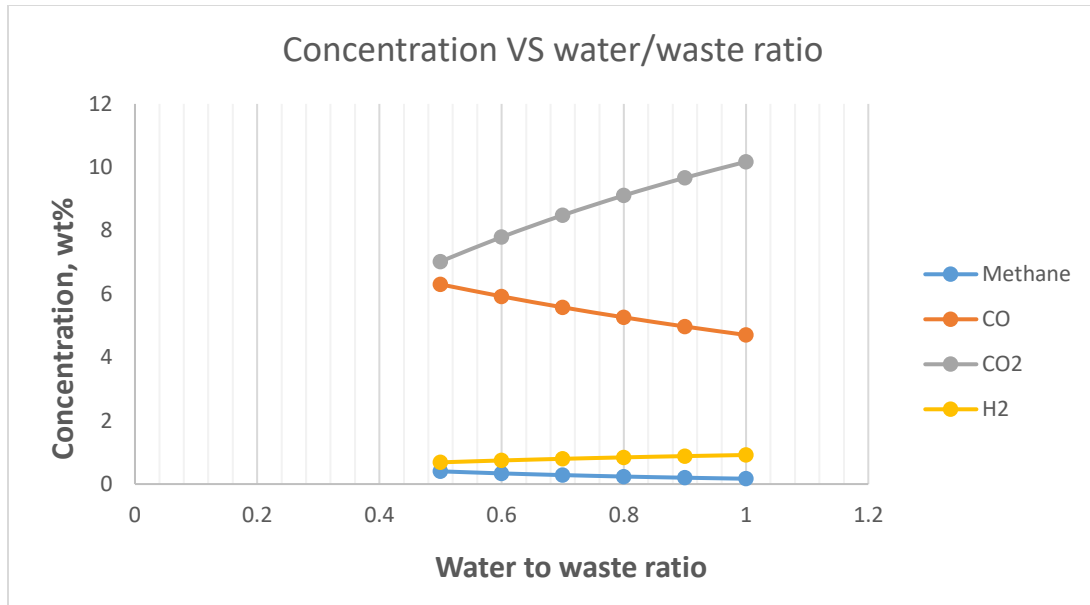Figure 5: Graphical presentation on water/waste ratio effect on produce gases at ER = 0.15 and T = 1200 F

**Experimental Results**:

Set 1: Feed rate = 10 kg/hr &

Equivalence ratio = 0.1

| Temperature (ºC) | 600 | 650 | 700 |
|---|---|---|---|
| Methane (%) | 1.025 | 1.018 | 1.099 |
| Carbon monoxide (%) | 2.896 | 2.912 | 3.003 |
| Carbon dioxide (%) | 3.006 | 3.012 | 3.051 |
| Hydrogen (%) | 1.289 | 1.315 | 1.316 |

**Set-2:** Feed rate = 10 kg/hr &

Equivalence ratio = 0.2

| Temperature (ºC) | 600 | 650 | 700 |
|---|---|---|---|
| Methane (%) | 1.025 | 1.022 | 1.095 |
| Carbon monoxide (%) | 3.020 | 3.150 | 3.155 |
| Carbon dioxide (%) | 3.225 | 3.250 | 3.242 |
| Hydrogen (%) | 1.290 | 1.316 | 1.318 |

Set-3: Feed rate = 10 kg/hr &

Equivalence ratio = 0.3

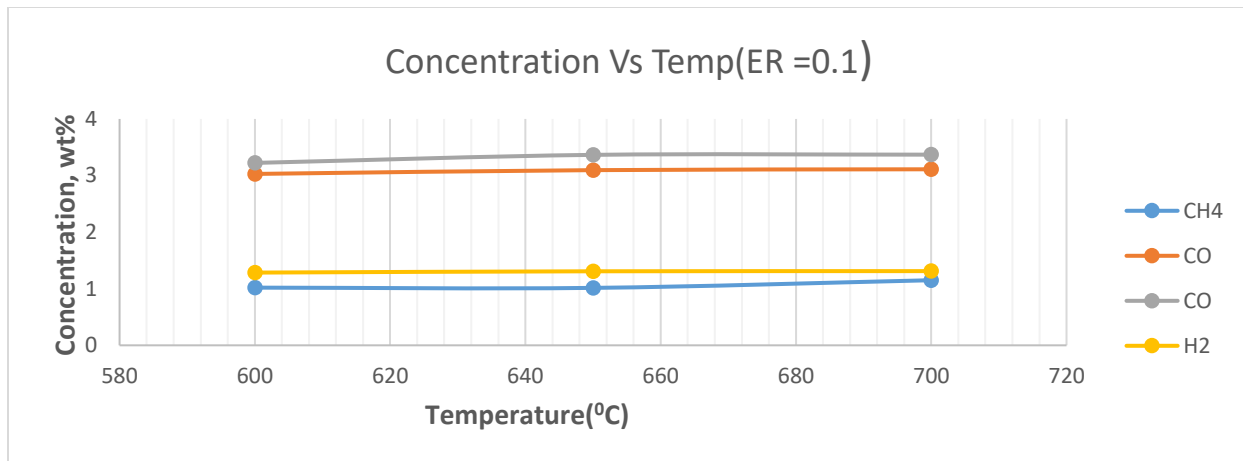| Temperature (ºC) | 600 | 650 | 700 |
|---|---|---|---|
| Methane (%) | 1.019 | 1.015 | 1.15 |
| Carbon monoxide (%) | 3.028 | 3.095 | 3.110 |
| Carbon dioxide (%) | 3.223 | 3.365 | 3.369 |
| Hydrogen (%) | 1.285 | 1.308 | 1.311 |

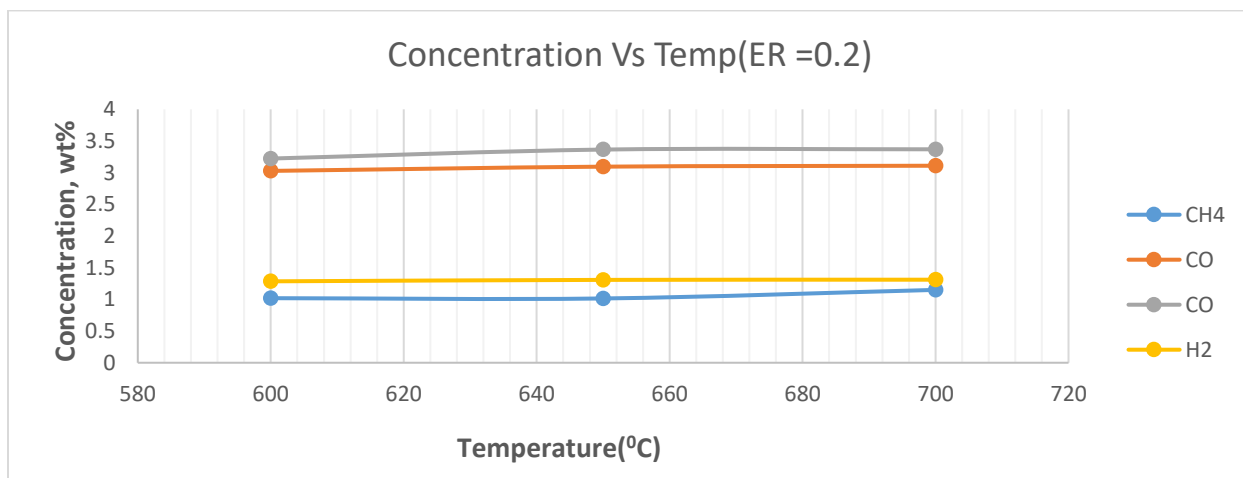Figure 6 Effect of temperature on syngas concentration at ER = 0.1



Figure 7 Effect of temperature on syngas concentration at ER = 0.2
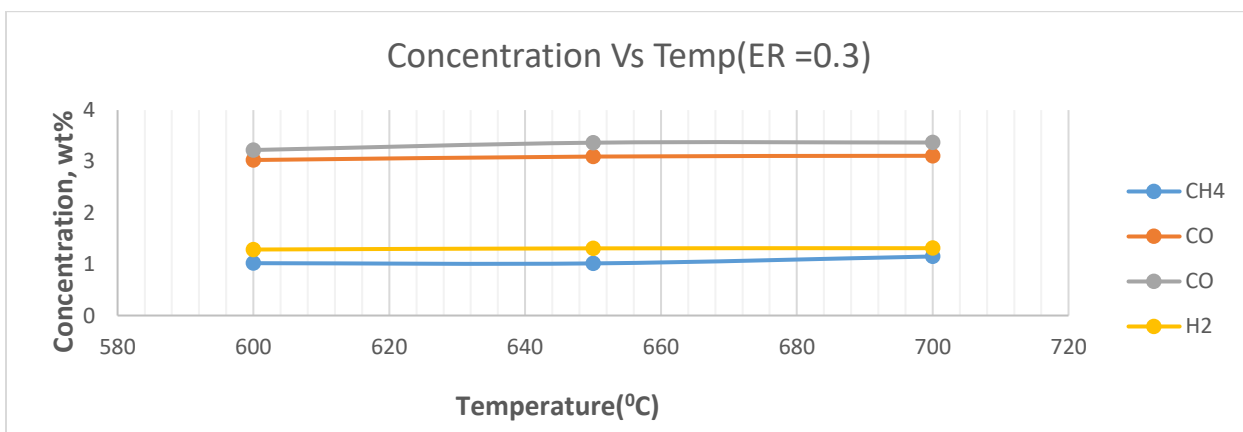


Figure 8 Effect of temperature on syngas concentration at ER = 0.3

## Effect of temperature

Temperature is considered one of the most affecting criteria in the gasification process. It has significant potential to alter the syngas composition and its calorific value. In this regards, to measure the effect of temperature on the syngas production, experiments were carried out with air at 600, 650 and 700 ℃. Also, then after doing the comparison of this data with the simulated data of syngas production. Figure 9 describes this effect on syngas production at ER 0.15 and 0.2 and It has identified that the vital concentration difference in syngas production in both cases.

It was found that in simulated data the concentration of carbon dioxide is decreased rapidly from 8.44%, 7.03% and 6.03% with temperature 593, 649 and 7040C. But in the experiment the concentration of carbon dioxide got higher than simulated data was 3.225%, 3.250% and 3.242% with temperature 600, 650 and 700 $^0$C, and also found that concentration of carbon dioxide in the experiment was an increase at 650 $^0$C and slightly decrease after 650 $^0$C.



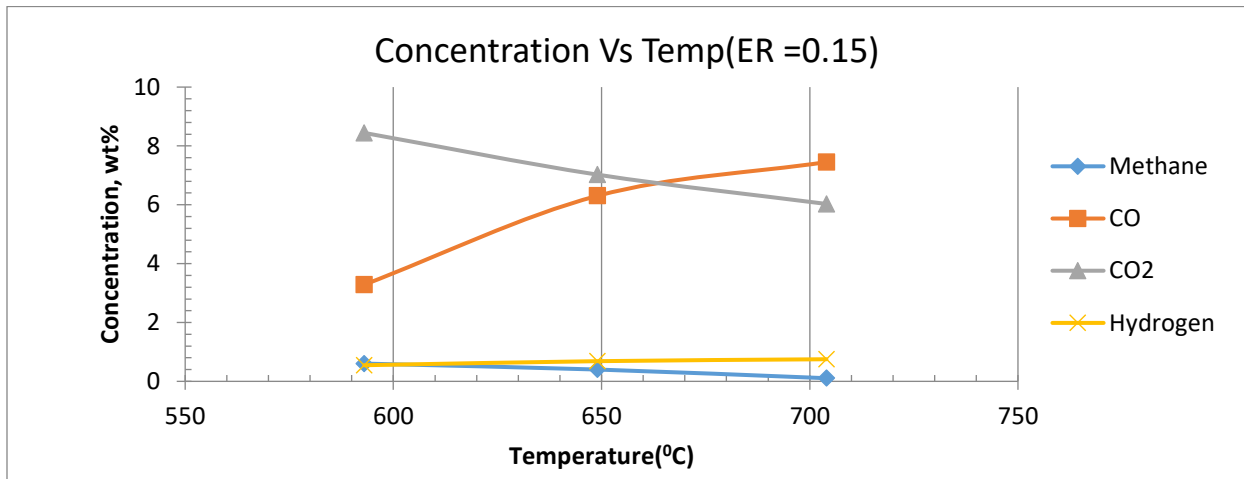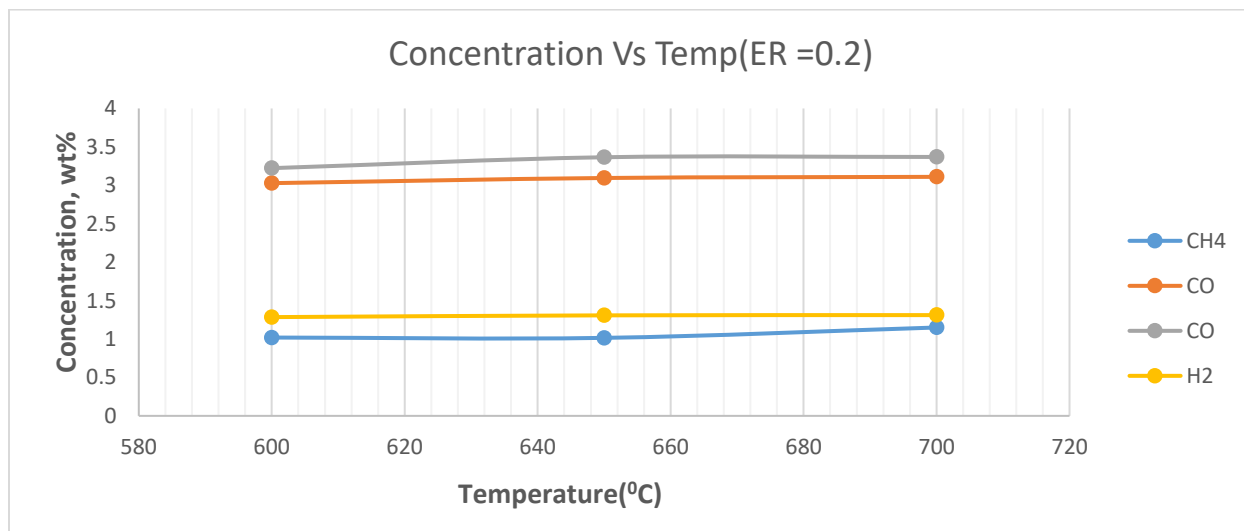Figure 9.1 Simulated data of syngas concentration on the different temperature at ER = 0.15



Figure 9.2Experimental data of syngas concentration on the different temperature at ER = 0.2

Figure 9: Comparison of the effect of temperature on syngas concentration at experimental and simulated data

For carbon monoxide concentration was increased with temperature in both cases. In simulated data, it increases rapidly with temperature to 3.29%, 6.3% and 7.45% and in experimental data, it shows the value increased slowly 3.020%, 3.150% and 3.155% as compared to simulated data.

In the case of methane and hydrogen for both cases, it shows the same behaviour. The concentration of methane decreased in both cases simulation and experimental data. It was found that the value decreased in simulated data to 0.60%, 0.40%, 0.11% and in experimental data 1.025%, 1.022%, 1.095%. The concentration of hydrogen increased in both cases simulation and experimental data. It was found that the value increased in simulated data to 0.55%, 0.69%, 0.75% and in experimental data 1.290%, 1.316%, 1.318%.

**Effect of equivalence ratio**

The another pivotal factor to decide the gauging of the consequences of air to mixed solid waste molar ratios in gasification.
To study the outcomes of air to mixed solid waste (ER) ratio on syngas production, composition gasification experiments were carried out using different ER ratios (0.1, 0.2 and 0.3). (Table 6 and figure 10.2 (b))

Feed rate = 10 kg/hr and Temperature = 650$^{\circ}$C

| Equivalence Ratio | 0.1 | 0.2 | 0.3 |
|---|---|---|---|
| Methane (%) | 1.018 | 1.022 | 1.015 |
| Carbon monoxide (%) | 2.912 | 3.150 | 3.095 |
| Carbon dioxide (%) | 3.012 | 3.250 | 3.365 |
| Hydrogen (%) | 1.315 | 1.316 | 1.308 |

Table 6: Effect of equivalence ratio on syngas production at T = 650$^{\circ}$C

Compare the syngas concentration data generated from a simulation with the data get from experiments. For methane, both cases saw different behaviour. The concentration of methane from simulation data was 0.45%, 0.40% and 0.29% for ER 0.1, 0.2 and 0.3. In experiments, it saw slightly increased in value at ER 0.15 and then decrease. The data was 1.018%, 1.022%, 1.015% at ER 0.1, 0.2 and 0.3.
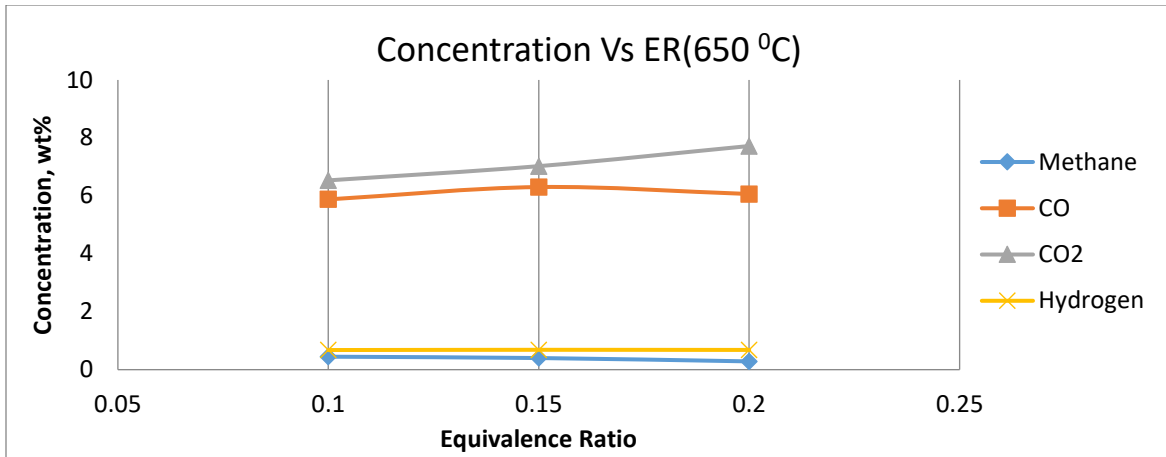
Figure 10.1 Simulated data of syngas concentration on different ER at $650^0$C
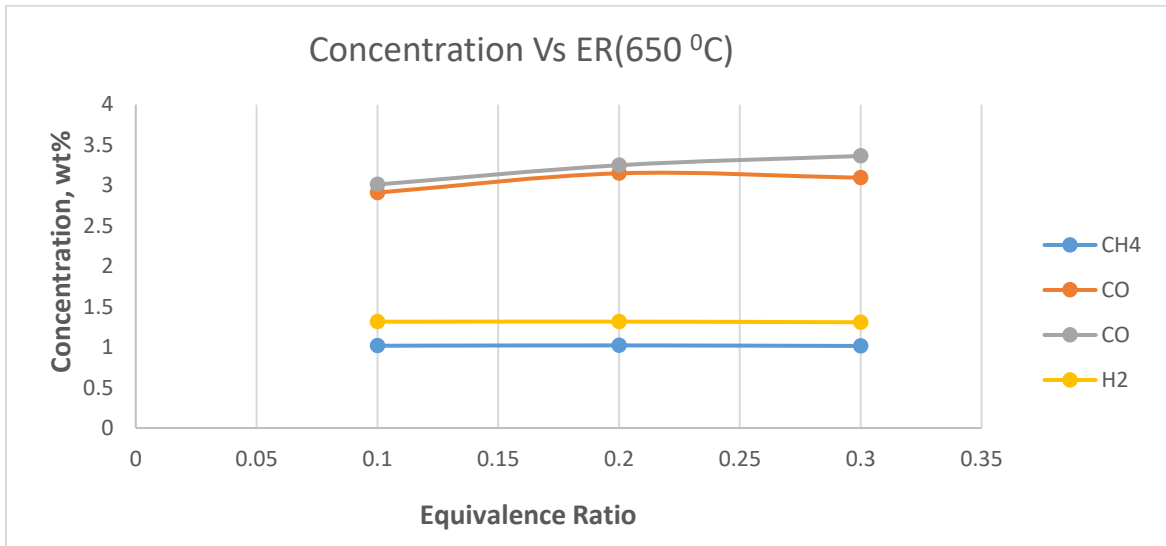


Figure 10.2 Experimental data of syngas concentration on different ER at $650^0$C

Figure 10: Comparison of the effect of ER on syngas concentration at experimental and simulated data

Carbon monoxide and carbon dioxide give the same behaviour in both cases. The concentration of carbon monoxide found in simulation and experimental data was 5.88%, 6.30%, 6.06% and 2.912%, 3.150%, 3.095% accordingly. The concentration of carbon dioxide found in simulation and experimental data was 6.53%, 7.02%, 7.72% and 3.012%, 3.250%, 3.365% accordingly.Hydrogen concentration was found slightly increased with ER in experimental data. The concentration of hydrogen found in simulation and experimental data was 0.68%, 0.69%, 0.68% and 1.315%, 1.316%, 1.308% accordingly.

**Conclusion:**

As the appropriate utilization of solid waste has always been a moot point; an alternative and renewable solid fuel can acknowledge a range of hindrances co-related to various waste production and its appropriate discard management. Numerous government all around the world have provided utmost significance to the RDF gasification as a part of their legislations in the waste management field. Nonetheless, owing to the considerable thermochemical complexity and implementation costs, this top-notch technology is not the choice of industrialists to be adapted globally.

This study contended to monitor the effect of temperature and different air ratios in syngas production, composition. To fulfil this, various practical experiments of Gasification have been performed with consideration of different ER ratios (0.1, 0.2 and 0.3) and different temperatures (600, 650 and 700ºC).

Results proved that air gasification is demonstrated to be more efficient at 650ºC. Results also proclaimed that in air gasification optimal air to mixed solid waste was found 0.2. At this temperature and ER, it gives a higher concentration of carbon monoxide and methane was 3.150% and 1.022% accordingly. Carbon dioxide and hydrogen concentration was found at 3.250% and 1.316% accordingly.

**References:**
a. Ajay K. Dalai a, Nishant Batta, I. Eswaramoorthi, Greg J. Schoenau, "Gasification of refuse-derived fuel in a fixed bed reactor for syngas production." Waste Management, 2009 (29), 252-258.
b. Umberto Arena, "Process and technological aspects of municipal solid waste gasification. A review." Waste management, 2011, 32: 625-639.
c. Qinglin Zhang , Liran Dor , Dikla Fenigshtein , Weihong Yang, Wlodzmierz Blasiak, "Gasification of municipal solid waste in the Plasma Gasification Melting process", Applied Energy · February 2012.
d. Hassan A. Arafat , Kenan Jijakli, "Modeling and comparative assessment of municipal solid waste gasification for energy production", Waste Management 33 (2013) 1704–1713.
e. Pauls, J.H., Mahinpey, N., Mostafavi, E., 2016. Simulation of air-steam gasification of woody biomass in a bubbling fluidized bed using Aspen Plus: a comprehensive model including pyrolysis, hydrodynamics and tar production. Bio. and Bioenerg. 95, 157–166.
f. Trirat Khosasaeng and Ratchaphon Suntivarakon, "Effect of Equivalence Ratio on an Efficiency of Single Throat Downdraft Gasifier Using RDF from Municipal solid waste". 2017 International Conference on Alternative Energy in Developing Countries and Emerging Economies 2017 AEDCEE, 25-26 May 2017, Bangkok, Thailand.
g. Puig-Gamero, M., Argudo-Santamaria, J., Valverde, J., S´anchez, P., Sanchez-Silva, L., 2018. Three integrated process simulation using aspen plus: pine gasification, syngas cleaning and methanol synthesis. Energ. Conv. Manag. 177, 416–427.

# Reformation of Existing Manufacturing Technologies Through the Concepts of Modular Chemical Process Intensification (MCPI)

*M Madhava Krishnan*[*]*, Sahaana R, Venkiteswaran P R, Dr Anu N*
*Department of Chemical Engineering, TKM College of Engineering, Kollam-691 005, Kerala, India*
*\*Corresponding Author: mmmadhavk99@gmail.com, +91 9747 199 851*

## ABSTRACT

Intensification and modularization of processes is a notion that appeared at the beginning of the last decade, but it is still regarded as a recent trend and concept in "Modern Chemical Engineering'. The application of PI strategies to industries is of utmost importance, by means of In process and equipment design, a paradigm shift is allowed by reducing operational functionality, cost of capital and capital, process performance increase, waste and emissions minimization and by enhancing safety. Industry modularization is the method of reducing the footprint (size) of industries and simplifying the scale-up of processes by numbering industries and separating industries into modules. The Modular Chemical Process Intensification analysis (MCPI) methods are in its exponential stage, many PI techniques are being applied in industries such as reactive distillation, split wall column, etc. In its application, the modularization of industries is just like the modularized processing of liquid chlorine. But PI and modularization are still applied in a few systems, and several studies are currently underway to propose different approaches for different industries. In the future, it is possible to change and equip an enterprise with zero waste and less footprint. The industry's economy is exemplified by MCPI because of its lowest capital expenditure (CAPEX) and operating expenditure. (OPEX) also addresses concerns related to the supply chain by modularization. MCPI is the future of the chemical industry, and the full inclusion of these principles fully removes environmental and safety issues.

Keywords: Process Intensification, Modularization, Sustainable Industry, Energy efficiency.

**List of Abbreviations**

CAPEX- Capital Expenditure

CFD- Computational Fluid Dynamics

DIMA-Decentralized Intelligence for Modular Applications

DWC- Divided Wall Column

EPC- Engineering, Procurement and Construction

MCPI-Modular Chemical Process Intensification

MTPP- Microwave Assisted Three Phase Partitioning

OPEX-Operating Expenditure

PI- Process Intensification

RAPID- Rapid Advancement in Process Intensification Deployment

RD- Reactive Distillation

R&D- Research and Development

SM- Static Mixer

TPP- Three Phase Partitioning

# 1.Introduction

The chemical, pharmaceutical and bio-based industries manufacture products that are critical for modernist civilization. Nevertheless, due to the need of developing sustainable products, these industries face tremendous challenges. Process Intensification is known as the method of optimizing the production process and equipment by boosting productivity as well as the costs of redundancy (Energy, material, time and space) [1]. The design of process facilities in numerous modules which is build off sites and are transported and assembled together is called Modular plant construction. The mixture of these ideas for ideal industrial development is referred to as Modular Chemical Process Intensification (MCPI). Currently, MCPI tackles several concerns prevailing in the manufacturing sector, such as sustainability and energy management. Examples in chemical engineering concepts include heat transfer, mass transfer reaction, fluid transfer, etc.

## 1.1 Process Intensification

Process Intensification (PI) drives significant improvements in production and processing across existing operating systems, that is being rethought into ones that are both more reliable and efficient than already established operations. PI often requires integrating individual unit operations, such as reaction and separation into a solitary piece of equipment to give more effective, convenient and feasible manufacturing process [2]. PI technologies are important at the molecular stage, it significantly improves mixing, which increases the mass and heat transfer, reaction kinetics, yields, and specificity. Such improvements result in decrease in the number of equipment, services, footprints and operation complexity, and in doing so minimizing risks and costs in chemical production facilities.

Process Intensification, in general, consists of the production of revolutionary equipment and techniques that are expected to drive dramatic improvements, as opposed to those widely used today, in production and processing, reducing equipment size significantly, production-capacity ratio, energy utilization, production of waste, and ultimately resulting in cheaper and more sustainable technologies[1].Or, to put this in a shorter form: any chemical engineering development that leads to a substantially smaller, cleaner, and more energy efficient technology is process intensification. Many definitions are proposed by many authors some of them are listed in Table 1.1. Sustainable design is accomplished through enhancements with respect to early stage design (also called reference design or base-case design). The role of the synthesis of processes in identifying early-stage design and/or more sustainable design is to generate alternatives to the feasible process [1]. It is possible to produce alternatives in various ways, such as trial and error, rule-based heuristics, process integration (mass and energy), optimization of processes, process intensification, and many more. Process intensification, which also involves process integration, is in this chapter (Fig 1.1).
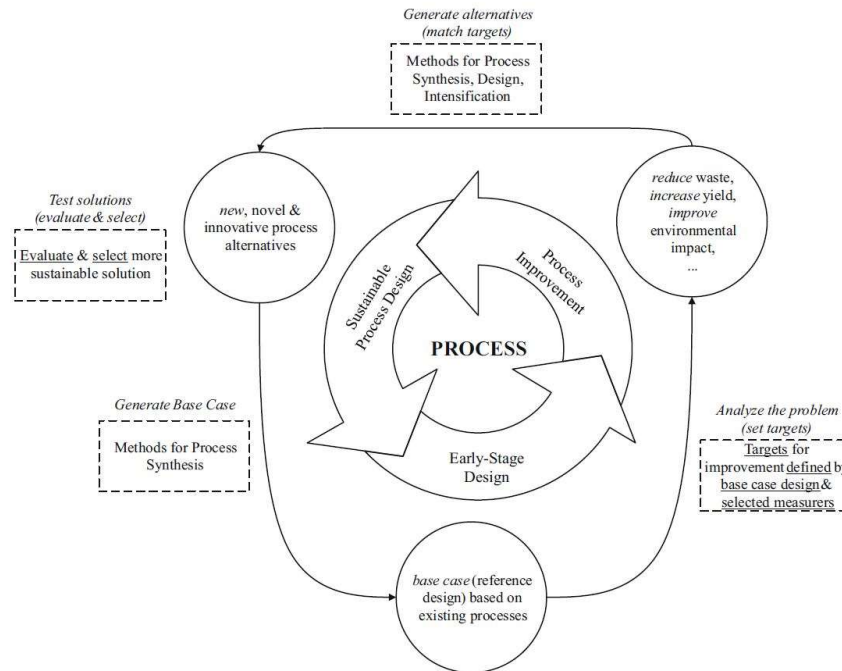
Fig.1.1: Role of process intensification within sustainable process design [3]

Table 1.1: Various definitions of PI

| Reference | Definition |
|---|---|
| **Ramshaw** | Devising exceedingly compact plant which reduces both the 'main plant item' and the installations costs. |
| **Stankiewicz & Moulijn** | Any chemical engineering development that leads to a substantially smaller, cleaner, and more energy efficient technology |
| **Tsouris & Porcelli** | Technologies that replace large, expensive, energy-intensive equipment or process with ones that are smaller, less costly, more efficient or that combine multiple operations into fewer devices (or a single apparatus). |
| **Portha et al.** | Holistic overall process based intensification in contrast to the classical approach of process intensification based on the use of techniques and methods for the drastic improvement of the efficiency of a single unit or device |
| **Baldea** | Any chemical engineering development that leads to substantially smaller, cleaner, safer and more energy efficient technology or that combine[s] multiple operations into fewer devices (or a single apparatus). |

## 1.2 Modularization

In general, the modularity of a product takes into account the final use and its architecture. More robust and efficient modularity can also be accomplished when the concept of modularity is extended to manufacturing processes. Modularity with regard to manufacturing requires an assessment of the different manufacturing processes encountered by each component [2]. Modularity requires maintaining the independence between components and processes in different modules, promoting the similarity of all module components and processes, and maintaining interchangeability between modules. These modules minimize development costs and lead time, thus reinforcing product families.

Process modularity is relatively a new concept. Complex production processes are divided into basic operation modules. To satisfy the changing requirements of new products, these modules are recombined. Process modularity is based on three principles:

I. standardization of processes, splitting the process into standard sub-processes that create standard base units and customization sub processes that further customize the base units;

II. resequencing the process, reordering the sub-processes so that standard sub-processes occur first while customization sub processes occur last;

III. process postponement, postponing customization sub processes until a customer order is received or place those sub processes in distribution centers to achieve maximum flexibility.

We define three different categories of modularity in the sense of chemical processing: modular fabrication and construction, modular design and modular manufacturing. Modular fabrication and construction refer to the situation where a single annual capacity P facility is constructed from (not necessarily identical) factory-preassembled blocks/modules, which are interconnected with minimal effort in the field, as opposed to a system that is essentially field-erected (also referred to as 'stick-built') [2]. These modules can include one conventional unit operation, multiple unit operations, or only part of a unit operation. Modular design is to designate a situation whereby production facility of annual capacity P is planned for and constructed with pre-specified, standardized building blocks. Modular output is referred to as the situation in which n equal or similar equipment (modules), each with capacity P/n, are used to meet processing capacity P [4].

## 2. Literature Review

Many new studies use the concepts of PI and modularization, especially in 2019 and 2019. This is due to a rise in sustainability and energy efficiency issues in 2020 (shown in fig 2.1). Many new equipment is used as part of process intensification, along with existing equipment that is less bulky than the prevailing equipment is often used with this new equipment. Some examples, including plate and frame heat exchangers that replace modular reactors with shell and tube heat exchangers, are ideal for many issues, including electricity, space and protection. The change to process intensification is important for many reasons, including changes in supply and demand, enhanced legislation, developments in technology,

financing mechanisms, etc. In modularization, several methods are tried by numbering and standardization [1].
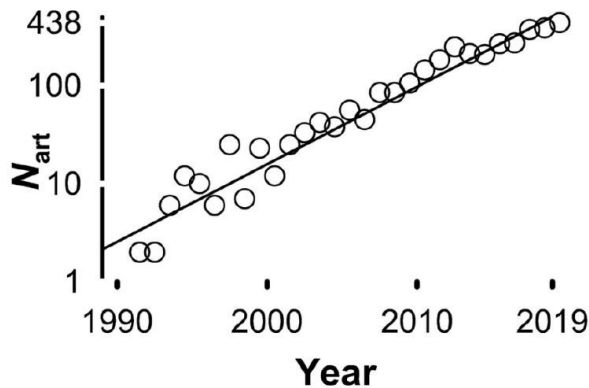


Fig 2.1: Number of articles on PI per year [1]

## 2.1 Prevailing Technologies in MCPI

MCPI is conventionally used as multiple devices such as static mixer, reactive distillation column, divided wall column, membrane reactors, and many others. Though the design of these equipment persists well before these industries are introduced or reformed, the application is not seen. Several responses such as Eastman's methyl acetate synthesis and FischerTropsh synthesis are in transition with these principles. In more processes, modern research is continuing to incorporate these principles, some of which are microwave reactor for extraction, membrane rector for separation of olefin-paraffin, microchannel reactor for production of biofuel. Industry modularization is accomplished only by intensification, by implementing the protection of modular industries, and problems can be eradicated because of the transport of hazardous chemicals.

### 2.1.1 Static Mixer

Static mixers (SM) are precision-engineered machines for continuous fluid mixing without the need for moving components. SM may be used for combining streams of liquid and gas, dispersing gas into liquid, or blending immiscible liquids. The energy required for fluid mixing efficiently comes from the pressure drop through the elements of the static mixer. Small volumes, low maintenance, easy installation and cleaning, and excellent reliability are the key advantages of static mixers. There are two major types of static mixers on the market and they are largely used on an industrial scale:

• Housed-elements type, consisting of mixer elements enclosed in a cylindrical (tube)(as shown in Fig 2.2) or squared housing. The static components continually mix the fluid materials as the streams pass through the mixer.

• Plate-type mixer. Mixing is achieved in the plate-type configuration by extreme turbulence in the flow. The static corrugated plate mixer is capable of mixing low-viscosity liquids, mixing

gases, dispersing immiscible liquids, and achieving gas-liquid dispersions over a short length with a very high degree of mixing.

Static mixers are now used for a wide range of applications, such as chemical refining, wastewater treatment, neutralization of acid-base, oxidation and bleaching, blending of gaseous reactants, blending of multicomponent drugs, preparation of fertilizers and pesticides, steam injection, organic-aqueous dispersions, and the oil and gas industry [3].
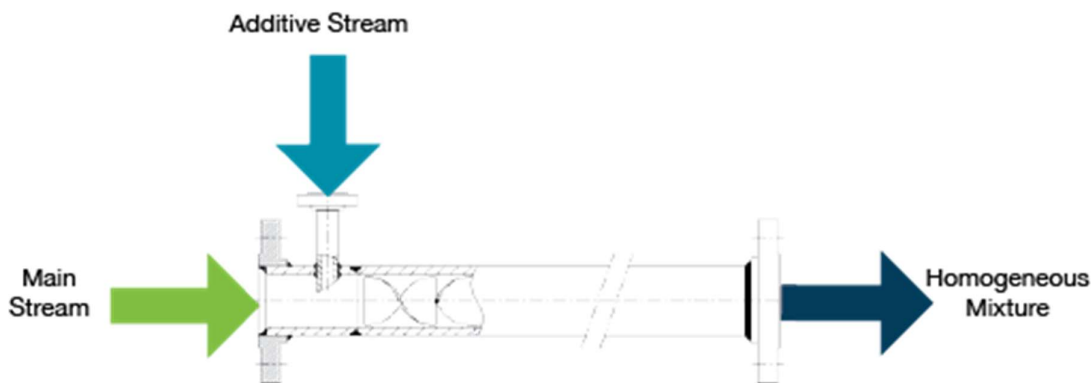


Fig 2.2 Schematic Representation of a static mixer [6]

## 2.1.2 Reactive Distillation Column

As a promising example of a process intensification technology for improved chemical processing, reactive distillation stands out. RD can be used in various ways to enhance chemical processing due to the synergic effect of combining reaction with separation (Schematic representation shown in Fig 2.3). The reduction in the excess of reactants relative to conventional methods is an additional benefit of the selective removal of products when conducting equilibrium reactions. As a consequence, for the same degree of conversion, the required catalyst loading is also reduced. In addition, by using heterogeneous catalysts and raw catalysts, materials are fed underneath the catalytic phases of an RD column, which helps protect the catalyst from deactivation caused by non-volatile impurities. Another synergistic advantage of RD system is linked to the use of heat, the incorporation of the heat from the reactions and the use of the distillation source [5].
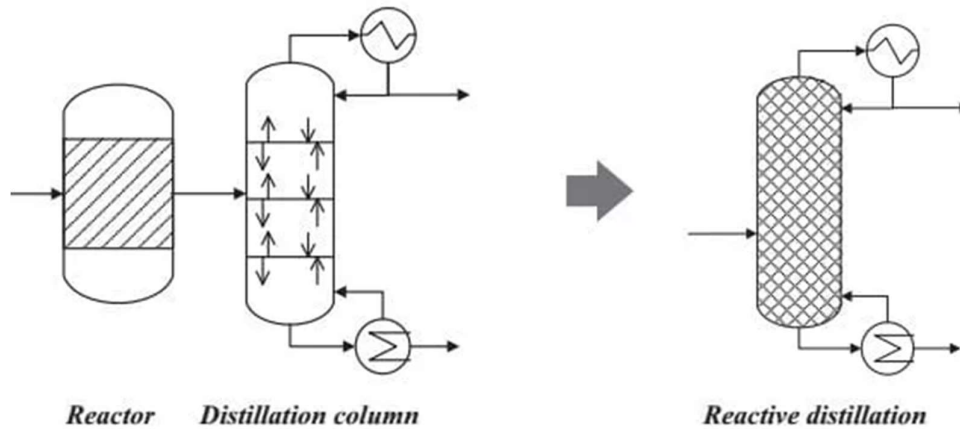
Fig 2.3 Schematic Representation of Reactive distillation [7]

## 2.1.3 Divided Wall Column

A direct or indirect series of at least two distillation columns usually includes the separation of an Azeotropic Ternary Mixture (ABC). The direct separation series has an inherent thermal inefficiency for certain mixtures (for example, when B is the major component and the split between A and B is as simple as the split between B and C), due to the remixing occurring for the mid-boiling component as shown in Fig 2.4. A DWC is capable of providing higher purity side product compared to classic columns with a side draw. The partition wall helps to prevent contamination of the column between the feed side and the side-draw section [6].
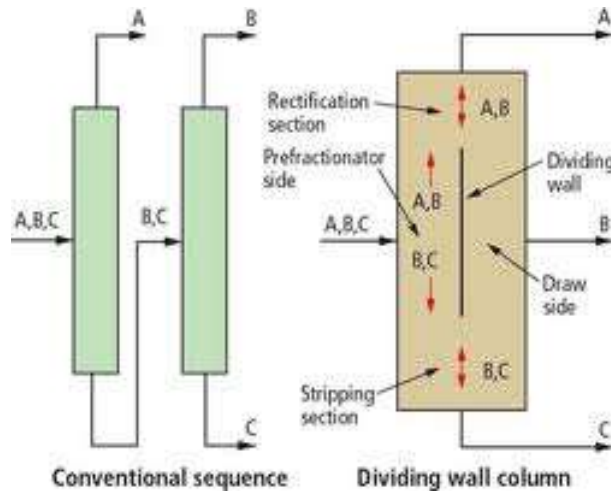


Fig 2.4: Comparison of Conventional DWC approach [8]

### 2.1.4 Microreactors

Another field covered by the process intensification literature is microreactor technology (PI). It is also related to green chemistry, organic synthesis, and flow chemistry because it represents a way of increasing energy and cost efficiency while minimizing waste by translating processes from batch to continuous, likely with enhanced technology such as microreactors. Above all, microreactors show considerable potential in the the pharmaceutical business. Microreactors may also be paired with other amplified technologies, such as irradiation through microwave and ultrasound, photochemistry, inductive heating, heat exchangers, etc., and electrochemical energy systems, such as a residence time module and a heat exchanger to incorporate a microreactor to be assembled in a unit composed of four microreactor elements [5,3].

### 2.2 New Technologies and Researches

In the food and petrochemical industries, recent inputs such as the microwave reactor in oil extraction and the separation of olefins and paraffin are the next step. Ultrasounds is the intensification of the tool used to decrease Custard apple waste, which is a big waste in the oil industry. Highly selective membranes are used in the case of the petrochemical industry to distinguish olefins and paraffin formed by the distillation column.

### 2.2.1 Microwave Reactor for The Separation of Oils

Microwave application has been observed to be an emerging method of intensification in the field of extraction. A recent extraction study shows the growing microwave prospectus as an integrated unit process with Three Phase Partitioning (TPP). The aim of this work is to determine the best microwave application mode for TPP assisted oil extraction from custard apple seeds, which as a biopesticide has significant industrial potential. Many ground-breaking efforts have been made by researchers to develop a method of rapid, effective, renewable, and economical extraction. The combination of intensification instruments and novel extraction methods is primarily incorporated into these processes. One of the techniques that separates oil and proteins simultaneously in different stages is three-phase partitioning (TPP). In contrast to conventional extraction methods, the method was also found to be economical, efficient, and green for the separation of bioactive molecules. To boost TPP, the researchers analysed intensification methods such as ultrasound, microwave, and high pressure. Among these intensification methods, a very versatile and effective extraction method was found to be the microwave. Ultrasound as a means of pre-treatment has recently been used as an intensification technique for improving the extraction of custard apple seed oil using TPP (Fig 2.5). With reduced extraction time, the use of ultrasound in TPP improved the extraction yield. Unlike traditional methods and innovative instruments such as ultrasound, based on its dipole rotation and ionic conduction, microwave radiation directly transfers heat to material, which in turn speeds up the heating process and minimizes losses. Although three-phase partitioning (MTPP) was supported by microwave researchers to study the separation of different biomolecules such as proteins (laccase), xanthonoid (mangiferin) diosgenin and steroidal saponins, no separation

of oil or lipid molecules is being investigated. Therefore, like ultrasound, there is a potential for exploring the possibility of microwave as a form of pre-treatment to increase the TPP-PPP yield [9].
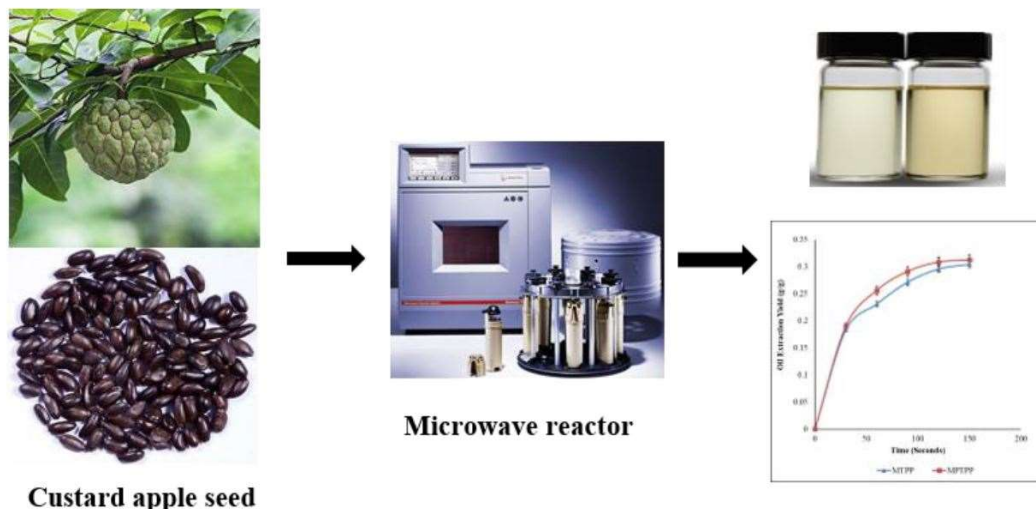


Fig 2.5 Process of Extraction of oil by Microwave reactor [9]

## 2.2.2 Olefin/Paraffin Separation Using Membranes

One of the most complex and energy-intensive methods is the separation of olefin and paraffin, which has gained more and more interest over the past few decades. Olefins are usually generated in the petrochemical industry through gasoline cracking or catalytic paraffin dehydrogenation. Olefins are therefore often followed by a small amount of paraffin, which must first be separated from the mixture in order to obtain olefin of a polymer grade (higher than 99.5 percent pure) before further use. Nevertheless, the isolation of the mixture of olefin/paraffin gas is due to their related physical and chemical properties, such as molecular size and boiling point, they are difficult [10]. Cryogenic distillation, which is an extremely energy-intensive process, is the most common technology for olefin/paraffin separation in the industry. To ease energy consumption, a more energy-efficient method for the separation of olefin/paraffin is urgently needed. Membrane technology has gained more and more interest and has proven promising for successful separation of olefin/paraffin. Metal salts were integrated into the membrane to form a facilitated transport polymer membrane to address the poor selectivity and permeability of the conventional polymer membranes. It is well known that, due to the unique interaction between the hybrid molecular orbital of the olefin and the atomic orbital of the metal, olefins are able to form reversible chemical bonds with transition metal ions. The advantage of chemical complexation is that the chemical bond formed between the transition metal ion and the olefin is stronger than the bond formed by the force of van der Waals [11]. High selectivity and high permeability can therefore be achieved in comparison

with traditional polymer membranes (Fig 2.6). Liquid membranes, membrane electrolytes and ionic liquid membranes are included in these facilitated transport polymer membranes.
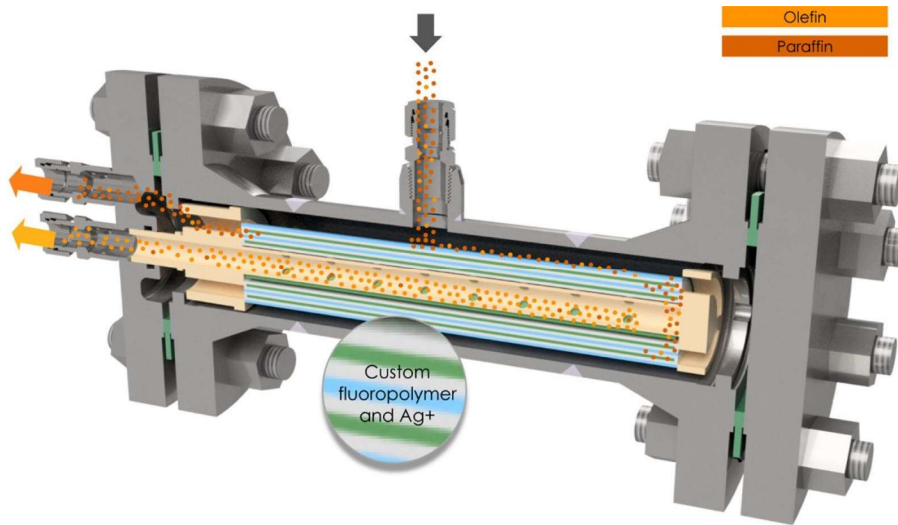


Fig 2.6: Example of membrane assisted separation of olefin/paraffin [12]

### 2.2.3 Intensification of Bio-fuel Production

### 2.2.3.1 Biodiesel

One of the areas explored in process intensification for the development of biodiesel is the use of novel reaction technology. A method of laminar flow is proposed for the simultaneous processing of biodiesel and the separation of by-products. The formation of two phases, in particular, allows the separation of biodiesel in the upper layer and of glycerol in the lower layer. The use of a static mixer reactor enhanced by ultrasound for esterification of an oil was recorded in other work. For the development of biodiesel, the use of microchannel reactors has also been documented. These reactors are small and, by adding more reactors in parallel, their scale-up can be accomplished. Simultaneous reaction and isolation is another approach to the intensification of the biodiesel processes. The membrane reactors are an example of this philosophy, where, as the reaction occurs, the tiny molecules selectively move through the membrane and hold the oil [3].

### 2.2.3.2 Bioethanol

The use of a two-stage bioreactor with cell-recycle, fermentation in an oscillatory baffled reactor are some intensification alternatives in the reactive phase. The proposed system substantially improved yields compared to a stirred tank reactor [3], according to the recorded results. To enhance enzymatic hydrolysis, the use of ultrasound has also been accounted. It has been documented that ultrasound helps increase yield, reducing processing time and consumption of enzymes. Intensification models are also suggested for the purification of fermented goods via the Azeotropic split wall column and Reactive distillation column.

### 2.2.3.3 Bio-Jet fuel

Since bio-jet fuel development is a relatively recent field of interest, there are only a small number of proposals for its intensification. Usage of microchannels and monolithic reactors to increase mass and heat transfer in hydroprocessing reactions for the reactive steps [3]. The authors report a higher selectivity for kerosene using a Ni-Mo catalyst backed by gamma alumina. In addition, it has been stated that, compared to the microchannel reactor, the monolithic reactor shows lower yields of oligomeric materials.

## 3.Conclusions

In chemical engineering, there are operations called chemical reaction engineering, solids handling and processing, separation technology, along with significant and wide areas such as thermodynamics, transport phenomena, and fluid mechanics. In all of these areas, PI plays a key role in developing and advancing research in these fields by various means (multifunctional reactors, microreactors, etc.). The synergistic relationship between process intensification and process systems engineering, in which PI is like a foundation stone or base from which different process systems are further revised and boosted, is a very prominent aspect. In this regard, PI offers the ability not only for model development to build a new platform for process systems engineering, but also provides space for new instruments and their processing methods, along with plant design and optimization. One can also think of PI at the molecular level. The rationale behind these is that PI provides different objectives, such as enhancing the effectiveness of intra- and intermolecular events to give each molecule the same treating experience and to increase the various dynamic forces in terms of increasing the surface to volume ratio, i.e., the interfacial area. Another boon in PI for chemical engineering is multifunctional reactors as well as microreactor technology. Microreactor technology enables any transport processes (mass transfer and reaction kinetics) to be enhanced due to the increased interfacial area and contact time between the specific phases chosen for the analysis. There is much more to this improvement than that of standard macro reactors. The method of highly active and selective catalysts, and optimization of feedstock utilization can lead to decrease in energy consumption per unit weight of product and hence the reduction in greenhouse gas emissions [13].

Multifunctional reactors can also be used to minimize energy in this respect, and this is achieved by combining multiple process steps into one. This involves extracting materials from the reaction zone in situ. It is also possible to stop a sequence of reactions using multifunctional reactors and a better reaction rate is achieved. PI also helps to minimize waste generation in the chemical industry. Advances in the production of catalysts and developments in reaction engineering may provide a roadmap for a new generation of multi-reactors that could help to disable some of the process industries' major engineering challenges.

### 3.1 Drivers and Barriers

### 3.1.1 Drivers

The production and implementation of modular chemical process intensification can be accelerated by several main factors, including energy consumption, cost savings, safety, environmental impacts, and investments. A significant driver of process intensification technologies is reducing energy consumption. Certain techniques can reduce the energy consumed by chemical and manufacturing processes. Cost savings are another strong benefit of process intensification technology, since lower costs mean higher profits for industry. Generally, process costs consist of costs for capital, energy, and raw materials. Savings in

capital and energy costs can result from reducing the process size and the amount of energy utilized, as well as increasing compactness. Process safety depends on the inventory of chemicals, flammability, explosivity, toxicity, temperature and pressure. Thus, for chemical and manufacturing processes handling dangerous, poisonous, corrosive, flammable, and explosive chemicals, safety is critical. Processes cannot be completely sterile because chemical inventories are complicated and contain vast quantities of hazardous chemicals. Via small processes that involve small chemical inventories and consume small quantities of chemicals, safety can be improved. Intensification of processes can eliminate hazardous chemicals from chemical inventories and can therefore offer inherent protection. Process Intensification can reduce the negative environmental consequences of chemical and production processes. For instance, intensified processes may emit less carbon dioxide by reducing energy consumption, which is suspected of causing global warming [2,3,13,14].

### 3.1.2 Barriers

The high risk associated in its investment is a major obstacle to the production of high-efficiency modular chemical processing devices. Process Intensification focuses on the creation of novel and innovative equipment and methods which greatly enhance operations. It may entail significant monetary investments to develop such equipment and methods, but it will often carry a high risk of failure, which increases the risk of investment.

Due to the possible effects on the environment and human health, safety can also be an obstacle to modular chemical process intensification. In chemical inventories, some intensified processes may contain harmful chemicals and are therefore not necessarily safe. New equipment and methods implemented in intensified modules cannot always be checked to ensure safe operation over a sufficiently long time. The chemical inventories of the chemical production processes can be complex. A safety risk may be generated when they are used due to a lack of knowledge on intensified modules [13,14].

### 3.1.3 Methods to overcome the barriers
### 3.1.3.1 Adopting investment opportunities

Investments are the essential part of research and development (R&D). Europe has continually made substantial R&D investments in process intensification since the late 1970s. The focus of investments was made to improve and implement process intensification in the field of chemical engineering [13]. Recently, the US Department of Energy has funded the Rapid Development in Process Intensification Implementation (RAPID) Manufacturing Institute. The RAPID Manufacturing Institute focuses on developing and implementing process intensification technologies to minimize costs, boost energy and resource quality, and increase overall productivity in manufacturing processes. Fig 3.1 Indicates other PI financing organizations.

Fig 3.1: Organisations funding for PI and related researches

## 3.1.3.2 Educating in PI
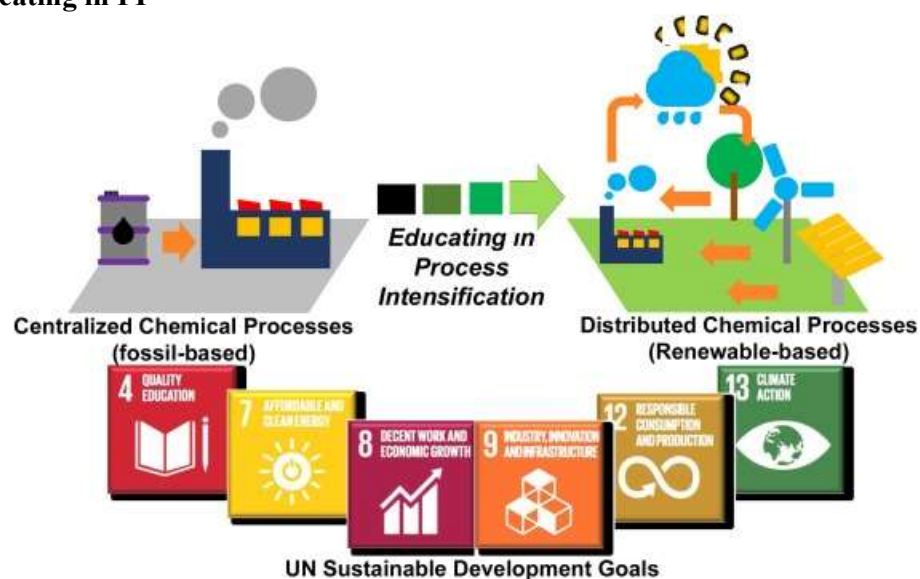


Fig 3.2: Interplay of education on process intensification and the United Nations Sustainable Development Goals. The chemical industry must change drastically to contribute to create sustainability. [16]

## 3.2 Future of MCPI

Modular chemical process intensification is a growing trend in chemical engineering and can substantially develop chemical and manufacturing processes substantially. Dramatic developments provide several advantages, including reduction in energy consumption, cost savings, improvements in safety and the minimization of environmental problems. These qualities are primary drivers and could accelerate future production and implementation of modular chemical processes intensification for the chemical industry, the pharmaceutical industry, materials, pulp and paper, petroleum, water treatment and desalination, and

environmental management, among other areas. In the future, process intensification is expected to involve a broad variety of academic and practical topics. Its diversity of applications [1,2,3,15] can be further expanded by a comprehensive definition of process intensification.

The core features of modular chemical process intensification are novelty, innovation, and creativity. The successful implementation of future process intensification technologies with these characteristics depends on a deeper understanding of molecular-scale thermodynamic, kinetic, and transport phenomena. Strong chemistry knowledge is crucial. Future process intensification work should also involve the creation of engineering approaches that that control different phenomena from the molecular to the process scale. Advanced manufacturing, e.g., three-dimensional printing of devices like micro mixing process equipment and droplet formation for liquid extraction and chemical synthesis and analysis reactors, is an emerging technique that can benefit process intensification. In the development of modular chemical process intensification, advanced manufacturing can be a major player, and process intensification can further stimulate the development of advanced manufacturing through process industry applications. There will be a need for interdisciplinary research and close collaboration between universities, research institutions and the industry. In chemical engineering, educational modules for process intensification, a curriculum to train researchers and professionals for future generations, must be incorporated.

Successful implementation of modular chemical process intensification relies on resolving several obstacles, high risk of failure, lack of scale-up knowledge and safety. Particularly,
To improve the efficiency of process intensification technologies, potential problems associated with the lack of scale-up knowledge should be prevented. In addressing scale-up, risk, and safety issues, mathematical modeling is expected to play a major role.
The intensification of processes requires several techniques to reduce manufacturing costs, energy intensity and pollution. Some methods include integrating several processes of reaction and separation into a single unit, improving chemical and physical driving forces, and internally sharing energy and waste streams in the process. By standardizing the manufacturing of small-scale processes, modular processing can handle investment risks to achieve similar economic benefits as output on a larger scale. These MCPI developments, when widely deployed, will reduce the national energy and carbon footprints of the chemical and petrochemical industry while also improving the economy. The focus area of MCPI on the conversion of renewable feedstocks holds the opportunities to realize long-term sustainability goals. Modular chemical processes for distributed processing of biofuels and bioproducts at feedstock availability sites will minimize long-haul transport costs and safety issues, increase feedstock energy density, and enhance local feedstock economies.

### 3.2.1 Modular Process Control
It is likely that the management of modular production architectures would involve the extension or alteration of the collection of control decisions usually enforced in process systems, where the supervisory controller meets plant-wide control objectives by directing the operation of the regulatory control layer, while the setpoints of the supervisory control system are determined by the optimization estimation. Development of specific architectures, such as Decentralized Intelligence for Modular Applications (DIMA) is being built under the umbrella of Industry 4.0 in Europe.  Future work to attain the plug & produce capability needed to build modular, cost-effective modules entails the development of scalable modules, compatible dynamic process models for model-based control. Such models could be developed by the

manufacturers of the modules themselves and delivered to the user in a very cost-effective manner together with the physical module [15].

MCPI's focus area on modelling and simulation uses these important technologies by collecting accurate data to enable better decision-making and by developing modelling tools for design, control, and analysis of processes and products. In particular, analyses can be applied with a systems perspective by using a model-based approach that integrates process simulation of new designs coupled with assessments across all sustainability dimensions. Ideally, analyses should be conducted with a lifecycle perspective in order to capture both upstream and downstream impacts in addition to the MCPI processes themselves. Analyses can be conducted early during conceptual design to screen alternatives and then later during detailed design when specific MCPI strategies are considered. Comparisons to "business-as-usual" designs and products can establish further justification for commercial deployment.

### 3.2.2 Towards Industry 4.0

Process-intensified reactors and components also have complex structures and geometry, such as static mixers, microchannel reactors, as well as multi-phase reactors, such as rotating packed and packed reactors, while at the same time striving to optimize mass, heat and momentum transfer. In order to understand micro mixing scales and measure the energy density of the intensified process, the combination of experimental data with advanced visual aids and/or computational fluid dynamics (CFD) modeling is necessary. We expect Industry 4.0 to accelerate the availability of new digital technologies for fast and efficient real-time use in this context. In addition to increase the consumer acceptance of PI technologies, Industry 4.0 will also make the workflow of engineering, procurement and construction companies (EPC) more effective when it comes to manufacturing and engineering modular units. This would be possible as it promotes the digitization of all production processes (smart manufacturing) and business processes that not only promise to improve the productivity of production, but also tackle the utilization of capital and waste elimination [3,15].

**REFERENCES**

1. Boffito, Daria C, Fernandez-Rivas, David, 2020, Process intensification connects scales and disciplines towards sustainability, The Canadian Journal of Chemical Engineering, 0008-4034

2. Kim, Yong-ha & Park, Lydia & Yiacoumi, Sotira & Tsouris, Costas. (2017). Modular Chemical Process Intensification: A Review. Annual Review of Chemical and Biomolecular Engineering. 8. 10.1146/annurev-chembioeng-060816-101354.

3. Juan Gabriel_Segovia-Hernández_Adrián_Bonilla-Petriciolet (2016) Process Intensification in Chemical Engineering Design: Optimization and Control. Springer Publications

4. Shaik, Abdul & Rao, Vaddi & Rao, Ch.Srinivasa. (2015). Development of modular manufacturing systems—a review. The International Journal of Advanced Manufacturing Technology. 76.  0.1007/s00170-014-6289-2.

5. Babi D.K., Cruz M.S., Gani R. (2016) Fundamentals of Process Intensification: A Process Systems Engineering View. In: Segovia-Hernández J., Bonilla-Petriciolet A. (eds) Process Intensification in Chemical Engineering. Springer, Cham.

6.https://www.aiche.org/resources/publications/cep/2018/march/employ-static-mixersprocessintensification 20/09/2020

7. https://www.epicmodularprocess.com/blog/what-is-process-intensification, 20/09/2020

8. http://seperationtechnology.com/dividing-wall-distillation/ , 20/09/2020

9. Dhanashree C. Panadare, Virendra K. Rathod, Process intensification of Three Phase Partition for extraction of custard apple seed oil using Microwave Pretreatment, Chemical Engineering and Processing - Process Intensification, 2020, 108095.

10. Miranda DM, Dutra LD, Way D, Amaral N, Wegenast F, Scaldaferri MC, Jesus N, Pinto JC. A Bibliometric Survey of Paraffin/Olefin Separation Using Membranes. Membranes. 2019:157.

11. Hou, Junjun and Liu, Pengchao and Jiang, Meihuizi and Yu, Lian and Li, Lianshan and Tang, Zhiyong, 2019, Olefin/paraffin separation through membranes: from mechanisms to critical materials, J. Mater. Chem. A, volume 7,41,23489-23511

12.https://www.aiche.org/rapid/news/08-05-2020/rapid-project-highlight-energyefficient-separationolefins-and-paraffins-through-membrane , 20/09/2020

13. Yuhe Tian, Iosif Pappas, Baris Burnak, Justin Katz, Efstratios N. Pistikopoulos, A Systematic Framework for the synthesis of operable process intensification systems – Reactive separation systems, Computers & Chemical Engineering,134, 2020, 106675,

14. Biswas, Koushik. (2018). Recent Trends of Process Intensification in Energy Domain.

15. Baldea, Michael & Edgar, Thomas & Stanley, Bill & Kiss, Anton. (2017). Modular Manufacturing Processes: Status, Challenges and Opportunities. AIChE Journal.

16. David Fernandez Rivas, Daria C. Boffito, Jimmy Faria-Albanese, Jarka Glassey, Nona

17. https://www.aiche.org/rapid/news/06-27-2019/rapid-spotlight-sustainability-and-process-intensification, 20/09/2020

# NUMERICAL PREDICTION AND FE ANALYSIS FOR STIFFNESS OPTIMIZATION OF HOLLOW TAPERED ROLLING ELEMENT BEARING

*Nilay Bhavsar[1], Gurmitsingh Bassan[2]*

[1]Assistant Professor, Mechanical Engineering Department, Dharmsinh Desai University, Nadiad, India

nmbhavssar.mech@ddu.ac.in

[2]Professor and Head, Mechanical Engineering Department, Dharmsinh Desai University, Nadiad, India

gdbassan.mech@ddu.ac.in

**Abstract:**

The increasing global environment consciousness, information by recent worldwide calls for control of climate change and greenhouse emissions, has placed significant new technical mandates for automotive to improve engine efficiency, which directly related to the production of carbon dioxide and a major greenhouse gases. Heat and friction has an adverse effect on bearing and automobiles system and leads to the problem as wear, tear and bad fuel economy, which leads to harmful environmental effects. The fatigue life of bearings mainly depends on many factors and variables, such as the size and direction of the loadings, the geometry and roughness of the contact surfaces, the kind of material, the operating temperature, applied lubricant, lubrication conditions and rolling speed. Investors have been proposed that under large normal loads a hollow element with a sufficiently thin wall thickness will deflect apparently more than a solid element of same size, further contact stress is reduced and minimize the generation of heat in bearing.

In present study Fatigue life investigation have been made using Numerical prediction and FE analysis for hollow tapered rolling element bearing, and 3D model has been made for 32212 tapered roller bearing with different hollowness percentage varying from 0% to 80% in interval of 10 to investigate the hollowness percentage that gives the highest fatigue life of bearing using the FEA package, ANSYS. It has been found that the stiffness is maximum at 60% hollowness and decrease up to at 70% hollowness, thus maximum value of stiffness lies between the 60% to 70% hollowness and in accordance to that fatigue life will be maximum in that range. Further, FE analysis has been carried out to obtain the optimum hollowness percentage and results suggests that the 65% hollowness is the optimum range to achieve sufficient roller flexibility and load carrying capacity.

**Keywords:** Hollow rolling element, Finite element analysis, Optimization, Bearing stiffness, Fatigue life

## 1. Introduction:

Bearing is a machine element that plays a vital role in transferring loads between two moving machine parts. The Rolling element bearing is a type of bearing in which the main load is transferred through elements which are in rolling contact rather than in sliding contact. Rolling element bearing are prominent because of their low starting torque and kinetic friction[1]. They are widely used for numerous applications like in locomotive, automobile, home appliances, industrial machines, electric motors, instruments, agricultural industries, textile industries, aerospace and many more.

The design of rolling element bearings has a great impact on the performance, life and reliability for specific application of bearings. The fatigue life of bearings mainly depends on many factors and variables, such as the size and direction of the loadings, the geometry and roughness of the contact surfaces, the kind of material, the operating temperature, applied lubricant, lubrication conditions and rolling speed[2]. However, it is anticipated that in future

the operating conditions of bearings will be much severe and more challenging for the parameters such as high speed revolution, huge load, high temperature, and high contact pressure and starved lubrication than at present[3]. Bearing may fail when used under such harsh conditions by different modes of bearing damages.

Design structure of tapered roller bearing mainly consists of rows of tapered rollers, cage, inner ring being called cone, outer ring being called cup and cage. These bearings are widely used in industrial applications such as automobiles. They have advantages in load carrying capacity and rigidity in comparison with ball bearings. Solid taper roller bearings have a large capacity to carry large radial loads and thrust load. In railway wagon they mainly used tapered roller bearings due to ability to withstand repeated shock loads.

The design of bearing has a great influence on performance and fatigue life of bearing. Further, tremendous work has been carried out for different types of bearing for different operating conditions. Furthermore, little or less work has been done for the bearing with the hollow rolling element. So here literature survey has been carried out to explore the scope of hollow rolling element in tapered roller bearing.

## 1.1 Definition of problem:

Bearing No: 32212 (Solid Tapered Roller Bearing)
Following are the major dimensions of the bearing:[4]

  Internal diameter of bearing: 60mm
  Outer diameter of bearing: 110mm
  Average outer diameter of inner ring: 76.09mm
  Average inner diameter of outer ring: 96.65mm
  Length of roller: 19.96mm
  Number of rollers: 19
  Applied load on bearing: 30KN
  Modulus of elasticity: 2.058 x 105 N/mm2
  Poisson's ratio: 0.3

Based on above geometric parameters of 32212 tapered roller baring and mechanical properties FEA is carried out for hollow rolling element bearing for the different hollowness percentage starting from 0% and 30% to 80% [4]
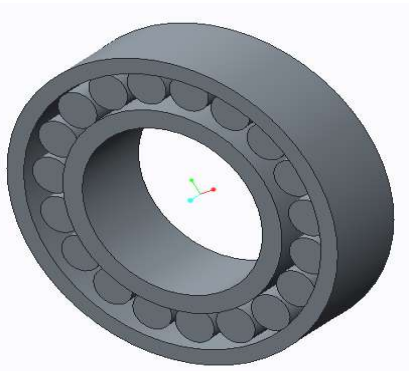


Figure 1: 3D model of Tapered Roller Bearing with 0% Hollowness

## 1.2 FEA for hollow rolling element:

The main objective of the present work is to study the stiffness optimization for the hollow tapered roller bearing. The contact stresses in solid roller bearing can be calculated using Hertz contact theory, but same theory cannot be apply applied to hollow roller bearing. Hence to

study the contact interaction between the rollers FEA approach has been carried out to determine the optimum percentage hollowness which gives longest fatigue life and radial stiffness for the tapered roller bearing.

Investigation have been made for hollow rollers in pure normal loading with different hollowness percentage starting from 0% and 30% to 80% using FEA software to find the maximum von-mises stress, maximum contact stress and maximum deflection[5]. Since hollow rollers deflect considerably more than the solid roller of the same size so contact stress will be less. Later on optimum radial stiffness which gives the longest fatigue life will be calculated using the result obtain through the FE analysis.
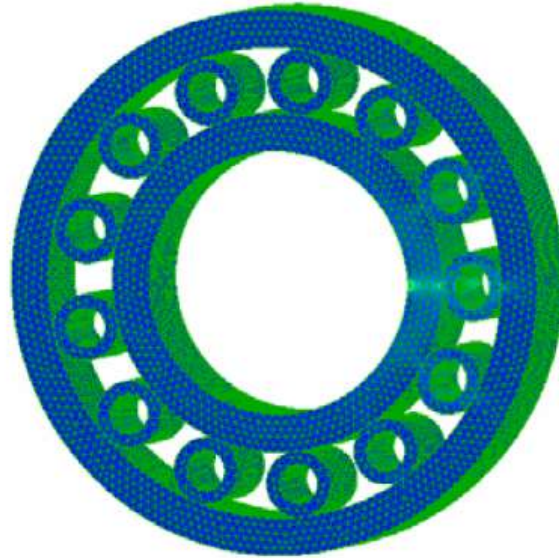


Figure 2: FE Analysis for 60% Hollowness

Table 1: Result of FEA for hollow rolling element

**Results of Finite Element Analysis**

| Hollowness % | Maximum Von-mises Stress (Mpa) | Maximum Contact Stress (Mpa) | Maximum Deflection (mm) |
|---|---|---|---|
| 0 | 714.493 | 1242.42 | 0.011164 |
| 30 | 575.491 | 1016.97 | 0.011212 |
| 40 | 523.92 | 933.628 | 0.012711 |
| 50 | 469.081 | 848.029 | 0.016263 |
| **60** | **433.314** | **743.757** | **0.024016** |
| **70** | **434.435** | **643.924** | **0.043082** |
| 80 | 572.492 | 542.375 | 0.102706 |

From the Table 1 we can observe that the maximum von-mises stress is continuously decreases and reach up to 433.314 (Mpa) by increasing the hollowness from 0% to 60%. There after it start increasing in the range of 60% to 70% hollowness. So contact stress is minimum in the range of 60% to 70% hollowness.

Table 2: value of radial stiffness with respect to hollowness %

| Hollowness % | Radial Stiffness (N/μm) |
|---|---|
| 0 | 317.86 |
| 30 | 318.01 |
| 40 | 322.43 |
| 50 | 331.29 |
| 60 | 345.943 |
| 70 | 298.67311 |
| 80 | 93.2777 |

As we know that bearing stiffness is inversely proportional to load carrying capacity. And fatigue life of bearing is directly proportional to the load carrying capacity. According to this Table 2 represents the radial stiffness at different hollowness of bearing.

From Table 2 we can observe that the stiffness is maximum 345.943(N/μm) at 60% hollowness and decreases up to 298.6731(N/μm) at 70 % hollowness. So the maximum stiffness value lies within the range of 60% to 70% hollowness. Further, the optimum hollowness percentage for the longest fatigue life lies within the range of 60% to 70%.

Now again FEA analysis has been carried out to identify the exact percentage of hollowness in the range of 60% to 70%

**Results and Discussion:**

Table 3: Result of FEA for hollow rolling element in between 60% to 70%

**Results of Finite Element Analysis**

| Hollowness % | Maximum Von-mises Stress (Mpa) | Maximum Contact Stress (Mpa) | Maximum Deflection (mm) |
|---|---|---|---|
| 60 | 433.314 | 8308.167088 | 0.024016 |
| 61 | 427.371 | 8750.815336 | 0.025135 |
| 62 | 425.521 | 9278.96641 | 0.026535 |
| 63 | 423.221 | 9861.552812 | 0.028042 |
| 64 | 422.678 | 10494.44123 | 0.029668 |
| **65** | **420.793** | **11151.01998** | **0.034335** |
| 66 | 425.578 | 11912.19041 | 0.033267 |
| 67 | 427.783 | 12830.30532 | 0.035603 |
| 68 | 428.07 | 13717.5867 | 0.037816 |
| 69 | 432.862 | 14799.44461 | 0.040524 |
| 70 | 434.435 | 15843.06084 | 0.043082 |

From the Table 3 we can observe that the maximum von-mises stress is continuously decreases and reach up to 420.793 (Mpa) at 65% hollowness. There after it start increasing in the range of 65% to 70% hollowness. So contact stress is minimum in the range of 65% to 70% hollowness.

Graph 1: Maximum Vonmises Stress Vs Hollowness %
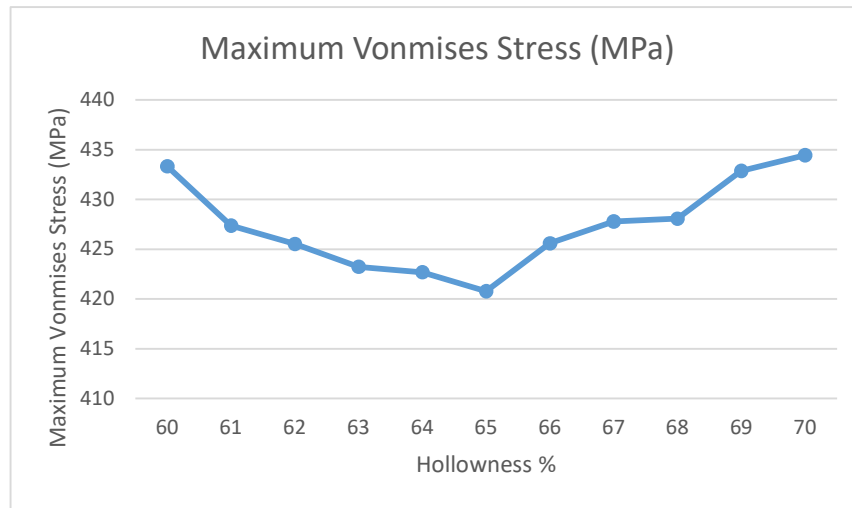


Graph 1 shows the relation between the Maximum von-mises stress (Mpa) Vs. Hollowness %. From graph we can observe that the maximum von-mises stress is continuously decreases up to 65% hollowness and then after it starts increases up to 70%. As we know that fatigue life is directly proportional to load carrying capacity, hence fatigue life will improve.

On the basis of above results calculating radial stiffness for hollow rolling element in the range of 60% to 70%.

Calculating radial stiffness for 60% hollowness[6].

➢ $K_1 = 7.86$ x $10^4$ $(l)^{8/9}$

   $= 7.86$ x $10^4$ $(19.96)^{8/9}$

   $= \mathbf{112.4917}$ x $\mathbf{10^4}$ $\mathbf{N/mm^{1.11}}$

➢ $K_n = 0.5^{1.11}$ x $K_1$

   $= 0.5^{1.11}$ x $112.4917$ x $10^4$

   $= \mathbf{52.1167}$ x $\mathbf{10^4}$ $\mathbf{N/mm^{1.11}}$

➢ $Q_{max} = K_n$ x $\S^{1.11}$

   $= 52.1167$ x $10^4$ x $(0.024016)^{1.11}$

   $= \mathbf{8308.167\ N}$

Accordingly calculation for bearing stiffness:

➢ $Ʌ = Q_{max}$ / $\S_{max}$

   $= 3548.60$ / $0.024016$

   $= \mathbf{345.943\ N/\mu m}$

Similarly, calculating radial stiffness for hollowness up to 70%.

Table 4: value of radial stiffness with respect to hollowness %

| Hollowness % | Radial Stiffness (N/µm) |
|---|---|
| 60 | 345.943 |
| 61 | 347.779 |
| 62 | 349.6878 |
| 63 | 351.6708 |
| 64 | 353.7293 |
| **65** | **355.8652** |
| 66 | 344.4256 |
| 67 | 332.9872 |
| 68 | 321.5488 |
| 69 | 310.1104 |
| 70 | 298.672 |

From the above table we can observe that the radial stiffness is maximum 355.865 N/µm at 65% hollowness and decrease up to 298.67311 N/µm at 70 % hollowness. Hence, the maximum radial stiffness value is at 65% hollowness. Therefore, the fatigue of hollow tapered roller bearing made up of chrome SAE 52100 bearing steel bearing will be maximum at 65% hollowness.

Graph 2: Radial stiffness (N/µm) Vs Hollowness %
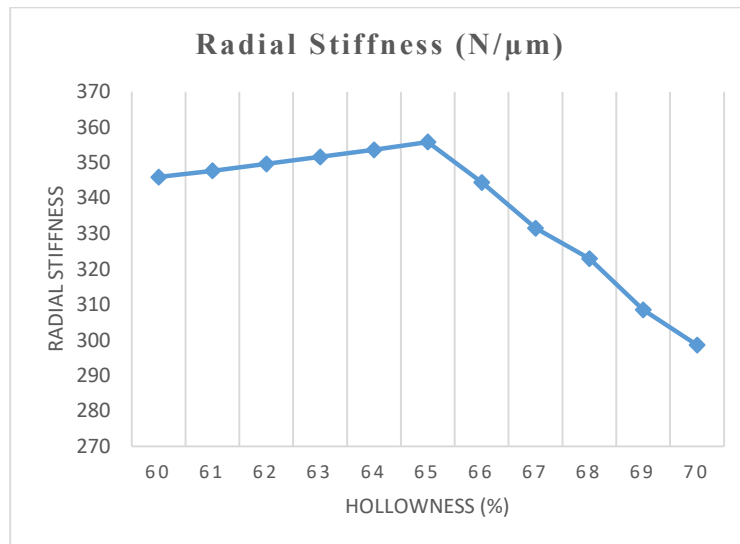


Graph 2 shows the relation between Radial stiffness (N/µm) Vs. Hollowness %. From graph we can observe that the Radial stiffness is continuously increases up to 65% hollowness and then after it deceasing and at 70% it has lowest stiffness value. Optimum value of radial stiffness lies is at 65% hollowness.

## 2. Conclusion:

In running condition bearings leads to heat and friction generation which has an adverse effect on bearing and automobiles system and leads to the problem as wear, tear and bad fuel economy, which leads to harmful environmental effects. Further, hollow rollers means less

weight, saving in material, permitted high speed, increase in stiffness, decrease in contact stress, longest fatigue life, less heat generation and more stability for the system.

Percentage of hollowness below 60% would be unusable for most application since there is no considerably advantage of using hollow roller bearing over solid roller bearing. On the other hand hollowness of 80% is having highest deflection value and limits the load carrying capacity. Thus 60% to 70% hollowness is the optimum range to achieve sufficient roller flexibility and load carrying capacity. Further, after observing the results 65% hollowness is the most desirable to impart sufficient roller flexibility and load carrying capacity for the roller made up of chrome SAE 52100 bearing steel. And by using a hollow rollers over solid rollers it improves heat dissipation by allowing the lubricant flow through the centre of the hollow rollers.

Hence, less heat generation can take place and it permits higher operating speed without affecting major losses in the engine due to the heat generation as well as with the high stiffness it serves the longest fatigue life by decreasing contact stress and improving load carrying capacity.

In present study, mechanical properties of chrome SAE 52100 bearing steel have been chosen. Optimum hollowness may differs based on the material of rollers. Further, harder the material higher the hollowness required to achieve the desired results and vice a versa.

**References:**

[1] B. G. Brothers and J. Halling (1965), "Effect of geometric conformity between rolling bodies on the slip and wear in the contact region", Proc Instn Mech Engrs, Vol. 179, p.p. 134-144.

[2] R. K. Upadhyay, L. A. Kumaraswamidhas, Md, Sikandar Azam (2013), "Rolling element bearing failire analysis: A case study", Engineering failure analysis, p.p. 15-17.

[3] Xiaolei Wang, Wei Liu, Fei Zhou and Di Zhu (2009), "Preliminary Investigation of the effect of dimple size on friction", Tribology International, p.p. 1118-1123.

[4] G. D. Bassan and D. P. Vakharia (2015), "Theoretical and Experimental Analysis of Tapered Roller Bearing for increasing Fatigue life", Proceeding of 1st International Conference on Tribology, TURKEYTRIB'15, Turkey, Paper ID-BET9.

[5] Shaik Mujeebur Rehman, Mulpur Sarat Babu, Yemineni Siva Siva Sankar Rao and TVRR Malleswara Rao (2016), "Fatigue, Model and Transient Analysis on the Tapered-Roller bearing", IJIRSET, p.p. 19108-19117.

[6] Tedric A. Harris, Rolling Element Bearing Analysis (John Wiley & Sons, New York, 2001)

# Influence of operating parameters on Biodiesel optimisation process using a heterogeneous catalyst in a membrane reactor

**O.A. Olagunju[1*], [2,3]P. Musonge**

[1]**Chemical Engineering Department, Durban University of Technology, Durban, South Africa.**

[2]**Institute of Systems Science, Durban University of Technology, Durban, South Africa.**

[3]**Faculty of Engineering, Mangosuthu University of Technology, Durban 4000, South Africa.**

*Corresponding author: gilbert4life2004@yahoo.com

## Abstract

The response surface methodology (RSM) was used to determine the optimal conditions for biodiesel production from soybean oil by using a central composite design. Four process variables were assessed ($2^4$ experimental designs). A total of 30 experiments were designed and conducted to study the effect of temperature, reaction time, methanol to oil molar ratio, and catalyst concentration (calcium oxide attached on activated carbon). Soybean oil methyl ester (SOME/biodiesel) yield of 96.9 % was obtained at different optimum conditions: 65 °C temperature, 90 min reaction time, 4.2:1 molar ratio of methanol to oil, and 3.0 wt. % catalyst concentration. A linear relationship between the experimental yield and predicted values of the biodiesel produced was developed. The biodiesel product was characterized and the fuel properties of the biodiesel such as kinematic viscosity, density, flash point, copper corrosion, calorific value, cloud point, pour point, ash content, and carbon residue were determined.

**Keywords:** Soybean oil, Biodiesel, Response surface methodology, Central composite design, Fuel properties.

## 1. INTRODUCTION

Fossil fuels are getting exhausted all over the world very fast due to increasing demand. Many countries in the world are in search of alternative sources of fuel for their energy need. In this regard, biodiesel is an alternative to diesel fuel due to several benefit such as biodegradability, non-toxic nature, and fewer emissions of CO, SO2, particulates, and hydrocarbons compared to conventional diesel (Yoosuk *et al*., 2010; Kafuku *et al*., 2010). Biodiesel can be produced from various sources like vegetable oils, greases, and animal fats. It is chemically known as fatty acid alkyl ester. Biodiesel can be produced by the transesterification of triglycerides with alcohol (commonly methanol) in the presence of acid or base catalyst into fatty acid methyl ester (FAME) (Dussan *et al*., 2010; TuThanh *et al*., 2010). Soyabean oil is one of the approved feedstocks for the production of biodiesel in South Africa and this serves as the basis for the use of the feedstock in this study. The government had approved large fertile land sites for the plantation of soya bean feedstock in Eastern Cape Province specifically for biodiesel production, thus eliminating the food-fuel debates (Amigun *et al*., 2011).

Primarily, the production of biodiesel has been by the conventional method. This involves the reaction of vegetable oil or animal fat with an alcohol (methanol) in the presence of

homogeneous basic catalysts (primarily sodium hydroxide or potassium hydroxide). Using a basic catalyst such as NaOH or KOH has a lot of disadvantages such as soap formation, difficulty in recovering which leads to downstream wastewater treatment and hence, increasing the cost of biodiesel production. The total cost of producing biodiesel using a homogenous catalyst is not sufficiently competitive enough compared to fuel produced from crude oil. Therefore, there is a need to consider an alternative process, which exhibits a less corrosive character leading to safer, cheaper, and more environment-friendly operation and eases the process of separating the catalyst from the product.

Heterogeneous catalysis with the use of a membrane reactor is an alternative process that can be used to overcome the challenges encountered by the homogenous process. In this process, the catalyst can be easily separated from the product and be further reused. There is also an integration of reaction and separations into a single process, thereby reducing separation costs and recycle requirements, resulting in higher conversions (Olagunju and Musonge, 2017).

Membrane separation technology has been extensively used in wastewater purification by various researchers because of its ability to carry out the separation of different components in a single process stream based on their molecular weight. In this process, reaction and separation take place within a single unit and therefore eliminates the need for a further purification step. Membrane reactors can selectively remove the product from the reaction mixture by allowing the component with lower molecular weight to pass through its pores while higher molecular weight components are rejected. This method also allows for proper contact between the immiscible reactants and catalyst and as a result, a higher yield of the product can be achieved (Westermann and Melin 2009).

South Africa is known to be a water-scarce country and the use of membrane technology to produce biodiesel will help to conserve water for other purposes as it will eliminate the use of water for purifying the product and makes the environment free from pollution. Baroutian *et al* (2011) had previously explored this technology, using potassium hydroxide as catalyst and palm oil as feedstock. However, the problem of membrane selectivity remains, which this study aims to address.

To find a solution to this problem of further purification step encountered with the use of membrane technology from previous studies, an estimation of the dispersed oil droplets size found in the permeate stream was carried out and then a suitable membrane pore size was selected. The minimum particle size in the oil-methanol emulsion can be estimated from the work of DeRoussel *et al* (2011) which showed that the average drop size for unreacted oil was 44 microns with a lower and upper size limit of 12 and 400 microns, respectively (DeRoussel *et al* 2011). Based on this finding, a membrane of 0.02 microns was selected for the current work, which was able to trap the unreacted oil within the membrane and allowed biodiesel and methanol to pass through it. The retention of free glycerol and unreacted oil in the reaction medium micro-filtrated by the 0.02 μm membrane eliminates the use of water in the process and therefore reduced the production cost.

Also, studying the optimization process is crucial for the development of maximizing the production of biodiesel. Conservatively, the optimization of the biodiesel production process was achieved with the variation of one factor at a time and the response is a function of a single parameter which is time overwhelming and excessive in cost (Olagunju and Musonge, 2017). This technique does not include interactive effects among the variables and it does not depict the complete effect of the parameters on the process (Olagunju and Musonge, 2017). However, the application of the response surface methodology (RSM) technique in a

multivariable system offers a research strategy in studying the interaction of the parameters using statistical methods.

The experiment model of biodiesel synthesis which is developed using response surface methodology can simulate the reaction under various transesterification conditions with good error estimation. This is helpful when mass production of biodiesel is needed.

Rashid *et al.* (2015) used RSM to optimize the process parameters in base catalytic methanolysis of sunflower seed oil for biodiesel production. In another study, Bojan *et al.* (2011) applied the same method for biodiesel production from high free fatty acid J. curcas oil. Response surface methodology was applied to optimize transesterification conditions for biodiesel production using acid oil and jajoba oil (Bouaid *et al.*, 2012; Chen *et al.*, 2013). In the present work, efforts were made to optimize the process conditions for transesterification reaction to increasing the yield of biodiesel from soybean oil in a membrane reactor. The influence of the variables such as temperature, reaction time, molar ratio, and catalyst concentration, on transesterification, was studied. The quality tests of the soybean oil methyl esters produced were also reported.

## 2. EXPERIMENTAL

### 2.1 Materials

Soybean oil was purchased from a local market. Methanol (99.8%) was supplied by Laboratory supplies co., South Africa. Pure calcium oxide (98.9%) was used as a catalyst for transesterification and was obtained from associated chemical enterprises, South Africa, and the activated carbon granules used as the catalyst support in this study were purchased from the same company.

### 2.2 Transesterification in the packed bed membrane reactor

Soybean oil and methanol were charged into the mixing tank separately. The volume ratio of oil to methanol was varied between 3:1 to 6:1 and the catalyst was packed into the membrane reactor. Methanol was charged continuously into the reactor using the circulating pump according to Olagunju and Musonge (2015) and the heat exchanger was started up to heat the reactants. Subsequently, the reactor was filled with the reactant. The pressure inside the membrane was monitored by two pressure gauges and was controlled at 100Kpa. The permeate stream containing biodiesel and methanol was collected in the beaker. After each run, the circulating pump and heat exchanger were switched off. Thereafter, the system was fully drained, the catalysts were taken out and the system was flushed for 30 min with methanol and then drained. Biodiesel yield in the present experiment was calculated by using the following equation (1):

*Biodiesel yield (%) = (Mass of the biodiesel / Mass of the oil used) \* 100%*       *(1)*

### 2.3 Experimental design

The effects of four transesterification variables on the yield of soybean oil methyl esters were evaluated using response surface methodology based on the central composite design (CCD)

with four factors varied at three levels: a high level, represented as (+1), a low level represented as (-1) and a middle point (0) consisting of 30 experiments. The design variables were temperature ($X_1$, $^{\circ}C$), reaction time ($X_2$, min), the molar ratio ($X_3$), and catalyst concentration ($X_4$) while the response variable was biodiesel yield (Y, %). The range and the levels of the independent variables chosen for the present study are presented in Table 1. Each experiment was performed in triplicates and the average yield of biodiesel was taken as the response variable Y.

**Table 1 – Experimental range and values for RSM**

| Variables | symbol | -1 | 0 | 1 |
|---|---|---|---|---|
| Temperature ($^{\circ}C$) | $X_1$ | 60 | 65 | 70 |
| Reaction time (minutes) | $X_2$ | 60 | 90 | 120 |
| Molar ratio | $X_3$ | 3:1 | 4:1 | 6:1 |
| Catalyst concentration | $X_4$ | 1 | 2.5 | 4 |
| Output | | | | |
| Biodiesel yield (%) | Y | | | |

### 2.4 Statistical analysis (ANOVA)

The polynomial equation raised to the order of two was then assigned to the obtained data by a multiple regression protocol. Thus complying with an empirical model which gives the nature between responses measured to the independent variables of the experiment. The empirical regression model equation for a four-factor system was taken as:

$$Y = \alpha 0 + \alpha 1X_1 + \alpha 2X_2 + \alpha 3X_3 + \alpha 4X_4 + \alpha 12X_1X_2 + \alpha 13X_1X_3 + \alpha 14X_1X_4 + \alpha 23X_2X_3$$
$$+ \alpha 24X_2X_4 + \alpha 34X_3X_4 + \alpha 11X_1^2 + \alpha 22X_2^2 + \alpha 33X_3^2 + \alpha 44X_4^2 \tag{2}$$

where $Y$ is the predicted response, $\alpha 0$ is the intercept, $\alpha 1$, $\alpha 2$, $\alpha 3$, $\alpha 4$ are linear coefficients, $\alpha 11$, $\alpha 22$, $\alpha 33$, $\alpha 44$ are squared coefficients, and $\alpha 12$, $\alpha 13$, $\alpha 14$, $\alpha 23$, $\alpha 24$, $\alpha 34$ are interaction coefficients and $X_1$ denoted temperature ($^{\circ}C$), $X_2$ was reaction time (min), $X_3$ was molar ratio and $X_4$ was catalyst concentration. The response of the CCD design was fitted with a second-order polynomial equation. Statistical analysis of the data was performed by Design-Expert version 10.0 (Stat Ease, Inc., Minneapolis, USA) to evaluate the analysis of variance (ANOVA), to determine the statistical significance of each term in the equation, the F value within the level of 95% and p-value of <0.05. The optimum values of the selected variables were obtained by analyzing the response surfaces and solving the regression equation. The fitted polynomial equation was expressed in the form of three-dimensional response surface plots to illustrate the main interactive effects of the independent variables.

## 3   RESULTS AND DISCUSSION

### 3.1 Experimental design based on central composite design

A central composite design was employed in this study to develop an experimental matrix of bio-organic reaction between temperature, reaction time, methanol: oil ratio, and catalyst concentration to maximize the biodiesel production by transesterification process in a

membrane reactor. The biodiesel yield varied between 48% to 96%. The application of the advanced multiple regression analysis was employed to obtain the polynomial equation with the coefficient of the full regression model equation and their statistical significance was determined. The equation of the significant terms obtained from the model in its coded form is as follows:

$$Y = 94.75 + 5.18X_1 + 3.60X_2 - 7.07X_3 + 4.24X_4 + 1.39X_1X_2 - 0.64X_1X_3 - 3.98X_1X_4 + 4.36X_2X_3 + 3.02X_2X_4 - 3.73X_3X_4 - 9.38X_1^2 - 1.50X_2^2 - 9.00X_3^2 - 3.63X_4^2 \tag{3}$$

Where Y is biodiesel yield and $X_1$, $X_2$, $X_3$, and $X_4$ were the coded forms of temperature ($^o$C), reaction time (min), methanol:oil ratio, catalyst concentration respectively. From the equation, the coefficient with one factor signifies the effect in an individual form while the coefficient which has two factors and second-order form signifies the interaction between themselves and other variables. The suffix symbols positive or negative (+/−) signifies the synergy and antagonistic effects, where the positive stands for synergistic effect and the negative stands for antagonistic effect (Joshi *et al.,* 2013). Then the model was analyzed by analysis of variance (ANOVA) for obtaining the fitness of the model employing the least square method. The study of this model variation is presented in Tables 2 and 3.

The statistical analysis of the regression equation by ANOVA showed that the R2 value (multiple correlation coefficient) was 0.9574 (R2 value >0.75 indicates fitness of the model). The obtained value presents the total variation of the data evaluated by our model and it is capable of explaining 95.74% of the total variation in the experimental observed parameters and their mutual interactions. The theoretical values of adj R2 and the pred R2 were 0.9176 and 0.8861 respectively, the difference between adjusted R2 and predicted R2 is less than 0.2 which signifies the model is good.

**Table 2: Experimental matrix results**

| Standard runs | Randomized runs | Coded factors | | | | Response Y |
|---|---|---|---|---|---|---|
| | | $X_1$ | $X_2$ | $X_3$ | $X_4$ | |
| 1 | 29 | -1 | -1 | -1 | -1 | 62 |
| 2 | 5 | 1 | -1 | -1 | -1 | 90 |
| 3 | 14 | -1 | 1 | -1 | -1 | 60 |
| 4 | 12 | -1 | 1 | -1 | -1 | 75 |
| 5 | 13 | -1 | -1 | 1 | -1 | 49 |
| 6 | 2 | 1 | -1 | 1 | -1 | 66 |
| 7 | 18 | -1 | 1 | 1 | -1 | 55 |
| 8 | 8 | 1 | 1 | 1 | -1 | 79 |
| 9 | 24 | -1 | -1 | -1 | 1 | 84 |
| 10 | 27 | 1 | -1 | -1 | 1 | 92 |
| 11 | 17 | -1 | 1 | -1 | 1 | 89 |
| 12 | 11 | 1 | 1 | -1 | 1 | 95 |
| 13 | 6 | -1 | -1 | 1 | 1 | 50 |
| 14 | 10 | 1 | -1 | 1 | 1 | 60 |
| 15 | 30 | -1 | 1 | 1 | 1 | 78 |
| 16 | 3 | 1 | 1 | 1 | 1 | 74 |
| 17 | 25 | -2 | 0 | 0 | 0 | 50 |
| 18 | 22 | 2 | 0 | 0 | 0 | 60 |
| 19 | 4 | 0 | -2 | 0 | 0 | 78 |
| 20 | 15 | 0 | 2 | 0 | 0 | 95 |
| 21 | 23 | 0 | 0 | -2 | 0 | 65 |
| 22 | 21 | 0 | 0 | 2 | 0 | 48 |
| 23 | 1 | 0 | 0 | 0 | -2 | 62 |
| 24 | 9 | 0 | 0 | 0 | 2 | 94 |
| 25 | 20 | 0 | 0 | 0 | 0 | 93 |
| 26 | 7 | 0 | 0 | 0 | 0 | 94 |
| 27 | 26 | 0 | 0 | 0 | 0 | 92 |
| 28 | 28 | 0 | 0 | 0 | 0 | 95 |
| 29 | 19 | 0 | 0 | 0 | 0 | 93 |
| 30 | 16 | 0 | 0 | 0 | 0 | 96 |

Fig. 3 represents the significant interaction between temperature (ºC) and reaction time (min), the variation in the biodiesel yield is depicted well in the plot; i.e. the biodiesel yield increases significantly by increasing both temperature and reaction time. The figure demonstrated that the conversion of oil to biodiesel increased as the reaction temperature and reaction time increased. This may be due to the reduction of viscosity of the oil as the temperature increases, which resulted in better mixing of oil with alcohol and faster separation of glycerol from biodiesel. This effect could be further explained using the Arrhenius equation which states that steady increases in reaction rate constant by temperature increase might cause the yield to increase. This result is in agreement with those reported in

the literature where higher reaction temperature and initial mixing of the immiscible reactants cause a higher production of biodiesel (Zabeti *et al.,* 2010).
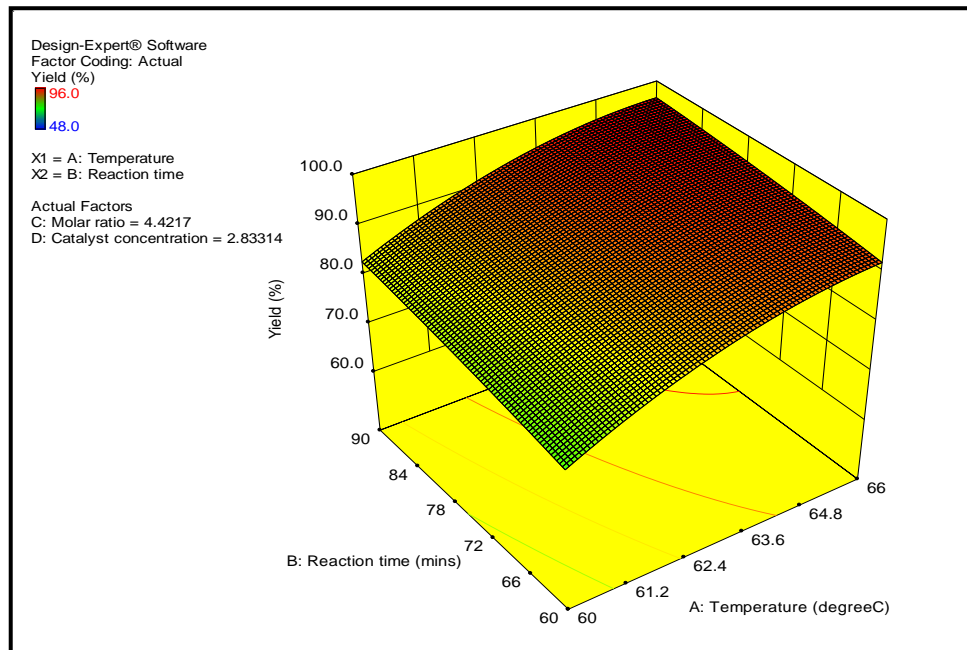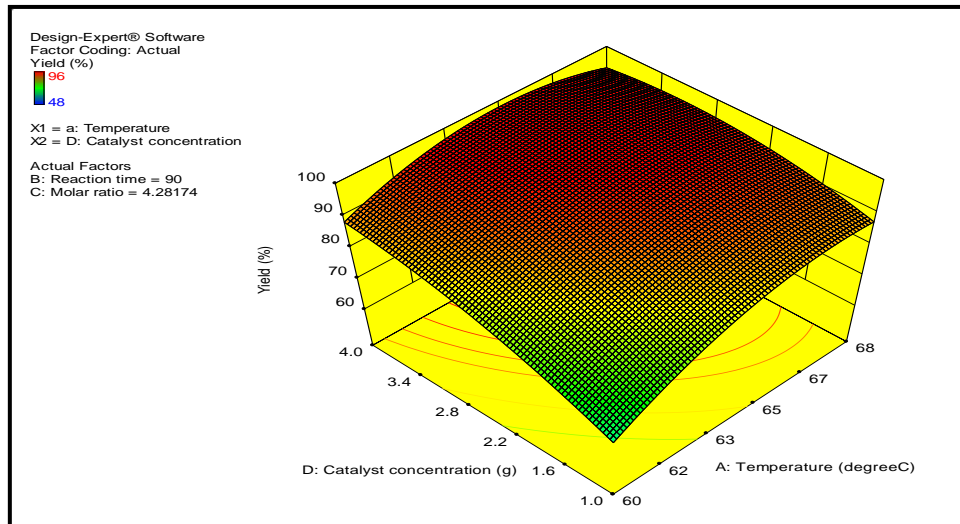


**Figure 3:** *Response surface 3D plot of predicted biodiesel yields versus reaction time and temperature*

Fig. 4 exhibits the effect of the catalyst concentration and reaction time at a temperature of 65 °C and a molar ratio of 4.4:1. The FAME yield increased with increasing catalyst concentration and reaction time. Then, there was a slight decrease when the reaction period was too long due to the influence of the reversible reaction in transesterification (Samart *et al.*, 2009). The 3D response curve reveals that there is a significant interaction effect between the catalyst concentration and reaction time on the FAME yield.
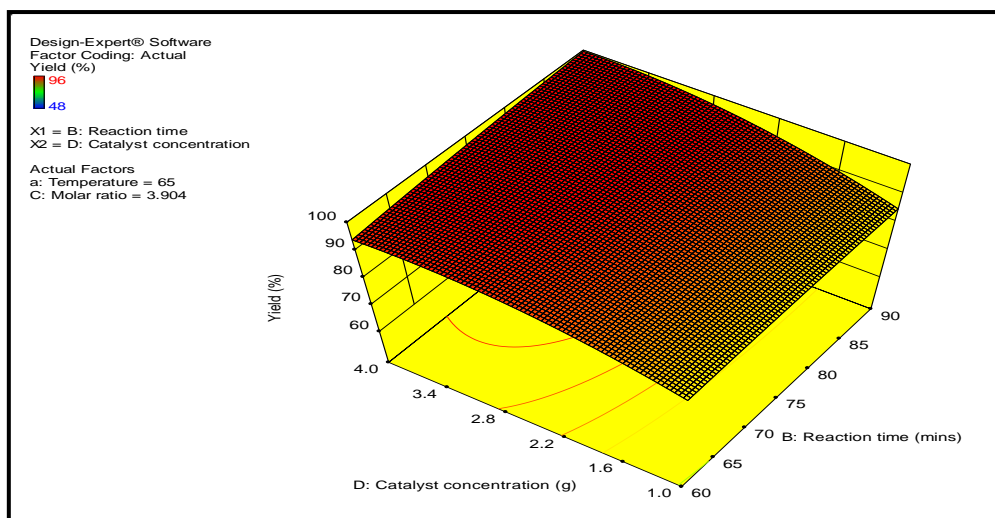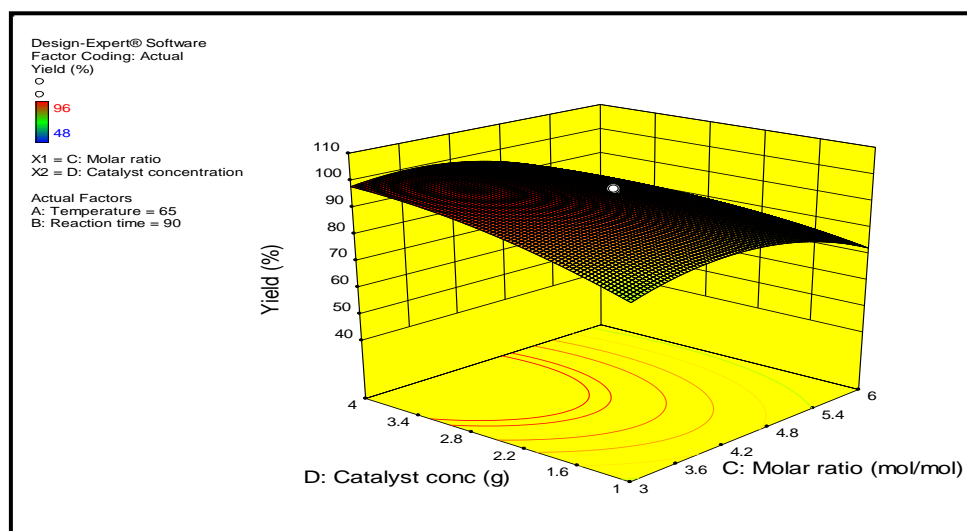


**Figure 4:** *Response surface 3D plot of predicted biodiesel yields versus reaction time and catalyst concentration*

Fig. 5 demonstrates that the conversion of feedstock to biodiesel increases as the reaction temperature and catalyst amount increase. However, at a higher catalyst amount, a reduction can be seen in the yield due to the catalyst concentration having a negative effect on the biodiesel produced. The decrease in yield at higher amounts of the catalyst can be attributed to the soap formation during the transesterification.



**Figure 5:** *Response surface 3D plot of predicted biodiesel yields versus temperature and catalyst concentration*

Fig. 6 shows the 3D contour plot at 90 min. reaction time and 65 °C. The FAME yield increases slightly with the increasing methanol-to-oil molar ratio and catalyst concentration. Then, the yield starts to decrease as the molar ratio increases. In general, a high molar ratio results in a higher rate of methyl ester formation and ensures completion of the reaction. However, overloading of methanol would inactivate the catalyst and reversed the reaction since transesterification is a reversible reaction (Wan Omar and Saidina Amin, 2011).



**Figure 6:** *Response surface 3D plot of predicted biodiesel yields versus molar ratio and Catalyst concentration*

**Table 4: Numerical optimization results and constraints for the factors/response.**

| Parameter | Goal | Experimental region | | Optimum condition | |
|---|---|---|---|---|---|
| | | Lower | Upper | Theoretical value | Experimental value |
| **Temperature (ºC)** | In range | 60 | 70 | 65 | 65 |
| **Reaction time (min)** | In range | 60 | 120 | 90 | 90 |
| **Catalyst concentration** | target | - | 3 | 3 | 3 |
| **Molar ratio** | In range | 3:1 | 6:1 | 4.2:1 | 4.2:1 |
| **Yield (%)** | Maximize | | | 97.7 | 96.9 |

### 3.2 Optimization study

Based on the model obtained and input criteria, the production of soybean biodiesel in the packed bed membrane reactor was optimized. The main objective of this study was to maximize the conversion of soybean oil to biodiesel. All the variables and responses with a respectively high and low limit to satisfy the creations defined for the optimum condition are listed in Table 4. To evaluate the accuracy of the developed model a transesterification experiment was carried out under the optimum conditions, the experiment was carried out three times, and the average was taken. The error values between the predicted and the observed results were less than 1% FAME yield indicating that the regression model was satisfactory.

## 4    CONCLUSION

In this study, we concluded experiments using RSM to determine the optimum reaction conditions for the production of biodiesel from soybean oil in a membrane reactor. The ceramic membrane with a pore size of 0.02 μm was very suitable for this reaction and separation process due to its high flux and the good quality of the permeate. High-quality biodiesel was produced without needing washing and purification steps. The effects of parameters including temperature, reaction time, molar ratio, and catalyst concentration were found significant. The highest conversion of 96.9 % was obtained at 65 ºC temperature, 90 min. reaction time, 4.2:1 molar ratio, and 3.0 wt. % catalyst concentration. The characteristics of the product under the optimum condition were within the ASTM standard and SANS standard.

## REFERENCES

Amigun, B., Musango, J.K. and Stafford, W. 2011. Biofuels and sustainability in Africa. *Renewable and Sustainable Energy Reviews 15(2):1360-1372.*

Baroutian, S., Aroua, M.K., Raman, A.A.A. and Sulaiman, N.M.N. 2011. A packed bed membrane reactor for production of biodiesel using activated carbon supported catalyst. *Bioresource Technology.* 102: 1095–1102.

Bojan, S.G., Chelladurai, S. and Durairaj, S.K. 2011. Response surface methodology for optimization of biodiesel production from high FFA Jatrophacurcas oil. *International Journal of Green Energy*. 8(6), 607–617.

Bouaid, A., Bajo, L., Martinez, M.and Aracil, J. 2012. Optimization of biodiesel production from jajoba oil Trans. Inst. Chemical Engineering. 85, 378–382.

Chen, X., Du, W.and Liu, D. 2013. Response surface optimization of biocatalytic biodiesel production with acid oil. *Biochemical Engineering Journal*. 40, 423–429.

DeRoussel, P., Khakhar, D. V. and Ottino, J. M. 2011. Mixing of viscous immiscible liquids. Part 2: over emulsification interpretation and use Chem. Eng. 56 5531

Dussan, K.J., Cardona, C.A., Giraldo, O.H., Gutierrez, L.F. and Perez, V.H. 2010. Analysis of a reactive extraction process for biodiesel production using a lipase immobilized on magnetic nanostructures. *Bioresource Technology*. 101, 9542–9549.

Guo, F., Peng, Z., Dai, J. and Xui, Z. 2010. Calcined sodium silicate as solid base catalyst for biodiesel production. *Fuel Processing Technology*, 91 (3):322.

Joshi, A., Pund, S., Nivsarkar, M., Vasu, K. and Shishoo, C. 2013. Dissolution test for site-specific release isoniazid pellets in USP apparatus 3 (reciprocating cylinder): optimization using response surface methodology. Eur. J. Pharm. Biopharm. 69 (2), 769–775.

Kafuku, G., Lam, M.K., Kansedo, J., Lee, K.T. and Mbarawa, M. 2010. Heterogeneous catalyzed biodiesel production from Moringaoleifera oil. *Fuel Processing Technology*. 91, 1525–1529.

Noordin, M.Y., Venkatesh, V.C., Sharif, S., Elting, S. and Abdullah, A. 2014. Application of response surface methodology in describing the performance of coated carbide tools when turning AISI 1045 steel. *Journal of Material Processing Technology*. 145 (1), 46–58.

Olagunju, O .A .and Musonge, P. 2015. The performance of a packed bed membrane reactor for the production of biodiesel 2nd Intl., Conf., on Composites, Biocomposites & Nanocomposites 28-30 October 2015 Durban University of Technology, South Africa.

Olagunju, O.A. and Musonge, P., 2017. Production of biodiesel using a membrane reactor to minimize separation cost. *Earth Environment science* .IOP Conference series. 78, 012019.

Rashid, U., Anwar, F. and Arif, M. 2015.Optimizationofbasecatalytic methanolysis of sunflower (*Helianthus annuus*) seed oil for biodiesel production by response surface methodology. *Industrial Engineering Chemical Resource*.48,1719–1726.

Samart, C., Sreetongkittikul, P. and Sookman, C. 2009. Heterogeneous catalysis of transesterification of soybean oil using KI/mesoporous silica. *Fuel Process Technology*,90:922–5.

TuThanh, L., Okitsu, K., Sadanaga, Y., Takenaka, N., Maeda, Y. and Bandow, H. 2010. Ultrasound-assisted production of biodiesel fuel from vegetable oils in a small scale circulation process. *Bioresource Technology*. 101, 639–645.

Wan Omar, W. N. N. and Saidina Amin, N. A. 2011. Optimization of heterogeneous biodiesel production from waste cooking palm oil via response surface methodology. Biomass and Bioenergy, vol. 35, no. 3, pp. 1329–1338.

Westermann, T. and Melin, T. 2009 Flow-through catalytic membrane reactors principles and applications Chem. Eng. Process. 48 17–28

Yoosuk, B., Krasae, P., Puttasawat, B., Udomsap, P., Viriya-empikul, N. and Faungnawakiji, K., 2010. Magnesia modified with strontium as a solid base catalyst for transesterification of palm olein. *Chemical Engineering Journal*. 162, 58–66.

Yuan, P., Liu, J., Zeng, G., Shi, J., Tong, J. and Huang, G. 2014. Optimization of conversion of waste rapeseed oil with high FFA to biodiesel using response surface methodology. *Renewable Energy*. 33 (7), 1678–1684.

Zabeti, M., WanDaud, W. M. A. and Aroua, M. K. 2010. Optimization of the activity of CaO/Al2O3 catalyst for biodiesel production using response surface methodology. *Applied Catalysis A*, 366:154–159.

# Optimizations of Electro-oxidation Process for the Treatment of Petrochemical RO reject using Response Surface Methodology

*Vishal Kumar Sandhwar[1]\*, Diksha Saxena[1], Shivendu Saxena[1]*

[1]Department of Chemical Engineering, Parul Institute of Technology, Parul University, Vadodara-391760, Gujarat, India

\*Corresponding author: vishal.sandhwar8850@paruluniversity.ac.in,

Mobile number: +91-8307070357

## Abstract

Even though reverse osmosis (RO) is one of the most prominent and effective techniques for wastewater treatment, but it also generates large amount of concentrated brine known as RO reject. The present work aimed to achieve maximum efficiency as well as optimal conditions for the treatment of petrochemical RO reject by electro-oxidation process using graphite electrodes. The Response Surface Methodology under Central Composite Design was utilized to examine the effect of various independent parameters such as reaction time, pH, current density and electrode distance on the removal efficiency. The maximum total dissolved solid (TDS) removal was obtained 51.16% at optimum conditions. 1st and 2nd order kinetic models were fitted to describe the best kinetic model for TDS removal.

**Keywords:** Electro-oxidation, RO reject, Total Dissolved Solid, Response Surface Methodology, Kinetic analysis

## 1. Introduction

Reverse osmosis (RO) is a highly efficient and eco-friendly membrane separation process to treat wide range of dissolved solids present in the aqueous solution. During RO treatment, approximately 50–80% of water is obtained as permeate (Sridhar et al., 2003) and rest of the amount (20-30%) formed as RO reject or also known concentrate and cannot be further treated by RO method because of high osmotic pressure. Huge amount of wastewater is generated during production of various petrochemical products such as High Density Polyethylene (HDPE), Mono Ethylene Glycol (MEG), Para xylene (PX), Purified Terephalic Acid (PTA) etc. (Verma et al., 2003). In some of petrochemical plants, RO efficiently treats generated wastewater but at the same time large quantity of RO reject forms having very high total dissolved solid (TDS) which need to be further treatment. Therefore, it is essential to treat RO reject or concentrate through an efficient treatment technique before its use or open discharge. Moreover, several conventional treatment techniques such as coagulation, flocculation, adsorption, advanced oxidation technologies, have been developed for the effective treatment/elimination of contaminants or pollutants from concentrate stream. Electrochemical methods have shown great potential for replacing or complementing conventional techniques since they are efficient, economical and eco-friendly. Electrochemical oxidation has several advantages for the treatment of RO reject as it can be used to treat RO concentrate streams with moderate to high salinity (Anglada et al., 2009), which favours good electric conductivity and also reduces the energy consumption (Van Hege et al., 2004; Dialynas et al., 2008; Zhou et al., 2011). Few studies have been reported for the treatment of RO rejects of different wastewaters such as textile, pharmaceutical etc. by different electrochemical methods (Urtiaga et al., 2013; Praneeth et al., 2014). The present study revealed the possibility of removal of TDS from petrochemical RO reject by electro-oxidation (EO) method using graphite electrodes. EO is an effective wastewater treatment technique where degradation takes place with the help of various oxidants such as nascent oxygen, hydrogen peroxide ($H_2O_2$), free chlorine and radicals. EO process occurs either as indirect EO method using electrochemically produced strong oxidants like hypochlorite/chlorine and $H_2O_2$ or as direct EO method in which oxidation takes place by physically adsorbed "active oxygen" (Maljaei et al., 2009). EO using graphite

electrodes takes place via combination of indirect oxidation of in-situ generated oxidizing agents as well as direct oxidation at anode surface (Cañizares et al., 2004; Raju et al., 2009). Further, an efficient optimization tool known as Response Surface Methodology was utilized to examine the effect of various independent parameters such as reaction time, pH, current density and electrolyte concentration to get maximum TDS removal.

## 2. Materials and Methods

### 2.1 Chemicals

Analytical grade chemicals were used in the entire study supplied by Ranbaxy Fine Chemical Limited, New Delhi, India as well as Loba Chemical Pvt. Ltd., Mumbai, India

### 2.2 Wastewater collection and characterization

Petrochemical RO reject was collected from the effluent treatment plant (ETP) of petrochemical complex in northern India. Entire pre-treatment characterizations were performed using standard methods prescribed by APHA (APHA, 1912). Initial TDS was found 3750 mg/L. Removal efficiency was calculated as follows.

$$\% \text{ Removal of TDS} = \frac{T_i - T_f}{T} \times 100 \tag{1}$$

Where, $T_i$- initial TDS, $T_f$- final TDS

## 3. Experimental

An open rectangular batch reactor was used to perform entire experiments. Graphite electrodes with an effective electrode area 131.2 cm$^2$ were used as anode and cathode during treatments. The schematic representation of experimental set up is shown in Fig.1. After each set of experiments, electrodes were cleaned by H$_2$SO$_4$ (5% v/v) and subsequently washed with water after each run.
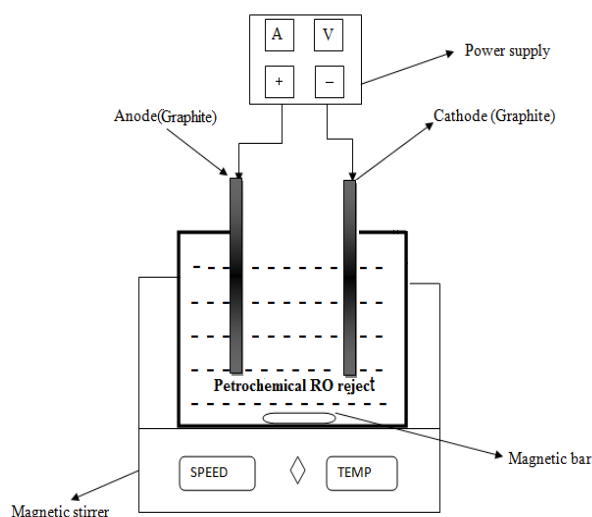


**Fig.1: Schematic diagram of experimental set up**

Optimization of independent parameters such as reaction time (20-100 min), pH: (1-9), current density (CD): (60.96-182.88 A/m$^2$), and electrode gap: (1-5 cm) was studied to get maximum TDS removal during EO treatment. The range for operating parameters during EO treatment is shown in Table 1.

**Table 1: Operating parameters and their levels obtained for EO treatment**

| | Central Composite Design characteristics | | | |
|---|---|---|---|---|
| Levels | Parameter (Range) | | | |
| | $X_1$ Time (min) (20→100) | $X_2$ pH (1-9) | $X_3$ CD (A/m$^2$) (60.96→182.88) | $X_4$ Electrode gap (cm) (1→5) |
| -2(-α) | 20 | 1 | 60.96 | 1 |
| -1 | 40 | 3 | 91.44 | 2 |
| 0 | 60 | 5 | 121.92 | 3 |
| +1 | 80 | 7 | 152.40 | 4 |
| +2(α) | 100 | 9 | 182.88 | 5 |

## 4. Results and Discussion

### 4.1 Influence of pH, current density, reaction time, and electrode gap on TDS removal

Oxidants such as hydrogen peroxide, nascent oxygen, free chlorine (Cl, ClO) and hydroxyl radicals (OH$^\bullet$) play pivotal role during EO treatment. At low pH, generation of strong oxidants like HOCl and $^\bullet$OH occurs rapidly (Guyot et al., 1990; Maljaei et al., 2009; Kushwaha et al., 2011) results higher removal. Formation of chlorate through oxidation of free chlorines and perchlorate through combination of HOCl and hypochlorite results lower removal at neutral pH. Hypochlorite ions are responsible for removal at high pH (Maljaei et al., 2009; Chen et al., 2003). In the Fig. 2 (a), it can be observed that TDS removal increased with pH and beyond optimum pH 5.32, it starts decreasing. Reaction time and current density (CD) are important parameters during EO treatment. Influences of current density and reaction time on TDS removal are shown in Figs. 2 (a) and 2 (b) respectively and observed that TDS removal continuously increases with CD and time. Increase in current density favours generation of electrons as well as H$_2$O$_2$ through catholic reduction of molecular oxygen results in higher removal [20, 54]. It was observed that beyond optimum conditions as mentioned in table 1, removal efficiencies start to decrease due to scavenging effect on available $^\bullet$OH radicals by excess amount of H$_2$O$_2$ (Raju et al., 2008; Maljaei et al., 2009).

$$H_2O_2 + {}^\bullet OH \rightarrow HO_2{}^\bullet + H_2O \tag{2}$$

Influence of electrode distance was also studied as shown in Fig. 2 (a). The optimum distance was found 4 cm. Based on the literatures, it can be said that there is a chance of higher electrical resistance due to accumulation of solid particles between electrodes results lower removal (Phalakornkule et al., 2010). Short electrode distance may also lead to short circuit due to presence of high current density between electrodes (Mameri et al., 1998). Removal of TDS starts to increases with electrode gap till optimum distance due to the slower movement of produced ions which favours more opportunity to aggregate and produce flocs. Beyond optimum electrode gap, due to weaker interaction of pollutants and flocs, efficiency decrease (Modirshahla et al., 2008).
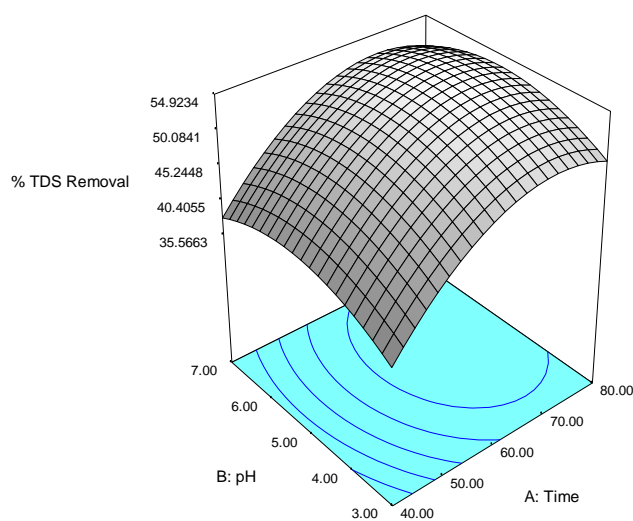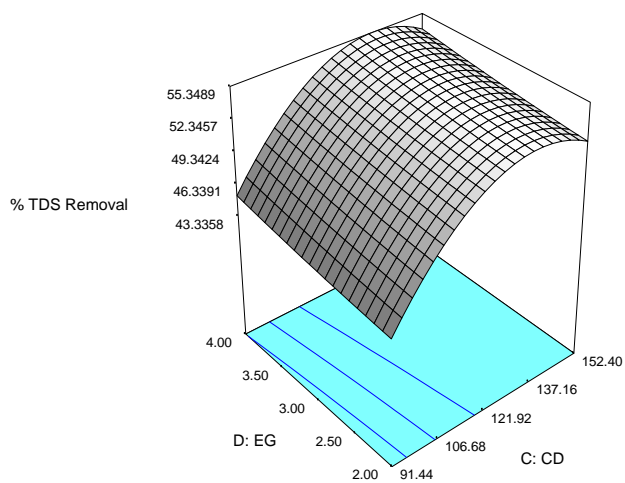
Figure 2 (a)



Figure 2 (b)

Figure 2. Effect of process parameters on % TDS removal

## 4.2 Optimization

Around thirty experiments based on the Central Composite Design (CCD) predicted set of operating parameters were performed to study the effect of operating variables such as reaction time, pH, CD, electrode gap on maximum removal of TDS. Table 2 indicates optimum variable conditions with CCD predicted and experimental results which also indicates an efficient CCD model.

Table 2 CCD predicted optimum operating conditions and their experimental and CCD predicted results

| | Time (min) | pH | CD (A/m$^2$) | Electrode gap (cm) | % Removal of TDS | |
| --- | --- | --- | --- | --- | --- | --- |
| | | | | | CCD (Pre.) | Test Run |
| EO | 72.03 | 5.32 | 139.55 | 4 | 57.69 | 51.16 |

where, T- TDS value, To= TDS at t = 0 and Tt= TDS at t = t, $k_1$ - Rate constant for 1st order, $k_2$ - Rate constant for 2nd order and t- time

## 5. Kinetic Study

The studies of kinetic during EO treatments at optimum parametric conditions as mentioned in Table 2 were shown in Figures 3 (a) and (b). First order and second order kinetic models were used to find best fit reaction order.

For 1$^{st}$ order: $\frac{-d\,(T)}{dt} = k_1(T_t)$ or $\ln\frac{T_o}{T_t} = k_1 t$ (3)

For 2$^n$ order: $\frac{-d\,(T_t)}{dt} = k_2(T_t)^2$ or $\frac{1}{T_t} - \frac{1}{T_o} = k_2 t$ (4)

Figs 3 (a) & (b) represents 1st & 2nd order plots for removal of TDS during EO treatments at optimum conditions. Higher rate constants (k) values indicates higher degradation rate, hence from the observed results it can be said that, TDS removal favours 2nd order rate kinetics due to high R$^2$ value as shown in Figures.
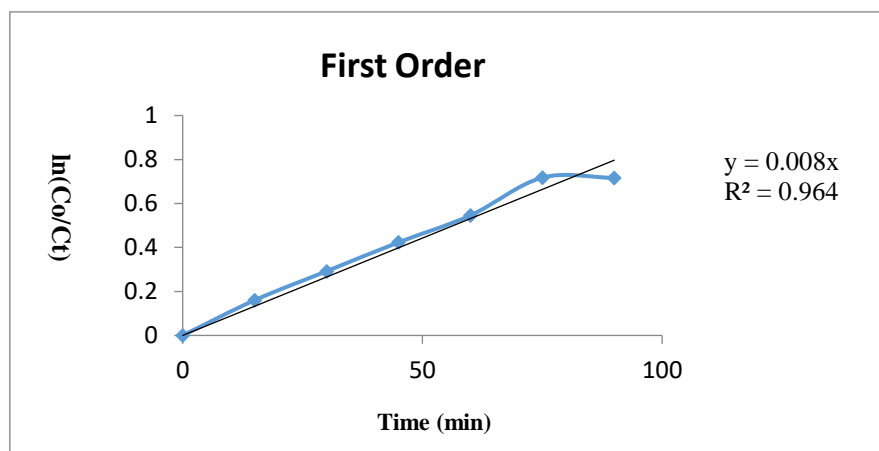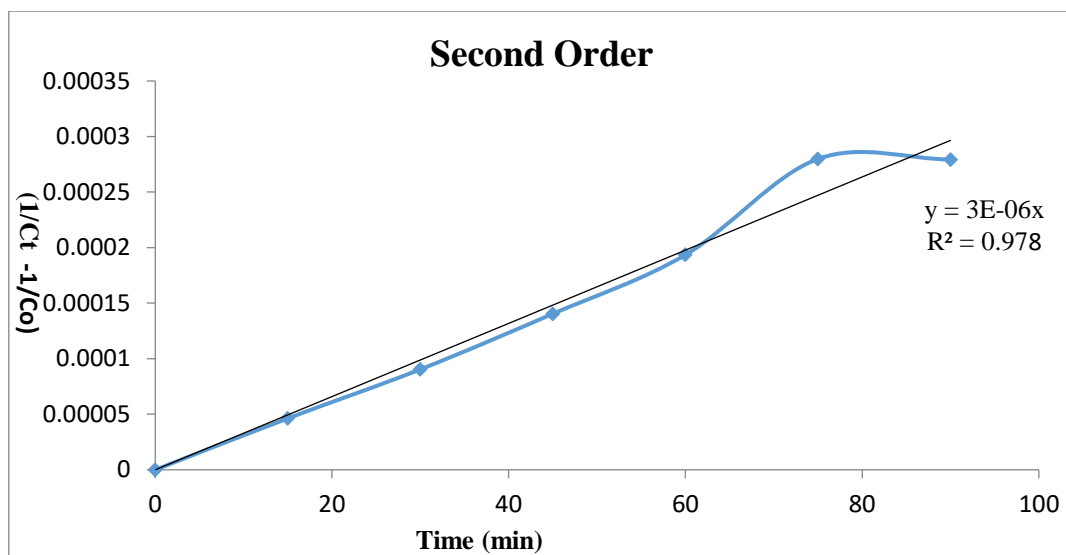


Figure 3 (a)

Figure 3 (b)

## 6. Conclusions

The performance of electro-oxidation treatment on the removal of TDS was investigated. It was observed that TDS removal is strongly dependent on solution reaction time, pH, current density and electrode gap during EO treatment. Maximum TDS removal 51.16% was obtained at optimum conditions such as pH 5.32, current density 139.55 A/m$^2$, reaction time 72.03 min and electrode gap 2 cm. Experimental and CCD predicted results shows an efficient CCD model. TDS removal favours 2$^{nd}$ order kinetic model.

## References:

1. Sridhar, S., Prasad, K.K., Murthy, G.S., Rao, A.G. and Khan, A.A., 2003. Processing of composite industrial effluent by reverse osmosis. *Journal of Chemical Technology & Biotechnology*, *78*(10), pp.1061-1067.
2. Verma, S., Prasad, B. and Mishra, I.M., 2010. Pretreatment of petrochemical wastewater by coagulation and flocculation and the sludge characteristics. *Journal of Hazardous materials*, *178*(1-3), pp.1055-1064.
3. Anglada, A., Urtiaga, A. and Ortiz, I., 2009. Contributions of electrochemical oxidation to waste-water treatment: fundamentals and review of applications. *Journal of Chemical Technology & Biotechnology*, *84*(12), pp.1747-1755.
4. Van Hege, K., Verhaege, M. and Verstraete, W., 2004. Electro-oxidative abatement of low-salinity reverse osmosis membrane concentrates. *Water Research*, *38*(6), pp.1550-1558.
5. Zhou, M., Liu, L., Jiao, Y., Wang, Q. and Tan, Q., 2011. Treatment of high-salinity reverse osmosis concentrate by electrochemical oxidation on BDD and DSA electrodes. *Desalination*, *277*(1-3), pp.201-206.
6. Dialynas, E., Mantzavinos, D. and Diamadopoulos, E., 2008. Advanced treatment of the reverse osmosis concentrate produced during reclamation of municipal wastewater. *Water research*, *42*(18), pp.4603-4608.
7. Praneeth, K., Manjunath, D., Bhargava, S.K., Tardio, J. and Sridhar, S., 2014. Economical treatment of reverse osmosis reject of textile industry effluent by electrodialysis–evaporation integrated process. *Desalination*, *333*(1), pp.82-91.
8. Urtiaga, A.M., Pérez, G., Ibáñez, R. and Ortiz, I., 2013. Removal of pharmaceuticals from

a WWTP secondary effluent by ultrafiltration/reverse osmosis followed by electrochemical oxidation of the RO concentrate. *Desalination*, *331*, pp.26-34.

9. Maljaei, A., Arami, M. and Mahmoodi, N.M., 2009. Decolorization and aromatic ring degradation of colored textile wastewater using indirect electrochemical oxidation method. *Desalination*, *249*(3), pp.1074-1078.

10. Raju, G.B., Karuppiah, M.T., Latha, S.S., Priya, D.L., Parvathy, S. and Prabhakar, S., 2009. Electrochemical pretreatment of textile effluents and effect of electrode materials on the removal of organics. *Desalination*, *249*(1), pp.167-174.

11. Cañizares, P., García-Gómez, J., Lobato, J. and Rodrigo, M.A., 2004. Modeling of wastewater electro-oxidation processes part II. Application to active electrodes. *Industrial & engineering chemistry research*, *43*(9), pp.1923-1931.

12. American Public Health Association, American Water Works Association, Water Pollution Control Federation and Water Environment Federation, 1912. *Standard methods for the examination of water and wastewater* (Vol. 2). American Public Health Association.

13. Guyot, J.P., Macarie, H. and Noyola, A., 1990. Anaerobic digestion of a petrochemical wastewater using the UASB process. *Applied Biochemistry and Biotechnology*, *24*(1), pp.579-589.

14. Prakash Kushwaha, J., Chandra Srivastava, V. and Deo Mall, I., 2011. Studies on electrochemical treatment of dairy wastewater using aluminum electrode. *AIChE journal*, *57*(9), pp.2589-2598.

15. Chen, X., Chen, G. and Yue, P.L., 2003. Anodic oxidation of dyes at novel Ti/B-diamond electrodes. *Chemical Engineering Science*, *58*(3-6), pp.995-1001.

16. Raju, G.B., Karuppiah, M.T., Latha, S.S., Parvathy, S. and Prabhakar, S., 2008. Treatment of wastewater from synthetic textile industry by electrocoagulation–electrooxidation. *Chemical Engineering Journal*, *144*(1), pp.51-58.

17. Phalakornkule, C., Polgumhang, S., Tongdaung, W., Karakat, B. and Nuyut, T., 2010. Electrocoagulation of blue reactive, red disperse and mixed dyes, and application in treating textile effluent. *Journal of environmental management*, *91*(4), pp.918-926.

18. Mameri, N., Yeddou, A.R., Lounici, H., Belhocine, D., Grib, H. and Bariou, B., 1998. Defluoridation of septentrional Sahara water of North Africa by electrocoagulation process using bipolar aluminium electrodes. *Water research*, *32*(5), pp.1604-1612.

19. Modirshahla, N., Behnajady, M.A. and Mohammadi-Aghdam, S., 2008. Investigation of the effect of different electrodes and their connections on the removal efficiency of 4-nitrophenol from aqueous solution by electrocoagulation. *Journal of Hazardous materials*, *154*(1-3), pp.778-786.

# Fluoride removal by capacitive deionization with rice husk waste derived microporous activated carbon electrode

*Mahendra S. Gaikwad [1*], Chandrajit Balomajumder[2]*

[1]Department of Chemical Engineering, Dharmsinh Desai University, Nadiad-387001, Gujarat, India.
[2]Department of Chemical Engineering, Indian Institute of Technology Roorkee, Roorkee-247667, Uttarakhand, India.

*Corresponding author. E-mail: mahendra14g@gmail.com

## Abstract

In the present work microporous rice husk activated carbon (MRHAC) electrode was fabricated from waste rice husk biomass which is easy available and largely generated in the agriculture field. This prepared MRHAC electrode was investigated in Fluoride electrosorption from the aqueous solution. The present MRHAC electrode shows maximum removal percentages of fluoride was found to 82.5% of initial feed concentration 10 mg/L at 1.2 V and flowrate 16 mL/min. The isotherm analysis study shows that Redlich Peterson and Langmuir isotherm models were fit with experimental results of the fluoride electrosorption. The rice husk waste derived microporous activated carbon was an effective electrode material for fluoride sorption from low concentrated aqueous solution.

**Keywords:** Fluoride, electrosorption, rice husk, electrode, capacitive deionization

## Nomenclatures

$C_e$    Concentration of adsorbate in solution at equilibrium (mg L$^{-1}$)
$Q_{e,i}^{exp}$    Experimental value of Qe (mg g$^{-1}$)
$Q_0$    Constant in Langmuir model (mg g$^{-1}$)
$Q_{e,i}^{cal}$    Predicted value of Qe (mg g$^{-1}$)
$K_{RP}$    Constant in R–P model (L g$^{-1}$)
$K_F$    Constant in Freundlich model (mg g$^{-1}$) / (mg L$^{-1}$)$^{1/n}$
$C_o$    Initial concentration of feed (mg L$^{-1}$)
$b$    Constant in Langmuir model (L mg$^{-1}$)
$V_f$    Feed volume in the feed tank (L)
$m$    mass of MRHAC electrode (g)
$n$    Constant in Freundlich model
$a_{RP}$    Constant in R–P model (L mg$^{-1}$)
$\beta$    Constant in R–P model
N    Number of observations in the experimental Isotherm
P    Number of parameter in regression model

## 1. Introduction

Fresh and pure drinking water is need of society. Global groundwater contamination with fluoride is also a serious issue (Amini et al., 2008). Fluoride present in several parts of the world groundwater. The areas most severely affected include East Africa, Middle East, Argentina, the United States, India, and China (Shen and Schäfer, 2014). Fluoride is geologically dispersed in the environment (Abe et al., 2004) and it is present in different rocks namely as basalt, granite, shale and syenite. These type of rocks can be responsible for contamination of groundwater with fluoride (Edmunds and Smedley, 2005). The anthropogenic process are also responsible environmental fluoride pollution. In general industries such as semiconductor manufacturing, electroplating, glass and ceramic production are responsible for the release of fluoride containing effluents (Shen et al., 2003). Fluoride cause the health

problems such as fluorosis problems, brittleness of bones and neurological damage (Fan et al., 2003). In recent years various techniques namely adsorption, electrochemical precipitation, ion exchange, reverse osmosis, membrane etc. have been used for the removal of fluoride although this technique is not ideal as it requires high energy, has a high operating cost and generate secondary waste (Fan et al., 2003; Gaikwad and Balomajumder, 2018). There is need to develop new technology to remove fluoride which work with less energy consumption. The development of sustainable electrode material for fluoride removal capacitive deionization is the greater challenge for the researcher. Recently, a few studies have identified related materials used for electrode preparation for fluoride removal by capacitive deionization (CDI) such as NiAl-layered metal oxide (Bai et al., 2019), Limonia acidissima shell activated carbon (Gaikwad and Balomajumder, 2018), Tea waste activated carbon (Gaikwad and Balomajumder, 2017a), Activated carbon (Mossad and Zou, 2012; Gaikwad and Balomajumder, 2017b) carbon (Pan et al., 2018), cellulose-derived and layer-by-layer stacked carbon fiber network (Pugazhenthiran et al., 2015). In the present study, main objective is fabrication of effective activated carbon electrode from waste rice husk for the treatment of fluoride contaminated water by CDI process.

## 2. Materials and method

### 2.1 Chemical and electrodes preparation

The waste rice husk was collected from the local agricultural place at Roorkee, India. The chemical and materials required for electrode preparation are graphite powder (Loba Chemie) polyvinylidene fluoride (HIMEDIA lab. Mumbai) N, N-dimethylacetamide (Loba Chemie). At the start whole collected waste rice husk was washed and dried. The acid treatment and thermal treatment for conversion of rice husk in to activated carbon and further its electrode preparation was carried out as mentioned in our previous study (Gaikwad and Balomajumder, 2020).

### 2.2 CDI experiment

The experiments were conducted with self-made CDI experimental set up shown in Fig.1. Two MRHAC electrodes were used in self-made CDI set up. The nylon net in placed between two MRHAC electrodes which provide channel for feed flow also it avoid any short circuits. Complete setup was closely packed with a Plexiglas sheet by nut and bolts. The fluoride aqueous feed was passed to CDI cell by a peristaltic pump (optimized flowrate 16 mL/min) and retransfer in a source tank. The 1.2 V potential supplied to MRHAC electrodes with DC power supply. The conductivity of solution was measured by digital conductive meter. The fluoride concentration was checked by ion chromatography (Metrohm compact IC, Switzerland). The electrosorption capacity was find at equilibrium $(q_e)$ by Eq. (1).
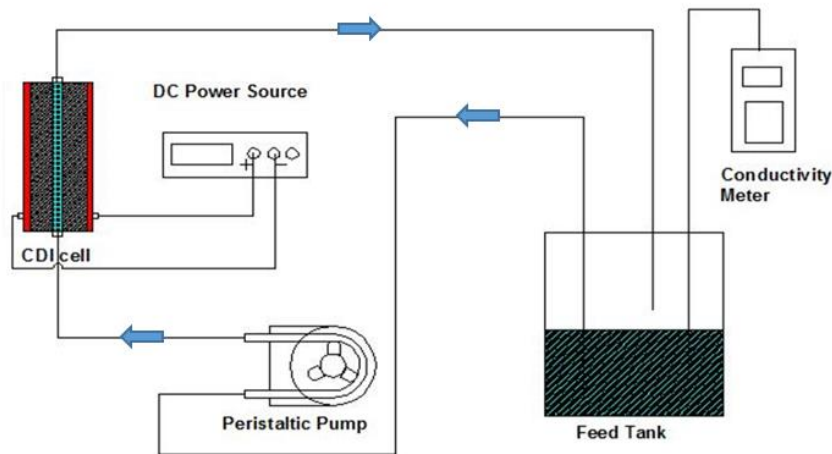
$$q_e = \frac{(C_o - C_e)V_f}{m} \qquad (1)$$

Figure 1. Schematics of self-made CDI experimental set up

## 3. Results and discussion

### 3.1 Fluoride removal by MRHAC electrode

The fluoride removal study conducted with self-made experimental set up of capacitive deionization with MRHAC electrode. The concentration rage of feed solution was varied from 10 mg/L to 100 mg/L. The graphical plot of maximum removal percentage at different feed concentration shown in Fig. 2. Maximum removal of fluoride was found to 82.5 % for 10 mg/L fluoride feed solution. The removal percentage decreases with increasing in feed concentration (Gaikwad and Balomajumder, 2017a, 2018).
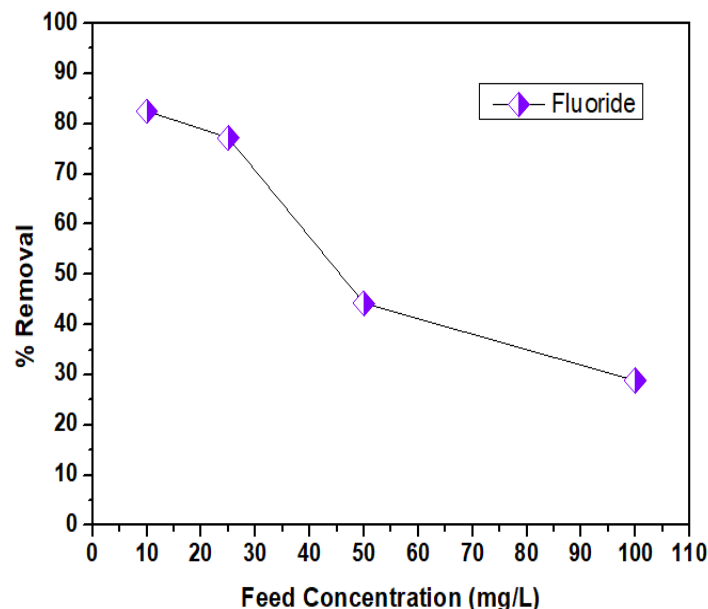


Figure 2. MRHAC electrode performance profile for Fluoride removal

### 3.2 Isotherm study

In the isotherm study, Langmuir, Freundlich, and Redlich Peterson models were used (Özkaya, 2006; Gaikwad and Balomajumder, 2017b) and mentioned below as eq. (2), (3) and (4) respectively.

$$q_e = (Q_0 b C_e)/(1 + b C_e) \qquad (2)$$

$$q_e = K_F C_e^{1/n} \qquad (3)$$

$$q_e = \frac{K_{RP} \times C_{eq}}{1 + a_{RP} \times C_{eq}^{\beta}} \qquad (4)$$

The Marquardt's sercent standard deviation (MPSD) was used in present study to find best fit isotherm model and equilibrium adsorption data (Annadurai et al., 2000; Gaikwad and Balomajumder, 2017b).

$$MPSD = 100 \sqrt{\frac{1}{N-P} \sum_{i=1}^{n} \left( \frac{Q_{e,i}^{exp} - Q_{e,i}^{cal}}{Q_{e,i}^{exp}} \right)^2} \qquad (5)$$

The isotherm modeling was done to find the best fit model with the experimental results. Comparative results of monocomponent isotherm models and experimental data are depited in Fig. 3. indicate that best fiiting isother model with experiemntal results. The Langmuir and Redlich Peterson models were found best fitting with experimental results.
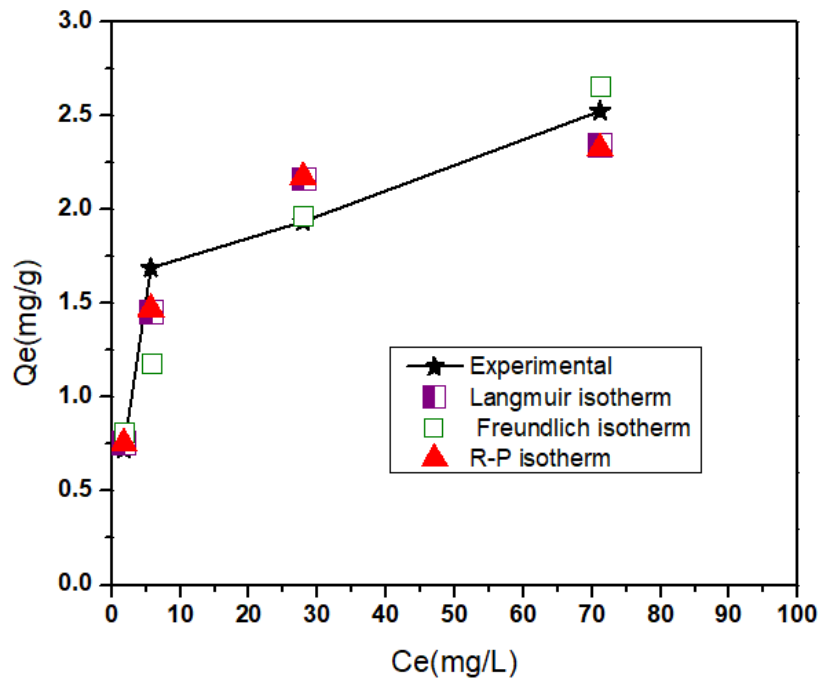


Figure 3. Isotherm model fitting with experimental data of fluoride removal by MRHAC electrode

## 4. Conclusions

The MRHAC electrode was made from rice husk activated carbon. It was found to very effective for fluoride removal (82.5 %) from the 10 mg L$^{-1}$ aqueous feed. The fluoride ion sorption process substantially follows the Langmuir and Redlich Peterson isotherm model trend. Thus, MRHAC CDI electrode could be a capable electrode for treatment of low concentrated fluoride feed.

**References**

1. Abe, I., Iwasaki, S., Tokimoto, T., Kawasaki, N., Nakamura, T., Tanada, S., 2004. Adsorption of fluoride ions onto carbonaceous materials. J. Colloid Interface Sci. 275, 35–39.
2. Amini, M., Mueller, K., Abbaspour, K.C., Rosenberg, T., Afyuni, M., Møller, K.N., Sarr, M., Johnson, C.A., 2008. Statistical modeling of global geogenic fluoride contamination in groundwaters. Environ. Sci. Technol. 42, 3662–3668.
3. Annadurai, G., Babu S.R., Mahesh, K.P.O., Murugesan, T., 2000. Adsorption and bio-degradation of phenol by chitosan-immobilized Pseudomonas putida (NICM 2174). Bioprocess Eng. 22(6), 493-501.
4. Bai, Z., Hu, C., Liu, H., Qu, J. 2019. Selective adsorption of fluoride from drinking water using NiAl-layered metal oxide film electrode. J. Colloid Interface Sci. 539, 146–151.
5. Edmunds, M., Smedley, P., 2005. Fluoride in natural waters. In Essentials of Medical Geology, Impacts of Natural Environment on Public Health, Elsevier Academic Press.
6. Fan, X., Parker, D.J., Smith, M.D., 2003. Adsorption kinetics of fluoride on low cost materials. Water Res. 37, 4929–4937.
7. Gaikwad, M.S., Balomajumder, C. 2017a. Tea waste biomass activated carbon electrode for simultaneous removal of Cr(VI) and fluoride by capacitive deionization. Chemosphere 184, 1141–1149.
8. Gaikwad, M.S., Balomajumder, C. 2017b. Simultaneous electrosorptive removal of chromium(VI) and fluoride ions by capacitive deionization(CDI): multicomponent isotherm modeling and kinetic study. Sep. Purif. Technol. 186, 272–281.
9. Gaikwad, M.S., Balomajumder, C. 2018. Removal of Cr(VI) and fluoride by membrane capacitive deionization with nanoporous and microporous Limonia acidissima (wood apple) shell activated carbon electrode. Sep. Purif. Technol. 195,305-313.
10. Gaikwad, M.S., Balomajumder, C., Tiwari, A.K. 2020. Acid treated RHWBAC electrode performance for Cr(VI) removal by capacitive deionization and CFD analysis study. Chemosphere 254, 126781.
11. Gupta, N., Balomajumder, C., Agarwal, V.K., 2012. Adsorption of cyanide ion on pressmud surface: a modeling approach. Chem. Eng. J. 191, 548-556.
12. Kumar, S., Zafar, M., Prajapati, J.K., Kumar, S., Kannepalli, S., 2011. Modeling studies on simultaneous adsorption of phenol and resorcinol onto granular activated carbon from simulated aqueous solution. J. Hazard Mater. 185, 287-294.
13. Mossad, M., Zou, L., 2012. A study of the capacitive deionisation performance under various operational conditions. J. Hazard. Mater. 213–214, 491–497.
14. Ozkaya, B., 2006. Adsorption and desorption of phenol on activated carbon and a comparison of isotherm models. J. Hazard Mater. 129, 158-163.
15. Pan, J., Zheng, Y., Ding, J., Gao, C., Van der Bruggen, B., Shen, J. 2018. Fluoride removal from water by membrane capacitive deionization with monovalent anion selective membrane. Ind. Eng. Chem. Res. 57(20), 7048–7053.
16. Pugazhenthiran, N., Sen Gupta, S., Prabhath, A., Manikandan, M., Swathy, J.R., Raman, V.K., Pradeep, T., 2015. Cellulose derived graphenic fibers for capacitive desalination of brackish water. Acs Appl. Mater. Inter. 7(36), 20156-20163.
17. Shen, F., Chen, X., Gao, P., Chen, G., 2003. Electrochemical removal of fluoride ions from industrial wastewater. Chem. Eng. Sci. 58, 987–993.
18. Shen, J. Schäfer, A. 2014. Removal of fluoride and uranium by nanofiltration and reverse osmosis:A review, Chemosphere 117,679–691.

# Optimization of the yield of mango wood pyrolysis oil produced using a semi-batch reactor

*Ajay Sharma [1,*], Bikash Mohanty [1]*

[1]Department of Chemical Engineering, Indian Institute of Technology Roorkee, India– 247667

*Corresponding author: asharma@ch.iitr.ac.in, 0133228–6371

**Abstract**

The present study deals with the pyrolysis of mango wood sawdust as a feedstock to produce pyrolysis oil. The study covers the optimization of process variables for the maximization of pyrolysis oil production. Three process variables with their operating ranges; particle diameter (0.2 to 0.6 mm), reaction temperature (450 to 650 °C), and $N_2$-gas flow rate (50 to 150 ml/min) have been selected to find their optimum values for maximization of pyrolysis oil production based on a set of nine experiments carried on a lab-scale semi-batch pyrolysis setup. The optimization results demonstrate maximum pyrolysis oil (44.5 mass%) production at a particle diameter of 0.6 mm, reaction temperature of 550 °C, and nitrogen gas flow rate of 100 ml/min. Further, the FT-IR and GC-MS analysis of pyrolysis oil has shown the presence of alcohols, acids, aldehydes, ketones, and carboxylic acids in it.

**Keywords:** Mango wood; Pyrolysis oil; Optimization; Semi-batch reactor; GC-MS.

## 1. Introduction

During the past few decades due to the changing scenario of the energy crisis, researchers have shown remarkable interest in the advancement of bio-fuel production. Interest in biomass fast pyrolysis is rapidly increasing all over the world as it is perceived to offer economic advantages over other thermal conversion processes. This is because the liquid product can be stored until required or readily transported to where it can be most effectively utilized. Pyrolysis, a process of thermochemical decomposition of organic material at elevated temperatures (>300 °C) in the absence of oxygen (or any $H_2$), is a promising technology to convert solid biomass to gasoline–range aromatics (a liquid fuel) directly that can be readily stored or transported.

Literature shows (Ahmad et al., 2020; Guedes et al., 2018; Mutsengerere et al., 2019; Qureshi et al., 2018) a limited number of systematic studies for optimizing process parameters for the production of pyrolysis oil in semi-batch pyrolysis reactor. Also, hardly any study has been carried out for the extraction yield of pyrolysis oil from mango wood along with maximization of pyrolysis oil yield based on a set of random run experiments. Thus, the present study is devoted to the extraction of pyrolysis oil from mango wood sawdust. Process parameters such as particle size, pyrolysis temperature and the inert gas ($N_2$) flow rate influence the yield of oil during pyrolysis in a semi-batch reactor. Thus, the effects of these parameters on pyrolysis oil yield have been investigated and the optimum condition obtained by a set of nine random experiments. Further, characterization of obtained pyrolysis oil have also been made using methods like Fourier transform infrared spectroscopy (FTIR) and gas chromatography-mass spectroscopy (GC–MS).

## 2. Materials and methods

### 2.1 Feedstock preparation

Mango wood sawdust used in the present study was collected from a sawmill at Meerut, Uttar Pradesh (India). It was then heated in an air oven at 105 °C for 30 minutes and separated as 0.2 mm, 0.4 mm, and 0.6 mm particle size groups using certified test sieves.

### 2.2 Pyrolysis setup

A lab-scale pyrolysis setup operating in a semi-batch mode is used for the extraction of oil from mango wood sawdust. The schematic of the experiment setup is shown in Fig. 1.
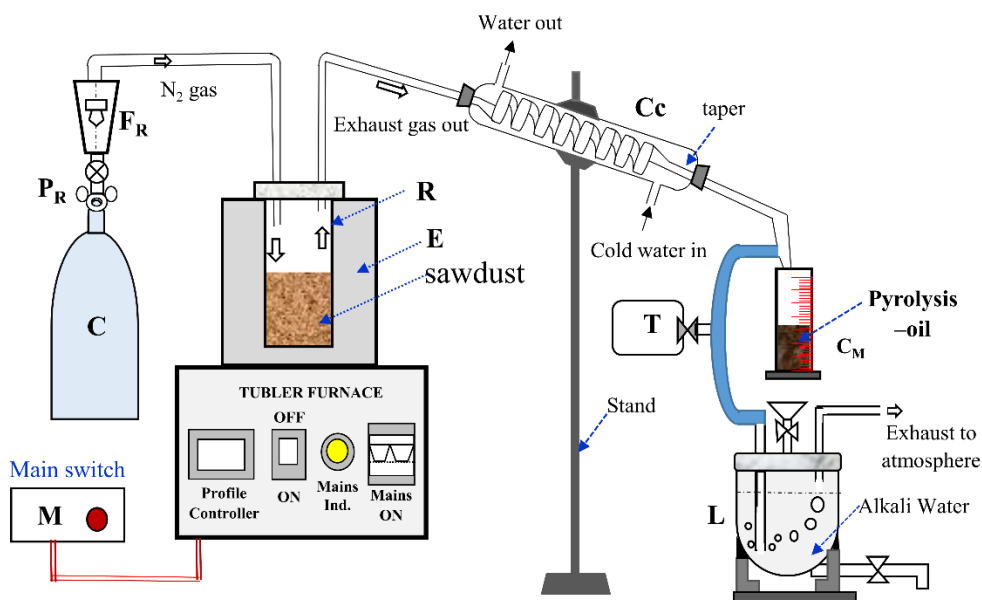


M–Main switch; C– gas cylinder; $P_R$– pressure regulator; $F_R$– gas flow rotameter;
R– pyrolysis reactor; E– electric furnace; Cc– glass coil condenser; T– Tedlar bag;
$C_M$– measuring cylinder; L– liquid tank

Figure 1. Schematic diagram of the pyrolysis setup

The details of the pyrolysis setup are given below:

$N_2$ gas from the gas cylinder (C) passed through pressure regulator ($P_R$) to gas flow rotameter ($F_R$) to control the flow rate of $N_2$ before it flows through the pyrolysis reactor (R) in which mango wood sawdust sample (25 g) was placed. The 304 stainless-steel semi-batch reactor (R) (5 cm I.D. and 16 cm length) has two openings at the top, one for inert gas ($N_2$) inlet and the other for pyrolysis vapors out. The reactor was heated by an electric furnace (E) to achieve the desired temperature (450 to 650 °C) of the sawdust material inside the reactor. The inside temperature of the reactor was measured with a K–type thermocouple and controlled by a PID controller.

### 2.3 Experimental Procedure

Initially, 25 g of mango wood sawdust sample was kept inside the reactor (R). Before each experimental run (given in Table 1), the semi-batch reactor (R) was purged with $N_2$-gas with a

flow rate of 100 ml/min for 7 minutes to create an oxygen-free environment. After that, $N_2$ gas flow rate (50, 100, and 150 ml/min) and reactor temperature (450, 550, and 650 °C) were set according to different experimental runs as detailed in Table 1. Once the temperature of reactor reached its set value, the reactor was kept at that temperature until no further release of pyrolysis vapors was observed. The condensable plus non-condensable gases coming out of the reactor (R) were cooled by a glass coil condenser ($C_C$) to condense the condensable part of the gas which provided a brown color liquid, which was collected in a measuring cylinder ($C_M$). The non-condensable gases coming out of the condenser ($C_C$) were collected in a Tedlar bag (T) for sampling and the remaining gases were vented to atmosphere after giving it an alkali wash in a tank (L). After the completion of the experiment, the bio-char was recovered from the bottom of the cooled reactor. The mass% yield of pyrolysis oil was calculated using Eq. (1) as given below:

$$\text{mass\% yield of pyrolysis oil} = \frac{\text{mass of pyrolysis oil}}{\text{mass of fed raw material}} \times 100 \tag{1}$$

## 2.4 Methodology used for the optimization of operating parameters for maximum pyrolysis oil production

A set, of nine experiments, was performed to find the maximum yield of pyrolysis oil as a function of three operating parameters. The first series of experiments (Runs -I, II, III) was performed to investigate the effect of particle diameters (0.2, 0.4, and 0.6 mm) of sawdust sample on the mass% yield of pyrolysis oil. For each experimental run (Runs -I, II, III), the feed sample was pyrolyzed at a fixed temperature of 550 °C and a gas flow rate of 100 ml/min. The second series of experiments (Runs -IV, V, VI) determined the effect of temperature (450, 550, 650 °C) on yield of pyrolysis oil while keeping the remaining two parameters fixed at 0.6 mm and 100 ml/min. The third series of experiments (Runs -VII, VIII, IX) investigated the effect of $N_2$-gas flow rate (50, 100, and 150 ml/min) on pyrolysis oil yield while keeping the remaining two parameters fixed at 0.6 mm and 550 °C.

Table 1 Experimental runs undertaken for the maximization of pyrolysis oil yield of mango wood sawdust

| Operating parameters with their ranges→ | Particle diameter (0.2 to 0.6) mm | Temperature (450 to 650) °C | $N_2$-gas flow rate (50 to 150) ml/min |
|---|---|---|---|
| Runs -I, II, III | 0.2, 0.4, 0.6 | 550 | 100 |
| Runs -IV, V, VI | 0.6 | 450, 550, 650 | 100 |
| Runs -VII, VIII, IX | 0.6 | 550 | 50, 100, 150 |
| For Example; | | | |
| Run I | 0.2 mm | 550 | 100 |
| Run IX | 0.6 | 550 | 150 |

## 3. Results and discussion

### 3.1 Influence of pyrolysis parameters on pyrolysis oil yield

A set, of nine experiments, has been performed for the pyrolysis of wood sawdust and the results obtained are shown in Fig. 2.

**550 °C, 100 ml/min**

(a)

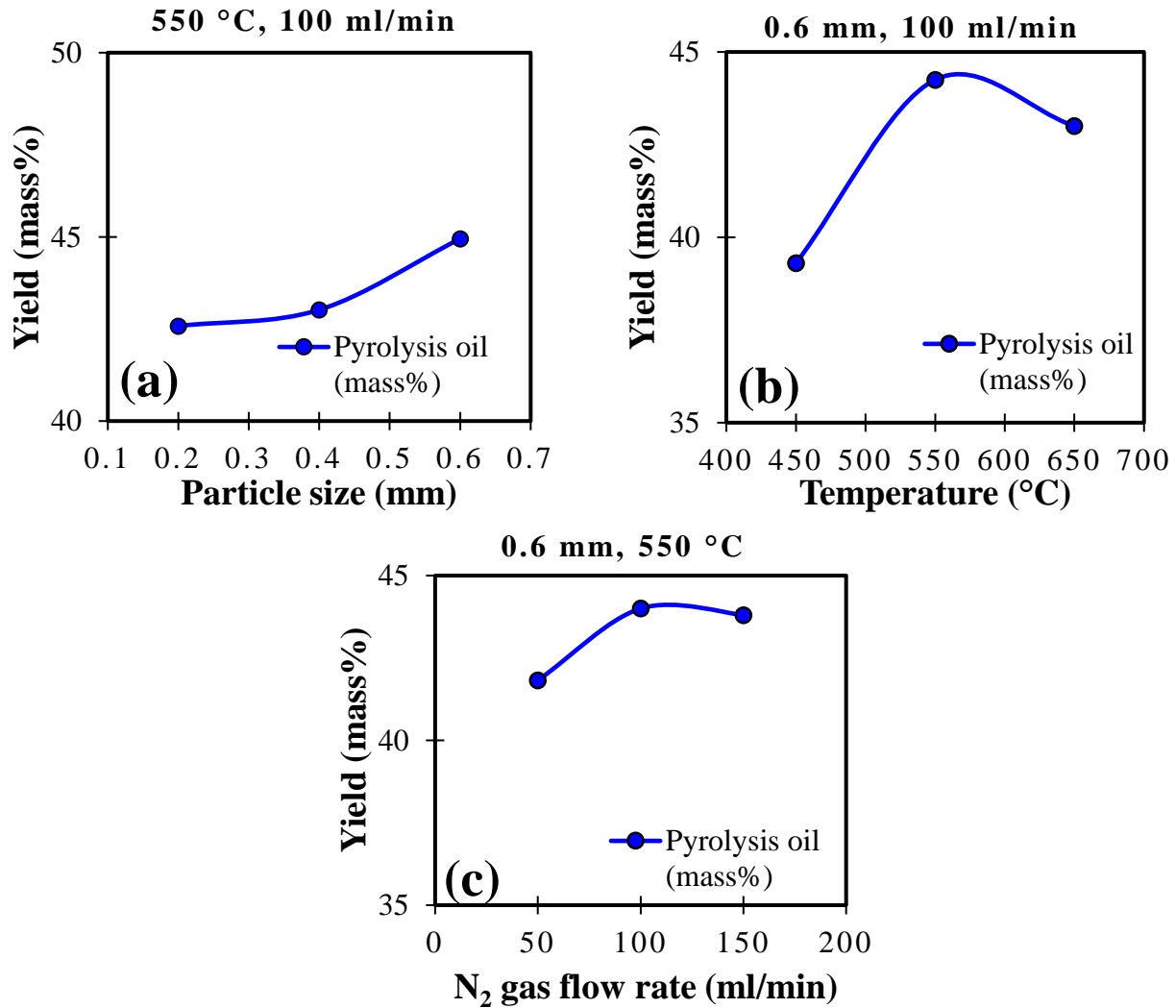**0.6 mm, 100 ml/min**

(b)

**0.6 mm, 550 °C**

(c)

Figure 2. Yield (mass%) of the pyrolysis oil released during the pyrolysis of mango wood sawdust from semi-batch pyrolysis unit; (a) Yield vs particle size (b) Yield vs temperature (c) Yield vs $N_2$-gas flow rate

The effects of three independent parameters (particle size, temperature, and $N_2$-gas flow rate) taking one at a time on the yield of pyrolysis oil while keeping the other two parameters fixed at their middle value are discussed below;

Fig. 2(a) showed that an increase in particle size from 0.2 to 0.6 mm, increased the pyrolysis oil yield. In this case, the flow rate of pyrolysis vapors from the reactor (R) depends on the porosity of the bed and penetration of heat into the solid particle within the bed. When the particle size is small, lumps of particles are formed in the reactor as the particles are not completely dry. This

inhibited proper penetration of heat into the lump and subsequent generation of pyrolysis vapors. Further, this also inhibited the $N_2$ gas to drive out pyrolysis vapor generated at the surface of the particle and thus accelerate the product formation process. However, when particle size is considerably high (> 0.4 mm) this does not happen and one gets a good porous bed leading to higher production of pyrolysis vapor. Fig. 2(b) indicates that with rise in temperature from 450 to 550 °C, pyrolysis oil yield increased and then it decreased up to 650 °C. The decrease in pyrolysis oil yield at higher temperatures (>550°C) is due to the cracking of pyrolysis vapor into non-condensable components (Zheng et al., 2008). Fig. 2(c) shows the effect of gas flow velocity on pyrolysis oil yield. An increase in gas velocity from 50 to 100 ml/min resulted in the continuous increase of pyrolysis oil yield. This increment in the yield is due to the continuous removal of gaseous condensable products from the hot zone (thereby shifting the equilibrium towards product formation) and to minimize secondary reactions such as thermal cracking and polymerization.

The maximum yield for pyrolysis oil obtained is 44.5 mass% at a reaction temperature of 550 °C, gas flow rate of 100 ml/min, and particle diameter of 0.6 mm.

## 3.2 FT-IR and GC-MS analysis of pyrolysis oil

Fourier transform infrared spectroscopy (FTIR) technique was used for the identification of the various functional groups (bonds) present in the mango wood pyrolysis oil. The IR spectra of pyrolysis oil was recorded in the frequency range of 450-4000 cm$^{-1}$ using FTIR instrument (Thermo Scientific- 6700). Further, in order to quantify the compounds present in mango wood pyrolysis oil, GC-MS analysis was performed. FTIR and GC–MS analysis showed the presence of mainly aromatics, phenolic and organic acid compounds such as serine, carbamic, propanoic and cyclobutanecarboxilic acids, imidazole, hexadecanal, cresol and phenol. Some of these compounds such as L-Serine (15%), carbamic acid (1.5%), and imidazole (3%) are of considerably high value and thus, for extraction of these compounds, mango wood pyrolysis oil can be used as an alternative raw material.

## 4. Conclusions

The following salient conclusions can be drawn from the present investigation;

1. Within the range of operating parameters, the maximum pyrolysis oil yield of 44.5 mass% has been obtained at a temperature of 550 °C, the particle size of 0.6 mm, and the N2–gas flow rate of 100 ml/min.
2. The detailed analysis of compounds present in sawdust pyrolysis oil via FTIR and GC-MS reveals the presence of alcohols, aldehydes, ketones, carboxylic acids, aromatics, esters, and phenols in which L-Serine (15%), carbamic acid (1.5%), and imidazole (3%) are of high value and thus, for the extraction of these compounds sawdust pyrolysis oil can be used.

## Acknowledgments

## References

1. Ahmad, S.F.K., Ali, U.F.M., Isa, K.M., 2020. Compilation of liquefaction and pyrolysis method used for bio-oil production from various biomass: A review. Environ. Eng. Res. 25, 18–28. https://doi.org/10.4491/eer.2018.419
2. Guedes, R.E., Luna, A.S., Torres, A.R., 2018. Operating parameters for bio-oil production in biomass pyrolysis: A review. J. Anal. Appl. Pyrolysis 129, 134–149. https://doi.org/10.1016/j.jaap.2017.11.019
3. Mutsengerere, S., Chihobo, C.H., Musademba, D., Nhapi, I., 2019. A review of operating parameters affecting bio-oil yield in microwave pyrolysis of lignocellulosic biomass. Renew. Sustain. Energy Rev. 104, 328–336. https://doi.org/10.1016/j.rser.2019.01.030
4. Qureshi, K.M., Kay Lup, A.N., Khan, S., Abnisa, F., Wan Daud, W.M.A., 2018. A technical review on semi-continuous and continuous pyrolysis process of biomass to bio-oil. J. Anal. Appl. Pyrolysis 131, 52–75. https://doi.org/10.1016/j.jaap.2018.02.010
5. Zheng, J. lu, Yi, W. ming, Wang, N. na, 2008. Bio-oil production from cotton stalk. Energy Convers. Manag. 49, 1724–1730. https://doi.org/10.1016/j.enconman.2007.11.005

# Separation technologies: A review of present and upcoming biorefining

*Hemant Kumar [1]\**

[1]Department of Chemical Engineering, Dharmsinh Desai University, Nadiad-387 001, Gujarat, India

*Corresponding author: hemantkumar.ch@ddu.ac.in

## Abstract:

In recent years, world energy demand is ever increasing. To cope up the present scenario new renewable technologies are required that provide alternatives to the depleting fossil fuels. In the modern world, one of the most important industries is biorefinery, as it provides a variety of precursor chemicals and bio-based materials. Biorefinery utilizes agriculture or forest biomass to produce energy comparable to the petroleum refineries products. Liquid fuels like bioethanol and biodegradable plastics like polyhydroxyalkanoates along with industrial chemicals like acetic acid can be formed from wood and other lignocellulosic biomass. Biorefineries utilizes a range of separation methods to produce high value co-products from the various feed streams. This paper reviews the different separation methods and technologies like pre-extraction of hemicellulose and other chemicals, detoxification of fermentation hydrolyzates, and separation and dehydration of ethanol products. Moreover, some of the challenges encountered during processing of biomaterials are analyzed in detail.

**Keywords:** Separation technologies; Biorefinery; Biofuels; Organic waste; Ethanol

## 1. Introduction

Energy demand is increasing gradually due to increasing GDP worldwide. As per the reports of the international agency out-look 2016, energy demand is projected to increase by 48% by the end of 2040, as shown in Fig. 1(Kumar H. et al., 2018). To deal with the energy need, renewable technologies are required. In recent years, biorefinery is one of the most important industries that provide precursor chemicals and bio-based materials. Along with bioethanol, biorefinery provides many industrial chemicals and biodegradable plastics. Biorefinery exploits the use of agricultural or forest biomass transforming to energy at par with the petroleum refineries products. Bioethanol is a promising future biorefineries product that has the possibility to be used as a transportation fuel. In this review a focus on conventional and innovative bioethanol production is emphasized. Blending of bioethanol with gasoline reduces not only the use of petroleum fuels but also reduces net price. Ethanol with high oxygen content makes it a cleaner fuel with respect to combustion. Therefore, in view of reducing objectionable emissions, blending of gasoline with ethanol saves urban environment. Biorefinery feed stock are wood and agro feedstocks (agricultural and forest resources), aquatic feed stocks and recycled materials and wastes. This paper reviews the production of ethanol from corn, lignocellulosic biomass and integrated lignocellulosic biomass.
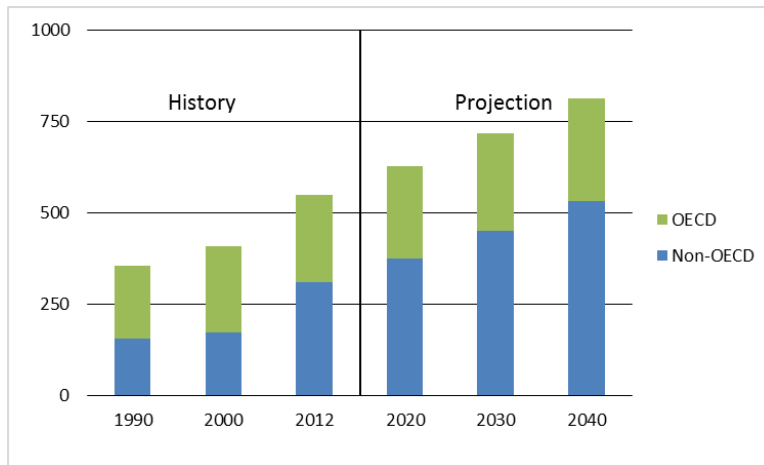
Figure 1. History and projection of world energy consumption (quadrillion Btu) (Kumar H. et al., 2018)

## 1.1 Bioethanol from corn

Two major methods viz. wet mill and dry grinding are applied to produce ethanol fuel from corn. Application of wet mill process (33%) provides co-products of high values like fiber, germ and gluten by applying pre-processing prior to fermentation. Therefore, wet mill process is a cost and energy consuming process. Conversely, usual drymill (67%) grind process involves the steps like grinding, cooking and liquefaction, followed by saccharification of the starch to sugars with enzymes, fermentation of sugar to ethanol with yeast. Distillation and dehydration of ethanol constitutes the last steps in dry mill processes (Heiningen, 2005). Solids retained at the bottom of distillation column after drying provides the feed stuff with proteins for animals. A recent modification in the dry mill process involves the separation of germ and fiber before fermentation process (agclassoom.org, 2021) aimed to reduce further cost. In this modified process cornkernel is treated with anhydrous ammonia resulting in the loosening of germ and fiber that serves a co-product as a food. A wet mill process involves corn cleaning, steeping and a de-germed process to obtain germ from which corn oil is extracted, defiberedfor obtaining fiber, and followed by separation of glutenand starch. Thereafter, the same steps follow like corn-grind process that includes saccharification, fermentation, distillation and dehydration of ethanol (Singh and Eckhoff, 1997).

## 1.2 Ethanol from lignocellulosic biomass

While considerable progress has been done for the conversion of lignocellulosic or cellulosic biomass to ethanol fuel, commercialization has not been done owing to prevailing technical and commercial constraints. On the other hand, cellulosic ethanol proved to be better effective and capable as an alternative renewable bio-fuel compared to corn ethanol in the end since a great reduction in the emissions of greenhouse gas along with apotential of displacing higher fossil fuel (Kszos, 2006). Feed for lignocellulosic biomass having large potential for producing fuel ethanol areagricultural residues like sugar cane bagasse, crop straws and corn stover etc.Vascular plants that have no persistent woody stemslike switchgrass, alfalfa etc. Forestry residue and wood wastes and paperwaste (Wyman, 1996). Steps for lignocellulosic biomass-to-ethanol conversion sequentially involves feedstock storage and handling, pretreatment andhydrolyzate

conditioning, saccharification and co-fermentation, separation of products (ethanol, waste gases, still solids, evaporative syrup etc.), wastewater treatment. Final step involves combustion oflignin for electricity production and steamgeneration.

## 1.3 Integrated biorefinery for lignocellulose

Forests are the massive resource of lignocellulosic materials. The major industry that can exploits the use of forest materials are Pulp mills, however, increased market competiveness has resulted in downsizing and mergers (Heiningen, 2006b). In the view of existing challenges, a new concept has been proposed that produces the fuels and chemicals along with existing pulp mills. The method involves the pre-extraction of hemicellulosic sugars before pulping operation. Separation of short and long fiber after the pulping operation has completed. Production of ethanol by converting hemicellulose and cellulose (short fiber) in two separate bioreactors. Long fiber cellulose is utilized for paper production along with other materials based on fiberslike bio-composites. After pulping operations, a further gasification of black liquor containing lignin can produce synthesis gas by gasification process. Moreover, syngas can be used in producing chemicals, fuels, electricity and steam. In short, the integrated bio-refinery utilizing forest resources exploita complete use of all the components of feed in producing value-added co-products. This scheme of optimized system can resemble with petroleum refinery and projects future resource for renewable energy.
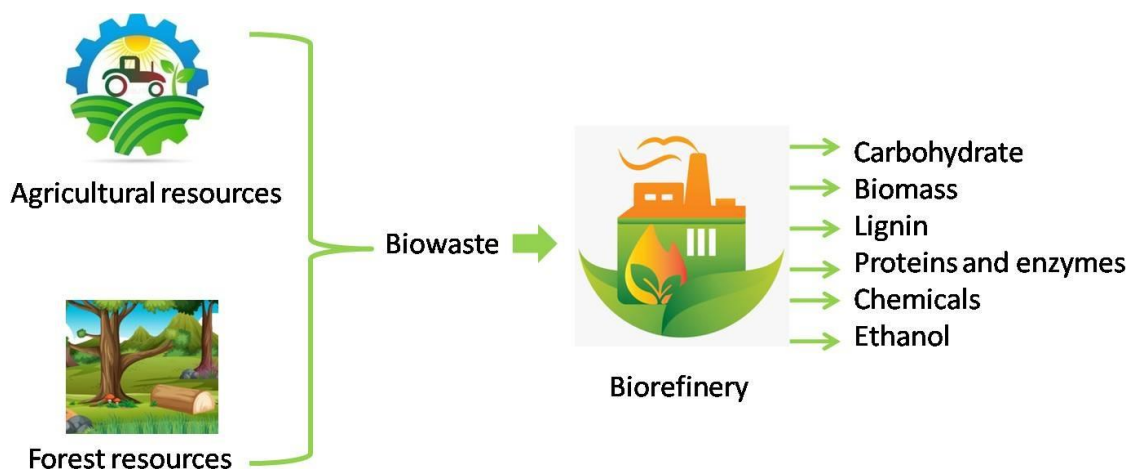


Figure 2. Schematic diagram of integrated biorefinery

## 2. Hemicellulose pre-extraction

## 2.1 Co-products extraction process

### 2.1.1 Corn germ

Extraction of co- product like corn germ is important in context of an additional value added products. The germ free of dermal lipids obtained from dry or wet grind processes are efficiently saccharified into glucose, xylose and arabinose by use of *Aureobasidiumsp.* enzymes. Later, these sugars are fermented to bio-ethanol. A profit enhancement therefore is achieved from extraction of germ.Conventionallyhydrocyclones are used for recovering germ that is obtained

after corn soaking from the wet milling degermination process. A quick germ method proposed by Singh and Eckhoff involves water soaking of whole corn, afterwards, usual wet milling degermination process takes place. It has been reported that the "Quick Germ" process modification produces additional value from co-products than the conventional dry grind process.

### 2.1.2   Corn fiber

Presently, norecovery of corn fiber persists, if existed it is mixed with low-value animal feeds compared to ethanol production (Bothastand Schlicher, 2005). A profitable use of corn fiber (or bran) is extraction of ethanol and fiber oil and fiber gum (Singh andMoreau, 1999, Donerand Hicks, 1997). Corn fiber can be separated either by hot water or steam fractionation, however, study suggests that hot water at the temperature of 215 ∘C with solids loadings of 5–to-10%, obtained very high pentosan recovery compared with steam at temperature of 210–220 ∘C with solids loading greater than 50%. A newly developed quick fiber process forcorn fiber recoveryinvolves pre grinding followed by extraction with hexane. The steps are: water soaking of corn, recovery of the germ, fiber separation. However, an addition of starch increases slurry density and fiber floats on the surface (Singh and Moreau, 1999).

## 2.2 Chemicals pre extraction

In the existing pulping process, black liquor is combusted for the generation of electricity and steam, however, low heating value of it due to the presence of hemicelluloses makes it uneconomical. Therefore, in an integrated bio refinery, hemicellusolse extraction is combined with the production of bioethnol and many more value added chemicals (Heiningen, 2005).

### 2.2.1   Hemicellulose pre extraction

Main fractions of lignocellulosic bio-mass consists 35 to 50% cellulose, 20 to 35% hemicelluloses and 10 to 25% lignin. Different methods are available for hydrolyzing and fractionating hemicellulose like acid treatment, extraction with hot water, extraction with steam and alkaline extraction. In one of the recent methods, wood chips with NaOH are extruded, centrifugation of liquid filtrate, vacuum evaporation, acidification, precipitation, filtration, washing followed by air drying extracts the hemicellulose.

### 2.2.2   Antioxidants pre extraction

Antioxidants like polyphenolics can be used as a low cost food additive as an antioxidant that can be extracted from lignocellulosic wood materials (Cruz et al., 1999, Gonzalez, et al., 2004). Mild acid hydrolysis process is applied to produce antioxidents.

## 3.   Inhibitors removal

Fermentation process is reduced in presence of inhibitors; therefore detoxification is required to increase productivity. Methods involves, pre treatment before fermentation like evaporation (Converti et al., 2000), solvent extraction (Cruz et al., 1999, Gonzalez, et al., 2004, Wilsonet al., 1989), treatment with activated charcoal (Chandel et al., 2007, Parajo et al., 1996, Canilha et al., 2004, Villarreal, 2006), treatment with ion exchange resins (Chandel et al., 2007), and enzymatic detoxificationetc.(Jonsson et al., 1998, Gutierrez et al., 2006).

## 4. Ethanol recovery

After fermentation process, the beer obtained contains 5 to 12 wt% ethanol beer, therefore, a dilute solution is obtained requiring very high energy to separate water from the solution. Distillation on the other side will be limited to azeotrope formation limit i.e. 95.6% by weight a temperature 78.15 °C. On the other hand, simple distillation in the range of 10 to 85% can be performed; however, near to 85 % distillation will become difficult since in the vicinity of azeotrope formation. Moreover, this condition will require high reflux ratios and many more consideration costing high. to overcome the persisting problem, nowadays, simple distillation is performed near to 90% and further dehydration steps taken into consideration are AD (azeotropic distillation), ED (extractive distillation), SE (solvent extraction), adsorption and Membrane separation.

Therefore, in order to concentrate the dilute solution of ethanol first simple distillation is performed near to 92%, thereafter; extractive distillation with high boiling point solvent is introduced with the feed in the upper part of the column. One of the solvents is gasoline for concentrating beer solution. Vacuum distillation may also be performed to break azeotrope formation but cost incurred in the process limits the use of method. The other choice is solvent extraction with salt added in the solution (Llano-Restrepoand Aguilar-Arias, 2003). Salts used are potassium acetate (Llano-Restrepoand Aguilar-Arias, 2003, Furter, 1972, Cookand Furter, 1968, Lynd and Grethlein, 1984), calcium chloride and sodium acetate (Furter, 1992). Extractive distillation with ionic liquids is a recent technique. Common ionic liquids used in the process are 1-butyl-3-methylimidazolium tetrafluoroborate, 1-butyl-3-methylimidazolium and 1-ethyl-3-methylimidazolium tetrafluoroborate. The other available methods are adsorption and membrane separation aimed to concentrate post fermentation process.

## 5. Conclusions

Different techniques regarding production of bio-ethanol through corn conversion are provided in this review. Along with lignocellulosic materials processing, an integrated biorefinery concept is discussed. Some modifications in wet mill and dry mill grinding process are discussed and recent methods are suggested that could not only enhance ethanol production but also provide different co-products of high economic values. Techniques of post formation process for separation of ethanol or concentrate the dilution ethanol solutions are proposed. Some of the challenges and future perspective regarding the conventional methods are discussed in detail. Overall biorefinery concept resembles the petroleum industry were along with profitable commodities, various co-products are generated.

**References**

1. A.V. Heiningen, Converting a kraft pulp mill into an Integrated Forest BioRefinery (IFBR), http://www.forestbioproducts.umaine.edu/ ForestBiorefinery.pdf (Feb. 20, 2021)
2. Bothast R.J., Schlicher M.A., 2005. Biotechnological processes for conversion of corn into ethanol. Appl. Microbiol. Biotechnol. 67, 19–25.
3. Canilha L. et al., 2004. Eucalyptus hydrolyzate detoxification with activated charcoal adsorption or ion-exchange resins for xylitol production. Process Biochem. 39, 1909–1912.
4. Chandel A.K. et al., 2007. Detoxification of sugarcane bagasse hydrolyzate improves ethanol production by Candida shehatae NCIM 3501. Bioresour. Technol. 98 (10), 1947–1950.
5. Converti A. et al., 2000. Wood hydrolysis and hydrolyzate detoxification for subsequent xylitol production. Chem. Eng. Technol. 23, 1013–1020.
6. Cook R.A., Furter W.F., 1968. Extractive distillation employing a dissolved salt as separating agent. Can. J. Chem. Eng. 46, 119–123.
7. Cruz, J.M. et al., 1999. Solvent extraction of hemicellulosic wood hydrolyzates: a procedure useful for obtaining both detoxified fermentation media and polyphenols with antioxidant activity. Food Chem. 67, 147–153.
8. Doner L.W., Hicks K.B., 1997. Isolation of hemicellulose from corn fiber by alkaline hydrogen peroxide extraction. Cereal Chem. 74, 176–181.
9. Furter W. F., 1972. Extractive distillation by salt effect, in: R.F. Gould (Ed.), Extractive and Azeotropic Distillation, Advances in Chemistry Series, pp. 35–45.
10. Gonzalez J. et al., 2004. Production of antioxidants from Eucalyptus globulus wood by solvent extraction of hemicellulose hydrolyzates. Food Chem. 84, 243–251.
11. Gutierrez T. et al., 2006. Purification and characterization of a furfural reductase (FFR) from Escherichia coli strain LYO1—an enzyme important in the detoxification of furfural during ethanol production. J. Biotechnol. 12, 154–164.
12. Jonsson L.J. et al., 1998. Detoxification of wood hydrolyzates with laccase and peroxidase from the white-rot fungus Trametesversicolor. Appl. Microbiol. Biotechnol. 49, 691–697.
13. Kumar H. et al., 2018. Water-in-Diesel Nanoemulsion Fuels for Diesel Engine: Combustion Properties and Emission Characteristics. In: Singh A., Agarwal R., Agarwal A., Dhar A., Shukla M. (eds) Prospects of Alternative Transportation Fuels. Energy, Environment, and Sustainability, Springer, Singapore, pp. 299-342.
14. L.A. Kszos, Bioenergy from switchgrass: reducing production costs by improving yield and optimizing crop management, website:
    http://www.ornl.gov/~webworks/cppr/y2001/pres/114121.pdf (Feb. 20, 2021)
15. L.R. Lynd, H.E. Grethlein, 1984. IHOSR/Extractive distillation for ethanol separation. Chem. Eng. Prog. 80, 59–62.
16. Llano-Restrepo M., J. Aguilar-Arias, 2003. Modeling and simulation of saline extractive distillation columns for the production of absolute ethanol. Comput. Chem. Eng. 27, 527–549.
17. New Milling Methods Improve Corn Ethanol Production, website: http://www.agclassroom.org/teen/ars pdf/tech/2004/07milling.pdf (Feb. 20, 2021)
18. Parajo J.C. et al., 1996. Charcoal adsorption of wood hydrolyzates for improving their fermentability: influence. Bioresour. Technol. 57, 179–185.
19. Singh V. et al., 1999. Recovery of fiber in the corn dry-grind ethanol process: a feedstock for valuable coproducts. Cereal Chem. 76 (6), 868–872.

20. Singh V., Eckhoff, S.R., 1997. Economics of germ preseparation for dry-grind ethanol facilities, Cereal Chem. 74 (4), 462–466.

21. V. Heiningen, Hemicellulose extraction and its integration in pulp production, in: Forest Products Industry of the Future, Quarterly Status Reports, September 30, 2005, U.S. Department of Energy website: http://www.eere.energy.gov/industry/forest/pdfs/quarterlyhighlights.pdf. (Feb. 21, 2021).

22. Villarreal M. L. M. et al., 2006. Detoxification procedures of eucalyptus hemicellulose hydrolyzate for xylitol production by Candida guilliermondii. Enzyme Microb. Technol. 40 (1), 17–24.

23. W.F. Furter, 1992. Extractive distillation by salt effect. Chem. Eng. Commun. 116, 35–40.

24. Wilson J.J. et al., 1989. Comparative fermentability of enzymatic and acid hydrolyzates of steam-pretreated aspenwood hemicellulose by Pichiastipitis CBS 5776. Appl. Microbiol. Biotechnol. 31, 592–596.

25. Wyman C.E., 1996. Ethanol production from lignocellulosic biomass: overview, in: C.E.Wyman (Ed.), Handbook on Bioethanol: Product Ion and Utilization, Taylor & Francis, Washington, DC, pp. 1–18.

# Characterisation and Assessment of the Adsorption Potential of Sugarcane Bagasse and Eggshells in Heavy Metal Removal

*C. Harripersadth[1], P. Musonge[1,2], Yusuf Isa[3]*

*[1] Institute of Systems Science, Durban University of Technology, Durban, South Africa,*

*[2] Faculty of Engineering, Mangosuthu University of Technology, Durban, South Africa,*

*[3] School of Chemical and Metallurgical Engineering, University of the Witwatersrand,*

*Johannesburg, South Africa.*

*paulm@dut.ac.za*

**Abstract:** The chemical constituents and bio-degradable features of agricultural waste have attracted increased attention as potential bio-sorbents in the water treatment industry. In this study, the physical and chemical characterisation of two types of agricultural waste, sugarcane bagasse and eggshells were investigated. The biosorbent properties were characterized using Fourier Transform Infrared Spectroscopy (FTIR), Scanning electron energy dispersive spectroscopy (SEM-EDX), X-ray diffraction (XRD) and Brunauer Emmett Teller (BET) analysis. Under the characterisation measurements investigated, the estimated composition of eggshells consists of calcium, oxygen and carbon atoms which constitutes carboxylic and carbonate functional groups. Carbon, hydrogen and oxygen atoms were prominent in bagasse with the defining functional groups due to hydroxyl and carbonyl groups. The surface area of bagasse was 1.0068 m²/g with a pore volume of 0.0023 cm³/g and a pore size of 8.17 nm and for eggshells, the surface area was 1.7114 m²/g with a pore volume of 0.01632 cm³/g and a pore size of 14.27 nm. Crystallographic information revealed a monoclinic lattice for bagasse with a rhombohedral lattice present in eggshells. The surface morphology of bagasse was found to exhibit an irregular surface, however for eggshells, the surface was densely packed with a layered surface. Further to this, it was found that the pore structures of both biomaterials belong to a typical Type III isotherm which are characteristic of materials with macropores or open voids.

## 1. Introduction

In recent decades, the increase in industrial activity and water usage worldwide have led to the release of various pollutants into the aquatic environment, such as toxic heavy metals, dyes, pesticides, humic substances and other persistent pollutants (Abdolali et al., 2014). A high degree of industrialization and urbanization has substantially enhanced the degradation of our aquatic environment through the discharge of industrial wastewaters and domestic wastes (Senthikumaar, 2000). Among these, anthropogenic sources are most common where pollutants such as heavy metals are distributed into the environment through the continuous discharge of sewage and industrial effluents (Lakherwal, 2014). The presence of these toxic and non-biodegradable pollutants in wastewater is a major cause of concern due to their adverse impacts on human health and the environment. Thus, governments have established environmental restrictions with regards to the quality of wastewater, forcing industries to treat waste effluent before discharging (Ronda et al., 2013). With sustainability at the forefront of

industrial operations, it is imperative for the industrial sector to comply with legislation. Many rural communities do not have access to potable water and therefore rely on these water sources.

Current treatment technologies used for the removal of hazardous pollutants include chemical precipitation, ion exchange, reverse osmosis and ultrafiltration, all of which have been reviewed by various researchers (Luptakova et al., 2012, Gaikwad et al., 2010, Buzzi et al., 2011). Although usable, the above processes are not suitable for applications with very low pollutant concentrations (Simate and Ndlovu, 2015). They are often ineffective, uneconomical or technically complicated when the target pollutant concentration falls below 100 mg/L. Additionally, some methods also have the disadvantages of high reagent usage, high energy requirements and toxic secondary sludge production (Abdolali et al., 2014).

In this regard, the process of adsorption has been widely researched for the removal of hazardous substances. The main attraction of adsorption is its cost effectiveness and good removal performance (Aksu and Gönen, 2004). Commercially available adsorbents such as activated carbon has restricted its widespread use due to its high cost (Malkoc et al., 2006) which therefore introduced the need to source low cost and easily available adsorbents. This gap has led to the investigation of materials of agricultural and biological origin (Aksu and Gönen, 2004). Raw and natural agricultural wastes are among some of the cheap adsorbents that are used. Two such agricultural-based adsorbents are eggshells and sugarcane bagasse.

Egg production amounts to a significant contribution to the agricultural sector and due to the large quantities produced, a considerable amount of shell residue is generated which is considered as waste (Oliveira et al., 2013). Additionally, the costs associated with the disposal of eggshells (mainly on landfill sites) are significant and is expected to continue increasing as landfill taxes increase (Carvalho et al., 2011). Another such waste is sugarcane bagasse, which is a by-product of the sugar industry. Disposal has also become a problem where some factories have resorted to landfills and incineration. Landfills, however pose a potential hazard due to the risk of spontaneous combustion as a result of microbial activity in the dumps (Mwasiswebe, 2005). As a countermeasure, using eggshells and sugarcane bagasse as potential biomaterials serves a twofold solution, it reduces the quantity of waste to be sent to landfills and has the potential to be used in the water treatment industry. Thus, the main objective of this study is to evaluate the physical and chemical properties of these biomaterials which make them suitable bio-sorbents to be used in the water treatment industry.

## 2. Materials and Methods

### 2.1 Materials

Five adsorbents were prepared for use which includes sugarcane bagasse, eggshells, adsorbent A which consisted of 25 % eggshells with 75% bagasse, adsorbent B consisting of 50% eggshells with 50% bagasse and adsorbent C consisting of 25% bagasse with 75% eggshells as seen in table 1. Waste sugarcane bagasse was sourced from Illovo Sugar, South Africa. After collection, it was washed with deionized water several times to remove the sand and dirt particles present. Following the methodology of Wong et al. (2009), bagasse was boiled in hot water for 1 hour which was then allowed to air dry followed by drying in an oven at 105°C until constant weight. After drying, the biomass was crushed using a coffee grinder to achieve the desired size of biosorbent material. It was crushed in 30 second intervals and sieved to achieve the particle size of <75 µm. for the preparation of eggshells, discarded chicken

eggshells were collected from local restaurants in Durban, South Africa. The shells were washed several times with deionized water to remove any debris and dirt particles. Following the drying method of Mao (2017), the biomass material was dried in an oven at 105 ℃ until constant weight. The dried eggshells were then crushed using a coffee grinder to achieve the desired particle size of biosorbent material where it was crushed in 30 second intervals until the particle size fraction of < 75 µm was achieved. To prepare adsorbents A – C, the 2 biomaterials were mixed together on a dry weight basis and the biosorbents were stored in an airtight container for use.

Table 1. Weight percentages used for the adsorbents

|  | Bagasse | Adsorbent A | Adsorbent B | Adsorbent C | Eggshells |
|---|---|---|---|---|---|
| Bagasse | 100% | 75% | 50% | 25% | - |
| Eggshells | - | 25% | 50% | 75% | 100% |

## 2.2 Methods of Characterisation

2.2.1 Surface Area, Pore Volume and Pore Size

The surface area, pore volume and pore size were obtained by measuring the nitrogen adsorption–desorption isotherms using a surface area and porosity analyzer (Micromeritics TriStar 3000). Brunnaer–Emmett–Teller surface area (BETs, $m^2/g$) and total pore volume (Vt, $cm^3/g$ at STP) were thus obtained by the Nitrogen adsorption data according to BET theory. The pore size was calculated based on differential pore volume of Barrett–Joyner–Halenda (BJH) adsorption–desorption isotherm data.

2.2.2 Scanning Electron Microscopy Analysis (SEM)

A FEI Nova Nano SEM 230 Scanning Electron Microscope was used to characterise the surface morphology of the biomass surface. An ETD and TLD detector was used with a high-resolution immersion lens. An EDS detector (Oxford X-Max equipped with INCA software Landing E 5.00KeV), HFW of 5.97- 298 µm, Spot of 3.5 and WD of 4.9 – 7.4 mm was used.

2.2.3 Fourier Transform Infrared Spectroscopy Analysis (FTIR)

The surface functional groups present on the surface of the biomass was qualitatively detected by Fourier Transform Infrared (FTIR) spectroscopy using a Perkin Elmer spectrum spectrophotometer. The spectrum was obtained in a frequency band range from 4000 to 400 $cm^{-1}$.

2.2.4 X-Ray Diffraction Analysis (XRD)

A Bruker D8 advance x-ray diffraction system using the Xpert data collector software was used to identify the crystalline materials and mineralogical composition of the biomass. The measurements were done continuously on a J-J scan in locked coupled mode and the tube was Cu-Ka radiation (lKa₁=1.5406Å). The measurement range was 4° to 69.997° with an increment (D2J: 0.034°) most of the time.

## 2.3 Batch Experiments

Synthetic stock solutions of Pb (II) and Cd (II) ions of 1000 mg/L concentration were prepared by dissolving appropriate amounts of lead nitrate $Pb(NO_3)_2$ and cadmium nitrate tetrahydrate $Cd(NO_3)_2.4H_2O$ salts in 1L deionised water. The stock solutions were subsequently diluted to the required concentrations using deionized water. All chemicals used in the experiments, $0.1\,M\,NaOH$ and $0.1\,M\,H_2SO_4$ (for pH adjustment) and $1N\,HNO_3$ which was used to clean the glassware, were of analytical reagent grade obtained from the Sigma Aldrich chemical company and were used without further purification.

A comparative performance study was performed to evaluate the performance of the adsorbents in batch studies. For each batch test, a $100\,\frac{mg}{L}$ concentrated adsorbate solution was prepared by diluting the stock solution with the addition of an appropriate amount of deionized water. For each experiment, $1.0\,g$ of adsorbent was mixed with $100\,mL$ of metal solution in a $1\,L$ glass beaker which was agitated at $150\,rpm$ for a duration of $120\,min$ to ensure equilibrium was reached. The pH of the aqueous solutions was maintained at 5.5 with $0.1\,M\,H_2SO_4$ or $0.1\,M\,NaOH$ respectively. All experiments were conducted at room temperature. After each experiment, the glassware used was cleaned with deionised water followed by $1N\,HNO_3$. The supernatant solution was filtered using $0.45\,\mu m$ syringe filters where a Varian Spectra AA 50B atomic absorption spectrophotometer (product of Spain) was used to determine the concentration of the samples. A calibration curve of Pb and Cd was plotted by measuring the absorbance at 283.3 nm for Pb and 228.8 nm for Cd at varying concentrations. Absorbance values with a standard deviation greater than 1% were discarded and an average value was taken from the duplicate results.

The adsorption uptake and percentage removal of metal ions from the aqueous solution (mg of adsorbate/g of adsorbent) was calculated using the following equations:

Amount Adsorbed:

$$q_e = \frac{C_o - C_t}{W}\,V \tag{1}$$

Percentage Removal:

$$q = \frac{100\,(C_o - C_t)}{C_o} \tag{2}$$

Where $q$ is the amount of metal ion adsorbed per gram of adsorbent $(\frac{mg}{g})$, $C_o$ (mg/L) is the initial metal ion concentration, $C_t$ (mg/L) is the metal ion concentration at time t, $W\,(g)$ is the mass of the adsorbent used and $V$ (L) is the volume of the solution.

## 3. Results and Discussion

3.1 Physical Characterization

3.1.1 Surface Area, Pore Volume and Pore Size

The data in Table 1 indicate the BET surface area, total pore volume, and pore size of the eggshells and bagasse.

Table 2. Biosorbent Surface Area, Pore Volume and Pore Size

| Biosorbent | BET Surface area ($m^2$/g) | Pore Volume ($cm^3$/g) | Pore size (nm) |
|---|---|---|---|
| Bagasse | 1.0068 | 0.0023 | 8.17 |
| Eggshell | 1.7114 | 0.01632 | 14.27 |

The surface area of bagasse was found to be 1.0068 m²/g with a pore volume of 0.0023 cm³/g and a pore size of 8.17 nm. The results obtained by Chao et al. (2014) reported a similar surface area of 1.19 $m^2$/g and the author demonstrated that the pore volume and surface area were not critical factors which influenced the adsorption process. It was postulated by the author that bio-sorbents uptake metal ions through their functional groups rather than diffusion through their pores as evidenced by their results. For eggshells, the surface area was determined to be 1.7114 $m^2$/g with a pore volume of 0.01632 cm³/g and a pore size of 14.27 nm. When compared to a surface area of 0.007 $m^2$/g, pore volume of 0.00022 $cm^3$/g and a pore size of 13.2 nm by Flores-Cano et al. (2013), the results from this study are significantly higher. To classify the porosity of the biomaterials, the International Union of Pure and Applied Chemistry (IUPAC) convention was used which classifies nanoporous materials into three groups; micropore (diameter <2 nm), mesopore (2–50 nm) and macropore (>50 nm). Based on the above conventions, the eggshell and bagasse biomaterials that were used in this study are classified as being mesoporous in nature. Generally, porosity and pore volume are not the primary determinants that governs the capability of a bio-sorbent since agricultural wastes possess an abundance of functional groups and usually uptake pollutants through their affinity to the biomass surface, that is through their functional groups.

As seen in figure 1, the adsorption-desorption isotherms of sugarcane bagasse and eggshell biomass exhibit very close values between adsorption and desorption at all P/Po values demonstrating that the isotherms are reversible. According to the institution of pure and applied chemists (IUPAC), both isotherms can be classified as a type III isotherm with no identifiable monolayer formation. Further to this, as explained by (Thommes et al., 2015), the adsorbent-adsorbate interactions are relatively weak with the adsorbed molecules clustered around the most favorable sites on the surface of a nonporous or macroporous solid.
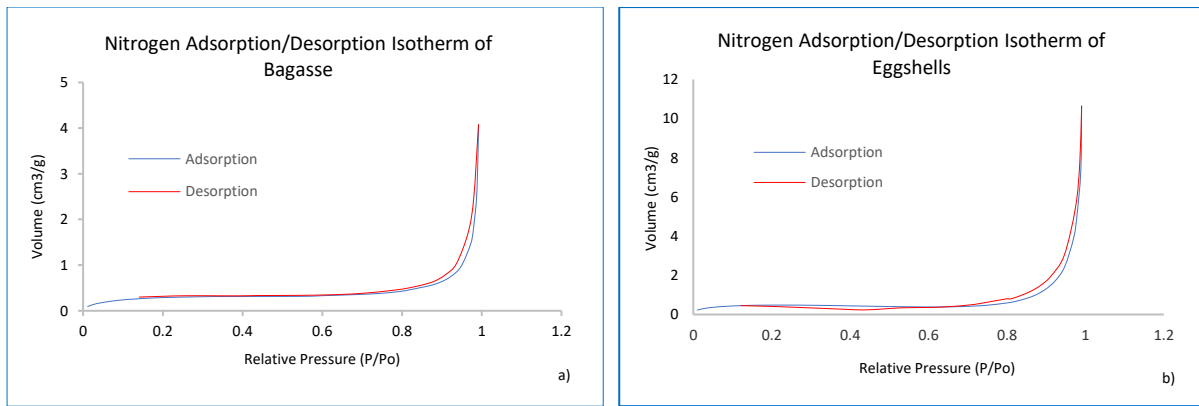
Figure 1. Nitrogen Adsorption Desorption Isotherms of Bagasse (a) and Eggshells (b)

### 3.1.2 Scanning Electron Microscopy Analysis (SEM)

The surface morphology of the biomaterials were characterised using scanning electron microscopy. The above analytical technique is used to provide a visual representation of the structure of the biomass surface.
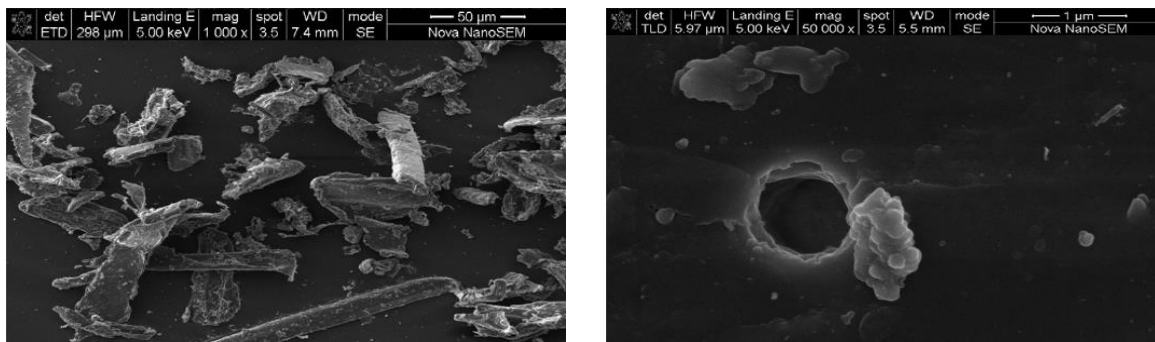


Figure 2: SEM Micrographs of Sugarcane Bagasse at a magnification of 1000 X and 50000X
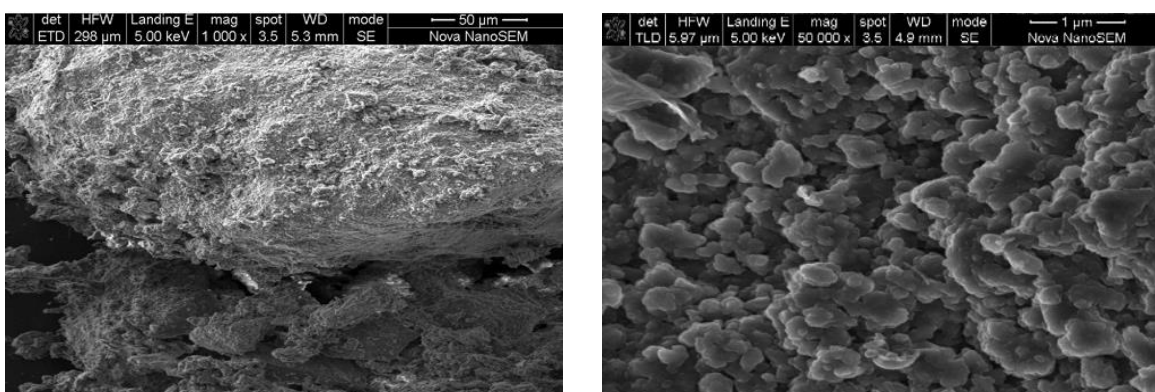


Figure 3: SEM Micrographs of Eggshells at a magnification of 1000 X and 50000X

The surface of the biomass in figure 2 depicts 1-dimensional rod like structures and particles which are randomly oriented. The fibrous fraction of bagasse is due to the notable predominance of particles of a high length to width ratio as evidenced above and supported by

Driemeier et al. (2011). The surface is non-uniform and jagged with loosely packed particles throughout the surface. The work of Leão et al. (2017) characterised these particles as globular wax particles, pectins and extractives in addition to the amorphous constituents such as lignin and hemicellulose present in bagasse. The SEM micrograph in figure 3 depicts definite structures which are densely packed on the surface of the biomass. The shape of the particles were mostly flake like grains with the majority being fine in size. On closer inspection, layered cloud like grains were visible with differing grain sizes. It is worthy to note that layered surfaces provide a larger surface area available when compared to flat 1-dimensional surfaces available for adsorption.

## 3.2. Chemical Characterisation

### 3.2.1 Energy Dispersive Spectroscopy Analysis (EDS)

Table 3. Elemental Composition of Eggshell and Bagasse obtained from the EDS Analysis

| Biosorbent | C (%) | O (%) | Ca (%) | Total |
|------------|-------|-------|--------|-------|
| Bagasse | 53,29 | 46,71 | ---- | 100 |
| Eggshell | 23,96 | 44,52 | 31,52 | 100 |

Energy Dispersive Spectroscopy (EDS) was used to determine the estimated composition of the biomaterials. The composition that constitutes sugarcane bagasse comprises mainly of carbon and oxygen atoms with approximately the same weight ratio. Cellulose is the main constituent in bagasse which is composed of oxygen, hydrogen and carbon atoms (Wong et al., 2014). However, in the above analysis, no hydrogen was detected. It is worthy to note that the use of analytical techniques involving x-rays are less sensitive to lighter atoms present in a compound, if they are located at all. Hence, in organic structures such as cellulose, $C_6H_{12}O_6$, the hydrogen atom positions are relatively inaccurate which is demonstrated by the lack of hydrogen present despite cellulose constituting hydrogen atoms. It is therefore recommended that an elemental analyser be used in conjunction with the above analysis to elucidate the above findings. Eggshell biomass consists mainly of calcium, oxygen and carbon atoms with a high amount of calcium and oxygen in comparison to carbon. Since eggshell biomass is composed mainly of calcium carbonate, $CaCO_3$, this is expected.

### 3.2.2 Fourier Transform Infrared Spectroscopy

Basic surface chemistry knowledge is useful in exploring the biosorption process especially in elucidating the adsorption mechanisms.
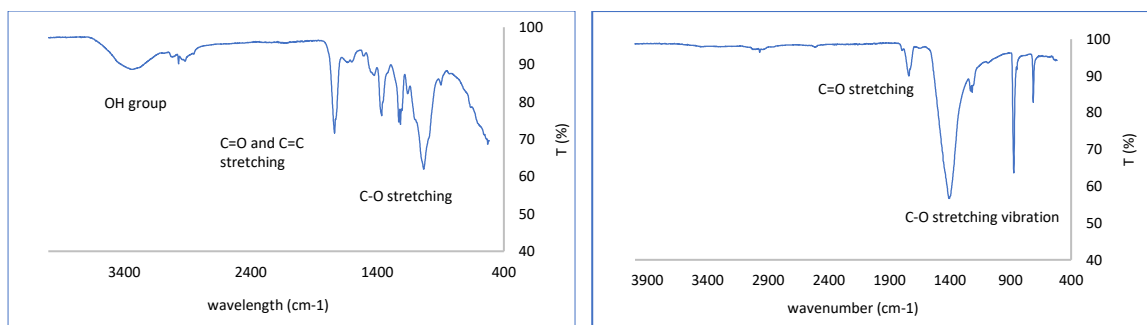
Figure 4: FTIR Spectra of Sugarcane Bagasse (Left) and Eggshell Biomass (Right)

The defining peaks identified in the FTIR spectra of sugarcane bagasse occur at the wavelengths of 3345 cm$^{-1}$, 1736 cm$^{-1}$, 1364 cm$^{-1}$, 1217 cm$^{-1}$, 1035 cm$^{-1}$ and 899 cm$^{-1}$. The broad absorbance band observed at 3345 cm$^{-1}$ is assigned to the hydroxyl groups present in bagasse (Zhang et al., 2011, Gurgel et al., 2008). In contrast, the sharp absorbance intensity at 1736 cm$^{-1}$ is representative of C=O carbonyl groups and the C=C stretching vibrations are due to the aromatic rings of lignin (Zhang et al., 2011). The high intensity bands within the range of 1364 cm$^{-1}$ – 1034 cm$^{-1}$ are due to the C-O stretching vibration of cellulose, lignin and hemicelluloses as supported by Gurgel et al. (2008) and Putra et al. (2014). The minor peak at 898 cm-1 may be assigned to the glycosidic bonds in cellulose as reported by (Lima et al., 2014). Thus, the FTIR spectra of bagasse indicates that the surface of the biomass is rich in polymeric hydroxyl, carbonyl and aromatic rings (Chao et al., 2014) which provides the necessary ion exchange and complexation sites for biosorption to occur.

For eggshells, the minor absorption band at 1740 cm$^{-1}$ is characteristic of the C=O stretching of carboxylic acid which has been further discussed by Flores-Cano et al. (2013). In addition, the sharp bands observed at 1405 cm$^{-1}$, 873 cm$^{-1}$ and 712 cm$^{-1}$ are characteristic of the mineral carbonate. According to Flores-Cano et al. (2013), the absorption band at this wavenumber is characteristic of the C−O bond in the carbonate due to a stretching vibration, showing a coordination bond between the oxygen atoms of the carbonate and the calcium atom. Further to this, the two sharp bands at 873 cm$^{-1}$ and 712 cm$^{-1}$ are due to the out-of-plane and in-plane deformation modes of carbonate, respectively. This can be further supported by Al-Ghouti and Salih (2018). It is the carboxylic acid and carbonate groups in eggshells that provide the necessary ion exchange and complexation sites for biosorption to occur.

3.2.3 X-Ray Diffraction (XRD) Analysis

With respect to the biosorption process, crystallographic information helps to determine the ease or difficulty required to break bonds within the atomic structure of a biomaterial. A crystalline material has a highly ordered arrangement making it difficult to break the bonds for adsorption to occur. On the other hand, amorphous materials are less ordered which require less energy to break the bonds.
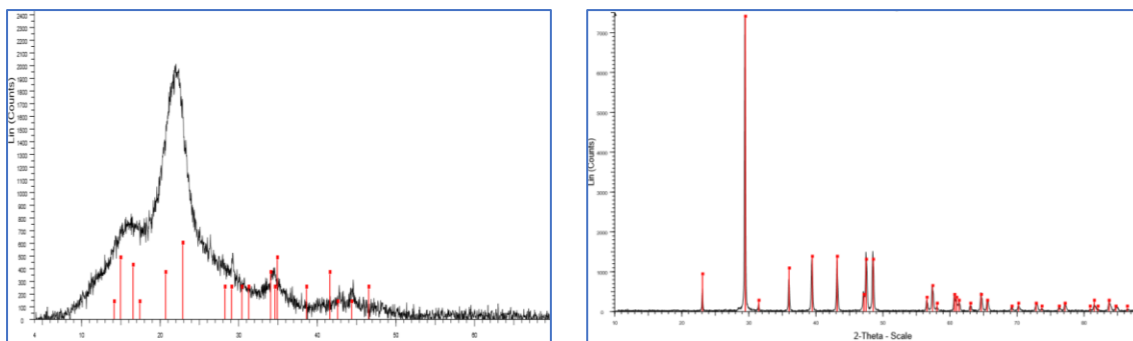
Figure 5: XRD Pattern of Sugarcane Bagasse (Left) and Eggshell biomass (Right)

For sugarcane bagasse, the diffraction pattern is not a good fit to the reference data and the lack of sharp diffraction peaks is characteristic of the amorphous constituents present in bagasse. This is mostly likely due to the lignin content present which is highly branched without a crystalline structure (Cagnon et al., 2009). With that said, the most noticeable peak that stands out occurs at a $2\theta$ value of $22°$. The peak formed at this angle is representative of native cellulose (Cellulose I). The work of Poletto et al. (2014) describes the pronounced peak range between $21.90°$ and $22.20°$ as the crystallographic plane of cellulose who further explains that it is the intramolecular and intermolecular hydrogen bonds of the free hydroxyl groups present in the cellulose macromolecules which give rise to this ordered crystalline arrangement. Further to this, Lopičić et al. (2016) supported the above results by assigning the $22.5°$ peak to the (002) plane of cellulose I. Sugarcane bagasse has both crystalline and amorphous regions with the cellulose constituent representing the crystalline region and lignin representing the amorphous one. Cellulose I, or native cellulose can exist as two polymorphs, a monoclinic structure $I_\beta$, which is the dominant polymorph in plants or a triclinic structure $I_\alpha$, which is more rare (Moon et al., 2011). Since bagasse is a lignocellulosic plant-based material, it is more likely that the monoclinic structure $I_\beta$ exists. It is worthy to note that the method of sample preparation is responsible for the development of texture in a sample which influences the relative intensities of the diffraction peaks and influences the crystallinity of a sample. This was demonstrated by Zhang et al. (2011) whose results showed that ball milled bagasse exhibited a lower crystallinity index compared to samples that were crushed using a cutter. It can therefore be assumed that the use of simple mechanical treatments such as grinding and crushing be used to improve the ratio of crystalline to amorphous regions in a sample which will inherently affect the accessible area available for adsorption.

The diffraction pattern of eggshells is a very good fit to the reference data highlighting the crystalline regions of the biomass. Eggshell waste is composed mainly of calcium carbonate (Ahmad et al., 2012) and the experimental evidence in figure 5 has demonstrated that the crystallographic lattice of calcium carbonate found in eggshells exists in the calcite phase with the highest peak observed at a $2\theta$ value of $29.38°$. This corresponds to the reference data found for the calcite phase of calcium carbonate crystals (AMCSD) which is also supported by the work of OK and co-workers (Ok et al., 2011). Generally, there are three possible polymorphs of calcium carbonate, namely vaterite, aragonite and calcite, listed in order of increasing thermodynamic stability. In eggshell waste, calcium carbonate exists predominantly in the calcite phase which typically assumes a rhombohedral structure.

### 3.3. Comparative Performance of the adsorbents

For the batch tests, a 100 mg/L concentrated adsorbate solution was prepared by diluting the stock solution with the addition of an appropriate amount of deionized water. For each experiment, 1.0 g of adsorbent was mixed with 100 mL of metal solution of < 75 µm particle size for a duration of 120 minutes to ensure equilibrium was reached. The pH was maintained at 5.5 for all experiments.
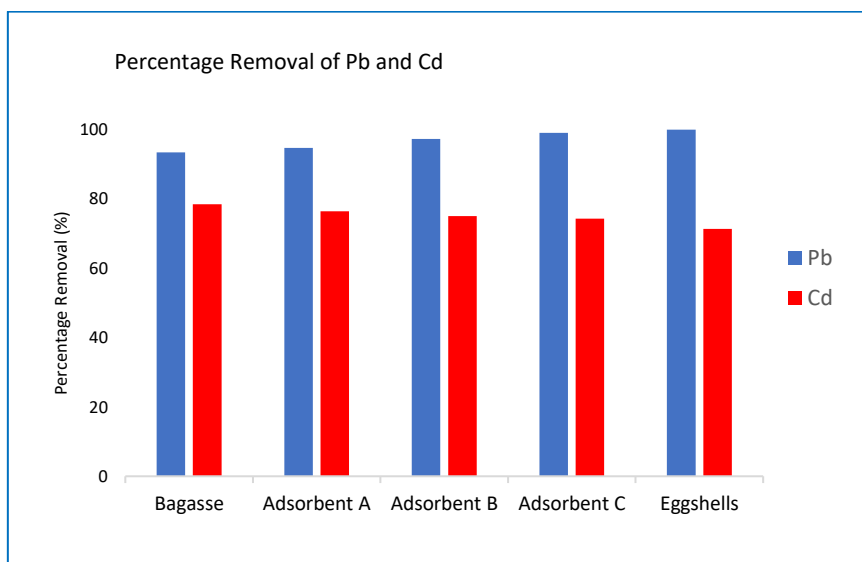


Figure 6. Batch Study: comparison of Pb and Cd removal

From the batch study, all adsorbents performed better in the removal of Pb than Cd. The percentage removal for Pb was in the range of 93 – 99 % with Cd removal remaining within the range of 70 – 75%. The order of efficiency for Pb removal were as follows: Eggshells > Adsorbent C > Adsorbent B> Adsorbent A> Bagasse. For Cd removal, Bagasse> Adsorbent A> Adsorbent B > Adsorbent C > Eggshells.

## 4. Conclusion

The surface properties of sugarcane bagasse and eggshell waste were identified using FTIR, XRD, BET and SEM-EDS analyses. Under the characterisation measurements investigated, eggshells were found to consist of calcium, oxygen and carbon atoms with carbon and oxygen atoms prominent in bagasse. This study shows that both biomaterials possess various functional groups that can function as cation exchange sites for the removal of pollutants from wastewater. Crystallographic information revealed a monoclinic lattice for bagasse with a rhombohedral lattice present in eggshells. The surface morphology of bagasse was found to exhibit an irregular surface however for eggshells, the surface was densely packed with a layered surface. The results strongly suggest the plausible reuse of both biomaterials in the treatment of wastewater through the biosorption process.

# 5. References

ABDOLALI, A., GUO, W. S., NGO, H. H., CHEN, S. S., NGUYEN, N. C. & TUNG, K. L. 2014. Typical lignocellulosic wastes and by-products for biosorption process in water and wastewater treatment: a critical review. *Bioresource technology,* 160**,** 57-66.

AHMAD, M., USMAN, A. R. A., LEE, S. S., KIM, S. C., JOO, J. H., YANG, J. E. & OK, Y. S. 2012. Eggshell and coral wastes as low cost sorbents for the removal of Pb2+, Cd2+ and Cu2+ from aqueous solutions. *Journal of industrial and engineering chemistry,* 18**,** 198-204.

AKSU, Z. & GÖNEN, F. 2004. Biosorption of phenol by immobilized activated sludge in a continuous packed bed: prediction of breakthrough curves. *Process Biochem.,* 5**,** 599–613.

AL-GHOUTI, M. A. & SALIH, N. R. 2018. Application of eggshell wastes for boron remediation from water. *Journal of Molecular Liquids,* 256**,** 599-610.

AMCSD. *American Mineralogist Crystal Structure Database* [Online]. Available: http://rruff.geo.arizona.edu/AMS/amcsd.php [Accessed 14/03/2020].

BUZZI, D. C., VIEGAS, L. S., SILVAS, F. P. C. & ESPINOSA, D. C. R. 2011. The use of Microfiltration and electrodialysis for Treatment of Acid Mine drainage. *IMWA***,** 287-292.

CAGNON, B., PY, X., GUILLOT, A., STOECKLI, F. & CHAMBAT, G. 2009. Contributions of hemicellulose, cellulose and lignin to the mass and the porous properties of chars and steam activated carbons from various lignocellulosic precursors. *Bioresource Technol***,** 292-298.

CARVALHO, J., RIBEIRO, A., GRAÇA, J., ARAÚJO, J., VILARINHO, C. & CASTRO, F. 2011. *Adsorption process onto an innovative eggshell-derived low-cost adsorbent in simulated effluent and real industrial effluents*.

CHAO, H. P., CHANG, C. C. & NIEVA, A. 2014. Biosorption of heavy metals on Citrus maxima peel, passion fruit shell, and sugarcane bagasse in a fixed-bed column. *Journal of industrial and engineering chemistry,* 20**,** 3408-3414.

DRIEMEIER, C., OLIVEIRA, M. M., MENDES, F. M. & GÓMEZ, E. O. 2011. Characterization of sugarcane bagasse powders. *Powder Technology,* 214**,** 111-116.

FLORES-CANO, J. V., LEYVA-RAMOS, R., MENDOZA-BARRON, J., GUERRERO-CORONADO, R. M., ARAGÓN-PIÑA, A. & LABRADA-DELGADO, G. J. 2013. Sorption mechanism of Cd(II) from water solution onto chicken eggshell. *Applied Surface Science,* 276**,** 682-690.

GAIKWAD, R. W., SAPKAL, V. S. S. & SAPKAL, R. S. S. 2010. Ion exchange system design for removal of heavy metals from acid mine drainage wastewater. *Acta Montanistica Slovaca***,** 298-304.

GURGEL, L. V. A., FREITAS, R. P. D. & GIL, L. F. 2008. Adsorption of Cu(II), Cd(II), and Pb(II) from aqueous single metal solutions by sugarcane bagasse and mercerized sugarcane bagasse chemically modified with succinic anhydride. *Carbohydrate Polymers,* 74**,** 922-929.

IUPAC. *International Union of Pure and Applied Chemistry* [Online]. Available: https://iupac.org/ [Accessed 02/05/2019].

LAKHERWAL, D. 2014. Adsorption of Heavy Metals: A Review *International Journal of Environmental Research and Development,* 4.

LEÃO, R. M., MILÉO, P. C., MAIA, J. M. L. L. & LUZ, S. M. 2017. Environmental and technical feasibility of cellulose nanocrystal manufacturing from sugarcane bagasse. *Carbohydrate Polymers,* 175**,** 518-529.

LIMA, M., D GOMEZ, L., G STEELE-KING, C., SIMISTER, R., BERNARDINELLI, O., CARVALHO, M., REZENDE, C., LABATE, C., DEAZEVEDO, E., J MCQUEEN-MASON, S. & POLIKARPOV, I. 2014. *Evaluating the Composition and Processing Potential of Novel Sources of Brazilian Biomass for Sustainable Biorenewables Production*.

LOPIČIĆ, Z. R., STOJANOVIĆ, M. D., MARKOVIĆ, S. B., MILOJKOVIĆ, J. V., MIHAJLOVIĆ, M. L., KALUĐEROVIĆ RADOIČIĆ, T. S. & KIJEVČANIN, M. L. J. 2016. Effects of different mechanical treatments on structural changes of lignocellulosic waste biomass and subsequent Cu(II) removal kinetics. *Arabian Journal of Chemistry*.

LUPTAKOVA, A., UBALDINI, S., FORNARI, P. & MACINGOVA, E. 2012. Physical, chemical and biological chemical methods for treatment of Acid mine drainage. *Journal of Chemical Engineering Transactions*.

MALKOC, E., NUHOGLU, Y. & ABALI, Y. 2006. Cr(VI) adsorption by waste acorn of Quercus ithaburensis in fixed beds: Prediction of breakthrough curves. *Chemical Engineering Journal,* 119**,** 61-68.

MAO, Y., MINGMING, S., XU, C., YANFANG, F., JINZHONG, W., KUAN, L., DA, T., MANQIANG, L., JUN, W., SCHWAB, A.P., AND XIN, J. 2017. Feasibility of sulfate-calcined eggshells for removing pathogenic bacteria and antibiotic resistance genes from landfill leachates. *Waste Management,* 63**,** 275-283.

MOON, R. J., MARTINI, A., NAIRN, J., SIMONSEN, J. & YOUNGBLOOD, J. 2011. Cellulose nanomaterials review: structure, properties and nanocomposites. *Chemical Society Reviews,* 40**,** 3941-3994.

MWASISWEBE, D. 2005. *Production of activated carbon from south african sugarcane bagasse.* Masters of Science in Engineering, University of KwaZulu-Natal, Durban.

OK, Y. S., LEE, S. S., JEON, W.-T., OH, S.-E., USMAN, A. & MOON, D. H. 2011. Application of Eggshell Waste for the Immobilization of Cadmium and Lead in a Contaminated Soil. *Environ Geochem Health,* 33 Suppl 1**,** 31-9.

OLIVEIRA, D., BENELLI, P. & AMANTE, E. 2013. *A literature review on adding value to solid residues: Egg shells*.

POLETTO, M., ORNAGHI JÚNIOR, H. L. & ZATTERA, A. J. 2014. Native Cellulose: Structure, Characterization and Thermal Properties. *Materials,* 7**,** 6105-6119.

PUTRA, W. P., KAMARI, A., YUSOFF, S. N. M., ISHAK, C. F., MOHAMED, A., HASHIM, N. & ISA, I. M. 2014. Biosorption of Cu(II), Pb(II) and Zn(II) Ions from Aqueous Solutions Using Selected Waste Materials: Adsorption and Characterisation Studies. *Journal of Encapsulation and Adsorption Sciences,* Vol.04No.01**,** 11.

RONDA, A., MARTÍN-LARA, M. A., DIONISIO, E., BLÁZQUEZ, G. & CALERO, M. 2013. Effect of lead in biosorption of copper by almond shell. *Journal of the Taiwan Institute of Chemical Engineers,* 44**,** 466-473.

SENTHIKUMAAR, S., BHARATHI, S., NITHYANANDHI, D., AND SUBBURAAM, C.V. 2000. Biosorption of toxic heavy metals from aqueous solutions *Bioresource Technology,* 75**,** 163-165.

SIMATE, G. S. & NDLOVU, S. 2015. The removal of heavy metals in a packed bed column using immobilized cassava peel waste biomass. *Journal of Industrial and Engineering Chemistry,* 21**,** 635-643.

THOMMES, M., KANEKO, K., NEIMARK ALEXANDER, V., OLIVIER JAMES, P., RODRIGUEZ-REINOSO, F., ROUQUEROL, J. & SING KENNETH, S. W. 2015. Physisorption of gases, with special reference to the evaluation of surface area and pore size distribution (IUPAC Technical Report). *Pure and Applied Chemistry.*

WONG, C.-W., BARFORD, J. P., CHEN, G. & MCKAY, G. 2014. Kinetics and equilibrium studies for the removal of cadmium ions by ion exchange resin. *Journal of Environmental Chemical Engineering,* 2**,** 698-707.

WONG, S. Y., TAN, Y. P., ABDULLAH, A. H. & ONG, S. T. 2009. REMOVAL OF BASIC BLUE 3 AND REACTIVE ORANGE 16 BY ADSORPTION ONTO QUARTENIZED SUGAR CANE BAGASSE. *The Malaysian Journal of Analytical Sciences,* 13**,** 185 - 193.

ZHANG, Z., MOGHADDAM, L., O'HARA, I. M. & DOHERTY, W. O. S. 2011. Congo Red adsorption by ball-milled sugarcane bagasse. *Chemical Engineering Journal,* 178**,** 122-128.

# Furfural Synthesis from Corn Cob & Pine Wood

*Ashish Baldania[1]\*, Bhalchandra Vibhute[2], Sachin Parikh[3]*

*\*[1]Faculty of Technology, R.K. University, Rajkot, India*
*[2]Faculty of Technology, R.K. University, Rajkot, India*
*[3]Chemical Engineering Department, L.D. Engineering College, Ahmedabad, India*
*Corresponding author: baldaniaashish@gmail.com, +91 9725668599

## Abstract

Furfural is a basic chemical which can be utilized in a variety of industries such as Chemical Industry, Refining Oil Industry, Food Industry and Agricultural Industry. This research work aims the use of Pine wood and Corn Cob for synthesis of furfural. The production of furfural by acid hydrolysis of Biomass is the focus area. Syntheses of the furanic compound at different Molar concentrations are used. With the help of GC – MS (Gas Chromatography) each step of product is analyzed. We focused on the hydrolysis in dilute Hydrochloric Acid (HCL) at specific temperature & reaction time. The experimental work is performed in a batch reactor system. A result shows maximum furfural (2.5 M HCL) yield 7.954 % is obtained for Corn Cob in comparison with pine wood.

*Keywords: Furfural, Acid Hydrolysis, Pine Wood, Corn Cob, GC – MS, Concentration.*

## 1. Introduction

Based on renewable resources chemical production has boomed over the past decade because of declining warehouses and commodity values in prices. Various types of biomass like crops, non-timber material and grasses are of particular focus because of their versatility, renewal, energy. Agricultural residues are mainly composed of three parts of the structure lignin, cellulose, and hemicellulose; each has specific structures designed for chemical production. Biomass in agricultural and forestry applications form a useful source for producing chemicals such as sugar reduction. All pentosan containing covers can, in a sense, as a raw material for the production of wool; however, an industrial furfural product requires a content of pentosans, 15 to 20%. About 1/3 of pentosans can be converted into fabric by production processes. Preferred solution for separating unsaturated chemicals in the refining of gas, diesel, and the high demand for its products, [1,2].

Two main types of technology to produce furfural, 1st is a one phase technology in which reduction of pentosans in xylose and dehydration goes hand in hand. 2nd is a two stage technology in which melting & decomposition of pentosan occur under mild conditions, followed by xylose to furfural drying. The advantage of the two stage technology is that the residual lignocellulose is slightly reduced and can convert other chemicals in the next step. [3,4].

Various researchers have investigated furfural production by hydrolysis of lignocellulosic residues in the presence of fatty acids such as catalyst, such as hydrochloric acid, nitric acid, sulfuric acid, and phosphoric acid. Among these acids like HCl, $H_2SO_4$, and $H_3PO_4$ produce a high wool yield, and $HNO_3$ is less active. The materials used for production of wool reported in the literature included, wood, sugarcane bagasse and rice husk. Several studies have been done using lignocellulosic materials such as feedstock for chemical production, In this case, Biorefinery concepts using pre-trade systematic biomass reconstruction aimed at chemical production and chemical products [5,6].

Pre-treatment of biomass, auto hydrolysis treatment detects high hemicellulose levels, converting them into soluble saccharides, while both cellulose and lignin are stored in a solid phase. The solid fraction obtained from auto hydrolysis treatment can produce bioethanol or other products with increased bio-based value. Hemicellulose-rich liquids can be used as raw material for the manufacture of wool, Hydroxymethylfurfural, the production of alcohol, and the removal of phenols from soluble components of lignin. In the anti-aging production by auto-hydrolysis Kraft. Burning such material is less expensive because its temperature is much lower and its load decreases overall stone production; it replaces the rescue boiler, which is bottled at most mills. Such items should be discarded, but this can create serious environmental issues. Therefore, its use for furfural production could be another exciting alternative [7].

Biomass has been accepted as practical Bio tool for production of petrol, various compounds, and chemicals for end products. The attractiveness of plat forming chemical products from renewable resources such as biomass has increased with fuel depots' depletion and rising prices. Carbohydrates produced by cellulose and hemicellulose from biomass can be refined into various additive products. However, hydrolysis decomposition/reaction to produce these products is a major challenge due to the high light cellulose [8,9].

Furfural, the main site for developing various platforms and additive chemical. Its greatest power lies in ingredients. It can be used to produce a variety of petroleum-based chemicals such as furan, tetrahydrofuran, and furfuryl alcohol, as well as in agricultural areas food, medicine. Furfural is produced by the hydrothermal process using a homogeneous acid catalyst that increases the hydrolysis of hemi cellulosic pentosans in biomass. Various types diverse elements used in production of furfural. Homogeneous regenerative elements, including mineral acids have been reported as effective stimulants for commercial art production. More expensive acids cause pipes corrosion and valves at higher temperatures, safety and environmental problems because of hazardous waste disposal. Mineral acid has cause undesirable side effects because of strong acidity. [10,11].

Process improvement is needed to remove such problems. Studies use organic acids to convert the mineral acids. Weak organic acids prefer to hydrolyze only weak bonds, leaving unchanged cellulose, lignin formation. Also, the organic acid is formic acid is alternative to Biorefinery because one of the products produced during the production of furfural is formic acid is from the formation of formyl group. Formic acid can be obtained from a moderate reaction after heat reaction, and neutral waste generating acid. [12].

Ethanol is a solvent which found in biomass production through biological or thermo chemical processes, has great potential for biodiversity production, especially under extreme conditions, as an effective biomass extinction source. The chemical and physical properties of high-quality liquids vary as a gas-like liquid by controlling its temperature and density, which affects its ionic production and dielectric flexibility, leading to increased attention to its use as a medium reaction [13].

Many batch processes have been performed with multiple batch operations using sulfuric acids as an acid catalyst and temperatures in the range of 160°C and 200°C. High costs and low efficiency associated with low yield ecosystems, less than 50%, led to the closure of crops designed for mass production in the 1990s. [12,13,14].

Furfural resinification is the process by which furfural reacts on its own, while condensation occurs. Furfural loss by condensation is higher than resinification loss in recent decades to reduce corruption and improve productivity. Corn Cob and Wood were hydrolyzed with acid to produce chemicals furfural. Biomass fossils found in agricultural and forestry applications form a source for producing chemicals. [14].

Agricultural waste containing pentosan in maize, rice and bagasse. Furfural is a solution produced from pentosans in plant tissue. The product helps to convert the extra supply of lignocelluloses feedstock into ethanol and its associated chemical products with high value. There are currently four important and potential applications for non-industrial products such as agrochemicals, Fuels. Corncobs as a material for furfural processing using the method of acid hydrolysis. Corncobs are heated with HCl at a temperature range of 180 -185 0C in an autoclave for about 45 mins. The Yield of furfural was found at about 7.75%. [13,14].

The corncob was heated with HCl at 180 0C in a press heater for about 30 minutes. Yield of furfural obtained was 1-1.5% and adhesive was 40-45%. The unit consists of a pressing, grinding unit with continuous column and cobs are soaked in water with a high-pressure vapor; the vapor is condensed to form a hair-soluble solution. The most effective conditions are pressure, 180 to 135 kg (180 ° C); water and grain ratio, 4: 1; digestion time, 2 hrs. The natural yield obtained is 6% of cob wt % used. The chemical compounds produced at the time of process are acetic acid, hydrochloric acid, and sulfuric acid with lactose, other iron oxides, mild oxidizing agents. To identify furfural presence GC, HPLC, and UV spectrophotometer are used. Small oxidizing agents does not affect the furfural yield, but the catalyst presence was affects the yield of furfural. [13,14].

## 2. Materials & Experimental Methods

### 2.1 Precursor Selection [15,16,17,18,19]

Selection of the precursor (raw material) for furfural production was apparently the first step in the research work. The available choices for precursor were:
1) Corn Cob (Morbi)
2) Pine Wood (Shri Krishna Vijay Saw Mill)



Figure 2.1 "Waste Corn Corb for Furfural Production"

Determining the superiority of the precursor compare to other precursors using a method like:
1) Proximate analysis

### 2.2 Characterization of Precursor [20,21,22,23]

In furfural production, raw material composition is a vital factor for determining the selection precursor. Precursor's chemical composition, especially the % of cellulose and lignin present in the pinewood, is crucial.

## 2.2.1 Cellulose Estimation

1.0 g of sample was mixed with 160 ml of 80% acetic acid + 10 ml of concentrated nitric acid and placed in a water bath for about 30 minutes with a temperature of 100°C. The collected residues were washed and for one hour soaked in 1 ml of 90% $H_2SO_4$. Afterward, 10 ml of anthrone was added to 1 ml of solution was diluted to 100 ml. For 15 minutes, tubes are heated in a water bath and measure absorption by 630 nm. 40 - 200 μg/L of cellulose is determined from the standard graph.

## 2.2.2 Estimation of Lignin

The sample (50 gm) was ground with ether until it was released from chlorophyll. The sediment was washed and rinsed. NaOH (1ml) was added to the residue, extracted at 80 °C for 12 hours. HCl (0.45 ml) was added, and using NaOH the pH was reduced to 7. The prepared solution was run by 2300 per minute. At 245 nm and 350 nm, absorbance was measured. The lignin amount is calculated between pH - 7.0 and pH - 12.

## 2.3 Preparation of Furfural product [25,26,27]

Specific amount (1 kg each) of Corn Cob (Morbi, Gujarat) and Pinewood (Same Material Used in the production of activated Carbon) is collected from a Local Area. It is then dried to in to the oven with temperature of 200°C for 2 days. It is then grinded into the mixture and sieved to a maximum 1mm size, is stored in a silica desiccator.

In a batch reactor, the experiment is carried out. The apparatus consists of a three-neck round bottom flask (3 liters) as a batch reactor, a column of 30 cm, a condenser, a mechanical stirrer, a flask, and a temperature measuring device (Figure 2.2). 1.50 liters of 1M aqueous HCl and 6.84 moles of 400 g NaCl were added to the flask, and 20 gms of Biomass. Based on that, different Molar Concentration of HCl has been prepared. The reaction mixture is continuously heated and stirred. The process of Steam distillation is carried out for 15 minutes at 107°C. 250 ml chloroform is added to the distillate into an extraction flask (Figure 2.3). As shown in (Figure 2.4), two layers are formed in which the aqueous layer at the top and the chloroformfurfural containing layer available at the bottom. [32, 42,53].

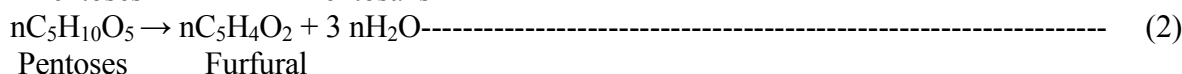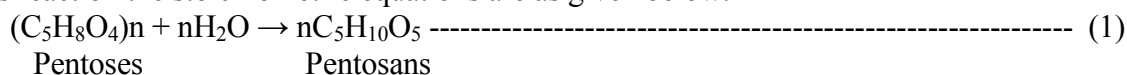For this reaction the stoichiometric equations are as given below.

$(C_5H_8O_4)n + nH_2O \rightarrow nC_5H_{10}O_5$ ------------------------------------------------------------ (1)

    Pentoses               Pentosans

$nC_5H_{10}O_5 \rightarrow nC_5H_4O_2 + 3 nH_2O$-------------------------------------------------------------- (2)

    Pentoses        Furfural

Figure 2.2. "Acid hydrolysis of biomass for synthesis of furfural"
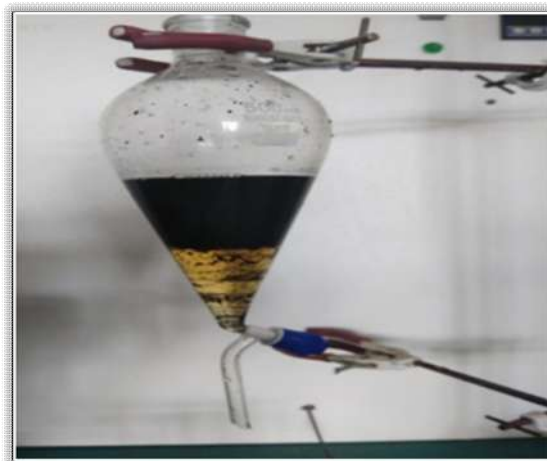


Figure 2.3 "Process of extraction after acid hydrolysis"


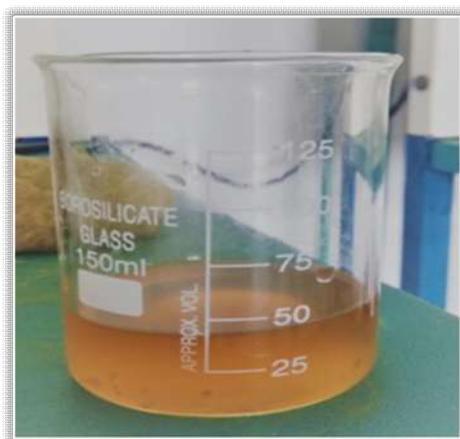
Figure 2.4 "Synthesized product after extraction"

## 2.4 Characterization of Furfural [8,9, 31,32]

2.4.1 Analytical Method

The extraction is carried out for the chloroform-furfural layer to remove the chloroform. The remaining liquid is yellowish. The product is then analyzed by GC-MS and is determined as furfural. In this analysis, Gas chromatograph is used which is equipped with a flame ionization detector. Injections were performed using an automatic sampler.

## 2.5 Application study of Furfural [12,30,33]

Catalyst like Sulfuric, hydrochloric, and phosphoric acid are used for furfural production. Furfural yields obtained in this study are in the range of 1.094 to 7.954 (dry weight). A 5.6% natural yield was obtained from oil palm at 198 °C for 11 minutes with dilute sulfuric acid. In the presence of nitric acid the furfural production was 3.5%. The highest furfural yield of 7.954% wt at 2.5 M HCl in the present study.

Table 2.1 "Comparison of various methods for production of furfural from biomass" [2,33,34]

| Sr. No. | Types of Method | Process | Operating conditions | Advantages |
|---|---|---|---|---|
| 1 | Physical | Chipping Grinding Milling Process | • Energy input < 30Kw per ton biomass<br>• Room temperature | Reduces cellulose critallinity |
| | | Steam pretreatment | • 160-260°C<br>• 5-15 min | • Causes hemicellulose auto hydrolysis and lignin transformation<br>• Cost-effective for hardwoods and agricultural residues |
| | | Ammonia fiber explosion method | • 1-2kg ammonia/kg dry biomass<br>• 0°C for 30 min. | • Increases accessible surface area<br>• Removes lignin and hemicellulose |
| | | Ammonia recycle percolation method | • for 14 min Fluid velocity 1cm/min<br>• 150-170°C | • Increases accessible surface area<br>• removes lignin and hemicellulose |
| | | CO2 explosion Process | 4kg CO2/kg fiber at 5.62 Mpa 160 bar for 90 min at 50 °C under supercritical carbon dioxide | Do not produce inhibitors for downstream processes. |
| | | Ozonolysis Process | Room temperature | • Reduce lignin content.<br>• Does not produce toxic residues |
| | | Wet oxidation Process | for 30 min, 148-200°C | • Removal of lignin<br>• low formation of inhibitors and low energy demand |
| 2 | Chemical | Acid hydrolysis: Dilute-Acid pretreatment Process | • Type I: T>160°, continuous-flow process for low solid loading 5-10 %,)<br>• Type II: | Alters lignin structure and Hydrolyzes hemicellulose to xylose and other sugar. |

| | | | T<160°C, batch process for high solid loadings (10-40%) | |
| --- | --- | --- | --- | --- |
| | | Alkaline Hydrolysis Process | Long time high Concentration of the base; For soybean straw at Low temperature, ammonia liquor (10%) for 24 h at room temperature | Removes hemicelluloses and lignin and increases accessible surface area |
| | | Organosolv Process | without addition of catalysts (oxalic, salicylic, acetylsalicylic acid) at 150-200 °C | Hydrolyzes lignin and hemicelluloses |
| 3 | Biological | Biological Treatment | brown-, white- and soft-rot fungi | • Degrades lignin and hemicelluloses <br> • low energy requirements |
| 4 | Electrical | Pulsed electrical field in the range of 5-20 kV/cm, | ~2000 pulses of 8 kV/cm | • Ambient conditions <br> • disrupts plant cells <br> • simple equipment |

# 3. Result & Discussion

## 3.1 Selection of Precursor [35,36,37]

The results reported is indicate that the Corn Cob has a low lignin content (16 %) , high cellulose content (40 %) and which is an important for Furfural preparation.

Table 3.1 "Chemical Composition of Corn Cob & Pine wood"

| Precursor | Cellulose | Hemicellulose + Others | Lignin |
| --- | --- | --- | --- |
| Corn Cob | 40% | 36% | 16% |
| Pine Wood | 40.7 % | 32.3 % | 27.0 % |

## 3.2 Acid Concentration Effect. [8,36,39]

The effect of acid concentration studies furfural yield. The different acid concentrations can be used, such as (0.5 M, 1.5 M & 2.5 M, 3.0 M). (Table 3.2) shows the effect of acid on yield of furfural. Increase in the furfural production as increase in the concentration of furfural. Highest yield is obtained at 2.5 M concentration of HCL when raw material is corn cob.

Table 3.2 "Furfural Concentration Results for Different Biomass Samples"

| Sr. No. | Different Biomass Samples | Wt% Furfural Concentration |
|---|---|---|
| 1 | 0.5 M HCL + Corncob (20 gms) | 1.092 |
| 2 | 1.5 M HCL + Corncob (20 gms) | 2.489 |
| 3 | 2.5 M HCL + Corncob (20 gms) | 7.954 |
| 4 | 3.0 M HCL + Corncob (20 gms) | 5.897 |
| 5 | 1.5 M HCL + Pine Wood (20 gms) | 1.525 |
| 6 | 2.5 M HCL + Pine Wood (20 gms) | 1.570 |
| 7 | 3.0 M HCL + Pine Wood (20 gms) | 1.426 |

## 3.3 GC – MS Analysis [19,20,38,40]

GC-MS Report for Identification of Furfural Concentration and Calibration Curve (Figure 3.1, 3.2) are showing that at 2.5 M Concentration of HCL along with Corn Cob as a raw material biomass is giving 7.957 % Wt of furfural which is highest among other concentration result and as well as with wood as raw material
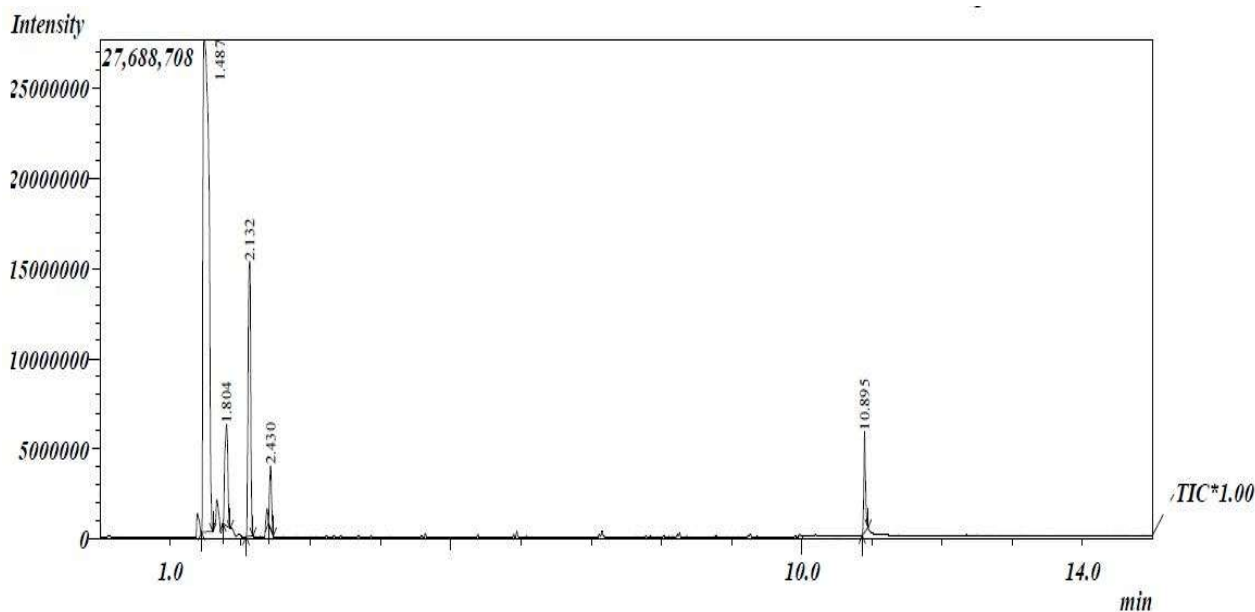


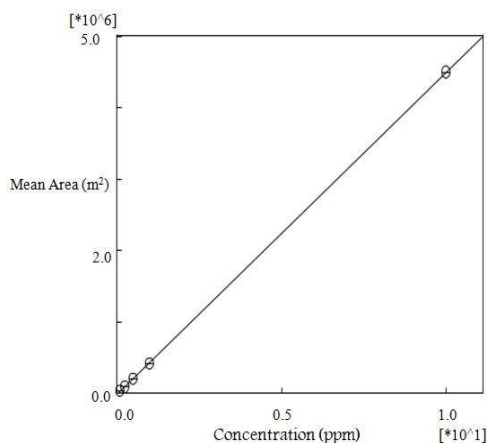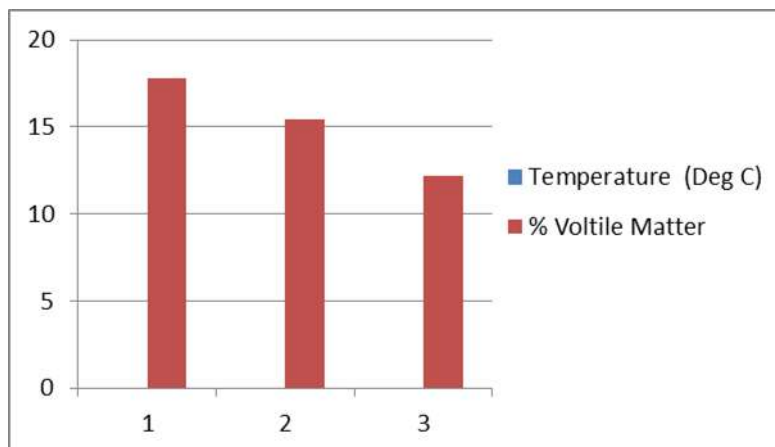Figure 3.1 "GC-MS Report for Identfication of Furfural Concentration"



Figure 3.2 "GC- MS Least Square Method Calibration Curve"

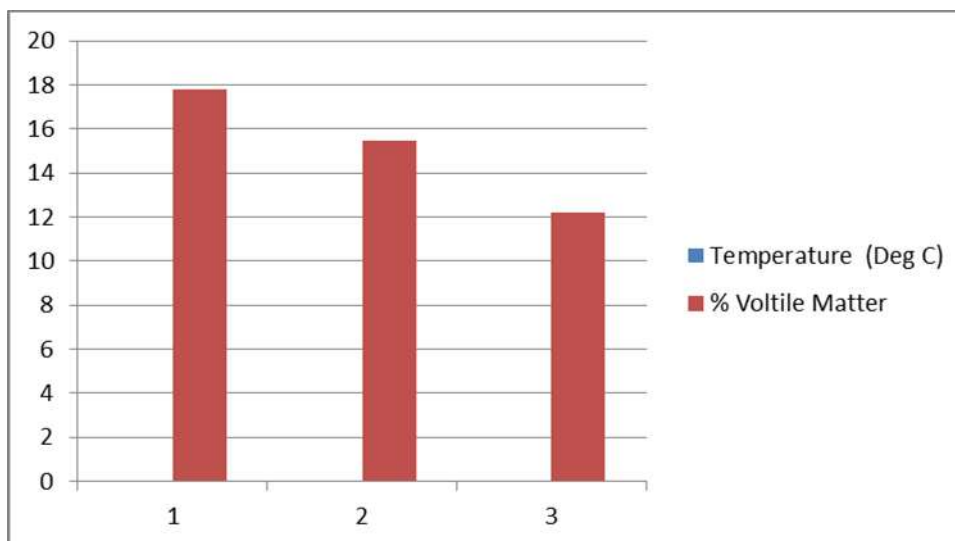## 3.4 Statistical optimization of Furfural production [10,38,39,42].

### 3.4.1 Effect of Acid Concentration on % Furfural for Corn Cob.



Graph 3.1 "Effect of Acid Concentration on % Furfural production for Corn Cob"

- Graphs 3.1 clearly shows that at 2.5 M HCl the % wt furfural concentration value is higher as compare to other HCL molar values. We can also analyze that after 2.5 M HCl if we further increase in HCL Molar values the % wt furfural concentration will decrease.

### 3.4.2 Effect of Acid Concentration on % Furfural for Pine Wood



Graph 3.2 "Effect of Acid Concentration on % Furfural production for Pine Wood"

- Graph 3.2 shows that at 2.5 M HCl the % wt furfural concentration value is higher as compare to other HCL molar values, But if we compare with Pine wood graph, here in this case there is not much differnce observed in % wt furfural as increase in Molar HCL value. We can also analyze that after 2.5 M HCl if we further increase in HCL Molar values the % wt furfural concentration will decrease.

3.4.3 Effect of Precursor on % Furfural
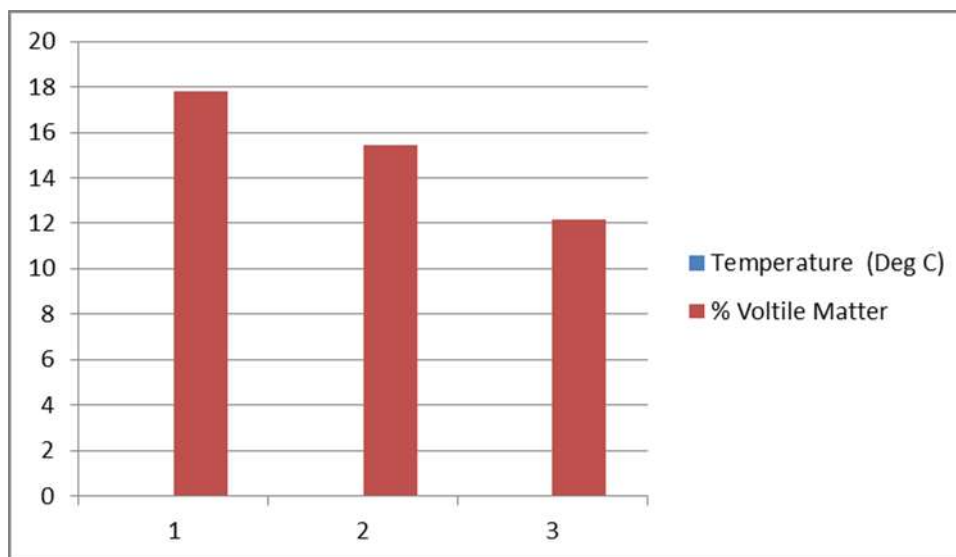


Graph 3.3 "Effect of Precursor on % Furfural Production"

- Graph 3.3 shows that at evey Molar value of HCl, the % wt furfural concentration value is higher in case of Corncob used as precursor as compare Pine wood. Higher wt% Furfural result at 2.5 M HCl when Corn cob is used as a precursor is 7.954 wt %.

## 4. Conclusion

Many new developments occur in acid hydrolysis and furfural use, such as synthesizing the family of solvents such as furfuryl alcohol and tetrahydrofuran in plastic manufacture and metal coatings. It plays an important role in insecticide manufacturing as well. Nowadays, the food industry is using furfural for flavouring as well. Researchers are working on the acid hydrolysis of lignocellulosic waste using various metal catalysts. In this study test, a good yield of 7.954 wt% furfural from Corn Cob was obtained, verified by various tests. Hence, from an environmental and economic point of view, furfural production from biomass could provide a less expensive alternative to commercially produced furfural.

## References

[1] Sarvamangala R. Patil A. Dayanand, *Production of pectinase from deseeded sunflower head by Aspergillusniger in submerged and solid-state conditions*, Bioresource Technology 97, 2054–2058, 2006.
[2] H. D. Mansilla, J. Baezu, S. Urzua, G. Muturana, J. Villasenor, and N. Duran," *Acid-catalyzed hydrolysis of rice hull: evaluation of furfural production",* Bioresource Technology, 66,189-193,1998.
[3] Salim S.A.L.Showiman, *Furfural from some edible plants Grown in Saudi Arabia*, J.King Saud Univ., Vol.10, 119-125, 1998.
[4] S. Abad, J. L. Alonso, V. Santos & J. C. Paraj, *Furfural From Wood In Catalyzed Acetic Acid Media: A Mathematical Assessment*, Bioresource Technology 62 , 115-122,1997.
[5] Claude Moreau, Robert Durand et.al., *Selective preparation of furfural from xylose over micro porous solid acid catalysts, Industrial Crops and Products* 7 , 95–99,1998.

[6] Hdctor D. Mansilla, Jaime Baeza, Sergio Urzfia , Gabriel Maturana h, Jorge Villasefior h & Nelson Durfin, *Acid-Catalyzed Hydrolysis Of Rice Hull: Evaluation of Furfural Production*, Bioresource Technology, 66 ,p.n.189- 19,1998.

[7] Daniel Montane, Joan Salvado, Carles Torras, Xavier Farriol, *High-temperature dilute-acid hydrolysis of olive stones for furfural production*, Biomass and Bioenergy ,22 ,295 – 304,2002.

[8] H.K. Ong and M. Sashikala, *Identification of furfural synthesized from pentosan in rice husk*, J. Trop. Agric. and Fd. Sc. 35(2)(2007): 305– 312,2007.

[9] Wirungrong Sangarunlert, Pornpote Piumsomboon et.al ,*Furfural production by acid hydrolysis and supercritical carbon dioxide extraction from rice husk* ,Korean J. Chem. Eng., 24(6), 936-941,2007.

[10] Manuel Vazque, Martha Oliva, Simon J. Tellez-Luis , Jose A. Ramırez, *Hydrolysis of sorghum straw using phosphoric acid: Evaluation of furfural production*, Bioresource Technology ,98 , 3053–3060,2007.

[11] Vittaya Punsuvon, Pilanee Vaithanomsat and Kenji Iiyama, *Simultaneous production of α-cellulose and furfural from bagasse by steam explosion pretreatment*, Mj. Int. J. Sci. Tech., 2(01), 182-191,2008.

[12] Masoud Kazemi and Mohammad Reza Zand-Monfared ,*Furfural production from pisthachio green hulls as agricultural residues,* JACR, Vol. 3, No. 12,2010.

[13] Cai, C. M.; Zhang, T.; Kumar, R.; Wyman, C. E. *Integrated furfural production as a renewable fuel and chemical platform from lignocellulosic biomass*. J. Chem. Technol. Biotechnol. 2014, 89 (1), 2− 10

[14] (3) Climent, M. J.; Corma, A.; Iborra, S. *Conversion of biomass platform molecules into fuel additives and liquid hydrocarbon fuels*. Green Chem. 2014, 16 (2), 516−547.

[15] Lange, J. P.; van der Heide, E.; van Buijtenen, J.; Price, R. *Furfural a promising platform for lignocellulosic biofuels*. ChemSusChem 2012, 5 (1), 150−166.

[16] Dutta, S.; De, S.; Saha, B.; Alam, M. I. *Advances in conversion of hemicellulosic biomass to furfural and upgrading to biofuels*. Catal. Sci. Technol. 2012, 2 (10), 2025−2036.

[17] Karinen, R.; Vilonen, K.; Niemela, M. *Biorefining: heteroge- ¨neously catalyzed reactions of carbohydrates for the production of furfural and hydroxymethylfurfural*. ChemSusChem 2011, 4 (8), 1002− 1016.

[18] Dashtban, M.; Gilbert, A.; Fatehi, P. *Production of furfural: overview and challenges*. J. Sci. Technol. Forest Prod. Process 2012, 2 (4), 44−53.

[19] Hurd, C. D.; Isenhour, L. L. *Pentose reactions. I. Furfural formation*. J. Am. Chem. Soc. 1932, 54 (1), 317−330.

[20] Dunlop, *A. Furfural formation and behavior*. Ind. Eng. Chem. 1948, 40 (2), 204−209

[21] Fulmer, E. I.; Christensen, L.; Hixon, R.; Foster, R. *The Production of Furfural from Xylose Solutions by Means of Hydrochloric Acid−Sodium Chloride Systems*. J. Phys. Chem. 1936, 40 (1), 133−141.

[22] Brownlee, H. J.; Miner, C. S. *Industrial development of furfural*. Ind. Eng. Chem. 1948, 40 (2), 201−204.

[23] Gü rbü z, E. I.; Gallo, J. M. R.; Alonso, D. M.; Wettstein, S. G.; Lim, W. Y.; Dumesic, J. A. *Conversion of Hemicellulose into Furfural Using Solid Acid Catalysts in γ-Valerolactone*. Angew. Chem., Int. Ed. 2013, 52 (4), 1270−1274

[24] Choudhary, V.; Pinar, A. B.; Sandler, S. I.; Vlachos, D. G.; Lobo, R. F. *Xylose isomerization to xylulose and its dehydration to furfural in aqueous media*. ACS Catal. 2011, 1 (12), 1724−1728.

[25] Amiri, H.; Karimi, K.; Roodpeyma, S. *Production of furans from rice straw by single-phase and biphasic systems*. Carbohydr. Res. 2010, 345 (15), 2133−2138

[26] Bhaumik, P.; Deepa, A.; Kane, T.; Dhepe, P. L. *Value addition to lignocellulosics and biomass-derived sugars: An insight into solid acid-based catalytic methods*. J. Chem. Sci. 2014, 126 (2), 373−385

[27] Luo, Y.; Hu, L.; Tong, D.; Hu, C. *Selective dissociation and conversion of hemicellulose in Phyllostachys heterocycla cv. var. pubescens to value-added monomers via solvent-thermal methods promoted by AlCl3*. RSC Adv. 2014, 4 (46), 24194−24206.

[28] Yang, Y.; Hu, C. W.; Abu-Omar, M. M. *Synthesis of furfural from xylose, xylan, and biomass using AlCl3· 6H2O in biphasic media via xylose isomerization to xylulose*. ChemSusChem 2012, 5 (2), 405− 410

[29] Yang, W.; Li, P.; Bo, D.; Chang, H.; Wang, X.; Zhu, T. *Optimization of furfural production from d-xylose with formic acid as catalyst in a reactive extraction system*. Bioresour. Technol. 2013, 133, 361−369.

[30] Yang, W.; Li, P.; Bo, D.; Chang, H. *The optimization of formic acid hydrolysis of xylose in furfural production*. Carbohydr. Res. 2012, 357, 53−61.

[31] Chheda, J. N.; Roman-Leshkov,́ Y.; Dumesic, J. *A. Production of 5-hydroxymethylfurfural and furfural by dehydration of biomassderived mono-and poly-saccharides*. Green Chem. 2007, 9 (4), 342− 350.

[32] Zhang, T.; Kumar, R.; Wyman, C. E. *Enhanced yields of furfural and other products by simultaneous solvent extraction during thermochemical treatment of cellulosic biomass*. RSC Adv. 2013, 3 (25), 9809−9819.

[33] Cai, C. M.; Zhang, T.; Kumar, R.; Wyman, C. E. *THF cosolvent enhances hydrocarbon fuel precursor yields from lignocellulosic biomass*. Green Chem. 2013, 15 (11), 3140−3145.

[34] Zeitsch, K. J. *Process for the Manufacture of Furfural*. U.S. Patent 6,743,928, Jun 1, 2004.

[35] Molina, M. C.; Mariscal, R.; Ojeda, M.; Granados, M. L. *Cyclopentyl methyl ether: A green co-solvent for the selective dehydration of lignocellulosic pentoses to furfural*. Bioresour. Technol. 2012, 126, 321−327.

[36] Kim, E. S.; Liu, S.; Abu-Omar, M. M.; Mosier, N. S. *Selective conversion of biomass hemicellulose to furfural using maleic acid with microwave heating*. Energy Fuels 2012, 26 (2), 1298−1304.

[37] Gü rbü z, E. I.; Wettstein, S. G.; Dumesic, J. A. *Conversion of hemicellulose to furfural and levulinic acid using biphasic reactors with alkylphenol solvents*. ChemSusChem 2012, 5 (2), 383−387.

[38] Xing, R.; Qi, W.; Huber, G. W. *Production of furfural and carboxylic acids from waste aqueous hemicellulose solutions from the pulp and paper and cellulosic ethanol industries*. Energy Environ. Sci. 2011, 4 (6), 2193−2205.

[39] Weingarten, R.; Cho, J.; Conner, W. C., Jr.; Huber, G. W. *Kinetics of furfural production by dehydration of xylose in a biphasic reactor with microwave heating*. Green Chem. 2010, 12 (8), 1423− 1429.

[40] Lessard, J.; Morin, J.-F.; Wehrung, J.-F.; Magnin, D.; Chornet, E. *High yield conversion of residual pentoses into furfural via zeolite catalysis and catalytic hydrogenation of furfural to 2-methylfuran*. Top. Catal. 2010, 53 (15−18), 1231−1234.

[41] Shekiro, J., III; Kuhn, E. M.; Nagle, N.; Tucker, M.; Elander, R.; Schell, D. *Characterization of pilot-scale dilute acid pretreatment performance using deacetylated corn stover. Biotechnol.* Biofuels 2014, 7, 23.

[42] Root, D. F.; Saeman, J. F.; Harris, J. F.; Neill, W. K. *Kinetics of the acid-catalyzed conversion of xylose to furfural*. Forest Prod. J. 1959, 9, 158−165.

# An Efficient Use of Mineral Base Oils by Improving Physico-Chemical Properties via Hydro-treatment Route

*Thummapalli Snigdha[a], Siddharth Modi[b], T Saritha[a], Meka Srinivasa Rao[b], TCSM Gupta[a]\**

*[a]R&D Centre, Apar Industries Limited., Mumbai, INDIA*

*[b]Department of Chemical Engineering , D. D. University (DDU), Nadiad, INDIA*

*\* Correspondence: tcsm.gupta@apar.com*

## ABSTRACT

The mineral oils used for process and lubricant applications are traditionally manufactured by treating the base oils using oleum treatment followed by solvent extraction to remove converted soluble acids from various unsaturates, such as aromatics, and heterocyclic compounds of sulphur and nitrogen. The hydro-treatment is one of the competing route to reduce the undesirable unsaturates. However, the efficacy of hydrogenation route in terms of improvement of product quality is not well reported. In the present study, the hydrogenation of base oils is evaluated based on four parameters namely reduction in aromatic content, improvement of physico-chemical properties,enhanced UV stability and better biodegradability. The percentage aromatic reduction was analysed using FTIR, whereas ultimate biodegradation was evaluated as per standard test of OECD 301B. The improvement in various physico-chemical properties like Viscosity Index (VI), aniline point, sulphur content, UV and oxidation stability were checked by respective ASTM standards. The base oil is observed to have reduced aromatics, enhanced bio-degradability and improved physico-chemical properties post hydro-treatment.

.

## KEYWORDS

Base oils, Physico-chemical properties, Biodegradability, UV and Oxidation stability, Hydro-treatment

# 1. Introduction

The mineral base oils are highly complex mixture of, paraffins, iso-paraffins, naphthenes aromatics and Polycyclic Aromatic Hydrocarbons (PAHs).The PAHs have two or more fused aromatic rings and is found to be probable carcinogens(Menzie and Potocki, 1992). The PAHsare also reported as potential environmental pollutants with genotoxic and mutagenic properties(Laheto et al, 2003).

The industries associated with mineral base oil processing perform hot oleum treatment to remove the aromatics and PAHs to meet the statutory norms. The hot oleum process generates lots of liquid effluent and subsequent solid waste for disposal in secured landfilling. This treatment also exhibits serious operational challenge due to liberation of huge amount of acidic vapors during the process. The European Union (EU) has labelled this hot oleum treated base oils as possible cancer hazard and use of such oil is prohibited for food and medicinal grade applications (EU regulation No 1223/2009).

To address this particular issue, two approaches namely hydrogenation and adsorption over acid clay are reported in literatureby various co-workers (Rausch, 1963; Gilbert, 1972; Kindwell Jr., 1977; Anstock, 1988; Corman, 1989; Powers, 1999; Hantzer, 2001; Lin et al, 2003; Germaine, 2005; Rosenbaum, 2015).The hydrogenation approach involves handling of hydrogen at elevated temperature and pressure condition but does not produce any waste at the end of process.Against this, the adsorptive process is relatively safer from operation point of view, however, it requires long contact hours and regeneration of adsorbents. The adsorbents have fixed life and after which they are required to be disposed in secured landfill. Thus both the approaches have some merits and demerits.

The hydrogenation approach is relatively cleaner approach among all with an added advantage of high through put. Due this, we have considered it as a potential method for PAH removal and evaluated the hydrogenation of naphthenic base oils based on four parameters namely reduction in aromatic content, improvement of physico-chemical properties, enhanced UV stability and better biodegradability. The safety evaluation of the hydrogenation process is separately addressed by us(Modi et al, 2020).

The structure of this paper is as follows. The section 2 discuss about base oil characteristics and analytical methods used to analyse the performance. The next section 3 evaluates the performance based on obtained results. The conclusions are derived in section 4.

## 2. Materials and Methods

### 2.1. Base Oil Characteristics

The naphthenic type of base oilwas considered for hydrogenation in range of 180 °C to 230 °C and 20 bar to 60 bar pressure. The hydrogenation was performed in both semi-batch mode and continuous mode using nickel based catalyst. Thesemi-batch mode experiments were performed till 18 hours of time span.

The base oil was observed to be C20 rich with highest aromatic content of 14% by mass. The physical appearance of base oil was clear, water white transparent and odourless. The density was obtained to be 0.86 gm/cm3, Viscosity Index (VI) of 71 and Refractive Index (RI) of 1.4788. The flash point, pour point and aniline point were 144 °C, -21 °C and 78 °C respectively before hydrogenation.

### 2.2.Characterisation Methods

Numerouscharacterisations were performed by us using well established standards. The most critical analysis ofPAH was performed as per ASTM D2269 followed by FTIR analysis utilizing DTGS TEC detector in range of 4000 cm$^{-1}$ to – 400 cm$^{-1}$.The other analysis were Viscosity Index (VI) by ASTM D2270, aniline point based on ASTM D611A,pour point determined by ASTM D97, flash point using ASTM D93, Refractive Index (RI) obtained by ASTM D1218 and sulphur content quantified by ASTM D2622.The biodegradabilitytestwas performed under standard condition mentioned by OECD 301B and the UV stability was measured by placing transparent glass bottle under direct sunlight for 8 hour and followed by Rotating Vessel Oxidation Test (RVOT) using ASTM D2112.

## 3. Results and Discussion

### 3.1. Aromatics Reduction

The first parameter to be measured was the %aromatics reductionpost hydro-treatment. The hydrogenation was performed till 18 hours in the range of 180 °C to 230 °C and 20 bar to 60 bar pressure with varying catalyst loading of 2 gm to 6 gm.The untreated base oil had 14% aromatics to be present in it.

## %Aromatics Reduction
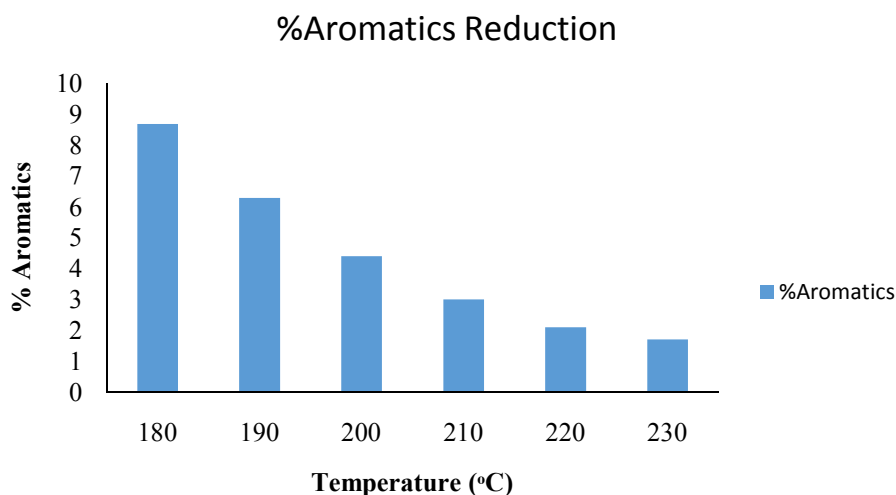
**Fig.1. %Aromatics reduction with respect toTemperatureChange**
**(Reaction condition: 60 bar,5gm of catalyst and 18 hours of reaction time)**

Fig.1 shows significantreduction in %aromatics post hydro-treatment to as low as 1.68% whereas the untreated oil had 14% aromatics to be present in it. The oil below 4% aromatics are suitable for various applications like circulating oil, lubricating oil and metal cutting oil type of applications.

### 3.2.Changes in Physico-chemical properties

After the removal of aromatics, the most important step is the evaluation of improvements in various physico-chemical properties.To evaluate this therelevant ASTM standards were adopted. Table-1, lists all useful physico-chemical properties of feedstock and product post hydro-treatment.

**Table-1 Physico-chemical properties of feedstock and product**

| Sr. No. | Characteristic Properties | Test Methods | Feed | Product |
|---|---|---|---|---|
| 1 | Density at 15°C | ASTM D 1298 | 0.8649 | 0.8636 |
| 2 | Viscosity at 40°C | ASTM D 7042 | 7.84 | 7.86 |
| 3 | Viscosity at 100°C | ASTM D 7042 | 2.12 | 2.20 |
| 4 | Viscosity Index | ASTM D 2270 | 50.7 | 76.8 |
| 5 | Aniline Point | ASTM D 611A | 77.2 | 81.8 |
| 6 | Flash Point | ASTM D 93 | 140.4 | 140.3 |
| 7 | Pour Point | ASTM D 97 | -39 | -39 |
| 8 | Refractive Index | ASTM D 1218 | 1.47 | 1.47 |
| 9 | PAH Test | ASTM D 2269 | 1.88% | 1.22% |
| 10 | Sulphur Content Test | ASTM D 2622 | 1.5 ppm | 0.85 ppm |
| 11 | RVOT Anti-Oxidant | ASTM D 2112 | 220 min | 400+ min |

From table-1, it can be seen that the VI increases from 50.7 to 76.8 which makes this treated oil more suitable for API grade I and II type of applications(Annexure-E, API, 2015).The aniline point also shows an improvement from 77.2 to 81.8, which means the paraffinic content of the treated oil is higher than the feed. The PAH test and sulphur content indicate reduction in poly-cyclic aromatics and sulphur content and thus fit for API grade I and II applications(Annexure-E, API, 2015). The oxidative response by RVOT test suggests approximately 90% improvement in the response time indicating improved stability of the product.The flash point, pour point and refractive index does show any change before and after the hydro-treatment.

## 3.3. UV stability study

The base oil with higher polycyclic aromatics and unsaturates is susceptible to UV degradation. On the exposure to sun light, it appears yellow leading to chromophores-conjugated aldehydes, ketone and esters. The formation of chromophores may be due to reaction of long chain lubricant hydrocarbon in presence of UV radiation and oxygen.

To study the improvement in UV stability of hydro-treated base oil, both untreated and treated oil samples were kept in transparent glass bottles under direct sunlight for 8 hours. The physical appearance is shown in Fig. 2(A-C).



**Fig.2. UV stability test (A) Untreated fresh base oil (B) Untreated base oil under 8 hour sunlight exposure (C) Hydro-treated base oil under 8 hour sunlight exposure**

By comparing Fig.2(B and C), it can be seen that the hydro-treated base oil is more stable due lower aromatics and higher paraffins and naphthenes presence leading to negative photo-oxidative response. The better UV stability of hydro-treated base oil improves the shelf life

and further lead to longer drain intervals. Thus this kind of oils can be suitable for insulating oil applications where higher electrical and photo-chemical stability are desirable.

## 3.4. Biodegradability Analysis

The biodegradation is the chemical breakdown or transformation of substance due to bacteria, fungi or enzyme. The biodegradability is classified according to the rate of degradation in three categories namely readily degradable, inherently degradable and persistent. The biodegradability for base oils refers to the microbial breakdown of oil in28 days standard test condition of OECD 301B.The readily degradable is one with 60 to 70 % oil degradation, the inherently degradable is 20 to 60% degradation and persistent is with less than 20% degradation(OECD 301B, 1992).

The biodegradability of any substance has to be on the higher side such that in case of direct disposal into environment, the substance will break down naturally under microbial action. The substance can be effortlessly disposed without much treatment if it readily or inherently biodegradable.



**Fig.3. Sample preparation and test setup (A) Microbial enumeration (B) Activated sludge and moist soil samplein blender and aerator (C) OECD test setup**

To study the biodegradability, a measured volume of inoculated mineral medium, containing known concentration of test substance (10-20 mg TOC/L) as the source of organic carbon was aerated by passing $CO_2$ free air at controlled rate in dark diffuse light. The degradation was followed over 28 days by determining amount of $CO_2$ produced. The $CO_2$ was then trapped in barium hydroxide and titrated for residual hydroxide. The amount of $CO_2$ produced from test was expressed as a $ThCO_2$.

The inoculum was prepared from activated sludge collected from effluent treatment plant and moist soil. It was homogenized by blender and aerated until ready for use. Later the microbial enumeration of the inoculum was performed. For the OECD test, four separate units of air supply, incubation, gas absorption and titrator were kept and placed on rotatory platform shaker during the period of study. The inoculum preparation part is shown in Fig. 3 (A and B), whereas the four units of OECD setup is shown in Fig. 3 (C).

**% Biodegradability as per OECD 301B**
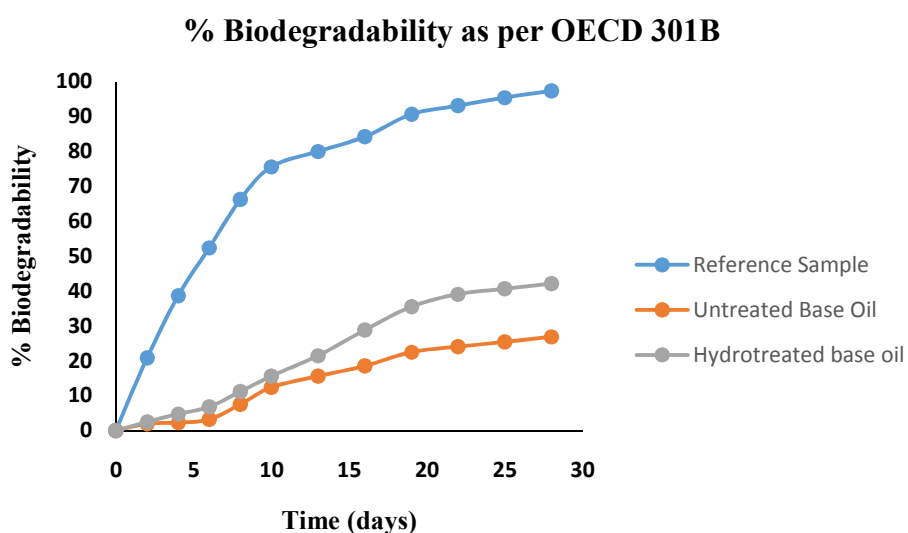


**Fig.4. %Biodegradability vs time for various samples as per OECD 301B**

The data for biodegradability were obtained from the titration and converted into $CO_2$ production and using same the percentage of biodegradation was determined. The % biodegradation for reference sample, untreated and treated base oils is plotted against time (in days till 28 days) as shown in Fig.4.

From the same figure, the performance of test method is validated as complete degradation of the reference sample is achieved. The untreated base oil achieves nearly 27% degradation whereas the treated base oil achieves more than 42% degradation as seen in Fig. 4. Thus the

hydro-treatment process has removed various undesirable polycyclic-aromatic compounds to the reasonable extent which are otherwise not easily biodegradable.

## 4. Conclusions

This paper evaluates the efficacy of the hydrogenation route for aromatics removal by evaluating four parameters. First is the aromatics removal in which almost up to 88 % of aromatics are removed along with slight reduction in sulphur content in semi-batch mode. The second parameter is the improvement of physico-chemical properties in which viscosity index and aniline point increases appreciably well whereas theflash point, pour point and refractive index does not show any changes. The third parameter is the UV stability,which is clearly observed to be better improved. Finally the biodegradability was assessed and the hydro-treated base oil is showing an increase of 15% in biodegradability. Thus the mild hydrogenation is better route for aromatics reduction then the traditional hot oleum and solvent extraction process. One can also compare the adsorptive route with respect to mild hydrogenation to compare the efficacy between this competing processes.

**References**

1. Charles Menzie, Bonie Potocki, 1992. The PAHs in the environment. Environ. Sci. Technol. 26(7), 1278-1284.

2. Kirsi-Maarit Laheto, J. A. Puhaka, H. Lemmetyinem, 2003. Biodegradation of selected UV-irradiatedand non-irradiated polycyclic aromatic hydrocarbons (PAHs). Biodegradation, 14, 249-263.

3. EU Regulation (EC) No 1223/2009 dated 30 November 2009 (published on 22 December 2009)

4. M. Rausch, S. Holland, Making A White Oil by Two Stages of Catalytic Hydrogenation, US Patent 3459656, 1969.

5. J. Gilbert, R. Kartzmark, Preparation of White Oils with Aluminum-Alkyl Activated Iron Group Metal Catalysts, US Patent 3658692, 1972.

6. L. E. Kindwell, Two Stage Process for Manufacturing of White Oils, US Patent 4055481, 1977.

7. T. Anstock, W. Himmel, M. Scharzmann, H. Dreyer, U. Lebert, A. Eisenbeis, Preparation of Medicinal White Oils and Medicinal Paraffins, US Patent 4786402, 1988.

8.  B. Corman, P. Korbach, K. Webber, Process Oil Manufacturing Process, US Patent 4801373, 1989.

9.  J. Powers, G. Prescott, J. Whiteman, Hydro-refining Process for Production of Base Oils, US Patent 5855767, 1999.

10. S. Hantzer, A. Ravella, I. Cody, D. Klein, Process for Production of Medicinal White Oil, US Patent 6187176B1, 2001.

11. W. Lin, J. M. Chen, J. Y. Chen, K. Tsai, Process for the Production of White Oil, US Patent 6508931B1, 2003.

12. G. R. B. Germaine, Process to Prepare Medicinal and Technical White Oil, US Patent 0258074A1, 2005.

13. J. Rosenbaum, B. Lok, K. Helling, S. Lee, R. Schexnaydre, Base Oil Manufacturing Plant, US Patent 8956581B2, 2015.

14. S. C. Modi, M. S. Rao, T. Snigdha, TCSM Gupta, Qualitative Analysis of Process Hazard for Hydro-treatment of Heavy Base Oils Using Combination of HAZOP and Network Analysis, International Conference on Advances in Chemical Engineering-2020 (AdChE-2020), Dehradun, India, 2020.

15. API-1509, ''API Base Oil Inter-changeability Guidelines'', Annexure-E, (March 2015)

16. OECD Guidelines for testing of chemicals (Ready Biodegradability), Test method 301B, 1992 (Revised 1996).

# Coordinated Control of Hybrid Renewable Power Generating System Applicable for DC Microgrid

*Siddharth Joshi[*], Vivek Pandya, Bhinal Mehta, Bhavya Pandya*
*Department of Electrical Engineering, Pandit Deendayal Energy University,*
*Gandhinagar, Gujarat, India.*
*\*Corresponding author: siddharth181285@gmail.com, +91-9427729739*

## Abstract

The current power sector scenario drives the world into eco-friendly power generation sources based system with fewer greenhouse emissions and lesser environmental pollution. This paper proposes a coordinated control of the Hybrid Renewable Power Generating System applicable for the standalone DC microgrids application. The incorporation of battery energy storage increases the reliability of the system. The simulation analysis is performed with the coordinated control of the wind turbine generating system, the photovoltaic system, and the battery energy storage system. To improve the performance of the renewable energy sources incorporation the maximum power point tracking algorithm is implemented with the integration of DC-DC boost converter to model wind turbine generating system and photovoltaic energy system. The bidirectional DC-DC converter is modeled and interfaced with a battery energy storage system. To validate the performance of the proposed scheme equivalent electrical residential loads modeled as DC load are considered in this work. The system is tested for various permutations and combinations in the climatic conditions and switching of the loads. The simulation results of the system indicate that the proposed hybrid system satisfies the power demand and regulates the DC bus voltage at the DC bus. This system plays a role as an implementation of small-scale DC microgrids to cater to the load demand and decrease the carbon footprint from the environment.

## Keywords

Battery energy storage system, DC Microgrid, Hybrid System, Photovoltaic System, Wind Turbine Generating System.

## 1. Introduction

Renewable energy sources like wind energy conversion systems and Photovoltaics are depending upon climate so intermittent in nature and, therefore, cannot be used as stand-alone systems for supplying power to remote areas. The inclusion of the battery storage banks improves the reliability of these systems due to the storage of excess energy in the battery bank. The hybrid system, formed by combining wind and PV, increases the reliability of this scheme and reduces the capacity of the storage elements. The hybrid small-scale DC system served as a DC microgrid to fulfill the local load demand. The variation in climatic conditions results in operational issues and introduces limitations in its applications. A microgrid can be defined as a power cluster of distributed generation, load, and energy storage devices accumulated together in the vicinity of each other [33]. The approximately 35MW wind power generation installed capacity and approximately 30MW solar power generation in the Indian grid is found and projected growth is almost 1.64 times and 3.38 times respectively for wind and solar power generation by the year 2022 reported by the International energy agency [25]. As of today the power generation scenario in MW and the installed capacity of renewable energy sources in the Indian power generation sector is shown in fig. 1 and fig. 2 respectively. Fig. 1 represents various means of power generating sources possibilities

available in India including renewable and non-renewable energy sources. Fig. 2 provides the bifurcation of renewable energy power generation sources that contributes power to the Indian grid. The manuscript is organized with introductory remarks, a mathematical modeling of the components of the hybrid system including the equivalent model of the converters, description of the hybrid system used in microgrid, and simulation results with analysis.
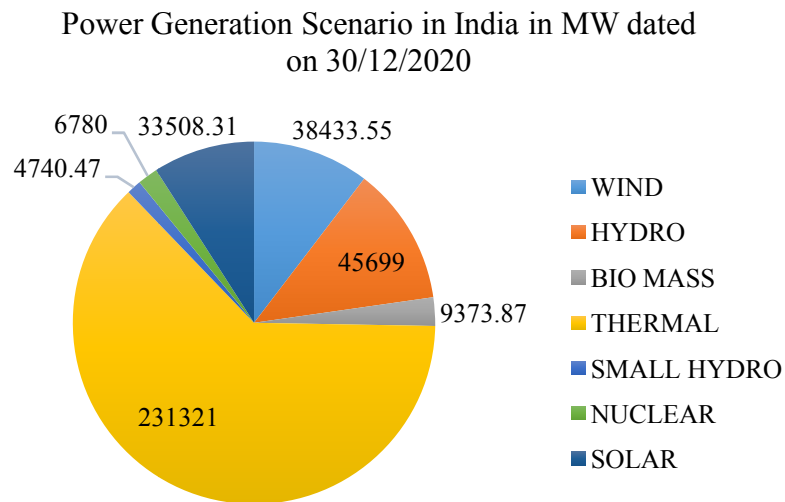
**Power Generation Scenario in India in MW dated on 30/12/2020**



Fig. 1 Current power generation scenario in India present day. [34, 35]

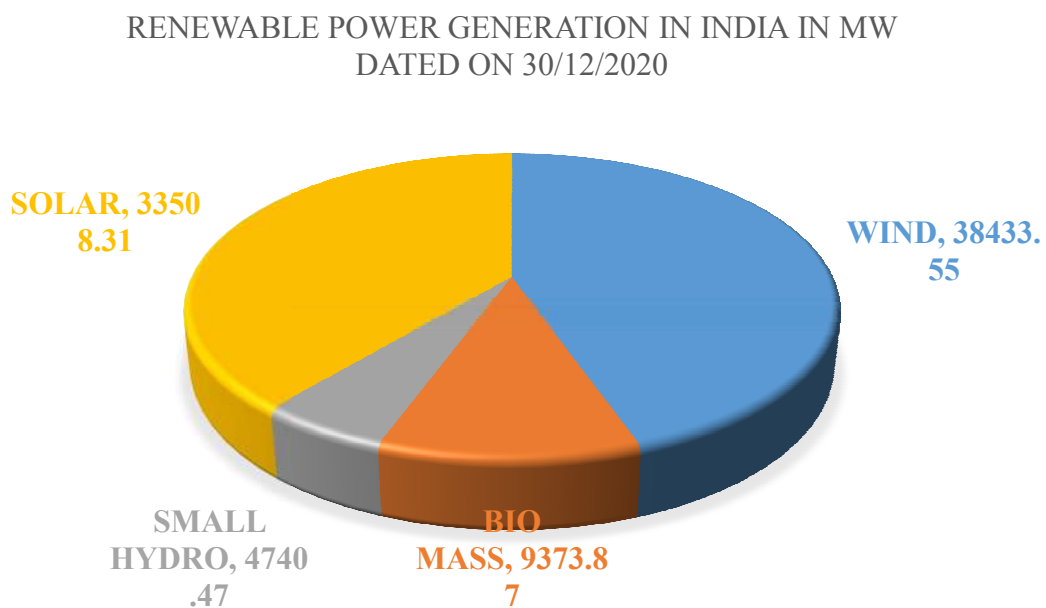**RENEWABLE POWER GENERATION IN INDIA IN MW DATED ON 30/12/2020**



Fig. 2 Contribution of Matured Renewable Energy sector in Current power generation scenario in India present day. [34, 35]

## 2. Modelling & Literature Review

### 2.1 Modelling of Hybrid System

The hybrid system comprises of wind turbine generating system, the photovoltaic system and the battery energy storage system. Each source contributes the power sharing to the load. This

subsection comprises of mathematical model of renewable energy sources and battery energy storage system with the incorporation of the power converters. The I-V modelled equation of PV module is mentioned in eq. (1), where $I_{PV}$ is the current at the load end, $I_{ph}$ is the current from photons, $I_{rs}$ is the reverse saturation current of the diode, $V_{PV}$ is the voltage across load, q is the charge of the electron, A is the diode ideality factor, k is the Boltzmann's constant, T is the absolute temperature of the cell, $R_s$ is the series resistance of photovoltaic cell/module, $R_{sh}$ is the shunt resistance of photovoltaic cell.

$$I_{PV} = I_{ph} - I_{rs}(e^{\frac{q(V_{pv}+I_{pv}R_s)}{AkT}} - 1) - \frac{V_{pv} + I_{pv}R_s}{R_{sh}} \quad (1)$$

The mechanical power available from the wind and the power captured by the blades of a wind turbine are given by eq. (2), where $P_{net}$ is the power from wind turbine in W, $\rho$ is the Air density (1.225kg/m$^3$), A is the swept area of wind turbine in m$^2$, v is the wind speed in m/s, $C_P$ is the power-coefficient of wind turbine, $\lambda$ is the TSR (tip speed ratio) of wind turbine, $\beta$ is termed as the blade pitch angle.

Power captured by the blades of a wind turbine is,

$$P_{net} = \frac{1}{2}\rho A C_p(\lambda, \beta)v^3 \quad (2)$$

Where, the power-coefficient $C_P$ depends upon the tip speed ratio and blade pitch angle of wind turbine. The tip speed ratio depends upon angular speed, radius of the rotor and wind speed. However, it also depends upon number of blades of wind turbine. The value of power-coefficient for low speed wind machines it ranges from 0.2 to 0.4 and for large wind machines up to 0.5 is the value observed in the field.

The basic modelling equation of the battery energy storage system is mentioned in eq. (3).

$$E = E_0 - K\frac{Q}{Q-it} + A\exp(-B*it) \quad (3)$$

Where; E = no-load voltage (V), $E0$ = battery constant voltage (V), K = polarisation voltage (V), Q = battery capacity (Ah), $\int idt$ = actual battery charge (Ah), A = exponential zone amplitude (V), B = exponential zone time constant inverse $(Ah)-1$, R = internal resistance ($\Omega$) and i = battery current (A).

The mathematical model of the boost converter is done using Laplace transform and the small signal model is developed in s domain. The equivalent matrix of the small signal model of the boost converter is as shown in eq. 4.

$$\begin{bmatrix} \dot{\hat{I}}_L \\ \dot{\hat{V}}_c \end{bmatrix} = \begin{bmatrix} 0 & \frac{-(1-D)}{L} \\ \frac{(1-D)}{C} & \frac{-1}{RC} \end{bmatrix} * \begin{bmatrix} \hat{I}_L \\ \hat{V}_c \end{bmatrix} + \begin{bmatrix} \frac{1}{L} & 0 & \frac{V_C}{C} \\ 0 & \frac{-1}{C} & \frac{-I_C}{C} \end{bmatrix} \begin{bmatrix} \hat{V}_g \\ \hat{I}_L \\ \hat{d} \end{bmatrix} \quad (4)$$

Where, D = Duty cycle, R = Load resistance, L = Inductance of the inductor, C = Capacitance of the capacitor, $V_c$ = Output voltage across converter, $I_L$ = Input current, $V_g$ = Input voltage.

## 2.2 Brief Literature Survey

The adaptive control algorithm to track MPPT is proposed in [1] for fast-changing in operating conditions by estimating the short circuit current of the module. The variable size of the perturbation for the sudden change in solar insolation is discussed in [2]. The value of reference photovoltaic current has been derived in [3] using upper and lower bounds of operating current limits. The authors proposed a reliable and cost-effective MPPT system in [4]. Adaptive perturb and observe algorithm is proposed for PV in [5] with boost converter and push-pull converters. Authors in [6, 7] and [8] proposed a novel technique for MPPT with a permanent magnet synchronous generator based standalone wind energy conversion system. Power coefficient analysis based MPPT tracking method is proposed in [9].

Remote Area Power Supply (RAPS) with a large rating of the battery and coordinated algorithms for wind generators have been proposed in [10]. Researchers also hybridized more than one source with the incorporation of the battery bank to provide uninterrupted power [11]. Model predictive control method for the hybrid system is also proposed. Authors in the literature suggested the concept of hybridization with permutations and combinations of type and capacity of loads [12, 13]. The authors proposed an approach of hybridization with the almost same amount of rating of wind and solar PV in [13]. In [14] PMSG based wind turbine with MPPT with the grid-connected system is discussed using double PWM. A case study from Algeria of hybrid Wind PV power system is reported in [15] for small-scale applications. Critical reviews of the renewable energy system are discussed in [16]. The author includes hybrid wind PV is discussed in [16], they have discussed various software used in hybridization methods with firm case studies. They have done the hybridization for the unit sizing of PV/wind hybrid renewable energy system (HRES) including meteorological data, load profile, modeling of the PV system, modeling of the wind energy system, modeling of the battery storage system, constraints of optimization, reliability analysis, economic analysis, converter and controller design, performance assessment and software tools. They have listed a summary of recent optimal sizing studies, software tools for HRES, a summary of a few location-specific studies, and a hybrid system review.

The hybrid solar systems for the off-grid rural electrification with various type of the load and capacity of the load is present in [17]. A review of different standalone hybrid solar systems for off-grid and rural electrification with load type, design capacity, and its outcome are presented in [18]. This review encompasses a study on solar PV as a standalone and hybrid generation system for off-grid locations. Different hybrid standalone systems, such as standalone solar PV systems, hybrid solar PV wind systems, hybrid solar PV diesel systems, and hybrid solar PV wind-diesel systems are also discussed in this review. They reviewed different standalone hybrid solar systems for off-grid and rural electrification with load type, design capacity, and its outcome in [17] across the world. The comparative analysis for hybrid standalone-solar and hybrid solar systems has been reported in the same reference. Initially, the authors explained global market availability based on photovoltaic and thermal types of solar energy systems. They have compared both types of systems in the context of their location, load type, design capacity, and outcome. The comparisons have been done for PV systems in the household, farm, and rural applications. Hybrid solar PV/wind systems reported in the same article for residential loads, government hospitals, institutions, shops, staff quarters, schools, public places, and village load, etc. The third aspect is hybrid solar/PV diesel systems for schools, colleges, and residential houses as well. The fourth comparison is with the incorporation of diesel with hybrid solar/PV for various loads in various premises.

Lots of MPPT algorithms have been proposed and implemented for photovoltaic system and wind energy system. The authors have provided an overview in [18] of various MPPT techniques for a PV system. They provided a comparison of different techniques with their

operating principles and variables used in different algorithms. They have compared various MPPT methods for robustness considering various aspects. They have also compared various MPPT methods for their operational characteristics for non-uniform irradiation conditions.

The authors have investigated by providing electrical energy Wind and PV hybrid system for in a remote location of Edirne one of the provinces of Turkey [19]. They reported the techno-economic feasibility of such a hybrid system using HOMER. They have taken monthly variations in solar radiation and wind speed for a remote location of Edirne, Turkey with daily and monthly load profiles. In this entire study, the remote residential region includes 50 houses and each one requires almost 2.5kW peak load indicates the possibility of hybrid system studies.

The authors proposed a novel algorithm in [20] to maintain DC link voltage irrespective of change in load or change in wind speed for PMSG based standalone WECS. Regulation of DC link voltage is very important especially significant in weak grids and isolated systems. An algorithm for regulating the DC link voltage irrespective of change in load or atmospheric conditions for wind energy system hybridized with the battery bank, fuel cell, and electrolyzer is proposed. They have proposed an effective control technique for the inverter based pulse width modulation (PWM) scheme, to make the line voltages balanced at the point of common coupling (PCC) during unbalanced loading conditions. They have also implemented an energy management algorithm by measuring the DC link voltage and state of charge (SoC) of the battery. By measuring the SoC of the battery, the algorithm can decide to charge the battery from a fuel cell or wind power as well if SoC is above a certain threshold the surplus power is given to dump load represents by the authors in this article.

The author has proposed simulation analysis with a hardware prototype of the MPPT connected with parallel connection for standalone PV system in [21]. Author proposed simulation and analysis with a prototype model for the MPPT system with parallel connection for PV standalone system. This topology reduces the power loss in the converter. They have used the bidirectional converter for MPPT implementation, and its function is to charge the battery for MPPT implementation and as a step-up converter. The authors proposed a simple bidirectional DC-DC power converter with MPPT for parallel-connected PV modules. First, they have compared the series connection of MPPT with parallel connections; then they have modeled series connected multiple parallel MPPT. They have verified the proposed MPPT controller in buck and boost mode of operation. They have also proposed a bidirectional power circuit with a battery and tested for five operation modes considering climatic conditions and load variation. The protections of overcharging and deep discharging are also discussed.

The authors proposed a control strategy in [22] for stable operation of DC micro-grid with different operating modes. Charge/discharge control of energy storages using DC microgrid with renewable is presented. The proposed control system demonstrates DC voltage control and quality power DC supply. The developed control architecture is used for both grid-connected and islanded mode. The system adapted presents effective charging of the battery from the microgrid. The stable operation has been observed during different modes of operation i.e., variation in DC link voltage and comparing the same with reference battery voltage. They have simulated four distinct modes for the battery charging and discharging process by comparing above said voltages. So, the control strategy has been developed for BESS (Battery energy storage system), RES (Renewable energy system), and load management including battery state of charge (SoC) with battery power limitations is proposed.

The authors presented a review of different hybrid systems used to generate power for a single house or a small community in [24]. The photovoltaic/wind/fuel cell hybrid power system for stand-alone applications has been demonstrated with a mobile house [25]. This concept

demonstrates renewable energy sources such as wind generators and PV are used simultaneously to power off-grid applications. PV and wind energy as a primary source and fuel cell act as a backup source in this mobile renewable house. They have considered 24V DC bus and 220V AC bus for this work.

This paper proposes the scheme of hybridization with the coordinated control for DC microgrids with the incorporation of the WTGS system, the PVS, and BESS. The values of AC loads are represented as equivalent DC resistance. The system used in this paper comprises of 12kW WTGS at rated wind speed is hybridized with 3.6kWp PVS at standard test condition (STC) and battery energy system (BES) (6 in numbers, 12V, 750Ah) are connected in series to form a battery bank. The WTGS and PVS are interfaced with the MPPT algorithm to ensure the maximum amount of available power to the load by considering various climatic conditions. In the present case, the permutation and combination of climatic conditions and loads are considered.

The permanent magnet synchronous generator (PMSG) based wind energy system is also interfaced with buck converter and then hybridized with the other conventional and non-conventional sources. Such kind of hybrid system is proposed in [27]. The comparative aspects of PMSG based wind energy conversion system with other wind power generating schemes are available in [4, 14]. In this article for WTGS, the diode bridge rectifier with boost converter is interfaced with WT and PMSG assembly with maximum power point tracking (MPPT) algorithm [6]. MPPT ensures the variation in duty cycle and operates WTGS at MPP for given wind speed. The characteristics of such MPP are mentioned in [27].

1. Description of the Hybrid Standalone DC Microgrid System

This hybrid DC microgrid used in this work comprises the wind turbine generating system (WTGS) and photovoltaic system (PS) with the incorporation of the battery energy storage system. The wind energy conversion system comprises the wind turbine interfaced with the PMSG. PMSGs are best suited for medium scale wind power applications. The WTGS (12kW) is the part of the hybrid system that is interfaced with a DC-DC boost converter and maximum power point tracking algorithm (MPPT) enabled. The other part of the hybrid system is PS. The PS is also comprised of a DC-DC boost converter interfaced with the MPPT algorithm. Series and parallel connection of PV modules are used to develop the strings. The 60W PV modules are used to develop the string, each string comprises 30 modules connected in series. The string of the same capacity and same configuration is connected in parallel makes the capacity of PS equals to 3.6kWp. The system is interfaced with Li-ion batteries of 12V, 750Ah, with a bi-directional DC-DC converter at a common DC bus. Six number of such batteries are connected in series develops BES. The loads with various power consumption rating are chosen in this work are listed in Table 1. The operation of the loads is tested with variations in climatic conditions and switching of the load. These operations are provided satisfactory results at DC bus voltage. The four cases have been discussed with the permutations and combinations of load, wind speed, and solar insolation. For these studies, the state of charge (SoC) is assumed as 0.8. The overall system block diagram applicable to the DC microgrid is shown in Fig. 3. The graphical abstract is as shown in Appendix.

The hybrid system is simulated in PSIM ® 9.3.4 with four case studies considering perturbations and combinations of switching of load and input conditions of the source [27, 32]. WTGS with the incorporation of perturb and observe MPPT method is proposed [6] used in this work. PVS interfaced with DC load, incorporated with the quasi double boost converter. The BES is connected with a DC bus using a bidirectional DC-DC converter. The Proportional Integrals (PI) associated with WTGS and PVS are fine-tuned to operate the converters. The battery bank is used to regulate the DC link voltage at the DC bus [26]. The bidirectional converter is used for which the value of the inductor is selected as 600mH [23].

The hybrid system incorporation is done using PSIM ® 9.3.4 software by refereeing documents available in the hard lock.

The reference voltage of the system is selected as 600V DC. To maintain the state of charge (SoC) of battery range of 0.4(minimum) and 1(maximum) is considered in simulations. These upper and lower limits are coded in the simplified C block available in PSIM. The control scheme for selecting the state of charge is taken from [10] in which inner current control and outer voltage control loops are used to control the state of charge of the battery.

The residential loads are shown in Table 1 taken from [33]. The performance of the hybrid system is analysed using these loads. The load is represented as its equivalent DC resistance at 600V DC. A total load of approximately 18kW is considered in this paper. Various cases of simulation studies with permutations and combinations of a load and climatic conditions are demonstrated. To introduce load variation in the hybrid system the 1kW cloth iron and 3kW air conditioner are turned ON & OFF at different times. These load variations are introduced to demonstrate that the DC link voltage is regulated at the reference value irrespective of load changes.

## 3. Simulation Results & Analysis

This section comprises of simulation outcome and its analysis for hybrid renewable system for DC microgrid. The simulation for various four cases are performed with permutations and combinations of load, wind speed and solar insolation assuming constant temperature of PV modules (25□). The coordinated control between WTGS, PS and BESS is done with an incorporation closed loop controller system.
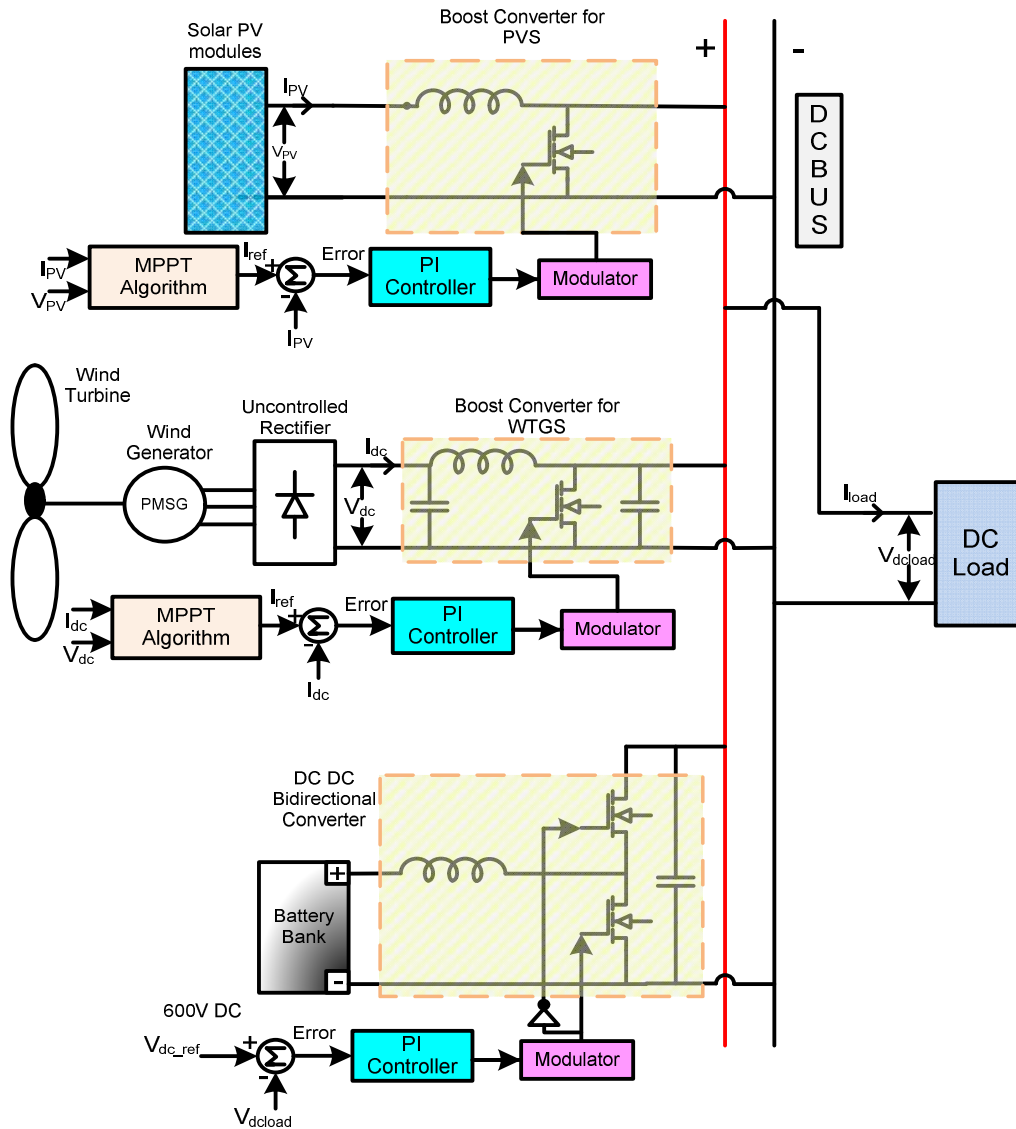
Fig. 3 Block diagram of DC Microgrid with Hybrid Renewable Energy System.

Table 1. Description of Load in Watt and the Value of the Resistance Used at 600V DC [33]

| Sr. No. | Type of Residential Load | Total No. of Units | Power Consumption in Watt | Value of resistance at 600V DC |
|---------|--------------------------|--------------------|--------------------------|-------------------------------|
| 1 | Refrigerator | 1 | 300W | 1200Ω |
| 2 | Dish washer | 1 | 1450W | 250Ω |
| 3 | Large Burner Cooking | 1 | 2100W | 175Ω |
| 4 | Fans (Celling/Wall mounted) | 4 | 100*4=400W | 900Ω |
| 5 | Iron | 1 | 1000W | 360Ω |
| 6 | Lights (Lamps) | 4 | 60*4=240W | 1500Ω |
| 7 | AC (Window) | 2 | 1200*2=2400W | 300Ω each |

| 8 | AC (3 Star) | 2 | 3000*2=6000W | 120Ω each |
|---|---|---|---|---|
| 9 | Television | 2 | 150*2=300W | 1200Ω for 2 units |
| 10 | Laptop/desktop | 4 | 450W | 800Ω |
| 11 | Water Pumping System | 1 | 450W | 260Ω |
| Net power | | | 18  kW | |

3.1 Variable wind speed, variable solar insolation and connection of maximum load with switching of loads

The hybrid DC microgrid power generation system is simulated for variable wind speed and variable solar insolation assuming constant temperature of 25□. The wind speed and solar insolation with their perturbations are shown in table II.

Table 2 Case 1 : Perturbation Applied for Wind Turbine Generating System in Wind Speed and for Photovoltaic System in Insolation.

| Sr. No. | Perturb applied for Wind turbine / PV | Value of perturbations |
|---|---|---|
| 1 | Wind Speed for wind turbine in m/s | 11.5m/s -10.5m/s-11.5m/s |
| 2 | Solar PV Insolation in $W/m^2$ for PV modules | $1000W/m^2$-$800W/m^2$-$1000W/m^2$ |



(a)
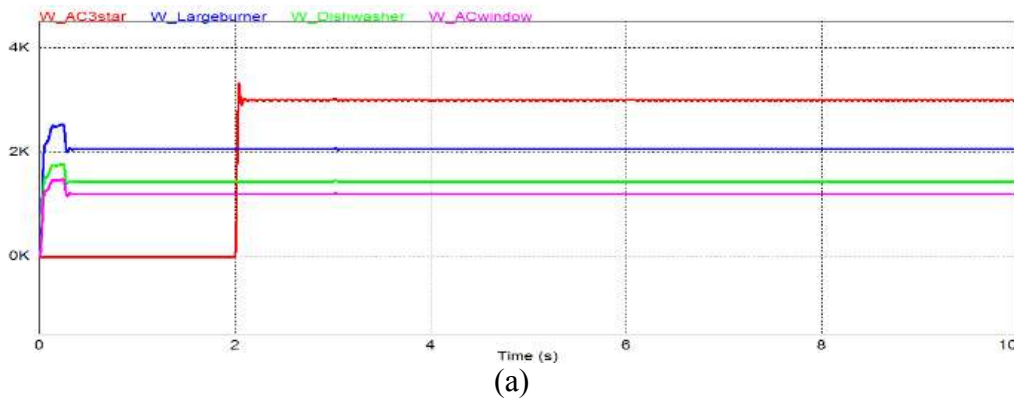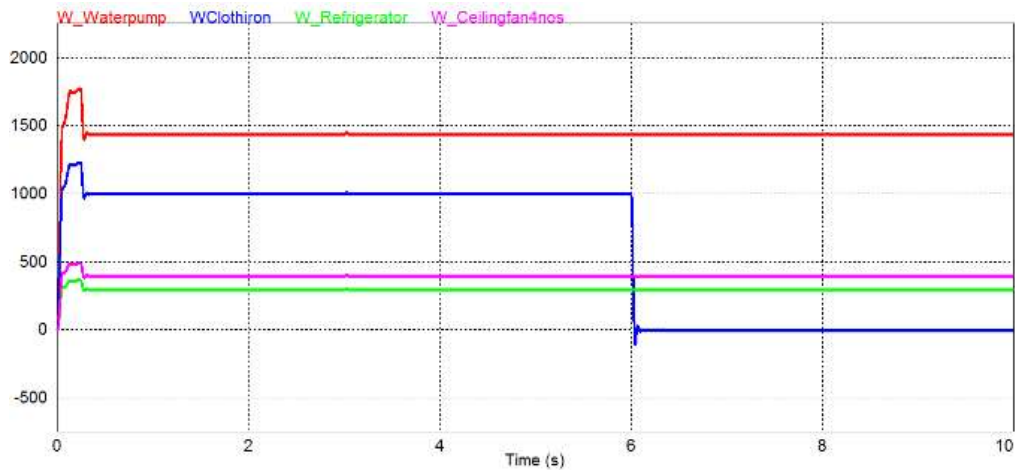
(b)
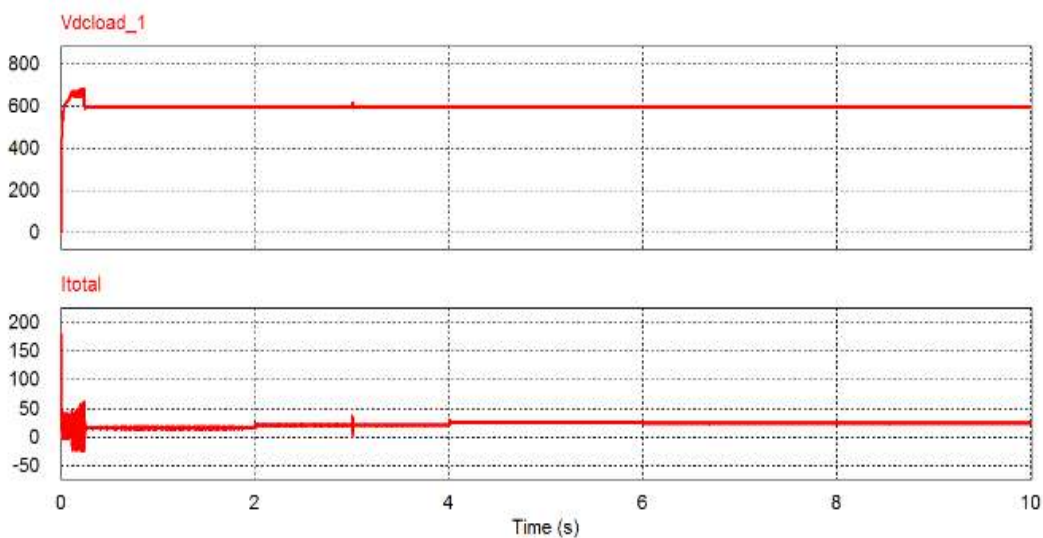


(c)

Fig. 4 Results of hybrid system for variable wind speed, variable solar insolation and connection of maximum load with switching of loads.
(a), (b) Power consumed by different loads (from top to bottom: 3 star air conditioner, large burner, dish washer, AC window) Power consumed by different loads (from top to bottom water pump, cloth iron, ceiling fans and refrigerators) and cloth iron switched off after 6 seconds, (c) Voltage across load (Vdcload_1) and total DC current drawn (Itotal) by load.

Fig. 4(a) and (b) depict simulation results under dynamic performance for the hybrid system under varying conditions in insolation and wind speed. Figs. 4(a) and (b) show the power consumption for the different load connected with the hybrid system, equivalent, DC load is considered for particular equipment in this study. The constant DC link voltage profile is maintained as shown in fig. 4(c). To make the system, dynamic switching ON and OFF the loads have made. Initially, load demand is set at 13.4kW, after t=2 second by connecting single unit of three-star AC (power rating has shown in table I) 3 star AC the load demand is set at 16.4kW and after t=6 second intentionally cloth iron is disconnected from the system at that time load demand is 15.4kW. Regarding wind speed from t=0 second wind speed is 11.5m/s and up to t=4 second, it will maintain at 11.5m/s. At t=4 second wind speed is decreased from 11.5m/s to 10.5m/s and at t=6 second wind speed is again increased at 11.5m/s. Similarly, perturbations are considered for solar insolation. At t=3 second insolation

from 1000W/m2 is decreased up to 800W/m2 and after t=8 second again insolation is increased at 1000W/m2. The change in the atmospheric conditions is as shown in table I. Fig. 5(a) and 5(b) are showing the constant DC link voltage due to sudden change in input parameters in terms of wind speed, insolation as well as a change in load. Boost converter connected with both the system maintains system DC link voltage constant. The constant load voltage profile is shown in fig. 5(c).

Itotal is the total current drawn by the load. In this case, 22A average current can be shared by WTGS and PVS and approximately 5A current can be provided by a battery. The value of L and C for the bidirectional converter is taken as of 200mH and 1000mF. The simulation results are satisfied for hybridization of the system with the change in atmospheric conditions and load. Similar responses have been plotted for various combinations of load, solar insolation, and wind speed for further cases.
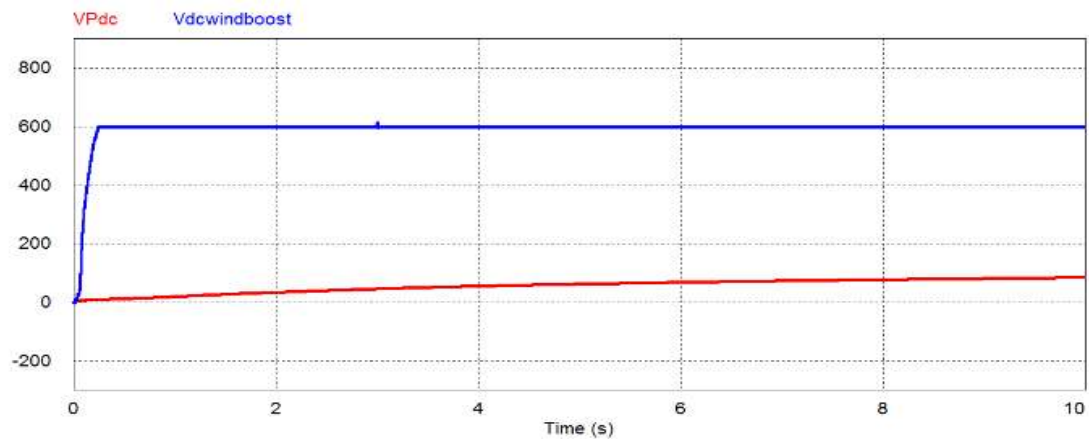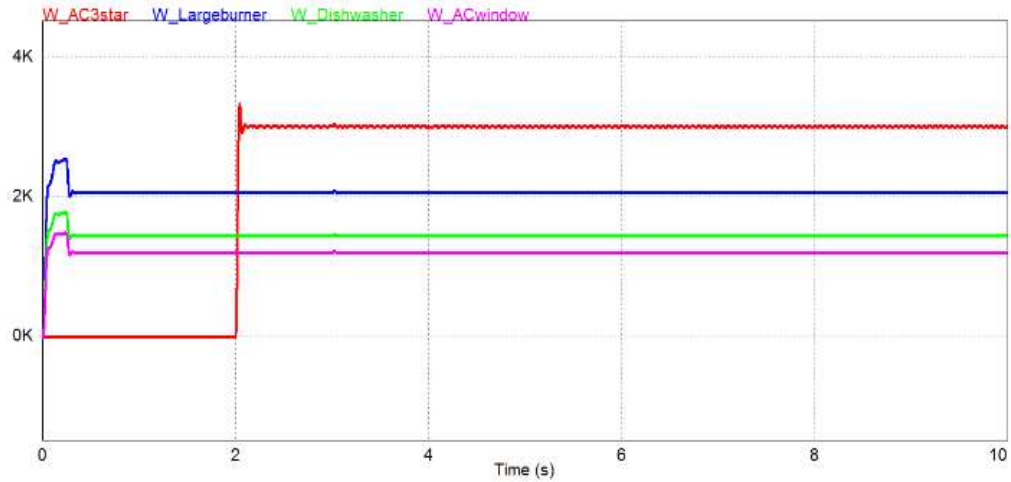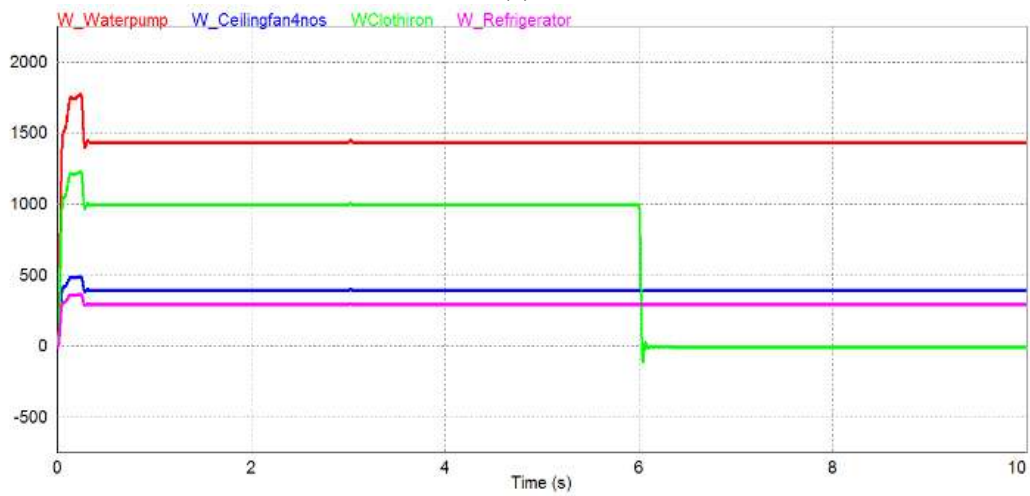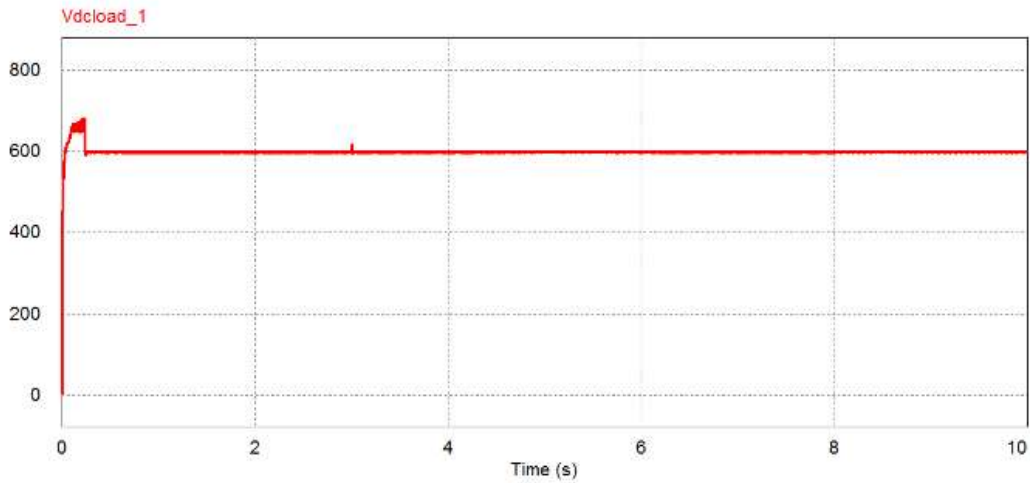


(a)
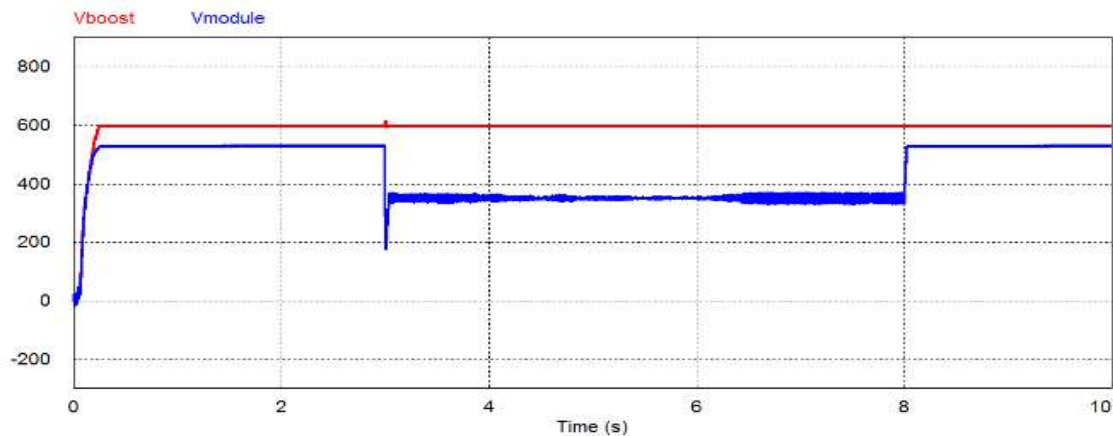


(b)
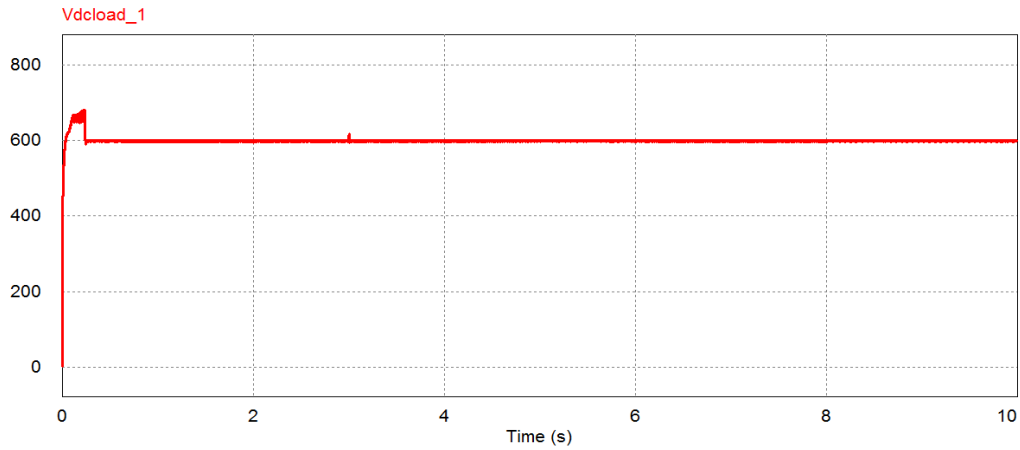
(c)

Fig. 5 Results for variable wind speed, variable solar insolation and connection of maximum load with switching of loads. (a) Rectifier voltage from wind energy conversion system (VPdc) and voltage after boost converter for wind (Vdcwindboost), (b)Voltage from boost converter of solar PV and actual module voltage, (c) Voltage profile across load.
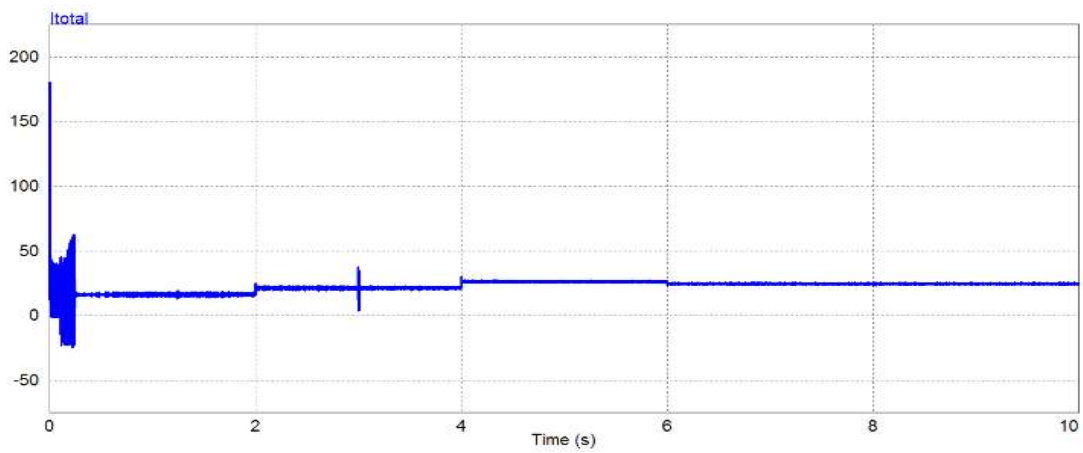


(a)



(b)

(c)

Fig 6. Results for constant wind speed, variable solar insolation and connection of maximum load with switching of loads.(a), (b) Power consumed by different loads (from top to bottom: 3 star air conditioner, large burner, dish washer, AC window, water pump, cloth iron, ceiling fans and refrigerators) and switching of 3 star AC after 2 seconds and cloth iron during 0 to 6 seconds, (c) Voltage across load.
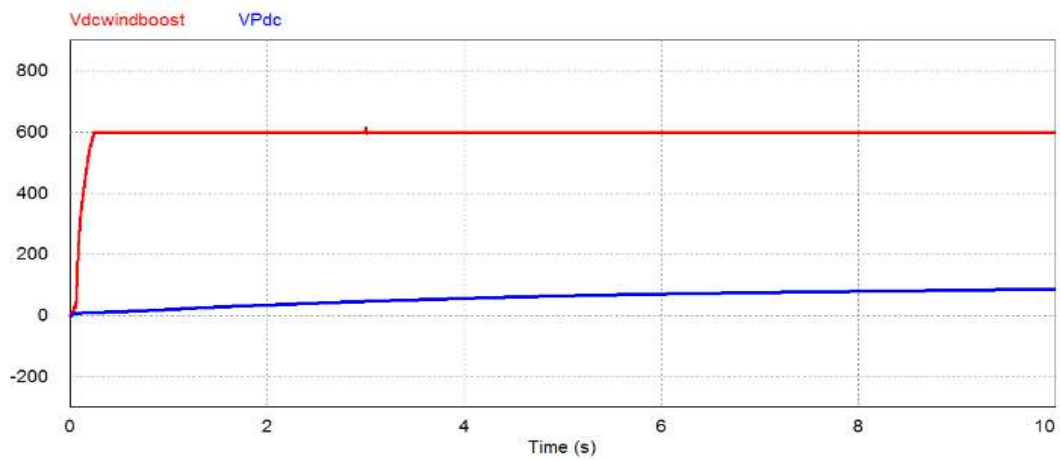


(a)



(b)

(c)

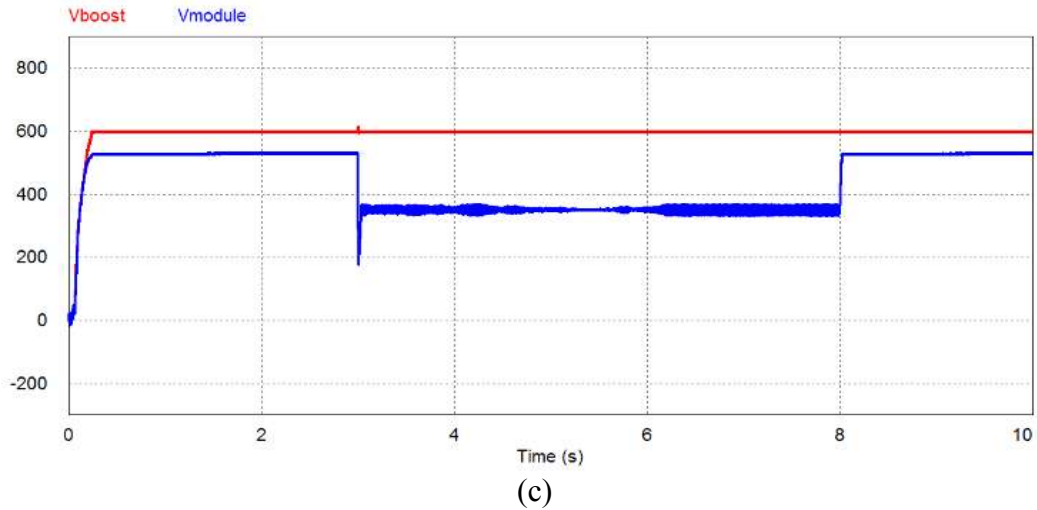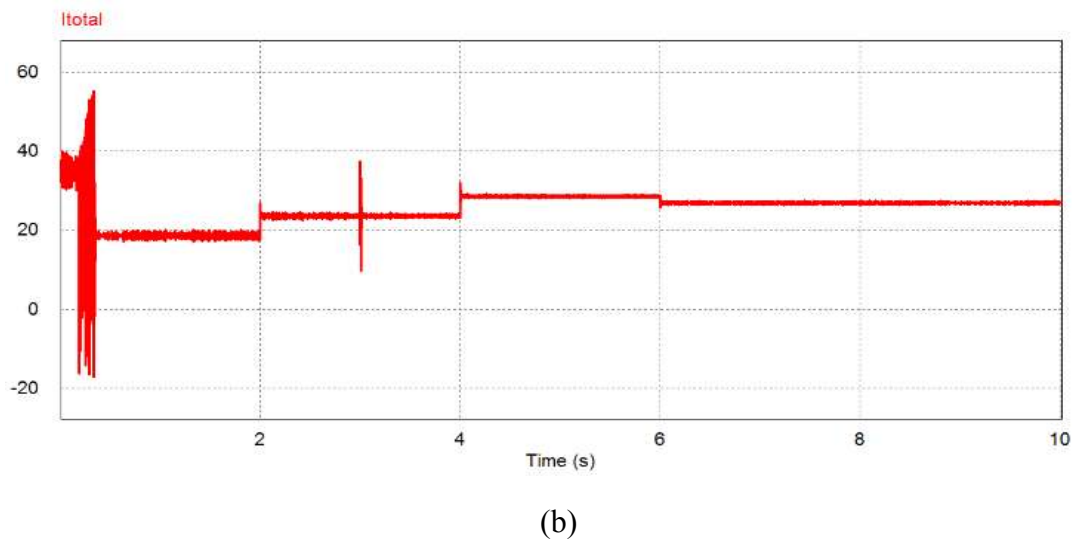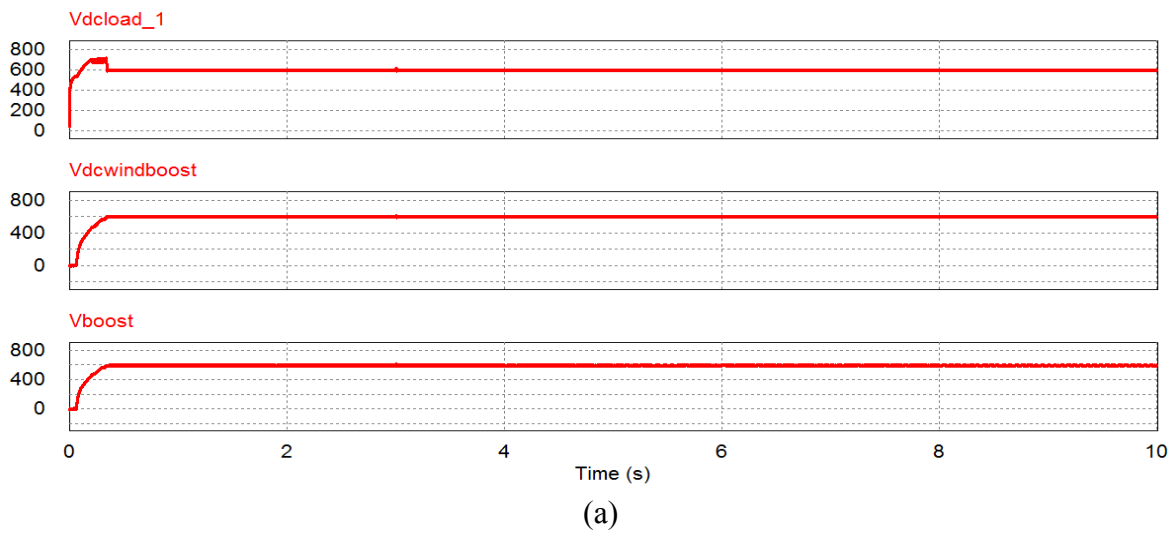Fig. 7 Results for constant wind speed, variable solar insolation and connection of maximum load with switching of loads. (a) Total current drawn by load, (b) Response of boost converter for wind energy conversion system (VPdc=Voltage at rectified end, Vdcwindboost = Boosted voltage from wind energy conversion system), (c) Response of boost converter for solar energy conversion system
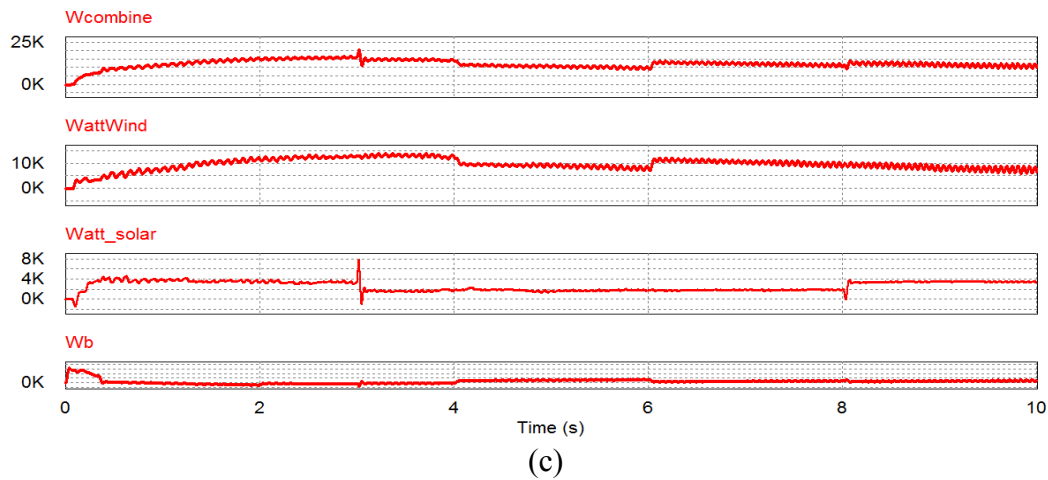


(a)



(b)

(c)

Fig. 8 Results for variable wind speed, constant solar insolation and connection for maximum connected load with switching of loads.(a) Voltage across load (Vdc_load1), Voltage from wind energy system (Vdcwindboost) and Voltage from Solar PV (Vboost), (b) Total current drawn from system, (c) Combine power from wind and solar (Wcombine =12.3kW), Power from wind (Wattwind =9.6kW), Power from solar PV (Watt_solar =2.6kW), Power from battery (Wb =4.2kW). The value of power shows average value with change in insolation, wind speed and load.

### 3.2 Constant wind speed, variable solar insolation, and connection of maximum load with the switching of loads

This case has simulated with variation in insolation as mentioned in Table II. and constant wind speed 11.5m/s with the switching of two loads as described in previous sections. Fig. 6(a) and (b) show the power consumed by different equipment with constant wind speed input and variable solar insolation. Fig. 6(c) shows the DC voltage profile across the load. Fig. 7(a) shows the total current drawn from the system which is almost 20A average as the load pattern remains the same. Figs. 7(b) and 7(c) show the response of the boost converter associated with the different systems.

### 3.3 Variable wind speed, constant solar insolation, and connection of maximum load with the switching of loads

his case has simulated with variation in wind speed as mentioned in table II, constant solar insolation, and switching of two loads as described in case 4.1. The results are shown in fig. 8(a), 8(b) and 8(c). Fig. 8(c) showing the result of power shared by WTGS, PVS, and BES. The results are showing that the DC link voltage remains constant. The BES is capable to provide a back up to 4.5kW power. Fig. 8(a) current profile and fig. 8 (b) and (c) typify coordinated voltage control between hybrid DC microgrids.

### 3.4 Constant wind speed, constant solar insolation, and connection of maximum load with the switching of loads

This case has simulated with constant wind speed 11.5 m/s and constant solar insolation, i.e. 1000W/m2 with the same change in switching of two loads as described in case A. The DC voltage profile remains constant across the load. The results are shown in Fig. 9(a) and 9(b). From the result, the voltage remains constant across the load with dynamic switching of the load.

The coordinated control is proposed for DC microgrid using a hybrid renewable energy source by keeping the constant voltage at the end of the DC bus. The results are obtained with various permutations and combinations of climatic conditions and switching of the loads signifies the coordinated control for the DC microgrid. The insertion of the energy storage increases the reliability of the system by supply the power when there are more fluctuations in the wind speed and solar radiations. In the case during the night where the insolation is almost zero and sudden load demand is increased then WTGS and BESS together cater the load demand. This coordinated control shows the overall effectiveness of hybrid renewable power generating system.
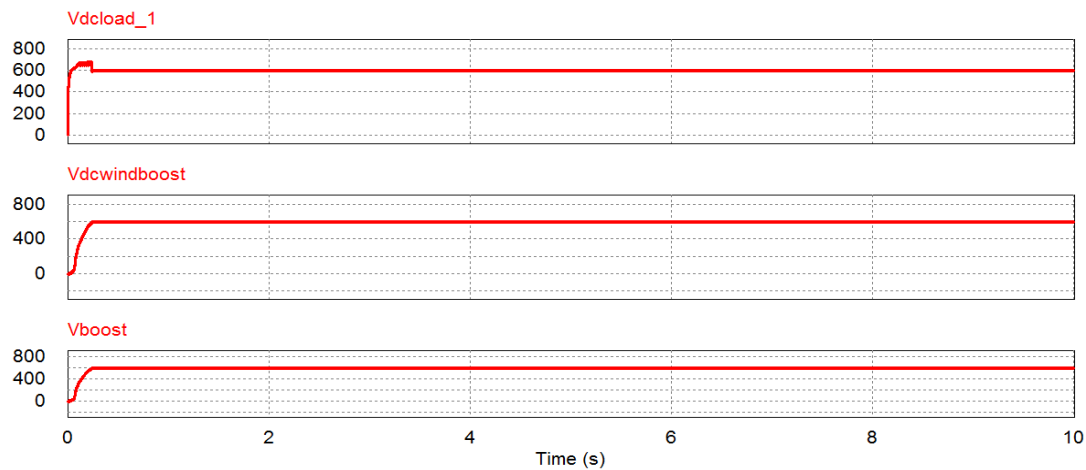


(a)
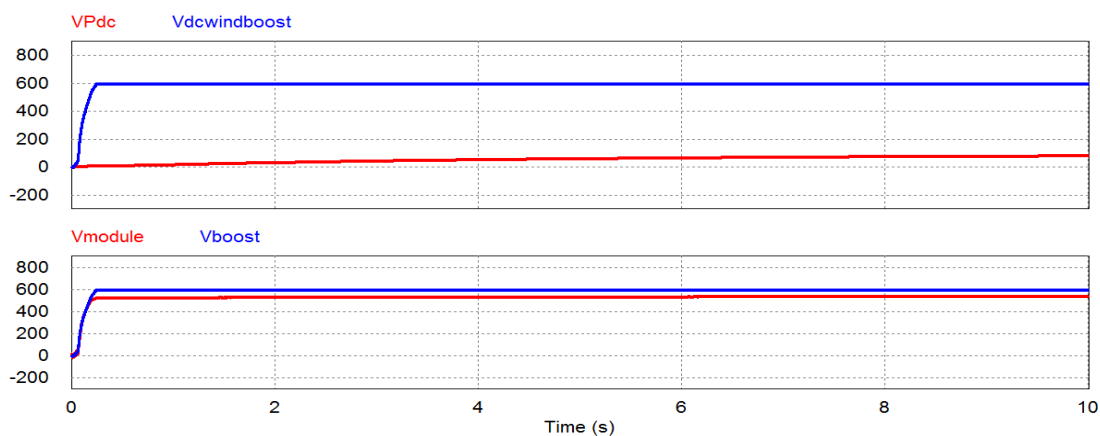


(b)

Fig. 9 Results for Constant wind speed, constant solar insolation and connection of maximum load with switching of loads. (a) Voltage across load (Vdc_load1), voltage after boost converter for wind (Vdcwindboost) and voltage from solar PV system (Vboost), (b) Rectifier voltage from wind energy conversion system (VPdc) with boosting of voltage, Voltage from boost converter of solar PV and actual module voltage (Vmodule).

**Concluding Remarks**

This paper describes the hybrid energy power generation system that combines the power from solar PV and wind turbine. The DC microgrid is formed with the help of WTGS, PS, and BESS. The simulation results demonstrate successful hybridization of the WTGS and PS with BESS. The effectiveness of the hybrid system in maintaining the constant voltage across the

load is demonstrated for variation in wind speed, solar insolation, and switching of type and patterns of loads. The BESS maintains the constant voltage by improving the DC link voltage profiles shown in the results. The incorporation of the MPPT algorithm for WTGS and PS ensures maximum power point with a change in climatic conditions. The DC link voltage is regulated using DC-DC converter, boost converter, and bidirectional DC-DC converter used in WTGS, PVS, and BESS respectively. The concept of hybridization applicable to DC microgrid is successfully demonstrated. However, the sharing of power by the sources is depending upon atmospheric conditions. The DC power itself serves the absence of an inverter so that overall conversion efficiency is increased. This kind of hybrid renewable DC system is helpful to the locations where the grid power is not accessible.

**References**

1. S. Kollimalla, Mishra, T., 2013. Novel adaptive P&O MPPT algorithm for photovoltaic system considering sudden changes in weather condition, Clean Electrical Power (ICCEP), pp. 653-658.
2. Kollimalla S, Mishra T., 2014. Variable Perturbation Size Adaptive P & O MPPT Algorithm for Sudden Changes in Irradiance. IEEE Transactions on Sustainable Energy, 5(3): pp. 718-728.
3. Kollimalla S, Mishra T., 2014. A Novel Adaptive P&O MPPT Algorithm Considering Sudden Changes in the Irradiance. IEEE Transactions on Energy Conversion, 29(3): 602-610.
4. Ahmed N, Miyatake M, Al-Othman A., 2008. Hybrid Solar Photovoltaic/Wind Turbine Energy Generation System with Voltage-Based Maximum Power Point Tracking. Electric Power Components and Systems, 37(1): 43-60.
5. Piegari, L., & Rizzo, R., 2010. Adaptive perturb and observe algorithm for photovoltaic maximum power point tracking. IET Renewable Power Generation, *4*(4), 317-328.
6. Dalala, Z. M., Zahid, Z. U., Yu, W., Cho, Y., & Lai, J. S. J., 2013. Design and analysis of an MPPT technique for small-scale wind energy conversion systems. *IEEE transactions on energy conversion*, *28*(3), 756-767.
7. Dalala, Z. M., Zahid, Z. U., & Lai, J. S., 2013. New overall control strategy for small-scale WECS in MPPT and stall regions with mode transfer control. *IEEE transactions on energy conversion*, *28*(4), 1082-1092.
8. Xia, Y., Ahmed, K. H., & Williams, B. W. 2011. A new maximum power point tracking technique for permanent magnet synchronous generator based wind energy conversion system. *IEEE Transactions on Power Electronics*, *26*(12), 3609-3620.
9. Xia, Y., Ahmed, K. H., & Williams, B. W., 2012. Wind turbine power coefficient analysis of a new maximum power point tracking technique. *IEEE transactions on industrial electronics*, *60*(3), 1122-1132.
10. Mendis, N., Muttaqi, K. M., Sayeef, S., & Perera, S., 2012. Standalone operation of wind turbine-based variable speed generators with maximum power extraction capability. *IEEE transactions on energy conversion*, *27*(4), 822-834.
11. Valenciaga, F., & Puleston, P. F., 2005. Supervisor control for a stand-alone hybrid generation system using wind and photovoltaic energy. *IEEE transactions on energy conversion*, *20*(2), 398-405.
12. Nehrir, M. H., LaMeres, B. J., Venkataramanan, G. et al., 2000. An approach to evaluate the general performance of stand-alone wind/photovoltaic generating systems. *IEEE Transactions on Energy conversion*, *15*(4), 433-439.
13. Hirose, T., & Matsuo, H., 2011. Standalone hybrid wind-solar power generation system applying dump power control without dump load. *IEEE transactions on industrial electronics*, *59*(2), 988-997.

14. Simões, M. G., Farret, F. A., & Blaabjerg, F., 2015. Small wind energy systems. *Electric Power Components and Systems*, *43*(12), 1388-1405.
15. Maouedj, R., Mammeri, A., Draou, M. D. et al., 2014. Performance evaluation of hybrid photovoltaic-wind power systems. *Energy Procedia*, *50*, 797-807.
16. Mahesh, A., & Sandhu, K. S., 2015. Hybrid wind/photovoltaic energy system developments: Critical review and findings. *Renewable and Sustainable Energy Reviews*, *52*, 1135-1147.
17. Akikur, R. K., Saidur, R., Ping, H. W. et al., 2013. Comparative study of stand-alone and hybrid solar energy systems suitable for off-grid rural electrification: A review. *Renewable and sustainable energy reviews*, *27*, 738-752.
18. Koutroulis, E., & Blaabjerg, F., 2015. Overview of maximum power point tracking techniques for photovoltaic energy production systems. *Electric Power Components and Systems*, *43*(12), 1329-1351.
19. Dursun, B., Gokcol, C., Umut, I., Ucar, E. et al., 2013. Techno-economic evaluation of a hybrid PV—Wind power generation system. *International Journal of Green Energy*, *10*(2), 117-136.
20. Bhende, C. N., Mishra, S., & Malla, S. G., 2011. Permanent magnet synchronous generator-based standalone wind energy supply system. *IEEE transactions on sustainable energy*, *2*(4), 361-373.
21. Gules, R., Pacheco, J. D. P., Hey, H. L. et al., 2008. A maximum power point tracking system with parallel connection for PV stand-alone applications. *IEEE transactions on industrial electronics*, *55*(7), 2674-2683.
22. Eghtedarpour, N., & Farjah, E., 2014. Distributed charge/discharge control of energy storages in a renewable-energy-based DC micro-grid. *IET Renewable Power Generation*, *8*(1), 45-57.
23. Michael G. Design Calculations for Buck-Boost Converters. Texas Instruments Inc., 2012.
24. Eroglu, M., Dursun, E., Sevencan, S., Song, J., Yazici, S., et al. 2011. A mobile renewable house using PV/wind/fuel cell hybrid power system. *International journal of hydrogen energy*, *36*(13), 7985-7992.
25. Report by International energy agency, 2018.
26. Senapati, M.K., Pradhan, C., Samantaray, S.R. and Nayak, P.K., 2018. Improved power management control strategy for renewable energy-based DC micro-grid with energy storage integration. IET Generation, Transmission & Distribution, 13(6), pp.838-849.
27. Solanki, C. S. 2013. *Solar photovoltaic technology and systems: a manual for technicians, trainers and engineers*. PHI Learning Pvt. Ltd.
28. PSIM ® 9.0 software user manual and hard lock kit.
29. Data sheet of solar PV module of 60W, http://www.solarelectricsupply.com/media/custom/upload/Solarex-MSX64.pdf.
30. Tutorials of PSIM, for battery bank and solar PV module. http://powersimtech.com/wp-content/uploads/2013/04/Tutorial-How-to-use-Lithium-Ion-battery-model.pdf (available with hard lock) http://powersimtech.com/wp-content/uploads/2013/04/Tutorial-Solar-Module-physical-model.pdf(available with hard lock)
31. Hummer 20kW Small Wind turbine, datasheet. http://www.hummerwindgenerator.com/20kw-projects/
32. Masters, G. M. 2013. *Renewable and efficient electric power systems*. John Wiley & Sons.

33. Lonkar, M., & Ponnaluri, S., 2015. An overview of DC microgrid operation and control,The Sixth International Renewable Energy Congress, pp. 1-6.

34. https://powermin.nic.in/en/content/power-sector-glance-all-indiaexcessed on January 2021.

35. https://mnre.gov.in/the-ministry/physical-progress excessed on January 2021.

**Appendix:**
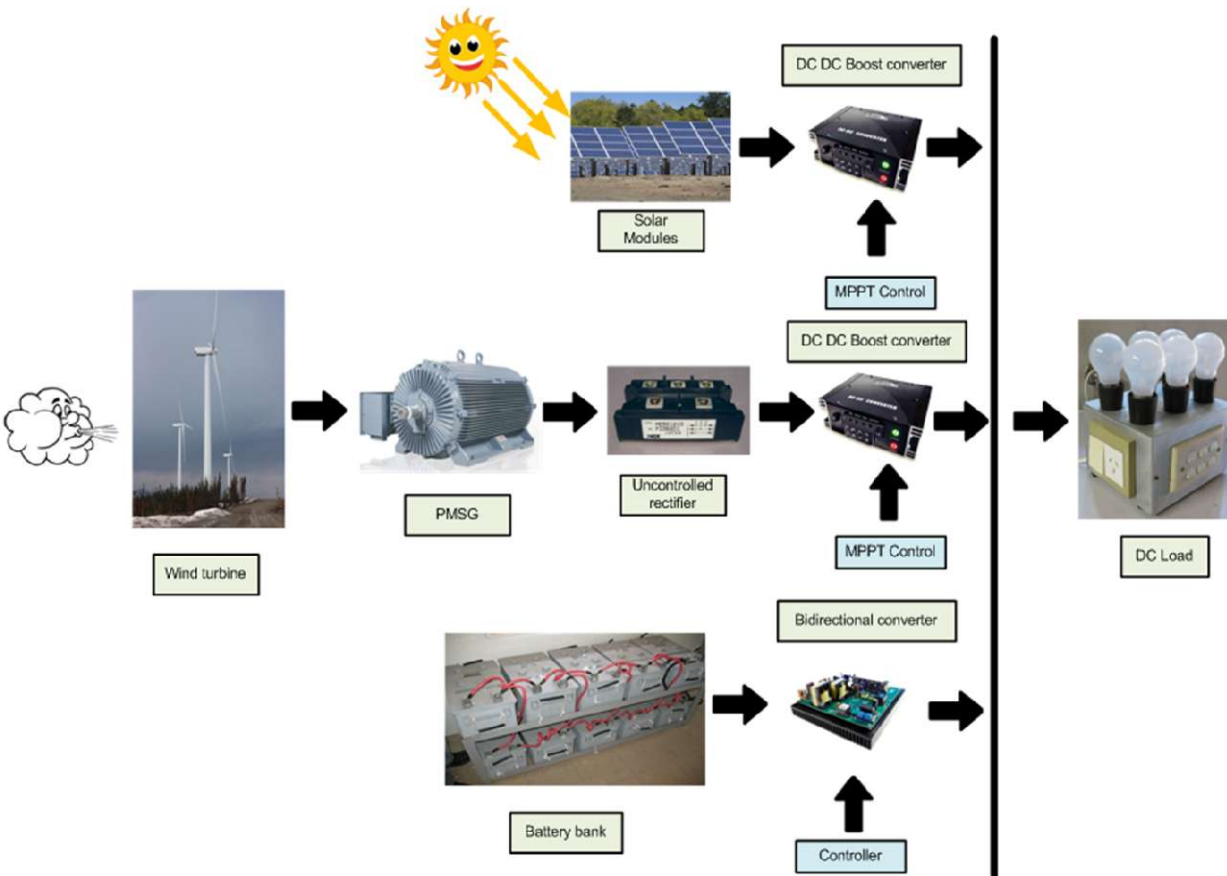
**Graphical Abstract**



Fig. 10 Graphical abstract for Coordinated Control of Hybrid Renewable Power Generating System Applicable for DC Microgrid.

# An Ultrasound-Assisted Process for the Optimization of Biodiesel Production from Waste Cottonseed Cooking Oil Using Response Surface Methodology

*Suvik Oza [1, 3], Nirav Prajapati [1, 3], Pravin Kodgire [1, 3*], Surendra Singh Kachhwaha [2, 3]*

1. Chemical Engineering Department, *Pandit Deendayal Energy University, Gandhinagar, Gujarat, India 382007.*
2. *Mechanical Engineering Department, Pandit Deendayal Energy University, Gandhinagar, Gujarat, India 382007.*
3. *Center for Biofuel and Bioenergy Studies, Pandit Deendayal Energy University, Gandhinagar, Gujarat, India 382007.*

* **Pravin Kodgire**: pravin.kodgire@sot.pdpu.ac.in, +91 8347564804 (O)

## Abstract

Biodiesel is a promising option instead of fossil energy, particularly when non-edible feedstocks are utilized in the production process. To limit the environmental effects of biodiesel production, the production method should be properly chosen and to optimize the process variables. Ultrasound-based biodiesel synthesis using waste cottonseed cooking oil (WCCO) is significant process it reduces reaction time and a highly energy-efficient process. This work focused on a comparison and analysis of optimization results using response surface methodology (RSM) based box-behnken design (BBD) and full factorial design (FFD) methods for a biodiesel production from waste cottonseed cooking oil (WCCO) catalyzed by KOH via an ultrasound (US) based transesterification process and also described the benefits to the environment caused by ultrasound method for producing biodiesel. For optimization of the biodiesel yield following parameters are considered: methyl alcohol: oil ratio (molar ratio) (A), KOH wt % (B), process temperature (C) and found to be methyl alcohol: oil molar ratio: 6:1, KOH wt %: 0.50 % reaction temperature: 50 $^0$C, with the process biodiesel yield: 98 %. Quadratic polynomial equations are obtained by analyzing experimental values for transesterification reaction. The impact of these parameters on biodiesel yield is inspected and analyzed by different plots. The process variables optimized for biodiesel yield were in a good match for BBD and FFD method.

## Keywords

Biodiesel, Optimization, Response surface methodology, Ultrasound (US) method, Waste cottonseed cooking oil (WCCO)

## 1. Introduction

The creation of biofuels, for example, biogas, bioethanol, biodiesel, and others, is an essential perspective when searching for energy, natural, social, and agronomic self-sufficiency among different aspects (Abdeshahian et al. 2010). Biodiesel is characterized as a fuel comprising of a combination of unsaturated fat methyl esters got from vegetable oils, waste cooking oil, or creature fats (Chuong et al. 2011). It is an enhancement or substitute to oil fuel, biodegradable, non-poisonous, has a high oxygen content (10 to 11%), high heat value, has a decent energy balance, and doesn't contain aromatic compounds and sulfur (Kulkarni et al.2006). The worldwide energy frameworks are profoundly subject to petroleum products. With rapid industrial and cosmopolitan development, the absolute global energy utilization is anticipated to enhance by 28% by the year 2040 (Ardabili et al.2020). Today, the most predominant assets for worldwide energy requirements are coal, flammable gas, and unrefined petroleum. These regular fuel sources are ceaselessly draining and non-sustainable. In this way, the scientists are centered on the issues to discover the substitute source (Sharma et al. 2020). For this, biodiesel helps in the insurance of the climate changes. Biodiesel is easy to utilize and safe as compared to fuel diesel. For biodiesel production, the main aspect is to choose the best, easily available, and low-cost raw material (Ardabili et al. 2020). The second-generation feedstocks have resolved the problems associated with first-generation biodiesel as the biodiesel made from edible oil will create a food security problem. The second-generation biodiesel product from non-edible oil plant sources is not utilized for human consumption (Keera et al. 2018b).

The Government of India taken up a countrywide biodiesel mission program in 2003 to produce biodiesel from second-generation feedstock using nonagricultural land (Sharma et al. 2020) , however, this missions couldn't succeed. Until this point of time, India has accomplished, just 0.12% biodiesel blending ( Keera et al. 2018b). India's national bio-fuel policy 2018 had specified a 5 percent biodiesel blending objective by year 2030. Being a feedstock with great accessibility for India, based on estimates waste/used cooking oil (WCO/UCO) can be seen as a conservative and cost-effective option (Kulkarni et al.2006). The worldwide UCO market size was esteemed at $ 6,041.2 million (42,288.4 crores in India) for the year 2018. Production of biodiesel from UCO may save 21% of fossil energy as compared with unrefined petroleum and hoards 96% of energy compared with petrodiesel manufacture (Rodionova et al. 2017).

Inspection exhibited that the use of the mechanical blending (MS) procedure for biodiesel creation requires a higher reaction time, a high proportion of process factors, and greater activation energy close to the extended post-processing time (Aghbashlo et al. 2019).Various PI-based biodiesel production techniques viz., membrane reactor, hydrodynamic cavitation (HC), ultrasonication (US), microwave irradiation (MW) and, the combination of the US and MW (Sharma et al. 2020). However, the use of process intensification (PI) especially US methods is energy-effective mostly due to lower process time and steps for purification of the product as well as removes the mass transfer limitation. Among the above methods, ultrasonication has an amazing process of interest. The US manages the beneficial outcome of ultra-sonication, which includes the production, development, and implosive breakdown of bubbles because of constant development and recompression in a fluid medium (Agarwal et al. 2012).

During biodiesel production, US irradiation causes bubble cavitation close to the phase boundary between the methanol and triglyceride phase, in this manner delivering an enormous number of micro-bubbles (Sharma et al. 2020). A few bubbles remain steady following the above cycle while others get exposed to brutal breakdown after growing to specific bubble size.

Enormous energy is conveyed upon the incredibly unbalanced breakdown of cavitation bubbles that ascent under ranges of 20 - 40 kHz (Oliveira et al. 2018). In such emulsions, at the interfacial area and mass exchange among the alcohol and oil phase increases. The homogeneous movement of reactants moves the equilibrium in a forward way via simultaneously giving physical and chemical influences in the transesterification. Further, the US gives physical blending to boost activation energy needed to initiate trans-esterification which enhances the reaction rate (Refaat et al. 2008). KOH catalyst is favored because of the nominal cost and readily available (Shinde et al. 2019). KOH catalyzed reaction has lesser process time, less utilization of catalyst, and is broadly utilized because of its ability to deliver the greatest yield under gentle temperature conditions (Quah et al. 2019).

For optimization of the process, researchers have used various methods such as response surface methodology (RSM), artificial neural network (ANN), extreme learning machine (ELM), however, the most used method is RSM (Shenbaga Vinayaga Moorthi et al. 2015). Response surface methodology (RSM) is a promising method for planning the experiments, developing models, analyzing the impacts of elements, and investigating the optimum conditions (Aydar 2018). The RSM method includes the techniques viz. box-behnken design (BBD) and full factorial design (FFD) which are widely used for optimization (Veljković et al. 2019). The analysis of variance (ANOVA) is commonly adopted to develop the mathematical model through the RSM techniques such as the BBD and FFD. Many researchers have utilized the RSM method and ANOVA to the results to carry examination. In the present study, the goal is to compare analysis obtained through the RSM coupled box-behnken design and full factorial design methods. Besides, it is critical to analyze the efficiency to reduce the resource accomplished through successful usage of these RSM techniques which can improve the viability of the process.

## 2. Material and Methodology

### 2.1 Raw materials

Waste cottonseed cooking oil (WCCO) is taken from neighborhood restaurant in Ahmedabad, Gujarat. Before experimentation, oil was filtered to separate the suspended food particles. Methyl alcohol (99 % pure, A.R. grade) and KOH pellets (99 % purity grade) were purchased from M/s fisher scientific, India.

### 2.2 Design of Experiment (DOE)

The biodiesel production from WCCO using KOH catalyst condition was optimized using RSM methods. Table 1 shown the process parameters (independent variables) and the range of levels used for experimentation. RSM-based BBD and FFD were used for studying the effects of process parameters on biodiesel yield. In the BBD approach total of fifteen experimental runs were designed, while in the FFD method a total of twenty-seven experimental runs were designed. A steady reaction time of 10 min and range of three levels were chosen based on preliminary performed experimentation.

Table 1 Independent variables and range of levels used for experimentation.

| Process variables | Levels for variables | | |
|---|---|---|---|
| | **-1** | **0** | **1** |
| Methyl alcohol/oil molar ratio; (A) | 4.5 | 6 | 7.5 |
| KOH, wt%; (B) | 0.3 | 0.5 | 0.7 |
| Temperature, ºC ; (C) | 40 | 50 | 60 |

## 2.3 Ultrasound-assisted transesterification reaction

Programmable sonicator (model no: VCX 500; M/s sonic vibracell, USA) was utilized for biodiesel production. Sonicator can vary power up to 500 W (amplitude range of 20-100%; for experimental runs 50% amplitude used) with a fixed frequency of 20 kHz. Three neck Borosil rector (250 ml capacity) was utilized as a reaction vessel with a 50 ml oil reactant. It was observed, that after completion of reaction, reaction mixture gets separated into two layers. The top layer comprises FAME with a trace of unconverted oil and the lower thick brown-colored layer is of glycerol. Three-time washing of biodiesel with distilled water was done to remove KOH catalyst and dried to eliminate water content.

## 2.4 Response Surface Methodology (RSM)

Response surface methodology (RSM) is a collection of statistical mathematical methods beneficial for evolving, refining, and optimizing process. The objective of the correct design of experimentation is to enhance a response that is influenced by numerous self-governing parameters. Based on the controlled value of independent variables the output is obtained from well-designed regression analysis (Khuri 2017). The design of the experiment (DOE) and response surface methodology (RSM) are broadly utilized in the optimization of the biodiesel production process (Aydar 2018). DOE technique is valuable for acquiring most extreme data from a negligible number of all-around arranged investigations by shifting at the same time all the cycle factor, while the RSM is an assortment of numerical and measurable parameters for building an experimental model associating result with the powerful process factors (Elango et al. 2019).

RSM has two models based on linearity or polynomial behavior that is a first-order model and the second-order model (Khuri 2017). Here, the regression analysis was performed on the experimental yield data to assess the response of biodiesel yield as y function (refer eq. 1) fitted for a quadratic second-order polynomial equation, given by;

$$y = \beta_0 + \sum_{i=1}^{n} \beta_i x_i + \sum_{i=1}^{n} \beta_{ii} x_i{}^2 + \sum_{i=1}^{n} \sum_{j=1}^{i-1} \beta_{ij} x_i x_j + \varepsilon_i \qquad (1)$$

Where y is the predicted response value, $B_i$ and $B_{ij}$ are regression coefficients obtained and interaction effect of $x_1$, $x_2$, and $x_3$ …, while n is the number of independent variables and ε is the random error.

Box-behnken design (BBD) and full factorial design (FFD) are the types of design methods of RSM. The BBD has treatment combinations at the mid-level of the edge of the experiment space and requires at least three continuous factors. The BBD ensures that all factors are not set to their high levels at the same time. For the development of BBD, the number of experiments (N) is

obtained by expression N= 2n (n-1) + m; where 'n' is the number of independent variables and 'm' denotes the number of center points (Ferreira et al. 2007; Soria-Figueroa et al. 2020). Here, both 'n' and 'm' have a value of 3. This makes BBD to have 15 experimental runs for 3 levels and 3 factors as shown in Table 2.

Table 2 List of observations considered in DOE for BBD. **(Bold term is maximum yield value)**

| Run order | Methyl alcohol: oil molar ratio (A) | KOH, wt% (B) | Temperature, °C (C) | Experimental yield % | Model Predicted yield % |
|---|---|---|---|---|---|
| 1 | 6.0 | 0.7 | 60.0 | 79.30 | 79.11 |
| 2 | 6.0 | 0.5 | 50.0 | 96.48 | 97.20 |
| 3 | 4.5 | 0.3 | 50.0 | 84.29 | 84.45 |
| 4 | 4.5 | 0.7 | 50.0 | 72.85 | 74.15 |
| 5 | 7.5 | 0.5 | 60.0 | 91.67 | 91.94 |
| 6 | 6.0 | 0.3 | 40.0 | 81.98 | 82.09 |
| 7 | 6.0 | 0.5 | 50.0 | **98.00** | **97.20** |
| 8 | 4.5 | 0.5 | 60.0 | 83.26 | 82.03 |
| 9 | 7.5 | 0.7 | 50.0 | 82.38 | 82.14 |
| 10 | 6.0 | 0.7 | 40.0 | 88.42 | 87.34 |
| 11 | 4.5 | 0.5 | 40.0 | 89.25 | 88.90 |
| 12 | 7.5 | 0.5 | 40.0 | 81.54 | 82.70 |
| 13 | 6.0 | 0.3 | 60.0 | 91.69 | 92.69 |
| 14 | 6.0 | 0.5 | 50.0 | 97.23 | 97.20 |
| 15 | 7.5 | 0.3 | 50.0 | 81.54 | 82.70 |

Full factorial design (FFD) used for the optimization process is part of the RSM method. This method connects both continuous factors and categorical factors with arbitrary numbers of levels. The FFD experiment combines all possible combinations of levels for all factors. The total number of experiments for studying k factor at 3- levels is $3^k$ (Sen 2016). In the FFD model, the total number of the experiment (N) is obtained by $N = 3^3 = 27$, for the 3 level and 3 independent variables. This makes FFD to have 27 experimental runs for 3 levels and 3 factors as shown in Table 3.

Using Design- expert® software (edition 11, stat-Ease Inc., USA), experimental yield data of both BBD (15 experimental runs) and FFD (27 experimental runs) were used as input to examine optimized biodiesel yield. ANOVA was carried out on the experiment yield values to determine the coefficient of the second-order polynomial model. ANOVA results give a relationship among the variations caused by experimental values and assert suitability of the predicted model. This is verified by analyzing the values of terms such as sum of the square root (SS), the mean square (MS), p-value, the fischer test (F-test), and the 'lack of fit' test (LOF). The evolution of the model is done by the coefficient of determination ($R^2$) and the accuracy of the obtained quadratic polynomial model is also evaluated. Significance of model coefficients are checked by F-test.

Table 3 List of observations considered in DOE for FFD. **(Bold term is maximum yield value)**

| Run order | Methyl alcohol: oil molar ratio(A) | KOH, wt% (B) | Temperature, °C (C) | Experimental yield % | Model Predicted yield % |
|---|---|---|---|---|---|
| 1 | 4.5 | 0.7 | 40.0 | 80.51 | 80.12 |
| 2 | 4.5 | 0.5 | 60.0 | 83.26 | 83.29 |
| 3 | 6.0 | 0.5 | 60.0 | 97.30 | 96.10 |
| 4 | 6.0 | 0.5 | 40.0 | 94.84 | 94.22 |
| 5 | 7.5 | 0.7 | 40.0 | 80.50 | 80.09 |
| 6 | 6.0 | 0.7 | 40.0 | 88.42 | 87.93 |
| 7 | 7.5 | 0.5 | 60.0 | 91.69 | 93.25 |
| 8 | 6.0 | 0.3 | 50.0 | 91.92 | 91.04 |
| 9 | 7.5 | 0.5 | 50.0 | 91.89 | 91.01 |
| 10 | 4.5 | 0.3 | 60.0 | 85.19 | 84.22 |
| 11 | 7.5 | 0.7 | 60.0 | 81.61 | 80.62 |
| 12 | 7.5 | 0.3 | 60.0 | 89.03 | 88.04 |
| 13 | 4.5 | 0.7 | 60.0 | 65.49 | 64.52 |
| 14 | 7.5 | 0.3 | 40.0 | 69.09 | 68.67 |
| 15 | 6.0 | 0.3 | 60.0 | 91.69 | 93.96 |
| 16 | 6.0 | 0.5 | 50.0 | **98.00** | **97.89** |
| 17 | 6.0 | 0.3 | 40.0 | 81.98 | 82.66 |
| 18 | 6.0 | 0.7 | 60.0 | 79.30 | 80.40 |
| 19 | 6.0 | 0.7 | 50.0 | 87.77 | 86.90 |
| 20 | 4.5 | 0.3 | 50.0 | 84.29 | 85.33 |
| 21 | 4.5 | 0.5 | 50.0 | 89.97 | 89.11 |
| 22 | 4.5 | 0.3 | 40.0 | 81.38 | 80.98 |
| 23 | 7.5 | 0.7 | 50.0 | 82.38 | 83.09 |
| 24 | 4.5 | 0.7 | 50.0 | 72.85 | 75.05 |
| 25 | 7.5 | 0.5 | 40.0 | 81.54 | 83.30 |
| 26 | 7.5 | 0.3 | 50.0 | 81.54 | 81.09 |
| 27 | 4.5 | 0.5 | 40.0 | 89.25 | 89.47 |

## 3. Result and Discussion

### 3.1 RSM statistical analysis:-

The design expert software (edition 11; Stat-Ease, Inc., USA) was used to optimize statistical process parameters to get maximize the biodiesel yield as per the process mentioned in section 2.4. The results of regression and analysis of variance (ANOVA) of biodiesel yield were dissected by selecting the best possible model either linear or quadratic. Second-order quadratic regression model was obtained to be the best fit for both RSM methods. As mentioned earlier, for three factors, fifteen factorial point experimental set was generated for the BBD model (refer to table.2) and twenty-seven factorial point for the FFD method (refer to table. 3). The two techniques

utilized the regression condition regarding uncoded factors created through the curve fitting utilizing the least square method to generate the predicated regression equation for BBD (refer to Eq.(2)) and FFD method (refer to Eq.(3)) which are mentions below,

The regression equation for the BBD method:

$$Y_{BBD} = -106.916 + 24.444A + 271.621B + 2.486C + 10.233AB + 0.269AC \\ - 2.354BC \quad - 3.531A^2 - 225.677B^2 - 0.028C^2 \tag{2}$$

The regression equation for the FFD method:

$$Y_{FFD} = -102.252 + 23.843A + 268.904B + 2.389C + 10.233AB + 0.269AC \\ - 2.354BC \quad - 3.481A^2 - 222.972B^2 - 0.027C^2 \tag{3}$$

Where A, B, and C are encoded forms of independent variables of methyl alcohol: oil molar ratio, KOH wt%, and temperature respectively. In both methods, over-all nine terms are generated in regression equation (refer to Eq.2 and Eq. 3), out of them, three liner term of A, B, C represents main effects; next three terms AB, BC, AC represents interaction effect among process variables, and remaining three terms $A^2$, $B^2$, $C^2$ represents quadratic effects of the factors. By utilizing the above equations Eq. 2 & 3 the predicted yield values for both models were obtained (refer to tables 2 & 3). The maximum experimental yield of 98% was obtained (refer to table 2 & table 3) for the BBD and FFD method respectively. The details of ANOVA parameters for BBD and FFD method are listed in Table 4 (a and b).

Table 4 Result of the ANOVA for the biodiesel production using (a) BBD & (b) FFD method. **(Bolt terms are significant).**

| Source of variables | df | a. Box-Behnken Design (BBD) | | | | df | b. Full Factorial Design (FFD) | | | |
|---|---|---|---|---|---|---|---|---|---|---|
| | | Sum of Squares | Mean square | F-value | p-value | | Sum of Squares | Mean square | F-value | p-value |
| Model | 9 | 741.62 | 82.4 | 40.98 | **0.0004** | 9 | 1573.88 | 174.88 | 103.73 | **< 0.0001** |
| A | 1 | 6.99 | 6.99 | 3.48 | 0.1212 | 1 | 16.21 | 16.21 | 9.61 | **0.0065** |
| B | 1 | 34.24 | 34.24 | 17.03 | **0.0091** | 1 | 77.21 | 77.21 | 45.8 | **< 0.0001** |
| C | 1 | 2.8 | 2.8 | 1.39 | 0.2913 | 1 | 16.15 | 16.15 | 9.58 | **0.0066** |
| AB | 1 | 37.7 | 37.7 | 18.75 | **0.0075** | 1 | 113.1 | 113.1 | 67.09 | **< 0.0001** |
| AC | 1 | 64.96 | 64.96 | 32.31 | **0.0023** | 1 | 195.21 | 195.21 | 115.8 | **< 0.0001** |
| BC | 1 | 88.64 | 88.64 | 44.08 | **0.0012** | 1 | 265.93 | 265.93 | 157.74 | **< 0.0001** |
| $A^2$ | 1 | 233.05 | 233.05 | 115.89 | **0.0001** | 1 | 368.06 | 368.06 | 218.33 | **< 0.0001** |
| $B^2$ | 1 | 300.88 | 300.88 | 149.63 | **<0.0001** | 1 | 477.28 | 477.28 | 283.11 | **< 0.0001** |
| $C^2$ | 1 | 30.25 | 30.25 | 15.04 | **0.0117** | 1 | 44.74 | 44.74 | 26.54 | **< 0.0001** |
| Lack of Fit | 3 | 8.9 | 2.97 | 5.14 | 0.1673 | - | - | - | - | - |
| Pure Error | 2 | 1.16 | 0.5776 | - | - | - | - | - | - | - |
| Residual | 5 | 10.05 | 2.01 | - | - | 17 | 28.66 | 1.69 | - | - |
| Total | 14 | 751.67 | - | - | - | 26 | 1602.54 | - | - | - |
| | | $R^2 = 98.66\%$; Adj.$R^2 = 96.25\%$; Adequate Precision=19.90 | | | | | $R^2 = 98.21\%$; Adj.$R^2 = 97.26\%$; Adequate Precision=42.23 | | | |

As per table 4 (a and b), the F-values of 40.98 for the BBD model and 103.73 for the FFD model were obtained with a corresponding p-value less than 0.05 (Veljković et al. 2019) indicating they are significant. The F- values can be higher, it indicate the model is significant. So, for the significance, the F-value is higher in the FFD model (103.73) as compare the BBD model (40.98). The 'lack of fit' of F-values is 5.14 (for BBD) and corresponding p-value is larger the 0.05 indicates that for lack of fit terms in F- values are insignificant in the models. The probability of F-value due to noise is 0.1673 (for BBD) found to be more than 0.05. In the FFD model, all the parameters are considered so that lack of fit and pure error terms are not required. This observation overall designates that the investigational data fitted satisfactorily with the proposed quadratic model.

The higher value of the coefficient of determination ($R^2$) indicate the accuracy and developed the model is the best fit with the predicted model data. The coefficient of determination ($R^2$) values of 98.66 % for BBD model and 98.21 % for FFD model were observed for KOH catalyzed US process. Additionally a term adjusted coefficient of determination (Adj.$R^2$) was also assessed (Sharma et al. 2020). Further, higher values of Adj.$R^2$ value of 96.21% for the BBD model, and 97.26% for the FFD model was observed which indicates that model is significant with best fitting.

As per the analysis of the developed quadratic model, as seen in table 4 (a) the significant model terms found in the BBD model were B, AB, AC, BC, $A^2$, $B^2$, $C^2$. While, table 4 (b) indicates that terms A, B, C, AB, AC, BC, $A^2$, $B^2$, $C^2$ are significant in FFD based model. As shown in table 4 (a) and (b), for the FFD model all the model terms is significant whereas for the BBD model terms A (methyl alcohol: oil molar ratio) and C (temperature) are insignificant. The $R^2$ value is higher in the BBD model compare to the FFD model.

Fig 1 (a and b) depicts distribution of experimental and model predicted yield data for BBD and FFD models. The biodiesel yield data are regularly distributed along the straight line of $45^0$ in both BBD & FFD respectively as seen in Fig. 1(a & b). The predicted yield values were dispersed reliably close to the real response and this verifies that developed regression models are best fit between the process variables and biodiesel yield. In both models the all the data points were distributed near the reference line, which indicate a good fit with the response. Fig. 1(c & d) shows the plots of the normal percentage probability versus residual data of biodiesel yield for the BBD & FFD models respectively. It shows a respectable connection between externally studentized residuals and their normal percentage probability rank position data. Fig. 1 (e & f) shows the plots of externally studentized residuals plotted against the predicted data of yield for the BBD & FFD models. In this plot, all the data points are randomly scatted to the reference line. It generally indicates that the regression model shows amazing adequacy of the biodiesel process. Fig. 1 (g & h) shows the pareto chart of the standardized effect for various terms for BBD and FFD models. In this graph, the quadric terms $B^2$ has a higher effect on the response (biodiesel yield) in both models. In the BBD model, the linear terms B and C and interaction term AC are insignificant, as the value does not cross the reference line (2.57 reference value), which can be seen in figure 1(g). In the FFD model, the interaction term AC is insignificant, as its value does not cross the reference line (2.11 reference value) (refer Fig. 1(h)).
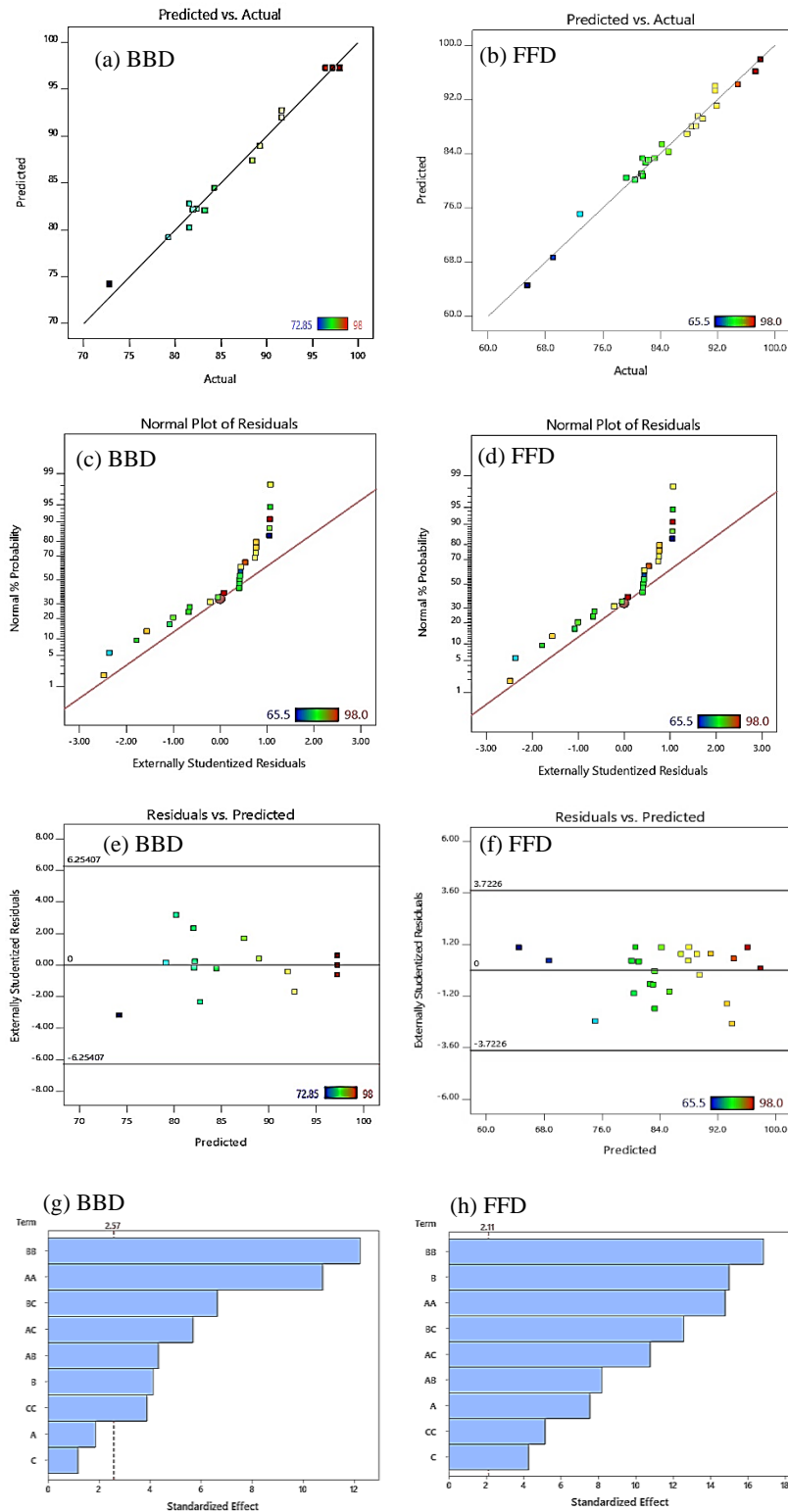
Figure 1 (a & b) Comparison of predicted vs. actual WCCO biodiesel yield conversion in percentage; (c & d) Normal probability plot of residuals; (e & f) externally studentized residuals plots; (g & h) Pareto chart of the standardized effects for both model of BBD and FFD respectively.
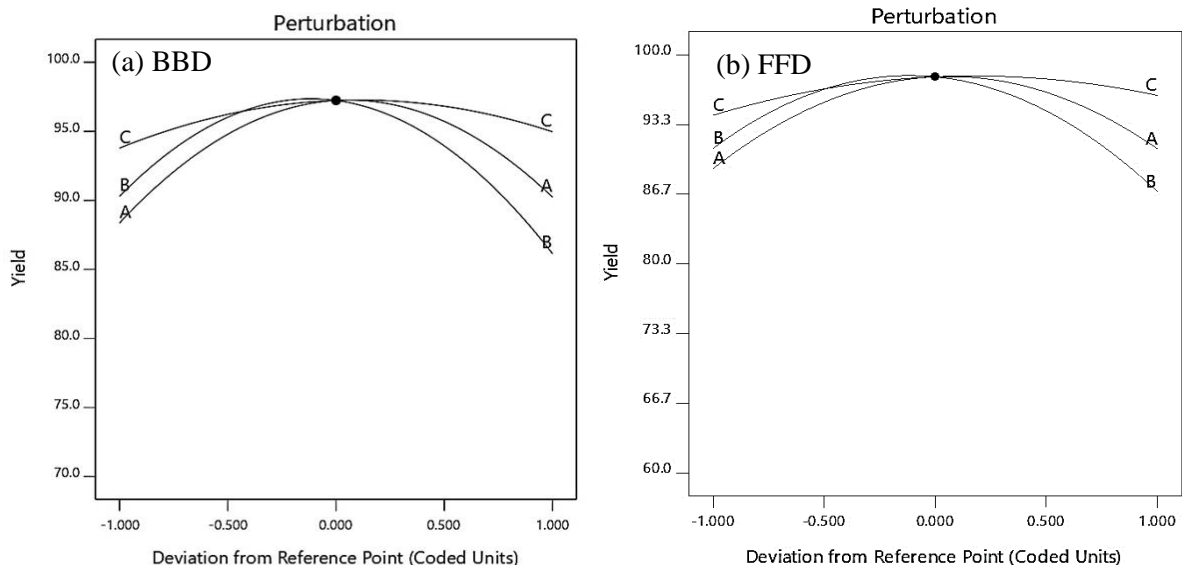
Figure 2 Perturbation plots for process variables for (a) BBD and (b) FFD method

Figure 2 (a & b) are the perturbation plots of process variables affecting biodiesel yield for both models BBD and FFD. The perturbation plot assists to assess the impacts of the multitude of factors at a specific point in the plan space. The response is plotted by changing just one factor over its reach, while holding the wide range of various components steady (Sharma et al. 2020). The nature of the factor which has a more inclined slope when contrasted with planner one indicates that it affects the biodiesel yield significantly. In the BBD model, (refer to Figure 2 (a)) process parameter A has the perturbation influence (exhibiting steep slope) between lower level (-1) to intermediary level (0) followed by the process variables B and C. Among intermediary and higher levels, parameter B presented overwhelming effects trailed by variables A and C. Overall higher slope associated with factor of B indicate, factor B is an influencing parameter in this model. Comparable approach exemplified in figure 2 (b) for FFD method, process parameter A has the sticking effect (i. e. steepest slope) between lower level (-1) to middle level (0) followed by the process variable B and C. Amongst intermediary and higher level, variable B displays governing effect trailed by the parameters A and C. Similar to the BBD model, in the FFD model also the factor of B is observed as influencing factor.

## 3.2 Effect of different parameters on biodiesel yield

The analysis of the effect of singular process variable on WCCO- biodiesel yield offers detailed understanding however is incapable to give an all-encompassing perspective concerning the variation in yield. As shown in pareto chart in fig. 1 (g & h) and perturbation plot in fig. 2 (a &b) linear/singular parameter effect can be observed on the biodiesel yield, however they alone will not provide the complete understanding of process. Hence their quadratic and interaction effects needs to be studied. In order to discover the impact among demonstrated variables, 3-D surfaces along with a 2-D contour plot need to be inspected.

Figure 3 (a) exhibits the interaction plot of WCCO-biodiesel yield for molar ratio and catalyst (KOH) wt% for BBD (@ keeping the temperature constant at the intermediary level). The elliptical shape of the yield profile represented the interaction between these parameters. The greater than 90% yield was obtained for a KOH wt% between 0.37% - 0.65% and molar ratio in the range of $5.2 - 6.9$ at a fixed temperature of 50 $^0$C. Figure 3 (b) shows an interaction plot of WCCO-biodiesel
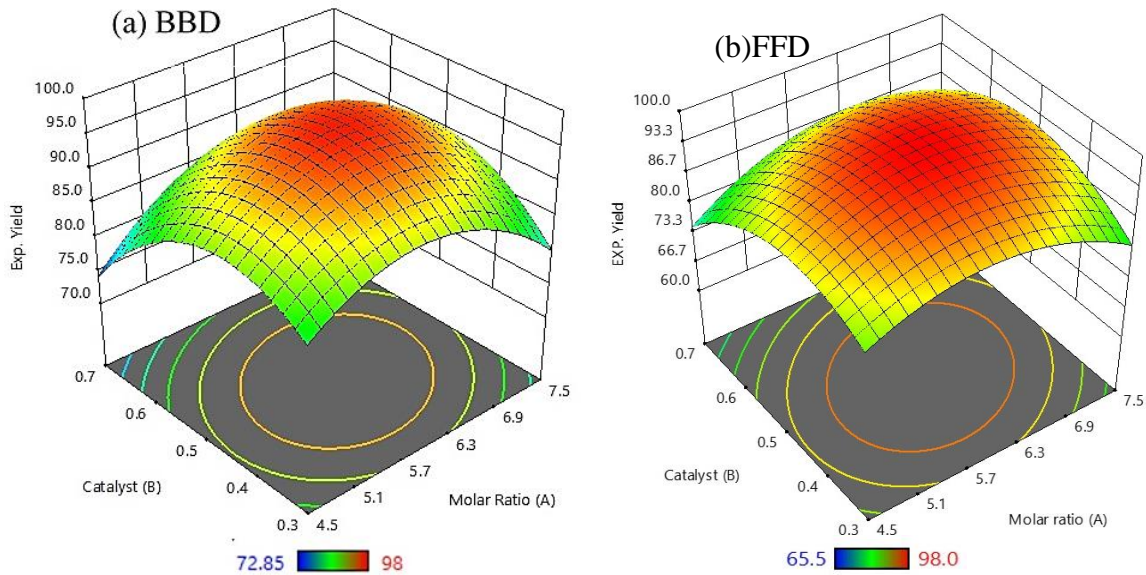
Figure 3 3-D surface plot and contour plot of interaction effect (molar ratio and catalyst (KOH) amount) on biodiesel yield for (a) BBD and (b) FFD model respectively.

yield concerning molar proportion and KOH wt% for FFD (@ keeping the temperature constant at the intermediary level). The greater than 90% yield was obtained for a catalyst KOH wt% in the range of 0.30% – 0.67% and molar proportion in the range of 4.5 – 7.5 at a constant temperature of $50^0$C. The residual region parts in the biodiesel yield decrease with an increase in the loading of the molar proportion and KOH amount. The higher amount of KOH wt% and molar ratio will lead to difficulty for the separation of produced biodiesel.

Figure 4 (a) presents the conjoint effect of process temperature and molar ratio for BBD. A yield profile region higher than 90 %, exists for a molar ratio in the range of 5.3 – 7.1 and temperature in the range of 42 $^0$C -60 $^0$C. Figure 4 (b) displayed the interaction effect of process temperature and molar proportion for FFD. Yield profile region more than 90 %, exists for a molar
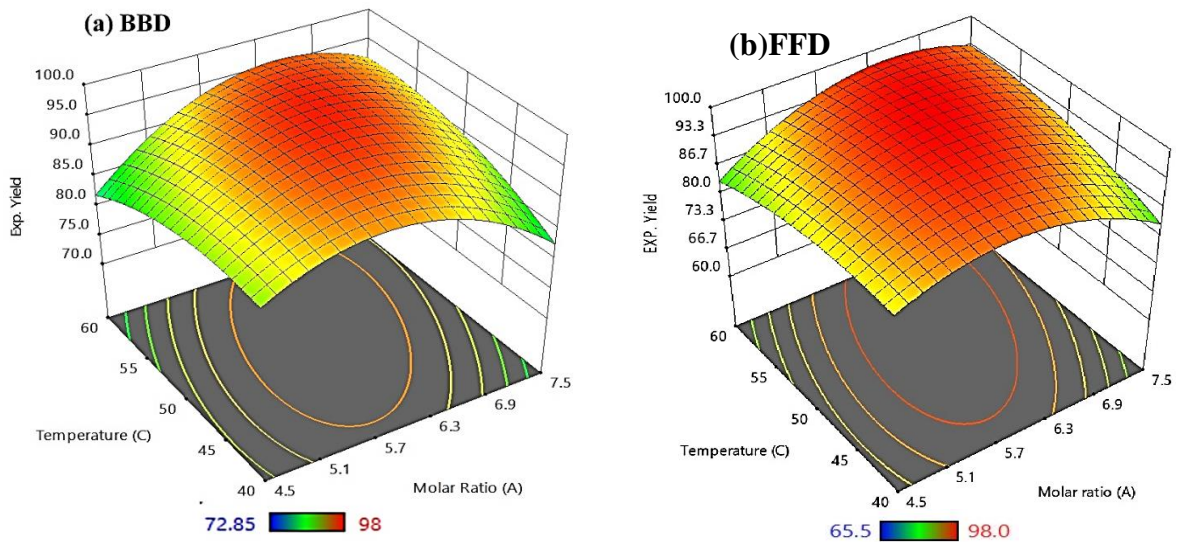


Figure 4 3-D surface plot and contour plot of interaction effect (molar ratio and temperature) on biodiesel yield for (a) BBD and (b) FFD method respectively.

proportion in the range of 4.5 – 7.5 and temperature in the range of $40^0C$ – $60^0C$. The higher molar ratio is not beneficial as glycerol dissolves with biodiesel at higher temperature.
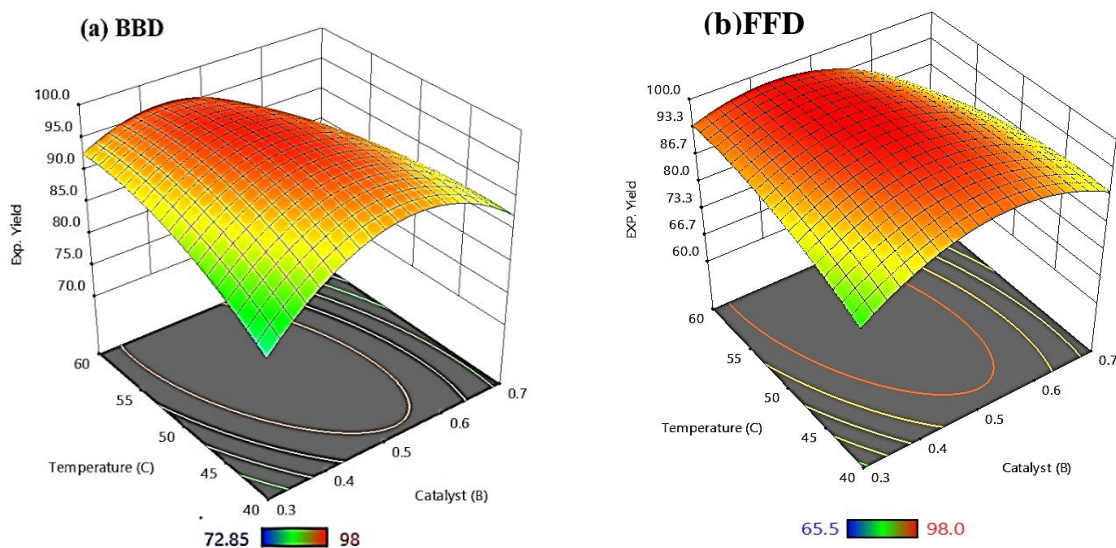


Figure 5 3-D surface plot and contour plot of interaction effect (catalyst (KOH) wt% and temperature) on biodiesel yield for (a) BBD and (b) FFD method respectively.

Figure 5 (a) shows the interaction effect of reaction temperature and catalyst (KOH) amount for BBD (molar ratio kept constant at the intermediate level). The realistic region for maximum yield ($\geq$ 90%) is 0.38% - 0.64% range of the catalyst wt % and temperature in the range of $40^0C$ - $60^0C$. Figure 5 (b) shown the interaction effect of process temperature and catalyst (KOH) amount for FFD (molar ratio kept constant at the intermediate level). The realistic region for higher yield ($\geq$ 90%) is 0.30% – 0.68% range of the KOH wt% and temperature in the range of $40^0C$ -$60^0C$. It was found that biodiesel yield increases with the increase in the operating factors until a specific value beyond which the biodiesel yield declined. The declined in biodiesel yield was because of the reversible response of the transesterification reaction.

## 3.3 Optimization of the process parameters

The RSM mathematical optimization procedure was used for investigating the ideal response conditions within the scope of the control factors by contemplating the standard blunder (StdErr) that occurred in the model (Talaghat et al. 2020). Fig. 6 shows that the lowest and higher limits of the range for all the parameters which are included in this optimization process. As indicated by the breaking point basis for biodiesel yield optimization, the second-order polynomial equation, i.e., Eq. (2) and (3) were applied to optimize the operating process conditions by utilizing mathematical RSM optimization in BBD and FFD approaches. By utilizing the design-expert software, various arrangements of various optimal operating factors and corresponding biodiesel yields were created. In the BBD model, the optimal solution of parameters found to be 6.160, 0.464 %, 53.274 $^0C$ respectively for molar ratio (A), KOH wt% (B), temperature (C), and at this optimal condition, the predicted yield is 97.57 % (where as
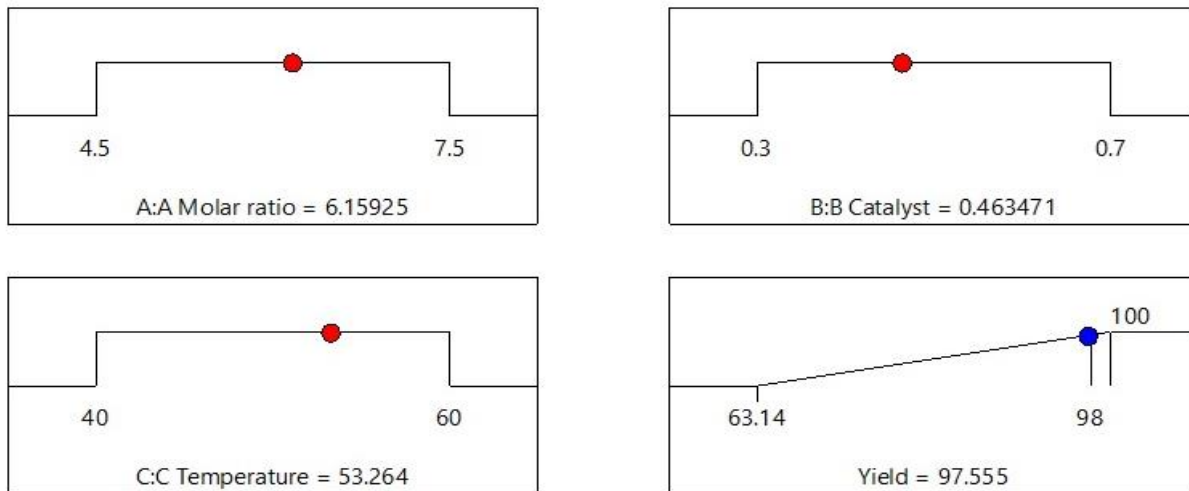
**Desirability = 0.934**

**(a)BBD**
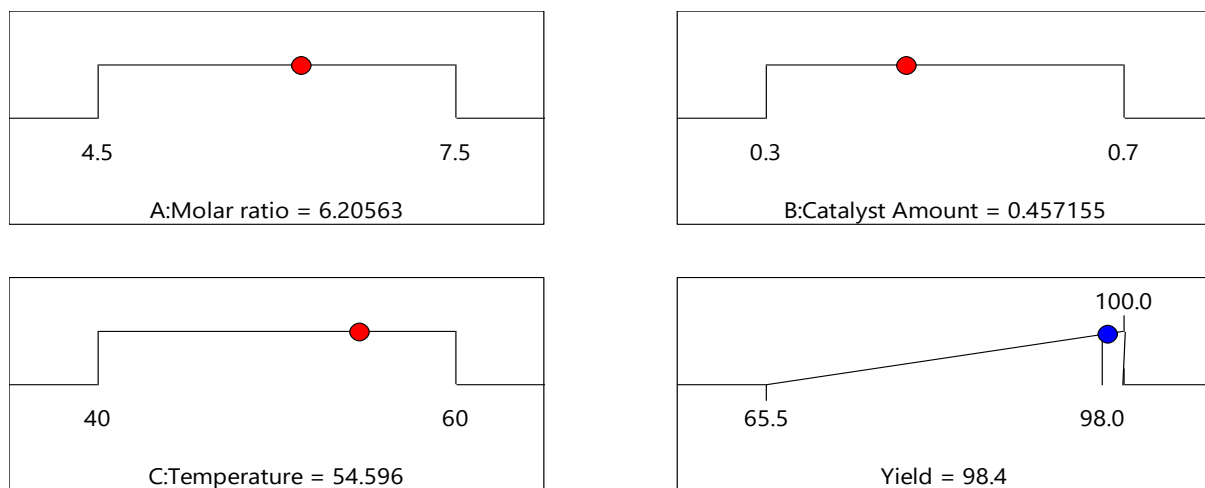


**Desirability = 0.954**

**(b) FFD**

Figure 6 the optimal reaction condition for (a) BBD and (b) FFD method

experimental yield is 98 %) as shown in Fig. 6 (a). For this BBD optimal conditions, the desirability values of 0.911 was observed which is close to the 1. In the FFD model, the optimal solution of parameters is 6.206, 0.457%, 54.596 $^0$C respectively for molar ratio (A), KOH wt% (B), temperature (C), and at this optimal condition, the predicted yield is 98.4% (where as experimental yield is 98 %) as shown in Fig. 6 (b). For this optimal condition, the desirability values of 0.954 was observed which is nearest to the 1. It is to mention here that experimental biodiesel yield of 98 % was obtained for both models i.e. BBD and FFD, while the optimal predicted biodiesel yield obtained is 98 % in the BBD model and 98.4% in the FFD model. This shows that, the experimental yield is nearest to the optimal yield.

## 3.4 Comparison of RSM method of BBD and FFD approach

In this study, both analytical tools of RSM i.e. BBD, and FFD approaches have given outstanding outputs for optimization of process variables of the transesterification process. Examination of the outcome indicated that the results obtained from both models of BBD and FFD of RSM statistical procedures were in agreement with one another. However, the sequence of the important parameters is not the same in both approaches. In the BBD, the liner terms of B, C and interaction terms of AC are insignificant, while in the FFD, all the terms are significant. The $R^2$ value is higher in the BBD (0.9866) compare to the FFD (0.9821). In the BBD, the experiment number of the set is fifteen while, in FFD twenty-seven number of the set of experiment. Hence, it is prescribed to utilize RSM to produce exact enhancement conditions in light of the fact that the necessity of bigger exploratory information in RSM gives low normal error towards modeling and experimental validation.

In the predicted versus actual graph of the BBD method in all the data point very closely the reference line to compare the FFD method plot. In the 3-D surface plots and contour plots of interaction effects of biodiesel, the yield was obtained the nearly close outcomes in both methods of BBD and FFD. The desirability value of 1 is indicated the optimal of the process gives accurate outcomes in the process. So, that here, the desirability values are obtained the 0.911 for the BBD method, 0.954 for the FFD method. RSM has indicated the quantifiable centrality of all potential blends of interaction and quadratic terms parameters dependent on a 95% certainty interval and this can help with perceiving the future course of an ideal reaction. Furthermore, the alluring work in RSM can without a very remarkable stretch choose the ideal operating process condition inside the extent of levels of components.

## 3.5 Application of ultrasound method for biodiesel production

It is found out that biodiesel is typically obtained by the transesterification of the fatty oils and fats with alcohol in the presence of the catalyst. This reaction is normally done utilizing mechanical blending, but this process is restrained by mass exchange among the numerous reactants. This restraint is normally overcome by increase blending, temperature, and reaction time to help in dissolvability between the reactants (Ishola et al. 2020). At first, the ultrasound was used in transesterification reactions to homogenize the two immiscible stages (triglyceride and alcohol). This homogenization is achieved by acoustic cavitation (Chuong et al. 2011). This phenomenon releases high levels of energy achieving high temperatures and pressure factors. There is no other application that includes the usage of non-destructive ultrasound for characterization and analysis of substances (Shinde et al. 2019). Ultrasound has been used for this cause for numerous many years in diverse industrial applications, such as chemical reactions. Ultrasound has been a good device in biodiesel production, due to the potential to take out the mass exchange obstruction and for being a proficient and easy technique. The fundamental viewpoint in the past was the utilization of gear accessible in any chemical research laboratory, with an ultrasonic wave of low recurrence and high force (Girish 2019). The process have shown bright prospects for commercialization for small scale applications with certain modifications (based on type of equipment) in process equipment and design parameters. Scale up studies are needed prior large scale production by achieving the strategy of rotating the reactants for a few times in the same reactor or by applying strategy of parallel reactor systems (Malani et al. 2019).

## 4 Conclusion

In this study, the process parameters were optimized using box-behnken design (BBD) and full factorial design (FFD) method of the RSM technique. Both BBD and FFD agreed that KOH wt% amount to be the most influencing factor in the biodiesel production from WCCO catalyzed by KOH. The optimum WCCO yield of 98 % was reached at a molar ratio of 6:1; KOH amount of 0.50 % w/w; process temperature of $50^0$C for BBD and FFD, respectively. These two techniques have given a decent expectation of the biodiesel yield with respect to molar proportion, KOH wt%, and process temperature. According to this study, the BBD has higher $R^2$ values to compare the other method of FFD. Both the models were given good outcomes of the optimal parameters.

## Acknowledgment

## References

Abdeshahian, P., M. G. Dashti, M. S. Kalil, and W. M.W. Yusoff. 2010. "Production of Biofuel Using Biomass as a Sustainable Biological Resource." *Biotechnology*.

Agarwal, Madhu, Garima Chauhan, S. P. Chaurasia, and Kailash Singh. 2012. "Study of Catalytic Behavior of KOH as Homogeneous and Heterogeneous Catalyst for Biodiesel Production." *Journal of the Taiwan Institute of Chemical Engineers* 43 (1): 89–94.

Aghbashlo, Mortaza, Soleiman Hosseinpour, Meisam Tabatabaei, and Mohamad Mojarab Soufiyan. 2019. "Multi-Objective Exergetic and Technical Optimization of a Piezoelectric Ultrasonic Reactor Applied to Synthesize Biodiesel from Waste Cooking Oil (WCO) Using Soft Computing Techniques." *Fuel* 235 : 100–112.

Ardabili Sina, Amir Mosavi, and Annamária R. Várkonyi-Kóczy. 2020. "Systematic Review of Deep Learning and Machine Learning Models in Biofuels Research." *Lecture Notes in Networks and Systems* 101: 19–32.

Aydar, Alev Yüksel. 2018. "Utilization of Response Surface Methodology in Optimization of Extraction of Plant Materials." *Statistical Approaches With Emphasis on Design of Experiments Applied to Chemical Processes*.

Chuong, T. V., L. Q.T. Dung, N. D.T. Luan, and T. T. Huy. 2011. "Application of Ultrasound for Nanomaterials Synthesis." *International Journal of Nanotechnology* 8 (3–5): 291–99.

Elango, Ragul Karthick, Kiruthika Sathiasivan, Chandrasekaran Muthukumaran, Viruthagiri Thangavelu, Mathur Rajesh, and Krishnamurthi Tamilarasan. 2019. "Transesterification of Castor Oil for Biodiesel Production: Process Optimization and Characterization." *Microchemical Journal* 145: 1162–68.

Ferreira, S. L.C., R. E. Bruns, H. S. Ferreira, G. D. Matos, J. M. David, G. C. Brandão, E. G.P. da Silva, et al. 2007. "Box-Behnken Design: An Alternative for the Optimization of Analytical Methods." *Analytica Chimica Acta* 597 (2): 179–86.

Girish, C. R. 2019. "Review of Various Technologies Used for Biodiesel Production." *International Journal of Mechanical and Production Engineering Research and Development* 9 (3): 1379–92.

Ishola, Felix, Damola Adelekan, Angela Mamudu, Temitope Abodunrin, Abraham Aworinde, Obafemi Olatunji, and Stephen Akinlabi. 2020. "Biodiesel Production from Palm Olein: A Sustainable Bioresource for Nigeria." *Heliyon* 6 (4): e03725.

Keera, S. T., S. M. El Sabagh, and A. R. Taman. 2018a. "Castor Oil Biodiesel Production and Optimization." *Egyptian Journal of Petroleum* 27 (4): 979–84.

Khuri, Andre I. 2017. "A General Overview of Response Surface Methodology." *Biometrics & Biostatistics International Journal* 5 (3): 87–93.

Kulkarni, Mangesh G., and Ajay K. Dalai. 2006. "Waste Cooking Oil - An Economical Source for Biodiesel: A Review." *Industrial and Engineering Chemistry Research* 45 (9): 2901–13.

Malani, Ritesh S., Sachin B. Umriwad, Karan Kumar, Arun Goyal, and Vijayanand S. Moholkar. 2019. "Ultrasound–Assisted Enzymatic Biodiesel Production Using Blended Feedstock of Non–Edible Oils: Kinetic Analysis." *Energy Conversion and Management* 188 (March): 142–50.

Oliveira, Pâmella A., Raphaela M. Baesso, Gabriel C. Moraes, André V. Alvarenga, and Rodrigo P.B. Costa-Félix. 2018. "Ultrasound Methods for Biodiesel Production and Analysis." *Biofuels - State of Development* 7.

Quah, Ray Vern, Yie Hua Tan, N. M. Mubarak, Mohammad Khalid, E. C. Abdullah, and Cirilo Nolasco-Hipolito. 2019. "An Overview of Biodiesel Production Using Recyclable Biomass and Non-Biomass Derived Magnetic Catalysts." *Journal of Environmental Chemical Engineering* 7 (4): 103219.

Refaat, A. A., and S. T. El Sheltawy. 2008. "Comparing Three Options for Biodiesel Production from Waste Vegetable Oil." *WIT Transactions on Ecology and the Environment* 109: 133–40.

Reza Talaghat, Mohammad, Shahin Mokhtari, and Mohammad Saadat. 2020. "Modeling and Optimization of Biodiesel Production from Microalgae in a Batch Reactor." *Fuel* 280 : 118578.

Rodionova, M. V., R. S. Poudyal, I. Tiwari, R. A. Voloshin, S. K. Zharmukhamedov, H. G. Nam, B. K. Zayadan, B. D. Bruce, H. J.M. Hou, and S. I. Allakhverdiev. 2017. "Biofuel Production: Challenges and Opportunities." *International Journal of Hydrogen Energy* 42 (12): 8450–61.

Sen, Gul Akar. 2016. "Application of Full Factorial Experimental Design and Response Surface Methodology for Chromite Beneficiation by Knelson Concentrator." *Minerals* 6 (1).

Anvita Sharma, Pravin Kodgire, and Surendra Singh Kachhwaha. 2020. "Investigation of Ultrasound-Assisted KOH and CaO Catalyzed Transesterification for Biodiesel Production from Waste Cotton-Seed Cooking Oil: Process Optimization and Conversion Rate Evaluation." *Journal of Cleaner Production* 259: 120982.

Shenbaga Vinayaga Moorthi, N., P. Arul Franco, and K. Ramesh. 2015. "Application of Design of Experiments and Artificial Neural Network in Optimization of Ultrasonic Energy-Assisted Transesterification of Sardinella Longiceps Fish Oil to Biodiesel." *Journal of the Chinese Institute of Engineers, Transactions of the Chinese Institute of Engineers,Series A* 38 (6): 731–41.

Shinde, Kiran, and Serge Kaliaguine. 2019. "A Comparative Study of Ultrasound Biodiesel Production Using Different Homogeneous Catalysts." *ChemEngineering* 3 (1): 1–10.

Soria-Figueroa, Erick, Violeta Y. Mena-Cervantes, Montserrat García-Solares, Raúl Hernández-Altamirano, and Jorge Vazquez-Arenas. 2020. "Statistical Optimization of Biodiesel Production from Waste Cooking Oil Using CaO as Catalyst in a Robinson-Mahoney Type Reactor." *Fuel* 282 (186): 118853.

Tan, Shiou Xuan, Steven Lim, Hwai Chyuan Ong, and Yean Ling Pang. 2019. "State of the Art Review on Development of Ultrasound-Assisted Catalytic Transesterification Process for Biodiesel Production." *Fuel* 235 : 886–907.

Tan, Yie Hua, Mohammad Omar Abdullah, Cirilo Nolasco-Hipolito, and Nur Syuhada Ahmad Zauzi. 2017. "Application of RSM and Taguchi Methods for Optimizing the Transesterification of Waste Cooking Oil Catalyzed by Solid Ostrich and Chicken-Eggshell Derived CaO." *Renewable Energy* 114 (PB): 437–47.

Veljković, Vlada B., Ana V. Veličković, Jelena M. Avramović, and Olivera S. Stamenković. 2019. "Modeling of Biodiesel Production: Performance Comparison of Box–Behnken, Face Central Composite and Full Factorial Design." *Chinese Journal of Chemical Engineering* 27 (7): 1690–98.

# Performance assessment & economic feasibility of dual axis solar Fresnel system for water boiling test

*A. J. Dere[1], S. R. Kalbande[2]*
*[1]SRF, Department of UCES&EE, Dr. PDKV,Akola.email-amardeep.dere2@gmail.com*
*[2]Proff & Head, Department of UCES&EE.  Dr. PDKV, Akola,*

## ABSTRACT

The performance of the system was evaluated in the term of water boiling test winter and summer season. The system successfully operated from 10 A. M. to 6 P. M. during water boiling test with cooking pot of 2-liter. Three type of oil were used having oil code 66, 68 and 15W40 for heat supply on indirect mode to the cooker. Among these the thermal performance of oil type 66 was found to be best as it achieved maximum temperature of 135℃ in winter and 145℃ in summer season, respectively. During the test run three types of flow rates were maintained as 0.5, 1 and 1.5 lpm in which the maximum heat achieved at flow rate of 1.5 lpm. also, three type of focal length were used for the performance was evaluated at focal length 1450, 1650 and 1850 mm for testing maximum temperature at focal point on heat exchanger to supply heat in cooking pot.It is conducted that the dual axis solar Fresnel lens system was found to be economical having the payback period 2 years, 11 months & 3 days and the system can be integrated in present energy scenario for cooking application where sunshine is available in abundance & throughout the year.installed capital cost and operation & maintenance cost was found to be Rs. 41,400 and Rs. 4,606 respectively. Therefore, the total energy saved per year was calculated to be Rs. 14,400.

**Keywords-** Fresnel lens, oil flow rate, solar radiation, cooking pot, solar cooker, dual axis.

## INTRODUCTION

Solar Energy for cooking heating and food processing consumes a significant amount of energy In many third-world regions people rely heavily on wood and biomass for houses heating and cooking food. Therefore, significant damage to the environment and smoke-related health problems are common consequences in the third-world. It has been well recognized worldwide that using less fossil fuels and implementing more sustainability in energy supplies are vitally important to the health and stability of the global economy, environment, and humanity. These facts result in an increasing demand of utilizing renewable energy for household heating and cooking.

## MATERAL AND METHODS

The steps in the process of manufacturing and assembling are outlined as follows:

1. FLSC system was fabricated using mild steel sheet, rods aluminum rods, glass, press brake machine and welding machine.
2. Heat exchanger was made up of stainless steel and 32 copper tubes were used to heat transfer and it was coated with black paint to absorb maximum solar radiation.
3. The size of cooking pots is 2 lit and it was made up of aluminum. It was insulated by polyurethane foam cover with Glass insulation.
4. The stand were fabricated with mild steel angle of $35 \times 35 \times 5$ mm to rest the Fresnel lens dual axis tracking system with connecting rods and heat exchanger  was kept vertical to the ground surface.
5. Glass required was cut and placed on the support and by using silica gel was fixed on heat exchanger. Rubber sealant was provided to hold toughened glass in contact with heat exchanger surfaces
6. The capacity of the hot oil flow meter was 1 liter per minute and required capacity of motor to circulate the oil was 90 watt.
7. Two numbers of motors with 15-watt capacity were used to rotate in east to west (zenithal) and north to south (azimuthally) direction in tracking system.
8. SPV panel were used to supply power to the temperature sensors and motor in tracking mechanism of the solar Fresnel lens system
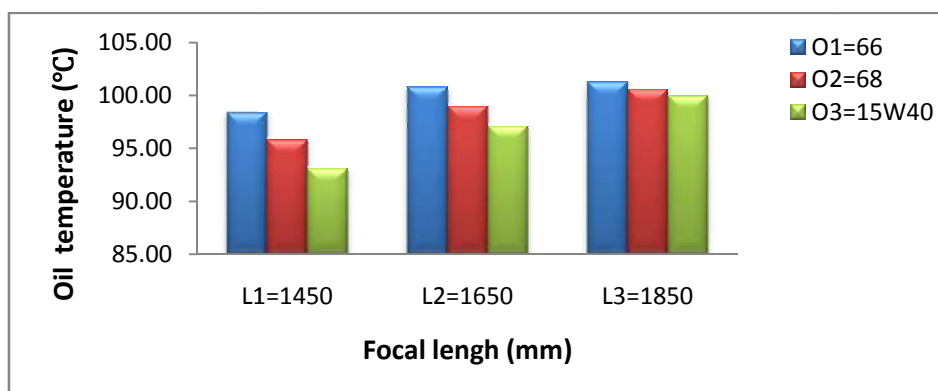
## Result & Discussion

### 1.1 Effect of type of oil and focal length of lens on temperature of cooking pot (°C)

The table 1.1 represents the effect of type of oil and focal length of lens on temperature of cooking pot (°C) in winter season (December to February 2018)

**Table 1.1 Effect of type of oil and focal length of lens on temperature of cooking pot (°C)**

| Sr. No. | Type of Oil | Focal length of lens (mm) | | |
|---------|-------------|------------|------------|------------|
| | | $L_1$=1450 | $L_2$=1650 | $L_3$=1850 |
| 1 | $O_1$=66 | 98.34 | 100.79 | 101.27 |
| 2 | $O_2$=68 | 95.77 | 98.96 | 100.58 |
| 3 | $O_3$=15W40 | 93.11 | 97.09 | 99.95 |
| | F test | Sig. | | |
| | SE(m)$\pm$ | 0.34 | | |
| | CD at 5 % | 0.98 | | |

The table 1.1 revealed the effect of type of oil and focal length of lens on temperature of cooking pot. It was observed that the focal length of lens increased from 1450 to 1850 mm, the temperature of cooking pot was found to be increased from 98.34 to 101.27, 95.77 to 100.58 and 93.11 to 99.95 °C by using the oil type 66 ($O_1$), oil type 68 ($O_2$) and oil type 15W40 ($O_3$), respectively. Also, it was observed that by using the oil type 66, the maximum temperature of cooking pot was obtained as 101.27°C than that of oil type 68 and oil type 15W40. The minimum temperature of cooking pot was obtained as 93.11°C by using the oil type 15W40.



**Fig 1.1 Effect of type of oil and focal length of lens on temperature of cooking pot (°C)**

Fig 1.1 shows that the per cent increase in the temperature of cooking pot (°C) was found to be 2.98, 5.02 and 7.35 from focal length 1450 to 1850 mm by using the oil type 66, oil type 68 and oil type 15W40, respectively. The combine effect of type of oil and focal length of the lens was found to be significant.

### 1.2 Effect of type of oil and flow rate of oil on temperature of cooking pot (°C)

The table 2.2 represents the combine effect type of oil and flow rate of oil on temperature of cooking pot (°C) in winter season (December 2018)

**Table 2.2 Effect of type of oil and flow rate of oil on temperature of cooking pot (°C)**

| Sr. No. | Type of Oil | Focal length of lens (mm) | | |
|---|---|---|---|---|
| | | $F_1=0.5$ | $F_2=1$ | $F_3=1.5$ |
| 1 | $O_1=66$ | 99.393 | 99.816 | 101.197 |
| 2 | $O_2=68$ | 97.718 | 98.258 | 99.333 |
| 3 | $O_3=15W40$ | 94.74 | 97.359 | 98.044 |
| | F test | Sig. | | |
| | SE(m)$\pm$ | 0.34 | | |
| | CD at 5 % | 0.98 | | |
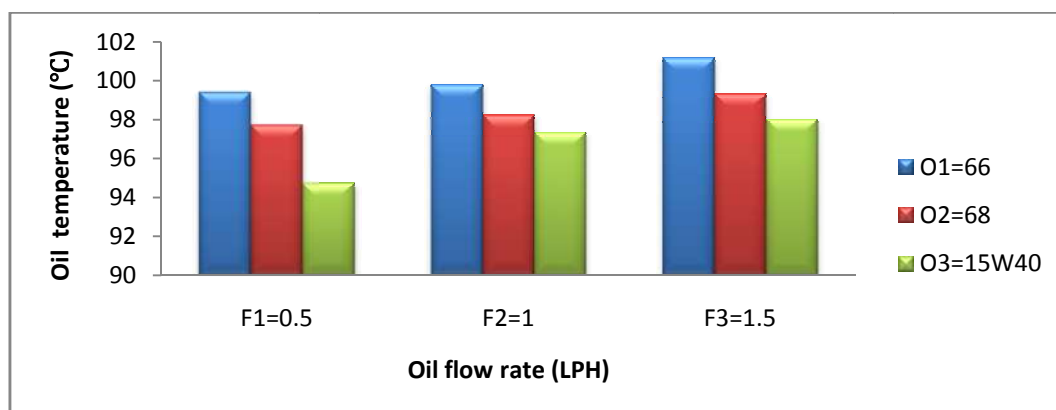


**Fig. 2.2 Effect of type of oil and flow rate of oil on temperature of cooking pot (°C)**

Fig 2.2 shows that the per cent in the cooking pot (°C) was found to be 1.81, 1.65 and 3.48 from flow rate 0.5 to 1.5 Lph by using oil type 66, 68 and 15W40 respectively. The combine effect of type of oil and flowrate was found to be significant.

**2.3 Effect of focal length and flow rate of the oil on the temperature of cooking pot (°C)**

The table 2.3 represent the effect of focal length and flow rate of the oil on the temperature of cooking pot (°C) in winter season (December to February 2018).

**Table 2.3 Effect of focal length and flow rate of the oil on the temperature of cooking pot (°C)**

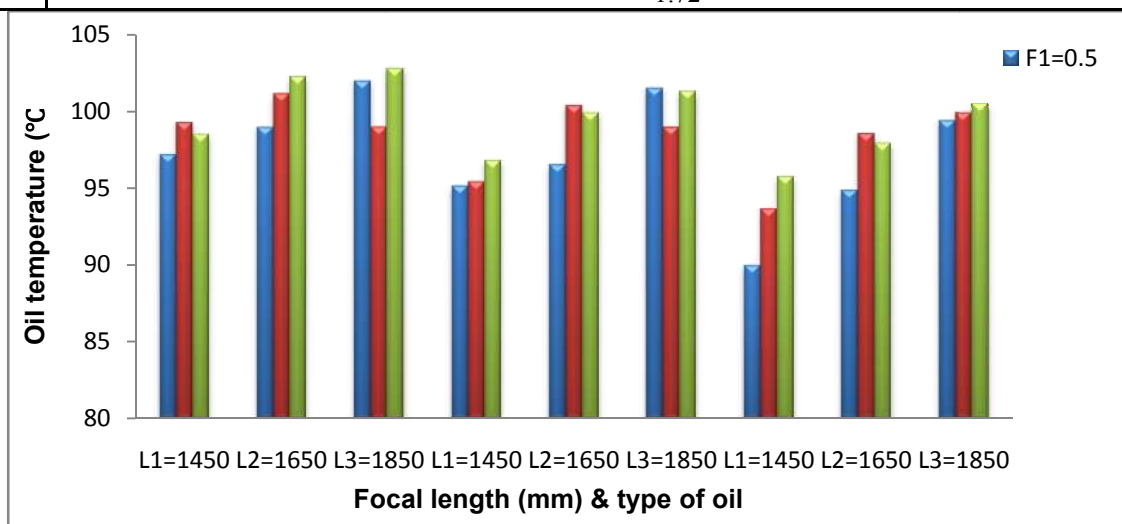| Sr. No. | Focal length (mm) | Flow rate of oil (LPH) | | |
|---|---|---|---|---|
| | | $F_1=0.5$ | $F_2=1$ | $F_3=1.5$ |
| 1 | $L_1=1450$ | 94.1 | 96.11 | 97.008 |
| 2 | $L_2=1650$ | 96.789 | 100.024 | 100.024 |
| 3 | $L_3=1850$ | 100.962 | 99.298 | 101.542 |
| | F test | Sig. | | |
| | SE(m)$\pm$ | 0.34 | | |
| | CD at 5 % | 0.98 | | |
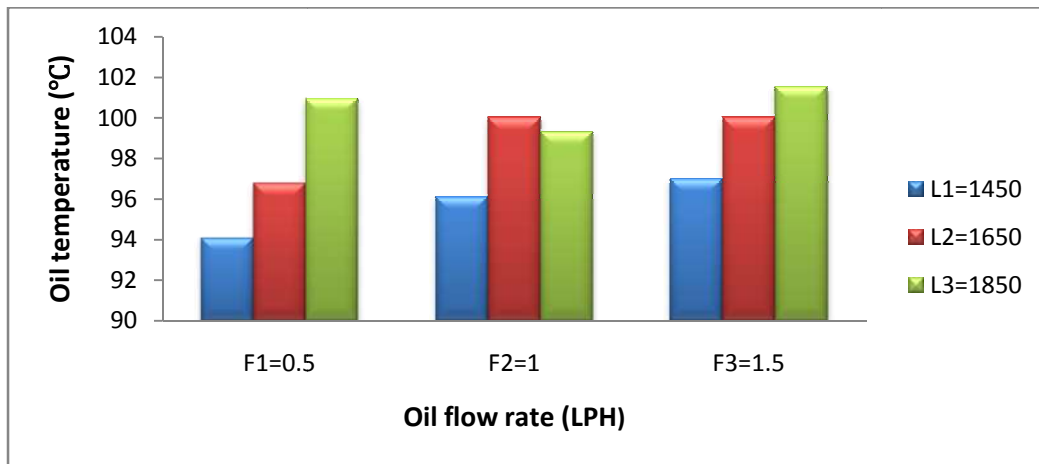
**Fig.2.3 Effect of focal length and flow rate of the oil on the temperature of cooking pot (°C)**

Fig. 2.3 shows that the per cent increase iin the temperature of cooking pot (°C) was found to be 3.08, 3.33 and 0.55 from the flow rate 0.5 to 1.5 LPH.

**2.4 Effect of oil flow rate, flow length of temperature of cook pot (°C).**

**Table 2.4 Effect of oil flow rate, flow length of temperature of cook pot (°C)**

| Oil flowrate (LPH) | Type of oil | | | | | | | | |
|---|---|---|---|---|---|---|---|---|---|
| | $O_1$=66 | | | $O_2$=68 | | | $O_3$=15W40 | | |
| | $L_1$=1450 | $L_2$=1650 | $L_3$=1850 | $L_1$=1450 | $L_2$=1650 | $L_3$=1850 | $L_1$=1450 | $L_2$=1650 | $L_3$=1850 |
| F1=0.5 | 97.22 | 98.96 | 102 | 95.117 | 96.557 | 101.48 | 89.963 | 94.85 | 99.407 |
| F2=1 | 99.293 | 101.15 | 99.003 | 95.403 | 100.407 | 98.963 | 93.633 | 98.517 | 99.927 |
| F3=1.5 | 98.52 | 102.257 | 102.813 | 96.78 | 99.927 | 101.293 | 95.723 | 97.89 | 100.52 |
| F test | Sig. | | | | | | | | |
| SE(m)+ | 0.604 | | | | | | | | |
| CD at 5 % | 1.72 | | | | | | | | |



**Fig 2.4 Effect of oil flow rate, flow length of temperature of cook pot.**

Fig. 2.4 shows that the per cent increase in the temperature of cook pot was found to be (102.813 – 97.22), (101.293 – 95.117) and (100.52 – 89.963) at flow rate 0.5 to 1.5 LPH, focal length 1450 to 1850 and with oil type 66 to 15W40 respectively.

**Economic assessment of the dual axis Fresnel lens solar concentrator (FLSC) system**

Following different economic indicators were used for economic analysis of dual axis Fresnel lens solar concentrator (FLSC) system for cooking application under the study.

1) Net present worth (NPW)
2) Benefit cost ratio (B/C ratio)
3) Payback period

**1 Net present worth (NPW)**

The difference between the present value of all returns and the present money require making an investment is the net present worth. The present value of the future returns was calculated through the use of discounting. Discounting essentially a technique by which future benefits and cost streams can be converted to their present worth.

$$NPW = \sum_{t=1}^{t=n} \frac{B_t - C_t}{(1+i)^t} \qquad \text{..... 4.10}$$

Where,

$C_t$ = Cost in each year
$B_t$ = Benefit in each year
t = 1, 2, 3................n
i = discount rate

**2 Benefit cost ratio**

This is the ratio obtained when the present worth of the benefit stream is divided by the present worth of the cost stream. The mathematical benefit-cost ratio can be expressed as

$$\text{Benefit-cost ratio} = \frac{\sum_{t=1}^{t=n} \frac{B_t}{(1+i)^t}}{\sum_{t=1}^{t=n} \frac{C_t}{(1+i)^t}} \qquad \text{.....4.11}$$

Where,

$C_t$ = Cost in each year

$B_t$ = Benefit in each year

t = 1, 2, 3................n (year)

i = discount rate

**3 Payback period**

The payback period is the length of time from the beginning of the project until the net value of the incremental production stream reaches the total amount of the capital investment. The payback period of the project is estimated by using the straight forward formula

$$P = \frac{I}{E} \qquad \text{... 4.12}$$

Where,

P = Payback period of the project in years,

I = Investment of the project in Rupees and

E = Annual net cash revenue in Rupees

### 4. Economic assumptions of dual axis FLSC system

Table 2 depicted the assumption considered for assessment of economical feasibility analysis.

**Table 2 Economic assumptions for dual axis FLSC system**

| Sr. no. | Description | Amount (Rs.) |
|---|---|---|
| **A** | **Fixed cost** | - |
| I | FLSC system | 35,000.00 |
| Ii | Solar photovoltaic panels | 6,400.00 |
| | **Total** | **41,400.00** |
| **B** | **Operating cost Rs/year** | - |
| I | Cost of Thremic oil | 520.00 |
| Ii | Repair and maintenance cost yr$^{-1}$ | 4,140.00 |
| | **Total** | **4,660.00** |
| **C** | **Electricity saving cost yr$^{-1}$** | **14,400.00** |

The following assumptions were considered for assessing the economic assessment of the dual axis Fresnel lens solar concentrator (FLSC) system.

1. The capacity of the cooker was 2 liter.
2. The fixed cost of dual axis Fresnel lens solar concentrator (FLSC) system was Rs. 35,000 and cost of photovoltaic system is Rs. 6,400.
3. The average price of electricity by using induction required to boil 2 liter of water is Rs. 14,400 per year which is saved by using FLSC system.
4. The operating days for the FLSC system was considered of 300 days yr$^{-1}$ i.e.10 months.
5. The annual repair and maintenance cost is 10% of the initial investment.
6. The useful life of solar Fresnel lens system is 10 years.
7. Rate of interest is 10 % on initial investment.

### 5. Economic assessment of the dual axis Fresnel lens solar concentrator (FLSC) system

The economic feasibility of dual axis Fresnel lens solar concentrator (FLSC) system for cooking application was calculated by considering investment, operating cost and average repair and maintenance cost of the system. Economics of dual axis FLSC system are summarized in Table 5.48 the details of cash inflow and outflow up to 10 year.

#### 5.1 Net present worth (NPW)

The present worth of total cash inflow and outflow for dual axis FLSC system for cooking application was found to be Rs. 88481.77 and 63889.12/- respectively. Based on NPW it could be concluded that the cooking on dual axis tracking system seems to be economical.

**Table 3 Economic assumptions of dual axis FLSC system**

| Sr. no. | Description | Amount (Rs.) |
|---|---|---|
| **I** | **Fixed cost** | - |
| 1 | FLSC system | 35,000.00 |
| 2 | Solar photovoltaic panels | 6,400.00 |
| | **Total** | **41,400.00** |
| **II** | **Operating cost Rs/year** | - |
| 1 | Cost of Oil | 520.00 |
| 2 | Repair and maintenance cost yr$^{-1}$ | 4,140.00 |
| | **Total** | **4,660.00** |
| **III** | **Electricity saving cost yr$^{-1}$** | **14,400.00** |

| IV | Net present worth | 49185.30 |
|---|---|---|
| V | Benefit- cost ratio | 1.38 |
| VI | Payback period | 2-year, 11 month & 3 days |

## 5.2 Benefit cost ratio

The BC ratio of the system was calculated by dividing present worth of benefit stream and present worth of cost stream. Table 5.48 revealed that the value of benefit cost ratio and it was found to be 1.38. Thus, it is concluded that investment was justified and dual axis FLSC system for cooking application was found to be economically viable.

## 5.3 Payback period

Payback period for dual axis FLSC system for cooking application was found to be 2 year, 11 month & 3 days (Appendix E). Apart from this, the FLSC cooking system can save the LPG, biomass, electricity. The use of solar energy in FLSC system is the green energy source there by it reduce the environmental pollution and ultimately save the environment.

## 6 Life cycle cost of dual axis FLSC system

The most comprehensive measure for cost of saving is life cycle cost. This measure incorporates all elements cost such as installed capital cost, cost of operation and maintenance over the life of installation and cost of subsystem replacement.

$$\text{Cost of cooking saved/yr} = \frac{ICC + FCR + O\&M + LRC}{\text{Eletricity saved /year}} \dots \dots \dots \dots 5.7$$

Where, ICC is the installed capital cost, FCR is the annual fixed charge rate, O&M is the annual operation and maintenance cost and LRC is the levelized replacement cost.

**Table 4 Capital statement of the dual axis FLSC system**

| Sr. No. | Particular | Parameter |
|---|---|---|
| 1 | Capacity of cooking pot (litre) | 2 |
| 2 | Installed capital cost (Rs.) | 41,400 |
| 3 | Annual operation and maintenance cost (Rs.) | 4,660 |
| 4 | Annual saving in the cost of cooking | 14400 |
| 5 | Discount rate (%) | 10 |
| 6 | Project life time, years | 10 |
| 7 | Levelized replacement cost (Rs.) | 25% on annual O & M cost |
| 8 | Annual fixed charge rate (%) | 10 |

Table 5.49 Shown that the installed capital cost and operation & maintenance cost was found to be Rs. 41,400 and Rs. 4,606 respectively. Therefore, the total energy saved per year was calculated to be Rs. 14,400.

**Table 5 Energy measures of FLSC system for cooking application**

| Energy measure | FLSC system | Electric system |
|---|---|---|
| Energy required to heat/boil the 10 lit of water per day (kWh) <br> $Q_p = W_p \times C_p \times \Delta T$ <br> Where, <br> $W_p$= weight of the product (kg), <br> $C_p$=specific heat of the product (kJ/kg °K), <br> $\Delta T$= difference of ambient temperature ($T_a$) and cabinet inside ($T_i$) temperature, K | 0.19 | 3.2 |
| Energy required to boil the water in a year (300 days), (kWh) | 57 | 960 |
| Electricity tariff required to boil 3000 lit water, Rs/yr. | - | 6720 |
| **Revenue saved using solar energy, Rs/yr** | **399** | **-** |

The Table 5 shows the energy measures for economic evaluation of FLSC system. The energy required to heat or boil water in FLSC system for 10 liter of water per day is 0.19 kWh. Revenue saved using solar energy is Rs. 399 and net profit from the system is Rs. 6720 per year. Apart from this, by using the solar energy i.e. green energy can be produced which ultimately reduces the environment pollution.

**CONCLUSION**

Economic indicators i.e. net present worth, benefit-cost ratio and payback period of the system was found to be Rs. 49185.30, 1.38 and 2 years, 11 months & 3 days, respectively which means that the dual axis FLSC system is economically viable, in the present context. As the solar energy was used for the cooking purpose, hence the use of green energy added extra benefit to the environmental. It is observed that the due to tracking system used in the system which consumes energy generated by SPV panel for its operation and contributing toward increasing the productivity of thermal energy required for the cooking.

**REFERENCES**

1) Anonymous, (2006) .Solar cooking Journal of Energy in Southern Africa. Vol18 No 3..

2) Kumar, V., Shrivastava, R. L., and Untawale S. P. (2015). Fresnel lens :Apromising alternative of reflectors in concentrated solar power. www.elsevier.com/locate/rser. Renewable and Sustainable Energy Reviews 44(2015)376–390.

3) Paul, A. J. (2013). Design and performance analysis of automated two axis solar tracking system for steam generation. IEEE, 432-437.

4) Udawant, R. R. (2016). Study of Performance of Fresnel Lens Solar Concentrator. International Journal of Energy Engineering, 6(1A): 14-22.

# Selection of Geometry for Improving Reactor Efficiency using Computational Fluid Dynamics

M.P.Shah, M.S.Rao,

Department of Chemical Engineering, Dharmsinh Desai University, Nadiad-387 001, Gujarat, INDIA
*Corresponding author: msrao@ddu.ac.in, m: (+91 94276 34725)

## Abstract

Sustainable industrial growth requires efficient reactor designs. Heat transfer and mass transfer play an inevitable part in improving conversions and yields in the reactor. One of the steps in improving heat and mass transfer is improving mixing characteristics in the reactor vessel. Increased heat and mass transfer, improves rate of reaction, conversion and yields of desired product.

Present work focuses on selection suitable geometry to increase the energy efficiency by enhanced mixing rate to increase the rate of reaction and yield of desired product. ANSYS platform was selected to carry out hydrodynamic study, generate temperature, pressure and concentration profile to calculate the final conversions for modeled geometries. Simulation studies were conducted to replace agitators with modified geometries with different entry and exit locations. Simulation results reveled that along with axial mixing, radial and tangential mixing also plays an important role in improving the mixing characteristics. Based on simulation results an efficient geometry, an annular cylindrical tube with multiple tangential entries and tangential is suggested.

**Keywords**: Computational Fluid Dynamics, Microwave, Synthesis Reaction, Conversion, Geometries.

## 1. Introduction

It is very much essential to have an appropriate model of green technology along with sustainable development for betterment of society. The world population demands more output in terms of end use product. This will force professionals to work hard, polluting environment to a large extent. Global problems of environmental degradation have forced authorities and professionals to identify the concept of sustainable development. New environmentally friendly technologies are fundamental to attain sustainable development. Various steps are being taken to maintain and improve the quality of environment by meeting the demand of society.

To meet the demand of higher throughput, chemical industries need to perform heterogeneous catalyzed reactions and are non-isothermal in nature. Especially synthesis reactions, associated with formation of long molecules are mostly endothermic in nature. The fluid-fluid or fluid-solid heterogeneous reactions need special focus on the rate of heat and mass transfer, as it directly affects the rate of reaction. Which in turn will decide reaction time and also economy of overall process plant.

Industrial reactors are working with heating or cooling jackets along with mechanical agitators. This will have direct effect on heat and mass transfer rates, which will increase the reaction time and also affect the overall conversion of desired products. It is essential to improve the rate of heat and mass transfer by improving mixing phenomena. This can be achieved by changing the mixing devise. by using alternative heat source or by modifying the reactor geometry.

Authors have suggested of using alternative heat source, Microwave (MW) Irradiations as green energy source, which directly interact with molecules of system by penetrating reaction vessel. The reactions time for reactions will be reduced due to direct interaction. This will allow reactions to be conducted in continuous mode thereby increasing the throughput of slow

synthesis reactions. The main issue with using MW cavity is that one can use any mechanical devise to enhance the mixing characteristics. So, it is essential to identify a geometry which will provide mixing without any mechanical agitator. In present work, authors have proposed a modified geometry which will have improved mixing characteristics to increase the rate of mass transfer. The study is based on simulation conducted using ANSYS. Modified geometries were simulated for reaction under microwave irradiations to study the effect of improved mixing on rate of reaction.

## 2. Problem definition

L. Estel *et.al.*[1] (2017) was the first one to clearly explained how to incorporate chemical engineering in the field of continuous microwave operations. They proposed various geometries from micro cm to few mm which can be fabricated from various MoC like PTFE or Teflon or Quartz. By varying T, P and inlet flow rate of reactants one can manipulate the residence time within the reactors. They also concluded that with the varying geometrical aspect one can achieve better hydrodynamic properties (mixing characteristics) and can improve the temperature distribution. They also showed effect of recycle with external cooling on overall operation. N.Haneishi *et.al.*[2] (2019) and Dela Hoz *et.al.*[3] (2005) shown creation of hot spot in heterogeneous reactions under microwave based synthesis. Zohu P. Et.al.[4] (2014) have studied effect of variation in geometry on heating characteristic of water as cheap solvent. They found more uniformity in the temperature profile when conventional reactor converted to micropipe on which MW was impacted by special rigid wave guide.

Based on Literature review, it was identified that researchers have put in efforts to modify geometries to use them effectively under MW irradiations. But they reported mixing issues required to be addressed, so present work focuses on geometrical modifications to enhance the mixing characteristics within geometries to improve heat and mass transfer in fluid-fluid or fluid-solid heterogeneous reactions.

Industrial reactors are either Pipe or tank with provision of mechanical agitators having heating or cooling facility. The material of construction of Reactor vessel will be a metal based on reacting species. The reaction vessel to selected for MW cavity can not have mechanical agitation facility and MoC of vessel has to be transparent to the MW irradiations. So it was decided to have pipe flow reactor to selected for current work.

It is essential to have proper mixing to enhance the rate of heat and rate mass transfer. This in turn will increase the overall rate of reaction. So, the problem under consideration is identification of a geometry which will have better mixing characteristics which can be used as microwave reactor.

The parameters and variables used for simulation are as follows:

$D_{Ro}$ = Outside diameter of reactor, mm
$D_{Ri}$ = Inside diameter of reactor, mm
$L_R$ = length of reactor, mm
$D_i$ = diameter of inlet nozzle, mm
$D_o$ = diameter of outlet nozzle, mm
$L_i$ = length of inlet nozzle, mm
$L_o$ = length of outlet nozzle, mm
$V_i$ = velocity normal to the inlet cross section, m/s
$Q_1$ = heat source, $W/m^2$
$Q_2$ = heat source, $W/m^3$
$V_R$ = volume of reactor, ml
$T_i$ = inlet temperature of process fluid = 288K
$L_h$ = length of heating section, 25 mm

**Table 2.1** Design parameter values

| Geometry No | $D_{Ro}$ | $D_{Ri}$ | $L_R$ | $V_R$ | $D_i/D_o$ | $L_i/L_o$ | $V_i$ | $Q_1$ | $Q_2$ |
|---|---|---|---|---|---|---|---|---|---|
| I | 25 | - | 154 | 75 | 10/10 | 100 | 0.00625 | - | |
| II | 25 | - | 150 | 75 | 6/6 | 100 | 0.00625 | - | |
| III | 22 | 12 | 150 | 40 | 6/6 | 30 | 0.00625 | 6000 | |
| IV | 22 | 12 | 150 | 40 | 6/6 | 30 | 0.693 | | 175000 |

As shown in Table 2.1, the parameters of geometry were changed after each simulation and results obtained were checked for tangential velocity profile within the reactor. To improve the hydrodynamics of the system, a new geometry was proposed.

## 3. Solution strategy

Computational Fluid Dynamics (CFD) involves the numerical solution of conservation equations for mass, momentum and energy in a flow geometry of interest. Additional sets of equations reflecting the problem at hand can be incorporated to customize the problem. Improved turbulence modelling and high-performance computing have a particularly important part to play in predicting conversions in this type of reactor.

Simulation studies were conducted using ANSYS-Fluent platform. The modeling started with a simple pipe flow (Plug Flow) reactor and then based on results; the modifications were proposed. Upon each simulation, the hydrodynamic and temperature profiles were generated. Those profiles helped to propose the modification in geometry, which was again simulated. The results obtained were compared with the previous mixing characteristic and improvements were observed. After many iterations in geometrical change, the final geometry with tangential entry and exit in annular flow was decided to be the best out of all.

## 4. Results and Discussion

Being fluid-fluid reactions, it is essential to have good mixing to avoid any hot spot. The simulation study was conducted to incorporate the flow patterns which will enhance the mixing of reaction mixture inside. As described in problem definition, the focus of the work is to propose a geometry which will have better mixing characteristics in comparison to base case discussed in case I. The outcome of simulated geometry results has been discussed and final geometry is proposed.

**Case I Cylindrical Pipe with one inlet and one outlet normal to flow direction**

First geometry proposed was having one inlet and one outlet normal to the pipe axis. To have 50seconds of residence time, 30ml/min of flow rate was set. That gave inlet velocity of fluid as 0.000625m/s normal to the cross section. There was large portion of the pipe having stagnant zone, which indicates non-ideality in mixing within geometry. Further only axial velocity component was present in the system, there was no tangential component. So, the improvement in the geometry was suggested to reduce the stagnant zone in the proposed geometry.

Based on the Figure 3.1, the modified geometry with inlet and outlet from opposite plane was decided and the simulation was run with same initial condition. The results showed similar stagnant zone as with first geometry and again the tangential velocity component was missing. Further, the geometry was modified with two inlets and one outlet, but the scenario was not improved much. The only difference was with residence time, due to variation in flow paths. But the large volume of reactor vessel shown stagnant zone and no presence of tangential

velocity. So, to incorporate tangential velocity component, same pipe flow geometry with lateral entry and tangential exit was proposed.
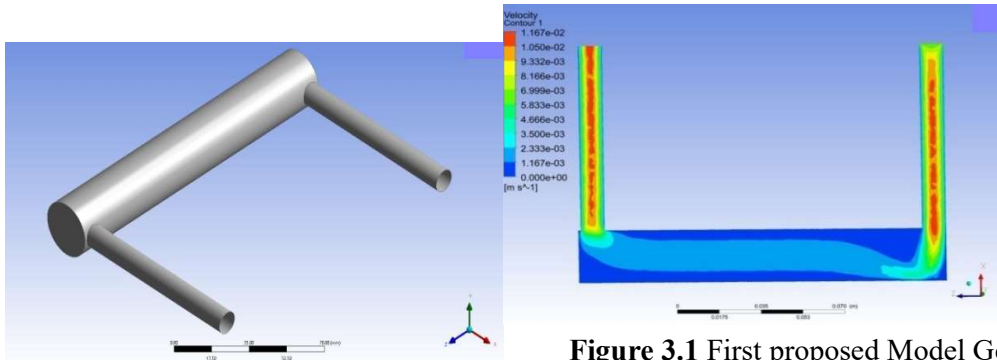


**Figure 3.1** First proposed Model Geometry

With new proposal, there was appreciable reduction in stagnant zone and for the first time a tangential velocity component was observed with magnitude of 0.00005m/s. Due to small magnitude the mixing length was 5mm only, there after the axial velocity component was dominating and flow became the same as it was with normal entry.

**Case II Cylindrical Pipe with three tangential entry and exits.**

Figure 3.2 shows the direction and plane in which entry and exit were attached. Figure 3.3 shows the velocity profile in axial and tangential directions. It clearly showed presence of good mixing characteristics for full length of geometry except at wall at which the velocity of fluid would be zero.
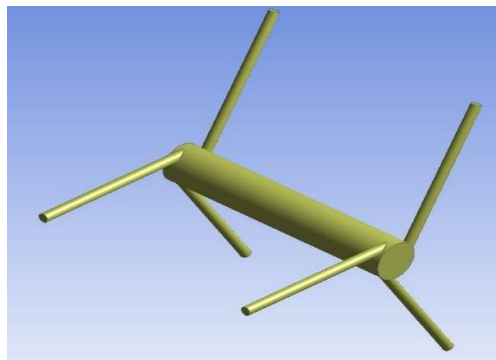


**Figure 3.2** Second Proposed Geometry
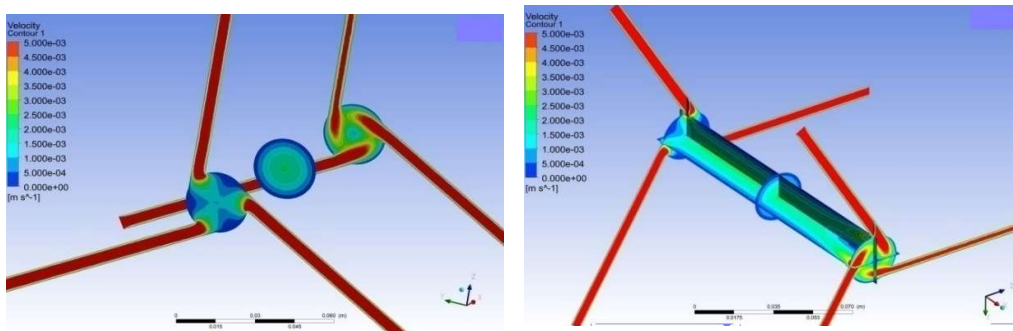


**Figure 3.3** Velocity profile in axial and tangential planes

Figure 3.4 shows the presence of tangential velocity component (0.00066m/s) on a plane at 75mm from inlet. The magnitude of tangential velocity was almost zero at middle of the plant and increases outward. Due to longer path, the residence time further increased to 4.2min. The streamlines in this geometry showed flow path fluid element follows, which is indicative of good mixing in the geometry with mixing length of 40mm from inlet, in comparison to 5mm in first proposed geometry.
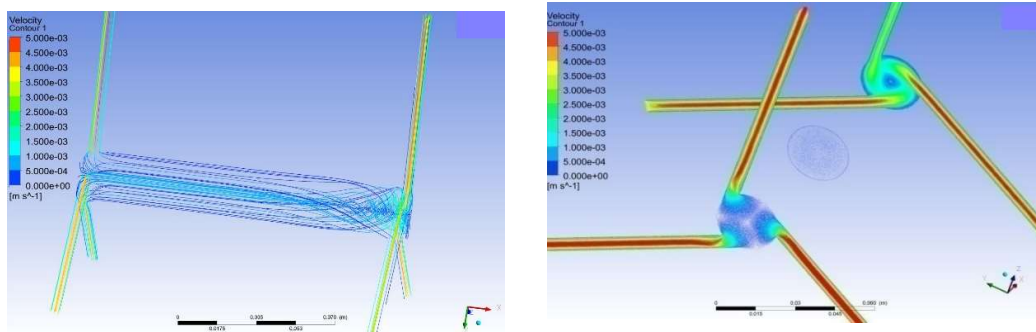


**Figure 3.4** Tangential Velocity component and velocity stream lines

The effect of tangential mixing along with lateral mixing was predominant in inlet area and was also present near exit. The effect towards exit was less due to middle bulk section of process fluid. So, simulation was carried out by doubling the inlet velocity. That showed improvement in mixing characteristics within geometry even in the middle section. As it is seen from the tangential velocity profile, the magnitude of velocity was very less in middle section of pipe, so it was proposed to have an annular geometry rather than a pipe flow.

**Case III Annular Pipe with three tangential inlets and three tangential outlets**
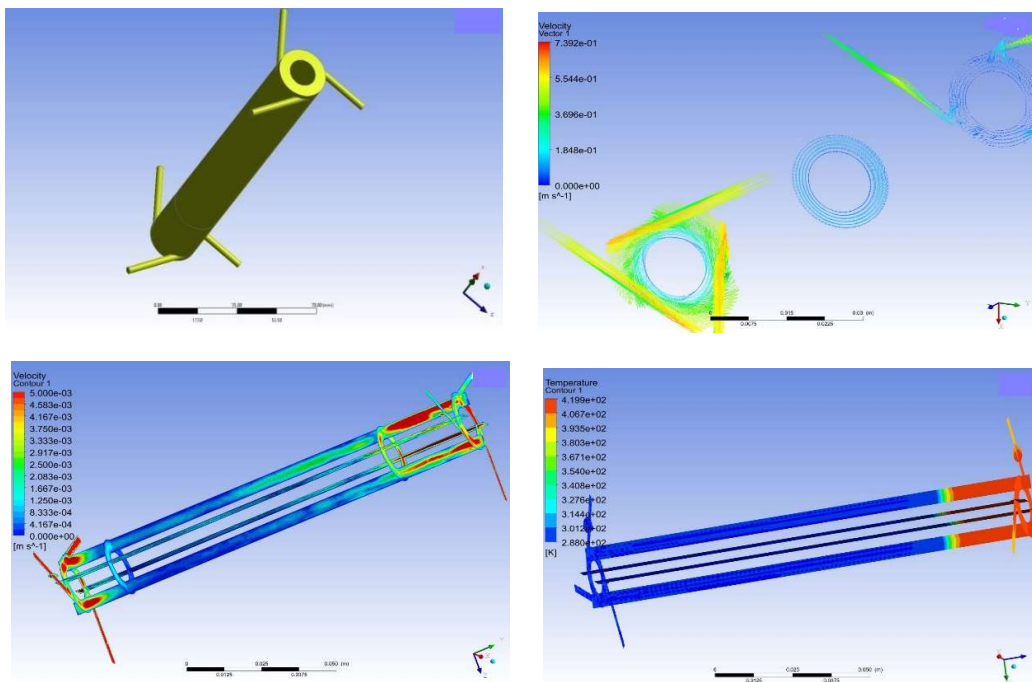


**Figure 3.5** Annular geometry with Tangential Entry and Exit

The geometry was simulated with higher velocity 0.5m/s with very less residence time to see hydrodynamics of the system. The figure below shows the geometry proposed and bulk velocity profile. The tangential velocity component was calculated from profile was having a value of 0.2m/s the plane 75mm from inlet. This shows a very good mixing without any mechanical agitator. Figure 3.5 shows the velocity profile. As the inlet velocity was very large, the simulation was done with the proposed velocity of 0.00625m/s (30ml/min) and 6000kJ/m$^2$ of heat flux was added. As heat source selected was heat flux, the temperature at the outer surface (320K) of geometry was higher than that of inner surface (300K). As was proposed in problem definition, to improve the mixing the geometry was modified so that it can be used within MW cavity.

**Case IV Annular flow with tangential entry and tangential exit with opposite direction with heat source and reaction.**

Based on previous simulation, the streamline (Figure 3.4) suggested, fluid entering should leave in same direction to have continuity in tangential velocity component. To incorporate that flow pattern, outlet nozzle direction was reversed. Both geometries are shown below for comparison.
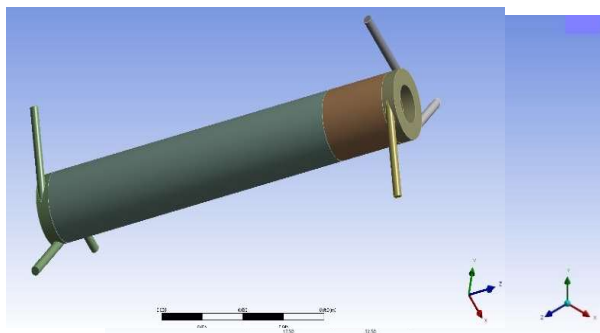


**Figure 3.6** Comparison of geometries with nozzle orientation

The mixing length in first proposed geometry was only 5mm for 30ml/min flow. To improve upon that, the geometry was simulated with 0.0693 m/s velocity (120ml/min inlet flow rate) and heat density of 175000W/m$^3$ (lower microwave intensity). The generated contours and vectors are showing good mixing within geometry and also a reasonable temperature profile. The average velocity was 0.03m/s with residence time of 10sec. The temperature in heating zone is uniform throughout the body of fluid, which shows the microwave heating with temperature value of 420K. The power law kinetic reaction was introduced along with reported values of pre exponential factor and activation energy [19] for saponification reaction.

$$NaOH + CH_3COOCH_2CH_3 \rightarrow CH_3COONa + CH_2CH_3OH$$
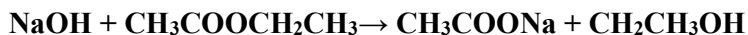
**[Kinetics Data:** T = 288K; II order reaction; $K_o$ = 1e7 [M$^{-1}$Sec$^{-1}$]; $E_a$ = 2.4e7 Kcal/kmol; $C_{A0}$ = 0.0018 (mass fraction)][19]

The concentration profile shows final conversion of 51% was obtained. The decrease in NaoH concentration was very fast in heating zone. The generated concentration profile is shown below in Figure 3.7. The mixing length found was 20mm in comparison to 5mm of base case. To increase the mixing length, inlet flow rate has to be increased, which intern will decrease the residence time. This will decrease the conversion, so large part of reaction mixture has to be recycled.
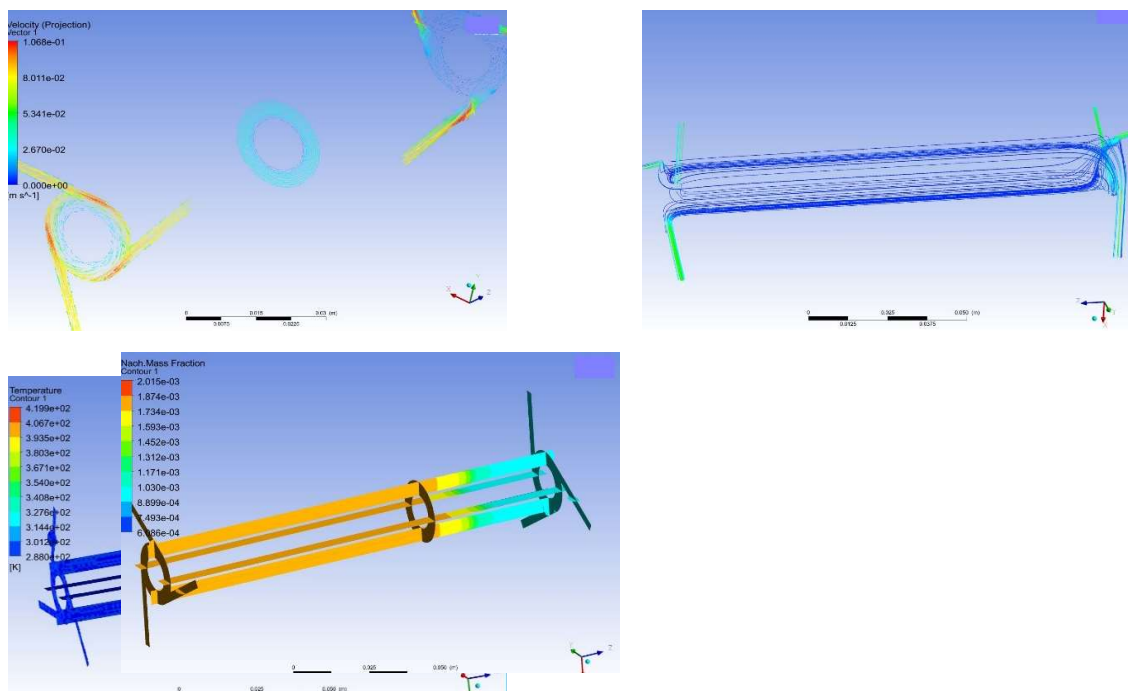
**Figure 3.7** Velocity, Temperature and concentration Profile of final geometry

After carrying simulations, the results have been obtained and generated profiles helped in making modifications in old geometries. The summary of results are shown in Table 3.2

**Table 3.2** Summary of results

| Case No | $V_i$ | $Q_1$ | $Q_2$ | Velocity (m/s) | Residence time, sec | Temp, K | Conversion(%) |
|---------|-------|-------|-------|----------------|---------------------|---------|---------------|
| I | 0.00625 | - | | 0.00281 | 55 | - | - |
| II | 0.00625 | - | | 0.00075 | 192 | - | - |
| III | 0.00625 | 6000 | | 0.00062 | 252 | 350 | - |
| IV | 0.0693 | | 175000 | 0.03 | 10 | 420 | 51 |

**Conclusions**

The Fluent Simulation tool will be a boon to predict the hydrodynamics and thermal condition within the selected geometry. Fluent will help in deciding the mixing characteristics of the geometry.

After conducting steady state simulation using Fluent, it was found that change in geometrical aspect will improve the mixing characteristics within geometry. Improved mixing will help heat and mass transfer rates for any chemical process. For conducting Fluid-fluid or fluid-solid heterogeneous synthesis reactions, the heat and mass transfer rate will affect the overall rate of reaction.

The proposed geometry was simulated for hydrodynamics and was found that to improve the mixing tangential component of velocity is required to be incorporated. All the effort in present work was to propose a geometry which will give good mixing without mechanical agitator.

The final selection of geometry with annular pipe having tangential entry and tangential exit in opposite direction higher tangential velocity, thereby giving good mixing. Same

geometry was simulated with two heat sources, one was based on conventional heating and second one based on microwave heating. The microwave heating mode gave better temperature distribution within geometry.

The rate of reaction was higher at elevated temperature. This was in good agreement with theory.

The simulation showed very small mixing length for selected flowrate and nozzle diameter. So the future work will be to increase the mixing length within geometry by making further modification.

## References

1. Estel, L.; Poux, M.; Benamara, N.; Polaert, I. Continuous Flow-Microwave Reactor: Where Are We? *Chemical Engineering and Processing: Process Intensification* **2017**, 113, 56–64.

2. Dąbrowska, S.; Chudoba, T.; Wojnarowicz, J.; Łojkowski, W. Current Trends in the Development of Microwave Reactors for the Synthesis of Nanomaterials in Laboratories and Industries: A Review. *Crystals* **2018**, 8(10), 379.

3. Haneishi, N.; Tsubaki, S.; Abe, E.; Maitani, M. M.; Suzuki, E.; Fujii, S.; Wada, Y. Enhancement of Fixed-bed Flow Reactions under Microwave Irradiation by Local Heating at the Vicinal Contact Points of Catalyst Particles. *Scientific Reports* **2019**, 9(1).

4. De la Hoz, A.; Díaz-Ortiz, Á.; Moreno, A. Microwaves in organic synthesis. Thermal and non-thermal microwave effects. *Chem. Soc. Rev.* **2005**, 34(2), 164–178.

5. Zhou, P.; Yang, X.; Huang, K.; Jia, G. *Microwave-Assisted Continuous-Flow Reactor Based on a Ridged Waveguide. Chemical Engineering & Technology* **2015**, *38(8), 1334–1339.*

6. Surati, M.A.; Jauhari, S.; Desai, K.R. A Brief Review: Microwave Assisted Organic Syntehsis. *Archives of Applies Science Research*. **2012,** 4(1), 645-66.

7. Joshi, A.V.; Baidoosi M.; Mukhopadhyay S. Nitration of Phenol and Substituted Phenols with Dilute Nitric Acid Using Phase-Transfer Catalysts. *Organic Process Research & Development* **2003,** 7(1), 95-97

8. Yadav, U.; Mande, H; Ghalsasi, P. Nitration of Phenols Using $Cu(NO_3)_2$: Green Chemistry Laboratory Experiment. *J. Chem. Educ.* **2012**, 89, 2, 268–270

9. Patneedi,C.B.; Durga Prasadu, K.; Sharma, R. S. K. ; Chandra Sekhar, D.; Venkata Rao, D.V. Microwave Mediated Synthesis In Pharmaceutical Chemistry. *Rasayan Jaournal of chemical engineering.* **2015**, 8(2), 176-185

10. Ravichandran, S.; Karthikeyan, E. Microwave Synthesis - A Potential Tool for Green Chemistry. *International Journal of Chemical Tech Research*. **2011**, 3(1), 466-470

11. Gedye, R.N.; Rank,W.; Westaway, K.C. The Rapid Synthesis Of Organic Compounds In Microwave Ovens. II. *Canadian Journal of Chemistry* **1991**, 69(4), 706–711.

12. Gedye, R.N.; Smith,F.E.; Westaway, K.C. The Rapid Synthesis Of Organic Compounds In Microwave Ovens. *Canadian Journal of Chemistry* **1988**, 66(1), 17–26

13. Kastratovic, V.; Bigovic M. Esterifcation Of Stearic Acid With Lower Mono hygroxylic Alcohols. *Chem. Ind. Chem. Eng.* **2018**, 24 (3) 283−291

14. Polshettiwar, V.; Varma R.S. Aqueous Microwave Assisted Chemistry Synthesis and Catalysis RCS green Chemistry Series,, *Royal Society of Chemistry*, Cambridge **2010**, Chapter 4.

15. Sauks, J.M. A Continuous Flow Microwave Reactor For Organic Synthesis. Ph.D. Thesis, *University of Toronto*, **2011**

**16.** National Materials Advisory Board Commission On Engineering And Technical Systems National Research Council, *National Academy Press*, Washington, D.C. **1994**

17. Gangurde, L.S. Process Intensification of Microwave Assisted Methane Dry Reforming, Ph.D. Thesis, *Delft University of Technology*, **2018**

18. Sharma, S. V.; Rama-sarma, G. V. S.; Suresh, B. More Chemistry: An Eco-friendly Technology. *Indian. J. Pham. Sci.* **2002**, 64, 337-344.

19. Ghobashy, M; Gadallah, M; El-Idreesy, T.T.; Sadek, M.A.; Elazab, H.A. Kinetic study of hydrolysis of ethyl acetate using caustic soda. *International Journal of Engineering & Technology* **2018**, 7(4), 1995-1999

# Study of Treated Recycled Aggregate on Strength properties of concrete

*Prof. Gaurav Vyas[1], Dr. D.N. Parekh[2], Prof. Prachi Pandya[3]*

*[1]Civil Engineering, Gujarat Power Engineering and Research Institute, Mewad, Mehsana, Gujarat, India: - 384460*

*[1]Email Id: - gaurav.vyas@gperi.ac.in, Mo:- 9033992273*

*[2]Applied Mechanics department, BPTI, Vidhyanagar, Bhavnagar, Gujarat, India: - 364002*

*[2]Email Id: - dnparekh@gmail.com, Mo:- 9428408308*

*[3]Civil Engineering department, RAI University, Saroda, dholka, Ahmedabad, Gujarat, India: - 382260*

*[3]Email id :-prachi25121994@gmail.com, Mo :- 9033964597*

## ABSTRACT

In India, many talks are being heard about sustainable construction and researchers are taking up studies here and there on use of unconventional construction materials that are aimed in using waste materials. However, focused attention on sustainability of materials for construction is needed. Though the time is not yet ripe for forming such an association in India, it is time for everyone concerned in the topic to start thinking about such a move. So here in this research main concern on the reuse of construction and demolition waste in conventional concrete. In this research use recycled coarse aggregate as well as recycled fine aggregate with replacement of natural aggregates. As per previous records there is considerably decrement in the strength property by using these kinds of recycled materials. This happen due to lower quality of recycled aggregates to improve the quality of R.A. here in this paper applies cement slurry treatment on the R.A. and use this Processed Recycled Aggregates (PRA) with fine recycled aggregates (FRA). In this research there is replacement, 10, 20, 30% RA with natural aggregates. Also replaced PRA 10, 20 and 30% with N.A. Also combine proportion of PRA and FRA and measure compressive, tensile and flexural strength of concrete. In the mix design water cement ratio used is 0.57 because there is higher water absorption of R.A.

## Keywords

Natural Coarse Aggregates (NCA), Recycled Coarse Aggregates (RCA), Recycled Fine Aggregates (R.F.A), Calcium Metasilicte (CM), Recycled Aggregates Concrete (RAC), Processed Recycled aggregates (PRA).

## 1.0 INTRODUCTION

Concrete has been proved to be a leading construction material for more than a century. It is estimated that the global production of concrete is at an annual rate of 1 m3 per capita (Neville 2003). The global consumption of natural aggregate will be in the range of 8–12 billion tones after 2010 (Tsung et al. 2006) Over 1 billion tonnes of construction and demolition waste (C&DW) is generated every year worldwide (Amnon 2004). The large-scale depletion of natural

aggregate and the increased amounts of C&DW going to landfill sites are causing significant damage to the environment and developing serious problems, denting the public and the environmentalist's aspirations for a waste-free society. The use of the recycled aggregates created from processing construction and demolition waste in new construction has become more important over the last two decades. There are many factors contributing to this, from the availability of new material and the damage caused by the quarrying of natural aggregate to the increased disposal costs of waste materials. Recently, these aggregates started to be used for intermediate utility applications, such as foundations for building sand roads. The advantages of recycling construction and demolition waste are (1) it reduces the amount of construction and demolition waste entering landfill sites; and (2) it reduces the use of natural resources in construction, contributes to the environment, provides a renewable source of construction material, and, if used in situ, reduces haulage costs. For economical and environmental reasons and because of the increased amount of recycled aggregates, there has been a growing global interest in maximizing the use of recycled aggregates in construction. In view of the increased volumes of construction, demolition waste, and industrial by-products such as fly ash (FA) and the advantages offered by the use of admixtures in modern concrete, it is considered very beneficial from different prospects with similar performance characteristics to natural aggregate concrete. When proved successful, recycled aggregate concrete (RAC) can be substituted for natural aggregate concrete in many concrete applications.

In the last 15 years, it has become clear that the availability of good quality natural aggregates is decreasing. The shortage of the resources of natural aggregates has opened the possibility for the use of recycled materials to replace part of the natural aggregates. As per record of news paper (23rd August2015) in India there is amount of construction waste generated.

| City | Construction waste (MT) |
|---|---|
| Delhi | 4600 |
| Mumbai | 2500 |
| Chennai | 2500 |
| Calcutta | 1600 |
| Bangalore | 875 |
| Ahmedabad | 700 |

As per Technology informational forecasting and assessment council estimated waste generation during construction 40 to 60 kg. Per sq. m. Similarly waste generation during renovation/ repair work is estimated to be 40 to 50 kg/Esq. of waste respectively.

Though it is now necessary to use of these recycled aggregates in place of natural ones. Properties of recycled aggregates have to be compared to those of natural aggregate to evaluate its suitability for applications in construction industry.

## 2.0  LITERATURE REVIEW
In the literature review there Is many papers studied and as per their view here following comparison carried out. Here studied natural and recycled aggregate properties and also parent concrete and RCA fresh and hardened properties. For the determining the various properties of aggregates the methods are in IS 2385 P-5.4

**2.1 Recycled Aggregates:** Aggregates can come from either natural or manufactured source. Natural aggregates are come from rock, of which there are three broad geological classifications. In our project work we collect R.A. from porbandar based C & D waste and used in the work.

**2.2 Abrasion Value:** Codal provision for abrasion value as per IS 2386 PART 5 is 30%. P.Saravana kumar et al (ASCE-0899- 1561/2012) reported that the abrasion value of natural aggregate is 12% for fine aggregate. Also Bhibhuti Bhusan et al (ASCE-0950-0618/2014) reported that abrasion value of natural aggregate is 19.72%. A.Akbarnerhad et al (ASCE-8099-1561/2013) reported on the crushing procedure of recycled aggregate and determine the abrasion value of R.A (recycled aggregate) varies from 31 to 39%. P.Saravana kumar et al. (ASCE -0899-1561/2012) reported on fine recycled aggregate abrasion value and observed that 7 to 10 % as per age of aggregates. Alla M. Rashall et al (ASCE -2013) reported on use of metakaoline in place of fine aggregate and observed that abrasion value 23.12% in MK content. Bhibhuti bhusan et al (ASCE-0950- 0618/2014) reported that abrasion value of RCA is 36.56%. Poblo pere et al (ASCE-2012) reported on cement treated recycled material and determine the abrasion value of RCA 38.00%.

**2.3 Impact value:** Codal provision for impact value as per IS- 2386 PART 5 is 30% for wearing surfaces and 45% for non wearing surface. P.Sarvana kumar et al. (ASCE-0899- 1561/2012) reported that impact value of N.A is 5.85% for F.A. And bhibhuti bhusan et al (ASCE-0950-0618/2014) reported that impact value 0f N.A. is 15.35%. P.Saravana kumar et al (ASCE-0899-1561/2012) reported that impact value of R.F.A is 9.66%, 12.79%, 18.45% after 5, 10, 15 years. Bhibhuti bhusan Mukharjee et al (ASCE- 0950-0618/2014) reported that impact value of R.C.A. 34.85%. Sallehan ismail et al (ASCE-0950-0618/2014) reported that impact value of R.C.A is higher than N.A by 13%.These results shows us that recycled fine and coarse aggregates are weaker than natural aggregates.

**2.4 Crushing value:** Codal provision for crushing value of aggregate as per IS-2386 part 5 is 30% for wearing surface and 45% for non wearing surface. P.Saravana kumar et al.(ASCE-0899-1561/2012) reported that crushing value of N.A is 17.75 for F.A. and Bhibhuti bhusan et al (ASCE-0950- 0618/2014) reported that crushing value of N,A is 15.1%. Sallehan ismail et al. (ASCE-0950-0618/2014) reported on the use of treated coarse recycled concrete aggregate and observed that crushing value higher than the N.A. Bhibhuti bhusan mukharjee et al (ASCE-0950-0618/2014) reported that crushing value of R.C.A is 31.52%.

**2.5 Specific Gravity:** Kunal rafat siddique et al (ASCE 2013) reported that specific gravity of natural coarse aggregate 2.59 and fine aggregate 2.62. Bhibhuti bhusan et al (ASCE-0950-0618/2014) also reported that specific gravity of NA P.Sarvana kumar (ASCE-0899-1561/2012) also reported same specific gravity of N.A 2.72. P.Saravana kumar et al. reported that specific gravity of recycled aggregate decrease with increase of the age of sourse of recycled aggregate specific gravity of R.A. varies from 2.63 to 2.68. S.K.singh et al (use of recycled aggregate-NBMCM-2011) reported that specific gravity of RA 2.35 to 2.58 which is lower than N.A. Bhibhuti bhusan Mukharjee et al (ASCE-0950-0618/2014) determined the values of specific gravity of RCA is 2.46.

**2.6 Water absorption:** Leonardo F.R. Miranda et al. (ASCE- 899-1561/2013) reported that water absorption value of fine aggregate is varies from 4.5% to 7.6%. While Kunal rafat Siddque et al (ASCE 2013) reported that water absorption of C.A 0.80 % and fine aggregate has 1.02 % of water absorption. Bhibhuti bhusan et al (ASCE-0950-0618/2014) reported that water absorption value for N.A is 0.5%. Valeria corinaldesiet et al. (ASCE 2010) reported on the behavior of beam-column joints made of recycled aggregate concrete under cyclic loading than water absorption value is 3.4% for N.A. Water absorption value of R.A is higher than 4% to 4.8%. Leonardo F.R. Miranda et al (ASCE-0899-1561/2013) reported that water absorption value of R.A is varies from 4.5 to 7.5%. A.Akbarnerhad et al (ASCE-8099-1561/2013) reported values vary from 2.7 to 5.1%. Sidnel H.C. et al (ASCE-0899-1561/2014) reported the value of water absorption varies from 1.65 to 6.2 % for recycled sand. Bhibhuti bhusan mukharjee et al (ASCCE-0950-0618/2014) determined the values of RCA are 4.6%. Valeria corinaldesi et al (ASSCE-2010) reported that water absorption value of RCA 7.0%. Poblo perez et al (ASCE-2012) reported that the value of water absorption is 4.72%.

**2.7 Treatment of Recycled Aggregates:**
Amnon Katz et al (ASCE 0899-1561/2008) studied on the treatments of recycled aggregates they applied two different treatment silica fume treatment and ultrasonic cleaning treatment. By used silica fume treatment compressive strength improve by 30 % and 15% after 7 & 28 days. And by using ultrasonic treatment compressive strength improved by 7% after 28 days. Kunal Rafat siddique et al (ASCE/2013) studied on the use of cement kiln dust replaced with fine aggregate and applied Bacterial treatment on CKD and then it replaced with F.A. CKD waste produced during cement production and it harmful for the nature and humans too so by applied bacterial treatment and then replaced with F.A. and compressive strength increased by 7.15% to 26.6% with 10% replacement. Erhan guneyisi et al (ASCE/2014) applied four different surface treatments on the properties of self compacting concrete with recycled aggregates. Treatments are I) Two stage mixing approaches ii) Pre- soaking in HCl solution. iii) Water glass dispersion IV) Cement silica fumes slurry. And they conclude that water glass dispersion treatment gives best result among all. Sallehan Ismail et al (ASCE-0950- 0618/2014) Studied on mechanical and drying shrinkage properties of concrete containing treated Recycled aggregates they firstly C.A. soaking in HCl 0.5 Molar solution then impregnated in calcium metasilicate (CM) to coat surface. 60% replaced with N.A. and conclude that there is increase in mechanical properties of aggregates and strength property by using treated aggregates.

**2.8 Properties of Concrete:** For concrete there are two main type of properties 1) Fresh concrete properties and 2) Hardened concrete properties. In this paper here compressive strength, split tensile strength, Flexural strength, Elastic modulus, workability, durability etc are analyzed for the parent concrete and Recycled aggregate concrete(RCA).

**2.9 Compressive strength:** Amnon katz (ASCE-0899- 1561/2008) studied on treatment of recycled aggregate and determine the compressive strength of RAC(Recycled aggregate concrete) reported that by applying silica fume treatment it increase 30 to 15% and by applying ultrasonic treatment it increase 7% after 28 days. P.Saravana kumar et al (ASCE/2012) reported that there is decrease in comp. strength about 5.5% in same mix proportion. Alla M. Rashall (ASCE/2013) studied on fine aggregate replacement with metakaoline and reported that there is increase in compressive strength up to 40% and then decrement start in compressive strength.

Jared R. wright et al (ASCE-1561/04014073/2013) studied on use of glasscrete and suggested that while use glass in concrete there is must be less W/C ratio. Sallehan Ismail et al (ASCE-0950-0618/2014) studied on mechanical strength properties of treated and untreated RAC and reported that there is increase in all properties of concrete compare to the untreated R.A. Bhibhuti bhusan mukharjee et al (ASCE-0950- 0618/2014) reported that there is decrease in compressive strength by using R.A. up to 8.9% but with using of nano silica as SP there is increase in compressive strength up to 12%. Macro pepe et al (ASCE/2014) reported that compressive strength of RA is 27.50 n/mm2.made of recycled aggregate concrete under cyclic loading (valeria corinaldesi et al. 2010)

**2.10 Split tensile strength:** P.Saravana kumar et al (ASCE/2012) reported that there is decrease in split tensile strength of 9%, 105, and 13.4% after 5,10,15 years aged R.A. Leonardo F.R. Miranda et al (ASCE-089901561/2013) studied on the use of recycled sand and determined the split tensile strength and it gives best results by using 50% replacement of recycled sand. Alla M.Raashall (ASCE/2013) studied on using of metakaoline(MK) reported that there is increase in split tensile strength up to use of MK 40% than there decrease in it by 15% of nominal split tensile strength. P.Pereira et al (ASCE/2013) studied on effect of super plasticizer on the mechanical performance of concrete made with recycled sand and suggested that there is decrease in split tensile strength by 15.6 to 24.5% without use of SP and with SP using there is increase in strength by 26.6% to 52.8%. Marco pepe et al (ASCE/2014) reported that split tensile strength of parent concrete 3.85 MPA and RAC is 3.36MPa.

**2.11 Flexural strength:** Valeria corinaldesi et al (ASCE 2010) studied on the behavior of the beam and column joints made with recycled aggregate concrete and reported that there is decreased in the flexural strength by 10%.

**2.12 Workability:** As in above water absorption properties we discussed and results added by them we can say that as water absorption increased by using R.A. there is create problem in the workability of RAC.( P.Saravana kumar et al ASCE/2012). Amnon katz (ASCE-0899-1561/2010) also reported that water absorption of R.A. increased due to old mortar on it because of high water absorption in R.A. There decreased in workability.

**3.0 EXPERIMENTAL PROGRAMME**
Firstly we collect recycled aggregates from C&D waste site and from it we separate R.C.A. with help of crusher and labour. After the separation we find out Natural aggregates and Recycled aggregates physical properties.

(Photo 1:- Construction and demolition site located at bhavnagar)

Then we used these aggregates by two ways directly uses of it and giving them process and uses of it. R.C.A. replacement of N.A. up to 10 to 30%.

### 3.1 Treatments to the R.A:
We applied cement slurry treatment to the R.A. to improve the properties of R.A. On the surface of R.A. there is old mortar adhere on it and due to this there is higher abrasion, impact and crushing value of aggregates. Also we observe in past research there is higher water absorption this happen due to on the surface of R.A. there is minute voids are available. By applied cement slurry treatment to the R.A. there is voids are poured and also old mortars are removed from the surface. In this treatment we used 1:10 ration of cement to water.


(Photo 2:- Applying treatment to the collected Recycled aggregates)

Make cement slurry as stated above proportion and put R.A. in to it for 24 hours. After 24 hours R.A. get out from the slurry and make them totally dry and then used in the concrete. Physical properties of N.A., R.A. and P.R.A. are finding out and compare each.

(Table 3.1 Properties of coarse aggregates)

| Property | NCA | RCA | PRA |
|---|---|---|---|
| Impact value | 17.18 | 26.58 | 24.5 |
| Abrasion value | 22.56 | 26.14 | 26 |
| Crushing value | 23.54 | 33.35 | 29.51 |
| Specific gravity | 2.61 | 2.56 | 2.6 |
| Water absorption | 0.48 | 4.02 | 1.09 |
| Fineness modulus | 7.42 | 7.02 | 7.12 |

(Table 3.2 Properties of fine aggregates)

| Properties | Sand | RFA |
|---|---|---|
| Fineness Modulus | 3.23 | 4.48 |
| Water Absorption | 0.38 | 5.1 |
| Specific gravity | 2.64 | 2.12 |
| Silt content | 1.07 | 5.56 |

## 4.0 RESULTS AND DISCUSSION

(Table 4.1 Compressive strength after 7 and 28 days)

| Sr. No. | Designation | Mix | Compressive strength after 7 days (N/mm$^2$) | Compressive strength after 28 days (N/mm$^2$) |
|---|---|---|---|---|
| 1 | NAC | A | 15.88 | 22.69 |
| 2 | 10%RA | B | 15.53 | 20.32 |
| 3 | 20%RA | C | 14.76 | 20.21 |
| 4 | 30%RA | D | 14.44 | 19.87 |
| 5 | 10%PRA | E | 17.27 | 26.01 |
| 6 | 20%PRA | F | 16.68 | 26.29 |
| 7 | 30%PRA | G | 16.35 | 26.78 |

(Table 4.2 Tensile strength After 7 and 28 days)

| Sr. No. | Designation | Mix | Tensile strength after 7 days (N/mm$^2$) | Tensile strength after 28 days (N/mm$^2$) |
|---|---|---|---|---|
| 1 | NAC | A | 1.95 | 2.299 |

| | | | | |
|---|---|---|---|---|
| 2 | 10%RA | B | 1.45 | 1.957 |
| 3 | 20%RA | C | 1.386 | 1.832 |
| 4 | 30%RA | D | 1.33 | 1.712 |
| 5 | 10%PRA | E | 1.723 | 1.979 |
| 6 | 20%PRA | F | 1.62 | 2.045 |
| 7 | 30%PRA | G | 1.41 | 2.144 |

(Table 4.3 Flexural strength after 7 and 28 days)

| Sr. No. | Designation | Mix | Flexural strength after 7 days (N/mm$^2$) | Flexural strength after 28 days (N/mm$^2$) |
|---|---|---|---|---|
| 1 | NAC | A | 3.94 | 5.73 |
| 2 | 10%RA | B | 3.58 | 5.31 |
| 3 | 20%RA | C | 3.21 | 4.76 |
| 4 | 30%RA | D | 2.68 | 4.06 |
| 5 | 10%PRA | E | 3.56 | 6.06 |
| 6 | 20%PRA | F | 3.72 | 6.69 |
| 7 | 30%PRA | G | 3.92 | 7.53 |

(Table 4.4 Workability and compaction factor test results)

| Sr. No. | Designation | Mix | Slump Value (mm) | Compaction factor |
|---|---|---|---|---|
| 1 | NAC | A | 85 | 0.920 |
| 2 | 10%RA | B | 70 | 0.890 |
| 3 | 20%RA | C | 68 | 0.886 |
| 4 | 30%RA | D | 69 | 0.875 |
| 5 | 10%PRA | E | 89 | 0.928 |
| 6 | 20%PRA | F | 91 | 0.932 |
| 7 | 30%PRA | G | 96 | 0.942 |

(Photo 3 :- Compressive strength measurement for the specimen)


(Photo 4:- Mixing ingredients for the concrete

## 5.0 CONCLUSION

- As discussed earlier we used normal R.A. and P.R.A. By using R.A. all the strength criteria are decreased. Compressive strength decreased up to 12 to 15% by using R.A. Same decreased in tensile strength and flexural strength.
- After then we applied Cement slurry treatment to the R.A. then we observe there is improve all the strength parameter.
- Also we measure workability and compaction factor of fresh concrete and there is lower workability of P.R.A.
- At the end we conclude that there is lower workability by using P.R.A. but there we get higher strength of concrete. Here we used W/C ratio 0.57 so if we modify mix design criteria or change in W/C ratio.
- As compressive strength, tensile strength and flexural strength gives better results by improving quality of recycled aggregates.
- By using recycled aggregate in construction industry many problem of environment might be solve.

## 6.0 REFERENCES

[1] A. Akbarrnezhad, et al (2013). "Effect of Parent concrete properties and crushing procedure on the properties of coarse recycled concrete aggregates". J. Mater. Civ. Eng. 2013.25:1795-1802.

[2] Amnon, K. (2004). "Treatments for the improvement of recycled aggregate." J. Mater. Civ. Eng., 16(6) (2004), 597–603.

[3] Apaeth Valeria (2013). "Improvement of recycled aggregate properties by polymer treatments". International Journal of Sustainable Built Environment 2 (2013) 143–152.

[4] Assia Djerbi tegguer (2013). "Improvement of recycled aggregate properties by polymer treatments". International Journal of Sustainable Built Environment 2 (2013) 143–152.

[5] Barai v. Sudhirkumar (2014) "Influence of incorporation of nano-silica and recycled aggregates on compressive strength and microstructure of concrete". Construction and Building Materials 71 (2014) 570–578.

[6] Corinaldesi Valeria, et al (2011) " Behavior of beam- Column joints made of recycled aggregate concrete under cyclic loading". Construction and Building Materials 25 (2011) 1877–1882.

[7] G. Dhinakaran (2012). "Effect of Admixed Recycled aggregate concrete on properties of fresh and hardened properties". J. Mater. Civ. Eng. 24 (2012):494-498.
[8] Guneyisi Erhan, et al (2014). "Effect of surface treatment methods on the properties of self-compacting concrete with recycled aggregates". Construction and Building Materials 64 (2014) 172–183.

[9] Ismail Sallehan, (2014). "Mechanical strength and drying shrinkage properties of concrete containing treated coarse recycled concrete aggregates". Construction and Building Materials 68 (2014) 726–739.

[10] Kou shi-cong, et al (2014). "Use of $CO_2$ curing step to improve the properties of concrete prepared with recycled aggregates". Cement & Concrete Composites 45 (2014) 22–28.

[11] Mahyuddin Ramil (2014). "Mechanical strength and drying shrinkage properties of concrete containing treated coarse recycled concrete aggregates". Construction and Building Materials 68 (2014) 726–739.

[12] Miranda F.R. Leonardo, et al (2012). "Use of recycled sand produced at construction sites in bedding mortars". J. Mater. Civ. Eng. 25 (2013):236-242.

[13] Miranda F.R. Leonardo,et al (2014). "Rational Procedure for Composition of Screed Mortar with Recycled Sand at a Construction Site" J. Mater. Civ. Eng.26 (2014):855-862.

[14] Mohamed Turki, et al (2012). "Influence of filler Addition on Mechanical behavior of cementations Mortar- Rubber Aggregates: Experimental study and Modeling". J. Mater. Civ. Eng. 24 (2012):1350-1358.

[15] Mukharjee B.B, (2014) "Influence of incorporation of nano-silica and recycled aggregates on compressive strength and microstructure of concrete". Construction and Building Materials 71 (2014) 570–578.

[16] P.Pereira, et al (2012). "The effect of super plasticizers on the mechanical performance of concrete made with fine recycled concrete aggregates".

[17] Cement & Concrete Composites 34 (2012) 1044–1052.

[18] P.saravana Kumar (2012). "Effect of Admixed Recycled aggregate concrete on properties of fresh and hardened properties". J. Mater. Civ. Eng. 24 (2012):494-498.

[19] Pepe Marco, et al (2014). "Alternative processing procedures for recycled aggregates in structural concrete." Construction and Building Materials 69 (2014) 124–132.

[20] Perez Pablo, et al (2013). " Application of cement treated recycled material in the construction of a section of road in Malaga, spain ". Construction and Building Materials 44 (2013) 593–599.

[21] Rajor Anita (2014). "Influence of bacterial treated cement kiln dust on the properties of concrete". Construction and Building Materials 52 (2014) 42–51.

[22] Rashad M. Alla (2013) "A preliminary study on effect of fine aggregate with metakaoline on strength and abrasion resistance of concrete". Construction and Building Materials 44 (2013) 487–495.

[23] Siddique Kunal, Rafat, (2014). "Influence of bacterial treated cement kiln dust on the properties of concrete". Construction and Building Materials 52 (2014) 42–51.

[24] T. sung, et al (2006). "Properties of HPC with recycled aggregates." Cem. Concr. Res., 36(5) (2014), 943–950.

[25] Tae Lee Seung, et al (2008). "Durability of mortars made with recycled fine aggregates exposed to sulphate solution". J. Mater. Civ. Eng. 20 (2008):63-70.

[26] Wright R. Jared, et al (2013). "Fresh and Hardened properties of concrete incorporating recycled glass as 100% sand replacement". J. Mater. Civ. Eng. 26. (2014): 04014073-1-11.

# Monitoring and Forecasting of Drought for North Gujarat Region

*Akshayrathod [1], Rajat.mishra [2]*

[1]Civil Engineering, Lukhdhirjiengineering college morbi-363641
[1]Email Id: - akrathod2421@gmail.com, Mo:-7383956503
[2]head of the department of civil engineering  saffrony institute of technological  Gujarat, India: - 384435
[2]Email Id: - rajat.mishra@saffrony.ac.in Mo:- 6355632102

## Abstract

One of the methods of mitigating the effect of drought is monitoring and assessment of drought and thus constituting the contingency plan to cater the adverse effect of drought. In the present study drought monitoring and assessment study is carried out using standard precipitation index values at a scale of 3 , 6 and 12  and  months using data 16 rain gauge stations in the north Gujarat region drought occurrence of different categories at different time scales in the past 30 years are assessed. Frequency of occurrence of drought is estimated. A trend analysis is carried out to estimate the trend of droughts. Minimum available precipitation values are estimated for kharif season at different degrees of dependability the study should help in management of irrigation resources in the region.

## Keywords

Drought, SPI, Monitoring, Trend Analysis, Monitoring, Drought indices, Assessment

## 1.INTRODUCTION

Water is one of the most important gifts to mankind by the nature. It is very much important for the various activities without which no development would have much occurred on the earth. Our daily lives depend on water. Throughout    the history of mankind civilization has developed where water is available. Water has always been fundamental to development in the form of food production and industrial activities. It is a key factor in the environment as  the universal medium for transport of nutrient and toxic elements. More than one – half of the country's major rivers are being seriously depleted and polluted, threatening the health and livelihood of the people who depend upon them for irrigation, drinking and industrial water . under the present condition of population pressure and regional disputes water can be the potential reason for the conflict between region of the country.

Natural disaster include drought ,flood, earthquake, tsunami, cyclone etc., which cause hazardous effect on various activities of the people. Water is directly related to first two i.e. drought and flood. the total water available remains constant on the earth but its distribution with respect to time and place is highly variable, which is the main reason for occurring drought and flood . also, it may very in space in such way that when one part of the country is facing drought the other part of the country may face the flood. Such occurrence of the drought and flood pose a great challenge for a people to face them and also for the government . among these two extreme drought is a non- event and creeping phenomenon. Its beginning is invisible, progress is hazardous and effect can be devastating . indeterminacy regarding its onset and uncertainty about its spread and severity rendered this phenomenon more harmful. Therefore, study about drought characteristics  and to be  ready by contingency plan is more important for mankind in general and government in particular.

According to map of district of Gujarat covered under area development programmes  provided by department of revenue , government of Gujarat , the whole north Gujarat region is prone to drought . in this aspect it is more important to monitor and forecast drought prior its occurrence to overcome the hazardous effects of drought.

There are several methods that have used in the past as the drought assessment tools such as measurement of lack of rainfall , shortage , of stream flow, reduced levels of water storage , and drought indices (DIs)of these, Dis are widely used for drought assessment now-

a-days. DI is a function of various hydro- meteorological variables i.e. rainfall and stream flow. A drought indices value is single number used  for decision making. To develop a suitable drought indices is not an easy task . So, to develop a suitable drought indices for a particular region to define drought condition is the first task in this thesis.

Historically little attention has been given to drought  forecasting aspect which is very important  from the point of view of drought preparedness and early warning in drought prone region another drought event is likely to occur before the region fully recover from the last event. another drought event is likely to occurs before the region fully recovers from the last event. However, early indication of drought condition could reduce future impacts. Therefore , the development of a drought forecasting tool that can be used for drought preparedness is considered as the second task in this thesis.

## Outline of the thesis

The outline of the thesis is given in figure
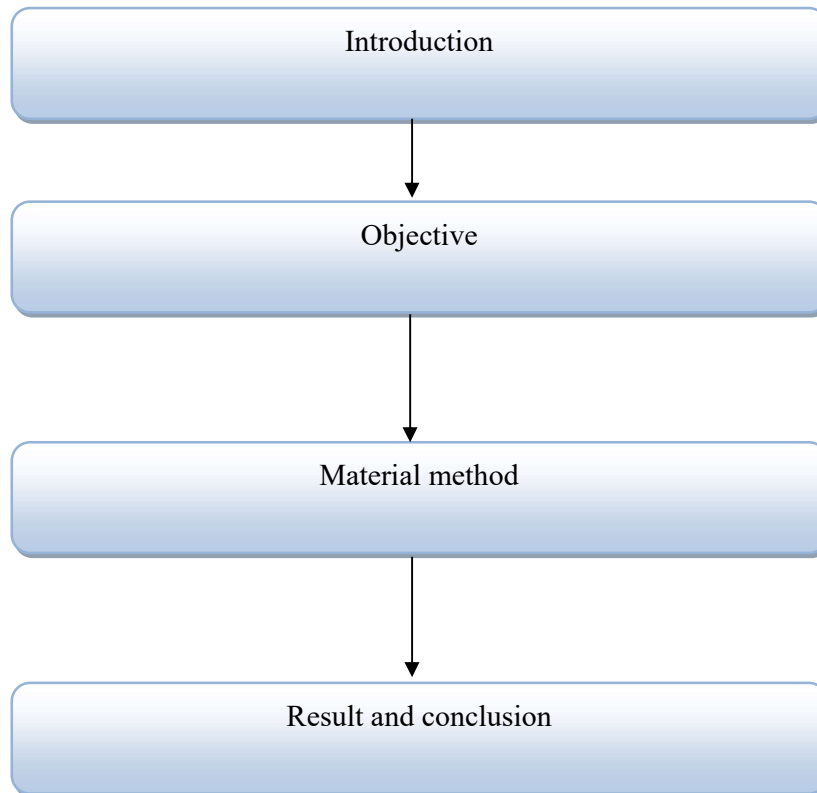
## 2.OBJECTIVES

1. To study Drought characteristics in North Gujarat region at different time scales in terms of Intensity, Duration, Frequency and Areal extent.
2. Probability analysis of minimum assured rainfall in the region with reference to the crops grown

## 3.MATERIALS AND METHODS

### 3.1 Methodology to Calculate Standard Precipitation Index

A  Monthly precipitation data set is prepared for a period of m months of a continuous period of  at least 30 years for the study area. A set of averaging periods are selected to determine a set of time scales of period is 3, 6, 12, and 24 months. The precipitation rate is then fitted man Kandel test is defined by its frequency or intensity function

The SPI was calculated using SPI generator Software developed by United states national drought mitigation centre to derive severity of drought in study area. The monthly time series of rainfall data from rain gauge station in the study area were used to derive SPI at 3 and 6 – Month time scales.

**Evaluation of probabilities of weekly rainfall for different dependability:**

 Many agricultural operations like crop sowing, crop harvesting, and pest control required daily or weekly probabilities rather than the information on average of rainfall or the normalized precipitation indices.. Therefore in addition to finding the pattern of drought using the Standard Precipitation Index values it was thought proper to find the probability of weekly rainfall patterns at different defensibilities such as 90%, 75% and 50% levels.

From the existing literature the probability distributions suitable for analysis of different hydrodrological events are recorded and tabulated as per Table A.1 below:

Table A.1

| Nature of Hydrological Data | Probability  Distributions |
|---|---|
| Annual Rainfall Data Series | Normal Distribution |
| Seasonal  Rainfall Data | Normal  Distribution |
| Weekly Rainfall series | Gama Distribution |
|  Daily  Rainfall series | Gama Distribution |
| Highest One Day Maximum Rainfall | Gumbel's Distribution |
| Monthly  Rainfall | Log Normal |
| Extreme Rainfall | Extreme  value Distribution |
| Floods | Log normal,Gumbel, Pearson |
| Low Hydrological Flows | Weibull Distribution |

Therefore to make a prediction of the weekly rainfall the gamma distribution is used in this study to estimate the probabilities of total weekly rainfall at the dependability's of 90, 75 and 50% for Ahmedabad station

The gamma distribution takes the form :

$$f(x, \alpha, \beta) = \frac{1}{\beta^\alpha \Gamma(\alpha)} x^{\alpha-1} e^{-\frac{x}{\beta}}$$

where $\alpha$, and $\beta$ are the parameters of the distribution. They are evaluated using the sample parameters of the weekly data using the relationships:

$\mu = \alpha\beta$ and

$\sigma = \alpha\beta^2$,

where $\mu$ and $\sigma$ relate to the sample parameters.

**Stationarity:**

In stochastic hydrology the basic assumption is that the time series is stationary that is the present data is independent of the past data and the randomness in the series is valid and so that the statistical properties such as mean , variance and higher order moments do not change over time. For the purpose of analysis, it is considered enough evidence of stationary if the auto correlation coefficient calculated from the sample data. Before the application of the theory of probability it is necessary to ascertain the stationary of the sample data. This can be done by calculating the value of serial correlation coefficient with lag one. The series is considered stationary with 5% level of significance if the lag one serial correlation coefficient value lies between $\frac{1.96}{\sqrt{N}}$ and $-\frac{1.96}{\sqrt{N}}$ , where N is the number of data points in the sample.

**3.2 Categorization of Droughts:**

Droughts are classified as mild, moderate, severe and extreme as per the SPI values in the table given below:

Classification of Drought as per the SPI values (McKee et al. 1993

Table A.2

| SPI Values | Drought Category |
|---|---|
| -0.5 to -0.99 | Mild |
| -1 to -1.49 | Moderate |
| -1.5 to -1.99 | Severe |
| <-2 | Extreme |

**Source**: McKee T. B. et al. "The relationship of drought frequency and duration to time scales", 8th Conf. on Applied Climatology, Anaheim C. A., 179-184.)
Using the above values and the calculated SPI values the number of droughts in the duration 1987 -2017 with reference to the above classification are tabulated below:

It is found that droughts of mild to moderate magnitudes have been occurring in the past 30 years and droughts of severe and extreme magnitude have not occurred. Moreover, it is found that there is a reduction in the value of dry as well as wet indices

## 3.3 drought trend analysis.

Sen (2012) have pointed out that the commonly used trend analysis methods namely the Mann Kendall method and the Spearman 's Rho test method have certain underlying assumptions such as independent structure of the series and normality of distribution in the time series which may not be valid under all circumstances for the hydrological or meteorological data. They have proposed an approach for trend

Table A.3

| Category of Drought | No of Droughts in N G Region SPI Time Scale (Months) | | |
|---|---|---|---|
| | 3 | 6 | 12 |
| Mild | 4 | 4 | 2 |
| Moderate | 0 | 0 | 3 |
| Severe | 0 | 0 | 0 |
| Extreme | 0 | 0 | 0 |

**analysis which is free of such restrictions. The method given by them has the following steps:**

1. Separate the  data into two parts of equal length. For odd number of records the middle value may be omitted.
2. Arrange the two parts in descending order
3. Plot  the two parts on a  simple graph . If the data fall along a forty five degree line they possibly have no trend . If they fall above the forty five degree line an increasing trend may be concluded if they fall below the forty five degree line there is a decreasing trend.

The above is a qualitative analysis. Richard H .McKuen has given some more steps to make a quantitative analysis of the trend at a particular level of significance. They have given the following steps for their analysis.

1. Fit an equation $y = mx$, where    $x$ and   $y$ represent the first and the second parts of the two data sets. Determine the value of $=$ using least square method. If  $m = 1$ it is concluded that there is no trend in the time series.
2. Calculate the critical value "C" given by :   $C = C_1 + C_2 \ e^{nC_3} n^{C_4}$
3. The value  $m$  is compared with "C" to take a decision rearding existance of trend. The value of the coefficients on the right handside of the above equation are given by a table given by R. H. McCuenn is the value of the length of the record.

Using the above method and a trend analysis is carried out for the SPI values at 3-month, 6 month ,12 month and 48-month time scale.

Using the SPI values contained in the table below the and using the method suggested by Zekai Sen (2012) the trends at different time scales are obtained as per the following figures no-A.4 are obtained:

Table A.4: SPI values at different Scales for North Gujarat Region

| Year | SPI3 | SPI6 | SPI12 |
|------|------|------|-------|
| 1987 | -0.66867 | -0.71933 | -0.68467 |
| 1988 | 0.072667 | -0.00867 | -1.126 |
| 1989 | 0.065333 | -0.10067 | 0.252667 |
| 1990 | 0.563333 | 0.638 | -0.04 |
| 1991 | -0.32333 | -0.48333 | 0.842667 |
| 1992 | 0.308 | 0.529333 | -0.25267 |
| 1993 | 0.144667 | 0.06 | 0.348 |
| 1994 | 0.732667 | 0.926 | 0.548 |
| 1995 | -0.06067 | -0.142 | 0.648 |
| 1996 | 0.102667 | 0.087333 | 0.072 |

| | | | |
|------|----------|----------|----------|
| 1997 | 0.674667 | 0.598667 | 0.316667 |
| 1998 | -0.30467 | 0.126 | -0.09933 |
| 1999 | -0.834 | -0.66133 | 0.301333 |
| 2000 | -0.53533 | -0.72067 | -1.09867 |
| 2001 | -0.22067 | -0.448 | -0.64267 |
| 2002 | -0.75 | -0.85667 | -0.23467 |
| 2003 | 0.324 | 0.208667 | -1.126 |
| 2004 | -0.01133 | -0.10467 | 0.319333 |
| 2005 | 0.098667 | 0.231333 | -0.068 |
| 2006 | 0.54 | 0.582667 | 0.262667 |
| 2007 | 0.422667 | 0.316667 | 0.532 |
| 2008 | 0.029333 | -0.17067 | 0.197333 |
| 2009 | 0.162 | 0.07 | -0.12333 |
| 2010 | -0.182 | -0.15333 | -0.22933 |
| 2011 | 0.55 | 0.616 | 0.043333 |
| 2012 | -0.12333 | 0.103333 | 0.432 |
| 2013 | 0.142667 | 0.345333 | 0.252667 |
| 2014 | 0.362667 | 0.232667 | -0.45333 |
| 2015 | 0.325333 | 0.149333 | 0.339333 |
| 2016 | -0.10467 | -0.308 | 0.359333 |
| 2017 | 0.188 | 0.350667 | -0.08667 |
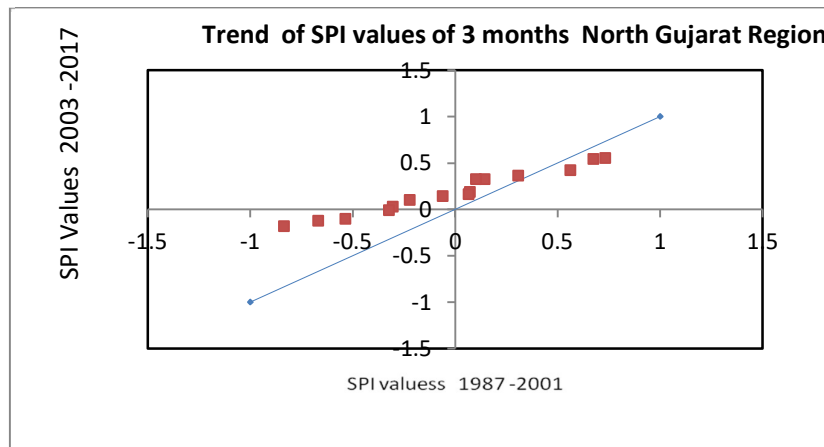


Figure A.1: Trend of SPI values of 3 month north Gujarat Region
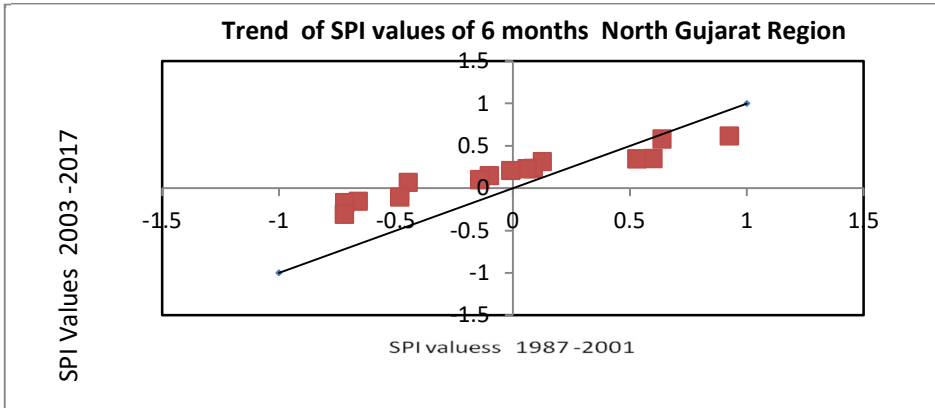
Figure A.2: Trend of SPI values of 6-month north Gujarat Region
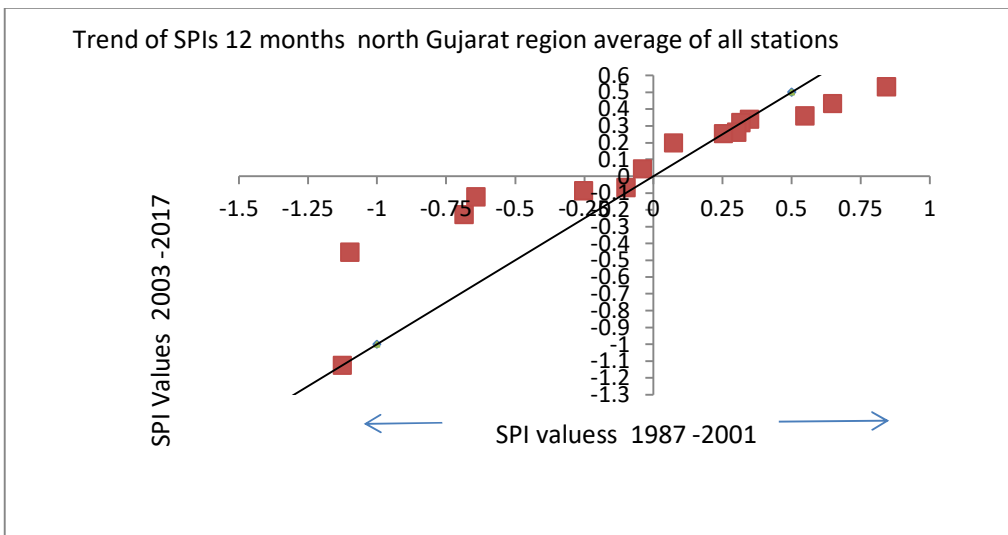


Figure A.3: Trend of SPI values of 12-month north Gujarat Region
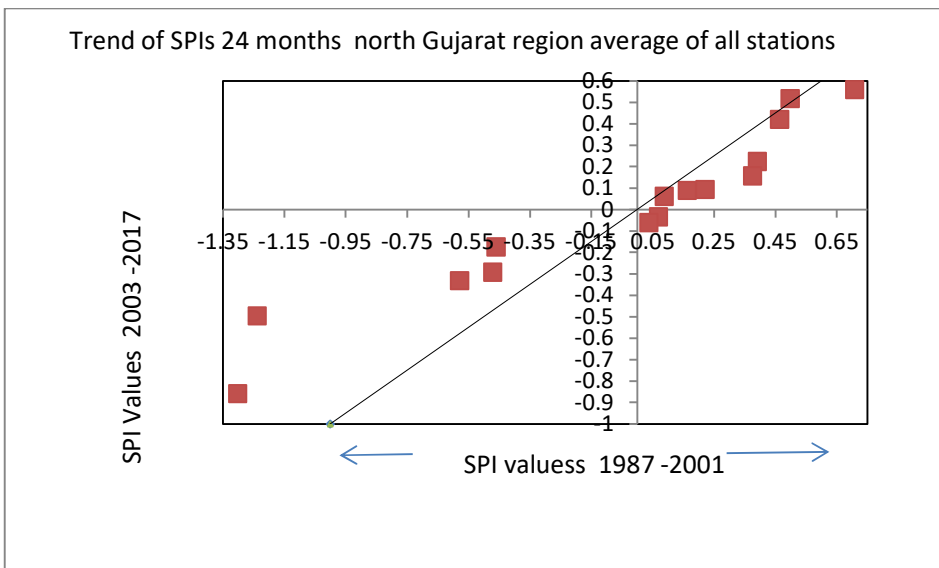
Table A.5

| Value of Coefficients | SPI3 | 6 | 12 |
|---|---|---|---|
| m | 0.472 | 0.476 | 0.635 |
| Lower critical value "C" | 0.89 | 0.89 | 0.89 |

On the visual observation of the above figure no – A.5 it is revealed that there is a decreasing trend in the in the absolute values of the SPIs at different scales.

A quantitative analysis is carried out. The "m" values are obtained by using the least square method and the critical values "C" is calculated as per R. H. McCuan (2018) at level of significance 5%.

The values of the coefficient "m" the calculated as per least square method for the SPI values and the critical value obtained by the method given by R. H. McCuan (2018) are tabulated as per table below:

Since the "m" values obtained are much less than the critical "m" values it is concluded that there is a decrease in the absolute values of the Standard Precipitation Indices at 5 % significance level. This means that dry and weight indices have shown a reduced trend.

**References**:

Innovative Trend Analysis Methodology, Journal of Hydrologic Engineering, Vol. 17, No. 9, September 1, 2012. ASCE.

Richard H. McCuen, Critical Values for Sen's Trend Analysis, J. Hydrol. Eng., 2018, 23(11):

## 3.4 Drought in different decades for period of 1987-2017

Plot of Decadal Values of Standard Precipitation Indices:

The 30-year period is divided into three ten-year periods starting from 1987 at all-time scales and the plots are as shown below**:**
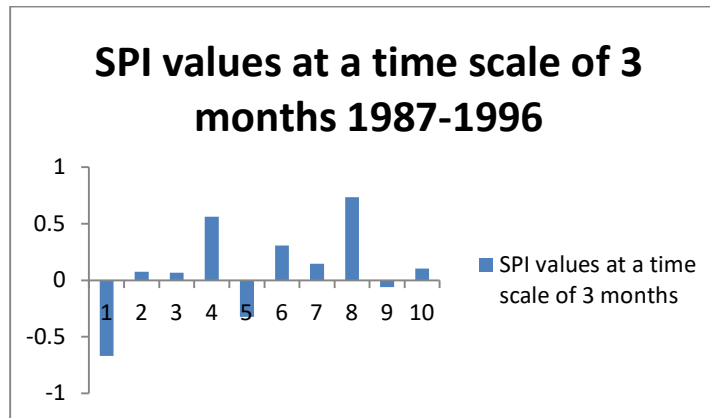
Figure A.4: SPI values at time scale of 3 months 1987-1996
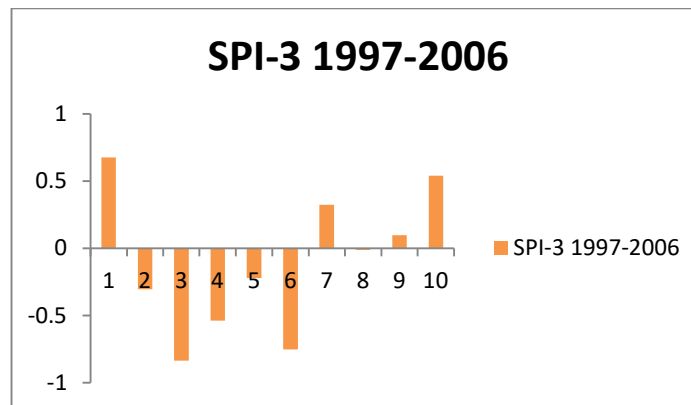


Figure A.5: SPI values at time scale of 3 months 1997-2006
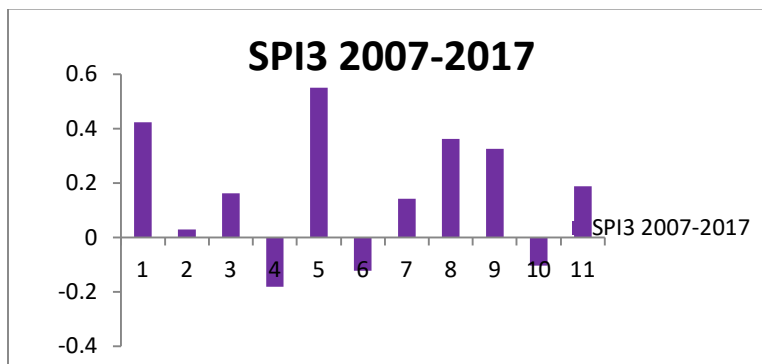


Figure A.6: SPI values at time scale of 3 months 2007-2017
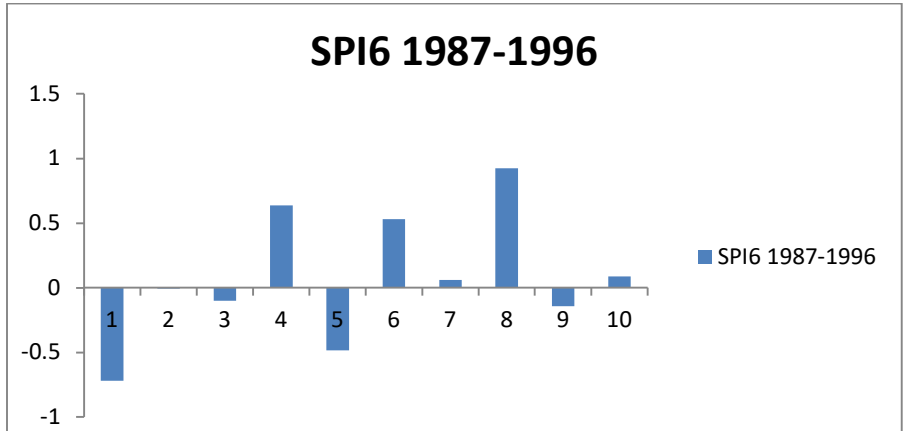
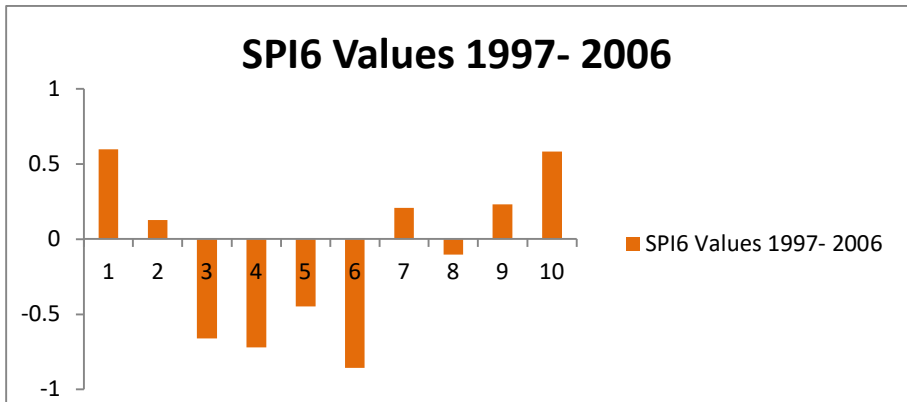Figure A.7: SPI values at time scale of 6 months 1987-1996



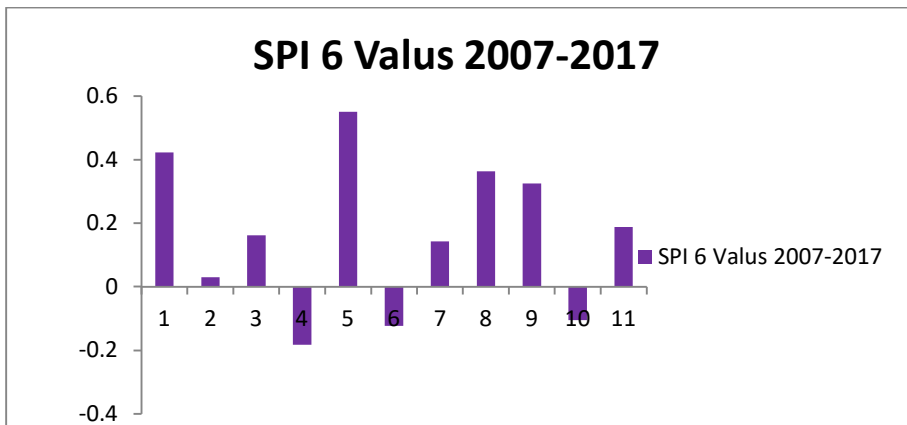Figure A.8: SPI values at time scale of 6 months 1997-2006



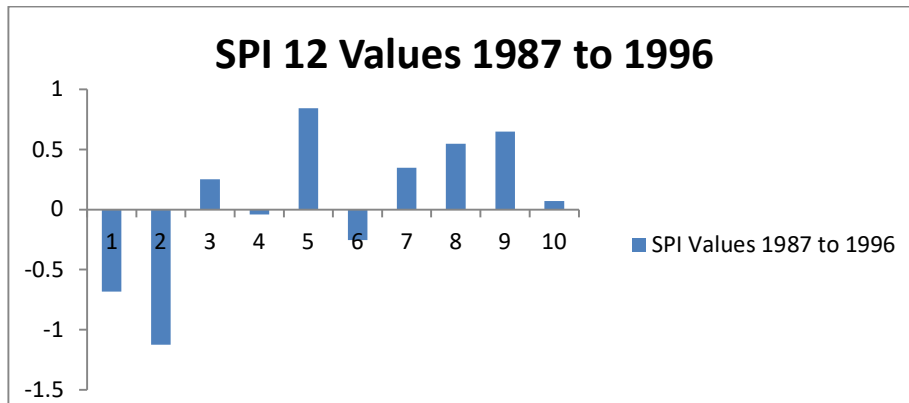Figure A.9: SPI values at time scale of 6 months 2007-2017

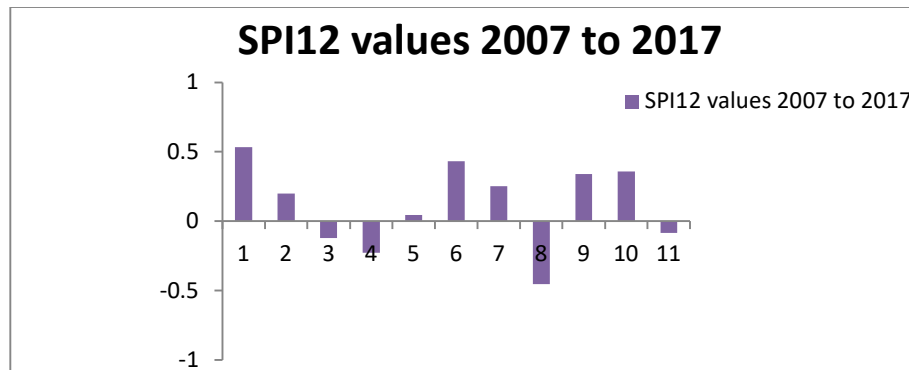Figure A.10: SPI values at time scale of 12 months 1987-1996



Figure A.11: SPI values at time scale of 12 months 2007-2017

The weekly rainfall data is extracted from the daily precipitation data for the last 30 years. the weekly precipitation data beginning from June first week through October second week are considered for the analysis. The serielcorrelaion values with lag 1 are tabulated in the table A.6 below:

Table No A.6: Correlation data week wise

| Week No | Correlation Coefficient with lag1 ($r_1$) |
|---------|------------------------------------------|
| 21      | -0.11243198                              |
| 22      | -0.132                                   |
| 23      | -0.06                                    |
| 24      | -0.11198734                              |
| 25      | -0.11513254                              |
| 26      | 0.22459073                               |
| 27      | -0.03194553                              |
| 28      | 0.2450662                                |
| 29      | -0.05007574                              |

| 30 | 0.20822175 |
|----|------------|
| 31 | 0.05416485 |
| 32 | -0.00399025 |
| 33 | 0.01693684 |
| 34 | -0.24467473 |
| 35 | -0.07064192 |
| 36 | -0.085479 |
| 37 | -0.03508995 |
| 38 | -0.02621067 |

It is observed that the $(r_1)$ values lie between the -0.35 and 0.35. Therefore the data is found to be stationary for probability analysis without any further transformations.

In India we have the monsoon type of climate and almost all the rainfall takes place from June to October. The analysis of daily and weekly rainfall is of much importance the Kharif crops. Data of corresponding weeks for the last 30 years are grouped together and a gamma distribution is fitted to the data of each week set separately. The exceedenceprobabilties of the various rainfall values are calculated using the grammatist function of excel mathematical functions.

A graph is plotted between weeks starting from first week of June till the second month of October at 90%, 75% and 50% exceedance probability. Such an estimation should be useful in planning and managing of water resources of the region for irrigating the crops.

## RESULT AND CONCLUSION

- As per our data the drought also measures to scale of SPI-3, SPI-6, SPI-12 so as per our study we take 16 rain gauge stations and all station have to past 30 years rainfall data and we observe for SPI-3 for all the station felt droughts average 15 years out of 30 years For SPI-6
- For all stations felt drought average 16 years out of 30 years for SPI-12 felt drought average 13 years out of 30 years and we have to data availability of 1987-2017.
- We observe to every station to felt normal drought to every two years
- All station to felt severe drought to every five-six years average
- We also study to all station then we conclude Out of sixteen rain gauge station eight rain gauge station to felt severe drought to last decade (2007-2017)
- We observe to every rain gauge to felt drought for every three or four years

## REFERENCES

1. Kironmala Chanda,and Rajib Maity(2015).'' Metrological Drought quantification With Standard Precipitation Anomly index for the region with strongly seasonal and periodic classification''. journal of hydrologic engineering ASCE.20(12),1-8.

2. T.Thomas P.C.Nayak and Aryan Ghost (2015). ''Spatiotemporal analysis of drought characteristics in the bundelkhand region of central India using the (SPI) method.'' J.Hydrol.Eng.,20(11),1-12.

3. Prakhar Modi and L.B.Roy (2017)"Drought and their analysis in West Bengal,India".The Indian Journal of Tech. Edu.40(3),64-73.

4. P.Guhathakurta Preetha Menon Pm Inkane Usha Krishanan S T Sable (2017) "Trend and variability of meteorological drought over the district of india using standard precipitation index"J.Earth Syst.Sci.,126:120,1-18.

5. Dimitris Tigkas, Harris Vangelis,George Tsakiris (2019)"Drought characterization based on agriculture-oriented standardized precipitation index"135;1435-1447.

# Application of synthesized selected South African kaolin deposit on catalytic pyrolysis of municipal plastic waste

*O.A. Olagunju, and  S.L. Kiambi.

Chemical Engineering Department Durban University of Technology, P.O. Box 1334, Durban 4000, South Africa.

*Corresponding Author: gilbert4life2004@yahoo.com

## Abstract
The rate of plastic waste production and consumption has been on the increase in the last five decades and this is as a result of increase in human population, continuous urbanization, rapid economic growth and a modern life style. The need to appropriately deal with this waste and harness the prospect of the abundance of renewable energy that can be produced from plastic waste validates the need of better and innovative recycling method. Therefore, this has led to the exploration of the use of synthesized catalyst for the catalytic pyrolysis of the municipal plastic waste in Durban, South Africa. Zeolite Socony Mobil–5 (ZSM-5) was synthesized after metakaolinizing South African kaolin deposit in Grahamstown and the use of sodium hydroxide (NaOH), Tetrapropylammoniumbromide (TPABr), sodium silicate pentahydrate ($Na_2SiO_3.5H_2O$) solution and deionized water. The synthesized zeolite was characterized by scanning electron microscopy (SEM), X-ray diffraction (XRD) and BET surface area. The results showed that the sample produced was of ZSM-5 phase. The effect of the temperature ranges between 400 ºC – 550 ºC and reaction time between 60 – 150 minutes on the plastic waste were investigated. Polystyrene wastes was selected as the source of plastic waste. The liquid fuel obtained from the catalytic pyrolysis was analyzed using GC–MS. The results showed effective conversion of the plastic waste to liquid fuels with significant hydrocarbons range obtained. ZSM-5 zeolite synthesized from kaolin of South African origin has shown great prospect as natural zeolite catalytic material for pyrolysis of plastic waste.

**Keywords**: South African Kaolin, ZSM-5, municipal plastic waste, catalytic pyrolysis process, hydrocarbons

## 1. INTRODUCTION

Plastic usage has played a vital role in every daily living although its continuous consumption has led to huge generation of plastic waste littering our environment for more than two decades now. The demand for plastics has increased over time because they are considered as alternative materials providing solutions to various sectors such as aerospace, engineering, medicals, and electronics (Al-salem *et al*., 2017). Polyethylene (PE), Polythene Terephthalate (PET) and Polystyrene (PS) plastics are non-biodegradable, flexible materials and are extremely important for technology advancement due to these properties.

 PE, PET and PS plastic wastes are the major constituent of municipal solid waste (MSW) and are been considered as one of the largest MSWs in the developing countries (Shah, 2010). The accumulation of this plastic waste (PW) over a length of time in conjunction with the inappropriate and conventional waste management strategies led to major health and environmental hazards such as greenhouse gas emissions, groundwater pollution, and several other human health problems (UNEP, 2009). In addition, developing countries such as South Africa, do not consider the

advantages of economic involved by utilizing certain recycling methods, but still depend solely on the conventional method of landfilling of MSW disposal.

There are mainly four different methods of recycling PW recycling namely primary recycling which involves waste scraps being processed into products with similar properties to the original products; secondary recycling has to do with waste/scrap plastics being processed into materials that have different properties to that of the initial product; tertiary methods deal with use of these waste scraps in the production of essential fuels and chemicals or as a segregated waste; and lastly quaternary recycling involves the burning of these plastics and retrieving energy contents afterward (Al-salem, 2009). Pyrolysis is a common method used to convert this plastic waste into energy, in the form of solid, liquid and gaseous fuels.

Pyrolysis is the thermal degradation of plastic waste at different temperatures (300 – 900 °C), in the absence of oxygen, to produced liquid oil (Rehan et al., 2017). Different kinds of catalysts have been used to improve the pyrolysis process of plastic waste overall and to enhance process efficiency. Catalysts have a very critical role in promoting process efficiency, targeting the specific reaction and reducing the process temperature and time (Serrano *et al*., 2012; Ratnasari *et al*., 2017). A wide range of catalysts have been employed in plastic pyrolysis processes, but the most extensively used catalysts are ZSM-5, FCC and MCM-41 (Ratnasari *et al*., 2017).

There are lots of previous work that have reported the use of microporous and mesoporous catalysts for the conversion of plastic waste into liquid fuel. Uemichi *et al*. (1998) carried out catalytic pyrolysis of polyethylene (PE) with HZSM-5 catalysts and reported increased liquid fuel production with the composition of aromatics and isoalkanes compounds. Gaca *et al*. (2008) carried out pyrolysis of plastic waste with modified MCM-41 and HZSM-5 and reported that use of HZSM-5 produced lighter hydrocarbons ($C_3$–$C_4$) with maximum aromatic compounds. Lin *et al*. (2004) used different kinds of catalysts and reported that even mixing of HZSM-5 with mesoporous $SiO_2$-$Al_2O_3$ resulted in maximum production of liquid oil with minimal gas production. The use of commercial catalysts enhanced the overall pyrolysis process and improved the quality of produced liquid oil. However, the use of commercial catalysts increased the overall cost of the pyrolysis process.

Zeolites are crystalline microporous aluminosilicate materials with an extra framework having ion exchange capabilities and thermal stability over a wide temperature range. They are currently used as catalysts for catalytic cracking of heavy hydrocarbons in many commercial processes; zeolite Y is a highly porous faujasite zeolite with Si/ l ratio of 1.5–3.8 (Sakaki *et al*., 2013; Auerbach *et al*., 2003). Zeolites are produced both naturally and synthetically. The synthesis of zeolites from clay as a source of silica and alumina is widely known and has yielded great achievement (Liu *et al*., 2003; Chandrasekhar and Pramada 1998). While ZSM-5 zeolite is generally synthesized using expensive chemicals, finding cheaper raw materials for zeolite synthesis could lead to cost effective and sustainable production as a whole. Recently, researchers have examined the use of natural cheaper minerals such as rice husk ash (Kordatos *et al*., 2008; Mohamed *et al*., 2008; Panpa and Jinawath, 2009), fly ash (Chareonpanich *et al*., 2004), kanemite (Salou *et al*., 2001), palygorskite (Jiang *et al*., 2014) and kaolinite (Feng *et al*., 2009a; Khatamian and Irani, 2009; Kovo *et al*., 2009; Wang *et al*., 2007) as raw materials in ZSM-5 synthesis. However, these minerals differ in their chemical and mineralogical composition and therefore, its likely to have

impact on the final product if used as a precursor for zeolite synthesis. In the earlier studies conducted by Jiang *et al* (2014) using high silica containing palygorskite and Panpa and Jinawath (2009) using rice husk as starting materials produced high silica ZSM-5 but the addition of aluminium to balance the Si/Al ratio was unfavorable and therefore prevented the formation of ZSM-5. Fly ash was found to be a feasible source for ZSM-5 synthesis (Chareonpanich *et al*., 2004). However high temperatures in excess of 200 °C are needed for synthesis of pure ZSM-5 and generally only low yields are obtained. The low product yield and energy needs due to high temperatures calls for improvement of the process. Kaolin has been used as a staring material and was successfully converted to a range of zeolites (Belviso *et al.,* 2013; Chandrasekhar and Pramada, 2008; Kovo and Holmes, 2010).

Kaolin-based zeolite is appraised as cheap and abundant catalytic material (Lijalem Ayele Regassa, 2016). Most studies performed have been on commercial kaolins either and mainly used in zeolite A synthesis. In the present work focus will be on synthesizing ZSM-5 zeolite from kaolin originating from Grahamstown, South Africa. The synthesis of ZSM-5 from kaolin in this geological area and its application as a catalyst in the process of pyrolysizing plastic wastes does not seem to have been reported in literature. Polystyrene, representing one of the common plastics usually present in high proportion in the plastic waste stream of municipal solid waste was selected as the feedstock.

The main objective of this study was to convert the waste plastics to oil products for use as a hydrocarbon fuel oil or raw chemical feedstock. The effects of temperature and reaction time have been studied to ascertain the optimum conditions necessary for the production of oil as well as to investigate the effects of these parameters on the compositions of reaction products, with a special emphasis on the oil.

## 2. EXPERIMENTAL

### 2.1 Materials and Methods

Polystyrene was used in this experiment. The Plastic wastes was obtained from waste bins and garbage from Durban University of Technology cafeterias, Durban, South Africa. They were sorted, cleaned to remove dirt, and then shredded into smaller particle sizes. As received kaolin from G&W minerals resources located in the Eastern Cape region of South Africa with Si/Al ratio 2.91, calcined at 600°C for 2h was used as a source of silica and alumina (66.58% $SiO_2$ and 22.81 % $Al_2O_3$ respectively). Sodium silicate 26.5% $SiO_2$ and 10.6% $Al_2O_3$ composition solution and TPABr. All the chemicals were procured from Sigma Aldrich except Nitric acid 55% which was obtained from Ace enterprises chemical association. The chemicals were applied as received with no additional purification.

### 2.2 Synthesis of Kaolin-based ZSM-5 Zeolite

In the preparation of kaolin-based ZSM-5, the required amount of G&W metakaolin and sodium hydroxide were dissolved in deionized (DI) water and TPABr were also mixed separately with the required amount of DI water. The solution of NaOH/Kaolin and sodium silicate solution were

added simultaneously to the solution of the TPABr while stirring. Nitric acid was used to control the pH until the solution mixture is homogenous. The synthesized gel was transferred to stainless steel Teflon lined autoclave cup and was hydrothermally treated at 180°C for two days. The resulting product was washed with DI until the pH is less than 8. The sample was dried overnight at 80°C and calcined for 5 hours at 550°C. The resulting powder was then characterized.

### 2.3 Characterization

X-ray diffraction (XRD) patterns and average crystallite size were collected with Bruker AXS, D8 Advance equipped with Tube (Cu-Ka radiation (lKa1=1.5406Å) and Detectors Lynx Eye (Position sensitive detector) at 40kV, 40mA and V20 variable slit. The measurements were carried out with a step width of 0.5° to 130° 2θ with an increment (Δ2θ of 0.034° and a scan rate of 0.5 sec per step. The diffraction data were analyzed using OriginPro 2018 software to give the estimation of the amount of each phase in the sample. The morphology was characterized by using scanning electron microscopy FEI Nova NanoSEM 230 with a field emission gun equipped with a high-resolution immersion lens. The EDS detector is an Oxford X-Max, using INCA software. Surface area, pore size, and pore volume measurements and analysis were determined by BET machine.

### 2.4 Experimental procedures

PS was collected and prepared by cutting into smaller particle sizes of 3–4 mm and charged into a packed bed pyrolysis reactor which was operated at set temperature and at atmospheric pressure. As shown in Fig. 1, the reactor is a lagged cylindrically shaped stainless steel vessel. The reactor was electrically heated with a 2 kW heating element equipped with an automatic temperature controller and connected to a coil condenser, and subsequently liquid collector. 100 g of polymer to 10 g of catalyst was used in the experiment and fed into the reactor, tightly closed, and purged with nitrogen gas at the start of each experiment at the rate of 20 ml/min for 10 min. The heating element was turned on and regulated to a specified temperature to pyrolyze the feedstock. The pyrolyzed PPW at the set temperature was vaporized. The vaporized PPW passed through the catalyst bed where reaction occurred. The vaporized product was finally condensed and collected for analysis. The solid (S), gaseous (G), and liquid product (L) yields were calculated using the formula given below as shown in Eqs. 1, 2, 3 (Patil *et al*., 2017)

$$L \ (wt\%) = \frac{weight \ of \ liquid \ product \times 100}{weight \ of \ plastic \ feed} \tag{1}$$

$$S \ (wt\%) = \frac{weight \ of \ solid \ product \times 100}{weight \ of \ plastic \ feed} \tag{2}$$

$$G \ (wt\%) = 100 - (L \ (wt\%) + S \ (wt\%)) \tag{3}$$

The pyrolyzed oil was analyzed using gas chromatography – mass spectrometry (GC–MS) to determine the chemical constituents of the hydrocarbon products.
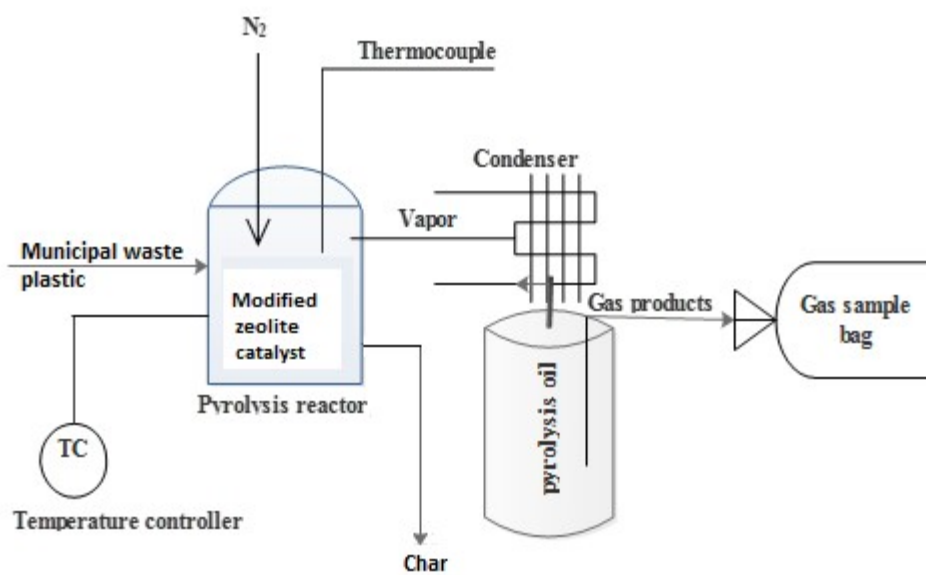
**Figure 1**: Schematic of  pyrolysis experimental set up

## 3. RESULTS AND DISCUSSION

### 3.1 X-ray diffraction (XRD) studies

The XRD pattern of ZSM-5 using metakaolin that was calcined at 650 ℃ for 2hour is shown in Fig. 2. The characteristic peaks of ZSM-5 are in the ranges of 7.9 to 23.1° 2θ which show nucleation with a sizable amount of quartz as an impurity at 20.9 and 26.6° 2θ clearly confirmed the formation of crystalline ZSM-5 phase (Mohiuddin *et al*., 2016; Salou *et al.,* 2001). The percentage (%) crystallinity and the average crystal (grain) size was evaluated using OriginPro 2018 version and found to be 87% crystallinity and 28 nm respectively. The two parameters are key to the pyrolysis process. The specific surface area, pore size and pore volume of 179.9 m2/g, 49.262A and 0.05 cm3/g respectively were deduced using BET surface area analyzer. The crystal size of the catalyst rises the specific surface area and intense surface porosity increases the outer surface area of the zeolite (Wibowo *et al*., 2017). The incorporation of the two parameters together influences the effective surface area. This shows that the synthesized kaolin-based ZSM-5 with a good surface area would promote high reaction rate potential and proficiency.

### 3.2 Scanning electron microscopy (SEM) studies

SEM is a technique used to interpret the morphology and distribution of crystals size of the zeolite phase. Typically, the configuration, formation, and structure of ZSM-5 crystals were highly controlled and depend on synthesis parameters such as crystallization temperature, time and aging. Mohiuddin (2016), conducted a study on the synthesis of ZSM-5 using impure kaolin under

various parameters resulting in different morphologies. The image of kaolin-based ZSM-5 nanocrystals synthesized under 180°C, 48hr and 48hr crystallization temperature, time and aging respectively were performed in this study and presented in Fig. 3. It can be seen clearly that the kaolin-based ZSM-5 is obviously orthogonal shape and highly crystallized with an average crystals size of 28 nm indicated that there is an intergrown crystal with some amorphous material present. The orthogonal nanocrystals are as a result of the aggregation of their high surface Gibbs free energy (Wu *et al.*, 2013).
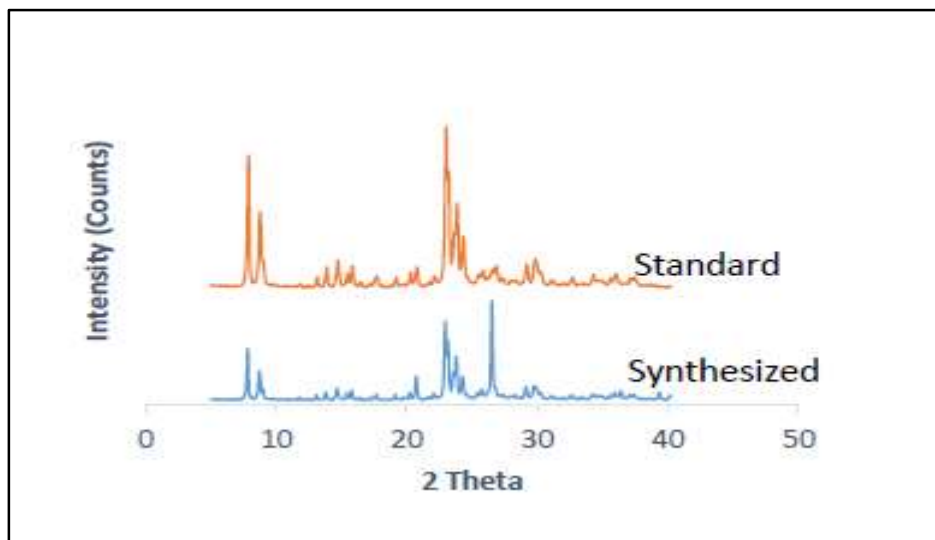


**Figure 2**: XRD pattern of standard and kaolin-based ZSM-5 zeolite and
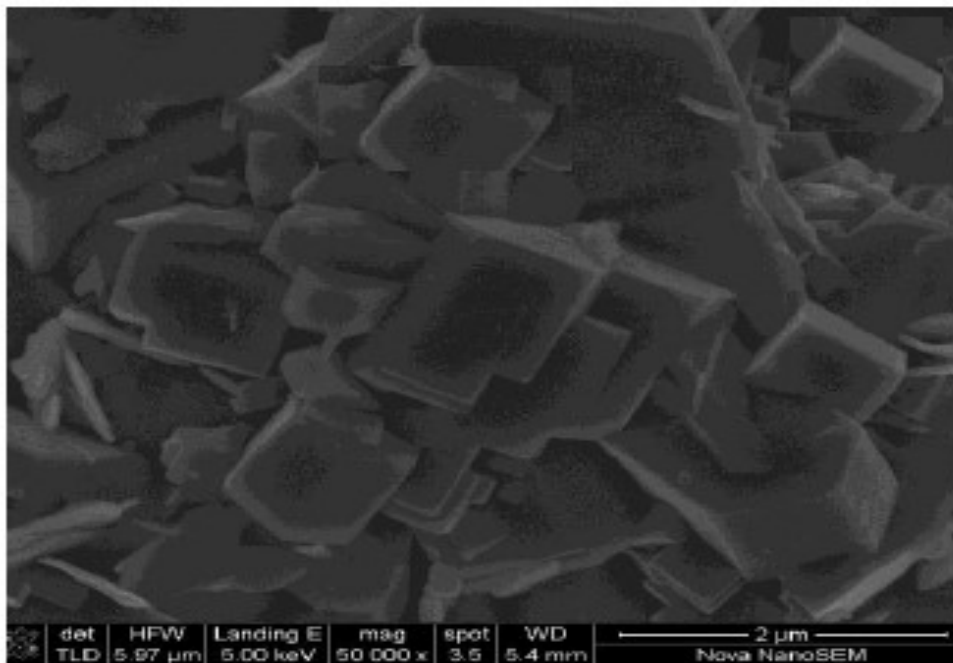


**Figure 3**: SEM image of synthesized kaolin-based ZSM-5 zeolite

### 3.3 Effect of temperature on the feedstock

Experiments were carried out at four different temperatures (400, 450, 500 and 550°C) to investigate the effect of temperature on the yield and quality of produced liquid oil. After determination of optimum temperature, experiments were carried out at four different reaction times (60, 90, 120 and 150 min) to investigate the effect on the feedstock decomposition and liquid oil. The purpose of using different temperature and reaction time was to find the optimum temperature and reaction time for pyrolysis of PS waste.

The study showed that PS started decomposing at 400°C and reached its maximum decomposition point of 56.8% at 500°C as shown in Fig. 4. Further increase in temperature did not improve the product yield, concluding the depolymerization of the feedstock with some residue (char) leftover. As more than 90% of the feedstock was achieved at up to 500°C in the experimental work it may be stated that optimum yield of the liquid oil was achieved at 500°C.

At 400 °C, the entire PS sample was completely degraded into highly viscous dark-coloured oil. Char formation was observed and a little amount of hydrocarbon gas was also formed. As the temperature increased above 400 °C and even up to 450 °C, there were significant decreases in the proportion of char formed and slight increase in gas formed, but the oil became less viscous. The amount of gas produced increased significantly as the reaction temperature was increased to 500 °C and then to 550 °C. The yield of produced liquid oil, especially styrene increased with an initial increase in temperature and time, and after a while, the oil yield started to decrease as shown in Figs. 4 and 5. Jung *et al*. (2013) and Mo *et al*. (2014) explained this phenomenon that after achieving optimum temperature, some secondary reactions such as polyaromatic formation reactions started during PS pyrolysis, which decrease the liquid oil and styrene yield. While the phenomenon of increased gas production at higher temperature was explained by Lopez *et al*. (2011), de Marco *et al*. (2009), and Artetxe *et al*. (2015) that the strong cracking of C-C bonds at higher temperature increases the production of lighter hydrocarbons with short carbon chain compounds. Moreover, according to Li *et al*. (1999), Hernández *et al*. (2007) and Lopez *et al*. (2011), temperature lower than 450°C increases the char and decreases the liquid oil yield and temperature in excess of 500°C increases the gases and lowers the liquid oil yield. Therefore, there is a strong relationship between the amounts of char and oil products formed from PS in relation to reaction temperature. This result may be explained by the presence of mainly aromatic compounds in the liquid degradation product of PS.
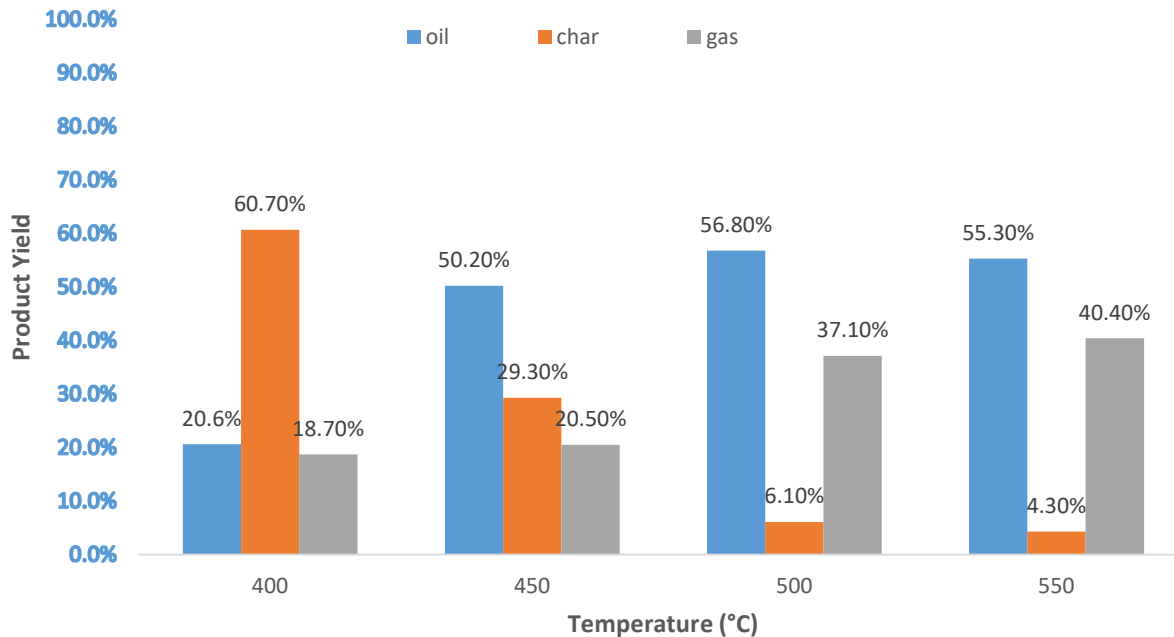
**Figure 4**: Effect of reaction temperature on pyrolysis liquid oil, char and gas product yields
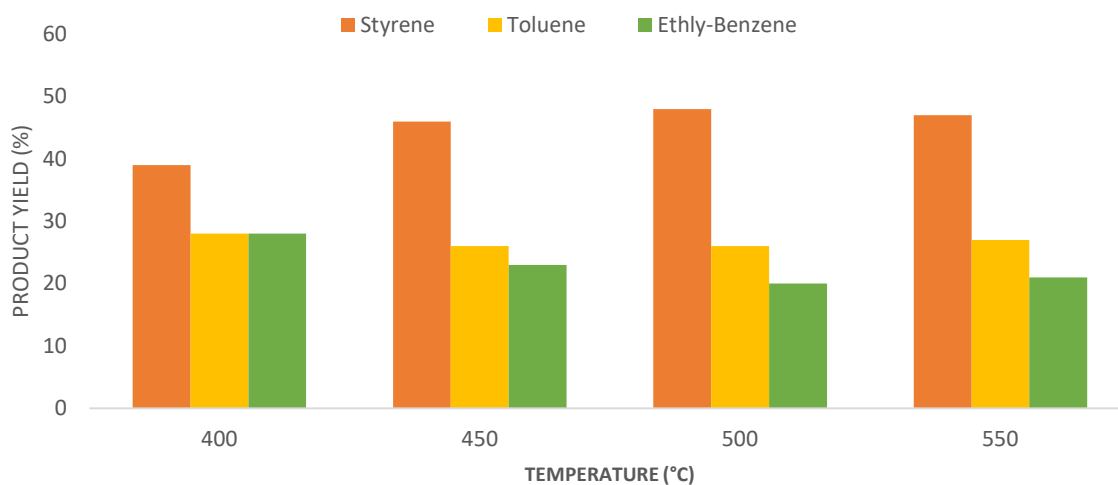
### 3.4 Effect of reaction time on liquid oil yield

The effect of reaction time on the liquid oil yield was studied against the optimum temperature of 500°C at 60, 90, 120 and150 min as shown in Fig. 5. The results showed insignificant difference in liquid oil production between the 90 and 150 min reaction times. The 90 min reaction time produced the maximum liquid oil yield of 56.8% as compared to 55.8% for a reaction time of 150 min. The char production was higher for a reaction time of 90 min as compared to 150 min (6.1 versus 4.3%). It can be stated that the oil yield at 90 min reaction time shows the maximum. Thus 90 min is suggested as the optimum reaction time. The lowest reaction time (60 min) produced more char and less liquid oil, suggesting that a 60 min reaction time is insufficient to convert the feedstock to liquid oil at maximum conversion efficiency. Similar results were observed and reported by Lopez *et al.* (2011) and Lee (2007) on the yield of liquid oil with different reaction times. However, the effect of reaction time on pyrolysis is also one of the functions of the reactor dimensions and the heat transfer rate from the heating elements to the PS feedstock within the reactor (Jung *et al.*, 2013; Ringer *et al.*, 2006). Therefore, the reaction time may change with other reactor configurations, especially in a continuous flow reactor, which would be the type of reactor that are mostly used in industrial application of the pyrolysis process (Chen *et al.*, 2014; Miandad *et al.*, 2016a, b).
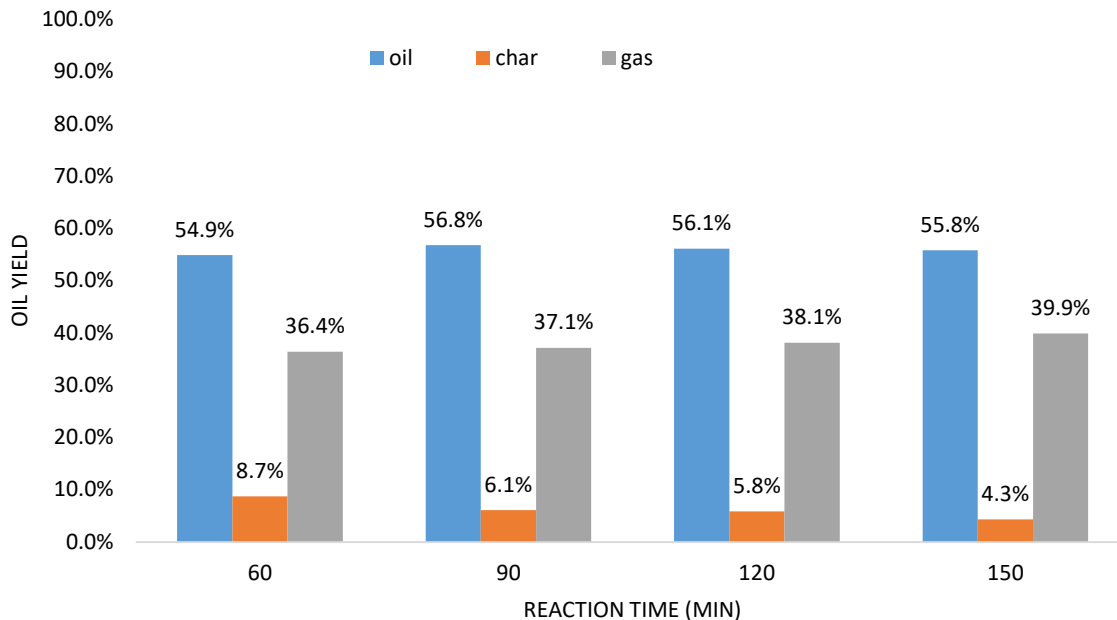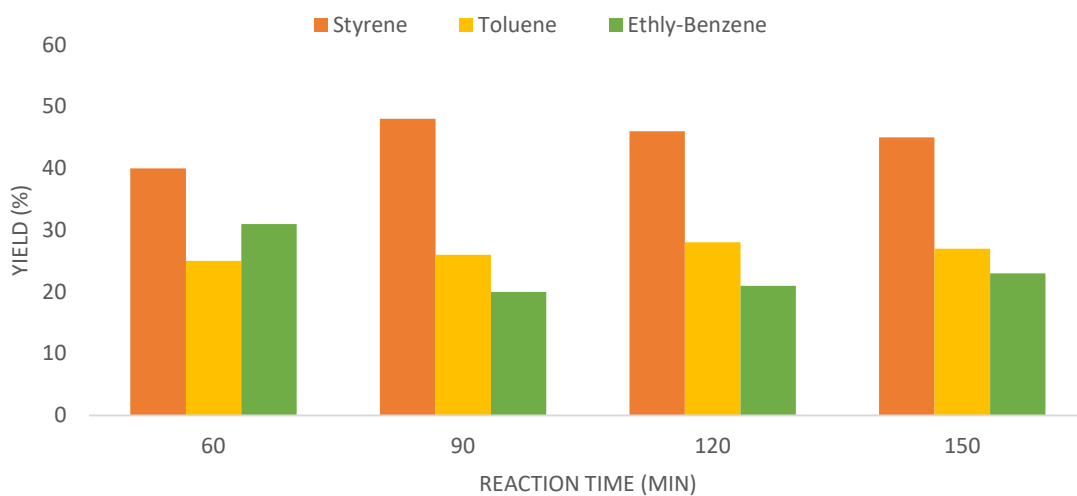
**Figure 5**: Effect of reaction time on pyrolysis liquid oil, char and gas product yields at 450 °C.

## 3.5 Characterization of liquid products

The results from the GC–MS analysis established the identification of quite a number of shorter chain carbons of the liquid fuel obtained from the catalytic pyrolysis of PS waste. The GC–MS analysis showed that the same aromatic compounds were found in the produced liquid oil but in different compositions at different temperatures and reaction times as shown in Figs. 6 and 7. Toluene, ethyl-benzene and styrene were found to be about 95%(by area) in all three samples produced at four different process temperatures. Styrene was found in more abundance than the other two compounds, starting from 39% and rising to 48% (at 400°C to 500°C respectively). The maximum value of 48% was achieved at optimum temperature (500°C) and reaction time (90 min) as shown in Figs. 6 and 7. Various other studies also reported similar results that styrene, toluene and ethylene benzene were the main compounds produced from PS waste (Artetxe et al.,2015; Frediani et al., 2014; Jung *et al*., 2013; Undri *et al*., 2013, 2014a). Onwudili *et al*. (2009) reported that there is no direct production of toluene and ethyl-benzene from the plastic waste feed-stock, however they may be produced by the reaction of styrene itself. It is reported that further increase in temperature leads to a decrease in styrene production with an increase in the production of toluene and ethyl-benzene (Onwudili et al., 2009; Demirbas, 2004).

**Figure 6**: GC–MS analysis showing the effect of temperature on composition of liquid oil (only the main products were reported).



**Figure 7**: GC–MS analysis showing the effect of reaction time (min) on composition of liquid oil (only the main products were reported).

This present study reveals that the catalytic pyrolysis of PS plastic has yielded a higher fraction of gaseous product and lesser liquid fraction when compared to our previous work on non-catalytic thermal cracking of this plastic waste. This also agrees with the work of Seo *et al*. (2003) that showed an increase of gaseous product using a catalyst for the pyrolysis reaction.

## 4. CONCLUSION

Kaolin-base ZSM-5 from south African local kaolin with specific surface area, pore size and pore volume of 179.9 m2/g, 49.262A and 0.05 cm3/g, respectively were successfully synthesized and applied as a catalyst. The catalytic cracking of the PS plastic wastes using zeolite has revealed the great usefulness of this waste as a rich source of raw materials for the production of a variety of chemicals and a good alternative to the production of automobile fuel. GC–MS showed the compositional analysis of the liquid fuel obtained containing mainly styrene (48%), toluene (26%) and ethyl-benzene (20%) compounds. The liquid products obtained have similar products to fossil fuels and can, therefore, be used as alternative fuels for a more sustainable and cleaner environment when necessary blending is done for upgrading.

## REFERENCE

Al-salem, S.M, Antelava, A, Constantinou, A, Manos, G and Dutta, A. 2017. A review on thermal and catalytic pyrolysis of plastic solid waste. J Environ Manage 197(1408):177–198.

Shah, S.H. 2010. Low temperature conversion of plastic waste into light hydrocarbons. J Hazard Mater 179(1–3):15–20.

UNEP 2009. Converting waste plastics into a resource. Osaka, pp. 1–15.

Al-Salem, S.M. 2009. Establishing an integrated databank for plastic manufacturers and converters in Kuwait. J Waste Manag 29:479–484.
Rehan, M., Miandad, R., Barakat, M. A., Ismail, I. M. I., Almeelbi, T., Gardy, J. 2017. Effect of zeolite catalysts on pyrolysis liquid oil. Int. Biodeterior.Biodegrad. 119, 162–175. doi: 10.1016/j.ibiod.2016.11.015.

Serrano, D. P., Aguado, J., and Escola, J. M. 2012. Developing advanced catalysts for the conversion of polyolefinic waste plastics into fuels and chemicals. ACS Catal. 2, 1924–1941. doi: 10.1021/cs3003403.

Ratnasari, D. K., Nahil, M. A., and Williams, P. T. 2017. Catalytic pyrolysis of waste plastics using staged catalysis for production of gasoline range hydrocarbon oils. J. Anal. Appl. Pyrolysis 124, 631–637. doi: 10.1016/j.jaap.2016.12.027.

Uemichi, Y., Hattori, M., Itoh, T., Nakamura, J., and Sugioka, M. 1998. Deactivation behaviors of Zeolite and Silica– Alumina catalysts in the degradation of polyethylene. Ind. Eng. Chem. Res. 37, 867–872. doi: 10.1021/ie970605c.

Gaca, P., Drzewiecka, M., Kaleta, W., Kozubek, H., and Nowinska, K. 2008. Catalytic degradation of polyethylene over mesoporous molecular sieve MCM-41 modified with heteropoly compounds. Polish J. Environ. Stud. 17, 25–35.

Lin, Y. H., Yang, M. H., Yeh, T. F., and Ger, M. D. (2004). Catalytic degradation of high density polyethylene over mesoporous and microporous catalysts in a fluidised-bed reactor. Polym. Degrad. Stab. 86, 121–128. doi: 10.1016/j.polymdegradstab.2004.02.015.

Sakaki AS, Roozbehani B, Shishesaz M, Nasrin A. 2013. Catalytic degradation of the mixed polyethylene and polypropylene into middle distillate products. Clean Technol Environ Policy 16:901–910.

Auerbach, S.M, Carrado KA, Dutta, P.K. 2003. Zeolite science and technology, New York, Basel, pp. 11–30.

Chandrasekhar S. and Pramada P.N. 1998. Investigation on the synthesis of zeolite NaX from Kerala kaolin. J Porous Mater 6:283–284.

Liu X, Yan Z, Wang, H. and Luo, Y. 2003. In-situ synthesis of NaY zeolite with coal-based kaolin. J Nat Gas Chem 12:63–70.

Kordatos, K., Gavela, S., Ntziouni, A., Pistiolas, K.N., Kyritsi, A., Kasselouri-Rigopoulou, V., 2008. Synthesis of highly siliceous ZSM-5 zeolite using silica from rice husk ash. Micropor. Mesopor. Mater. 115, 189–196.

Mohamed, M.M., Zidan, F.I., Thabt, M., 2008. Synthesis of ZSM-5 zeolite from rice husk ash: characterization and implications for photocatalytic degradation catalysts. Micropor. Mesopor. Mater. 108, 193–203.

Panpa,W., Jinawath, S., 2009. Synthesis of ZSM-5 zeolite and silicalite from rice husk ash. Appl. Catal. Environ. 90, 389–394.

Chareonpanich, M., Namto, T., Kongkachuichay, P., Limtrakul, J., 2004. Synthesis of ZSM-5 zeolite from lignite fly ash and rice husk ash. Fuel Process. Technol. 85, 1623–1634.

Salou, M., Kooli, F., Kiyozumi, Y., Mikamizu, F., 2001. Effect of aluminium source and content on the synthesis of zeolite ZSM-5 from kanemite via solid-state transformation. J. Mater. Chem. 11, 1476–1481.

Jiang, J., Duanmu, C., Yang, Y., Gu, X., Chen, J., 2014. Synthesis and characterization of high siliceous ZSM-5 zeolite from acid-treated palygorskite. Powder Technol. 251, 9–14.

Feng, H., Li, C., Shan, H., 2009a. Effect of calcination temperature of kaolin microspheres on the in situ synthesis of ZSM-5. Catal. Lett. 129, 71–78.

Khatamian, M., Irani,M., 2009. Preparation and characterization of nanosized ZSM-5 zeolite using kaolin and investigation of kaolin content, crystallization time and temperature changes on the size and crystallinity of products. J. Iran. Chem. Soc. 6, 187–194.

Kovo, A.S., Hernandez, O., Holmes, S.M., 2009. Synthesis and characterization of zeolite Y and ZSM-5 from Nigerian Ahoko Kaolin using a novel, lower temperature, metakaolinization technique. J. Mater. Chem. 19, 6207–6212.

Wang, P., Shen, B., Shen, D., Peng, T., Gao, J., 2007. Synthesis of ZSM-5 zeolite from expanded perlite/kaolin and its catalytic performance for FCC naphtha aromatization. Cat. Comm. 8, 1452–1456.

Belviso, C., Cavalcante, F., Lettino, A., Fiore, S., 2013. A and X-type zeolites synthesized from kaolinite at low temperature. Appl. Clay Sci. 80-81, 162–168.

Chandrasekhar, S., Pramada, P.N., 2008. Microwave assisted synthesis of zeolite A from metakaolin. Micropor. Mesopor. Mater. 108, 152–161.

Kovo, A.S., Holmes, S.M., 2010. Effect of aging on kaolin-based zeolite Y from Ahoko Nigeria using a novel metakaolinization technique. J. Disper Sci Technol. 31, 442–448.

Lijalem Ayele Regassa 2016. Synthesis and Characterization of Zeolite A Studies of its application as detergent builder and in tannery wastewater treatment Lijalem Ayele Regassa A Thesis Submitted to Department of Chemistry Presented in Fulfillment of the R.

Patil L, Varma K, Gajendra S, Mondal P. 2017. Thermocatalytic degradation of high density polyethylene into liquid product. J Polym Environ 1–10.

Salou, M., Kooli, F., Kiyozumi, Y., Mikamizu, F., 2001. Effect of aluminium source and content on the synthesis of zeolite ZSM-5 from kanemite via solid-state transformation. J. Mater. Chem. 11, 1476–1481.

Wibowo, E., Sutisna, Rokhmat, M., Murniati, R., Khairurrijal and Abdullah, M. 2017 Utilization of Natural Zeolite as Sorbent Material for Seawater Desalination, Procedia Engineering. The Author(s), 170, pp. 8□13. doi: 10.1016/j.proeng.2017.03.002.

Mohiuddin, E., Isa, Y. M., Mdleleni, M. M., Sincadu, N., Key, D. and Tshabalala, T. 2016. Synthesis of ZSM-5 from impure and beneficiated Grahamstown kaolin: Effect of kaolinite content, crystallisation temperatures and time, Applied Clay Science, 119(November), pp. 213-221. doi: 10.1016/j.clay.2015.10.008.

Wu, G., Wu, W., Wang, X., Zan, W., Wang, W. and Li, C. 2013. Nanosized ZSM-5 zeolites: Seed-induced synthesis and the relation between the physicochemical properties and the catalytic performance in the alkylation of naphthalene, Microporous and Mesoporous Materials. Elsevier Inc., 180, pp. 187□195. doi: 10.1016/j.micromeso.2012.11.011.

Jung, S.H., Kim, S.J., Kim, J.S. 2013. The influence of reaction parameters on characteristics of pyrolysis oils from waste high impact polystyrene and acrylonitrile–butadiene–styrene using a fluidized bed reactor. Fuel Process. Technol. 116, 123–129.

Mo, Y., Zhao, L., Wang, Z., Chen, C.L., Tan, G.Y.A., Wang, J.Y. 2014. Enhanced styrene recovery from waste polystyrene pyrolysis using response surface methodology coupled with Box-Behnken design. Waste Manage. 34, 763–769.

Lopez, A., Marco, D.I., Caballero, B.M., Laresgoiti, M.F., Adrados, A. 2011. Influence of time and temperature on pyrolysis of plastic wastes in a semi-batch reactor. Chem. Eng. J. 173, 62-67.

de Marco, I., Caballero, B.M., López, A., Laresgoiti, M.F., Torres, A., Chomón, M.J. 2009. Pyrolysis of the rejects of a waste packaging separation and classification plant. J. Anal. Appl. Pyrol. 85 (1–2), 384–391.

Artetxe, M., Lopez, G., Amutio, M., Barbarias, I., Arregi, A., Aguado, R., Bilbao, J., Olazar, M. 2015. Styrene recovery from polystyrene by flash pyrolysis in a conical spouted bed reactor. Waste Manage. 45, 126–133.
Li, A.M., Li, X.D., Li, S.Q., Ren, Y., Chi, Y., Yan, J.H., Cen, K.F. 1999. Pyrolysis of solid waste in a rotary kiln: influence of final pyrolysis temperature on the pyrolysis products. J. Anal. Appl. Pyrol. 50, 149–162.

Hernández, M.R., Gómez, A., García, A.N., Agulló, J., Marcilla, A. 2007. Effect of the temperature in the nature and extension of the primary and secondary reactions in the thermal and HZSM-5 catalytic pyrolysis of HDPE. Appl. Catal. A 317, 183–194.

Lee, S., Yoshida, K., Yoshikawa, K. 2015. Application of waste plastic pyrolysis oil in a direct injection diesel engine: for a small scale non-grid electrification. Energy Environ. Res. 5 (1). 1927-0569.

Ringer, M., Putsche, V., Scahill, J. 2006. Large-scale pyrolysis oil production: a technology assessment and economic analysis. A technical report by National Renewable Energy Laboratory (NREL), US. NREL/TP-510-37779. Available from: <http://www.nrel.gov/docs/fy07osti/37779.pdf>.

Chen, D., Yin, L., Wang, H., He, P. 2014. Pyrolysis technologies for municipal solid waste: a review. Waste Manage. 34, 2466–2486.

Miandad, R., Barakat, M.A., Aburiazaiza, A.S., Rehan, M., Nizami, A.S. 2016a. Catalytic pyrolysis of plastic waste: a review. Process Saf. Environ. Prot. 102, 822–838. http://dx.doi.org/10.1016/j.psep.2016.06.022.

Miandad, R., Barakat, M., Rehan, M., Ismail, I.M.I., Nizami, A.S. 2016b. The energy and value-added products from pyrolysis of waste plastics. In Book, 'Recycling of Solid Waste for Biofuels and Bio-chemicals' under Series Title: Environmental Footprints and Eco-design of Products and

Processes. Springer Science+Business Media, Singapore. http://dx.doi.org/10.1007/978-981-10-0150-5_12.

Undri, A., Meini, S., Rosi, L., Frediani, M., Frediani, P. 2013. Microwave pyrolysis of polymeric materials: waste tires treatment and characterization of the valueadded products. J. Anal. Appl. Pyrol. 103, 149–158.

Frediani, P., Undri, A., Rosi, L., Frediani, M. 2014. Waste/Contaminated Polystyrene Recycling through Reverse Polymerization. Lynwood ed., Nova Publisher. ISBN: 978-1-63321-371-5.

Onwudili, J.A., Insura, N., Williams, P.T. 2009. Composition of products from the pyrolysis of polyethylene and polystyrene in a closed batch reactor: effects of temperature and residence time. J. Anal. Appl. Pyrol. 86, 293–303.

Demirbas, A. 2004. Pyrolysis of municipal plastic wastes for recovery of gasoline range hydrocarbons. J. Anal. Appl. Pyrol. 72, 97–102.

Undri, A., Frediani, M., Rosi, L., Frediani, P. 2014a. Reverse polymerization of waste polystyrene through microwave assisted pyrolysis. J. Anal. Appl. Pyrol. 105, 35– 42.
Seo, Y.H., Lee, K.H., Shin, D.H. 2003. Investigation of catalytic degradation of high-density polyethylene by hydrocarbon group type analysis. J Anal Appl Pyrolysis 70:383–398.

# Society involvement as a sustainable initiative to Municipal Solid Waste management

*Kinjal Patel[1], Dr. Monika Swami[1]*
[1]Department of Chemical Engineering, Sal Engineering & Technical Institute(SETI),
[2]Department of Chemical Engineering, Sal College of Engineering (SCE),
Sal Education, Ahmedabad-380060, Gujarat, INDIA
[1]chem.kinjal@gmail.com, +91 9974407792

**Abstract:**

Integrated solid waste management is the term used to describe activities associated with the management of society's waste. Municipal solid waste management (MSWM) comes out as a big challenge because of the environmental and health concerns as well as the extent of waste generated. The major obstacles are door to door waste collection, segregation of waste, technologies for the processing of waste, reuse and/or sale of recovered materials and disposal methods. The municipalities in each region can implement the regional solid waste-resource management plan. The stakeholders do not have clarity and apprehension that give rise to failure of the programe and policies regarding MSWM. The present paper provides a study of an existing solid waste-resource management facility in India and highlights some major local issues. There is a need to drive behavioral change among citizens and persistent collaboration of the community to SWM. The paper provides different local practices that can greatly influence the operations at hierarchical levels in solid waste management.

**Keywords:**

sustainable development, solid waste management, community involvement, segregation of waste, source reduction.

## 1. Introduction

Today, solid waste management has become one of the major global problems among climate change and public health concerns. It has become the need of the hour to have detailed research into solid waste generated in the society and the disposal facility available to accommodate such a huge volume of waste. As per MOEF annual report 2019-20, generation of MSW is 1,52,076 TPD in India. Therefore the effective management of such escalating loads becomes more complex day by day (Tchobanoglous, 2015). It is observed that there are major challenges in Municipal solid waste management on the grounds of rate of generation and the mixed nature of its composition. (Bhide & Sundaresan 1983). The rate of generation of MSW in developing countries has been increased because of industrialization, urbanization and lifestyle of community. For the sustainable use of resources, it is recommended to use the 4Rs concept in solid waste management. In the study conducted by Parekh et al. for the two big cities of india named Surat in Gujarat and Ghaziabad in Uttar Pradesh, evaluated the performance of municipal waste management system by identifying 44 indicators and assigned weight fraction to them. The study reports that performance of Urban Local Bodies is quite good in terms of collection and transportation however segregation aspects need more attention and for that society participation should be inspired.(Parekh et al., 2015). SWM problems are concealed in the creator's way of life. Waste generated if treated as a resource can become income at personal level but to circulate this idea among people requires mass awareness campaigns by the media aimed at school children, NGOs, Municipal Corporation, Panchayat village, etc(Kuniyal et al., 1998). Srivastava et al. had conducted SWOT analysis for successful MSWM in Lucknow- India

and had identified a major weakness parameters as public attitude towards segregation of waste and lack of environmental awareness amongst society(Srivastava et al., 2005). Generally, women and childrens(CPHEEO, 2016) are involved in waste picking and sorting activities that too without any Personal protective equipment(PPE) thus effective solid waste management plan should be perceived by the community with concern to their health.

The present study focuses on existing waste management facilities in India and society involvement therein. It stressed on the source reduction the top most hierarchical level in solid waste management. The reviews from different research articles have been taken as baseline to the study. It drives to the public participation in MSWM as a major contributing factor to explore in Municipal solid waste management. The study describes various outlooks regarding how public involvement can lessen the burden of SWM.

## 2. Theory:

Some major environmental effects due to improper solid waste disposal are soil acidity, water contamination, bad odour,deterioration of air quality above the dump area and birds menace. So the solid waste mangemnet is a major research area. This section includes major obstacles and current scenario of SWM in India. It also covers source reduction techniques and highlights on waste segregation.

### 2.1 Obstacles

Guerrero et al. conducted a comprehensive analysis on stakeholders regarding challenges in SWM in mixed culture cities of India and arrived at the major challenge that local public in the region is equally responsible with the municipality for solid waste management.(Guerrero et al., 2013). Chakrabarti et al. had studied Public-community participation in household waste management for the Baranagar area of Kolkata in India and suggested that the door to door collection is not proper and emphasized on a society involvement as the public residing in the area are well educated(Chakrabarti et al., 2009). Some major obstacles from the literatures are as below

- Failure of program/policies: Although separate categories have been specified for wet, dry, hazardous and C & D wastes, a separate category for sanitary waste is missing(Mani & Singh, 2016). Therefore there is a need to modify categorization of waste. According to a case study of Puducherry, a coastal city of India, a Strong solid waste management system is required for heritage places in India (Rajamanikam et al., 2014).
- Behaviour and public attitude: Generally people have unwillingness to cooperate as they are not aware of severity and problems in Solid waste management. Stakeholder-based SWOT analysis in Lucknow-India explains society's Not in My Backyard (NIMBY) syndrome and Who cares syndrome, they wait for action from government (Srivastava et al., 2005). They can be directed by local policies on the daily amount of waste generated (Mani & Singh, 2016).
- Household segregation of waste: Though local authorities recommended separating dry and wet waste, it is not practiced in some cities. This is the responsibility of the waste generator. Therefore a strong and independent authority is needed and there is a need to raise responsibility by awareness programs to regulate waste management.(Kumar et al., 2017).

- Lack of environmental awareness: There is a gap in information and communication between local management and society people. Public participation at the early stage of SWM can minimize the risks and increase their awareness of waste management (Ma & Hipel, 2016). There should be environmental education, awareness and training programs for sanitary workers and community people. There is a need to increase knowledge about problems faced in MSW management through media efforts by television or newspapers targeting waste reduction techniques at personal level because just by public awareness campaigning over some period of time will not work to change the behavior of society(Huang, 2016). Now when they are aware of the issues, they require some help to convert the knowledge to actions. Community can not notice the link between increased waste generation and filling and closing of costly landfill sites (Lober, 1996).
- COVID 19 pandemic: There are some challenges in solid waste management during and after COVID 19 pandemic which demands a great attention of the government. Some waste management priorities include clear communication regarding safe practice of handling and disposal of waste, making sure that workers involved at all stages are well equipped with PPE and there is a dire need to study the dynamics of solid waste generated(Sharma et al., 2020).

## 2.2 Current Scenario

Municipal solid waste is of mixed nature and includes varied waste components. For the management of such mixed waste streams, it cannot be described by a single approach so the Environmental Protection Agency developed a hierarchical structure for MSW. It is made up of four levels ordered from most favored-source reduction and reuse, recycling or composting, energy recovery, treatment and disposal. Source reduction is at the highest rank. This includes reducing the waste at the source level which results not only in reduction of the burden on successive stages of collection, transportation and disposal but also its environmental impacts.

The Ministry of Environment and Forests (MoEF) is taking care of the issues related to solid waste management together with Central and State Pollution Control Boards. Status of the Municipal Solid Waste Management at different stages in all States/UTs of India is given below
Solid Waste Generation:1,52,076 TPD
Solid Waste Collection:1,49,748TPD
MSW Treated:55,759 TPD
Landfilled:50,161 TPD
Total Landfill Sites:21 Nos operational

According to the annual report-2019 of MOEF, there is lack of coordination between Urban Development Departments (UDDs), Urban Local Bodies (ULBs) & State Pollution Control Boards (SPCBs) and other stakeholders, who are involved in implementation of SWM Rules, 2016. In addition, MSW dumped to the landfill sites is mixed waste without segregation which causes open fire for example it happened at Ahmedabad's Pirana landfill site in 2017 and it took 3 days to put out the fire. Apart from these, in many cities of India, management of landfill sites and related health and environmental hazards becomes a critical issue. Some programmes of environmental awareness like segregation of dry and wet waste and no use of 'single-use' plastic items are operational under MOEF. Some tools used to develop mass awareness are rallies, door-

to-door campaigns and environmental film festivals. Ahluwalia & Patel had collected data as given in Table 1 on source segregation and collection of waste for some cities as reported by cities themselves. It shows that there is no segregation at source in large cities and some medium sized cities. Therefore there is a need to investigate for sorting of waste at source in India. The various treatment methods practiced in India for MSW and other similar types of waste are: Composting, landfills, Thermal processes (incineration, pyrolysis) etc.

| City | State | Population (million) | segregation at source(%) | City | State | Population (million) | segregation at source(%) |
|------|-------|----------------------|--------------------------|------|-------|----------------------|--------------------------|
| Mumbai | Maharastra | 20 | - | Ludhiana | Punjab | 1.7 | - |
| Delhi | - | 19.1 | - | Chandigarh | - | 1.2 | - |
| Bengaluru | Karnataka | 10.4 | 50 | Mysuru | Karnataka | 1 | 55 |
| Channai | Tamil Nadu | 10 | - | Warangal | Telangana | 0.9 | NA |
| Hyderabad | Telangana | 9.1 | - | Tirunelveli | Tamil Nadu | 0.5 | 100 |
| Ahmedabad | Gujarat | 7.5 | - | Alappuzha | Kerala | 0.2 | 76 |
| Surat | Gujarat | 5.8 | 12 | Suryapet | Telangana | 0.1 | NA |
| Pune | Maharastra | 5.8 | 52 | Gangtok | Sikkim | 0.1 | 30 |
| Indore | Madhya Pradesh | 2.5 | 53 | Panaji | Goa | 0.07 | 90 |
| Bhopal | Madhya Pradesh | 2.1 | NA | | | | |

Table 1: estimation of source segregation for some cities of India (Ahluwalia & Patel, 2018)

### 2.3 Source Reduction

It is the most fascinating technique for waste management as it does not incur any cost at all. MSW contains paper, textiles, leather, plastic, metal parts, glass, ash and others. The composition varies depending on weather, the location, and living standards of community. The household MSW consists of a major portion of compostable matters and plastic. Plastic is an inevitable part of MSW. Studies show that some fungi for example Aspergillus niger can degrade plastic up to some extent (Nandan et al., 2017). It can also be used in road construction to some extent however still today there are no proper alternatives to plastic waste. Source reduction can be by following ways,

- Least use of virgin materials: The practice of following industry standards for product packaging and manufacturing that call for the use of less materials and by passing the laws related to minimum use of virgin material in production.
- Sorting at source: For source segregation, public actions can become very helpful in successive waste processing. The sorting can be of everyday newspaper items, electronics items, metal parts, plastic bags. Mandatory sorting for the public by authorities and allocation of service and equipment for the same can be considered. Recycling and processing at source assist in waste reduction at source. For example garden waste and fruits and vegetables waste can be composted locally. Community compost plants can be

one of the approach to reduce the cost of waste processing at different stage according to the optimization model developed for Mumbai city in India (Rathi, 2007).

- Penalty and incentives: Charging of fees for the generator in case of increasing waste quantity and variable rate per ton of waste which impulse the generator to reduce the amount of waste. Besides, a scheme of providing incentives to those who use recyclable materials and contribute in some way to minimization of solid waste as if reducing plastic footprint. There can be a more discounted rate for the purchase of products in concentrated form for example laundry detergents and different cleaners. This will also reduce related packing materials.

## 2.4 Waste segregation

It is one of the major obstacles in MSW management. In India, MSW is actually a mixed waste because of lack of community awareness (Nandan et al., 2017). Although some plastic, paper waste and electronic waste are separately taken up by scrap dealers, it seems that the community is less involved in managing it this way. MSW is divided into dry recyclable materials e.g. glass, paper, plastics, cans etc., bio-waste and garden waste, hazardous materials, construction and demolition waste, and mixed waste. The waste collection and sorting points-Dhalaos are running short of space to compile the amount of waste coming to the point and it becomes an obligation for the municipality to remove it. The rag pickers involved here are women and children with unhygienic conditions. Thus New Delhi Municipal council (NDMC) had started converting these dhalaos to scientific transfer stations (CPHEEO, 2016). To avoid such situations, some actions are required at the source level where it is generated. It can be sorting of waste and recycling from household level and composting at the local level. There is a need to develop a waste management plan that impulses the public to segregate their waste and a facility for local composting can contribute a lot to waste management. Community response in one of the studies is that they do not have space to keep many dustbins at home for segregation of waste (Rajamanikam et al.2014). Design of dustbin for segregation of waste is one of the research areas.

## 3. Results and Discussion

The principal observations as a concern to public involvement to municipal solid waste management from the review are summarized here. Literatures suggest that society participation is the most demanding situation in SWM. Public-private partnership can improve the service provided and efficiency of SWM to some extent (Ahmed and Ali, 2004) but less cooperation of people lead to failure of their policies. Waste can be sorted majorly as kitchen waste, recyclable items, garden waste and hazardous waste. Some recyclables like paper, plastics, metal were sold as scrap items though it is not followed by majority of people. Some waste items like textiles, rubber, ceramics and garden waste are always remain unrecovered and increase waste.

- One of the concern for sorting of waste is design of waste bins should be such that it mandate public to segregate waste i.e. Compartmental waste bin. Timing of waste collection is also one of the issue as generally morning time is the busy schedule for everyone. Moreover, ''No Segregation, No Collection'' slogan can work effectively.
- Behavior and attitude of public can be changed by awareness and realization of the problems in SWM. For these, mass Celebration of important environmental days and short film making competition can work. Hand in Hand India, An international NGO

based in Tamilnadu, the annual report 2019-20 depicts involvement of women in converting garbage vulnerable points to beautiful rangoli as a solution to trash accumulation to make Bhargah in Odisa a cleaner place. Such plan can be implemented in all states of India.

- There can be local landfill sites and small pits in each area which will serve the purpose of realization of solid waste generated in cities. Therefore decentralized disposal of MSW is suggested.

- At an individual level, public can bring their own bag for groceries, use of refill packs, buying concentrated form of cleaners, borrow/sharing of  rare used items, donate unwanted items, use of rechargeable batteries.

- Waste reduction urges national, state and local level policy interference regarding packaging materials, E-waste, biomedical waste, restrictions on certain non decomposable materials, incentives for reducing plastic footprint and for rewards against returning recyclables. There should be program which link buyers and sellers for secondhand items. The non-decomposable items should be banned.

- Suppliers for a product are responsible for generating waste related to packging of product under the Extended Producer Responsibility. This is applied to equipments like refrigeration, air conditioners, computers, newspapers and milk pouch. Milk is used vastly in all household and commercial buildings and at many places it is not segregated from other household waste therefore there can be policy that ask consumer to return milk pouch before buying.

## 4. Conclusion

Solid state management is important for public health and also to preserve natural environment. It is recognized that many policies and programs fail due to transparency and awareness between stakeholders and local government. Waste disposal is end of pipe treatment approach instead source reduction should be emphasized. Source reduction especially public involvement has influence on all successive stages of SWM. Apprehension of SWM problems by public is the top most priority for maximum participation. The study opens the way for designing local composting practice and design of compartmental waste collection bins at household level. Such transformation can function for environmentally strong solid waste management system and for sustainable development of Indian cities.

**References:**

Ahluwalia, I. J., & Patel, U. (2018). Solid Waste Management in India An Assessment of Resource Recovery and Environmental Impact. *Indian Council for Research on International Economic Relations*, *356*, 1–48.

Bhide, A. D., Sundaresan, B. B. (1983). Solid    Waste    Management    in    Developing Countries. India: Indian National Scientific Documentation Centre, New Delhi.

Chakrabarti, S., Majumder, A., & Chakrabarti, S. (2009). Public-community participation in household waste management in India: An operational approach. *Habitat International*, *33*(1), 125–130. https://doi.org/10.1016/j.habitatint.2008.05.009

CPHEEO. (2016). MUNICIPAL SOLID WASTE Part I. *Ministry of Urban Development*, 1–96. http://www.smmurban.com/uploads/swm/SWM Manual/Book 1.pdf

Guerrero, L. A., Maas, G., & Hogland, W. (2013). Solid waste management challenges for cities in developing countries. *Waste Management*, *33*(1), 220–232. https://doi.org/10.1016/j.wasman.2012.09.008

Huang, H. (2016). Media use, environmental beliefs, self-efficacy, and pro-environmental behavior. *Journal of Business Research*, *69*(6), 2206–2212. https://doi.org/10.1016/j.jbusres.2015.12.031

Kumar, S., Smith, S. R., Fowler, G., Velis, C., Kumar, S. J., Arya, S., Rena, Kumar, R., & Cheeseman, C. (2017). Challenges and opportunities associated with waste management in India. *Royal Society Open Science*, *4*(3). https://doi.org/10.1098/rsos.160764

Kuniyal, J. C., Jain, A. P., & Shannigrahi, A. S. (1998). Public involvement in solid waste management in Himalayan trails in and around the Valley of Flowers, India. *Resources, Conservation and Recycling*, *24*(3–4), 299–322. https://doi.org/10.1016/S0921-3449(98)00056-1

Lober, D. J. (1996). Municipal Solid Waste Policy and Public Participation in Household Source Reduction. *Waste Management & Research*, *14*(2), 125–143. https://doi.org/10.1177/0734242x9601400203

Ma, J., & Hipel, K. W. (2016). Exploring social dimensions of municipal solid waste management around the globe – A systematic literature review. *Waste Management*, *56*, 3–12. https://doi.org/10.1016/j.wasman.2016.06.041

Mani, S., & Singh, S. (2016). Sustainable Municipal Solid Waste Management in India: A Policy Agenda. *Procedia Environmental Sciences*, *35*, 150–157. https://doi.org/10.1016/j.proenv.2016.07.064

Ministry of Environment and Forest, G. of I. (2019). Annual Report 2019-2020. *Current*, 252.

Miranville, A. (2020). Annual report 2019. *AIMS Mathematics*, *5*(1), i–v. https://doi.org/10.3934/math.2020i

Nandan, A., Yadav, B. P., Baksi, S., & Bose, D. (2017). Recent Scenario of Solid Waste Management in India. *World Scientific News*, *66*, 56–74. www.worldscientificnews.com

Narayana, T. (2009). Municipal solid waste management in India: From waste disposal to recovery of resources? *Waste Management*, *29*(3), 1163–1166. https://doi.org/10.1016/j.wasman.2008.06.038

Parekh, H., Yadav, K., Yadav, S., & Shah, N. (2015). Identification and assigning weight of indicator influencing performance of municipal solid waste management using AHP. *KSCE Journal of Civil Engineering*, *19*(1), 36–45. https://doi.org/10.1007/s12205-014-2356-3

Rajamanikam, R., Poyyamoli, G., Kumar, S., & Lekshmi, R. (2014). The role of non-governmental organizations in residential solid waste management: A case study of

Puducherry, a coastal city of India. *Waste Management and Research*, *32*(9), 867–881. https://doi.org/10.1177/0734242X14544353

Rathi, S. (2007). Optimization model for integrated municipal solid waste management in Mumbai, India. *Environment and Development Economics*, *12*(1), 105–121. https://doi.org/10.1017/S1355770X0600341X

Sharma, H. B., Vanapalli, K. R., Cheela, V. S., Ranjan, V. P., Jaglan, A. K., Dubey, B., Goel, S., & Bhattacharya, J. (2020). Challenges, opportunities, and innovations for effective solid waste management during and post COVID-19 pandemic. *Resources, Conservation and Recycling*, *162*(May), 105052. https://doi.org/10.1016/j.resconrec.2020.105052

Srivastava, P. K., Kulshreshtha, K., Mohanty, C. S., Pushpangadan, P., & Singh, A. (2005). Stakeholder-based SWOT analysis for successful municipal solid waste management in Lucknow, India. *Waste Management*, *25*(5), 531–537. https://doi.org/10.1016/j.wasman.2004.08.010

Tchobanoglous, G., Theisen, H., & Vigil, S. A. (2015). Integrated solid waste management: engineering principles and management issues. McGraw-Hill(India) Private limited

# Influence of Eco-Friendly Chemicals on Swell, Shrinkage and Strength Characteristics of Alluvial Soil

*Manisha C. Solanki, Dr. Manish V. Shah*

Department of Civil Engineering, Engineering College Tuwa-Godhra, Godhra-389 001, Gujarat, INDIA
Department of Applied Mechanics, L. D. College of Engineering, Ahmedabad-320 008, Gujarat, INDIA
mannu721996@gmail.com, mobile number- (+91) 7777930984
drmvshah@ldce.ac.in, mobile number- (+91) 94267 24617

## Abstract

In soil stabilization methods, many chemicals are used in geotechnical engineering field to improve soil properties. But the use of certain chemicals is hazardous to the environment, such as the use of lime emits carbon dioxide and if we use cement or flyash it also harms the environment, so the use of such chemicals is not appropriate.  In this present work, using Potassium Carbonate and Calcium Disodium EDTA to increased alluvial soil properties and this chemicals are does not harm the environment, which means that the use of those chemicals are eco-friendly.  After observing the natural characteristics of alluvial soil, the alluvial soil properties are increased by adding some chemical for increase its strength and other relevant characteristics such as Atterberg limits, swelling and shrinkage characteristics, Maximum Dry Density and Optimum Moisture Content. In this research paper, using Potassium Carbonate and Calcium Disodium EDTA as a chemical admixture in alluvial soil and observed the behavior of alluvial soil. After the adding chemical in different various proportion such as 0, 1.0, 1.5 and 2.0 percent respectively, the value of maximum improved on characteristics of soil in adding 1.0 percent of Potassium Carbonate and as well as also improved by adding 1%  of Calcium Disodium EDTA. Thus present study reflects effective use of such chemicals based on soil surface chemistry and proves to be eco-friendly.

## Keywords

Alluvial soil, shrinkage, swell, MDD &OMC, Potassium Carbonate, Calcium Disodium EDTA;

## 1. Introduction

In geotechnical engineering works, huge amount of soil material is widely used in many structures such as, railway embankment, highway embankment, dams, canals, filling low laying areas, backfilling of retaining walls and many more civil structures. The need for soil is high for all the construction works, so its availability is also required in large quantities. If there is construction work in urban areas, it is difficult to get the soil and even in this, soil availability in good quality is a challenge. Due to all these difficulties, we should use soft soil, but when it comes to soft soil like alluvial soil its strength is not so good, so its quality is enhanced by using some kind of additive admixtures to increase its characteristics and it is then used in civil construction works. Stabilization of soil is one of the techniques to improve the quality of the subgrade soil. Many admixtures are used to increase soil characteristics. But some admixtures are harmful to the environment. For example, in the production of lime, carbon dioxide ($CO_2$) gas is emitted in large quantities and also in the production of cement, carbon dioxide ($CO_2$) gas

is emitted. One ton of cement production produces one ton of carbon dioxide ($CO_2$) gas, which is harmful to the environment, and certain chemicals such as aluminium chloride ($AlCl_3$), ferric chloride ($FeCl_2$) and ammonium chloride ($NH_4Cl$) and fly ash also are harmful to the environment.

From the past literature study, Bujang B. K. Huat et al.(2005), in his study to treated the soil by using cement and lime chemical admixtures and improved the soil strength and engineering properties of the soil.N. L. Hussey et al.(2010), in their study, taken flyash, cement kiln dust and lime as a chemical admixture and recommended that the surface area is perhaps the most important factor in determining if chemical additive will be effective for soil stabilization. P. Ramesh, A.V. Narasimha Rao et al.(2012), observed the efficacy of sodium carbonate and calcium carbonate is stabilizing a black cotton soil. The efficacy of calcium carbonate is much better than sodium carbonate from strength and stability point of view. Both the chemicals ($Na_2CO_3$ and $CaCO_3$) are equally effective at optimum percentage of the chemical in reducing the plasticity characteristics of expansive soil.A. Athanasopoulou et al.(2014), in his study using lime and flyash as an admixture in highway subgrade soil and results that the improved California bearing ratio value and also increased bearing capacity of the soil. G. Radhakrishnan et al.(2014), in his investigation, Magnesium Chloride ($MgCl_2$), Aluminum Chloride ($AlCl_3$) and also flyash are taken as a chemical admixture and treated the expansive soil subgrade. And observed the results that effective use of these chemicals are increased soil properties. L.S. Subramanyam et al.(2015), in their investigation, using ferric chloride as an additive admixture in soil and observed that this chemical is very effective in improved of strength and deformation characteristics expansive soil subgrade of Konaseema Region.M. V. Shah and Deepika Rathore et al.(2016), in their studies, to taken polyvinyl alcohol (PVA) and polyvinyl chloride (PVC) and β- Cyclodextrin by treated the expansive soil and improved the swelling and shrinkage characteristics of the soil. Magdi M. E. Zumrawi et al.(2016), in their studies, used three types of chloride salts such as $AlCl_3$, $FeCl_2$ and $NH_4Cl$ in various proportion on expansive clay and observed results that improved the expansive soil characteristics. Roop Kishor et al.(2017), studied that used rice husk ash, sugar cane, bagasse ash and cow dung in road subgrade soil, and observed results that are significantly improved in CBR value and UCS value of subgrade soil. Dr. M.V. Shah et al.(2017), studied that use of chemical additives in bentonite clay and observed the behaviour of soil then he was concluded that the use of chemicals is very improved the swelling and shrinkage characteristics of bentonite clay. Haibo Wang et al.(2017), in their research work found that the various proportion of cement, lime and fly ash are used in alluvial soil and it was very effective on properties of soil and increased unconfined compression strength of alluvial soil. Rodrigo Beck Saldanha et al.(2018), in their studies, using industrial residues such as carbide lime for soil stabilization.Mohammed N. J. Alzaidy et al.(2019), recommend that the cement, lime and flyash are very effective chemicals in alluvial soil properties and it is increased workability, durability, strength and also improved in swelling and shrinkage characteristics of the alluvial soil.Vishal Narnoli et. al.(2019), in his studies, used lime, marble dust and burnt brick dust in various proportion in soil and showed the results that increased the strength of alluvial soil properties and it was used in road construction works. S. K. Belal Hossen et al.(2020), in their investigation, using fine content, lime content and carbonation process in the soil. And observed that increased unconfined compressive strength of the soil.

Most of all above the chemicals are generally affected to environment by direct or indirect manner. In this research study, the alluvial soil is modified with using different chemical

admixtures such as, Potassium Carbonate ($K_2CO_3$) and Calcium Disodium EDTA.The Calcium Disodium EDTA is safe as used in cosmetic formulation (Rebecca S. Lanigan,2002). And the Potassium Carbonate as low hazard to the environment. Potassium and Carbonate ions are naturally found widely in the environment, and thus the substance will have little impact (Evonic Industries, 2014).Which means that the Potassium Carbonate is slightly harmful to the aquatic environment but the Calcium Disodium EDTA is safe for environment.For this reason, the Calcium Disodium EDTA is more eco-friendly chemical compared to the Potassium Carbonate.These chemicals are used in various proportion such as 0%, 1.0%, 1.5% and 2.0% respectively by weight of the alluvial soil.

## 2. Materials and Methods

### 2.1 Materials

Alluvial soil, Potassium Carbonate and Calcium Disodium EDTA

1. **Alluvial Soil:** Alluvial soil was collected from Mahisagar River, Anand District, Gujarat. The alluvial soil is fine-grained fertile soil deposited by flowing water, over flood plains or in river beds. Alluvial soil is generally formed by almost eroding rock through water and flowing with water and deposited, where the stream or river are slows down. It consists of silty and clayey and some part of the sand are present. The present of mineral is generally kaolinite. The classification of soil is CL type.

2. **Potassium Carbonate:** The chemical formula of Potassium Carbonate is $K_2CO_3$. It is inorganic compound. It is also known as Carbonate of Potash or Dipotassium Carbonate or Carbonate of Pearl ash. Potassium Carbonate is made by potassium hydroxide with carbon dioxide.  The use of potassium carbonate in made of glass, soap and china production. The application of potassium carbonate is used as an ingredient in welding fluxes, and in the flux coating on arc-welding rods, as an animal feed ingredient to satisfy the potassium requirements of farmed animals such as broiler breeders.

3. **Calcium Disodium EDTA:** The full form of EDTA is Ethylenediaminetetraacetate. It is used in food ingredient such as flavor of foods, color and texture. It is also used in production of cosmetic material and industrial production. Soaps, shampoos, lotions and contact lens solutions are examples of cosmetic and personal care products that may contain calcium disodium EDTA. It is also used in chelation therapy.

### 2.2 Methods

The finding of the natural properties of Alluvial soil such as natural water content, specific gravity, liquid limit, plastic limit, shrinkage limit, swelling pressure, free swell index, maximum dry density, optimum moisture content and unconfined compressive strength by laboratory performance using Indian Standard code IS: 2720.
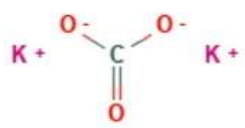
## 2.3 Properties of Alluvial Soil

Table 2.1: Properties of Alluvial soil

| Sr. No. | Parameter | Alluvial soil | Unit |
|---|---|---|---|
| 1. | Natural Water Content | 20.31 | % |
| 2. | Liquid Limit | 32.8 | % |
| 3. | Plastic Limit | 17.5 | % |
| 4. | Classification | CL | - |
| 5. | Shrinkage Limit | 12.01 | % |
| 6. | Volumetric Shrinkage | 29.97 | % |
| 7. | Linear Shrinkage | 12.28 | % |
| 8. | Shrinkage Ratio | 1.69 | - |
| 9. | Swell Pressure | 0.22 | kg/ cm$^2$ |
| 10. | Free Swell Index | 20 | % |
| 11. | Specific Gravity | 2.0 | - |
| 12. | Maximum Dry Density | 1.952 | g/cc |
| 13. | Optimum Moisture Content | 14.58 | % |
| 14. | Unconfined Compressive Strength | 0.94 | Kg / cm$^2$ |

## 2.4 Properties of Chemical Admixture

Table 2.2: Properties of Chemical Admixture

| Sr. No. | Parameters | Calcium Disodium EDTA | Potassium Carbonate |
|---|---|---|---|
| 1. | Chemical formula | $C_{10}H_{14}CaN_2O_8$ | $K_2CO_3$ |
| 2. | 2D Structure |  |  |
| 3. | pH | 6.5-7.5 | 11.6 |
| 4. | Density | - | 2.29 g/cc |
| 5. | Molecular Weight | 376.286 g/mol | 138.205 g/mol |

| 6. | Market price | Rs. 1100/- per 500 gm | Rs. 320/- per 500 gm |
|---|---|---|---|

## 2.5 Preparation of Chemical Solution:

The chemicals such as Potassium Carbonate and Calcium Disodium EDTA are used in different proportion in Alluvial soil, such as 0%, 1.0%, 1.5% and 2.0% respectively.

1. **Potassium Carbonate Solution:** Take 1 gm of Potassium Carbonate in solid form and add 1.25 ml distilled water in it and dilute it. After some time, the solution is cooled position, then we can used the solution in different proportion such as 0%, 1.0%, 1.5% and 2.0% respectively.
2. **Calcium Disodium EDTA Solution:** Take 1 gm of Calcium Disodium EDTA in solid form and add 5 ml distilled water in it and dilute it. After some time, the solution is cooled position, then we can used in different percentage in Alluvial soil.

## 3. Results, Analysis and Discussion

According to adding various doses of both the chemical solutions in alluvial soil, obtained the results are given below:

1. Liquid Limit:

Table 3.1: Comparison of Liquid limit of Alluvial soil, $K_2CO_3$ and Calcium Disodium EDTA

| Soil Sample | $K_2CO_3$ (%) | Calcium Disodium EDTA (%) |
|---|---|---|
| **Untreated, 0%** | 32.8 | 32.8 |
| **1%** | 26.1 | 26.9 |
| **1.5%** | 27.9 | 33.1 |
| **2%** | 33.4 | 33.4 |
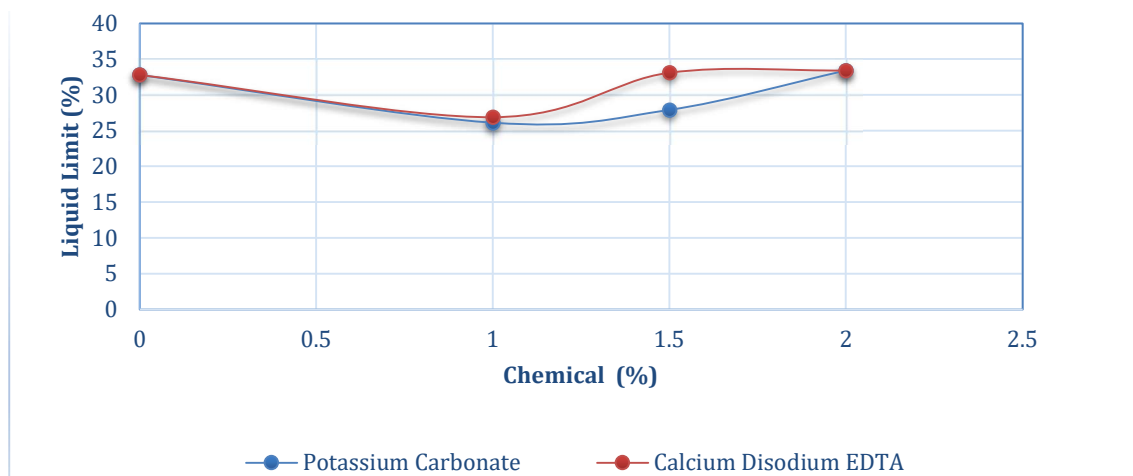


Fig. 3.1 Liquid limit VS Chemical in % of Alluvial soil

From the Fig. 3.1, observed that the potassium carbonate and calcium disodium EDTA reduce liquid limit by 20.42% and 17.98% respectively by addition of 1.0% of chemicals.
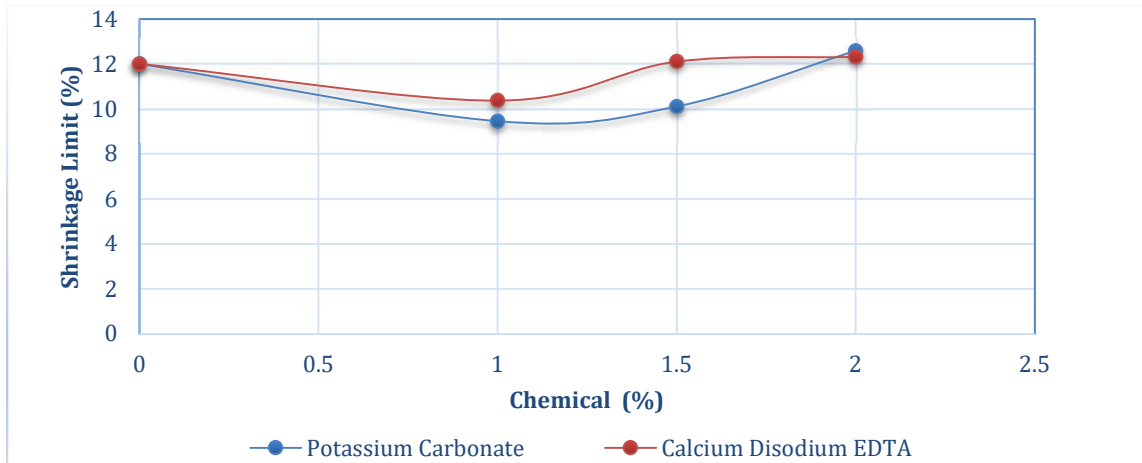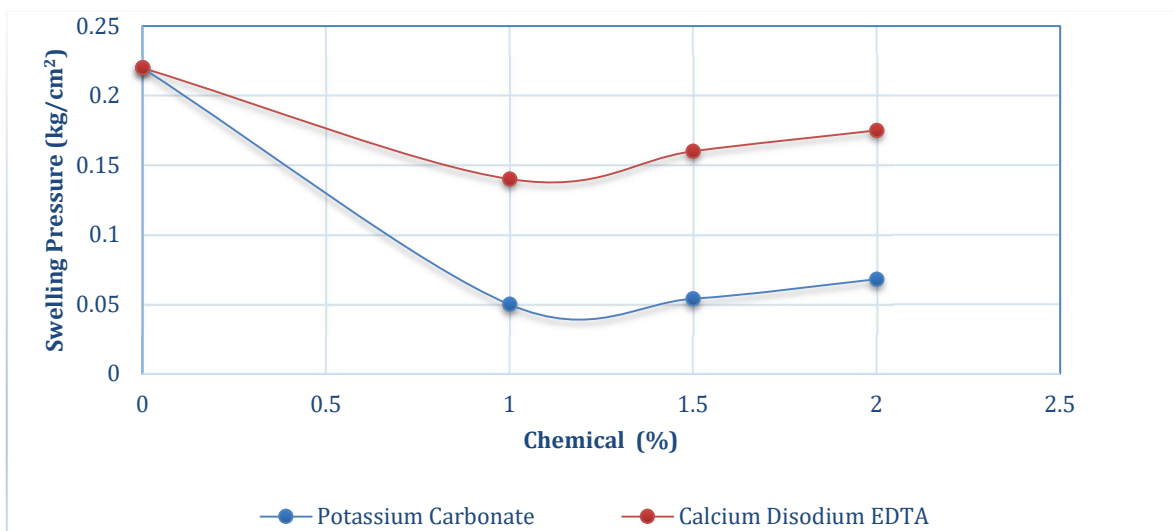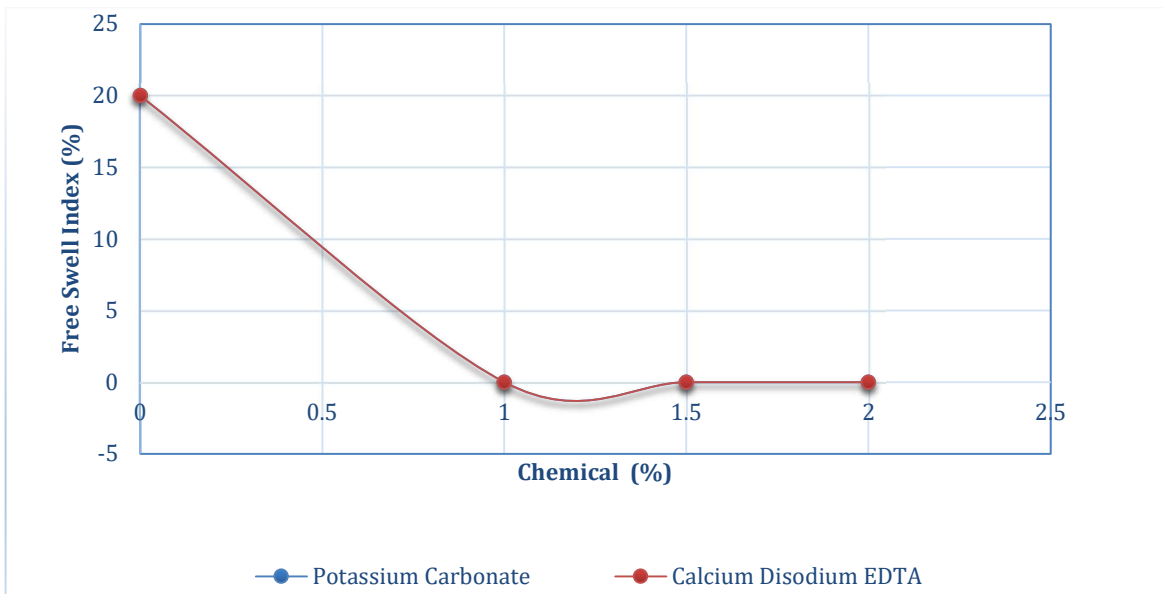
2. Plastic Limit:

Table 3.2: Comparison of Plastic limit of Alluvial soil, $K_2CO_3$ and Calcium Disodium EDTA

| Soil Sample | $K_2CO_3$ (%) | Calcium Disodium EDTA (%) |
|---|---|---|
| Untreated, 0% | 17.5 | 17.5 |
| 1% | 15.2 | 15.8 |
| 1.5% | 15.8 | 17.6 |
| 2% | 18.1 | 17.9 |
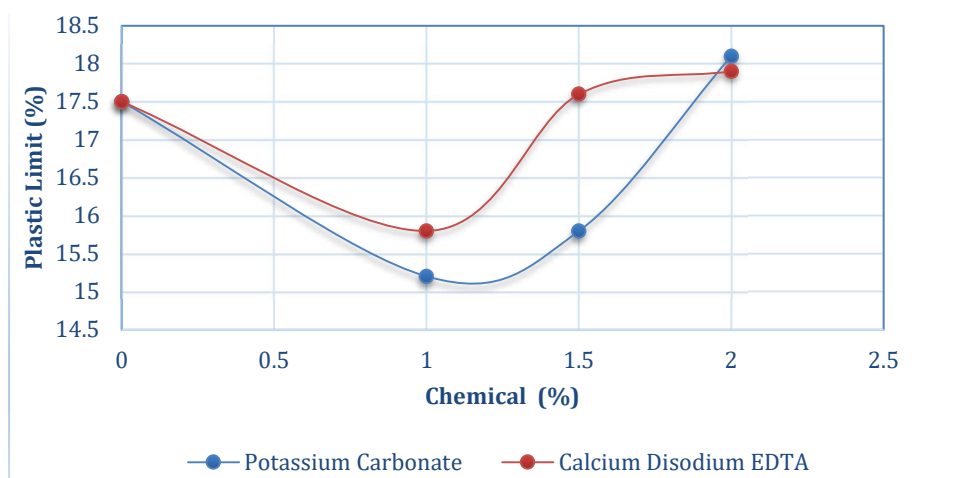


Fig. 3.2 Plastic limit VS Chemical in % of Alluvial soil

From the Fig. 3.2, observed that the potassium carbonate and calcium disodium EDTA reduce plastic limit by 13.14% and 9.71% respectively by addition of 1.0% of chemicals.

3. Shrinkage Limit:

Table 3.3: Comparison of Shrinkage limit of Alluvial soil, $K_2CO_3$ and Calcium Disodium EDTA.

| Soil Sample | $K_2CO_3$ (%) | Calcium Disodium EDTA (%) |
|---|---|---|
| Untreated, 0% | 12.01 | 12.01 |
| 1% | 9.46 | 10.38 |
| 1.5% | 10.12 | 12.12 |
| 2% | 12.59 | 12.32 |

From the Fig. 3.3, it is observed that the potassium carbonate and calcium disodium EDTA reduce shrinkage limit by 21.23% and 13.57% respectively by addition of 1.0% of chemicals.

Fig. 3.3 Shrinkage limit VS Chemical in % of Alluvial soil

4. Swell Pressure:

Table 3.4: Comparison of Swelling Pressure of Alluvial soil, $K_2CO_3$ and Calcium Disodium EDTA

| Soil Sample | $K_2CO_3$ (kg/cm$^2$) | Calcium Disodium EDTA (kg/cm$^2$) |
|---|---|---|
| Untreated, 0% | 0.22 | 0.22 |
| 1% | 0.05 | 0.14 |
| 1.5% | 0.054 | 0.16 |
| 2% | 0.068 | 0.175 |



Fig.. 3.4 Swell pressure VS Chemical in % of Alluvial soil

From the Fig. 3.4, it is observed that the potassium carbonate and calcium disodium EDTA reduce swelling pressure by 77.27% and 36.36% respectively by addition of 1.0% of chemicals.

5. Free Swell Index:

Table 3.5: Comparison of Free Swell Index of Alluvial soil, $K_2CO_3$ and Calcium Disodium EDTA

| Soil Sample | $K_2CO_3$ (%) | Calcium Disodium EDTA (%) |
|---|---|---|
| Untreated, 0% | 20 | 20 |
| 1% | 0 | 0 |
| 1.5% | 0 | 0 |
| 2% | 0 | 0 |



Fig.3.5 Free swell index VS Chemical in % of Alluvial soil

From the Fig. 3.5, it is observed that the potassium carbonate and calcium disodium EDTA reduce free swell index by 100% with addition of 1.0%, 1.5% and 2.0% of chemicals respectively.

6. Maximum Dry Density:

Table 3.6: Comparison of Maximum Dry Density of Alluvial soil, $K_2CO_3$ and Calcium Disodium EDTA

| Soil Sample | $K_2CO_3$(g/cc) | Calcium Disodium EDTA (g/cc) |
|---|---|---|
| Untreated, 0% | 1.952 | 1.952 |
| 1% | 1.975 | 1.968 |
| 1.5% | 1.915 | 1.945 |
| 2% | 1.923 | 1.920 |
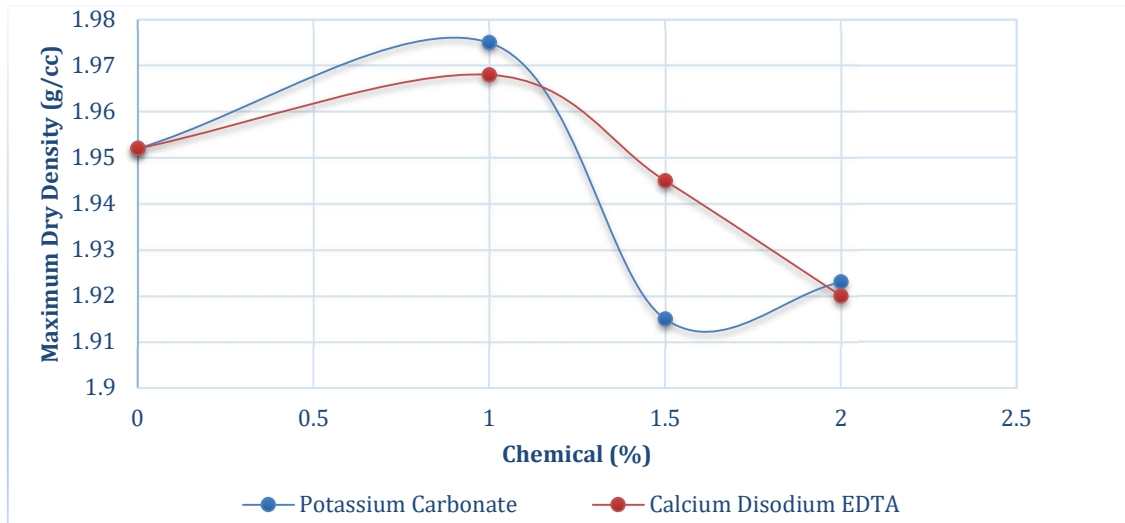
Fig. 3.6 Maximum Dry Density VS Chemical in % of Alluvial soil

From the Fig. 3.6, it is observed that the potassium carbonate and calcium disodium EDTA increasis maximum dry density by 1.18% and 0.88% respectively by addition of 1.0% of chemicals.

7. Optimum Moisture Content:

Table 3.7: Comparison of Optimum Moisture Content of Alluvial soil, $K_2CO_3$ and Calcium Disodium EDTA

| Soil Sample | $K_2CO_3$ (%) | Calcium Disodium EDTA (%) |
|---|---|---|
| Untreated, 0% | 14.58 | 14.58 |
| 1% | 13.49 | 13.65 |
| 1.5% | 14.38 | 14.42 |
| 2% | 15.03 | 14.89 |
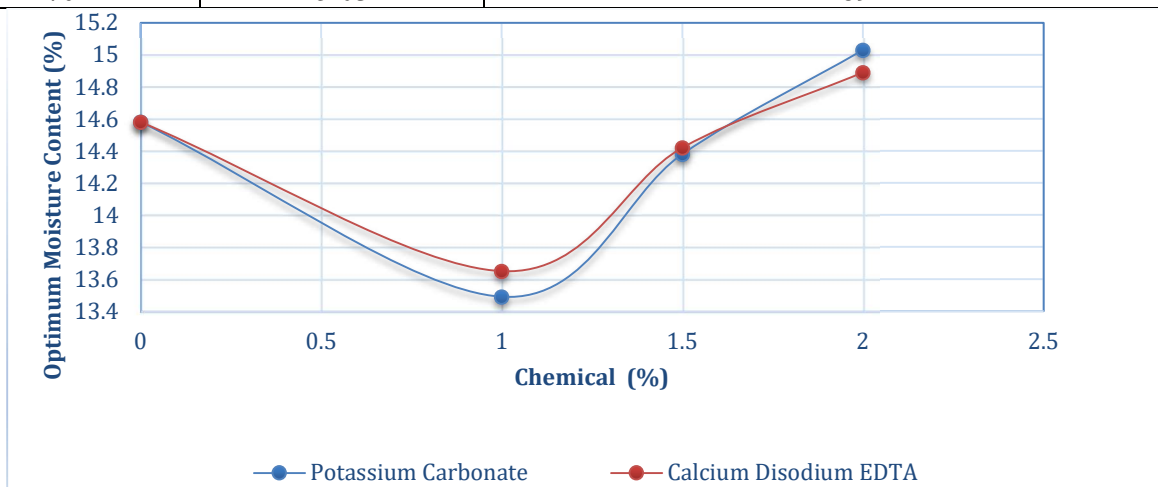


Fig. 3.7 Optimum Moisture Content VS Chemical in % of Alluvial soil

From the Fig. 3.7, it is observed that the potassium carbonate and calcium disodium EDTA are reduce optimum moisture content by 7.47% and 6.38% respectively by addition of 1.0% of chemicals.

## 4.Conclusions

It is revealed from the above study that chemicals have good potential for use in geotechnical applications.  The soilchemistry interaction gives true insight of ions responsible for swelling and shrinkage. In present study use of chemicals viz. Potassium Carbonate and Calcium Disodium EDTA gives very effective results in reducing shrinkage and swell characteristics of alluvial soil.

The following conclusions were drawn from experimental works:

- The illite mineral consists of an alumina sheet sandwiched between the silica sheets, forming a structural unit. The silica sheets are joined by the oxygen atom and the presence of potassium as bonding material between two structural units makes the minerals swell less.
- When potassium carbonate ($K_2CO_3$) is added to the soil, the potassium ($K^+$) ion forms a KOH ion by chemical reaction with the hydroxyl ($OH^-$) of aluminium sheet. Due to which water cannot enter the structure of the soil and this reduces the swelling and shrinkage characteristics of alluvial soil.
- Similarly, when Calcium Disodium EDTA is added to the soil, sodium($Na^+$) ion chemically reacts with the hydroxyl ($OH^-$) of aluminium sheet to form NaOH ion, which prevents water from entering the soil structure and significantly reduces soil swelling and shrinkage characteristics.
- This chemical reaction greatly improves the swelling and shrinkage characteristics of alluvial soil.
- Adding 1.0 percent of both chemicals is seen to maximize soil characterization. Both of these chemicals make a very effective change in alluvial soil.
- Present study reveals the use of such chemicals as they are eco-friendly and non-toxic in nature. Use of potassium and carbonate are found naturally and results indicate their effective in reducing swelling and shrinkage characteristics of alluvial soils. The results overall promote the use of chemicals based on surface chemistry and its interaction with active ions can play vital role in mitigating shrinkage and swelling potential of weak soils.

**References**

1. A. Athanasopoulpu (April-2014), "Addition of Lime and Fly Ash to Improve Highway Subgrade Soils", by Published in Journal of Materials in Civil Engineering, Vol. 26, No. 4, ASCE, ISSN 0899-1561.
2. Bujang B. K. Huat (2005), "Effect OF Chemical Admixtures on the Engineering Properties of Tropical Peat Soils", American Journal of Applied Sciences2(7):1113-1120, ISSN 1546-9239.

3. Dr. M. V. Shah, Dr. H. J. Pandya and A. D. Shukla (2017), "Influence of chemical additives on Shrinkage and Swelling characteristics of Bentonite clay'', by Published in journal of Science Direct.

4. Evonik Industries AG (2014), GPS Safety Summery $K_2CO_3$.

5. G. Radhakrishnan, Dr. M. Anjan Kumar and Dr. GVR Prasada Raju (2014), "Swelling Properties of Expansive Soils Treated with Chemical and Flyash'', Published in American Journal of Engineering Research.

6. Haibo Wang, An Deng and Ping Yang February-2017, "Strength and Stiffness of Stabilized Alluvial Silt under Frost Action", by Published in Advances in Materia; Science and Engineering, Volume 2017, Article Id-5605471.

7. L. S. Subramanyam, Y. S.G. Govind Babu, Dr. D. S. V. Prasad and G. V. R. Prasada Raju (2015), "Influence of Ferric Chloride on Strength and Deformation Characteristics of Expansive Soil Sub Grades in Konaseema", Published in International Journal of Innovative Research in Science, Engineering and Technology, Vol. 4, Issue. 11.

8. M. V. Shah and Deepika Rathore (2016), "Influence of Polymers on the Swelling and Shrinkage Characteristics of Montmorillonite Clays.",Geo-China, GSP 265 246, © ASCE Journal.

9. Magdi M. E. Zumravi, AllaM. M. Mahjoub and Iman M. Alnour (2016), "Effect of Some Chloride Salts on Swelling Properties of Expansive Soil" by Published in Journal of Research Gate.

10. Mohammed N. J. Alzaidy (January-2019), "Stabilization of Soils Using Chemical Admixtures: A Review", Article in Journal of University of Babylon for Engineering Sciences, Vol. (27), No. (1).

11. N. L. Hussey and A. B. Cerato (2010), "An Assessment of Soil Parameters Governing Soil Strength Increases with Chemical Additives", by Published in Advances in Analysis, Modeling and Design, Geo Florida 2010, GSP 199, ASCE Journal.

12. P. Ramesh, A.V. Narasimha  Rao and N. Krishna Murthy (2012), "Efficacy of Sodium Carbonate and Calcium Carbonate in Stabilizing a Black Cotton Soil.", Published in International Journal of Emerging Technology and Advanced Engineering, ISSN 2250-2459, Vol. 2, Issue 10.

13. Rebecca S. Lannigan and Torill A. Yamarik (2002),"Final Report on the safety Assessment of EDTA, Calcium Disodium EDTA, Diammonium EDTA, Dipotassium EDTA, Disodium EDTA, TEA-EDTA, Tetrasodium EDTA, Tripotassium EDTA, Trisodium EDTA, HEDTA and Trisodium HEDTA", by Published in International Journal of Toxicology.

14. Rodrigo Beck Saldanha and Hugo CarloseScheuemann Filho (2018), "Physical Mineralogical-Chemical Characterization of Carbide Lime: An Environment-Friendly Chemical Additive for Soil Stabilization", by Published in Journal of Civil Engineering, ASCE, ISSN 0899-1561.

15. Roop Kishor and S. K. Suman (February-2017), "Stabilization of Alluvial Soil for Subgrade using Rice Husk Ash, Sugarcane Bagasse Ash and Cow Dung Ash for Rural Road", by Published in Science Direct, 254-261.

16. S. K. Belal Hossen (2020), "Elemental Testing of Carbonated Silty Sand Treated with Lime", Geo Congress, GSP 315, ASCE Journal.

17. Vishal Narnoli and Rajnish Kumar (March-2019), "Stabilization of Alluvial Soil using Marble Dust, Lime and Burnt Brick Dust for Road Construction", Indian Conference on Geotechnical and Geo-Environmental Engineering, by Published in Research Gate.

18. Bryan AJ (1988), "Criteria for the suitability of soil for cement stabilization", Building and Environment 23(4): 309-319.

19. British Geological Survey Heeral, M., SadaiahEggadi and Uma Maheswara Rao, O. (2006), Article of "Ground Shrinking and Swelling", "Stabilization of Poorly Graded sand with Lime-Flyash", Proceedings of Indian Geotechnical Conference IGS, Volume 2, pp. 755-757.

20. Sivapullaiah P.V. and Han Prasad Reddy P. (December 2006), "Stabilization of soil containing interstratified minerals with KOH", Proceedings of Indian Geotechnical Conference IGS-2006,Volume 2, 1416, IIT, Madras, Chennai, Organized by Indian Geotechnical Society Chennai Chapter, pp. 883-886.

21. Tapash Kumar Roy, B. C. Chattopadhyay and S, H, Roy (2010), "Effect of Alternative Materials on Engineering Properties of Alluvial Soil for Construction of Road Subgrade", by Published in Traffic and Transportation Studies, ASCE Journal.

22. Wei Wang, Zongwei CHEN and Tao LIU (2012), "Potential Impacts of Different Chemical Deicing Salts on Soil Health along Roadsides", CICPT 2012, ASCE Journal.

23. Belabbaci, Z., Mamoune, S.M.A. and Bekkouche A. (2013), "Laboratory study of the influence of mineral salts on swelling (KCl, $MgCl_2$).", Earth Science Research. Vol.2, (Issue 2), pp.135-142.

24. Ciancio D, Jaquin P, Walker P (2013), "Advances on the assessment of soil suitability for rammed earth", Construction and Building Materials 42: 40-47.

25. S. Boudaghpour and F. Majdzadeh (2014), "Environmental Effects Lime on Mechanical Characteristics of Stabilized Closed Texture", by Published in International Journal of Geology, Vol:8.

# Influence of blending proportion on properties of melt spun monofilaments produced from virgin PET and recycled PET blend

*Nabo Kumar Barman, S. S. Bhattacharya, Aadhar A. Mandot*

Department of Textile Engineering, Faculty of Technology and Engineering,
The Maharaja Sayajirao University of Baroda, Kalabhavan, Vadodara – 390 001, Gujarat, India

*Corresponding Author: nabo.barman@gmail.com

## Abstract

Mechanical recycling of post-consumer polyethylene terephthalate (PET) bottles provides a sustainable, green, environmental friendly and cost-effective solution. In the present study, influence of blending recycled PET flakes with virgin PET on melt flow rate, boiling water shrinkage, tensile properties, melting behavior, crystalline behavior, molecular confirmation and yellowing effect is reported. The virgin-PET/recycled-PET blended yarn samples are produced by introducing R-PET in the proportions of 0%, 50%, 60%, 70%, 80%, 90% and 100%. The blend homogenization, melt spinning and drawing is carried out sequentially to produce monofilament yarn samples. The virgin PET sample has highest intrinsic viscosity, boiling water shrinkage stability, molecular weight, and crystallinity. The blended yarn samples with R-PET content of 50-80% have performed marginally similar in terms of tensile stress and strain. The loss of tensile stress and strain is significant when R-PET content in blend is above 80%. IR spectra confirmed presence of hydroxyl and carboxyl groups with –OH links which induces thermo-mechanical degradation of PET. The whiteness, brightness and reflectance values decreases in contrast to yellowing index which increases on introducing R-PET content in blend. This study recommends blend produced from mechanical recycling process should restrict the recycled PET content to 70-80%, in order to accomplish minimum desired yarn properties for average strength applications with cost-reduction, minimising environmental impact and raw material conservation.

## Keywords

PET bottle recycling, mechanical recycling, virgin PET, recycled PET, blending, PET monofilaments.

## Abbreviations

PET - polyethylene terephthalate

PP – polypropylene

PE – polyethylene

PA – polyamide

PC-PET (PET-bg) – post-consumer polyethylene terephthalate bottle grade

R-PET (rPET) – recycled polyethylene terephthalate bottle flake

V-PET (vPET) – virgin polyethylene terephthalate pellet

DMT – dimethyl terephthalate

TPA – terephthalic acid

EG – ethylene glycol

BHET – bis(hydroxyethyl) terephthalate

NERU – non-renewable energy use

GHG – greenhouse gas

GWP – global warming potential

V-PET/R-PET – virgin PET and recycled PET blend (proportions in weight)

MFR – melt flow rate (gram/10 minute)

IV – intrinsic viscosity (dL/gram)

## 1. Introduction

Polyethylene terephthalate (PET) is classified as a semi-crystalline thermoplastic polymer produced from either Dimethyl terephthalate method (DMT) or Terephthalic acid (TPA) method. In the former method, the product bis(hydroxyethyl) terephthalate (BHET) is obtained from ethylene glycol (EG) and dimethyl terephthalate (DMT) by transesterification reaction. In the latter method, bis(hydroxyethyl) terephthalate (BHET) is obtained from ethylene glycol (EG) and terephthalic acid (TPA) by esterification reaction. Further, the polymerization of BHET yields polyethylene terephthalate often recognized as PET. PET bottles are produced through blow moulding process by air blowing and stretching the amorphous PET perform (Awaja & Pavel, 2005).

PET possess good barrier, chemical, thermal and mechanical properties. It is used worldwide to produce range of products such as bottle and food containers, textiles (fiber and fabric), nets, strappings, foils, films, resins, automotive parts, electrical insulation, acoustics, packaging material, civil engineering, geotechnical and industrial applications (American Chemistry Council, 2016). The identification of PET resin can be done with the code printed on various products as represented in Figure 1. The modest cost along with associated properties such as clear and transparent color, light weight, absence of Bisphenol-A, good impact behavior, shelf life, chemical resistance and barrier properties against light, gas, and microorganisms made PET favorable for application in water or beverage bottles. Food grade application recommends use of virgin PET due to health concern. Therefore, more often post-consumer PET (PC-PET) bottles are considered as a single use material. A major share of the PC-PET bottles are discarded which contributes in landfills and ocean pollution. The slow rate of natural decomposition of PET poses threat to manage the quantum of solid waste. The photolytic and hydrolytic degradation under natural environment more often alters surface chemistry; the bulk polymer under accelerated ageing requires a temperature closer to glass transition temperature for possible decomposition reaction (Sang et al., 2020). The biological degradation entails intricate process and is economically not viable (Awaja & Pavel, 2005). The PET waste management can be regulated by opting for either incineration or recycling process. The incineration process with energy recovery is an acceptable solution considering its lower acidification potential with reduced burden on fossil fuel requirement (Aryan et al., 2019). However, recycling is advantageous in contrast to incineration considering low emission of pollutant particles, greenhouse gas, heavy metal, and dioxins with considerable quantity of raw material savings (Aryan et al., 2019; Chilton et al., 2010). The thermoplastic nature of PET polymer makes it worthy for remoulding and recycling process. There is a growing intent towards sustainability by implementing 3-R concept – reduce, recycle and reuse. Recycling of PET into fibers and filaments is advisable considering improved societal

awareness, responsibility and imposition of stringent law and regulations for environmental protection. PC-PET recycling provides a sustainable solution by second life to product, solid waste management, availability of R-PET at cheaper rates, limits virgin raw material dependency, reduced energy requirement, and lower processing cost.

According to the data obtained from National Association for PET Container Resources (NAPCOR), PET bottle recycling in United States stands at 29.2% in 2017. The major share 47% of the R-PET produced was used in fiber production. The other uses includes 21% as food and beverage bottles, 19% in sheet and film production, 8% as strappings, 4% in non-food bottles and 1% others (NAPCOR (National Association for PET Container), 2018). Globally, out of the total PC-PET flakes collected, fiber production and bottle to bottle conversion contributes to 72% and 10%, respectively (Shen et al., 2010, 2011). The European nations have made significant progress in PET recycling compared to the rest of the world. The recycling of PC-PET bottle is greatly influenced by the type and the concentration of foreign matter (contaminants) such as water, colouring matter, acetaldehyde, PVC, PA, PP, PE, acid generating substances, pesticides, and detergents (Awaja & Pavel, 2005; Itim & Philip, 2015). Appropriate means of waste collection system, sorting and segregation methods is of utmost importance involved in PET recycling. According to (Gomes et al., 2019), there is a need for consideration of social and economic analysis and energy efficient recovery routes apart from the environmental impact for selecting PET recycling methods.

The recycling of PC-PET is broadly categorized into primary (re-extrusion), secondary (mechanical), tertiary (chemical) and quaternary (incineration with energy recovery) recycling methods. The mechanical recycling method is again sub-categorized as – flake to fiber conversion process (mechanical recycling), flake to pellets and pellets to fiber conversion process (semi-mechanical recycling) (Shen et al., 2010). The tertiary recycling method is sub-categorized as – hydrolysis (disintegration into TPA and EG), methanolysis (break down into monomers- DMT and EG), glycolysis (disintegration into oligomer-BHET), aminolyis and ammonolysis (Shen et al., 2010; Sinha et al., 2010). Among the chemical recycling methods, glyclolysis method is the elementary, and economical method and it should be assisted by catalyst (Campanelli et al., 1994; Chen & Chen, 1999). Methanolysis process yields superior PET grade, but has the highest environmental impact compared to glycolysis, mechanical and semi-mechanical recycling methods (Shen et al., 2010). The chemical recycling involves disintegration of PET molecule into the monomers or oligomers. This process can yield PET with high purity and has a wider application range. The chemical recycling method is recommended for bottle to bottle recycling due to fulfilment of food grade packaging safety standards. The PC-PET to fiber conversion using chemical recycling is expensive in contrast to mechanical recycling process (Shen et al., 2010). The bottle to bottle recycling through super-clean recycling processes is not a very economical means considering insignificant cost reduction in contrast to the processing cost involved for bottle production from virgin PET. However, the major push to bottle to bottle recycling is due to increased awareness and reforms for environmental conservation and sustainability (Welle, 2011). Implementation of European Recycling Regulation 282/2008 has made it mandatory for individual recycling process to get acceptance from European Food Safety Authority (EFSA). The super-clean recycling processes involving bottle to bottle recycling has been considered hazard-free (Welle, 2013). The life cycle analysis and social life cycle analysis of PC-PET bottles in Mauritius was studied (Foolmaun & Ramjeeawon, 2013). The option included landfilling, incineration with energy recovery, flake production and their combinations. They reported that, environmental and social impacts were least for case considering 75% PC-PET flake production and 25% landfilling.

Mechanical recycling is recognized as green technology due to its considerable lower environmental impact. The chemistry of material is not changed during mechanical recycling process. It involves collection of PC-PET bottles, segregation, bailing, flake conversion, cleaning, and melt extrusion. Shen et al. (2010) studied life cycle analysis of PC-PET bottle to fiber conversion. They reported that compared to virgin PET fiber production, PC-PET flake to fiber conversion has a reduced NERU and GWP impact by 40-85% and 25-75% respectively, subjected to recycling method and boundary conditions. Mechanical and semi-mechanical recycling has lower environmental impact in contrast to chemical recycling (via glycolysis method). The mechanical recycling offers substantial environmental protection by regulating parameters such as abiotic depletion, acidification, eutrophication, human toxicity and aquatic toxicity, global warming potential (GWP), and non-renewable energy use (NREU) (Shen et al., 2010). Shen et al. (2011) further reported PC-PET to fiber recycling has lesser environmental impact compared to PC-PET to bottle recycling. The use of bio-based feedstock for PET production minimizes NERU by 21% and GHG by 25%. The recycled bio-based PET has the least impact of NERU and GHG by 35% and 37% respectively. The increase in R-PET content when used for PET production will have positive impact on environment. Multiple recycling of R-PET can have 26% reduction in environmental impacts, which is insignificant after third time recycling (Shen et al., 2011). However, there are certain limitations of mechanical recycling method such as reduction in molecular weight which is assisted by presence of water and other impurities causing chain-scission reactions. They are less often recommended for food-grade applications (Sinha et al., 2010).

Mechanical recycling of PET offers advantage in form of environment and economic considerations. Fann et al. (1997) reported V-PET has higher crystallinity in contrast to R-PET when both are spun at similar speed. However, at high spinning speed crystallinity reduces with increase in R-PET content due to strain induced crystallization. They reported marginal boiling water shrinkage for crystalline structures. The tensile strength increases and elongation decreases when R-PET is spun at higher speed. The drawing process improves tensile properties, but R-PET possesses poor ability for drawing as compared to V-PET. The fully drawn R-PET irrespective of possessing 70% of tensile strength compared to V-PET can be suitably used to meet requirements of industrial applications (Fann et al., 1997). V-PET/R-PET blend has exhibited good compatibility and miscibility without phase separation. The static, dynamic and cyclic fatigue behavior of V-PET/R-PET blend offers acceptable properties. Increase in R-PET content has offered an increase in tensile strength with minor enhancement in crystallinity and reduced elongation (Elamri et al., 2007). According to the investigation by Lee et al. (2013) R-PET exhibited a faster rate of crystallization and lower thermal stability as compared to V-PET. Melting temperature decreases on increasing R-PET content in blend. Drawn fiber yield higher tensile strength, modulus and birefringence with lower elongation, attributed to improved orientation. The V-PET/R-PET blend with 70% composition exhibited similar mechanical behavior as compared to 100% V-PET (Lee et al., 2013).

The increase in number of extrusion cycles causes break in ester bond of PET dominated chain scission leads to reduced molecular weight of polymer, viscosity, modulus and toughness. PET degradation is associated with formation of cyclic oligomeric species (with glycol unit) increases evident from forth reprocessing cycle (López et al., 2014). Repeated reprocessing cycle leads to increase in crystallinity, reduced melt flow rate with reduction of plastic deformation ability was reported (Badía et al., 2009). The thermal behavior of R-PET contaminated with PP was studied along with the effect of multiple extrusion cycles (Itim & Philip, 2015). A reduction in nucleation rate, spherulite development and crystallinity with increase in molecular movement (melt flow) was observed both for PP contaminated R-PET

and multiple extrusion cycles and was attributed to cross-linking of PP with R-PET, copolymer grafting, chain scission and extension. Eccentric rotor extruder based on elongational flow field was employed to recycle PET was reported (Wu et al., 2019). The R-PET produced was found to have superior mechanical properties except toughness, retaining molecular weight of polymer in contrast to R-PET processed on a twin-screw extruder with shear flow field. Another study investigated the possibility of R-PET flakes to be reused for food packaging applications. They observed yellowing of the R-PET, without any hazardous metal traces. They suggested use of R-PET is safe to consider for food grade packaging application (Masmoudi et al., 2018). An intensive study was carried out by Berg et al. (2016) to understand the discoloration of R-PET. The presence of grey color in R-PET is attributed to the presence of antinomy metal based catalyst residues. However, yellow color is associated with the either thermo-oxidative reaction during PET extrusion or formation of azomethine structures on exposing polyamide (used as barrier layers in PET bottles) to higher temperature (Berg et al., 2016).

Efforts were made by various researchers to understand the mechanical, thermal, and rheological behavior of R-PET material. This paper is intended to improve the understanding on the influence of R-PET content in blended yarn subjected to melt flow rate analysis, viscosity measurement, hot water thermal stability, tensile test, melting and crystallization, absorption behavior and molecular confirmation through IR spectrum, and color change (yellowing effect). This study is intended to estimate the optimum amount of R-PET which can be accommodated in V-PET/R-PET blend without compromising the minimum property requirement suited for average tenacity applications.



Figure 1. Resin code for identification of PET product (American Chemistry Council, 2016).

## 2. Materials and methods

### 2.1 Raw materials

The virgin PET fiber grade polymer pellets was scoured from Reliance Industries, Gujarat, India. The R-PET bottles (transparent in color) were supplied by a local supplier.

### 2.2 Material Processing

#### 2.2.1 Impurities removal

The process for R-PET bottles into flakes conversion followed by decontamination and cleaning of R-PET flakes has been shown in Figure 2. The removal of impurities and moisture from R-PET flakes has a significant role in mechanical properties of R-PET yarn.
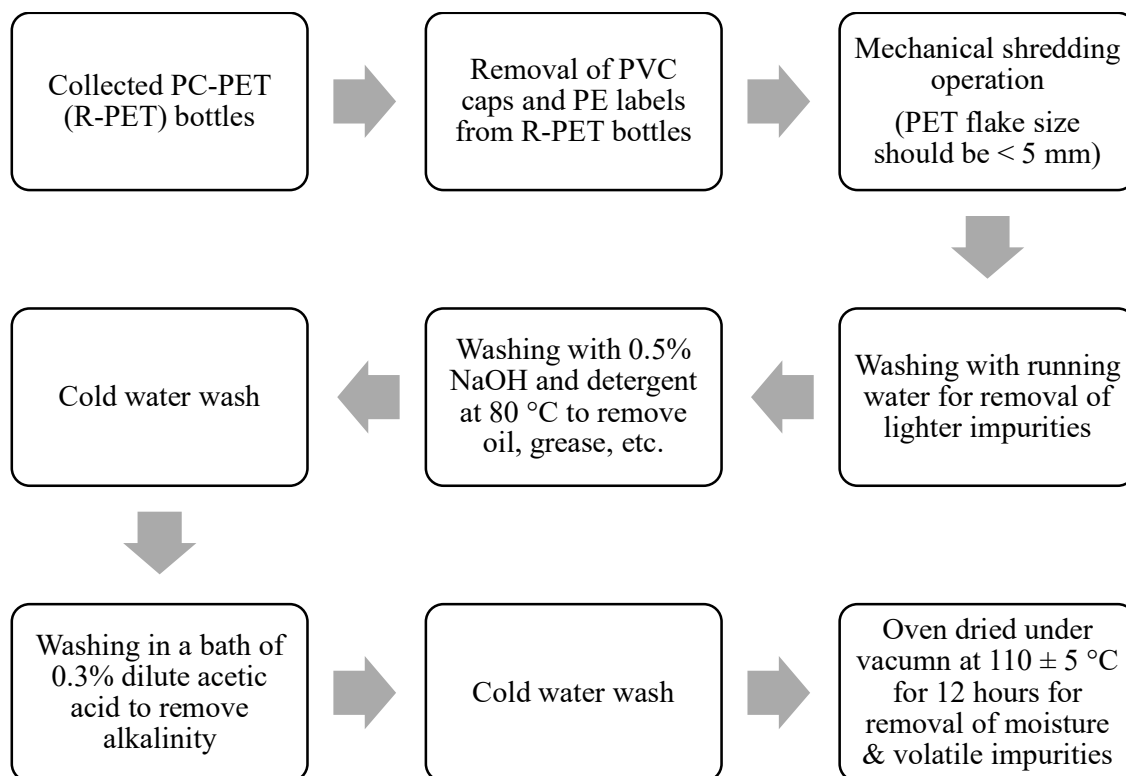
Figure 2. Process flow showing R-PET bottle to flake conversion and removal of impurities (decontamination) from R-PET flakes (Barman et al., 2015).

### 2.2.2 Pelletizing

The pilot scale twin screw extruder was employed to yield good blend homogenization of V-PET and R-PET. A total of five V-PET/R-PET samples were produced at blending proportions of 50/50, 40/60, 30/70, 20/80, and 10/90. The screws with 20 mm diameter were rotating in coaxial direction with 30 rpm speed and temperature was set at $270 \pm 5$ °C. This was followed by pelletizing process where V-PET/R-PET pellets were formed. The pellets were oven dried at 100 °C for 12 Hours to remove the residual moisture.

### 2.2.3 Monofilament production

Melt spinning is carried out for seven samples out of which five samples were in blended pellet form and two additional samples of V-PET/R-PET in following compositions 100/0 (100% V-PET) and 0/100 (100% R-PET). A single extruder pilot melt-spinning machine with a single spinneret hole (0.5 mm nozzle diameter) was employed. The screw was set to rotate at 100 rpm, spinning speed 1500 mpm and temperature was set for extrusion and spinning regions at 275 and 280 °C, respectively. The filament was passed through a cold water bath for quenching of filament. To improve the molecular orientation inside the PET monofilament it was drawn with the aid of hot godet rollers (draw ratio 2.5) and finally wound on package. The melt spinning prototype machine and different zones of the screw extruder are shown in Figures 3 and 4, respectively.
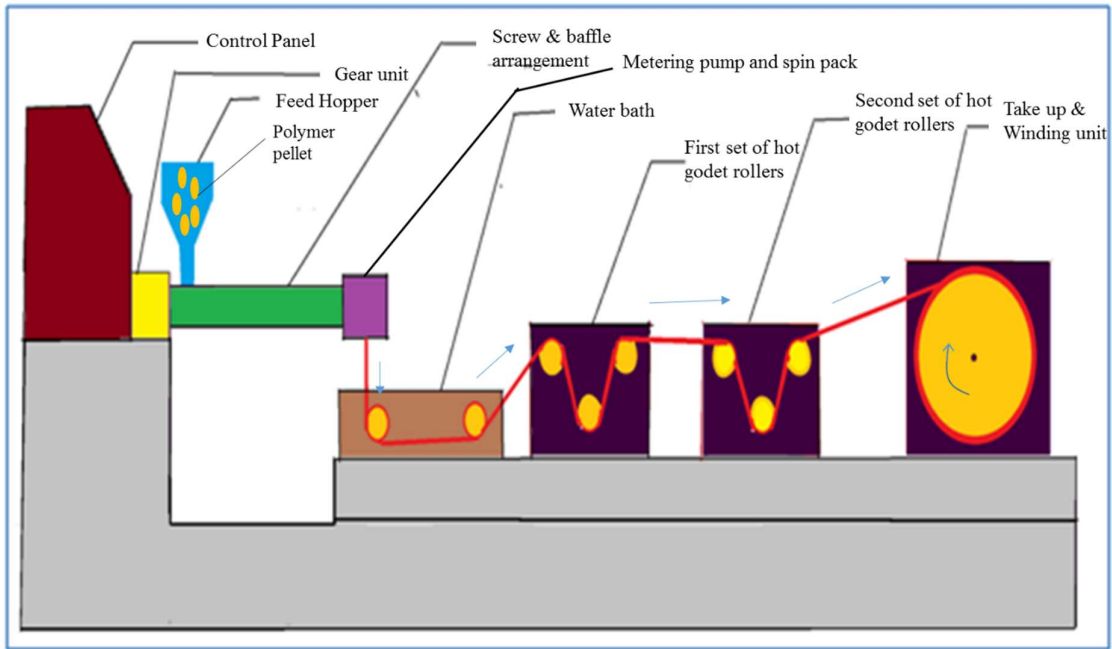
Figure 3. Schematic representation of a pilot scale melt-spinning machine for producing PET mono-filament.
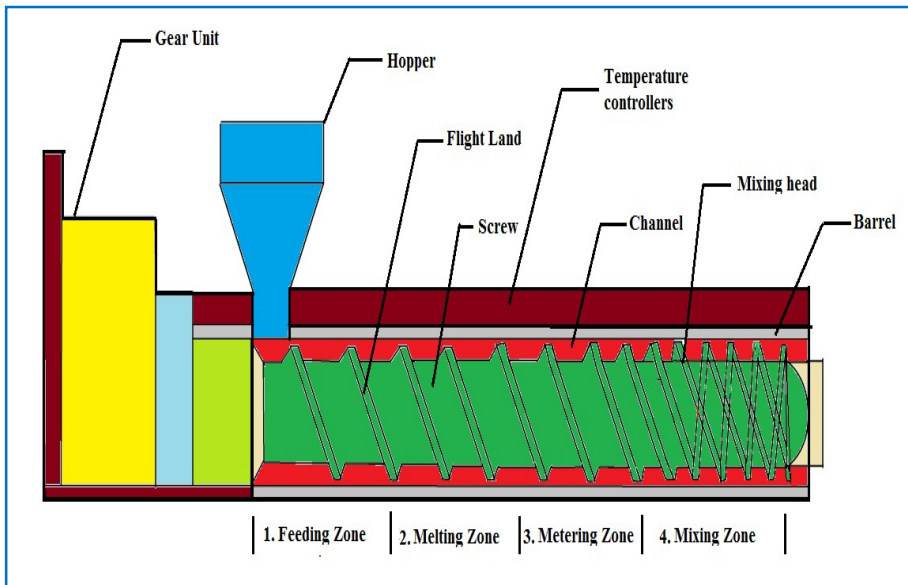


Figure 4. Schematic representation of the different regions inside the screw extruder.

## 2.3 Material test methods

### 2.3.1 Denier measurement

The test was carried out as per ASTM D1907 test method using a wrap reel and weighing balance. It is a representation of linear density of the yarn sample. It is defined as the weight in grams of 9000 meters yarn length. Average of ten reading was considered. The linear density of the yarn sample was 400±3 denier.

### 2.3.2 Melt flow rate and intrinsic viscosity

This melt flow analysis was performed as per ASTM D1238 using extrusion plastometer by Hem- Tech Corporation. The melt flow rate (grams/10 min) was recorded and average of five readings was considered.

Polymer viscosity was measured as per ASTM D4603 test method in an Ubbelohde viscometer. A dilute solution (0.5% ) of phenol and 1,1,2,2- tetrachloroethane was formed at 60/40 (v/v) composition at temperature of 30 °C for dissolution of PET polymer. The intrinsic viscosity was computed using Billmeyer equation as followed in previous research (Berkowitz, 1984).

### 2.3.3 Boiling water shrinkage

This test was performed as per ASTM D2259 on A-one Scientific equipment. The percentage shrinkage (%) of the different monofilament yarn samples was observed when subjected to hot water immersion at 90 °C for 30 minutes.

### 2.3.4 Tensile properties

The test was performed as per ASTM D2256 method on Lloyd LRX material testing machine. Test parameters includes gauge length-250 mm, Test speed-25 mm/min, breaking time-20 ± 3 sec. Average of ten reading was considered.

### 2.3.5 Thermal characterisation

Thermographs of different blended samples were obtained using differential scanning calorimeter of make and model – Perkin Elmer DSC 6000. The test involves a heating run from 20-300 °C, followed by a thermal treatment at 300 °C for 180 seconds to eradicate the previous history and thereafter cooling run (crystallisation) back to 30 °C. The heating and cooling cycle was carried out at a rate of 10 °C/minute, 3 bar pressure and gas flow of 10 mL/minute. The crystallinity (% Xc) of the blended samples was computed using the standard equation (1).

$$X_c(\%) = \frac{\Delta H_m - |H_c|}{\Delta H_m^\circ} \times 100 \quad \text{.... (1)}$$

Where, $\Delta H_m^\circ$ is the heat of fusion of 100% crystalline PET ($\Delta H_m^\circ$= 135.8 J g$^{-1}$) (Starkweather et al., 1983), enthalpy of crystallization ($\Delta H_c$), and enthalpy of melting ($\Delta H_m$).

### 2.3.6 Fourier Transform Infrared (FTIR) Spectroscopy

A computer-assisted Fourier Transform Infrared (FTIR) Nicolet-10 Spectrophotometer (Thermo Scientific) is used in the absorption mode and was set in the range 4000-400 cm$^{-1}$.

### 2.3.7 Whiteness, yellowness, brightness indices reflectance and K/S value

The whiteness, yellowness, brightness indices, and reflectance value of the different PET blended yarn samples were measured using Premier Colour Scan – 5100 Spectrophotometer connected with computer colour matching (CCM) system. The test was done with following test methods- Stephensen (for whiteness), ASTM D1925 (for yellowness) and TAPPI 452/ ISO 2470 (for brightness). The sample was prepared by wrapping the PET monofilament yarn samples on a white hard paper board (50 mm X 40 mm).  The yarn was wrapped in parallel configuration with no interspacing between the adjacent yarn wraps, and that can be correlated as a close packed structure.

## 3. Results and discussion

### 3.1 Influence of V-PET/R-PET blending on Melt flow rate and intrinsic viscosity

The melt flow rate analysis shows an upward trend on increase in R-PET content in the blend, opposite behaviour is found for intrinsic viscosity as shown in Figure 5. The 100% R-PET sample has offered highest MFR value of 85 grams/10 min and lowest IV value of 0.59 dL/grams, respectively. The increase in MFR values is associated with lower molecular weight of R-PET which is attributed to thermo-mechanical degradation and shortening of molecular structure due to chain scission reactions of PET caused during reprocessing which is confirmed through IR analysis. This effect is more evident when PET is subjected to higher reprocessed cycles (Badía et al., 2009).
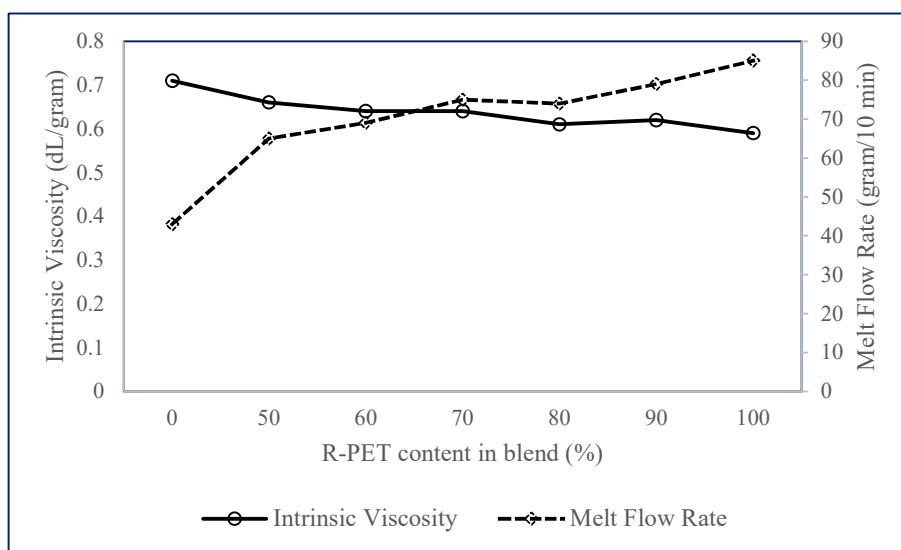


Figure 5. The influence of R-PET content (%) on IV and MFR for V-PET/R-PET blended pellet samples.

### 3.2 Influence of V-PET/R-PET blending on Boiling water shrinkage

There is a marginal change in shrinkage behaviour of blended yarn samples when subjected to hot water as shown in Figure 6. The shrinkage was highest for 100% R-PET yarn sample and lowest for 100% V-PET sample at 6.7% and 5.1%, respectively. This behaviour is attributed to lower thermal stability, orientation and crystallinity of R-PET sample which is confirmed through DSC, IR analysis. On the contrary, R-PET sample has lower molecular weight, shorter length chains and increased molecular mobility due to chain scission reactions which makes the specimen sensitive to boiling shrinkage. The raw material characteristics and composition in blend has an influence on shrinkage (Fann et al., 1997).

### 3.3 Influence of V-PET/R-PET blending on tensile properties

The change in tensile stress and strain values with increasing R-PET content in blended yarn has been shown in Figure 7. The 100% V-PET sample has exhibited the highest tensile stress and strain at 306.7 MPa and 30.17%, respectively. The effect is attributed to the presence of higher molecular weight in V-PET, ordered and crystalline structure, and relatively longer molecular chain. On the contrary, 100% R-PET sample has offered the lowest tensile stress

and strain at 114.40 MPa and 13.24%, respectively. This explanation to this behavior is R-PET has lower molecular weight, short molecular chains, and reprocessing under higher temperature has caused removal of plastic deformation ability. The blended yarn samples with R-PET content of 50%, 60%, 70% and 80% have performed comparable in terms of tensile stress and strain. The loss of tensile stress and strain is significant when blend possess V-PET content less than 20%.
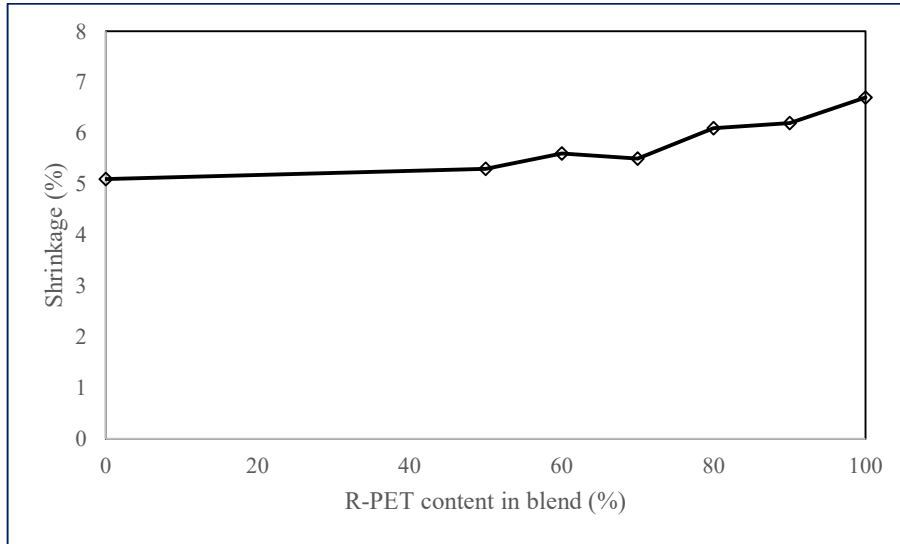


Figure 6. The influence of R-PET content (%) on boiling shrinkage (%) for V-PET/R-PET yarn.



| R-PET content in blend (%) | 0 | 50 | 60 | 70 | 80 | 90 | 100 |
|---|---|---|---|---|---|---|---|
| Tenacity (MPa) | 306.71 | 175.44 | 159.49 | 164.40 | 157.04 | 141.09 | 114.10 |
| Breaking Strain (%) | 30.17 | 18.2 | 16.54 | 17.16 | 16.05 | 15.19 | 13.24 |
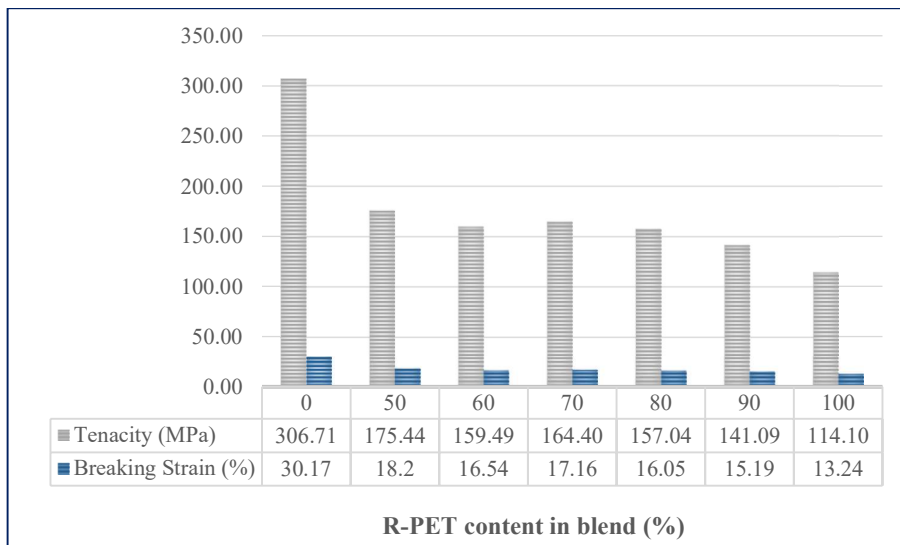
Figure 7. The influence of R-PET content (%) on tenacity (MPa) and breaking strain (%) for V-PET/R-PET yarn.

## 3.4 Influence of V-PET/R-PET blending on melting and crystallisation behavior

The DSC thermographs involving heating and cooling scan for different blend compositions has been shown in Figure 8. The effect of increasing R-PET content in blend on glass

transition temperature, crystalline temperature and melting temperature has been graphically represented in Figure 9. The crystallisation temperature also marginally increases with increase in R-PET content in blend. On observation, it was found that increasing amount of R-PET content in blend causes formation of narrow and long melt-crystallisation peaks. This behaviour is attributed to the faster rate of crystallisation for the R-PET samples in contrast to the V-PET samples. The presence of contaminants in form of traces of metals, chain scission reaction products and oligomers and associated thermal treatment during recycling process opens up the molecular chain to release the residual strain leads to rapid crystallisation of R-PET (Lee et al., 2013). There is a marginal increase in melting temperature with increase in R-PET content in blend. This behavior may attributed to the chain scission reaction occurred during reprocessing of R-PET which may induce crystallization with modification and separation of crystal populations based on crystal dimensions (Badía et al., 2009). Another explanation to this behavior is shorter length molecular chains get accommodated in the long chain polymer network, require high temperature for melting phenomena (Sängerlaub et al., 2020). The glass transition temperature which constitute molecular movement in amorphous region remains almost unaffected except higher glass transition temperature for 100% R-PET sample. The thermographs of all the blended samples have single prominent crystallization and melting peak which confirms the good compatibility and homogeneity within a single phase for both V-PET and R-PET components (Elamri et al., 2007).
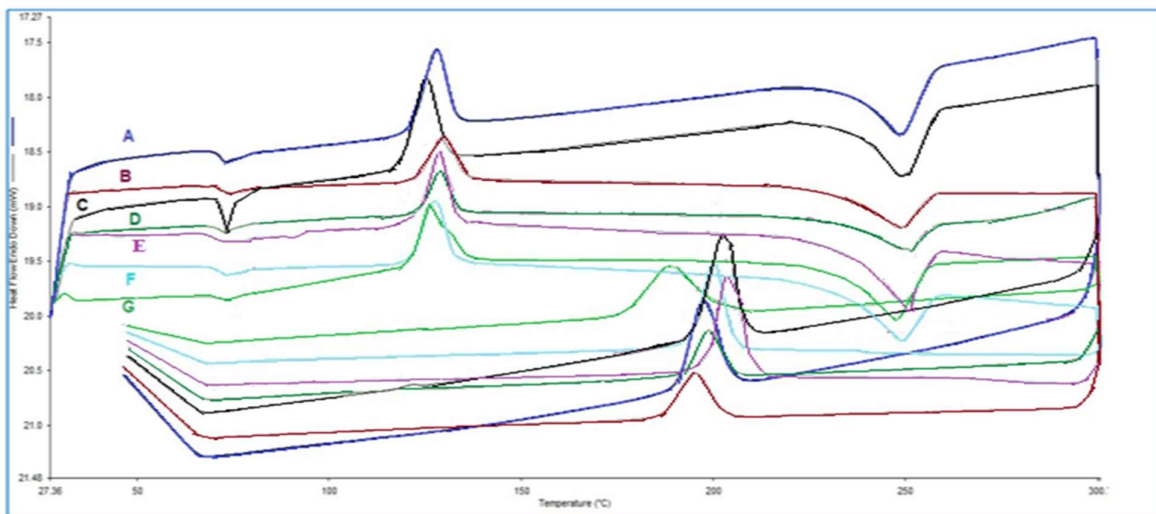


A – V-PET/R-PET (40/60); B – V-PET/R-PET (50/50); C – V-PET/R-PET (10/90); D – V-PET/R-PET (30/70); E – V-PET/R-PET (0/100); F – V-PET/R-PET (20/80); G – V-PET/R-PET (100/0)

Figure 8. DSC Thermographs showing heating and cooling scan for V-PET/R-PET pellets.

The crystallinity (%) of the samples obtained from DSC indicates that crystallinity content in sample gradually reduces with incorporation of R-PET in blend. The 100% V-PET sample have exhibited highest crystallinity of 36.55% and 100% R-PET sample has lowest crystallinity of 17.19%. This result is attributed to the presence of dense closely packed molecular configuration, higher molecular weight and longer molecular chain in V-PET. V-PET achieves high degree of crystallinity through strain induced crystallization during thermal drawing and spinning operation (Fann et al., 1997).
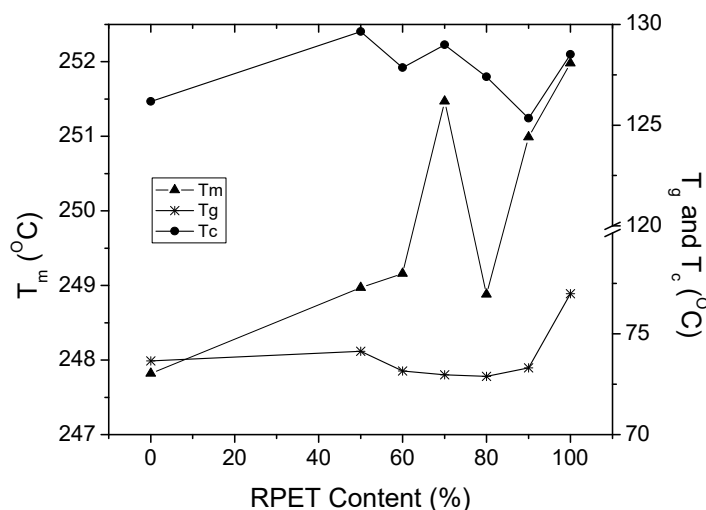
Figure 9. The influence of R-PET content (%) on glass transition temperature, crystalline temperature and melting temperature for V-PET/R-PET pellets.
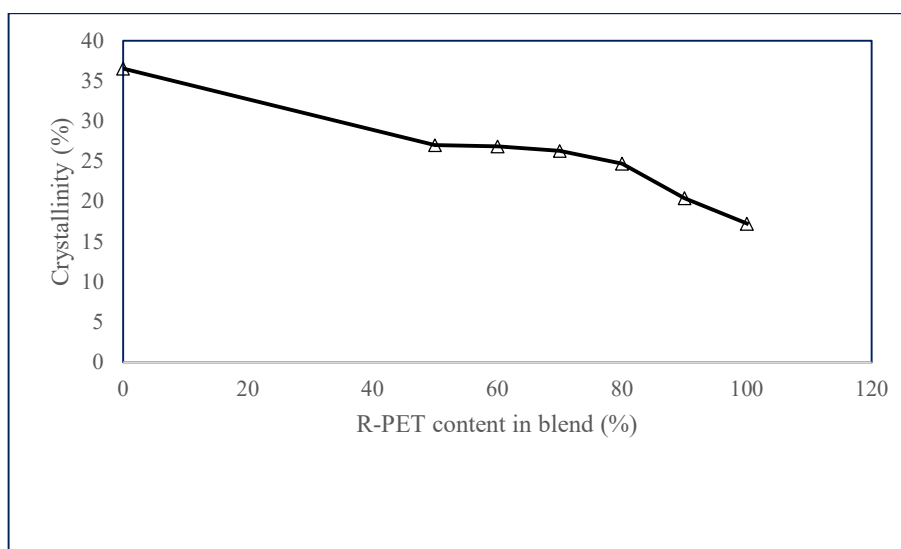


Figure 10. The influence of R-PET content (%) on crystallinity (%) of the V-PET/R-PET pellets.

## 3.5 Influence of V-PET/R-PET blending on Fourier Transform Infrared (FTIR) Spectroscopy

The FTIR spectra of the 100% V-PET and 100% R-PET samples have been shown in Figure 11 and 12, respectively. The spectrum is helpful to investigate molecular conformation of PET, presence of functional groups, orientation, and change in molecular structure (stretching, vibration, bending of bonds).

The IR spectra for 100% V-PET and 100% R-PET show almost similar absorption peaks. The spectra confirm the presence of characteristic absorption peak for PET as shown in Table 1. In contrast to the 100% R-PET sample, 100% V-PET has exhibited higher absorption value

at all the corresponding absorption peaks. This behaviour is attributed to presence of higher crystallinity (%) in V-PET, otherwise also confirmed by DSC result analysis. Similar findings was reported by (Acar et al., 2006).

Formation of new absorption peaks were observed for 100% R-PET sample at 3566 cm$^{-1}$ and 3613 cm$^{-1}$. This behaviour is due to the availability of hydroxyl and carboxyl groups with – OH links, which may be produced due to chain scission (chain cleavage) reaction. This acts as catalyst and causes thermo-mechanical degradation of PET with reduction of molecular weight and viscosity associated with higher polymer mobility (Badia et al., 2012). The increase in – OH species are also responsible for presence of yellow hue in sample and causes discoloration of PET sample. Hydroxyl ions induces hydroxylation of terephthalate ring (Ladasiu Ciolacu et al., 2006).

Table 1. IR peak detection in FTIR spectra for V-PET and R-PET specimen.

| Absorption peak detection at corresponding Wavenumber (cm$^{-1}$) for 100% V-PET sample | Absorption peak detection at corresponding Wavenumber (cm$^{-1}$) for 100% R-PET sample | Explanation (Acar et al., 2006; Badia et al., 2012; Holland & Hay, 2002; Varma et al., 1998) |
|---|---|---|
| 723.50 | 723.39 | Out of plane distortion or bending of two carbonyl substitute on aromatic ring |
| 872.91 | 872.98 | Vibration of aromatic ring with C – H deformation of adjacent hydrogen atoms |
| 1016.20 | 1016.32 | In plane vibration of aromatic ring |
| 1041.71 | | 1, 4-substitution of aromatic ring |
| 1092.31 | 1092.22 | Stretching vibration of C – O bonds associated with semi-crystalline structure of PET |
| - | 1174.38 | Bending vibration of – $CH_2$ group |
| 1239.06 | 1239.17 | Stretching vibration of C – O bonds, associated with parallel dichroism |
| 1339.37 | 1339.28 | Bending vibration of – $CH_2$ group, trans, extended, crystalline. Wagging of the ethyl unit |
| 1370.95 | 1370.96 | $CH_2$ wagging mode of the gauche-conformer, relaxed, amorphous. |
| 1408.24 | 1408.26 | Vibration of aromatic ring |
| 1456.11 | 1456.66 | Reduced intensity in crystallisation process, gauche-conformation of the EG. |
| 1505.50 | 1506.01 | Formation of conjugated aromatic structure |
| 1577.22 | 1577.16 | Formation of conjugated aromatic structure |
| 1715.22 | 1715.46 | Stretching vibration of carbonyl C=O bonds in ester linkage, connected |

| | | with perpendicular dichroism |
|---|---|---|
| 2958.21 | 2962.22 | Aliphatic C – H stretching vibration |
| - | 3566.76 | Associated with moisture absorption or availability of hydroxyl and carboxyl groups with – OH links due to thermo-mechanical degradation |
| - | 3613.14 | Associated with moisture absorption or availability of hydroxyl and carboxyl groups with – OH links due to thermo-mechanical degradation |
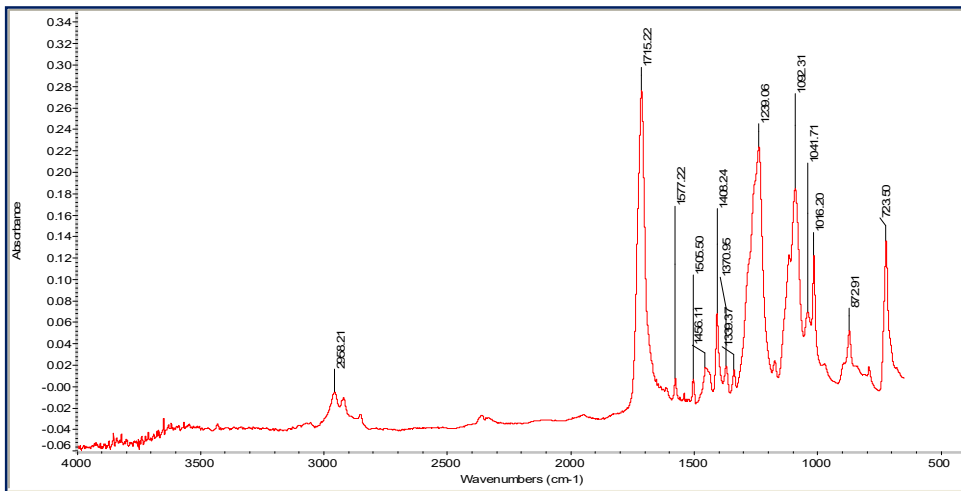


Figure 11. Infra-red spectrum for 100% V-PET sample.
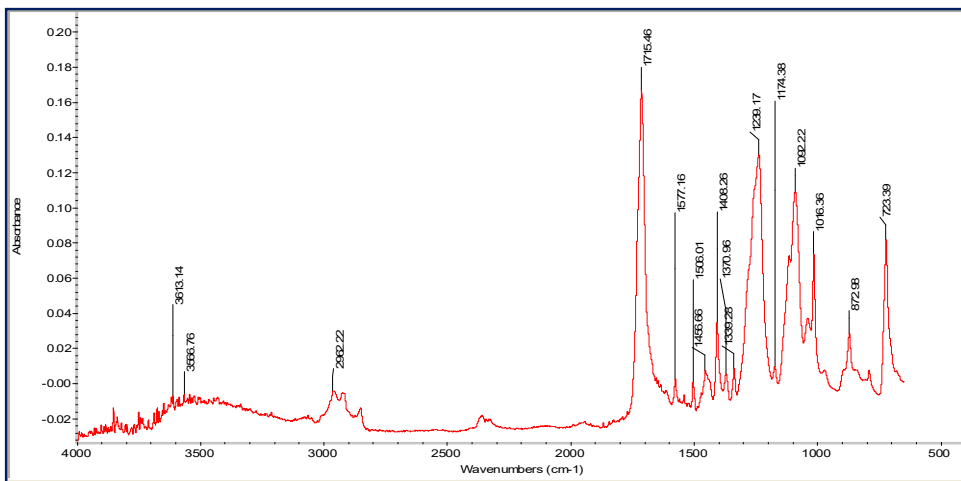


Figure 12. Infra-red spectrum for 100% R-PET sample.

## 3.6 Influence of V-PET/R-PET blending on whiteness, yellowness, brightness indices and reflectance

The influence of increasing R-PET content in the whiteness, yellowness and brightness values of the samples is shown in Figure 13. Moreover, influence of increasing R-PET

content in the reflectance values of the blended samples is shown in Figure 14. There is a reduction in whiteness, brightness and reflectance values on increase in R-PET content in blend. Contrary behaviour is observed for yellow index, which increases with incorporation of R-PET in blend. Yellowing of R-PET makes it less acceptable in food grade packaging applications. The yellowness hue in R-PET is attributed to the chain scission reaction or thermo-oxidative reaction during PET extrusion which produces – OH species which causes hydroxylation of terephthalate ring (Badia et al., 2012; Ladasiu Ciolacu et al., 2006). This behaviour was also confirmed through FTIR analysis. Another reason for yellowing of R-PET is formation of azomethine structures on exposing polyamide (used as barrier layers in PET bottles) to higher temperature (Berg et al., 2016).
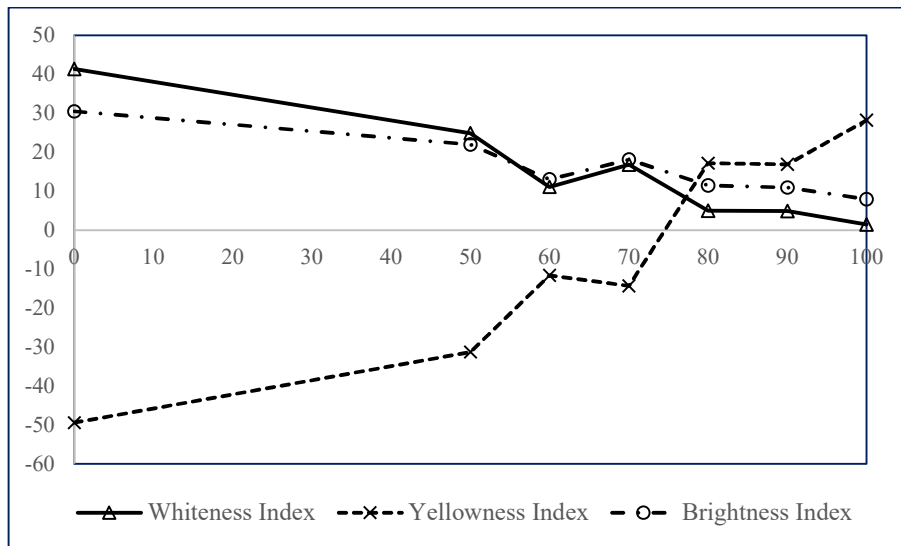


Figure 13. The influence of R-PET content (%) on whiteness, yellowness and brightness indices of the V-PET/R-PET monofilaments.
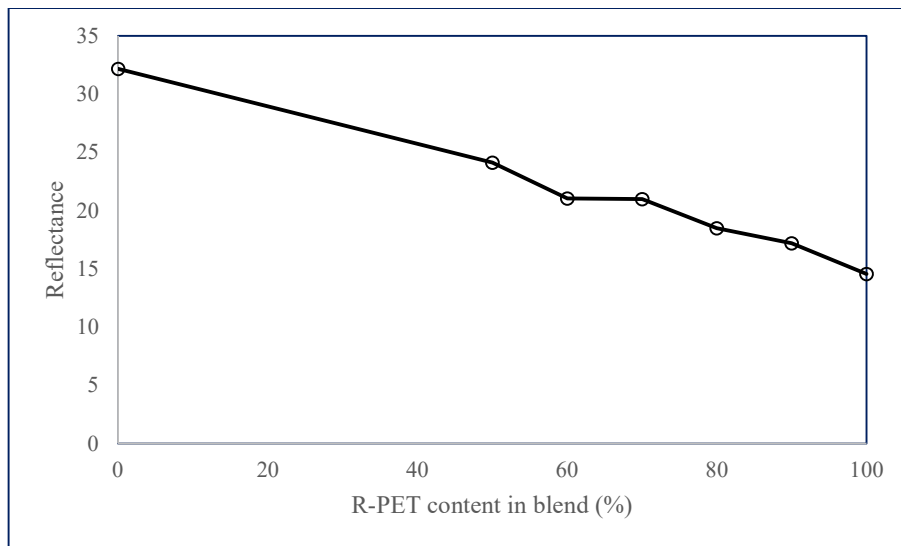


Figure 14. The inflence of R-PET content (%) on reflectance value of the V-PET/R-PET monofilaments.

## 4. Conclusions

The V-PET/R-PET yarn properties were investigated by varying the proportion of R-PET content in blend (0%, 50%, 60%, 70%, 80%, 90% and 100%). The 100% R-PET sample has offered highest MFR values and lowest IV, confirming the reduction in molecular weight and increase molecular mobility of specimen due to chain scission reaction occurred during thermo-mechanical degradation, confirmed through IR analysis. The thermal stability of V-PET sample was highest which is attributed to the presence of higher molecular weight, longer molecular chains and high crystallinity and more oriented structure. The tensile stress and strain are recorded lowest for 100% R-PET sample. This explanation to this behavior is R-PET has lower molecular weight, short molecular chains, and reprocessing under higher temperature has led to removal of plastic deformation ability. The blended yarn samples with R-PET content of 50-80% have performed marginally similar in terms of tensile stress and strain. The loss of tensile stress and strain is significant when R-PET content in blend is above 80%. Thermal characterisation of R-PET specimen confirmed presence of narrow and long melt-crystallisation peaks, which indicates faster rate of crystallisation for R-PET in contrast to V-PET. The thermographs of all the blended samples have single prominent crystallization and melting peak which confirms the good compatibility and homogeneity within a single phase for both V-PET and R-PET components. The crystallinity (%) of the samples obtained from DSC, indicates that crystallinity content in sample gradually reduces with increase in R-PET content. The IR analysis suggested a higher absorption value for 100% V-PET at all the corresponding absorption peaks. This behaviour is attributed to presence of higher crystallinity (%) in V-PET. New absorption peaks were detected for 100% R-PET sample at 3566 cm$^{-1}$ and 3613 cm$^{-1}$. This is attributed to the presence of hydroxyl and carboxyl groups with – OH links causes thermo-mechanical degradation of PET. There is a decrease in whiteness, brightness and reflectance values and increase in yellow index on incorporation of R-PET content in blend. The yellowness is attributed to the chain scission reaction or thermo-oxidative reaction during PET extrusion which produces – OH species which incite hydroxylation of terephthalate ring.

The 100% V-PET sample have performed superior in comparison to other V-PET/R-PET blended samples. However, in order to reduce cost, environmental impact, and raw material requirement it is advisable to incorporate R-PET in such a manner that the minimum desired property requirement is achieved. In this study it was found that, V-PET/R-PET blended yarn produced through mechanical recycling process should not contain less than 20-30% of V-PET, suitable for average tenacity applications. Optimizing V-PET/R-PET blend ratio in mechanical recycling provides a sustainable alternative to obtain minimum desirable filament characteristics with significant cost reduction.

## References

Acar, I., Kaşgöz, A., Özgümüş, S., & Orbay, M. (2006). Modification of Waste Poly(Ethylene Terephthalate) (PET) by Using Poly(L-Lactic Acid) (PLA) and Hydrolytic Stability. *Polymer-Plastics Technology and Engineering*, *45*(3), 351–359. https://doi.org/10.1080/03602550600553267

American Chemistry Council. (2016). *Plastic Packaging Resins*. 3. https://plastics.americanchemistry.com/Plastic-Resin-Codes-PDF/

Aryan, Y., Yadav, P., & Samadder, S. R. (2019). Life Cycle Assessment of the existing and proposed plastic waste management options in India: A case study. *Journal of Cleaner Production*, *211*, 1268–1283. https://doi.org/10.1016/j.jclepro.2018.11.236

Awaja, F., & Pavel, D. (2005). Recycling of PET. *European Polymer Journal*, *41*(7), 1453–1477. https://doi.org/10.1016/j.eurpolymj.2005.02.005

Badia, J. D., Strömberg, E., Karlsson, S., & Ribes-Greus, A. (2012). The role of crystalline, mobile amorphous and rigid amorphous fractions in the performance of recycled poly (ethylene terephthalate) (PET). *Polymer Degradation and Stability*, *97*(1), 98–107. https://doi.org/10.1016/j.polymdegradstab.2011.10.008

Badía, J. D., Vilaplana, F., Karlsson, S., & Ribes-Greus, A. (2009). Thermal analysis as a quality tool for assessing the influence of thermo-mechanical degradation on recycled poly(ethylene terephthalate). *Polymer Testing*, *28*(2), 169–175. https://doi.org/10.1016/j.polymertesting.2008.11.010

Barman, N. K., Bhattacharya, S. S., & Mandot, A. (2015). Mechanical Properties of melt-spun Monofilaments Produced From Virgin and Recycyled Poly (ethylene terephthalate ) Blends. *International Journal of Recent Scientific Research*, *6*(6), 4517–4525.

Berg, D., Schaefer, K., Koerner, A., Kaufmann, R., Tillmann, W., & Moeller, M. (2016). Reasons for the Discoloration of Postconsumer Poly(ethylene terephthalate) during Reprocessing. *Macromolecular Materials and Engineering*, *301*(12), 1454–1467. https://doi.org/10.1002/mame.201600313

Berkowitz, S. (1984). Viscosity–molecular weight relationships for poly(ethylene terephthalate) in hexafluoroisopropanol–pentafluorophenol using SEC–LALLS. *Journal of Applied Polymer Science*, *29*(12), 4353–4361. https://doi.org/10.1002/app.1984.070291264

Campanelli, J. R., Kamal, M. R., & Cooper, D. G. (1994). Kinetics of glycolysis of poly(ethylene terephthalate) melts. *Journal of Applied Polymer Science*, *54*(11), 1731–1740. https://doi.org/10.1002/app.1994.070541115

Chen, J.-W., & Chen, L.-W. (1999). The glycolysis of poly(ethylene terephthalate). *Journal of Applied Polymer Science*, *73*(1), 35–40. https://doi.org/10.1002/(SICI)1097-4628(19990705)73:1<35::AID-APP4>3.0.CO;2-W

Chilton, T., Burnley, S., & Nesaratnam, S. (2010). A life cycle assessment of the closed-loop recycling and thermal recovery of post-consumer PET. *Resources, Conservation and Recycling*, *54*(12), 1241–1249. https://doi.org/10.1016/j.resconrec.2010.04.002

Elamri, A., Lallam, A., Harzallah, O., & Bencheikh, L. (2007). Mechanical characterization of melt spun fibers from recycled and virgin PET blends. *Journal of Materials Science*, *42*(19), 8271–8278. https://doi.org/10.1007/s10853-007-1590-1

Fann, D.-M., Huang, S. K., & Lee, J.-Y. (1997). Processing Characteristics of Recycled Poly(Ethylene Terephthalate) as Melt Spun Fibers. *Textile Research Journal*, *67*(12), 891–896. https://doi.org/10.1177/004051759706701205

Foolmaun, R. K., & Ramjeeawon, T. (2013). Comparative life cycle assessment and social life cycle assessment of used polyethylene terephthalate (PET) bottles in Mauritius. *The International Journal of Life Cycle Assessment*, *18*(1), 155–171. https://doi.org/10.1007/s11367-012-0447-2

Gomes, T. S., Visconte, L. L. Y., & Pacheco, E. B. A. V. (2019). Life Cycle Assessment of Polyethylene Terephthalate Packaging: An Overview. *Journal of Polymers and the Environment*, *27*(3), 533–548. https://doi.org/10.1007/s10924-019-01375-5

Holland, B. ., & Hay, J. . (2002). The thermal degradation of PET and analogous polyesters measured by thermal analysis–Fourier transform infrared spectroscopy. *Polymer*, *43*(6), 1835–1847. https://doi.org/10.1016/S0032-3861(01)00775-3

Itim, B., & Philip, M. (2015). Effect of multiple extrusions and influence of PP contamination on the thermal characteristics of bottle grade recycled PET. *Polymer Degradation and Stability*, *117*, 84–89. https://doi.org/10.1016/j.polymdegradstab.2015.04.004

Ladasiu Ciolacu, C. F., Roy Choudhury, N., & Dutta, N. K. (2006). Colour formation in

poly(ethylene terephthalate) during melt processing. *Polymer Degradation and Stability*, *91*(4), 875–885. https://doi.org/10.1016/j.polymdegradstab.2005.06.021

Lee, J. H., Lim, K. S., Hahm, W. G., & Kim, S. H. (2013). Properties of recycled and virgin poly(ethylene terephthalate) blend fibers. *Journal of Applied Polymer Science*, *128*(2), 1250–1256. https://doi.org/10.1002/app.38502

López, M. del M. C., Ares Pernas, A. I., Abad López, M. J., Latorre, A. L., López Vilariño, J. M., & González Rodríguez, M. V. (2014). Assessing changes on poly(ethylene terephthalate) properties after recycling: Mechanical recycling in laboratory versus postconsumer recycled material. *Materials Chemistry and Physics*, *147*(3), 884–894. https://doi.org/10.1016/j.matchemphys.2014.06.034

Masmoudi, F., Fenouillot, F., Mehri, A., Jaziri, M., & Ammar, E. (2018). Characterization and quality assessment of recycled post-consumption poly(ethylene terephthalate) (PET). *Environmental Science and Pollution Research*, *25*(23), 23307–23314. https://doi.org/10.1007/s11356-018-2390-7

NAPCOR (National Association for PET Container). (2018). *Report on postconsumer PET container recycling activity in 2017*. 13. https://napcor.com/wp-content/uploads/2018/11/NAPCOR_2017RateReport_FINAL.pdf

Sang, T., Wallis, C. J., Hill, G., & Britovsek, G. J. P. (2020). Polyethylene terephthalate degradation under natural and accelerated weathering conditions. *European Polymer Journal*, *136*(July), 109873. https://doi.org/10.1016/j.eurpolymj.2020.109873

Sängerlaub, S., Glas, C. E., Schlemmer, D., & Müller, K. (2020). Influence of multiple extrusions of blends made of polyethylene terephthalate and an oxygen scavenger on processing and packaging-related properties. *Journal of Plastic Film & Sheeting*, *36*(3), 260–284. https://doi.org/10.1177/8756087919886893

Shen, L., Nieuwlaar, E., Worrell, E., & Patel, M. K. (2011). Life cycle energy and GHG emissions of PET recycling: change-oriented effects. *The International Journal of Life Cycle Assessment*, *16*(6), 522–536. https://doi.org/10.1007/s11367-011-0296-4

Shen, L., Worrell, E., & Patel, M. K. (2010). Open-loop recycling: A LCA case study of PET bottle-to-fibre recycling. *Resources, Conservation and Recycling*, *55*(1), 34–52. https://doi.org/10.1016/j.resconrec.2010.06.014

Sinha, V., Patel, M. R., & Patel, J. V. (2010). Pet Waste Management by Chemical Recycling: A Review. *Journal of Polymers and the Environment*, *18*(1), 8–25. https://doi.org/10.1007/s10924-008-0106-7

Starkweather, H. W., Zoller, P., & Jones, G. A. (1983). The heat of fusion of poly(ethylene terephthalate). *Journal of Polymer Science: Polymer Physics Edition*, *21*(2), 295–299. https://doi.org/10.1002/pol.1983.180210211

Varma, P., Lofgren, E. A., & Jabarin, S. A. (1998). Properties and kinetics of thermally crystallized oriented poly(ethylene terephthalate) (PET). I: Kinetics of crystallization. *Polymer Engineering & Science*, *38*(2), 237–244. https://doi.org/10.1002/pen.10184

Welle, F. (2011). Twenty years of PET bottle to bottle recycling—An overview. *Resources, Conservation and Recycling*, *55*(11), 865–875. https://doi.org/10.1016/j.resconrec.2011.04.009

Welle, F. (2013). Is PET bottle-to-bottle recycling safe? Evaluation of post-consumer recycling processes according to the EFSA guidelines. *Resources, Conservation and Recycling*, *73*, 41–45. https://doi.org/10.1016/j.resconrec.2013.01.012

Wu, H., Lv, S., He, Y., & Qu, J. P. (2019). The study of the thermomechanical degradation and mechanical properties of PET recycled by industrial-scale elongational processing. *Polymer Testing*, *77*(December 2018), 105882. https://doi.org/10.1016/j.polymertesting.2019.04.029

# NaBH₄ Reduced Black TiO₂ for Photocatalytic Degradation of Organic Pollutants in Wastewater

**T. S. Rajaraman[1,2], Vimal G. Gandhi[3], Sachin P. Parikh[1,2*]**

[1]Chemical Engineering Department, L. D. College of Engineering, Ahmedabad-38 0015, Gujarat, INDIA

[2]Gujarat Technological University, Chandkheda, Ahmedabad-382424, Gujarat, INDIA

[3]Department of Chemical Engineering, Dharmsinh Desai University, Nadiad-387 001, Gujarat, INDIA

*Corresponding author: sachinparikh@ldce.ac.in, Mobile number: +91 9925611525

## Abstract

Black titanium dioxide (TiO₂) has captured significant attention among the scientific community since its discovery in 2011. The enhanced visible light absorption along with superior photocatalytic properties have led to widespread research on it for various applications like wastewater treatment, hydrogen production, photocatalytic $CO_2$ reduction etc. The superior activity of black TiO₂ over the white counterpart has often been attributed to the various defects species like $Ti^{3+}$ species, oxygen vacancies, Ti-H bonds, Ti-OH groups etc. Numerous methods for synthesis of black TiO₂, other than the commonly reported hydrogenation method, have been developed and are available in literature. NaBH₄ reduction technique is one of the simplest ways of synthesizing black TiO₂. In this paper, Black TiO₂ (brownish-grey and black) has been synthesized using a modified NaBH₄ route under simplest of operating conditions. The colour of the reduced product could be tuned from brown to black by altering the time of reduction. Characterization revealed physicochemical properties including the higher concentration of defect species like $Ti^{3+}$ and oxygen vacancies leading to a reduced band gap and increased visible light absorption. The as prepared samples were tested for their photocatalytic efficiency in the degradation of toxic organic pollutant fuchsin basic dye solution under UV-Vis light. The brownish-grey TiO₂ was found to be the better sample with its photoactivity higher than the white TiO₂ and black TiO₂.

**Keywords:** Photocatalysis; Black TiO₂; Wastewater Degradation, Defect Species; NaBH₄ Reduction

## 1. Introduction

Photocatalysis has become one of the most active research areas in many applications. The prospect of utilization of sunlight to carry out reactions which aid in the degradation of pollutants, production of hydrogen etc. has captured increased attention among the scientific community (Dincer and Acar 2017) (Varma et al. 2021). Titanium Dioxide (TiO₂) based photocatalysts have long been successfully tested for their photocatalytic activity. However, lower visible light activity and charge carrier recombination acted as two of the major drawbacks of the conventional standalone TiO₂ photocatalysts (Chung et al. 2018; Hernández-Alonso et al. 2009). Metal and non metal doped TiO₂ were developed in an effort to counter these inherent limitations of standalone TiO₂ (Chen and Mao 2007). Although, visible light activity has been greatly improved by such methodologies, the recombination problem still persisted in such photocatalysts. Ever since its discovery in 2011, Black TiO₂ has revolutionised the research on TiO₂ based photocatalysis. Black TiO₂ was first synthesized by Chen et al. (Chen et al. 2011) through high pressure hydrogenation which introduced lattice disorder in the white TiO₂ thereby changing its colour to black which enhanced the absorption of visible radiation. Superior photocatalytic properties of black TiO₂ due to increased visible light absorption and reduced charge carrier recombination have led to extensive research in applications like hydrogen production through water splitting and wastewater

remediation (Bagheri and Muhd Julkapli 2018). Subsequently, many different synthetic routes have been developed in the last decade and almost all such studies have reported the presence of defect species like $Ti^{3+}$ and oxygen vacancies which are responsible for the change in physicochemical properties of the sample (Lin et al. 2017; Ullattil et al. 2018). However, most synthetic routes involve harsh conditions involving multiple steps and require sophisticated facilities like hydrogenation at high pressure and temperature, plasma discharge, laser irradiation etc. (Chen et al. 2011; Wang et al. 2019).

In this work, Black $TiO_2$ photocatalysts have been synthesized through a modified solid state $NaBH_4$ reduction method. Although $NaBH_4$ reduction method has been reported previously in literature, the modified route discussed in this work enables use of low molar ratios of $NaBH_4$ /$TiO_2$ for reduction without the need of inert atmosphere during annealing. The time of reduction affected the colour of the sample and the extent of reduction. The samples were then tested for their photocatalytic activity under UV-Vis light for the decolourization of fuchsin basic dyes. Defects like $Ti^{3+}$ and oxygen vacancies were responsible for the change in optical properties following the reduction step.

## 2. Materials and Methods

### 2.1 Materials

Titanium Isopropoxide (TTIP), Acetic Acid (Glacial), Hydrochloric Acid (HCl) Diethylene Glycol, Deionized water, Diethyl Ether, Ethanol (Absolute alcohol), Methanol, $NaBH_4$, Aluminium Foil, Fuchsin basic dye. All chemicals were purchased from Astron Chemicals (India).

### 2.2 Synthesis of white $TiO_2$ nanoparticles

Synthesis of pristine white $TiO_2$ nanoparticles were based on a previously reported one pot gel combustion method (Ullattil and Periyat 2016). 32 g of Titanium Isopropoxide (TTIP) was first added to 80 ml of Diethylene Glycol (DEG) (1:10 molar ratio of TTIP and DEG). The resulting solution was thoroughly mixed at 70 °C for 2 hours to form Titanium Glycolate (TG) gel which was a transparent pale yellow liquid. 78 ml of deionized water (40 molar times that of TTIP) was then added to this TG leading to the formation of an opaque gel. The gel was then heated in an oven at 250 °C to remove the unreacted DEG and alcoholic by-products and was then calcined in muffle furnace at 500 °C for 4 hours to produce white $TiO_2$ nanoparticles (Figure 1(b)).
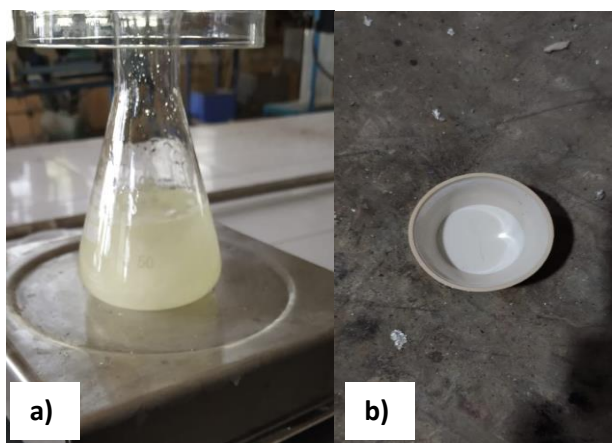


Figure 1. a) Titanium Glycolate gel; b) White anatase $TiO_2$ powder after calcination at 500 °C

## 2.3 Synthesis of Black TiO₂ nanoparticles

In a typical synthesis procedure, 2 g of the as synthesized white $TiO_2$ nanoparticles was taken and thoroughly ground and mixed with 0.19 g of $NaBH_4$ powder ($NaBH_4/TiO_2$ molar ratio of 0.2). The resulting fine white powdered mixture was then wrapped in an Aluminium foil and folded multiple times to form a tightly sealed rectangular pack as shown in Figure 2(a). Two such different packs containing same amount of mixed powder were made and were then placed inside muffle furnace and heated to 400 ℃ for 30 min and 120 min respectively. The packings, subjected to different reduction times, were carefully opened and brownish-grey and black powders were obtained for 30 min and 120 min reduction times respectively. The resulting samples were thoroughly washed with 0.1 M HCl solution, methanol and deionized water to remove any sodium and borate impurities and further dried in oven at 80 ℃ overnight to get reduced brownish-grey and black $TiO_2$ powders.
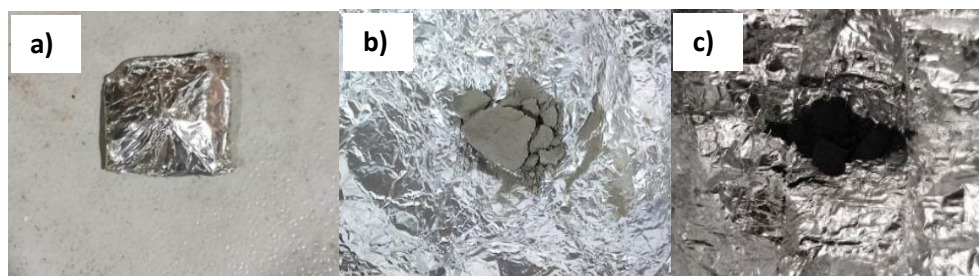


Figure 2. a) Tightly sealed Al foil pack consisting of homogenous mixture of $NaBH_4$ and white $TiO_2$ powders, b) Reduced grey $TiO_2$ after a reduction time of 30 min, c) Reduced black $TiO_2$ after a reduction time of 120 min.

## 2.4 Characterization

The prepared samples were characterized by X-ray diffraction (XRD) (Japan, SMartlabSE) with X-Ray Generator- 40 kV, 30 mA and Cu-K-Beta filter. The surface composition and electronic state was measured by an X-ray Photoelectron Spectrometer (XPS, Kratos Axis Ultra DLD). UV-Vis-NIR Spectrophotometer (Shimadzu UV-3600) equipped with an integrating sphere was used to measure the light absorbance.

## 2.5 Photocatalytic Experiments

Photocatalytic experiments were carried out under UV-Vis light for degradation of Fuchsin basic dye. A 250 W UV-Vis Xenon lamp was used for photocatalytic experiments (Figure 3). A 1 litre quartz photoreactor consisting of an annulus for placing UV-Vis lamps was used. 200 ml of 5 ppm solutions of Fuchsin basic dye was taken. 0.2 g of the as prepared white and reduced $TiO_2$ samples were taken for each run. Initially, a dark experiment was performed for 1 hr to remove the effect of dye adsorption on the photocatalyst particle surface. Magnetic stirring was used throughout all experiments. Samples were thereafter taken every 30 minutes in sample tubes and the change in colour of the dye solution was observed periodically over a 5 hr irradiation time.

Figure 3. Photoreactor with 250 W Xenon UV-Vis lamp for degradation of fuchsin basic dye

## 3. Theory

Black $TiO_2$ has attracted the attention of the scientific community mainly due to the fact that the photocatalytic activity could be improved without the introduction of any foreign substances (metals/non metals except hydrogen). The term "Black $TiO_2$" can be a little hazy in the sense that phrases like "hydrogenated $TiO_2$", "reduced $TiO_2$", "defective $TiO_2$ /$TiO_{2-x}$" etc. have also been reported in literature. Additionally, some studies report many different coloured $TiO_2$ (like brown, grey, yellow, blue etc.) obtained by tuning the reduction parameters. White and black $TiO_2$ seem to represent two extreme ends of the spectrum (white being the unreduced and black being the most reduced sample) with other different colours obtained at intermediate reducing conditions. Nevertheless, most of the above studies report the same traits like increased visible light absorption, reduced band gap, presence of one or more defect species/disorder, enhanced photocatalytic activity etc. This commonality in properties enables us to bring all such studies under one roof of "Black $TiO_2$". However, it may be noted that samples turning black due to doping/addition of foreign elements (metals/non metals except H) or due to composite formation with other compounds cannot be considered as black $TiO_2$. This clearly draws the line where black $TiO_2$ is essentially a result of changes in intrinsic aspects of $TiO_2$ rather than due to the presence of some foreign species. (Rajaraman et al. 2020).

Titanium Glycolate based method for the synthesis of white $TiO_2$ offers many advantages compared to conventional sol-gel based route. Titanium glycolate is first produced as an intermediate followed by calcination step to yield $TiO_2$. It has been previously reported that Titanium Glycolate can act as a better precursor towards synthesizing $TiO_2$ nanoparticles owing to its resistance to air and moisture unlike the titanium alkoxide precursors which are highly sensitive to air and moisture (Niederberger and Garnweitner 2006). Moreover, glycolate precursors are very stable and can be kept for several years without any phase transformation (Wei et al. 2018).

Previous studies on $NaBH_4$ reduction for black $TiO_2$ have been either carried out as solution based reduction (Fang et al. 2014; Xing et al. 2013) or solid state reduction. The solid state $NaBH_4$ reduction has been reported to be an effective method for Black $TiO_2$ synthesis (Ariyanti et al. 2017; He et al. 2019; Shang et al. 2019; Tan et al. 2014). However, these studies have reported high molar ratios of $NaBH_4$ to $TiO_2$ as part of solid mixture which is annealed in inert atmospheres like Nitrogen and Argon in most cases. In this work, $NaBH_4/TiO_2$ molar ratios as low as 0.2 have been found to be sufficient to cause significant reduction in the sample. The lower ratio decreases the chances of contamination of sample by unreacted $NaBH_4$ and other borate impurities. Moreover, the constricted environment provided by wrapping tightly in Al foil aids the reduction process thereby eliminating the need for inert atmosphere.

Sodium Borohydride ($NaBH_4$) is a commonly used reducing agent which generates active hydrogen during thermal decomposition. This active hydrogen leads to the creation of defects (oxygen vacancies) in the $TiO_2$ lattice (Ariyanti et al. 2017). It has also been reported that the active hydrogen produced by $NaBH_4$ decomposition is more reactive than $H_2$ and other reductants (Tan et al. 2014). The overall equation can be represented as follows:

$$NaBH_4 \rightarrow \sum_i solid_i (Na, B, H) \ + \ \sum_j gas_j (B, H)$$
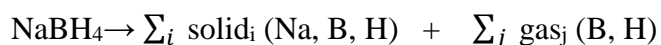
where the solid residue and the unreacted reactant can be removed by washing with HCl solution and DI water.

Pristine white titanium dioxide (Anatase phase) has a band gap energy of 3.0-3.2 eV which means that a light of wavelength $<= 387$ nm is needed to excite the electrons from valence band (VB) to conduction band (CB) which eventually take part in photocatalytic reactions (Ullattil et al. 2018; Yan et al. 2017). Due to this inability to utilize the visible region of the spectrum, modification in $TiO_2$ in desired to bring down the band gap and hence increase the absorption in the visible spectrum which constitutes 42 % of natural sunlight incident on earth as compared to just 4% contribution of the UV region (Byrne et al. 2017). Most studies on black $TiO_2$ have shown that defect species like $Ti^{3+}$ and oxygen vacancies formed during the reduction step lead to change in the optical properties of the sample thereby reducing the band gap (Jiang et al. 2012). These defect species result in creation of VB and CB tailing as shown in Figure 4 (b). This results in enhanced visible light absorption by the black samples and higher photocatalytic activities.

However, too many defects have also been reported to cause reduction in the photocatalytic activity as $Ti^{3+}$ have been known to act as recombination centres for photogenerated electron and hole pairs (Leshuk et al. 2013; Ohtani et al. 1997; Xu et al. 2015). Moreover, it has been reported that dark colouration of the samples due to excess defect and increased visible light absorption does not necessarily mean higher photocatalytic activities. There is some optimal defect concentration (extent of reduction) for highest photocatalytic activity (He et al. 2019; Wang et al. 2018).
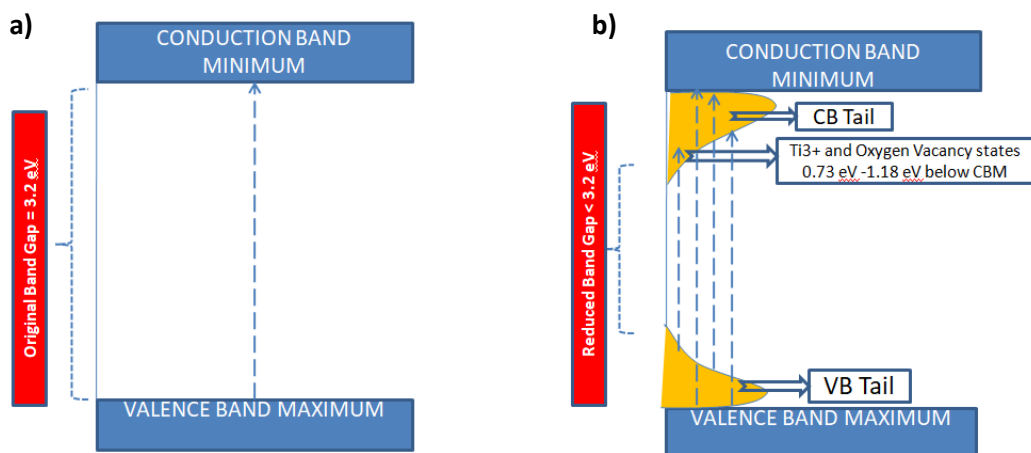
Figure 4. Comparison of Energy Band Diagrams (Density of States) of a) White and b) Black TiO$_2$

## 4. Results and Discussion

### 4.1 Characterization of Black and Brownish-grey TiO$_2$

X-Ray diffraction spectra enabled better understanding of the crystal structure and phase. The diffraction spectra is shown in Figure 5 and it can be seen that the spectra for both white and black samples are very similar in nature. The characteristic peaks at $2\theta$ = 25.4, 37.8, 48.14 confirm the anatase polymorph of TiO$_2$ in both the samples (Beegam et al. 2018; Ullattil and Periyat 2016). Moreover, there is no noticeable change in the peak intensities of both the samples which suggests that the degree of crystallinity was not affected during the reduction process. The crystallite size of the black and white samples are 28.4 nm and 28.8 nm respectively w.r.t to the main peak at 25.4$^0$ for Anatase TiO$_2$ thereby indicating that the particle size did not change appreciably during the reduction process by agglomeration or any other factor. Additionally, the absence of specific peaks for NaBH$_4$ or other borate impurities underlines the fact that the impurities adsorbed on the black TiO$_2$ surface have been thoroughly removed with HCl and DI water washing.
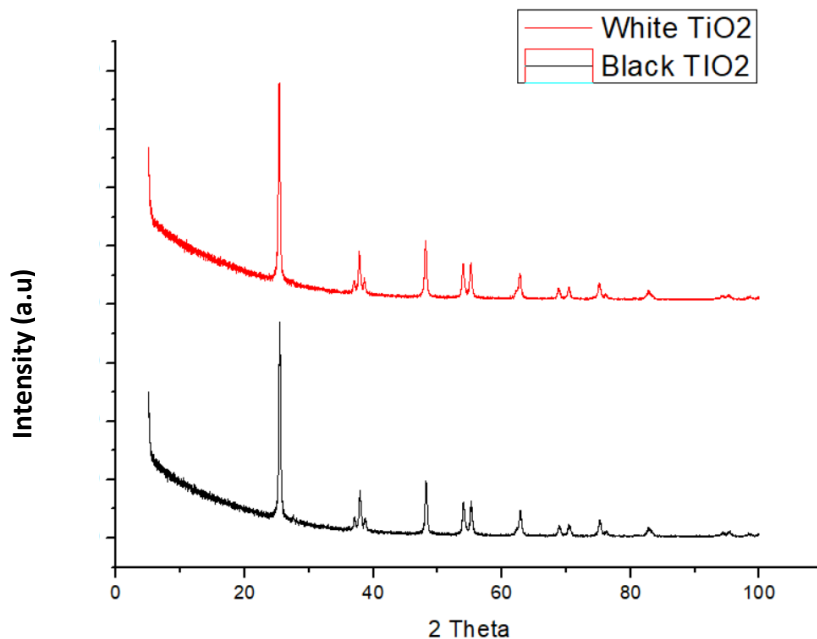
Figure 5. X-Ray Diffraction spectra of white and black $TiO_2$ powders

X-Ray photoelectron spectroscopy results revealed the surface characteristics of the samples. Figure 6(b) shows the Ti 2p spectra where a characteristic peak at 458.8 eV suggests the presence of $Ti^{4+}$–O bond along with another peak at 464.48 eV for white $TiO_2$. For Black $TiO_2$, however, these peaks shift to lower binding energies of 458.48 eV and 464.1 eV respectively which suggest the presence of $Ti^{3+}$–O bonds (Ariyanti et al. 2017; Si et al. 2019).

In the O1s spectra of Figure 6 (c), the peaks at 530.08 eV for both the samples can be ascribed to the Ti-O bonds. The broad shoulder peak at 531.38 eV depicts the presence of surface adsorbed oxygen which in turn denotes the presence of oxygen vacancies (Fang et al. 2014; He et al. 2019). It can be clearly seen that the shoulder peak is broader in case of the black $TiO_2$ as compared to white which suggests the higher concentration of oxygen vacancies.

Moreover, the XPS survey spectra of Figure 6 (a) for both these samples reveal that there are no impurities of boron or sodium suggesting that these impurities have been thoroughly removed through ethanol, HCl and DI water washing. HCl washing has been reported to be effective in the removal of boron based impurities (Fang et al. 2014; Xing et al. 2013).

Additionally, the C1s peaks at 284.78 eV and 288 eV have been reported in literature to be due to adventitious carbon impurity from natural environment (Xing et al. 2013; Zhang et al. 2018).
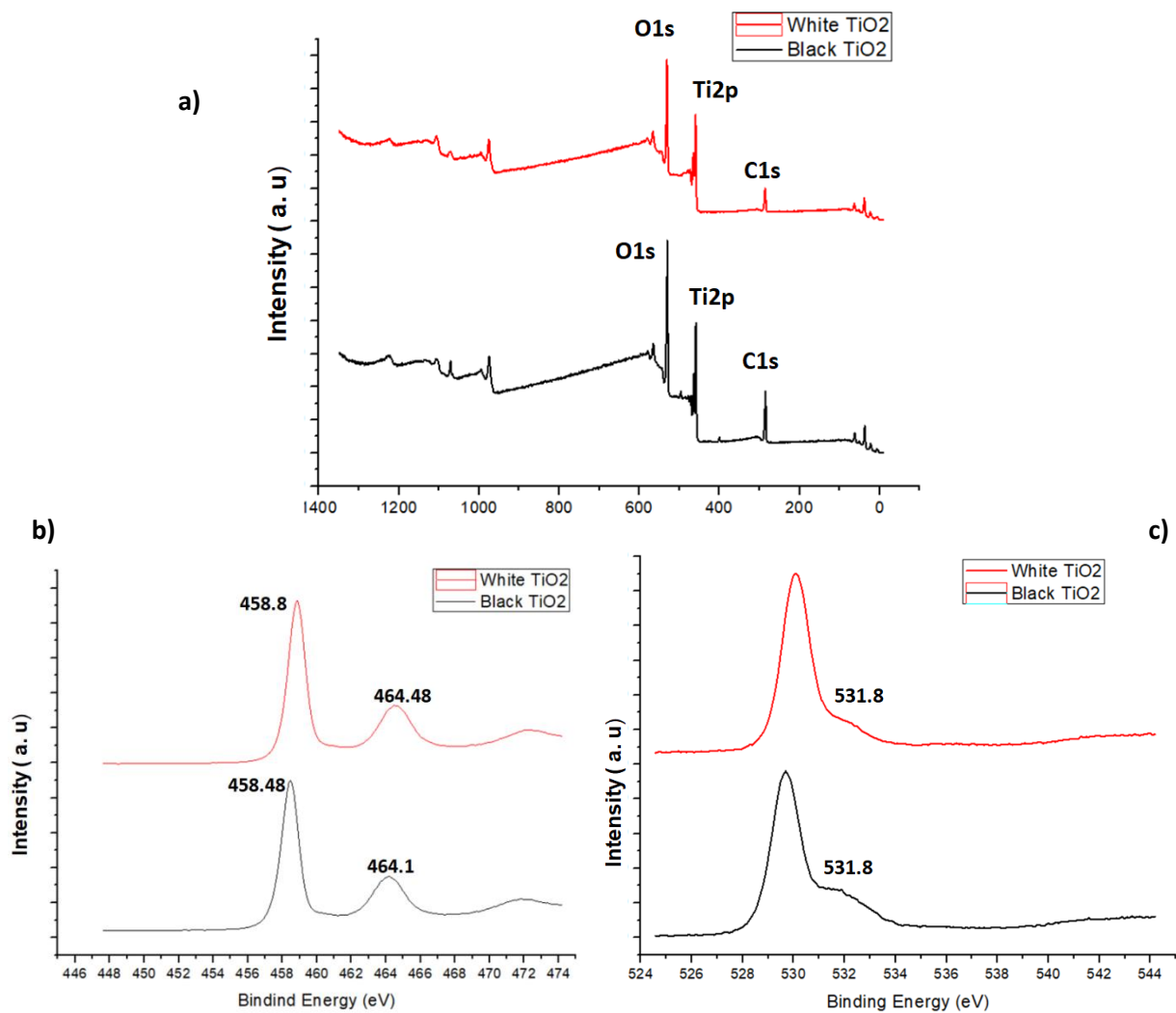
Figure 6. a) XPS survey spectra and black and white $TiO_2$, b) Ti 2p spectra of black and white $TiO_2$, c) O 1s spectra of black and white $TiO_2$

The absorbance of the black, brownish-grey and white samples are shown in Figure 7 (a). It can be clearly seen that the visible light absorption of the white sample follows the typical pristine white $TiO_2$ pattern with a sharp decline in the absorption of incident light of wavelengths in excess of 400 nm which matches well with those reported in literature (He et al. 2019). For the brownish-grey and black samples, the absorption spectra reveals higher visible light absorption with the black sample exhibiting the highest absorption out of the three. Even for brownish grey sample, the absorbance in the visible region is appreciably higher as compared to the pristine white sample.

The band gap energy for all the three samples were computed using the Tauc-plot as shown in Figure 7 (b). The band gap energies of the white, brownish-grey and black samples were found to be 3.01 eV, 2.98 eV and 2.81 eV respectively. The reduction in the band gap energies of brownish-grey and black samples can be attributed to the introduction of defect levels due to $Ti^{3+}$ and oxygen vacancies which matches well with the XPS findings.
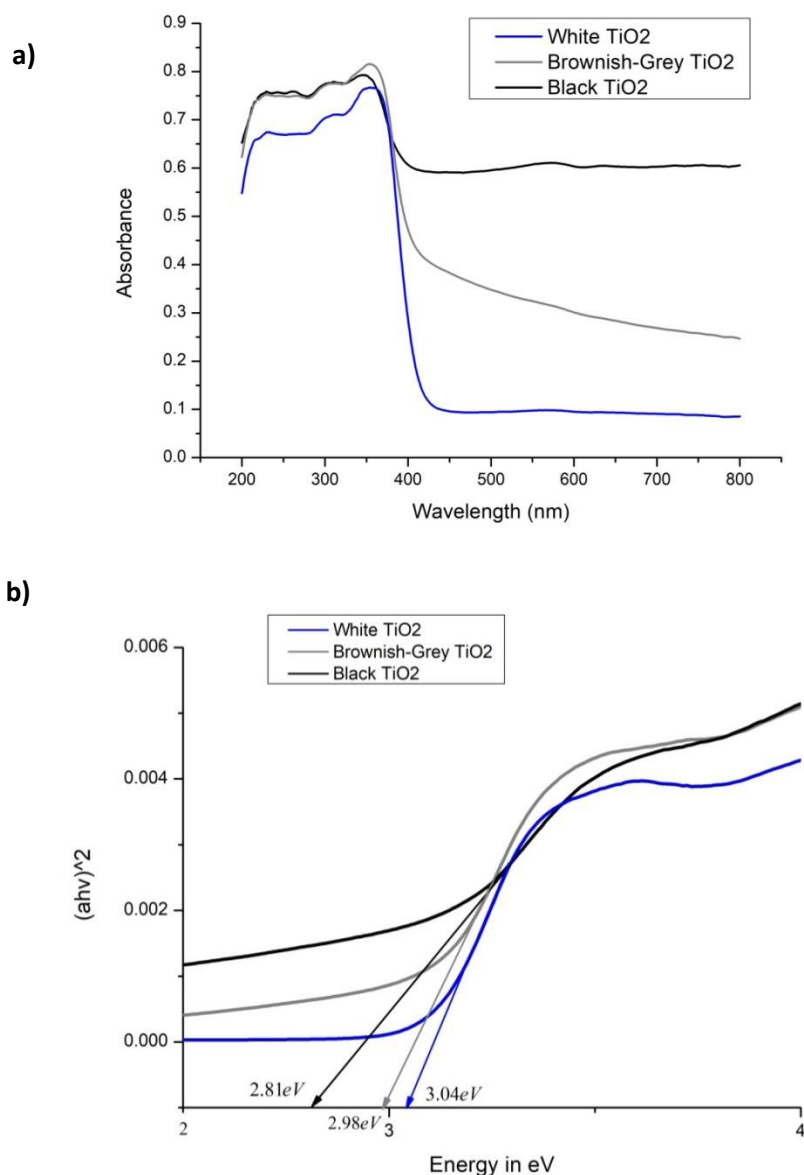
Figure 7. a) UV-Vis absorbance spectra of black, brownish-grey and white $TiO_2$ samples, b) Tauc plot for computing the band-gap energy of black, brownish-grey and white $TiO_2$ samples.

## 4.2 Photocatalytic Degradation of fuchsin basic dye under UV-Vis light

Photocatalytic experiment under UV-Vis light was carried out as mentioned above in section 2.5. Photocatalytic experiments carried out between white and black $TiO_2$ reveal no noticeable change in the decolorization of fuchsin basic dye solution over regular intervals of 30 min as shown in Figure 8 (a). As mentioned above, presence of excess defects might have caused the defect species to act as recombination centres which in turn counteracts the positive effect of increased visible light absorption.
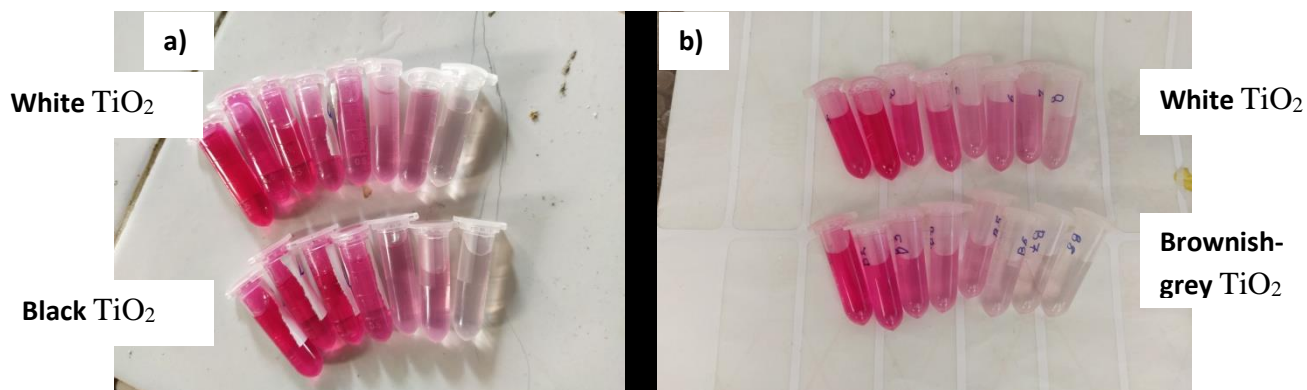
Figure 8. Comparison of decolorization of fuchsin basic dye solution by a) white and black $TiO_2$, b) white and brownish-grey $TiO_2$

For brownish-grey $TiO_2$, however, a clear difference in the activity could be noticed through the decolourization of the dye solution. As shown in Figure 8 (b), the brownish-grey $TiO_2$ displayed superior degradation rate as compared to the pristine white samples. In spite of a higher band gap energy value and lower visible light absorbance, the brownish-grey $TiO_2$ outperformed the black sample. The white and black samples seem to represent to extreme ends of activities where the photocatalytic degradation rates are lower due to less visible light activity in case of white $TiO_2$ and higher recombination centres for photogenerated electrons in case of black $TiO_2$.

## 5. Conclusions

Black $TiO_2$ nanoparticles were successfully synthesized using a modified $NaBH_4$ reduction method where Aluminium foil wrapping was used to create a constricted oxygen free environment without the need of inert atmosphere. The low $NaBH_4/TiO_2$ molar ratio of 0.2 was found to be sufficient to cause defects in the $TiO_2$ lattice as seen in the characterization results. Oxygen vacancies and $Ti^{3+}$ species were found to be the main defects in the black samples as indicated by the XPS results. The extent of reduction (concentration of defects) was found to vary with the reduction time. The band gap energy of the white, brownish-grey and black samples were found to be 3.04 eV, 2.98 eV and 2.81 eV respectively and the decreased values for the reduced samples are believed to be due to the introduction of defect states in between the VB and CB. In spite of lower visible light absorption as compared to black sample, the brownish-grey $TiO_2$ exhibited the best photocatalytic activity for degradation of fuchsin basic dye whereas the white and black samples showed similar decolorization rates. As reported in the literature, too high a concentration of the defect species reduces the activity of the $TiO_2$ samples. The modified low cost reduction method without the need of inert environment, expensive chemicals and harsh operating conditions promises to be offer great prospects in various photocatalytic applications like wastewater remediation and hydrogen production.

**Acknowledgement**

**References**

1. Ariyanti, Dessy, Laura Mills, Junzhe Dong, Yao Yao, and Wei Gao. 2017. $NaBH_4$ Modified $TiO_2$: Defect Site Enhancement Related to Its Photocatalytic Activity. Materials Chemistry and Physics. 199, 571-576.
2. Bagheri, S., & Julkapli, N. M. 2018. Black Titania for Photodecomposition of Organic Compounds. In: Nanocatalysts in Environmental Applications, Springer, Cham, pp. 37-50.
3. Beegam, M. S. , Sanjay Gopal Ullattil, and Pradeepan Periyat. 2018. Selective Solar Photocatalysis by High Temperature Stable Anatase $TiO_2$. Solar Energy 160, 10–17.
4. Byrne, Ciara, Gokulakrishnan Subramanian, and Suresh C. Pillai. 2017. Recent Advances in Photocatalysis for Environmental Applications. Journal of Environmental Chemical Engineering 6(3), 3531-3555.
5. Chen, Xiaobo, Lei Liu, Peter Y. Yu, and Samuel S. Mao. 2011. Increasing Solar Absorption for Photocatalysis with Black Hydrogenated Titanium Dioxide Nanocrystals. Science 331(6018), 746–50.
6. Chen, Xiaobo and Samuel S. Mao. 2007. Titanium Dioxide Nanomaterials: Synthesis, Properties, Modifications and Applications. Chemical Reviews 107(7):2891–2959.
7. Chung, Woo Jin, Dinh Duc Nguyen, Xuan Thanh Bui, Sang Woo An, J. Rajesh Banu, Sang Moon Lee, Sung Su Kim, Dea Hyun Moon, Byong Hun Jeon, and Soon Woong Chang. 2018. A Magnetically Separable and Recyclable Ag-Supported Magnetic $TiO_2$ composite Catalyst: Fabrication, Characterization, and Photocatalytic Activity. Journal of Environmental Management 213, 541–48.
8. Dincer, Ibrahim and Canan Acar. 2017. Innovation in Hydrogen Production. International Journal of Hydrogen Energy 42(22), 14843–64.
9. Fang, Wenzhang, Mingyang Xing, and Jinlong Zhang. 2014. A New Approach to Prepare $Ti^{3+}$ Self-Doped $TiO_2$ via $NaBH_4$ Reduction and Hydrochloric Acid Treatment. Applied Catalysis B: Environmental 160, 240–46.
10. He, Miao, Jian Ji, Biyuan Liu, and Haibao Huang. 2019. Reduced $TiO_2$ with Tunable Oxygen Vacancies for Catalytic Oxidation of Formaldehyde at Room Temperature. Applied Surface Science, 473, 934-942.
11. Hernández-Alonso, María D., Fernando Fresno, Silvia Suárez, and Juan M. Coronado. 2009. Development of Alternative Photocatalysts to TiO2: Challenges and Opportunities. Energy & Environmental Science 2(12), 1231–57.
12. Jiang, Xudong, Yupeng Zhang, Jing Jiang, Yongsen Rong, Yancheng Wang, Yichu Wu, and Chunxu Pan. 2012. Characterization of Oxygen Vacancy Associates within Hydrogenated $TiO_2$: A Positron Annihilation Study. Journal of Physical Chemistry C. 116(42), 22619-22624.
13. Leshuk, Tim, Roozbeh Parviz, Perry Everett, Harish Krishnakumar, Robert A. Varin, and

Frank Gu. 2013. Photocatalytic Activity of Hydrogenated TiO$_2$. ACS Applied Materials and Interfaces 5(6), 1892–95.

14. Lin, Liangxu, Juntong Huang, Xifei Li, Monsuru A. Abass, and Shaowei Zhang. 2017. Effective Surface Disorder Engineering of Metal Oxide Nanocrystals for Improved Photocatalysis. Applied Catalysis B: Environmental 203, 615–24.

15. Niederberger, Markus and Georg Garnweitner. 2006. Organic Reaction Pathways in the Nonaqueous Synthesis of Metal Oxide Nanoparticles. Chemistry - A European Journal 12(28), 7282–7302.

16. Ohtani, Bunsho, Yoshimasa Ogawa, and Sei-ichi Nishimoto. 1997. Photocatalytic Activity of Amorphous-Anatase Mixture of Titanium(IV) Oxide Particles Suspended in Aqueous Solutions. The Journal of Physical Chemistry B 67(6), 3746–52.

17. Rajaraman, T. S., S. P. Parikh, and V. G. Gandhi. 2020. Black TiO$_2$: A Review of Its Properties and Conflicting Trends. Chemical Engineering Journal 389, 123918

18. Shang, Huan, Meiqi Li, Hao Li, Shun Huang, Chengliang Mao, Zhihui Ai, and Lizhi Zhang. 2019. Oxygen Vacancies Promoted the Selective Photocatalytic Removal of NO with Blue TiO$_2$ via Simultaneous Molecular Oxygen Activation and Photogenerated Hole Annihilation. Environmental Science and Technology 53(11), 6444–53.

19. Si, Dawei, Zhenbiao Dong, Ting Li, Dongyan Ding, and Congqin Ning. 2019. Surface-Reduced Si-Doped TiO$_2$ Nanotubes for High-Efficiency Photoelectrochemical Water Splitting. Functional Materials Letters 12(6), 3–6.

20. Tan, Huaqiao, Zhao Zhao, Mang Niu, Chengyu Mao, Dapeng Cao, Daojian Cheng, Pingyun Feng, and Zaicheng Sun. 2014. A Facile and Versatile Method for Preparation of Colored TiO$_2$ with Enhanced Solar-Driven Photocatalytic Activity. Nanoscale 6(17), 10216–23.

21. Ullattil, Sanjay Gopal, Soumya B. Narendranath, Suresh C. Pillai, and Pradeepan Periyat. 2018. Black TiO$_2$ Nanomaterials: A Review of Recent Advances. Chemical Engineering Journal 343, 708–36.

22. Ullattil, Sanjay Gopal and Pradeepan Periyat. 2016. A 'One Pot' Gel Combustion Strategy towards Ti$^{3+}$ Self-Doped 'Black' Anatase TiO$_{2-x}$ Solar Photocatalyst. J. Mater. Chem. A 4(16), 5854–58.

23. Varma, K. S., Bharatiya, B., Tayade, R. J., Shukla, A. D., Joshi, P. A., & Gandhi, V. Degradation of Pharmaceutical Pollutants under UV Light using TiO$_2$ Nanomaterial Synthesized through Reverse Micelle Nanodomains. Advances in Wastewater Treatment I, 91(2021), 87-110.

24. Wang, Shanchi, Jingsheng Cai, Jiajun Mao, Shuhui Li, Jiali Shen, Shouwei Gao, Jianying Huang, Xiaoqin Wang, Ivan P. Parkin, and Yuekun Lai. 2019. Defective Black Ti$^{3+}$ Self-Doped TiO$_2$ and Reduced Graphene Oxide Composite Nanoparticles for Boosting Visible-Light Driven Photocatalytic and Photoelectrochemical Activity. Applied Surface Science 467, 45–55.

25. Wang, Xiangdong, Rong Fu, Qianqian Yin, Han Wu, Xiaoling Guo, Ruohan Xu, and Qianyun Zhong. 2018. Black TiO$_2$ Synthesized via Magnesiothermic Reduction for Enhanced Photocatalytic Activity. Journal of Nanoparticle Research 20(4), 1-10.

26. Wei, Yi, Jiaxin Zhu, Yixin Gan, and Gang Cheng. 2018. Titanium Glycolate-Derived TiO$_2$ Nanomaterials: Synthesis and Applications . Advanced Powder Technology. 29(10), 2289-2311.

27. Xing, Mingyang, Wenzhang Fang, Muhammad Nasir, Yunfei Ma, Jinlong Zhang, and Masakazu Anpo. 2013. Self-Doped Ti$^{3+}$-Enhanced TiO$_2$ Nanoparticles with a High-

Performance Photocatalysis. Journal of Catalysis 297, 236–43.

28. Xu, Jijian, Guilian Zhu, Tianquan Lin, Zhanglian Hong, Juan Wang, and Fuqiang Huang. 2015. Molten Salt Assisted Synthesis of Black Titania Hexagonal Nanosheets with Tuneable Phase Composition and Morphology. RSC Advances 5(104), 85928–32.

29. Yan, Xiaodong, Yong Li, and Ting Xia. 2017. Black Titanium Dioxide Nanomaterials in Photocatalysis. International Journal of Photoenergy 2017.

30. Zhang, Dandan, Gang Liu, Hong Lu, Shaodan Wang, and Qiang Wei. 2018. Preparation and Photocatalytic Activities of Black $TiO_2$ in Vacuum and Ambient Temperature Environment . Journal of Nanoscience and Nanotechnology, 19(1), 81–90.

# Solar light-responsive spinel and spinel composites for photocatalytic dye degradation: Review

*Parth Shah[†]\*, Kartik Joshi[†], Manan Shah^, Ashish Unnarkat^, Femina J. Patel[†]*

[†] *Department of Chemical Engineering, Vishwakarma Government Engineering College, Ahmedabad, Gujarat, India*

^ *Department of Chemical Engineering, School of Technology, Pandit Deendayal Petroleum University, Gandhinagar, Gujarat, India.*

*\*Corresponding author: shahparth2100@gmail.com, mobile number: +91 8866582715*

## Abstract

Coloured wastewater is of great concern due to its adverse effects on aquatic flora-fauna and human health. Among all available processes such as physical, chemical, biological, and electrochemical methods, photocatalysis can be a promising solution because of its ability to degrade colour-causing compounds completely by converting them into simpler molecules ($H_2O$, $CO_2$) depending on dye structure. In this review, spinel and their nanocomposites are studied as photocatalysts for dye degradation. Spinel and their nanocomposites show better separation ability, catalytic activity, relatively narrow bandgap, utilises large parts of the sunlight spectrum and better retardation of photoinduced charge carriers. Innovative techniques needed for surface modification and improving photocatalytic efficiency of spinel and their nanocomposites towards different pollutant degradation are briefly reviewed. Finally, challenges, gaps and future research need in order to improve the photocatalytic application of spinel and their nanocomposites are addressed.

**Keywords:** Photocatalytic dye degradation, Solar light-responsive, spinel, spinel composite

## 1. Introduction

Water is an essential component for life on the earth, though plenty of water is available on earth, only 0.03% of it is useful for human activities. (Osman 2014; Ahmed, Sushil, and Krishna 2012) Improving life standards, industrialization has adversely affected water quality. (Rajaram and Das 2008; Seow et al. 2016) In particular dye wastewater has a significant contribution to the deterioration of water quality as a large amount of water is consumed by dyes and related industries. The wet dying process causes maximum dye lost and contamination of effluent. (Robinson et al. 2000) This effluent contains 99.94% water and 0.06% are other pollutants by weight, though they have a significant effect on water quality. (Shivnarayan Singh 2015) Wastewater quality can be checked by certain physicochemical parameters such as pH, colour, Total Dissolved Solids (TDS), Total Suspended Solids (TSS), electrical conductivity, total solids (TS), Dissolved oxygen (DO), Chemical oxygen demand (COD), Biological oxygen demand (BOD), total alkalinity, total hardness and chloride content, phosphorous content, fluoride content, sulphur and heavy metal content. (Ahmed, Sushil, and Krishna 2012)

Dyes are the coloured compounds with the basic structure of skeleton, chromophore (causes colour), auxochrome (enhances the colour), and soluble part (make dyes soluble in solvents, optional). (Kiernan 2001) Dyes have a large area of application such as pharmaceuticals, foods, textiles, cosmetics, photoelectrochemical cell, paper and many more. (Forgacs, Cserháti, and Oros 2004; Khehra et al. 2006) More than 0.7 million tons of organic synthetic dyes are produced yearly, worldwide (Jonstrup et al. 2011). Also, over 10,000 different dyes are known

and have their applications in various industries. Studies indicate that approximately 10 % of synthetic dyes produced per year are lost to the environment during manufacturing and processing operations (S et al. 2005). Dyes can be classified according to their application and chemical structure. It is composed of a group of atoms responsible for the dye colour, called chromophores, as well as an electron-withdrawing or donating substituents that cause or intensify the colour of the chromophores, called auxochromes. The most important chromophores are azo (–N=N–), carbonyl (–C=O), ethylene (–C=C–), carbon-nitrogen group (–C=NH–), nitro (–NO$_2$–), and quinoid groups. The most important auxochromes are amines (–NH$_2$), carboxyl (–COOH), sulphonate (–SO$_3$H), and hydroxyl (–OH). The auxochromes can belong to the classes of reactive, acid, direct, basic, mordant, disperse, sulphur, and vat dyes based on the method of application (Klaus Hunger 2008; Mansoor 2008; Popli and Patel 2015). Base on structure dyes can be classified as Azo, Nitro, Indigoid, Anthraquinone, Phthalein, triphenyl methyl, Nitroso, Arylmethane and many other types are known. (Benkhaya, Souad, and El 2020; Kiernan 2001) And based on application dyes can be classified as acid, azoic, basic, direct, disperse, fluorescent brighteners, natural, solvent, sulfur, vat, reactive, mordant etc. (Gregory, n.d.)

For dyes removal from dye wastewater, different methods are available. Mainly three types of methods are available for dyes removal from dyes wastewater such as physical methods(Katheresan, Kansedo, and Lau 2018; Hethnawi et al. 2017; Yagub et al. 2014) (coagulation-flocculation(Liang et al. 2014), membrane separation, adsorption(Yagub et al. 2014; Salleh et al. 2011; Adegoke and Bello 2015; Zhou et al. 2018)), biological methods(Chacko and Subramaniam 2011; Mojsov et al. 2016; Manavi, Kazemi, and Bonakdarpour 2017; Srinivasan and Viraraghavan 2010), chemical methods (Advance oxidation processes, electrochemical destruction, direct oxidation etc.)(Forgacs, Cserháti, and Oros 2004; Gusain et al. 2019; Joshi, Bansal, and Purwar 2004; Nidheesh, Zhou, and Oturan 2018). Among these AOPs are novel and relatively better performing methods. AOPs cover many processes such as Fenton, ozonation, oxidation using H$_2$O$_2$, photocatalysis using metal-nonmetal semiconductors or spinel or combined catalyst. Physical methods do not destroy the dyes but carry out the mass transfer from the liquid phase into the solid phase commonly, hence there are the chances of colour regain after some time. While in biological processes only limited dyes can be degraded, because of the involvement of living organisms which can be killed by some compounds and have a limited range of pH and temperature. Even though biological processes are used at maximum extent for effluent treatment in ETP plant, but it has a limitation of time which makes it impractical for dyes degradation. And Chemical processes can destroy in lesser time then biological processes, hence these processes can be a promising option for dyes removal. Typically, with AOPs complete mineralization and partial oxidation to inert and less concerning products such as H$_2$O, CO$_2$ and other simpler products. (Anwer et al. 2019a; Babuponnusami and Muthukumar 2014; Hodges, Cates, and Kim 2018) Various AOPs are there such as Fenton, Photocatalysis, Hydrogen peroxide oxidation, Ultrasonic treatment, Ozonation, UV irradiation, Electrochemical and electron beam irradiation, and combination of these processes. Among these processes, Photocatalysis serve as a promising method as it makes use of sunlight possible and relatively cheaper process than other methods as separation of catalyst is possible. (Joseph et al. 2009; Verma and Samanta 2018; S Krishnan, H Rawindran, C M Sinnathambi 2017; Paździor, Bilińska, and Ledakowicz 2018; Anwer et al. 2019a; Babuponnusami and Muthukumar 2014)

This review aims to discuss photocatalytic dye degradation using spinel, spinel composite with other photocatalysts such as metal or non-metal based semiconductors. In successive sections basics of photocatalysts and afterwards, different spinels and composites are reported.

## 2. Photocatalysis

The word photocatalysis is combined with the prefix photo, characterized as 'light', and catalysis, characterized as a material that alters the rate of the chemical reaction. Thus, photocatalysis is a response that uses light to trigger a material that alters the rate of a chemical reaction without included itself. The mechanism is depicted in scheme 1 below. Irradiation of light causes excitation of electrons from Valance band (VB) to Conduction Band (CB) and causes the formation of holes in VB. (Kirankumar and Sumathi 2020)

$$\text{Photocatalyst} + h\nu \rightarrow hVB+ + eCB- \tag{1}$$

$$h_{VB}^+ + e_{CB}^- \rightarrow \text{energy (heat)} \tag{2}$$

$$H_2O + h_{VB}^+ \rightarrow \bullet OH \text{ (hydroxyl radical)} + H^+ \tag{3}$$

$$O_2 + e_{CB}^- \rightarrow \bullet O_2^- \text{ (superoxide radical)} \tag{4}$$

$$\bullet OH + \text{pollutant} \rightarrow \text{Intermediates} \rightarrow H_2O + CO_2 \tag{5}$$

$$\bullet O_2^- + \text{pollutant} \rightarrow \text{Intermediates} \rightarrow H_2O + CO_2 \tag{6}$$

*Scheme_1 Photocatalytic reaction steps* (Bora and Mewada 2017; Jo, Wan-Kuen 2014)

Photocatalysis follows two different pathways namely, (i) direct photocatalysis which further follows two processes, a. Heterogeneous photocatalysis-the Langmuir-Hinshelwood process, b. the Eley - Rideal process- photo-generated holes trapped by surface defects and (ii) Indirect photocatalysis, in later process photogenerated holes are trapped by a water molecule and converted in too the hydroxyl radicals. (Rauf and Ashraf 2009)

Different types of photocatalysts are investigated since the staring of this century, namely semiconductors- metal and non-metal type, perovskite, ilmenite, spinel and doped spinel and many more. Refer to the following table 1 to have an overview of photocatalytic dye degradation using different types of catalysts.

Table 1 Different types of photocatalysts for dye degradation

| Sr. No. | Catalyst | Bandgap (eV) | Synthesis method | Dye | Light source | Catalyst dosage (mg) | Dye Concentration (ppm) | Dye degradation (%) | Time (min) | Ref. |
|---|---|---|---|---|---|---|---|---|---|---|
| 1. | LaNiO$_{3-\delta}$ | - | Sol-gel | Methyl Orange | Under Dark condition | 150 | 5 | 94.3 | 240 | (Zhong et al. 2018) |
| 2. | CsPbI$_3$ | 1.89 | hydrothermal | Methyl violet | Osram lamp 150 W | 100 | 5 | 81.7 | | (Karami et al. 2020) |
| 3. | La$_{0.5}$Sr$_{0.5}$CoO$_3$ | 1.6 | Pechini method | Methyl Orange | UV light 4 W Philips TUV | 25 | 20 | 99.7 | 25 | (Verduzco et al. 2020) |
| 4. | LaCoO$_3$ hollow spheres | 2.07 | surface-ion adsorption method | Methylene Blue | 30 W UV-light | 10 | 10 | 87 | 100 | (Fu et al. 2013) |
| 5. | LaMnO$_3$ | 2.2 | Sol-gel | Methyl Orange | Visible light | | 6.5 | 100 | 60 | (Rekavandi, Malekzadeh, and Ghiasi 2019) |
| 6. | BaFeO$_{3-x}$ | | Sol-gel | Methyl Orange | Philips 250W | 10 | 20 | | | (Mengmeng Sun et al. 2010) |
| 7. | SrTiO$_3$/ BiOI | | Microwave-assisted Solvothermal method | Methyl Orange | Visible light- 250 W metal halide lamp | 40 | 1.22 *10$^{-4}$M | 180 | 94.6 | (C. Hu et al. 2019) |
| 8. | NaTaO$_{3-x}$N$_x$ | | One step Hydrothermal method | Methyl Orange | Sunlight | 100 | 20 | 100 with 95.21 % COD removal | 840 | (Liu, Jiang, and Gao 2011) |
| 9. | SrTiO$_3$ | 3.063 @12h reaction | Hydrothermal | CR | 150W Xe lamp | 1000 | 1 | 84 | 180 | (Gao, Yang, and Wang 2018) |
| 10. | Ag$_2$CO$_3$/ Bi$_2$O$_2$CO$_3$ | 2.28/ 3.35 | Solution method-precipitation | Rhodamine B | Visible light | 100 | 10 | 94% | 120 min | (Li et al. 2016) |
| 11. | Fe$_2$BiSbO$_7$ | N/A | Solid-State Reaction of Fe$_2$O$_3$, Bi$_2$O$_3$, and Sb$_2$O$_5$ | Methylene Blue | 500W Xenon lamp Visible light | 300 | 0.025 mM | 96.59& | 230 min | (Luan and Hu 2012) |

## 3. Semiconductors

A large variety of photocatalysts are known today, for example, metal oxides, metals, semiconductors, carbon-based nanostructures, quantum dots, metal-organic frameworks (MOFs). Among these majority of research work is done on the metal oxides which can be classified as i) first-generation- single-component oxides, sulphides, nitrides and phosphates are considers under this category e.g. $TiO_2$, ZnO, $ZrO_2$, ZnS, $SnO_2$, and NiO, but the problem with this catalysts is that their wider bandgap makes them effective only under UV light; ii) the Second generation- Composites fall under this category, here benefits of both the components are combined and more efficient catalyst is developed, but the separation is the main issue, even though filtration is used but some loss occurs during filtration hence loss of catalyst is a major problem at the end of the process; iii) the third generation – to overcome the problem immobilization of catalyst is done on some substrates via two approaches- binder through and binderless. Though the third generation can overcome the drawback of former generation catalyst at the cost of surface area and active sites, this methods reduces the total active sites available and uses costlier methods for fabrication of catalyst. Mechanism of all three generation s is shown in. (Anwer et al. 2019b)

More work is tabulated in table2.

Table 2 Semiconductors for photocatalytic dye degradation

| Sr. No. | Catalyst | Bandgap (eV) | Synthesis method | Dye | Light source | Catalyst dosage (mg) | Dye Concentration (ppm) | Dye degradation (%) | Time (min) | Ref. |
|---|---|---|---|---|---|---|---|---|---|---|
| 1. | $CdS/CdWO_4$ | 1.67/3.8 | Ultrasonic method | Malachite Green | 1 kW Xe lamp | 30 | 100 | 97 | 100 | (Cui et al. 2018) |
| 2. | core-shell structured $TiO_2$ | 3 | - | Methylene blue | 500 W Xe Lamp | | 5 | 81 | 150 | (H. Hu, Lin, and Hu 2020) |
| 3. | $LaNiO_3/TiO_2$ | 2.24/3.20 | Sol-gel | Methyl Orange | UV- light 300W high-pressure Hg lamp | 50 | 20 | 92 | 150 | (Chen et al. 2020) |
| 4. | ZnO | 3.37 | (Procured) | Methylene blue | Sunlight | 150 | 15 | 98% | 90 min | (Marcella and Melo 2019) |
| 5. | ZnO / Polyaniline | 2.99, 2.67, 2.59 | precipitation followed by sonication | Methyl Orange | UV-Visible light | 100. | - | 98.3 % | 180 min | (Saravanan et al. 2016) |
| 6. | $SMHAC/TiO_2 + H_2O_2$ | | | RR120 | UV light | 30/200 | 100 | 80% | 70 min | (Mahmoodi 2014) |
| 7. | CdS–grapheme | 2.15 (1:0.05 mol ratio) 2.15 | Hydrothermal method | Methyl Orange | 200 Xe lamp-Visible light | 50 | 10 | 95% | 60 min | (A. Ye et al. 2012) |
| 8. | CdS–CNT nanocomposites | 2.15 (1:0.05 mol ratio) | Hydrothermal | Methyl Orange | Visible light | 50 | 10 | 88% | 60 min | (A. Ye et al. 2012) |
| 9. | $g-C_3N_4 / Ag_3VO_4$ | 2.2/2.7 | Facile precipitation method | basic fuchsine | Visible light | 50 | 20 | 95% | 2.5 hr | (Shaomang Wang et al. 2014) |
| 10. | N-doped $TiO_2$ | 2.5 | Sol-gel method | Methylene Blue | Visible light | 30 | 9 | 80 | 300 | (Sacco et al. 2012) |
| 11. | ZnO NPs | 3.7 | Sol-gel method | Reactive Blue 21 | UV light | 50 | 20 | ~90 % | 270 min | (Davar, Majedi, and Mirzaei 2015) |
| 12. | $Fe_2O_3/Cu_2O$ | 1.85 | Hydrothermal method | Janus green | UV light | 100 | 9 mM | 79.15% | 120 min | (Abhilash 2019) |
| 13. | ZnO | 3.37 | Procured | Reactive Blue | UV-light | 800 | 50 | 99% | 240 min | (Pardiwala, Patel, and Patel 2017) |

## 4. Spinel

Spinels are a class of mixed metal oxide of chemical composition $AB_2O_4$, where $A^{2+}$ represents divalent metal ion, $B3þ$ denotes trivalent metal ion, and $O^{2-}$ anions. The crystal system of spinel oxide has cubic symmetry with an $Fd_3m$ space group (EIICHI HANAMURA et al. 2003). The spinel oxide unit cell containing 32 $O^{2-}$, 8 $A^{2+}$, and 16 $B^{3+}$, in which 32 $O^{2-}$ anions frame a face-centred cubic system by 8 cations involving 64 tetrahedral interstices ($A^{2+}$ sites) and the rest of the 16 cations involving 32 octahedral interstices ($B^{3+}$ locations). An aggregate of 24 cations possesses the accessible 96 interstices inside the spinel oxide unit cell, leaving the important quantity of vacant interstitial voids and letting for the movement of cations among voids [11]. (Kirankumar and Sumathi 2020) Ion on A is divalent (+2 charge) and on B is trivalent (+3 charge). Very common A site ions are $Zn^{+2}$, $Ni^{+2}$, $Mg^{+2}$, $Cu^{+2}$, $Co^{+2}$, $Mn^{+2}$, $Ag^{+2}$, $Ce^{+2}$, $V^{+2}$ last three are rarely investigated and for B site, $Fe^{+3}$, $Al^{+3}$, $Cr^{+3}$, $Mn^{+3}$, $Ga^{+3}$, $Ru^{+3}$, $Ti^{+3}$, $Co^{+3}$, first two are investigated extensively among all type of B site metal ions. Spinel structure is shown in the following figure.1 And Table 3 has tabulated some spinels for photocatalytic dye degradation
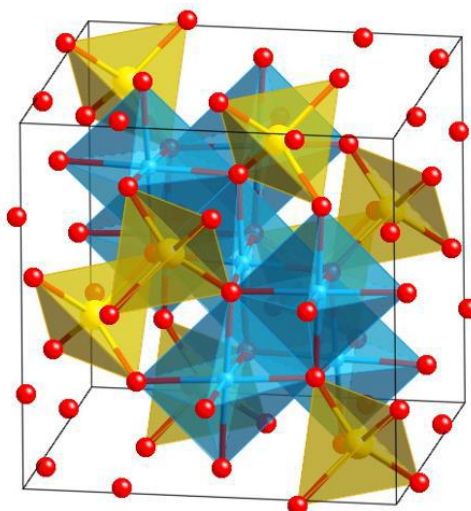


Figure 1 Spinel structure(Kefeni and Mamba 2019)

Table 3 Spinel photocatalysts for dye degradation

| Sr. No. | Catalyst | Bandgap (eV) | Synthesis method | Dye | Light source | Catalyst dosage (mg) | Dye Concentration (ppm) | Dye degradation (%) | Time (min) | Ref. |
|---|---|---|---|---|---|---|---|---|---|---|
| 1. | $MgFeCrO_4$ | 1.67 | Sol-gel method | direct black 122 | Visible light | 40 | 40 | 96% | 60 s | Moradnia et al. (2020) |
| 2. | $Ni_{0.6}Mn_{0.4}Fe_2O_4$ | 2.19 | Microwave irradiation method | Methylene Blue | UV-light | 300 | - | 96.73% | 270 min | Mathubala et al. (2016) |
| 3. | $ZnGa_2S_4$ | 2.33 | Co-precipitation method–Thiourea reduction reaction | Methylene Blue | Visible light | 600 | 100 | 99.2% | 60 min. | Peng et al. (2015) |
| 4. | $ZnAl_2O_4$ | | Co-precipitation | Direct Black 38 | UV- visible | 1000 | 80 | 99% | 240 min | (Battiston et al. 2014) |
| 5. | $MnFe_2O_4$: $Cu^{2+}$ (3 mol%) | 2 | Solution Combustion | malachite green | sunlight | 60 | 20 | ~ 92 | 120 | (Meena et al. 2017) |
| 6. | $MgAl_2O_4$:Ce:Mn | 2.95 | gamma-ray irradiation-assisted polyacrylamide gel method | Methylene Blue | Sunlight | | | 90 | 180 | (Shifa Wang et al. 2019) |
| 7. | $CoFe_2O_4$ | | Co-Precipitation | Rhodamine B | Sunlight | 0.1 | 5 | 63.62 | 90 | (Revathi et al., n.d.) |
| 8. | $Zn_{0.25}Co_{0.75}FeMnO_4$ | 2.41 | Sol-Gel | Methylene Blue | sunlight | 200 | 10 | 99 | 20 | (Jangam et al. 2020) |
| 9. | $CuFe_{2-x}Ce_xO_4$ | 2.8 | AC | Methyl Orange | UV-light | 100 | 10 | 66 | 60 | (Rahimi-nasrabadi and Sobhani-nasab 2016) |
| 10. | $CoAl_{0.3}Fe_{1.7}O_4$ | | Sol-gel | Methylene Blue | Visible light | 100 | 10 | 93 | 120 | (N. Abbas et al., n.d.) |
| 11. | $NiRu_{0.4}Fe_{1.6}O_4$ | 1.42 | Sol-Gel | RDR | Visible light | 50 | 60 | ~ 90 | 10 | (Sneha Singh et al. 2019) |

## 5. Composite catalysts (spinel with semiconductors)

Need for composite arises, because of separation issues of non-magnetic semiconductors ($TiO_2$, ZnO, ZnS, etc.) after treatment, because of small size separation is difficult, expensive and time-consuming too, even complete separation is also not possible hence there is a loss of catalyst (Mamba and Mishra 2016). Because of this loss, additional environmental pollutants are added. These problems reduce the practical application at large scales. Along with separation issues bandgap of these semiconductors are wide and needs irradiation of UV light, this also makes this technique inapplicable at large scale. Hence incorporation of spinels in semiconductors creates a different type of junctions and reduces the bandgap and if the spinel is magnetic it will make composite magnetically separable. Along with these advantages, this incorporation improves the relative stability in acidic and basic conditions while parent catalyst alone can perform well with some specific conductions only. These all advantages add on one more and very important advantage of better degradation of dyes. (Govan and Gun'ko 2014; Gawande et al. 2015; Johnson 2017; Parsons et al. 2009; Zhang et al. 2010; D. Wang and Astruc 2017; Meijuan Sun, Han, and Chen 2019)

Jing et al.(2016) have investigated the photocatalytic performance of $Ag/Ag_3VO_4$ and 5% $CoFe_2O_4/Ag/Ag_3VO_4$ composite. The result has shown that 49.75% and 61.48% tetracycline was photo-degraded, respectively. This shows that incorporation of $CoFe_2O_4$ improves the activity, and even composite shows magnetic separability. They have confirmed the better performance for several runs.

Another example is Fenton like a catalyst- $Fe_3O_4@SiO_2$ for the decomposition of methylene blue dye in presence of $H_2O_2$. Results show higher activity than $Fe_3O_4$ alone. (Yang et al. 2015) In one more study 99% degradation of methylene blue with $Fe_3O_4@TiO_2$ with $H_2O_2$ within 5 minutes. M. Abbas et al. (2014)  While another study shows a degradation of methylene blue with $Fe_3O_4$/chitosan/$TiO_2$ nanocomposites, results shows 93% degradation within 40 min. (Xiang et al. 2015). Shekofteh-Gohari and Habibi-Yangjeh (2016) have also investigated Fe3O4/ZnO/CuWO4 for photodegradation of Rhodamine B dyes and it shows better performance than binary composites Fe3O4/ZnO or Fe3O4/CuWO4, the reason is the same as discussed earlier.

Photocatalytic activity of core-shell structured $Fe_3O_4/SiO_2/TiO_2$ nanocomposites synthesised using the sol-gel process was compared with $SiO_2$ $TiO_2$ by Ye et al. (M. Ye et al. 2010), This composite shows additional advantages of high chemical stability, fast magnetic separation and maintenance of the photocatalytic activity for at least eighteen cycles. Similarly, Wang et al.(R. Wang et al. 2012) synthesised $Fe_3O_4/SiO_2/TiO_2$ NCs using the sol-gel method and investigated its photocatalytic activity on MB that was present in an aqueous solution at room temperature and pH = 10. Under UV irradiation, the NCs showed higher photodegradation of MB (78%) within 5 min. Here in table 3 some of the other composites are briefed.

Table 4 Composites for photocatalytic dye degradation

| Sr. No. | Catalyst | Bandgap (eV) | Synthesis method | Dye | Light source | Catalyst dosage (mg) | Dye Concentration (ppm) | Dye degradation (%) | Time (min) | Ref. |
|---|---|---|---|---|---|---|---|---|---|---|
| 1. | $CoCr_2O_4/TiO_2$ (7:10)<br>$CoCr_2O_4$ | | Sol-gel | Methyl Orange | UV light | 20 | 5 | 95<br>80 | 90 | (Shojaei, Tabari, and Loghmani 2013) |
| 2. | $Ni_{0.65}Zn_{0.35}Fe_2O_4$/r-GO<br>$Ni_{0.65}Zn_{0.35}Fe_2O_4$ | 1.84<br>1.91 | Ultrasonic approach<br>Co-precipitation | Methylene Blue | Visible light | 100 | 5 | 95<br>55 | 56 | (Javed et al. 2019) |
| 3. | $Zf_{0.06}Mg_{0.197}Co_{0.797}Fe_2O_4$-rGo<br>$Zf_{0.06}Mg_{0.197}Co_{0.797}Fe_2O_4$ | | Ultra-sonication<br>Co-precipitation | Methylene Blue | UV-Visible light | 100 | 10 | 75<br>60 | 100 | (Shabbir et al. 2019) |
| 4. | $NiFe_2O_4/TiO_2$ (40%) | | Sol-gel | Methyl Orange | UV light | 100 | 8 | 90 | 90 | (Baig, Pervaiz, and Afzal 2020) |
| 5. | $La_2O_2CO_3/ZnFe_2O_4$/r-GO | 3.4/1.9 | Hydrothermal induced precipitation | Rhodamine B | UV light | 100 | 30 | 90 | 180 | (Jun et al. 2020) |
| 6. | $TiO_2/ZnCr_2O_4$ | 3.0 | Precipitation | Methylene Blue | UV-light | 50 | 30 | 99 | 120 | (Salehi, Eshaghi, and Tajizadegan 2019) |
| 7. | $ZnCr_2O_4/ZnS$ | 2.76/3.71 | Wet precipitation | Methyl Orange | Visible light | 40 | 40 | 96.88 | 105 | (Palanisamy et al. 2020) |
| 8. | $ZnO/ZnAl_2O_4$/0.06 mol KOH | | Co-precipitation | Methylene Blue | Visible light | 60 | 35 | 100 | 240 | (Somraksa, Amornpitoksuk, and Suwanboon 2019) |
| 9. | $NiAl_2O_4$/GQDs | | co-precipitation | RhB ($2 \times 10^{-5}$ mol $L^{-1}$) | Solar light | 1500 | 20 ml | 70 | 120 | (Regulska, Breczko, and Basa 2019) |
| 10. | $CoFe_2O_4/ZnO$/Ag<br>$CoFe_2O_4/ZnO$ | | Auto combustion + Sonication | Acid violet | UV light | 50 | 25 | 25<br>76 | 100 | (Ferdosi, Bahiraei, and Ghanbari 2019) |

## 6. Conclusion

It can be observed that composite type catalyst adds on the benefits of both types of catalysts, spinel and semiconductors. To add the magnetic nature to composites ferrite of ferromagnetic spinels should be taken as one of the parent catalysts. Because if incorporation of spinel in semiconductors it improves the magnetic properties and reduces the band gap because of formation of junctions between the catalysts which enhance the formation of hydroxyl radical and oxygen radicals which finally increase the degradation efficiency. Still, further work can be done with industrial effluent as very less or no work has been carried out with industrial effluent, and if done it didn't show that much efficiency.

## Acknowledgement

**References**

1. Abbas, Mohamed, B. Parvatheeswara Rao, Venu Reddy, and Cheolgi Kim. 2014. "Fe3O4/TiO2 Core/Shell Nanocubes: Single-Batch Surfactantless Synthesis, Characterization and Efficient Catalysts for Methylene Blue Degradation." *Ceramics International* 40 (7): 11177–86. https://doi.org/10.1016/j.ceramint.2014.03.148.

2. Abbas, Naseem, Nida Rubab, Natasha Sadiq, Suryyia Manzoor, Muhammad Imran Khan, Javier Fernandez Garcia, Isaias Barbosa Aragao, Muhammad Tariq, Zeeshan Akhtar, and Ghazala Yasmin. n.d. "Aluminum-Doped Cobalt Ferrite as an Efficient Photocatalyst for the Abatement of Methylene Blue."

3. Abhilash, Mavinakere Ramesh. 2019. "RSC Advances Photocatalytic Dye Degradation and Biological," 8557–68. https://doi.org/10.1039/c8ra09929d.

4. Adegoke, Kayode Adesina, and Olugbenga Solomon Bello. 2015. "Dye Sequestration Using Agricultural Wastes as Adsorbents." *Water Resources and Industry* 12: 8–24. https://doi.org/10.1016/j.wri.2015.09.002.

5. Ahmed, Thoker Farook, Mandira Sushil, and Manderia Krishna. 2012. "Impact of Dye Industrial Effluent on Physicochemical Characteristics of Kshipra River, Ujjain City, India" 1 (June): 41–45.

6. Anwer, Hassan, Asad Mahmood, Jechan Lee, Ki-Hyun Kim, Jae-woo Park, and Alex C K Yip. 2019a. "Photocatalysts for Degradation of Dyes in Industrial Effluents : Opportunities and Challenges" 12 (1).

7. ———. 2019b. "Photocatalysts for Degradation of Dyes in Industrial Effluents : Opportunities and Challenges" 12 (5): 955–72.

8. Babuponnusami, Arjunan, and Karuppan Muthukumar. 2014. "A Review on Fenton and improvements to the Fenton Process for Wastewater Treatment." *Journal of Environmental Chemical Engineering* 2 (1): 557–72. https://doi.org/10.1016/j.jece.2013.10.011.

9. Baig, Mutawara Mahmood, Erum Pervaiz, and Muhammad Junaid Afzal. 2020. "Catalytic Activity and Kinetic Studies of Core @ Shell Nanostructure NiFe 2 O 4 @ TiO 2 for Photocatalytic Degradation of Methyl Orange Dye" 42 (04): 531–41.

10. Battiston, Suellen, Caroline Rigo, Cruz Severo, and Marcio Antonio. 2014. "Synthesis of Zinc Aluminate ( ZnAl 2 O 4 ) Spinel and Its Application as Photocatalyst" 17 (3): 734–38.

11. Benkhaya, Said, M Souad, and Ahmed El. 2020. "Classifications, Properties, Recent Synthesis and Applications of Azo Dyes" 6 (October 2019). https://doi.org/10.1016/j.heliyon.2020.e03271.

12. Bora, Leena V, and Rajubhai K Mewada. 2017. "Visible / Solar Light Active Photocatalysts for Organic eFFL Unit Treatment : Fundamentals, Mechanisms and Parametric Review." *Renewable and Sustainable Energy Reviews* 76 (April): 1393–1421. https://doi.org/10.1016/j.rser.2017.01.130.

13. Chacko, Joshni T, and Kalidass Subramaniam. 2011. "Enzymatic Degradation of Azo Dyes – A Review." *International Journal Of Environmental Sciences* 1 (6): 1250–60. https://doi.org/10.6088/ijes.00106020018.

14. Chen, Chen, Jialing Zhou, Junfeng Geng, Ruiyu Bao, Zhonghua Wang, Jianxin Xia, and Hua Li. 2020. "Perovskite LaNiO3/TiO2 Step-Scheme Heterojunction with Enhanced Photocatalytic Activity." *Applied Surface Science* 503. https://doi.org/10.1016/j.apsusc.2019.144287.

15. Cui, Haojie, Beibei Li, Zhongyu Li, Xiazhang Li, and Song Xu. 2018. "Z-scheme Based CdS/CdWO 4 Heterojunction Visible Light Photocatalyst for Dye Degradation and Hydrogen Evolution." *Applied Surface Science* 455 (May): 831–40. https://doi.org/10.1016/j.apsusc.2018.06.054.

16. Davar, Fatemeh, Ali Majedi, and Alireza Mirzaei. 2015. "Green Synthesis of ZnO Nanoparticles and Its Application in the Degradation of Some Dyes" 1746: 1739–46. https://doi.org/10.1111/jace.13467.

17. EIICHI HANAMURA, YUTAKA KAWABE, HIDEAKI TAKASHIMA, TOKUSHI SATO, and AYANA TOMITA. 2003. "Optical Properties of Transition-Metal Doped Spinels" 12 (4): 467–73.

18. Ferdosi, E., H. Bahiraei, and D. Ghanbari. 2019. "Investigation the Photocatalytic Activity of CoFe2O4/ZnO and CoFe2O4/ZnO/Ag Nanocomposites for Purification of Dye Pollutants." *Separation and Purification Technology* 211: 35–39. https://doi.org/10.1016/j.seppur.2018.09.054.

19. Forgacs, Esther, Tibor Cserháti, and Gyula Oros. 2004. "Removal of Synthetic Dyes from Wastewaters: A Review." *Environment International* 30 (7): 953–71. https://doi.org/10.1016/j.envint.2004.02.001.

20. Fu, Shasha, Helin Niu, Zhiyin Tao, Jiming Song, Changjie Mao, Shengyi Zhang, Changle Chen, and Dong Wang. 2013. "Low-Temperature Synthesis and Photocatalytic Property of Perovskitetype LaCoO3 Hollow Spheres." *Journal of Alloys and Compounds* 576: 5–12. https://doi.org/10.1016/j.jallcom.2013.04.092.

21. Gao, Huajing, Hua Yang, and Shifa Wang. 2018. "Hydrothermal Synthesis, Growth Mechanism, Optical Properties and Photocatalytic Activity of Cubic SrTiO3 Particles for the Degradation of Cationic and Anionic Dyes." *Optik* 175: 237–49. https://doi.org/10.1016/j.ijleo.2018.09.027.

22. Gawande, Manoj B., Yukti Monga, Radek Zboril, and R. K. Sharma. 2015. "Silica-Decorated Magnetic Nanocomposites for Catalytic Applications." *Coordination Chemistry Reviews* 288: 118–43. https://doi.org/10.1016/j.ccr.2015.01.001.

23. Govan, Joseph, and Yurii Gun'ko. 2014. "Recent Advances in the Application of Magnetic Nanoparticles as a Support for Homogeneous Catalysts." *Nanomaterials* 4 (2): 222–41. https://doi.org/10.3390/nano4020222.

24. Gregory, Peter. n.d. "Dye and Dye Intermediates," no. Ci: 1–16.

25. Gusain, Rashi, Kanika Gupta, Pratiksha Joshi, and Om P Khatri. 2019. "Adsorptive Removal and Photocatalytic Degradation of Organic Pollutants Using Metal Oxides and Their Composites : A Comprehensive Review Adsorptive Removal and Photocatalytic Degradation of Organic Pollutants Using Metal Oxides and Their Composites : A Co." *Advances in Colloid and Interface Science* 272 (August): 102009. https://doi.org/10.1016/j.cis.2019.102009.

26. Hethnawi, Afif, Nashaat N. Nassar, Abdallah D. Manasrah, and Gerardo Vitale. 2017. *Polyethylenimine-Functionalized Pyroxene Nanoparticles Embedded on Diatomite for Adsorptive Removal of Dye from Textile Wastewater in a Fixed-Bed Column. Chemical Engineering Journal.* Vol. 320. Elsevier B.V. https://doi.org/10.1016/j.cej.2017.03.057.

27. Hodges, Brenna C., Ezra L. Cates, and Jae Hong Kim. 2018. "Challenges and Prospects of Advanced Oxidation Water Treatment Processes Using Catalytic Nanomaterials." *Nature Nanotechnology* 13 (8): 642–50. https://doi.org/10.1038/s41565-018-0216-x.

28. Hu, Chechia, Hui Xin Huang, Yi Feng Lin, Masaaki Yoshida, and Tzu Hsin Chen. 2019. "Decoration of SrTiO 3 Nanofibers by BiOI for Photocatalytic Methyl Orange Degradation under Visible Light Irradiation." *Journal of the Taiwan Institute of Chemical Engineers* 96 (xxxx): 264–72. https://doi.org/10.1016/j.jtice.2018.11.020.

29. Hu, Haiyang, Yan Lin, and Yun Hang Hu. 2020. "Core-Shell Structured TiO2 as Highly Efficient Visible Light Photocatalyst for Dye Degradation." *Catalysis Today* 341 (October 2018): 90–95. https://doi.org/10.1016/j.cattod.2019.01.077.

30. Jangam, Kundan, Kundan Patil, Sagar Balgude, Sunil Patange, and Paresh More. 2020. "Jo Ur Na l P Re Of." *Journal of Physics and Chemistry of Solids*, 109700. https://doi.org/10.1016/j.jpcs.2020.109700.

31. Javed, Hafsa, Abdul Rehman, Sara Mussadiq, Muhammad Shahid, Muhammad Azhar Khan, Imran Shakir, Philips Olaleye Agboola, Mohamed F.Aly Aboud, and Muhammad Farooq Warsi. 2019. "Reduced Graphene Oxide-Spinel Ferrite Nano-Hybrids as Magnetically Separable and Recyclable Visible Light-Driven Photocatalyst." *Synthetic Metals* 254 (February): 1–9. https://doi.org/10.1016/j.synthmet.2019.05.013.

32. Jing, Liquan, Yuanguo Xu, Shuquan Huang, Meng Xie, Minqiang He, Hui Xu, Huaming Li, and Qi Zhang. 2016. "Novel Magnetic CoFe2O4/Ag/Ag3VO4 Composites: Highly Efficient Visible Light Photocatalytic and Antibacterial Activity." *Applied Catalysis B: Environmental* 199: 11–22. https://doi.org/10.1016/j.apcatb.2016.05.049.

33. Jo, Wan-Kuen, Rajesh J. ayade. 2014. "Recent Developments in Photocatalytic Dye Degradation upon Irradiation with Energy - Efficient Light Emitting Diodes" 35 (11): 1781–92. https://doi.org/10.1016/S1872.

34. Johnson, Brian F.G. 2017. "Model Nanoparticles in Catalysis." *Metal Nanoparticles and Clusters: Advances in Synthesis, Properties and Applications* 24 (October): 165–99. https://doi.org/10.1007/978-3-319-68053-8_5.

35. Jonstrup, M., N. Kumar, M. Murto, and B. Mattiasson. 2011. "Sequential Anaerobic-Aerobic Treatment of Azo Dyes: Decolourisation and Amine Degradability." *Desalination* 280 (1–3): 339–46. https://doi.org/10.1016/j.desal.2011.07.022.

36. Joseph, Collin G., Gianluca Li Puma, Awang Bono, and Duduku Krishnaiah. 2009. "Sonophotocatalysis in Advanced Oxidation Process: A Short Review." *Ultrasonics Sonochemistry* 16 (5): 583–89. https://doi.org/10.1016/j.ultsonch.2009.02.002.

37. Joshi, M, R Bansal, and R Purwar. 2004. "Colour Removal from Textile Effluents." *Indian Journal of Fibre & Textile Research* 29 (June): 239–59.

38. Jun, Byung Moon, S. SD Elanchezhiyan, Yeomin Yoon, Dengjun Wang, Soonhyun Kim, Subbaiah Muthu Prabhu, and Chang Min Park. 2020. "Accelerated Photocatalytic Degradation of Organic Pollutants over Carbonate-Rich Lanthanum-Substituted Zinc Spinel Ferrite Assembled Reduced Graphene Oxide by Ultraviolet (UV)-Activated Persulfate." *Chemical Engineering Journal* 393 (February): 124733. https://doi.org/10.1016/j.cej.2020.124733.

39. Karami, Maryam, Mojgan Ghanbari, Omid Amiri, and Masoud Salavati-Niasari. 2020. "Enhanced Antibacterial Activity and Photocatalytic Degradation of Organic Dyes under Visible Light Using Cesium Lead Iodide Perovskite Nanostructures Prepared by Hydrothermal Method." *Separation and Purification Technology* 253 (July): 117526. https://doi.org/10.1016/j.seppur.2020.117526.

40. Katheresan, Vanitha, Jibrail Kansedo, and Sie Yon Lau. 2018. "Efficiency of Various Recent Wastewater Dye Removal Methods : A Review" 6 (June): 4676–97. https://doi.org/10.1016/j.jece.2018.06.060.

41. Kefeni, Kebede Keterew, and Bhekie Brilliance Mamba. 2019. "Photocatalytic Application of Spinel Ferrite Nanoparticles and Nanocomposites in Wastewater Treatment: Review Kebede." *Sustainable Materials and Technologies*, e00140. https://doi.org/10.1016/j.susmat.2019.e00140.

42. Khehra, Manjinder Singh, Harvinder Singh Saini, Deepak Kumar Sharma, Bhupinder Singh Chadha, and Swapandeep Singh Chimni. 2006. "Biodegradation of Azo Dye C.I. Acid Red 88 by an Anoxic - Aerobic Sequential Bioreactor." *Dyes and Pigments* 70 (1): 1–7. https://doi.org/10.1016/j.dyepig.2004.12.021.

43. Kiernan, J A. 2001. "Classification and Naming of Dyes, Stains and Fluorochromes" 2111: 261–78.

44. Kirankumar, V. S., and S. Sumathi. 2020. "A Review on Photodegradation of Organic Pollutants Using Spinel Oxide." *Materials Today Chemistry* 18: 100355. https://doi.org/10.1016/j.mtchem.2020.100355.

45. Klaus Hunger, ed. 2008. *Industrial Dyes: Chemistry, Properties, Applications*.

46. Li, Tingting, Xiaolong Hu, Chaochao Liu, Chunming Tang, Xinkai Wang, and Shenglian Luo. 2016. "Efficient Photocatalytic Degradation of Organic Dyes and Reaction Mechanism with Ag2CO3/Bi2O2CO3 Photocatalyst under Visible Light Irradiation." *"Journal of Molecular Catalysis. A Chemical."* https://doi.org/10.1016/j.molcata.2016.10.001.

47. Liang, Can Zeng, Shi Peng Sun, Fu Yun Li, Yee Kang Ong, and Tai Shung Chung. 2014. "Treatment of Highly Concentrated Wastewater Containing Multiple Synthetic Dyes by a Combined Process of Coagulation/Flocculation and Nanofiltration." *Journal of Membrane Science* 469: 306–15. https://doi.org/10.1016/j.memsci.2014.06.057.

48. Liu, Da Rui, Yin Shan Jiang, and Gui Mei Gao. 2011. "Photocatalytic Degradation of an Azo Dye Using N-Doped NaTaO3 Synthesized by One-Step Hydrothermal Process." *Chemosphere* 83 (11): 1546–52. https://doi.org/10.1016/j.chemosphere.2011.01.033.

49. Luan, Jingfei, and Zhitian Hu. 2012. "Synthesis, Property Characterization, and Photocatalytic Activity of Novel Visible Light-Responsive Photocatalyst Fe 2 BiSbO 7" 2012. https://doi.org/10.1155/2012/301954.

50. Mahmoodi, Niyaz Mohammad. 2014. "Binary Catalyst System Dye Degradation Using Photocatalysis" 15 (2): 273–80. https://doi.org/10.1007/s12221-014-0273-1.

51. Mamba, Gcina, and Ajay Mishra. 2016. "Advances in Magnetically Separable Photocatalysts: Smart, Recyclable Materials for Water Pollution Mitigation." *Catalysts* 6 (6): 1–34. https://doi.org/10.3390/catal6060079.

52. Manavi, Narges, Amir Sadegh Kazemi, and Babak Bonakdarpour. 2017. "The Development of Aerobic Granules from Conventional Activated Sludge under Anaerobic-Aerobic Cycles and Their Adaptation for Treatment of Dyeing Wastewater." *Chemical Engineering Journal* 312: 375–84. https://doi.org/10.1016/j.cej.2016.11.155.

53. Mansoor, Iqbal. 2008. "Textile Dyes." *REHBAR PUBLISHERS KARACHI*.

54. Marcella, Maria, and Medeiros Melo. 2019. "Solar Heterogeneous Photocatalysis ( ZnO / UV ) for Textile Dyes Removal," 65–71. https://doi.org/10.1002/tqem.21584.

55. Mathubala, G, A Manikandan, S Arul Antony, and P Ramar. 2016. "Photocatalytic Degradation of Methylene Blue Dye and Magneto- Optical Studies of Magnetically Recyclable Spinel Ni x Mn 1-x Fe 2 O 4 ( x ¼ 0 . 0 e 1 . 0 ) Nanoparticles" 1113: 79–87. https://doi.org/10.1016/j.molstruc.2016.02.032.

56. Meena, S, L Renuka, K S Anantharaju, Y S Vidya, and H P Nagaswarupa. 2017. "Optical , Electrochemical and Photocatalytic Properties of Sunlight Driven Cu Doped Manganese Ferrite Synthesized By Solution Combustion Synthesis." *Materials Today: Proceedings* 4 (11): 11773–81. https://doi.org/10.1016/j.matpr.2017.09.094.

57. Mojsov, Kiro D, Darko Andronikov, Aco Janevski, Aco Kuzelov, and Stevan Gaber. 2016. "The Application of Enzymes for the Removal of Dyes From." *Advanced Technologies* 5 (1): 81–86.

58. Moradnia, Farzaneh, Saeid Taghavi, Ali Ramazani, and Vinod Kumar. 2020. "Green Synthesis of Recyclable MgFeCrO 4 Spinel Nanoparticles for Rapid Photodegradation of Direct Black 122 Dye." *Journal of Photochemistry & Photobiology, A: Chemistry* 392 (November 2019): 112433. https://doi.org/10.1016/j.jphotochem.2020.112433.

59. Nidheesh, P. V., Minghua Zhou, and Mehmet A. Oturan. 2018. "An Overview on the Removal of Synthetic Dyes from Water by Electrochemical Advanced Oxidation Processes." *Chemosphere* 197: 210–27. https://doi.org/10.1016/j.chemosphere.2017.12.195.

60. Osman, Mohamed. 2014. "Waste Water Treatment in Chemical Industries: The Concept and Current Technologies." *Journal of Waste Water Treatment & Analysis* 05 (01): 1–12. https://doi.org/10.4172/2157-7587.1000164.

61. Palanisamy, G., T. Pazhanivel, K. Bhuvaneswari, G. Bharathi, G. Marimuthu, and T. Maiyalagan. 2020. "Spinel Oxide ZnCr2O4 Incorporated with ZnS Quantum Dots for Application on Visible Light Driven Photocatalyst Azo Dye Degradation." *Colloids and Surfaces A: Physicochemical and Engineering Aspects* 590 (December 2019): 124505. https://doi.org/10.1016/j.colsurfa.2020.124505.

62. Pardiwala, Julie M, Femina J Patel, and Sanjay S Patel. 2017. "PHOTOCATALYTIC DEGRADATION OF RB21 DYE BY TIO 2 AND Z N O UNDER NATURAL SUNLIGHT , MICROWAVE IRRADIATION AND UV-REACTOR" 8 (1): 8–16.

63. Parsons, J. G., M. L. Lopez, J. R. Peralta-Videa, and J. L. Gardea-Torresdey. 2009. "Determination of Arsenic(III) and Arsenic(V) Binding to Microwave Assisted Hydrothermal Synthetically Prepared Fe3O4, Mn3O4, and MnFe2O4 Nanoadsorbents." *Microchemical Journal* 91 (1): 100–106. https://doi.org/10.1016/j.microc.2008.08.012.

64. Paździor, Katarzyna, Lucyna Bilińska, and Stanisław Ledakowicz. 2018. "A Review of the Existing and Emerging Technologies in the Combination of AOPs and Biological Processes in Industrial Textile Wastewater Treatment." *Chemical Engineering Journal*. https://doi.org/10.1016/j.cej.2018.12.057.

65. Peng, Ding, Zhang Min, Xie Zhonglei, and Cao Lihong. 2015. "Synthesis of the ZnGa 2 S 4 Nanocrystals and Their Visible-Light Photocatalytic Degradation Property" 2015.

66. Popli, S., and Upendra D. Patel. 2015. "Destruction of Azo Dyes by Anaerobic–Aerobic Sequential Biological Treatment: A Review." *International Journal of Environmental Science and Technology* 12 (1): 405–20. https://doi.org/10.1007/s13762-014-0499-x.

67. Rahimi-nasrabadi, Mehdi, and Mohsen Behpour Ali Sobhani-nasab. 2016. "Nanocrystalline Ce-Doped Copper Ferrite : Synthesis , Characterization , and Its Photocatalyst Application." https://doi.org/10.1007/s10854-016-5305-8.

68. Rajaram, T Ã, and Ashutosh Das. 2008. "Water Pollution by Industrial Effluents in India : Discharge Scenarios and Case for Participatory Ecosystem Specific Local Regulation" 40: 56–69. https://doi.org/10.1016/j.futures.2007.06.002.

69. Rauf, M A, and S Salman Ashraf. 2009. "Fundamental Principles and Application of Heterogeneous Photocatalytic Degradation of Dyes in Solution Fundamental Principles and Application of Heterogeneous Photocatalytic Degradation of Dyes in Solution," no. June 2019. https://doi.org/10.1016/j.cej.2009.02.026.

70. Regulska, Elzbieta, Joanna Breczko, and Anna Basa. 2019. "Pristine and Graphene-Quantum-Dots-Decorated Spinel Nickel Aluminate for Water Remediation from Dyes and Toxic Pollutants." *Water (Switzerland)* 11 (5). https://doi.org/10.3390/w11050953.

71. Rekavandi, Neda, Azim Malekzadeh, and Elham Ghiasi. 2019. "Methyl Orange Degradation Using Nano-LaMnO3 as a Green Catalyst under the Mild Conditions." *Nanochem Res* 4 (1): 1–10. https://doi.org/10.22036/ncr.2019.01.001.

72. Revathi, J., M. John Abel, V. Archana, T. Sumithra, R. Thiruneelakandan, and J. Joseph Prince. n.d. "Synthesis and Characterization of CoFe2O4 and Ni-Doped CoFe2O4 Nanoparticles by Chemical Co-Precipitation Technique for Photo-Degradation of Organic Dyestuffs under Direct Sunlight."

73. Robinson, Tim, Geoff McMullan, Roger Marchant, and Poonam Nigam. 2000. "Remediation of Dyes in Textile effluent: A Critical Review on Current Treatment Technologies with a Proposed Alternative." *Bioresource Technology* 21 (3): 211–22. https://doi.org/10.1504/IJEP.2004.004190.

74. S Krishnan, H Rawindran, C M Sinnathambi, J W Lim. 2017. "Comparison of Various Advanced Oxidation Processes Used in Remediation of Industrial Wastewater Laden with Recalcitrant Pollutants Comparison of Various Advanced Oxidation Processes Used in Remediation of Industrial Wastewater Laden with Recalcitrant Poll." https://doi.org/10.1088/1757-899X/206/1/012089.

75. S, Sandhya, Padmavathy S, Swaminathan K, Subrahmanyam Y, and Kaul S. 2005. "Microaerophilic–Aerobic Sequential Batch Reactor for Treatment of Azo Dyes Containing Simulated Wastewater." Proc Biochem.

76. Sacco, Olga, Marco Stoller, Vincenzo Vaiano, Paolo Ciambelli, Angelo Chianese, and Diana Sannino. 2012. "Photocatalytic Degradation of Organic Dyes under Visible Light on N-Doped TiO 2 Photocatalysts" 2012. https://doi.org/10.1155/2012/626759.

77. Salehi, Mozhgan, Akbar Eshaghi, and Hamid Tajizadegan. 2019. "Synthesis and Characterization of TiO2/ZnCr2O4 Core-Shell Structure and Its Photocatalytic and Antibacterial Activity." *Journal of Alloys and Compounds* 778: 148–55. https://doi.org/10.1016/j.jallcom.2018.11.025.

78. Salleh, Mohamad Amran Mohd, Dalia Khalid Mahmoud, Wan Azlina Wan Abdul Karim, and Azni Idris. 2011. "Cationic and Anionic Dye Adsorption by Agricultural Solid Wastes: A Comprehensive Review." *Desalination* 280 (1–3): 1–13. https://doi.org/10.1016/j.desal.2011.07.019.

79. Saravanan, R, Elisban Sacari, F Gracia, Mohammad Mansoob, E Mosquera, and Vinod Kumar. 2016. "Conducting PANI Stimulated ZnO System for Visible Light Photocatalytic Degradation of Coloured Dyes." *Journal of Molecular Liquids* 221: 1029–33. https://doi.org/10.1016/j.molliq.2016.06.074.

80. Seow, Ta, Chi Lim, MHM Nor, MFM Mubarak, Chi Lam, Adibah Yahya, and Zaharah Ibrahim. 2016. "Review on Wastewater Treatment Technologies." *International Journal of Applied Environmental Sciences* 11 (1): 111–26.

81. Shabbir, Aneela, Sara Ajmal, Muhammad Shahid, Imran Shakir, Philips Olaleye Agboola, and Muhammad Farooq Warsi. 2019. "Zirconium Substituted Spinel Nano-Ferrite Mg0.2Co0.8Fe2O4 Particles and Their Hybrids with Reduced Graphene Oxide for Photocatalytic and Other Potential Applications." *Ceramics International* 45 (13): 16121–29. https://doi.org/10.1016/j.ceramint.2019.05.130.

82. Shekofteh-Gohari, Maryam, and Aziz Habibi-Yangjeh. 2016. "Fabrication of Novel Magnetically Separable Visible-Light-Driven Photocatalysts through Photosensitization of Fe3O4/ZnO with CuWO4." *Journal of Industrial and Engineering Chemistry* 44: 174–84. https://doi.org/10.1016/j.jiec.2016.08.028.

83. Shojaei, Abdollah Fallah, Atefeh Roshan Tabari, and Mohammad Hassan Loghmani. 2013. "Normal Spinel CoCr2O4 and CoCr2O 4/TiO2 Nanocomposite as Novel Photocatalysts, for Degradation of Dyes." *Micro and Nano Letters* 8 (8): 426–31. https://doi.org/10.1049/mnl.2013.0114.

84. Singh, Shivnarayan. 2015. "Study of Waste Water Effluent Characteristics Generated from Paper Industries" 2 (17): 1505–9.

85. Singh, Sneha, Paramdeep Kaur, Sandeep Bansal, and Sonal Singhal. 2019. "Enhanced Photocatalytic Performance of Ru-Doped Spinel Nanoferrites for Treating Recalcitrant Organic Pollutants in Wastewater." *Journal of Sol-Gel Science and Technology*. https://doi.org/10.1007/s10971-019-05142-9.

86. Somraksa, Wararat, Pongsaton Amornpitoksuk, and Sumetha Suwanboon. 2019. "และสมบ ั ต ก ิ ารเร ่ งปฏ ิ ก ิ ร ิ ยาด ้ วยแสง Influence of KOH Concentration on ZnO / ZnAl 2 O 4 Composite Formation and Its Photocatalytic Activity" 24 (ฉบับที่ 3): 1071–84.

87. Srinivasan, Asha, and Thiruvenkatachari Viraraghavan. 2010. "Decolorization of Dye Wastewaters by Biosorbents: A Review." *Journal of Environmental Management* 91 (10): 1915–29. https://doi.org/10.1016/j.jenvman.2010.05.003.

88. Sun, Meijuan, Xiulin Han, and Shuguang Chen. 2019. "Synthesis and Photocatalytic Activity of Nano-Cobalt Ferrite Catalyst for the Photo-Degradation Various Dyes under Simulated Sunlight Irradiation." *Materials Science in Semiconductor Processing* 91 (May 2018): 367–76. https://doi.org/10.1016/j.mssp.2018.12.005.

89. Sun, Mengmeng, Yinshan Jiang, Fangfei Li, Maosheng Xia, Bing Xue, and Darui Liu. 2010. "Structure, Dye Degradation Activity and Stability of Oxygen Defective BaFeO3-X." *Materials Transactions* 51 (11): 1981–89. https://doi.org/10.2320/matertrans.M2010206.

90. Verduzco, L. E., R. Garcia-Díaz, A. I. Martinez, R. Almanza Salgado, F. Méndez-Arriaga, S. A. Lozano-Morales, M. Avendaño-Alejo, and K. P. Padmasree. 2020. "Degradation Efficiency of Methyl Orange Dye by La0.5Sr0.5CoO3 Perovskite Oxide under Dark and UV Irradiated Conditions." *Dyes and Pigments* 183 (March). https://doi.org/10.1016/j.dyepig.2020.108743.

91. Verma, Priyanshu, and Sujoy Kumar Samanta. 2018. *Microwave-Enhanced Advanced Oxidation Processes for the Degradation of Dyes in Water*. *Environmental Chemistry Letters*. Vol. 16. Springer International Publishing. https://doi.org/10.1007/s10311-018-0739-2.

92. Wang, Dong, and Didier Astruc. 2017. "The Recent Development of Efficient Earth-Abundant Transition-Metal Nanocatalysts." *Chemical Society Reviews* 46 (3): 816–54. https://doi.org/10.1039/c6cs00629a.

93. Wang, Rijing, Xiaohong Wang, Xiaoguang Xi, Ruanbing Hu, and Guohua Jiang. 2012. "Preparation and Photocatalytic Activity of Magnetic Fe3O 4/SiO2/TiO2 Composites." *Advances in Materials Science and Engineering* 2012. https://doi.org/10.1155/2012/409379.

94. Wang, Shaomang, Dinglong Li, Cheng Sun, Shaogui Yang, Yuan Guan, and Huan He. 2014. "Applied Catalysis B : Environmental Synthesis and Characterization of g-C 3 N 4 / Ag 3 VO 4 Composites with Significantly Enhanced Visible-Light Photocatalytic Activity for Triphenylmethane Dye Degradation." *"Applied Catalysis B, Environmental"* 144: 885–92. https://doi.org/10.1016/j.apcatb.2013.08.008.

95. Wang, Shifa, Chaoli Chen, Yanwu Li, Qing Zhang, Yanlan Li, and Huajing Gao. 2019. "Synergistic Effects of Optical and Photoluminescence Properties , Charge Transfer , and Photocatalytic Activity in MgAl 2 O 4 : Ce and Mn-Codoped MgAl 2 O 4 : Ce Phosphors." https://doi.org/10.1007/s11664-019-07479-x.

96. Xiang, Ying, Hui Wang, Yu He, and Gongwu Song. 2015. "Efficient Degradation of Methylene Blue by Magnetically Separable Fe3O4/Chitosan/TiO2 Nanocomposites." *Desalination and Water Treatment* 55 (4): 1018–25. https://doi.org/10.1080/19443994.2014.922441.

97. Yagub, Mustafa T., Tushar Kanti Sen, Sharmeen Afroze, and H. M. Ang. 2014. "Dye and Its Removal from Aqueous Solution by Adsorption: A Review." *Advances in Colloid and Interface Science* 209: 172–84. https://doi.org/10.1016/j.cis.2014.04.002.

98. Yang, Sheng Tao, Wu Zhang, Jingru Xie, Rong Liao, Xiaoliang Zhang, Baowei Yu, Ruihan Wu, Xiaoyang Liu, Hongliang Li, and Zhen Guo. 2015. "Fe3O4@SiO2

Nanoparticles as a High-Performance Fenton-like Catalyst in a Neutral Environment." *RSC Advances* 5 (7): 5458–63. https://doi.org/10.1039/c4ra10207j.

99. Ye, Aihua, Wenqing Fan, Qinghong Zhang, Weiping Deng, and Ye Wang. 2012. "Catalysis Science & Technology PAPER CdS – Graphene and CdS – CNT Nanocomposites as Visible-Light Photocatalysts for Hydrogen Evolution and Organic Dye Degradation," 969–78. https://doi.org/10.1039/c2cy20027a.

100.     Ye, Miaomiao, Qiao Zhang, Yongxing Hu, Jianping Ge, Zhenda Lu, Le He, Zhonglin Chen, and Yadong Yin. 2010. "Magnetically Recoverable Core-Shell Nanocomposites with Enhanced Photocatalytic Activity." *Chemistry - A European Journal* 16 (21): 6243–50. https://doi.org/10.1002/chem.200903516.

101.     Zhang, Shengxiao, Hongyun Niu, Yaqi Cai, Xiaoli Zhao, and Yali Shi. 2010. "Arsenite and Arsenate Adsorption on Coprecipitated Bimetal Oxide Magnetic Nanomaterials: MnFe2O4 and CoFe2O4." *Chemical Engineering Journal* 158 (3): 599–607. https://doi.org/10.1016/j.cej.2010.02.013.

102.     Zhong, Wei, Ting Jiang, Yanliu Dang, Junkai He, Sheng Yu Chen, Chung Hao Kuo, David Kriz, Yongtao Meng, Andrew G. Meguerdichian, and Steven L. Suib. 2018. "Mechanism Studies on Methyl Orange Dye Degradation by Perovskite-Type LaNiO3-Δ under Dark Ambient Conditions." *Applied Catalysis A: General* 549: 302–9. https://doi.org/10.1016/j.apcata.2017.10.013.

103.     Zhou, Yanbo, Yonghua Hu, Weiwei Huang, Guang Cheng, Changzheng Cui, and Jun Lu. 2018. "A Novel Amphoteric B-Cyclodextrin-Based Adsorbent for Simultaneous Removal of Cationic/Anionic Dyes and Bisphenol A." *Chemical Engineering Journal* 341: 47–57. https://doi.org/10.1016/j.cej.2018.01.155.

# Anti-photocorrosion property enhancement of photocatalysts by combining with graphene and its derivatives in photocatalysis applications-Review

*Rutuja S. Bhoje\* and Parag R. Nemade*

*Department of Chemical Engineering, Institute of Chemical Technology Matunga, Mumbai - 400019. \*Corresponding author: [rutujabhoje.15@gmail.com](mailto:rutujabhoje.15@gmail.com), 91-8928370845*

## Abstract

Photocatalysis is a promising technology for many useful environmental applications that include removing or diluting hazardous environmental pollutants and solving the energy shortage issue by producing sustainable energy using a light source and a photocatalyst. However, many catalysts utilized in photocatalysis suffer from an intrinsic drawback: Photocorrosion, i.e., photoinduced decomposition, which mainly affects the life span of the catalyst, results in lower catalytic efficiency. Graphene and its derivatives have proved their importance in different photocatalytic processes and opened new opportunities in this field with its unique structure and excellent optical, electrical, and physicochemical properties. This review will briefly discuss the specific mechanisms for the heterogeneous photocatalysis using graphene and its derivatives in many photocatalytic processes used by different researchers. Dedicated attention is put on the photocorrosion mechanism of semiconductors, the strategies and rules for improving the anticorrosion property of the semiconductor for better photocatalytic efficiency by using photocatalysis related properties of graphene and its derivatives via doping, hybridization with different semiconductors, etc. The photocatalytic applications discussed in this paper are dye degradation, $H_2$ generation, $CO_2$ reduction.

## Keywords:

Photocatalysis, photocorrosion, anti-photocorrosion, graphene, graphene oxide, reduced graphene oxide.

## 1. Introduction

The Photocatalysis process occurs in a light source, which interacts with the surface of the photocatalyst to generate electrons and holes (Lee and Gouma, 2012). The photocatalyst is nothing but a semiconductor, which plays a vital role in photocatalysis, as it changes the rate of reaction when it gets exposed to the light source. There are simultaneous two types of reactions that takes place in the photocatalysis process; one is a reduction from photogenerated electrons, and the second is oxidation from photogenerated holes. Photocatalysis generally controlled by three main steps, (1) Absorption of light energy by photocatalyst to form electron and hole generation, (2) charge separation and transportation, which defines the efficiency of the process, (3) charge consumptions, which mainly enhances the surface adsorption activation edges on the catalyst. Due to ease in photocatalysis technology, it covers a wide area of applications. With the excellent results in photocatalysis, photocatalytic performance and stability are the crucial issues caused due to the recombination of photogenerated holes and electrons and "Photocorrosion' of photocatalyst (Sudhai et al., 2018). Various techniques are evolved to suppress the photocorrosion of photocatalyst like the use of composite catalyst, surface modification of catalyst, etc. A major limitation in achieving efficiency for a photocatalytic process is the recombination of the charge carriers (a photogenerated hole and electron). A surface redox reaction is responsible for the photocatalytic activity, but recombination has much faster kinetics than this reaction, which results in a reduction in the quantum efficiency of photocatalysis. Photocorrosion is nothing but the deactivation or reduction of the activity of the photocatalyst.

The carbon-based nanomaterials have gained tremendous interest in the photocatalytic process due to their specific characteristics such as large surface area, good electronic conductivity, high chemical and thermal stability, and low synthesis cost (An and Yu, 2011; Xia et al., 2017; Yang et al., 2014). Graphene and its derivatives have been widely studied as effective modifiers for many catalysts over the last ten years (Yu et al., 2005; Zhao et al., 1998).The advantages of graphene and its derivatives over other members in the carbon family in the light activation photocatalytic processes. Graphene has excellent physical and chemical properties with a 2D honeycomb like structure, making it a preferable candidate for designing efficient photocatalytic material (Madkour, 2019). Graphene also has an essential property that is excellent mobility of charge carriers at room temperature, attracting researchers' attention in the photocatalysis field (Novoselov et al., 2004). These properties and the structure of graphene helps in the reduction of photocorrosion, which is studied by many researchers. This review focused on the effect of graphene and its derivates on the photocorrosion effect in different photocatalytic processes.

## 2. Mechanism of photocatalysis

Photocatalytic reaction mainly depends on a specific wavelength of light and the catalyst. Generally, semiconductors are used as a photocatalyst. When light interacts with the surface of a semiconductor, it stimulates the redox reaction (Hagen, 2005). The photocatalysis reaction mechanism is shown in Fig1.A valance electron is the one that forms the bond. When the amount of bonded atoms is high, the energy value of electrons is created a specific range, which is nothing but an 'energy gap'. The energy gap is the gap between the valance band and conduction band. The electron in the valence band gets excited and jumps into the conduction band. The gap between the valance band and the conduction band is called the bandgap (Khan et al., 2015; Rehman et al., 2009).
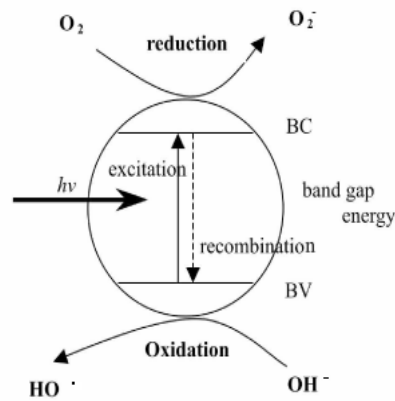
Fig 1.Mechanism of photocatalysis (Silva et al., 2002)

The photocatalytic oxidation or reduction happens due to the absorption of light energy equal to or more than the energy of the bandgap of the respective photocatalyst. Photogenerated electrons are responsible for forming holes and electrons in the valance band and conduction band, respectively. These holes and electrons could undergo oxidation and reduction reactions with any material or species, respectively. This redox reaction gives the necessary product in the photocatalytic process (Kaneco et al., 1998; Wen et al., 2002).

## 2.1 Mechanism of Photocorrosion
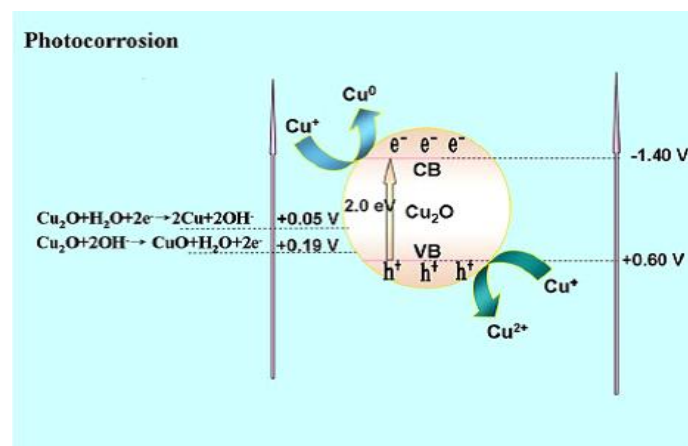


Fig 2. Mechanism Photocorrosion of $Cu_2O$(D. Wang et al., 2015)

The photocorrosion mechanism is explained with the example in Fig 2., where the Copper oxide -Titanium dioxide ($Cu_2O$-$TiO_2$) combination was used to decrease the photocorrosion and increase the photocatalytic efficiency (D. Wang et al., 2015). This example demonstrates that the reduction and oxidation potential of $Cu_2O$ into $Cu^0$ and $Cu_2O$ lies in the bandgap, as shown in Fig. 2. $Cu_2O$ experienced a photocorrosion effect in the liquid media experiments (Tran et al., 2012) rather than a modified $Cu_2O$-$TiO_2$ catalyst that offers stability without deactivation in the gaseous experiments. During the photocatalytic reaction, the photogenerated electrons in $Cu_2O$ were precisely captured by oxygen molecule (Huang et al., 2009). The reduction potential of $O_2$ or $OH^-$ is +0.4 V, which is lower than the margin level of the conduction band of $Cu_2O$ and more extensive than the reduction potential of $Cu^+$ or CuO is 0.05 V (Huang et al., 2009). This leads to the $O_2$ reduction by the photogenerated electrons of $Cu_2O$ then the self-reduction reaction, of $Cu^+$ reduces to CuO. So, the self-reduction reaction of $Cu_2O$ was controlled (Huang et al., 2009). Inhibition of photocorrosion or increase in the

photostability of $Cu_2O$ depends on how to consume the photo-excited holes effectively to diminish the self-oxidation reaction.

## 3.Application of graphene and its products for anti-photocorrosion /stability of photocatalyst

### 3.1 Dye degradation

Various photocatalysts and combinations have already been studied and proved their performance in the dye degradation process (Adegoke et al., 2019; C. Chen et al., 2016; Najafidoust et al., 2019; Pung et al., 2012). Graphene and its derivatives based photocatalyst is studied widely in dye degradation application. ASilver phosphate ($AgPO_4$)/Silver Iodide AgI /Graphene composite photocatalyst was synthesized using a chemical coprecipitation method for the degradation of carbamazepine (CBZ) dye under artificial visible light and sunlight (Duan et al., 2019). The results show that the small amount of graphene presence leads to high photocatalytic efficiency compared to pristine $AgPO_4$. The highest rate constant of photocatalytic dye degradation is observed for $Ag_3PO_4$/AgI-3%Graphene composite catalyst, which is 0.124 $min^{-1}$, and it is 9.5 and 2.1 folds more elevated than the pristine $Ag_3PO_4$, 0.013 $min^{-1}$ and $Ag_3PO_4$/AgI, 0.060 $min^{-1}$, respectively.
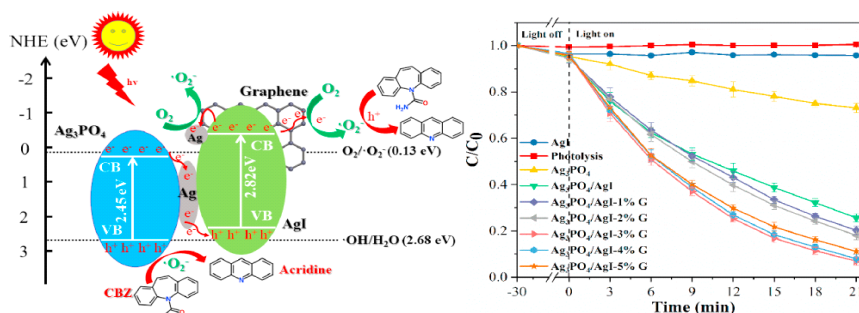


Fig 3. Schematic dye degradation reaction mechanism for $AgPO_4$/AgI -Graphene composite photocatalyst and Photocatalytic degradation of CBZ over the prepared samples (Duan et al., 2019).
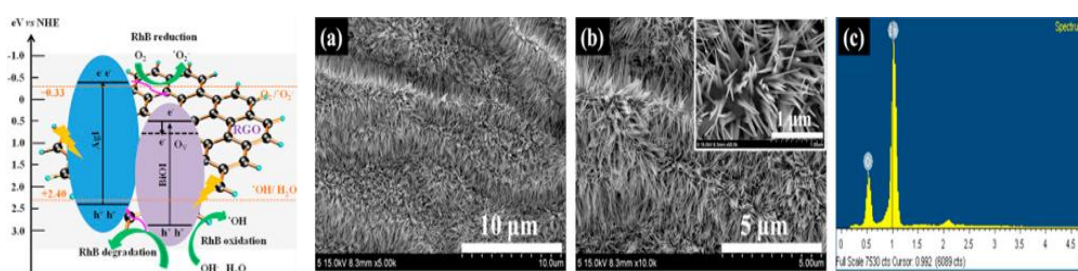


Fig. 4. Schematic dye degradation reaction mechanism RGO/BiOI/AgI (Islam et al., 2016) and (a) and high-magnification FE-SEM (b) FESEM images of ZNNs (c) EDS. Spectrum of as-synthesized Z.N.N.s. The inset in (a) shows the high-magnification FESEM image of ZNNs.(Tripathy et al., 2014)

BiOI (Bismuth iodide oxide) is the most promising visible-light-driven photocatalyst due to its narrow bandgap and efficiency in attempting utilization of enough energy from sunlight (Feng et al., 2016), and AgI is a very promising photocatalyst in the degradation organic pollutants (An et al., 2016). A combination of these two can show an application in the degradation of organic pollutants/ contaminants in the presence of sunlight. But the photocorrosion is the main

drawback in the efficiency of this catalyst. Using graphene-based catalyst with BiOI helps in the separation of photogenerated charge carriers efficiently (Cheng et al., 2013; He et al., 2015). Reduced graphene oxide (RGO)/BiOI/AgI combination photocatalyst was synthesized by simple precipitation method, used in the degradation of rhodamine B under sunlight irradiation (Islam et al., 2016). Photogenerated holes assisted in the oxidation reaction directly or producing $OH^-$ radicle, and photogenerated electrons of AgI reduces $O_2$ to $O_2^-$ radicle. In this system, rhodamine B dye molecule adsorbed on the surface of the RGO sheet was oxidized by the photogenerated holes. At the same time, the photogenerated electrons were trapped in the RGO sheet, which indicates that RGO sheet helps in inhibition of the recombination of the photogenerated charge carriers. RGO also generates a positive photothermal effect, which is an additional point to increase the separation of photoinduced charge carriers.

ZnO (Zinc Oxide) is a highly studied photocatalyst in the dye degradation process (Nagaraja et al., 2012; Tripathy et al., 2014) but mainly suffers photocorrosion effect. Graphene and its derivative used along with ZnO show high stability and photocatalytic efficiency in many research works. The combination of ZnO-graphene composite was synthesized by hydrothermal method (Fan et al., 2012), ZnO-Graphene nanorod was synthesized using the facile hydrothermal reaction of graphene oxide (Chen et al., 2013) and ZnO/graphene composite by chemical precipitation method (Gayathri et al., 2014) for the study of degradation of methylene blue dye under UV visible light irradiation. The photocatalytic performance observed that the ZnO/graphene composite photocatalyst shows the highest photocatalytic performance for the photodegradation process compared to the pure ZnO. The reason behind this was the graphene sheet act as the electronic conductive channel and responsible for the effective separation of the photogenerated hole and electron pairs of ZnO. This results in inhibition on the recombination of these charge carriers by transferring them to the surface of the methylene blue dye molecule. The ratio of 50:1 for the ZnO/graphene nanorods shows the highest photocatalytic efficiency.
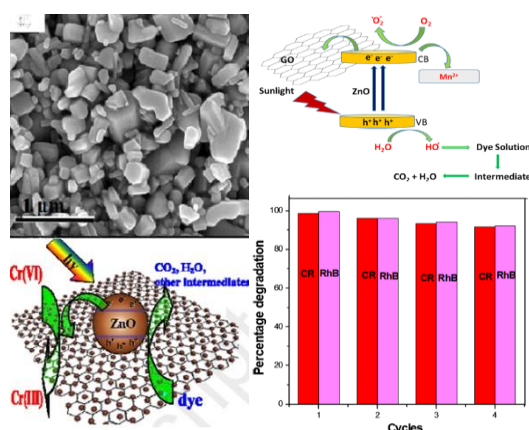


Fig 5 SEM images of and schematic dye degradation reaction mechanism of ZnO/reduced graphene oxide composite photocatalyst (Peng et al., 2015) and schematic dye degradation reaction mechanism and performance study of Mn-doped ZnO/ reduced graphene oxide composite photocatalyst (Zhang et al., 2013)

ZnO and RGO composite was synthesized by the in situ growth of the ultrasound-assisted method, which was utilized to degrade methylene blue and CI acid red 249 aqueous dyes solutions under UV light irradiation (Peng et al., 2015). The dye degradation performance is enhanced by 8.6% and 14.7% for methylene blue and CI acid red 249 after using ZnO/reduced

graphene oxide composite photocatalyst. The photocorrosion suppression is observed for the ZnO/RGO composite catalyst due to the higher rate in the separation of photoinduced charge carriers at the interface of ZnO and reduced graphene oxide, as well as a reduction in the activation of oxygen on the ZnO surface. A similar catalyst has been studied (Zhang et al., 2013) and concludes nearly identical results. The composite ZnO/RGO and manganese have been studied (Labhane et al., 2018)and conclude that this Mn-doped ZnO/ RGO composite enhanced the stability of the photocatalyst.

CdS (Cadmium sulfide) is used in dye degradation applications (Kothari et al., 2009; Negi, 2013). Graphene and its derivatives helps in enhancing photocatalytic performance. Cadmium sulfide nanoparticles/reduced graphene oxide composite photocatalyst synthesized by pulsed laser ablation in liquid technique for methylene blue dye degradation under visible light irradiation (Moqbel et al., 2018). There is a 2.65 fold increase in the photocatalytic efficiency for the reduced graphene oxide/CdS with 5% reduced graphene oxide weight loading than the pure CdS performance. CdS microspheres wrapped in RGO type photocatalyst was synthesized by a two-step hydrothermal method for the which used in the application of Rhodamine B dye degradation under visible light irradiation(Liu et al., 2014).
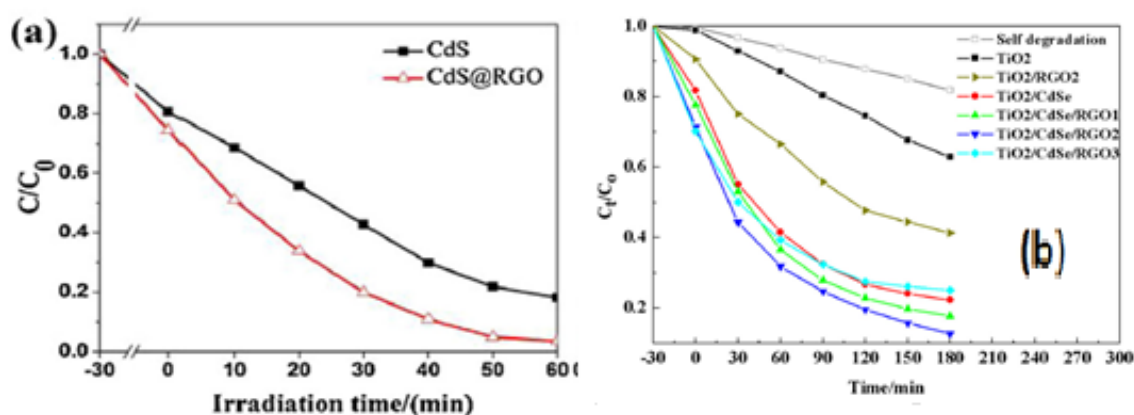


Fig.6 (a)The degradation rate of RhB, (C/C0) as the function of irradiation time(Liu et al., 2014) and, (b) Photocatalytic degradation of MB on different film electrodes under visible light irradiation(Shen et al., 2019).

RGO sheets responsible for enhancing the surface area and stepwise structure of energy level result in an increase in the adsorption performance of dye molecule and reduction in the rate of recombination of photoinduced charge carriers. The unique design of this catalyst protects the CdS microsphere from photocorrosion, which is inside the shell of graphene oxide. $TiO_2$/CdSe (Titanium oxide/Cadmium selenide) composite catalyst has achieved outstanding photocatalytic performance in UV and Visible light irradiation, but CdSe faces a high photocorrosion effect. $TiO_2$/CdSe was combined with reduced graphene oxide by spin coating and used in the methylene blue dye degradation process (Shen et al., 2019). RGO acts as an electron acceptor that was generated on the ZnO surface, which leads to improvement in the separation efficiency of photogenerated charge carriers. Secondly, RGO also helps to avoid direct contact between CdSe nanocatalyst and dissolved oxygen in the solution, which avoids the reaction between CdSe and oxygen to generate $Cd^{2+}$ and $SeO_4^{2-}$. So graphene is not only helping in increasing photocatalytic performance but also shows anti-photocorrosion effect.

## 3.2 Hydrogen ($H_2$) production

For the photocatalytic $H_2$ production reaction, the photocatalysts should cross the energy bandgaps of the reduction potential of water. For the generation of $H_2$ gas, photocatalytic water

splitting is an attractive and very well-used process for future energy sources (Ahmad et al., 2015). Graphene and its derivatives used along with other catalysts have been studied and proved as an efficient photocatalyst for inhibiting the recombination of the charge carriers. AgInZnS (Silver/Indium /Zinc Sulphide) / $MoS_2$-Graphene (Molybdenum disulfide-graphene) composite photocatalyst was synthesized by a facile two-step hydrothermal method used for the $H_2$ generation under visible light irradiation(Huang et al., 2018). In this work, $MoS_2$-Graphene is used as a co-catalyst with the primary Ag/In/ZnS catalyst. From the results, 1 wt%, $MoS_2$-GO loading amount in this composite gives the highest $H_2$ evolution rate, 1302 $\mu mol \cdot h^{-1}$. The enhancement of the photocatalytic performance and photocorrosion rate reduction was caused due to graphene, which can provide an active site of the $MoS_2$ and provide strong electron transfer abilities.
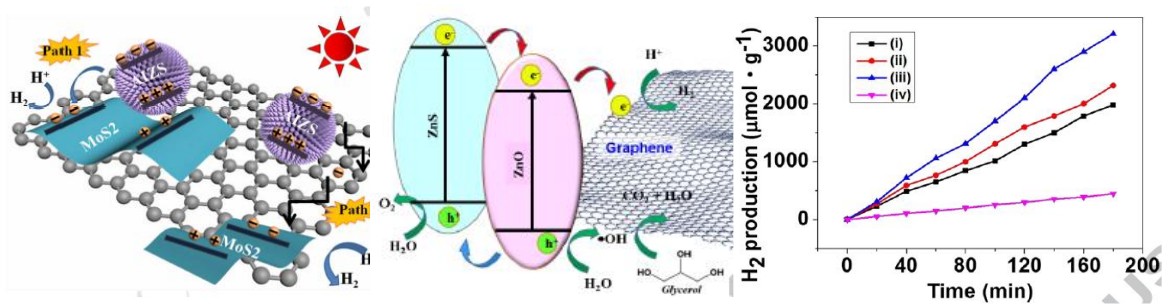


Fig 7.Schematic mechanism of $H_2$ generation using A.I.Z.S./$MoS_2$ catalyst(Huang et al., 2018) with Schematic mechanism of $H_2$ generation using ZnO/ZnS/graphene and $H_2$ production rate(Chang et al., 2018).

Hydrogen production from the aqueous glycerol solution using ZnO/ZnS/graphene photocatalyst was synthesized at room temperature (Chang et al., 2018). ZnO/ZnS/graphene photocatalyst shows a high photocatalytic $H_2$ production rate 1070 $\mu mol \cdot h^{-1}$ which indicates graphene promotes the fast transport of photoinduced electrons from ZnO-ZnS composite catalyst and increase in the light absorption capacity.

$TiO_2$ is well established catalyst in the photocatalytic $H_2$ production process (Cai et al., 2019; Reisner et al., 2009), and how its surface texture supports the photocatalytic $H_2$ evolution is also studied (Pellegrino et al., 2019). But $TiO_2$ suffers from a high photocorrosion effect and rapid recombination of photogenerated charge carriers.$TiO_2$ modified with nanosphere-reduced graphene photocatalyst was studied for $H_2$ generation( Chen et al., 2016).
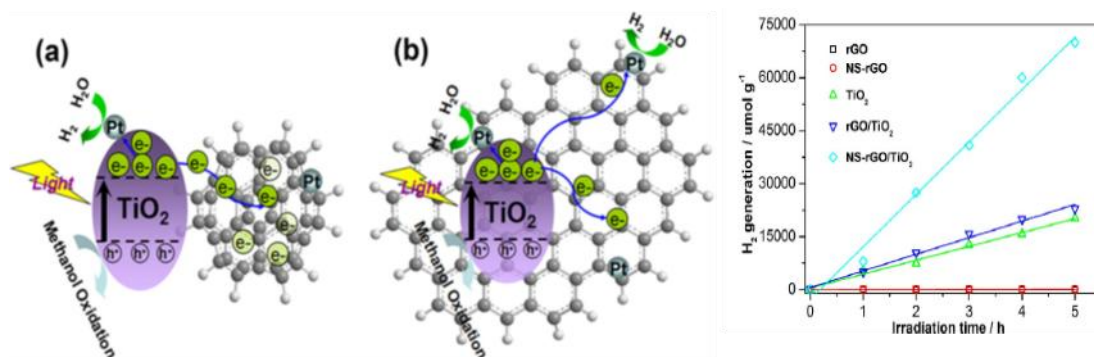


Fig 8. Illustration of the working mechanism of  (**a**) NS-rGO/$TiO_2$ (**b**) rGO/$TiO_2$ and photocatalytic system for hydrogen production.Reaction time profiles of hydrogen production

under UV-Vis light illumination over TiO2, rGO/TiO$_2$, and NS-rGO/TiO$_2$ compositions for comparison (D. Chen et al., 2016).

This TiO$_2$/RGO photocatalyst shows a remarkable improvement in the adsorption of visible light, creates a narrow bandgap and shows an increase in charge collection and separation rate. The highest performance for the photocatalytic H$_2$ production rate was observed for TiO$_2$/ nanosphere-reduced graphene oxide, which is 13996 $\mu$mol g$^{-1}$ h$^{-1}$, which is 3.45 and 3.05 times higher as compared to pure TiO$_2$ and TiO$_2$ / graphene sheets, respectively. Nanosphere reduced graphene oxide acts as an efficient electron collector and transporter. TiO$_2$/graphene composite photocatalysts used in the photocatalytic hydrogen generation from H$_2$O and H$_2$S were investigated (Lv et al., 2012). From the result, TiO$_2$/graphene composites photocatalyst helps in enhancing the photocatalytic performance. Graphene acts as a co-catalyst attached to TiO$_2$ surfaces, allowing the enhancement of the hydrogen evolution from H$_2$O and H$_2$S compared to the TiO$_2$/platinum composite catalyst under similar experimental conditions.

CdS and CdS based photocatalysts in the form of powder, nanorod, quantum dots, and suspension have been studied for the photocatalytic H$_2$ generation (Q. Wang et al., 2015; Yuan et al., 2018; Zhang et al., 2014). CdS show advantages like better absorption capacity in visible light, exceptional electronic charge transfer, and appropriate band edge levels. Still, CdS provides a fast recombination rate of photogenerated charge carriers, leading to a lack of H$_2$ evolution, which indicates CdS alone as photocatalyst is not the right choice for H$_2$ generation application. CdS suffer from a severe photocorrosion effect, making its applications limited.
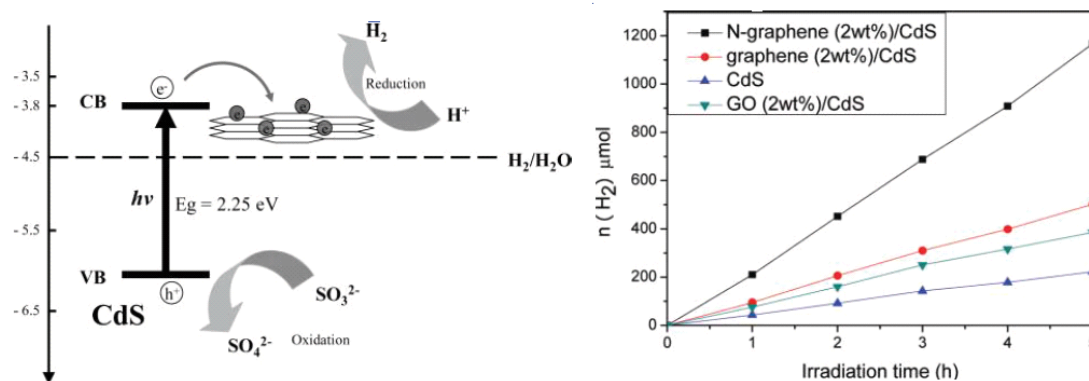


Fig 9. The energy level diagram for N-graphene/CdS nanocomposites and Photocatalytic H$_2$ production activity(Jia et al., 2011)

ZnS/CdS/graphene oxide composite was synthesized by light irradiation-assisted process and studied for photocatalytic H$_2$ generation(Wang et al., 2015) under UV–visible or visible light irradiation. Nitrogen-doped graphene/CdS composite catalyst was synthesized by calcination method and studied for photocatalytic evolution of H$_2$ from water (Jia et al., 2011)under visible light irradiation at $\lambda \geq 420$ nm. A Photoelectrochemical test device was used to measure the transient photocurrent, which shows transient photocurrent of nitrogen-doped graphene/CdS catalyst has increased than the pure CdS. The photogenerated electron from CdS surface has ideally transferred that electron to the nitrogen-doped graphene, the photoinduced hole which resists the recombination of e and electron and results in an increase in the photocatalytic efficiency. 2 wt% nitrogen-doped graphene with CdS amount in combination photocatalyst was proved to be the optimum which gives the highest activity. In the same work, graphene/CdS, graphene oxide/CdS composite photocatalyst were also studied. RGO/CdS/MoS$_2$ composite photocatalyst was investigated for H$_2$ generation (Ben Ali et al.,

2017) CdS nanorod/RGO/molybdenum sulfide synthesized using a hydrothermal process, which helps to increase the interfacial contact between CdS and $MoS_2$. The maximum photocurrent density was observed for the CdS/reduced graphene oxide/$MoS_2$ compared to CdS/$MoS_2$. Electron and hole recombination rate suppression was observed from the fluorescence quenching. Reduced graphene oxide surface area makes a way to transfer an electron from CdS to $MoS_2$ due to the intimate interfacial contact. 20 wt% reduced graphene oxide in composite catalyst shows highest amount $H_2$ evolution which 7.1 mmol $h^{-1}g^{-1}$.
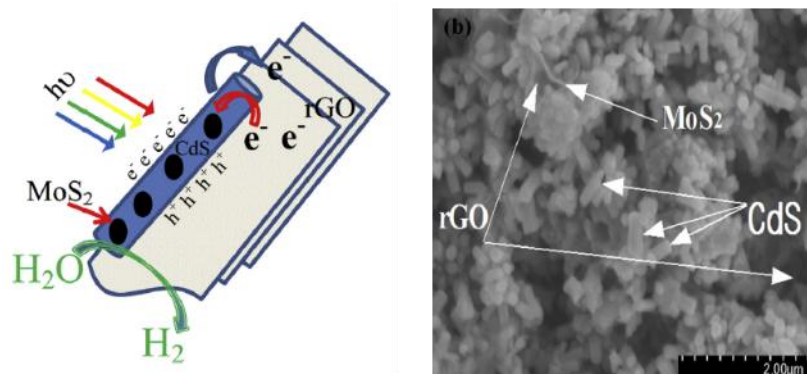


Fig.10.Schematic diagram illustrating the system used for $H_2$ evolution and the proposed charge transfer in CdS-rGO-$MoS_2$., ) FE-SEM images of CdS-rGO-$MoS_2$(Ben Ali et al., 2017)

Copper oxide(CuO) shown affinity toward $H_2$ generation, but it also suffers from photocorrosion effect. When reduced, graphene oxide is combined with copper oxide to form a composite photocatalyst to enhance the photocatalytic $H_2$ generation (Tran et al., 2012). RGO act as an electron acceptor generated by $Cu_2O$, which suppresses the recombination rate of electron and hole.

### 3.3 CO₂ (Carbon dioxide) reduction

Photocatalytic $CO_2$ reduction is the process where $CO_2$ gets converted into fuels and chemicals using light energy. This process gives two advantages like one is the reduction of atmospheric $CO_2$ level, which reduces the health hazard, and the second is the production of fuels and chemicals by utilizing $CO_2$ can satisfy the energy demand (Roy et al., 2010; Yang et al., 2010; Yang and Xu, 2016).

CdS is a visible-light-driven catalyst, and CdS based catalysts are also studied for photocatalytic reduction of $CO_2$ (Ijaz et al., 2016; Li et al., 2011; Wei et al., 2018) but its faces photocorrosion effect. RGO and CdS nanorod composite catalyst was prepared by a one-step microwave-hydrothermal method for photocatalytic $CO_2$ reduction in visible light irradiation (Yu et al., 2014). RGO/CdS composite catalyst shows the highest performance for reduction of the $CO_2$ into methane ($CH_4$) without using platinum as a co-catalyst. The optimum amount of reduced graphene oxide was found to be 0.5 wt% in RGO/CdS composite photocatalyst, which shows the maximum $CH_4$ production rate (2.51 mmol $h^{-1}$ $g^{-1}$ ), which is ten folds higher than that of pure CdS nanorods. RGO/CdS composite photocatalyst shows an efficient electron-hole separation due to the proper band structure and high electron conductivity of RGO.
The RGO not only improves the adsorption and stabilization of $CO_2$ molecules but also leads to formation of  large number of photogenerated electrons on its surface. This results in the reduction of recombination rate of charge carriers, which leads to suppress the photocorrosion effect and an enhancement of the $CO_2$ reduction performance for the RGO /CdS composite photocatalyst.
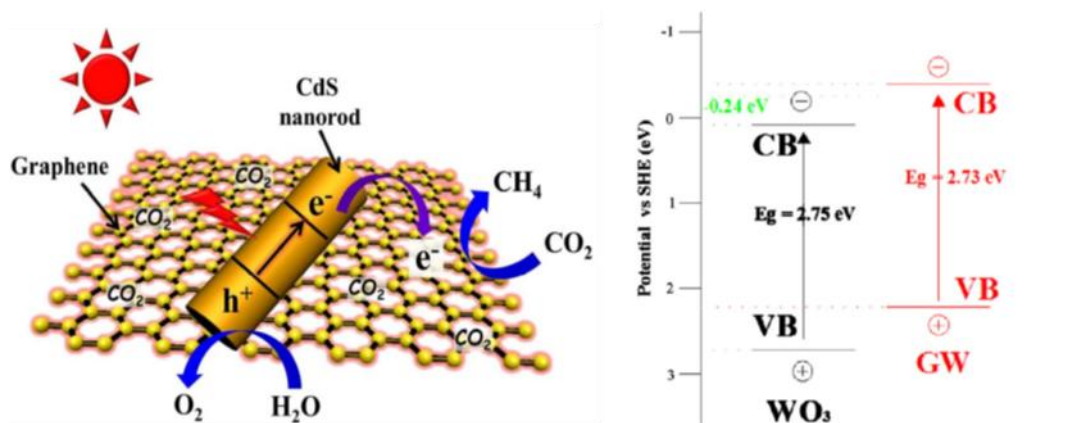
Fig 11.Schematic representation for the photocatalytic $CO_2$ reduction mechanism of CdS nanorod/graphene composites (Yu et al., 2014) and the schematic representation of valence band and conduction band edges of $WO_3$ and GW versus NHE (Wang et al., 2013).

Cuprous oxide ($Cu_2O$) and tungsten oxide($WO_3$) used in $CO_2$ photoreduction (Shi et al., 2020), but to avoid photocorrosion of these enhance the photocatalytic efficiency and catalyst stability, photocatalyst graphene was employed with them. Graphene– Tungsten trioxide nanobelt composites were synthesized by facile hydrothermal method for the photocatalytic reduction of $CO_2$ (Wang et al., 2013). $WO_3$ alone can not show any photocatalytic $CO_2$ reduction capability due to its low conduction. In this work, it is found that graphene raises the conduction band of $WO_3$ about -0.24 eV for the photocatalytic reduction of the $CO_2$ process under visible-light irradiation. The rise of the conduction band is caused due to electron transfer from graphene to $WO_3$.

$Cu_2O$/reduced graphene oxide composite was synthesized by a facile one-step microwave-assisted chemical method for the $CO_2$ reduction under UV and Visible light irradiation(An et al., 2014) at ambient conditions. RGO coating on $Cu_2O$ results in an increase in the activity of $Cu_2O$ for the photoreduction of $CO_2$. The composite catalyst shows around six times higher activity than the optimized pure $Cu_2O$ and, in the $20^{th}$ hour,50 times higher activity than the $Cu_2O/RuO_x$ junction. Reduced graphene oxide has good electronic conductivity, providing good $Cu_2O$ to, $Cu_2O$/ reduced graphene oxide shows low photoinduced charge recombination rate and high surface active sites. This composite catalyst offers high photocatalytic performance and increased stability.

$TiO_2$ and its derivatives are widely used in different structures as photocatalysts for $CO_2$ photoreduction due to its wide bandgap, low cost, availability, and chemical stability(Kar et al., 2019; Thompson et al., 2018; Xie et al., 2001). It will suffer from photocorrosion drawback if it is used alone.

Graphene/$TiO_2$ nanosheet is synthesized in a binary ethylenediamine/$H_2O$ solvent by reduction-hydrolysis technique for the photocatalytic $CO_2$ reduction application (Tu et al., 2013). This 2D sandwich-like nanostructure photocatalyst was formed due to the simultaneous reduction-hydrolysis (SRH) technique. The second one is $TiO_2$ nanoparticle synthesis via hydrolysis of titanium (IV) bis(ammonium lactato) dihydroxide. $TiO_2$ nanoparticles formed and can be in situ loaded onto the graphene nanosheet-like 2D sandwich structure through the chemical bonds shown in fig.11.
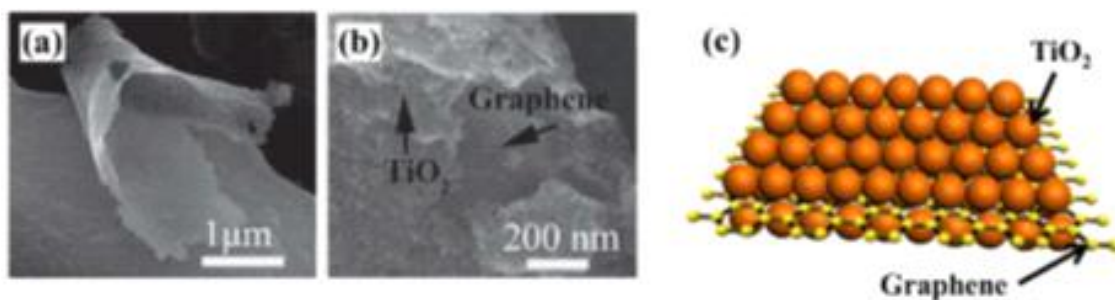
Fig 11. SEM images of Graphene/TiO$_2$ nanosheet, schematic representation of graphene/TiO$_2$ photocatalyst.(Tu et al., 2013)

This slit-like porous structure avoids TiO$_2$ nanoparticle agglomeration and restacking of graphene nanosheets. This composite catalyst shows a specific surface area than the pure TiO$_2$, thus gives more adsorption and active sites on the photocatalyst surface. On the surface of composite photocatalyst Ti$^{3+}$ was found, which acts as a photoinduced electron acceptor, and suppresses the electron-hole recombination rate. Graphene/TiO$_2$ photocatalyst shows higher photocatalytic CO$_2$ reduction into ethane production performance, which is 16.8 µmolg$^{-1}$h$^{-1}$, than pure TiO$_2$, which is 7.2 µmolg$^{-1}$h$^{-1}$.

CdS /RGO /TiO$_2$ core-shell catalyst synthesized by the versatile kinetics-controlled coating method and used as a Z-scheme system for CO$_2$ photoreduction into useful solar fuels (Kuai et al., 2015). This composite catalyst shows an efficient result as compared to pure CdS and CdS/TiO$_2$ catalyst. Electron generated in the conduction band of TiO$_2$ transfers to reduced graphene oxide sheet, as the conduction edges of TiO$_2$ are more negative than the fermi level of reduced graphene oxide. Then the transferred electron moves via reduced graphene oxide to combine with the holes of the CdS. Holes of CdS accept the electron from TiO$_2$ then this action suppresses electron recombination, which was generated by CdS itself. This mechanism accumulated the electron in CdS for CO$_2$ reduction. In this process hole density of CdS reduces, which results in inhibition in photocorrosion of CdS.
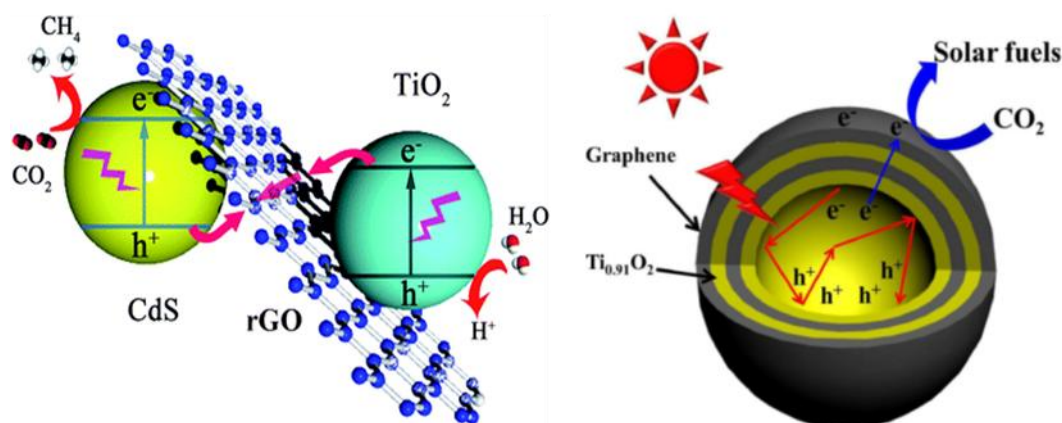


Fig. 12 Schematic illustration of photocatalytic reduction of CO$_2$ over CdS NSs/rGO/TiO$_2$ Z-scheme system (Kuai et al., 2015) and Proposed mechanism for photocatalytic CO$_2$ reduction activity over the titania/graphene hollow sphere composite system (Low et al., 2015)

A similar catalyst with the platinum combination was also studied (Benedetti et al., 2015). TiO$_2$/CdS/RGO /Pt, the quaternary nanocomposite photocatalyst was synthesized for the photocatalytic reduction of CO$_2$ to methane CH$_4$ under visible light illumination. The results show that 0.11 µmol of CH$_4$ was produced from the quaternary nanocomposite photocatalyst 5

hrs of light irradiation with an average production rate of 0.0867 μmol h$^{-1}$, which is higher than the yield of CH$_4$ produced from the TiO$_2$/CdS and the TiO$_2$/CdS/Pt composite photocatalyst. Photocatalytic performance enhancement is the result of fast electron transport and the inhibition of electron-hole recombination due to the properties of RGO.

Graphene and titania-based 2D-2D structure composite photocatalyst was synthesized and studied for photocatalytic reduction of CO$_2$ (Tu et al., 2012). Robust hollow spheres structure arranged by alternating titania (Ti$_{0.91}$O$_2$) nanosheets and graphene nanosheets was prepared by using layer-by-layer assembly technique. This structure provides an extensive and close contact interface, allowing the photogenerated electron transfer from titania nanosheet to graphene nanosheet. This results in inhibition in electron-hole recombination and improvement in photocatalytic activity of the composite catalyst. The hollow structure also helps to utilize maximum light energy due to its unique light scattering ability. The production rate of CO from CO$_2$ by the composite catalyst which is nine times higher than that of P25 TiO$_2$.

## 4.Conclusion

Different types of graphene and its derivatives based composite photocatalyst for the photocatalytic dye degradation, H2 generation, and CO$_2$ reduction applications are discussed in deatil. The potential of graphene and its derivatives in the stability and the anti-photocorrosion effect of the photocatalyst is reviewed thouroghly . The primary mechanism of photocorrosion and photocatalytic performance enhancement mechanism after the use of graphene and its derivatives in composite has been discussed with examples. This review will help to generate and develop a new stable photocatalyst that can be used in commercial applications. The incorporation of graphene and its derivatives in various nanocomposites can improve their photocatalytic efficiency by adding them in a small amount to show superior properties, like high surface area, enhancement in adsorption (dye molecule/CO$_2$), high visible light absorption capacity, and fast separation and transportation of photoinduced electron. To make this graphene-based composite catalyst used photocatalytic processes more feasible on a commercial scale, there is a need for precise engineering of the respective photocatalyst to gain a higher photocatalytic yield.

## References

1. Adegoke, K.A., Iqbal, M., Louis, H., Bello, O.S., 2019. Synthesis, characterization and application of CdS/ZnO nanorod heterostructure for the photodegradation of Rhodamine B dye. Materials Science for Energy Technologies 2, 329–336. https://doi.org/10.1016/j.mset.2019.02.008

2. Ahmad, H., Kamarudin, S.K., Minggu, LJ, Kassim, M., 2015. Hydrogen from photocatalytic water splitting process: A review. Renewable and Sustainable Energy Reviews 43, 599–610. https://doi.org/10.1016/j.rser.2014.10.101

3. An, C., Wang, S., Sun, Y., Zhang, Q., Zhang, J., Wang, C., Fang, J., 2016. Plasmonic silver incorporated silver halides for efficient photocatalysis. J. Mater. Chem. A 4, 4336–4352. https://doi.org/10.1039/C5TA07719B

4. An, X., Li, K., Tang, J., 2014. Cu$_2$O/Reduced Graphene Oxide Composites for the Photocatalytic Conversion of CO$_2$. ChemSusChem 7, 1086–1093. https://doi.org/10.1002/cssc.201301194

5. An, X., Yu, J.C., 2011. Graphene-based photocatalytic composites. RSC Adv. 1, 1426–1434. https://doi.org/10.1039/C1RA00382H

6. Ben Ali, M., Jo, W.-K., Elhouichet, H., Boukherroub, R., 2017. Reduced graphene oxide as an efficient support for CdS-MoS$_2$ heterostructures for enhanced photocatalytic H2 evolution. International Journal of Hydrogen Energy 42, 16449–16458. https://doi.org/10.1016/j.ijhydene.2017.05.225

7. Benedetti, J.E., Bernardo, D.R., Morais, A., Bettini, J., Nogueira, A.F., 2015. Synthesis and character ization of a quaternary nanocomposite based on $TiO_2/CdS/rGO/Pt$ and its application in the photoreduction of $CO_2$ to methane under visible light. RSC Adv. 5, 33914–33922. https://doi.org/10.1039/C4RA15605F

8. Cai, J., Shen, J., Zhang, X., Ng, Y.H., Huang, J., Guo, W., Lin, C., Lai, Y., 2019. Light-Driven Sustainable Hydrogen Production Utilizing $TiO_2$ Nanostructures: A Review. wiley online library 3.

9. Chang, C.-J., Lin, Y.-G., Weng, H.-T., Wei, Y.-H., 2018. Photocatalytic hydrogen production from glycerol solution at room temperature by ZnO-ZnS/graphene photocatalysts. Applied Surface Science 451, 198–206. https://doi.org/10.1016/j.apsusc.2018.05.004

10. Chen, C., Li, Z., Lin, H., Wang, G., Liao, J., Li, M., Lv, S., Li, W., 2016. Enhanced visible light photocatalytic performance of ZnO nanowires integrated with CdS and Ag2S. Dalton Trans. 45, 3750–3758. https://doi.org/10.1039/C5DT04533A

11. Chen, D., Zou, L., Li, S., Zheng, F., 2016. Nanospherical like reduced graphene oxide decorated TiO 2 nanoparticles: an advanced catalyst for the hydrogen evolution reaction. Scientific Reports 6, 20335. https://doi.org/10.1038/srep20335

12. Chen, J., Yao, B., Li, C., Shi, G., 2013. An improved Hummers method for eco-friendly synthesis of graphene oxide. Carbon 64, 225–229. https://doi.org/10.1016/j.carbon.2013.07.055

13. Cheng, H., Wang, W., Huang, B., Wang, Z., Zhan, J., Qin, X., Xiaoyang, Z., Dai, Y., 2013. Tailoring AgI nanoparticles for the assembly of AgI/BiOI hierarchical hybrids with size-dependent photocatalytic activities - Journal of Materials Chemistry A (RSC Publishing). Journal of Materials Chemistry A 7131–7136.

14. Duan, Y., Deng, L., Shi, Z., Zhu, L., Li, G., 2019. Assembly of graphene on $Ag_3PO_4/AgI$ for effective degradation of carbamazepine under Visible-light irradiation: Mechanism and degradation pathways. Chemical Engineering Journal 359, 1379–1390. https://doi.org/10.1016/j.cej.2018.11.040

15. Fan, H., Zhao, X., Yang, J., Shan, X., Yang, L., Zhang, Y., Li, X., Gao, M., 2012. ZnO–graphene composite for photocatalytic degradation of methylene blue dye. Catalysis Communications 29, 29–34. https://doi.org/10.1016/j.catcom.2012.09.013

16. Feng, Y., Liu, C., Che, H., Chen, J., Huang, K., Huang, C., Shi, W., 2016. The highly improved visible light photocatalytic activity of BiOI through fabricating a novel p–n heterojunction BiOI/WO3 nanocomposite. CrystEngComm 18, 1790–1799. https://doi.org/10.1039/C5CE02244D

17. Gayathri, S., Jayabal, P., Kottaisamy, M., Ramakrishnan, V., 2014. Synthesis of ZnO decorated graphene nanocomposite for enhanced photocatalytic properties. Journal of Applied Physics 115, 173504. https://doi.org/10.1063/1.4874877

18. Hagen, J., 2005. Industrial Catalysis: A Practical Approach, 3rd Edition | Wiley. Wiley.com.

19. He, R., Cao, S., Guo, D., Cheng, B., Wageh, S., A.Al-Ghamdi, A., Yu, J., 2015. 3D BiOI–GO composite with enhanced photocatalytic performance for phenol degradation under visible-light - ScienceDirect. Ceramics International 41, 3511–3517.

20. Huang, L., Peng, F., Wang, H., Yu, H., Li, Z., 2009. Preparation and characterization of Cu2O/TiO2 nano–nano heterostructure photocatalysts. Catalysis Communications 10, 1839–1843. https://doi.org/10.1016/j.catcom.2009.06.011

21. Huang, T., Hua, Y., Yao, J., Luo, Y., Liu, X., 2018. The synergetic effect of graphene and $MoS_2$ on AgInZnS for visible-light driven photocatalytic $H_2$ evolution. Materials Chemistry and Physics 212, 506–512. https://doi.org/10.1016/j.matchemphys.2018.03.068

22. Ijaz, S., Ehsan, MF, Ashiq, M.N., Karamat, N., He, T., 2016. Preparation of CdS@CeO$_2$ core/shell composite for photocatalytic reduction of CO2 under visible-light irradiation. Applied Surface Science 390, 550–559. https://doi.org/10.1016/j.apsusc.2016.08.098
23. Islam, M.J., Reddy, D.A., Ma, R., Kim, Y., Kim, T.K., 2016. Reduced-graphene-oxide-wrapped BiOI-AgI heterostructured nanocomposite as a high-performance photocatalyst for dye degradation under solar light irradiation. Solid State Sciences 61, 32–39. https://doi.org/10.1016/j.solidstatesciences.2016.09.006
24. Jia, L., Wang, D.-H., Huang, Y.-X., Xu, A.-W., Yu, H.-Q., 2011. Highly Durable N-Doped Graphene/CdS Nanocomposites with Enhanced Photocatalytic Hydrogen Evolution from Water under Visible Light Irradiation | The Journal of Physical Chemistry C. ACS publication 115, 11466–11473.
25. Kaneco, S., Shimizu, Y., Ohta, K., Mizuno, T., 1998. Photocatalytic reduction of high pressure carbon dioxide using TiO$_2$ powders with a positive hole scavenger. Journal of Photochemistry and Photobiology A: Chemistry 115, 223–226. https://doi.org/10.1016/S1010-6030(98)00274-3
26. Kar, P., Zeng, S., Zhang, Y., Vahidzadeh, E., Manuel, A., Kisslinger, R., Alam, K.M., Thakur, U.K., Mahdi, N., Kumar, P., Shankar, K., 2019. High rate CO$_2$ photoreduction using flame annealed TiO2 nanotubes. Applied Catalysis B: Environmental 243, 522–536. https://doi.org/10.1016/j.apcatb.2018.08.002
27. Khan, M.M., Adil, S.F., Al-Mayouf, A., 2015. Metal oxides as photocatalysts. Journal of Saudi Chemical Society, Special Issue: Nanomaterials as Photocatalysts 19, 462–464. https://doi.org/10.1016/j.jscs.2015.04.003
28. Kothari, S., Kumar, A., Vyas, R., Ameta, R., Punjabi, PB, 2009. Cadmium sulfide photocatalysed reduction of malachite green by ascorbic acid and EDTA as reductants. Journal of the Brazilian Chemical Society 20, 1821–1826. https://doi.org/10.1590/S0103-50532009001000008
29. Kuai, L., Zhou, Y., Tu, W., Li, P., Li, H., Xu, Q., Tang, L., Wang, X., Xiao, M., Zou, Z., 2015. Rational construction of a CdS/reduced graphene oxide/TiO2 core–shell nanostructure as an all-solid-state Z-scheme system for CO$_2$ photoreduction into solar fuels. RSC Adv. 5, 88409–88413. https://doi.org/10.1039/C5RA14374H
30. Labhane, P.K., Patle, L.B., Sonawane, G.H., Sonawane, S.H., 2018. Fabrication of ternary Mn doped ZnO nanoparticles grafted on reduced graphene oxide (RGO) sheet as an efficient solar light driven photocatalyst. Chemical Physics Letters 710, 70–77. https://doi.org/10.1016/j.cplett.2018.08.066
31. Lee, J., Gouma, P.I., 2012. Sol-Gel Processed Oxide Photocatalysts, in: Aparicio, M., Jitianu, A., Klein, L.C. (Eds.), Sol-Gel Processing for Conventional and Alternative Energy, Advances in Sol-Gel Derived Materials and Technologies. Springer US, Boston, MA, pp. 217–237. https://doi.org/10.1007/978-1-4614-1957-0_11
32. Li, X., Chen, J., Li, H., Li, J., Xu, Y., Liu, Y., Zhou, J., 2011. Photoreduction of CO$_2$ to methanol over Bi2S3/CdS photocatalyst under visible light irradiation. Journal of Natural Gas Chemistry 20, 413–417. https://doi.org/10.1016/S1003-9953(10)60212-5
33. Liu, H., Lv, T., Wu, X., Zhu, C., Zhu, Z., 2014. Preparation and enhanced photocatalytic activity of CdS@RGO core–shell structural microspheres. Applied Surface Science 305, 242–246. https://doi.org/10.1016/j.apsusc.2014.03.045
34. Low, J., Yu, J., Ho, W., 2015. Graphene-Based Photocatalysts for CO$_2$ Reduction to Solar Fuel. The Journal of Physical Chemistry Letters 6, 4244–4251. https://doi.org/10.1021/acs.jpclett.5b01610
35. Lv, X., Zhang, G., Fu, W., 2012. Highly Efficient Hydrogen Evolution Using TiO$_2$/Graphene Composite Photocatalysts. Procedia Engineering, 2011 Chinese Materials Conference 27, 570–576. https://doi.org/10.1016/j.proeng.2011.12.489

36. Madkour, L., 2019. Carbon Nanomaterials and Two-Dimensional Transition Metal Dichalcogenides (2D TMDCs). pp. 165–245. https://doi.org/10.1007/978-3-030-21621-4_7

37. Moqbel, R.A., Gondal, M.A., Qahtan, T.F., Lais, A., 2018. Photocatalytic application of CdS nanoparticles and CdS/R.G.O. hybrid composite synthesized by pulsed laser ablation method. Presented at the sixth saudi international meeting on frontiers of physics 2018 (SIMFP2018), Gizan, Saudi Arabia, p. 020015. https://doi.org/10.1063/1.5042382

38. Nagaraja, R., Kottam, N., Girija, C.R., Nagabhushana, B.M., 2012. Photocatalytic degradation of Rhodamine B dye under U.V./solar light using ZnO nanopowder synthesized by solution combustion route. Powder Technology 215–216, 91–97. https://doi.org/10.1016/j.powtec.2011.09.014

39. Najafidoust, A., Haghighi, M., Abbasi Asl, E., Bananifard, H., 2019. Sono-solvothermal design of nanostructured flowerlike BiOI photocatalyst over silica-aerogel with enhanced solar-light-driven property for degradation of organic dyes. Separation and Purification Technology 221, 101–113. https://doi.org/10.1016/j.seppur.2019.03.075

40. Negi, DPS, 2013. Photocatalytic Degradation of Rhodamine B Dye Using Histidine-Stabilized CdS Quantum Dots. Asian J. Chem. 25, 4.

41. Ning, X., Lu, G., 2020. Photocorrosion inhibition of CdS-based catalysts for photocatalytic overall water splitting. Nanoscale 12, 1213–1223. https://doi.org/10.1039/C9NR09183A

42. Novoselov, K.S., Geim, A.K., Morozov, S.V., Jiang, D., Zhang, Y., Dubonos, S.V., Grigorieva, I.V., Firsov, A.A., 2004. Electric Field Effect in Atomically Thin Carbon Films. Science 306, 666–669. https://doi.org/10.1126/science.1102896

43. Pellegrino, F., Sordello, F., Minella, M., Minero, C., Maurino, V., 2019. The Role of Surface Texture on the Photocatalytic $H_2$ Production on TiO2. Catalysts 9, 32. https://doi.org/10.3390/catal9010032

44. Peng, Y., Ji, J., Chen, D., 2015. Ultrasound assisted synthesis of ZnO/reduced graphene oxide composites with enhanced photocatalytic activity and anti-photocorrosion. Applied Surface Science 356, 762–768. https://doi.org/10.1016/j.apsusc.2015.08.070

45. Pung, S.-Y., Lee, W.-P., Aziz, A., 2012. Kinetic Study of Organic Dye Degradation Using ZnO Particles with Different Morphologies as a Photocatalyst [WWW Document]. International Journal of Inorganic Chemistry. https://doi.org/10.1155/2012/608183

46. Rehman, S., Ullah, R., Butt, A.M., Gohar, ND, 2009. Strategies of making TiO2 and ZnO visible light active. Journal of Hazardous Materials 170, 560–569. https://doi.org/10.1016/j.jhazmat.2009.05.064

47. Reisner, E., Powell, D.J., Cavazza, C., Fontecilla-Camps, J.C., Armstrong*, FA, 2009. Visible Light-Driven H2 Production by Hydrogenases Attached to Dye-Sensitized TiO2 Nanoparticles | Journal of the American Chemical Society. ACS publication 131, 18457–18466.

48. Roy, S.C., Varghese, O.K., Paulose, M., Grimes, C.A., 2010. Toward Solar Fuels: Photocatalytic Conversion of Carbon Dioxide to Hydrocarbons | ACS. Nano. ACS publication 4, 1259–1278.

49. Shen, Q., Wang, Y., Xue, J., Gao, G., Liu, X., Jia, H., Li, Q., Xu, B., 2019. The dual effects of RGO films in TiO2/CdSe heterojunction: Enhancing photocatalytic activity and improving photocorrosion resistance. Applied Surface Science 481, 1515–1523. https://doi.org/10.1016/j.apsusc.2019.03.136

50. Shi, W., Guo, X., Wang, J.-C., Liub, Y., Hou, Y., Li, Y., Lou, H., 2020. Enhanced photocatalytic 3D/2D architecture for $CO_2$ reduction over cuprous oxide octahedrons supported on hexagonal phase tungsten oxide nanoflakes - ScienceDirect. Journal of Alloys and Compounds 830.

51. Silva, M.K., Marques, R.G., Machado, NRCF, Santos, O. a. A., 2002. Evaluation of $Nb_2O_5$ and $Ag/Nb_2O_5$ in the photocatalytic degradation of dyes from textile industries. Brazilian Journal of Chemical Engineering 19, 359–363. https://doi.org/10.1590/S0104-66322002000400001

52. Sudhai, A., Raizada, P., Shandilya, P., Jeong, D.-Y., Lim, J.-H., Singh, P., 2018. Review on fabrication of graphitic carbon nitride based efficient nanocomposites for photodegradation of aqueous phase organic pollutants - ScienceDirect. Journal of Industrial and Engineering Chemistry 67, 28–51.

53. Thompson, W.A., Perier, C., Maroto-Valer, M.M., 2018. Systematic study of sol-gel parameters on $TiO_2$ coating for $CO_2$ photoreduction. Applied Catalysis B: Environmental 238, 136–146. https://doi.org/10.1016/j.apcatb.2018.07.018

54. Tran, P.D., Batabyal, S.K., Pramana, S.S., Barber, J., Wong, L.H., Loo, S.C.J., 2012. A cuprous oxide–reduced graphene oxide ($Cu_2O$–rGO) composite photocatalyst for hydrogen generation: employing rGO as an electron acceptor to enhance the photocatalytic activity and stability of $Cu_2O$ - Nanoscale (RSC Publishing). Nanoscale 4, 3875–3878.

55. Tripathy, N., Ahmad, R., Eun Song, J., Ah Ko, H., Hahn, Y.-B., Khang, G., 2014. Photocatalytic degradation of methyl orange dye by ZnO nanoneedle under UV irradiation. Materials Letters 136, 171–174. https://doi.org/10.1016/j.matlet.2014.08.064

56. Tu, W., Zhou, Y., Liu, Q., Tian, Z., Gao, J., Chen, X., Zhang, H., Liu, J., Zou, Z., 2012. Robust Hollow Spheres Consisting of Alternating Titania Nanosheets and Graphene Nanosheets with High Photocatalytic Activity for $CO_2$ Conversion into Renewable Fuels. Advanced Functional Materials 22, 1215–1221. https://doi.org/10.1002/adfm.201102566

57. Tu, W., Zhou, Y., Liu, Q., Yan, S., Bao, S., Wang, X., Xiao, M., Zou, Z., 2013. An In Situ Simultaneous Reduction-Hydrolysis Technique for Fabrication of $TiO_2$-Graphene 2D Sandwich-Like Hybrid Nanosheets: Graphene-Promoted Selectivity of Photocatalytic-Driven Hydrogenation and Coupling of $CO_2$ into Methane and Ethane. Advanced Functional Materials 23, 1743–1749. https://doi.org/10.1002/adfm.201202349

58. Wang, D., Pan, X., Wang, G., Yi, Z., 2015. Improved propane photooxidation activities upon nano $Cu2O/TiO2$ heterojunction semiconductors at room temperature. RSC Adv. 5. https://doi.org/10.1039/C4RA15215H

59. Wang, P.-Q., Bai, Y., Luo, P.-Y., Liu, J.-Y., 2013. Graphene–$WO_3$ nanobelt composite: Elevated conduction band toward photocatalytic reduction of $CO_2$ into hydrocarbon fuels. Catalysis Communications 38, 82–85. https://doi.org/10.1016/j.catcom.2013.04.020

60. Wang, Q., Lian, J., Li, J., Wang, R., Huang, H., Su, B., Lei, Z., 2015. Highly Efficient Photocatalytic Hydrogen Production of Flower-like Cadmium Sulfide Decorated by Histidine. Scientific Reports 5, 13593. https://doi.org/10.1038/srep13593

61. Wang, X., Yuan, B., Xie, Z., Wang, D., Zhang, R., 2015. ZnS–CdS/Graphene oxide heterostructures prepared by a light irradiation-assisted method for effective photocatalytic hydrogen generation. Journal of Colloid and Interface Science 446, 150–154. https://doi.org/10.1016/j.jcis.2015.01.051

62. Wei, Z.-H., Wang, Y.-F., Li, Y.-Y., Zhang, L., Yao, H.-C., Li, Z.-J., 2018. Enhanced photocatalytic $CO_2$ reduction activity of Z-scheme CdS/BiVO4 nanocomposite with thinner BiVO4 nanosheets - ScienceDirect. Journal of $CO_2$ Utilization 28, 15–25.

63. Wen, S., Zhao, J., Sheng, G., Fu, J., Peng, P., 2002. Photocatalytic reactions of phenanthrene at $TiO_2$/water interfaces. Chemosphere 46, 871–877. https://doi.org/10.1016/S0045-6535(01)00149-7

64. Xia, Y., Li, Q., Lv, K., Tang, D., Li, M., 2017. Superiority of graphene over carbon analogs for enhanced photocatalytic $H_2$-production activity of $ZnIn_2S_4$. Applied Catalysis B: Environmental 206, 344–352. https://doi.org/10.1016/j.apcatb.2017.01.060

65. Xie, T., Wang, D., Zhu, L., Li, T., Xu, Y., 2001. Application of surface photovoltage technique in photocatalysis studies on modified $TiO_2$ photocatalysts for photo-reduction of $CO_2$. Materials Chemistry and Physics 70, 103–106. https://doi.org/10.1016/S0254-0584(00)00475-2

66. Yang, C.-C., Yu, Y.-H., van der Linden, B., Wu, J.C.S., Mul, G., 2010. Artificial Photosynthesis over Crystalline $TiO_2$-Based Catalysts: Fact or Fiction? J. Am. Chem. Soc. 132, 8398–8406. https://doi.org/10.1021/ja101318k

67. Yang, M.-Q., Xu, Y.-J., 2016. Photocatalytic conversion of $CO_2$ over graphene-based composites: current status and future perspective. Nanoscale Horiz. 1, 185–200. https://doi.org/10.1039/C5NH00113G

68. Yang, M.-Q., Zhang, N., Pagliaro, M., Xu, Y.-J., 2014. Artificial photosynthesis over graphene–semiconductor composites. Are we getting better? Chem. Soc. Rev. 43, 8240–8254. https://doi.org/10.1039/C4CS00213J

69. Yu, J., Jin, J., Cheng, B., Jaroniec, M., 2014. A noble metal-free reduced graphene oxide–CdS nanorod composite for the enhanced visible-light photocatalytic reduction of $CO_2$ to solar fuel. J. Mater. Chem. A 2, 3407–3416. https://doi.org/10.1039/C3TA14493C

70. Yu, J., Xiong, J., Cheng, B., Liu, S., 2005. Fabrication and characterization of Ag–$TiO_2$ multiphase nanocomposite thin films with enhanced photocatalytic activity. Applied Catalysis B: Environmental 60, 211–221. https://doi.org/10.1016/j.apcatb.2005.03.009

71. Yuan, Y.-J., Chen, D., Yu, Z.-T., Zou, Z.-G., 2018. Cadmium sulfide-based nanomaterials for photocatalytic hydrogen production. J. Mater. Chem. A 6, 11606–11630. https://doi.org/10.1039/C8TA00671G

72. Zhang, L.J., Zheng, Rui., Li, Shuo., Liu, B.K., Wang, D.J., Wang, L.L., Xie, T.F., 2014. Enhanced Photocatalytic $H_2$ Generation on Cadmium Sulfide Nanorods with Cobalt Hydroxide as Co-catalyst and Insights into Their Photogenerated Charge Transfer Properties. ACS Appl. Mater. Interfaces 6, 13406–13412. https://doi.org/10.1021/am501216b

73. Zhang, Y., Chen, Z., Liu, S., Xu, Y.-J., 2013. Size effect induced activity enhancement and anti-photocorrosion of reduced graphene oxide/ZnO composites for degradation of organic dyes and reduction of Cr(VI) in water. Applied Catalysis B: Environmental 140–141, 598–607. https://doi.org/10.1016/j.apcatb.2013.04.059

74. Zhao, J., Wu, T., Wu, K., Oikawa, K., Hidaka, H., Serpone, N., 1998. Photoassisted Degradation of Dye Pollutants. 3. Degradation of the Cationic Dye Rhodamine B in Aqueous Anionic Surfactant/$TiO_2$ Dispersions under Visible Light Irradiation: Evidence for the Need of Substrate Adsorption on $TiO_2$ Particles. Environ. Sci. Technol. 32, 2394–2400. https://doi.org/10.1021/es9707926.

# TiO₂/graphene oxide nanocomposite with enhanced photocatalytic capacity for degradation of 2, 4-dichlorophenoxyacetic acid herbicide

*Thillai Sivakumar Natarajan[a, b], Kalithasan Natarajan[a], Praveen Kumar Gopi [a], Hari C Bajaj[a] and Rajesh J Tayade[a]\**

[a]Inorganic Materials and Catalysis Division, CSIR-Central Salt and Marine Chemicals Research Institute (CSIR-CSMCRI), Gijubhai Badheka Marg, Bhavnagar 364 002, Gujarat, India.
[b]Environmental Science Laboratory, CSIR-Central Leather Research Institute (CSIR-CLRI), Sardar Patel Road, Adyar, Chennai-600 020, India.
*Corresponding author: tayade@csmcri.res.in, rtayade@gmail.com

## Abstract

The present study investigates the photocatalytic degradation of 2, 4-Dichlorophenoxyacetic acid (2, 4-D), hazardous herbicides using $TiO_2$/Graphene oxide nanocomposite photocatalysts. The nanocomposite photocatalysts were synthesized using the solvothermal method by varying the weight percentage amount of graphene oxide. The nanocomposite photocatalysts were examined by X-ray diffraction (XRD), scanning electron microscopy (SEM), Bruner Emmet Teller (BET), FTIR and UV-visible-diffuse reflectance spectroscopy (UV-Vis-DRS) analysis. The XRD pattern of nanocomposite was found unaltered, whereas a significant change that is around 33 to 91% was observed in the surface area of the nanocomposites as compared to pristine $TiO_2$. The ultraviolet diffuse reflectance study showed that there was a blue shift in the band edge of the composites in the range of 21-29 nm. The complete photocatalytic degradation of 2, 4-D was achieved using $TiO_2/GO_{7\%}$ catalyst within 4 h of reaction under UV-light irradiation. The photocatalytic activity of the synthesized nanocomposite photocatalysts was also compared with the standard Degussa P-25 $TiO_2$ photocatalyst. The order of photocatalytic activity of the synthesized photocatalysts was $TiO_2/GO_{7\%}$> P25-$TiO_2$> $TiO_2/GO_{5\%}$> $TiO_2/GO_{2\%}$ > $TiO_2/GO_{1\%}$ > $TiO_2/GO_{10\%}$ > $TiO_2/GO_{1\%}$ > $TiO_2/GO_{0.5\%}$ > Pristine-$TiO_2$. This study offers a better platform for the synthesis of new composite photocatalytic materials for environment abatement by the degradation of organic pollutants.

*Keyword:* $TiO_2$, Graphene oxide, Nanocomposite, 2, 4-Dichlorophenoxyacetic acid, Photocatalysis, Degradation.

# 1. Introduction

An increase in demand for food resulted in higher use of low cost herbicides in the agricultural field to control the broad-leaved weeds and pests (Aksu and Kabasakal, 2004; Khoshnood and Azizian, 2012). 2, 4-Dichlorophenoxyacetic acid (2, 4-D) is one of the most widely used herbicides in the agriculture field, phenoxy organic compound and toxic to living organisms. Exposure to 2, 4-D can generate unintended impacts on wildlife food chains. Toxic effects on nervous tissue i.e., peripheral nerves and the brain were found for 2, 4-D. However, the specific toxicity levels for human beings were not yet studied clearly. This hazardous pesticide was easily being absorbed by soil and water bodies which pollutes environmental resources. The extensive use of pesticides in agriculture is not only compromising soil and water quality, but also the consumption of the contaminated water by living organism could lead to cancer, growth rate reduction, reproductive problems, and even death of non-target species including plants, animals, and human beings, respectively (Benli et al. 2007; Aronzon et al. 2011; Bondada, 2011; Huy et al. 2017; Singh et al. 2017). Moreover, numerous studies have proven that 2, 4-D might be an environmental hazard (Celik and Tuluce, 2007; Li et al. 2017). Based on the World Health Organization (WHO) regulation, the maximum allowable concentration of 2, 4-D is 30 µg/L in drinking water (Salman and Hameed, 2011). Wijnja $et$ $al.$, (2014) reported that 2, 4-D is the most frequently detected herbicide in the suburban surface waters in the United States during 1999-2010, with the highest concentration of 0.46 mg/L, respectively. Therefore, it is highly necessary to treat the wastewater before discharging it into the environment.

Various physical, chemical, thermal, biological, and advanced oxidation processes have been applied for the treatment of wastewater (Kang et al. 2001; Meshko et al. 2001; Rosal et al. 2010; Hakimelahi et al. 2012; Rodrigues et al. 2013; Natarajan et al. 2018) and 2,4,-D as well (Kundu et al. 2005; Cai et al. 2018; Kermani et al. 2018; Cruz González et al. 2018). Among these, advanced oxidation process such as photocatalysis using $TiO_2$ catalyst is one of the effective technologies for degradation of organic pollutants because of its high photocatalytic activity, chemical stability, and nontoxicity in nature, respectively (Fujishima and Honda, 1972; Mills et al. 1993; Hoffmann et al. 1995; Bhatkhande et al. 2002; Kamble et al. 2004; Carp et al. 2004; Tayade et al. 2006). Nevertheless, the higher band gap (3.2 eV) and poor surface area of $TiO_2$ and high recombination of photogenerated charge carriers on the $TiO_2$ surface limiting its practical applicability. Various modification on $TiO_2$ have been performed, among that synthesis of nanocomposites of $TiO_2$ with graphene oxide significantly enhances its surface area and suppress the recombination rate of charge carriers which leads to higher photocatalytic activity in degradation of organic pollutants (Zhang et al. 2010; Jiang et al. 2011; Morales-Torres et al. 2012; Gao et al. 2012; Ghosh et al. 2013; Pu et al. 2013; Jo et al. 2014; Atchudan et al. 2017; Thomas et al. 2017; Iliev et al. 2018). Ton et al. (2018) reported one-pot synthesis of $TiO_2$/graphene nanocomposites for the degradation of methylene blue dye degradation. Martins et al. (2018) developed $TiO_2$/graphene and $TiO_2$/graphene oxide nanocomposite for ciprofloxacin degradation under UV light irradiation. However, the $TiO_2$/graphene oxide based photocatalysts for the degradation of herbicide, 2, 4-Dichlorophenoxyacetic acid (2, 4-D) is rarely studied. Sandeep et al. (2018) evaluated the photocatalytic efficiency of hydrothermally synthesized $TiO_2$ for 2, 4-D degradation and compared the efficiency with commercial $TiO_2$.

Therefore, in the present study, we report the application of modified $TiO_2$ by developing the heterojunction between n-type semiconductor $TiO_2$ and p-type graphene oxide by the solvothermal method. To understand the role of interface between the p-n junction the nanocomposite photocatalysts were synthesized by varying the weight percentage amount of

p-type graphene (0.5%, 1%, 2%, 5%, 7%, and 10%) with respect to $TiO_2$. The synthesized photocatalysts were thoroughly characterized to determine their structural, morphological, textural and electronic properties. The result demonstrated that the optimal photocatalytic activity was demonstrated by composite contains 7% graphene oxide. The optimized synthesized photocatalyst showed the higher photocatalytic degradation of 2, 4-D as compared to Degussa P-25 $TiO_2$ photocatalysts, and complete degradation of 2, 4-D within 4 hours was observed in the presence of ultraviolet light irradiation using current experimental conditions.

## 2. Experimental section

### 2.1. Materials

Degussa P-25 $TiO_2$ was purchased from Degussa Corporation, Germany. Graphite powder, 2, 4-dichlorophenoxy acetic acid, titanium (IV) isopropoxide (TTIP), isopropyl alcohol (IPA), potassium permanganate ($KMnO_4$), hydrogen peroxide ($H_2O_2$), terephthalic acid (Benzene-1, 4-Dicarboxylic acid, BDC), and acetic acid ($CH_3COOH$) were purchased from Sigma-Aldrich and used without any further purification. Analytical double distilled (DD) water was used to prepare the experimental solutions.

### 2.2. Synthesis of graphene oxide

Graphene oxide was synthesized using modified Hummer's method as followed by Chen et al. (2009). 2 g of graphite powder and 8 g of $KMnO_4$ have added into the 100 mL of concentrated sulphuric acid, and then the beaker was placed into an ice bath with continues stirring. After removal from the ice bath, the mixture was changed into a water bath and continuously stirred for 1h under 35 °C. Then the mixture was diluted with distilled water and stirred for 1h at room temperature. Afterward, 20 mL of 30% $H_2O_2$ was added to reduce the residual $KMnO_4$ (the color changes from brown residue to brilliant yellow). The mixture was further washed with 5% HCl solution, and a copious amount of distilled water to neutralize the product. Finally, the obtained solid was dried at 60 °C for 24 h, and the material was denoted as GO.

### 2.3. Synthesis of TiO$_2$-Graphene oxide composites

The $TiO_2$-graphene oxide composites were synthesized via the solvothermal method. Typically, 70 mL of IPA and 5 mL of acetic acid was taken in 250 mL round-bottomed flask with different weight percentage (0.5, 1, 2, 5, 7, 10 %) of GO was added into the solution under vigorous stirring up to 5 min. The complete dispersion of GO with the reaction mixture was carried out using sonication for 30 min. Afterward, the 10 mL of TTIP was added into a well-dispersed GO solution and vigorously stirred for 2 h. The obtained reaction mixture was transferred into Teflon lined autoclave and heated in a hot air oven at 120 °C for 24 h. Subsequently, the autoclave was allowed to cool down to room temperature. The obtained product was collected by centrifugation and then washed with deionized water and ethanol several times. The final product was dried at 70 °C for 12 h for complete evaporation of the solvent. The as-synthesized $TiO_2$/GO composites were allowed to the annealing process at 500 °C for 3 h with a ramping rate of 2 °C min$^{-1}$ under nitrogen atmosphere in a tubular furnace system. Finally, the obtained products were denoted as $TiO_2$/GO$_{0.5\%}$, $TiO_2$/GO$_{1\%}$, $TiO_2$/GO$_{2\%}$, $TiO_2$/GO$_{5\%}$, $TiO_2$/GO$_{7\%}$ and $TiO_2$/GO$_{10\%}$, respectively. Similarly, the $TiO_2$ was synthesized without the addition of GO during the hydrothermal synthesis.

## 2.4. Characterization

The structural properties of as-synthesized photocatalysts were measured using Rigaku miniflexII Desktop X-ray diffractometer equipped with a Cu Kα1 ($\lambda$ = 0.154056 nm) radiation source. The surface morphology and elemental composition of $TiO_2$/GO composites were examined using scanning electron microscopy (SEM, Leo Series VP1430; INCA, EDX). The surface area of the photocatalyst was analyzed using Bruner Emmet Teller analysis (BET, ASAP-2020, Micromeritics, USA) at -196 °C. The FT-IR spectrums of synthesized composites were recorded using Perkin Elmer (FT-1730) spectrophotometer. The band edge and bandgap energy of $TiO_2$ with different weight percentages of GO were analyzed using ultraviolet-diffuse reflectance spectroscopy analysis (Shimadzu UV-2550, $BaSO_4$ as a reference). Chemical oxygen demand (COD) of 2, 4-D solution before and after degradation was analyzed via COD analyzer.

## 2.5. Photocatalytic degradation experimental setup

Photocatalytic degradation of the environmental pollutant (2, 4-D) was analyzed by using as-synthesized photocatalysts under irradiation of ultraviolet light (Medium pressure Mercury lamp, 125W with the presence of UV-light). The photocatalytic reactor which we have used in our earlier studies (Tayade et al. 2006) was used to determine the photocatalytic efficiency of the synthesized photocatalysts. First, a 200 mL aqueous solution of 2, 4-D (50 ppm) and synthesized photocatalyst (25 mg) was taken outer part of the reaction vessel and the photocatalyst particles were dispersed by sonicating the reaction mixture for few minutes. After this, the reaction mixture was continuously stirred for up to 30 min under the dark condition to obtain complete adsorption of the pollutant on the surface of the photocatalyst. Then the solution was kept under the UV light irradiation by switching on the UV-light source. During this process, the reactor temperature level was maintained around 20 °C by continuous circulation of water. Moreover, the reaction mixture has allowing continues stirring for up to 240 min for the complete reaction. Afterward, the reaction mixture was collected (5 mL) via the sample collection port every 10 min, for the first 1 hour and then after every 60 minutes and the catalyst particles were separated by centrifugation to analyze the catalytic behavior of as-prepared $TiO_2$/GO composite. Finally, the concentration of toxic pollutant (2, 4-D) was determined by measuring the absorbance of the degraded solution at λmax 229 nm using a UV-vis spectrophotometer.

## 2.6. Determination of hydroxyl (•OH) radical formation

The formation of hydroxyl radical (•OH) during the photocatalytic degradation of 2, 4- D using synthesised composite catalyst ($TiO_2$/$GO_{7\%}$) and P25 $TiO_2$ under UV light irradiation was detected by a fluorescence technique with terephthalic acid as a probe molecule (excitation wavelength, 315 nm). It is well-known from the literature that the terephthalic acid readily reacts with •OH radicals formed in the reaction to produce a highly fluorescent product, 2-hydroxyterephthalic acid. The detailed experimental procedures are reported in our earlier reports (Natarajan et al. 2013).

## 3. Result and Discussion

### 3.1. Structural analysis

The X-ray diffraction pattern of graphite and graphene oxide was shown in Fig. 1(A). The characteristic peak at 2θ=26.55° corresponds to the (0 0 2) plane of graphite can be seen

in Fig. 1(A), which was disappeared during the solvothermal reduction process and new peak at 2θ= 11.09° which corresponds to (0 0 1) plane of graphene oxide was observed indicating the complete transformation of graphite to graphene oxide. The diffraction pattern of synthesized $TiO_2$ and $TiO_2$/GO composites with a different weight percentage of GO are shown in Fig. 1(B). The diffraction peaks at 2θ = 25.5°, 37.1°, 37.9°, 38.8°, 48.3°, 54.1°, 55.3°, 62.9°, 68.9°, 70.5° and 75.3° are corresponded to planes of anatase phase of $TiO_2$ respectively (JCPDS No.21-1272). From the diffraction pattern of $TiO_2$ (Fig. 1(B)) with a different weight percentage of GO (0.5%, 1%, 2%, 5%, 7%, and 10%), it is observed that there was no alteration in the X-ray diffraction pattern of $TiO_2$, also no other additional peak related to graphene oxide in the $TiO_2$/GO. This indicates that the formation of composite materials without any impurities and alteration in the crystallite phase of $TiO_2$. However, the crystallite sizes calculated from the full width at half maximum (FWHM) of $TiO_2$ at (101) plane using Scherer formula showed that reduction in the crystallite size in the range of 5.15 - 7.25 nm (Table 1). It is further observed that the introduction of GO results in widening of diffraction peaks for (101) plane of $TiO_2$ and slight shifting in the diffraction angle indicates that the $TiO_2$ in $TiO_2$/GO composites possesses a lesser crystallite size. It is found that the crystallite size of $TiO_2$/GO composites was in the range of ~13-15 nm and it was lower than that of pristine $TiO_2$ (~20 nm). This may be presumably due to the addition of GO, which forms the thick graphene layer on the $TiO_2$ surface which suppressed the crystal growth of $TiO_2$ under solvothermal conditions. The transformation of graphite powder to GO was further confirmed by BET surface area and SEM analysis.

## 3.2. Morphological analysis

The surface morphology of the synthesized nanocomposites was examined using scanning electron microscopy analysis. As can be seen in Fig.2 (A), the synthesized GO revealed the wrinkled morphology with the complete transformation of graphite powder into layered GO. Fig. 2 (B) shows that the synthesized $TiO_2$ consists of the unique sphere-like structure with uniform distribution. Fig. 2 (C-H) shows that the different weight percentages of GO have interconnected with $TiO_2$ nanospheres. This was proved further from EDX analysis (results not shown here), which clearly shows the presence of C, Ti, and O on the as-synthesized composite which confirms the successful synthesis of nanocomposites.

## 3.3. UV-Vis-DRS analysis

The band edge and bandgap energy of the catalyst are essential features for photocatalytic degradation reaction. The band edge and bandgap energy of synthesized $TiO_2$ and $TiO_2$/GO composite catalysts were analyzed using UV-vis DRS spectroscopy analysis. The DRS spectrum recorded for different synthesized photocatalysts is shown in Fig. 3. The band edge and band gap of the synthesized photocatalysts were determined precisely by differentiation of UV-vis DRS spectrum curve of respective catalysts and the results are shown in Table 1.

The result demonstrated that, $TiO_2$/GO (0.5%, 1%, 2%, 5%, 7% and 10%) composite absorption edge extended towards blue region. The composition of $TiO_2$/GO$_{5\%}$ and $TiO_2$/GO$_{7\%}$ was observed the shifts up to 30 nm, which has revealed that the band edge decreased. The results revealed that the band gap values of the synthesized different composites are increasing while comparing with $TiO_2$. Herein, GO plays a crucial role in as-synthesized different composites. The increase in bandgap values leads to the decrease in the recombination rates of electron-hole, which shows the feasibility of enhancing the photocatalytic degradation of environmental pollutants. This is in accordance with our results and demonstrated the higher photocatalytic activity at a higher amount of GO up to

7% and then decreased as compared to pristine TiO₂. The decrease in photocatalytic activity of synthesised photocatalysts above 7 % loading of GO may be attributed to inhibiting the light penetration on the TiO₂ by GO.

### 3.4. FT-IR analysis

FT-IR spectra of GO, TiO₂ and TiO₂ with GO (0.5%, 1%, 2%, 5%, 7%, and 10%) are shown in Fig. 4. The broad peak at 3000–3500 $cm^{-1}$ in the spectra of GO corresponds to the –OH stretching vibrations of adsorbed water molecules and the vibration at 1626 $cm^{-1}$ can be attributed to -OH bending vibrations. Moreover, the very weak peak at ~1727 $cm^{-1}$ and 1033 $cm^{-1}$ as assigned to C=O stretching of carboxylic acid. The FT-IR of TiO₂ showed characteristic vibrations about ~500-900 $cm^{-1}$, the broadband corresponds to the inorganic Ti-O-Ti network, respectively. Furthermore, the broad vibration around 500-900 $cm^{-1}$ in the series of different composites shifted towards a high wavenumber. This peak may be the combination of Ti-O-Ti vibration and Ti-O-C vibration (798 $cm^{-1}$). The presence of Ti-O-C bonds indicated that the GO and carboxylic acid interacted with the surface hydroxyl groups of TiO₂ under hydrothermal conditions. These factors revealed that the formation of TiO₂/GO composite chemically bonded.

### 3.5. BET analysis

The photocatalytic activity strongly depends on the specific surface area of the photocatalyst. Thus, the surface area and pore size distribution of TiO₂ with a different weight percentage of GO (0.5%, 1%, 2%, 5%, 7% and 10%) were evaluated by BET (N₂ adsorption/desorption) isotherm analysis, the results are tabulated in Table 1. Fig. 5 (A-C) shows the N₂ adsorption/desorption isotherm of GO, TiO₂, and TiO₂/GO₇% composites, respectively. The results clearly shows that the series of GO affected the surface area of the as-prepared composites and the surface area of the catalysts such as pristine TiO₂, GO, TiO₂/GO₀.₅%,TiO₂/GO₁%, TiO₂/GO₂%, TiO₂/GO₅%, TiO₂/GO₇%, and TiO₂/GO₁₀% were 1.06, 2011.16, 63.58, 35.57, 73.57, 80.56, 97.08, and 92.55 $m^2/g$ respectively. Moreover, the surface area and pore size distribution are varying with the composition and reach maximum for TiO₂/GO₇% composition. The enhancement in surface area, pore size, and pore volume has a significant influence on the degradation ability while comparing other compositions of the GO series with TiO₂.

### 3.6. Photocatalytic degradation analysis

Photocatalytic activity of Degussa P25-TiO₂, pristine TiO₂ and TiO₂/GO (0.5%, 1%, 2%, 5%, 7%, and 10%) composites were evaluated by the degradation of 2, 4-D under the UV light irradiation. The percentage degradation of 2, 4-D (50 ppm) in the presence of Degussa P25-TiO₂, without catalyst, TiO₂ and TiO₂/GO (0.5%, 1%, 2%, 5%, 7%, and 10%) composites and UV light irradiation are shown in Fig. 6A and B. Fig. 6(A) shows that the complete degradation of 2, 4-D (50 ppm) was obtained in the presence of Degussa P-25 TiO₂ after 4h only, however, 17% of 2,4-D was degraded in the initial 10 minutes of reaction. Furthermore, 57 and 62% of 2, 4-D was degraded after 240 min in the absence of photocatalyst and hydrothermally synthesized TiO₂ under UV irradiation. The results further demonstrated that 69 %, 82.4 %, 82.4 % 86.4 % and 79% of 2, 4-D degraded in the presence of TiO₂/GO₀.₅%, TiO₂/GO₁%, TiO₂/GO₂%, TiO₂/GO₅% and TiO₂/GO₁₀% composites, respectively, under UV light illumination. Furthermore, complete degradation (100%) of 2, 4-D was observed using the TiO₂/GO₇% catalyst under UV light illumination (Fig. 6(B)). The results revealed that GO plays a crucial performance in the degradation of 2, 4-D by effective

suppression of photogenerated electron hole recombination rates while comparing to pristine $TiO_2$. It is further observed that the significant suppression of photogenerated electron-hole pair recombination leads to 85% of 2, 4-D degradation was observed within 60 minutes using 7% of GO loaded composite as compared to pristine $TiO_2$. Furthermore, the increase in GO loading to 10% showed 79% of degradation was observed, however, the decrease in percentage degradation might be due to that higher concentration of GO covered the $TiO_2$ surface which leads to photon scattering and blocks the active surface of $TiO_2$ (Huang et al. 2016; Thomas et al. 2017). The percentage degradation of 2, 4-D follows the order $(TiO_2/GO_{7\%})$ > Degussa P-25 $TiO_2$ > $(TiO_2/GO_{5\%})$ > $(TiO_2/GO_{2\%})$ > $(TiO_2/GO_{1\%})$ > $(TiO_2/GO_{10\%})$ > $(TiO_2/GO_{0.5\%})$ > pristine-$TiO_2$, respectively. The higher photocatalytic activity of $TiO_2/GO_{7\%}$ due to its lower crystallite size, which leads to high surface area (97 $m^2/g$) and pore volume (0.26 $cm^3/g$) as compared with other composites, Degussa P-25 $TiO_2$ and pristine $TiO_2$. So, in the presence $TiO_2/GO_{7\%}$ photocatalyst, the generated photogenerated charge carriers are effectively separated and the higher concentration of reactive radicals are generated (Scheme 1) which leads to complete degradation of 2, 4-D. Similarly, Huang et al. (2016) reported that graphene/$TiO_2$ composite nanomaterials showed higher photocatalytic activity as compared to $TiO_2$ in 2, 4-D degradation.

## 3.7. Chemical oxygen demand (COD) analysis

Photocatalytic degradation of 2, 4-D was further confirmed by COD analysis. 3 mL of different time interval sample was mixed with COD reagents and then digested at 150 °C for 2 h. After 2 h the samples were cooled down to room temperature, and COD was measured using HACH spectrophotometer and the results are shown in Fig. 7. The results demonstrated that a 97 % decrease in the COD values was observed for $TiO_2/GO_{7\%}$ composite which corroborates the results obtained by the UV-visible spectrophotometer. These results further demonstrated that the presence of photocatalysts and UV light irradiation essential for the degradation of environmental pollutant (2, 4-D).

## 3.8. Hydroxyl radicals ($^\bullet$OH) determination

The highest photocatalytic activity of $TiO_2/GO_{7\%}$ composite under UV light irradiation and the reactive radicals responsible for the degradation was carried out by hydroxyl radical ($\bullet$OH) determination during the reaction using fluorescence technique (Ishibashi et al. 2000; Xiao et al. 2008). In this regard, the hydroxyl radical formation was analyzed using terephthalic acid (TPA) as a probe molecule in the presence of $TiO_2/GO_{7\%}$ catalysts and results are shown in Fig. 8. Generally, the rate of hydroxyl radical ($\bullet$OH) formation directly proportional to the reaction time; the concentration of $\bullet$OH increasing with increasing irradiation time which is observed by the increase in the intensity of peak at 425 nm in the fluorescence spectroscopy corresponds to 2-hydroxyterephthalic acid product. The results demonstrated that the intensity of peak at 425 nm on the fluorescence spectra is decreased with an increase in the irradiation time. This may be due to the quenching of $\bullet$OH radicals was observed during photocatalytic degradation which leads to superoxide radical anions is the dominant reactive species responsible for the degradation of 2, 4-D in the presence of $TiO_2/GO_{7\%}$ composite in the present approach (Sahni and Locke, 2006).

## 3.9. Photocatalytic degradation mechanism

Irradiation of $TiO_2$ photocatalyst with energy higher than the bandgap energy of $TiO_2$ allows the electrons to move from valance band (VB) to conduction band (CB) by leaving holes. The photogenerated electrons get trapped by loaded GO leads to a decrease in the

recombination of photogenerated charge carriers. The generated positive holes move towards the surface of the catalyst where it reacts with adsorbed water molecules and produces hydroxyl radical ($^•OH$). Likewise, the trapped electrons undergo a reaction with oxygen ($O_2$) and form superoxide radical anion ($O_2^{•-}$). Thus, both reactive radicals react with water pollutant (2, 4- D) and produces range of intermediates which are ultimately mineralized into carbon dioxide ($CO_2$) and water ($H_2O$), respectively. The proposed photogenerated electron-hole pairs separation mechanism and their reaction with water pollutants is given in Fig. 9.

The possible intermediates generation during 2, 4-D degradation and the mineralization of formed intermediates using the composite catalysts are given in Scheme 1. It is understood from the literature that 2, 4-D undergoes both oxidative and reductive degradation reaction produces a range of intermediates followed by hydroxylation, ring-opening, and mineralization of formed intermediates occurs (Chen et al. 2009; Abdennouri et al. 2015). The photogenerated reactive radical species attacks the 2, 4-D water pollutant and produces 2, 4-dichlorophenol followed by fragmented into 2-chlorophenol intermediates. Then the electrophilic attack by $^•OH$ radicals generates mono and polyhydroxylated intermediate compounds (2-chlorobenze-1, 4-diol, benzene-1, 2, 4-triol, 3, 5-dichlorobenzene-1, 2-diol and phenol). Subsequently, the $^•OH$ radicals attack the hydroxylated intermediate compounds leads to the opening of the benzene ring and generates carboxylic acids which further mineralized into $CO_2$ and $H_2O$ (Scheme 1). The photocatalytic degradation efficiency of developed composite systems is compared with the literature available on the 2, 4-D water pollutant degradation and the results are given in Table 2. The results demonstrated that the $TiO_2/GO_{7\%}$ composite catalyst showed effective degradation of 2, 4-D as compared to the literature data under current experimental conditions.

## 4. Conclusion

$TiO_2$ and $TiO_2/GO$ composites with a different weight percentage of GO (0.5%, 1%, 2%, 5%, 7%, and 10%) were synthesized successfully via a solvothermal method. The structural and textural properties, surface morphology and bandgap energy of the composites were studied using various analytical techniques. The results demonstrated $TiO_2/GO$ composites were successfully formed which leads to a significant improvement in the photocatalyst performance. The bandgap energy analysis demonstrated that the bandgap energy value is increasing with a different weight percentage of GO and decreased the recombination rate of charge carriers after incorporation of GO. The photocatalytic degradation results demonstrated that the photocatalyst $TiO_2/GO7\%$ showed complete degradation of environmental pollutant (2, 4-D) under UV light irradiation. The percentage degradation of 2, 4-D follows the order ($TiO_2/GO_{7\%}$) > Degussa P-25 $TiO_2$ > ($TiO_2/GO_{5\%}$) > ($TiO_2/GO_{2\%}$) > ($TiO_2/GO_{1\%}$) > ($TiO_2/GO_{10\%}$) > ($TiO_2/GO_{0.5\%}$) > pristine-$TiO_2$, respectively. The enhanced photocatalytic activity of $TiO_2/GO_{7\%}$ is attributed to the high surface area, decreased recombination rate of photogenerated charge carriers and formation of higher concentration of reactive radicals as compared to other composites, pristine $TiO_2$ and Degussa P25 $TiO_2$ photocatalyst under present reaction conditions.

## Conflicts of interest

There are no conflicts to declare.

## Acknowledgements

## References

Abdennouri, M., Elhalil, A., Farnane, M., Tounsadi, H., Mahjoubi, F.Z., Elmoubarki, R., Sadiq, M., Khamar, L., Galadi, A., Baâlala, M., Bensitel, M., El Hafiane, Y., Smith, A., Barka, N., 2015. Photocatalytic degradation of 2,4-D and 2,4-DP herbicides on Pt/TiO$_2$ nanoparticles. J. Saudi Chem. Soc. 19, 485–493.

Aksu, Z., Kabasakal, E., 2004. Batch adsorption of 2, 4-dichlorophenoxy-acetic acid (2, 4-D) from aqueous solution by granular activated carbon. Sep. Purif. Technol. 35, 223-240.

Aronzon, C. M., Sandoval, M.T., Herkovits, J., Perez-Coll, C.S., 2011. Stage-dependent toxicity of 2, 4-dichlorophenoxyacetic on the embryonic development of a South American toad, Rhinella arenarum. Environ. Toxicol., 26, 373-381.

Atchudan, R., Edison, T.N.J.I., Perumal, S., Karthikeyan, D., Lee, Y.R. 2017. Effective photocatalytic degradation of anthropogenic dyes using graphene oxide grafting titanium dioxide nanoparticles under UV-light irradiation. J. Photochem, Photobiol. A: Chem. 333, 92-104.

Benli, A. Ç. K., Sarikaya, R., Sepici-Dincel, A., Selvi, M., Shain, D., Erkoc, F., 2007. Investigation of acute toxicity of (2, 4-dichlorophenoxy) acetic acid (2, 4-D) herbicide on crayfish (Astacus leptodactylus Esch. 1823). Pesticide Biochem. Physiology, 88, 296-299.

Bhatkhande, D. S., Pangarkar, V.G., Beenackers ACM.A., 2002. Photocatalytic degradation for environmental applications - a review. Journal of Chemical Technology & Biotechnology. 77, 102-116.

Bian, X., Chen, J., Ji, R., 2013. Degradation of 2,4-dichlorophenoxyacetic acid (2,4-D) by novel photocatalytic material of tourmaline-coated TiO$_2$ nanoparticles: Kinetic study and model. Materials (Basel). 6, 1530-1542.

Bondada, B. R., 2011. Micromorpho-anatomical examination of 2, 4-D phytotoxicity in grapevine (Vitis vinifera L.) leaves. Journal of Plant Growth Regulation 30, 185-198.

Cai, J., Zhou, M., Yang, W., Pan, Y., Lu, X., Groenen, K., 2018. Degradation and mechanism of 2 , 4-dichlorophenoxyacetic acid ( 2 , 4- D ) by thermally activated persulfate oxidation. Chemosphere 212, 784–793.

Carp, O., Huisman, C.L., Reller, A., 2004. Photoinduced reactivity of titanium dioxide. Prog. Solid State Chem. 32, 33–177.

Celik, I., Tuluce, Y., 2007. Determination of toxicity of subacute treatment of some plant growth regulators on rats. Environ. Toxicol., 22, 613-619.

Chen, T., Zeng, B., Liu, J.L., Dong, J.H., Liu, X.Q., Wu, Z., Yang, X.Z., Li, Z.M., 2009. High throughput exfoliation of graphene oxide from expanded graphite with assistance of strong oxidant in modified Hummers method. J. Phys. Conf. Ser. 188.

Cruz González, G., Julcour, C., Chaumat, H., Jáuregui-Haza, U., Delmas, H., 2018. Degradation of 2,4-dichlorophenoxyacetic acid by photolysis and photo-Fenton oxidation. J. Environ. Chem. Eng. 6, 874–882.

Fujishima, A., Honda, K., 1972. Electrochemical Photolysis of Water at a Semiconductor

electrode. Nature 238, 37–38.

Galindo, F., Gómez, R., Aguilar, M., 2008. Photodegradation of the herbicide 2,4-dichlorophenoxyacetic acid on nanocrystalline $TiO_2$-$CeO_2$ sol-gel catalysts. J. Mol. Catal. A Chem. 281, 119–125.

Gao, Y., Pu, X., Zhang, D., Ding, G., Shao, X., Ma, J., 2012. Combustion synthesis of graphene oxide-$TiO_2$ hybrid materials for photodegradation of methyl orange. Carbon 50, 4093–4101.

Ghosh, T., Cho, K.Y., Ullah, K., Nikam, V., Park, C.Y., Meng, Z. Da, Oh, W.C., 2013. High photonic effect of organic dye degradation by CdSe-graphene-$TiO_2$ particles. J. Ind. Eng. Chem. 19, 797–805.

Hakimelahi, M., Moghaddam, M.R.A., Hashemi, S.H., 2012. Biological treatment of wastewater containing an azo dye using mixed culture in alternating anaerobic/aerobic sequencing batch reactors. Biotechnol. Bioproc. Eng. 17, 875-880.

Hoffmann, M.R., Martin, S.T., Choi, W., Bahnemann, D.W., 1995. Environmental Applications of Semiconductor Photocatalysis. Chem. Rev. 95, 69–96.

Huang, D., Yang, T., Mo, Z., Guo, Q., Quan, S., Luo, C., Liu, L., 2016. Preparation of Graphene/$TiO_2$ Composite Nanomaterials and Its Photocatalytic Performance for the Degradation of 2, 4-Dichlorophenoxyacetic Acid, J. Nanomaterials, 2016, Article ID 5858906, 11 pages.

Huy, B. T., Jung, D.S., Phuong, N.T.K., Lee, Y. I., 2017. Enhanced photodegradation of 2, 4-dichlorophenoxyacetic acid using a novel $TiO_2$@ $MgFe_2O_4$ core@ shell structure. Chemosphere, 184, 849-856.

Iliev, V., Tomova, D., Bilyarska, L., 2018. Promoting the oxidative removal rate of 2 , 4-dichlorophenoxyacetic acid on gold-doped $WO_3$/$TiO_2$/reduced graphene oxide photocatalysts under UV light irradiation. J. Photochem. Photobiol. A Chem. 351, 69–77.

Ishibashi, K., Fujishima, A., Watanabe, T., Hashimoto, K., 2000. Detection of active oxidative species in $TiO_2$ photocatalysis using the fluorescence technique. Electrochem Commun 2, 207-210.

Jiang, G., Lin, Z., Chen, C., Zhu, L., Chang, Q., Wang, N., Wei, W., Tang, H., 2011. $TiO_2$ nanoparticles assembled on graphene oxide nanosheets with high photocatalytic activity for removal of pollutants. Carbon 49, 2693–2701.

Jo, W.K., Won, Y., Hwang, I., Tayade, R. J. 2014. Enhanced Photocatalytic Degradation of Aqueous Nitrobenzene Using Graphitic Carbon−$TiO_2$ Composites. Ind. Eng. Chem. Res. 53, 3455-3461.

Kamble, S. P., Sawant, S.B., Pangarkar, V.G., 2004. Novel solar-based photocatalytic reactor for degradation of refractory pollutants. AIChE Journal. 50, 1647-1650.

Kang, S.F., Liao, C.H., Po, S.T. 2001. Decolorization of textile wastewater by photo Fenton oxidation technology. Chemosphere 41, 1287-1297.

Kermani, M., Mohammadi, F., Kakavandi, B., Esrafili, A., Rostamifasih, Z. 2018. Simultaneous catalytic degradation of 2, 4-D and MCPA herbicides using sulfate radical-based heterogeneous oxidation over persulfate activated by natural hematite ($\alpha$-$Fe_2O_3$/PS), J Physics Chem. Solids 117, 49-59.

Khoshnood, M., Azizian, S., 2012. Adsorption of 2, 4-dichlorophenoxyacetic acid pesticide by graphitic carbon nanostructures prepared from biomasses. J Ind. Eng. Chem. 18, 1796-

1800.

Kundu, S., Pal, A., Dikshit, A.K., 2005. UV induced degradation of herbicide 2, 4-D : kinetics , mechanism and effect of various conditions on the degradation, Sep. Purif. Technol., 44, 121–129.

Li, K., Wu, J.Q., Jiang, L.L., Shen, L.Z., Li, J.Y., He, Z.H., Wei, P., Lv, Z., He, M.R., 2017. Developmental toxicity of 2, 4-dichlorophenoxyacetic acid in zebrafish embryos. Chemosphere, 171, 40-48.

Martins, P.M., Ferreira, C.G., Silva, A.R., Magalhães, B., Alves, M.M., Pereira, L., Marques, P.A.A.P., Melle-Franco, M., Lanceros-Méndez, S. (2018) $TiO_2$/graphene and $TiO_2$/graphene oxide nanocomposites for photocatalytic applications: A computer modeling and experimental study. Composites Part B: Eng. 145, 39-46.

Meshko, V., Markovska, L., Mincheva, M., Rodrigues, A.E. 2001. Adsorption of basic dyes on granular activated carbon and natural zeolite. Water Res. 35, 3357-3366.

Mills, A., Davis, R.H., Worsley, D., 1993. Water Purification by Semiconductor Photocatalysis. Chem. Soc. Rev. 22, 417-425.

Morales-Torres, S., Pastrana-Martínez, L.M., Figueiredo, J.L., Faria, J.L., Silva, A.M.T., 2012. Design of graphene-based $TiO_2$ photocatalysts-a review. Environ. Sci. Pollut. Res. 19, 3676–3687;

Natarajan, S., Bajaj, H. C., Tayade, R. J., 2018. Recent advances based on the synergetic effect of adsorption for removal of dyes from waste water using photocatalytic process. J. Environ. Sci., 65, 201-222.

Natarajan, T.S., Bajaj, H.C., Tayade, R.J. 2013, Enhanced direct sunlight photocatalytic oxidation of methanol using nanocrystalline $TiO_2$ calcined at different temperature. J Nanopart. Res. 16:2713, 1-16.

Piera, E., Calpe, J.C., Brillas, E., Domènech, X., Peral, J., 2000. 2,4-Dichlorophenoxyacetic acid degradation by catalyzed ozonation: $TiO_2$/UVA/$O_3$ and FE(II)/UVA/$O_3$ systems. Appl. Catal. B Environ. 27, 169–177.

Pu, X., Zhang, D., Gao, Y., Shao, X., Ding, G., Li, S., Zhao, S., 2013. One-pot microwave-assisted combustion synthesis of graphene oxide-$TiO_2$ hybrids for photodegradation of methyl orange. J. Alloys Compd. 551, 382–388.

Rodrigues, C.S.D., Madeira, L.M., Boaventura, R.A.R. 2013. Treatment of textile dye wastewaters using ferrous sulphate in a chemical coagulation/flocculation process. Environ. Technol. 34, 719-729.

Rosal, R., Rodriguez, A., Perdigon-Melon, J.A., Petre, A., Garcia-Calvo, E., Gomez, J.M., Aguera, A., Fernandez-Alba, A.R., 2010. Occurrence of emerging pollutants in urban wastewater and their removal through biological treatment followed by ozonation. Water Res. 44**,** 578-88;

Sahni, M., Locke, B. R. 2006. Quantification of Hydroxyl Radicals Produced in Aqueous Phase Pulsed Electrical Discharge Reactors, Ind. Eng. Chem. Res. 45, 17, 5819–5825

Salman, J., Hameed, B. J. D., 2010. Adsorption of 2, 4-dichlorophenoxyacetic acid and carbofuran pesticides onto granular activated carbon. Desalination 256, 129-135.

Sandeep, S., Nagashree, K.L., Maiyalagan, T., Keerthiga, G., 2018. Photocatalytic degradation of 2,4-dichlorophenoxyacetic acid - A comparative study in hydrothermal $TiO_2$ and commercial $TiO_2$. Appl. Surf. Sci. 449, 371–379.

Shankar, M.V., Anandan, S., Venkatachalam, N., Arabindoo, B., 2006. Fine route for an efficient removal of 2,4-dichlorophenoxyacetic acid (2,4-D) by zeolite-supported $TiO_2$. Chemosphere, 63, 1014-1021.

Singh, R. K., Philip, L., Ramanujam, S., 2017. Removal of 2, 4-dichlorophenoxyacetic acid in aqueous solution by pulsed corona discharge treatment: effect of different water constituents, degradation pathway and toxicity assay. Chemosphere 184, 207-214.

Tayade, R. J., Kulkarni, R. G., Jasra, R. V. 2006. Photocatalytic Degradation of Aqueous Nitrobenzene by Nanocrystalline $TiO_2$. Ind. Eng. Chem. Res. 45, 922-927.

Thomas, M., Natarajan, T. S., Sheikha, M. U. D., Banoa, M., Khana, F. 2017. Self-organized graphene oxide and $TiO_2$ nanoparticles incorporated alginate/carboxymethyl cellulose nanocomposites with efficient photocatalytic activity under direct sunlight. J. Photochem. Photobio. A: Chem. 346,113-125.

Ton, N. N. T., Dao, A. T. N., Kato, K., Ikenaga, T., Trinh, D. X., Taniike, T. 2018. One-pot synthesis of $TiO_2$/graphene nanocomposites for excellent visible light photocatalysis based on chemical exfoliation method. Carbon 133, 109-117.

Wijnja, H., Doherty, J.J., Safie, S.A., 2014. Changes in pesticide occurrence in suburban surface waters in Massachusetts, USA, 1999–2010. Bull Environ Contam Toxicol. 93, 228-232.

Xiao, Q., Si, Z., Zhang. J., Xiao. C., Tan, X., 2008. Photoinduced hydroxyl radical and photocatalytic activity of samarium doped $TiO_2$ nanocrystalline. J Hazard Mater 150, 62–67

Zhang, H., Lv, X., Li, Y., Wang, Y., Li, J. 2010. P25-Graphene Composite as a High Performance Photocatalyst. ACS Nano 4, 380-386.

**Fig. 1.**



**Fig. 2.**



**Fig. 3.**

**Fig. 4.**



**Fig. 5.**

Fig. 6.
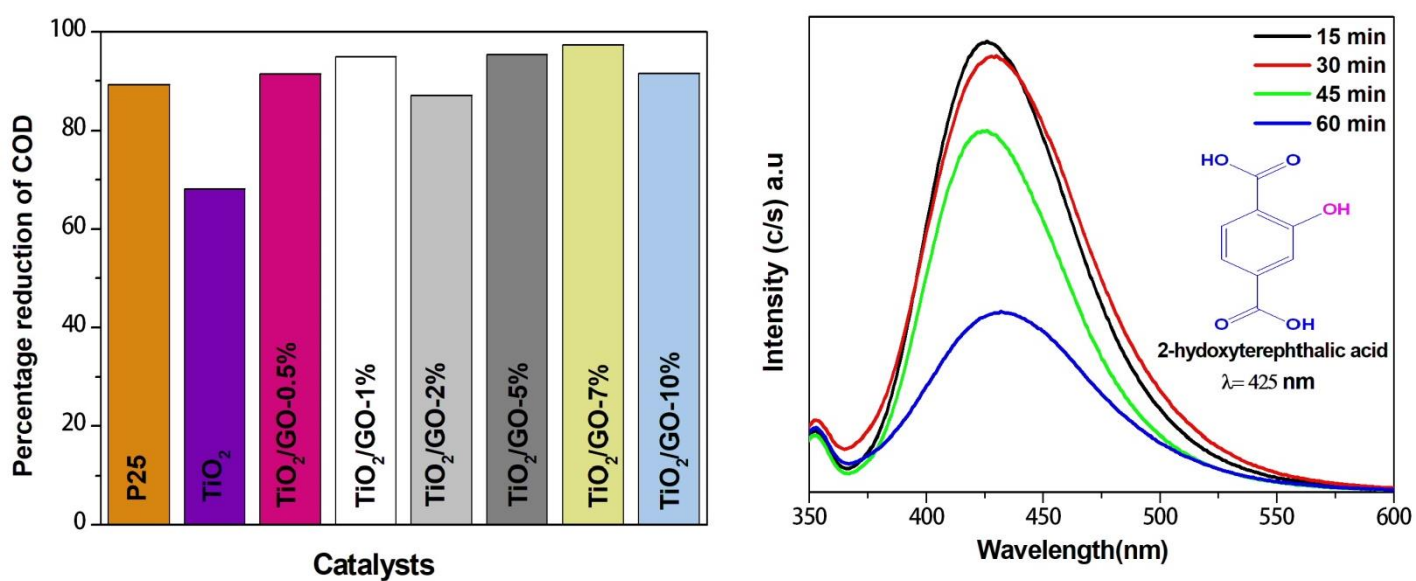


Fig. 7.



Fig. 8.
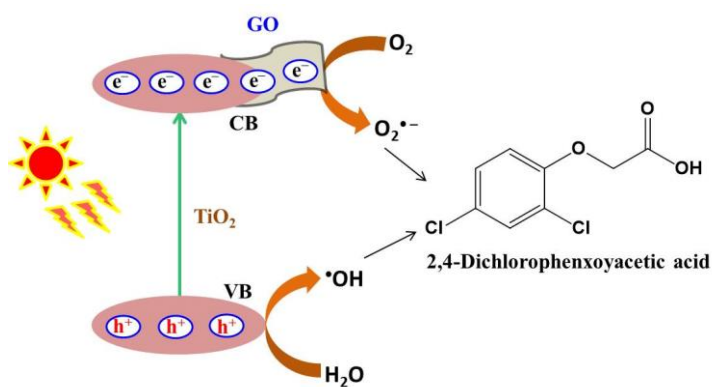


Fig.9.
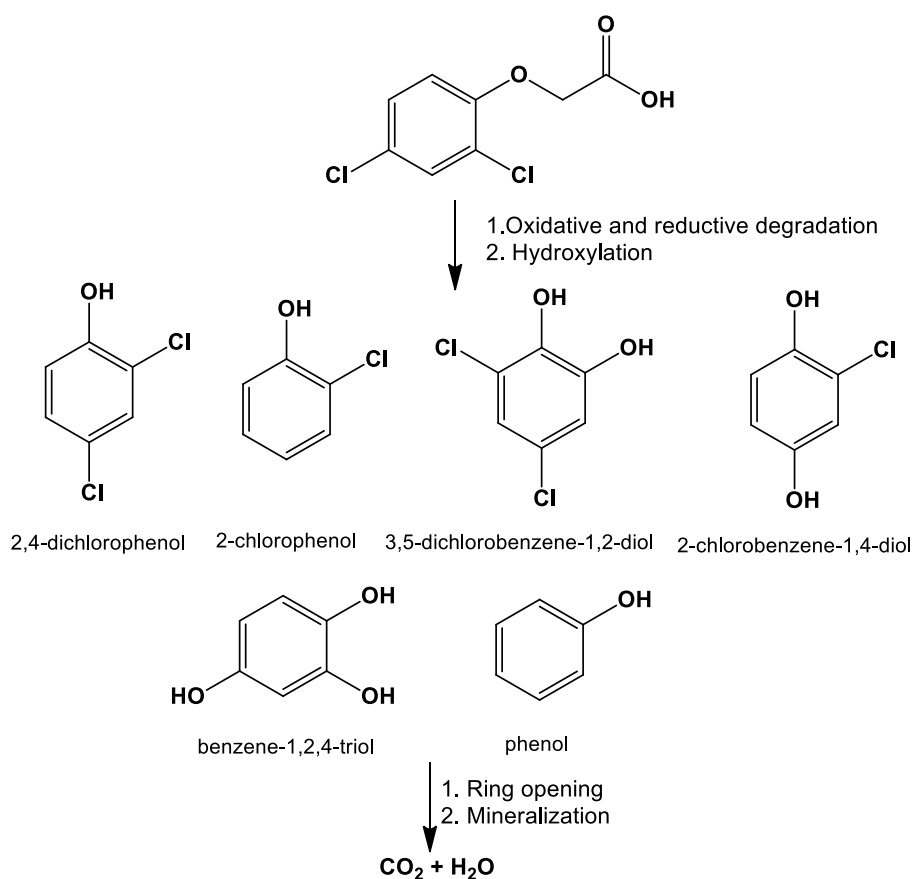
**Scheme 1.**

**Table 1.** The structural, textural and electronic properties of the synthesized photocatalysts.

| Catalysts | Crystallite Size ( nm) | BET surface area ($m^2$/g) | Pore Size (Å) | Pore volume ($cm^3$/g) | Band edge (nm) | Bandgap (eV) |
|---|---|---|---|---|---|---|
| $TiO_2$ | 20.4 | 1.06 | 52.03 | 2.4 | 391.1 | 3.16 |
| GO | 23 | 2011 | 52.93 | 0.02 | - | - |
| $TiO_2/GO_{0.5\%}$ | 13.15 | 63.58 | 36.9 | 0.11 | 369.5 | 3.36 |
| $TiO_2/GO_{1\%}$ | 15.25 | 35.57 | 14.09 | 0.29 | 363.6 | 3.41 |
| $TiO_2/GO_{2\%}$ | 13.8 | 73.57 | 32.8 | 0.12 | 364.4 | 3.40 |
| $TiO_2/GO_{5\%}$ | 13.4 | 80.56 | - | 0.25 | 361.7 | 3.43 |
| $TiO_2/GO_{7\%}$ | 13.17 | 97.08 | 60.67 | 0.26 | 361.6 | 3.43 |
| $TiO_2/GO_{10\%}$ | 13.29 | 92.55 | 35.4 | 0.16 | 363.6 | 3.41 |

**Table 2** Comparison of degradation efficiency of present system with literature data on 2, 4-D degradation

| Photocatalysts | Light source | Concentration of 2, 4-D | Volume/catalyst (mL):(mg) | Degradation (%) and Time (min) | Ref. |
|---|---|---|---|---|---|
| $TiO_2$/UVA/$O_3$ and Fe(II)/UVA/$O_3$ | Black-light fluorescent lamp | $2 \times 10^{-3}$ mol $dm^{-3}$ | 100:NA | 100:45 | Piera et al. 2000 |
| $TiO_2$/$CeO_2$ | UV Pen-Ray (UVP) lamp | 30 ppm | 250:250 | 68 :240 | Galindo et al. 2008 |
| $TiO_2$/Zeolite | Low-pressure mercury lamp | 200 mg/L | 100:200 | 100:300 | Shankar et al. 2006 |
| Tourmaline coated $TiO_2$ | UV light | 20 mg/L | 3000:1500 | >90:40 | Bian et al. 2013 |
| Pt/$TiO_2$ | medium pressure mercury-lamp | 20 mg/L | 800:120 | 100:90 | Abdennouri et al. 2015 |
| Graphene /$TiO_2$ | UV lamp | 50 mg/L | 1000:800 | >90:15 h | Huang et al. 2016 |
| Au/$WO_3$/$TiO_2$/ RGO | UV lamp | $3.2 \times 10^{-3}$ mol $L^{-1}$ | 350:35 | 100:150 | Iliev et al. 2018 |
| Graphene/$TiO_2$ | UV-light | 50 ppm | 1000:400 | 96:120 | Sandeep et al. 2018 |
| $TiO_2$/$GO_{7\%}$ | High pressure mercury vapor lamp | 50 mg/L | 200:25 | 100:240 | Present work |

*NA-Data not available

# EXTRACTION OF PHA FROM MOLASSES

*Prathyusha Nair*

Department of Chemical Engineering, Shroff Rotatry Institute of Chemical Technology,Ankleswar – Valia road,Vataria 393135, Gujarat, INDIA

prathyushagnair6606@gmail.com, 919409472054

## Abstract

Polyhydroxyalkaonate (PHA) is a biodegradable polymer obtained through organic sources. The aim of this work was to study the production of polyhyroxyalkanoates from waste material called molasses. Molasses is an agricultural waste which acts as a cheap carbon source for PHA production. The experiments had been carried out with mixed culture of *Bacillus subtilis*, *Escherichia coli* and *Enterobacter*and obtained as pure culture. Molasses had characteristics of 14.5 g/*l* volatile fatty acid, 65% reducing sugar and pH 5 ± 0.5. The effect of different parameters such as inoculum concentration, molasses concentration, fermentation time, nitrogen and phosphorous sources were studied.

## Keywords

Biopolymer, polyhydroxyalkanoate, molasses, biodegradable, cost effective, mixed culture

## 1. Introduction

Petrochemical plastics has blended finely in our day-to-day lives in the form of machinery, utensils, packaging and many other accessories. But plastic could not blend so easily with nature as its degradation rate is very low. Due to the short-term applications or single-time use plastics, it has been accumulated in large amount causing difficulty in disposing in landfills.

Polyhydroxyalkanote is a natural, sustainable and biodegradable biopolymer. Other naturally obtained biopolymers are silk, leather and cellulose. These have been replaced by synthetic polymers which is causing environmental problems. Problems are faced due to their non-biodegradable nature. In order to reduce the amount of plastic waste, recycling is one solution. Another solution is the development of biodegradable biopolymer. Polyhydroxyalkanoate is gaining major attention for its biocompatibility. PHAs are thermoplastics that are synthesized from carbon storing materials by bacteria. It is accumulated intra-cellularly in bacteria as a carbon and/or energy storage material (Eman 2014)

The major challenge in the production of polyhydroxyalkanoates is to reduce the production cost. Available carbon source has a large impact on production cost. So continuous researches are being carried out to find cost effective carbon sources. Food and agricultural wastes such as whey, legume waste, waste oil, and sugar industry wastes have carbon content (Chad et al 2017). India being the second largest producer of sugar, has a rich source of molasses which considered as a by-product from sugarcane industry. Molasses is rich in minerals and carbohydrates. These serve as a good source of nutrients and energy for microbes to grow. Microbes need nitrogen and phosphorus rich media for growth.PHA accumulating microorganisms of pure cultures mainly bacteria are used such as Alcaligeneslatus, Cupriavidusnecator and Escherichia coli.

Polyhydroxyalkanoates have mechanical properties similar to conventional plastics. So it can be spun into monofilaments and made into films. It can also be used to make heteropolymers with other synthetic polymers and many more applications in agriculture, packing, and medical field being biodegradable and also immunologically compatible with human tissue. Recently PHA is used in drug delivery systems (Anupama 2013) and biofuels (Kanokphorn et al. 2019).

The main objective of this work was to extract polyhydroxyalkanoates from a mixed strain of bacteria using molasses as a cost-effective carbon source. Also to study the effect of parameter like concentration of molasses, inoculum size, incubation time, and various proportions of nutrients on yield of PHA as well as to study and identify auxiliary carbon sources.

## 2. Materials and methods

### 2.1. Characterization of molasses

Molasses sample was obtained from Ganesh sugar factory, Ankleshwar. Primary characterization of molasses was done to know its properties. Reducing sugar test was performed by Benedict's titration method. 10gm of anhydrous $Na_2CO_3$ and 25ml Benedict's solution was taken in a conical flask and boiled until the salt dissolves. Molasses is diluted and taken in burette and titrated with Benedict's solution being heated throughout. A color from blue to brick red is observed and the volume of molasses is noted.

Total organic carbon and total nitrogen was performed in automatic analyzers. Volatile fatty acid test was performed by pH point titration from 3 to 7 pH using 0.1 N HCL and 0.1 N NaOH. Other tests include total suspended solids, total dissolved solids, and total reducing sugar following standard laboratory procedures.

### 2.2. Growth of mixed culture microbes

Pure cultures of *Bacillus subtilis*, *Escherichia coli* and *Enterobacter* was obtained from EnviroTechnology Ltd, Ankleshwar. They were sub-cultured by streaking method. Media used was agar agar powder(14 gm in 500ml distilled water) and agar powder. Streaked petri dished are incubated at 37.6°C for 2 days and stored in refrigerator for further use. Later, microbes are scraped using saline solution to form a mixed culture inoculum.

### 2.3. Nitrogen source

From a detailed literature study (Eman, 2014; El-Sayed et al,2017) it was found that the best nitrogen sources are ammonium nitrate, ammonium sulphate and ammonium chloride. This work uses ammonium sulphate to study its effect with different quantities.

### 2. 4.Salts

Different proportions of potassium dihydrogen phosphate ($KH_2PO_4$) and disodium phosphate ($Na_2HPO_4$) were used in this work. Eman (2014) has proved that there is no significant effect of MgSO4 and CaCl2 on either PHA concentration or cellular growth.

### 2.5. Polyhydroxyalkanoates production

Molasses is diluted (20%) and centrifuged at 5000 rpm for 10 minutes. 100 ml of centrifuged solution is taken in 250ml bottle. pH is maintained to 7 using 0.1 N HCL and 0.1 N NaOHand 2ml of inoculum is added. This mixture is then incubated at 36.6°C for different time periods. PHA is accumulated in the cells of bacteria. Resultant liquid is first sterilized

and then centrifuged at 10,000 rpm for 15 minutes. PHA pallets are obtained which is filtered out.More batches are prepared to study the optimum quantity of nitrogen and phosphorous sources and its effect on PHA production.

### 3.Theory

PHAs are regarded as a renewable resources-based alternative to petrochemical polymers. The advantageous character of PHAs lies in its environmental biodegradability and biocompatibility (Muhammadi *et al.* 2015). PHAs cover a large scale of biological polyesters having properties in the range from thermoplastic to elastomers (Koller 2018). The first identified and still the most investigated PHA is poly(3-hydroxybutyrate) (PHB). The chemical structure of formed PHA is primarily influenced by the microbial strains, carbon source, and eventually by the addition of precursors (Braunegg *et al.* 2002).

PHA obtained from molasses is a sugar-based biopolymer. Feedstock used for sugar-based fermentation processes, dedicated plant crops (e.g., sugarcane and cereal grains) are the preferred ones, followed by agriculture residues (e.g., sugarcane bagasse, wheat straw, corn stover), forestry residues, agro-industrial by-products, and bio-wastes. This biomass can also be categorized based on their carbohydrate composition as mono-, di-, or oligosaccharides (e.g., glucose and sucrose), polysaccharides (e.g., starch, cellulose, hemicellulose), or a mixture of those. All sugar-based biomass requires a certain level of upstream processing to make its sugar content available for efficient microbial fermentation processes. Biomass containing mono- or disaccharides (e.g., sugarcane and sugar beet) needs minimal crushing/extraction upstream processing to obtain a sugar solution (Nag 2008).

<table>
<tr><td>Figure 1. Saline solution</td><td>Figure 2. Molasses solution</td></tr>
</table>



The cost of PHA production can be effectively reduced by using molasses which is a cheap and easily available agro-industrial waste. Conventionally, molasses has very high sugar content of 60-70%. Molasses also has high amount of organic carbon and nitrogen which proves to be very useful for microbial growth as well as PHA production.

## 4. Results and Discussion

Prior to PHA production, knowing the characteristics of the raw material is quite essential. Parameters like volatile fatty acid, pH and reducing sugar content is crucial to be known beforehand. These parameters vary after the fermentation process, for example reducing sugar reduces accounting the amount sugar used up by the microbes. Molasses sample obtained from Ganesh Sugar Factory, Ankleshwarhad tested for following parameters and results are tabulated below:

Table 1. List of tested parameters of molasses

| Sr. no. | Property | Quantity |
|---|---|---|
| 1 | Color | Dark brown |
| 2 | pH | 5.08 |
| 3 | Reducing sugar | 65.8% |
| 4 | Total Reducing Sugar | 79.78% |
| 5 | Sucrose Content | 13.3% |
| 6 | Total Suspended Solids | 0.820 g/l |
| 7 | Volatile Suspended Solids | 41.024g/l |
| 8 | Total Dissolved Solids | 6.037 g/l |
| 9 | Total Organic content | 273.040 g/l |
| 10 | Total Nitrogen Content | 6.156 g/l |
| 11 | Volatile Fatty Acid | 14.865 g/l |

Several batches were tested for PHA can with molasses solely with no added salts and maintaining the pH neutral as well as using different amount of salts. Incubation temperature was 36.6°C with inoculum size 2ml. the results obtained are tabulated as follows:

Table 2. PHA obtained using molasses as a sole carbon source without other salts and chemicals in the form of nutrients.

| Sr. No. | pH | Volatile Fatty acid (g/l) | Dry Cell Weight (g/l) | Incubation time(hrs) |
|---|---|---|---|---|
| 1 | 4.51 | 2.021 | 1.347 | 24 |
| 2 | 4.49 | 3.537 | 2.19 | 48 |
| 3 | 4.24 | 9.171 | 1.475 | 72 |
| 4 | 4.04 | 14.227 | 1.401 | 96 |
| 5 | 4.33 | 11.334 | 0.915 | 120 |

Table 3. PHA obtained using molasses with 0.5g/l ammonium sulphate, 0.25g/l potassium dihydrogen phosphate and 0.25g/l disodium phosphate.

| Sr. No. | pH | Volatile Fatty acid (g/l) | Dry Cell Weight (g/l) | Incubation time(hrs) |
|---------|------|--------|-------|-----|
| 1 | 4.81 | 7.463 | 0.963 | 24 |
| 2 | 4.88 | 9.154 | 0.933 | 48 |
| 3 | 4.52 | 5.163 | 0.932 | 72 |
| 4 | 4.58 | 7.900 | 1.511 | 96 |
| 5 | 4.4 | 8.425 | 1.81 | 120 |

Table 4. PHA obtained using molasses with 0.1g/l ammonium sulphate, 0.5g/l potassium dihydrogen phosphate and 0.5g/l disodium phosphate

| Sr. No. | pH | Volatile Fatty acid (g/l) | Dry Cell Weight (g/l) | Incubation time(hrs) |
|---------|------|--------|-------|-----|
| 1 | 5.03 | 7.64 | 1.288 | 24 |
| 2 | 4.71 | 12.74 | 1.766 | 48 |
| 3 | 4.46 | 11.55 | 1.642 | 72 |
| 4 | 4.41 | 14.2 | 1.356 | 96 |
| 5 | 4.76 | 7.89 | 3.666 | 120 |
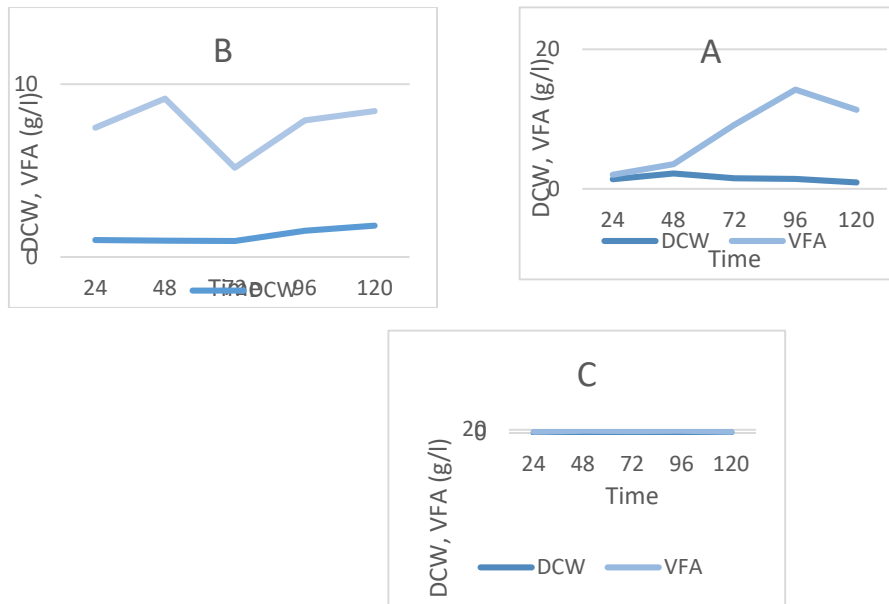


Figure 3. Variations in dry cell weight and volatile fatty acid is shown in the figure obtained from table 2, 3 and 4 respectively.

The highest amount of PHA is seen to have obtained when the microbes are provided with sufficient amount of nitrogen and phosphorous sources which is 0.5 g/l of potassium dihydrogen phosphate and disodium phosphate, and 0.1 g/l of ammonium sulphate.

## 5. Conclusion

This work represents the production of polyhydroxyalkanoates from sugarcane molasses as a cheap carbon source by mixed cultures of *Bacillus subtilis*, *Escherichia coli* and *Enterobacter.* Molasses concentration during the entire work was 20%. Maximum DCW of PHA obtained with molasses was 2.19g/l achieved after 48 hours without using any additional nutrients. Furthermore, 3.66g/l DCW is achieved using 0.1g/l ammonium sulphate, 0.5g/l potassium dihydrogen phosphate and 0.5g/l disodium phosphate. Thus it can be concluded that significant amount of PHA can be accumulated from this cheap carbon source.

## Acknowledgements

## References

1. A K H NorAslan, M D Mohd Ali, N A Morad and P Tamunaidu (2016). Polyhydroxyalkanoates production from waste biomass
2. Adriana Kovalcik, StanislavObruca, Ines Fritz, Ivana Marova(2019) Polyhydroxyalkanoates: Their Importance and Future
3. AnupamaShrivastav, Hae-YeongKim,and Young-Rok Kim (2013)Advances in the Applications of Polyhydroxyalkanoate Nanoparticles for Novel Drug Delivery System
4. C.S.K. Reddy, R. Ghai, Rashmi, V.C. Kalia (2003). Polyhydroxyalkanoates: an overview
5. Chad Nielsen, Asif Rahman, Asad Ur Rehman, Marie K. Walsh and Charles D. Miller (2017). Food waste conversion to microbial polyhydroxyalkanoates
6. *E. Bugnicourt*1*, P. Cinelli*2*, A. Lazzeri*2*, V. Alvarez*3(2014). Polyhydroxyalkanoate (PHA): Review of synthesis, characteristics, processing and potential applications in packaging
7. EmanZakariaGomaa (2014). Production of Polyhydroxyalkanoates (PHAs) By *Bacillus subtilis*and *Escherichia coli* Grown on Cane Molasses Fortified with Ethanol
8. GerhartBraunegg, Rodolfo Bona, Florian Schellauf, Elisabeth Wallner(2002) Polyhydroxyalkanoates (PHAs): Sustainable biopolyester production
9. Guo-Qiang Chena, XinyuChenc, FuqingWua, Jinchun Chena (2019). Polyhydroxyalkanoates (PHA) Toward Cost Competitiveness and Functionality
10. Hussein Reda Hussein, Mohamed A. Hassan, S. G. Ali, ElsayedKhalafBakhiet (2016) Production and characterization of polyhydroxybutyrate (PHB) produced by Bacillus sp. isolated from Egypt
11. Jaciane Lutz Ienczak, WillibaldoSchmidell, Gla´ucia Maria Falca˜o de Araga˜o (2013). High-cell-density culture tstrategies for polyhydroxyalkanoate production: a review

12. Jai Shanker Pillai, Naveen Danesh, Puttaiah.E.T, Girish. K (2011). Microbial diversity in solid waste molasses of Sugar Indusry, Aranthangi, Tamilnadu
13. Lai, S.-M., Sun, W.-W. & Don, T.-M. (2015) Preparation and characterization of biodegradable polymer blends from poly(3-hydroxybutyrate)/poly(vinyl acetate)-modified corn starch.
14. M. Geethu, R. Vrundha, S. Raja, H. Raghu Chandrashekar, M. S. Divyashree (2019). Improvement of the Production and Characterisation of Polyhydroxyalkanoate by *Bacillus endophyticus*Using Inexpensive Carbon Feedstock
15. M.G.E. Albuquerque, M. Eiroa, C. Torres, B.R. Nunes, M.A.M. Reis (2007). Strategies for the development of a side stream process for polyhydroxyalkanoate (PHA) production from sugar cane molasses
16. Mamtesh Singh, PrasunKumar,SanjayPatel,Vipin Chandra Kalia(2013) Production of Polyhydroxyalkanoate Co-polymer by Bacillus thuringiensis
17. Martin Koller (2018)A Review on Established and Emerging Fermentation Schemes for Microbial Production of Polyhydroxyalkanoate (PHA) Biopolyesters
18. Muhammadi, Shabina, Muhammad Afzal, Shafqat Hameed (2015) Bacterial polyhydroxyalkanoates-eco-friendly next generation plastic: Production, biocompatibility, biodegradation, physical properties and applications
19. NarisaBinhayeeding, SappasithKlomklao, PoonsukPrasertsan, KanokphornSangkharak (2020) Improvement of biodiesel production using waste cooking oil and applying single and mixed immobilised lipases on polyhydroxyalkanoate
20. NighatNaheed, Nazia Jamil (2013). Optimization of biodegradable plastic production on sugar cane molasses in *Enterobacter*sp. SEL2
21. PalmiroPoltronieri, Prasun Kumar (2017)Polyhydroxyalkanoates (PHAs) in industrial applications
22. Said El-SayedDesouky, Mohamed Ali Abdel-Rahman, Mohamed Salah Azab, Mahmoud E. Esmael (2017) Batch and fed-batch production of polyhydroxyalkanoates from sugarcane molasses by *Bacillus flexus*Azu-A2
23. Shashi Kant Bhatia. Yung-Hun Yang (2017). Microbial production of volatile fatty acids: current status and future perspectives
24. Simon Bengtssona, Ana R. Pisco, Peter Johansson, Paulo C. Lemos, Maria A.M. Reis (2010). Molecular weight and thermal properties of polyhydroxyalkanoates produced from fermented sugar molasses by open mixed cultures
25. Zibiao Li, Jing Yang, and Xian Jun Loh (2016). Polyhydroxyalkanoates: opening doors for a sustainable future

# Review Paper

## on

## "Bio Compostable Plastics: A New Generation of Environment Friendly Plastics"

*Bharati G Basantani [1] & Prof. [Dr.] Alok Gautam [2]*

*[1]Asso. Prof. & Head – Plastic Technology , L.D college of  Engineering, Ahmedabad,*
*[2]Prof. & Head – Department of Chemical Engineering, Shroff S R Rotary Institute of  Chemical Technology, Ankleshwar, Gujarat*

**Abstract:** The current threat to the use of plastics, particularly single –use, is a threat to Animals, Environment, Plastic Industry as a whole and its beneficiaries. The intent of this review paper is to highlight the current scenario and possible solutions. Although great deal of research is done on Biodegradable plastics, but the composting time is higher. To solve current issues, Lot of research work is needed in the area of compostable plastics to bring forth an amicable solution to the existing problem.

**Key Words:** Bioplastics, Biodegradable Plastics, Compostable Plastics, Biodegradation, Compostibility , Packaging , Composites

## 1. Introduction

Petroleum-based plastics are the third highest used product extracted from petroleum. India has become one of the biggest centers of plastic usage with over 15,000 tons of plastic waste generated every year, of which only 60% is re-processed. Countries all over the globe have begun to take steps on curbing its usage. Bangladesh has prohibited plastic bags countrywide, Ireland has imposed a tax on plastic bags, while the UK and other European countries are contemplating about taxing them as well.  There is now 5.25 trillion macro and micro pieces of plastic in our ocean & 46,000 pieces in every square mile of ocean, weighing up to 269,000 tonnes. Every day around 8 million pieces of plastic makes their way into our oceans.

The India Packaging Market was valued at USD 50.5 billion in 2019, and it is expected to reach USD 204.81 billion by 2025, registering a CAGR of 26.7% during the period of 2020-2025. The Indian plastics market is comprised of around 25,000 companies and employs 3 million people.

Corresponding Author: Bharati Basantani
bharati64053@gmail.com, (+91) 9824064053

1.1 Current Scenario in Plastics Industry

The current situation in India stands at BAN OF SINGLE USE plastics. There is an insistence on finding alternate materials.

1.2 Impact on society and Industry

Newly established plastic units finding it difficult to pay EMI on machinery hence shutting down and moving on to newer businesses. It is estimated that approx 6 lakhs jobs would be lost due to this.

1.3 Where Is The Problem?
➢ Lack of education in handling plastics.
➢ No proper system for collecting plastics by giving incentives.
➢ Litter resulting in animals eating them and getting sick.

1.4 What is the Solution?

The best solution is the use of Bioplastics, Biodegradable Plastics and BioCompostible Plastics

## 2. BIOPLASTICS, BIODEGRADABLE PLASTICS, BIOCOMPOSTIBLE PLASTICS

➢ Biopolymer or organic plastic is a form of plastic derived from renewable biomass sources such as vegetable oil, starch, proteins etc, unlike fossil fuel plastics which are derived from petroleum.

➢ BioDegradable polymers (BDPs) or biodegradable plastics refer to polymeric materials that are 'capable of undergoing decomposition into carbon dioxide, methane, water, inorganic compounds, or biomass in which the predominant mechanism is the enzymatic action of microorganisms, that can be measured by standardized tests, in a specified period of time, reflecting available disposal condition' (ASTM standard D6813).

➢ Bio Compostible Plastic is plastic which is "capable of undergoing biological decomposition in a compost site as part of an available program, such that the plastic is not visually distinguishable and breaks down to carbon dioxide, water, inorganic compounds, and biomass, at a rate consistent with known compostable materials (*e.g.* cellulose) and leaves no toxic residue. In order for a plastic to be called compostable, three criteria need to be met:

a. Biodegrade - break down into carbon dioxide, water, biomass at the same rate as cellulose (paper).
b. Disintegrate - the material is indistinguishable in the compost, that it is not visible and needs to be screened out

c. Eco-toxicity - the biodegradation does not produce any toxic material and the compost can support plant growth.

## 3. Biodegradability and Bio Compostibility

A substance or a material is biodegradable if it is broken down by micro-organisms such as bacteria, protozoa, fungi, or enzymes. The micro-organisms use the substances as nutrients or a source of energy. The remain- der of the broken down substance consists of carbon dioxide ($CO_2$), water and mineral salts of the other elements present (mineralisation)

Compostable Plastics are a new generation of plastics which are biodegradable through composting. They are derived generally from renewable raw materials like starch (e.g. corn, potato, tapioca etc), cellulose, soy protein, lactic acid etc., are not hazardous/toxic in production and decompose back into carbon dioxide, water, biomass etc. when composted. Some compostable plastics may not be derived from renewable materials, but instead derived made from petroleum or made by bacteria through a process of microbial fermentation.

## Composting

A managed process that controls the biological decomposition and transformation of biodegradable materials into a humus-like substance called compost: the aerobic mesophilic and thermophilic degradation of organic matter to make compost, the transformation of biologically decomposable material through a controlled process of biooxidation that proceeds through mesophilic and thermophilic phases and results in the production of carbon dioxide, water, minerals and stabilized organic matter (compost or humus). Composting uses a natural process to stabilize mixed decomposable organic material recovered from municipal solid waste, yard trimmings, biosolids (digested sewage sludge), certain industrial residues and commercial residues.

**Degradable Plastic** is plastic which will undergo a significant change in its chemical structure under specific environmental conditions resulting in a loss of some properties. Please note that there is no requirement that the plastic has to be degrade from the action of "naturally occurring microorganism" or any of the other criteria required for compostable plastics.

A plastic therefore may be degradable but not biodegradable or it may be biodegradable but not compostable (that is, it breaks down too slowly to be called compostable or leaves toxic residue).

Table 1. Estimated Composting Times

| Product | Home Composting | Commercial Composting |
|---|---|---|
| Wheat Straw or Sugarcane Fiber  Plates, Takeout Contianers, Bowls, Cups and Trays | Upto 6 months | 1-3 Months |
| Ingeo Cold Cups, Clear Containers, Straws | Not recommended | 3-6 Months |
| TPLA Heat Resistant & Non Heat Resistant Utensils | Not recommended | 3-6 Months |
| Trash/Kitchen Bags | Upto 1 year | 2-4 Months |

The rate of biodegration for different biocompostables is dependent upon the composition and thickness of the material as well as composting conditions. Commercial composting facilities grind the materials, turn over the piles and reach high temperatures, thus reducing the amount of time it takes to compost and, is thus, the recommended method for composting these products. Home composting rates are slower and can vary, depending on how frequently the pile is turned over, the moisture and material content and the temperature.

Making or calling a product biodegradable has no inherent value if the product, after use by the customer, does not end up in a waste management system that uses the biodegradability features (Narayan 1993, 1994). Figure 1[ref illustrates the integration of biodegradable plastics with disposal infrastructures that use this biodegradable function of the plastic product.
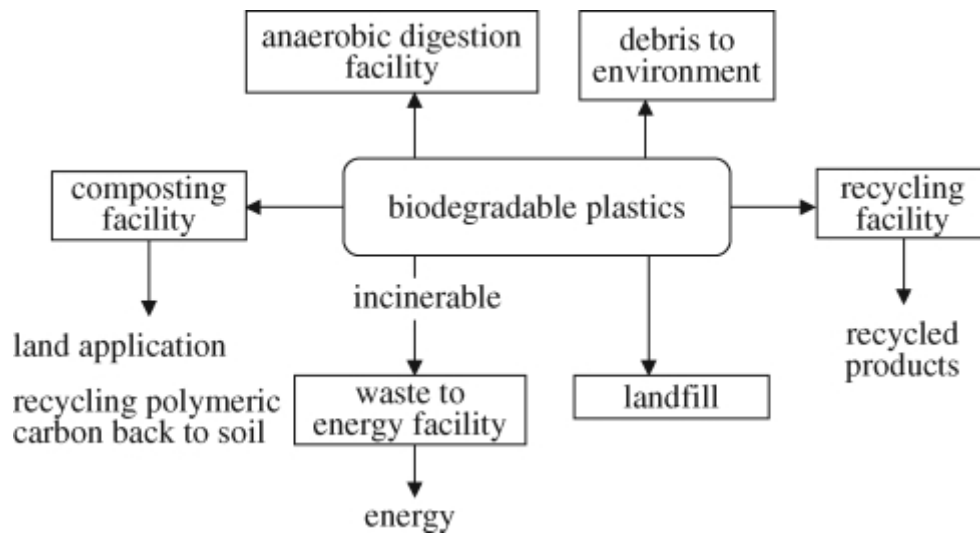


Figure 1.  Integration of biodegradable plastics with disposal infrastructures.[ref21]

# Biodegradation of polymers in aerobic and anaerobic conditions
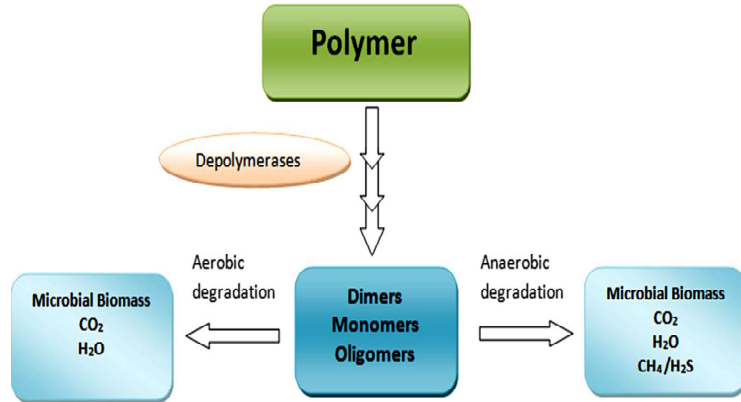


**Figure 2. Illustrates Biodegradation of polymers in aerobic and anaerobic conditions.**

# Cradle to grave life cycle flowchart of plastic mulch films



Conventional mulch films are **reused, recycled, incinerated, and/or landfilled**.

Biodegradable mulch provides the end-of-life scenario routes which can be **composted.**

Figure 3. Cradle to gate, grave, and cradle life cycle flowchart of plastic mulch films. After removal of conventional mulch films, they can be reused, recycled, incinerated, and/or landfilled. Biodegradable mulch provides the same end-of-life scenario routes and also can be composted.[ref.18]
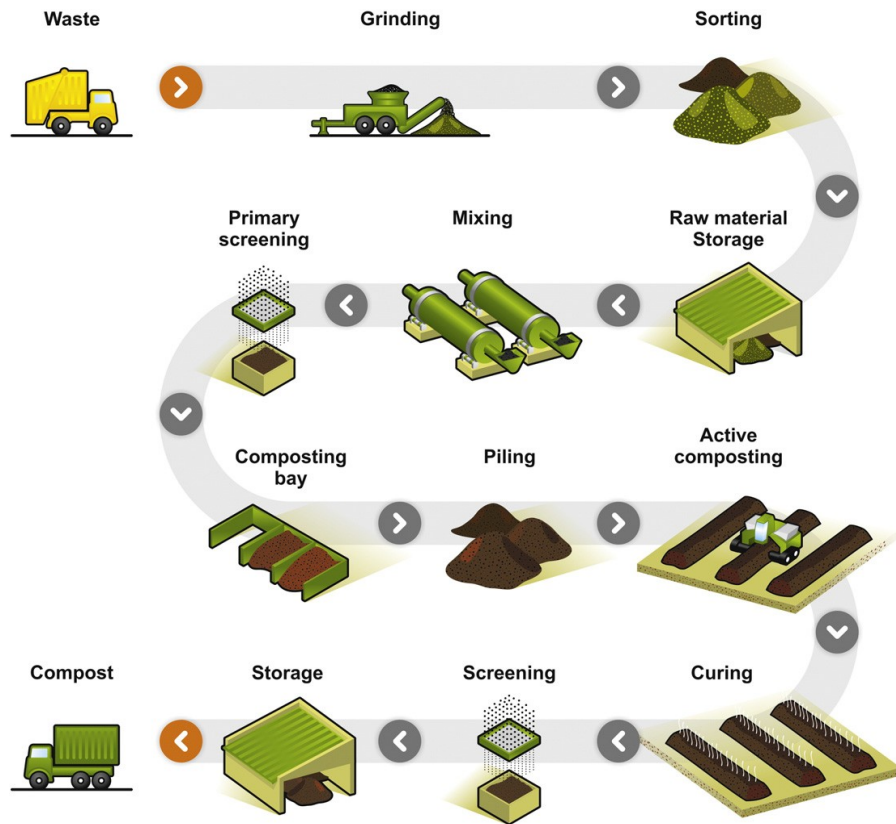
**Figure 4 :** **Large-scale commercial composting process.** "Reprinted from Polymer International, 57, Kijchavengkul et al., Compostability of polymers, 793–804[ref.18]

## 4. Standards

There are currently few international organizations which have established standards and testing methods for compostability, namely:

- American Society for Testing and Materials    ASTM-6400-99
- European Standardization Committee (CEN)  EN13432
- International Standards Organization (ISO)   ISO14855 (only for biodegradation)
- German Institute for Standardization (DIN)  DIN V49000

**Table 2. Comparison of key requirements of composting standards [ Ewa Rudnik]**

| Standard | Biodegradation | Disintegration | Safety |
|---|---|---|---|
| ASTM D 6400 | *For products consisting of a single polymer (homopolymer or random copolymer),60% of the organic carbon must be converted to carbon dioxide within 180 days. *For products consisting of more than one polymer (block copolymers, segmented copolymers blends or addition of low molecular weight), 90% of the organic carbon must be converted to carbon dioxide within180 days | No more than 10% of its original dry weight remains after sieving on a 2.0 mm sieve after controlled laboratory scale composting | * No adverse impact on ability of compost to support plant growth *Low levels of heavy metals |
| ISO/DIS 117088 | • For products consisting of a homopolymer, 60% of the organic carbon must be converted to carbon dioxide within 180 days • For all other polymers (e.g. copolymers or blends), 90% of the organic carbon must be converted to carbon dioxide within 180 days | No more than 10% of its original dry mass remains after sieving on a 2.0 mm sieve after 84 days in a controlled composting test | • Low levels of heavy metals • A minimum of 50% of volatile solids • Ecotoxicological test on two different plant species following modified OECD guideline 208) |
| EN 13432 | At least 90% of biodegradation within six months | No more than 10% of the residues from the packaging waste should be larger than 2 mm | *Low levels of heavy Physical / chemical analysis of resulting compost *Ecotoxicological assessment (plant growth) test on two different plant species following modified OECD guideline 208) |

The ASTM, CEN and DIN standards specify the criteria for biodegradation, disintegration and eco-toxicity for a plastic to be called compostable.

- Biodegradability is determined by measuring the amount of $CO_2$ produced over a certain time period by the biodegrading plastic. The standards require 60% conversion of carbon into carbon dioxide within 180 days for resins made from single

polymer and 90% conversion of carbon into carbon dioxide for co-polymers or polymer mixes.

- Disintegration is measured by sieving the material to determine the biodegraded size and less than 10% should remain on a 2mm screen within 120 days.

Eco toxicity is measured by having concentrations of heavy metals below the limits set by the standards and by testing plant growth by mixing the compost with soil in different concentrations and comparing it with controlled compost.

a.

b.

| between 20 and 40 % Biobased | between 40 and 60% Biobased | between 60 and 80 % Biobased | more than 80 % Biobased |
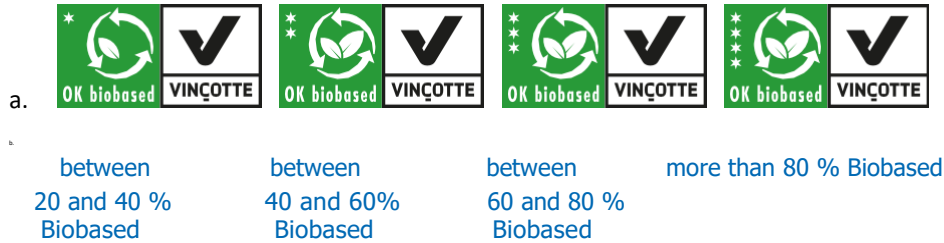
Figure 5. *OK-biobased Logo with indication of the carbon share*[ref1]

## 5. Comparative Advantage of Bioplastics

**Table 3. Comparison of Petroleum based plastics v/s. Bioplastics[ref23]**

| Characteristics | Petroleum based Plastics | BioPlastics |
| --- | --- | --- |
| Energy consumption in production | High | 48% lower than petroleum based plastic production |
| Raw Materials | Petroleum, a non-renewable resource | Biomass obtained from starch of corn, sugarcane, potato and other renewable crops |
| Carbon Footprint | High as petroleum is involved | 62% less emission of CO2 which is significantly less than traditional plastics |
| Presence of chemicals | Presence of Bisphenol A (BPA) which is a potential hormone disrupting chemical | No presence of any toxic chemical |
| Physical properties | Highly stable and thermo-plastic | Equally stable with high thermo-plasticity as traditional plastics |
| Biodegradability | Could take more than 500 years to decompose completely; needs to be recycled | Decomposes inside 180 days if decomposed in the right environment; releases methane on decomposition which can be harnessed to produce energy |
| Effect on holding contents | Fails to retain the flavor and scent of the food stored in them; potentially releases harmful substances in the food on long exposures | Retains the original flavor and scent of the food being carried in them |
| Price | Low | 3 times higher than traditional plastics |

## 6. Different classes of polymers which are biobased
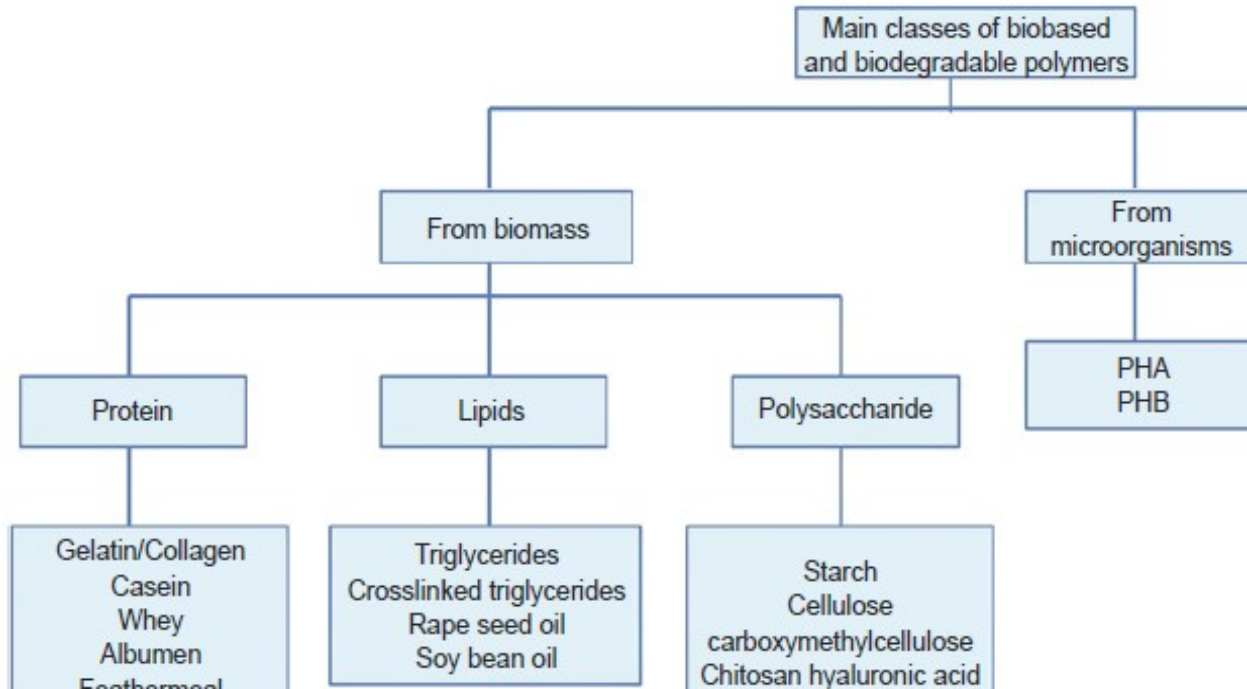


**Figure 6. Different classes of polymers which are biobased and biodegradable**

## 7. Commercially available Biodegradable Polymers

The range of biodegradable plastics available include

Starch based products including thermoplastic starch, starch and synthetic aliphatic polyester blends, and starch and PVOH blends.

- Naturally produced polyesters including PVB, PHB and PHBH.

- Renewable resource polyesters such as PLA.

- Synthetic aliphatic polyesters including PCL and PBS.

- Aliphatic-aromatic (AAC) copolyesters.

- Hydro-biodegradable polyester such as modified PET.

- Water soluble polymer such as polyvinyl alcohol and ethylene vinyl alcohol.

  - Photo-biodegradable plastics.
  - Controlled degradation additive masterbatches

## BIODEGRADABLE POLYESTERS

Polyesters play a predominant role as biodegradable plastics due to their potentially hydrolysable ester bonds. As shown in Figure 7 below, the polyester family is made of two major groups – aliphatic (linear) polyesters and aromatic (aromatic rings) polyesters. Biodegradable polyesters which have been developed commercially and are in commercial development are as follows:

PHA – polyhydroxyalkanoates PHB – polyhydroxybutyrate

PHH – polyhydroxyhexanoate PHV - polyhydroxyvalerate

PLA – polylactic acid PCL – polycaprolactone

PBS – polybutylene succinate PBSA - polybutylene succinate adipate

AAC – Aliphatic-Aromatic copolyesters PET – polyethylene terephthalate

PBAT – polybutylene adipate/terephthalate PTMAT- polymethylene adipate/terephthalate
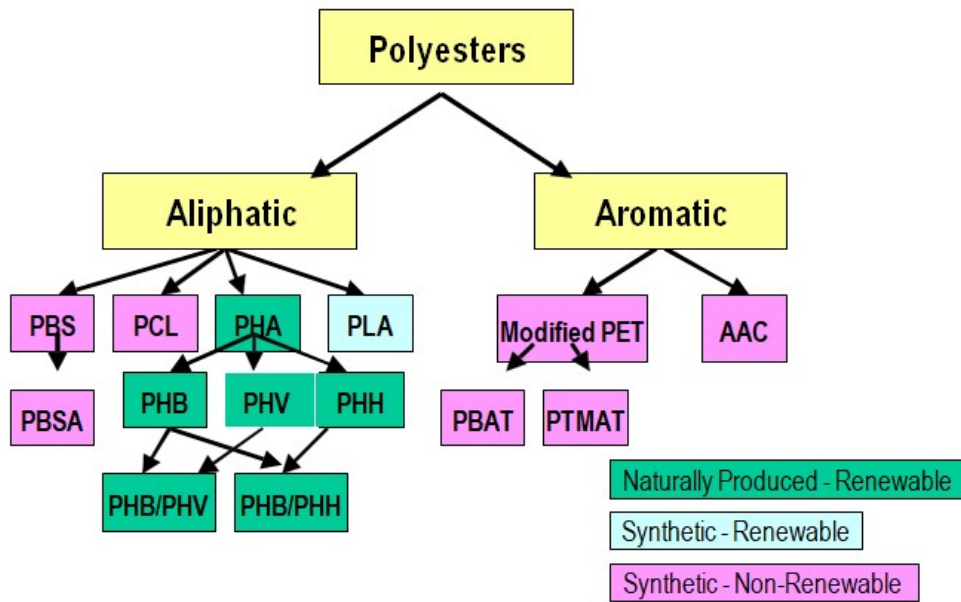
Figure 7. Biodegradable Polyester Family [Ref. Australian report on Biodegradable plastics]

## 8. Applications

**Table 4. Applications of commercially used biopolymers.**

| Chemical branch | Biopolymer | Application |
|---|---|---|
| Poly-(hydroxy acid) | Poly(lactic acid)<br><br>Poly(glycolic acid) | Food packaging, bags, cutlery products, sheets, floor mats, containers<br><br>Medical devices, surgical sutures, pharmaceutical supplies |
| Polyhydroxyalkonoate | Poly(3-hydroxybutyrate)<br><br>Poly($\beta$-malic acid) | Disposable films, gloves, medical applications<br>Biomedical devices, biomaterial applications |
| Poly-(alkylene dicarboxylate) | Poly(butylene succinate)<br><br>Poly(butylene adipate-*co*-terephthalate)<br>Poly(ethylene terephthalate) | Injection molding, disposable products like sheets, fibers, films<br>Packaging films, compost and plastic bags, agricultural films Bottles, sheet components, containers for food commodities, pharmaceutical products |
| Poly-(ether ester) | Polydioxanone | Medical sutures and implants for slow tissue-healing process |

## 9. Studies on Blends of Bio- Degradable/ Compostible polymers

**A.** PLA/SOY PROTEIN[ref 22] was blended using adipic anhydride as a plasticizer. For all samples studied a single Tg was observed in DSC, indicating acompatible blend. The major drawback of this plastic is the high water sensitivity, which has been reported to increase the weight of soy protein sheets by more than 180% water when submerged in water. Another common issue is that the protein films are often quite stiff and brittle because of extensive intermolecular interactions between molecular chains. Work done focused on resolving aforementioned issues by plasticizers, in order to induce flexibility and water resistance of soy protein based plastics.

**B.** A series of biodegradable plastics from soy protein isolate (SPI) and lignosulfonate (LS)[ref.6] with a weight ratio of 0:10 to 6:4 were prepared with 40 wt % glycerol as a plasticizer. The results indicated that the introduction of a moderate LS content from 30 to 40 parts in the blends could simultaneously enhance the tensile strength, elongation, and Young's modulus of soy protein plastics. Studies of the water sensitivity of the materials suggested that the strong interaction between LS and SPI could restrict the effect of water on the swelling and the damage of the materials, resulting in lower water absorption.

**C.** PHA/PA blends[ref 9] were melt blended using a twin screw extruder, in order to improve the toughness of PHA and investigate a variety of fundamental properties on the blends. For all of the samples studied by SEM, biphasic separation was observed, indicating that PHA was not miscible with PA in the melt. DMA results confirmed that the blend is an immiscible two-phase system. Rheological results revealed that the melt viscosity of the blends increased with the content of PHA. On the basis of DSC results, both of the melting and crystallization temperatures of the blends systematically decreased as the concentration of the PA increased. TGA curves depicted that the thermal stability of the blends increased significantly at high temperatures as PA loadings increased. In addition the tensile toughness of the PHA blend was greatly enhanced by the addition of PA.

**D.** The processability and the performance of a biodegradable polymer, Mater-Bi, and of its blends with either a sample of poly (hydroxy alkanoates) (PHA) or with bacterial biomass containing PHAs were compared. Adding PHA or directly the biomass containing it allows improving the processability of the matrix. Moreover, the mechanical behavior of the systems was compared considering two different preparation methods, namely compression and injection molding. The injection molded samples show poorer mechanical performances than those of the compression molded systems. The impact strength significantly improves when PHA is added while it reduces when bacterial biomass is used instead.[ref 14]

**E.** Thermoplastic Starch and blends of Thermoplastic starch studied. TPS bioplastics are completely biodegradable and compostable. The innovation of this bioplastic technology is an excellent example for a sustainable development, which means the responsible use of available natural resources and production processes that take environmental aspects and natural circulations into consideration.[ref 19]

## 10. Conclusion

Intensive studies done on PLA based bioplastics and blends and biodegradability is studied. However, more work needs to be done on completely compostible materials. Blends of PHA with various substrates like starch, soy protein,etc needs lot of work. Also needed is the development of fully compostible plastic materials so that the current problems can be solved.

**References:**

1. Fachagentur Nachwachsende Rohstoffe e. V. (FNR)  "BIOPLASTICS "  Published by Agency for Renewable Resources OT Gülzow, Hofplatz 1 18276 Gülzow-Prüzen
2. Compostible Plastics  [World  Centric]
3. Australian report on  Biodegradable Plastics –  Developments and Environmental Impacts OCTOBER, 2002 Prepared in association with ExcelPlas Australia
4. Shengzhe Yang, "Novel bio-based and biodegradable polymer blends", Iowa State University,2014
5. Ashish George  , M.R. Sanjay , Rapeeporn Srisuk  , Jyotishkumar Parameswaranpillai  , Suchart Siengchin ," A comprehensive review on chemical properties and applications of biopolymers and their composites , International Journal of Biological Macromolecules 154 (2020) 329–338
6. Jin Huang, Lina Zhang, Fangeng Chen," Effects of lignin as a filler on properties of soy protein plastics. I. Lignosulfonate", Journal of Applied Polymer Science, 17th April, 2003
7.  V. M. GHORPADE,.A. GENNADIOS,M. A. HANNA, and C. L. WELLER, "Soy Protein Isolate/Poly(ethylene oxide) films" , University of Nebraska – Lincoln, e Biological Systems Engineering
8.  Mekonnen, T., et al., Progress in bio-based plastics and plasticizing modifications. Journal of Materials Chemistry A, 2013. **1**(43): p. 13379-13398
9. Shengzhe Yang, James A. Schrader, Kenneth G. McCabe, David Grewell , Michael R. Kessler  Samy A. Madbouly[*]," PROCESSING AND CHARACTERIZATION OF BIO-BASED POLYHYDROXYALKANOTE [PHA] /POLYAMIDE [PA] BLENDS Chapter 2, Novel bio-based and biodegradable polymer blends, Iowa State University,Iowa, 2014
10. Imre, B. and B. Pukanszky, Compatibilization in bio-based and biodegradable polymer blends. European Polymer Journal, 2013. **49**(6): p. 1215-1233
11. Wang, D. and G. Sun, *Novel Polymer Blends from Polyester and Bio-Based Cellulose Ester.* Journal of Applied Polymer Science, 2011. **119**(4): p. 2302-2309.
12. Feng, F. and L. Ye, *Structure and Property of Polylactide/Polyamide Blends.* Journal of Macromolecular Science Part B-Physics, 2010. **49**(6): p. 1117-1127
13. Kucharczyk, P., et al., *Correlation of Morphology and Viscoelastic Properties of Partially Biodegradable Polymer Blends Based on Polyamide 6 and Polylactide Copolyester.* Polymer-Plastics Technology and Engineering, 2012. **51**(14): p. 1432-1442
14. . Scaffaro • N. Tz. Dintcheva • R. Marino • F. P. La Mantia," Processing and Properties of Biopolymer/Polyhydroxyalkanoates Blends" , J Polym Environ (2012) 20:267–272
15. E. Bugnicourt , P. Cinelli, A. Lazzeri, V. Alvarez," Polyhydroxyalkanoate (PHA): Review of synthesis, characteristics, processing and potential applications in  packaging" , eXPRESS Polymer Letters Vol.8, No.11 (2014) 791–808
16. Ramani Narayan  & Sunder Balakrishnan , "DRIVERS FOR  BIODEGRADABLE / COMPOSTABLE PLASTICS & ROLE OF COMPOSTING IN WASTE MANAGEMENT & SUSTAINABLE AGRICULTURE" , SYMPOSIUM PROCEEDINGS, February 15, 2007 The New College, Chennai 600 014, India
17. BEAUTY OF BIOPLASTICS

18. E. Castro-Aguirre , F. Iñiguez-Franco , H. Samsudin , X. Fang , R. Auras , "Poly(lactic acid)—Mass production, processing, industrial applications and end of life", Advanced Drug Delivery Reviews, journal homepage: www.elsevier.com/locate/addr

19. Jurgen Lorcks, "Properties and applications of compostable starch-based plastic material", Polymer Degradation and Stability, Elsevier, Volume 59, Issues 1-3, 3 Janurary 1998, Pages 245-249

20. Ewa Rudnik," Compostible Polymer Materials", Elsevier 2008

21. J. H. Song, R. J. Murphy, R. Narayan, and G. B. H. Davies," Biodegradable and compostable alternatives to conventional plastics," The Royal Society Publishing, 2009,jul 27

22. Shengzhe Yang, James A. Schrader, Kenneth G. McCabe, David Grewell, Michael R. Kessler, Samy A. Madbouly , "CHARACTERIZATION AND BIODEGRADATION BEHAVIOR OF BIO-BASED POLY(LACTIC ACID) [PLA] AND SOY PROTEIN BLENDS, Novel bio-based and biodegradable polymer blends, Iowa State University,Iowa, 2014

# Carbohydrates (Starch & Maltose) from Biological Waste Materials

*Saikrushna Jena and Ram Singh\**

Department of Applied Chemistry, Delhi Technological University, Delhi-110 042, India
ramsingh@dtu.ac.in

## Abstract

A sustained and healthy society needs proper utilization of the waste material to deal with the increasing pollution rate. Several works are successfully done on this note, and till now, several strategies have been developed for the production of bio-chemicals from biological waste. In other words, value has been added to the waste materials. The biochemicals like starch, maltose, amylose, etc. have been isolated from the biological waste. Starch is an anion-reducing homo-polysaccharide consisting of 10 D-glucose units; it can be amylase and amylopectin whereas maltose (4-$\alpha$-D-glucopyranosido-D-glucopyranose) a reducing sweet white crystal which is a disaccharide; consisting of 2 D-glucose unit linked by glycosidic bonds. Starch upon hydrolysis by enzymes like amylase forms maltose.

In our day-to-day life, most of the food sources comprised of starch, and maltose like bread, grains, cereals, pasta, rice, sweet potatoes, corn, fruits, vegetables are wasted due to partial consumption. The leftover and expired food when discarded, create public health threat due to the fungal growth. According to FAO (Food and Agriculture Organization) of UN, around 1.3 billion food wastes are generated annually. So, proper utilization of these food wastes for the isolation of carbohydrates like starch and maltose, which can be further used as the precursor for many biological products, will create a great area of research with proper cost-effectiveness.

Here in this paper, the extraction of carbohydrates, mainly starch and maltose, from the waste biological materials such as food waste will be discussed.

**Keywords**: Starch, maltose, waste, isolation, food waste, carbohydrate

13

## 1.    Introduction

Wastes are anything that is not of humans use. Waste management (WM) is a serious problem for both urban and local bodies. Effective WM is the requirement of sustainable life. There are various effective methods that can be applied for better WM (Figure 1) (Kumar et al. 2017). There are a lot of barriers to effective WM, which posed both challenges and opportunities for the researchers to work scientifically in this area. The waste has been classified and analyzed on the basis of different aspects; the important one is the basis of the source (Ghoushchi et al. 2020).

Biological waste is usually grouped as wastes that is generated from natural sources. One of the most talked, and researched natural waste is agricultural wastes. The important types of agricultural wastes include field-based waste, associated animal waste, and agro-industrial wastes (Obi et al. 2016). Agricultural products like crops, fruits, vegetables many times become agricultural waste either as raw material or during the processing of raw materials. Food waste is an example of agro-industrial waste. They are produced through agricultural operations or household consumption.
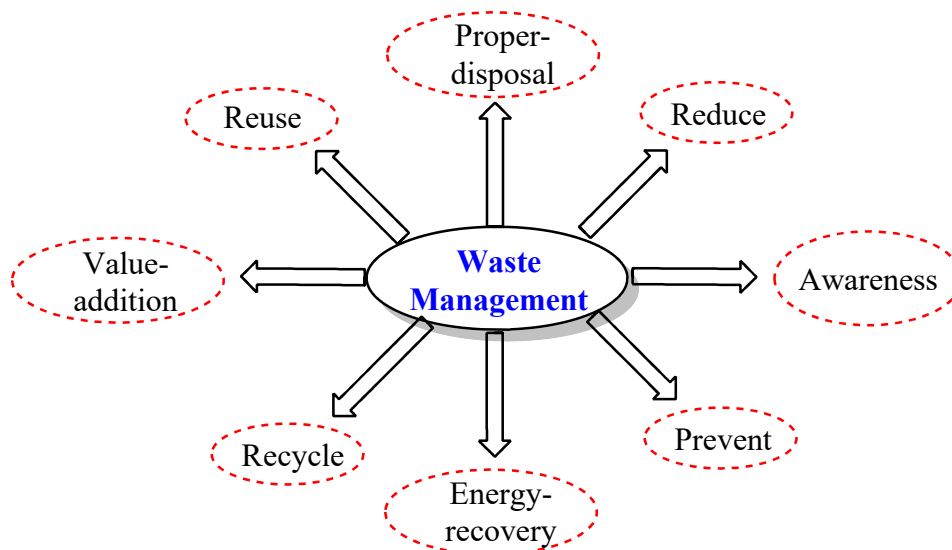
**Figure 1**. Methods of waste management

### *General information about food waste*

Sustainability is much needed for surviving. Sustainability means configuring and planning the present-day human activity so that the future generation will not face any difficulty.

13

Due to the increase in the global population; there is a proportional increase in food requirements (Dugmore et al. 2017). The increase in consumption of material is proportional to the increase in wastage. It was estimated in 2011 by the Food and Agriculture Organization of United Nation (FAO) that the food waste per year is about $1/3^{rd}$ of the world's food (www.fao.org ).

It was reported that the discarded food waste is more than enough to feed 815 million hunger people globally. In general, food wastage can be any type of food loss or food waste. Although both the terms are used, they seem to be identical but quite different, employing definition and meaning. According to FAO "Food loss is the decrease in the quantity or quality of food resulting from decisions and actions by food suppliers in the chain, excluding retailers, food service providers and consumers."

In simple word, food loss is defined as any food that is disposed or discarded unenviably along the supply chain of food at the time of harvesting or storage or transportation. This does not include the retail level, and any other productive utilization. "Food waste refers to the decrease in the quantity or quality of food resulting from decisions and actions by retailers, food service providers and consumers." However, it can be wasted through many ways:

- Fresh product that are discarded during sorting operations in terms of color, shape or size or any type of consideration that is not fulfilled by the product.
- Expired or close to expiry date food products are mostly discarded by retailers and consumers.
- Large quantities of unused or left-over edible foods are discarded from household kitchens or from eating establishments.

As production of food is resourceful so when food is discarded, it is not just the food that has been discarded, but all the water, land, hard work of the farmer or laborers, fuels, transport costs, everything is discarded. Moreover, food wastage also causes lots of environmental impacts like soil erosion, deforestation, water and air pollution. Also, after disposal or at the time of production, also it causes the emission of greenhouse gases. It is calculated that the amount of food that is discarded is produced in approximately 28% of the world's agricultural area i.e., 1.4 billion hectors of agro-based land (annually) (Kumar et al. 2017).

In recent decades, food waste has become an emerging area of interest from urban, rural, national and international level organizations and policymakers. Many research centers, academics, NGOs show their concern about utilizing food waste as valuable resources of many

bio-active molecules and for minimizing its harmful environmental effects like soil erosion, deforestations, water, and air pollution & most importantly the greenhouse gas emission (Mourad, 2016). Food waste has become global problem now-days. Many factors like slow progress in the development of effective waste management, public carelessness, easy excess to food, much wealthier to afford sufficient food and unnecessarily throwing them into garbage, while still being consumable (Melikoglu et al. 2013).

However, food waste is generated all along the food supply chain, but at the household level highest amount of food waste is generated (BIOIS, 2010). Million tons of food waste is generated globally, and it is very hard to quantify each of them and control them in a recycling manner in a due short time. However, we can manage to utilize them as resources of some of the important bio-active molecules like complex carbohydrates, proteins, lipids, and nutraceuticals (Salimi et al. 2020). Some studies reported that the extraction of bulk chemicals from food waste is more profitable than converting into biofuels (Tuck et al. 2012). Based on the above facts, in this paper, the extraction of bio-active molecule, carbohydrates mainly starch and maltose, from food waste, a biological waste material, have been compiled. This study will help in food waste management and isolation of useful chemicals from them.

## 2.    Sources of food loss

From farm to home, in every sector i.e., during harvesting, processing, transportation and distribution, in restaurants and even at home food is wasted along the food chain.

### 2.1    Food loss on farms

Farms are the first place of food chain. However, many times farmers harvest more crops on seeing the demand of consumer but due to so many reasons like lack of storage facility, lack of transportation facilities or sometime due to sudden down of market demand of that product leads to wastage. Another unavoidable source of food waste from farm is the unwanted parts of the crops like in case of wheat only the seed is consumed but other parts like head, stem, leaves and roots are generated as waste material. It was found that 20 billion pounds of product is lost on farms every year (Melikoglu et al. 2013). In recent cases due to the COVID-19 pandemic lockdown has occurred which causes a huge loss to the farmers along with creating lots of food waste.

## 2.2    Food loss during Manufacturing

Food waste at manufacturing sector mostly causes at the time of trimming off the edible portions like peels, skins, fats or crusts from food. Although some are used to feed the animals and some are reused but most of the parts are just thrown away which ultimately causes serious environmental issues. For example, in the juice factory the peel of orange and mango are discarded. Sometimes overproduction, product damage and some kind of technical issues, production trials, packaging defects, trial runs, and wrong sizes and weights lead to food waste in a large quantity (Melikoglu et al. 2013; Kringel et al. 2019).

## 2.3    Food loss in Transportation & distribution

Food waste during transportation is most vulnerable mostly in Developing countries as there are lack of good transportation means, adequate and reliable storage system and good infrastructure. However sometimes due to carelessness of the driver accidents are occurred and cause both food loss along with life loss.

## 2.4    Food waste in retail business

Retail stores or supermarkets are another source of food waste. The main drivers for food loss in supermarkets are overstocked products, color, shape and size issue, damaged product, expired products etc.

## 2.5    Food waste in restaurants and Home kitchens

Restaurants and home kitchens are the main source of food wastage. Households are responsible for the largest portion of all food waste.

## 3.    Value-addition to food waste

Food waste is present everywhere and many valuable molecules have been isolated from this (Schanes et al. 2018; Paritosh et al. 2017; Ravindran and Jaiswal 2016; Galanakis et al. 2012). Traditionally, they have been disposed only through landfills but with the development of analytical techniques and isolation methods, values have been added to them. This is an important part of food waste management. The biochemicals like starch, maltose, amylose etc.

13

have been isolated from the biological waste. Starch is anion-reducing homo-polysaccharide consisting of 10 D-glucose units; can be amylase and amylopectin whereas, maltose (4-$\alpha$-D-glucopyranosido-D-glucopyranose) a reducing sweet white crystal which is a disaccharide; consisting of 2 D-glucose unit linked by glycosidic bonds. Starch upon hydrolysis by enzyme like amylase forms maltose.

Torres et al. (2020) used low sized or irregular shaped discarded potatoes from three varieties like agria, kennebec, and neiker, as raw material for extraction of starch through subcritical method. The % of starch yields are 24.4 for agria, 22.1 for kennebec and 18.5 for neiker (Torres et al. 2020). Li et al. (2017) extracted starch from core and pericap of fallen ripen kiwifruit with yield % 34.6 to 40.7 and 38.6 to 51.8 respectively. Shehzad et al. (2018) extracted maltose by utilizing food waste like damaged wheat grain with 21.7 % yield. Nakthong et al. (2017) used waste pineapple stem as a significant resource for the extraction of good amount of starch by mechanical extraction method. The % yield of starch and amylose are 30.0 and 34.4 respectively.

Guo et al. (2015) isolated starch from the kernels of jack fruit, longan, loquat, and litchi and mango fruits. The % of yield of starch from litchi is 53 and from longan and loquat yield % are 59.0 & 71.0 respectively. Jaiswal et al. (2016) isolated starch from shahi litchi seeds using both acidic and alkaline extraction method got 11% and 12.6% yield respectively. Lists of different food waste and carbohydrates isolated from them are listed in table 1.

**Table 1.** Carbohydrates isolated from food waste

| S. No. | Source | Waste residue | Carbohydrates (%) | Reference |
|---|---|---|---|---|
| 1 | Potato | Low-sized or irregular shape discarded potatoes from Agria | Amylose (29.3) | Torres et al. 2020 |
| 2 | Potato | Low-sized or irregular shape discarded | Amylose (27.3) | Torres et al. 2020 |

13

| | | potatoes from Kennebec | | |
|---|---|---|---|---|
| 3 | Potato | Low-sized or irregular shape discarded potatoes from Neiker | Amylose (23.0) | Torres et al. 2020 |
| 4 | Fallen kiwifruit during ripening | Core tissue | Starch (38.6-51.8) | Li et al. 2017 |
| 5 | Fallen kiwifruit during ripening | Pericarp | Starch (34.6-40.7) | Li et al. 2017 |
| 6 | Fallen kiwifruit during ripening | Core tissue | Amylose (15.5-17.8) | Li et al. 2017 |
| 7 | Fallen kiwifruit during ripening | Pericarp | Amylose (20.7- 23.3) | Li et al. 2017 |
| 8 | Mango | Kernel flour | Starch (44.9) | Nakthong et al. 2017 |
| 9 | Mango | Kernel flour | Amylose (9.1-16.3) | Nakthong et al. 2017 |
| 10 | Pineapple | Stem | Starch (30.0) | Ferraz et al. 2019 |
| 11 | Pineapple | Stem | Amylose (34.4) | Ferraz et al. 2019 |
| 12 | Mango | Kernel flour | Starch (44.9) | Kaur et al. 2004 |
| 13 | Mango | Kernel flour | Amylose (9.1-16.3) | Kaur et al. 2004 |
| 14 | Mango | Kernel | Starch (75.6-80) | Sandhu et al. 2008 |
| 15 | Litchi | Seeds | Starch (53) | Jaiswal et |

13

| | | | | al. 2015 |
|---|---|---|---|---|
| 16 | Litchi | Seeds (acidic method) Seeds (alkaline method | Starch (11) Amylose (9.60) Starch (12.6) Amylose (7.60) | Guo et al. 2018 |
| 17 | Litchi | Seeds | Amylose (19.2) | Thory and Sandhu 2017 |
| 18 | Jackfruit | Seeds | Starch (60-80) Amylose (22.10-38.34) | Zhang et al. 2019 |
| 19 | Tamarind | Seeds | Amylose (14.2) | Kaur et al. 2016 |
| 20 | Longan | Kernel | Starch (59.0) | Guo et al. 2018 |
| 21 | Loquat | Kernel | Starch (71.0) | Guo et al. 2018 |
| 22 | Annatto | Seeds | Starch (66) Amylose (24) | Kringel et al. 2019 |
| 23 | Avocado | Seeds | Starch (27.5-29.8) Starch (wet milled) (19.7) | Lacerda et al. 2014 |
| 24 | Apple | Immature apples | Starch (44-53) Amylose (26-29.3) | Stevenson et al 2006 |
| 25 | Banana (unripe) | Pulp | Starch (70-80) | Reyes-Atrizco et al. 2019 |
| 26 | Banana (unripe) | Peel | Starch (29) | Franklin et al. 2017 |
| 27 | Banana | Flesh | Starch (69.5) | Li et al. |

13

| | | | Amylose (21.3) | 2018 |
|---|---|---|---|---|
| 28 | Banana (unripe) | Peel | Starch (22.6) Amylose (25.7) | Ralet et al. 2005 |
| 29 | Apple | Dry apple | Pectin (10-15) | Bhushan et al. 2008 |
| 30 | Citrus fruits | | Pectin (20-30) | Bhushan et al. 2008 |
| 31 | Apple | Pomace | Carbohydrates (48-62) | Mahmood et al. 1998 |
| 32 | Orange | Peel, pulp, seeds | Carbohydrates (47) | Kossori et al. 1998 |
| 33 | Pear | Pulp | Carbohydrates (62.8) | Wang et al. 2014 |
| 34 | Cabbage | Frozen edamame | Maltose (9-12) | Shehzad et al. 2018 |
| 35 | Wheat | White wheat flour | Maltose (2.2- 9) | Shehzad et al. 2018 |
| 36 | Barley | Spaghetti | Maltose (19.6) | Shehzad et al. 2018 |
| 37 | Wheat | Damaged wheat grains | Maltose (21.7) | Shehzad et al. 2018 |

## 4.    Conclusions

To develop the eco-sustainability, value addition to waste materials is important and widely used in recent times. However, there is still lot of research is required to isolate biochemicals from waste. The use of food waste for the isolation of biochemicals has been exploited by many researchers, which reduces the burden on landfill. The commercial exploitation is not very prevalent due to the cost of production. Keeping this in mind, this field is wide open to work.

## 5. References

Bhushan, S., Kalia, K., Sharma, M., Singh, B., Ahuja, P.S., 2008. Processing of apple pomace for bioactive molecules. Crit. Rev. Biotech. 28, 285–296.

BIOIS, 2010. Preparatory Study on Food Waste across EU 27. European Commission (DG ENV) Directorate C-Industry. 2010. Final Report. ISBN: 978-92-79-22138-5.

Dugmore, T.I.J., Clark J.H., Bustamante J., Houghton J.A., Matharu A.S., 2017. Valorisation of Biowastes for the Production of Green Materials Using Chemical Methods. In: Lin C. (eds) Chemistry and Chemical Technologies in Waste Valorization. Topics in Current Chemistry Collections. Springer, Cham.

El Kossori, R.L., Villaume, C., El Boustani, E., Sauvaire, Y., Mejean, L., 1998. Composition of pulp, skin and seeds of prickly pears fruit (*Opuntia ficus indica* sp.) Plant Food Human Nutr. 52, 263–270.

Ferraz, C.A., Fontes, R.L.S., Fontes-SantAna, G.C., Calado, V., Lopez, E.O., Rocha-Leao, M.H.M., 2019. Extraction, modification, and chemical, thermal and morphological characterization of starch from the agro-industrial residue of mango (*Mangifera indica L*) var. Ubá. Starch. 71, 1800023.

Galanakis, C.M., 2012. Recovery of high added-value components from food wastes: Conventional, emerging technologies and commercialized applications. Trends Food Sci. Tech. 26, 68–87.

Ghoushchi, S.J., Dorosti, S., Moghaddam, S.H., 2020. Qualitative and quantitative analysis of waste management literature from 2000 to 2015. Int. J. Environ Waste Manag. 26, 471-486.

Guo, K., Lin, L., Fan, X., Zhang, L., 2018. Comparison of structural and functional properties of starches from five fruit kernels. Food Chem. 257, 75–82.

Hernández-Carmona, F., Morales-Matos, Y., Lambis-Miranda, H., Pasqualino, J., 2017. Starch extraction potential from plantain peel wastes. J. Environ. Chem. Eng. 5, 4980-4985.

13

http://www.fao.org/save-food/resources/keyfindings/en/ (retrieved on 20th Jan 2021)

Jaiswal, P., Kumar, K.J., 2015, Physicochemical properties and release characteristics of starches from seeds of Indian Shahi Litchi. Int. J. Biol. Macromol. 79, 256–261.

Kaur, M., Singh, N., Sandhu, K.S., Guraya, H.S., 2004. Physicochemical, morphological, thermal and rheological properties of starches separated from kernels of some Indian mango cultivars (*Mangifera indica* L.). Food Chem. 85, 131–140.

Kaur, M., Singh, S., 2016. Physicochemical, morphological, pasting, and rheological properties of tamarind (Tamarindus indica L.) Kernel Starch. Int. J. Food Prop. 19, 2432-2442.

Kringel, D.H., Dias, A.R.G., Zavareze, E.R., Gandra, E.A., 2019. Fruit wastes as promising sources of starch: Extraction, properties, and applications. Wiley Online Library.

Kumar, K., Yadav, A.N., Kumar, V., Vyas, P., Dhaliwal, H.S.,2017. Food waste: a potential bioresource for extraction of nutraceuticals and bioactive compounds. Biores. Bioproc. 4, 18.

Kumar, S., Smith, S.R., Fowler, G., Velis, C., Kumar, S.J., Arya, S.R., Kumar, R., Cheeseman, C. 2017. Challenges and opportunities associated with waste management in India. R. Soc. Open Sci. 4:160764.

Lacerda, L.G., Colman, T.A.D., Bauab, T., da Silva, M.A., Filho, C., Demiate, I.M., de Vasconcelos, E.C., Schnitzler, E., 2014. Thermal, structural and rheological properties of starch from avocado seeds (*Persea americana*, Miller) modified with standard sodium hypochlorite solutions. J. Ther. Anal. Calori. 115, 1893–1899.

Li, D., Zhu, F., 2017. Physicochemical properties of kiwifruit starch. Food Chem. 220, 129-136.

Li, Z., Guo, K., Lin, L., He, W., Zhang, L., Wei, C., 2018. Comparison of physicochemical properties of starches from flesh and peel of green banana fruit. Molecules. 23, 2312.

Mahmood, A.U., Greenman, J., Scragg, A.H., 1998. Orange and potato peel extracts: Analysis and use as *Bacillus* substrates for the production of extracellular enzymes in continuous culture. Enz. Microb. Tech. 22, 130–137.

Melikoglu, M., Lin, C. S. K., Webb, C., 2013. Analysing global food waste problem: pinpointing the facts and estimating the energy content. Central Eur. J. Eng. 3, 157–164.

Mourad, M., 2016. Recycling, recovering and preventing "food waste": competing solutions for food systems sustainability in the United States and France. J. Clean. Prod. 126, 461- 477.

13

Nakthong, N., Wongsagonsup, R., Amornsakchai, T., 2017. Characteristics and potential utilizations of starch from pineapple stem waste. Ind. Crops Prod., 105, 74–82.

Obi, F.O., Ugwuishiwu, B.O., Nwakaire, J.N., 2016. Agricultural waste concept, generation, utilization and management. Nigerian J. Tech. (NIJOTECH). 35, 957– 964.

Paritosh, K., Kushwaha, S.K., Yadav, M., Pareek, N., Chawade, A., Vivekanand, V., 2017. Food waste to energy: An overview of sustainable approaches for food waste management and nutrient recycling. BioMed Res. Int. Article ID 2370927, 19 pages.

Ralet, M.C., Bonnin, E., Thibault, J.F., 2005. Polysaccharides and polyamides in the food industry: Properties, production, and patents, ed. A. Steinbuchel and S. Ki Rhee, Wiley- VCH, Weinheim, vol. 1, ch. 10, pp. 351–386.

Ravindran, R., Jaiswal, A.K., 2016. Exploitation of food industry waste for high-value products. Trends Biotech. 34, 58–69.

Reyes-Atrizco, J.N., Agama-Acevedo, E., Bello-Perez, L.A., Alvarez-Ramirez, J., 2019. Morphological, molecular evolution an in vitro digestibility of filamentous granules of banana starch during fruit development. Int. J. Biol. Macromol. 132, 119-125.

Salimi, M., Taheri, M.E., Passadis, K., Novacovic. J., Barampouti, E.M., Mai, S., Moustakas, K., Malamis, D., Loizidou, M., 2020. Valorization of restaurant food waste under the concept of a bio-refinery. Biomass Conv.  Bioref. In press.

Sandhu, K.S., Lim, S-T., 2008. Structural characteristics and in vitro digestibility of Mango kernel starches (*Mangifera indica* L.). Food Chem. 107, 92–97.

Schanes, K., Dobernig, K., Gozet, B., 2018. Food waste matters - A systematic review of household food waste practices and their policy implications. J. Clean. Prod. 182, 978-991.

Shehzad, A., Ahmad, N., Hussain, Z., Haider, M.S., Rashid, N., 2018. Valorization of waste foods using pullulan hydrolase from *Thermococcus kodakarensis*. Amylase, 2, 39–43.

Stevenson, D.G., Domoto, P.A., Jane, J-L., 2006. Structures and functional properties of apple (*Malus domestica*Borkh) fruit starch. Carbohydr. Polym. 63, 432–441.

Thory, R., Sandhu, K.S., 2017. A Comparison of mango kernel starch with a novel starch from litchi (Litchi chinensis) kernel: Physicochemical, morphological, pasting, and rheological properties. Int. J. Food Prop. 20, 911-921.

13

Torres, M.D., Fradinho, P., Rodriguez, P., Falque, E., Santos, V., Dominguez, H., 2020. Biorefinery concept for discarded potatoes: Recovery of starch and bioactive compounds. J. Food Eng. 275, 109886.

Tuck, C.O., Pérez, E., Horváth, I.T., Sheldon, R.A., Poliakoff, M., 2012. Valorization of biomass: deriving more value from waste. Science. 337, 695–699.

Wang, X., Chen, Q., Lu, X., 2014. Pectin extracted from apple pomace and citrus peel by subcritical water. Food Hydrocolloids. 38, 129–137.

Zhang, Y., Li, B., Zhang, Y., Xu, F., Zhu, K., Li, S., Tan, L., Wu, G., Dong, W., 2019. Effect of degree of polymerization of amylopectin on the gelatinization properties of jackfruit seed starch. Food Chem. 289, 152–159.

# Microwave-Assisted Green Synthesis of Isoalloxazines

*Yogesh B. Khairnar, Ram Singh\**

*Department of Applied Chemistry, Delhi Technological University, Delhi-110 042, India ramsingh@dtu.ac.in*

**Abstract**

Isoalloxazine is a heterocyclic compound with the molecular formula $C_{10}H_6N_4O_2$, yellow in color solid, which is a structural component of flavins framework. Isoalloxazine derivatives are reported for various biological importance and their applications have reported in various fields in recent years. Isoalloxazine heterocycle consists of three closed rings system, pyrazine ring and pyrimidine ring fused to form pteridine. Considering its biological importance & physicochemical parameters, and similarity of structural features of tacrine and donepezil which are available drug treatments for Alzheimer's disease, the isoalloxazine ring would be considered to develop as an anti-Alzheimer's agents. The researchers have explored Isoalloxazine synthesis by using traditional methods, solvents & harsh conditions. The present article highlights & enriches the applications of microwave-assisted green chemistry synthesis of Isoalloxazine & enhance the existing literature about the subject.

**Keywords**: Isoalloxazine, Green synthesis, Microwave, Montmorillonite clays, Acidic alumina.

## 1. Introduction

Microwave heating plays an important role in organic chemical transformation by providing a highly effective heating source to accelerate the rate of the reaction with improved quality and quantity of the product because it's uniform and selective heating, simple, eco-friendly, cost effective, successful approach. With help of dry media, solid support, solid phase catalyst, acidic alumina, clay, nanocatalyst, etc; solvent-free reaction protocol with microwave-assisted reaction is a convenient way toward the goal of green chemistry, these reactions are highly compatibles, convenient with green solvents like water, ionic liquids & alcohols which help us to reduce the environmental load. Since the first report published on microwave heating on organic chemical transformation reported by Giguere, R. J; et al & Gedye R, et al.[1,2]; recently the use of microwaves-assisted chemical transformation has been reviewed and published [3] in this exciting field. Microwave radiation discovered as a method of heating in firstly in 1946 and the later, first commercial domestic microwave oven was introduced in 1947, In 1978 the first microwave laboratory instrument was developed by CEM corporation for analysis & in 1986's articles were published relating to microwave radiation in chemical synthesis using a microwave oven, then later the CEM corporation has developed the signal mode cavity system used for chemical synthesis in the 1990s and recently in 2000 the first commercial microwave synthesizer was introduced to conduct chemical synthesis [4].

In the conventional organic transformation method usually take place with the hot plate, use of oil bath and reaction vessel, the walls of the oil bath get heated first then the solvent, which require a longer heating time to heat the subsequent apparatus then reaction medium & the vessel, there is always a difference in the temperature/heat, at source to reaction vessel. Tedious apparatus setup which results in higher production cost, use of excessive solvents or reagent in conventional methods leads to the environmental load and in the other hand use of green chemistry approach, process with the support of microwave, the instrument plays an important role to eliminate the use of and generation of hazardous chemicals, waste & solvents which may have an adverse effect on

environmental and human health. The benefits of Microwave assisted reaction are summarized in the following table-1; over the conventional approach [5 to 18].

Table- 1. Advantages of microwave-assisted chemical transformation vs conventional approach.

| Sr.No | Advantages of microwave-asssited chemical transformation over conventional chemical transformation | |
| --- | --- | --- |
| | **Microwave appraoch** | **Conventional appraoch** |
| 1 | **Faster reaction**<br>a) Reactions are completed in few minutes instead of hours | Longer reaction time |
| 2 | **Improved yield and higher purity**<br>a) Less formation of side products thus the product recovery is good<br>b) Purification step is faster and easier | Formation of side products |
| 3 | **Energy-saving:**<br>**a)** Microwaves heat up just the sample and not the apparatus thus energy consumption is less | Energy consumption is more |
| 4 | **Uniform and selective heating:**<br>**a)** In microwave heating only the solvent and the solute particles are excited which results in uniform heating of the solvent. | Uneven distribution of heat |
| 5 | **Reproducibility:**<br>a) Uniform heating and better control of process parameters<br>b) Easy monitoring of chemical reaction temperature | Not easily reproducible |
| 6 | **Eco-friendly**<br>a) Reactions are cleaner and more environmental friendly in microwave<br>b) Heat the compound directly therefore usage of solvents in the chemical reaction can be reduced or eliminated | Non-eco friendly |

Similarly; the use of microwave radiation is useful in analytical-chemistry in the following application;

**Ashing: -** Ashing is the process to calculate the ash content of the sample. The microwave heating is used to heat the sample at high temperature to calculate the ash contain, then microwave-assisted muffle furnaces are more efficient, safe, and successful method as compared to conventional muffle furnaces, with this high temperature achieve easily and a large number of samples can be performed simultaneously [19].

**Digestion:** - Digestion is the chemical process in which a test sample is broken down into its basic chemical constituent for analysis. The microwave digestion system is used with the microwave radiation to break down the sample decomposition and preparation, with the use of the pressurized vessel, a higher temperature is easily achieved in a short period of time which increases the speed of digestion [20].

**Moisture analysis: -** The use of microwave-assisted moisture analysis has been extended in various filed like chemical, food, beverage and pharmaceutical industries and found is highly effective with reduction of testing time, its can be useful in all stage of research like raw material testing, intermediate and final products [20].

These emerging applications and usefulness of microwave radiation in chemistry; trigger us to highlight & enrich the subject knowledge about the topic.

## 2. Importance of Isoalloxazine:

Isoalloxazine is a yellow, tricyclic nitrogen-heterocyclic compound that is the structural component of flavins and other derivatives. Flavins are biologically important due to their involvement in biosynthesis and a biological pathway [21, 22] also plays an important role in the versatile redox reaction and active in antimalarial activity [23, 24]. Considering its biological importance & physicochemical parameters, and similarity of structural features of tacrine and donepezil which are available drug treatments for Alzheimer's disease, the isoalloxazine ring would be considered to be developed as an anti-Alzheimer's agents. The research group Kanhed et al., in 2015 has reported synthesis & its inhibitory activity against AChE and BChE inhibitors with standard drug tacrine and donepezil [25]. However the structure–activity *relationships* between Isoalloxazine and AChE inhibitors not fully reveal [26]. It creates an interest in the researchers to synthesize Isoalloxazine derivatives rapidly, with a high yield and eco-friendly manner to fill the research gap.

## 3. Conventional methods for synthesis of Isoalloxazine:

In the literature, the isoalloxazines synthesis has been described and formed by the condensation of *ortho*-substituted anilines with pyrimidines. The various synthetic methodologies employed for the synthesis of isoalloxazines was discussed in the following section.

**a) Using Barbituric Acid: -** The synthesis was reported by Max Tishler et al. in 1947, the condensation reaction was carried out in between in 2-amino azo compound with barbituric acid under acidic condition in presence of an organic solvent. The weak organic acid like acetic acid was used for this condensation. The presence of mineral acid or strong acid slow-down the reaction progess also it rapidly destroys the azo compound [27].

**b) Using Violuric Acid:-** The condensation reaction was carried in between violuric acid with aniline in an acidic condition in presence of organic solvent gave substituted isoalloxazines was reported by P. Hemmerich et al. [28].

**c) Using Quinoxaline: -** The condensation reaction was carried out in between quinoxaline with guanidine under control condition (under a nitrogen atmosphere and dark place) in presence of alcoholic solvent [29, 30].

**d) Using Uracils:-** The synthesis was achieved by carrying reaction in between substituted uracil with aniline gave us the aniline-uracil intermediate which further subjected to nitrosation in acetic acid with an excess sodium nitrite gave substituted isoalloxazine N-oxide, which was further reduced with sodium dithionite in water gave us isoalloxazines [31,32].

**e) Using Alloxan Monohydrate: -** Using alloxan Monohydrate was the most widely useful method for the synthesis of substituted isoalloxazines. The reaction was carried out in between N-substituted ortho-phenylenediamine and alloxan monohydrate under acidic conditions gave isoalloxazines [33, 34, & 35]. The cyclo condensation of a diamine with alloxan (alloxan, alloxan monohydrate, alloxan tetrahydrate are considered to be equivalent) was carried out in aqueous medium or in an alcoholic solvent with the presence of weak and mineral acid, even 30% sulfuric acid solution reaction was successful.

Furthermore modification of reaction condition was done by the reaction between diamine with alloxan monohydrate with boric acid, dilute acetic acid, & hydrochloric acid has been very successful & condensation carried out by mixing the components, shaking them, or refluxing for few hours and leaving them at room temperature for 1 or 2 days.

These conventional methods having some of the drawbacks; 1) Longer reaction time 2) less yield 3) Use of hazardous chemical and reagent 4) Limitation of handling the reagent 5) Tedious reaction setup & 6) High production cost, etc.

## 4. Microwave assisted synthesis of Isoalloxazine:

To overcome above challenges of conventional methods the research group of S. M. S. Chauhan et.al has reported the microwave-assisted synthesis of isoalloxazine [36], has a unique reaction environments leading to improved product yield, reduction in reaction time, clean reaction profile. The cyclo condensation was carried out in between 2-substituted aminoanilines (1) with alloxan or substituted-alloxan monohydrate (2) in the presence of solid acids [37, 38] under microwave irradiation gave the desired product in good yield [39] in scheme-1.



Scheme-1. synthesis of isoalloxazine under microwave irradiation
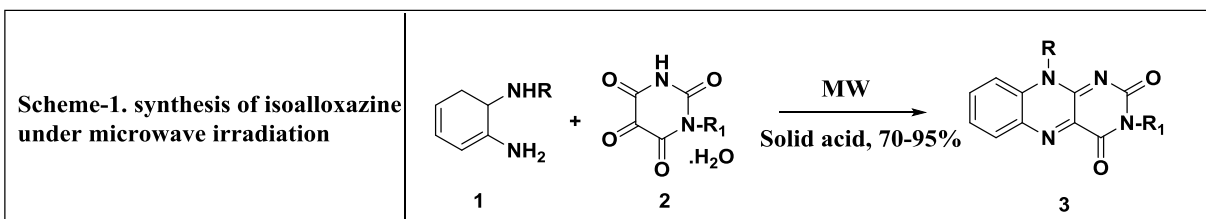
They carried-out and performed the sequential experimental studies of isoalloxazine synthesis, was summarized in table-2

Table- 2. Synthesis of isoalloxazine under different reaction conditions.

| Sr. No | Cyclocondensation of (1)+(2) | Reagent | Reaction approach | Yield |
|--------|------------------------------|---------|-------------------|-------|
| 1 | Method-1 | Boric acid+acetic acid | Conventional method | 39-55 % |
| 2 | Method-2 | Boric acid+acetic acid | Under microwave irradiation | 74-84 % |
| 3 | Method-3 | Acidic alumina | Under microwave irradiation | 88–97% |
| 4 | Method-4 | Montmorillonite KSF | Under microwave irradiation | 79-87 % |
| 5 | Method-5 | Montmorillonite $K_{10}$ | Under microwave irradiation | 81-90 % |

The cyclo condensation was carried in between 2-substituted aminoanilines (1) with alloxan (2) in boric acid and acetic acid under the conventional method gave isoalloxazines in 39–55% yields (method-1). Whereas a similar reaction was performed under microwave irradiation in a minimum amount of acetic acid gave us products in 74–84% yields (method-2). Further, the mixture of 1 and 2 were irradiated under microwave irradiation in the presence of acidic alumina afforded the product in 88–97% yield (method-3). Moreover, the reaction of 1 and 2 was carried under microwave irradiation in the presence of montmorillonite KSF and $K_{10}$ gave us products 80-90% & 83-90% yields (method-4 and method-5) respectively.

The improvements in the yield of the solid-phase reactions in comparison with the other methods 1 & 2 were observed; overall acidic alumina gave better yield (method-3) in comparison to other methods. Therefore, microwave-assisted reaction with solid acids was an easy and convenient protocol for the synthesis.

## 5. Conclusion

The microwave-assisted reaction is a convenient and a more efficient way to performed organic chemical transformation in a shorter time, with improved yield, which has advantage of energy-saving, uniform heating, with reduction of production cost over conventional technology. Microwave-assisted reaction with solid support, acidic alumina; solvent-free reaction protocol is a convenient way forward to achieve the goal of green chemistry. The advantages of microwave assisted technology have been useful towards the context of multistep total synthesis, medicinal chemistry/drug discovery. To achieve further modification and development in the area of novel technology and instruments, which give rise to reproducible performances and that constitute a minimal hazard should be used instead of the domestic microwave oven.

**References:**
1. Giguere, R. J., Bray, T. L., Duncan, S. M., & Majetich, G. 1986. Application of commercial microwave ovens to organic synthesis. Tetrahedron Letters, 27 (41), 4945-4948.
2. Gedye R, Smith F, Westaway K, Ali H, Baldisera L, Laberge L, Rousell J., 1986. The use of microwave ovens for rapid organic synthesis. Tetrahedron Lett., 27:279–282.
3. (a) A. de la Hoz and A. Loupy., 2012. Microwaves in Organic Synthesis, Wiley-VCH, Weinheim (b) R. Sanghi and V. Singh, Wiley, Hoboken, 2012. Green Chemistry for Environmental Remediation (c) M. P. Pollastri and W. G. Devine, *Microwave Synthesis In Green Techniques for Organic Synthesis and Medicinal Chemistry*, W. Zhang and B. Cue., 2012. Wiley, Chichester, pp. 325–342 (d) S. Horikoshi and N. Serpone., 2013. Microwaves in Nanoparticles Synthesis: Fundamentals and Applications, Wiley-VCH, Weinheim (e) J. P. Tierney and P. Lidström., 2009. Microwave Assisted Organic Synthesis, Blackwell Publishing Ltd., Oxford. (f) P. Knochel and G. Molander, N. E. Leadbeater., 2014. Organic Synthesis Using Microwave Heating, Comprehensive Organic Synthesis: Second Edition , Elsevier Ltd., Oxford, pp. 234–286 (g) C. O. Kappe and A. Stadler Weinheim., 2012. Microwaves in Organic and Medicinal Chemistry, Wiley (h) R. B. N. Baig and R. S. Varma., 2012. Chem. Soc. Rev., 41 , 1559-1584 (i) S. L. Pedersen , A. P. Tofteng , L. Malik and K. J. Jensen., 2012. Chem. Soc. Rev., 41, 1826-1844 (j) S. R. Takkellapati., 2013. Curr. Org. Chem., 17, 2305-2322 (k) C. O. Kappe., 2013. Chem. Soc. Rev.,42 ,4977-4990 (l) Z. Wu , E. Borreto , J. Medlock , W. Bonrath and G. Cravotto., 2014. Chem Cat Chem, 6, 2762-2783 (m) G. D. Stefanidis, A. N. Muñoz, G. S. J. Sturm and A. Stankiewicz., 2014. Rev. Chem. Eng., 30, 233-259 (o) A. de la Hoz , A.Díaz-Ortiz and A. Moreno., 2005. Chem. Soc. Rev., 34 , 164 -178
4. Gupta M, Paul S, Gupta R., 2009. General characteristics and applications of microwaves in organic synthesis. Acta Chim Slov; 56: 749–764.
5. P.T. Anastas, J.C. Warner., 2000. Green Chemistry: Theory and Practice, Oxford University Press, Oxford, 2, p 124.
6. M. Lancaster., 2016. Green Chemistry 3rd Ed: An Introductory Text, Royal Society of Chemistry: Cambridge, 1, p 58.
7. U.J. Joshi, K.M. Gokhale, A.P. Kanitkar., 2011. *Indian J. Pharm. Edu. Res.*, *45*, 168-174.

8.  J.H. Clark, D.J. Macquarrie, 2008.  *Handbook of Green Chemistry and Technology*, John Wiley & Sons.  pp.10-27.
9.  S. Ravichandran, E. Karthikeyan., 2011. *Int. J. Chem. Tech. Res. 3*, 466-470.
10.  J.L. Krstenansky, I. Cotterill., 2000. *Curr Opin Drug Discov Devel*, *3*, 454-461.
11. B.S. Sekhon., 2010.  *Int. J. PharmTech. Res*. *2*, 827-833.
12. H. Rajak, P. Mishra., 2004. *J. Sci. Ind. Res*., *63*, 641-654.
13. B. Wathey, J. Tierney, P. Lidström, J. Westman., 2002. *Drug Discov Today*, 7, 373-380.
14. P. Lidström, J. Tierney, B. Wathey, J. Westman., 2001. *Tetrahedron*, *57*, 9225-9283.
15.  E.H. Grant, B.J. Halstead., 1998. *Chem. Soc. Rev*., *27*, 213-224.
16.  C.R. Strauss, R.W. Trainor., 1995.  *Aust. J. Chem*., *48*, 1665-1692.
17.  Loupy A, Petit A, Hamelin J, Texier-Boullet F, Jacquault P, Mathe D., 1998. New solvent-free organic synthesis using focused microwaves. Synthesis 9:1213-1234.
18. Baghurst DR, Mingos DMP., 1992. Superheating effects associated with microwave dielectric heating. J Chem Soc Chem Commun 9: 674–677.
19.  Glasnov TN, Kappe CO., 2007. Microwave-assisted synthesis under continuous-flow conditions. Macromolecular Rapid Communications. 28(4): 395–410.
20.  Qinhan J, Feng L, Hanqi Z, Liwei Z, Yanfu H, Daqian S., 1999. Applications of microwave techniques in analytical chemistry. Trends in Analytical Chemistry; 18: 479-484.
21. N.S. Lewis, D.G. Nocera., 2006. Powering the planet: chemical challenges in solar energy utilization, Proc. Natl. Acad. Sci. USA 103, 15729–15735.
22. K. Itagaki, G.T. Carver, R.M. Philpot., 1996. Expression and characterization of a modified flavin-containing monooxygenases 4 from humans, J. Biol. Chem. 271, 20102–20107.
23. Poulsen, L.L.; Ziegler, D.M., 1995. Multisubstrate flavin-containing monooxygenases: applications of mechanism to specificity. Chemico- Biological Interactions 96 (1), 57–73.
24. Cowden, W.B.; Halladay, P.K.; Cunningham, R.B.; Hunt, N.H.; Clark, I.A., 1991. Flavins as potential antimalarials. 2, 3-methyl-10- (substitutedphenyl) flavins. J. Med. Chem. 34 (6), 1818–1822.
25. Kanhed, A. M., et al., 2015. *Discovery of isoalloxazine derivatives as a new class of potential anti-Alzheimer agents and their synthesis. Bioorganic Chemistry, 61, 7–12.*
26. Identification of molecular descriptors for design of novel Isoalloxazine derivatives as potential Acetylcholinesterase inhibitors against Alzheimer's disease, 2017. *J. Biomol. Struct. Dyn.* Jun; 35 (8):1729-1742.
27. M. Tishler 3rd, K. Pfister, R.D. Babson, K. Ladenburg, A.J., 1947. Fleming, The reaction between *o*-aminoazo compounds and barbituric acid. A new synthesis of riboflavin, J. Am. Chem. Soc. 69. 1487–1492.
28. P. Hemmerich, S. Fallab, H. Erlenmeyer., 1956. Synthesen in der lumiflavinreine, Helv. Chim. Acta. 39. 1242–1252.
29. R.M. Cresswell., 1959. A.C. Hill, H.C.S. Wood, Pteridine derivatives. Part VII. The synthesis of riboflavin 2-Imine and related isoalloxazine 2-Imines, J. Chem. Soc. 698–704.
30. J. Davoll, D.D. Evans., 1960. The synthesis of 9-glycitylpurins, 3-glycityl-[1,2,3]-triazolo[d]-pyrimidines, 8-glycitylpteridines and 10-glycitylbenzo[g]pteridines including riboflavin and riboflavin-2-Imine, J. Chem. Soc., 5041–5049.
31. A. Niemz, J. Imbriglio, V.M. Rotello., 1997. Model systems for flavoenzyme activity: One- and two-electron reduction of flavins in aprotic hydrophobic environments, J. Am. Chem. Soc. 119, 887–892.

32. F. Yoneda, K. Tsukuda., 1979. A new synthesis of 10-arylisoalloxazines (10-arylflavins), J. Heterocycl. Chem. 16, 1365–1367.

33. V. Awasthi, A. Awasthi, S.M.S. Chauhan., 1992. Synthesis of newer amphiphilic 10-(aminoalkyl)-benzo[g]pteridines and related compounds, Ind. J. Heterocycl. Chem. 2 11–14.

34. S.M.S. Chauhan, Geetanjali, R. Singh., 2000. A mild and efficient synthesis of 10-substituted isoalloxazines in the presence of solid acids, Ind. J. Heterocycl. Chem. 10,157–158.

35. Geetanjali, R. Singh., 2006. Synthesis of Selected Novel 7-Methoxycarbonyl-10-substituted Isoalloxazines, J. Serb. Chem. Soc. 71. 575–579.

36. Chauhan, S. M. S., Singh, R., & Geetanjali., 2003. *Microwave-Assisted Synthesis of 10-Substituted Isoalloxazines in the Presence of Solid Acids. Synthetic Communications, 33(7), 1179–1184.*

37. Hofmann U., 1968. On the chemistry of clay. Angew. Chem. Int. Ed. Engl. 7 (9), 681–692.

38. Posner, G.H., 1978. Organic reactions at alumina surfaces. Angew. Chem. Int. Ed. Engl.17 (7), 487–496.

39. Strauss, C.R., 1999. A combinatorial approach to the development of environmentally benign organic chemical preparations. Australian J. Chem. 52 (1), 83–96.

# Applications of Continuous Flow Packed Bed Reactor in Biotransformations using Lipase Enzyme as Biocatalyst for production of Chiral Intermediates

*Shalini Basetty[a,b], Thenkrishnan Kumaraguru[a,b]\* and Subhash Ghosh[a,b]\**

*[a]Department of Organic Synthesis & Process Chemistry, CSIR-Indian Institute of Chemical Technology, Uppal Road, Habsiguda, Hyderabad, 500007, India.*
*[b]Academy of Scientific and Innovative Research (AcSIR), Ghaziabad, Uttar Pradesh, 201002, India.*
*Tel. 91-40-27191629, Fax: 91-40-27160512. E-mail: kumaraguru@iict.res.in*

## Abstract

Bioreactor is a manufacturing device used to perform reactions using enzymes. Numerous types of bioreactors are currently used at laboratory or industrial scale such as stirred-tank reactor (STR), packed-bed reactor (PBR), fluidized-bed reactor (FBR) and membrane reactor (MR). Among these reactors, PBR are intensively used at small and large scale due to their simple construction, lower cost for operation and maintenance, facile automatization and scaling-up. As a case studies, enzymatic production of (S)-7-((tert-butyldiphenylsilyl) oxy) hept-1-yn-4-ol (**I**), a key intermediate for Eribulin synthesis and (5S)-5-aminocarbonyl-4, 5-dihydro-1H-pyrrole-1-carboxylic acid, 1-(1, 1-dimethylethyl) ester (**II**), a key intermediate for Saxagliptin synthesis were studied in PBR.

In the case of intermediate (**I**), Amano lipase from *Pseudomonas fluorescens* was used for the enantioselective acylation in MTBE. The estimated kinetic parameters were $V_{max}$ 3.463($\pm$0.173) mM/h/g and apparent $K_m$ value, $K_{m,app}$ = 582.1($\pm$ 29.1) mM (correlation coeff. r =0.9614). At substrate concentration of 10 mg/mL (272 mM) and flow rate of 0.1 mL/min, the both the isomers are obtained in > 95 % theoretical yield and > 99 % *e.e* at steady state in a column (30 cm x 0.92 cm) packed with 3.6 g enzyme.

In the case of intermediate (**II**), Immobilized *Candida antarctica* Lipase B (CAL B) was used for the amidation of corresponding ester without loss of its enantiopurity. The estimated kinetic parameters were $V_{max}$ 40 $\pm$ 4.4 mM h$^{-1}$g$^{-1}$, $K_m$ (216 $\pm$ 22 mM) and $K_i$ 303 $\pm$ 31 mM. At substrate concentration of 30 mg/mL (132 mM) and flow rate of 0.1 mL/min, the product is obtained in > 98% yield and 98.5 % purity at steady state in a column (100 cm x 1.2 cm) packed with 40 g enzyme.

The enzyme can be recovered and reused in at least 10 times by using in a continuous mode operation in a packed bed reactor for both reactions. The reactions were scaled up to pilot scale level.

**Keywords:** biocatalysts, packed bed reactor, continuous flow, lipase, eribulin, saxagliptin, kinetics, and optimization and scale up.

## 1. Introduction

Enzyme-catalyzed reactions (biocatalysis) are often highly enantioselective, regioselective and diastereoselective and they can distinguish between functional groups with different chemical environments. Another advantage of enzymatic reactions is that the enzymatic reactions can be carried out at ambient temperature and atmospheric pressure, thus avoiding the use of more extreme conditions which could cause problems with isomerization, racemization, epimerization, and rearrangement. Besides, biocatalysts are environmentally acceptable, being completely degraded in the environment. At the manufacturing scale using

immobilized heterogeneous biocatalysts is preferred. The benefits of immobilizing an enzyme are:

> 1. Convenience: The ability to stop the reaction rapidly by removing the enzyme from the reaction solution (or vice versa). Product is not contaminated with the enzyme.
> 2. Economical: easily removed from the reaction and reused (especially useful in food and pharmaceutical industries).
> 3. Stability: Enhancement of enzyme stability against pH, temperature, solvents, contaminants, and impurities.

Despite decades of intense research in enzyme immobilization and the impressive advances that have been achieved, studies with bioreactors is still an active area of research and development owing to its significant technological impact. Numerous types of bioreactors are currently used at laboratory or industrial scale such as Batch stirred-tank reactor (STR), packed-bed reactor (PBR), fluidized-bed reactor (FBR) and membrane reactor (MR), Basket reactor etc. Usually, a stirred tank reactor is used in industry/laboratory for reactions. However, immobilized biocatalysts are so fine due to attrition of immobilized enzyme due to mechanical friction with stirrer blades there will be loss of enzyme in a stirred tank reactor where the particles are quickly broken up into very small pieces. This will cause a complete loss of enzyme. Most of immobilized enzyme reactions wear carried out in fixed/packed bed bioreactors in continuous, semi continuous or fed-batch systems. Among these bioreactors, those with packed bed of biocatalysts are intensively used at small and large scale due to their simple construction, lower cost for operation and maintenance, facile automatization and scaling-up. The bioreactors with fixed beds of biocatalysts promote the intimate contact between the phases and their easier separation, the products with inhibitory effect being removed from the reaction zone (fixed bed), this leading to the reutilization of the biocatalyst without its preliminary regeneration. As a case studies, enzymatic production of (S)-7-((tert-butyldiphenylsilyl) oxy) hept-1-yn-4-ol (**I**), a key intermediate for Eribulin synthesis and (5S)-5-aminocarbonyl-4, 5-dihydro-1H-pyrrole-1-carboxylic acid, 1-(1, 1-dimethylethyl) ester (**II**), a key intermediate for Saxagliptin synthesis were studied in PBR.

In the case of intermediate (**I**) Eribulin, a truncated version of marine natural product halichondrin B is used for the treatment of metastatic breast cancer. Currently Esai sells this drug in the trade name Halaven® or E7389. Several strategies have been developed for the synthesis of Eribulin and its intermediates.[1a-k] 4-Methylene tetrahydrofuran compound **1** is an essential building block (C14-C26) of Eribulin (Scheme 1) and enantiomerically pure homopropargyl alcohol (S)-**4** is used for its synthesis. From commercial point of view, synthesis of both the enantiomers of **4** in enantiomerically pure form with less number of steps is an attractive option.



(S)-7-((tert-butyldiphenylsilyl)oxy)hept-1-yn-4-ol
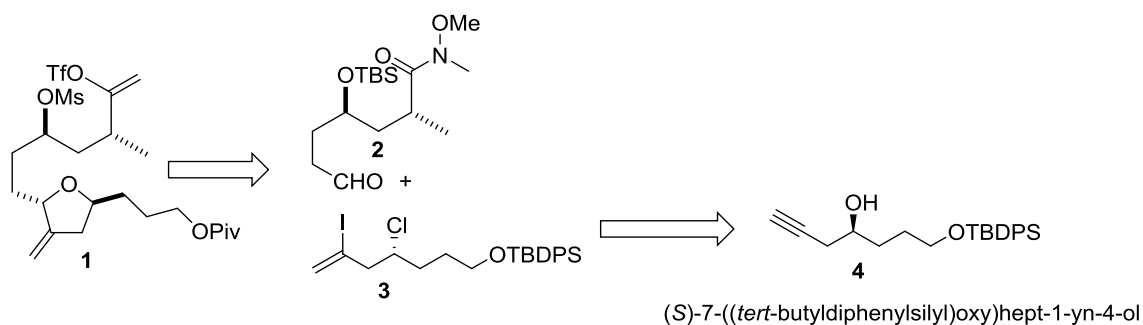
**Scheme 1.** Retro synthesis of C14-C26 building block of eribulin.

Preparation of (*S*)-**4** has been carried out by CrBr₃ mediated asymmetric propargylation of an aldehyde with a propargyl halide with 78% yield and 90 % *e.e.*  The enantiomeric purity was further improved by enantioselective hydrolysis of corresponding acetate derivates catalyzed by Amano lipase at 50 °C over a period of 43 h. This reaction was carried out with the enzyme dissolved in aqueous buffer from which enzyme recovery and recycle is difficult. Here we reported preparation of (*S*)-4 by enantioselective enzymatic acylation of (+/-)-**4** in organic solvent in 95 % yield and with *e.e.*  >99 % (Scheme 1). The enzymatic reaction was carried out in a continuous mode in a packed bed reactor for 5 days with productivity of 1.1198 mM/h/g  g product /g enzyme/h. The reaction was scaled up to 300 g. The unwanted isomer (*R*)-**4** was converted into required (*S*)-**4** through Mitsunobu inversion.

In the case of intermediate (**II**) Saxagliptin is a well known dipeptidyl peptidase IV (DPP4) inhibitor and is marketed under the trade name ONGLYZA® by Bristol-Myers Squibb for the treatment of type 2 diabetes. The amide (5*S*)-5-aminocarbonyl-4,5-dihydro-1H-pyrrole-1-carboxylic acid, 1-(1,1-dimethylethyl) ester **6**, is an important intermediate in its synthesis. The preparation of **6** by direct amidation with ammonia suffers from amide racemization and side-product formation while a two-step conversion via coupling reagents under mild conditions leads to low yields (57-64%).  In comparison, several reports of enzymatic amidation without formation of side products and racemization have also been made.
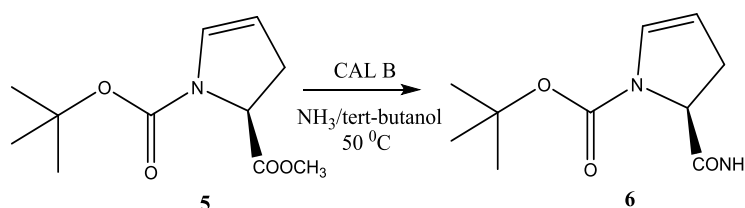


**Scheme 2.** CAL B catalyzed ammonolysis of ester **5**

In present work, we have simplified the overall process by performing the ammonolysis reaction with immobilized CAL B (Novozyme 435) in a catalytic packed bed reactor (PBR) (Fig.1.). The reactor essentially consists of a jacketed glass column maintained at 50 °C with a circulating water bath. The column is filled with immobilized enzyme beads and substrate dissolved in anhydrous *tert*-butanol containing 1.25 M ammonia is pumped at a fixed flow rate from the bottom of the reactor. The product stream is collected from top and analysed for monitoring the reaction.

## 2. Materials and methods

Amano Lipase from *Pseudomonas fluorescens* (≥ 20,000 U/g) was purchased from Sigma Aldrich. Novozyme 435 was a gift from Novozymes, Bangalore, India. Gum arabic (cat. no. 51198) was obtained from Sigma-Aldrich, Bangalore, India. All other chemicals and reagents were obtained from Sigma Aldrich, Himedia. IR spectra were recorded on a Perkin- Elmer RX-1 FT-IR system. ¹H NMR (300 MHz) and ¹³C NMR (75 MHz) spectra were recorded on Bruker Avance-300 MHz spectrometer. HPLC analyses were carried out on Shimadzu HPLC Unit LC 20 AD with diode array detector. Chiral HPLC columns were obtained from Daicel Chemical Corporation, Japan. For reverse phase Column C-18 (250 x 5 mm), Chrompack, Netherlands. Optical rotations were measured with a Horiba-SEPA-300 digital polarimeter. Mass spectra were recorded on a Q STAR mass spectrometer (Applied Biosystems, USA).

## 3. Results and Discussion

### 3.1 In the case of intermediate (1), Eribulin Enzymatic reaction in a stirred tank reactor.

Initially, the reaction was carried out in a 250 mL jacketed vessel maintained at 27 °C. Reactants were continuously stirred with an overhead mechanical stirrer at 150 rpm. The progress of the reaction was monitored by taking samples at regular intervals and analyzed through chiral HPLC. The reaction was continued till the reaction was completed (24-30 h). The enzyme kinetics follows a typical first order exponential path (Figure 1) with apparent $k_{obsd} = 0.0279$ h$^{-1}$ (correlation coeff. $r = 0.9519$).
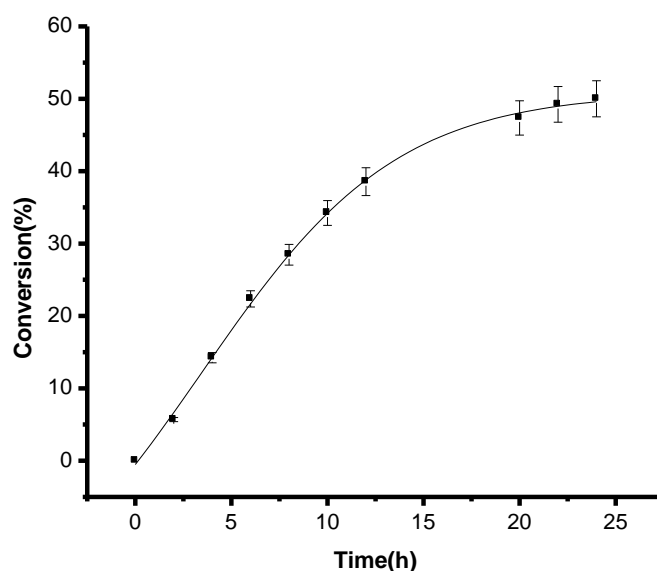


**Figure 1.** Kinetics of the reaction: [S] 5g (13.64 mmol), vinyl acetate = 3.14 mL (34.06 mmol), MTBE = 60ml, enzyme = 500 mg (10 % w/w) stirred at 27 °C.

**Advantages of a continuous packed-bed reactor over stirred tank reactor.** The major advantage of the resolution reaction carried out in packed bed reactor is to increase productivity by shortening the reaction time. It will also circumvents the problems associated with mechanical disruption of the biocatalysts, loss of enzyme & its activity during handling such as filtration, washing and drying at commercial scale.

**Packed bed reactor.** Continuous kinetic resolution was carried out in a jacketed stainless steel reactor with length and diameter of (250mm* 4mm). Temperature of the packed bed reactor was maintained at 27 °C with circulating water bath. After draining excess solvent, mixture of the substrate **4** and vinyl acetate dissolved in the MTBE was pumped from the bottom of the reactor and product stream was collected from top at steady state (Figure 2).
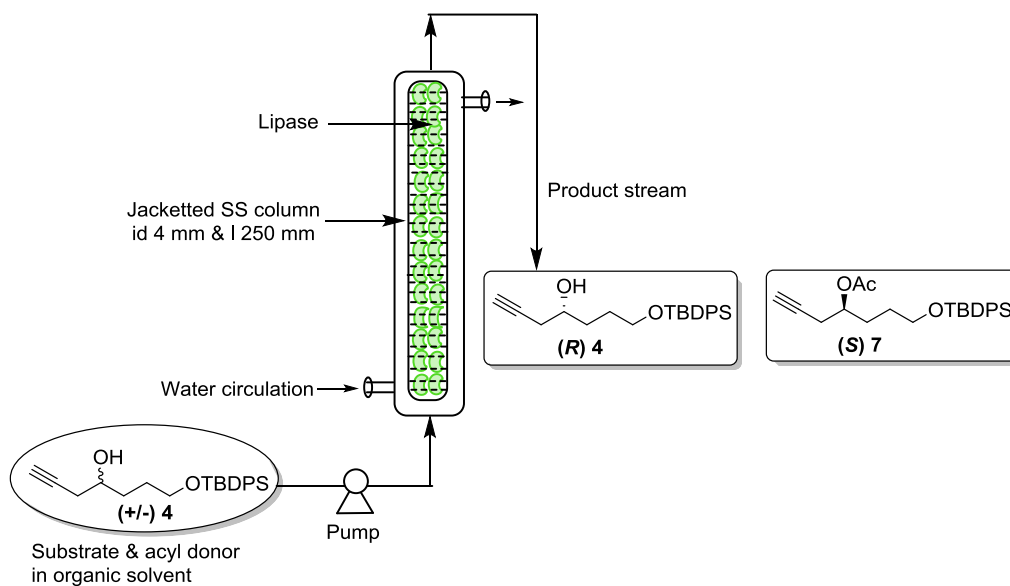
**Figure 2.** Schematic representation of packed bed reactor.

**Reactor performance**. In a packed bed reactor the flow is in axial direction. Assuming uniform velocity with no radial variation in reaction rate, the reaction rate is given by its performance equation (eqn 1) at steady state condition.

$$-r_A = \frac{dX_A}{dW/F_{A0}} \quad \ldots\ldots\text{eqn (1)}$$

Where, $X_A$ = Fraction of product converted; W = Weight of catalyst required; $F_{A0}$= Volumetric flow rate.

**Effect of flow rate on conversion.** Effect of flow rate was studied to investigate reactor performance. Reaction is carried out using 2 g enzyme in packed bed reactor. At fixed substrate concentration (0.136 M), the reactants were pumped at different flow rates (0.1 to 0.5 ml/min) and the product from PBR was analyzed using HPLC. As expected for a PBR, increase in flow rate caused decrease in conversion due to lower residence time.

The enzymatic reaction is of first order and at steady state; the product formation in packed reactor is given by eqn (2)

$$k_{obsd.} \ \tau = -\ln(1-X) \ \ldots\ldots\text{eqn (2)}$$

where '$\tau$' is residence time defined as '$\tau$' = reactor volume/flow rate; $X$ is the mole fraction of the product and '$k_{obsd}$' is the observed first-order rate constant.

The plot of '$\tau$' *vs* mole fraction of product, [$X$], followed an exponential curve expected for a first-order reaction with $k_{obsd} = 0.028 \ h^{-1} \pm 0.0014 \ min^{-1}$ (Figure 3).
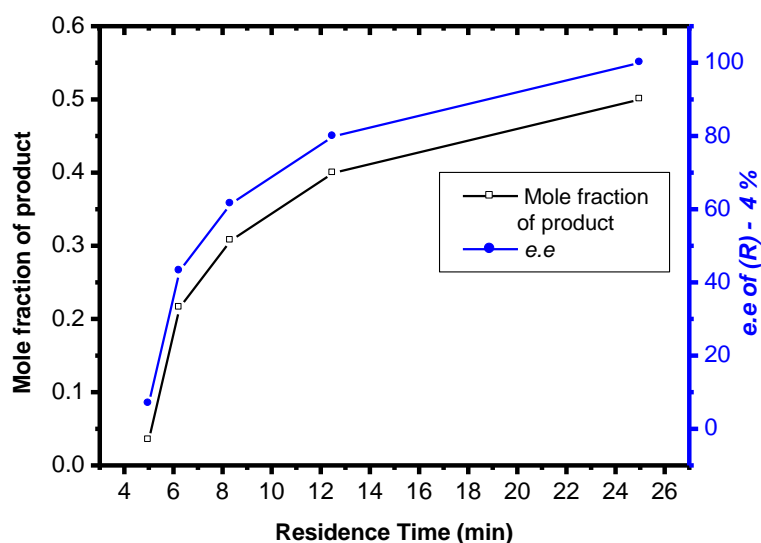
**Figure 3.** Effect of residence time on conversion and *e.e* at 27 °C. Reaction Condition [S] 0.136 M in MTBE, 1 eq vinyl acetate, 2 g Amano lipase from *Pseudomonas fluorescens* (bed volume 2.5ml).

**Effect of substrate concentration on reaction.** Effect of substrate concentration on rate of the reaction at steady state was studied in the packed bed reactor with fixed amount of lipase (2g) and fixed flow rate of 0.1 mL/min. As expected for an enzymatic reaction in a tubular reactor, increasing substrate concentration (from 50 mg/mL, 0.14 M, to 500 mg/mL, 1.0 M) causes increase in the rate of the reaction in the outflow (Figure 6). Analysis of the data using Michaelis-Menten equation provided the apparent $V_{max}$ value, $V_{max,app} = 3.46$ mM/h/g and apparent $K_m$ value, $K_{m,app} = 582$ mM (correlation coeff. $r = 0.9614$).
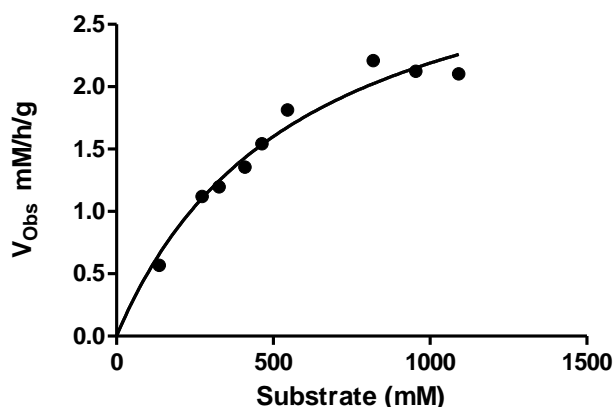


**Figure 4.** Effect of substrate concentration for resolution of *rac*-homopropargylic alcohol by using 2g of Amano Lipase from *Pseudomonas fluorescens* in PBR. *Reaction conditions:* Substrate concentration (136 mM -1091 mM) in MTBE at 27 °C at 0.1ml/min flow rate.

From the Micheleis - Menten kinetic parameters (assuming isothermal reactor without pressure drop and catalyst inhibition), a theoretical model can be used to calculate the weight

of the catalyst required to achieve 50% conversion at different substrate concentrations (Figure 5).
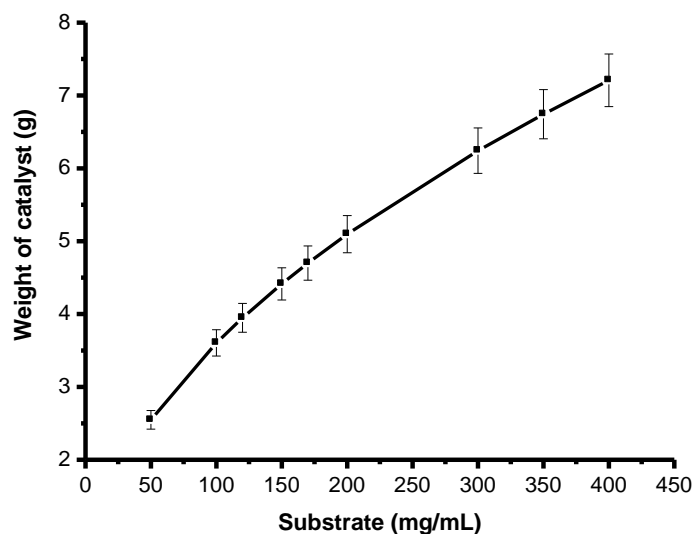


**Figure 5.** Theoretical requirement of Amano Lipase from *Pseudomonas fluorescens* for resolution of *rac*-homopropargylic alcohol at various substrate concentrations (50-400 mg/ml).

The model was tested with packed bed reactor consisting of two columns of dimensions 250 mm×4 mm connected in series. Total weight of enzyme in the packed bed was 3.6 g. 10 g of substrate (272 mM) dissolved in 100 mL MTBE and 2.77 mL of vinyl acetate (30 mM) was pumped from bottom using dosing pump at 27 °C. The flow rate was maintained at 0.1 mL/min. Analysis of the sample from top of the reactor showed *e.e* of > 99%The enzyme filled in the reactor was used continuously for one week without significant change in productivity. The productivity achieved by us is 1.1198 mM/h/g with advantage of using enzyme in a continuous reactor which can provide the product (combined isolated yield 10.2 g, > 96%) of high enantiomeric purity (> 99 % *e.e*).

### 3.2 In the case of intermediate (II), Saxagliptin

Glass column reactors of different lengths (10 cm to 60 cm) were fashioned out of double walled laboratory condensers of 8 mm internal diameter. Temperature was maintained at 50 °C with a circulating water bath. Slurry of immobilized enzyme in *tert*-butanol was poured into the column, and the enzyme bed was allowed to settle. After draining excess solvent, the bed was equilibrated with 1.25 M ammonia solution in *tert*-butanol. As reported earlier by Patel and co-workers, we too have observed that amide yield was negligible at 30 C, increased with temperature and was maximum at 50 ºC. The product quality and yield decreased on further increase in temperature. Thus further investigations were carried out at 50 °C. The substrate dissolved in the ammoniacal *tert*-butanol was pumped from the bottom of the reactor and product stream was collected from top.
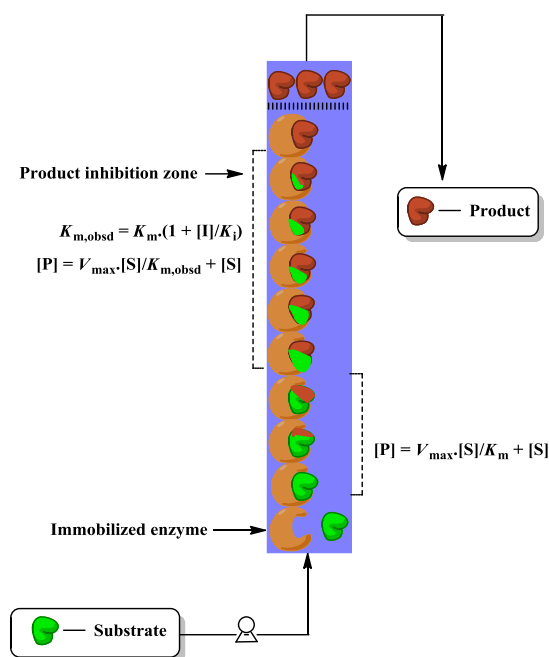
**Figure 5. A schematic representation of enzymatic reactions in a Packed bed reactor (PBR).**

## Effect of flow rate on conversion

A series of experiments were performed to investigate the effect of flow rate on reactor performance. For each experiment, reactions were carried out with 1.25 g immobilized enzyme (bed volume 3.1 mL). Substrate solution (25 mg/mL, 0.11 M) dissolved in *tert*-butanol containing 1.25 M ammonia was pumped at flow rates ranging from 0.1 mL/min to 0.5 mL/min and product stream was analysed by HPLC. At steady state, the conversion decreased with increasing flow rate due to decreased residence time (Fig. 6).
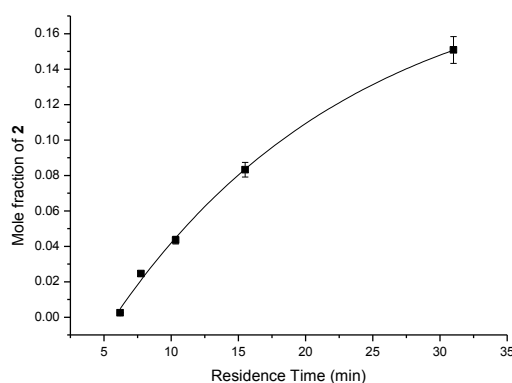


**Fig. 6.** Effect of residence time on conversion at 50 °C. [1] = 0.11 M in dry *tert*-butanol containing 1.25 M ammonia. [Immobilized enzyme] = 1.25 g (bed volume 3.1 mL).

## Effect of substrate concentration

Effect of substrate concentration on conversion at steady state was studied in the fixed bed reactor at fixed feed rate of 0.1 mL/min. As expected for enzymatic reaction in a tubular reactor, increasing substrate concentration (from 5 mg/mL, 0.022M, to 30 mg/mL, 0.132M)

causes increase in the product concentration in the outflow. The data for [S] against conversion was analysed in terms of Michaelis-Menten kinetics and the values of $V_{max} = 4 \pm 0.4$ mM min$^{-1}$g$^{-1}$ and $K_m = 0.215$ M $\pm 0.022$ M were obtained by non-linear analysis.

**Effect of enzyme concentration**

One simple way to achieve near 100% conversion in a single pass is to use a series of reactors. To evaluate this possibility, the substrate solution was passed through a series of 9 reactors, each with a bed of 1.2 g catalyst. Initial substrate concentration was changed from (5 mg/mL, 0.022 M) to (50 mg/mL, 0.22 M) while the flow rate was kept constant at 0.1 mL/min. Product concentration in the outflow of each bed was determined by HPLC. Plots of catalyst weight against product concentration were curved instead of being linear at all substrate concentrations (Fig. 7) indicating that the reaction was accompanied by product inhibition.
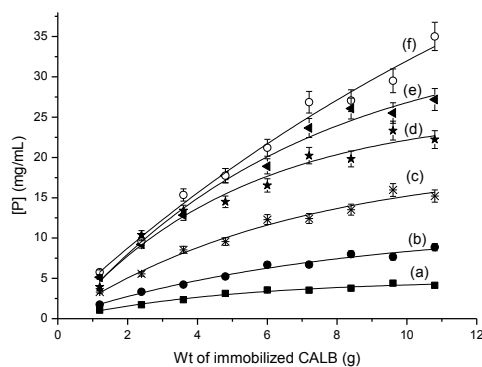


**Fig. 7.** Experimentally observed changes in product concentration profile due to product inhibition in serially connected packed bed reactors (9 beds with 1.2 g catalyst each). Substrate concentration (a) 5 mg/mL; (b) 10 mg/mL; (c) 20 mg/mL; (d) 30 mg/mL; (e) 40 mg/mL; (f) 50 mg/mL.

Using the Michaelis-Menten kinetic parameters estimated earlier with single catalyst bed of 1.2 g, the inhibition constant $K_i$ that would fit the data in Fig. was theoretically calculated. The product stream of first bed served as substrate + inhibitor solution for the next bed. The concentration of product, Y, was calculated using the equations (3) and (4):

$$K_{m,obsd} = K_m.(1 + [I]/K_i) \qquad ………(3) \qquad \text{and}$$

$$Y = V_{max}.X/(K_{m,obsd} + X) …….(4)$$

Where, $K_i$ is the inhibition constant, $V_{max}$ is the maximum enzyme velocity in the absence of inhibitor, $K_m$ is the Michaelis-Menten constant in absence of inhibitor and $K_{m,obsd}$ is the Michaelis-Menten constant in presence of inhibitor. X is the substrate concentration and Y is product concentration. An ideal plug flow was assumed. A value of $K_i = = 0.30 \pm 0.03$ M was estimated. The model predicted the amount of enzyme required to achieve > 99% conversion at different substrate concentrations (Fig. 8).
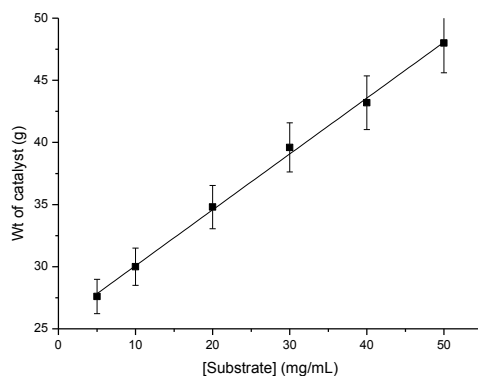
**Fig. 8.** Theoretical requirement of immobilized CAL B to achieve > 99% conversion at various initial substrate concentrations

The model was tested with a larger reactor (100 cm x 1.2 cm) with 40 g immobilized enzyme and 10 g of substrate (0.04 M) dissolved in 350 mL ammoniacal *tert*-butanol at 50 °C. The flow rate was maintained at 0.1 mL/min. and the solution was passed through a pre-heater at 50 °C before entering the enzyme reactor. The product stream contained 98.5% amide, 0.2% starting material and 1.3% of other impurities. The reactor was used continuously for one week without significant change in productivity. Based on enzyme loading of 40 mg/g, the productivity achieved by us (125 mg/h/g) is higher than that reported in literature (105 ± 15 mg/h/g) with advantage of using immobilized enzyme which can provide the product (isolated yield 9 g, 96%) of high purity in a continuous reactor.

## 4. Enzyme recyclability

After completion of every batch, a sample of enzyme was collected (50 mg) and its activity was assayed after washing. The reactor was used continuously for one week for 5 batches without significant change in productivity and change in activity of the enzyme.

## 5. Conclusion

We have developed a sustainable and improved process for the preparation of pure Intermediates using packed bed reactor to increase the productivity and avoid the enzyme deactivation by rupture and prolonged contact with substrate, product and solvents. The both reactions were scaled up to pilot scale level.

# Microalgae production using combinations of agricultural grade fertilizers and enhanced lipid recovery under nutrient stress

Swapnaja Kabirrao *Jadhav*[1*], Anil Kumar *Dubey*[2], Ankur *Nagori*[3], Mayuri *Gupta*[4] and Sachin *Gajendra*[5]

[1,2,3,4,5] *Agricultural Energy and Power Division, Central Institute of Agricultural Engineering, Bhopal, 462038, MP, INDIA.*
*Corresponding author: Email id- swapnaja20kjadhav@gmail.com, Mobile No. 9589110049; Tele No. 0755 252 1121, Address: 205, AEPD, ICAR- Central Institute of Agricultural Engineering, Nabibagh, Berasia Road, Bhopal-462038.*

## Abstract

Microalgae are unicellular, photosynthetic organism and rich in lipids which are being used as renewable source for biofuel production. However, microalgae biomass is still unconventional source in most of the countries. The major reason is cost occured on production process. Microalgae based biofuels will become more feasible with reduced cost of production and higher lipid recovery. In this work, locally available micro algae strains were isolated viz. *scendesmus obliqqus* and *chlorella vulgaris*. A pilot scale modified fibre reinforced plastic race way pond of 2.5 m$^3$ capacity was developed and cultivation of microalgae *chlorella sp.* was studied at normal and nutrient stress condition in Indian sub tropical condition of Bhopal. Growth medium was prepared by using different combinations of low cost agriculture grade fertilizers and compared based on microalgae biomass yield with standard growth media. Micro algae production was up scaled gradually in the laboratory using polyethylene bags and PVC container to prepare culture for race way pond. Fresh water micro algae grown in pond produced at the rate of 1.2 to 1.6 g.l$^{-1}$ after 14 to 18 days. Lipid content of micro algae was observed to be increased at nutrient - nitrogen stress condition by 47 to 86%. Cost expenditure occurred on the growth media was drastically reduced using these combinations of fertilizers; fibre reinforced plastic pond and nutrient stress condition.

**Key wards: microalgae, bio fuel, nutrient stress, lipid, growth media.**

# 1. Introduction

Energy demand of the world is being increased with industrialization and modernization. Petroleum fuels are basic requirement of the internal combustion based engines for transportation fuel, pumping, furnace and as an aviation fuel. Since bio fuels produced from oil crops and waste oils cannot alone meet the existing demand for fuel, microalgae seems to be a more promising feedstock alternative (Chisti, 2007). Micro algae based third generation bio fuel has attracted attention worldwide for its unexploited benefits over fossil fuels. However the production of micro algae has been started since 50 years and then large scale production in Japan followed by United States, Israel, India and other Asian countries by 1980s as a protein source (Borowitzka, 1999). Micro algae biomass is not only source of oil, ethanol, bio methane but also a potential source of other high value products (Yen and Brune, 2007; Seefeldt, 2007; Huntley and Redalje, 2007; Zhou et. al., 2011 ). Many developed countries already have micro algae based bio fuel plants and waste water treatments plants (Abdel-Raouf, 2012; Christenson and Sims, 2011, Markou and Georgakakis, 2011; Molinuevo-Salces *et al*. 2010; Subashchandrabose *et. al*., 2013; Park et. al 2011; Paul *et al*. 2014; Zhu, 2014)

Micro algae are a diverse group of unicellular, photosynthetic organism which is capable to grow in fresh, brackish and salty water. Microalgae include eukaryotic and prokaryotic cynobacteria having size ranging between 3 to 30 µm (Guo et al. 2013) with different shapes and capable of growing in very different environments. It has millions of strains which can grow in any type of water and on a moist surface having adequate nutrients, pH (7 to 9), aeration and light intensity (1000 to 10000 lux) (Randrianarison and Ashraf, 2017). Micro algae are reportedly having higher photosynthesis efficiency and have ability to utilize 1.6 to 2 kg of $CO_2$ per kg of dry weight of algal biomass per year during process (Bai, *et al*. 2017) and use of algal biofilm can be done for $CO_2$ fixation at the rate of 110 ton per ha per year (Miyauchi, et. al., 2020). Compared to terrestrial oilseed crops, micro algae can produce 5 to 10 times biomass considering land, energy, time requirement due to higher growth rate and short life span of algae. Thus, algae being a non food source have a big potential of recycling water, liquid waste or gaseous waste streams back to organic biomass efficiently than conventional crops by utilizing nitrates, phosphates and other inorganic elements (Abdel-Raouf *et al.,* 2012).

Though micro algae can grow in the natural habitat as lake; pond; river; coastal streams; and backwater streams, isolated structures are necessary for commercial production and harvesting. The established popular structures used worldwide are open pond (Race way and circular pond) and closed systems called as photo bioreactors. In closed systems, micro algae can be cultivated in continuous mode and with higher photosynthetic efficiency as a result of controlled growth factor. However, only disadvantage of closed systems is cost of operation and sophisticated way of production which is mainly used for high end product (Singh and Gu, 2010 and Darzins, *et. al*., 2010). Open pond structures are inexpensive (Benemann, 2013) and simple in fabrication and operation, however, more vulnerable for contamination and environmental conditions than closed systems for bulk production of micro algae (Khan *et al.,* 2018). These systems are more suitable for locally dominant strain provided preventive measures are taken to avoid contamination (Anthony and Runge, 2014).

Micronutrients required in trace amounts include silica, calcium, magnesium, potassium, iron, manganese, sulfur, zinc, copper, and cobalt, etc. Algae cultivation does not require herbicides or pesticides application providing advantage to environment. Composition of the algae can be altered by varying growth conditions, and thus significantly boosting the oil yield up to 60% of their dry mass making them potential future bio fuel (Hu *et al.* 2012). While growing microalgae at laboratory scale by various researchers, growth media used

were F/2 nutrient enrichment for saline water (Andersen et. al. 2005),  BG 11 and TAP culture medium for different micro algal species such as *Synechococcus* PCC 7002, C. *reinhardtii* and *Synechococcus* 7942. For outdoor cultivation commercial fertilizer 'Mor' was used which contained (in m equiv.) 703 $NO_3^-$, 268 $NH_4^-$, 213 $P_2O_5$, 771 $K_2O$, 604 $Ca^{+2}$, 229 $Mg^{+2}$, 13 $Fe^{+2}$, 6.6 $Mn^{+2}$, 2.8 $Zn^{+2}$, 0.4 $Cu^{+2}$, 0.2 Mo (Guillard and Ryther, 1962). The general nutrient medium F/2 was supplemented with nitrogen and phosphorus by adding Miracle Grow plant food at a final concentration of 0.1 g/L for fresh water micro algae cultivation by Lee et.al. (2014). Also a growth medium was prepared using commercial fertilizer for nitrate and phosphate source and studied to grow marine micro algae and *chlorella sp.* which was found at par to F/2 media and N-8 media (Ashraf *et al.* 2011 and Rofidi, 2017).

While adequate nutrient supply is necessary for algal growth which ultimately leads to biomass production, research interest lies in higher lipid content in the microalgae. Therefore along with the culture media, studies were focused on strategies for enhancing the lipid content ( Gour et al. 2018; Khoo et al. 2020).  Nutrient deprivation, temperature and light intensity has a distinguishing effect on the biomass and lipid production of micro algae (Converti, et al. 2009; Liu *et.al*, 2016; Minhas *et al.* 2016 ). Nutrient stress like nitrogen, phosphorous, silicon and sulfur helps in lipid accumulation. Among those, Nitrogen deprivation has better effect on lipid accumulation in microalgae. The lipid accumulation under variable nitrate concentration has been reported increase in lipid accumulation by 15-85%. Most chlorella species accumulate lipids under Nitrogen stress (Alishah Aratboni et al. 2019).


For Indian conditions, micro algae is produced on commercial level as a protein source especially *Spirulina sp.* For production of bio fuel, micro algae are produced only on pilot scale and very few micro algae based waste water treatment plants for agro industries are in operation. Micro algae are not yet seriously considered on commercial level for bio fuel production in India (Hemaiswarya *et al.* 2012). The cost involved in micro algae production are mainly on installation and operation of cultivation structure, nutrient media, harvesting, drying and oil extraction which can vary depending on biomass yield, oil content, scale of production systems, and efficiency of oil recovery from microalgae biomass (Hannon *et al.* 2010, Lundquist, *et. al.* 2010; Norsker *et al.* 2011).

Thus, In this study we have given emphasis on isolation of locally dominant micro algae strain of Indian sub-tropical region, growth media preparation from commercially available agricultural grade fertilizers, varying growth conditions for high lipid accumulation and development of up scaled modified race way pond to reduce contamination and cost.

## 2. Material and methods

The research work began with identification of lipid producing microalgae strains. This work was carried out at Bhopal, Madhya Pradesh, India (Lattitude 23.2599°N, 77.4126° E longitude:.) Bhopal has humid subtropical climate with the lowest temperature varies from 11ºC in winter and to 45 °**C** in summer**.** Therefore, to tolerate such a varying weather, locally available strains were selected**.**

### 2.1    Isolation and Identification of local microalgae strains

Microalgae *Scendesmus sp. and chlorella sp.* were isolated from the water samples collected from water bodies such as a dam, pond, waste water streams, farm pond located nearby Bhopal region in 50 ml tubes and refrigerated until brought to lab. Strains were isolated by the serial dilution method. In order to isolate single microalgal species from the field water samples, standard plating methods were used to separate algal populations (Lee, 2014). BG-11 and BBM media recipes were utilized to isolate the colonies. For algae production at

laboratory scale, growth chamber was developed for micro algae where temperature was maintained at 20 °C and fluorescent lamps were used as a light source.

## 2.2 Maintenance of isolated microalgae strains

For growing micro algae in to 250 ml flasks, arbitrary shaker operating at 50 rpm was used to ensure turbulence and aeration of media. For assessing the performance of culture media and selection of suitable media for the growth and up scaling of micro algae, experiment was conducted using different media. Both BG-11 and Bold's Basal medium (BBM) media were prepared and inoculated with the isolated *Scendesmus sp.* and *chlorella sp.* and assessed for the average growth of microalgae.

## 2.3 Microalgae growth kinetics

In various microalgae cultivation experiment using different growth medium, the growth rate of microalgae was measured in the form of optical density using UV–visible spectrophotometer (LAMBDA 850+ UV/Vis Spectrophotometer) at 680 nm. The microalgae cell suspension in the medium creates turbidity to the liquid which scatters the light resulting in relatively higher optical density than transparent liquid. A UV-visible spectrophotometer was used after calibrating it with a sample of the BG-11 media as blank reading. Biomass yield was measured by harvesting biomass through centrifuge at 6000 rpm for 2 min (Chojnacka, 2005) followed by oven drying at specific interval. The microalgal biomass harvested and dried to achieve dry algal biomass. The standard graph for microalgae of known dry algal biomass weight and optical density was plotted for both species for growth study.

## 2.4 Optimization of fertilizer based medium for cultivation of fresh water microalgae

As micro algae need mainly Nitrogen and Phosphorous and other micro nutrients in traces. *Scendesmus sp.* mainly utilizes these two nutrients (Shi et. al. 2002). Various agriculture grade fertilizers contain single or mixed macro and micro nutrient sources in different proportions. Agriculture grade fertilizers were procured from local market and their solutions were prepared which are equivalent to the proportion of a particular nutrient present in the BG 11 growth media solutio (Stanier et al. 1979).

Table 1: chemical composition of different fertilizer used

| S.No. | Fertilizer | Content | Amount equivalent to BG-11 medium, g/l |
|---|---|---|---|
| 1. | Urea | 46 % Nitrogen | 0.5 |
| 2. | N:P:K (19:19:19) | 19% Nitrogen, 19 % Phosphorus, 19 % Potassium | 1.3 |
| 3. | 00:52:34 | 0% Nitrogent, 52% Phosphorus, 34 % Potassium | 0.1 |
| 4. | Calcium nitrate | 15.5 % Nitrogen, 26.5% CaO, 18.8% Ca, 14.4% $NO_3$-N and 1.1% $NH_4$-N | 0.25 |
| 5. | Single Super Phosphate (SSP) | Phosphate fertilizer | 0.05 |
| 6. | Rich Kombi-F | FeEDTA – 5%, MnEDTA – 2.5%, ZnEDTA – 3.5%, CuEDTA – 1%, Boron – 0.65%, Molybdenum – 0.3% | 0.005 |

Na$_2$CO$_3$ added as Carbon source. The medium was prepared by using different combinations of commercially available fertilizers mentioned in Table 1 to assess the suitable, low cost growth medium for microalgae. Since the commercial fertilizers have particular chemicals in specific proportion, four combinations were prepared using fertilizers solutions to approximately match the standard medium composition. The microalgae growth experiments were conducted to select the better combination and compared with the microalgae growth in BG-11 growth medium.

## 2.5 Nutrient stress on algae growth for high lipid yield

The algae were studied for growth and lipid content in different concentrations of nitrate. Micro algae were grown in the initial nitrogen source of NaNO$_3$ with 0.5 g L$^{-1}$ concentration in the medium.The microalgae were partially harvested after 7 days of growth in original media by centrifugation at 2000 rpm for 5 minutes. Harvested cells were re-suspended in media prepared with 0, 0.25, 0.5, 0.75 times of the original nitrogen source concentration of 0.5g/L NaNO$_3$ as a control. The effect of initial and experimental nitrogen concentration on the micro algal growth and lipid content was investigated. Total lipid extraction carried out by Folch et al. (1957) method. The experiment was performed in with three replications.

## 2.6 Up-scaling of micro-algae production

The up-scaling of pure strains of selected species of microalgae was started from 10 ml using standard media and proceeds through various steps up to the mass production in polyethylene (PE) bags up to 20 litre and final growth in small race way pond (2500 litre).

Each step involves an increase of the culture volume prepared to inoculate in higher volume media after a log phase. The cultures were continuously aerated through bubbling using air pumps. Each algal culture sample was monitored alternate day for cellular growth rates by measuring optical density. After up-scaling in a 5 litre flask, a synthetic media was replaced by the selected combination of fertilizers. For 20 to 40 litre micro algae media cultivation, polythene tubing is cut to a suitable length and width (70x50 cm$^2$) and sealed carefully at both ends and checked for leakage. Three holes (diameter of 1 cm) made in the upper surface to facilitate the aeration by inserting pipe of 1 cm diameter. The total biomass yield was also assessed by the standard graph plotted for the both species. Hemocytometer was used to count the cells.

## 2.7 Production of microalgae in modified pilot scale raceway pond

Race way ponds are easy to construct and there is no involvement of pumps, air bubbling and cleaning which makes their operating cost less than closed systems. Most of the race way ponds are constructed up to 30-40 cm below land level using concrete and liners at the edges. There are chances of these ponds getting contaminated with dust, and bacterial contamination. Therefore, pond was constructed 90 cm above the ground level, however this may add 50-65% more cost for construction. The material used for pond construction was **4 mm** thick FRP (Fibre Reinforced Plastic) sheets and was placed on mild steel raiser which avoided use of expensive liners and its cleaning. FRP is light weight, durable material and can be moulded in any shape and has resistance to the temperature. The capacity of FRP pond constructed is 2.00 m$^3$ having height of 40 cm so that sufficient sunlight penetration may facilitate. Paddle wheel was made up of 5 mm thick FRP sheets with 10 rpm rotational speed driven by 0.25 hp geared motor to achieve mixing velocity between 0.2 to 0.25m/s (Lundquist, *et. al.,* 2010 ). In summer season, evaporation loss of medium was observed and studied.

# 3 Result and discussion

## 3.1 **Isolation and Identification of local microalgae strains**

Chlorella sp. and *scendesmus sp.* were identified on the basis of morphology ( Lortou 2019) as a *dominant* species from the isolation and used in further study. Chlorella species is widely cultivated for lipid production and has lipid content in the range of 58% (Rodolfi et. al., 2009; Gouveia and Oliveira, 2009; Miao and Wu, 2004 and Peng, et. al., 2001). *Scenedesmus sp.* is very common in all kinds of fresh water. Both BG-11 and Bold's Basal medium (BBM) media were prepared and inoculated with the isolated *Scendesmus sp. and chlorella sp.* and assessed for the average growth of microalgae using optical density and biomass yield as presented in Figure 1.
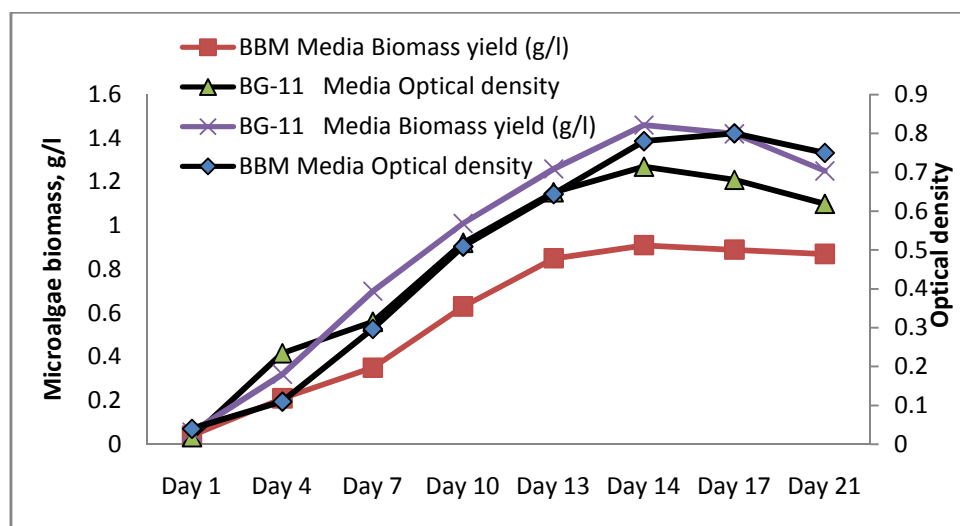


Fig. 1 Growth kinetics of micro algae BG-11 and Bold's Basal medium (BBM) media

The biomass content of microalgae on day 14 was observed to be 48.42 percent more in BG-11 media in comparison to BBM media and therefore BG-11 media was selected for further growth and scaling experiments. There is maximum growth during Day 14 to 17 having maximum optical density, and beyond that the optical density starts reducing as during the final stage, nutrients level get depleted and therefore cell density eventually collapses.

## 3.2 **Optimization of fertilizer based medium for cultivation of fresh water microalgae**

Commercially available agricultural grade fertilizer were selected for the supply of macronutrient mainly considering nitrate and phosphate source and Kombi F solution for micronutrients. Four different combinations of fertilizers were prepared as shown in Table 2 and the growth experiments were conducted comparable with BG-11 growth medium.

Table 2. Combinations of fertilizers under different treatments

| S.N. | Treatment | Composition |
|------|-----------|-------------|
| 1. | Treatment - 1 | NPK 19:19:19 - 1.3 g/ L + 10 ml/L of 0.5% Kombi-F solution + 0.02g $Na_2CO_3$ |
| 2. | Treatment - 2 | NPK 00:52:34 – 0.05 g/ L + $CaNO_3$ fertilizer–0.25g/L + 10 ml/L of 0.5% Kombi-F solution + 0.02g $Na_2CO_3$ |
| 3. | Treatment- 3 | $CaNO_3$ fertilizer – 0.25g/L + SSP -0.05g/L + 10 ml/L of 0.5% Kombi-F solution + 0.02g $Na_2CO_3$ |
| 4. | Treatment-4 | Urea – 0.5g/L + SSP – 0.05g/L + 10 ml/L of 0.5% Kombi-F solution + 0.02g $Na_2CO_3$ |

The fertilizer concentration mentioned in Table 2 is equivalent with the concentration of nitrate and phosphates concentration of BG-11 medium. The water soluble micronutrient fertilizer Kombi-F was used as micronutrient source for the medium. Micro algal biomass obtained using different fertilizer combination is presented in Figure 2. Treatment 3 and 4 has produced 1.21 and 1.47 g/l biomass at par that of BG 11 that is 1.5 g/l on 17th day. It was observed that pure form of fertilizer urea which contains 45% of nitrates had better effect on the microalgae growth. Lower growth of microalgae was observed in the Treatment 1 and Treatment 2 which contain Potassium which excludes in Treatment 3 and 4. Therefore, for open race way pond cultivation, Treatment 4 was selected.
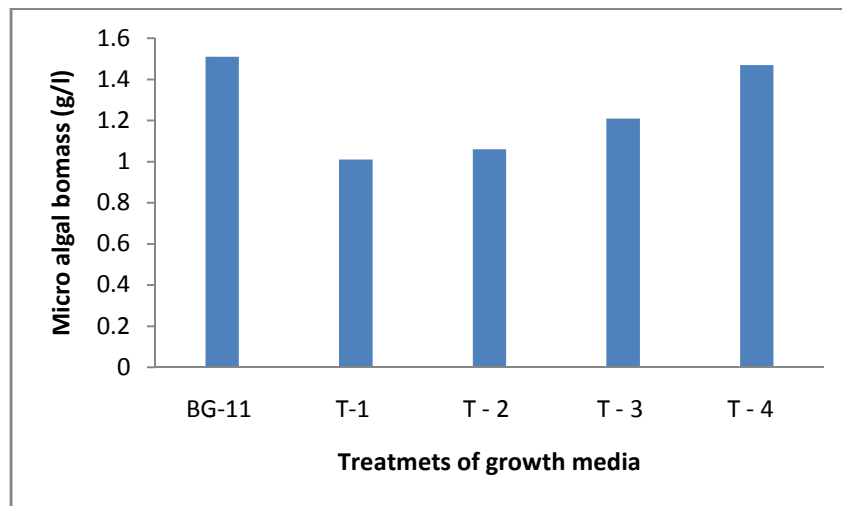


Fig. 2. Micro algal biomass (g/l) obtained using growth media prepared from different combinations of fertilizer.

### 3.3 Up-scaling of micro-algae production

The isolated microalgae culture was up scaled gradually from Petri dish to 10 ml flask by adding 5% of culture initially and then 2% of culture from the 10 ml flask to 250 ml flask and same process was followed for up-scaling in 5 litre and 20 litre and then finally in the FRP race way pond in 2 $m^3$ of growth medium. The flowchart of up-scaling of isolated microalgae culture is shown in Figure 3. Once the culture was up-scaled, the cultivated microalga was used for further cultivation. The growth of both the microalgae in the polythene bags was observed at par that of in the flasks and shown in Figure 4.
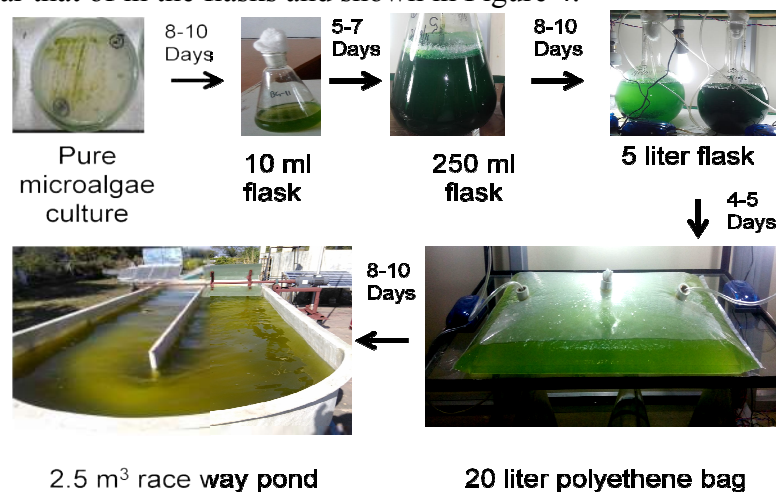


Fig. 3: Scaling up of micro algae culture for race way pond cultivation
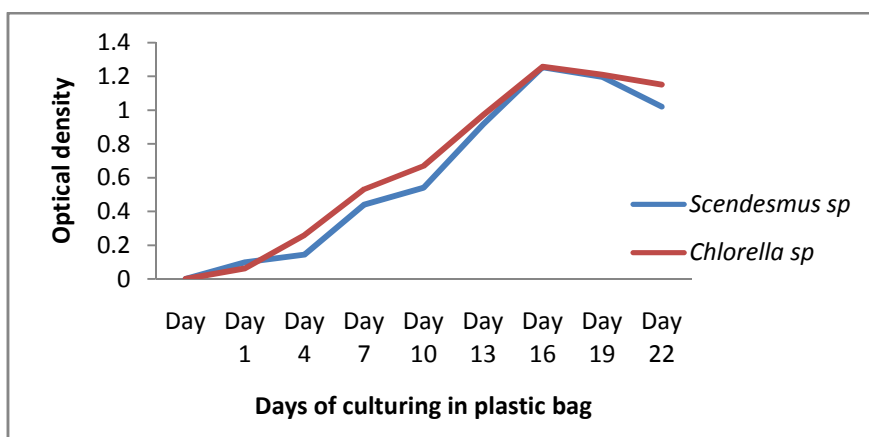
Fig.4  Growth of *Scendesmus sp.* and *chlorella sp.* in 20 litre plastic bags in lab.

## 3.4 Production of microalgae in modified pilot scale raceway pond

A race way pond was fabricated using fibre reinforced race way pond raised from ground at 90 am height and also covered with partial net to avoid any dust falling in the pond. As a result no contamination issue occurred throughout the year. The geared motor of 0.25 hp was sufficient to circulate the medium. Installation and handling of the race way pond was easy due to its low weight. The growth media prepared from fertilizer combination Treatment 4 was used for race way pond cultivation.  Further the up-scaling was done in tank of 2000 liter capacity. Optical density of *Scendesmus sp* and *Chlorella sp* grown in race way pond was measured at the interval of alternate day and the graph was plotted between the optical density and dried algal biomass in g/L. An equation was derived from the graph and then utilized for assessment of concentration of microalgae biomass for further experiments is shown in the Figure 5.



$y_{chorella} = 0.2205x - 0.2266$
$R^2 = 0.9819$

$y_{scendesmus} = 0.1801x - 0.2669$
$R^2 = 0.9833$
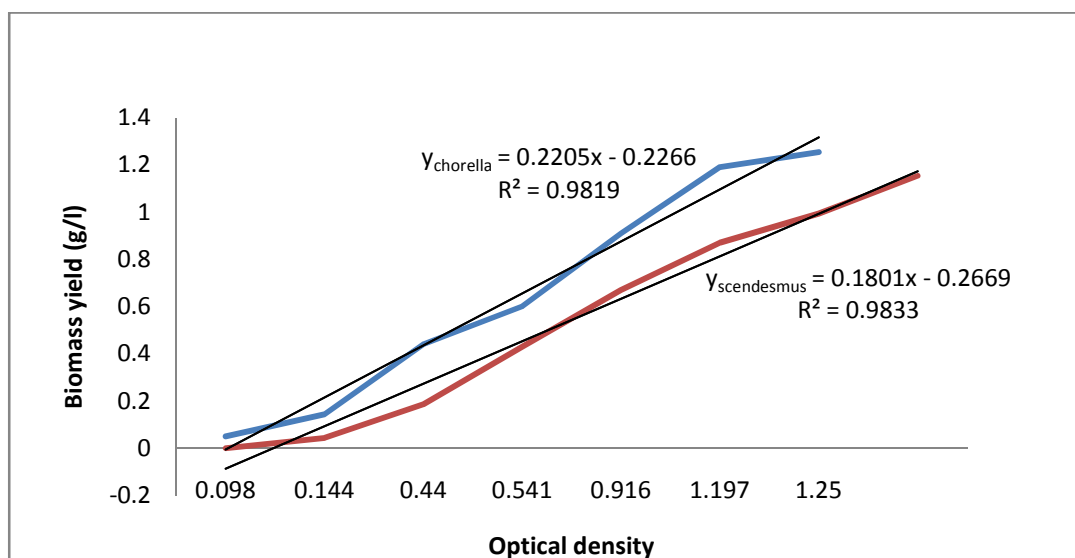
Fig. 5 Biomass yield of *Scendesmus sp. and Chlorella sp.* against an optical density in race way pond

The biomass yield of both the microalgae grown in race way pond was calculated from the optical density of using the derived standard equation. The biomass yield was observed slightly less than the laboratory yield due to environmental parameters like temperature

variation, evaporation and pH variation of tap water. *Chlorella sp.* showed higher growth than *Scendesmus sp.* in the open race way pond as shown in Figure 6.
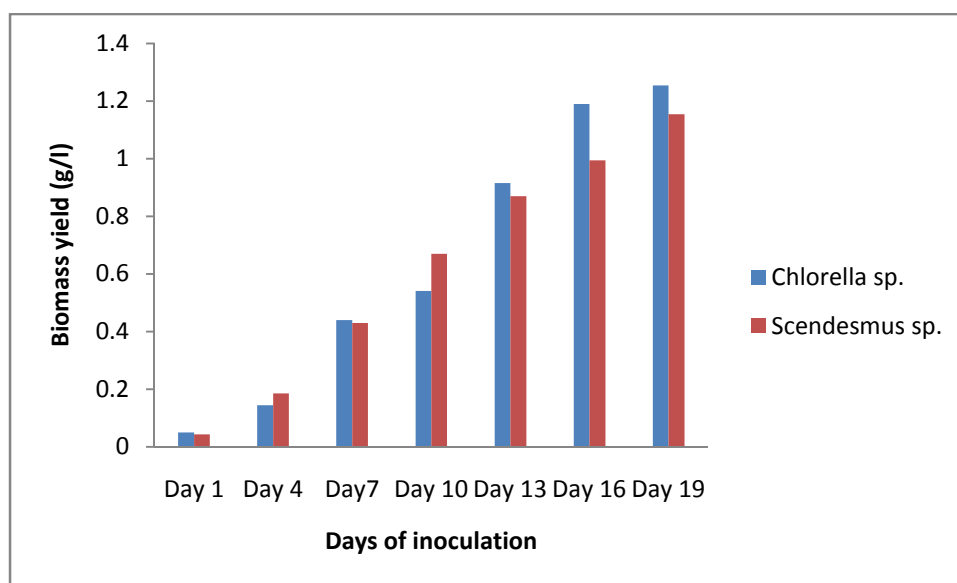


Figure 6. Biomass yield of microalgae cultivated in open raceway pond

During summer, rise in temperature, evaporation loss and contamination was observed in open pond microalgae cultivation. Therefore shed net was used to cover the pond and protect it from contamination and also to reduce the evaporation loss of algal medium. The growth study during summer in month of May was carried and effect on the evaporation loss per unit surface area and pH was observed as shown in the Table. 3. It was observed that pH of culture medium was continuously increased as the alkalinity increases along with the utilization of nutrients and microalgal growth and the evaporation. Almost 25% of water was evaporated during 10 days of culturing. Evaporation loss from the surface of the pond of area 8 m$^2$ was calculated by marking on the wall of pond. The increased wind was also one of the reasons for evaporation along with the raised temperature.

Table 3: Growth study of microalgae and evaporation loss assessment

| S.N. | Day | Atm. Temperature, °C | Pond water temperature, °C | Evaporation loss, litre/m$^2$ | pH | Optical density |
|------|-----|------|------|------|------|------|
| 1 | Day 1 | 42 | 33 | 6.3375 | 7.8 | 0.06 |
| 2 | Day 2 | 42 | 33 | 6.75 | 8.9 | 0.087 |
| 3 | Day 3 | 43 | 34 | 7.5 | 9.18 | 0.12 |
| 4 | Day 4 | 43 | 33 | 8 | 9.22 | 0.18 |
| 5 | Day 5 | 40 | 28 | 6.25 | 9.26 | 0.258 |
| 6 | Day 6 | 41 | 30 | 7.25 | 9.27 | 0.391 |
| 7 | Day 7 | 41 | 30 | 7.25 | 9.43 | 0.541 |
| 8 | Day 8 | 42 | 32 | 6.75 | 9.48 | 0.73 |
| 9 | Day 9 | 42 | 30 | 6.25 | 9.9 | 0.925 |
| 10 | Day 10 | 43 | 32 | 8.5 | 10.1 | 0.965 |

It was observed that micro algae biomass yield varies in the range of 0.7 to 1.5 g/l throughout the year due to environmental conditions. Biomass yield was observed lower in summer due to high temperature (Ras et al. 2013) and evaporation losses and in rainy season due to low sun light intensity than in winter season. In summer, water level may decrease below the paddle height leading stagnation and sedimentation and eventually retarding algae growth. Regular addition of fresh water was necessary to level the media in the summer.

**3.5 Nutrient stress on algae growth for high lipid yield**

The nitrogen concentration in the original culture was maintained as 0.5 g/l. Nutrient stress factors applied were in the range of 0 to 0.75. The biomass yield was measured in the stress condition. On the basis of experiments, the best suitable concentrations were selected which showed higher lipid content in microalgae. Lipid content of the micro algae samples grown under nutrient stress were measured and compared for each concentration as shown in Table. 5.

Table 5: Lipid content of chlorella sp. under nitrogen stress condition

| S.N. | Original Nitrate Conc. Of the culture media**(g/l)** | Nutrient stress factor of original concentration | Sodium Nitrate Conc.(g/l) | Biomass yield, (g/l) | % Lipid content in after 10 days | % Lipid content after 18 Days |
|---|---|---|---|---|---|---|
| 1 | 0.5 | 0 | 0 | 0.4163 | 3.85 | 5.03 |
| 2 | 0.5 | 0.25 | 0.125 | 0.98 | 6.96 | 8.13 |
| 3 | 0.5 | 0.5 | 0.25 | 1.2399 | 6.78 | 14.016 |
| 4 | 0.5 | 0.75 | 0.375 | 1.1859 | 18.88 | 21.3 |

The lipid content of microalgae grown in nitrogen stressed condition was measured during the exponential phase after 10 days and 18 days, the highest lipid content was estimated to be 18.8% and 21.3% respectively in nitrate ($NO_3$) concentrations of 0.375 g/l.

**4. Conclusion**

A locally available strain can tolerate environmental and water quality conditions if grown in artificial open pond resulting in less maintenance and higher production. Fibre reinforced plastic ponds is better alternative for brick and concrete ponds. Use of commercially available low cost agricultural grade fertilizers for microalgae can reduce overall operating cost of bio fuel production. A nitrogen stress can enhance the lipid content in fresh water microalgae. Evaporation loss is major problem for open pond cultivation resulting in higher water requirement for microalgae cultivation in sub tropical climate conditions. The production and harvesting process is not yet simplified and it requires multidisciplinary technical skills. A lot of research is lacking in identification of locally unexploited micro algae strain in different Indian conditions.

**References:**

Abdel-Raouf, N., Al-Homaidan, A. A., Ibraheem, I.B.M. 2012. Microalgae and wastewater treatment. Saudi Journal of Biologial Science.19 (3), 2, 57-75. https://doi.org/10.1016/j.sjbs.2012.04.005

Alishah Aratboni, H., Rafiei, N., Garcia-Granados, R. *et al.* 2019. Biomass and lipid induction strategies in microalgae for biofuel production and other applications. *Microb Cell Fact.* **18,** 178  https://doi.org/10.1186/s12934-019-1228-4

Andersen, R.A., Berges, J. A, Harrison JP, Watanabe MM. 2005. Appendix A: Recipes for freshwater and seawater media. Algal culturing techniques. Burlington Elsevier San Diego and London: Academic Press;. pp: 429–532. Available online file:///C:/Users/Administrator/Downloads/epdf.pub_algal-culturing-techniques.pdf. Accessed on 5th April 2019.

Anthony, R., Runge, T. 2014. An Approach to Microalgal Production Systems for Commodities. Oceanography 2, 116. doi:10.4172/2332-2632.1000116

Ashraf, M., M. Javaid, T. Rashid, M. Ayub, A. Zafar and S. Ali, 2011. Replacement of expensive pure nutritive media with low cost commercial fertilizers for mass culture of freshwater algae, Chlorella vulgaris. Int. J. Agric. Biol., 13, 484–490.

Bai, A., Popp, J.,  Pet, K., Szoke, I., Harangi-Rákos, M. and Gabnai, Z. 2017. The Significance of Forests and Algae in CO2 Balance: A Hungarian Case Study. Sustainability. 9, 857. http:///doi:10.3390/su9050857

Benemann, J. 2013. Microalgae for Biofuels and Animal Feeds. Energies. 6, 5869-5886.

Borowitzka, M. A. 1999. Commercial production of microalgae: ponds, tanks, tubes and fomenters. Journal of Biotechnology. 70, 313–321. https://doi.org/10.1016/S0079-6352(99)80123-4

Chisti, Y. 2007. Biodiesel from microalgae. Biotechnology Advances 25, 294–306. http://dx.doi.org/10.1016/j.biotechadv.2007.02.001

Chojnacka K, Chojnacki A, Górecka H. 2005. Biosorption of Cr3+, Cd2+ and Cu2+ ions by blue-green algae Spirulina sp.: kinetics, equilibrium and the mechanism of the process. Chemosphere. 59 (1), 75-84.

Christenson, L., Sims, R. 2011. Production and harvesting of microalgae for wastewater treatment, biofuels and bioproducts. Biotechnology Adv. 29(6), 686-702.

Converti A., Casazza A.A., Ortiz E.Y., Perego P., del Borghi M. 2009.Effect of temperature and nitrogen concentration on the growth and lipid content of *Nannochloropsis oculata* and *Chlorella vulgaris* for biodiesel production. Chem. Eng. Process. 48, 1146–1151. doi: 10.1016/j.cep.2009.03.006.

Darzins, A., Pienkos, P.T., Edye, L. 2010. Current status and potential for algal bio fuels production. IEA Bioenergy Task. 39, 1-131. Available online http://task39.org/files/2013/05/IEA-Task-39-Current-Status-and-Potential-of-Algal-biofuels-1.pdf . Accessed on 9 th April 2020.

Folch J., Lees M., Stanley G.H.S .1957. A simple method for the isolation and purification of total lipides from animal tissues. *The Journal of Biological Chemistry.* 226, 497–509.

Gour, R.S., Bairagi, M., Garlapati, V. K. and Kant, A. 2018. Enhanced microalgal lipid production with media engineering of potassium nitrate as a nitrogen source, Bioengineered, 9 (1), 98-107, DOI: 10.1080/21655979.2017.1316440

Gouveia L, Oliveira AC. 2009.Microalgae as a raw material for biofuels production. J Ind Microbiol Biotechnol 36(2), 69-74. https://doi.org/10.1007/s10295-008-0495-6

Guillard, R.R.L. and J.H. Ryther. 1962. Studies of marine planktonic diatoms. I. Cyclotella nana Hustedt and Detonula confervacea Cleve. Can. J. Microbiol. 8, 229-239.

Guo S. L., Zhao X. Q., Wan C., Huang, Z. Y., Yang, Y. L., Alam, M. A., Ho, S. H., Bai, F.W., Chang, J.S. 2013. Characterization of flocculating agent from the self flocculating microalga *Scenedesmus obliquus* AS61 for efficient biomass harvest. *Bioresource Technology* 145, 285–289. https://doi.org/10.1016/j.biortech.2013.01.120

Hannon, M., Gimpel, J., Tran, M., Rasala, B., Mayfield, S. 2010. Biofuels from algae: challenges and potential. *Biofuels*, *1*(5), 763–784. https://doi.org/10.4155/bfs.10.44

Hemaiswarya, S., Raja, R., Carvalho, I. S. *et al.* 2012. An Indian scenario on renewable and sustainable energy sources with emphasis on algae. *Appl Microbiol Biotechnol.* 96, 1125–1135. https://doi.org/10.1007/s00253-012-4487-0

Hu, B., Min, M., Zhou, W., Du, Z., Mohr, M., et al. 2012. Enhanced Mixotrophic Growthof Microalga *Chlorella* sp. on Pretreated Swine Manure for Simultaneous Biofuel Feedstock Production and Nutrient Removal. Bioresour Technol 126, 71-79.

Huntley, M. E., Redalje, D. G. 2007. CO2 mitigation and renewable oil from photosynthetic microbes: a new appraisal. Mitigation Adaption Strategies Global Change. 12, 573 - 608. Available online https://digitalcommons.calpoly.edu/cgi/viewcontent.cgi?article=1189&context=cenv_fac. Accessed on 9th April 2020.

Khan, M. I., Shin, J. H.1 and Kim, J. D. 2018. The promising future of microalgae: current status, challenges, and optimization of a sustainable and renewable industry for biofuels, feed, and other products. Microb Cell Fact, 17, 36. https://doi.org/10.1186/s12934-018-0879-x

Khoo, K. S. Chew, K. W., Yew, G. Y. Hong Leong, W. Chai, Y. H. Show, P. L. and Chen,W. H. 2020. Recent advances in downstream processing of microalgae lipid recovery for biofuel production. Bioresource Technology. 304, 122996.

Lee, K., Eisterhold, M. L., Rindi, F., Palanisami, S., Nam, P. K. 2014. Isolation and screening of microalgae from natural habitats in the midwestern United States of America for biomass and biodiesel sources. J Nat Sci Biol Med. 5, 333–339. https://dx.doi.org/10.4103%2F0976-9668.136178

Liu J., Mao X., Zhou W., Guarnieri M.T. 2016. Simultaneous production of triacylglycerol and high-value carotenoids by the astaxanthin-producing oleaginous green microalga *Chlorella zofingiensis*. Bioresour. Technol. 214, 319–327. https://doi.org/10.1016/j.biortech.2016.04.112

Lortou, U., and Gkelis, S. 2019. Polyphasic taxonomy of green algae strains isolated from Mediterranean freshwaters. *Journal of biological research*, *26*, 11. https://doi.org/10.1186/s40709-019-0105-y

Lundquist T.J., Woertz. I. C., Quinn N. W.T., Benemann, J.R. 2010. A realistic technology and engineering assessment of algae biofuel production. Berkeley, California: Energy Biosciences Institute. Available online https://digitalcommons.calpoly.edu/cgi/viewcontent.cgi?article=1189&context=cenv_fac. Accessed on 9th April 2010.

Markou G., Georgakakis, D. 2011.Cultivation of filamentous cyanobacteria (blue green algae) in agro-industrial wastes and wastewaters: a review. Applied Energy. 88 (10), 3, 3389-3401. https://doi.org/10.1016/j.apenergy.2010.12.042

Miao, X.L. and Wu, Q. Y. 2004. High yield bio-oil production from fast pyrolysis by metabolic controlling of *Chlorella protothecoides*. J Biotechnol. 110, 85-93. https://doi.org/10.1016/j.jbiotec.2004.01.013

Minhas, A. K., Hodgson, P., Barrow, C. J., Adholeya, A. 2016. A review on the assessment of stress conditions for simultaneous production of microalgal lipids and carotenoids. Front. Microbiol. 7, 546. doi: 10.3389/fmicb.2016.00546.

Miyauchi, H., Okada, K., Fujiwara, S. and Tsuzuki. M, 2020. Characterization of $CO_2$ fixation on algal biofilms with an infrared gas analyzer and importance of a space-rich structure on the surface. Algal Research. 46, 101814. https://doi.org/10.1016/j.algal.2020.101814

Molinuevo-Salces B, García-González MC, González-Fernández C. 2010. Performance comparison of two photobioreactors configurations (open and closed to the atmosphere) treating anaerobically degraded swine slurry. Bioresour Technol. 101(14), 5144–9.

Norsker, N. H., Barbosa, M. J., Vermuë, M. H and Wijffels, R. H. 2011. Microalgal production--a close look at the economics. Biotechnol Adv. 29(1), 24-27. https://doi.org/10.1016/j.biotechadv.2010.08.005

Park, J. B. K., Craggs, R. J., Shilton, A.N. 2011.Wastewater treatment high rate algal ponds for biofuel production. BioresourceTechnology. 102 (1), 35-42. https://doi.org/10.1016/j.biortech.2010.06.158

Paul, M., Patel, A. J., and Rajan, A. P. 2014. Algae Oil: A Sustainable Renewable Fuel of Future. Biotechnology Research International, 2090-3138. https://doi.org/10.1155/2014/272814

Peng, W., Wu, Q., Tu, P., Zhao, N. 2001. Pyrolytic characteristics of microalgae as renewable energy source determined by thermogravimetric analysis. Bioresource Technology. 80 (1), 1-7. http://doi.org/10.1016/s0960-8524(01)00072-4

Randrianarison, G. and Ashraf, M. A. 2017. Microalgae: a potential plant for energy production, Geology, Ecology, and Landscapes, 1 (2), 104-120 https://doi.org/10.1080/24749508.2017.1332853

Ras, M., Steyer, J.P., Bernard, O. 2013.Temperature effect on microalgae: A crucial factor for outdoor production. Rev. Environ. Sci. Biotechnol. 12, 153–164. http://doi: 10.1007/s11157-013-9310-6

Rodolfi, L, Chini Zittelli, G., Bassi, N., Padovani, G., Biondi, N., Bonini, G., Tredici, M. R. 2009. Microalgae for oil: strain selection, induction of lipid synthesis and outdoor mass cultivation in a low-cost photobioreactor. Biotechnol Bioeng.102 (1), 100-12. https://doi.org/10.1002/bit.22033

Rofidi, I. M. (2017). Commercial Fertilizer as Cheaper Alternative Culture Medium for Microalgal Growth (Chlorella sp.). Undergraduate thesis, Bachelor of Science (Marine Biology), School of Marine and Environmental Sciences, Universiti Malaysia Terengganu, Terengganu, 34. Online available on a website accessed on 6th April 2020. https://www.researchgate.net/publication/318201032_Commercial_Fertilizer_as_Cheaper_Alternative_Culture_Medium_for_Microalgal_Growth_Chlorella_sp

Seefeldt, L. C. 2007. Utah group plans to make biodiesel from algae. Ind Bioprocess. 29, 5-6.

Shi, X.-M., Jiang, Y., Chen, F. 2002. High-yield production of lutein by the green microalga *Chlorella* protothecoides in heterotrophic fed-batch culture. Biotechnol. Prog. 18, 723–727. doi: 10.1021/bp0101987.

Singh, J., Gu, S. 2010. Commercialization potential of microalgae for bio fuels production. Renewable Sustainable Energy Review. 14 (9), 2596-610. https://doi.org/10.1016/j.rser.2010.06.014

Stanier RY, Deruelles J, Rippka R, Herdman M, Waterbury J.B. 1979. Generic assignments, strain histories and properties of pure cultures of cyanobacteria. microbiology.111, 1–61.

Subashchandrabose, S.R, Ramakrishnan, B., Megharaj, M., Venkateswarlu, K., Naidu, R. 2013. Mixotrophic cyanobacteria and microalgae as distinctive biological agents for organic pollutant degradation. Environ Int. 51, 59-72. https://doi.org/10.1016/j.envint.2012.10.007

Yen, H. W. and Brune, D. E. 2007. Anaerobic co-digestion of algal sludge and waste paper to produce methane. Bioresource Technology. 98(1), 130-134. https://doi.org/10.1016/j.biortech.2005.11.010

Zhou N, Zhang Y, Wu X, Gong X, Wang Q. 2011. Hydrolysis of Chlorella biomass for fermentable sugars in the presence of HCl and $MgCl_2$. Bioresource Technology. 102 (21), 10158-61. https://doi.org/10.1016/j.biortech.2011.08.051

Zhu L. 2014. The combined production of ethanol and biogas from microalgal residuals to sustain microalgal biodiesel: a theoretical evaluation. Biofuels Bioprod Biorefin. 8, (1) 7–15.

# Hydrogel forming glucogalactan/sodium alginate blend-*graft*-polyacrylamide: Synthesis and characterization

[1, 2]Mihir D Oza* [2]A K Siddhanta

[1] Department of Chemistry, Gyanmanjari Science College
30-Sidsar Road, Near Iscon Eleven, Bhavnagar 364 060, Gujarat, India
[2]Marine Biotechnology & Ecology Discipline
Central Salt & Marine Chemicals Research Institute
CSIR-Council of Scientific & Industrial Research
Bhavnagar 364 002, Gujarat, India
[[1,2]Correspondence: E-mail: mihircs2@gmail.com]

## Abstract

Polyacrylamide grafted agar/sodium alginate (Agar/Na-Alg-graft-PAAm) has been synthesized in the presence of potassium persulphate as a free radical initiator. By varying the reaction parameters, e.g., concentrations of acrylamide monomer and $K_2S_2O_8$, reaction time and temperature, the optimum grafting conditions have been identified. The blend and grafted products have been characterized by FT-IR, TGA, XRD and SEM analysis. The swelling capacities of hydrogels of agaroid of *Gracilaria textorii* and *Gelidiella acerosa* (Meena *et al.*, 2008) were 5.1 g/g and 5 g/g in aqueous medium (pH 7.0) respectively. Due to the presence of 6-*O*Me group in *Gelidiella acerosa* agar and *Gracilaria textorii* agaroid making it relatively more hydrophobic, (Oza *et al.*, 2011). Sulphate content and molecular weight of the latter was 0.2% and $8.25 \times 10^5$ Da as against 1.5% sulphate and $3.5 \times 10^5$ Da of *Gelidiella acerosa* agar (Prasad *et al.*, 2007), respectively. The swelling capacities of blend and grafted copolymer hydrogels were significantly lower in comparison to the dewatered parent agaroid hydrogel used in this study. Agars of different sources can have potentially useful effects on the blend as well as on its derivatives, offering rewarding opportunities in new application domains and bioprospecting work leading to materials and resources security.

**Keywords:** Polymers, Graft polymers, Copolymers, Biopolymers, Alginates, Polyacrylamide, Hydrogels

## 1. Introduction

Hydrogels which can undergo a reversible and yet discontinuous volume phase change in response to various external physicochemical factors, such as pH, metabolites and ionic factors, will alter the molecular interactions between polymer chains, or between polymer chain and solutes present in a system called smart or stimuli responsive hydrogels. Hydrogel technology has focused on developing biocompatible, non-toxic materials for pharmaceutical and biomedical applications (Qui and Park, 2002; Chen *et al.,* 2003; Bhattarai *et. al.,* 2005; Ju *et al*., 2009). Hydrogels are three dimensional networks consisting of predominantly hydrophilic group that can swell upon exposure to water, yet maintain their physical shape. For more than two decades, research on development of smart hydrogel materials have been receiving considerable attention due to their potential for significant technological and biomedical applications (Serizawa *et al*., 2002; Plunkett *et al*., 2005; Bhattarai *et al*., 2005; Alarcon *et al*., 2005). The structural feature of these materials dominates its surface properties, perm selectivity, and permeability, giving hydrogels their unique, interesting properties and the similarity of their physical properties to those of living tissues (Bae, 1997; Dong & Hoffman, 1991). Hydrogel technology supports a wide range of applications such as in biomedical, tissue engineering, pharmaceuticals and personal care products, agriculture as a water retentive (Nishi & Kotaka, 1989; Zhang & Nicholas, 2000; Sershen & West, 2002; Kikuchi and Okano, 2002; Yamato *et al.,* 2002; Hu *et al*., 2007; Yeo and Kohane, 2008).

Agar, the red seaweed gelling linear homopolysaccharides consisted of alternating 1,3-linked β-D-galactose and 1,4-linked α-L-3,6 anhydro galactose residues (Figure 1) (Araki, 1966). Alginate is a high-molecular mass polysaccharide extracted from various species of brown seaweeds (Ertesvag & Valla, 1998). Alginates are also produced extracellularly by *Pseudomonas aeruginosa* and *Azetobacter vinelandii* (Johnson *et al*., 1997). Alginate is a linear, anionic block copolymer heteropolysaccharide consisting of β-D-mannuronic acid (M) and α-L-guluronic acid (G) (Figure 2). The relative amount and sequential distribution of homogeneous M-M segments (M-blocks), homogeneous G-G segments (G-blocks) and alternating M-G segments (MG-blocks), which represent the primary structure of alginate, depend on the producing species, and for marine sources, on seasonal and geographical variations. Both the polysaccharides agar and alginate are biodegradable and widely used in the food, pharmaceutical and cosmetics industries and biological applications.

Meena *et al.* (2008) reported the synthesis of robust hydrogel by grafting the blend of agar and sodium alginate with polyacrylamide (PAAm). The agar was extracted from the seaweed *Gelidiella acerosa* and alginate was from *Sargassum tenerrimum* of Indian waters. The polysaccharide extracted from *Gracilaria textorii* was found to be glucogalactan type of polymer having weak gelling properties, and may be called agaroid (Oza *et al*., 2011). For evaluating the effect of agaroid in the agaroid / alginate - *graft*-PAAm product as opposed agaroid / alginate - *graft*-PAAm, mentioned above (Meena *et al.*, 2008), it was decided to use of this polysaccharide of *Gracilaria textorii* Division-Rhodophyta (Class-Rhodophyceae, Order-Gracilariales, Family- Gracilaraceae, Genus-*Gracilaria*, and Species-*textorii*) (www.algaebase.org), a little known agarophyte of Indian waters. This study will be described in this study.

In an ongoing program of the author's laboratory on modification of seaweed polysaccharides for preparing new materials with improved functional properties (Prasad *et al*., 2005a,b; Prasad *et al*., 2006a, b; Meena *et al*., 2006; Meena *et al*., 2007a,b; Meena *et al*., 2008; Meena *et al.,* 2009; Prasad *et al*., 2009; Chhatbar *et al*., 2009; Oza *et al*., 2010; Siddhanta *et al.,*

2010; Meena *et al.,* 2011; Chhatbar *et al.,* 2011; Mehta *et al*., 2011., Oza *et al*., 2012a, b; Chhatbar *et al.,* 2012a, b) the agaroid of *Gracilaria textorii* was employed in the blending with sodium alginate (Sigma; M/G 0.32) followed by grafting reaction with polyacrylamide (PAAm). This reaction was carried out for the first time on *G. textorii* agaroid, the low gelling polysaccharide. The ultimate objective of this work is bioprospecting of agaroid-yielding seaweeds of Indian waters and their value addition.

## 2. Materials and Methods

### 2.1 Materials and Instruments

The agaroid polysaccharide (glucogalatan) used in this investigation was extracted from the red seaweed *Gracilaria textorii* which was harvested from the west coast of India. *G. textorii* used in this study was collected during December, 2006 to January, 2006 from Okha (22º 28.580' N, 69º 04.254' E), the inter-tidal zone in the west coast of India in Gujarat. Sodium alginate and potassium persulphate (AR) were purchased from Sigma-Aldrich, Mumbai. Laboratory grade acrylamide (AAm) and isopropanol (IPA) were purchased from Ranbaxy Chemicals, Mumbai, India.

### *Apparatus*

Milestone Start S (Italy) programmable microwave reactor system with integral magnetic stirrer and IR-temperature sensor (Model No.: Start S; Terminal T260; Line Voltage 230V; Magnetron S.N. 131528; Frequency 2450 MHz) was used for the grafting reactions.

### Extraction of agaroid from *G. textorii*

Dry *G. textorii* (20 g each) weresoaked in 600 mL water for 1 h at room temperature.The soaked seaweed was cooked in an autoclave withDM water (1:30 w/v) for 1.5 h at 120°C. The cookedseaweed was then homogenized in a kitchen grinder, boiled with Celite and charcoal and filtered over a Celite bed under vacuum to obtain a clear extract. The clear extract was kept at room temperature for gel formation and gelled material was then frozen in the freezer at -15°C for 15 h and then thawed at room temperature. Finally, the thawed polysaccharide was air dried for 24 h at ambient conditions and then dried in an oven at 50°C for 2 h to obtain the native polysaccharide.

### *Preparation of alkali treated Polysaccharide*

Alkali pre-treatment of *G. textorii* was carried out using 5% and 10% aqueous NaOH solution following the procedure described in our previous work on *Gracilaria* species (Mehta *et al*. 2010). Sample of *G. textorii* (20 g dry each) was soaked in 600 mL tap water for 1 h at room temperature and then treated with 600 mL of aqueous NaOH solutions at 80°C on a water-bath for 2 h. After the alkali treatment, excess alkali was removed by water washing till pH of the washings was in the range of 7–8. The seaweed was then autoclaved with distilled water (1:30 w/v) at 120°C for 1.5 h. Afterwards the alkali-treated agar was obtained by using a similar process as mentioned for the native agar by freezing-thawing. The alkali (NaOH) used in this study can be recycled and reused for subsequent batches for the preparation of alkali treated agar (cf Mehta *et al*. 2008). The percentage yields of dried native and alkali treated agars were calculated on the basis of dry as received seaweed with respect to nil moisture content in the seaweed. Native and alkali pretreated extractions were repeated three times with both the seaweed species. All the above mentioned galactan samples were treated with

a-amylase to remove floridean starch (cf. Falshaw *et al*. 2005), and then they were characterized.

## 2.2 Preparation of agaroid/alginate blend hydrogel

Blends of agaroid/alginate containing different ratios (agaroid : alginate, 1:0.5, 1:1, 1:1.5, 1:2 w/w) were prepared in demineralized (DM) water. In a typical experiment, 1.5 g agaroid was dissolved in 50 ml DM water using an autoclave at 120°C for 30 min. Sodium alginate (0.75 g) was dissolved in 50 ml DM water at ambient temperature under stirring for 10 min. The agaroid/alginate blend was prepared by mixing both the solutions in hot condition (at ca 70°C) to prevent the gel formation during the addition. The resulting blend sample was allowed to cool at ambient temperature for gel formation followed by curing at 10-15°C for 12 h in a refrigerator. Stabilized blend gel was cut into the pieces (ca. 2 cm$^3$) by a knife and dehydrated with isopropanol (IPA) (1:2 w/w) for 24 h. The dewatered gel pieces were collected by straining off the liquid and dried at ambient temperature followed by drying in an oven at 50°C 1 h. The dried blend sample was saved in a closed plastic bottle. The ratio of agaroid and alginate was optimized on the basis of stability of the gel sample in aqueous media (pH 1.2, 7.0 and pH 12.5) during the equilibrium swelling (ES) study.

## 2.3 Synthesis of agaroid/alginate blend-*graft*-PAAm hydrogel

Grafting reaction was carried out in a 250 ml round bottom flask (RBF) in a microwave reactor following the procedure described earlier in the literature (Shah *et al*., 1995; Prasad *et al.,* 2006a,b; Meena *et al*., 2008) (Scheme 3). Optimized agaroid/alginate blend (1.0 g) was dissolved in 40 ml DM water at 90° C for 5 min in the microwave reactor under stirring condition. The free radical initiator potassium per sulphate ($K_2S_2O_8$; 0.03 % w/w wrt agar/alginate blend) was added to the reaction mixture in the RBF with constant stirring and MW-irradiated at 90°C for 0.5 min. Acrylamide (AAm) was added in different ratios [(agaroid/alginate blend) : AAm, 1:0.5, 1:1, 1:1.5] in 10 ml DM water to the reaction mixture in separate experiments for optimization, wherein the optimized ratio was found to be (agaroid/alginate blend) : AAm, on the basis of maximum swelling. The grafting reaction, under optimized condition was carried out at 90°C for 2 min microwave irradiation. The reaction mixture turned colorless to light yellow color, which was cooled to 45°C followed by precipitation in isopropyl alcohol (1:2 v/v). The products were separated by centrifugation at 8000 rpm for 10 min. The grafted product [(agaroid/alginate blend)-*graft*-PAAm] was purified by washing with 90 % (v/v) IPA (10 ml × 3; under constant stirring for 15 min) followed by pure IPA (20 ml) for complete removal of homopolymer and unreacted substrates. The removal of homo polymer and unreacted substrates was ensured by FT-IR spectra of the final wash, wherein no IR bands of the substrate were obtained. The product was dried in a vacuum desiccator over blue silica gel overnight followed by oven drying at 50°C for 1 h.

The hydrogel agaroid/alginate blend-*graft*-PAAm was prepared from the dried grafted product. The grafted product (1.5 % w/v) was dissolved in DM water at 90°C for 2 min. The resulting solution was allowed to cool at ambient temperature for gel formation followed by curing at 10-15°C for 12 h in a refrigerator. Cured agaroid/alginate blend-*graft*-PAAm hydrogel was cut into the pieces (ca. 2.0 cm$^3$) by a knife and dehydrated with isopropanol (IPA) for 24 h. The dewatered gel pieces were collected by straining off the liquid, dried in the air at ambient temperature followed by drying in an oven at 50°C. The dried blend sample was saved in a closed plastic bottle.

## 2.4 Grafting parameters

Grafting parameters, such as conversion percentage (C %), grafting percentage (G %) and grafting efficiency (E %) were determined using the equations 1 to 3, reported in the literature (cf. Bajpai *et al*., 1988; Athawale and Padwaldesai, 1999; Meena *et al.,* 2006; Meena *et al*., 2008).

Equations for grafting parameters,

$$C \% = \left( \frac{\text{Total weight of polymerized substrate}}{\text{Weight of polymeric substrate charged}} \right) \times 100 \quad \text{.......(1)}$$

$$G \% = \left( \frac{\text{Weight of grafted polymer}}{\text{Weight of blend}} \right) \times 100 \quad \text{...................(2)}$$

$$E \% = \left( \frac{\text{Weight of grafted polymer}}{\text{Weight of polymeric substrate charged}} \right) \times 100 \text{.........(3)}$$

## 2.5 Characterization

The grafted product (agaroid/alginate blend-*graft*-PAAm) was characterized by Fourier transform infrared (FTIR) analysis on KBr plates on a Perkin-Elmer Spectrum GX FTIR system (USA) by taking 2.0 mg of sample in 600 mg of KBr. All spectra were an average of two counts with 10 scans each and a resolution of 5 cm$^{-1}$. Apparent viscosity was measured using a Brookfield Viscometer (DV-II +Pro) at 80$^{\circ}$C. Spindle SC4-18 was used for all measurement at 60 rpm. The pH was measured on a model-535 pH meter from Systronics Scientific Instruments (India). The gel strength (g/cm$^2$) was measured using a Nikkansui-type gel tester (Kiya Seisakusho Ltd.Tokyo, Japan). In this study gelling and melting temperatures of copolymer gels were measured as described by Craigie and Leigh, (1978). Thermogravimetric analysis was carried out on a Mettler Toledo TGA system (Switzerland), using dynamic temperature program (50$^{\circ}$C to 800$^{\circ}$C @ 10$^{\circ}$C/min) in air atmosphere. Powder X-ray diffractions were recorded on a Philips X'pert MPD X-ray powder diffractometer using 2θ = 5$^{\circ}$-60$^{\circ}$. The surface morphology of the samples was analyzed on a scanning electron microscope (SEM) instrument (Carl-Zeiss Leo VP 1430) applying an accelerating voltage of 20 kV and magnification 1 to 38 K respectively. Each vacuum oven dried samples were mounted on a sample holder and coated with gold under vacuum prior to the studies.

## 2.6 Equilibrium Swelling (ES)

An accurately weighed dried hydrogel pieces of *G. textorii* agaroid, agaroid/alginate blend and agaroid/alginate blend-*graft*-PAAm product was immersed in the aqueous media having different pHs (pH 1.2, 7.0 and 12.5) in separate experiments. The swollen gel pieces were wiped dry with a tissue paper by removing the adhering water from the surface of the gel and weighed at regular intervals until equilibrium (constant weight) was achieved up to 24 h. Stability of hydrogels in different at pH media (pH 1.2, 7.0 and 12.5) were observed for one week. Equilibrium swelling (ES) capacity was calculated as described by Meena *et al.,* (2008) using the following equation (4).

$ES = W_s - W_d / W_d$ ………………… (4)

Where,

$W_s$ weight of the swollen hydrogel sample
$W_d$ weight of dried hydrogel sample

## 3. Results and Discussion

### 3.1    Equilibrium swelling (ES) and agaroid/alginate blend ratio

The ratio of *G. textorii* agaroid and alginate in the blends were optimized by measuring the equilibrium swelling (ES) ability and stability of hydrogels in all aqueous media pHs (pH 1.2, 7.0, 12.5). The results of ES and stability are shown in Figure 4 & Table 1. The swelling capacity of the blend and grafted copolymer was lower in comparison to the dewatered parent agaroid hyrogel used in this study. The parent agaroid and agaroid/alginate blend (1:0.25) hydrogels exhibited greatest ES in pH 7.0 (5.1 g/g and 5.0 g/g) and pH 12.5 (6.2 g/g and 4.7 g/g) media during 14 h and were found to be stable for more than week. In acidic pH 1.2 medium both the gels collapsed and started dispersing within 2 h presumably due to the acid lability of agaroid present in blends. The hydrogel of the blend (agaroid : alginate, 1:0.75) exhibited relatively greater ES in pH 1.2 (1.6 g/g) and pH 12.5 (5.7 g/g) which was stable for more than a week.  However in neutral pH 7.0 media the gel got dispersed after 10 min perhaps due to the presence of relatively greater amount of hydrophilic alginate present in the gel composition (cf. Meena *et al*., 2008). Hydrogel having blend ratio - agaroid : alginate, 1:0.5  was found to be stable more than a week in all aqueous media exhibiting greatest ES in pH 1.2 (1.8 g/g), pH 7.0 (5.0 g/g) and pH 12.5 (5.9 g/g) media (Figure 4; Table 1). This may be due to the enhanced stability of the blend preventing protons from penetrating the blend matrix lowering thereby the swelling of the material as a direct consequence of low degree of ion transport phenomenon. Likewise, reverse was the case when the relative proportion of the sodium alginate was lower (cf. De *et al*., 2002).

On the basis of the superior stability and swelling ability in all pHs media agaroid/alginate blend ratio (agaroid : alginate, 1:0.5) was employed for grafting reaction. Agaroid/Alginate blend was grafted with PAAm in different ratios (Blend : AAm, 1:0.5; 1:1 and 1:1.5) for swelling study. The hydrogels prepared from grafted product (Blend : AAm,  1:1 and 1:1.5 w/w) exhibited lower ES in acidic (1.5 g/g; 1.3 g/g) and got dispersed, basic (3.9 g/g, 3.8 g/g) aqueous media than the agaroid/alginate blend (1:0.5, 5.65 g/g, 12.0) while it decreased in neutral (4.2 g/g; 4.0 g/g) aqueous media respectively (Figure 5; Table 1).

The swelling capacity significantly decreased in the blend and grafted copolymer in comparison to the parent agaroid used in this study. The blend (1:0.5) and grafted copolymer hydrogel (Agaroid/Na-Alg-*graft*-PAAm 1:1) exhibited low swelling (180% in blend and 150% in grafted product) while it remained in swelled condition more than 24 h in neutral and alkaline media

When compared with the ES performance of the hydrogels agar/alginate-*graft*-PAAm reported by Meena *et al.* (2008) with those of the present study it was observed that the hydrogels described in this investigation exhibited poorer ES performance (Table 1).  This was apparently due to the poor gelling quality of the agaroid that was employed in this study.

### 3.2    Physical properties and grafting parameters

The physical properties of agaroid, alginate, agaroid/alginate blends and agaroid/alginate blend-*graft*-PAAm copolymers are depicted in Table 2. The apparent viscosity increased with the increasing proportion of acrylamide (AAm) with respect to the blend (Table 2). This may

be due to the increase in stiffness and hydrodynamic volume of the copolymers in the presence of higher level of PAAm (Sharma *et al*., 2003; Meena *et al.,* 2008).

The values of gel strength, gelling and melting temperatures were found to be lower in agaroid/alginate blends and blend-*graft*-PAAm with the increase of alginate and AAm contents in the respective products (Table 2). It may be partly due to the enhanced hydrophilicity along with interruption of hydrogen bonding caused by the grafted residues resulting in lower gel strenght (Meena *et al.,* 2008). The optimized hydrogels of the products [agaroid/alginate blend and (agaroid/alginate blend)-*graft*-PAAm] exhibited low swelling capacity and stability in all pHs media as well as weak gel strengths <100 g cm$^{-2}$ (Table 2).

Significantly lower viscosity of this blend and blend grafted product (cf. agar/alginate-*graft*-PAAm reported by Meena et al., 2008) was obviously due to the quality of the agaroid since it was consisted of certain amount of glucose (branched) and methylated galactose as well as low amount of 3,6-anhydrogalactose (Oza *et al*., 2011), which imparted fair amount of hydrophobicity precluding hydrogel network formation as a consequence of reduced hydrogen bonding interaction phenomena.

Grafting parameters, conversion percent (C%) and grafting percent (G%) increased while grafting efficiency percent (E%) decreased with the increasing amount of the monomer (AAm) in grafted products (Table 2). The copolymer hydrogel prepared under optimum grafting conditions with C% = 86%, G% = 81% and E% = 81% exhibited low swelling abilities 1.5± 0.2 g/g, 4.2± 0.2 g/g and 3.9± 0.2 g/g in acidic, neutral and alkaline media, respectively (Tables 1 & 2). Optimized concentration of free radical initiator potassium per sulfate (KPS) 0.03 (w/w) with respect to blend was used for all reactions (Meena *et al.,* 2008).

In the absence of the water soluble initiator the grafting reaction did not take place (Prasad *et al.,* 2006 & Meena *et al.,* 2006). The maximum values of C% = 90% and G% = 122% were obtained with ratio blend : AAm, 1:1.5 (Table 1). A plausible reaction mechanism for the formation of the graft copolymer is proposed in Scheme 3 (Meena *et al*., 2008). The free radical initiator KPS generated sulphate anion radicals under microwave heating which attacked the hydroxyl groups of agar/alginate blend to form alkoxy radicals. This per sulfate-blend redox system resulted in active centers on the substrate to radically initiate polymerization of AAm leading to the graft copolymer formation (Scheme 3) (Pourjavadi *et al.,* 2007; Meena *et al*., 2008).

### 3.3   Characterization of (agaroid/alginate blend)-*graft*-PAAm copolymer

The grafted product (agaroid/alginate blend)-*graft*-PAAm copolymer was characterized by FT-IR, TGA, XRD and SEM analysis. The FT-IR spectra of the parent polysaccharides and graft copolymer are shown in Figure 6. The absorption band at 1670 cm$^{-1}$ for (C=O stretching) and at 1455 cm$^{-1}$ for C-N stretching indicated the insertion of PAAm in agaroid/alginate blend.

The comparative thermogram of parent polysaccharides and grafted copolymer are shown in Figures 7. Thermogravimetric analysis revealed that mass loss occurred in three steps in all samples.

For agaroid, in first step 100-84.5% (15.5 %) mass loss occurred in the temperature range 50º-165ºC, may be due to the moisture contents. In second and third steps 85.0 -35.5% (50.5 %) and C 35.5-3.0% (32.5%) mass losses occurred in temperature range 237-384ºC and 384-

551ºC, respectively and 3.0% mass remained thermally stable up to 800ºC.  In second step maximum thermal degradation (50.5%) took place in the temperature range 237-384ºC.

Similarly, in case of sodium alginate, in the temperature range 36.7º-152.6ºC, mass loss 100-90.7 % (9.3%) occurred in the first step may be due to the moisture contents. In second and third steps 90.7-42.3% (48.4%) and 42.3-19.8% (22.5%)  mass losses occurred in the temperature range 152.6-438.5ºC and 438.5-747ºC, respectively, and 19.8% mass remained thermally stable up to 800ºC.

For the graft copolymer (agaroid/alginate blend-*graft*-PAAm, 1:0.5:1) and agaroid/alginate blend (1:0.5) mass losses occurred in three steps. In the first step 100-87.6% (12.4 %) and 100- 84.6% (15.4%) mass losses occurred in the temperature range 35.3º-148.5ºC and 36.7º-170ºC, respectively may be due to the moisture contents. In the second step 87.6-69.8% (17.8%) and 84.6-67.0% (17.6%) mass losses occurred in the temperature range 148º-203.7ºC and 170-218ºC, respectively. In this step mass loss occurred more rapidly in a narrow temperature range for both the products. In the third step gradual 69.8-14.1% (55.7%) and 67.0-12.97% (49.4%) mass losses occurred in the temperature range 203.7º-522.7ºC and 218.9º-612.5ºC. In this step maximum thermal degradation took place in both the products (Figure 7). The pattern of the mass losses of the grafted copolymer was different showing lower values than the blend, while the corresponding temperatures were almost identical, indicating the occurrence of grafting. The TGA pattern of the blend copolymer presumably reflected the modified macromolecular entangled architecture of the copolymer.

The X-ray diffraction pattern showed that the crystallinity of alginate and acrylamide disappeared in the blend polysaccharide as well as in the grafted copolymer (Figure 8) indicating happening of the graft reaction destroying the ordered structures of alginate and acrylamide (Prasad *et al*., 2006b).

The scanning electron microscopy (SEM) images of the graft copolymer confirmed grafting when compared to those of parent polysaccharides, PAAm and Agaroid-Na-Alg blend (Figure 9). The morphology of the agaroid/alginate blend and graft copolymer appeared more composed than those of the parent polysaccharides indicating modified molecular associations in products.

## 4.   Conclusions

It may be noted that the swelling capacities of hydrogels of agaroid of *Gracilaria textorii* (present investigation) and *Gelidiella acerosa* (Meena *et al.*, 2008) were 5.1 g/g and 5 g/g in aqueous medium (pH 7.0) respectively. This may primarily be due to the presence of 6-*O*Me group in *Gelidiella acerosa* agar and *Gracilaria textorii* agaroid making it relatively more hydrophobic, (Oza *et al.*, 2011). Sulphate content and molecular weight of the latter was 0.2% and $8.25 \times 10^5$ Da as against 1.5% sulphate and $3.5 \times 10^5$ Da of *Gelidiella acerosa* agar (Prasad *et al.*, 2007), respectively.  This compositional variation appears to be playing a role in the difference of the properties of the grafted materials obtained in the present study and the one described by Meena *et al.* (2008) (Table 2).

The swelling capacities of blend and grafted copolymer hydrogels were significantly lower in comparison to the dewatered parent agaroid hydrogel used in this study. The optimized blend and grafted product exhibited different pattern of swelling capacities in aqueous media, in the

order pH 7.0 > 12.0 > 1.2 and pH 12.0 > 7.0 > 1.2 respectively. However, the ones (blend and grafted product) reported by Meena *et al*. (2008), exhibited greater swelling capacities than that of the parent polysaccharides. In this case, both the optimized blend and the grafted copolymer exhibited identical order of swelling pH 1.2 > 7.0 > 12.0 in aqueous medium (Table 2).

All other properties e.g. apparent viscosity, gel strength, gelling and melting temperatures of blend and grafted copolymer of the present study exhibited similar trend as reported by Meena *et al*. (2008) (Table 2).

Therefore, this study brings forth the fact that agars of different sources can have potentially useful effects on the blend as well as on its derivatives, offering rewarding opportunities in new application domains. This study further reassures the merits of bioprospecting work leading to materials and resources security.

## Acknowledgements

## References

1. Alarcon, C. D. L., Pennadam, S., Alexander, C., 2005. Stimuli responsive polymers for biomedical applications. Chem. Soc. Rev.,*34*, 276.

2. Araki, C., 1966. Some recent studies on the polysaccharides of agarophytes. Proc. Int. Seaweed Symp*., 5,* 3.

3. Athawale, V. D. and Padwaldesai, M. P., 1999**.** Free radical graft copolymerization of methacrylamide onto agar European Polymer Journal, 35, 1237.

4. Bae, Y. H., 1997. ''Controlled Drug Delivery, Challenge and Strategies,''American Chemical Society, Washington, DC.

5. Bajpai, S. K. and Thankhiwale, R., 2006. Investigation of water uptake behavior and stability of calcium alginate/chitosan bi-polymeric beads: Part-1. Reactive & Functional Polymers*,* 66, 645.

6. Bhattarai, N., Ramay, H. R., Gunn, J., Matsen,F. A., M. Zhang, 2005. PEG-grafted chitosan as an injectable thermosensitive hydrogel for sustained protein release. J. Controlled Release*, 103*, 609.

7. Chhatbar, M. U., Godiya, C. B., Siddhanta, A. K. 2012a. Functional modification of agarose: A facile synthesis of an agarose-saccharate derivative. Carbohydr. Polym*., 88,* 1123.

8. Chhatbar, M.U., Meena, R., Prasad, K. and Siddhanta, A.K. 2009. Agar/sodium alginate-graft -polyacrylonitrile, a stable hydrogel system. Ind. J. Chem*., 48A*, 1085.

9. Chhatbar, M. U., Meena, R., Prasad, K., Chejara, D. R. & Siddhanta, A. K. 2011. Microwave induced facile synthesis of watersoluble fluorogenic alginic acid derivatives. Carbohydrate Research, 346(5), 527–533.

10. Chhatbar, M. U., Prasad, K., Chejara, D. R., Siddhanta, A. K. 2012b. Synthesis of sodium alginate based sprayable new soft gel system. Soft matter, 8 1837-1844.

11. Chhatbar, M. U., Meena, R., Prasad, K. & Siddhanta, A. K. 2009. Microwave assisted rapid method for hydrolysis of sodium alginate for M/G ratio determination. Carbohydrate. Polymers, 76, 650–665.

12. Chen, T., Embree, H. D., Brown, E. M., Taylor, M. M., Payne, G. F. 2003. Enzyme-catalyzed gel formation of gelatin and chitosan: potential for in situ applications. Biomaterials*, 24*, 2831.

13. Craigie, J. S. and Leigh, C., 1978. Carrageenans and Agars.  In Hellebust JA, Craigie JS (eds), Handbook of Phycological Methods. Cambridge Univ. Press, Cambridge, 109.

14. De, S. K., Aluru, N. R*.,* Johnson, B., Crone, W. C., Beebe, D. J*.,* Moore, J., 2002. Equilibrium swelling and kinetics of pH-responsive hydrogels: Models, experiments, and simulations. J Microelectromechanical Systems, 11(5)*,* 544.

15. Dong, L. C., Hoffman, A. S. J. 1991. A novel approach for preparation of pH-sensitive hydrogels for enteric drug delivery. *Controlled Release, 15*,141.

16. Ertesvag, H., Valla, S. 1998. Biosynthesis and applications of alginates. Polym. Degrad*. Stabil., 59,* 85.

17. Hu, S. H. Liu,T. Y., Liu, D. M., Chen, S. Y. 2007. Controlled pulsatile drug release from a ferrogel by a high-frequency magnetic field. Macromolecules, *40(19)*, 6786.

18. Johnson, F.A., Craig, D.Q.M. Mercer, A.D. 1997.  Characterization of the block structure and molecular weight of sodium alginates. J. Pharm. Pharmacol*., 49,* 639.

19. Ju, X., Xie, R., Yang, L., & Chu, L., *Expert Opin. Ther. Patents,* **2009**, *19(5),* 683. Kikuchi, A., Okano, T. 2002. Biodegradable 'intelligent'materials in response to chemical stimuli for biomedical applications. Adv. Drug Del. Rev., *54(1),* 53.

20. Meena, R., Chhatbar, M., Prasad, K. & Siddhanta, A. K. 2008. Development of a robust hydrogel system based on agar and sodium alginate blend. Polym Int, 57, 329–336.

21. Meena, R., Prasad, K. & Siddhanta, A. K. 2007. Effect of genipin, a naturally occurring crosslinker on the properties of kappacarrageenan. J Appl Polym Sci, 104, 290–296.

22. Meena, R., Prasad, K., Siddhanta, A. K. 2009. Development of a stable hydrogel network based on agar–kappa-carrageenan blend cross-linked with genipin. Food Hydr, *23*, 497.

23. Meena, R., Chhatbar, M.U., Prasad, K. and Siddhanta A.K., 2011. Microwave assisted synthesis of pH-responsive swellable adducts of chitosan–polyuronic acids. *Carbohydrate Polymers*, *83*, 1402.

24. Mehta, G. K., Meena, R., Prasad, K., Ganesan, M. and Siddhanta, A. K. 2010. Preparation of galactans from *Gracilaria debilis* and *Gracilaria salicornia* (Gracilariales, Rhodophyta) of Indian waters. *J. Appl. Phycol.* 22: 623–7.

25. Mehta, G. K., Kondaveeti S., Siddhanta A. K. 2011. Facile synthesis of agarose-l-phenylalanine ester hydrogels. *Polym.Chem.*, *2*, 2340.

26. Mehta, A. S., Mody, K. H., Iyer, A., Ghosh, P. K., *Ind. J. Chem. Tech.,* **2008**, *15*, 45.

27. Mehta, A. S., Mody, K. H., Iyer, A. and Ghosh, P. K. 2008. Preparation of semi-refined k-carrageenan: recycling of alkali solution and recovery of alkali from spent liquor. Ind. J. Chem. Tech. 15: 45–52.

28. Nishi, S., Kotaka,T. 1989. Complex-forming polyoxyethylene: poly (acrylic acid) interpenetrating polymer networks III. Swelling and mechanochemical behavior. *Polym. J.*, *21*, 393.

29. Oza, M. D., Mehta G. K., Kumar S., Meena, R.., & Siddhanta, A. K. 2011. Galactans from Gracilaria millardetii and G textorii (Gracilariales, Rhodophyta) of Indian waters. *Phycological Research*, *59,* 249.

30. Oza, M. D., Meena, R., Prasad, K., Paul, P. & Siddhanta, A. K. 2010. Functional modification of agarose: A facile synthesis of a fluorescent agarose–guanine derivative. Carbohydrate Polymers, 81, 878–884.

31. Oza, M. D., Meena, R., Siddhanta, A.K. 2012a. Facile synthesis of fluorescent polysaccharides: Cytosine grafted agarose and kcarrageenan. Carbohydrate Polymers, *87,* 1979.

32. Oza, M. D., Prasad, K., Siddhanta, A. K. 2012b. One-pot synthesis of fluorescent polysaccharides: adenine grafted agarose and carrageenan. Carbohydrate Research, *357*, 23-31.

33. Plunkett, K. N., Berkowski, K. L., Moore, J. S. 2005. Chymotrypsin responsive hydrogel: application of a disulfide exchange protocol for the preparation of methacrylamide containing peptides *Biomacromolecules, 06,* 632.

34. Pourjavadi, A., Barzegar, S., Zeidabadi, F. 2007. Synthesis and properties of biodegradable hydrogels of κ-carrageenan grafted acrylic acid-co-2-acrylamido-2-methylpropanesulfonic acid as candidates for drug. Reactive & Functional Polymers, *67*, 644.

35. Prasad, G., Prasad, K., Meena, R., Siddhanta, A. K. 2009. Facile preparation of Chaetomorpha antennina based porous polysaccharide–PMMA hybrid material by radical polymerization under microwave irradiation. J. Mat. Sci. *44*, 4062.

36. Prasad, K., Meena, R. and Siddhanta, A. K. 2006a. Microwave induced rapid onepot synthesis of kcarrageenangPMMA copolymer by potassium persulphate initiating system. J Appl polym Sci*., 101*, 161.

37. Prasad, K., Mehta, G., Meena, R. and Siddhanta, A. K. 2006b .Hydrogelforming agar*graft*PVP and kcarrageenan*graft*PVP blends: Rapid synthesis and characterization. J Appl polym Sci*., 102,* 3654.

*38.* Prasad, K., Siddhanta, A. K., Rakshit, A. K., Bhattacharya, A. and Ghosh, P. K. 2005a. On the properties of agar gel containing ionic and non ionic surfactants. Int J Biol Macromol*., 35*, 135.

39. Prasad, K., Trivedi, K., Meena, R. and Siddhanta, A. K., 2005b. Physical modification of agar: Formation of agarfatty acid complexes. Polymer Journal, *37,* 826.

40. Qiu, Y., Park, K. *2001.* Environment-sensitive hydrogels for drug delivery. Adv. Drug Deliv. Rev. *53*, 321.

41. Sershen, S., West, J. 2002 Implantable, polymeric systems for modulated drug delivery. *Adv. Drug Deliv. Rev., 54*, 1225.

42. Serizawa, T., Wakita, K., Akashi, M. 2002. Rapid Deswelling of Porous Poly(N-isopropylacrylamide) Hydrogels Prepared by Incorporation of Silica Particles. Macromolecules*, 35*, 10.

43. Shah, S. B., Patel, C. P. and Trivedi, H. C. 1995. Ceric-induced grafting of acrylate monomers onto sodium alginate. *Carbohy. Polym.*, *26,* 61.

44. Sharma, B. R., Kumar, V. and Soni, P. L. 2003. Carbamoylethylation of Cassia tora gum. Carbohy. Polym*., 54,* 143.

45. Siddhanta, A.K., Meena, R., Prasad, G., Chhatbar, M.U., Mehta, G.K., Oza, M.D., Kumar, S., Prasad, K., Development of carbohydrate polymer based new hydrogel materials derived from seaweed polysaccharides in ″Handbook of Carbohydrate

Polymers: Development, Properties and Applications" Ito, Ryouichi and Matsuo, Youta (Eds), Chapter 17. Series: Polymer Science and Technology, ISBN: 978-1-60876-367-2. NOVA Science Publishers Inc., New York, **2010**, pp 555-582.

46. Yamato, M., Konno, C., Utsumi, M., Kikuci,A., Okano,T. 2002. Thermally responsive polymer-grafted surfaces facilitate patterned cell seeding and co-culture. Biomaterials, *23,* 561.

47. Yeo, Y., Kohane,D. S. 2008. Polymers in the prevention of peritoneal adhesions. *Eur. J. Pharm. Biopharm.*, *68(1)*, 57.

48. Zhang, J., Nicholas, A. 2000. Synthesis and Characterization of pH- and Temperature-Sensitive Poly(methacrylic acid)/Poly(N-isopropylacrylamide) Interpenetrating Polymeric Networks*Macromolecules*, *33*, 102.

**Figure captions**

**Figure 1** Repeating dimeric unit of agaroid

**Figure 2** Repeating unit of MG block of sodium alginate

**Figure 3** Reaction scheme for graft copolymerization

**Figure 4** Equilibrium swelling (ES) behavior of agaroid/alginate blends in aqueous media (a) in pH 1.2, (b) pH 7.0 and (c) pH 12.5.

**Figure 4** Equilibrium swelling (ES) behavior of agaroid/alginate blends in aqueous media (a) in pH 1.2, (b) pH 7.0 and (c) pH 12.5

**Figure 5** Equilibrium swelling (ES) behavior of agaroid/alginate blends-*graft*-PAAm in aqueous media (a) in pH 1.2, (b) pH 7.0 and (c) pH 12.5

**Figure 5** Equilibrium swelling (ES) behavior of agaroid/alginate blends-*graft*-PAAm in aqueous media (a) in pH 1.2, (b) pH 7.0 and (c) pH 12.5

**Figure 6** FT-IR spectra of (a) sodium alginate, (b) agaroid (c) agaroid/alginate blend, (d) (agaroid/alginate)-*graft*-PAAm, (e) AAm

**Figure 7** TGA of parent polysaccharides and grafted copolymer

**Figure 8** X-ray diffraction patterns of agaroid, sodium alginate and (agaroid/alginate blend)-*graft*-PAAm

**Figure 9** SEM images of (a) agaroid (b) sodium alginate (c) agaroid/alginate blend (d) PAAm and (e) agaroid/alginate blend-*graft*-PAAm.

**Figure 1** Repeating dimeric unit of agaroid

1, 3 linked-β-D-galactose

1, 4 linked-α-L-3, 6 anhydro galactose



L-Guluronic acid

D-Mannuronic acid

**Figure 2** Repeating unit of MG block of sodium alginate

**(a)**

pH 1.2
- Agar hydrogel
- Blend (agar:alginate 1:0.25) hydrogel
- Blend (agar:alginate 1:0.50) hydrogel
- Blend (agar:alginate 1:0.75) hydrogel

**(b)**

pH 7.0
- Agar hydrogel
- Blend (agar:alginate 1:0.25) hydrogel
- Blend (agar:alginate 1:0.50) hydrogel
- Blend (agar:alginate 1:0.75) hydrogel

**Figure 4** Equilibrium swelling (ES) behavior of agaroid/alginate blends in aqueous media (a) in pH 1.2, (b) pH 7.0 and (c) pH 12.5
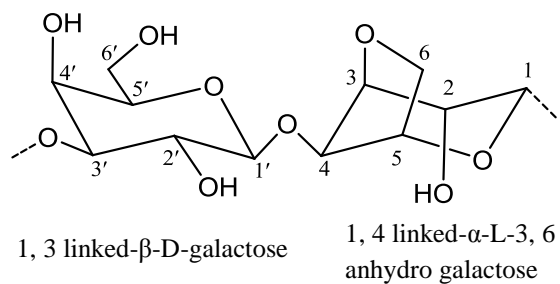
**Figure 5** Equilibrium swelling (ES) behavior of agaroid/alginate blends-*graft*-PAAm in aqueous media (a) in pH 1.2, (b) pH 7.0 and (c) pH 12.5

**Figure 6** FT-IR spectra of (a) sodium alginate, (b) agaroid (c) agaroid/alginate blend, (d) (agaroid/alginate)-*graft*-PAAm, (e) AAm
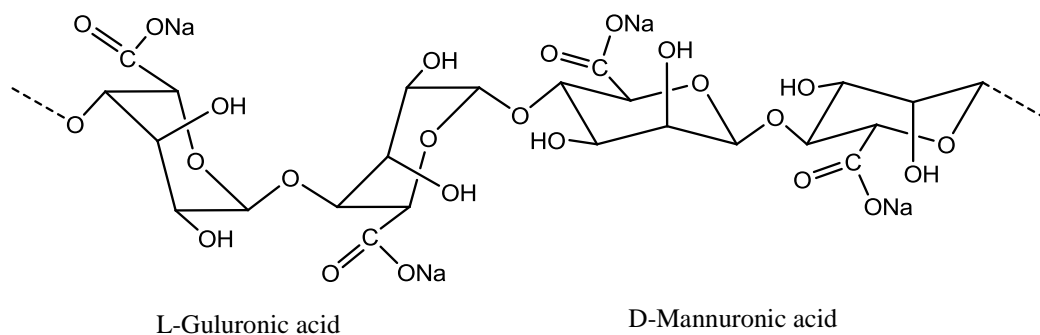


**Figure 7** TGA of parent polysaccharides and grafted copolymer

**Figure 8** X-ray diffraction patterns of agaroid, sodium alginate and (agaroid/alginate blend)-*graft*-PAAm
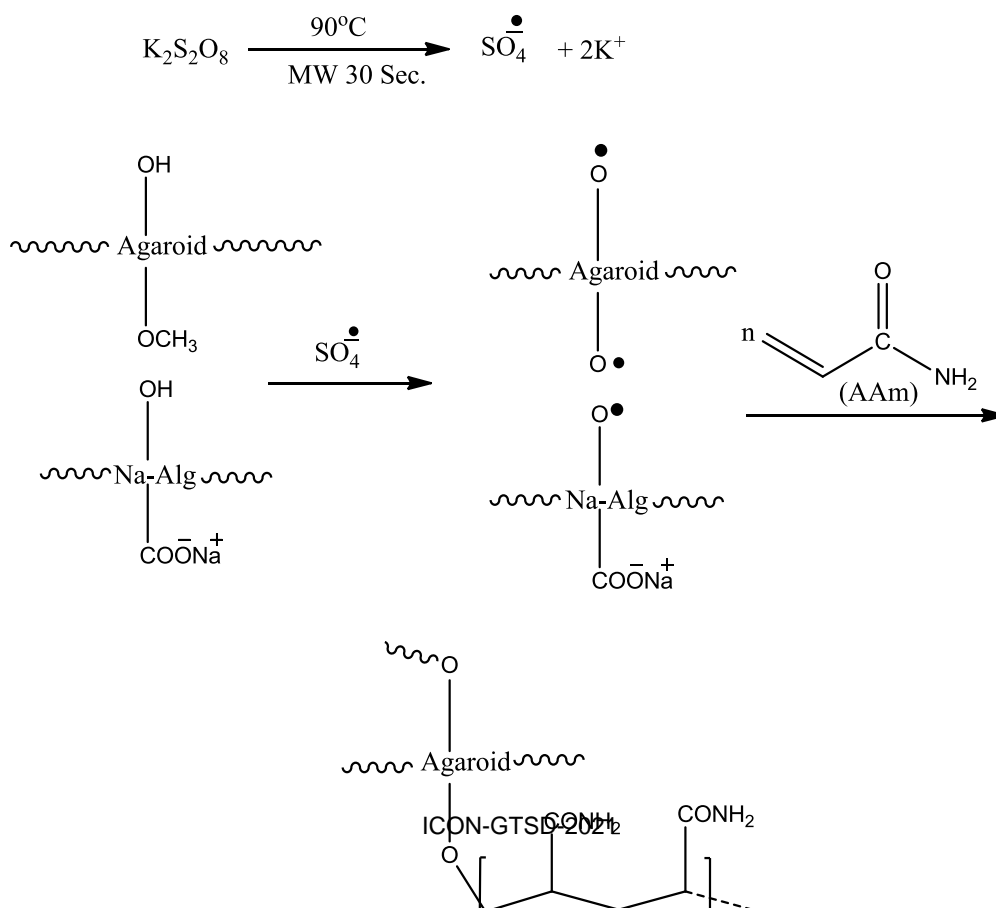


**Figure 9** SEM images of (a) agaroid (b) sodium alginate (c) agaroid/alginate blend (d) PAAm and (e) agaroid/alginate blend-*graft*-PAAm.
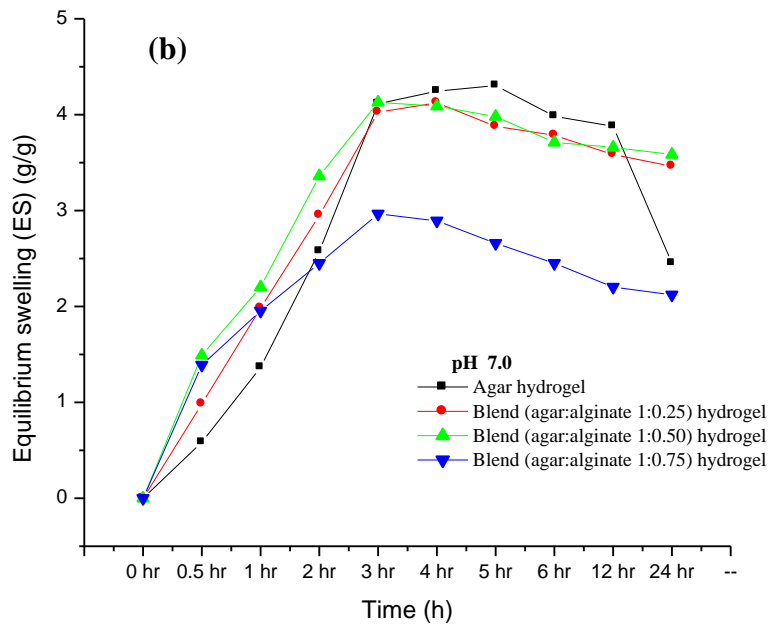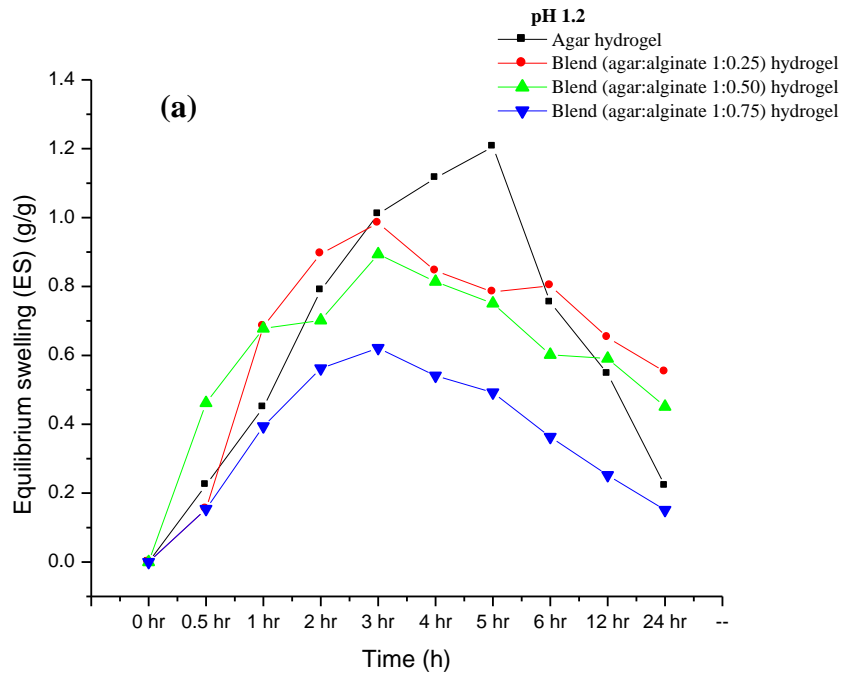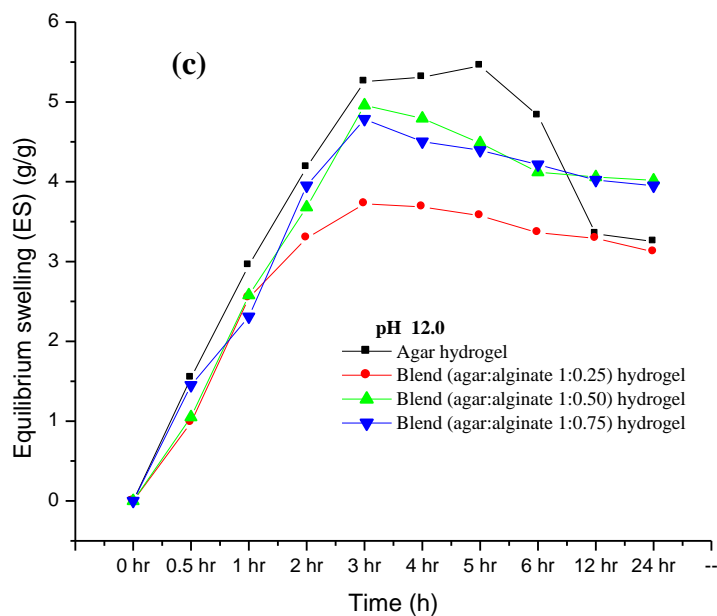
**Table 1** Equilibrium swelling (ES) values of agaroid and agaroid/alginate blend hydrogel samples [a]

| Hydrogel products | ES (g/g) pH 1.2 | ES (g/g) pH 7.0 | ES (g/g) pH 12.5 |
|---|---|---|---|
| Agaroid | 2.0[b] ± 0.2 | 5.1 ± 0.2 | 6.2 ± 0.2 |
| Sodium alginate (Na-Alg) | DNS | D | D |
| Agaroid/Alginate blend (1:0.25) | 1.9[b] ± 0.2 | 5.0 ± 0.2 | 4.7 ± 0.2 |
| **Agaroid/Alginate blend (1:0.5)** | **1.8 ± 0.2** | **5.0 ± 0.2** | **5.9 ± 0.2** |
| Agaroid/Alginate blend (1:0.75) | 1.6 ± 0.2 | 3.9 ± 0.2[c] | 5.7 ± 0.2 |
| Agaroid/Alginate blend-*graft*-PAAm (1: 0.5 : 0.5) | 1.25± 0.2 | 4.1 ± 0.2 | 5.8± 0.2 |
| **Agaroid/Alginate blend-*graft*-PAAm (1: 0.5 : 1)** | **1.5± 0.2** | **4.2± 0.2** | **3.9± 0.2** |
| Agaroid/Alginate blend-*graft*-PAAm (1: 0.5 : 1.5) | 1.3± 0.2 | 4.0± 0.2 | 3.8± 0.2 |
| **(Meena *et al.*, 2008)** | | | |
| Agar | 6.0± 0.4 | 5.0±0.2 | 5.0±0.2 |
| Agar /Alginate blend | 14.0± 0.6 | 12.0± 0.4 | 8.5± 0.42 |
| **Agar /Alginate blend-*graft*-PAAm (1:1.2:0.03)** | 24.0± 0.4 | 18.0± 0.2 | 11.0± 0.5 |

[a]Data presented are mean of triplicate measurements; [b,c] products got dispersed after 2 h and 0.16 h swelling in respective aqueous media; DNS=did not swell;  D= Dispersed

**Table 2** Physical properties of the agaroid, alginate, agaroid/alginate blends and (agaroid/alginate blend)-*graft*-PAAm and grafting parameters[e]

| Product | App. Visc.[a,b] (cp) | pH[b] | Gel strength[a,c] (g cm^{-2}) | Gelling temp. (°C) | Melting temp. (°C) | Grafting parameters C% | G% | E% |
|---|---|---|---|---|---|---|---|---|
| Agaroid | 6.6 ± 1 | 7.4± 0.1 | <100 | 38 ± 0.5 | 83±0.5 | NA[d] | NA[d] | NA[d] |
| Sodium alginate | 19.1 ± 1 | 7.1± 0.1 | NA[d] | NA[d] | NA[d] | NA[d] | NA[d] | NA[d] |
| Agaroid /alginate blend (1:0.25) | 6.2 ± 1 | 7.1± 0.1 | <100 | 36±0.5 | 79 ± 0.5 | NA[d] | NA[d] | NA[d] |
| **Agaroid /alginate blend (1:0.5)** | **6.0 ± 1** | **7.1± 0.1** | <100 | **34±0.5** | **66 ±0.5** | **NA[d]** | **NA[d]** | **NA[d]** |
| Agaroid /alginate blend (1:0.75) | 5.8 ± 1 | 7.2± 0.1 | < 100 | 31±0.5 | 66 ±0.5 | NA[d] | NA[d] | NA[d] |
| Agaroid /alginate blend -*graft*-PAAm (1:0.5:0.5) | 6.4 ± 1 | 6.9± 0.1 | <100 | 30±0.5 | 71±0.5 | 84 ± 0.5 | 40.0± 0.5 | 80.0± 0.5 |
| **Agaroid /alginate blend -*graft*-PAAm (1:0.5:1)** | **7.2 ± 1** | **6.8± 0.1** | <100 | **28±0.5** | **57±0.5** | **86.0 ± 0.5** | **81.0 ± 0.5** | **81.0 ± 0.5** |
| Agaroid /alginate blend -*graft*-PAAm (1:0.5:1.5) | 7.2 ± 1 | 6.8± 0.1 | < 100 | 28 ±0.5 | 56±0.5 | 90.0 ± 0.5 | 118± 0.5 | 78.6± 0.5 |

# Pretreatment of biopolymer composite to manufacture sustainable green geotextile: A Review

Prof. Samirsinh P Parmar*, Dr. Atindra Shukla[2]

[1] Dharmasinh Desai University, Nadiad.
spp.cl@ddu.ac.in, (+91-9427619628)
[2]Shah-Schulman Nano technology and Surface science center, Dharmasinh Desai University, Nadiad, Gujarat, India.

**Abstract**

Application of geotextile for various geotechnical projects are increasing and hence geotextiles are subjected to the severe exposure conditions. The disintegration of polymeric geotextile creates pollution in environment. The present world order advocates use of natural geotextile material with additional pretreatment to maintain sustainability and lesser carbon footprint. The attempts were made to treat the natural polymers by chemicals as well as blending them with synthetic polymers by researchers in last two decades. The synthetic and natural polymers were treated by various chemicals by conventional coating techniques. The resultant product can be designated as "biopolymer composite". With the extended use of nanotechnology, the coating of biopolymers started by nano material. The present paper describes about the attempts made by researchers for nano technology application to treat biopolymer composites and the effect of pretreatment of the same. The effect of pretreatment by nanotechnology indicates improvement in physical and mechanical properties of biopolymer composite can be used to manufacture sustainable geotextile.

*Key words:* *Natural fibers, green geotextile, sustainable material, nano-modified geotextile, properties of nano-modified geotextiles.*

## 1. Introduction:

Geotextile materials are textile materials manufactured by either synthetic or natural polymeric fibers. The Geotextile Market size is projected to reach $10 billion by 2025, with CAGR growth of 9.6 per cent by 2020-2025. Polymeric geotextile lefts huge carbon footprint and remains there in the buried soil for years even after failure and degradation. The small fragments of broken geotextiles can act as a pollutant for soil. The application of natural geotextile is now a days enhanced for moderately durability governed projects in geotechnical engineering. Figure – describes classification of fibers and its derivation from various resources, which can be used to manufacture geotextiles. Natural geotextile materials are used to achieve economy in a geotechnical project to perform various functions. The major shortcoming of the natural geotextiles is physical degradation, bio degradable and highly susceptible to chemicals. The durability of Natural geotextiles is less compared to polymeric geotextiles.
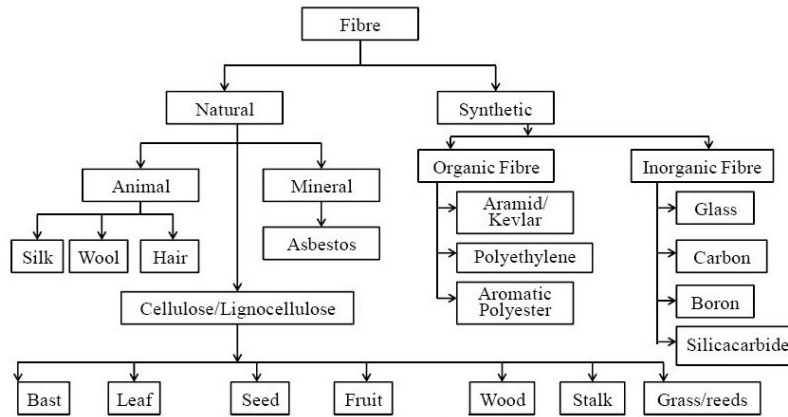
**Fig. 1. Classification of natural and synthetic fibers. (After Jawaid M., 2011)**

Zhu J. et al. (2013) studied and summarized the advantages and shortcomings of both natural and synthetic fibers, used to manufacture geotextile basically applicable for the function of soil reinforcement. The comparison of pros and cons of both natural versus synthetic fibers are tabulated in table-1.

**Table-1 comparative properties of natural versus synthetic geotextiles.**

| Geotextile | Advantages | Disadvantages |
|---|---|---|
| Geotextile from Natural fibres | Biodegradable | Biodegradable - Moderately durable |
| | Low density | Non homogeneous material |
| | Economical | Dimensional irregularity |
| | Natural Availability | Attracts moisture |
| | UV resistant | Not wrinkle free |
| | Less skill required to manufacture | inherent Modification is not possible |
| Geotextile from Synthetic fibres | Moisture resistance | Difficult to recycle |
| | Controlled mechanical properties | Relatively high price |
| | Designed as per Desirable mechanical properties | High carbon footprint |
| | Mostly hydrophobic | UV Susceptible |
| | Inherent Modification is possible | |
| | Non bio degradable | |

## 1.1.Base Material of natural geotextiles:

There are three types of natural fibers: plant fibers, animal fibers, and mineral fibers. Among these fibers, plant fibers have become the first option for natural geotextiles due to rich sources, fast extraction, low cost and superior efficiency.

The properties of natural fibers differ from type to type. Natural geotextiles commonly prefer natural fibers with high mechanical properties as raw materials. Table-2 details the structure and properties of natural fibers widely used for the development of natural geotextiles. Among the fabrics, the jute and coir fibers, because of their superior performance become the best research materials for natural geotextiles, and many commercial products are available.

**Table 2 Composition and properties of natural fibers commonly used to make natural geotextiles. (after Arifuzzaman, 2009)**

| Type of fiber | Cellulose (wt.%) | Lignin (wt.%) | Hemicellulose (wt.%) | Density (g/m3) | Strain at Break (%) | Tensile Strength (Mpa) | Youngs Modulus (Mpa) |
|---|---|---|---|---|---|---|---|
| Flex | 71-78 | 2.2 | 18.6 - 20.6 | 1.4 - 1.5 | 1.2 -3.2 | 345 -1500 | 27.6 - 80 |
| Hemp | 57-77 | 3.7-13 | 14 - 22.4 | 1.48 | 1.6 | 550 - 900 | 70 |
| Jute | 45-71.5 | 12-26 | 13.6 - 21 | 1.3 - 1.46 | 1.5 -1.8 | 393 - 800 | 10 - 30 |
| Kenaf | 31-57 | 15-19 | 21.5 - 23 | 1.2 | 2.7 - 6.9 | 295 - 930 | 22 -60 |
| Ramie | 68.6-76.2 | 0.6 -0.7 | 5 - 16.7 | 1.5 | 2 - 3.8 | 220 - 938 | 44 -128 |
| Nettle | 86 | 5.4 | 4 | 1.51 | 1.7 | 650 | 38 |
| Sisal | 47-78 | 7-11 | 10 -24 | 1.33 -1.5 | 2 -14 | 400 - 700 | 9 -38 |
| Abaca | 56-63 | 7-9 | 21.7 | 1.5 | 2.9 | 430 - 813 | 33.1 - 33.6 |
| Cotton | 85-90 | 0.7-1.6 | 5.7 | 1.21 | 3 -10 | 287 - 597 | 5.5 - 12.6 |
| Coir | 36-43 | 41-45 | 0.15 - 0.25 | 1.2 | 15 - 30 | 175 - 220 | 4 - 6 |

Due to the biodegradability of natural fibres, the performance of natural geotextiles will decrease with the passage of time, which will lead to the failure of later reinforcement when used in road construction (Basu G., 2019). In recent years, scholars have found that the long-term durability of natural geotextiles is not particularly crucial for strengthening the stability of rural highway subgrade. In India, a growing number of natural geotextiles are used to strengthen the subgrade of rural roads (Sarsby R.W., 2007). This is because the natural geotextiles have high initial tensile strength, which makes the subgrade bear low stress during the construction and operation period of the road. Then, with the passage of time, the consolidation and compaction of the subgrade soil occur under the traffic load, so the bearing capacity is enhanced.

Natural geotextiles may also be used for medium and short-term filtration or drainage and natural fibers have the potential to extract heavy metals Abbar et al. (2017,18). Abbar et al. (2019) Analyzed of the effect of linen geotextile on soluble heavy metals using sand-filter and flax geotextile filters. The results showed that flax geotextile enhanced the ability of the filter to maintain soluble metals, and Inserted heavy metals. Natural geotextiles therefore have significant advantages in the filtration of soluble heavy metals. However, the hygroscopicity of plant fibers entails crucial problems in the absorption and expansion of water. It is found that jute geotextile, as a drainage medium, is feasible and economical to deal with drainage problems encountered in geotechnical engineering (Chattopadhyay B. 2009). Owing to the high-water absorption, the pore diameter of the filter is diminished significantly. In the worst case, this will lead to filter plugging and an absolute loss of permeability.

## 2. Modification of natural geotextiles

### 2.1. Chemical modification and blending of synthetic fibers.

According to the above application of natural geotextiles, it can be found that the early biodegradation of natural geotextiles is the primary problem that restricts the further functionality of natural geotextiles (Prambauer M., 2019). Most of the research done in natural geotextiles over the last two decades has concentrated at how to enhance the durability of natural geotextiles. Table 4. outlines the methods used to improve the efficiency of natural geotextiles in recent years.

**Table 3 Study on improving the properties of natural geotextiles by chemical modification.**

| Method | Type of Geotextile | Sr. No. | Research | Effect | Ref. |
|---|---|---|---|---|---|
| **Chemical Modification** | **Jute Geotextiles** | 1 | Esterification of Jute Geotextiles | Stretching and chemical degradation resistance enhanced | Saha P. et al. (2012), Midha V.K. et al. (2017) |
| | | 2 | Laccase treatment of Jute geotextile | Physical properties and Surface hydrophobicity are improved | Dong A. et al. (2016) |
| | | 3 | Isothiazoline and Fluorocarbon derivatives | Improvement of Antimicrobial and Water-proof performance | Chakrabarti S. et al. (2016) |
| | **Coir Geotextiles** | 1 | Durability studies of Surface modified geotextiles | The surface modified geotextiles retained more than 70% of their initial tensile strength after one year. | Sumi S. et al. (2016), Sumi S. et al. (2017), Sumi S. et al. (2018) |
| | | 2 | Lime treatment | Lime treatment promotes the initial retention of cellulose in natural fibers compared with untreated Kenaf. | Liehr S. et al. (2008) |
| | **Kenaf Geotextiles** | 1 | Alkaline Treated | The tensile strength of the geotextile treated with 6% NaOH is increased by 51.0 %. | Shirazi, M.G et al. (2019) |

At present, the main methods for enhancing the properties of natural geotextile are the incorporation of a certain quantity of synthetic fiber or the chemical treatment of natural geotextile. Adding a certain quantity of synthetic fiber will enhance the physical and mechanical properties of natural geotextiles. These natural fiber/polymer composite geotextiles, such as jute/PET geotextiles, jute/PP geotextiles and nettle/polylactic acid geotextiles, exhibit excellent performance in various tests.

**Table 4 Study on improving the properties of natural geotextiles by blending.**

| Method | Types of Geotextiles | Research | Effect | References |
|---|---|---|---|---|
| **Blending synthetic fiber** | Nettle/ PLA geotextiles | Tests on tensile strength, biodegradability and soil fertility enhancement | The geotextiles are promising for slope stabilization application | Kumar N. et al. (2018) |
| | Jute/ Polypropylene geotextiles | Treatment of jute/PP Nonwoven Geotextile with Alkali | Tensile properties and puncture resistance were improved | Jaafar J. et al. (2019), Koohestani B. et al. (2019) |
| | | Mechanical Properties and Damage analysis of Jute/Polypropylene Nonwoven Geotextile | Compared with PP geotextiles, 40/60 jute/PP geotextiles have higher tensile strength and secant modulus | Rawal A. et al. (2014) |

The reinforcing benefits of treated coir fiber and lime on the engineering properties of marine clay have been studied by Vivi Angrainni et.al;(2016). Results from the experimental investigation showed that the shear strength and durability of natural coir fibers were enhanced by lime and treated fibers. Moreover, an improvement in the effective stress internal friction angle and the cohesion intercept were observed. Table-4 deliniates the types of pretreatment carried out on natural fibers and its effects on geotextile product.

The effect of treated coir fiber on the tensile strength of the soil and its contact with the soil was studied in N. Farzadnia, H. Jahangirian et.al;(2016). Various tests, such as unconfined compressive strength tests, indirect tensile strength tests, flexural strength tests, and triaxial compressive strength tests, have been carried out. Because of the tensile strength of the enhanced fibers, the findings showed that treated fibers improved the mechanical properties of the lime-treated clay soil. The findings showed that the compressive strength increased by 64%, while the indirect tensile strength increased by 122% and the flexural strength increased by 56% of samples treated with modified coir compared to those treated with unmodified fibers.

Vishwas N. Khatri, Rakesh K. Dutta et.al., (2015), investigated the effect on the shear strength action of clay of treated coir fibers. The findings showed that the tension of the deviator at the failure of the clay could be increased by inserting coir fiber treated in the clay. A substantial increase was also observed in shear strength parameters with different percentages of clay reinforced with coir fibers. The clay reinforced with untreated/treated coir fibers has shown improved strength behavior, it can be used for short term stability problems.

## 2.1 Natural and synthetic polymers composites:

Hybrid bio composites are designed primarily and processed by a conjunction of synthetic fiber and natural fiber (biofiber) in a matrix or by a fusion of multiple natural fibers/biofibers in a matrix. The behavior of composite materials is the weighted sum of the individual components. Hybrid composite properties are exclusively governed by the length of the individual fibers, the orientation, the fiber to the matrix bonding, the content, the extent of the intermingling of the fibers and the arrangement of the two fibers. The rule of mixtures may be used to determine the properties of a hybrid system consisting of two components. In addition, the successful use of hybrid composites is determined by the mechanical, chemical and physical stability of the fiber/matrix system. Several researchers have developed hybrid composites by combining natural fibers with polyurethane resins, phenolic, polyester, epoxy, polyvinyl ester, etc. as polymeric matrices. Table 6 shows the reported and exclusive work on cellulose/synthetic and cellulose/cellulose reinforced hybrid composites.

**Table 5 Reported work on hybrid Composites**.

| Sr. No. | Natural Fiber | Polymer Matrix | References | References |
|---------|---------------|----------------|------------|------------|
| 1 | Palmyra/glass | Roofilite resin | 91,92 | Velmurugan, R.; et al. (2005), Velmurugan, R.; et al. (2007) |
| 2 | Bamboo/glass | Vinyl ester | 93 | Mandal, S.et al. (2010) |
| 3 | Coir | Phenolic resin | 96 | Kumar, N.et al. (2009) |
| 4 | Jute/Glass | Polyester (isothalic) | 94,95 | Ahmed, K.S.et al. (2007), Ahmed, K.S.et al. (2008) |
| 5 | Jute/Glass | Polypropylene (PP) | 105 | Esfandiari, A.et al. (2007) |
| 6 | Jute/biomass | Bisphenol-C-Formaldehyde | 99 | Mehta, N.M.et al. (2006) |
| 7 | Jute/Cotton | Novolac phenolic | 104 | De Medeiros, E.S.et al. (2005) |
| 8 | Cotton/waste Silk | Polycarbonate (PC) | 108 | Taşdemır, M.et al. (2008) |
| 9 | Sisal/Kapok | Unsaturated Polymer | 100 | Venkata Reddy, G.et al. (2009) |
| 10 | Oil Palm/ Jute | Epoxy resin | 101 | Jawaid, M. et al. (2010) |
| 11 | Kenaf/ Glass | Epoxy resin | 102 | Davoodi, M.M.et al. (2010) |
| 12 | Kenaf/ Glass | Natural Rubber | 107 | Wan Busu, W.N.et al. (2010) |

| 13 | Banana/ Kenaf | Polyester | 97 | Thiruchitrambalam, M.et al. (2009) |
|----|---------------|-----------|----|-----------------------------------|
| 14 | Cellulose /Glass | Epoxy resin | 103 | Kong, K. et al. (2009) |
| 15 | Flax/Glass | Polypropylene (PP) | 106 | Arbelaiz, A.et al. (2005) |
| 16 | Wood flour/glass | Polyvinyl Chloride (PVC) | 109 | Jiang, H. et al. (2003) |

## 2.2 Natural filler reinforced polymer nanocomposites

Nanocomposites are considered to belong to groups called nanomaterials, where a nano-object (particle) is distributed in a matrix (Marquis, D.M.et al. 2011). Generally speaking, nanocomposite is a multi-phase dense material in which at least one of its phases has either one, two or three dimensions of less than 100 nm (Ajayan, P.M. et al. 2003). Nanocomposites have unique characteristics and comparatively better properties than conventional or traditional composites such as glass fiber reinforced composites (Biswas, M.& Ray, S.S. 2001). Nowadays, a significant amount of research and study is underway towards various fillers to form a wide range of nanocomposites. Nano filters in nanocomposite materials are the key components and can be made up of inorganic/inorganic, inorganic/organic, or organic/organic sources. Polymer nanocomposites are polymers (thermoplastics, thermosets or elastomers) which have been reinforced with small quantities (less than 5% by weight) of nano-sized particles having high aspect ratios (L/h > 300) (Denault, J.; Labrecque, B, 2004). The reinforcement of polymeric matrix materials (thermoplastics or thermosets) with nano-sizes, such as nano-size particles, carbon nanotubes or intercalated layers to form nanocomposites, is considered to be an attractive and active area of research. In general, polymer/layer nanocomposites can be classified into three different types, (i) intercalated nanocomposites, (ii) flocculated nanocomposites and (iii) exfoliated nanocomposites (Wypych, F.et al. 2005 and Ray, S.S. et al./ 2003). Significantly larger interfacial matrix material surface (interphase) is presented by nanocomposites, the characteristics of which are quite different from the bulk polymer produced by the high specific surface area of the nanofiller (Schadler, L.S.2007 & Hari, J. 2011). Thus, when the dimensions of polymer fiber materials are restricted or reduced from micrometers to submicron's or nanometers, there are numerous unique characteristics, such as flexibility in surface functionality, a higher surface area to volume ratio (this ratio of nanofiber can be as large as 103 times that of microfiber) and superior mechanical performance (such as stiffness and tensile strength). Recognizing the morphological and mechanical benefits of nanofillers, a number of researchers produced nanocomposites using different polymer matrixes and reinforcing a wide range of clays with enhanced properties. Reported nanocomposite work is shown in Table 8 for a review of nano-and micro-scale particle reinforcement technology in several polymeric fiber reinforced systems, including polyamide (PA), polyimide (PI), polyarylacetylene (PAA), poly (ether ketone) (PEEK), epoxy resin (ER), polyester, polyurethane (PU), and polyp-phenylenebenzobisoxazole (PBO). Researchers demonstrated the different processing techniques in nanocomposites and their corresponding characterization techniques

. Nanocomposites show improvements in mechanical, electrical, thermal and resistant (barrier) properties over conventional composites. In addition, nanoparticles cause a significant reduction in flammability and also preserve the transparency or clarity of the polymer matrix.

**Table 6 List of reported work on nanocomposite type from different polymeric matrix with natural fiber /nanofiller.**

| Sr. No. | Polymer Matrix | Natural Fiber / Nanofiller | References | References |
|---|---|---|---|---|
| 1 | Polyamide 11 (PA-11) | Nano-Clay | 54 | Lin.T et al. (2003) |
| 2 | Polyamide (PA-6) | Montmorillonite (MMT) | 56 | Linconln D.M. et al. (2001) |
| 3 | Polyamide (PA-6) | Organically modified MMT (OMMT) | 57-59 | Fong H. et al. (2001) |
| 4 | Polyamide (PA-6) | Fe2O3 particles | 60 | Liang, Y. et al. (2007) |
| 5 | Polyurethanes (PU) | Carbon nanotube | 61 | Chen W. et al. (2006) |
| 6 | Polyaniline and sulfonated urethane | Carbon nanotube | 62 | Poulin P. et al. (2002) |
| 7 | Polypropylene (PP) | Nano-Clay | 63 | Roy S. et al. (2004) |
| 8 | Polypropylene (PP) | Nano carbon fiber | 64 | Kumar S. et al. (2002) |
| 9 | Polypropylene (PP) | Nano-Clay | 65 | Zhang X. et al. (2007) |
| 10 | Poly(ethylene) (PE) | Carbon nanotube | 66 | Ruan S.L. et al. (2003) |
| 11 | Ultra-high MW poly(ethylene) (UHMWPE) | Carbon nanotube | 67 | Ruan S.L. et al. (2006) |
| 12 | Polystyrene (PS) | Carbon nanotube | 68 | Ji Y. et al. (2006) |
| 13 | Polystyrene (PS) | Carbon nanotube | 69 | Qian D. et al. (2000) |
| 14 | Poly (ether ether ketone) (PEEK) | Nanoparticles of SiO2 | 70 | Jen M.H.R. et al. (2005) |
| 15 | Poly (ether ether ketone) (PEEK) | Carbon nanofibers CNFs | 71 | Sandler J. et al. (2002) |
| 16 | Poly (ether ether ketone) (PEEK) | organo-alkoxysilanes | 72 | Schmidt, H. et al. (1994) |
| 17 | Poly (ether ether ketone) (PEEK) | SiC nanoparticles. | 73,74 | Lin J. et al. (1992), Wang Q.H. et al. (2000) |
| 18 | Phenyl ethynyl-terminated imide (PI) | multi-walled carbon nanotube | 75 | Ogasawara, T. et al. (2004) |
| 19 | Polyarylacetylene (PAA) | Carbon fiber | 76 | Fu, H.J. et al. (2004) |
| 20 | Polyarylacetylene (PAA) | carbon fiber/LiAlH4 | 77 | Lin, Z. et al. (201) |
| 21 | Polyarylacetylene (PAA) | Carbon fiber | 78 | Zhang, S. et al. (2007) |
| 22 | Poly p-phenylenebenzobisoxazole (PBO) | SWNT (Single-walled nanotubes) | 79 | Singh, A.P. et al. (2007) |
| 23 | Epoxy resin (ER) | Coir-fiber nano filler | 80 | Sen, A.K. et al. (2010) |

## 2.3 Nano filler (nano-clay) - natural fibre hybrid composites

Natural fiber-reinforced polymer composites have formed an enormous attraction and concern as an innovative material in a number of applications. Although natural fiber–plastic composites have been commercialized, their potential for use in many industries has been limited. The majority of studies in this area therefore focus on improving the physio-mechanical properties and impact resistance of the composites. One way to improve the mechanical properties of bio composites is to develop hybrid composites by combining several types of reinforcement/fillers, such as nano clay with polymers. Nano clay materials are commonly identified for their specific dimension and high aspect ratio in most of the research work (Babaei, I. et al.2014) (Table 8).

**Table 7 Reported work on fiber/ nanofiller hybrid composites.**

| Sr. No. | Matrix | Filler | Reference |
|---|---|---|---|
| 1 | Polyamide (PA-6) | Carbon fiber/ Nano-clay | Wu et al. (2001) |
| 2 | Polyamide (PA-6) | Carbon fiber/glass fiber/ Nano-clay | Wu et al. (2001) |
| 3 | Polyamide (PA-6) | Chopped glass fibers/hectorite-type clays (nano size) | Akkapeddi M.K. et al. (2000) |
| 4 | Polyamide (PA-6) | Glass fiber/layered silicate | Vlasveld D.P. et al. (2005) |

| 5 | Polyamide (PA-12) | Carbon nanotubes and nanofibers | Sandler J.K. et al. (2004) |
|---|---|---|---|
| 6 | Polyester | Nano-clay/ glass fiber | Jawahar P. et al. (2006) |
| 7 | Polyvinyl ester | Organoclay/glass fiber mats | Chandradass J. (2007) |
| 8 | High density polyethylene (HDPE) | Nano-clay/ rice husk | Kord B. (2011) |
| 9 | Ethylene-propylene copolymer | Nano-clay/ cellulose | Singh A.P. et al. (2007) |
| 10 | Polyarylacetylene | Carbon fiber/LiAlH$_4$ | Lin Z. et al (2001) |

## 2.4 Nano modified natural fibers:

Hari and Pukanzsky (2011) and Henrique et al. (2009) have studied that the general idea of nanocomposites is predicated on the notion of creating a very large interface between nanoscale building blocks and the polymer matrix. Very often, the homogeneous distribution of nano-sized particles is problematic. Nanocomposites, a high-performance material, exhibit unusual properties, combinations and unique design capabilities. Aggregation phenomenon is a major issue in composites with spherical nanoparticles. Due to the nanoscale size of the reinforcement phase, the interface-to-volume ratio is significantly higher than in conventional composites. As a result, the volume fraction of the second phase can be reduced, without

Chaudhary B.S. et al. (2012) Studied effect of Nano TiO2 pretreatment on functional properties of cotton fibers. Cotton fabric was prepared by Nano TiO2 particles by Pad-dry-cure technique and the fabric was observed by SEM and elementary analyzed oxford-Inca software using SEM. The pretreatment by nano-TiO2 improved antimicrobial property, UV transmission percentage, tensile strength and self-cleaning action.

Rahman R. et al. (2012) carried out experimental investigation on bamboo fiber polypropylene composites treated with nano-clay. Bamboo fibers were modified with sodium Meta-periodate. Bamboo fiber weight into the nano clay and polypropylene mix was increased from 5 %, 10 %, 15%, 20% and 25 % gradually. Tensile strength test and flexural strength test was carried out for the raw bamboo fibers, bamboo fibers plus clay and bamboo fibers treated with nano clay.

Azam Ali et al. (2016) made comprehensive review for hydrophobic treatment on natural fibers and influence of treatment on its engineering properties were documented. Various hydrophobic treatments such as SiO2, Silane, Acetylation, Mercerization, treatment with isocyanate, Enzyme, Pre-oxide treatment, Benzoylatio, Plasma treatment, Ozone treatment and grafting were discussed thoroughly with respective chemical reactions. Comparison of pre-treatment on natural fiber composite were listed in table-8. Below.

Divya J et al. (2016) prepared cellulose nanofibers from agricultural waste and carried out characterization of the same. Cellulose nanofibers were isolated from a variety of natural fibers like bamboo, pine and neem by chemical treatment, which comprises length of 500nm -10μm. They measured moisture sorption of pine is 1.61 %, neem is 18.425 % and bamboo is 26.185 %.

**Table 8 Type of pretreatment on natural fibers and its effect.**

| Sr. No. | Type of Pre-treatment | Material | Effect | References |
|---|---|---|---|---|
| 1 | Sodium Chlorite treatment | Jute fiber | Significant improvement in tensile strength, young's modulus and extension at break | Arifuzzaman et al. (2009) |

| 2 | Treatment with meta-acrylate | Jute fiber | Improvement in flexural and tensile strength | Cantero G. et al. (2003) |
|---|---|---|---|---|
| 3 | Silane treatment | Flax fibers | Improvement in hydrophobic and mechanical properties | Alix S. et al. (2011) |
| 4 | Acetylation | Flax fibers | Increase in tensile strength and flexural strength | Rao K.M. (2007) |
| 5 | Mercerization | Jute, Flax fibers | Reduction in moisture regain due to better interface and improvement in mechanical properties | Sreekala M. et al. (2000) |
| 6 | Treatment with isocyanate | Flax fibers | Surface modification | Joseph K & Thomast S, (1996) |
| 7 | Enzyme | Flax fibers | Decrease in lignin contents from 35 % to 24 % | Gronqvist S. et al (2003) |
| 8 | Per-oxide treatment | Natural fibers | Decrease in moisture regain | Sreekala M. et al. (2000) |
| 9 | Benzoylation | Sisal fibers | Surface modification and improvement in hydrophobicity | Joseph K. et al. (2000) |
| 10 | Plasma treatment | Natural fibers | Surface modification and improvement in hydrophobicity | Maldas D. et al. (1989) |
| 11 | Ozone treatment | Natural fibers, pulp | Increased the strength properties of polyethylene and pulp composites | Chtourou H. et al. (1997) |
| 12 | Grafting | Natural fibers, wood | Surface modification and improvement in ultraviolet protection properties, hydrophobicity and mechanical properties | |

Pappu A & Thakur V. (2017) invented sustainable micro and nano composites from fly ash and natural fibers for multi-functional applications. Sisal cellulose fibers along with silica and alumina in fly ash was used to manufacture biofiber. The bio composite polymer was tested for reinforcement property indicates good tensile strength. The same bio-polymer was analyzed for biodegradation characteristics, which exhibits recyclable possibilities. The nanoscale biopolymer can be applicable as ingredient in epoxy resins which is used for creating glossy look in interior designing.

**Applications of nano polymers in geotextile engineering**

The sustainable green geotextile is possible solution overcome problem of recycling. The nano modified bio composite is relatively biodegradable and perform superior compared to conventional pure geotextiles made out of either natural or syntenic polymers. There are three ways to incorporate nano technology to manufacture sustainable green geotextiles, which is (i) nano coated natural geotextiles (ii) Nano coating of biopolymer composites geotextile, and (iii) Inclusion of biopolymer or biopolymer composite with nano material (i.e., Nano Clay, nanotube etc.) while manufacture of geotextiles. The variables such as type of natural fibers, nano coating techniques, requirement of synthetic polymers, quantity of addition of nano materials etc. governs the strength and quantitative improvement of the modified fibers. Depend on the severity of exposure condition and requirement of biodegradability the inclusion of material and modification methods can be altered.

The research work reviewed here delineate the improvement in performance of biopolymer composites. The biopolymer admixed with synthetic polymer results into improved thermal stability, flexibility, surface energy, coefficient of friction, hydrophobicity and the like. Tougheners, plasticizers, polymer compatibilizers, impact modifiers, UV shielding agents, and/or stabilizers may be such polymer modifiers.
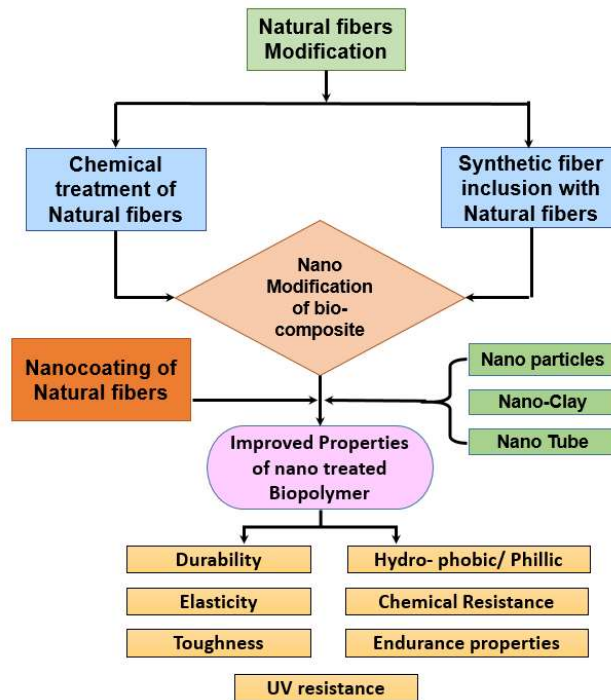
**Fig. 2. Flowchart indicating nanomodification of geotextile and improvement in properties.**

Conventional ingredients include anti-blocking agents, anti-static agents, antioxidants, blowing agents, polymer compatibilizers, crystallization aids, dyes, flame retardants, fillers, impact inhibitors, mold releasing agents, oils, pigments, performance additives, plasticizers, manufacturing agents, reinforcing agents, polymer stabilizers, UV light absorbers, UV light absorber photo stabilizers. The use of the Nano composites described herein and recycled bio-polymer nano composites in geotechnical applications is an important feature of the compositions, papers and methods described herein. Water protection, flood control, pollution control of waste materials, soil stability, green building, and the like are examples of geotechnical applications. Specifically, this factor relates to major changes in the materials used in geotechnical applications. Increasing the tensile strength of the materials, the flexural modulus of the materials, increasing the puncture strength of the materials, decreasing material changes due to time-dependent loading (creep), decreasing the coefficient of linear thermal expansion of the materials, decreasing the transmission of gas through the materials, and increasing the transmission of gas through the materials.

When an intelligent geotextile is applied to the reinforcement of the geotechnical structure, a health monitoring of the geotechnical structure can be carried out in order to ensure that the geotechnical structure and its location of probable failure, and risk of damage can be identified at an early stage. Prevention and repair in advance are conducive to it. The capacity of the intelligent geotextile to track depends on the characteristics of the sensor. At present, the fiber optic sensors assimilated into geotextile comprise mainly fiber optic sensors based on Fiber Bragg grating, fiber optic sensors based on Brillouin scattering, and polymer fiber optic sensors with their own pros and cons. On the other hand, POF sensors with high elasticity, high fracture strain and measuring strain (more than 40%) are more suitable for intelligent geotextiles. In addition to optical fiber sensors, there are several other technologies, such as graphene technology, which can make geotextiles smart.
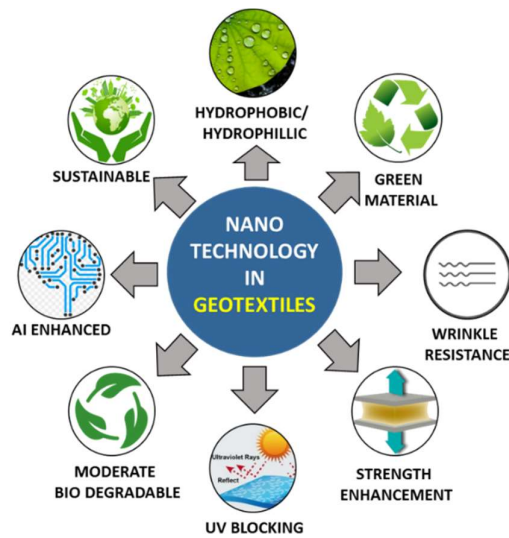
Fig. 3. Applications of Nano-modified fibers as next gen. Geotextiles.

## Conclusion

Partially green to fully green geotextiles are possible to manufacture today. Incorporation of nanotechnology by various techniques at different stages and inclusion of nano materials to natural fibers can enhance the physical, mechanical and chemical properties of geotextiles. Based on exposure condition of geotextile material in various geotechnical projects, the nano material inclusion percentage and coating techniques alters. It has been observed that natural fiber along with synthetic fibers composite are treated with nano materials and improvements in various properties. Nano clay adopted as a nano material in manufacturing biopolymer composites in large number. Soil to geotextile interfacial behavior can be better controlled by incorporation of nanotechnology as surface engineering. The soil treated with nano materials and incorporation of nano treated bio composite can be the next generation reinforced earth.

The surface treatment of natural fibers has been of interest to numerous studies in order to make full use of the advantages of natural fibers in composite materials and to successfully utilize them in various applications.

However, research in this area is quite diversified and the existing literature talks about a range of techniques, including various physical, chemical and biological modes. Therefore, a thorough review of the existing literature and critical analysis of outcomes is extremely important in order to know the advantages and disadvantages of each treatment and to identify the right one according to the requirements. On the basis of this review, further researches are recommended to investigate the effects of nano modification of matrix and fiber, and the properties of resulting bio polymer composites as probable next generation Geotextile material.

## References

[1]    Abbar, B.; Alem, A.; Pantet, A.; Marcotte, S.; Ahfir, N.-D.; Duriatti, D. Experimental investigation on removal of suspended particles from water using flax fibre geotextiles. Environ. Technol. 2017, 38, 2964–2978.

[2]    Abbar, B.; Alem, A.; Pantet, A.; Marcotte, S.; Ahfir, N.-D.;Wang, H.; Ouahbi, T.; Duchemin, B.; Duriatti, D. Nonwoven flax fibres geotextiles e_ects on solute heavy metals transport in porous media. Environ. Technol. 2018

[3]    Abbar, B.; Alem, A.; Pantet, A.; Ahfir, N.-D.; Marcotte, S.; Wang, H.; Duchemin, B. E_ect of natural geotextile on the cotransport of heavy metals (Cu2+, Pb2+, and Zn2+) and kaolinite particles. Environ. Technol. 2019.

[4]    Adhikari J. et al., Lignocellulosic materials for geotextile and geocomposites for engineering applications. Springer series on polymer, 2018, 357-388.

[5]    Ahmed, K.S.; Vijayarangan, S.; Kumar, A. Low velocity impact damage characterization of woven jute glass fabric reinforced isothalic polyester hybrid composites. J. Reinf. Plast. Compos. 2007, 26, 959–976.

[6]    Ahmed, K.S.; Vijayarangan, S. Tensile, flexural and interlaminar shear properties of woven jute and jute-glass fabric reinforced polyester composites. J. Mater. Process. Technol. 2008, 207, 330–335.

[7]    A. Hegde & T. G. Sitharam, Experimental and Analytical Studies on Soft Clay Beds Reinforced with Bamboo Cells and Geocells, Int. J. of Geosynth. and Ground Eng. (2015) 1-13.

[8]    Ajayan, P.M.; Schadler, L.S.; Braun, P.V. Nanocomposite Science and Technology; Wiley-VCH Verlag GmBH & Co.: Winheim, Germany, 2003; p. 239.

[9]    Akkapeddi, M.K. Glass fiber reinforced polyamide-6 nanocomposites. Polym. Compos. 2000, 21, 576–585.

[10]   Alix S, Lebrun L, Morvan C, et al. Study of water behavior of chemically treated flax fibers-based composites: A way to approach the hydric interface. Compos Sci Technol 2011; 71: 893–899.

[11]   "Aracri E, Fillat A, Colom JF, et al. Enzymatic grafting of simple phenols on flax and sisal pulp fibres using laccases. Bioresour Technol 2010; 101: 8211–8216."

[12]   Arbelaiz, A.; Fernandez, B.; Cantero, G.; Llano-Ponte, R.; Valea, A.; Mondragon, I. Mechanical properties of flax fiber/polypropylene composites. Influence of fiber/matrix modification and glass fiber hybridization. Compos. A Appl. Sci. Manuf. 2005, 36, 1637–1644.

[13]   Arifuzzaman Khan GM, Shaheruzzaman M, Rahman MH, et al. Surface modification of okra bast fiber and its physio-chemical characteristics. Fibers Polym 2009; 10: 65–70.

[14]   Arrakhiz, F.Z.; Benmoussa, K.; Bouhfid, R.; Qaiss, A. Pine cone fiber/clay hybrid composite: Mechanical and thermal properties. Mater. Des. 2013, 50, 376–381.

[15]   Basu, G.; Roy, A.; Sanyal, P.; Mitra, K.; Mishra, L.; Ghosh, S. Bioengineering of river earth embankment using natural fiber-based composite-structured geotextiles. Geotext. Geomembr. 2019, 47, 493–501.

[16]   Bartos, P.; Hughes, J.; Trtik, P.; Zhu, W. Freedonia Group; Freedonia Group: Cleveland, OH, USA, 2009; p. 174.

[17]   Biswas, M.; Ray, S.S. Recent progress in synthesis and evaluation of polymer-montmorillonite nanocomposites. Adv. Polym. Sci. 2001, 155, 167–221.

[18] Bledzki AK, Fink H and Specht K. Unidirectional hemp and flax EP- and PP-composites: Influence of defined fiber treatments. J Appl Polym. Sci 2004; 93: 2150–2156.

[19] Cantero G, Arbelaiz A, Llano-Ponte R, et al. Effects of fiber treatment on wettability and mechanical behaviour of flax/polypropylene composites. Compos Sci Technol 2003;63: 1247–1254.

[20] Chakrabarti, S.; Saha, S.; Paul, P.; Dewan, A.; Das, K.; Chowdhury, P.; Gon, D.; Ray, P. Specially treated woven jute geotextiles for river bank protection. IJFTR 2016, 41, 207–211.

[21] Chandradass, J.; Kumar, M.R.; Velmurugan, R. Effect of nano clay addition on vibration properties of glass fiber reinforced vinyl ester composites. Mater. Lett. 2007, 61, 4385–4388.

[22] Chattopadhyay, B.; Chakravarty, S. Application of jute geotextiles as facilitator in drainage. Geotext. Geomembr. 2009, 27, 156–161.

[23] Chaturvedi, S.; Dave, P.N. Design process for nanomaterials. J. Mater. Sci. 2013, 48, 3605–3622.

[24] Chaudhary B.S. et al., Effect of nano TiO2 pretreatment on functional properties of cotton fabric, IJERD, ISSN: 2278-067X, Vol.1, Issue 9, 2012, 24-29.

[25] Chen, W.; Tao, X.; Liu, Y. Carbon nanotube-reinforced polyurethane composite fibers. Compos. Sci. Technol. 2006, 66, 3029–3034.

[26] Chtourou H, Riedl B and Kokta BV. Strength properties of wood-PE composites: Influence of pulp ratio and pretreatment of PE fibers. TAPPI J 1997; 80: 141–151.

[27] Cicala, G.; Cristaldi, G.; Recca, G.; Ziegmann, G.; El-Sabbagh, A.; Dickert, M. Properties and performances of various hybrid glass/natural fiber composites for curved pipes. Mater. Des. 2009, 30, 2538–2542.

[28] Cruz Juliana & Fangueiro R., Surface modification of natural fibers: A review. Procedia Engg., 155, 2016, 285-288.

[29] Davoodi, M.M.; Sapuan, S.M.; Ahmad, D.; Ali, A.; Khalina, A.; Jonoobi, M. Mechanical properties of hybrid kenaf/glass reinforced epoxy composite for passenger car bumper beam. Mater. Des. 2010, 31, 4927–4932.

[30] Dixon et al., Sustainability aspect of using geotextiles. From design to applications. Woodhead publishing, 2016, 577-596.

[31] De Medeiros, E.S.; Agnelli, J.A.M.; Joseph, K.; De Carvalho, L.H.; Mattoso, L.H.C. Mechanical properties of phenolic composites reinforced with Jute/cotton hybrid fabrics. Polym. Compos. 2005, 26, 1–11.

[32] Denault, J.; Labrecque, B. Technology Group on Polymer Nanocomposites; Boucherville: Québec, QC, Canada, 2004.

[33] Dong, A.; Fan, X.;Wang, Q.; Yu, Y.; Cavaco-Paulo, A. Enzymatic treatments to improve mechanical properties and surface hydrophobicity of jute fiber membranes. BioResources 2016, 11, 3289–3302.

[34] Esfandiari, A. Mechanical properties of PP/Jute and glass fibers composites: The statistical investigation. J. Appl. Sci. 2007, 7, 3943–3950.

[35] Fangueiro R. & Rana S., Innovative fibrous materials for geotechnical applications. ACEM'12, Seoul, Korea, 2012, 1279-1290.

[36] Fillat A, Gallardo O, Vidal T, et al. enzymatic grafting of natural phenols to flax fibers: Development of antimicrobial properties. Carbohydr. Polym. 2012; 87: 146–152.

[37]    Fong, H.; Liu, W.; Wang, C.S.; Vaia, R.A. Generation of electro spun fibers of nylon 6 and nylon 6-montmorillonite nanocomposite. Polymer 2001, 43, 775–780.

[38]    Fornes, T.D.; Paul, D.R. Crystallization behavior of nylon 6 nanocomposites. Polymer 2003, 44, 3945–3961.

[39]    Gacitua, W.; Ballerini, A.; Zhang, J. Polymer nanocomposites: Synthetic and natural fillers a review. Maderas Cienc. Y Tecnol. 2005, 7, 159–178.

[40]    Gaurav Mago, Suprakas Sinha Ray, Meisha L. Shofner, Shanfeng Wang, and Jin Zhang, Polymer Nanocomposite Processing, Characterization, and Applications, Journal of Nanomaterials, Volume 2014, Article ID 403492, 2 pages.

[41]    Gronqvist S, Buchert J, Rantanen K, et al. Activity of laccase on unbleached and bleached thermomechanical pulp. Enzyme Microb. Technol. 2003; 32: 439–445.

[42]    Gosh M et al., Sustainability of natural fibers in geotextile applications, IGC Guntur, 2009, 479-501.

[43]    Hanus M.J. & Harris A.T., Nanotechnology innovations for the construction industry. Progress in material science. Elesvier, 58(2013), 1056-1102.

[44]    Hari, J.; Pukanzsky, B. Nanocomposites: Preparation, structure, properties. In Applied Plastics Engine Handbook: Processing Materials; Kutz, M., Ed.; Elsevier Inc.: Waltham, MA, USA,2011; pp. 109–142.Henrique, P.; Camargo, C.; Satyanarayana, K.G.; Wypych, F. Nanocomposites: Synthesis, structure, properties and new application opportunities. Mater. Res. 2009, 12, 1–39.

[45]    Hejazi S.M. et al., A simple review of soil reinforcement by using natural and synthetic fibers. Cons and Buil. Mat. Elsevier, 30, 2012, 100-116.

[46]    Henrique,P. et al., Nanocomposites: Synthesis, structure, properties and new application opportunities. Mater. Res. 2009, 12, 1-39.

[47]    Holem Ian, Innovative technologies for high performance textiles. Journal compilation, Color.Technol., 123, 2007, 59-73.

[48]    Ibrahim I.D. et al., Impact of surface modification and nanoparticle on sisal fiber reinforced polypropylene nanocomposites,.Hindawi, Journal of Nanotechnology, 1-9.

[49]    Jaafar, J.; Siregar, J.P.; Salleh, S.M.; Hamdan, M.H.M.; Cionita, T.; Rihayat, T. Important considerations in manufacturing of natural fiber composites: A review. Int. J. Precis. Eng. Manuf. Technol. 2019, 6, 647–664.

[50]    Jadoun S. et al., Modification of textiles via Nanomaterials and their applications, Front. Of text. Mat. Scrivener Pub. 2020, 135-152.

[51]    Jawahar, P.; Balasubramanian, M. Influence of nanosized clay platelets on the mechanical properties of glass fiber reinforced polyester composites. J. Nanosci. Nanotechnol. 2006, 6, 3973–3976.

[52]    Jawaid, M.; Abdul Khalil, H.P.S.; Abu Bakar, A. Mechanical performance of oil palm empty fruit bunches/jute fibers reinforced epoxy hybrid composites. Mater. Sci. Eng. A 2010, 527, 7944–7949.

[53]    Jawaid, M.; Abdul Khalil, H.P.S. Cellulosic/synthetic fiber reinforced polymer hybrid composites: A review. Carbohydr. Polym. ,6, 2011, 86, 1–18.

[54]    Jawaid M. & Saba N., A review on potentiality of nano filler/ Natural fiber filled polymer hybrid composites., Polymers, 2014, 2247-2273.

[55]    Jen, M.H.R.; Tseng, Y.C.; Wu, C.H. Manufacturing and mechanical response of nanocomposite laminates. Compos. Sci. Technol. 2005, 65, 775–779.

[56] Jiang, H.; Kamdem, D.P. Mechanical properties of poly (vinyl chloride)/wood flour/glass fiber hybrid composites. J. Vinyl 2003, 9, 138–145.

[57] Ji, Y.; Li, B.; Ge, S.; Sokolov, J.C.; Rafailovich, M.H. Structure and nanomechanical characterization of electrospun PS/clay nanocomposite fibers. Langmuir 2006, 22, 1321–1328.

[58] Joseph K and Thomast S. Effect of chemical treatment on the tensile properties of short sisal fiber-reinforced polyethylene composites. Polymer (Guildf) 1996; 37: 5139–5149.

[59] Joseph K, Mattoso LHC, Toledo RD, et al. Natural fiber reinforced thermoplastic composites. Nat Polym Agrofibers Compos 2000; 159: 159–201.

[60] Kim S and Cavaco-Paulo A. Laccase-catalyzed protein-flavonoid conjugates for flax Fiber modification. J Appl Microbiol 2012; 93: 585–600.

[61] Koichi Goda & Yong Cao, Research and development of fully green composites reinforced with natural fibers. Jour. of solid Mech. & Mat. Engg. Vol.1, No.9, 2007, 1073-1084.

[62] Kong, K.; Hejda, M.; Young, R.J.; Eichhorn, S.J. Deformation micromechanics of a model cellulose/glass fiber hybrid composite. Compos. Sci. Technol. 2009, 69, 2218–2224.

[63] Koohestani, B.; Darban, A.; Mokhtari, P.; Yilmaz, E.; Darezereshki, E. Comparison of different natural fiber treatments: A literature review. Int. J. Environ. Sci. Technol. 2019, 16, 629–642.

[64] Kord, B. [a.] Nanofiller reinforcement effects on the thermal, dynamic mechanical, and morphological behavior of HDPE/rice husk flour composites. Bio-Resources 2011, 6, 1351–1358.

[65] Kord, B. [b.]; Kiakojouri, S. Effect of nano clay dispersion on physical and mechanical properties of wood flour/polypropylene/glass fiber hybrid composites. Bio-Resources 2011, 6, 1741–1751.

[66] Kord, B. Effect of nanoparticles loading on properties of polymeric composite based on Hemp Fiber/Polypropylene. J. Thermoplast. Compos. Mater. 2012, 25, 793–806.

[67] Kudanga T, Nyanhongo GS, Guebitz GM, et al. Potential applications of laccase mediated coupling and grafting reactions: A review. Enzyme Microb. Technol 2011; 48: 195–208.

[68] Kumar, N.M.; Reddy, G.V.; Naidu, S.V.; Rani, T.S.; Subha, M.C.S. Mechanical properties of coir/glass fiber phenolic resin-based composites. J. Reinf. Plast. Compos. 2009, 28, 2605–2613.

[69] Kumar, N.; Das, D. Nonwoven geotextiles from nettle and poly (lactic acid) fibers for slope stabilization using bioengineering approach. Geotext. Geomembr. 2018, 46, 206–213.

[70] Kumar S. Chemical modification of wood. Wood Fiber Sci 1994; 26: 270–280.

[71] Kumar, S.; Dang, T.D.; Arnold, F.E.; Bhattacharyya, A.R.; Min, B.G.; Zhang, X.; Vaia, R.A.; Park, C.; Adams, W.W.; Hauge, R.H.; et al. Synthesis, structure, and properties of PBO/SWNT composites. Macromolecules 2002, 35, 9039–9043.

[72] Li, L.; Bellan, L.M.; Craighead, H.G.; Frey, M.W. Formation and properties of nylon-6 and nylon-6/montmorillonite composite nanofibers. Polymer 2006, 47, 6208–6217.

[73] Liang, Y.; Xia, X.; Luo, Y.; Jia, Z. Synthesis and performances of Fe2O3/PA-6 nanocomposite fiber. Mater. Lett. 2007, 61, 3269–3272.

[74] Liany, Y.; Tabei, A.; Farsi, M.; Madanipour, M. Effect of nanoclay and magnesium hydroxide on some properties of HDPE/wheat straw composites. Fibers Polym. 2013, 14, 304–310.

[75] Liehr, S.; Lenke, P.; Krebber, K.; Seeger, M.; Thiele, E.; Metschies, H.; Gebreselassie, B.; Münich, J.C.;Stempniewski, L. Distributed strain measurement with polymer optical fibers integrated into multifunctional geotextiles. In Proceedings of the Optical Sensors, Strasbourg, France, 7–10 April 2008; p. 700302

[76] Lin, J. In situ Syntheses and Phase Behavior Investigations of Inorganic Materials in Orgamic Polymer Solid Matrices; The Pennsylvania State University: Nittany Valley Central County, PA, USA, 1992.

[77] Lin, Z.; Ye, W.; Du, K.; Zeng, H. Homogenization of functional groups on surface of carbon fiber and its surface energy. J. Huaqiao Univ. Sci. 2001, 22, 261–263.

[78] Lin, Z.; Ye, W.; Du, K.; Zeng, H. Homogenization of functional groups on surface of carbon fiber and its surface energy. J. Huaqiao Univ. Sci. 2001, 22, 261–263.

[79] Lincoln, D.M.; Vaia, R.A.; Wang, Z.; Hsiao, B.S. Secondary structure and elevated temperature crystallite morphology of nylon-6/layered silicate nanocomposites. Polymer 2001, 42, 1621–1631

[80] Liu, T.; Lim, K.P.; Tjiu, W.C.; Pramoda, K.P.; Chen, Z.K. Preparation and characterization of nylon 11/organoclay nanocomposites. Polymer 2003, 44, 3529–3535.

[81] Maldas D, Kokta B and Daneault C. Influence of coupling agents and treatments on the mechanical properties of cellulose fiber–polystyrene composites. J Appl Polym Sci. 1989; 37: 751–775.

[82] Mandal, S.; Alam, S.; Varma, I.K.; Maiti, S.N. Studies on bamboo/glass fiber reinforced USP and VE resin. J. Reinf. Plast. Compos. 2010, 29, 43–51.

[83] Marquis, D.M.; Guillaume, É.; Chivas-Joly, C. Properties of nanofillers in polymer.In Nanocomposites and Polymers with Analytical Methods; Cuppoletti, J., Ed.; Intech Publishing: Rijeka, Croatia, 2011; pp. 261–284.

[84] Matsuda H. Chemical modification of solid wood, 1st edn. New York, NY: Marcel Dekker Inc., 1996.

[85] Mehta, N.M.; Parsania, P.H. Fabrication and evaluation of some mechanical and electrical properties of jute-biomass based hybrid composites. J. Appl. Polym. Sci. 2006, 100, 1754–1758.

[86] Midha, V.K.; Joshi, S.; Kumar, S.S. Performance of chemically treated jute geotextile in unpaved roads at different in situ conditions. J. Inst. Eng. (India) Series E 2017, 98, 47–54.

[87] Mishra S, Misra M, Tripathy SS, et al. Influence of chemical surface modification on the performance of sisal-polyester bio composites. Polym Compos 2002; 23: 164.

[88] Montazer M. & Seifollahzadeh Samira, Enhanced self-cleaning, antimicrobial and UV protection properties of Nano $TiO_2$ treated textile through enzymatic pretreatment. Photo & Photo, 87, 2011, 877-883.

[89] Na Sim and Seong Ok Han, Effect on modified nanoclay on dynamic mechanical and thermomechanical properties of natural fiber/polypropylene bio composites., Journal of Adhesion science and technology, Vol. 27, No.12, 2013, 1313-1323.

[90] Najafi1, A.; Kord, B.; Abdi, A.; Ranaee, S. The impact of the nature of nano clay on physical and mechanical properties of polypropylene/reed flour nanocomposites. J. Thermoplast. Compos. 2012, 25, 717–727.

[91] Nazzal M.D. et al. The use of green polymer nano composites in Geo-infrastructure. Geo-Chicago, 2016, 488-497.

[92] Negi Y.S. et al., Recent development in natural fiber reinforced polypropylene composites. Jour. of reinf. Plastics and Comp. Vol.28, No. 10, 2009, 1169-1189.

[93] Ogasawara, T.; Ishida, Y.; Ishikawa, T.; Yokota, R. Characterization of multi-walled carbon nanotube/phenyl ethynyl terminated polyimide composites. Compos. Appl. Sci. Manuf.2004, 35, 67–74.

[94] Ogbuagu J.O & Akubue P.C., Achieving sustainable development goals through nanotechnology in polymer and textile, Eu. Jour. Of Engg. & tech. Vol.3, No. 7. 2015, 30-39.

[95] Omrani E. et al., State of the art on tribological behavior if polymer matrix composites reinforced with natural fibers in the green materials world. Engg. Sci. Tech. an int. journal, 19 (2016) , 717-736.

[96] Pappu A. & Thakur V.K., Towards sustainable micro and nano composites from fly ash and natural fibers for multifunctional applications

[97] Patra J.K. & Gouda S., Applications of nanotechnology in textile engineering: An overview, JETR, Vol.5 (5), 2013, 104-111.

[98] Podgorski I and Roux M. Wood modification to improve the durability of coatings. Surf Coat Int 1999; 82: 590–596.

[99] Poulin, P.; Vigolo, B.; Launois, P. Films and fibers of oriented single wall nanotubes. Carbon 2002, 40, 1741–1749.

[100] Prambauer, M.; Wendeler, C.; Weitzenböck, J.; Burgstaller, C. Biodegradable geotextiles–An overview of existing and potential materials. Geotext. Geomembr. 2019, 47, 48–59.

[101] Qian, D.; Dickey, E.C.; Andrews, R.; Rantell, T. Load transfer and deformation mechanisms in carbon nanotube-polystyrene composites. Appl. Phys. Lett. 2000, 76, 2868–2870.

[102] Rahman R. et al., Bamboo fiber polypropylene composites: effect of fiber treatment and nano clay on mechanical and thermal properties. Jour. of Vinyl & Add. Tech., 2014, 1-6.

[103] Rajini N. et al., Dynamic mechanical analysis and free vibration behavior in chemical modifications of coconut sheath/nanoclay reinforced hybrid polyester composite. Jour. of Comp. Material, 47(24), 2012, 3105-3121.

[104] Ramakrishnan S. et al. An experimental study on the effect of nano-clay addition on mechanical and water absorption behavior of jute fiber reinforced epoxy composites. SAGE, 2018.

[105] Ramakrishanan S. et al., Dynamic mechanical properties and free vibration characteristics of surface modified jute fiber/ Nanoclay reinforced epoxy composites. Jour. Of Poly. & Env., 2020, 1-13.

[106] Ramu P. et al. Mechanical characteristics and terminological behavior study on natural fiber nano reinforced polymer composite- A Review. Materials today: Proceedings, 16, 2019, 1287-1296.

[107] Rattanasom, N.; Saowapark, T.; Deeprasertkul, C. Reinforcement of natural rubber with silica/carbon black hybrid filler. Polym. Test. 2007, 26, 369–377.

[108] Rao KMM and Rao KM. Extraction and tensile properties of natural fibers: Vakka, date and bamboo. Compos Struct 2007; 77: 288–295.

[109] Rawal, A.; Sayeed, M. Tailoring the structure and properties of jute blended nonwoven geotextiles via alkali treatment of jute fibers. Mater. Des. 2014, 53, 701–705.

[110] Ray, S.S.; Okamoto, M. Polymer/layered silicate nanocomposites: A review from preparation to processing. Prog. Polym. Sci. 2003, 28, 1539–1641.

[111] Roy, S.; Vengadassalam, K.; Hussain, F.; Lu, H. Compressive strength enhancement of pultruded thermoplastic composites using nano clay reinforce. In Proceedings of the 45th AIAA/ASME/ASCE/AHS/ASC Structures, Structural Dynamics & Materials Conference, Long Beach, CA, USA, 19–22 April 2004; pp. 2245–2259.

[112] Roco, M.C.; Mirkin, C.A.; Hersam, M.C. Nanotechnology research directions for societal needs in 2020: Summary of international study. J. Nanopart. Res. 2011, 13, 897–919.

[113] Ruan, S.L.; Gao, P.; Yang, X.G.; Yu, T.X. Toughening high performance ultrahigh molecular weight polyethylene using multiwalled carbon nanotubes. Polymer 2003, 44, 5643–5654.

[114] Ruan, S.; Gao, P.; Yu, T.X. Ultra-strong gel-spun UHMWPE fibers reinforced using multiwalled carbon nanotubes. Polymer 2006, 47, 1604–1611.

[115] Saha, P.; Roy, D.; Manna, S.; Adhikari, B.; Sen, R.; Roy, S. Durability of trans-esterified jute geotextiles. Geotext.Geomember.2012, 35,69-75.

[116] Sakata I, Morita M, Furuichi H, et al. Improvement of ply bond strength of paperboard by corona treatment. J Appl Polym 1991; 42: 2099–2104

[117] Sandler, J.; Werner, P.; Shaffer, M.S.P.; Demchuk, V.; Altstädt, V.; Windle, A.H. Carbon-nanofiber-reinforced poly (ether ether ketone) composites. Compos. A Appl. Sci. Manuf. 2002, 33, 1033–1039.

[118] Sandler, J.K.W.; Pegel, S.; Cadek, M.; Gojny, F.; van Es, M.; Lohmar, J.; Blau, W.J.; Schulte, K.;Windle, A.H.; Shaffer, M.S.P. A comparative study of melt spun polyamide-12 fibers reinforced with carbon nanotubes and nanofibers. Polymer 2004, 45, 2001–2015.

[119] Sarsby, R.W. Use of 'Limited Life Geotextiles'(LLGs) for basal reinforcement of embankments built on soft clay. Geotext. Geomembr. 2007, 25, 302–310.

[120] Sawhney A.P.S. et al., Modern applications of nanotechnology in textiles, Textile. Res. Jou. 2012, 731-739.

[121] Schmidt, H. Multifunctional inorganic-organic composite sol-gel coatings for glass surfaces. J. Non-Cryst. Solids 1994, 178, 302–312.

[122] Schadler, L.S.; Brinson, L.C.; Sawyer, W.G. Polymer nanocomposites: A small part of the story. JOM 2007, 59, 53–60.

[123] Sen, A.K.; Kumar, S. Coir-fiber-based fire-retardant nano filler for epoxy composites. J. Therm. Anal. Calorim. 2010, 101, 265–271.

[124] Shah S.G., An overview of applications of nanotechnology for geotechnical engineering- A future scope, AGE-2014, App. Mech. Dept., SVNIT, 2014, 69-78.

[125] Shipra K. Applications of nanotechnology in textile. AJHS, Vol.9., Issue 2, 2014, 580-583.

[126] Shirazi, M.G.; Rashid, A.S.A.; Nazir, R.B.; Rashid, A.H.A.; Kassim, A.; Horpibulsuk, S. Investigation of tensile strength on alkaline treated and untreated kenaf geotextile under dry and wet conditions. Geotext. Geomembr. 2019, 47, 522–529.

[127] Shukla S.K., Chapter-2, "Basic description of fibre-reinforced soil. Springer, Basic description of fibre-reinforced soil engineering, 2017, 23-40.

[128] Sindhu A.R. & Justin K.Joseph, Effect of compaction characteristics and shear strength parameters of expansive soil reinforced with nanomodified coir fiber and lime, IRJET, 2017, 2450-2459.

[129] Singh, A.P.; Pal, K.R. Novel hybrid of clay, cellulose, and thermoplastics. I. Preparation and characterization of composites of ethylene–propylene copolymer. J. Appl. Polym. Sci. 2007, 104, 2672–2682.

[130] Singh, A.P.; Pal, K.R. Novel hybrid of clay, cellulose, and thermoplastics. I. Preparation and characterization of composites of ethylene–propylene copolymer. J. Appl. Polym. Sci.2007, 104, 2672–2682.

[131] Singh J.I., Study of effect of surface treatment on mechanical properties of natural fiber reinforced composites. Materials today: proceedings, 4. (2017), 2793-2799.

[132] Sreekala M, Kumaran M, Joseph S, et al. Oil palm fiber reinforced phenol formaldehyde composites: Influence of fiber surface modifications on the mechanical performance. Appl Compos Mater 2000; 7: 295–329.

[133] Subhash Anand, Designer natural fiber geotextiles- A new concept., Ind. Jour. Of Fiber and textile research, Vol.33, sept 208, 339-344.

[134] Sumi, S.; Unnikrishnan, N.; Mathew, L. Experimental Investigations on Biological Resistance of Surface Modified Coir Geotextiles. Int. J. Geosynth. Ground Eng. 2016, 2, 31.

[135] Sumi, S.; Unnikrishnan, N.; Mathew, L. Surface modification of coir fibers for extended hydrophobicity and antimicrobial property for possible geotextile application. J. Nat. Fibers 2017, 14, 335–345.

[136] Sumi, S.; Unnikrishnan, N.; Mathew, L. Durability studies of surface-modified coir geotextiles. Geotext. Geomembr. 2018, 46, 699–706.

[137] Taha M.R., Recent Development in nanomaterials for geotechnical and geoenvironmental engineering, MATEC Web of Conf. 149, 02004(2018) CMSS-2017.

[138] Taşdemır, M.; Koçak, D.; Usta, İ.; Akalin, M.; Merdan, N. Properties of recycled polycarbonate/waste silk and cotton fiber polymer composites. Int. J. Polym. Mater. 2008, 57, 797–805.

[139] Thiruchitrambalam, M.; Alavudeen, A.; Athijayamani, A.; Venkateshwaran, N.; Perumal, A.E. Improving mechanical properties of banana/kenaf polyester hybrid composites using sodium lauryl sulfate treatment. Mater. Phys. Mech. 2009, 8, 165–173.

[140] Uehara T and Sakata I. Effect of corona discharge treatment on cellulose prepared from beech wood. J Appl Polym Sci 1990; 41: 1695–1706.

[141] Velmurugan, R.; Manikandan, V. Mechanical properties of glass/palmyra fiber waste sandwich composites. Indian J. Eng. Mater. Sci. 2005, 12, 563–570.

[142] Velmurugan, R.; Manikandan, V. Mechanical properties of palmyra/glass fiber hybrid composites. Compos. A Appl. Sci. Manuf. 2007, 38, 2216–2226.

[143] Venkata Reddy, G.; Shobha Rani, T.; Chowdoji Rao, K.; Venkata Naidu, S. Flexural, compressive, and interlaminar shear strength properties of kapok/glass composites. J. Reinf. Plast. Compos. 2009, 28, 1665–1677.

[144] Vlasveld, D.P.N.; Parlevliet, P.P.; Bersee, H.E.N.; Picken, S.J. Fibre-matrix adhesion in glass-fiber reinforced polyamide-6 silicate nanocomposites. Compos. A Appl. Sci. Manuf. 2005, 36, 1–11.

[145] Wan Busu, W.N.; Anuar, H.; Ahmad, S.H.; Rasid, R.; Jamal, N.A. The mechanical and physical properties of thermoplastic natural rubber hybrid composites reinforced with hibiscus cannabinus, L and short glass fiber. Polym. Plast. Technol. Eng. 2010, 49, 1315–1322.

[146] Wang, Q.H.; Xue, Q.J.; Liu, W.M.; Chen, J.M. The friction and wear characteristics of nanometer SiC and polytetrafluoroethylene filled polyether ether ketone. Wear 2000, 243, 140–146. Ogasawara, T.; Ishida, Y.; Ishikawa, T.; Yokota, R. Characterization of multi-walled carbon nanotube/phenyl ethynyl terminated polyimide composites. Compos. A Appl. Sci. Manuf. 2004, 35, 67–74.

[147] Wallace G. et al., Smart nanotextiles: A review of materials and applications, 2007, 343-442.

[148] Wu, S.-H.; Wang, F.Y.; Ma, C.C.M.; Chang, W.C. Mechanical, thermal and morphological properties of glass fiber and carbon fiber reinforced polyamide-6 and polyamide-6/clay nano composites. Mater. Lett. 2001, 49, 327–333.

[149] Wypych, F.; Satyanarayana, K.G. Functionalization of single layers and nanofibers: A new strategy to produce polymer nanocomposites with optimized properties. J. Colloid Interface Sci. 2005, 285, 532–543.

[150] Zhang, S.; Hull, T.R.; Horrocks, A.R.; Smart, G.; Kandola, B.K.; Ebdon, J.; Joseph, P.; Hunt, B. Thermal degradation analysis and XRD characterization of fiber-forming synthetic polypropylene containing nanoclay. Polym. Degrad. Stab. 2007, 92, 727–732.

[151] Zhang, X.; Huang, Y.; Wang, T.; Liu, L. Influence of fiber surface oxidation-reduction followed by silsesquioxane coating treatment on interfacial mechanical properties of carbon fiber/polyarylacetylene composites. Compos. A Appl. Sci. Manuf. 2007, 38, 936–944.

[152] Zhong, Y.; Poloso, T.; Hetzer, M.; de Kee1, D. Enhancement of wood/polyethylene composites via compatibilization and incorporation of organoclay particles. Polym. Eng. Sci. 2007, 47, 797–803.

[153] Zhu J, Zhu H, Njuguna J, et al. Recent development of flax fibers and their reinforced composites based on different polymeric matrices. Materials (Basel) 2013; 6: 5171–5198.

[154] https://www.merzconstruction.co.nz/products/coir-matting-and-coir-geo-cells/

# Potential of green heterogeneous catalyst derived from the fusion of eggshells and pawpaw peels in the optimised transesterification of linseed oil methyl ester

**A. O. Etim[1*], P. Musonge[1,2] and A. C. Eloka-Eboka [3]**

[1]*Institute of Systems Science, Durban University of Technology, Durban, South Africa.*
[2]*Faculty of Engineering, Mangosuthu University of Technology, Durban, South Africa*
[3] *School of Chemical and Minerals Engineering, North West University, Potchefstroom, South Africa.*
*Corresponding author: etimanietie@yahoo.com*

## Abstract

Heterogeneous catalysts derived from calcium and potassium-rich biological sources have become prominent in biodiesel production due to easy synthesis from waste available animal shells and agricultural materials. In this study, the potential of fused eggshells and pawpaw peels derived heterogeneous catalyst was tested in the transesterification reaction of linseed oil. The waste materials were dried and calcined at different temperatures of 900ºC and 700ºC for 3 hrs to obtain their individual calcined ashes (calcined eggshells (CES) and calcined pawpaw peels (CPP)) respectively. The CES and CPP were then bonded by wet impregnation method (by dissolving each ash at weight concentration of 7:3 CES/CPP in 100 ml warm distilled water and further calcined at 600ºC for 2 hrs). The developed catalyst was characterized using SEM-EDX and FT-IR. The Box Behnken design was applied to generate 15 experimental runs which were used to investigate the effect of the operational parameters such as methanol-to-oil molar ratio, catalyst loading and reaction time. Characterization results obtained show that the ash is highly rich in Ca and K ions. The best reaction condition for the transesterification process was found to be methanol/oil molar ratio of 14.9:1, catalyst loading of 3.78 wt%, process reaction time of 79.9 min at constant reaction temperature of 65ºC with a biodiesel maximum yield of 91.2 wt%. The physicochemical properties of the produced biodiesel were measured and found to meet the ASTM and EN and SANS biodiesel quality standards. The fused catalyst can be reused up to 5 cycles with little decrease in yields. The study demonstrates the potential of utilizing biomass feedstock in developing effective and sustainable biodiesel fuels.

**Keywords**: biodiesel, transesterification, heterogeneous catalyst, waste biomass materials, optimization

## 1    Introduction

Fossil fuel is the global primary source of energy upon which most countries depend for economic development. Constant release of greenhouse gases during fossil fuel combustion contributes tremendously in environmental pollution, health problems and global warming (Aleman-Ramirez et al., 2021; Kataria et al., 2019). Biodiesel appears to be the most convenient and sustainable fuel source which can be used as a long-term substitute in minimising the harmful emission encountered with the use of fossil fuels. Biodiesel is characterized with biodegradability, non-toxicity, low $CO_2$ emission, zero sulphur, low hydrocarbons, excellent lubricity, high flash points and cetane numbers. Biodiesel have similar chemical properties with petroleum diesel but different in emission generation and it can be utilised in the same infrastructure as diesel engine without modifications.

Biodiesel is produced via transesterification reaction using vegetable oils, animal fats and algal oils as the main lipid source, together with alcohols and catalysts. Alcohols such as methanol is needed to achieve the required physiochemical properties of the biodiesel produced. Transesterification is a reversible reaction, while alcohol is required in excess to change the direction of equilibrium to the favour of the product, catalyst is used to facilitate and hasten the reaction process to completion. Other factors also considered to enhance the success of the process are temperature, time and applied technologies. In transesterification process, there are several factors that influences the operation conditions of the biodiesel production and the yields. These factors include; oil/alcohol molar ratio, reaction time, temperature and catalyst concentration. However, to study the effect of interaction of these factors and to describe the relationship between the variables and the response in order to establish the optimal operation conditions, modelling tools such Box Behnken design (BBD) can be applied. BBD has been used as one of the effective experimental designs in studying the interaction of variables and also to determine the most influential optimisation factors in an experiment.

Transesterification is a slow process due to the immiscibility of oil and methanol. Catalyst is therefore introduced to the system to quicken the conversion process. Catalyst used in transesterification is divided into three: the homogenous, heterogenous and enzymes. Homogenous catalyst is widely used for this purpose but it is linked to some technical issues which are not economical to the system. Issues such as soap formation, difficulties in separation and purification of product, equipment corrosion, spent water generation, non-recoverability and reusability of the catalyst are associated with the use of homogenous catalysts. Heterogenous catalyst are used to offset the inconveniences in the use of homogenous catalysts. Other than chemical base heterogenous catalysts, research focus has been shifted to the exploration and development of new heterogenous catalysts from biomass sources mostly waste materials. This is another advantage as an added measure to reduce environmental pollution. Catalysts derived from biomass sources have special characteristics such as non-toxicity, biodegradability, renewability and eco-friendliness. In addition, catalysts derived from biomass contain varieties of mineral components and their surface areas and pore structures can be modified (Etim et al., 2020).

Several biomass waste materials used in some published works include: eggshell chicken bones, scallop, mussels, cockle shells (Buasri et al., 2014; Farooq et al., 2015; Kirubakaran and Selvan, 2018), banana peels, papaya peels, coco pod husks, tucuma peels, plantain peels, moringa leaves (Aleman-Ramirez et al., 2021; Betiku et al., 2017; Etim et al., 2018, 2021a; Etim et al., 2021b; Mendonça et al., 2019). These materials have been used in the development of heterogenous catalysts for biodiesel production and they can be reused severally. Animal shells and bones are rich sources of natural CaO derived catalysts while waste plant materials are chief sources of potassium derived compounds such as $K_2O$, $KCl$, $K_2SO_4$ and so on. It is therefore reported that the CaO, MgO and ZnO catalysts are confronted with some problems during transesterification reaction such as: longer reaction time, difficulty in catalyst separation and impure biodiesel products (Etim et al., 2020; Kirubakaran and Arul Mozhi Selvan, 2018). Although there are few reports on different biomass mixtures in order to achieve effective heterogenous catalyst where mostly agro-waste materials are used (Adedayo et al., 2020; Adepoju, 2020). The fusion of chicken and fish bones was also investigated by (Tan et al. (2019a). From the literature point of view, information regarding biogenic fusion of heterogenous catalysts for biodiesel conversion has not been explored and presented.

In the present study, heterogenous catalyst prepared from waste eggshells and pawpaw peels was investigated in the transesterification of linseed oil for methyl ester production. To the best of our knowledge, the fusion of these green waste materials for the development of heterogenous catalysts for biodiesel production has not been investigated, hence this study. The synthesized catalyst was characterised to examine the active elements and compounds responsible for the high catalytic activity in the conversion process. Response surface methodology (RSM) based on Box Behnken design (BBD) was used to analyse the effect of the operational parameters of the transesterification process in order to determine the optimal conditions for the best conversion yields. The physiochemical properties of the linseed oil biodiesel were also compared with the ASTM D 6751 standards.

## 2 Experimental methods

### 2.1 Materials and Reagents

The chemical reagents used in this study were: methanol, ethanol (98%), potassium hydroxide, diethyl ether, potassium iodide, cyclohexane, sodium sulphate, chloroform and phenolphthalein indicator. They were all analytical grades, supplied by United Scientific SA CC, Congella, South Africa.

### 2.2 Preparation of the fused catalyst

The waste materials (eggshells and papaya peels) were thoroughly washed with distilled water to remove all debris attached on the surface of the materials. The washed materials were then dried in the oven at 80°C for 48 hrs. The dried materials were milled separately to powder particle size of <50 mm and further calcined in the furnace at different temperature range (900°C and 700°C; eggshell at 900°C and papaya peel at 700°C) for 3 hrs, to obtain their individual ash respectively. The calcined ashes were then fused by wet impregnation: 7g of calcined eggshell (CES) and 3g of calcined papaya peels (CPP) were measured and dissolved in 100 ml warm distilled water. The mixture was stirred vigorously at 600 rpm for 1 hr. The slurry was further dried in the oven at 120 °C for 24 hrs to obtain a dried cake which was further pulverised and activated in the furnace at 600°C for 1 hr. The developed catalyst was then stored in a tight container for biodiesel production and for further analysis.

### 2.3 Characterization of the fusion catalyst from calcined eggshells and pawpaw peels

The developed fusion catalyst was analysed for the Fourier transform infrared (FT-IR) spectra at the range of 4000 – 500 cm$^{-1}$ using Perkin Elmer spectrum (version 10.5.4) to determine the active surface functional groups present in the catalyst. Also, a high-resolution scanning electron microscope (SEM) by AURIGA (Zeiss Germany) fitted to the energy dispersive X-ray (EDX) detector was used for the elemental composition and the surface morphology of the calcined fusion catalyst.

### 2.4 Experimental Design for Transesterification Process using the fused catalyst

Response surface methodology (RSM) was used for the modelling and optimization of the transesterification process parameters. The applied BBD was used to generate 15 experimental runs which was afterwards carried out in the laboratory. The independent factors selected for the optimization include, catalyst loading, reaction time and methanol-to-oil molar ratio. The impact of unexpected variability in the actual responses was reduced by the randomization of the standard order of the experimental conditions. Table 1 shows the levels and the actual

values of the independent variables while the BBD of the experimental conditions are shown in Table 2. The quadratic polynomial model coefficient of the responses was fitted using multiple regression. The test of significance and the analysis of variance (ANOVA) at 95% confident level were used to assess the fit quality of the model and to investigate the significance of the process parameters. The equation that described the model fitness is given in Equation 1.

$$Y = \beta_0 + \sum_{i=1}^{n} \beta_i W_i + \sum_{i=i}^{n} \beta_{ii} W_i^2 + \sum_{i=1}^{n-1} \sum_{j=2}^{n} \beta_{ij} W_i W_j + h \tag{1}$$

Where $Y$ is the biodiesel yield, $\beta_0$ is the intercept, $\beta_i$ is the first order coefficient, $\beta_{ii}$ is the quadratic coefficient, $\beta_{ij}$ and $W_i$ is the interaction effect coefficient and $h$ is the random error.

Both the regression equation and response surfaces were analysed to obtain the optimal value for the selected independent parameters. Other factors such as probability value ($P$-value), Fisher's test ($F$-value), determination coefficient ($R^2$), the adjusted $R^2$ and predicted $R^2$ were also examined for predicting the responses. The actual and predicted values were plotted on a straight line in a normal probability plot to also evaluate the fit of the model.

Table 1: Process parameters and values considered at different levels

| Factors | Symbols | Coded factor levels | | |
|---|---|---|---|---|
| | | -1 | 0 | 1 |
| Reaction time (min) | $W_1$ | 60 | 70 | 80 |
| Catalyst loading (wt%) | $W_2$ | 2.5 | 3.5 | 4.5 |
| Methanol/oil molar ratio | $W_3$ | 9:1 | 12:1 | 15:1 |

Table 2:Experimental matrix and LSOME yield for transesterification process

| Standard order | Run | $W_1$ | $W_2$ | $W_3$ | LSOME | RSM Prediction |
|---|---|---|---|---|---|---|
| 4 | 1 | 80 | 4.5 | 12 | 78.50 | 77.64 |
| 10 | 2 | 70 | 4.5 | 9 | 55.50 | 56.31 |
| 1 | 3 | 60 | 2.5 | 12 | 72.30 | 73.16 |
| 3 | 4 | 60 | 4.5 | 12 | 79.50 | 78.56 |
| 9 | 5 | 70 | 2.5 | 9 | 64.20 | 63.21 |
| 14 | 6 | 70 | 3.5 | 12 | 77.80 | 78.33 |
| 12 | 7 | 70 | 4.5 | 15 | 82.50 | 83.49 |
| 5 | 8 | 60 | 3.5 | 9 | 67.40 | 67.53 |
| 13 | 9 | 70 | 3.5 | 12 | 78.10 | 78.33 |
| 6 | 10 | 80 | 3.5 | 9 | 72.80 | 72.85 |
| 11 | 11 | 70 | 2.5 | 15 | 75.30 | 74.49 |
| 7 | 12 | 60 | 3.5 | 15 | 88.70 | 88.65 |
| 8 | 13 | 80 | 3.5 | 15 | 90.30 | 90.17 |
| 2 | 14 | 80 | 2.5 | 12 | 80.00 | 80.94 |
| 15 | 15 | 70 | 3.5 | 12 | 79.10 | 78.33 |

## 2.5 Transesterification of linseed oil using the synthesized fusion catalyst

The transesterification process of LSO with the calcined fusion catalyst of eggshells and pawpaw peels was performed in a 250 ml three-necked round bottom flask equipped with a thermometer and a water-cool condenser. The magnetic hot plate was used as a source of heat and agitation to enhance a uniform temperature and proper mixing of the reactants. The temperature of the reaction was kept constant at 65°C and at a stirring speed of 800 rpm. The reaction was carried out at different runs of parametric conditions according to the design matrix allotted by BBD as shown in Table 2. The linseed oil of a given quantity was discharged into the reactor and allowed to heat up to a desired temperature. Appropriate amount of methanol and catalyst was then added and allowed to run according to the specified reaction time provided in the design guide. After completion, the reaction mixture was transferred into the separating funnels and allowed to settle by gravitation for 12 h, forming three-layer phases; the crude biodiesel, glycerol and catalyst, arranged according to their differences in densities. The glycerol and catalyst layers were decanted and the crude biodiesel layer was purified by wet-washing with warm distilled water and heating to remove any traces of glycerol, methanol, catalyst and water. The purified LSOME was subjected to fuel characterization for the physicochemical properties following the ASTM standards. The yield of LSOME produced was determined using Eq. 2.

$$LSOME = \frac{weight\ of\ biodiesel\ produced}{weight\ of\ oil\ sample\ used}\ x\ 100 \qquad (2)$$

## 3 Results and Discussion

### 3.1 Characterization of the catalyst

#### 3.1.1 FT-IR Analysis

Fig. 1a shows the FT-IR plot for the calcined fusion of eggshell and pawpaw peels catalyst. The peak at 3641 cm$^{-1}$ was attributed to hydroxyl (-OH) group which corresponds to Ca (OH)$_2$ due to the absorption of moisture from the atmosphere. However, the intensity of this peak was decreased after high temperature of calcination where the water content is removed from the catalyst resulting in calcium oxide formation. The occurrence of band at 1412 cm$^{-1}$ and 1050 cm$^{-1}$ are attributed to the metal oxide such as Ca-O and K-O. The small peak at 870 cm$^{-1}$ is ascribed to O-C-O stretching peak of carbonate ions. The bandwidth around 500 cm$^{-1}$ also identified the presence of Ca-O. The minority inorganic compounds such as magnesium, phosphorus and sulphur are found in the range of 1500 – 2500 cm$^{-1}$. The FT-IR spectrum of calcined fusion of eggshell/pawpaw peels agrees with Kirubakaran and Arul Mozhi Selvan, (2018), Tan et al. (2019b), Xie and Zhao, (20.13).

#### 3.1.2 SEM with EDS analysis

Fig. 1(b) shows the SEM image of the surface morphology of the synthesized fuse catalyst. The particles are arranged in irregular shape. The porous and spongy nature of the ash particles is as a result of high temperature of calcination which led to sintering of small mineral aggregate and agglomeration of the particles (Betiku et al., 2017). The non-uniform structure of the particle size distribution might form as a result of the merging of the particle size structure of the two waste materials during the catalyst synthesis. After calcination, a fine

powdered form crystal was observed which suggests the efficacy of good catalytic performance due to the increase in surface area of the catalyst. The elemental composition from the EDS result in Table 1, clearly showed that Ca (40.96 %) has the highest percentage mass fraction followed by potassium (8.57%).
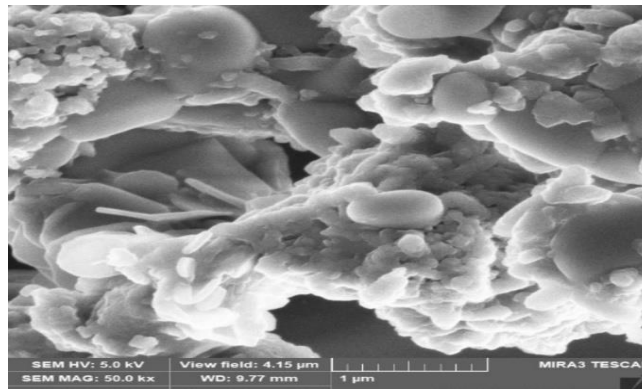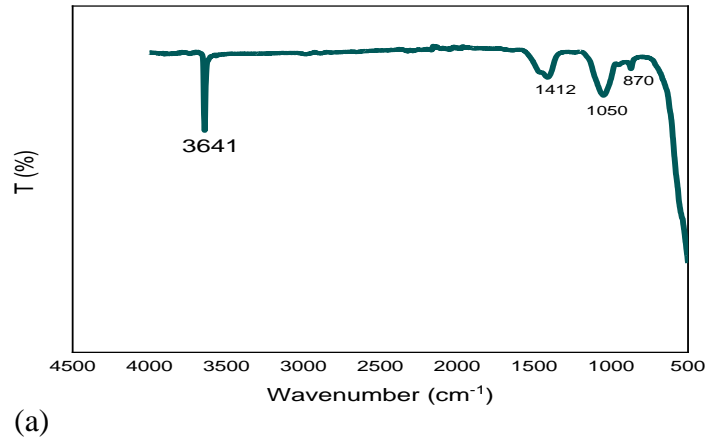


(a)



(b)

Figure 1(a,b): Shows (a) the FT-IR, (b) SEM-EDS of the synthesized fusion catalyst

Table 3: Elemental composition of the eggshells and pawpaw peel fusion catalyst

| Element | Mass fraction (%) |
| --- | --- |
| Ca | 40.96 |
| K | 8.57 |
| P | 0.62 |
| Mg | 0.52 |
| S | 0.3 |
| O | 49.03 |

## 3.2 Experimental design and statistical analysis

The interaction effect of the key operational parameters such as reaction time, catalyst loading and methanol to oil molar ratio on the transesterification process of linseed oil was examined using RSM. Box Behnken design (BBD) with three factors 3 levels was used for modelling and optimization of the transesterification process as shown in Table 1. Fifteen experimental

runs were generated with one response (LSOME) which was carried out successfully following the design matrix and the results are presented in Table 2. The experimental runs were randomised to reduce the variability in the responses. The quadratic model was developed at 95 % confident level to predict the experimental results. The response model presented in Eq. (3), which includes the coefficient of individual terms ($W_1$, $W_2$ and $W_3$), interactive terms ($W_1 W_2$, $W_1 W_3$, $W_2 W_3$ and quadratic terms ($W_1^2$, $W_2^2$, $W_3^2$) is:

$$Y = 78.33 + 1.71W_1 + 0.5250W_2 + 9.61W_3 - 2.17W_1W_2 - 0.9500W_1W_3 + 3.98W_2W_3 +$$
$$4.83W_1^2 - 5.59W_2^2 - 3.37W_3^2 \qquad\qquad\qquad\qquad\qquad\qquad \text{Eq.} \qquad (3)$$

The significance of the individual term, interaction and quadratic terms were determined by *F*-test and probability, *p*-value. The subsequent decreasing order of independent terms effect was $W_3 > W_1 > W_2$. The order of interaction effect was $W_2W_3 > W_1W_2 > W_1W_3$. The correlation between the actual experimental results and the predicted values are shown in Fig. 2. The obtained data were well fitted on the quadratic model, which indicates that the model results were in a reasonable agreement with the experimental results within the design range. The test of significance of the model was carried out by the analysis of variance (ANOVA) and it is presented in Table 4. The significance of the regression coefficients of the parameters is determined by the F-value. The F-value of 82.44 with a p-value of $< 0.0001$ signifies that the model is significant. There is only 0.01% chance that an F-value this large could occur due to noise. The prediction regression coefficient ($R^2 = 0.9933$) was high and it is close to unity, 1. The adjusted $R^2$ (0.9813) and predicted $R^2$ (0.9043) value differences was less than 2 which implies that they were in justifiable agreement. The precision ratio of 33.910 obtained was adequate and desirable to define the correlation between the operational parameters and the response. The low coefficient of variance of 1.61% also confirmed the predictive accuracy of the model. The parity plot that shows the correlation between the actual and predicted values is represented in Fig.2 which also confirmed the good fit of the model.

Table 4: Test of significance of ANOVA

| Source | Sum of Squares | df | Mean Square | F-value | p-value | |
|---|---|---|---|---|---|---|
| Model | 1109.91 | 9 | 123.32 | 82.44 | $< 0.0001$ | Significant |
| $W_1$-Reaction time | 23.46 | 1 | 23.46 | 15.68 | 0.0107 | |
| $W_2$-Catalyst loading | 2.20 | 1 | 2.20 | 1.47 | 0.2789 | |
| $W_3$-Methanol/oil ratio | 739.20 | 1 | 739.20 | 494.17 | $< 0.0001$ | |
| $W_1W_2$ | 18.92 | 1 | 18.92 | 12.65 | 0.0163 | |
| $W_1W_3$ | 3.61 | 1 | 3.61 | 2.41 | 0.1810 | |
| $W_2W_3$ | 63.20 | 1 | 63.20 | 42.25 | 0.0013 | |
| $W_1^2$ | 86.26 | 1 | 86.26 | 57.66 | 0.0006 | |
| $W_2^2$ | 115.45 | 1 | 115.45 | 77.18 | 0.0003 | |
| $W_3^2$ | 41.85 | 1 | 41.85 | 27.98 | 0.0032 | |
| Residual | 7.48 | 5 | 1.50 | | | |
| Lack of Fit | 6.55 | 3 | 2.18 | 4.71 | 0.1800 | Not significant |

| | | | |
|---|---|---|---|
| Pure Error | 0.9267 | 2 | 0.4633 |
| Cor Total | 1117.39 | 14 | |

$R^2 = 0.9933$; Adjusted $R^2 = 0.9813$; Predicted $R^2 = 0.9043$; Adequate precision 33.9096; Mean 76.13; CV% 1.61; Std dev. 1.22
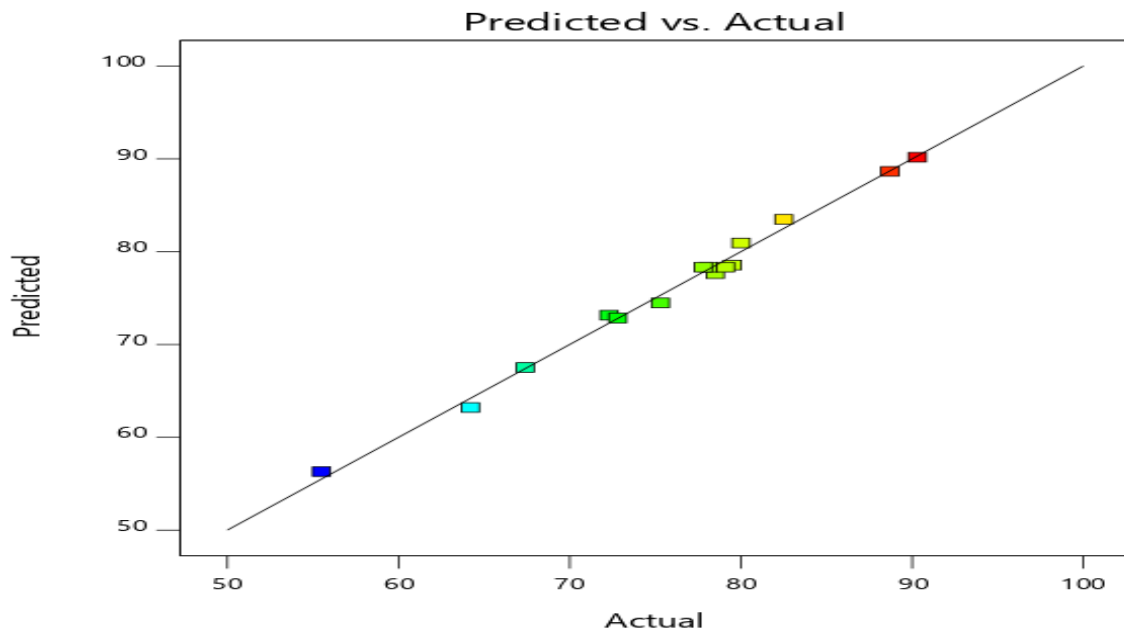


Figure 2: A plot of actual value against predicted value for LSOME produced using calcined eggshells and pawpaw fusion catalyst

## 3.3 Interaction effect of the process parameter on LSOME yield for the transesterification process

The effects of interaction of the three independent parameters on LSOME yield in the transesterification process using the calcined fusion eggshells and pawpaw peels catalyst were investigated. The three-dimensional plots are shown in Fig 3(a-c). Fig 3a. shows the surface plot of LSOME yield as a function of catalyst concentration and reaction time. The surface plot shows that the maximum LSOME yield was attained at highest reaction time and the catalyst concentration within the range of 3 – 4 wt%. Fig 3b. depicts the interaction between methanol/oil ratio and reaction time in regards to LSOME yield. The plot illustrates that increase in both methanol/io ratio and time increases LSOME yield. The maximum yield of LSOME was achieved at the highest methanol/oil ratio and reaction time. Fig 3c. revealed the interaction of methanol/oil and catalyst concentration. The plot shows that maximum biodiesel yield was attained at highest methanol/oil ratio of 15:1 and catalyst concentration of 3.7wt%. This is so because excess methanol/oil favours the FAME yield while highest catalysts favour the triglyceride.

## 3.4 Optimization of the process parameters

The DOE software was used to perform the numerical optimization of LSOME based on experimental results. The optimal condition was achieved by setting LSOME yield at

maximum and the three independent parameters in range. The optimal condition established for LSOME synthesis for the calcined fusion eggshells and pawpaw peels catalysed transesterification reaction was reaction time of 79.9 min, catalyst concentration of 3.78 wt%, and methanol /oil molar ratio of 14.94:1 with the predicted LSOME yield of 90.32 wt%. This condition was further verified by carrying out three independent experimental replicate and the average LSOME yield was computed for the process, which was observed to be 91. 2 wt%. This indicates that the developed model is adequate to describe the transesterification process investigated.
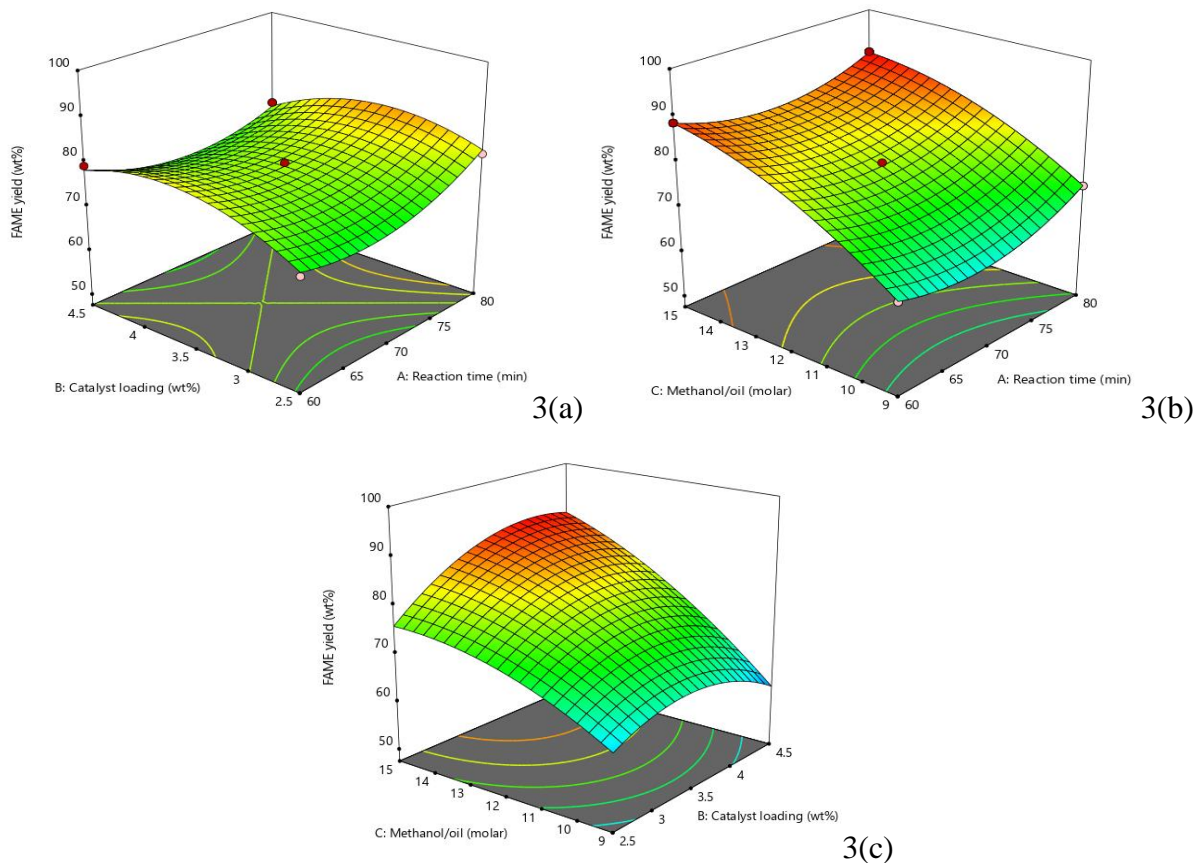


Figure 3(a,b,c): show the surface plot of the interaction effect of the process parameters on the LSOME

## 4    Reusability of calcined eggshells and pawpaw peels fusion catalyst

The most important economical aspect in using heterogenous catalyst is the potential for reusability. The process of reusability of the calcined fusion catalyst was performed at optimized parametric conditions as established by the BBD. The catalyst was separated from the biodiesel mixture after each run via centrifugation. This was then washed with hexane to remove impurities and further calcined at 800°C for 1 h. The reusability of the calcined catalyst was studied over five consecutive transesterifications using the same optimum condition. The first three cycles showed no significant drop in the catalytic activity of the catalyst. Significant decrease in the biodiesel yield occurred at the 4th and 5th cycles. This might be due to the deactivation of the catalyst by oil, moisture, $CO_2$ and other absorbed impurities on the surface of the catalyst (Tan et al., 2019b).

## 5    Physiochemical properties of LSOME

The important physical and chemical properties of the LSOME obtained from the calcined eggshells and pawpaw peels fusion catalysed transesterification process was determined and compared with the ASTM and EN standards. The results are presented in Table 5, which shows that all the properties of the produced LSOME satisfied both standard specification for biodiesel quality. This implies that the biodiesel produced using this protocol can be used as viable fuel substitute for petrol diesel.

Table 5: Physiochemical properties of LSOME

| Property | Units | LSOME | ASTM D6751 | EN 14214 |
|---|---|---|---|---|
| Physical state/colour | - | Liquid/light brown | - | - |
| Density @ 25ºC | g/cm$^3$ | 0.897 | 0.86 – 0.90 | 0.85 |
| Kinematic Viscosity @ 40 ºC | mm$^2$/s | 3.57 | 1.9 – 6.0 | 3.5 – 5.0 |
| Acid Value | mg KOH/g | 0.45 | 0.5 max | 0.5 max |
| FFA | % | 0.23 | - | - |
| Iodine Value | g I$_2$/100 g | 60.30 | - | 120 max |
| Calorific value | MJ/kg | 42.92 | - | - |
| Cetane number | | 62.89 | 47 min | 51 min |

## 6    Conclusion

The present study evaluates the potential of heterogenous bio-waste catalyst derived from the calcined eggshells and pawpaw peels fusion catalyst for the transesterification of LSOME. The characterization of the synthesized catalyst showed that calcium (40.96%) and K (8.57%) are the main active elements responsible for the high catalytic function of the developed catalyst. The modelling and optimization of the transesterification process was accomplished by RSM. Box Behnken Design based on three levels three factors was employed to obtain the possible interaction of the process variables which include reaction time, catalyst concentration and methanol to oil ratio. The optimal condition of the reaction time of 79.9 min, catalyst concentration of 3.78 wt%, and methanol/oil ratio of 14.9 :1, showed that the LSOME yield > 91 wt% could be achieved. The statistical evaluation of the developed model showed high accuracy and good predictions. The LSOME produced satisfied the ASTM D 6751 and EN 14214 specification standards. The study demonstrated that eggshells, pawpaw peels and LSO could serve as viable raw materials for biodiesel production.

## References

Adedayo et al., 2020. Cocoa pod husk-plantain peel blend as a novel green heterogeneous catalyst for renewable and sustainable honne oil biodiesel synthesis : A case of biowastes-to-wealth. Renew. Energy 166, 163–175. https://doi.org/10.1016/j.renene.2020.11.131

Adepoju, T.F., 2020. Optimization processes of biodiesel production from pig and neem (Azadirachta indica a . Juss) seeds blend oil using alternative catalysts from waste biomass. Ind. Crop. Prod. 149, 112334. https://doi.org/10.1016/j.indcrop.2020.112334

Aleman-Ramirez et al., 2021. Preparation of a heterogeneous catalyst from moringa leaves as a sustainable precursor for biodiesel production. Fuel 284, 118983. https://doi.org/10.1016/j.fuel.2020.118983

Betiku et al., 2017. Two-Step Conversion of Neem ( Azadirachta indica ) Seed Oil into Fatty Methyl Esters Using a Heterogeneous Biomass-Based Catalyst: An Example of Cocoa Pod Husk. Energy & Fuels 31, 6182–6193. https://doi.org/10.1021/acs.energyfuels.7b00604

Buasri et al., 2014. Utilization of Scallop Waste Shell for Biodiesel Production from Palm Oil – Optimization Using Taguchi Method. APCBEE Procedia 8, 216–221. https://doi.org/10.1016/j.apcbee.2014.03.030

Etim et al., 2018. Potential of Ripe Plantain Fruit Peels as an Ecofriendly Catalyst for Biodiesel Synthesis: Optimization by Artificial Neural Network Integrated with Genetic Algorithm. Sustainability 10, 707. https://doi.org/10.3390/su10030707

Etim et al., 2021a. Potential of Carica papaya peels as effective biocatalyst in the optimized parametric transesterification of used vegetable oil. Environ. Eng. Res. 26, 200–299. https://doi.org/10.4491/eer.2020.299

Etim et al., 2021b. Transesterification via Parametric Modelling and Optimization of Marula ( Sclerocarya birrea ) Seed Oil Methyl Ester Synthesis. J. Oleo Sci. 93, 77–93.

Etim et al., 2020. Effectiveness of biogenic waste-derived heterogeneous catalysts and feedstock hybridization techniques in biodiesel production. Biofuels, Bioprod. Biorefining 14, 620–649. https://doi.org/10.1002/bbb.2094

Farooq, M., Ramli, A., Naeem, A., 2015. Biodiesel production from low FFA waste cooking oil using heterogeneous catalyst derived from chicken bones. Renew. Energy 76, 362–368. https://doi.org/10.1016/j.renene.2014.11.042

Kataria et al., 2019. Biodiesel production from waste cooking oil using heterogeneous catalysts and its operational characteristics on variable compression ratio CI engine. J. Energy Inst. 92, 275–287. https://doi.org/10.1016/j.joei.2018.01.008

Kirubakaran, K., Arul Mozhi Selvan, V., 2018. Eggshell as heterogeneous catalyst for synthesis of biodiesel from high free fatty acid chicken fat and its working characteristics on a CI engine. J. Environ. Chem. Eng. 6, 4490–4503. https://doi.org/10.1016/j.jece.2018.06.027

Kirubakaran, M., Selvan, V.A.M., 2018. A comprehensive review of low cost biodiesel production from waste chicken fat. Renew. Sustain. Energy Rev. 82, 390–401. https://doi.org/10.1016/j.rser.2017.09.039

Mendonça et al., 2019. New heterogeneous catalyst for biodiesel production from waste tucumã peels (Astrocaryum aculeatum Meyer): Parameters optimization study. Renew.

Energy 130, 103–110. https://doi.org/10.1016/j.renene.2018.06.059

Tan et al., 2019a. Biodiesel production from used cooking oil using green solid catalyst derived from calcined fusion waste chicken and fish bones. Renew. Energy 139, 696–706. https://doi.org/10.1016/j.renene.2019.02.110

Tan et al., 2019b. Biodiesel production from used cooking oil using green solid catalyst derived from calcined fusion waste chicken and fish bones. Renew. Energy 139, 696–706. https://doi.org/10.1016/j.renene.2019.02.110

Xie, W., Zhao, L., 2013. Production of biodiesel by transesterification of soybean oil using calcium supported tin oxides as heterogeneous catalysts. Energy Convers. Manag. 76, 55–62. https://doi.org/10.1016/j.enconman.2013.07.027

# Effect of mineral waste on CO$_2$ Capture: Critical Review

*Hetal J. Suvar, Dr. M.V. Shah, Dr. Attindra Shukla*

*Applied Mechanics Department, L.D. College of Engineering, Gujarat Technological University, Ahmedabad 380015, Department of Chemical Engineering, Dharmsinh Desai University, Nadiad-387001, Gujarat, INDIA*

*Corresponding author:* suvarhetal@gmail.com, mvs2212@yahoo.com.co.in, atindra@gmail.com
*+919537635506, +919426724617, +919904020338*

## Abstract

The literature review is for assessment of various methodologies for CO$_2$ capture and it deals with the analysis of experimental model used for CO$_2$ capture, study of the catalysts such as CaO, Waste Marble Powder for enhancing CO$_2$ uptake capacity. This also includes critically examining several Carbon Capture and Storage Technologies used at industrial level providing great extent of positive results towards net removal of CO$_2$ from the atmosphere. Besides, it involves the assessment of advantage and disadvantage of CO$_2$ sorbent (mineral waste) furthermore study of the activation of activated carbon for high CO$_2$ uptake capacity. This study shows that Ca enrich catalyst shows the better enhancement in capture capacity of CO$_2$ of virgin waste materials. In comparison to different kinds of CCS technologies for CO$_2$ capture most widely accepted are BECCS, WTE, Carbon Mineralization, et al. This paper also includes analysis of waste material activation of three kinds steam activation, CO$_2$ activation and Potassium hydroxide (KOH) activation for enhancement of CO$_2$ uptake capacity.

**Keywords:** Municipal solid waste, CO$_2$ capture, Negative emission, Activated carbon, Microspores, Catalyst, Mesopores, waste materials, breakthrough analysis

## 1. Introduction

CO$_2$ is the main greenhouse gas emitted following human activities. CO$_2$ is mainly released to the atmosphere from the combustion of fossil fuels (coal, natural gas, and oil) for energy and transportation, although certain industrial processes (cement production, chemical, petrochemical, and refining processes) and land-use changes also emit CO$_2$. Reducing emissions of CO$_2$ is of great importance to the scientific community. The emissions of CO$_2$ from MSWI plants are important source of greenhouse gas. With the need to reduce CO$_2$ emissions, controlling the production of CO$_2$ inside incineration plants is important. Power plants are a popular target for carbon capture since they are a large, stationary source of CO$_2$ emissions. Municipal solid waste, an inevitable by-product of urban life, is known to contain high proportion of hydrocarbon, which has become an attractive alternative for energy recovery.

Carbon Capture and Storage (CCS) technology can significantly reduce the impacts of climate change by capturing the CO$_2$ produced from the combustion of fossil fuels. The captured CO$_2$ must then be transported to an underground storage site, where it will be stored away from the atmosphere for a very long time. However, full large-scale integrated demonstration projects and numerical simulations are still required to enhance the knowledge on long-term geological storage of CO$_2$ before the wider deployment of CCS in geological formations takes place. Due to slow progress in the deployment of technologies that store CO$_2$ underground, and the fact that access to underground storage may not be entirely feasible, or even possible in some parts of the world, there has been an increasing interest in mineral carbonation.

The literature review is covered in five sections. The first section deals with use of equipment to assess the CO$_2$ capture capacity is examined for hydrous conditions and anhydrous

conditions with pure $CO_2$ and simulated incineration flue gas. BECCS, CCS, LFG-CCS, MSW-CCS, WTE technologies for net removal of $CO_2$ from the atmosphere and its evaluation as the environmental and economic implications is studied in second section. In third section catalyst such as CaO and activated carbon as a $CO_2$ sorbent were studied parallel studying the activation of activated carbon for high $CO_2$ capture. In fourth section the prepared different components municipal solid wastes based carbons were used to investigate the adsorption of $CO_2$ were studied. The work reviews the using mineral wastes for CCS and their potential in $CO_2$ abatement and study Carbon Capture and Storage by Mineralization (CCSM) in fifth section. The objective of the work is to critical assess the various methodologies for $CO_2$ capture using waste materials. The study of the various catalysts such as CaO, Waste marble powder used as a $CO_2$ absorbent to enhance capture capacity. Study of experimental modelling used for $CO_2$ capture.

## 2. Methodology

Many researchers has done extensive research work in the field of $CO_2$ capture with utilization of waste material in various different ways. Besides, research work has also been done in utilization of Ca enrich catalysts and $CO_2$ sorbent to enhance $CO_2$ uptake capacity of waste materials. Following group of research is being critically reviewed are mentioned below.

### 2.1. $CO_2$ capture based on experimental modeling

Jian-guo Jiang, et al. (2009) worked on the Novel dynamic equipment with gas in and out continuously was developed to study the capture capacity of $CO_2$. Municipal solid waste incineration (MSWI) fly ash has a high capture rate of $CO_2$ in $CO_2$ -rich gas. Fly ash can sequester pure $CO_2$ rapidly, and its capacity is examined for hydrous conditions and anhydrous conditions with pure $CO_2$ and simulated incineration flue gas. Chemical tests were performed to examine its chemical behaviour such as SEM, XRD, XRF, et al.In this study, novel dynamic equipment with gas in and out continuously was designed and used to examine the sequestration capacity of $CO_2$ in the form of pure $CO_2$ and simulated incineration emissions.

### Theory/calculation

Comparing the results under the four conditions the fly ash had a high sequestration capacity for $CO_2$; the capture rate was fast for pure $CO_2$, but relatively slow for the simulated incineration emissions. In practice, the possibility exists that fly ash with some additives could be formed into porous material to capture incineration emissions, allowing the release of pure $CO_2$ and the reuse of the porous material. This technology should thus facilitate a reduction in the amount of $CO_2$ entering the atmosphere. The SEM images revealed distinct differences in the morphology of the samples before and after carbonation.

Raw fly ash (×12,000)  Raw fly ash (×60,000)

Carbonated fly ash (×12,000)  Carbonated fly ash (×60,000)

Raw fly ash

Carbonated fly ash
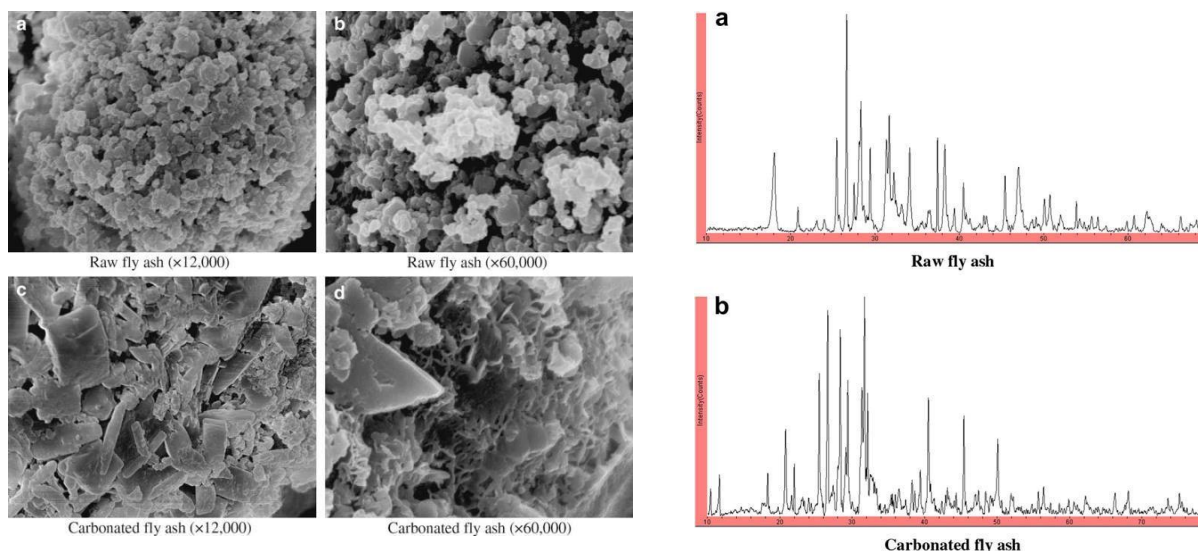
## 2.2. Comparative study of technologies to be used for net removal of $CO_2$

Nasim Pour, et al. (2018) examined the global potential for using municipal solid waste as a resource for bioenergy with carbon capture and storage (BECCS) and to compare the feasibility of two specific BECCS options: municipal solid waste incineration with carbon capture and storage (MSW-CCS), and landfill gas combusted in a gas turbine with carbon capture and storage (LFG- CCS).  Bioenergy with Carbon Capture and Storage (BECCS) is a carbon removal technology that offers permanent net removal of carbon dioxide ($CO_2$) from the atmosphere. One of the significant bioenergy resources is organic waste collected from municipal solid waste (MSW). The goal of this to assess the feasibility of MSW-based BECCS options, techno-economic and environmental impact assessments were conducted.

## Theory/calculation

Environmental impact assessment Life cycle assessment (LCA) was carried out ,the LCA study includes four main steps; defining the goal and scope, life cycle inventory of all the inputs and outputs, lifecycle impact assessment, and interpretation of the results. Allocation modelling was applied to assess the environmental impacts of the two waste – based BECCS systems with the same functional unit of 1 kg of the wet waste delivered to the landfill. The corresponding data for the electricity mix, construction materials and background processes, changes for each context. All the other data regarding operational conditions of the plants are the same. In the case of business-as-usual with no emission policy in effect, both BECCS options are more costly than coal-based power generation. Since BECCS options in this modelling had higher net $CO_2$ avoided, the total cost of avoided emission was lower than coal-CCS technology. Environmental impact assessment of the proposed BECCS models showed that both systems are environmentally benign with considerable potential for net $CO_2$-eq emission reduction.

## 2.3. Evaluation of catalysts/ $CO_2$ sorbent to enhance $CO_2$ uptake capacity of waste material

### 2.3.1 Study of CaO and activated carbons as a $CO_2$ sorbent

Mian Hu, et al. (2015) carried out research work in order to enhance energy recovery

efficiency from MSW (municipal solid waste), an in-situ steam gasification method for hydrogen production where CaO was used as $CO_2$ sorbent and catalyst in the process was proposed. The effects of moisture content, the molar ratio of CaO to carbon in wet MSW ([Ca]/[C]) and reactor temperature on H2 yield and gas composition were investigated. The proposed direct gasification of wet MSW with in situ $CO_2$ capture process may be a promising route to produce hydrogen rich fuel gas using MSW.

Jarosław Serafin, et al. (2017) reports on the preparation and examination of biomass-derived activated carbons featuring high $CO_2$ adsorption capacity. A detailed micropore structure analysis and surface characterization were performed using nitrogen adsorption isotherms and carbon dioxide isotherms. At 273 K and 1 bar only micropores were mainly effective for $CO_2$ adsorption. When the temperature increased the ranges of effective micropores for $CO_2$ adsorption at 1 bar decreased. For the typical flue gas conditions, micropores in the range of 0.30–0.57 nm were mainly effective for $CO_2$ adsorption. Activated carbon prepared from pomegranate peels showed the highest $CO_2$ adsorption and selectivity ($CO_2$ / $N_2$).Biomass-derived activated carbons with high $CO_2$ adsorption were successfully prepared through the KOH activation and carbonization. The precursor had a strong effect on the textural properties of the resulting carbon. The activated carbons with different sizes of micropores showed various sensitivity to the adsorption temperatures and pressures. Activated carbon prepared from pomegranate peels showed the highest $CO_2$ adsorption and selectivity.

### 2.3.3 Application of APC residue to assess $CO_2$ uptake capacity of ash

Renato Baciocchi, et al. (2009) study on accelerated carbonation of incinerator air pollution control residues, with a particular focus on the modifications in the leaching behaviour of the ash. Aqueous carbonation experiments were carried out using 100% $CO_2$ at different temperatures, pressures and liquid-to-solid ratios, in order to assess their influence on process kinetics, $CO_2$ uptake and the leaching behaviour of major and trace elements. The main effects of carbonation on trace metal leaching involved a significant decrease in mobility for Pb, Zn and Cu at high pH values, a slight change or mobilization for Cr and Sb, and no major effects on the release of As and soluble salts. Geochemical modelling of leachates indicated solubility control by different minerals after carbonation. In particular, in the stability pH range of carbonates, solubility control by a number of metal carbonates was clearly suggested by modelling results.

In the present work we aimed at investigating the effects of accelerated carbonation on humidified samples of APC residues to assess the $CO_2$ storage capacity of the ash and the influence of the main operational parameters on the kinetics of the reaction as well as the leaching-controlling mechanisms for carbonated APC residues, motivating the effects of carbonation on metal release by means of geochemical modelling. Furthermore, the works regarding the effects of accelerated carbonation on the mechanisms controlling the leaching behaviour of the ash, generally do not elaborate on the outcome of the treatment in terms of the $CO_2$ uptake, the achieved calcium conversion yield and the kinetics of the process.

### 2.4. Examining the different components of municipal solid wastes based carbons used to investigate the adsorption of $CO_2$

Thiruvenkatachari, et al. (2009) has done research work to obtain the ideal adsorbents for $CO_2$ adsorption, have carried out a series of research on carbon materials. The prepared different components municipal solid wastes based carbons were used to investigate the adsorption of $CO_2$. The optimum conditions for $CO_2$ adsorption were investigated firstly. And then, the $CO_2$

adsorption performance of different components based carbon adsorbents were compared with each other under the optimum parameters. The results illustrated that the triple components (pinewood, acrylic textile, and tire) based carbon exhibited the best adsorption performance. Besides, to further approach to the actual gas, the influence of additional $O_2$ and $SO_2$ on $CO_2$ adsorption properties of ternary-component-based carbon was investigated. For the excellent adsorption performance, activated carbons are widely applied for $CO_2$ adsorption. But the expensive cost of carbon adsorbent restricts its application for $CO_2$ removal. So the researchers turn to the low-cost adsorbents from cheap materials such as municipal solid wastes (MSWs). In this study, the $CO_2$ adsorption performances of the prepared different components MSW-based carbon were compared. The influence of experiment conditions on adsorption properties was conducted firstly. The ideal experiment parameters such as adsorption temperature, $CO_2$ concentration, and flow rate were determined by $CO_2$ adsorption capacity. Then the $CO_2$ adsorption capacities for different components MSW-based carbons were tested and the best group was selected. Besides, the competitive adsorption from different inlet gases was verified and the adsorption mechanism for $CO_2$ was illustrated.

**Theory/calculation**

The adsorption capacity could be calculated with

$$q_e = \frac{(C_i \times t \div 60 - S) \times u \times A \times 60 \times 10^{-3}}{m_{AC} \times 44},$$

Eq. (1) where qe is the $CO_2$ adsorption capacity (mmol/g), Ci is the inlet concentration of $CO_2$ (mg/L), t is the adsorption equilibrium time(s), S is the integration area between the breakthrough curve and the abscissa (m2), u is the gas velocity (m/s), A is the cross-sectional area of adsorption column (m2), and mAC represents the mass of the once used carbon adsorbent (g).

The prepared pinewood-based carbon adsorbent was applied for $CO_2$ adsorption firstly to acquire the optimal adsorption experiment conditions. The prepared different component-based carbon adsorbents were used for $CO_2$ adsorption. The mixture of pinewood, acrylic textile, and tire exhibited the best $CO_2$ adsorption capacity which is comparable to the commercial activated carbon. The $SO_2$ exert great inhibited effect on $CO_2$ adsorption and reduced the equilibrium adsorption capacity obviously. The results illustrate that $O_2$ concentration exerts little effect on adsorption capacity. $SO_2$ plays the dominated role in the competitive adsorption effect.

**2.5. Analysis the effects of methods of activation on $CO_2$ adsorption performance of activated carbon**

Sepideh Shahkarami, et al. (2015) study the effects of different methods of activation on $CO_2$ adsorption performance of activated carbon were studied. Activated carbons were prepared from biochar, obtained from fast pyrolysis of white wood, using three different activation methods of steam activation, $CO_2$ activation and Potassium hydroxide (KOH) activation. $CO_2$ adsorption behavior of the produced activated carbons was studied in a fixed-bed reactor set-up to determine the effects of the surface area, porosity and surface chemistry on adsorption capacity of the samples. Characterization of the micropore and mesopore texture was carried

out using $N_2$ and $CO_2$ adsorption at 77 and 273 K, respectively. Central composite design was used to evaluate the combined effects of temperature and concentration of $CO_2$ on the adsorption behavior of the adsorbents. The performance of the adsorbents in multi-cyclic adsorption process was also assessed and the adsorption capacity of KOH and $CO_2$ activated carbons remained remarkably stable after 50 cycles with low temperature (160°C) regeneration.

As the breakthrough continues the $CCO_2$ in the outlet increases gradually to the inlet concentration. At this point, no more adsorption can take place in the bed. Adsorption results demonstrate that, in this range of parameters, the adsorption behavior of activated carbon can be mainly influenced by porosity of the adsorbent. Steam activated carbon and $CO_2$ activated carbon with the close range of surface area, the total porosity, micro porosity and similar surface chemistry present the same adsorption behaviour, indicating the fact that activation agent is not a significant factor on performance of activated carbon for $CO_2$ capture under these operating conditions. Overall, KOH activated carbon with higher surface area and porosity can be considered as the best option for $CO_2$ capture at atmospheric pressure and low temperature of $CO_2$. It has been shown that the KOH activated carbon does not offer any advantages at higher temperature.

## 2.6. Assessment of mineral wastes to be used for CCS and review of its potential applications

Aimaro Sanna, et al. (2012) deals with using mineral wastes for CCS and their potential in $CO_2$ abatement, highlighting the potential applications and scenarios. This study indicates that a variety of inorganic waste materials such as pulverised fuel ash, municipal solid waste ash, cement kiln dust, biomass and paper sludge ash and sewage sludge ash are available feedstocks for Carbon Capture and Storage by Mineralisation (CCSM) in the UK. The high variability of both the waste amounts and chemical composition represent a major obstacle to the deployment of these materials in CCSM. Inorganic waste as a CCSM resource is in many ways more complex than the use of natural minerals due to uncertainty on future availability and high chemical variability and might be viable only in niche applications. The parameters used to assess the current and the future potential of the mineral wastes as a resource for CCSM are: 1. Amounts available (including predicted future trends); 2. Content of calcium, magnesium and other elements.

### Theory/calculation

The 'theoretical' maximum $CO_2$ uptake ($TCO_2$ uptake) expressed in wt% was calculated for each potential UK CCSM resource from its total Ca and Mg concentrations using a modified Steinour formula:

$$TCO_{2\ uptake} = 0.785 \times (\%CaO - 0.56 \times \%CaCO_3 - 0.7 \times \%SO_3) + 1.091 \times \%MgO + 0.71 \times \%Na_2O + 0.468 \times (\%K_2O - 0.632 \times \%KCl)$$

This method is based on the assumption that the total amount of Ca and Mg can be extracted from the waste and subsequently carbonated. $TCO_2$ uptake and the annual production of the waste in the UK were then used to calculate its 'theoretical' annual maximum $CO_2$ storage

potential ($TCO_2$ capture; expressed in Mt $CO_2$/year) as follows;

$$TCO_{2\ capture}(A) = \text{Waste available}(A) \times TCO_{2\ uptake}(A)$$

Where (A) represents potential waste resources in the UK for CCSM and the waste available stands for the amount of waste that is currently not reused in other applications (i.e. sent to landfill). The experimental $CO_2$ capture ($ECO_2$ capture) considering the experimental $CO_2$ uptake ($ECO_2$ uptake) was calculated.

For this study, the $ECO_2$ uptake and not the conversion yield is considered of primary importance, because its final aim is to evaluate the potential of UK wastes as feedstock for CCSM and not to compare the different mineral carbonation technologies available. Overall, the use of waste resources for CCSM should be considered as a niche market that could utilize relatively small amounts of feed material for CCSM. They may have the advantage to be often located close to the $CO_2$ emission site.

## 3. Materials and methods

### 3.1 Material

MSW from disposal sites, KOH, Waste marble powder, CaO, Activated Carbon, mineral wastes, Organic fractions (paper, textile, wood and plastic) were selected as the experimental materials.

### 3.2 Methods

Equipment uses fixed bed reactor for absorbance test with continues monitoring of pressure and temperature. The assembly consisted of the fixed bed reactor and associated auxiliary equipment which included electric furnace heater, temperature controller cabinet and gas purification unit. The work also involves to study the methods used as industrial level such as Carbon Capture and Storage, Waste to Energy coupled with CCS, Landfill Gas Combustion and MSW-incineration comparing the effectiveness of each by study its techno-economical analysis. Chemical behavior of waste material is examined by various chemical tests such as SEM, XRD, XRF, TGA to study structural changes, elemental composition, chemical composition, $CO_2$ absorbed by material, Leaching tests to study the behavior of leachate produced by Municipal Solid Waste. Methods for the activation of activated carbon were thoroughly studied with analyzing the changes in $CO_2$ capture capacity of it.

## 4. Critical Comment and Gap

The use of Carbon Capture and storage (CCS) technologies imparts the great extent of removal of $CO_2$ from the atmosphere.

• Ca enrich compounds can increase the Cation Exchange Capacity of waste material so that material can act as potential $CO_2$ absorbent.

• Waste materials having more percentage of Ca element should be thoroughly studied such as waste concrete, kiln dust, etc.

• Carbon Capture and Utilization (CCU) Technologies are more beneficial than some of the

CCS technologies. The study of $CO_2$ capture was limited to certain temperature and pressure ranges only.

• Geological storage involves injecting captured $CO_2$ from industrial processes into rock formations deep underground, thereby permanently removing it from the atmosphere. The geological investigations regarding changes in strength and structural characteristics of the rock needs to be encouraged and further reclamation strategies need to be developed.

• The research work for mineral carbonation should be done to convert Ca-enrich waste materials into reusable carbonates.

• Study of organic parts and effects of heavy metals presents in MSW and their effects on Carbon Capture was not studied.

• The research work related to creating strong permanent chemical bonds which provide the facility to captured $CO_2$ to be permanently stored or release the $CO_2$ on very high temperature ranges only needs to be studied.

## 5. Conclusions

Theoretical review of the potential applications of the technologies using waste material to be useful for carbon capture and storage.

- There could be probability of using some additives/ Catalyst with Fly ash to enhance its capturing capacity by dealing with its specific surface area and pore size. Also, it can be converted it into porous material that allows release of captured $CO_2$ and reuse the fly ash.

- Considering economic factor BECCS options are more costly than coal- based power generation. Besides, global requirements are more focused on Carbon Capture and Utilization (CCU) than Carbon Capture and Storage (CCS).

- Both the technologies MSW-CCS and LFG-CCS shows equal and positive results in environmental- impact assessment.

- Use of CaO for carbon capture and $H_2$ enrich Gas can be promising technique. But, possibility of using captured Carbon for construction applications, ethanol blending, etc. needed to be further study.

- Biomass-derived activated carbons with high $CO_2$ adsorption were successfully prepared through the KOH activation and carbonization. Further study can be done by altering activation method such as thermal activation which could provide positive results towards absorption capacity for carbon capture.

- The experimental work for accelerated carbonation of incinerator air pollution control (APC) residues has successfully done with a particular focus on the modifications in the leaching behavior of the ash with using 100% $CO_2$. Further research work can be done using actual amount of $CO_2$ in flue gas (contain 12% $CO_2$) and compare with the results obtain in existed study.

- Activated carbon show excellent adsorption performance and are widely applied for $CO_2$ adsorption. But the expensive cost of carbon adsorbent restricts its application for $CO_2$ removal.

- Applications of three different types of activation of activated carbon, KOH and $CO_2$ activated carbons remained remarkably stable after 50 cycles with low temperature (160°C) regeneration. The Characterization of the micropores and mesopores texture has been carried out in detail till the point has reached where no more adsorption can take place.

- Use of variety of waste materials such as pulverised fuel ash, municipal solid waste ash, cement kiln dust, biomass and paper sludge ash and sewage sludge ash for $CO_2$ capture is a great initiative as Carbon Capture and Storage by Mineralisation (CCSM) technique. The study also provides the possibility to use it for permanently storage of captured $CO_2$.

## Acknowledgements

## References

1. Anthony, E.J., Jia, L.,Woods, J., Roque,W., Burwell, S., 2000. Pacification of high calcic residues using carbon dioxide. Waste Manag. 20, 1–13.

2. Atis, C.D., 2003. Accelerated carbonation and testing of concrete made with fly ash. Construct. Build. Mater. 17, 147–152.

3. Aaron, D., Tsouris, C., 2005. Separation of $CO_2$ from flue gas: a review. Sep. Sci. Technol. 40, 321–348.

4. Abu-Zahra, M., Schneiders, L., Niederer, J., Feron, P., Versteeg, G., 2007. $CO_2$ capture from power plants Part I. A parametric study of the technical performance based on monoethanolamine. Int. J. Greenh. Gas Control 1, 37–46.

5. Bodénan, F., Deniard, Ph., 2003. Characterization of flue gas cleaning residues from European solid waste incinerators: assessment of various Ca-based sorbent processes. Chemosphere 51, 335–347.

6. Bodénan, F., Azaroual, M., Piantone, P., 2000. Forecasting the longterm behaviour of municipal solid waste incineration bottom ash: rapid combined tests. In:Woolley, G.R., Goumans, J.J.J.M., Wainwright, P. (Eds.), Waste Materials in Construction. Studies in Environmental Sciences, vol. 71. Elsevier Science,Amsterdam, pp. 475–482.

7. Bone, B.D., Knox, K., Picken, A., Robinson, H.D., 2003. The effect of carbonation on leachate quality from landfilled municipal solid waste (MSW) incinerator residues.

8.  Christensen, T.H., Cossu, R., Stegmann, R. (Eds.), Proceedings Sardinia 2003, Ninth International Waste Management and Landfill Symposium (on CD ROM).

9.  Cheng, T.W., 2003. Combined glassification of EAF dust and incinerator fly ash. Chemosphere 50,47–51.

10. Ecke H. Sequestration of metals in carbonated municipal solid waste incineration (MSWI) fly ash. Waste Manage 2003;23:631–40.

11. Fernandez Bertos M, Li X, Simons SJR, Hills CD, Carey PJ. Investigation of accelerated carbonation for the stabilisation of MSW incinerator ashes and the sequestration of $CO_2$. Green Chem 2004;6:428–36.

12. Johnson DC. Accelerated carbonation of waste calcium silicate materials. SCI Lect Pap Ser 2000;108:1–10.

13. Polettini, A., Pomi, R., 2004. The leaching behaviour of incineration bottom ash as affected by accelerated ageing. Journal of Hazardous Materials B113, 209–215.

14. Prigiobbe, V., Polettini, A., Baciocchi, R., 2009. Gas–solid carbonation kinetics of air pollution control residues for $CO_2$ storage. Chemical Engineering Journal 148, 270–278.

15. Zhu TY, Zhang SY, Hung JJ, Wang Y. Effect of calcium oxide on pyrolysis of coal in a fluidized bed. Fuel Process Technol 2000;64:271e84.

# OUR SPONSORERS: